UCRL-ID-152852

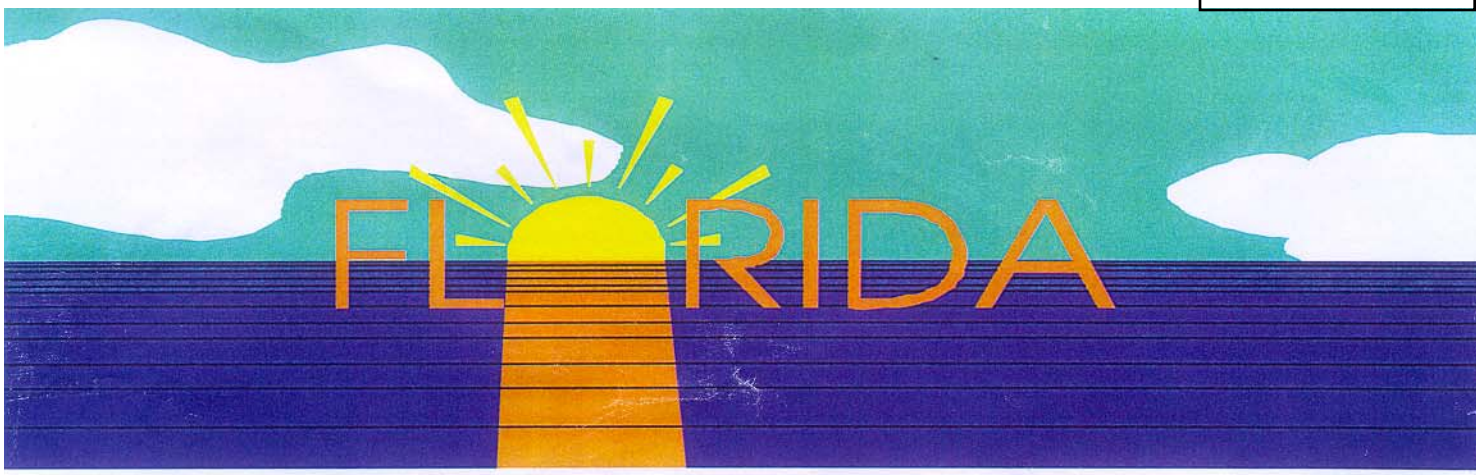

6TH WORKSHOP ON FAST IGNITION OF FUSION TARGETS

NOVEMBER 16-19, 2002

DOLPHIN BEACH RESORT

ST. PETES BEACH, FLORIDA

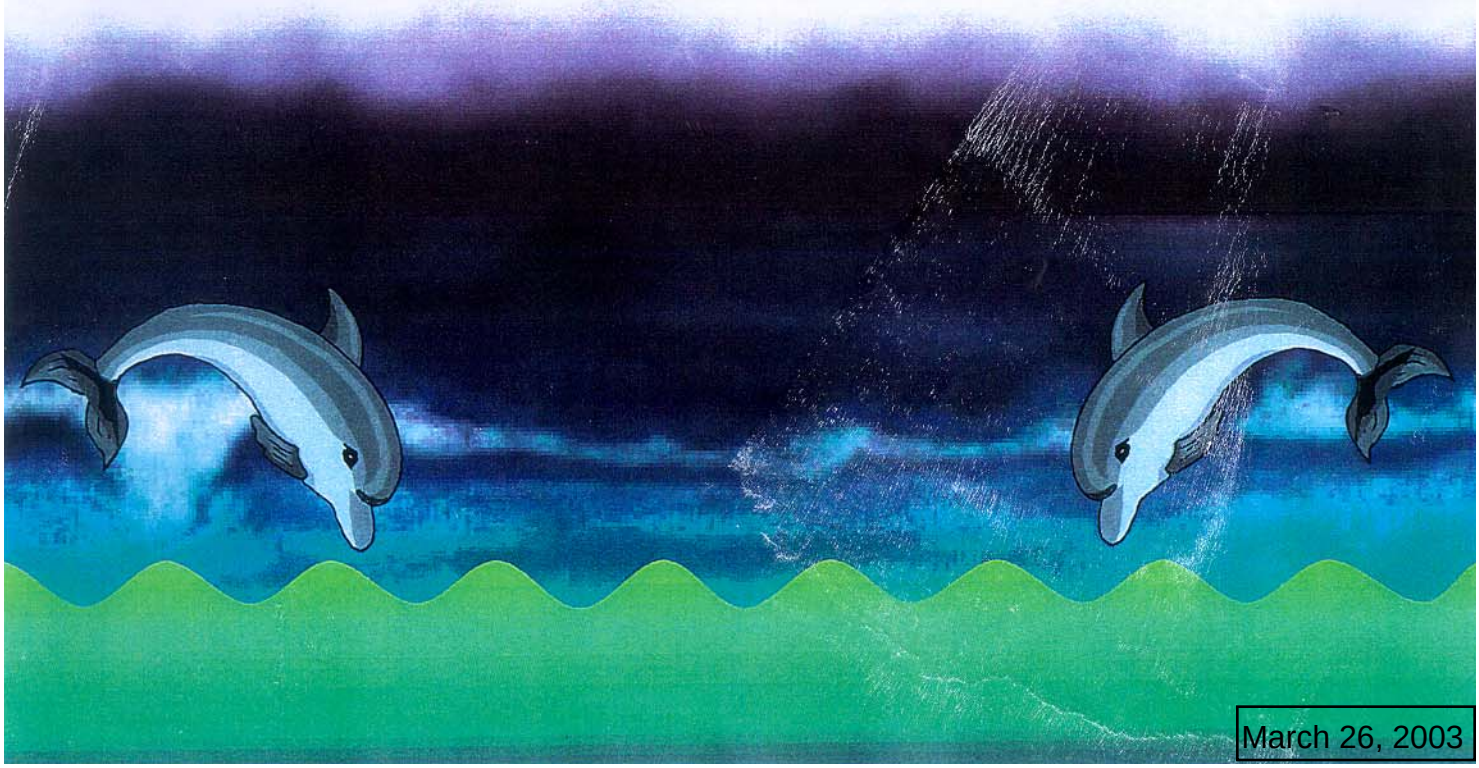

March 26, 2003

This document was prepared as an account of work sponsored by an agency of the United States Government. Neither the United States Government nor the University of California nor any of their employees, makes any warranty, express or implied, or assumes any legal liability or responsibility for the accuracy, completeness, or usefulness of any information, apparatus, product, or process disclosed, or represents that its use would not infringe privately owned rights. Reference herein to any specific commercial product, process, or service by trade name, trademark, manufacturer, or otherwise, does not necessarily constitute or imply its endorsement, recommendation, or favoring by the United States Government or the University of California. The views and opinions of authors expressed herein do not necessarily state or reflect those of the United States Government or the University of California, and shall not be used for advertising or product endorsement purposes.

This work was performed under the auspices of the U.S. Department of Energy by University of California, Lawrence Livermore National Laboratory under Contract W-7405-Eng-48.

FIW2002

6th Workshop on Fast Ignition of Fusion Targets
November 16, 2002 - November 19, 2002
Dolphin Beach Resort
St. Petes Beach, Florida, USA

Kirk Flippo - poster prize winner

Lawrence Livermore National Laboratory
Making History Making a Difference
1952-2002

NIF Programs
P.O. Box 808
Livermore, CA 94550

Dear FIW2002 participants,

The 6th Workshop on Fast Ignition of Fusion targets had 72 participants whose affiliation and e-mail addresses are listed in the attached spreadsheet. The scientific presentations gave a wide-ranging and up to day summary of work related to fast ignition. You have all been most cooperative in supplying electronic copies of your presentations and these are attached in this CD and should provide us all with a valuable source of information.

This mailing is the final action of the organizers of the conference. I would like to use this opportunity to reiterate my thanks to the members of the local organizing committee and the international organizing committee. Their names are listed after this note. I would like to remind you also of the sponsorship which we received from General Atomics and the National Science Foundation.

The conference would not have been a success without significant administrative support and you will remember the contribution at the meeting of Connie Oakley and Sharon Hornstein. The heavier lifting was however done behind the scenes and I would like particularly to express thanks to Lynnette Gomez for undertaking most of the conference administration and to Bill Meyer for his expert management of the website.

Please find attached also an electronic photograph of us all on the beach at St. Pete's as a final reminded of the meeting.

The next conference will be organized by our Japanese colleagues and I have heard talk of an enjoyable venue with hot springs somewhere in the south of Japan in the spring time of 2004

Yours sincerely,

M.H. Key
Conference Chairman

FIW2002

6th Workshop on Fast Ignition of Fusion Targets
November 16, 2002 - November 19, 2002
Dolphin Beach Resort
St. Petes Beach, Florida, USA

Program Committee

International Committee

Allen Offenberger	Canada	aao@ee.ualberta.ca
Jie Zhang	China	jzhang@aphy.iphy.ac.cn
Xianto He	China	xthe@mail.iapcm.ac.cn
Jean-Claude J. Gauthier	France	jean-claude.gauthier@polytechnique.fr
Jean-Claude Adam	France	adam@cpht.polytechnique.fr
Oswald Willi	Germany	oswald.willi@laserphy.uni-duesseldorf.de
Juergen Meyer-ter Vehn	Germany	Juergen.Meyer-ter-Vehn@mpq.mpg.de
Dimitri Batani	Italy	batani@mib.infn.it
Kazuo Tanaka	Japan	katanaka@ile.osaka-u.ac.jp
Kunioki Mima	Japan	mima@ile.osaka-u.ac.jp
Luis Silva	Portugal	luis.silva@ist.utl.pt
Boris Sharkov	Russia	Boris.Sharkov@itep.ru
Jose Javier Honrubia	Spain	honrubia@etsii.upm.es
Peter Norreys	UK	P.A.Norreys@rl.ac.uk
Malcolm Haines	UK	m.haines@ic.ac.uk
Mike Campbell	US	Mike.campbell@gat.com
Mike Key	US	Key1@llnl.gov

Local Organizing Committee

Mike Key	Lawrence Livermore National Laboratory	Key1@llnl.gov
Steve Hatchett	Lawrence Livermore National Laboratory	hatchett1@llnl.gov
Grant Logan	Lawrence Berkeley Laboratory	bglogan@lbl.gov
Rodney Mason	Los Alamos National Laboratory	mason@lanl.gov
Stephen Slutz	Sandia National Laboratory	saslutz@sandia.gov
Rich Stephens	General Atomics, San Diego	rich.stephens@gat.com
Nat Fisch	Princeton University	nfisch@pppl.gov

Rick Freeman	University of California, Davis	Rrfree@ucdavis.edu
Warren Mori	University of California, Los Angeles	mori@physics.ucla.edu
Don Umstadter	University of Michigan	dpu@umich.edu
Christian Stoeckl	University of Rochester	csto@lle.rochester.edu
Todd Ditmire	University of Texas	tditmire@physics.utexas.edu

FIW2002

6th Workshop on Fast Ignition of Fusion Targets
November 16, 2002 - November 19, 2002
Dolphin Beach Resort
St. Petes Beach, Florida, USA

Workshop Program

You may view all the abstracts sorted by first author. The titles for the oral talks below link to the pdf files if available.

Saturday, November 16, 2002

6:00-8:00 PM		Registration and Welcome Reception hosted by General Atomics

Sunday, November 17, 2002

Conference Overview (8:00 AM- 9:50 AM) Session Chair - K. Tanaka		
8:05-8:45	M. Tabak	Review of the theory and modeling basis of fast ignition (tutorial)
8:45-9:10	R. Kodama	Petawatt laser heating of high-density plasmas
9:10-9:50	M. Key	Review of the experimental basis of fast ignition (tutorial)
9:50-10:10	Morning Break	Continental Breakfast
Electron Transport (10:10 AM-12:15 PM) Session Chair - W. Kruer		
10:10-10:35	J. Adam	Angular dispersion of energetic electrons generated by interaction of an ultra-intense laser with an overdense plasma
10:35-11:00	K. Krushelnick	Laboratory measurements of GigaGauss range magnetic fields generated during high intensity laser interactions with dense plasmas
11:00-11:15	J. Delettrez	Transport of relativistic electrons for modeling fast ignition in the 2-D hydrocode DRACO
11:15-11:30	S. Baton	Evidence of sub-picosecond electron bunches in solid matter irradiated by ultra-high intensity laser
11:30-11:45	J. Koch	Monochromatic x-ray imaging as a diagnostic of relativistic electron flow in ultra-high-intensity laser irradiated targets.
11:45-7:00	INFORMAL DISCUSSIONS-LUNCH/DINNER ON YOUR OWN	
7:00-9:00 PM	**Evening Poster Session**/Judging of posters (Dessert and hot beverage will be served)	

Monday, November 18, 2002

Proton Beams (8:00 AM-10:00 AM) Session Chair - H. Hutchinson		
8:00 -8:15.	P. Patel	Experimental observation of isochoric heating with a ballistically focused laser-generated proton beam
8:15-8:30	M. Roth	Laser accelerated ions for fusion research
8:30-8:45	J. Fernandez	Ion acceleration experiments with the new short-pulse capability on Trident
8:45-9:00	M. Zepf	Proton acceleration from high intensity laser interactions with thin foil targets
9:00-9:15	A. MacKinnon	Development of advanced proton diagnostics for probing plasmas and shocked materials
9:15-9:30	M. Allen	Proton and ion acceleration from laser-plasma interactions with thin foils
9:30-9:45	D. Gericke	Energy deposition of laser-produced ions in fusion plasmas
9:45-10:00	K. Flippo	Laser produced proton beam characteristics
10:00-10:20	Morning Break	Refreshments served
Electron Transport (10:20 AM- 12:15 PM) Session Chair - G. Laval		
10:20-10:45	H. Sakagami	PIC, Fokker Planck and hydro simulation studies on implosion and heating process of cone-shell target fast ignition
10:45-11:00	M. Wei	Experimental observations of the filamentary instability in high intensity laser solid interactions
11:00-11:15	K. Tanaka	Investigation of coherent transition radiation from energetic electron beam produced in laser solid interaction
11:15-11:30	P. Mulser	Super-intense laser-pellet interaction and it's implications for fast ignition
11:30-11:45	R. Town	Calculations of electron transport in fast ignition targets
11:45-12:00	R. Freeman	What we've learned and haven't learned from recent electron transport experiments
12:00-12:15	R. Campbell	Propagation of petawatt laser-generated electron beams through solid density plasma
12:15-4:00	INFORMAL DISCUSSIONS-LUNCH ON YOUR OWN	
Electron Transport (4:00 PM-5:00 PM) Session Chair - G. Logan		
4:00-4:15	A. Macksimchuk	Electromagnetic emission from short-laser-pulse interaction with high density plasmas
4:15-4:30	P. Mora	Plasma expansion into a vacuum

4:30-4:45	J. Fuchs	Short-pulse high-power lsaer propagation in hollow plasma channel
4:45-5:00	J. Fuchs	Imaging ultra-high current electron transport in metals and insulators by laser-accelerated protons
6:30 PM	Conference Dinner	

Tuesday, November 19, 2002

Electron Transport (8:00 AM- 9:40 AM) Session Chair - J. Adam		
8:00-8:25	L. Silva	Collisionless electron transport and ion acceleration in laser-solid interactions
8:25-8:40	V. Malkin	Fast ignition utilizing collective deceleration of relativistic electrons produced by ultra-intense laser
8:40-8:55	R. Snavely	Relativistic electron beam transport and characteristics in solid density plasmas
8:55-9:10	C. Deutsch	Penetration of charged intense particle beams in precompressed DT fuels
9:10-9:25	A. Offenberger	Measurement of ultra-high magnetic fields in petawatt laser experiments
9:25-9:40	B. Logan	Application of fast ignition to heavy-ion fusion
9:40-10:00	Morning Break	Refreshments served
Integrated modeling and experiments (10:00 AM-11:55 PM) Session Chair - A. Offenberger		
10:00-10:15	H. Hutchinson	The Vulcan Petawatt Interaction Facility
10:15-10:30	S. Hatchett	Designs for Sub-Ignition Cone-Focused Experiments
10:30-10:55	P. Norreys	Relativistic laser-plasma experiments relevant to advanced fast ignition
10:55-11:10	C. Stoeckl	Integrated fast-ignitor experiments on the proposed OMEGA-EP facility at LLE
11:10-11:25	S. Slutz	Fast ignition capsules using liquid cryogenic fuel
11:25-11:40	R. Stephens	Implosion hydro of indirect drive FI targets.
11:40-11:55	D. Hanson	Hemispherical capsule implosions in a Z-pinch-driven fast ignitor fuel compression geometry
11:55-2:00	LUNCH ON YOUR OWN	
Full scale fast ignition (2:00 PM-4:00 PM) Session Chair - M. Roth		
2:00-2:25	C. Barty	High energy petawatt lasers for fast ignition
2:25-2:50	R. Stephens	Fast ignition targets for fusion energy
2:50-3:15	H. Azechi	Fast ignition Power plant concepts
3:15-3:30	A. Andreev	Laser fast ignition for dynamic hohlraum ICF scheme
3:30-3:45	J. DeGroot	Conceptual design of an Z-pinch fast ignitor power plant

3:45-4:00	Afternoon Break	Refreshments served
4:00-5:30	**Wrap-up/Summary**	

* All papers will be displayed as posters throughout the conference program. In addition to the oral presentations, the following papers will be presented as posters only.

Posters	
F. Alouani-Bibi	FOKKER-PLANCK SIMULATIONS OF HOT ELECTRON TRANSPORT IN SOLID DENSITY PLASMA
R. Bingham	Bremsstrahlung losses in inertially confined fusion targets
H. Habara	Neutron spectroscopy for plasma heating measurements in cone guided shell implosions on VULCAN
J.A. King	A preliminary study of picosecond K-Alpha backlighting of a 6-beam directly driven implosion
W. Kruer	Some features of relativistic electron transport for fast ignition
B. Lasinski	Ion beams in short-pulse, high intensity laser matter interactions
M. Marti	Ion acceleration in laser-thin target interactions: parametric study
J. Myatt	Fast-electron transport in dense plasmas in the context of fast ignition studies at LLE
C. Ren	Fast electron penetration and return current flow into plasma pellets with and without a hollow wedge
H. Sakagami	Fast ignition integrated interconnecting code project
K. Shigemori	Direct drive implosion experiments of plastic shell targets with gold cone for fast ignition research
G. Shvets	Self-similar superradiant amplification: from one-dimensional
M. Tabak	The effect of runaway electrons on transport in fast ignition targets
M. Tabak	Effect of relative costs of long pulse and short pulse coupled energy on optimized target designs for fast ignition
E. Takahashi	High intensity KrF laser pulse interaction with solid targets
Y. Urzhumov	Collective stopping of relativistic electron beams in dense plasma by Weibel and Tearing instabilities
N. Yugami	Short pulse microwave generation from interactions between ultra short laser and weakly magnetized plasma

FIW 2002
6TH WORKSHOP ON FAST IGNITION OF FUSION TARGETS
November 16 - 19, 2002
Dolphin Beach Resort
St. Petes Beach, Florida USA

ATTENDEES	E-MAIL	AFFILIATION
Adam, Jean Claude	adam@cpht.polytechnique.fr	LULI Ecole Polytechnique (France)
Allen, Matthew M.	mallen2nuc.berkeley.edu	Lawrence Livermore National Laboratory (USA)
Andreev, Alexander	andreev@ilph.spb.su	Institute for Laser Physics (Russia)
Azechi, Hiroshi	azechi@ile.osaka-u.ac.jp	Institue of Laser Engineering, Osaka Universityn (Japan)
Barty, Chris	barty1@llnl.gov	Lawrence Livermore National Laboratory (USA)
Baton, Sophie D.	sophie.baton@polytechnique.fr	LULI Ecole Polytechnique (France)
Bingham, Robert	R.Bingham@rl.ac.uk	Rutherford Appleton Laboratory (United Kingdom)
Campbell, Robert B.	rbcampb@sandia.gov	Sandia National Laboratories (USA)
Clark, Eugene L.	eugene.clark@awe.co.uk	AWE plc - Plasma Physics Department (United Kingdom)
Cuneo, Michael E.	mecuneo@sandia.gov	Sandia National Laboratories (USA)
DeGroot, John S.	jsdegroot@ucdavis.edu	University of California, Davis (USA)
Delettrez, Jacques	jdel@lle.rochester.edu	Laboratory for Laser Energetics - Theoretical (Rochester, NY)
Deutsch, Claude	claude.deutsch@lpgp.u-psud.fr	LPGP (France)
Fernandez, Juan C.	juanc@lanl.gov	Los Alamos National Laboratories (USA)
Flippo, Kirk A.	firpo2@llnl.gov	University of Michigan (USA)
Freeman, Richard R.	rrfree@ucdavis.edu	University of California, Davis (USA)
Fuchs, Julien	fuchsj@fusion.gat.com	General Atomics - Fusion Group (USA)
Garbett, Warren J.	Warren.J.Garbett@awe.co.uk	AWE (United Kingdom)
Gericke, Dirk O.	gericke@lanl.gov	Los Alamos National Laboratories (USA)
Habara, Hideaki	h.habara@rl.ac.uk	Rutherford Appleton Laboratory (United Kingdom)
Hanson, David L.	dlhanso@sandia.gov	Sandia National Laboratories (USA)
Hatchett, Stephen P.	hatchett1@llnl.gov	Lawrence Livermore National Laboratory (USA)
Hutchinson, Henry	h.hutchinson@rl.ac.uk	CLRC - Rutherford Appleton Laboratory (United Kingdom)
Izumi, Nobuhiko	izumi2@llnl.gov	Lawrence Livermore National Laboratory (USA)
Johnston, Tudor W.	johnston@inrs-ener.uquebec.ca	INRS-EMT (Canada)
Key, Michael H.	key1@llnl.gov	Lawrence Livermore National Laboratory (USA)
King, James A.	king55@llnl.gov	University of California, Davis (USA)
Koch, Jeffrey A.	koch1@llnl.gov	Lawrence Livermore National Laboratory (USA)
Kodama, Ryosuke	ryo@ile.osaka-u.ac.jp	Institue of Laser Engineering, Osaka Universityn (Japan)
Koenig, Michel	michel.koenig@polytechnique.fr	Laboratoire LULI/Ecole Polytechnique (France)
Kruer, William L.	kruer1@llnl.gov	Lawrence Livermore National Laboratory (USA)

FIW 2002
6TH WORKSHOP ON FAST IGNITION OF FUSION TARGETS
November 16 - 19, 2002
Dolphin Beach Resort
St. Petes Beach, Florida USA

ATTENDEES	E-MAIL	AFFILIATION
Adam, Jean Claude	adam@cpht.polytechnique.fr	LULI Ecole Polytechnique (France)
Krushelnick, Karl M.	kmkr@ic.ac.uk	Imperial College - Physics (United Kingdom)
Langdon, Bruce	blangdon@llnl.gov	Lawrence Livermore National Laboratory (USA)
Lasinski, Barbara F.	lasinski1@llnl.gov	Lawrence Livermore National Laboratory (USA)
Laval, Guy C.	laval@cpht.polytechnique.fr	CNRS-CPHT/Ecole Polytechnique (France)
Lindberg, Ryan	rl236@socrates.berkeley.edu	University of California, Berkeley (USA)
Logan, Grant	bglogan@lbl.gov	Lawrence Berkeley National Laboratory (USA)
Mackinnon, Andrew J.	mackinnon2@llnl.gov	Lawrence Livermore National Laboratory (USA)
Maksimchuck, Tolya	tolya@engin.umich.edu	University of Michigan (USA)
Malkin, Vladimir M.	malkin@astro.Princeton.EDU	Princeton University (USA)
Mason, Rod	mason@lanl.gov	Los Alamos National Laboratories - Group X-1 (USA)
Maximov, Andrei	amax@lle.rochester.edu	Laboratory for Laser Energetics (Rochester, NY, USA)
McKnight, Ronald	ronald.mcknight@science.doe.gov	US Department of Energy (USA)
Mehlhorn, Thomas A.	tamehlh@sandia.gov	Sandia National Laboratories (USA)
Mora, Patrick	patrick.mora@cpht.polytechnique.fr	Centre de Physique Theorique/Ecole Polytechnique (France)
Mulser, Peter	peter.mulser@physik.tu-darmstadt.de	Darmstadt University of Technology - Physics (Germany)
Myatt, Jason	jmya@lle.rochester.edu	University of Rochester (USA)
Norreys, Peter A.	p.norreys@rl.ac.uk	CCLRC Rutherford Appleton Laboratory (United Kingdom)
Offenberger, Allan A.	aao@ee.ualberta.ca	University of Alberta (Canada)
Patel, Pravesh K.	pravpatel@llnl.gov	Lawrence Livermore National Laboratory (USA)
Porter, John L.	jlporte@sandia.gov	Sandia National Laboratories (Albuquerque, NM)
Ren, Chuang	ren@physics.ucla.edu	University of California, Los Angeles
Roth, Markus	m.roth@gsi.de	Gesellschaft fr Schwerionenforschung mbH - Plasmaphysik (Germany)
Laurence E. Ruggles	leruggl@sandia.gov	Sandia National Laboratories (USA)
Sakagami, Hitoshi	sakagami@comp.eng.himeji-tech.ac.jp	Himeji Institute of Technology - Computer Engineering (Japan)
Shigemori, K.	shige@ile.osaka-u.ac.jp	Institue of Laser Engineering, Osaka Universityn (Japan)
Silva, Luis Oliveira	luis.silva@ist.utl.pt	Instituto Superior Tecnico (Portugal)
Slutz, Stephen A.	saslutz@sandia.gov	Sandia National Laboratories (USA)
Snavely, Richard A.	rasnavely@llnl.gov	Lawrence Livermore National Laboratory (USA)
Stephens, Richard B.	rich.stephens@gat.com	General Atomics (USA)

FIW 2002
6TH WORKSHOP ON FAST IGNITION OF FUSION TARGETS
November 16 - 19, 2002
Dolphin Beach Resort
St. Petes Beach, Florida USA

ATTENDEES	E-MAIL	AFFILIATION
Adam, Jean Claude	adam@cpht.polytechnique.fr	LULI Ecole Polytechnique (France)
Stoeckl, Christian	csto@lle.rochester.edu	University of Rochester
Tabak, Max	tabak1@llnl.gov	Lawrence Livermore National Laboratory (USA)
Takahashi, Eiichi	eiichi-takahashi@aist.go.jp	AIST - Central 2 1-1-1 Umezono (Japan)
Tanaka, Kazuo	katanaka@ile.osaka-u.ac.jp	Institue of Laser Engineering, Osaka Universityn (Japan)
Town, Richard PJ	town2@llnl.gov	Lawrence Livermore National Laboratory (USA)
Umstadter, Donald P.	dpu@umich.edu	University of Michigan - EECS/CUOS
Urzhumov, Yaroslav A.	urzhyar@iit.edu	Illinois Institute of Technology - (UA)
Vesey, Roger A.	ravesey@sandia.gov	Sandia National Laboratories (Albuquerque, NM)
Woolsey, Nigel C.	ncw2@york.ac.uk	University of York - Physics (United Kingdom)
Yasuike, Kazuhito	yasuike@apr.jaeri.go.jp	JAERI (Japan)
Yugami, Noboru	yugami@cc.utsunomiya-u.ac.jp	Utsunomiya University (Japan)
Zepf, Matthew	m.zepf@qub.ac.uk	Queen's University Belfast - Physics Dept (United Kingdom)

Angular dispersion of energetic electrons generated by the interaction of ultra intense laser pulses with overdense plasma

JC Adam, A Héron, G Laval

CPHT, Ecole Polytechnique

Introduction

As usual when dealing with simulations of electron genereration and transport, one has to make choices, and has to let aside some part of the physics. We have favored system size at the expense of the number of dimensions.

This leads us to stick to 2D PIC EM simulations with large simulation box.

This allow us to follow the time evolution of the system on long time scale without boundaries problems and to realize high accuracy simulations without compromize on the mesh size.

Parameter space covered (over years) by the study

Pulse Shape : Uniform in space or
Gaussian(FWHM in space 3 to 20 µm)
Flat plateau or Gaussian in time

Fluxes : ranging from 10^{18}W/cm^2 up to 10^{21}W/cm^2

Initial density profiles : steep gradient or linear ramp

Transverse boundary conditions : periodic or
isolated in space

Two common points to all the simulations performed with a steep density gradient

All of the simulations show a **strong divergence** of the beam of hot electrons with an **angle of emission of approximatively 40°.**

This divergence of the beam **appears very early in time**, **much before** any significant **hole boring** occurs**.**

It seems to be **correlated** to the apparition of a **strong filamented magnetic field** close to the plasma/vacuum interface.

All of the simulations show that **the return current is not cold** but corresponds to electrons with a spectrum of energy ranging from the initial plasma temperature up to 100 KeV.

A big simulation

920 x 1060 k_0^{-1}
$dx=dy=0.2k_0^{-1}$
$dt\sim0.2?\ _0^{-1}$
T_e=10KeV

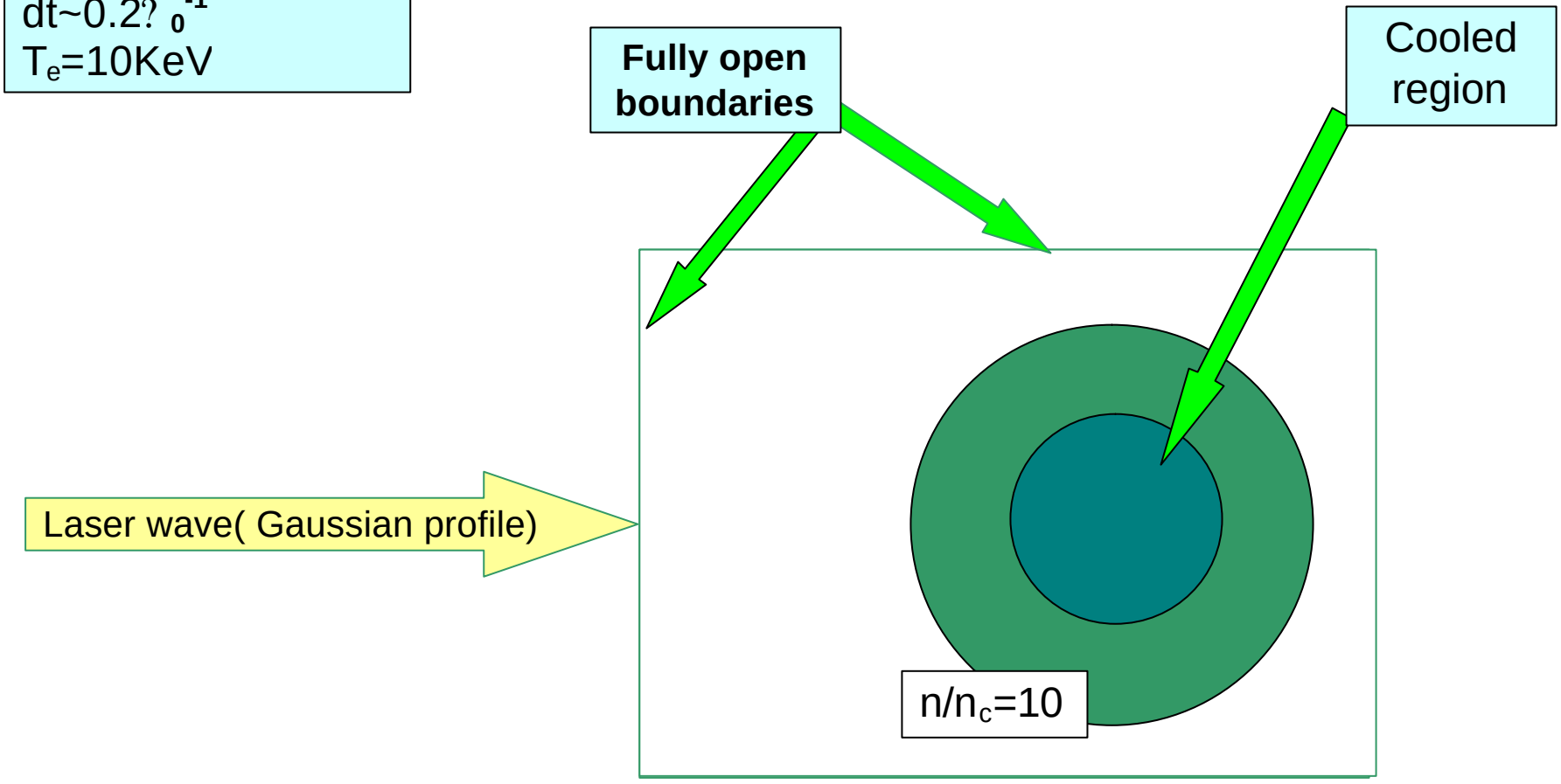

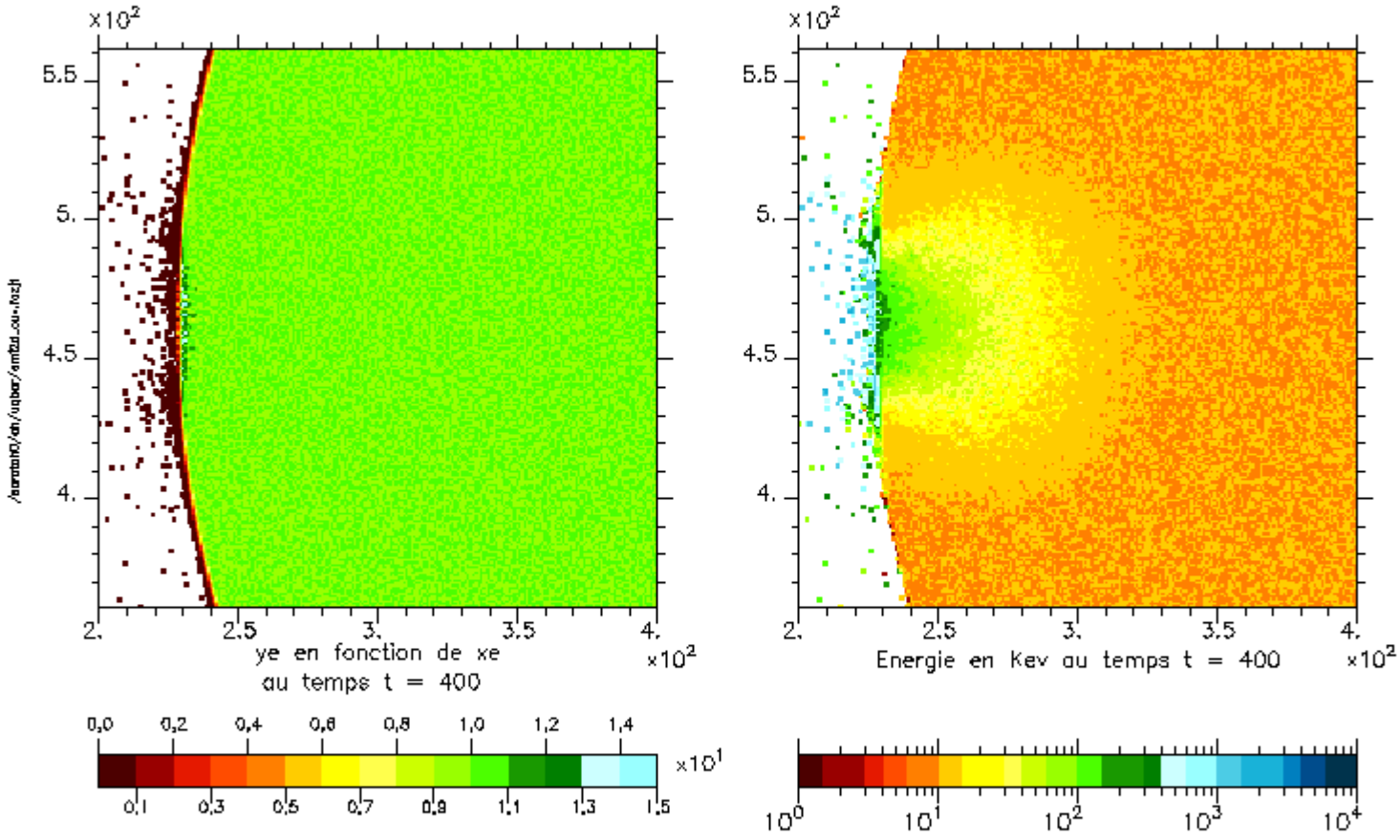
x10^2
5.5
5.
4.5
4.
2.
2.5
3.
3.5
4.
x10^2
ye en fonction de xe
au temps t = 400
0,0
0,2
0,4
0,6
0,8
1,0
1,2
1,4
x10^1
0,1
0,3
0,5
0,7
0,9
1,1
1,3
1,5
x10^2
5.5
5.
4.5
4.
2.
2.5
3.
3.5
4.
x10^2
Energie en Kev au temps t = 400
10^0
10^1
10^2
10^3
10^4

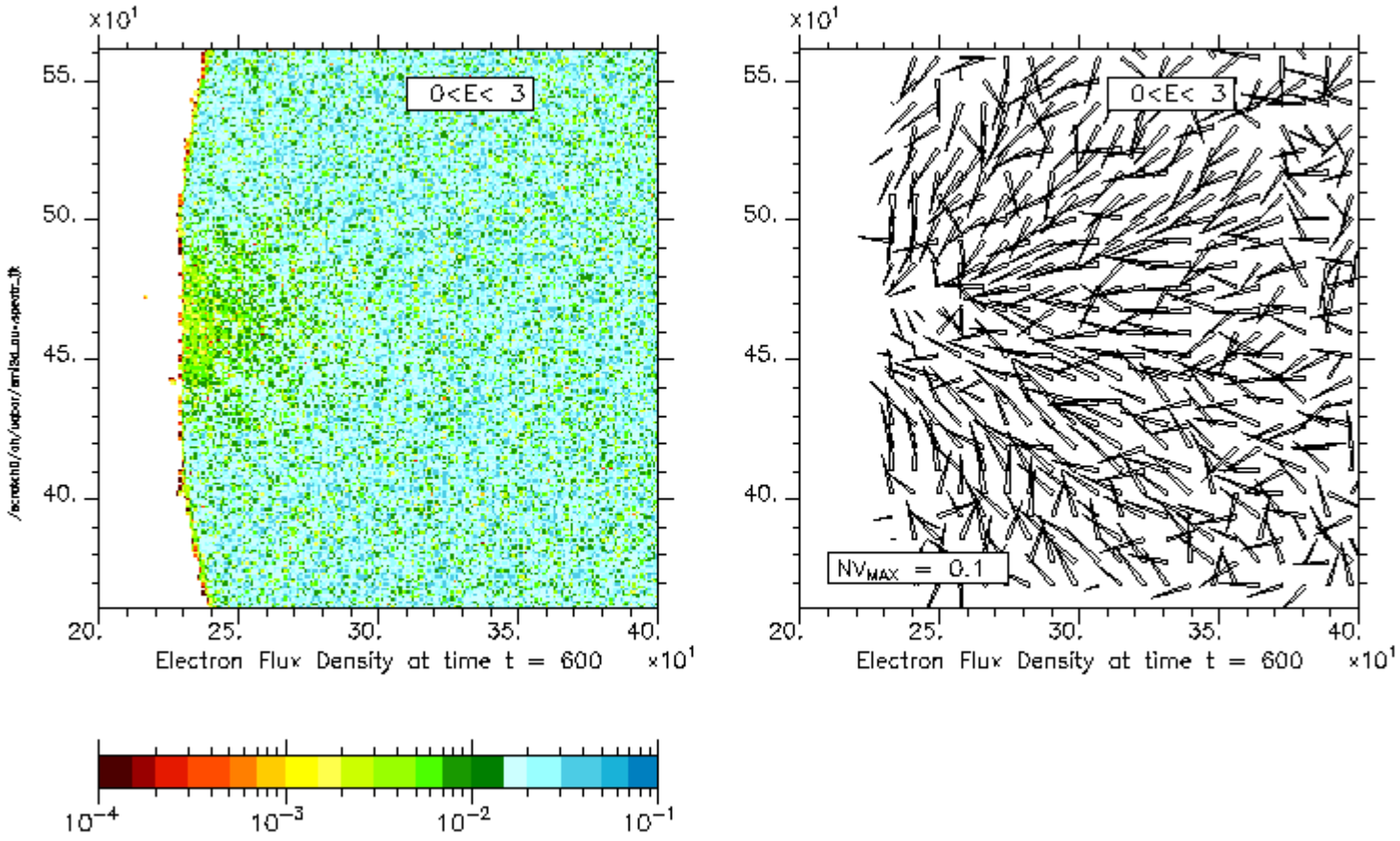
x10¹
55.
50.
45.
40.
0<E< 3
20.
25.
30.
35.
40.
Electron Flux Density at time t = 600
x10¹
x10¹
55.
50.
45.
40.
0<E< 3
NV_MAX = 0.1
20.
25.
30.
35.
40.
Electron Flux Density at time t = 600
x10¹
10⁻⁴
10⁻³
10⁻²
10⁻¹

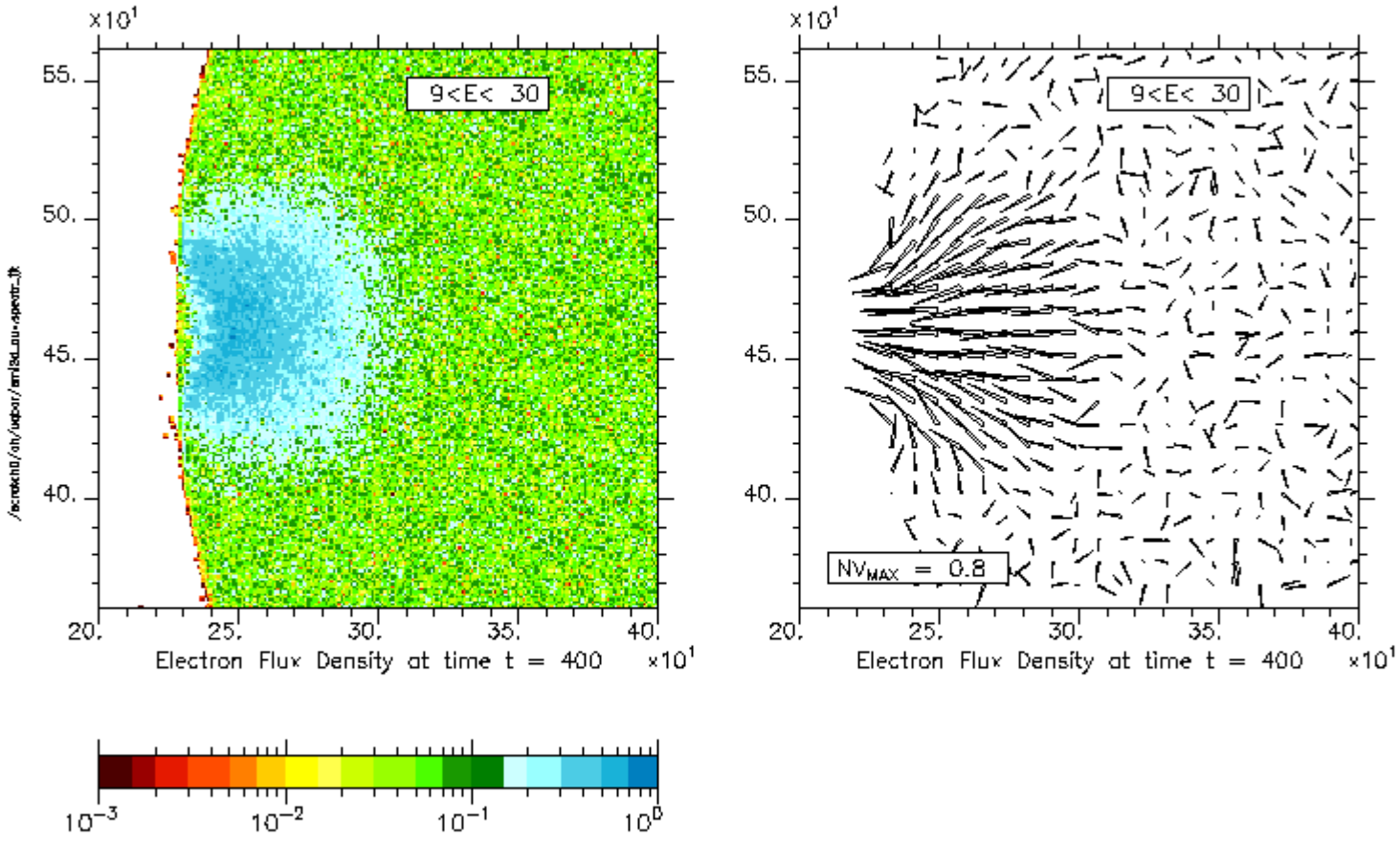
x10¹
55.
50.
45.
40.
9<E< 30
20.
25.
30.
35.
40.
Electron Flux Density at time t = 400
x10¹
x10¹
55.
50.
45.
40.
9<E< 30
NV_MAX = 0.8
20.
25.
30.
35.
40.
Electron Flux Density at time t = 400
x10¹
10⁻³
10⁻²
10⁻¹
10⁰

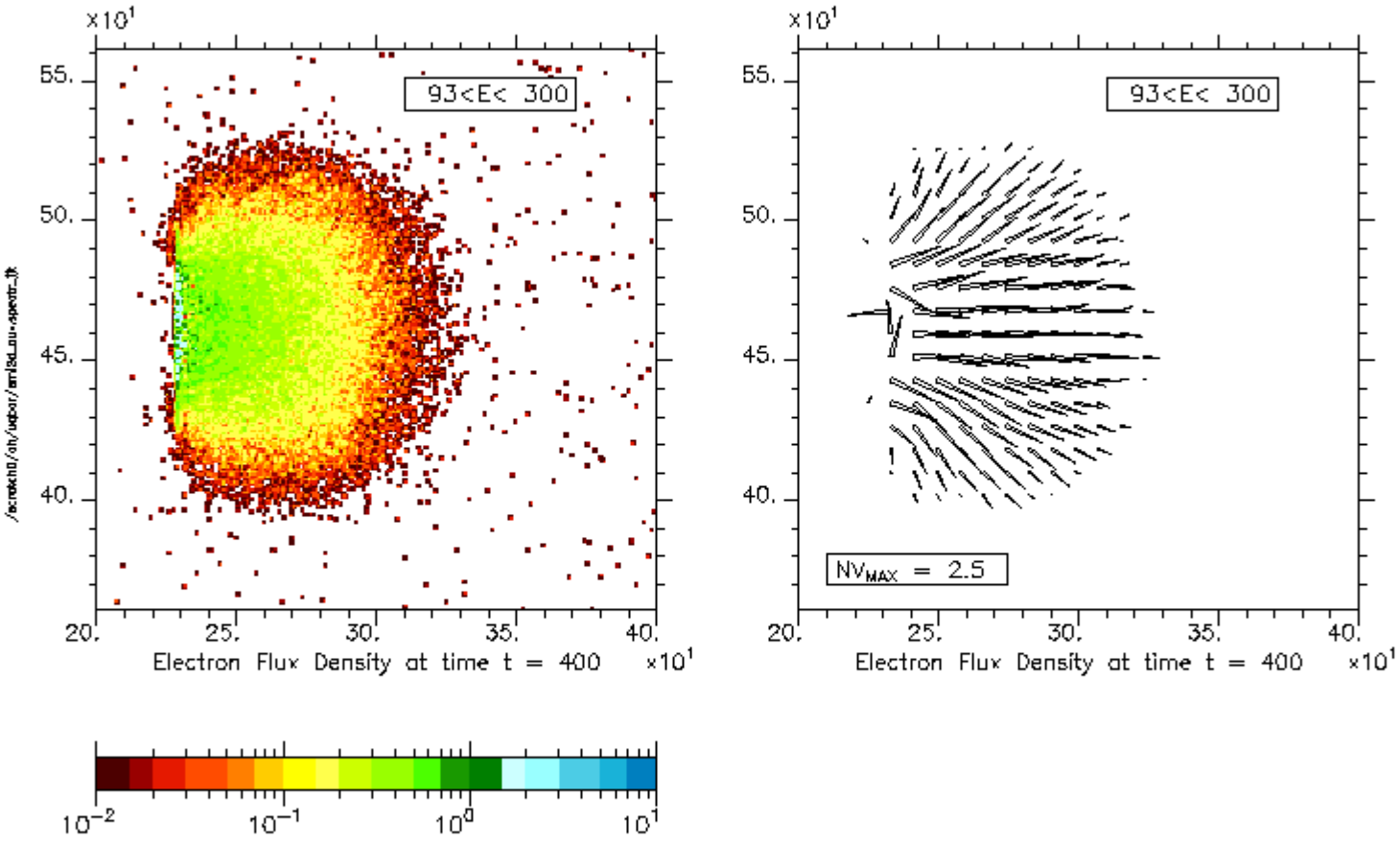
x10¹
55.
50.
45.
40.
93<E< 300
20.
25.
30.
35.
40.
Electron Flux Density at time t = 400
x10¹
x10¹
55.
50.
45.
40.
93<E< 300
NV_MAX = 2.5
20.
25.
30.
35.
40.
Electron Flux Density at time t = 400
x10¹
10⁻²
10⁻¹
10⁰
10¹

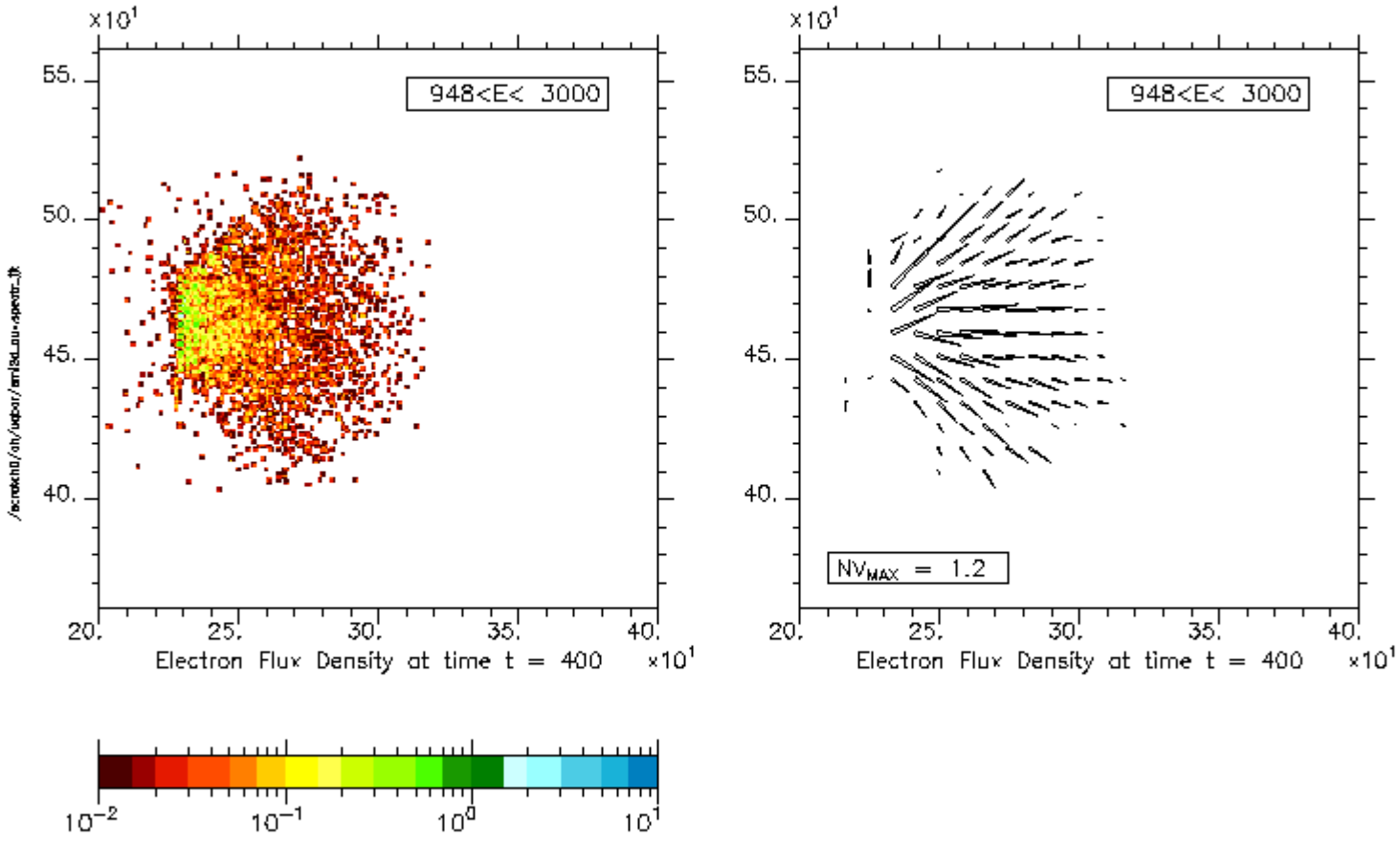
x10¹
55.
50.
45.
40.
948<E< 3000
20.
25.
30.
35.
40.
Electron Flux Density at time t = 400
x10¹
NV_MAX = 1.2
10⁻²
10⁻¹
10⁰
10¹

A very simple simulation system

In order to identify the mecanisms responsible of the beam divergence we have study the tranverse heating generated by the **interaction of plane EM wave with a slab of plasma** using periodic boundary conditions in the transverse direction. Simulations used both mobile and immobile ions.

The density step was varied from **4 times** critical **up to 80 times critical.**

The fluxes where varied from **10^{17}W/cm^2 up to 10^{21}W/cm^2.**

The initial temperature of the plasma was varied **from 250 eV up to 1 Kev** (These low temperature allows to make a clear distinction between particules coming from the bulk of the distribution function and the one that must have accelerated).

This requests very small mesh size (**up to 180 mesh points per wave length were used**) and correspondingly small time steps.(this allows also to describe high order harmonics).

A very simple simulation system

90/180 points per laser wavelength

90/180 time steps per laser period

10 particles/cells

~15 x 10^6 grid points

~200 x 10^6 particles of each species

simulation box size ~12? x50?

250eV<Te<1000eV

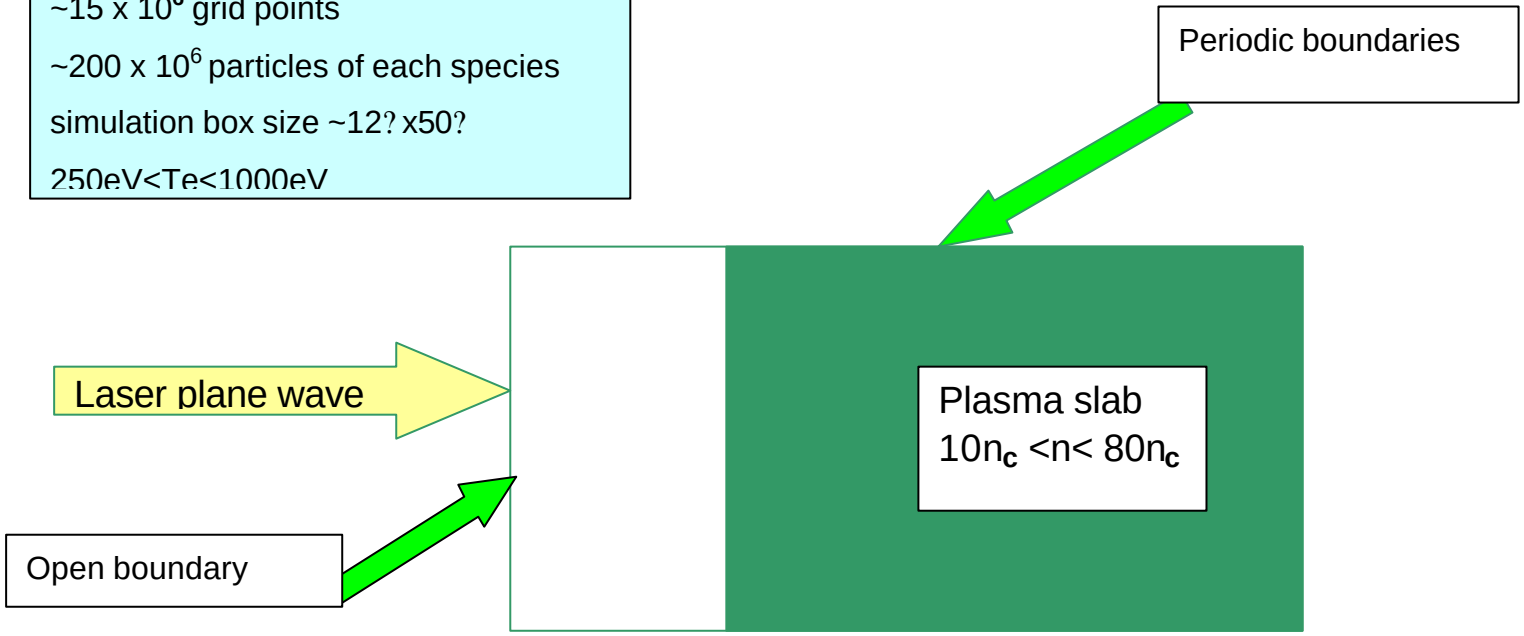

Main results (1)

All the simulations **show a strong tranverse heating** as soon as the simluation is 2D (Simulations keeping only mode $k_Y=0$ show no transverse heating as it should be, because of conservation of tranverse momentum).

Longitudinal heating appears as soon as the amplitude of the wave is large enough even in the absence of any underdense plasma.

This heating appears to be related to some kind of jXB heating, which implies that a significant fraction of EM wave penetrate inside the plasma.

Transverse heating appears very early in time but **increases with** the developpment of **the filamented magnetic field**.

Main results (2)

This low frequency magnetic field decreases very rapidly inside the overdense plasma typically less than 1µm for $n/n_c=10$ and ? $=10^{19}$W/cm^2. (Also observed by Sentoku et al in 3D simulations).

A careful examination of phase space projections reveals the emission of jets of energetic particles corresponding to jxB acceleration (frequency of emission 2? $_0$) but **also jets of energetic particles in the transverse direction** (frequency of emission ? $_0$) with velocity alternating in sign.

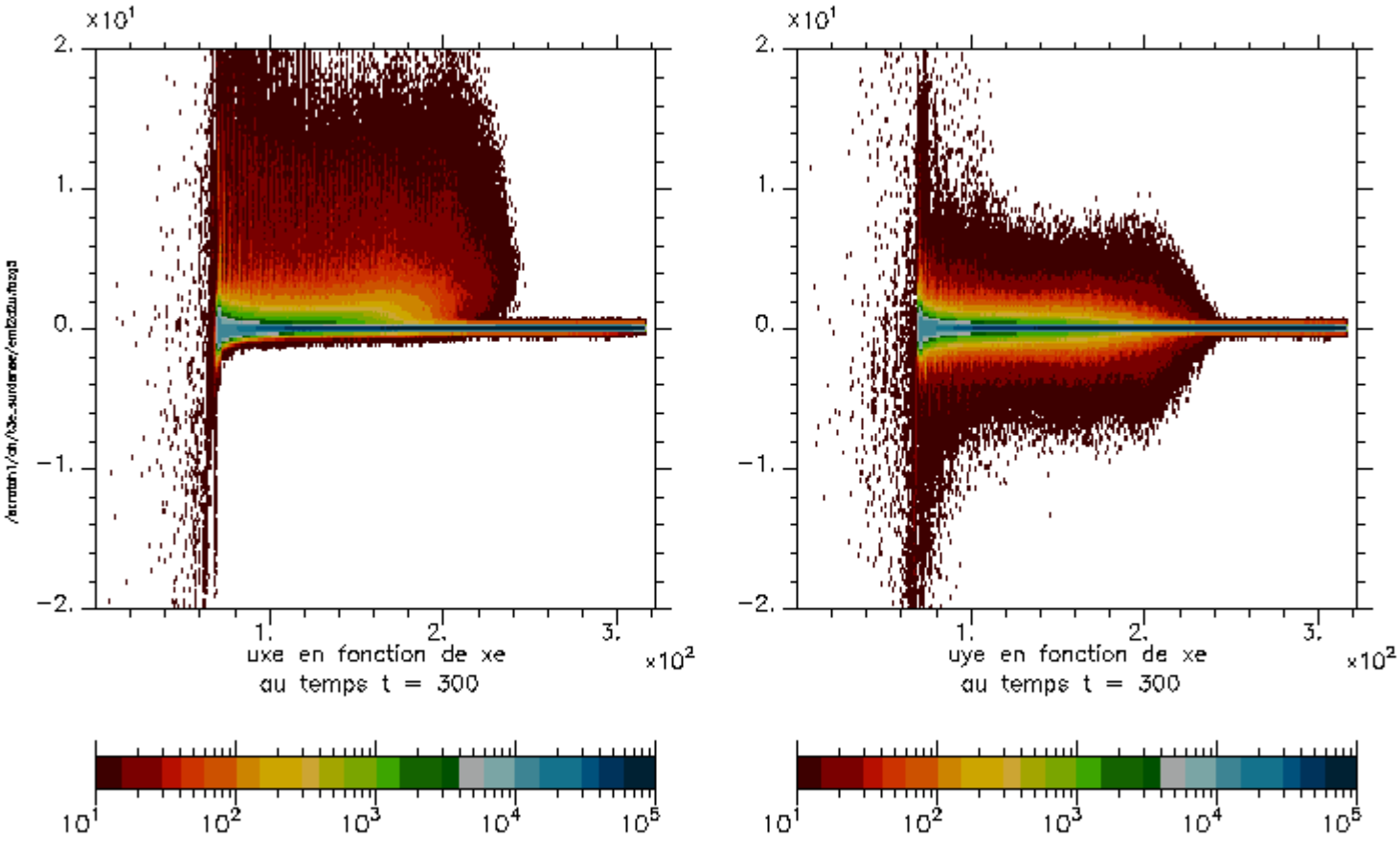
x10¹
2.
1.
0.
−1.
−2.
1.
2.
3.
x10²
uxe en fonction de xe
au temps t = 300
10¹
10²
10³
10⁴
10⁵
x10¹
2.
1.
0.
−1.
−2.
1.
2.
3.
x10²
uye en fonction de xe
au temps t = 300
10¹
10²
10³
10⁴
10⁵

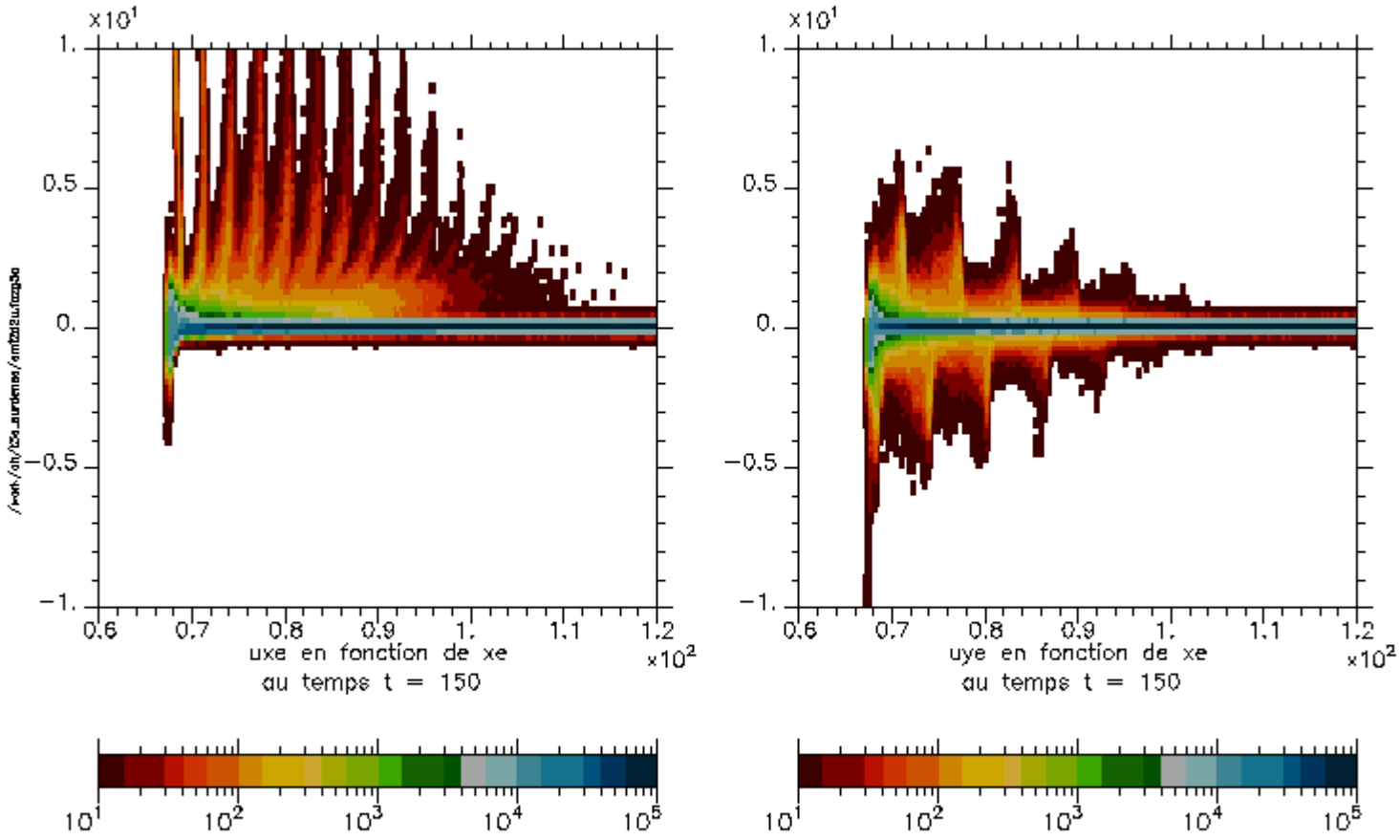
x10¹
1.
0.5
0.
−0.5
−1.
0.6
0.7
0.8
0.9
1.
1.1
1.2
x10²
uxe en fonction de xe
au temps t = 150
uye en fonction de xe
au temps t = 150
10¹
10²
10³
10⁴
10⁵

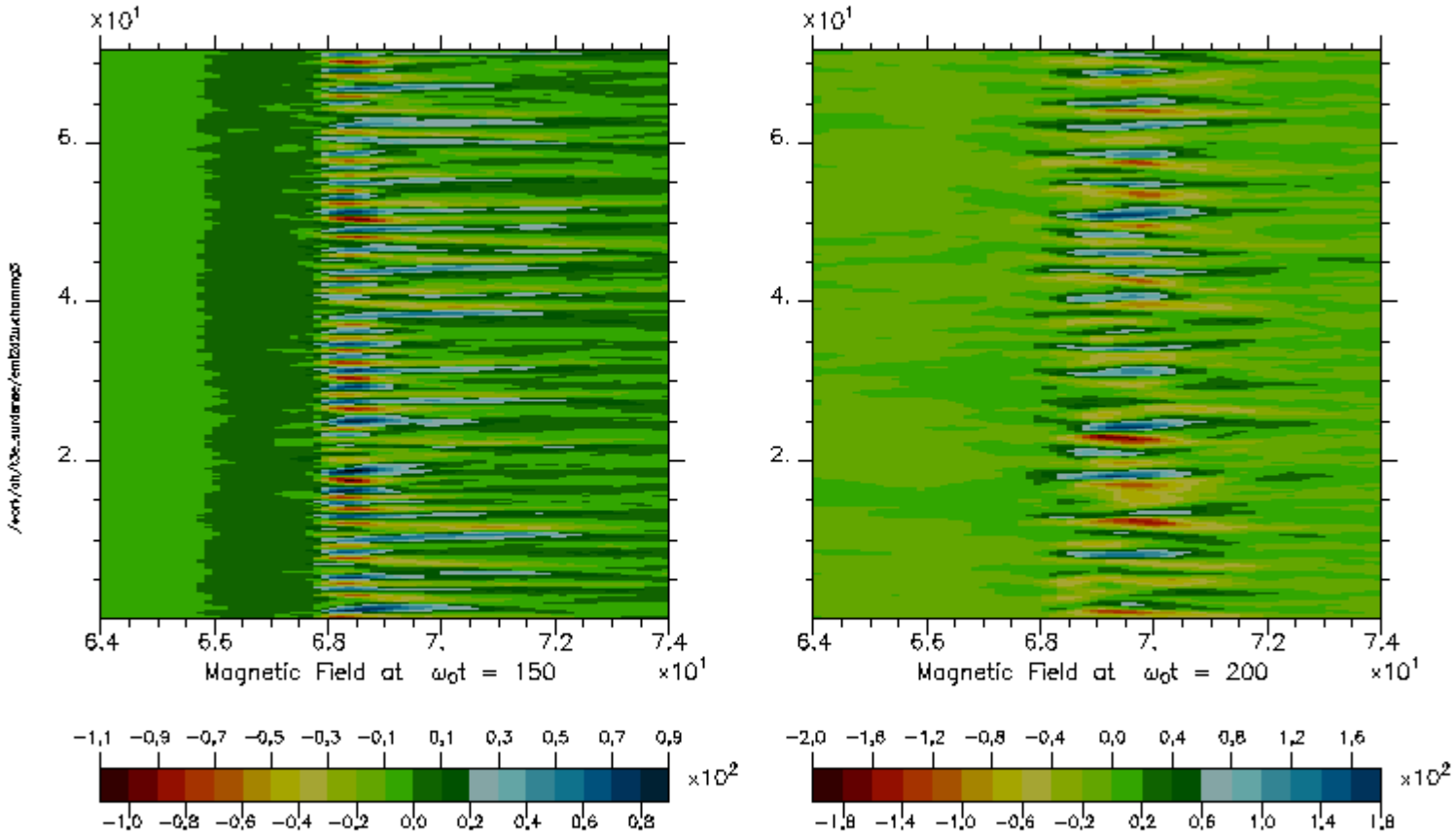
x10¹
6.
4.
2.
6.4
6.6
6.8
7.
7.2
7.4
Magnetic Field at ω₀t = 150
x10¹
−1,1 −0,9 −0,7 −0,5 −0,3 −0,1 0,1 0,3 0,5 0,7 0,9
x10²
−1,0 −0,8 −0,6 −0,4 −0,2 0,0 0,2 0,4 0,6 0,8
x10¹
6.
4.
2.
6.4
6.6
6.8
7.
7.2
7.4
Magnetic Field at ω₀t = 200
x10¹
−2,0 −1,6 −1,2 −0,8 −0,4 0,0 0,4 0,8 1,2 1,6
x10²
−1,8 −1,4 −1,0 −0,6 −0,2 0,2 0,6 1,0 1,4 1,8

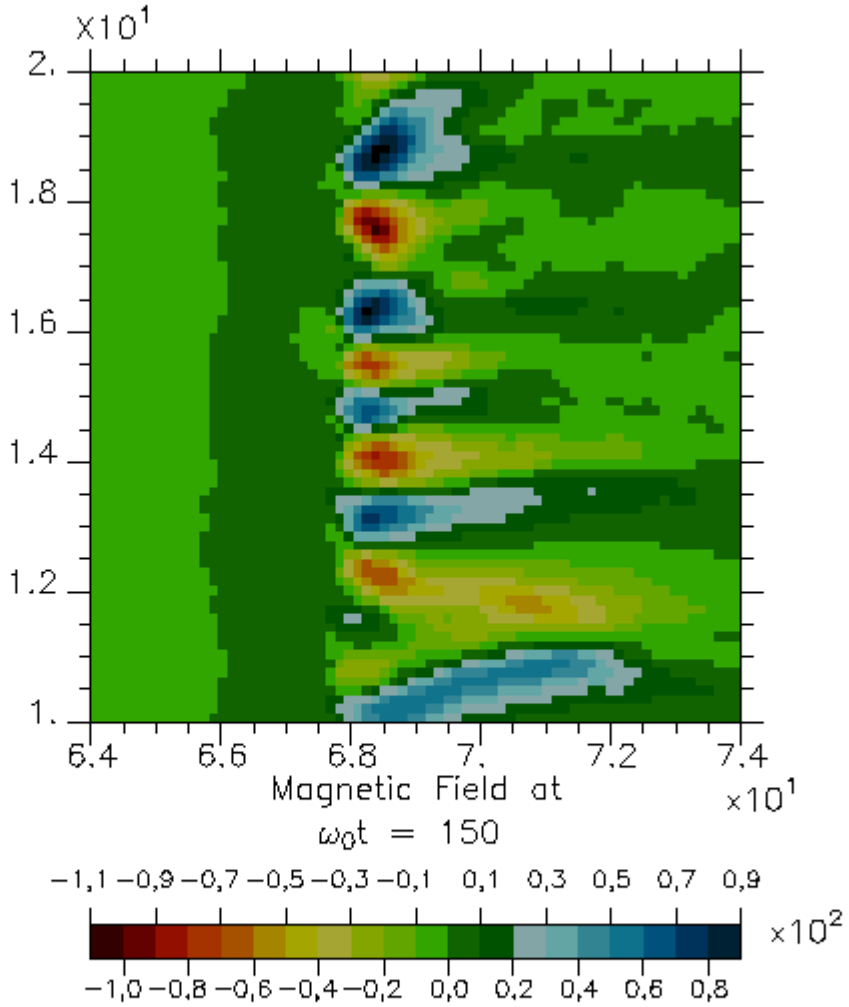
X10^1
2.
1.8
1.6
1.4
1.2
1.
6.4
6.6
6.8
7.
7.2
7.4
Magnetic Field at
×10^1
ω0t = 150
−1,1 −0,9 −0,7 −0,5 −0,3 −0,1 0,1 0,3 0,5 0,7 0,9
×10^2
−1,0 −0,8 −0,6 −0,4 −0,2 0,0 0,2 0,4 0,6 0,8

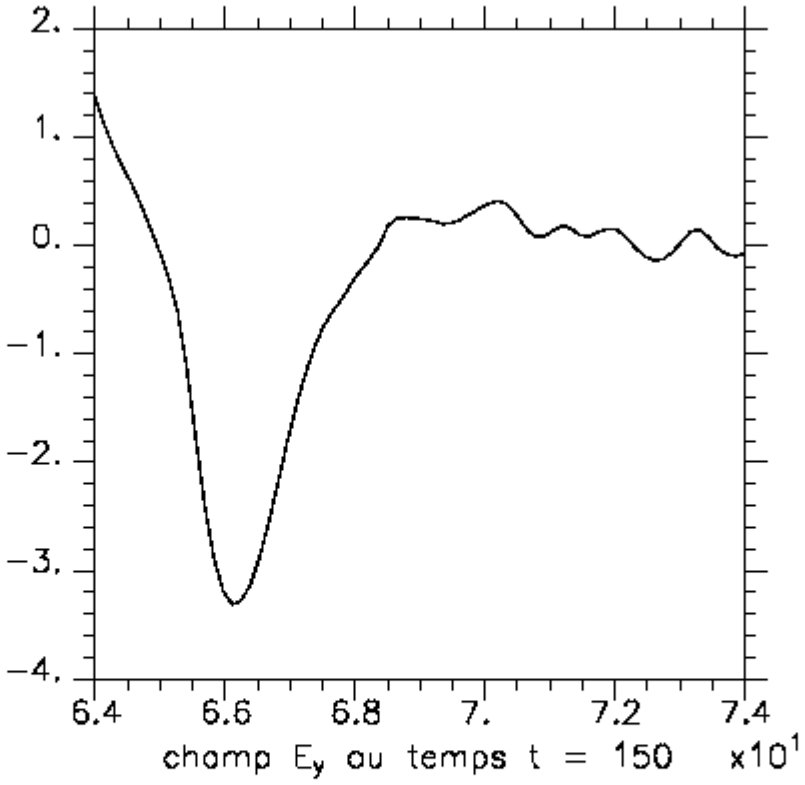

/work/ch/h3e_aunderee/embb/zu.champ5

A proposed scenario for the transverse heating

The longitudinal electric filed present in skin depth extract particles that are accelerated by a jXB mecanism.

This creates a beam in the distribution function that makes it unstable with respect to a Weibel instability (Pegoraro, Sentoku. et al,…).

This instability has a very large growth rate and develops rapidly yielding a strong quasi static magnetic field close to the edge of the plasma.

This magnetic field in turn scatter the particles in the transverse direction yielding the observed transverse heating. This affects the shape of the distribution function and changes the nature of the instability yielding a much weaker magnetic field.

Main results (3)

A residual low frequency magnetic field is present everywhere from the edge of the plasma slab up to the front of propagation of fast particles with an amplitude typically one order of magnitude less than the one at the edge.

This residual magnetic field is too small to inhibit the transport of energetic particles (> 300KeV), but it is large enough to affect the transport of the particles belonging to the return current (< 100KeV)

A strong low frequency electric field is present everywhere from the edge of the plasma slab up to the front of propagation of fast particles.

This electric field is responsible for the anomalous stopping power of fast particles and the acceleration of the thermal one up to 100KeV

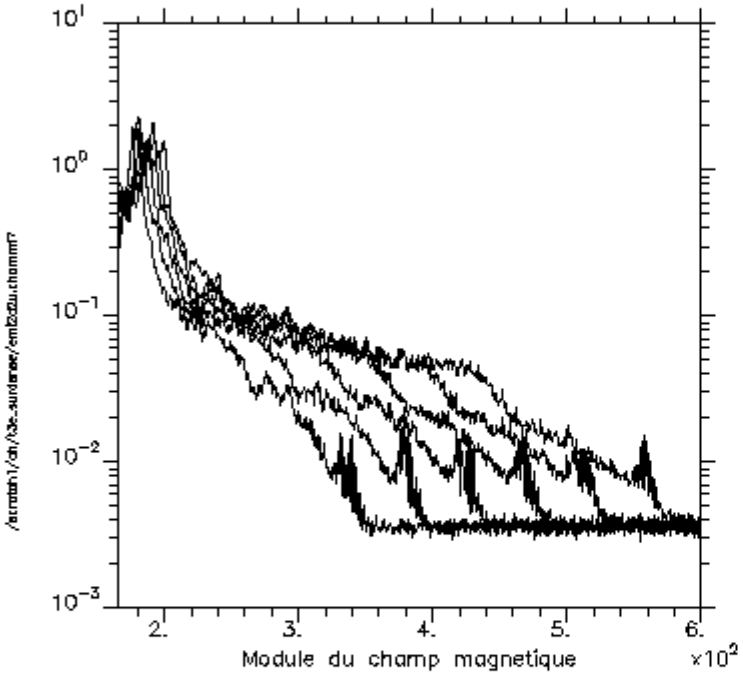
10^1
10^0
10^{-1}
10^{-2}
10^{-3}
2.
3.
4.
5.
6.
Module du champ magnetique
$\times 10^2$

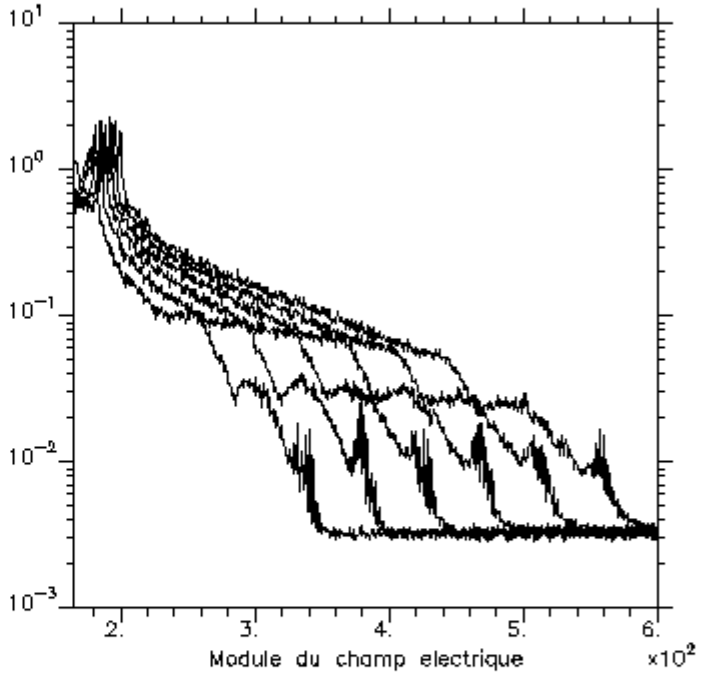
10^1
10^0
10^{-1}
10^{-2}
10^{-3}
2.
3.
4.
5.
6.
Module du champ electrique
$\times 10^2$

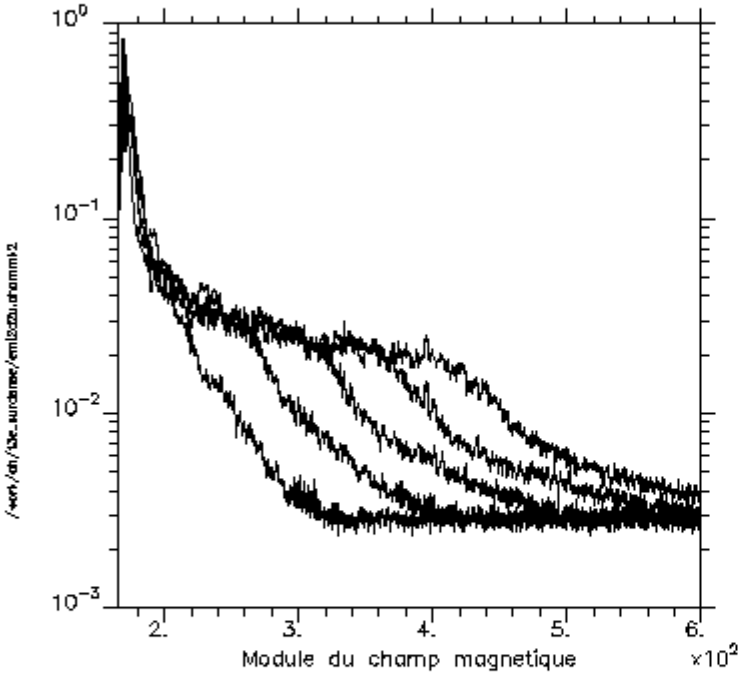
10^0
10^{-1}
10^{-2}
10^{-3}
2.
3.
4.
5.
6.
Module du champ magnetique
$\times 10^2$

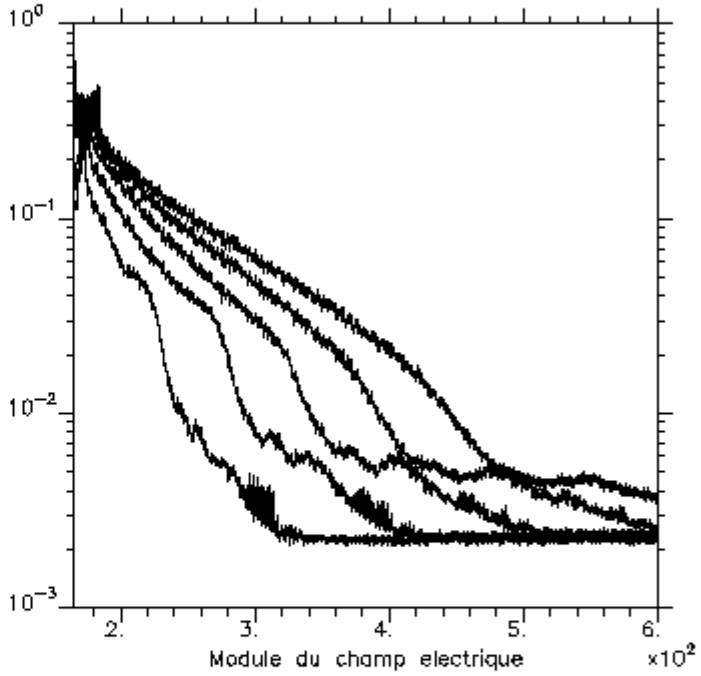
10^0
10^{-1}
10^{-2}
10^{-3}
2.
3.
4.
5.
6.
Module du champ electrique
$\times 10^2$

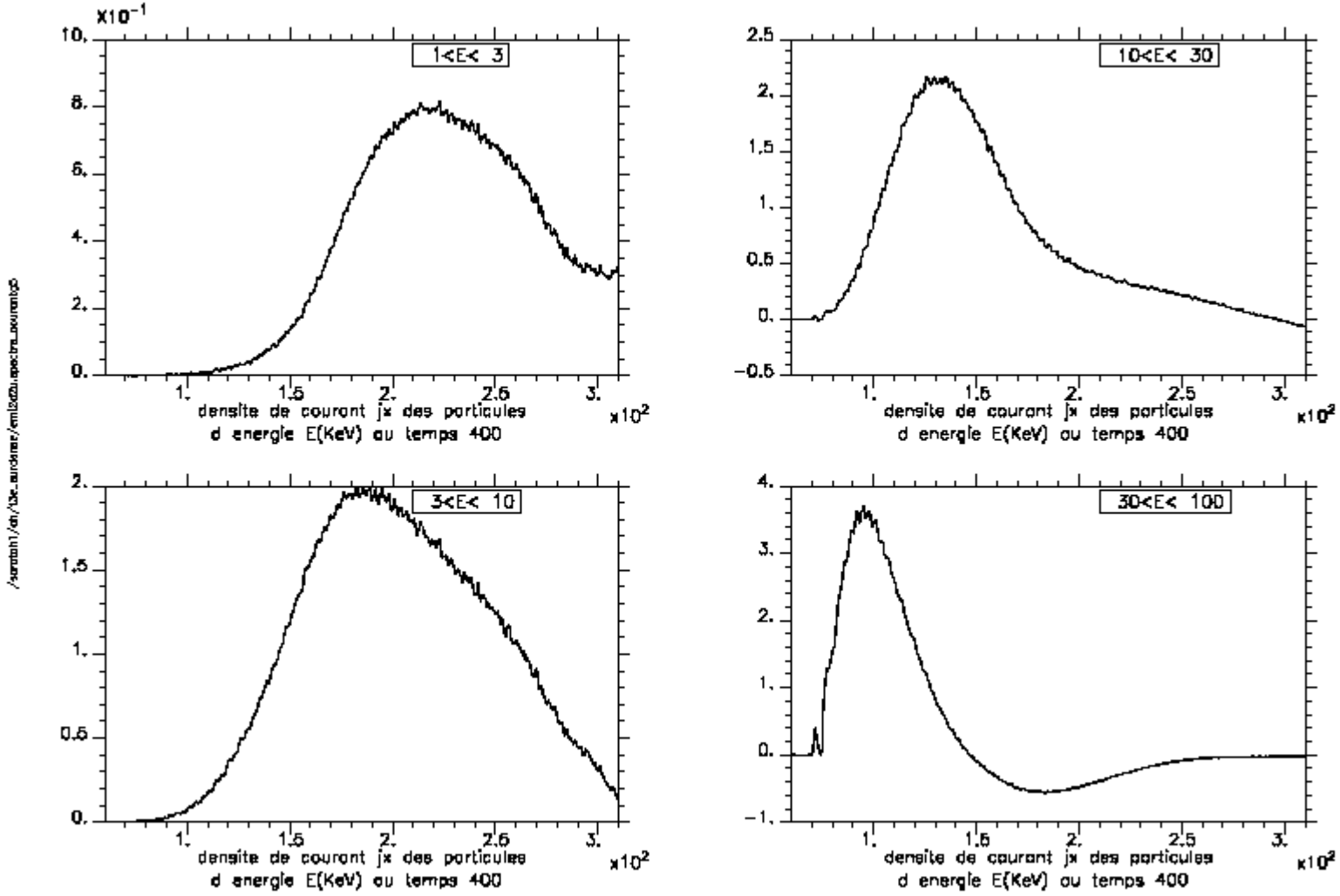
x10⁻¹
1<E< 3
10<E< 30
3<E< 10
30<E< 100
densite de courant jx des particules
d energie E(KeV) au temps 400
x10²

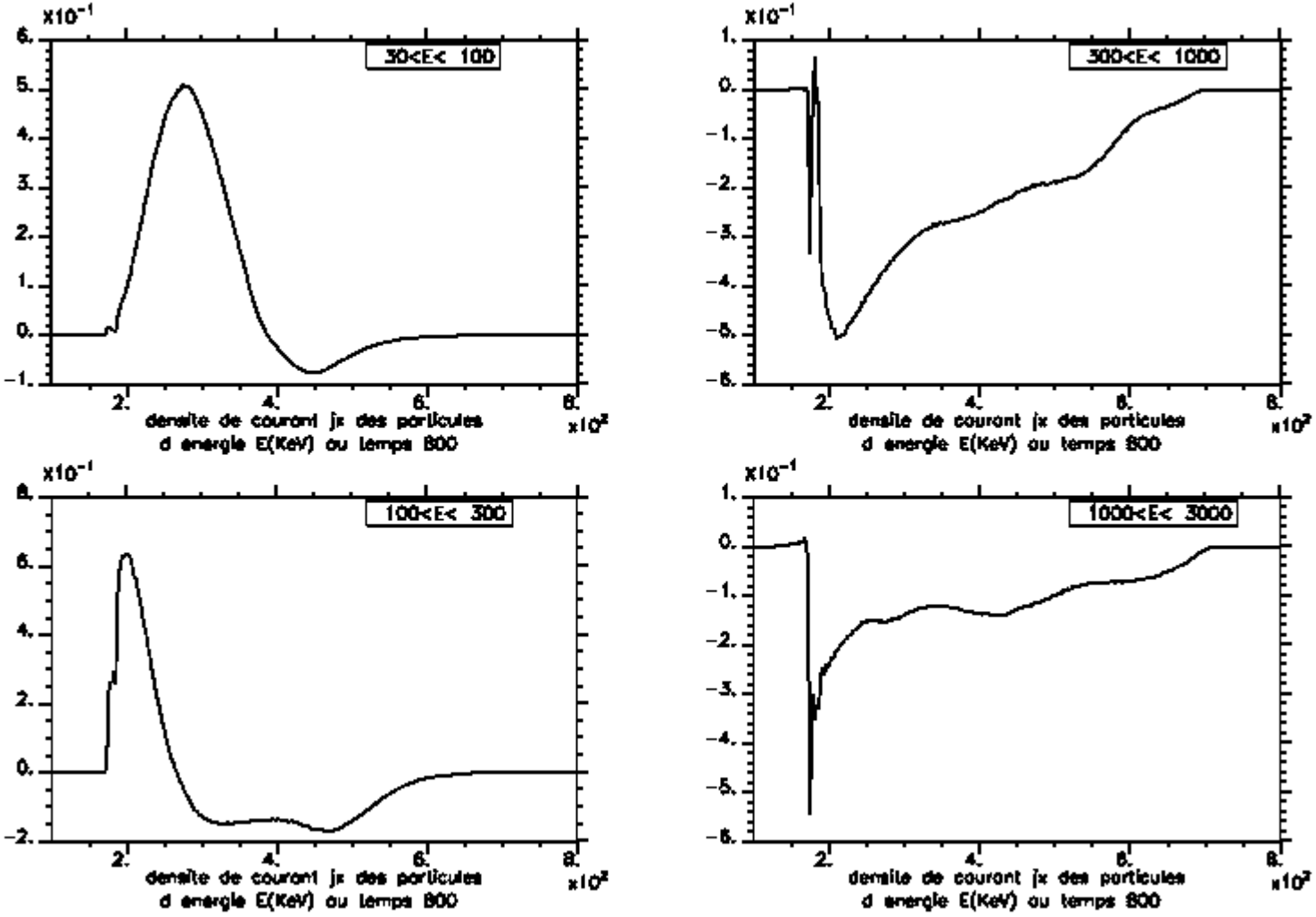
30<E< 100
300<E< 1000
100<E< 300
1000<E< 3000
x10⁻¹
x10²
densite de courant jx des particules
d energie E(KeV) au temps 800

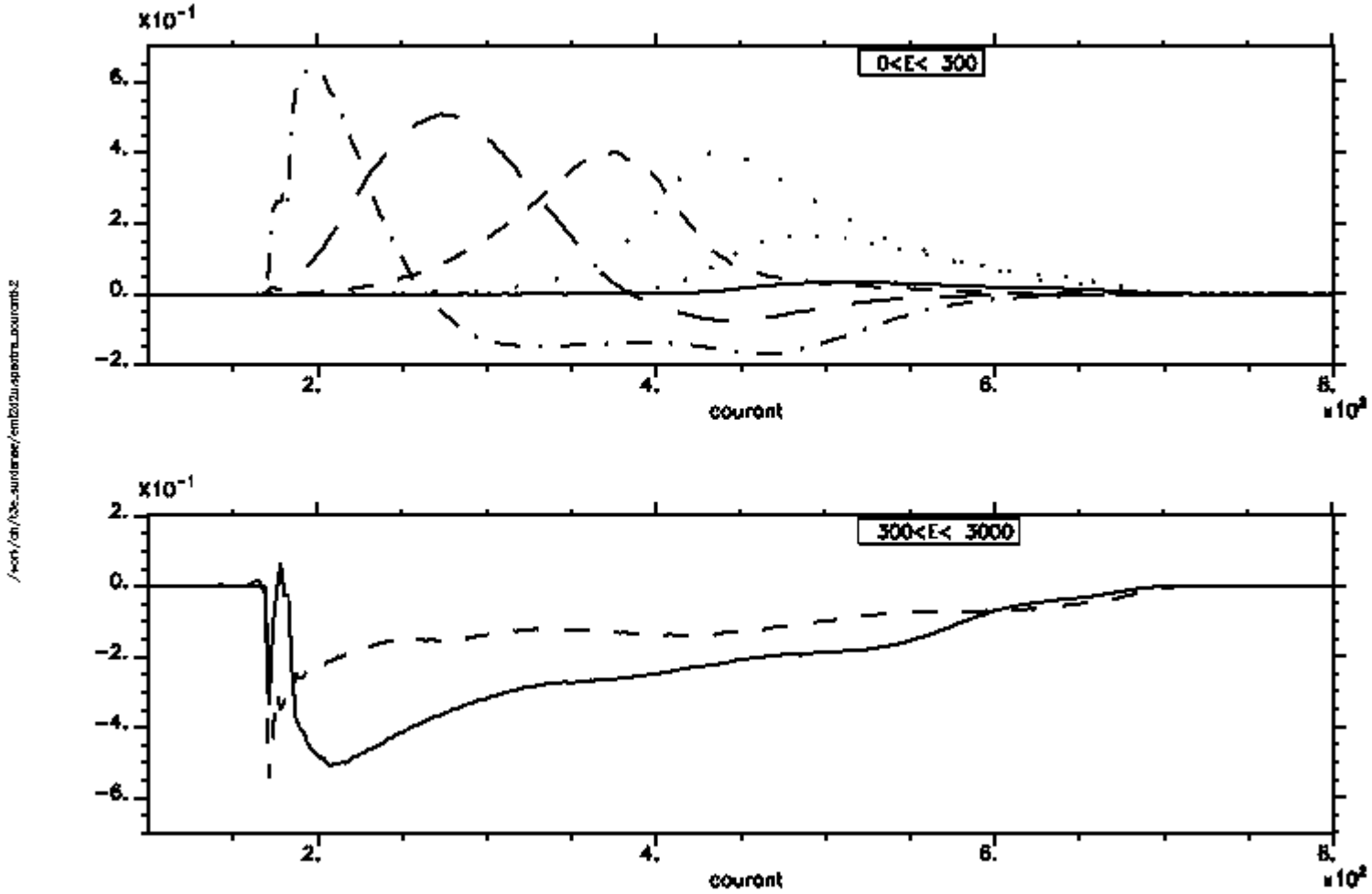
x10⁻¹
0<E< 300
6.
4.
2.
0.
-2.
2.
4.
6.
8.
x10²
courant
x10⁻¹
300<E< 3000
2.
0.
-2.
-4.
-6.
2.
4.
6.
8.
x10²
courant

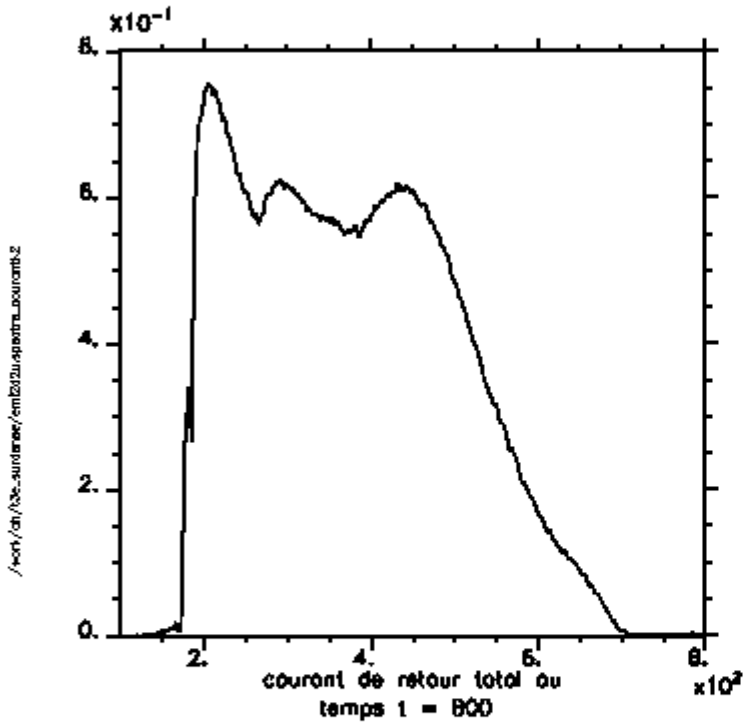
x10⁻¹
8.
6.
4.
2.
0.
2.
4.
6.
8.
x10²
courant de retour total au
temps t = 800

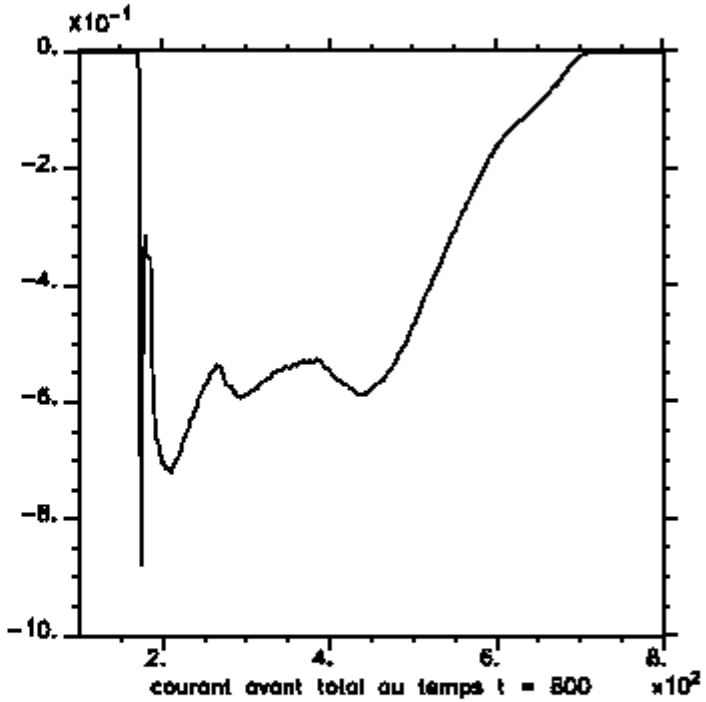
x10⁻¹
0.
-2.
-4.
-6.
-8.
-10.
2.
4.
6.
8.
x10²
courant avant total au temps t = 800

Conclusions(1)

We have shown that the transverse heating is inherent to any system with more then one dimension (we do not expect that going from 2D to 3D will kill this effect!).

A consequence of this heating is that the divergence of particles is independent of hole boring. It is an intrinsic property of the interaction.

The strong filamented magnetic field that appears at the interface of interaction seems to be responsible of this heating.(this effect may be weaker in 3D than in 2D because the volume occupied by the filament may be smaller than in 2D).

Conclusions(2)

We have observed the existence of a residual magnetic in all the space where energetic electrons have been injected as well as strong electric field due to the limitation of the mobility of cold electron by this magnetic field

The combined effect of the magnetic field and the electric yield a warm electron return current that may not be affected by collisions

Nuclear Physics on the JanUSP Laser

Physics & Advanced Technologies

Lawrence Livermore National Laboratory

M. Allen[1], P. Patel[2], D. Price[2], M. Stoyer[2], N. Izumi[2], E. Morse[1]

1. *Dept. Nuclear Eng., University of California, Berkeley, California 94720*
2. *Lawrence Livermore National Laboratory, Livermore, California 94550*

This work was performed under the auspices of the U. S. Department of Energy by the University of California, Lawrence Livermore National Laboratory under Contract No. W-7405-Eng-48.

Controllable Laser-ion Beams Will Have Many Applications

- Isotope Production
- Materials Damage
- Fast Ignitor (ICF)
- Proton Radiography
- Neutron Source

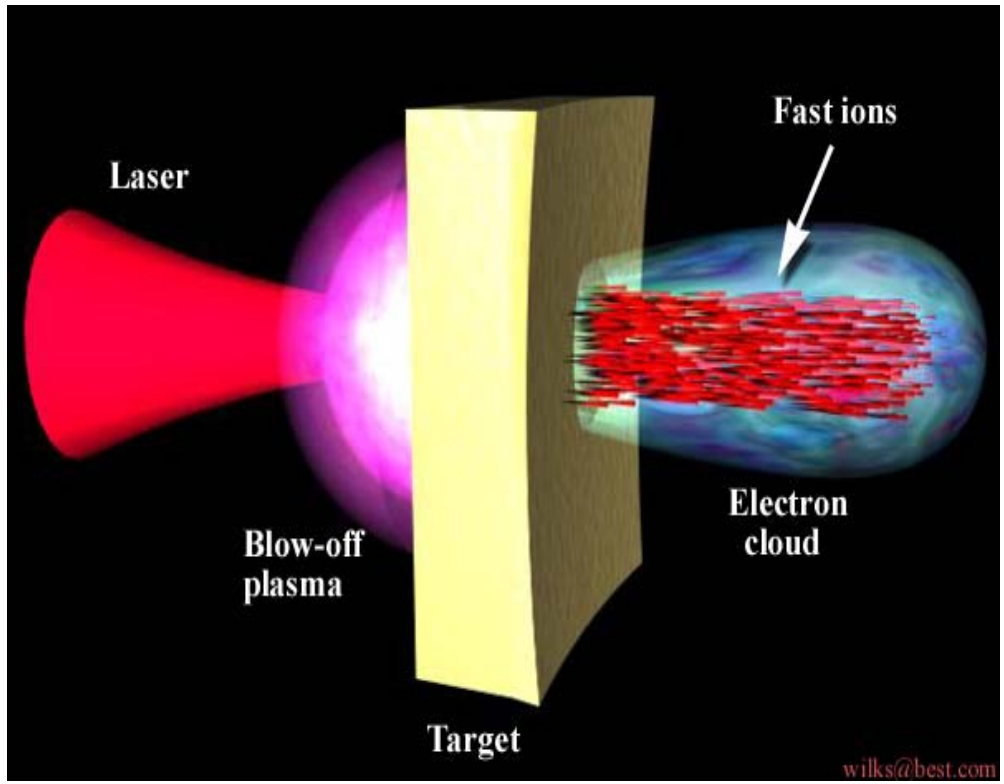

R.A. Snavely *et al*., *Phys Rev. Lett.* **84,** 2945 (2000).

M. Roth *et al*., *Phys. Rev. Lett.* **86,** 436 (2001).

The DT Experiment: Short Pulse, 14 MeV Neutron Source

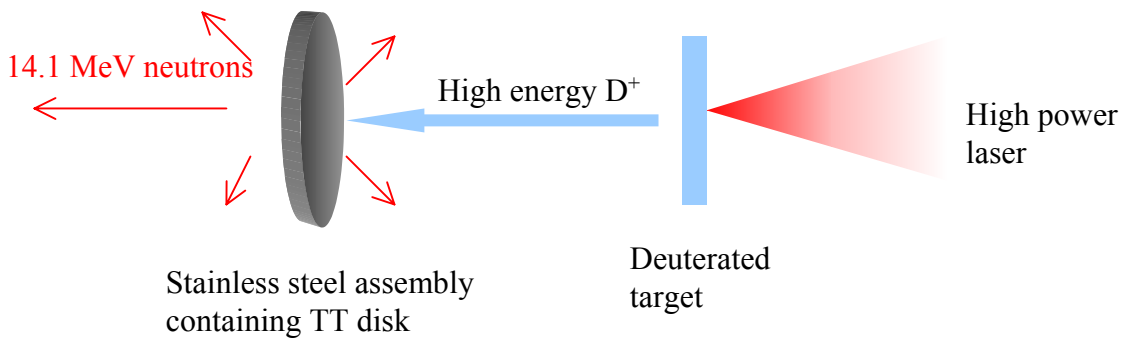

- Laser target fabrication
- Ion beam characterization
- Sealed tritium target
- Uniquely identify DT neutrons

Laser Target Fabrication of Doped Metal Foils (Ti, Pd)

Electrolysis

- Low current (12 mA), room temp
- Heavy Water

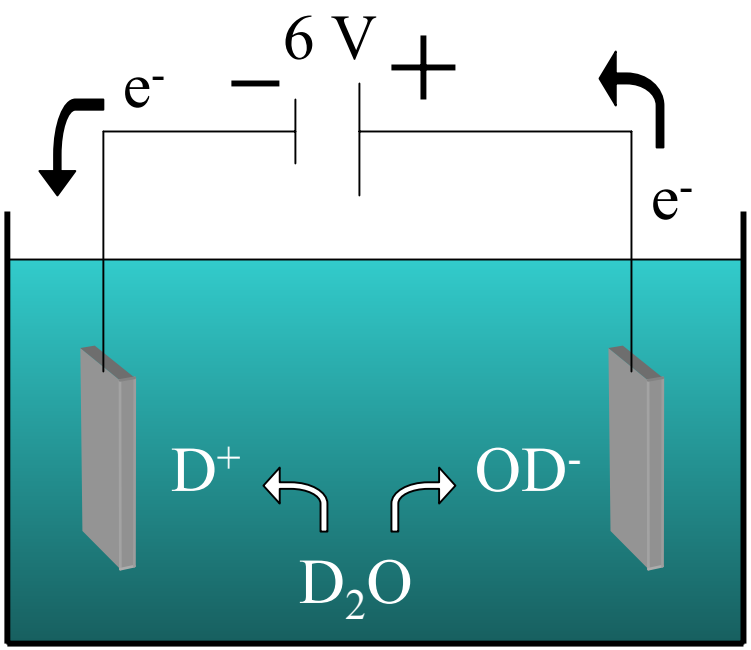

M. Fleischmann S. Pons, *J. Electroanal. Chem.* **261**, 301 (1989).
S.E. Jones *et al., Nature* **338**, 737 (1989).

Gaseous diffusion

- Ohmically heat ~ 700^0 C
- 1 ATM deuterium gas

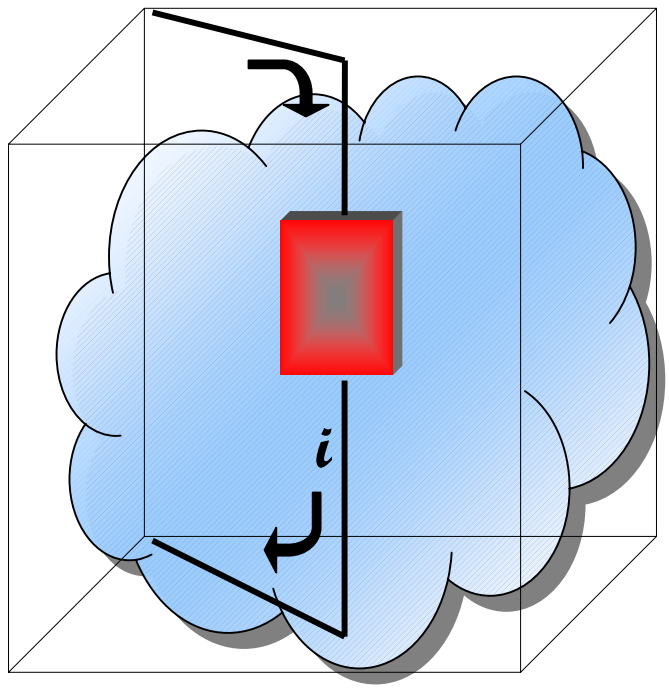

M.G. Olayo *et al., Int. J. Hydrogen Energy* **23**, 15 (1998).
William Mueller, *Metal Hydrides* (1968).

Experimental Setup

Radiochromic Film
Al blast shield

Laser-target
$\theta_{incident} = 22.3^0$

$f/2$ Parabolic mirror

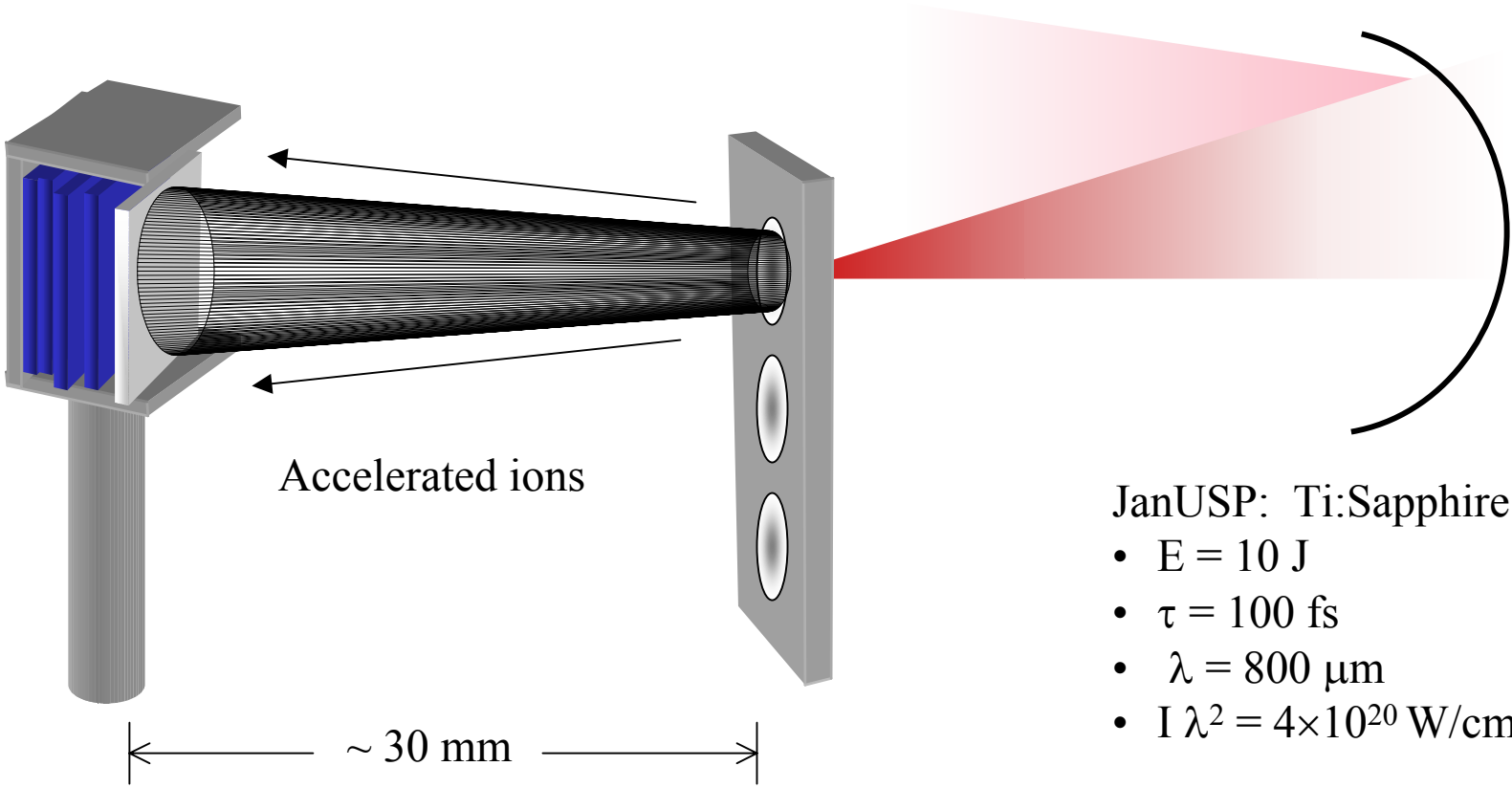

JanUSP: Ti:Sapphire

- E = 10 J
- τ = 100 fs
- λ = 800 μm
- $I\lambda^2 = 4\times10^{20}$ W/cm^2 μm ^{2}

Physics & Advanced Technologies

A Simple Radiative Heater

- Hydrogenous contaminants *must* be removed before other ions can effectively be accelerated.
- Small 40W bulb with the glass cut off.
- TC temperature on back of foil ~ 250^0C.
- Heater ~ 2-3mm from foil, for 20 minutes.

Laser-target

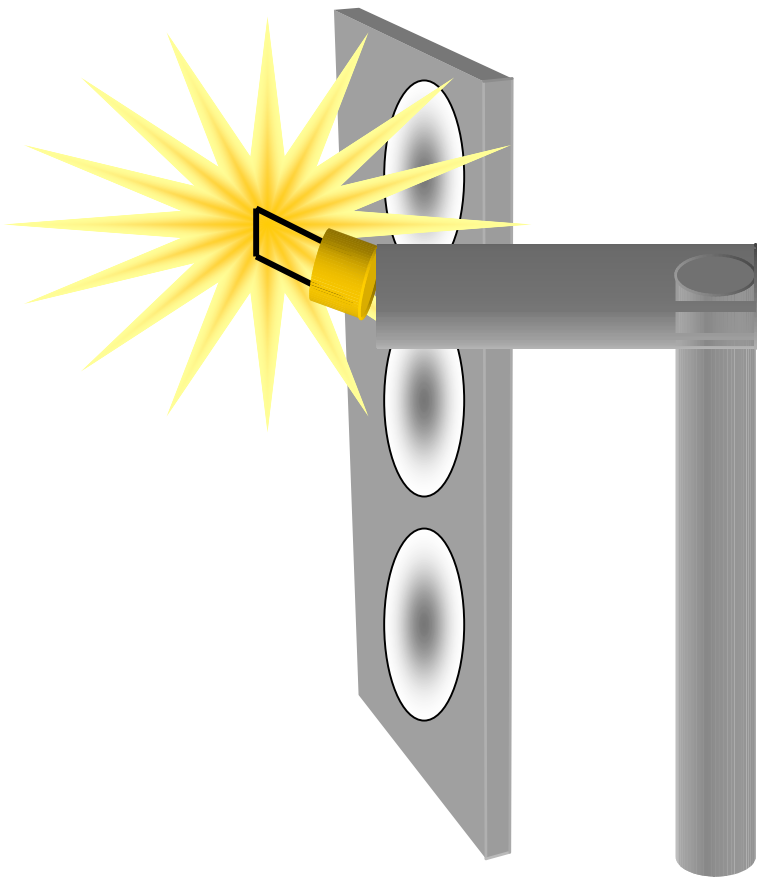

Radiative Heating Can Be Very Effective

<u>Shot #10011605</u>
Target: Pd 25 μm
E_L = 10.7 J
E_{ion} > 17 MeV

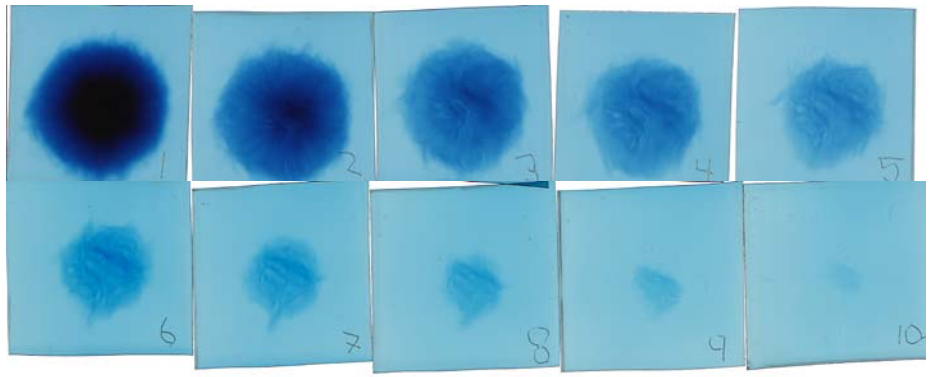

<u>Shot #10021550</u>
Target: Pd 25 μm
Heated
E_L = 10.7 J
E_{ion} > 8 MeV

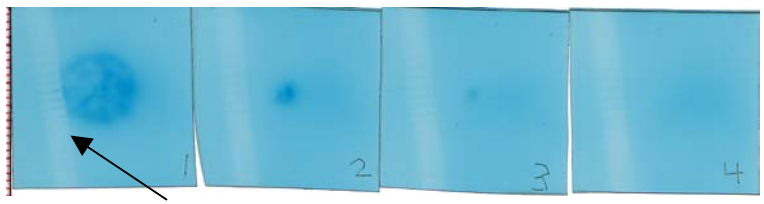

Radiograph of heating filament

<u>Shot # 10021630</u>
Target: Pd 25 μm (doped H)
Heated
E_L = 9.7 J
E_{ion} > 13 MeV

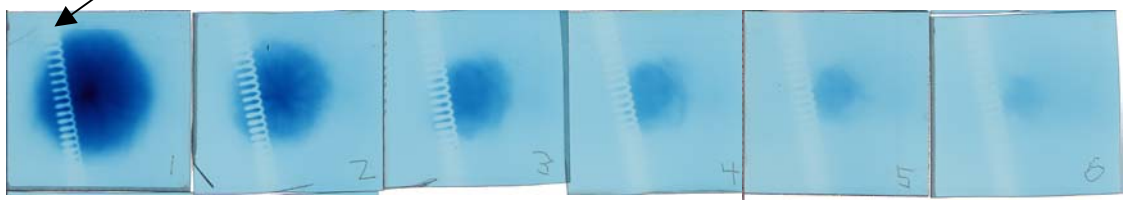

Ion-beam Target: Sealed Tritium Source

<u>Tritiated-titanium disk</u>
1 inch round
$TiT_{1.6}$
Activity ~ 1.6 Ci

(Al blast shield requires
D^+ > 4 MeV)

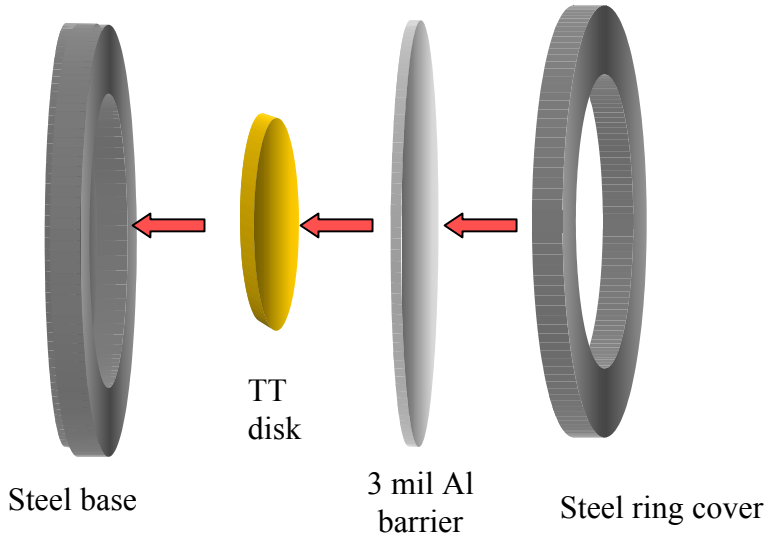

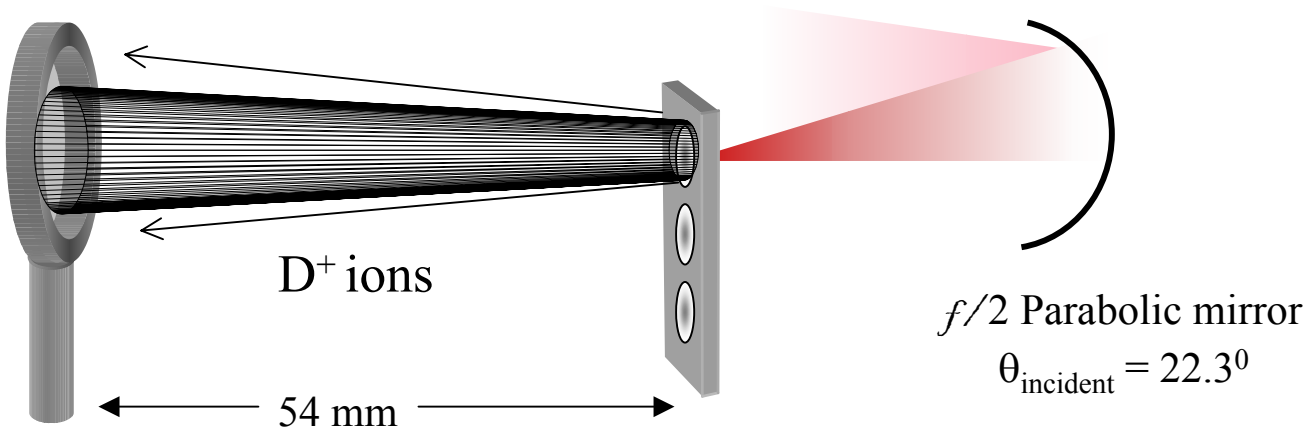

Nuclear Physics/diagnostics

- Thin foil activation counting
- Silver activation detectors
- Time of Flight (TOF) spectroscopy

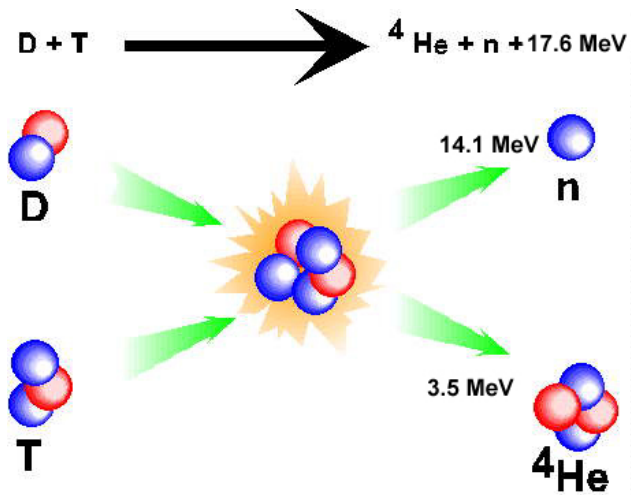

Competing reactions include:

$$D + D \xrightarrow{50\%} n + {}^{3}He$$

And various (γ,n) and (ion,n) reactions

Physics & Advanced Technologies

Nuclear Activation Cross Sections of ^{197}Au

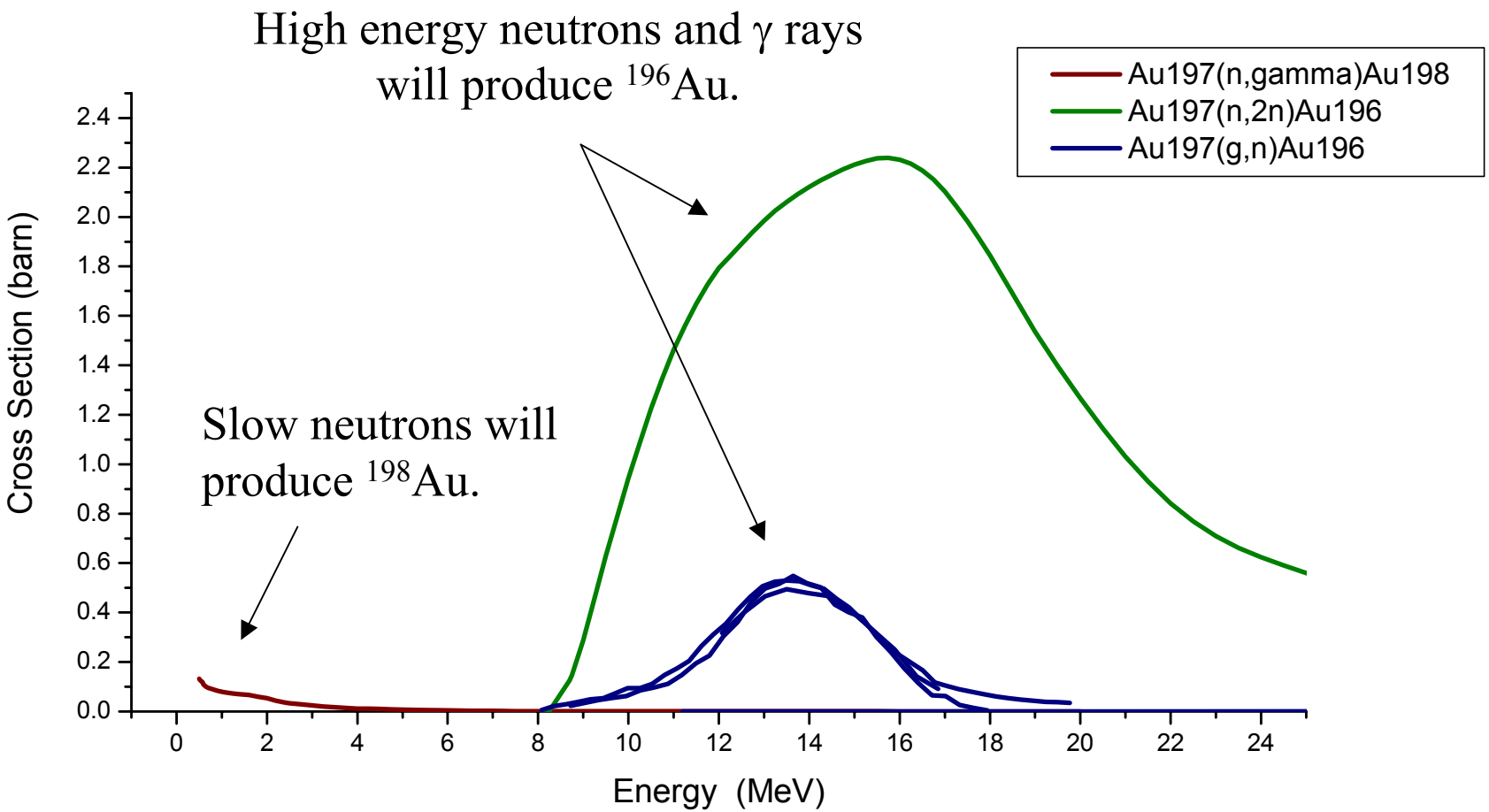

Presence of ^{198}Au gives evidence of (ion,n) reactions in target chamber

Laser incident on gold block

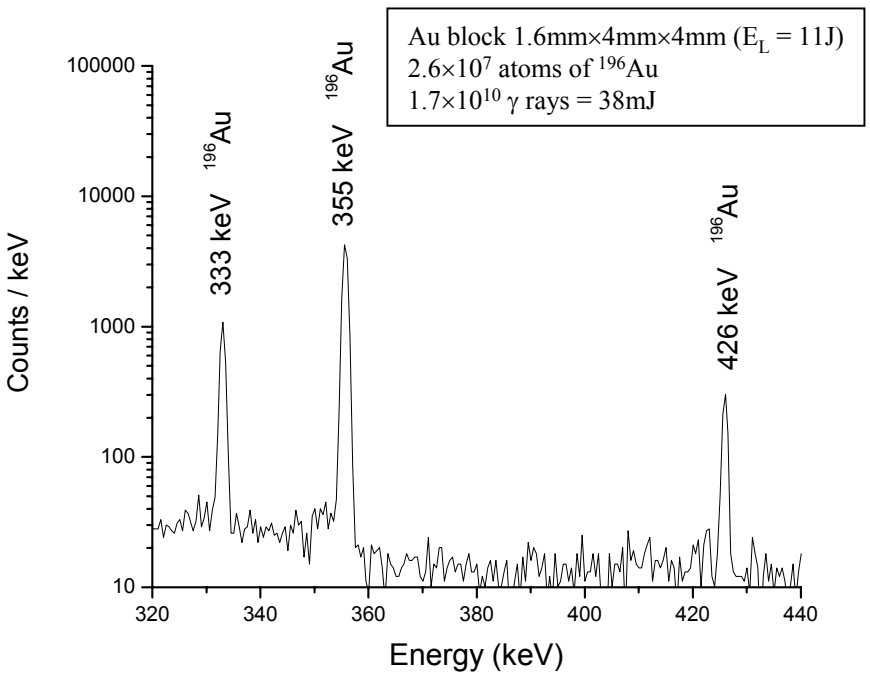

Laser incident on Pd target

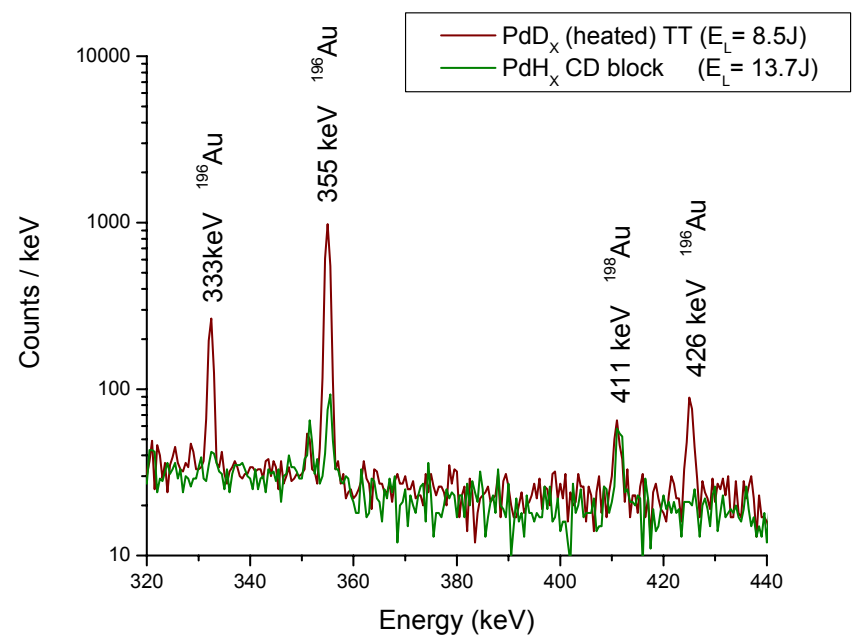

Increased presence of ^{196}Au may indicate neutrons with E > 8 MeV

— PdD_X (heated) TT (E_L = 8.5J)

^{196}Au: 6.02×10^5
^{198}Au: 1.58×10^4

— PdH_X CD block (E_L = 13.7J)

^{196}Au: 3.38×10^4
^{198}Au: 1.33×10^4

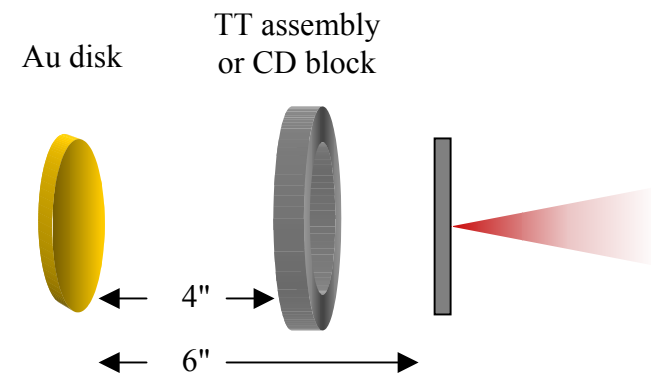

$$Yield = \frac{counts}{d\Omega / \Omega} \longrightarrow$$

Neutrons: 3.6×10^7
γ – rays: 9.0×10^7

$$\#\ particles = \frac{Yield}{\int N\sigma dx} \longrightarrow$$

Deuterons: 1.1×10^{12}
γ – rays: 1.3×10^{10}

8.3% of E_L into D > 4 MeV
0.2% of E_L into γ > 8 MeV

Physics & Advanced Technologies

CONCLUSION

- Metal targets doped with hydrogen isotopes can be fabricated effectively and cheaply.

- Radiative heating can be an effective method of removing hydrogenous contaminants from the target surface.

- Evidence of energetic deuterons (> 4 MeV) may be inferred from an increase in activated Au samples sensitive to high energy neutrons and γ rays.

Silver Activation Detectors

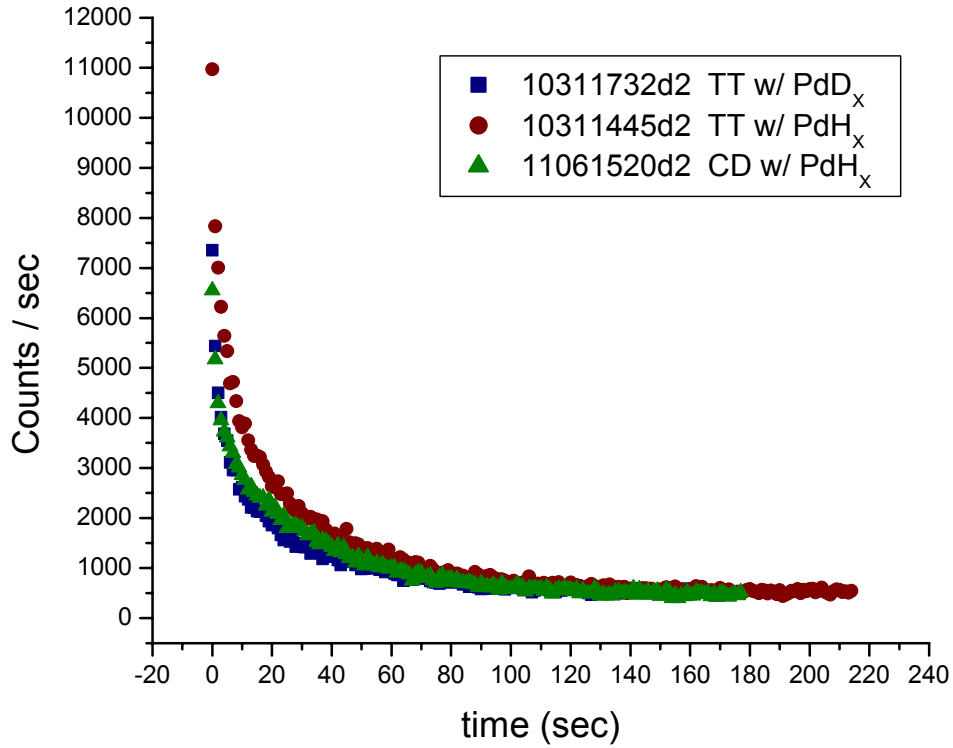

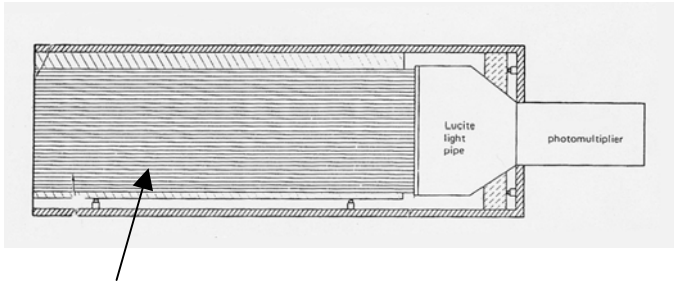

31 silver foils alternating NE110

^{108}Ag $\tau_{1/2}$ = 24 sec
^{110}Ag $\tau_{1/2}$ = 2.4 min

Statistics were too low to accurately fit data, implying neutron yield < 10^8.

D.R. Slaughter and W.L. Pickles, *Nucl. Instr. Methods* **160**, 87 (1979).

Fast Ignition Reactor Concepts

H. Azechi
Institute of Laser Engineering
Osaka University

6th Fast Ignition Workshop
Nov. 16-19, 2002
Dolphin Beach Resort
St. Petes Beach, Florida

For fast ignition we need high density compression as well as efficient heating.

ILE OSAKA

Required energy for ignition is given by

$$\eta E_{laser} = \frac{4\pi}{3} R^3 \rho \cdot \varepsilon_h = \frac{4\pi}{3} \frac{(\rho R)^3}{\rho^2} \varepsilon_h$$

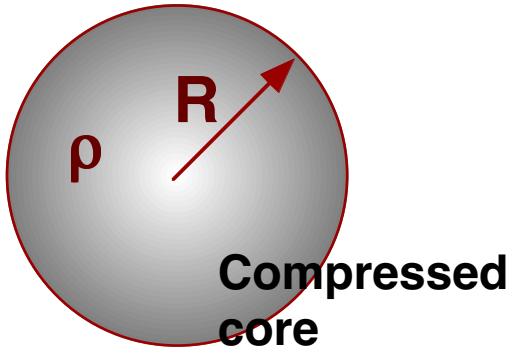

where

$\rho R \approx \alpha$ particle range = 0.3 g/cm^2

$\varepsilon_h = 2(3/2)T/m_{dt}$=1.15 GJ/g @T=10 keV.

To achieve fast ignition with reasonable size of $E_{laser} \approx$ 10's kJ, we need

- efficient heating of $\eta \approx$ 0.2-0.3
- high density of $\rho \approx$ 1000-1500 times liquid density.

Recent fast ignition exp't at Osaka has demonstrated efficient heating of $\eta \approx 0.2$ at the ignition equivalent laser intensity.

ILE OSAKA

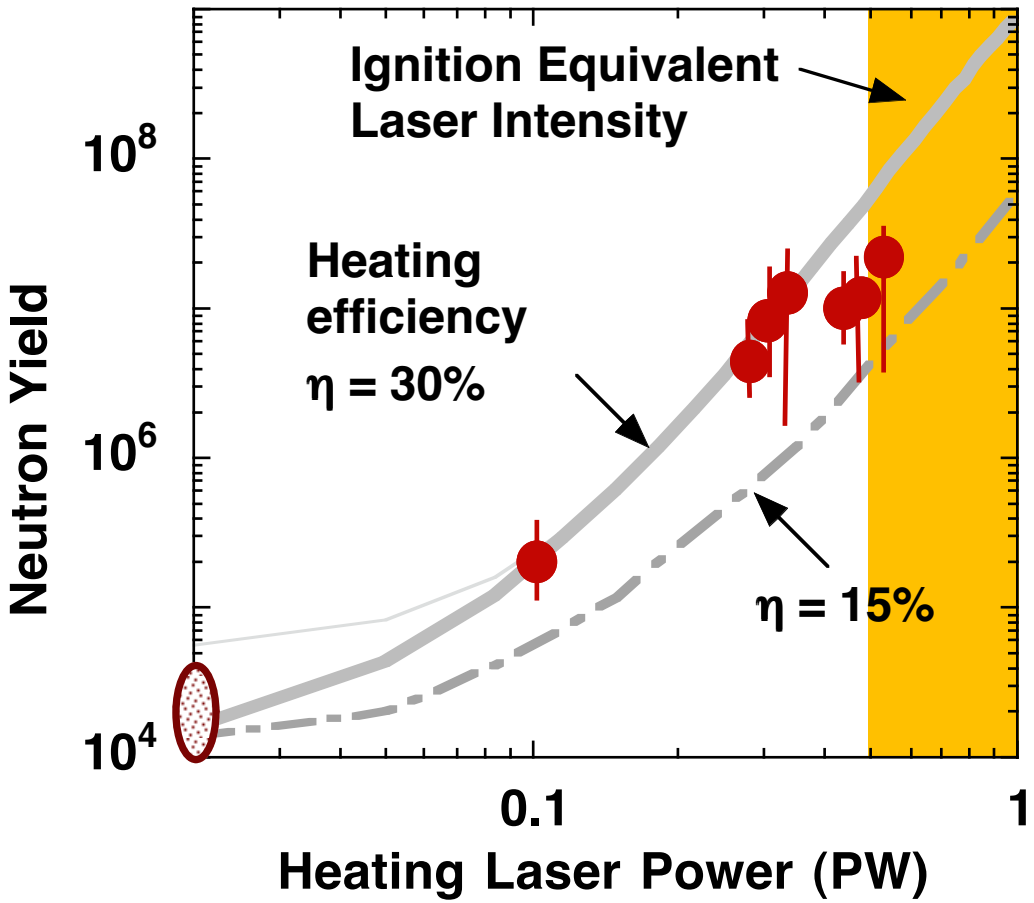

Neutron time-of-flight spectra showing Ti ≈ 1kev

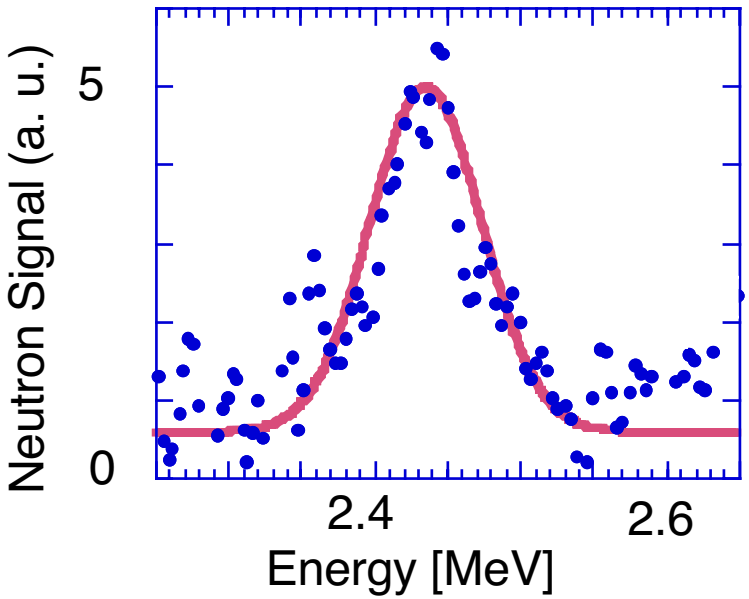

R. Kodama et al., Natue 2002

High density compression of ρ ≈ 1500 times liquid density needs to be demonstrated.

ILE OSAKA

This is about three times higher density than that ever achieved.

Average density ≈ 600 XLD

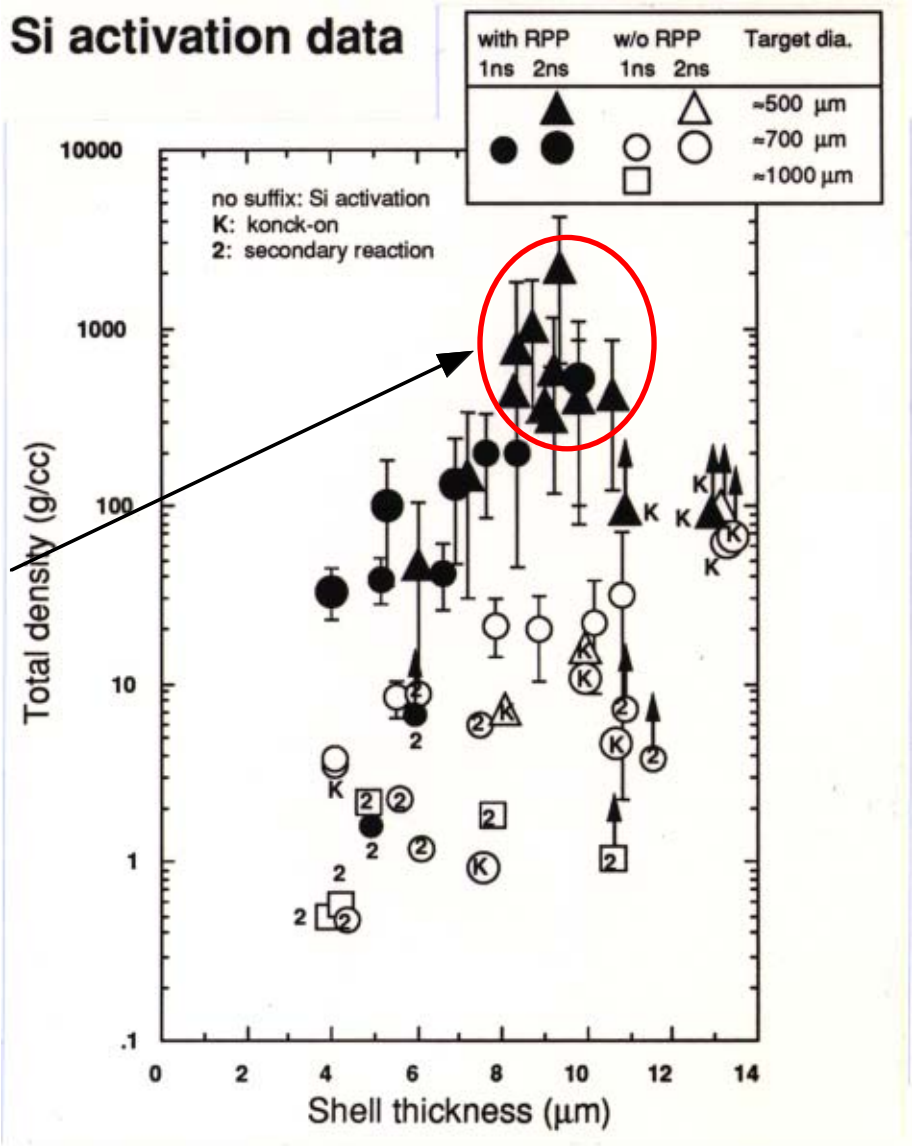

Azechi et al., Laser Part. Beam 1991.

Proposed FIREX

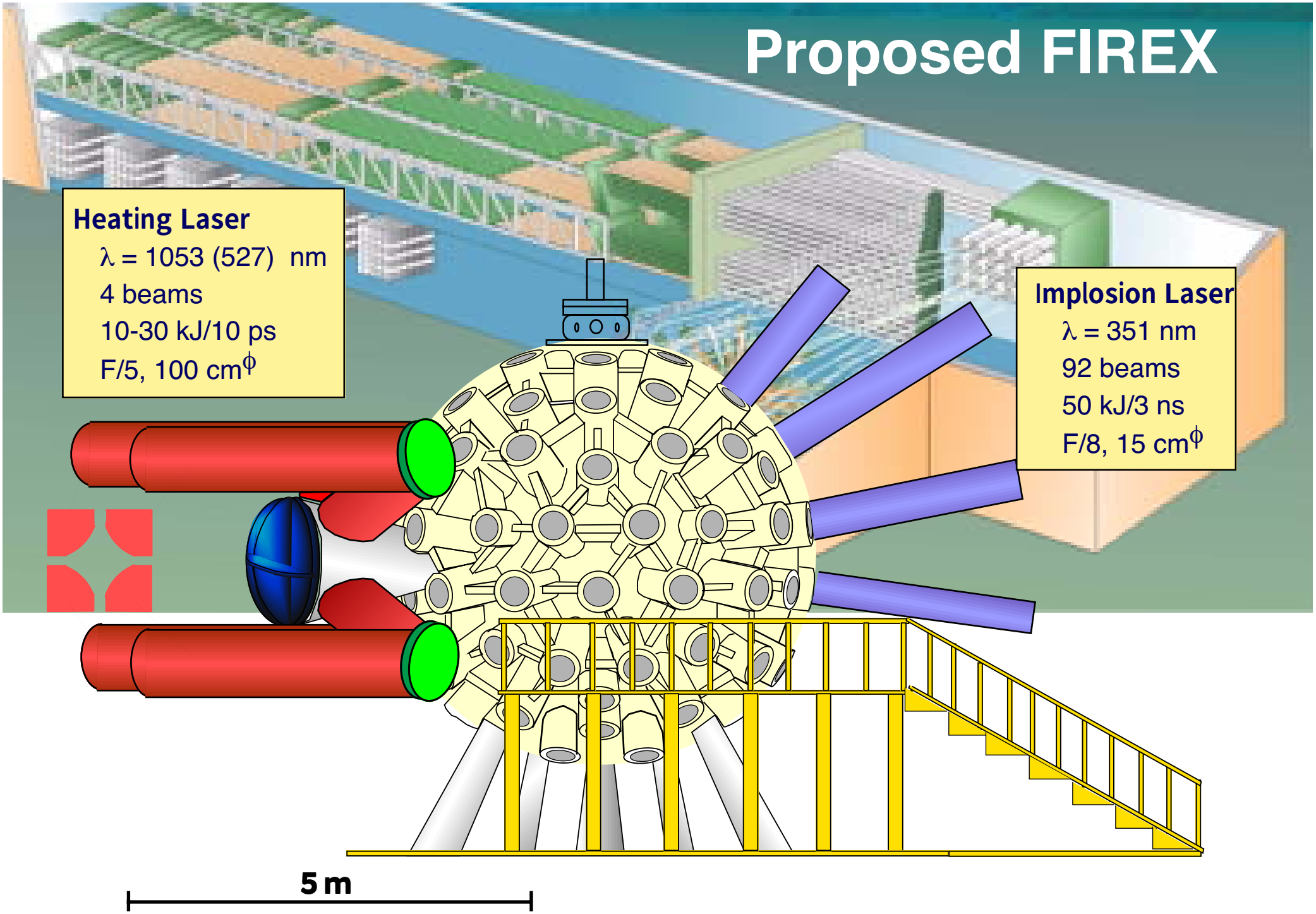

Once ignition is achieved by FIREX, getting high gain is rather straight forward.

ILE OSAKA

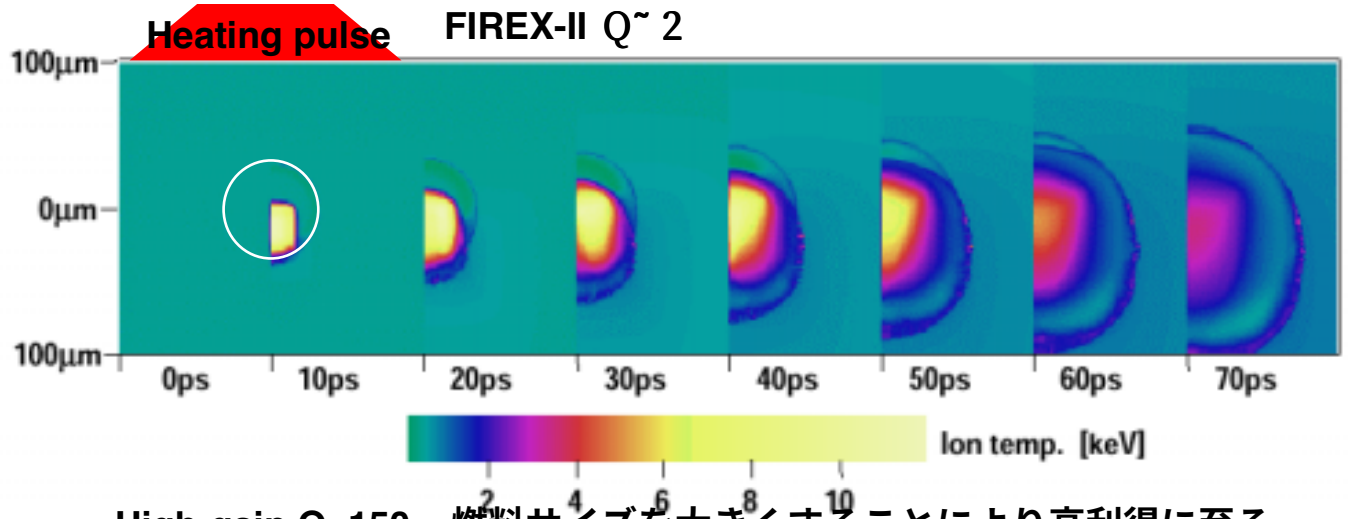

High-gain Q~150　燃料サイズを大きくすることにより高利得に至る.

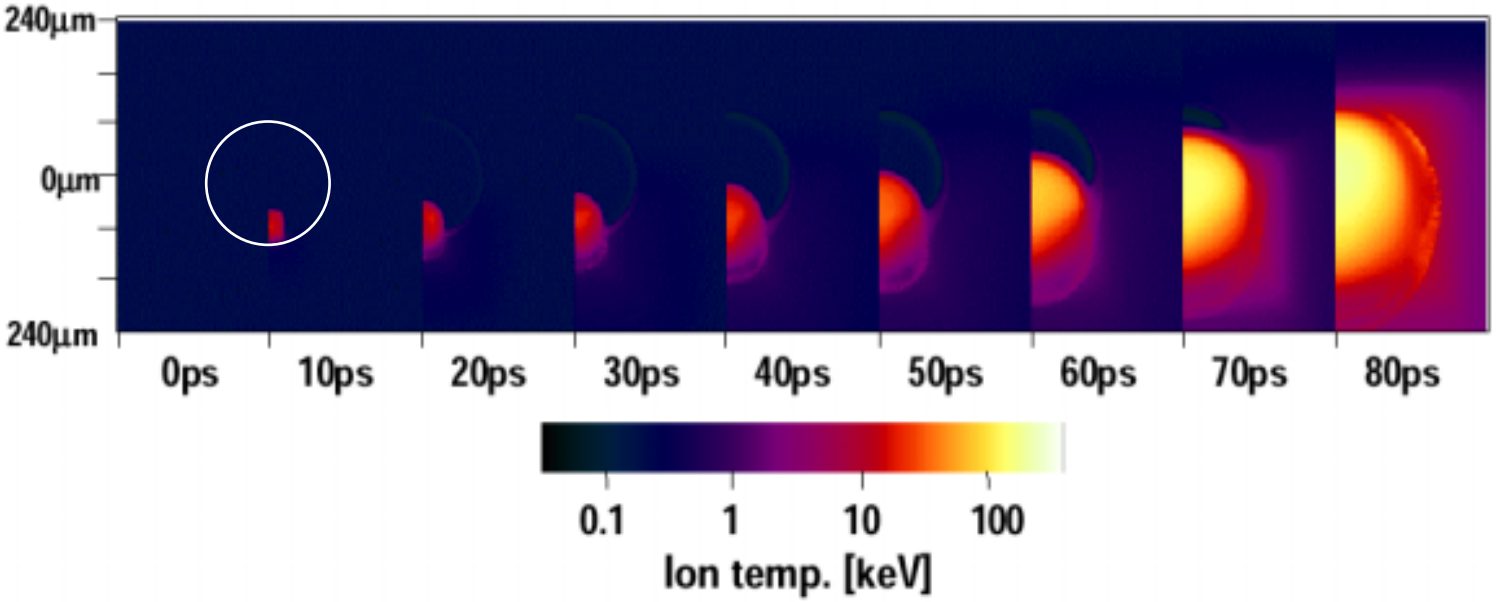

The major difference from FIREX-II to high-gain is only the size of the fuel.

Fast ignition gain curve

ILE OSAKA

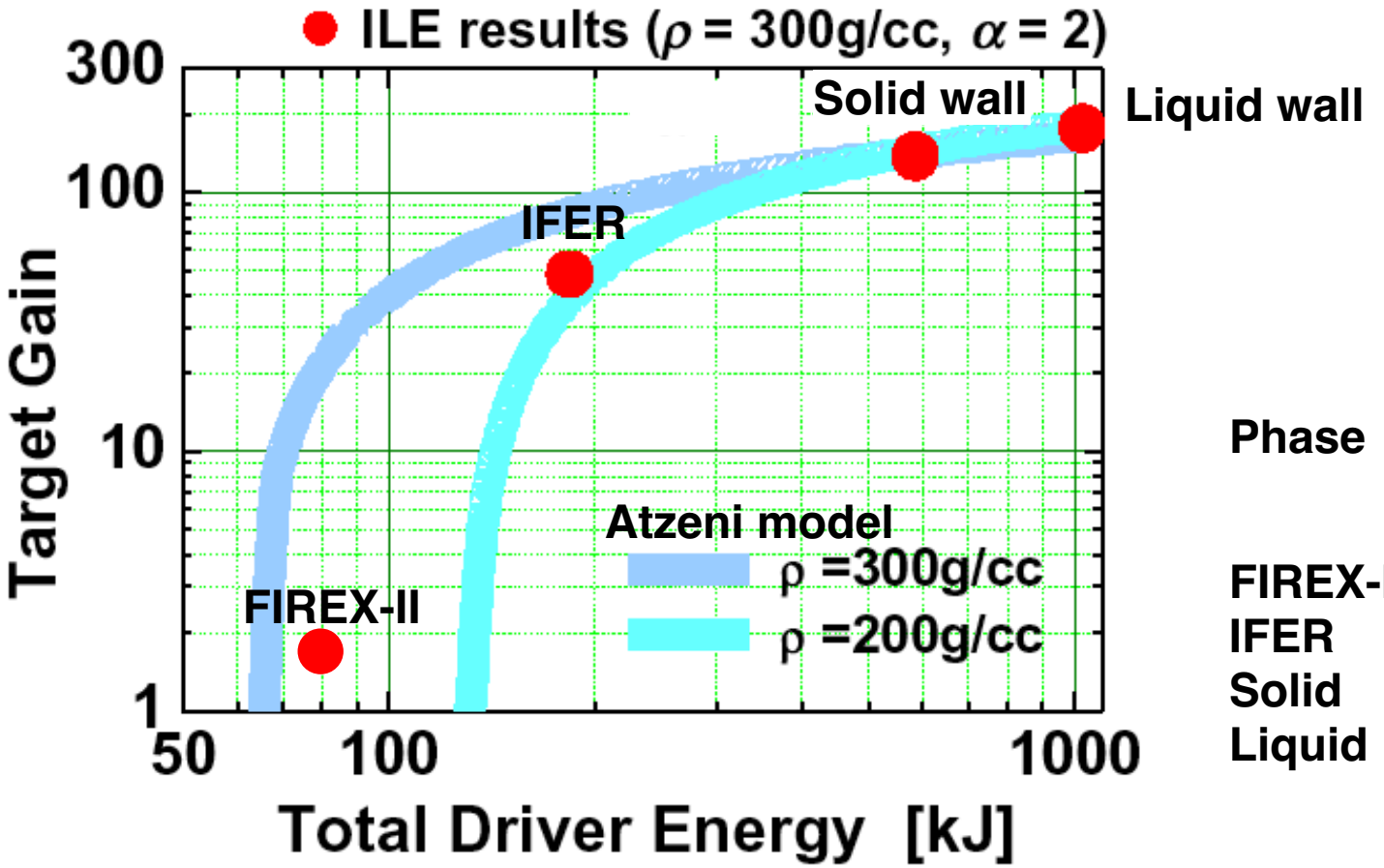

Phase	I_{REB} 10^{20}W/cm^2
FIREX-II	1.4
IFER	1.4
Solid	2.6
Liquid	2.6

This workshop and the comming Japanese conference are the good opportunity to consider from the goal.

Is fast ignition compatible to power plants?

ILE OSAKA

Fast ignition, if it is feasible, has a potential to completely change the strategy towards inertial fusion energy reactor.

・The market prefers small power plants of~ 100 MW.
・Small size of experimental reactors and demo reactors enables quick and inexpensive development.

However, FI might bring additional drawbacks (hopefully, advantages too.)

・Does heating beams propagate in a reactor chamber in which evaporated gas is filled? How much fill gas can be accepted?
・What is the compatibility of the cone targets to power plants?
  Isn't the cone damaging to the optics?
  How can we inject cone pellet?
  How can beam steering be made?

etc.

How small fast ignition reactors are!

IFE (Laser)

Fusion gain G ⇨ laser energy

power balance $\eta G \geqq 10$

⇨ laser cost

pulsed operation ⇨ pulse rep-rate

geometry ⇨ separability

⇨ final optics

MFE (DT)

plasma β ⇨ magnet cost

neutron wall loading

⇨ reactor size

geometry ⇨ complex

⇨ maintainability

Central ignition 700 MWe

Fast ignition 200 MWe

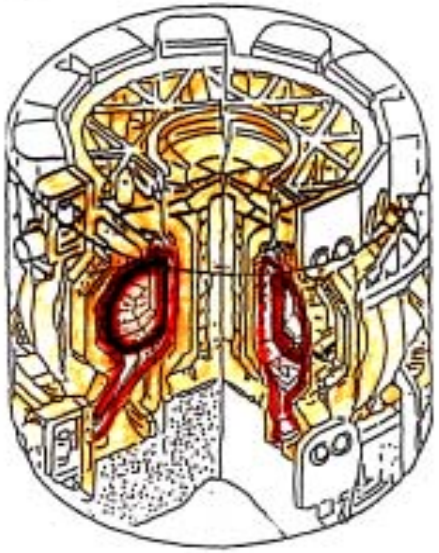

TOKAMAK 1200 MWe

LWR 1100MWe

20 m

[Comparison of reactor size]

How fast fast ignition reactor development is!

ILE OSAKA

２０１５年頃に高速点火研究成果及び欧米の中心点火研究成果を踏まえ、並行に推進する高繰り返しレーザー技術、燃料の繰り返し投入・炉技術の成果のもとに、実験炉の段階に進むことができる。

その後、商用を視野に入れた条件を満足する先進レーザー技術開発、先進炉技術の開発により原型炉へと進むことができる。

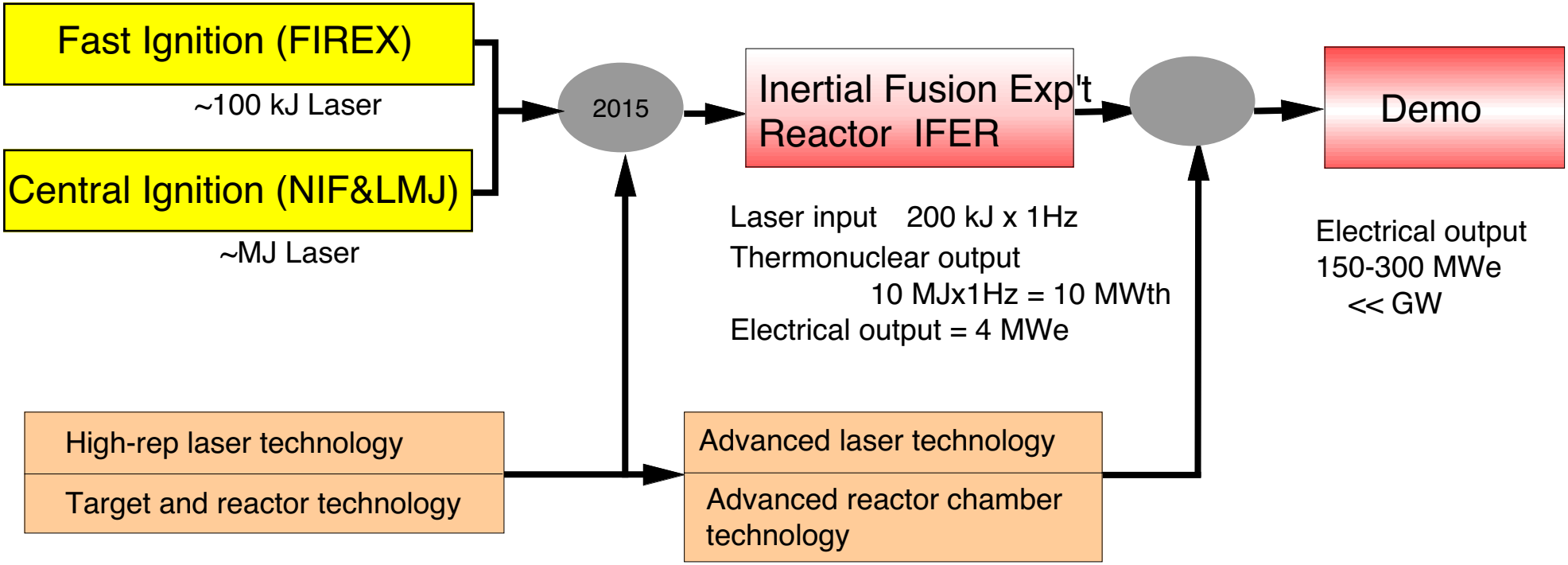

Fast Ignition Reactor Engineering-High Rep FIRE-HR

- High Rep. laser 10kJ ×1Hz
- Cryo. Target
- Pellet injection and beam steering

How inexpensive the development cost is!

ILE OSAKA

1） Cost of Laser Diode（LD）

・Required LD output per 1J pulse laser
=1J/Excitation efficiency 0.25=4J

・Laser medium needs to be excited within half life time.
Required LD power=4J/0.5 τ =24kW

・From the predicted LD cost at year 2015
LD cost＝1440$/J

・ For 200kJ IFER laser（350 kJ effective)
LD cost =500M$

2） LD Power supply+Cooling= 100 M$

3） Optics ect. (NIF60$/J) = 200 M$

Total 800 M$

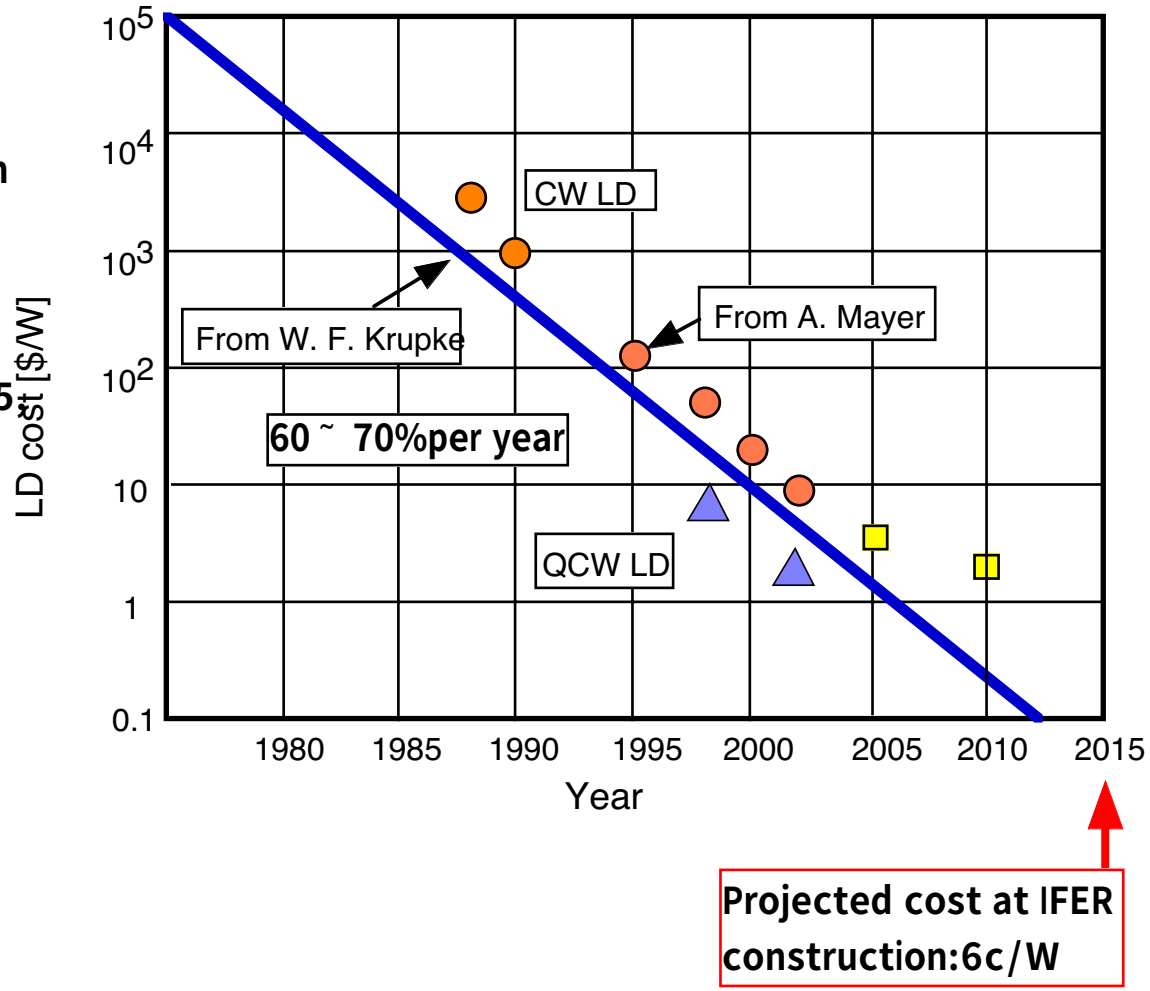

Cost estimate of major facilities for FI reactors (M$)

ILE OSAKA

Facilities	IFER	DEMO	COMMERCIAL
Laser energy	200kJ(inc.100kJ heating)	800 kJ	800 kJ
Fusion output	20 MJ	200 MJ	200 MJ
Rep. rate	1Hz	3 Hz	3 Hz×5
Fusion output	10 MWth	240 MWe	1200 MWe
Laser system cost	800	1500	1500
Items LD	500	900	900
Optics	200	400	400
Power supply	50	100	100
Cooling system	50	100	100
Reactor chamber	Solid 200 (+Liquid 200)	300	900
Fuel pellet	100	100	200
Peripherals	200 (+Power system200)	400	1200
Total	1300 (+400)	2300	3800

Assumption
LD cost 6c/W
Optics 60$/J

Assumption
LD cost 3c/W
Optics 30$/J

However, FI might bring additional drawbacks (hopefully, advantages too.)

Liquid and solid wall are both considered.

ILE OSAKA

1） Liquid wall

- Chamber wall protection by liquid metal (LiPb)
- Laser energy 1MJ， Pellet gain 200
- Fusion output 200MJ， Rep rate 3Hz， 600 MWth, 240 MWe
- If necessary, 5 modular plant--> 1.2 GWe

2） Solid wall

- Chamber wall unprotected. (W+SiC)
- Laser energy 0.6MJ， Pellet gain 150
- Fusion output 90MJ， Rep rate 6.7Hz， 600 MWth, 240 MWe

Liquid wall reactor concept

ILE OSAKA

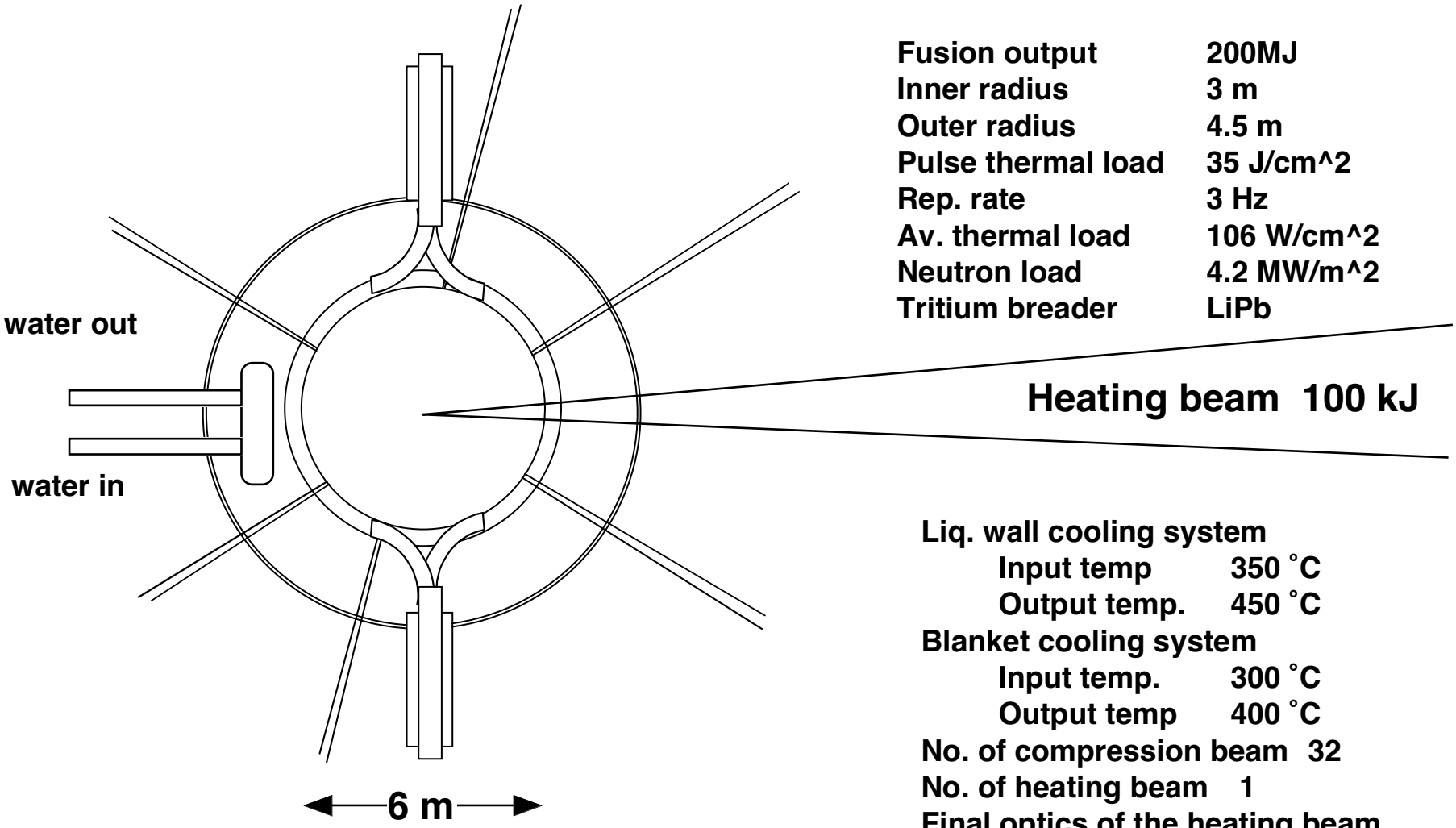

Fusion output	200MJ
Inner radius	3 m
Outer radius	4.5 m
Pulse thermal load	35 J/cm^2
Rep. rate	3 Hz
Av. thermal load	106 W/cm^2
Neutron load	4.2 MW/m^2
Tritium breader	LiPb

Liq. wall cooling system
- Input temp 350 ˚C
- Output temp. 450 ˚C

Blanket cooling system
- Input temp. 300 ˚C
- Output temp 400 ˚C

No. of compression beam 32

No. of heating beam 1

Final optics of the heating beam
- position from the center 30 m
- optics size 10 m^2

How much fill gas can be accepted?

ILE OSAKA

1. Nonlinear refractive index determines pressure allowed in reactor chambers.

2. If high pressure gas fill is allowed, filling Xe or Kr gas in solid-wall chamber may considerably reduce the thermal load by ions.

3. Alphas are not absorbed in the gas. How much alphas are accumulated in the reactor life?

4. Absorption of ion energy generates a blast wave. How strong is it?

Distortion of electron cloud causing nonlinear dielectroc "constant"

ILE OSAKA

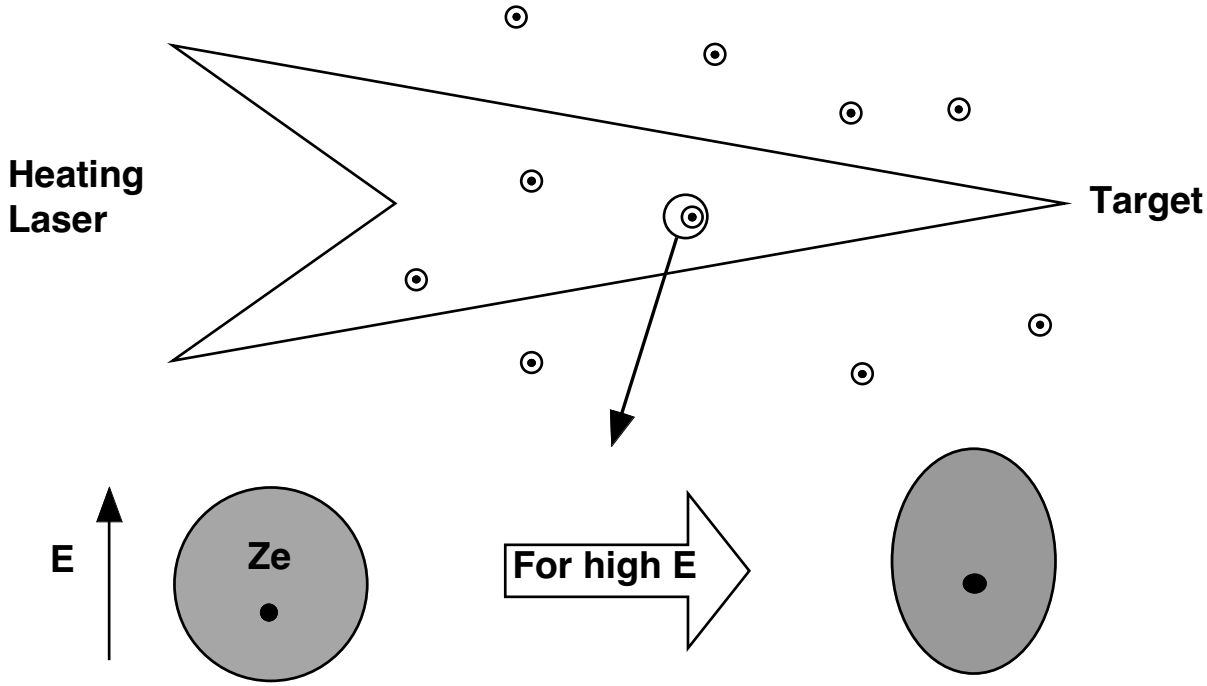

$$\varepsilon = 1 + \left(\frac{\omega_b}{\omega_0}\right)^2$$

$$\varepsilon = 1 + \left(\frac{\omega_b}{\omega'_0}\right)^2$$

$$\omega_b^2 = \frac{4\pi n_b e^2}{m_e},$$

$$h\omega'_0 = h\omega_0 - \frac{1}{2} p \cdot E$$

$\omega_0 =$ ionization potential/h

$\omega =$ laser frequency

Before catastrophic increase of the nonlinearity, field ionization takes place

ILE OSAKA

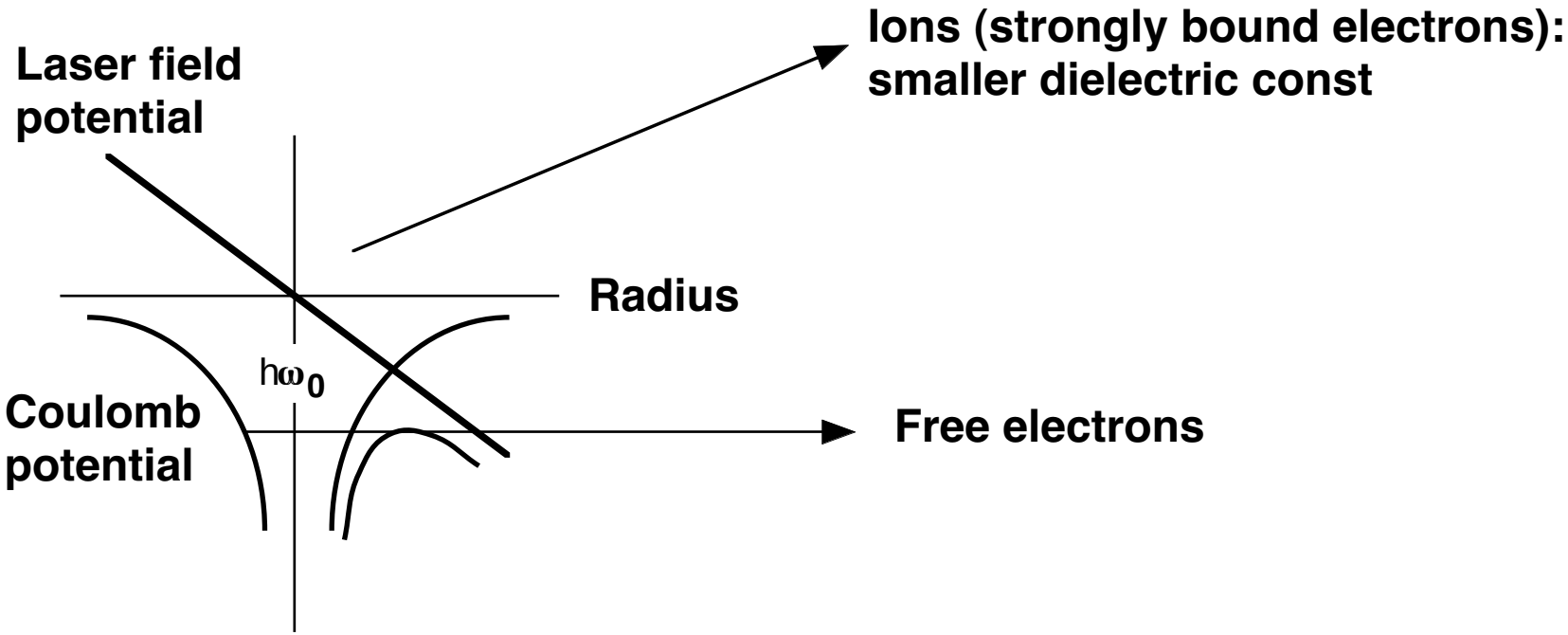

Polarization is dominated by free electrons

ILE OSAKA

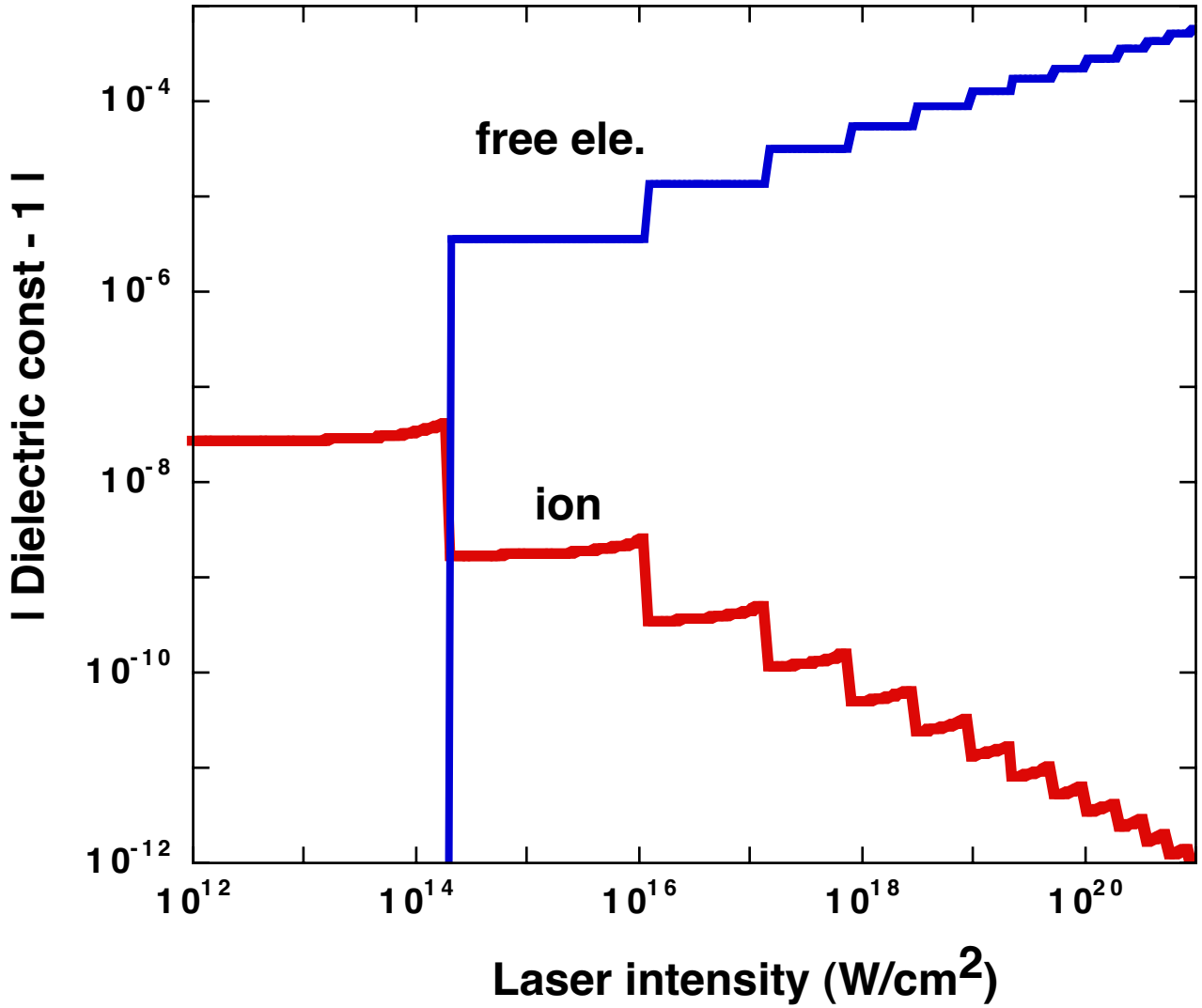

Effect of nonlinear refractive index is NOT a major concern at gas pressure below 0.1 Torr.

ILE OSAKA

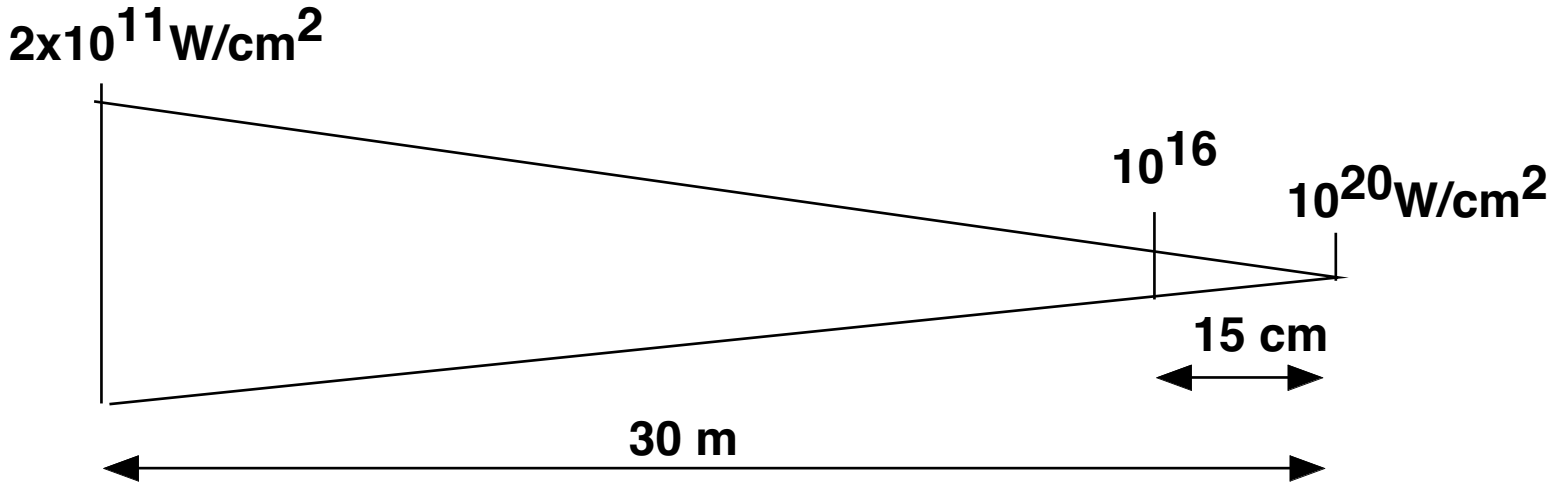

Nonlinear refractive index

$$\delta n = \sqrt{\varepsilon(I)} - 1$$

Optical length

$$\frac{\int \delta n dz}{\lambda_L} \approx 1 \text{ @0.03Torr Xe}$$

Acceptable gas pressure is about 0.03 Torr for a 30-m path length.

Ion range from high gain reactor core

ILE OSAKA

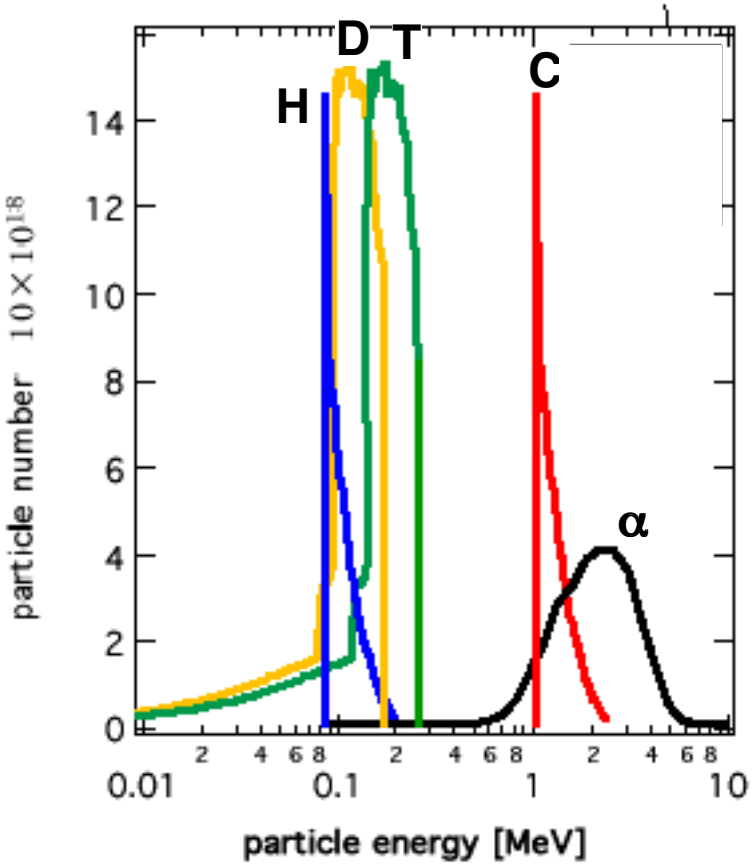

Ion spectra from a central ignition target (E_{fusion}=400MJ)

Same spectra is assumed for FI

Ion range in 0.1Torr-Xe

- 0.2-MeV proton = 8 m
- 0.18-MeVdeuteron=7 m
- 0.25-MeV triton =10 m
- 2.4-MeV carbon = 16 m
- 3.5-MeV alpha =100 m

All ions except alphas can be stopped.

Thermal load can be significantly reduced by stopping ion flux.

ILE OSAKA

Energy flux

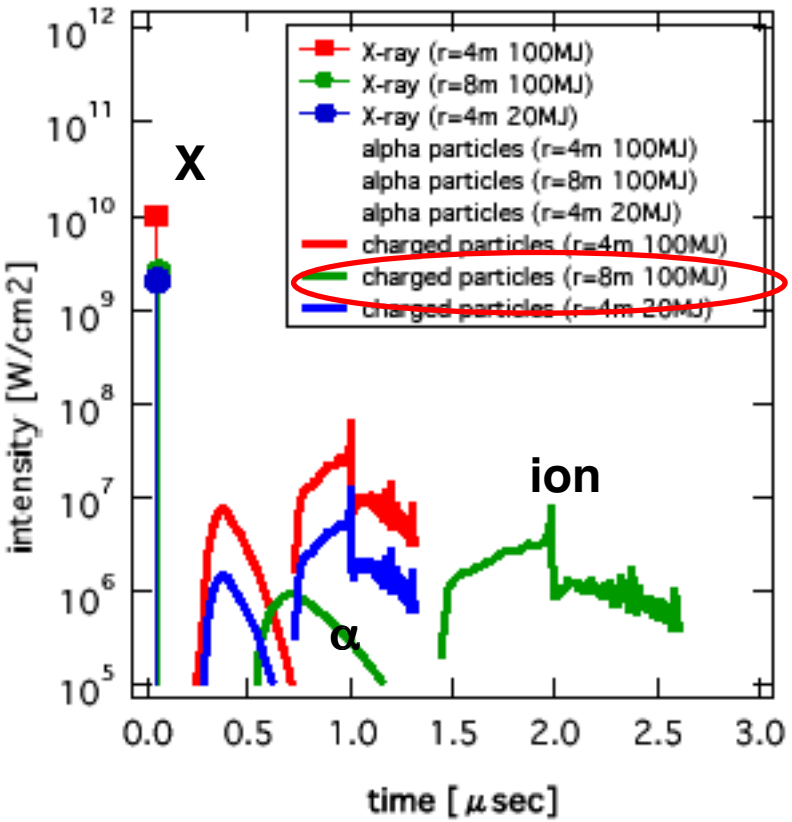

Wall temperature

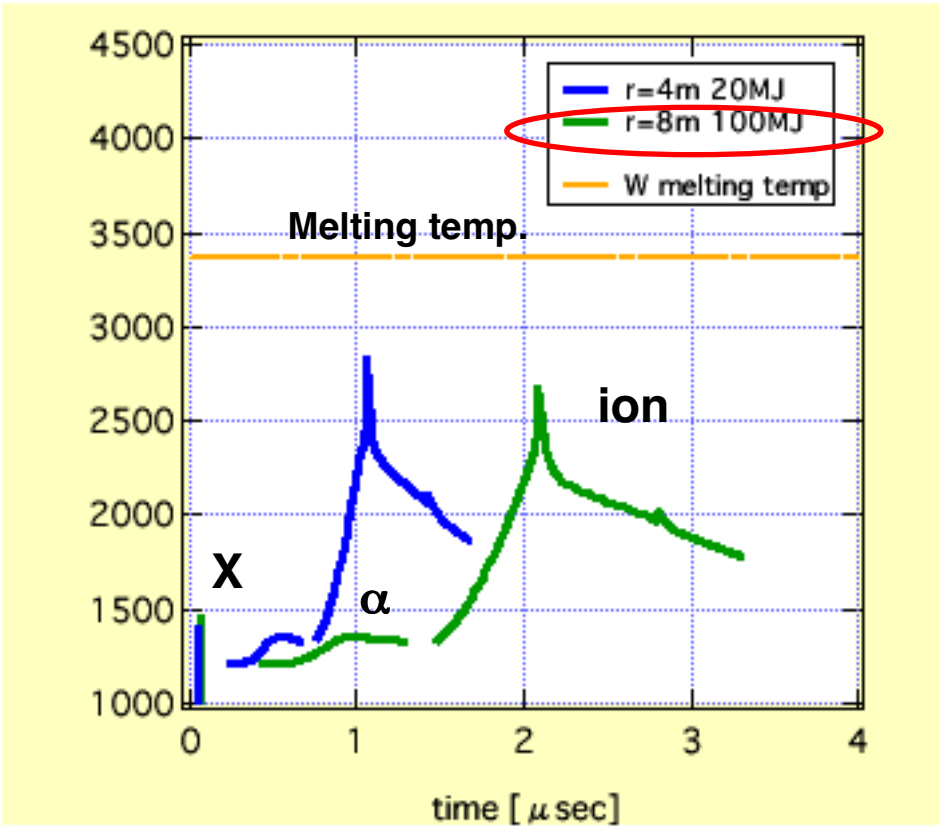

Y. Kozaki, April 6-7, 2002

Accumulation of alphas in the wall

ILE OSAKA

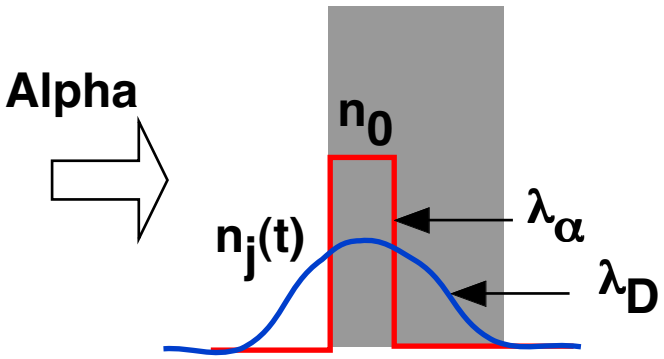

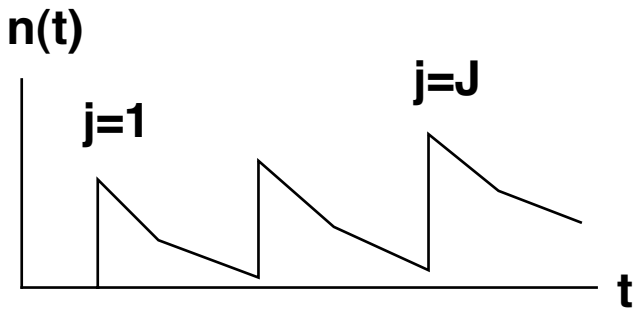

n_0 = initial alpha density

$$n_j(t) = n_0 \frac{\lambda\alpha}{\lambda_D(t)}$$

λ_α = α rang

$\lambda_D(t)$ = diffusion length = $\sqrt{\chi t}$

χ = thermal diffusibity = $\frac{l_{mfp} v_{th}}{3}$

v_{th} = thermal velocity of alpha at T = 1000 K

$$n(t) = \sum n_j(t)$$

Simple estimation shows that the accumulated alpha density is only 10^{-4} of the solid density even after 10^{10} shots (Elusion = 100 MJ, R=10m).

But material experts expect that α particles accumulate much more.

Compatibility of the cone target to power plants

Cone target size and mass

- considering protection of chamber wall and optics -

r (cone) = 1.7 mm
M(cone) = 40 mg Pb

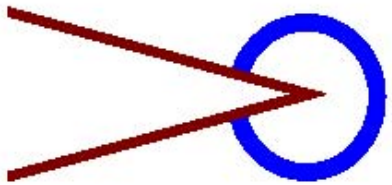

90 MJ cone target

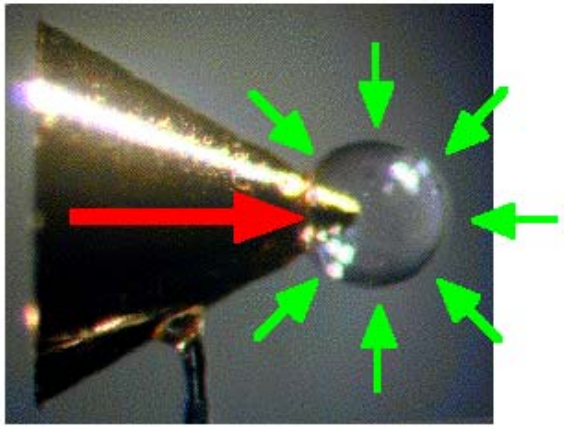

Cone Target Experiment

The cone must be long enough for the corona plasma not to interfere the heating beam.
---> 5 mm

The cone must be thick enough for the 100-Mbar shock not to transit within the implosion time.
--->200 μm

Cone angle = 30° ---> Cone mass = 40 mg for Pb

How much energy does the cone get from the core?

ILE OSAKA

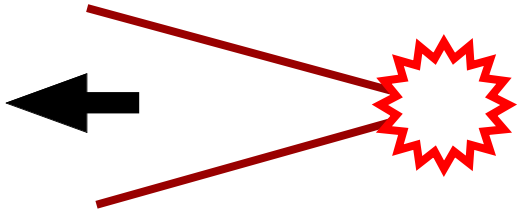

The cone could be accelerated by the core pressure.--> It might shoot the final optics like a bullet.

But

If the target ignites, the pressure is so high that the cone will be vaporized completely.

If the target fails to ignite, since the thermal energy of the core is converted to kinetic energy of radial motion, the core pressure can accelerate the cone only in the very beginning. The cone gets only a very small fraction of energy on the order of 100 J, even if the cone completely survives.

If it is still concern, we may stop the cone by force.
----debris clearing by laser

Fueling is probably faster and safer.

ILE OSAKA

Faster because fueling through a pipe. Safer because minimum T inventry

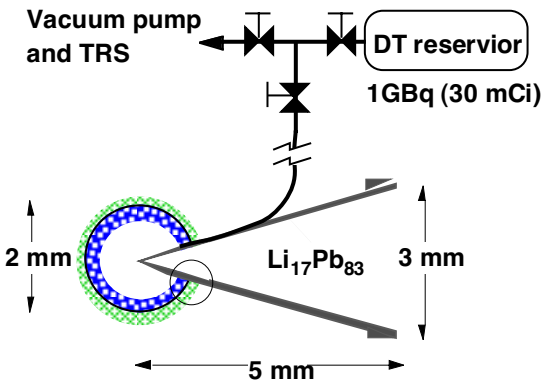

↑FireX-II用コーン付きDTクライオターゲット概念図

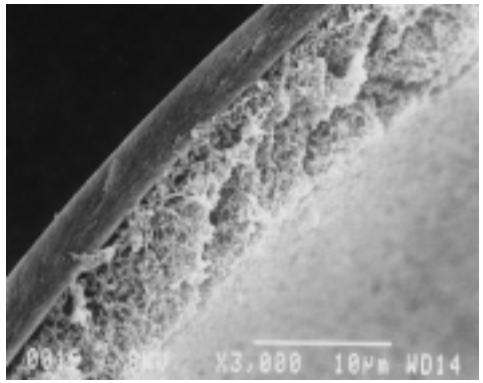

↑フォームシェルはエマルション法で製作可能

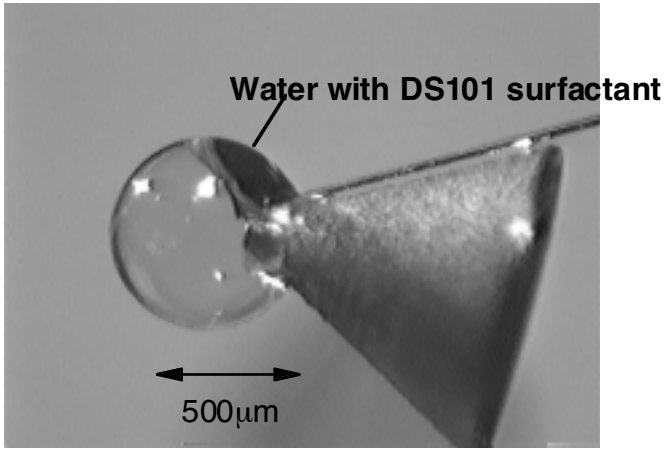

↑直径30μmのガス導入管で水を充填した例。

　ガス導入管を用いることにより、充填時間の短縮、インベントリー低減、安全性向上などが期待される。

→フォーム層で均一な厚さの液体重水素層を製作。

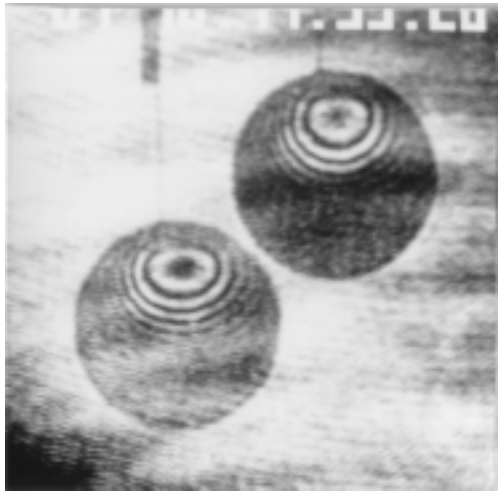

フォーム無し↑有り↓

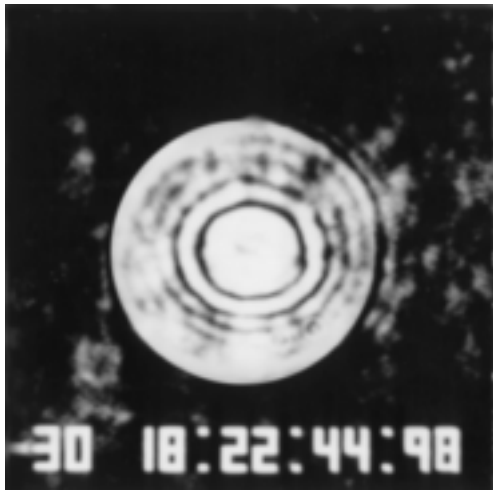

In the case of a fast ignition target, thermal load is concentrated on the leading side.

ILE OSAKA

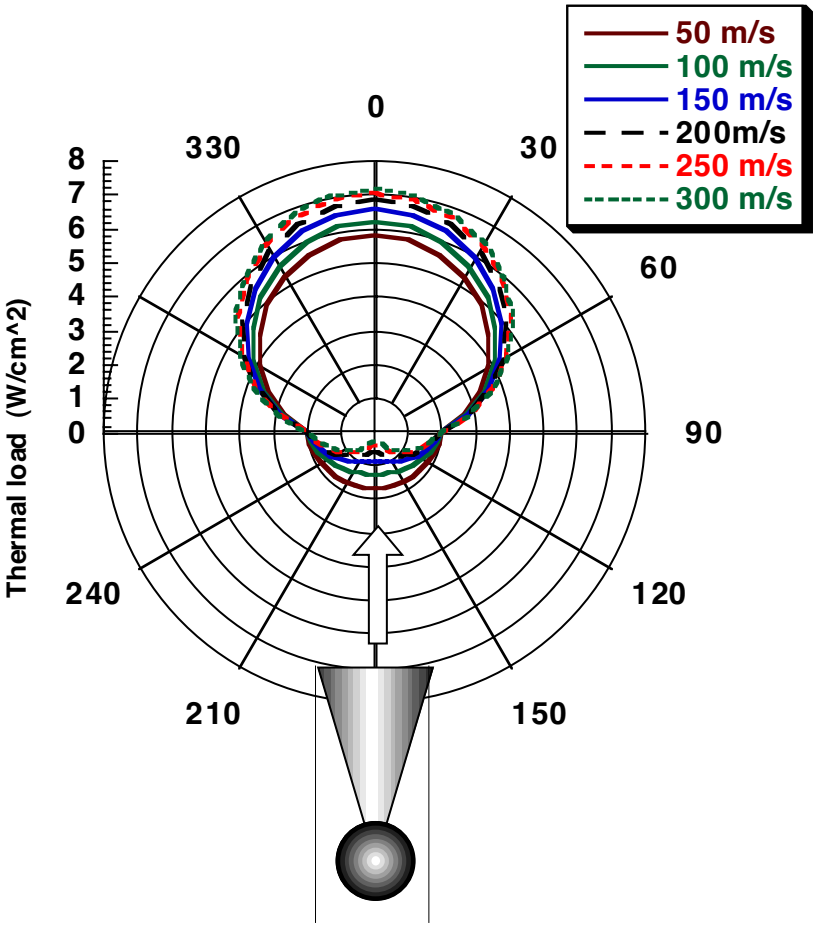

- When a target is injected into 650 C, 0.05 Torr Pb vapor at 300 m/s, the thermal load on the leading side exceeds Black body radiation.
- The cone works as a wake shield that reduces the thermal load due to the dynamic component.
- Because of large thermal conductivity of lead, the cryogenic layer would melt away.

Moreover, inertia of the cone reduces fluctuation of the target position

Is fast ignition compatible to power plants?
The answer is hopefully YES.

ILE OSAKA

Fast ignition, if it is feasible, has a potential to completely change the strategy towards inertial fusion energy reactor.

・The market prefers small power plants of~ 100 MW.
・Small size of experimental reactors and demo reactors enables quick and inexpensive development.

However, FI might bring additional drawbacks (hopefully, advantages too.)

・Does heating beams propagate in a reactor chamber in which evaporated gas is filled? Yes.
How much fill gas to reduce the wall load can be accepted?
about 0.03 Torr for a 30-m path
・What is the compatibility of the cone guided targets to power plants?
Isn't the cone damaging to the optics? No.
How can we inject cone pellet?
How can beam steering be made?

etc.

High Energy Petawatt Lasers For Fast Ignition

6th Workshop on Fast Ignition of Fusion Targets

St. Pete Beach, Florida

November 19, 2002

C. P. J. Barty
Chief Scientist
Laser Science and Technology Program
Lawrence Livermore National Laboratory

This work was performed under the auspices of the US Department of Energy by the University of California, Lawrence Livermore National Laboratory under contract No. W-7405-Eng-48

Outline

The National Ignition Facility

- Introduction to High Energy Petawatt Lasers (HEPW)
- Enabling R&D for HEPW Beams
- Prospects on NIF and beyond
- Summary

3 Goals of Solid-State, Short-Pulse Amplification

The National Ignition Facility

Highest Efficiency

Saturated Amplification
>1 photon/cross section
$J > J_{sat} = h\nu/\sigma$

Shortest Pulse Duration

Bandwidth-Limited Duration
$\Delta t_{min} \sim 0.5/\Delta\nu_{fluorescence}$

No Damage

Avoid Intensity Dependent Damage
Field Ionization
Avalanche Ionization
And Self focusing

$I_{max} = J_{sat}/\Delta t_{min}$

$J_{sat} = 6\ J/cm^2$ and $\Delta t_{min} = 60\ fs$

$I_{max} > 10^{14}\ W/cm^2$

$I_{max} < 10^{10}\ W/cm^2$

DAMAGE!

Chirped Pulse Amplification

The National Ignition Facility

Stictland & Mourou, Opt. Comm.56, 219, 1985

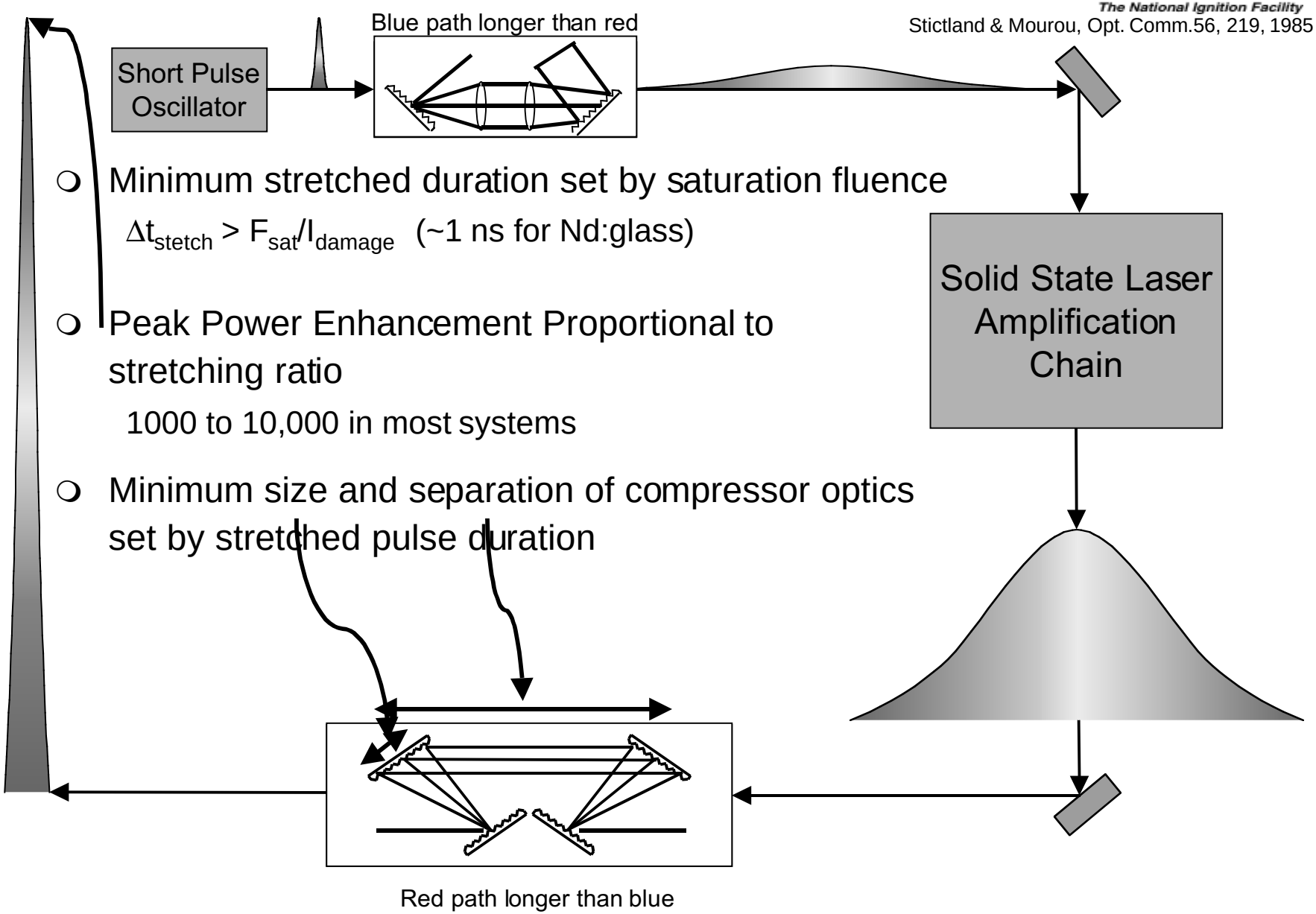

- Minimum stretched duration set by saturation fluence

  $\Delta t_{stetch} > F_{sat}/I_{damage}$ (~1 ns for Nd:glass)

- Peak Power Enhancement Proportional to stretching ratio

  1000 to 10,000 in most systems

- Minimum size and separation of compressor optics set by stretched pulse duration

Three Classes of Petawatt Lasers

The National Ignition Facility

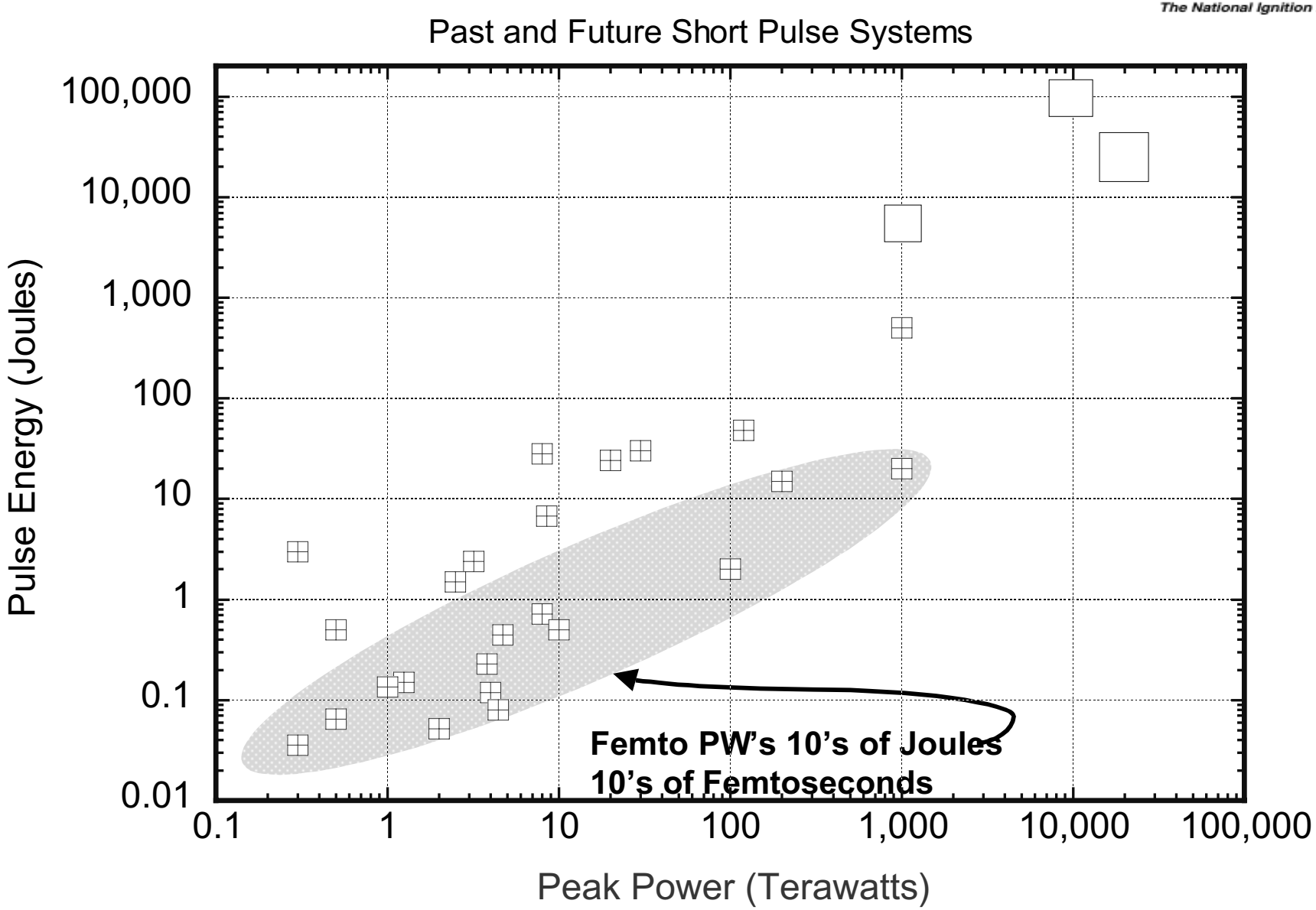

CPA State of the Art (Femto systems)

The National Ignition Facility

- Femtosecond systems are progressing steadily toward PW powers

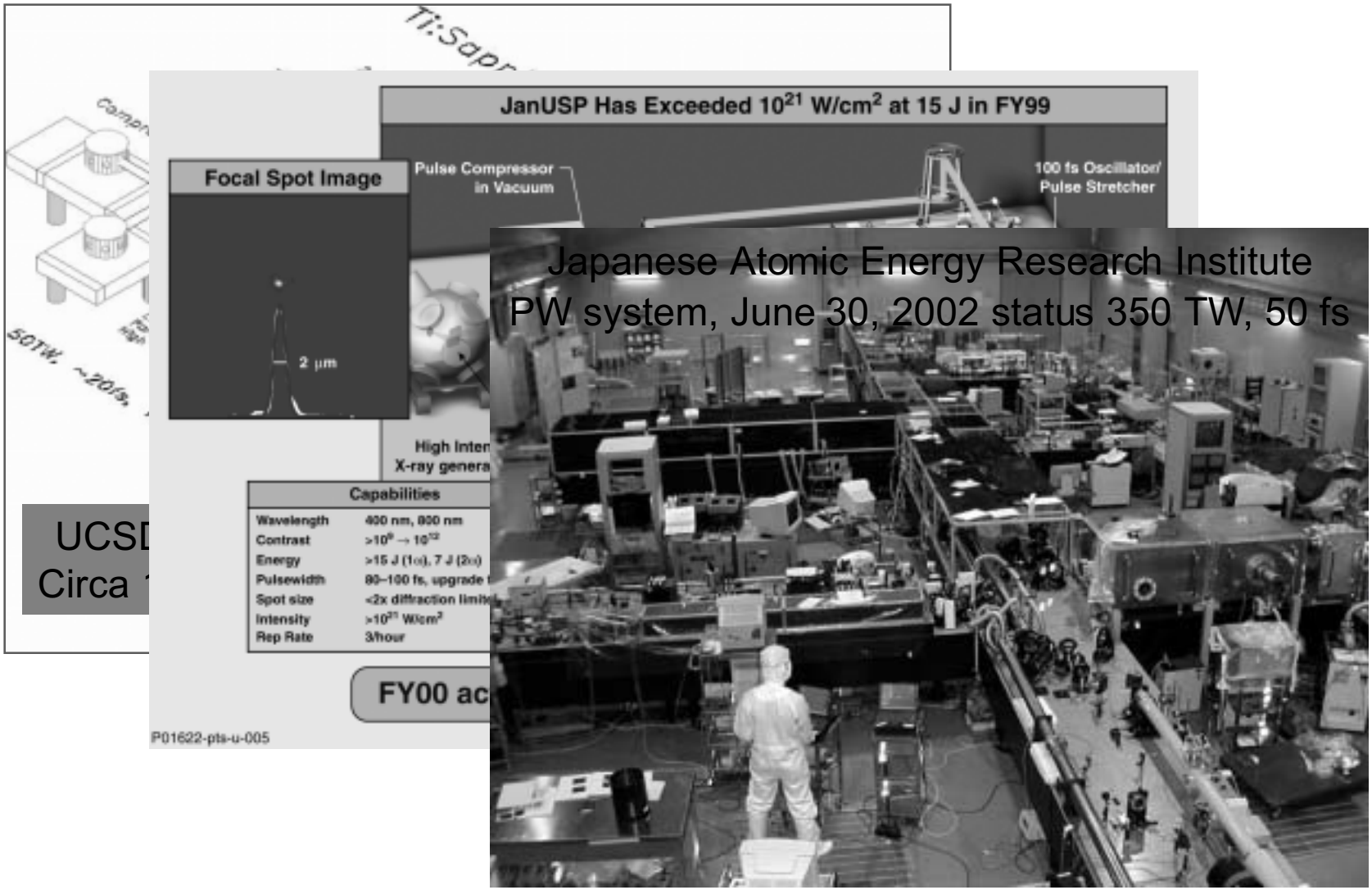

Three Classes of Petawatt Lasers

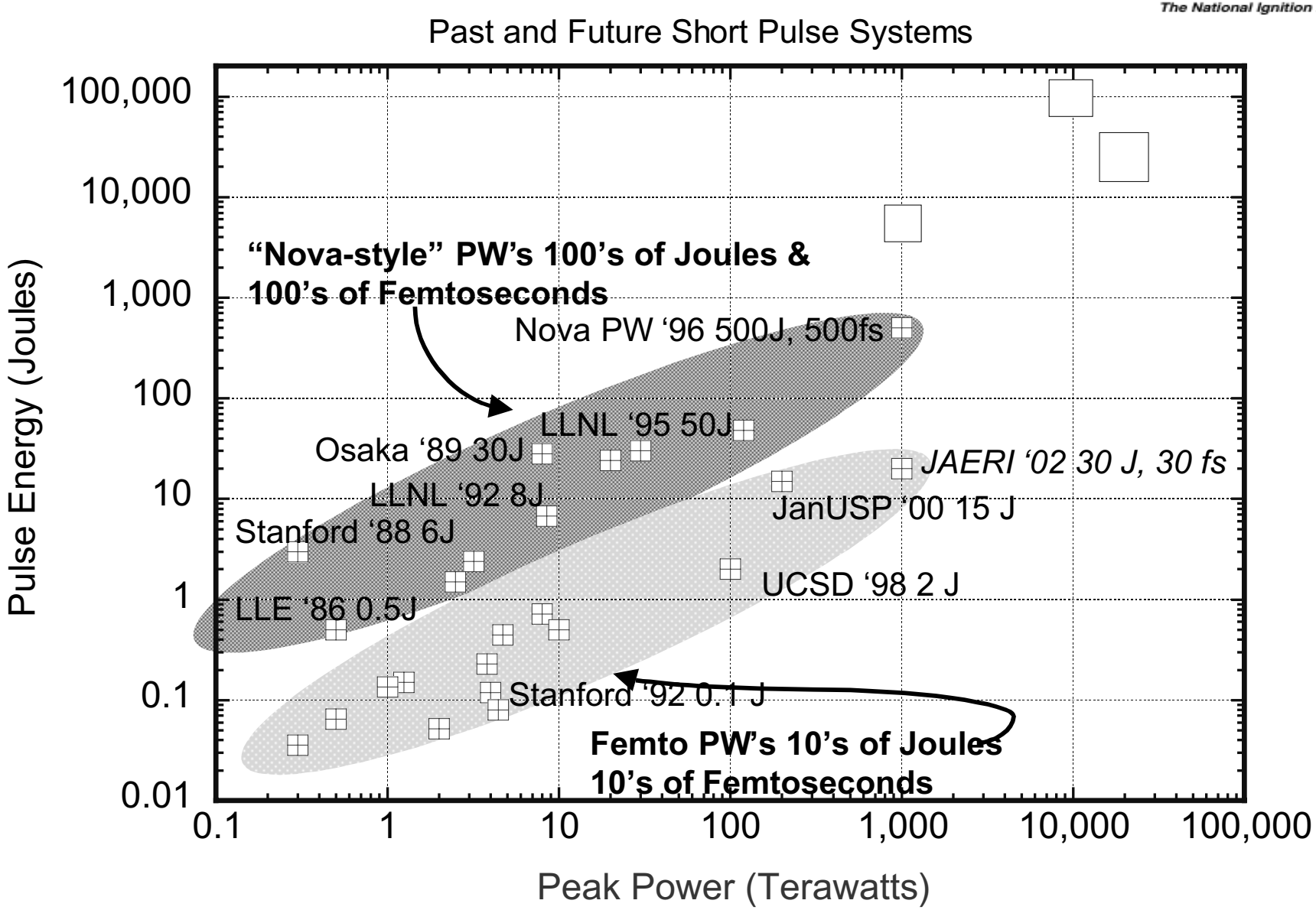

CPA State fo the Art (Nd:glass systems)

The National Ignition Facility

- Nova-style PW lasers are being built and used at labs outside the US

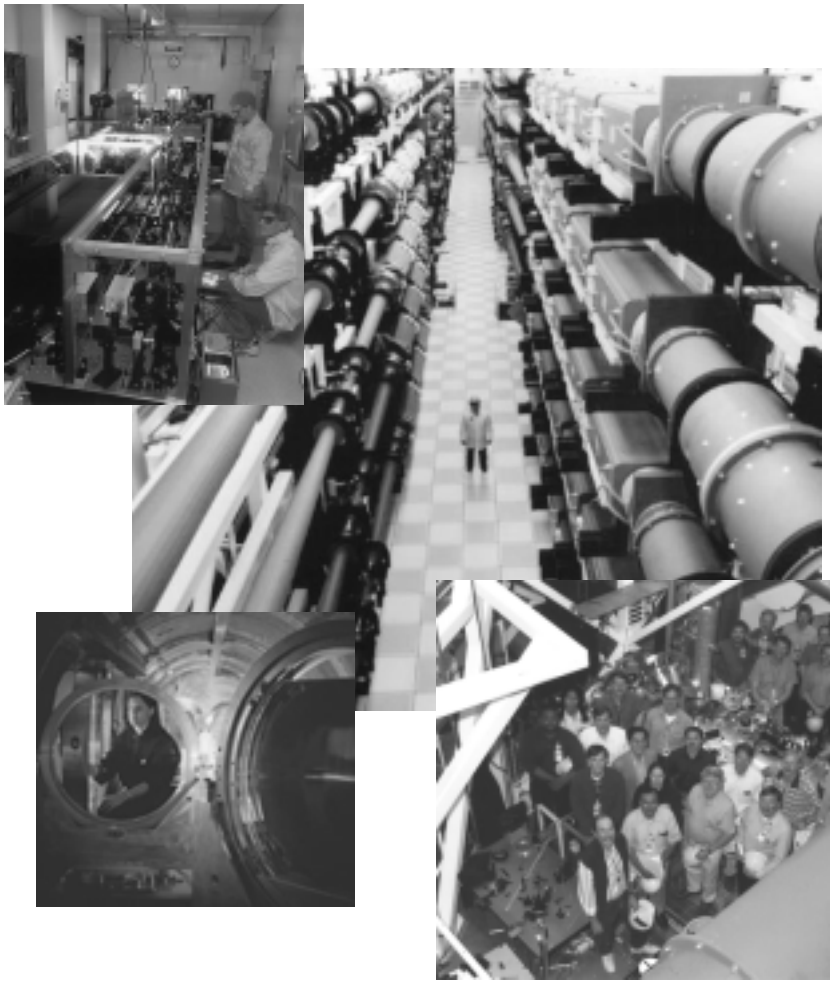

Nova PW 1996 ~500J, ~500fs

Three Classes of Petawatt Lasers

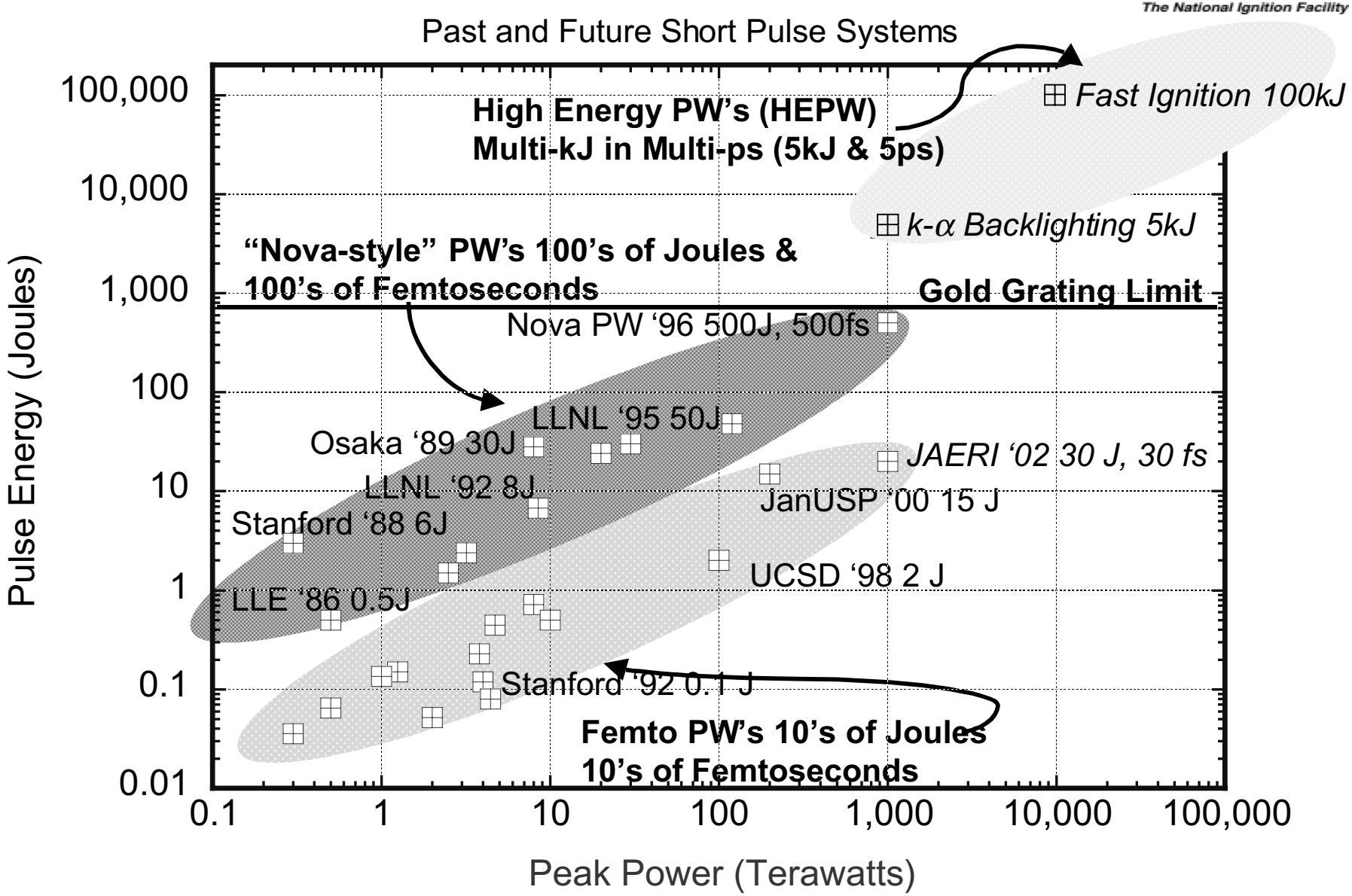

HEPW Potential of Advanced Nd:Glass Lasers

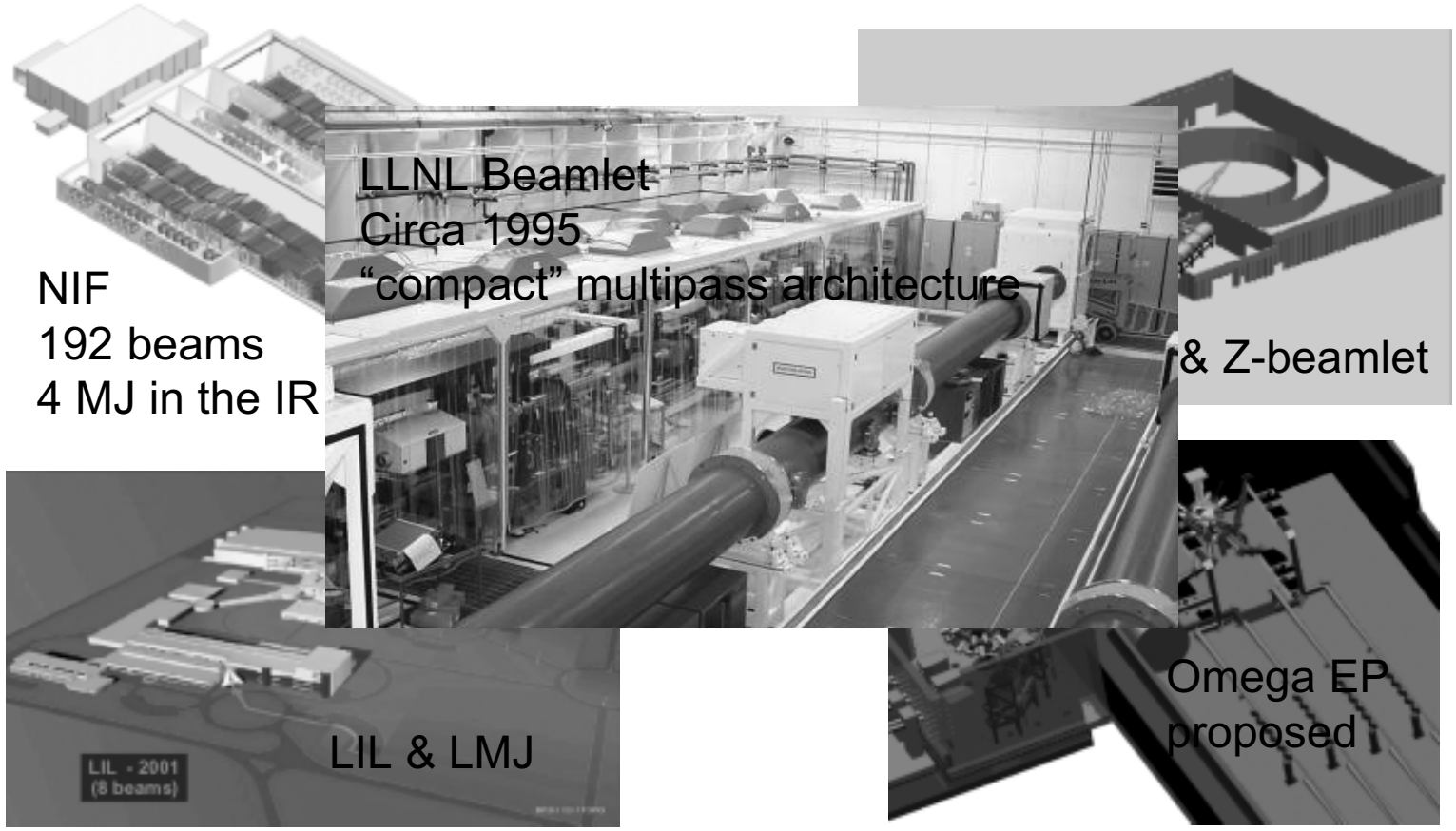

- All have similar multipass architecture and nominal 35cm x35cm beam aperture
- Beam line “Potential” is of order 20 kJ energy and 100 fs bandwidth (200 PW)
- Compressed Pulse duration limited by final optic damage & set by mission needs
- Extractable Energy is determined by Stretched Pulse Duration (~5 kJ @ 1 ns)

Possible HEPW requirements for NIF

The National Ignition Facility

- Advanced backlighting of dense targets will require **multi-kJ's**
  - Thickness of targets and signal to noise dictates energy requirement
  - Events radiographed are relatively "slow" ps-ns

20-100 keV X rays required for NIF-scale targets

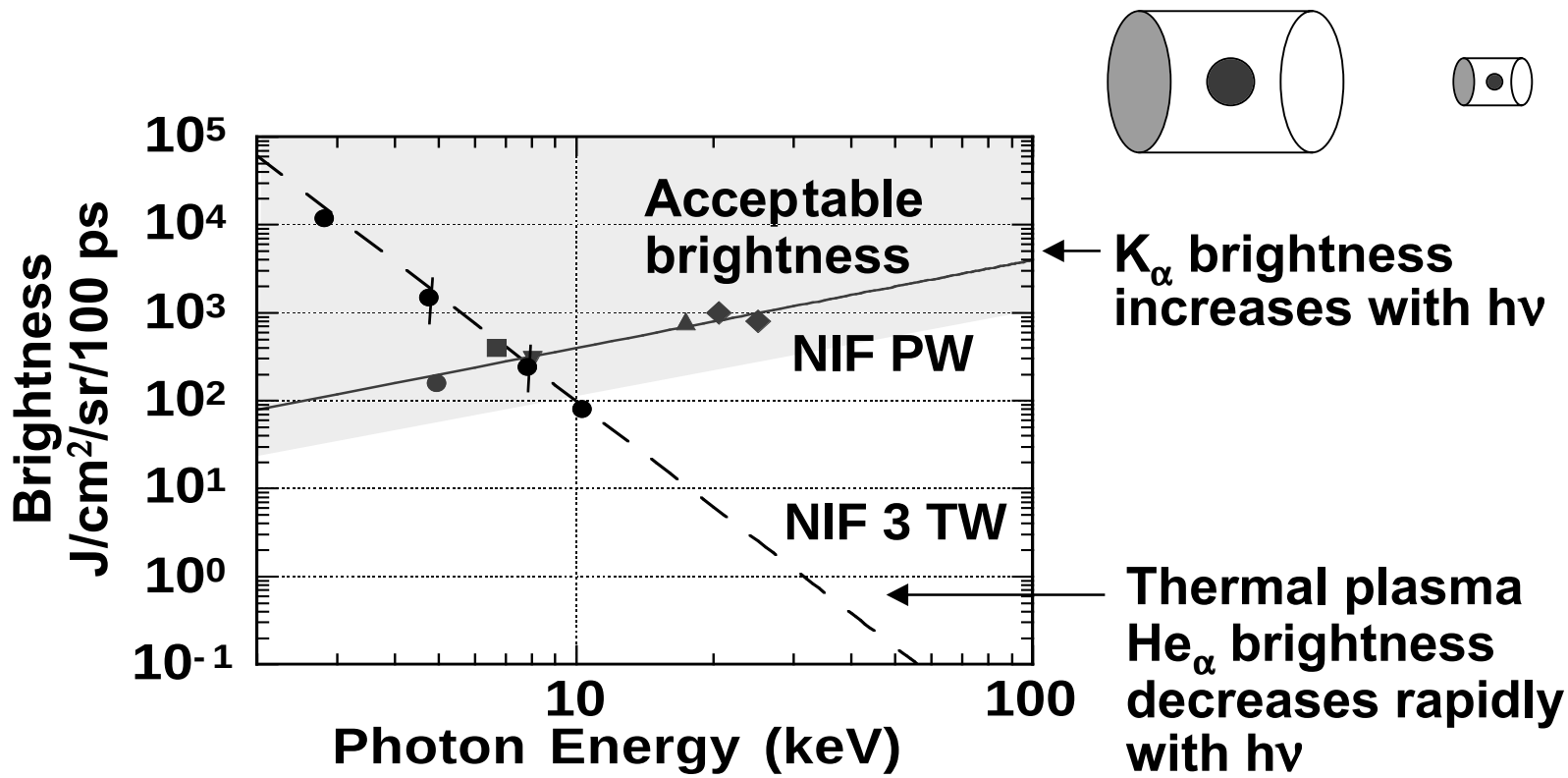

- NIF targets are >250 times larger volume than Nova targets
- Higher energy X rays, >> 10 keV are needed for imaging
- Some concepts call for use of 60 beams to drive one “thermal backlighter”
- One, 5-kJ, 5-ps driven, K-alpha source could do the same job!
  But this would be one order beyond the present state of the art

Possible HEPW requirements for NIF

The National Ignition Facility

- Advanced backlighting of dense targets will require **multi-kJ's**
  - Thickness of targets and signal to noise dictates energy requirement
  - Events radiographed are relatively "slow" ps-ns
- Fast Ignition demonstration predicted to require ~**100 kJ**
  - Energy estimate depends heavily on conversion of laser light to energetic particles and coupling efficiency to dense target
  - Optimal pulse length of order 10 ps
- Proton beams and radiography and heating with them
  - Conversion efficiency and beam brightness point to desire for high energy
  - Not strongly dependent upon pulse duration. Picoseconds OK
- All require **mulit-kilojoule, few picosecond** pulses, i.e.HEPW lasers

Two R&D Efforts of NIF HEPW Strategic Initiative

The National Ignition Facility

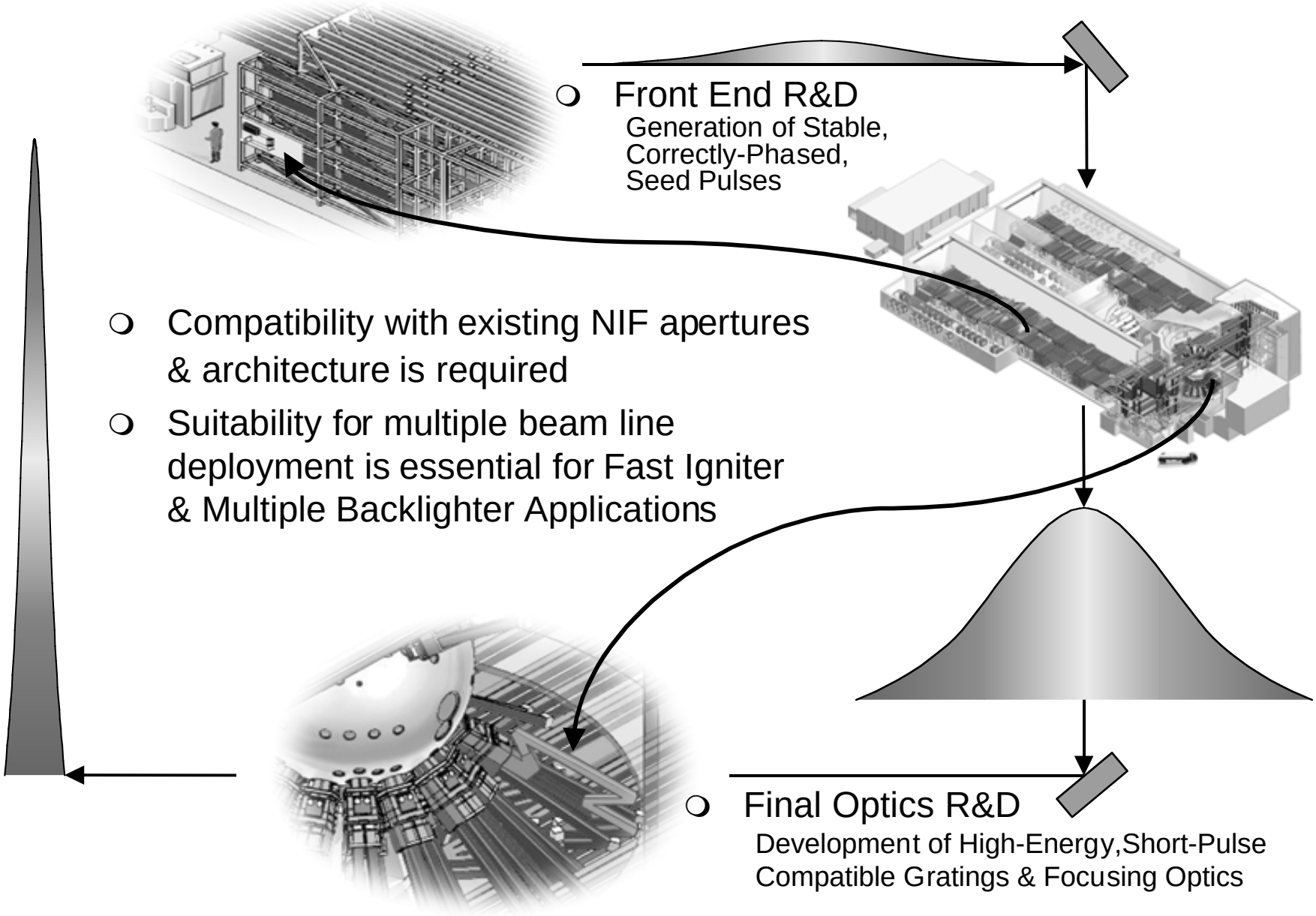

Required R&D for HEPW Production

The National Ignition Facility

Device or Task	Risk	Comments
Stable, seed laser	L	Commercial options available at 100-fs pulse duration
Timing synchronization	L	Issue has been addressed at the ps level in laser-electron interaction experiments at accelerator facilities
Multi-nanosecond pulse stretcher	L	Designs exist, telecom components may allow reduction in size and complexity
Broadband preamplifiers	M	OPCPA has been demo'd in research environment. Improvements in stability could be made
Active Phase and amplitude control	M	Important for pedestal control and pre-compensation of gain saturation effects. Commercial devices exist but have not been tested
Bandwidth failsafe	L	Prevents short pulse injection and subsequent damage. Commercial solutions available
Chirp failsafe	M	Prevents accidental production of transform limited compressed pulses and damage to final optics and gratings
Prepulse control	M	Necessary to prevent target preconditioning

Nova-style 1 μm Ti:sapphire Regenerative Amp

Perry & Shore Petawatt Laser Report UCRL 124933, 1996

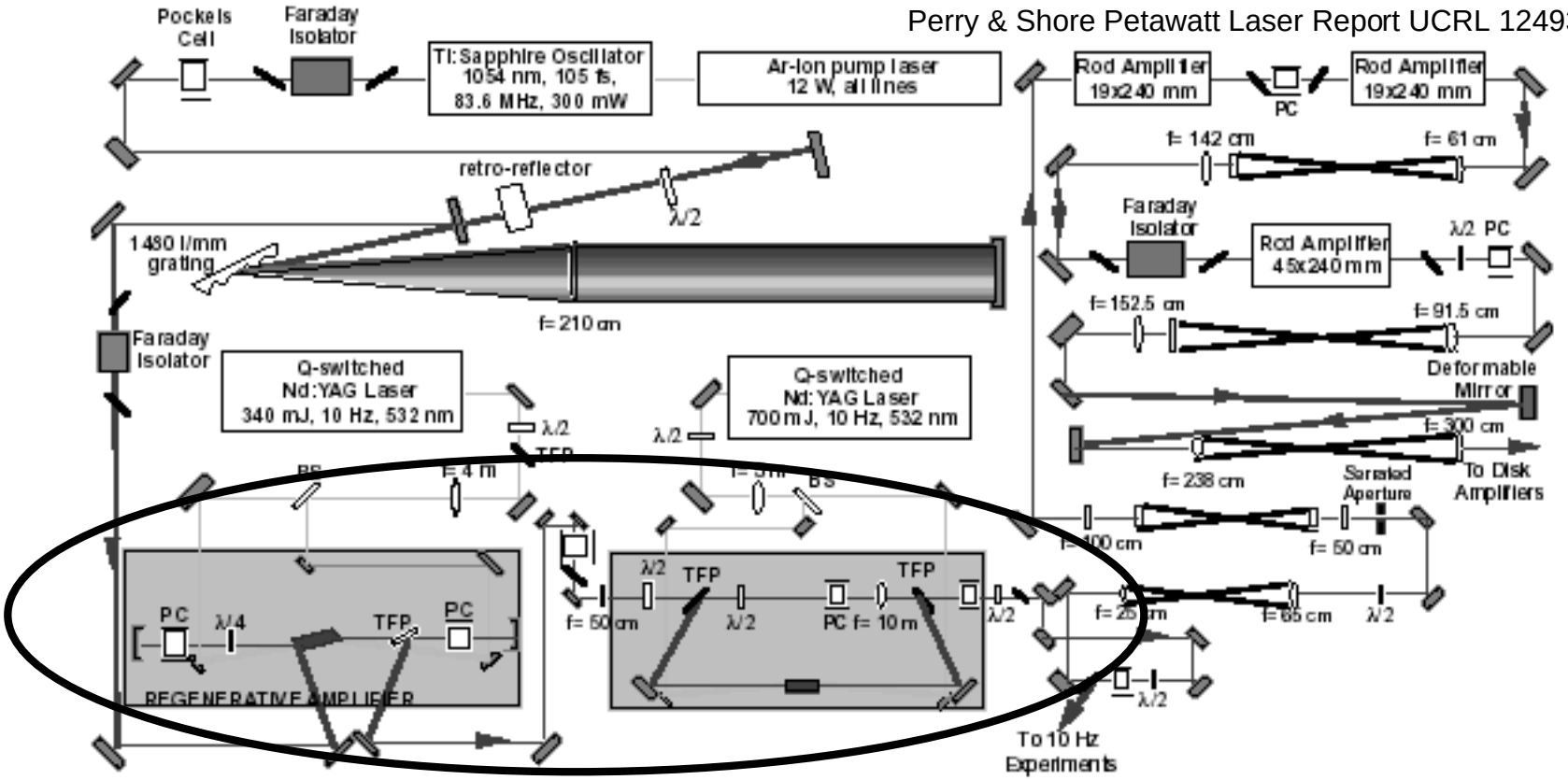

- Regenerative amplifier provides multiple passes of the gain media
- 10-mJ output and 100-fs compatible
- Low gain and oscillation at 800-nm a problem require special design
- Leakage pulses are amplified and can effect experiments

Prepulses from Regens

Intracavity pulse build up

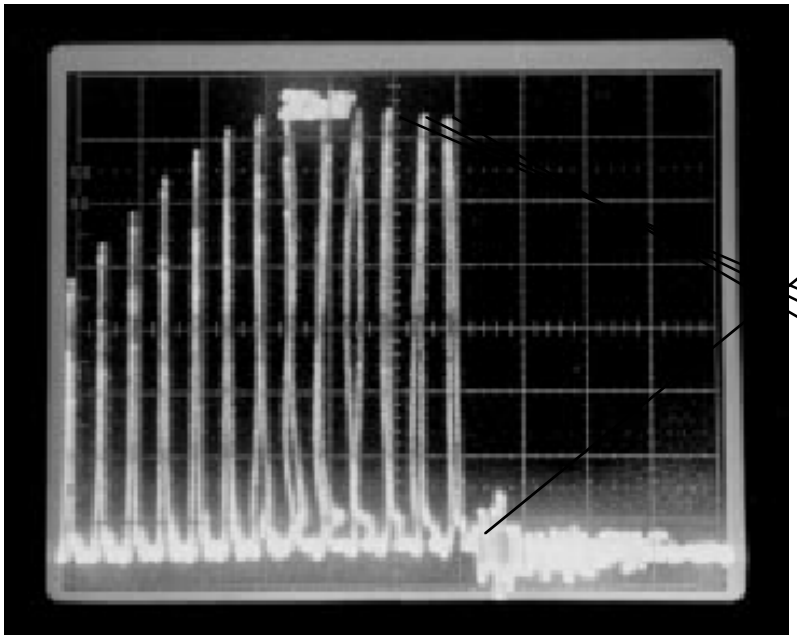

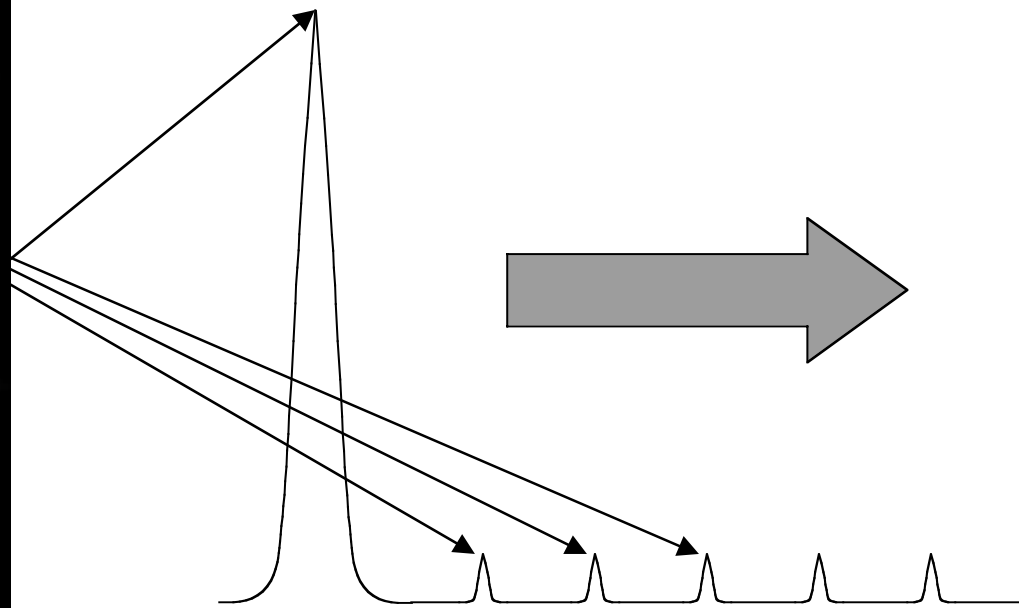

- Some leakage of the buildup pulses occurs in the regen before the main pulse is ejected
- At 10^{21} W/cm^2 peak intensity, prepulses must be suppressed ~9 orders of magnitude in order to conduct “clean” experiments

Optical Parametric Preamp

- Replace the pre-amp gain media with an Optical Parametric Amplifier

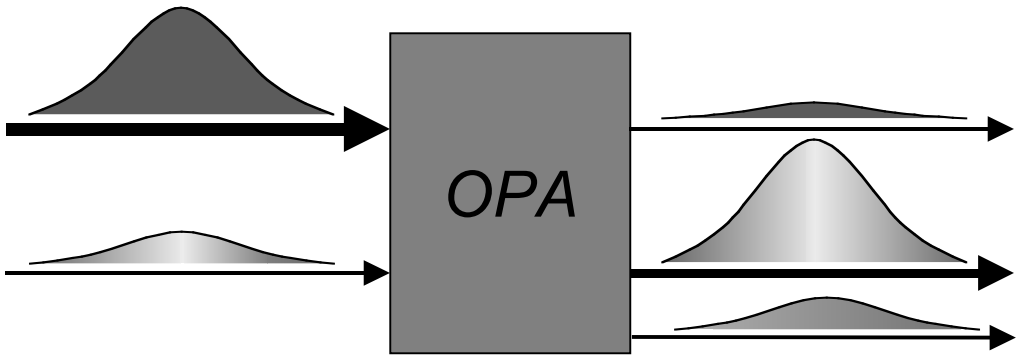

- Very high gain per pass (single or few pass amps)
- Very high amplification bandwidth
- Very Little thermal loading since no heat deposited in the material
- ASE reduced by a order of magnitude
- Prepulses reduced by 6 to 7 orders of magnitude prior to main amp
- Much less material dispersion in the overall amplification chain

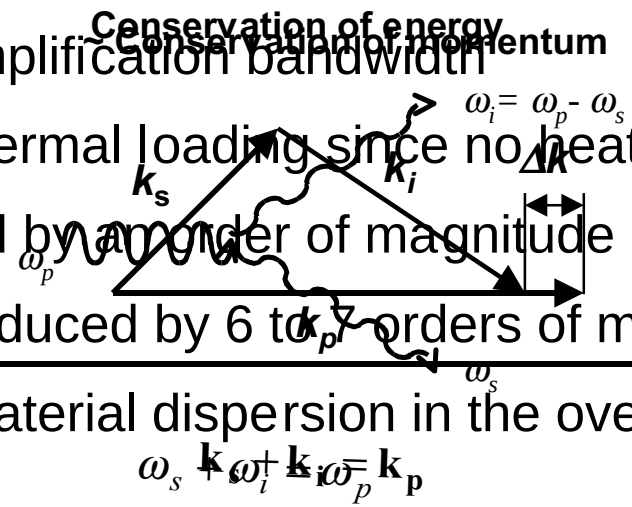

A. Dubietis, G. Jonasauskas, and A. Piskarskas, Opt. Commun. **88**, 437 (1992)

I. N. Ross, P. Matousek, M. Towrie, A. J. Langley, and J. L. Collier, Opt. Commun. **144**, 125 (1997)

LLNL 1 micron OPCPA demonstration

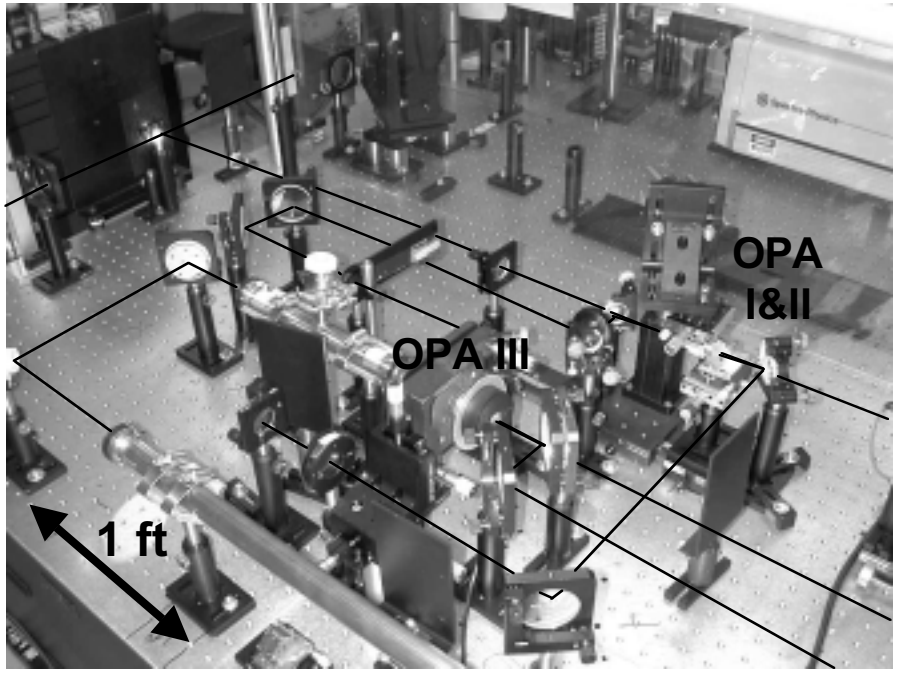

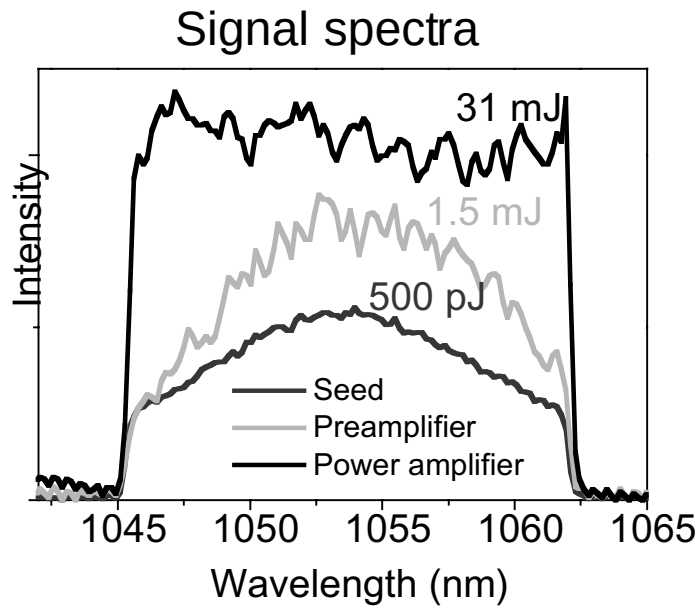

- Compact and no electro-optic components required
- Gain “broadening” occurs for proper conditions
- Instantaneous gain produces ~10^7 prepulse contrast
- Good beam quality and pulse stability (±5%)
- 6% efficiency with commercial pump lasers

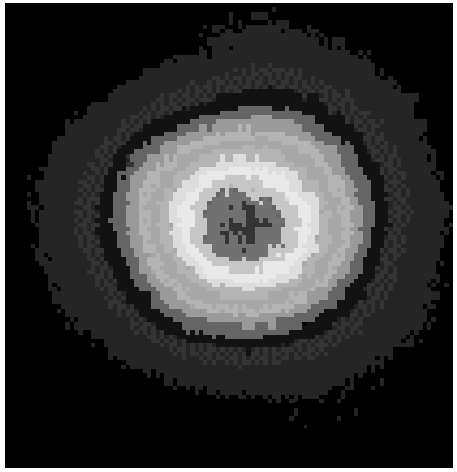

Osaka PW uses OPCPA as front end

The National Ignition Facility

System layout

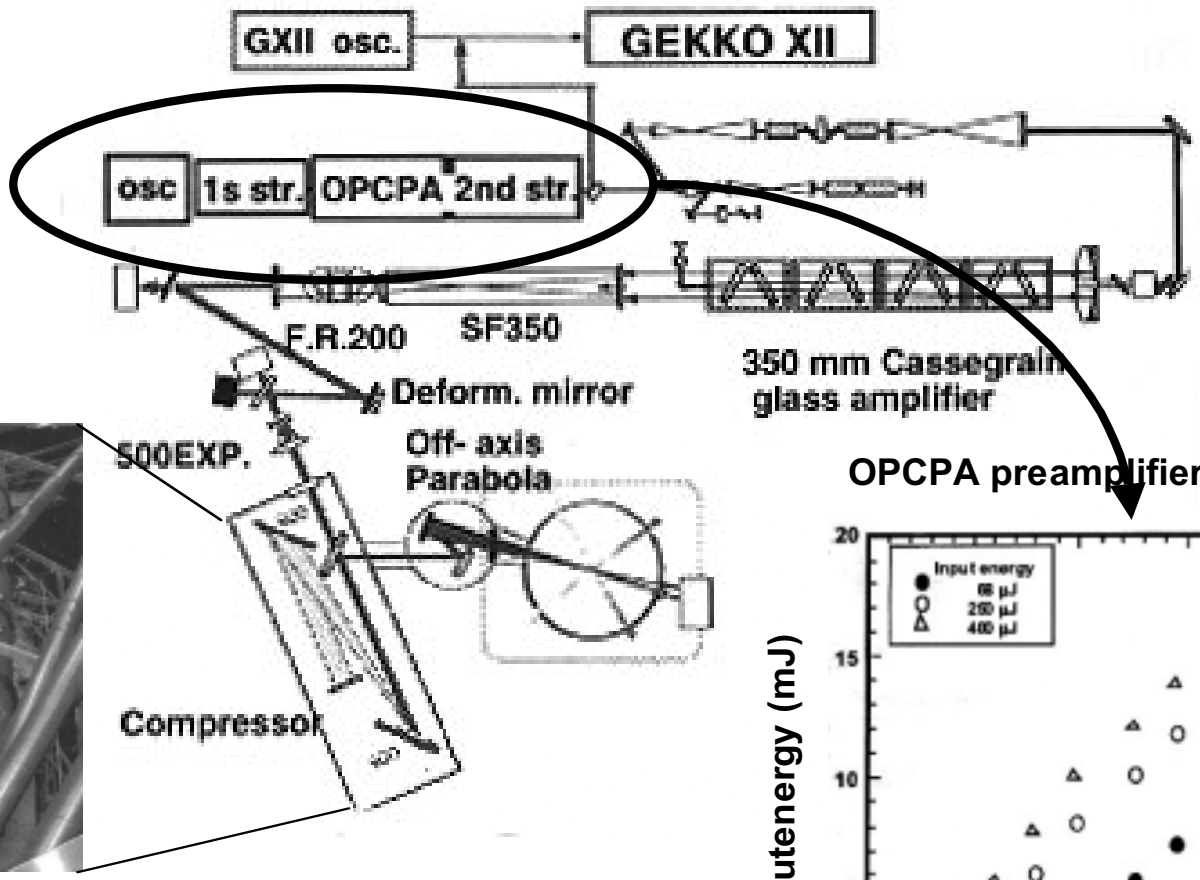

Compressor chamber

OPCPA preamplifier results

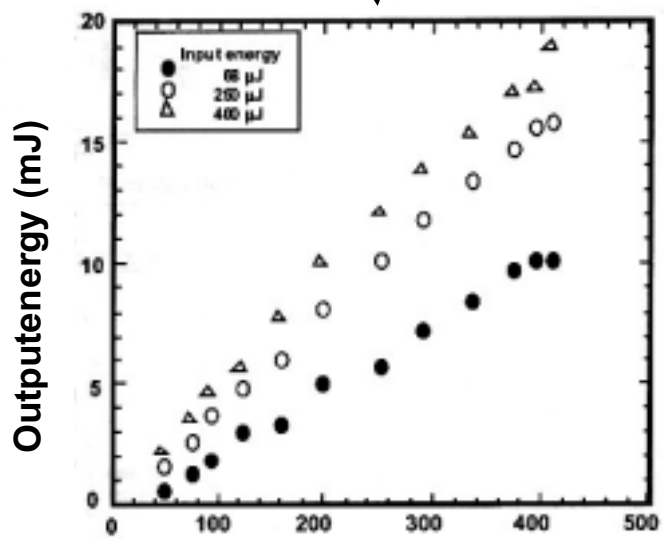

Required R&D for HEPW Production

The National Ignition Facility

Device or Task	Risk	Comments
Damage resistant gratings	**H**	**Need high dispersion, high efficiency and 1 order higher threshold than gold**
Scaling of grating aperture	**H**	**Techniques need to be developed for production of gratings or arrays of gratings with multi-meter dimensions**
Damage resistant coatings	**H**	**Focusing and turning optics after the compressor see high intensity**
Compact compressors	**M**	**To minimize cost and/or fit within existing facilities**
Adaptive beam control	**M**	**Intensity goes as square of beam quality**
Focusing optics	**M**	**Different optics are needed for integrated experiments**
Debris control	**M**	**Existing shields are too thick**
Back reflection mitigation	**M**	**Additional consideration of amplifier protection needed. Compressor acts as a good spectral filter**

CPA Doesn't Eliminate Final Optic Damage

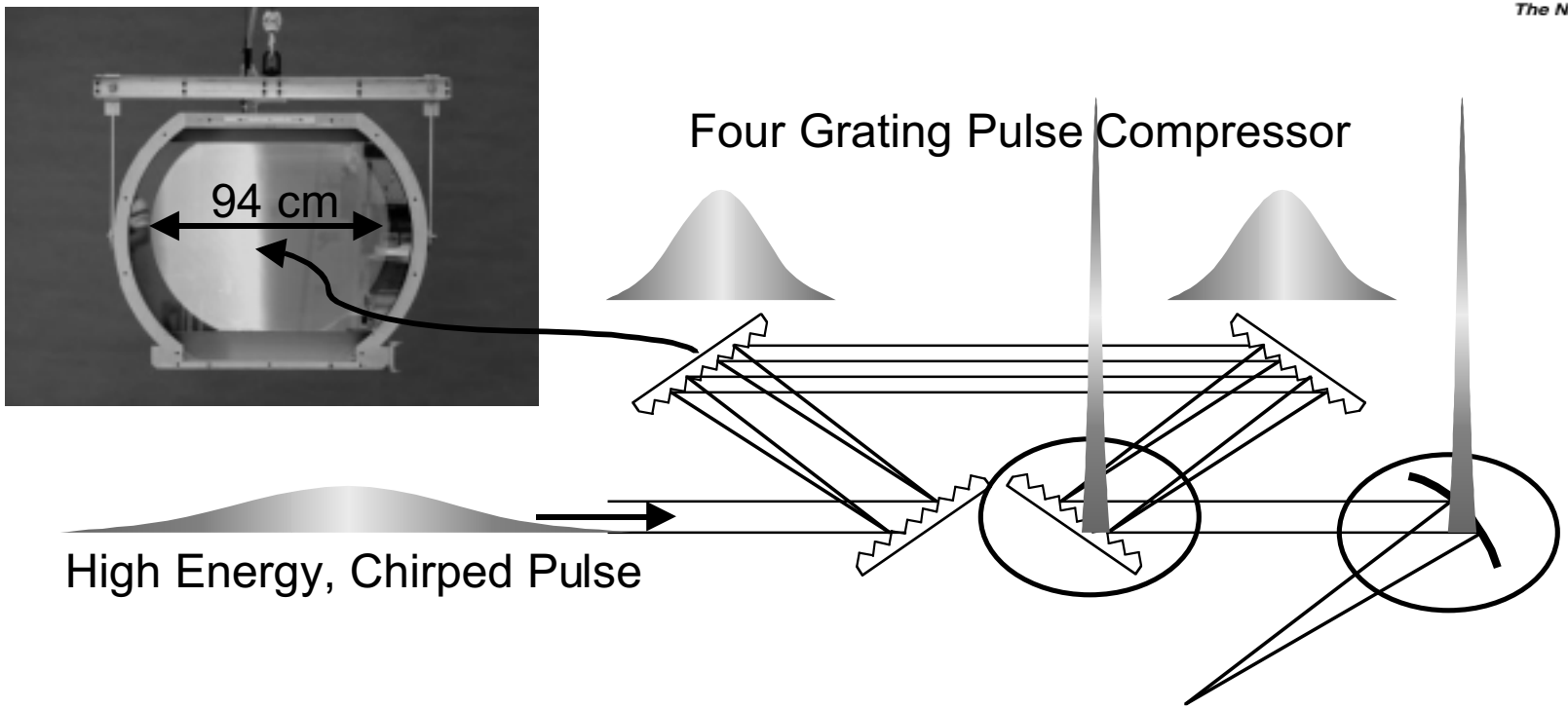

- Pulse is SHORT and energy is HIGH on the Final Grating and Focusing Optic
- Intensity dependent damage of "Final Optics" is THE BIG problem
- Nova PW solution was to scale metal coated gratings to large aperture
- Multi-kJ PW pulses would require "garage door" size gold optics, fabrication technology and vacuum enclosures!

Dielectric Final Optics for ps HEPW pulses

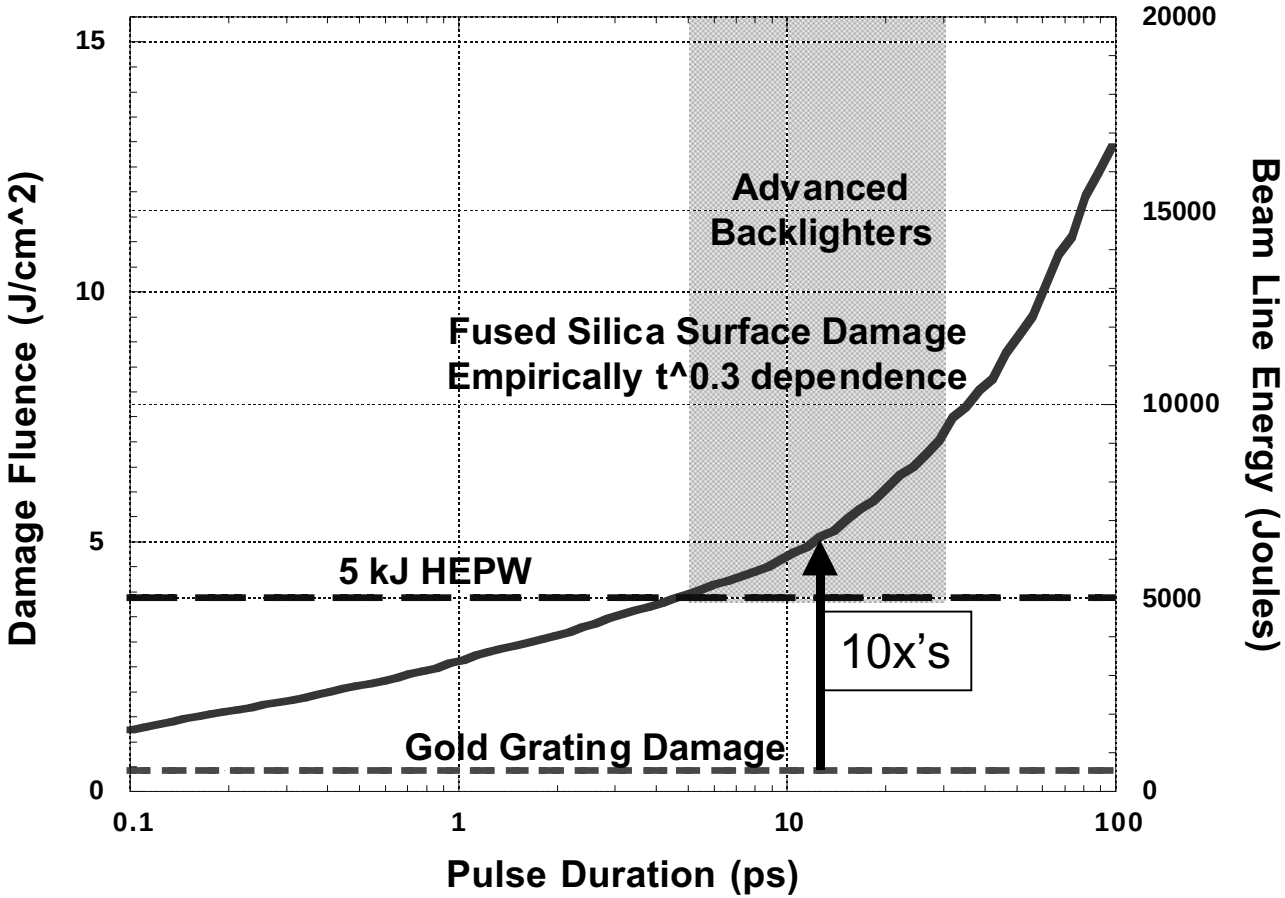

- Move away from gold coated optics
- For fixed aperture, higher energy is obtained at increased pulse duration

High energy short pulse grating design

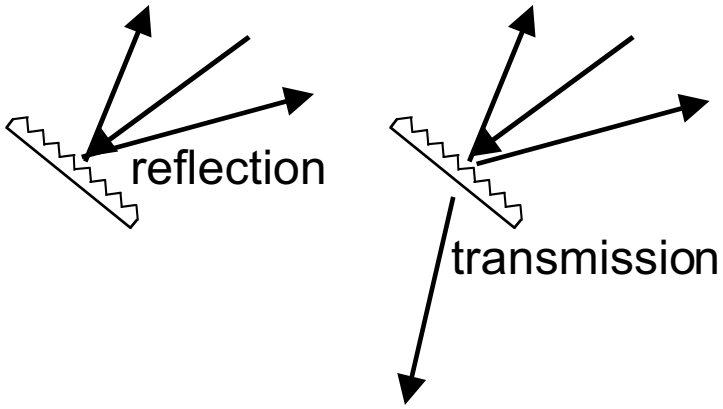

- Possible dielectric grating configurations
  - Reflection has less loss & better wave front
- Possible grating construction
  - Multi-layer dielectric (MLD)
  - Polymer surface relief
  - Volume holographic
  - Disposable materials
- MLD gratings
  - High efficiency
  - Can be constructed from high damage materials
  - Technology is scalable in area
  - Low wavefront distortions
- Optimization and/or testing of high damage gratings is being pursued by several organizations
  - LLNL, LLE, LULI (France), GA, Jobin Yvon (France) etc.

Dielectric Final Optics for ps HEPW pulses

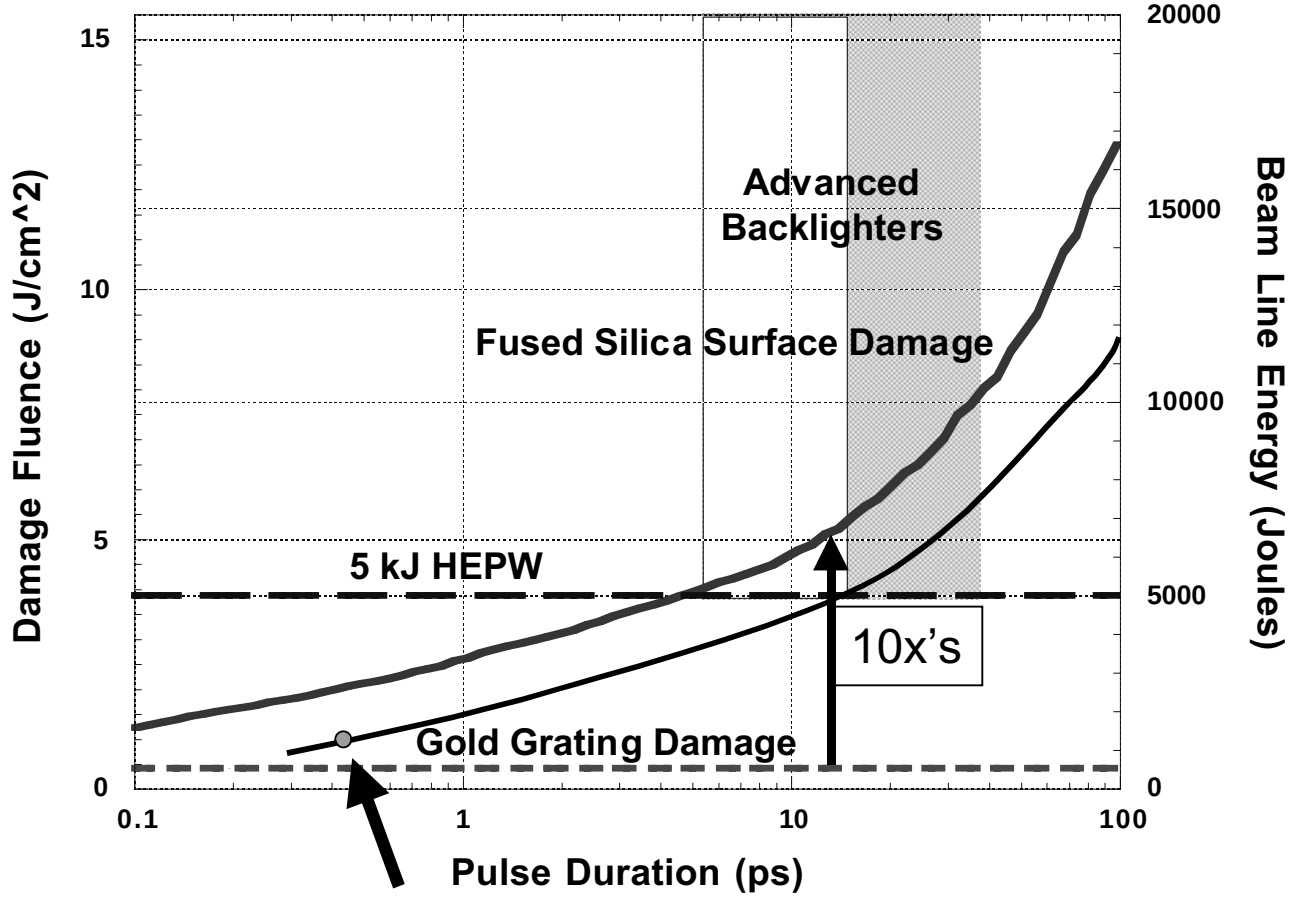

- LULI damage testing in 2000: MLD grating from Jobin Yvon had twice the capacity of gold optics at 0.5 ps duration
- Reduction from ideal dielectric due to "structure" effects
- Structure effects can be controlled with proper groove design

Multilayer Dielectric Gratings

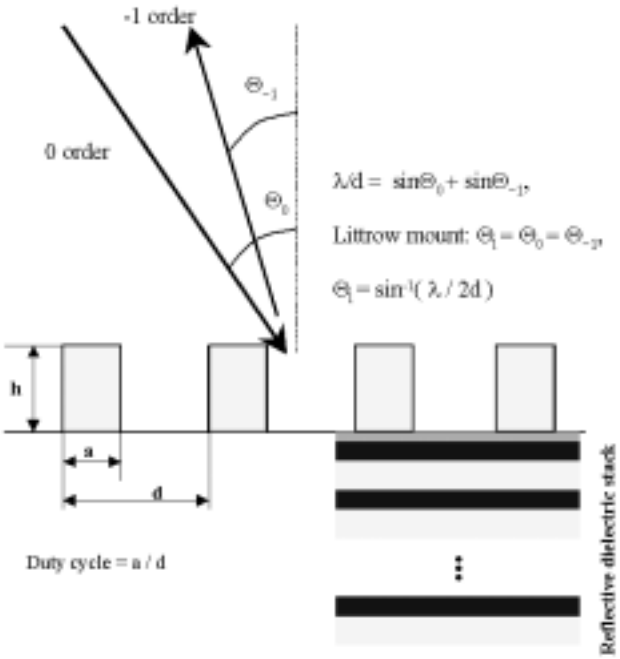

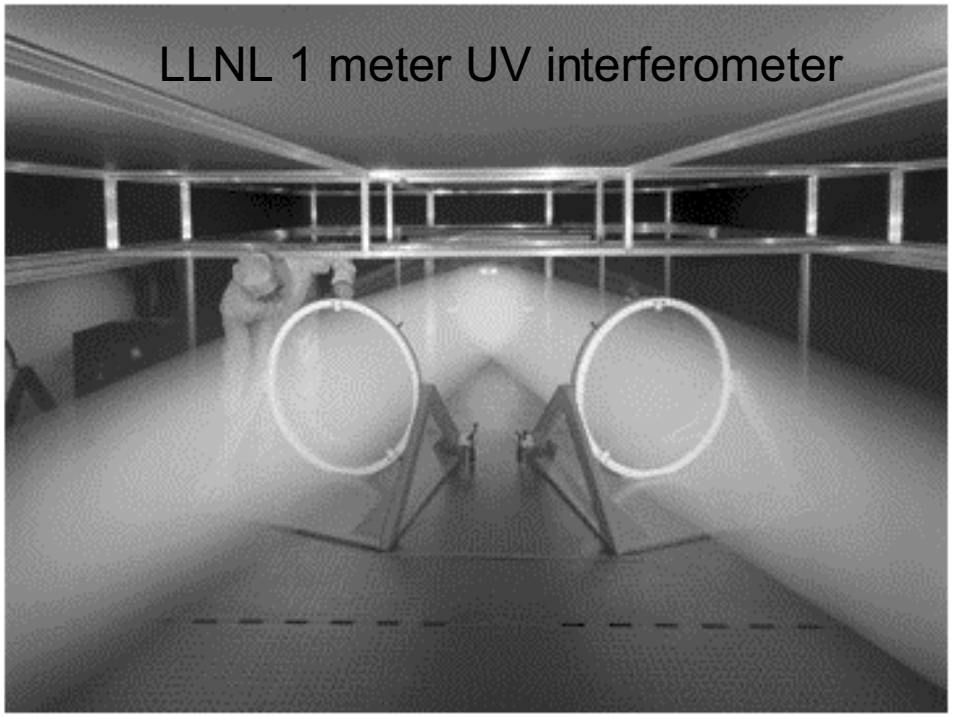

- Grating is etched into top layer of multilayer dielectric stack
- Stack provides enhanced reflectivity at wavelength and angle of operation
- Top layer grating structure is produced with lithographic technology

Multilayer Dielectric Gratings

The National Ignition Facility

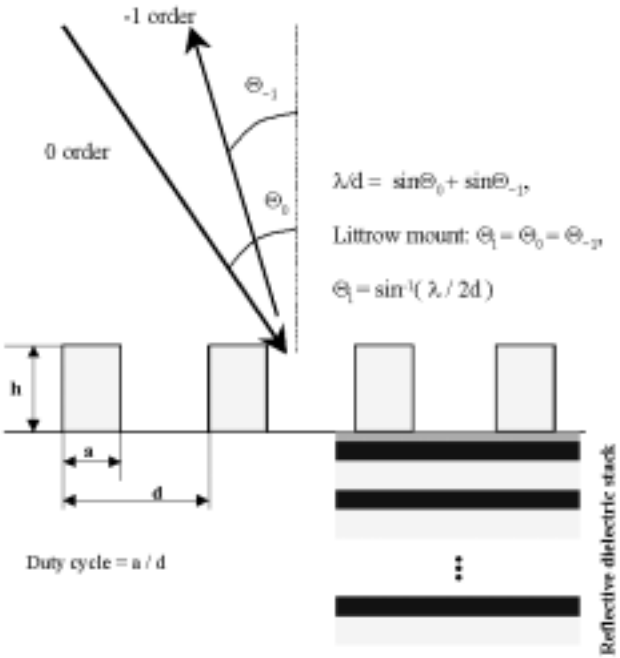

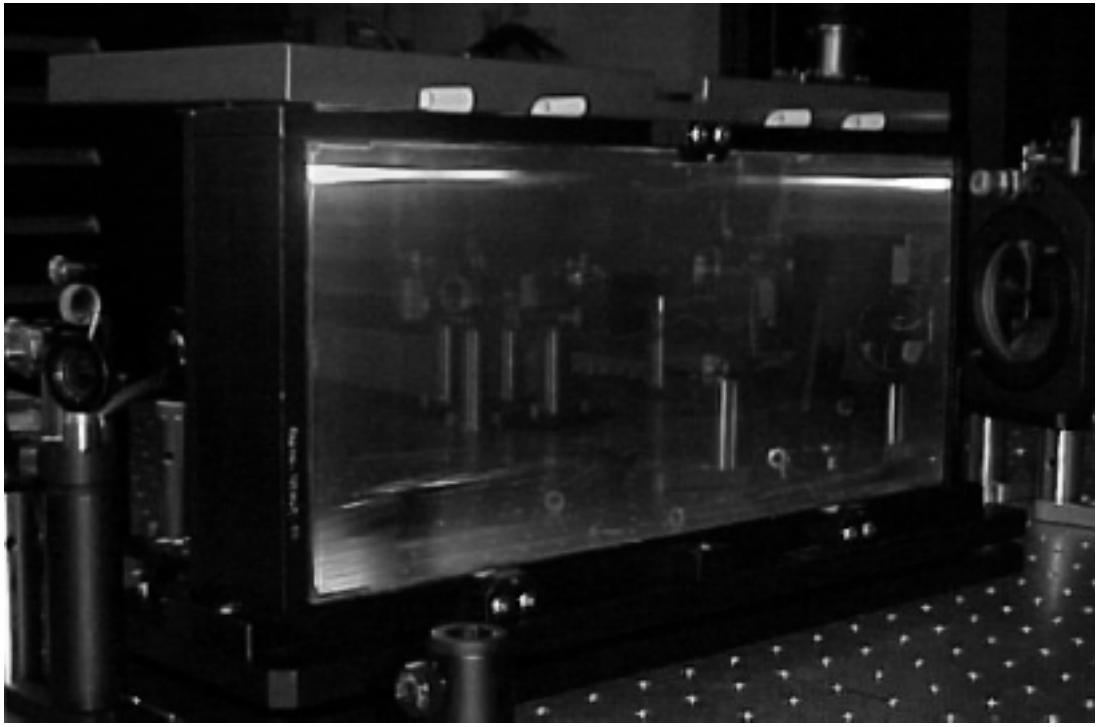

- Grating is etched into top layer of multilayer dielectric stack
- Stack provides enhanced reflectivity at wavelength and angle of operation
- Top layer grating structure is produced with lithographic technology
- Width and height of grooves determines diffraction efficiency

Multilayer Dielectric Gratings

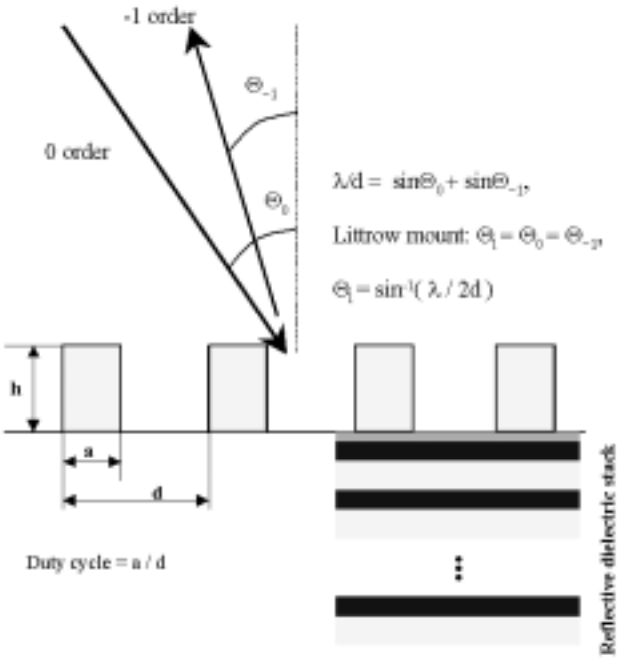

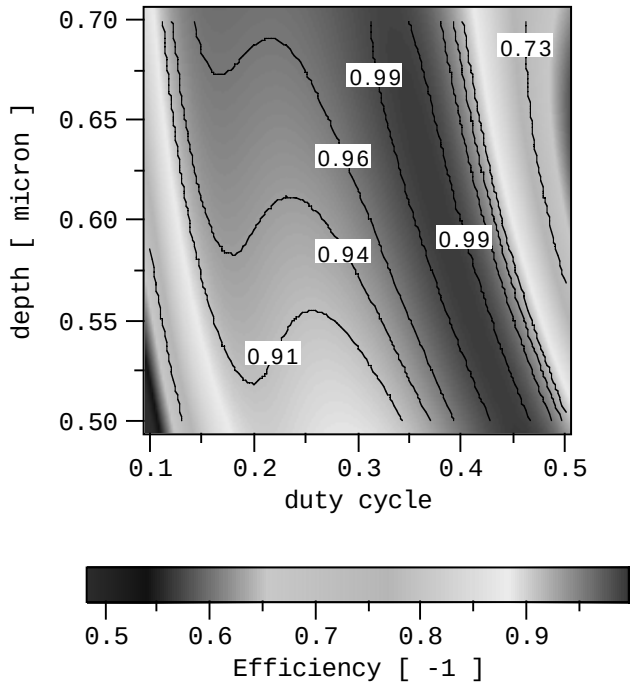

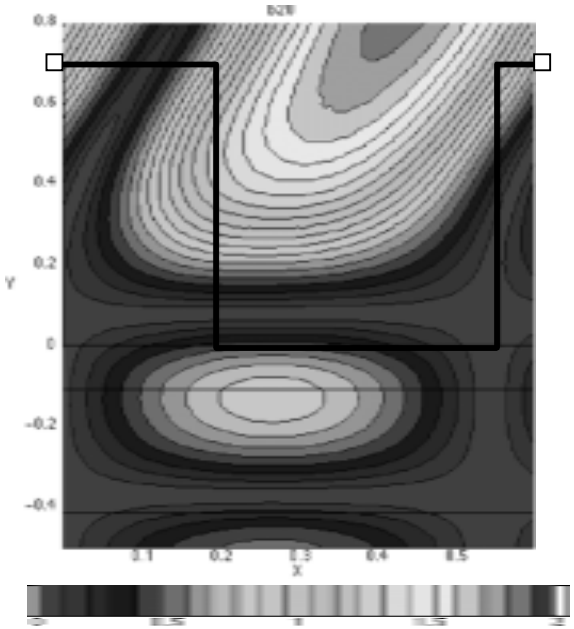

Field strength

- Grating is etched into top layer of multilayer dielectric stack
- Stack provides enhanced reflectivity at wavelength and angle of operation
- Top layer grating structure is produced with lithographic technology
- Width and height of grooves determines diffraction efficiency
- Field structure in the grooves will dictate damage (intensity dependent)

1780 gr/mm final grating design

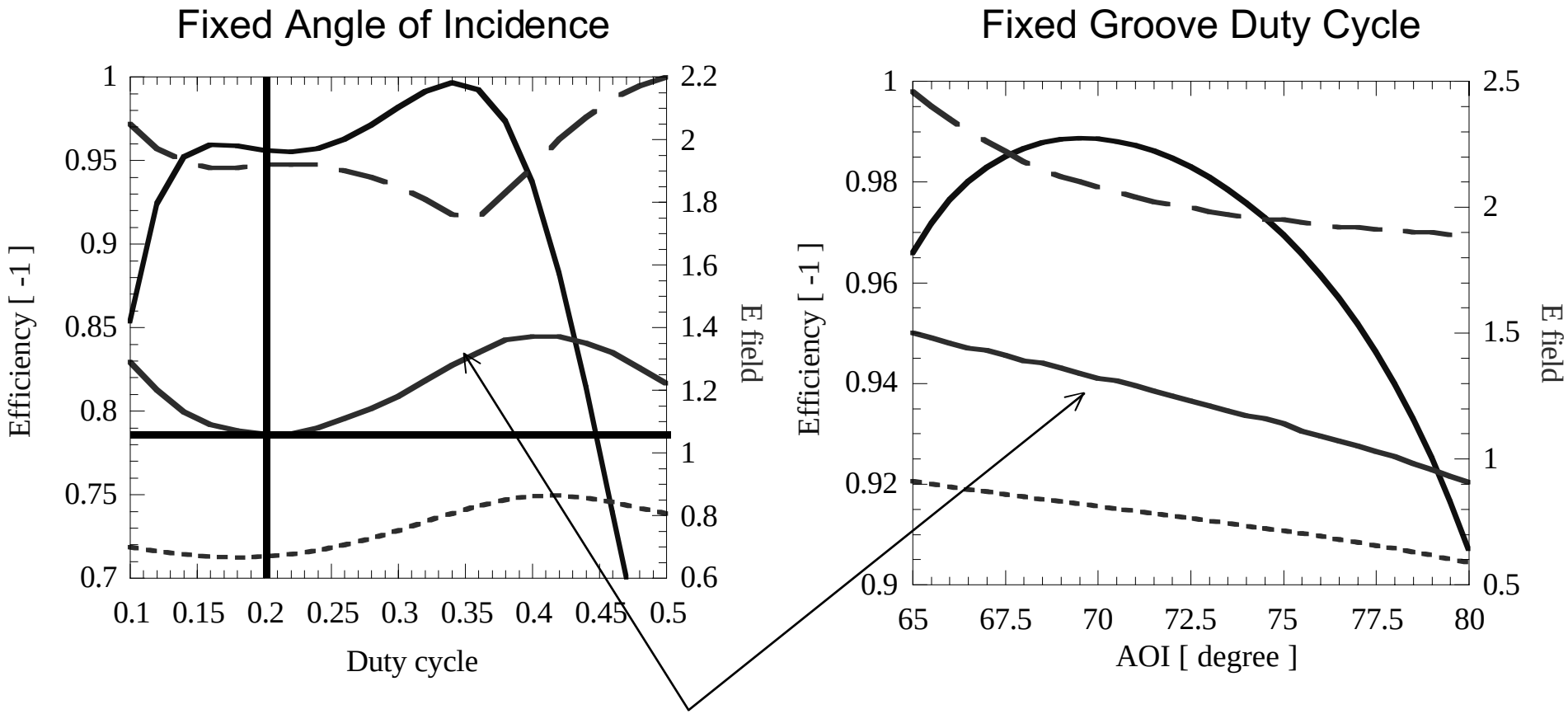

Max E-field at the edge of the grooves

- For duty cycle of 0.2, field enhancement in the grooves is 1.1
- Note strong dependence on angle of incidence

Intra-groove field enhancement drives damage

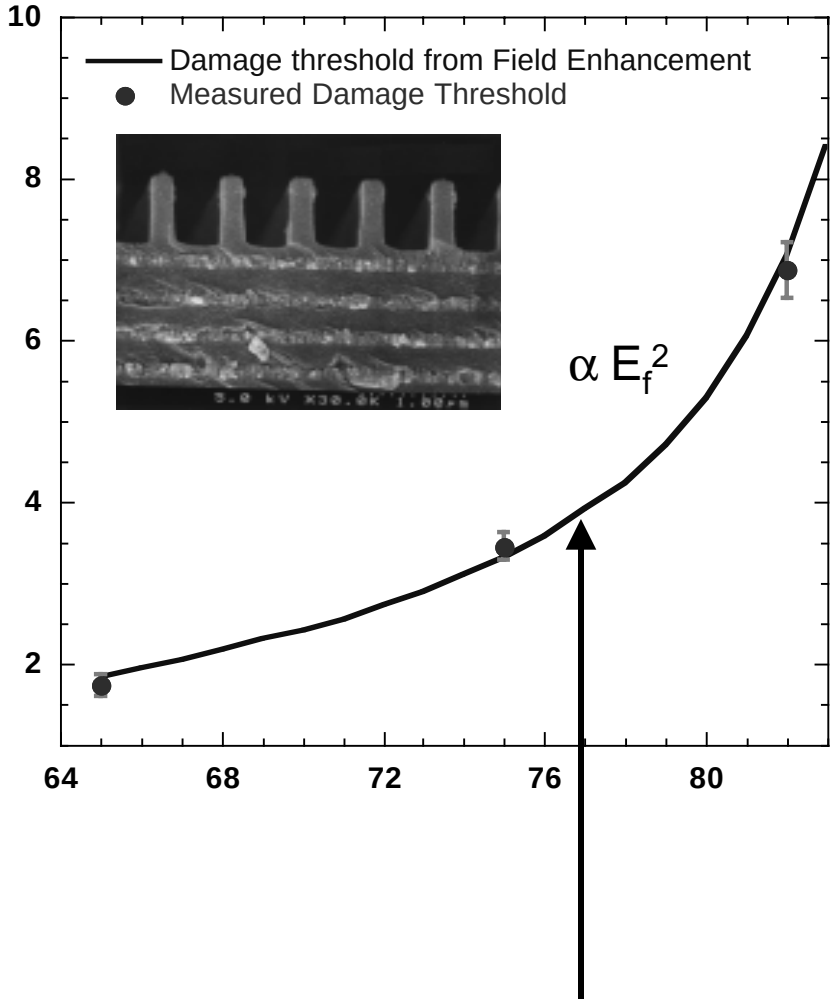

Field structure in the grooves is a strong function of angle of incidence

Preliminary damage tests at LLNL confirm a square dependence on E-field on the groove surface

35 cm aperture and 77 degree incidence will require a 2 meter grating surface and presents new technical challenges

Compressor grating scalability

The National Ignition Facility

- Two approaches: Monolithic and Segmented

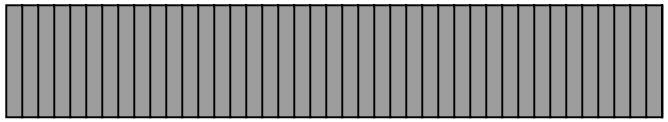

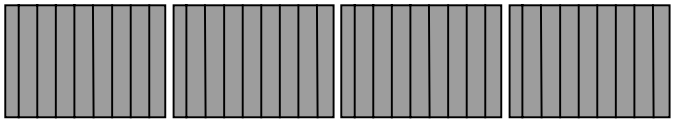

- Issues for multi-meter monolithic grating production
  - Substrate thickness
  - Substrate weight
  - Coating of large substrates
  - Exposure of large substrates
  - Etching of large substrates
- Issues for segmented grating structures
  - Development of high resolution and stability adjustable mounts
  - Development of precision alignment schemes
  - Control of damage at grating interfaces

2 meter class MLD etching device

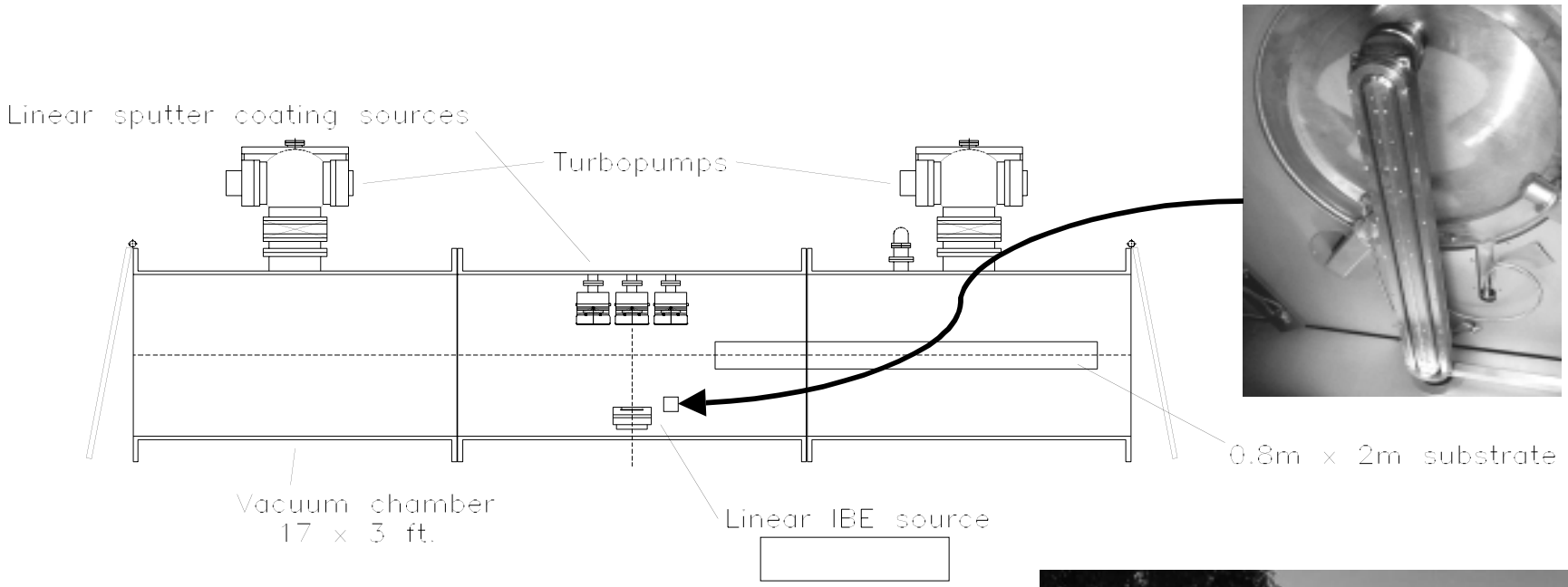

- Linear Ion sources can be adapted to provide 2 meter-scale etching capability

Tolerances for a segmented grating mosaic

The National Ignition Facility

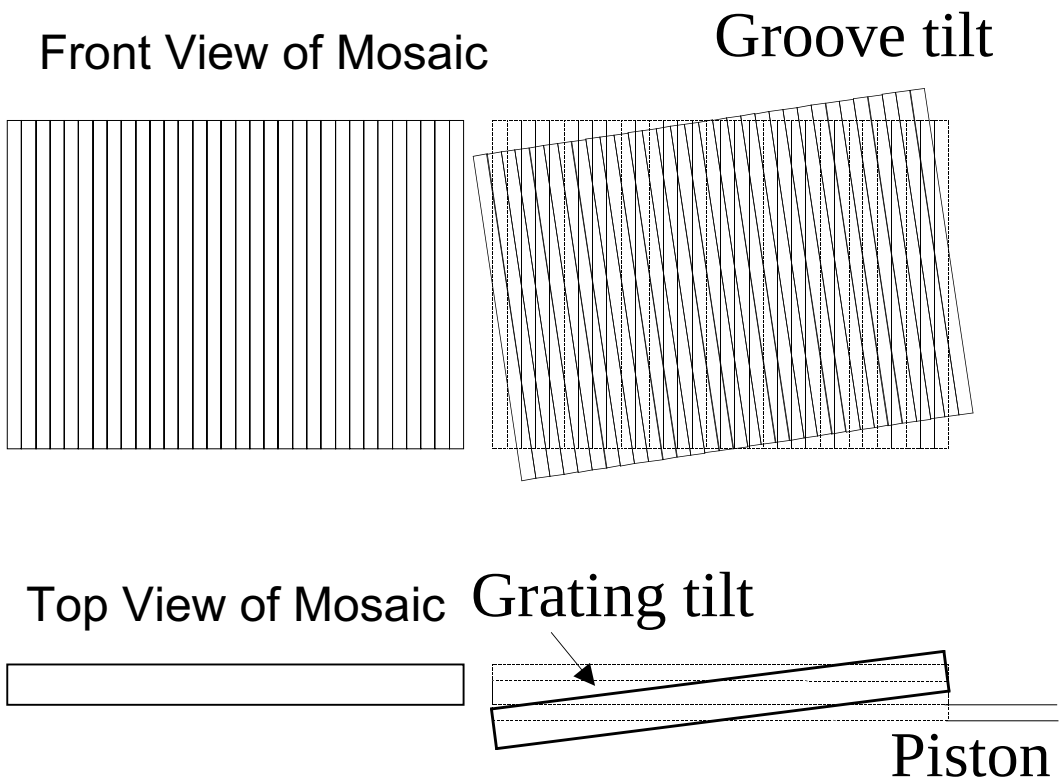

Three effects will induce aberrations on the laser beam

Tolerances on grating and groove tilt

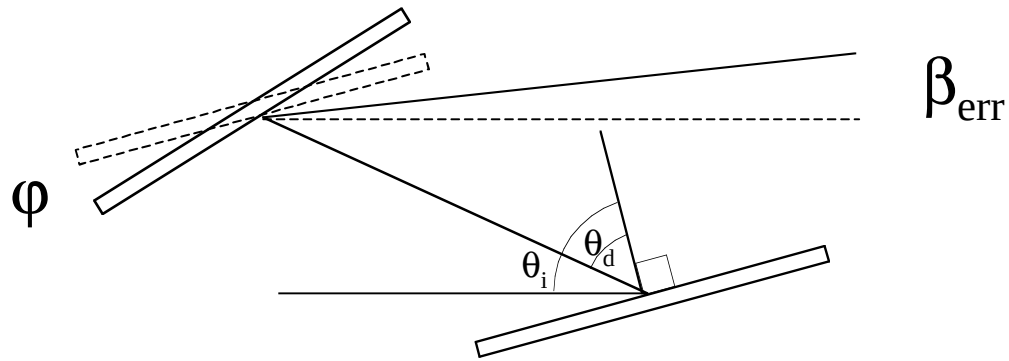

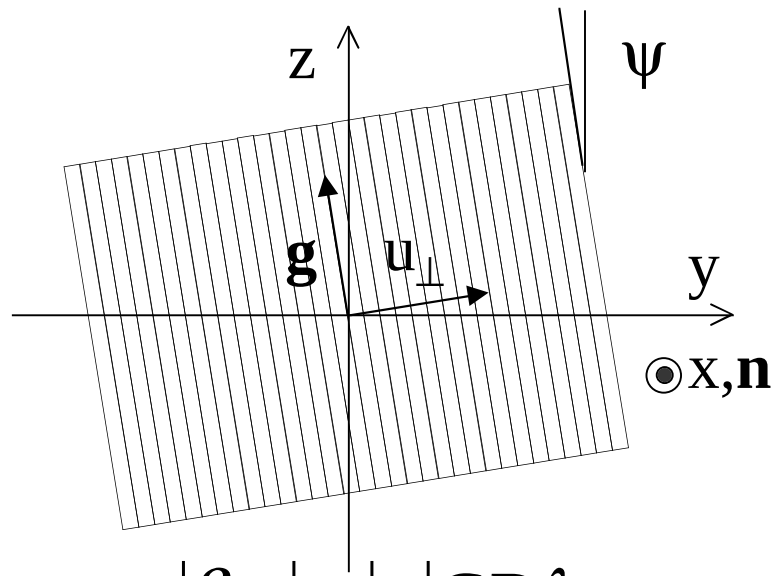

$$|\beta_{err}| = |\varphi| \frac{\cos\theta_d}{\cos\theta_i}$$

$$\boxed{\varphi_{\max} = 2.0x10^{-6} rad}$$

With θ_i=76.7° and θ_d=64.3°

$$|\beta_{err}| = |\psi| GD\lambda$$

$$\boxed{\psi_{\max} = 2.0x10^{-6} rad}$$

With GD =1.780 μm^{-1} (groove density)

Estimated deviations required to produce spots separated at the focus by half the focal spot area

Tolerances for a segmented grating mosaic

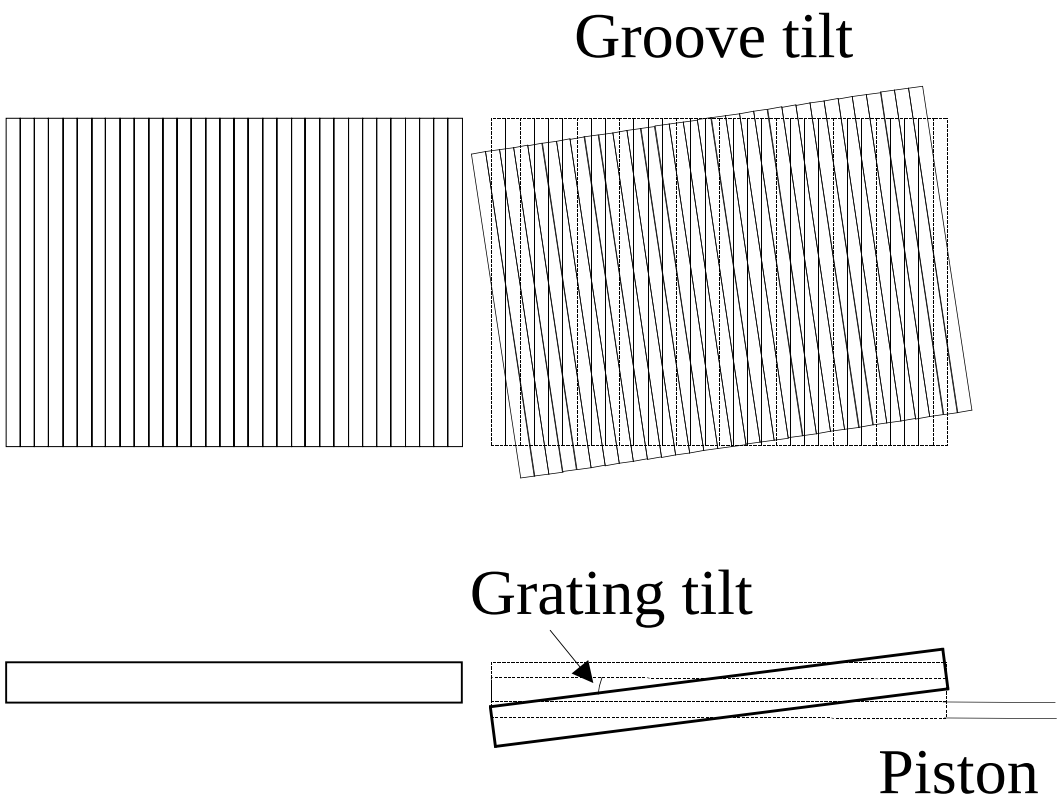

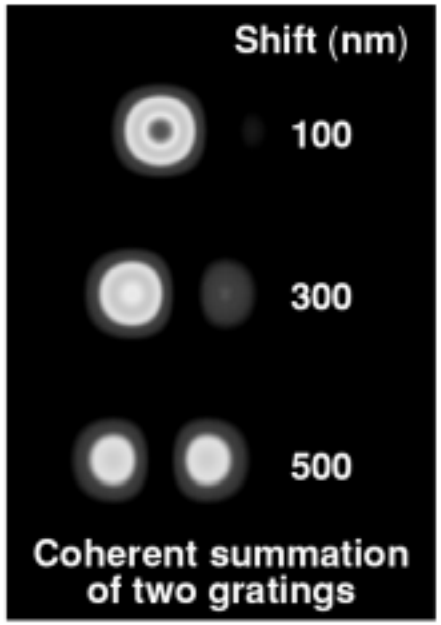

For 40 cm sub-gratings, alignment requirements are of order 0.2 micron for grating and groove tilt and of order 0.1 micron for piston

New Compressor Designs Also Needed

- HEPW pulse stretching will require > twice dispersion of Nova PW class lasers
  - Nova PW compressor grating separation at this stretched pulse duration would be 20 meters

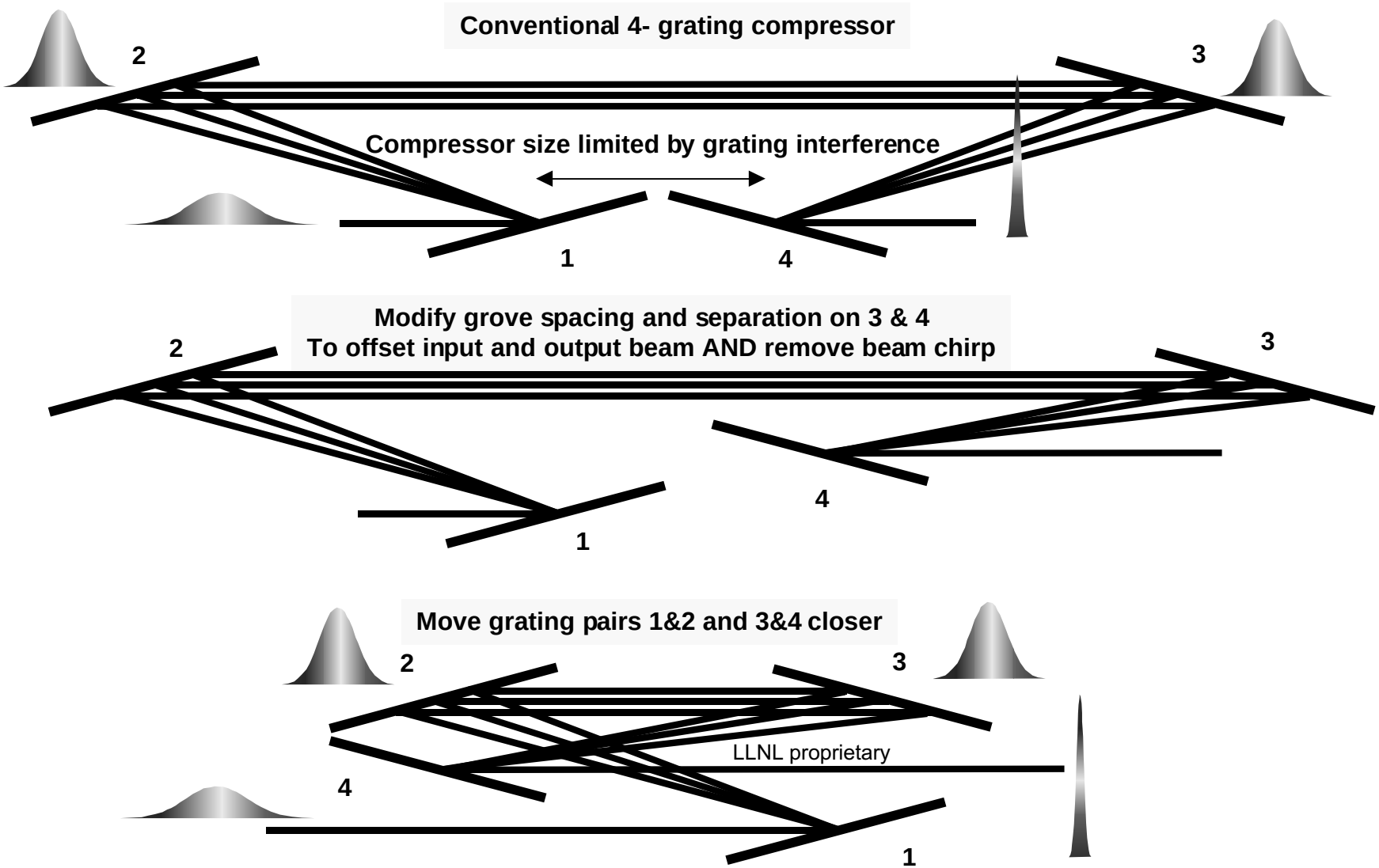

LLNL proprietary

Typical Path for 4 of NIF's 192 Beams

The National Ignition Facility

Indirect Drive Focusing

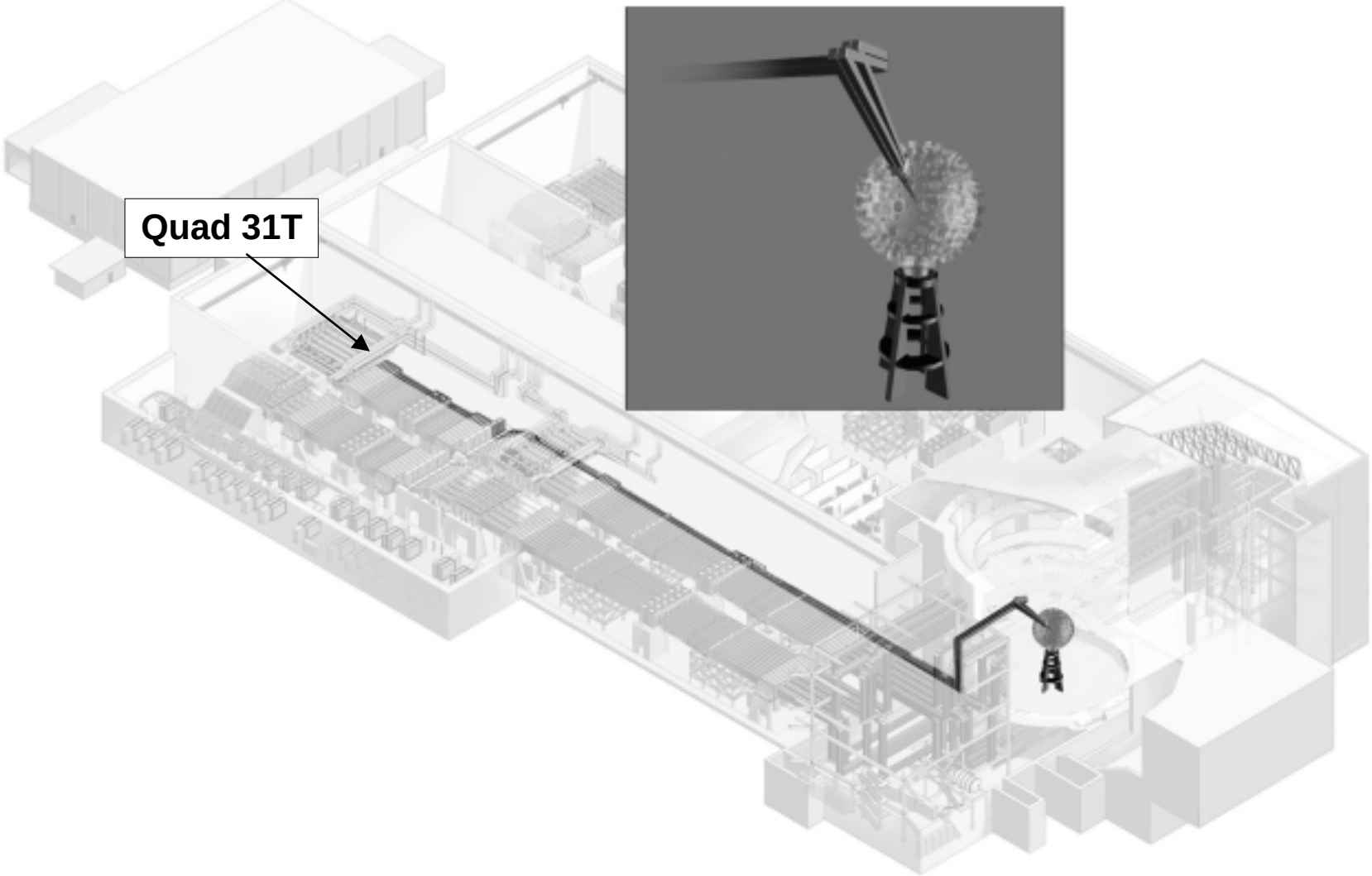

HEPW deployment could use DD equatorial ports

The National Ignition Facility

Indirect drive configuration

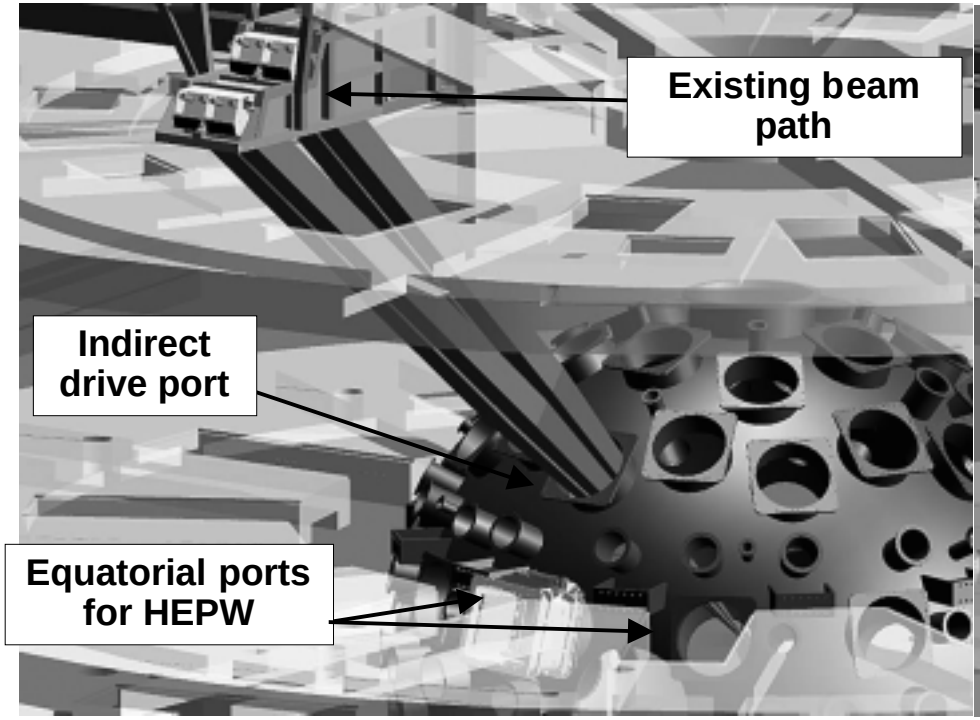

HEPW Configuration

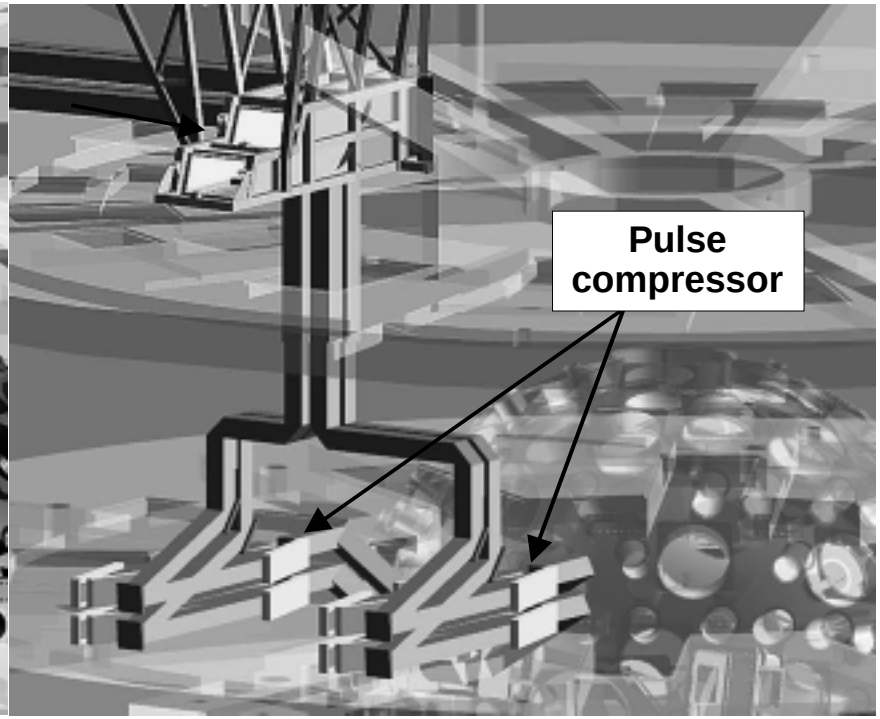

For HEPW up to 4 beams could be redirected to two dual beam, compact compressors and sent to one equatorial port

Desired HEPW Deployment Schedule on NIF

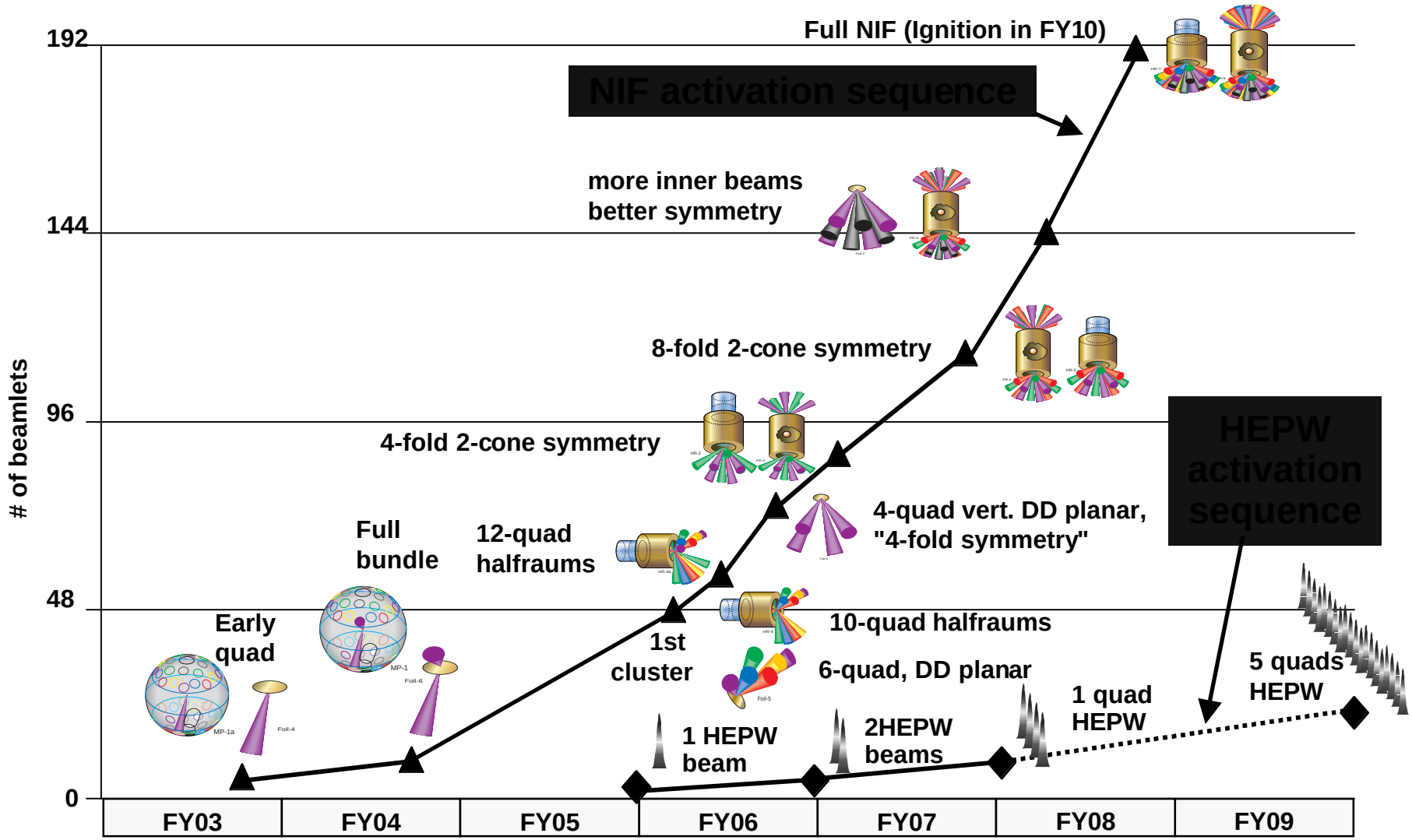

Concept for 100-kJ FI deployment

The National Ignition Facility

Max cone angle:
± 12.5 deg vertically
± 15 deg horizontally

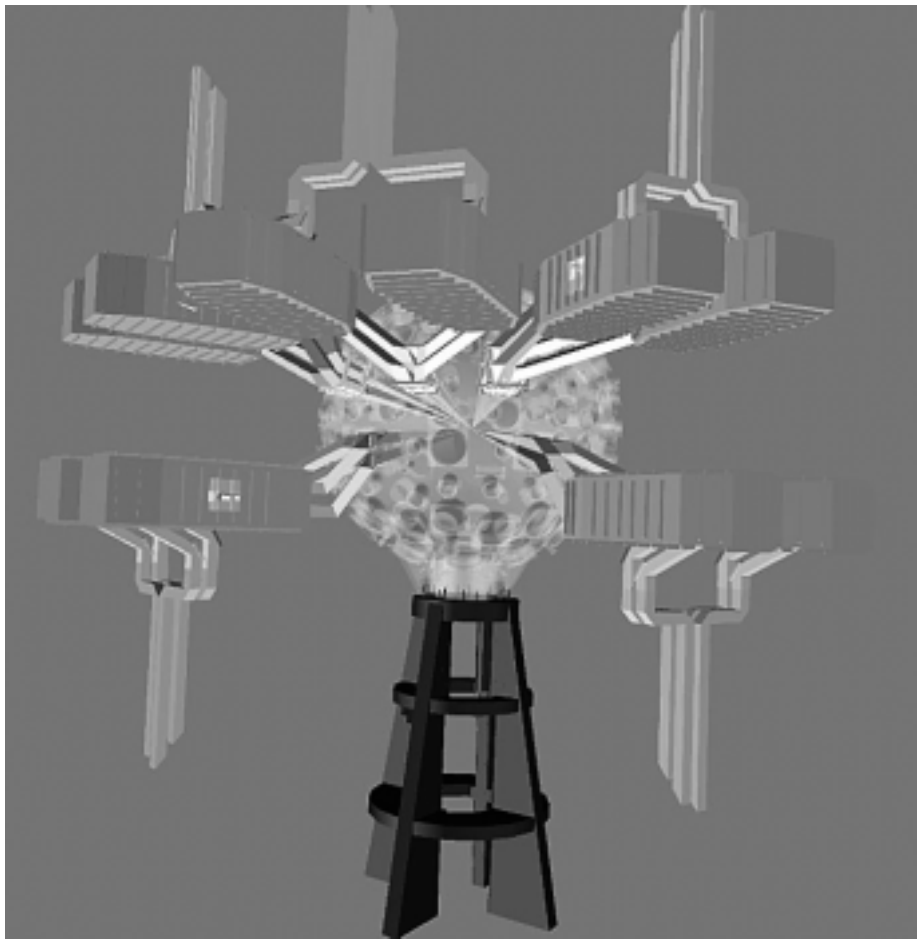

Summary

The National Ignition Facility

- 0.5 kJ Nova PW technology is deployable on existing Nd:glass lasers
  - Systems integration endeavor
- There is strong HEDP mission leverage at higher energy
  - Hard x-ray backlighting, fast ignition, etc. require multi-kJ's to 100 kJ
- HEPW lasers are fundamentally limited by final optic damage
  - Aperture scaling of past technology not practical
- Dielectric final optics and longer pulse duration should allow needed multi-kJ pulse production

Evidence of sub-picosecond electron bunches in solid matter irradiated by ultra-high intensity laser

S.D. Baton, **J.J. Santos, F. Amiranoff, H. Popescu, L. Gremillet, M. Koenig, E. Martinolli**

LULI, CNRS-CEA-Ecole Polytechnique-Paris VI, Palaiseau, France

C. Rousseaux, M. Rabec Le Gloahec

CEA Bruyères-le-Châtel, France

T. Hall

University of Essex, Colchester, UK

D. Batani, E. Perelli, F. Scianitti

Università di Milano and INFM, Italy

T. Cowan

General Atomics, San Diego, CA, USA

This work has been supported by the European contracts TMR ERBFMGE-CT95-0044 and LULI ACCESS HPRI-1999-CT 00052 and by Grant E1127 from Région Ile-de-France

Development of a numerical and experimental program to study *electron transport* and *target heating* in the fast-ignitor context

Important issues :

- Conversion efficiency laser / electrons
- Electron transport and collimation
- Energy deposition and target heating

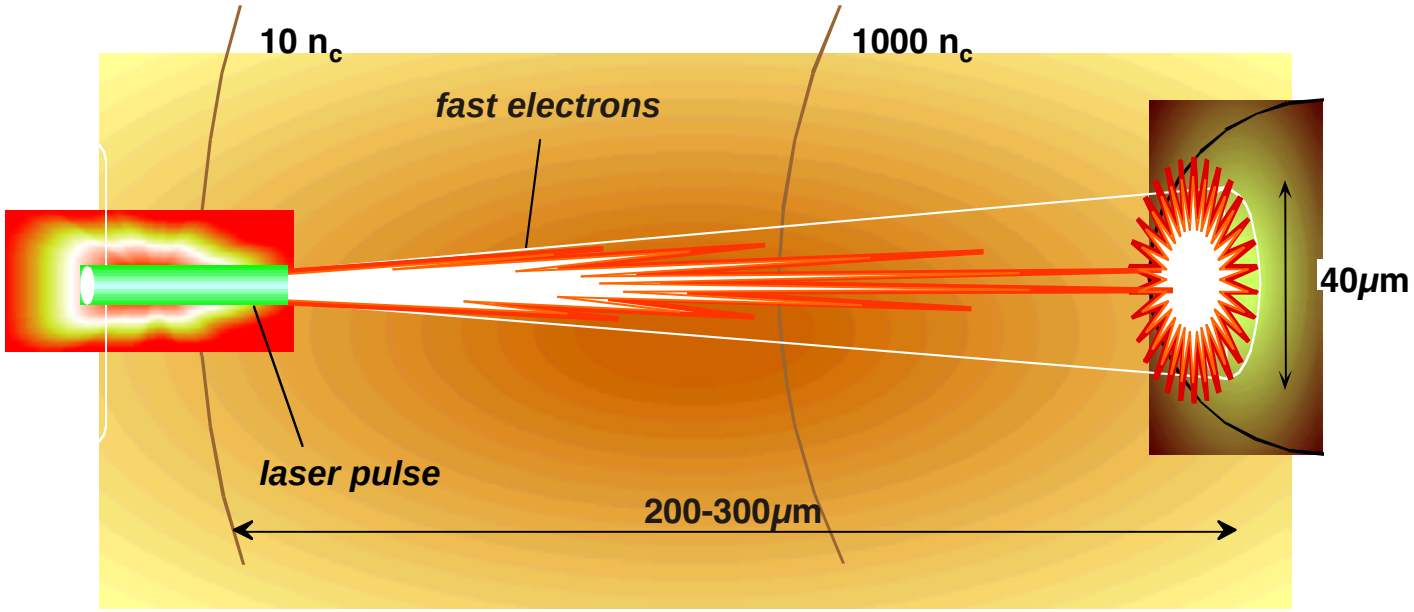

Aspect ratio = 1

Summary

- Two electron populations at rear side
  - coherent electrons in bunches
  - incoherent electrons

- CTR is a good diagnostic of ultrashort electron bunches but only sensitive to high-energy electrons

Rear-side optical visible emission : diagnostic of outgoing electrons at rear-side

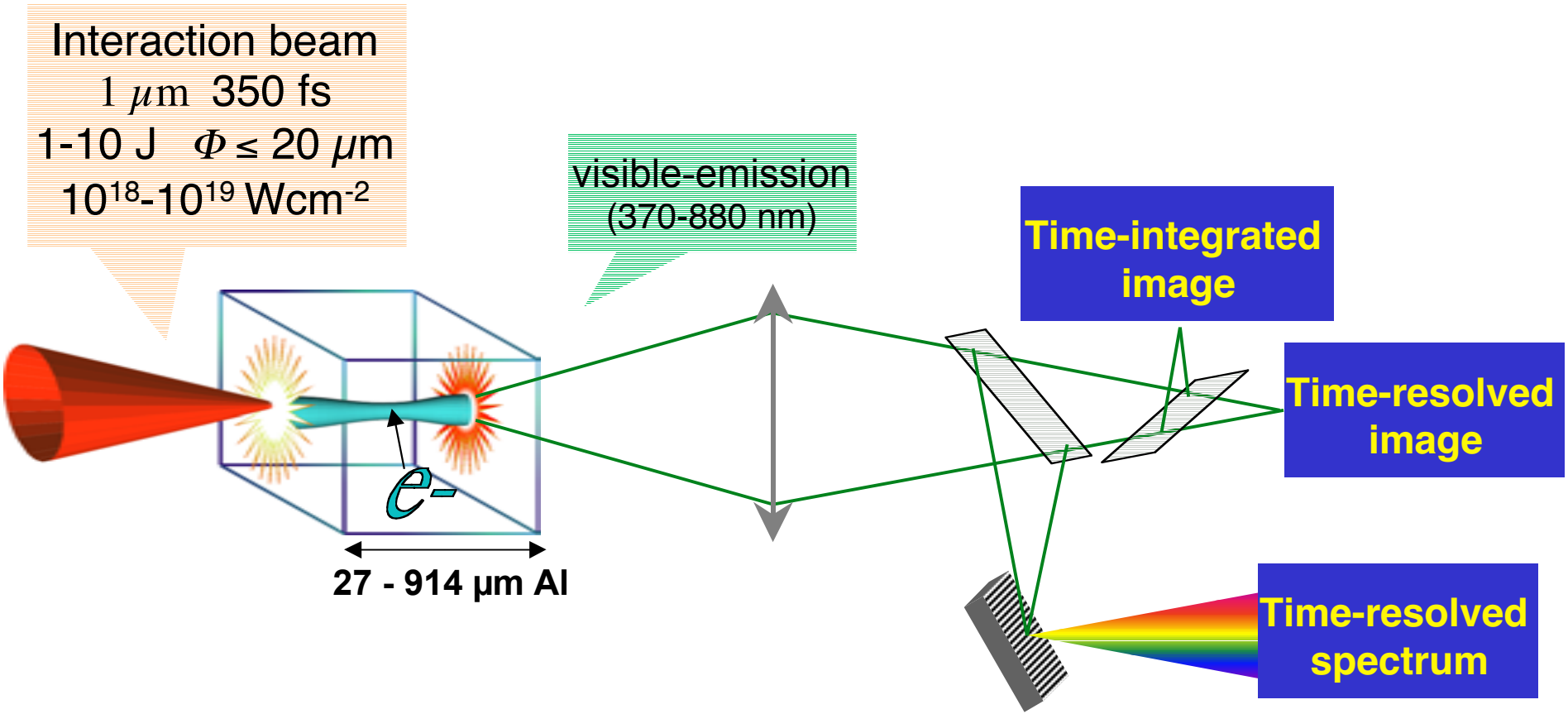

Brief and bright visible emission at rear side of Al target : Optical Transition Radiation (OTR)*

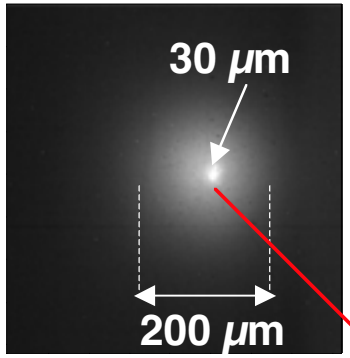

Time-integrated image

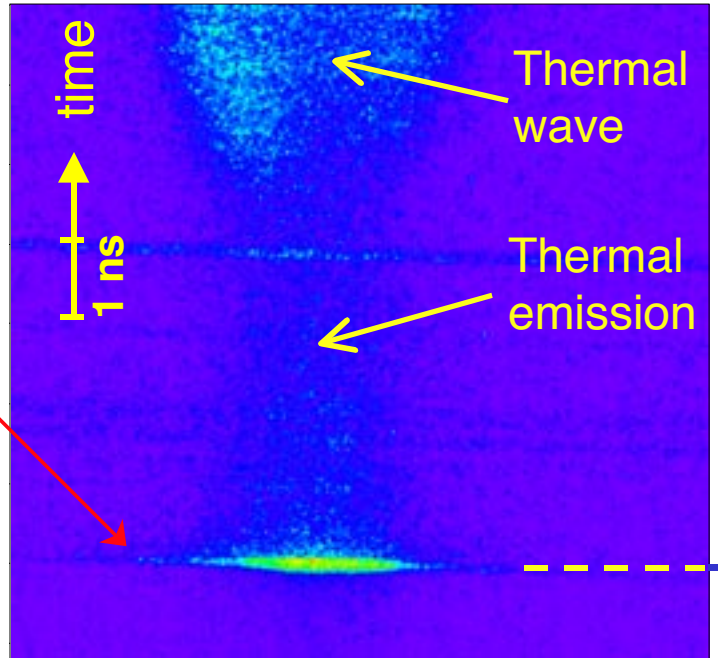

Time-resolved image
75 μm Al target

Short-duration signal ≤ 10 ps

Electron jets

*J.J. Santos *et al*., Phys. Rev. Lett., 89, 025001 (2002)

Bright and narrow 2ω emission at the rear of the targets superimposed on wide spectrum

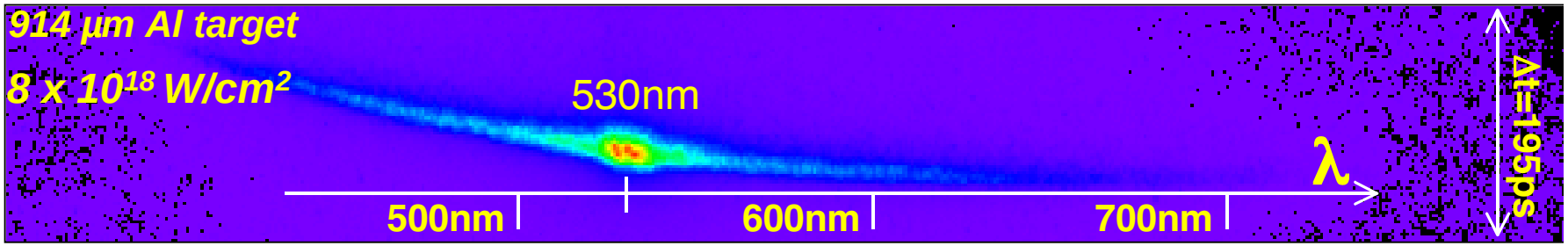

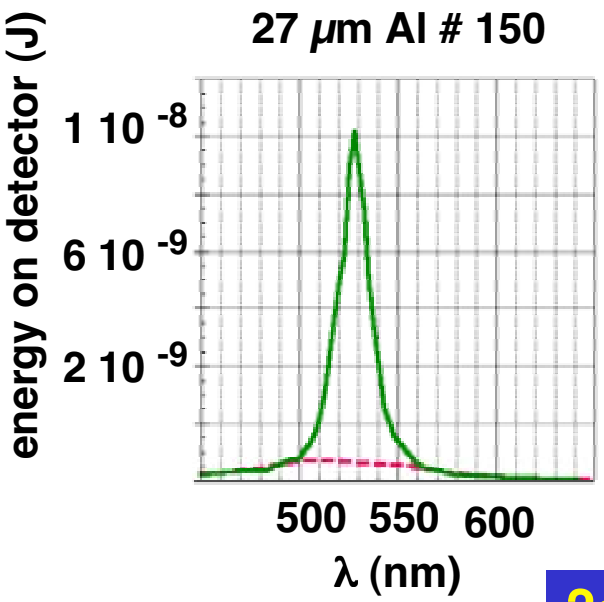

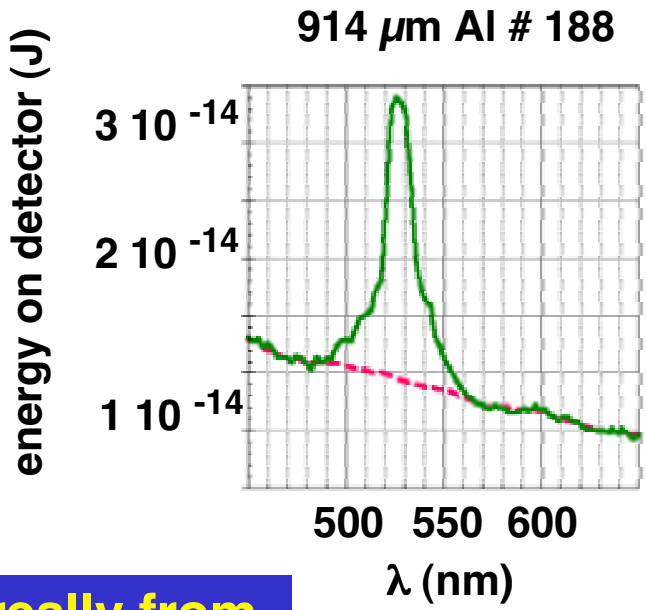

2ω comes really from the rear side!

OTR consistent with two electron populations : incoherent and coherent

wide spectrum :
Incoherent Transition Radiation (ITR)

10^{13} outgoing electrons
~ 1 J
T_h ~ a few hundreds of keV

3D hybrid code PâRIS

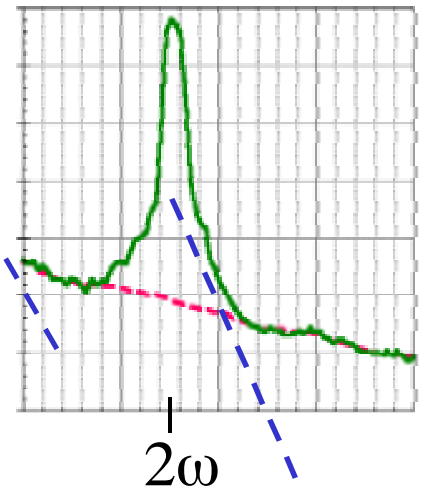

2ω line : Coherent Transition Radiation (CTR) generated by ultrashort electron bunches

Evidence of bunches at 2ω in numerical simulations

W. Yu *et al.*, Phys. Rev. Lett. **85**, 570 (2000)

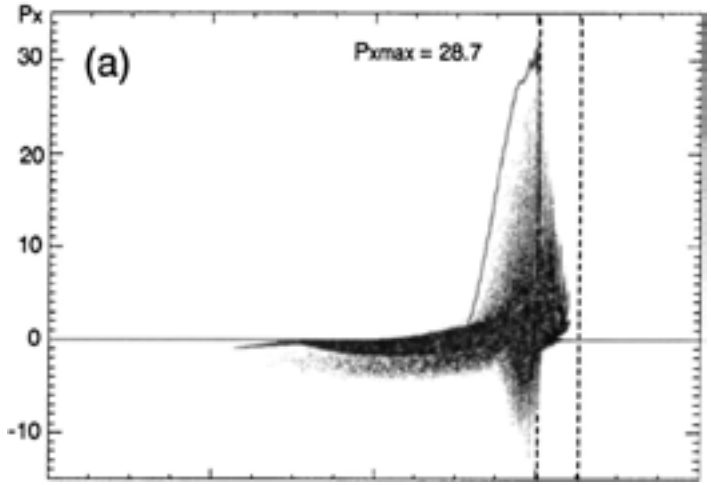

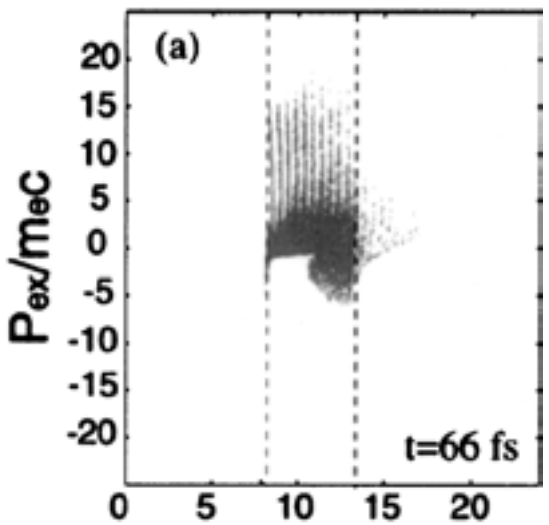

A.J. Mackinnon *et al.*,
Phys. Rev. Lett. **88**, 215006 (2002)

B.F. Lasinski *et al.*,
Phys. Plasmas **6**, 2041 (1999)

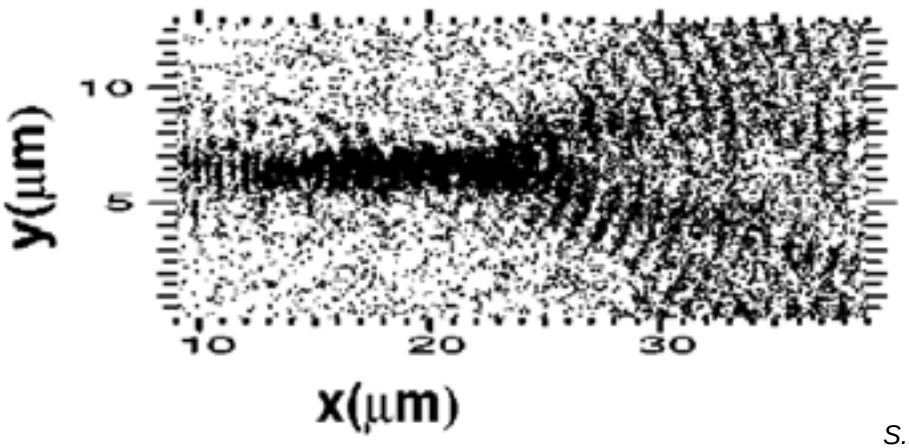

2ω component due to bunches of electrons at 2ω generated by vxB force or vacuum heating

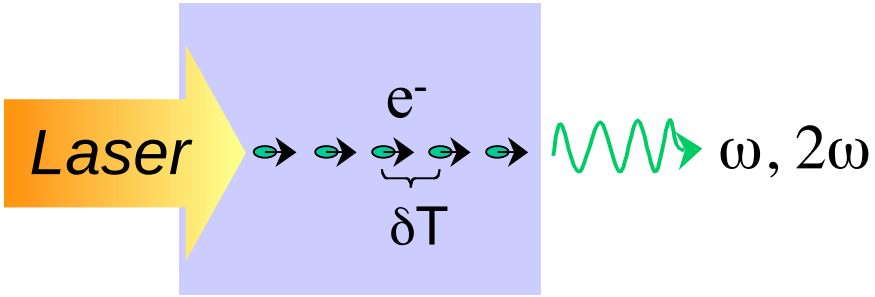

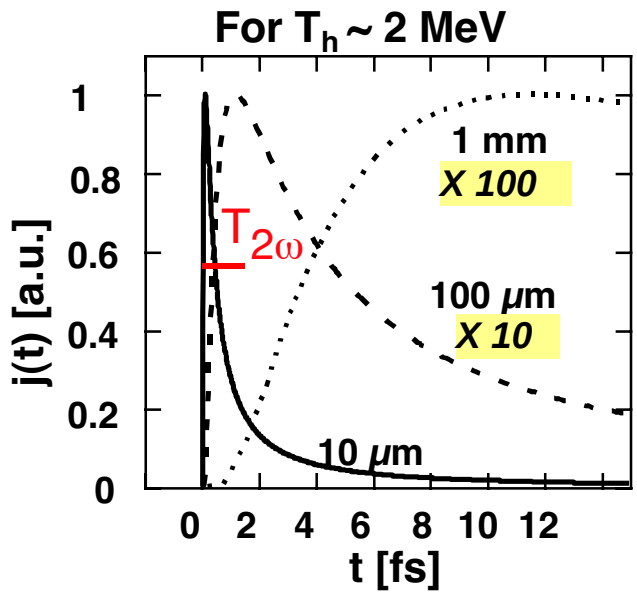

$$I(\omega) = P^2 \,.\, \eta\,(E_c,\omega) \,.\, |i(\omega)|^2 \,.\, \frac{\sin^2(M\omega\delta T/2)}{\sin^2(\omega\delta T/2)}$$

# of e-/ bunch

OTR efficiency

FT of i(t)

Interferences between M bunches

Good fit for CTR signal is obtained for $T_h \sim 2$ MeV and ~ 1 mJ with 15 or 30 bunches

Good fit obtained with

$T_h \sim 2$ MeV

if vxB ➡ 30 bunches x 38 μJ

if v. h. ➡ 15 bunches x 76 μJ

~ 1mJ in e- bunches

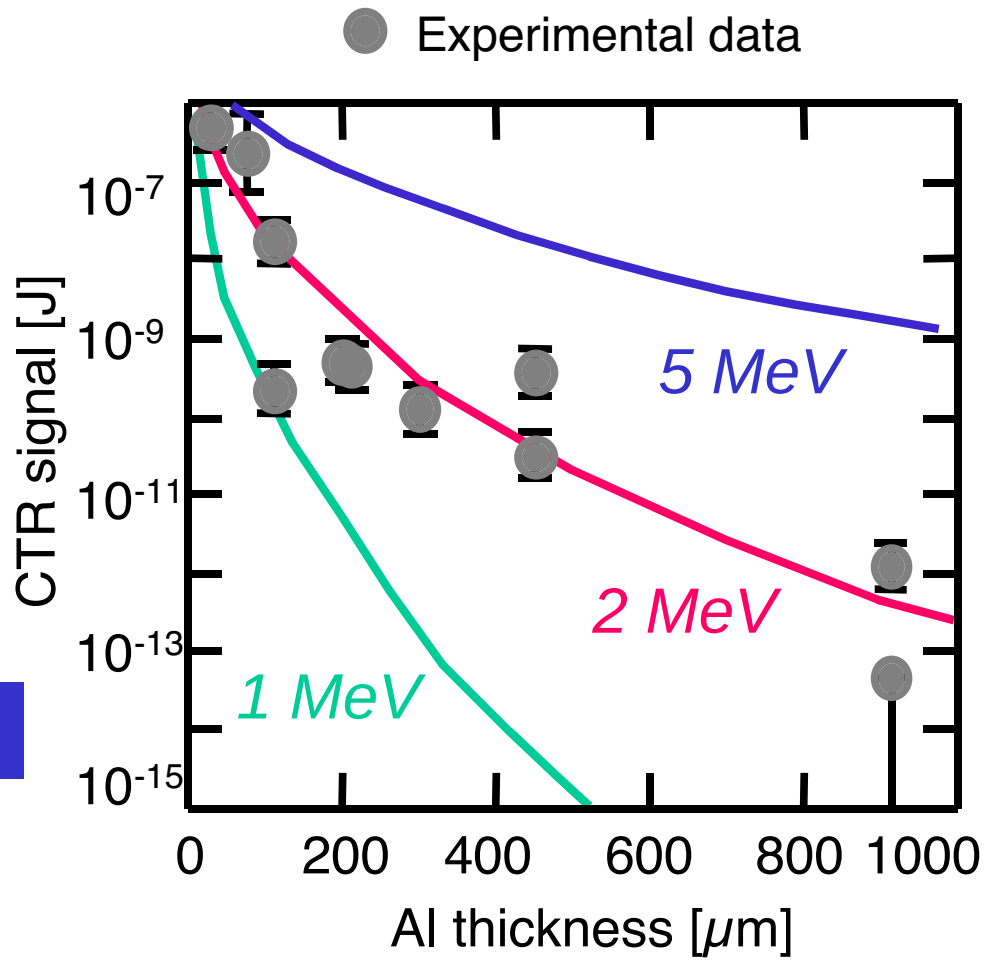

Summary:

- **two electron populations at rear side**
- **CTR is a good diagnostic of ultrashort electron bunches but only sensitive to high-energy electrons**

Incoherent

~ 1 J in 10^{13} outgoing e^-
T_h ~ a few hundreds of keV

for 10 J laser

Coherent

≥ 1 mJ with 10^7 - 10^8 e^- / bunch
T_h ~ 2 MeV

More precise calculations (energy losses, angular deviations, angular divergence …) are in progress

FIW2002 Workshop in Florida

FOKKER-PLANCK SIMULATIONS OF HOT ELECTRON TRANSPORT IN SOLID DENSITY PLASMA

F. Alouani-Bibi, J-P. Matte and J-C. Kieffer

INRS Énergie et Matériaux Varennes, Québec, Canada. J3X-1S2

Tel: (Canada) 450-929-8183

Fax: (Canada) 450-929-8102

Email: Alouani@inrs-ener.uquebec.ca

INTRODUCTION

- Intense (³ 10^{19} W/cm^2), short laser pulses (£1 psec) on solid targets.

- Experiments and simulations ongoing in several laboratories:

LLNL (USA), RAL(UK), ILE(Jap), LULI(Fr), Jena (De),

Motivation : Fast Ignitor development

INRS(Québec,Canada) J.C. Kieffer group (Our simulation parameters)

Motivation : Ultra-short hard X-ray source

-Absorption mostly into hot electrons (T_{HOT} ³ 20 keV)

Intense (³ 5 10^{16} W/cm^2)* flux of hots penetrates deep into solid.

Space charge E-field Cold return current Joule heating.

(Fast Ignitor: **T_{HOT} > 100 keV ; I_{HOT} >** 10^{19} W/cm^2 : need relativistic code)

-Previous modeling:

2-D code: Fully kinetic (PIC or Vlasov); n_e 10-20 n_c

[Several groups]

2-D code: Kinetic (PIC) for hots; (T_{Hot} and I_{Hot} assumed)

Fluid for thermals (with classical resistivity)

[J.R. Davies *et al*., Phys. Rev. E **59**, 6032 (1999)]

* For small focal spots: Fast electrons do complex trajectories in vacuum, before being pulled back by space charge field. Magnetic field effects.

Flux spread over longer time, larger area than incident laser pulse.

(INRS Experiments)

** For large focal spots: Fast electrons penetrate the target directly.

Flux spread over same time and area as incident laser pulse.

(Fast Ignitor experiments at LLNL, ILE, etc.)

We do **not** model this physics.

Only assume a hot electron flux incident on the solid target, replacing some of the thermals.

PHYSICAL MODEL

Electron kinetic code "FPI".

1-D in space ; Non relativistic ;

2-D in V-space ($V, \mu = V_x/V$), Legendre expansion for μ.

Includes:

- Advection (transport term: V_x F/ x)
- Electric field for quasi-neutrality, and acceleration ($-eE/m$ F/ V_x)
- Fokker-Planck term for e-i and e-e collisions
- Atomic physics: average ion model,

  fully coupled to electron kinetics with:
  - ionization (incl. stepwise), 3-body recombination.
  - excitation, collisional and radiative deexcitation.
  - pressure ionization.

Turned off: Hydrodynamic motion ; Collisional (IB) heating

Added: Hot electron source. T_{Hot} = 20-40 keV, in first 4 cells.

$F(E= m_e V^2/2)$ μ $E^n \exp[-E/T_{Hot}]$

(n= -1/2 : "1-D Maxwellian" ; n= +1/2 : ("3-D Maxwellian")

(N.B. $< m_e V^2/2>_{n=-1/2}$ ~ $(1/3) < m_e V^2/2>_{n=+3/2}$ = $(3/2)\, k_B T_{Hot}$)

<u>Isotropic</u>, ($F_{L>0Hot}$ =0) or Beam-like. (F_{LHot} =$(2L+1)F_{0Hot}$, L even)

Assume $T_{Hot}(t)/T_{0Hot}$ μ $(I_{Hot}(t)/I_{0Hot})^{(1/3)}$

SIMULATION PARAMETERS

- Solid Al. $N_i = 6\ 10^{22}\ cm^{-3}$.
- At t=0: $T_e = 10$ eV; $\langle Z \rangle = 3.15$ (LTE at this T_e and density)
- $I_{Hot} = 5\ 10^{16}\ W/cm^2$ - $10^{18}\ W/cm^2$
- FWHM = 0.30, 0.60, and 1.2 psec.
- Pulse peak: $t_0 = 0.45$, 0.90, and 1.8 psec, respectively.

Here, four cases will be compared:

1) $I_{Hot} = 5\ 10^{16}\ W/cm^2$, $T_{Hot} = 20$ keV , FWHM = 1.2 psec , n=-1/2,

Isotropic hots.

2) $I_{Hot} = 5\ 10^{16}\ W/cm^2$, $T_{Hot} = 20$ keV , FWHM = 1.2 psec , n=-1/2,

Beam-like hots. (most relevant to INRS experiments)

3) $I_{Hot} = 10^{18}\ W/cm^2$, $T_{Hot} = 40$ keV , FWHM = 0.6 psec , n=+1/2,

Beam-like hots.

4) $I_{Hot} = 10^{18}\ W/cm^2$, $T_{Hot} = 30$ keV , FWHM = 0.3 psec , n=-1/2,

Beam-like hots.

Density , Temperature and Energy Flux.

1) $I_{0Hot} = 5\ 10^{16}$ W/cm^2, $T_{0Hot} = 20$ keV, n=-1/2, **Isotropic**

FWHM: 1.2 ps, t = peak + 100 fs

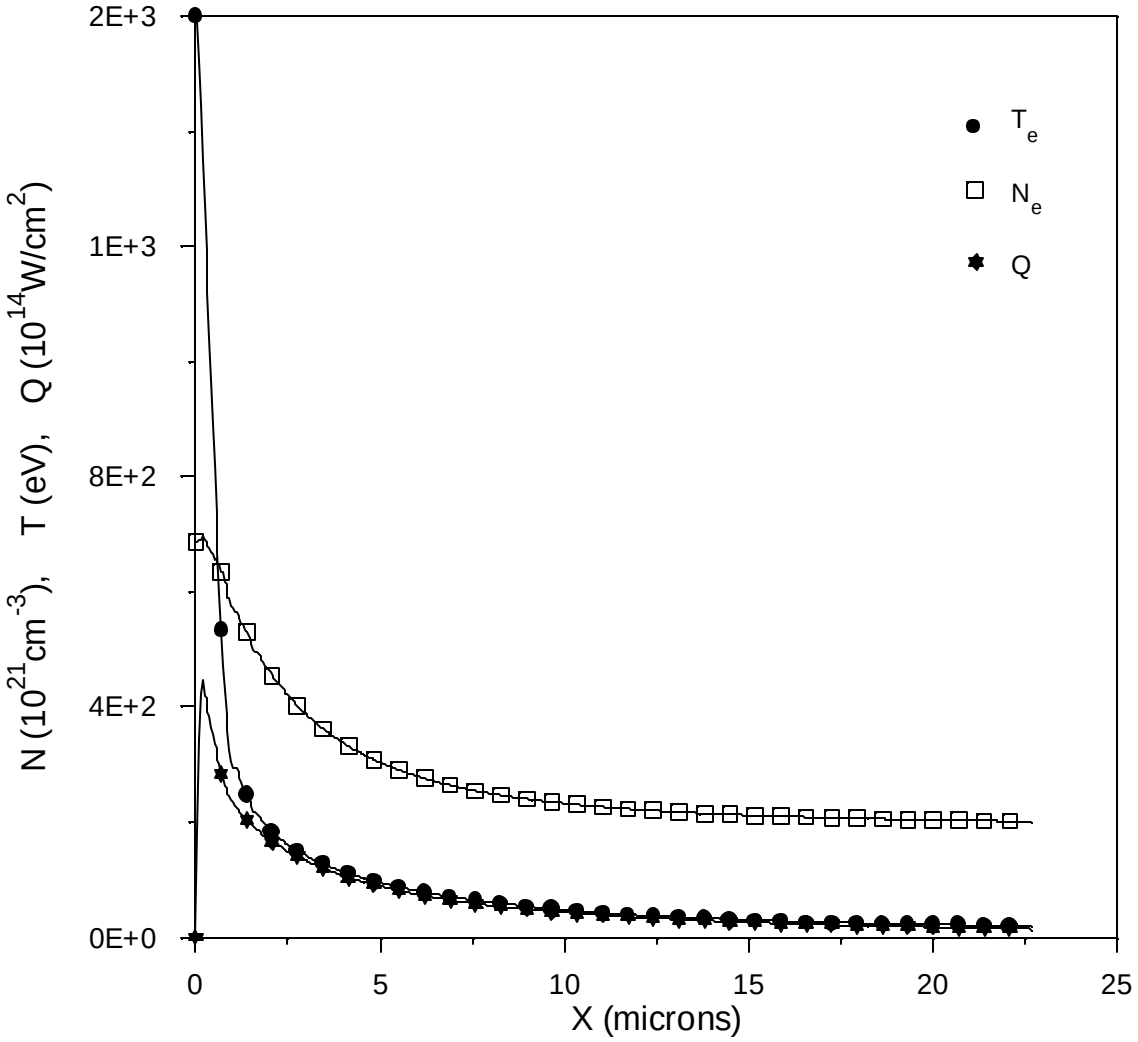

Density , Temperature and Energy Flux.

2) $I_{0Hot} = 5\ 10^{16}$ W/cm^2, $T_{0Hot} = 20$ keV, n=-1/2, Beam-like

FWHM: 1.2 ps, t = peak + 100 fs

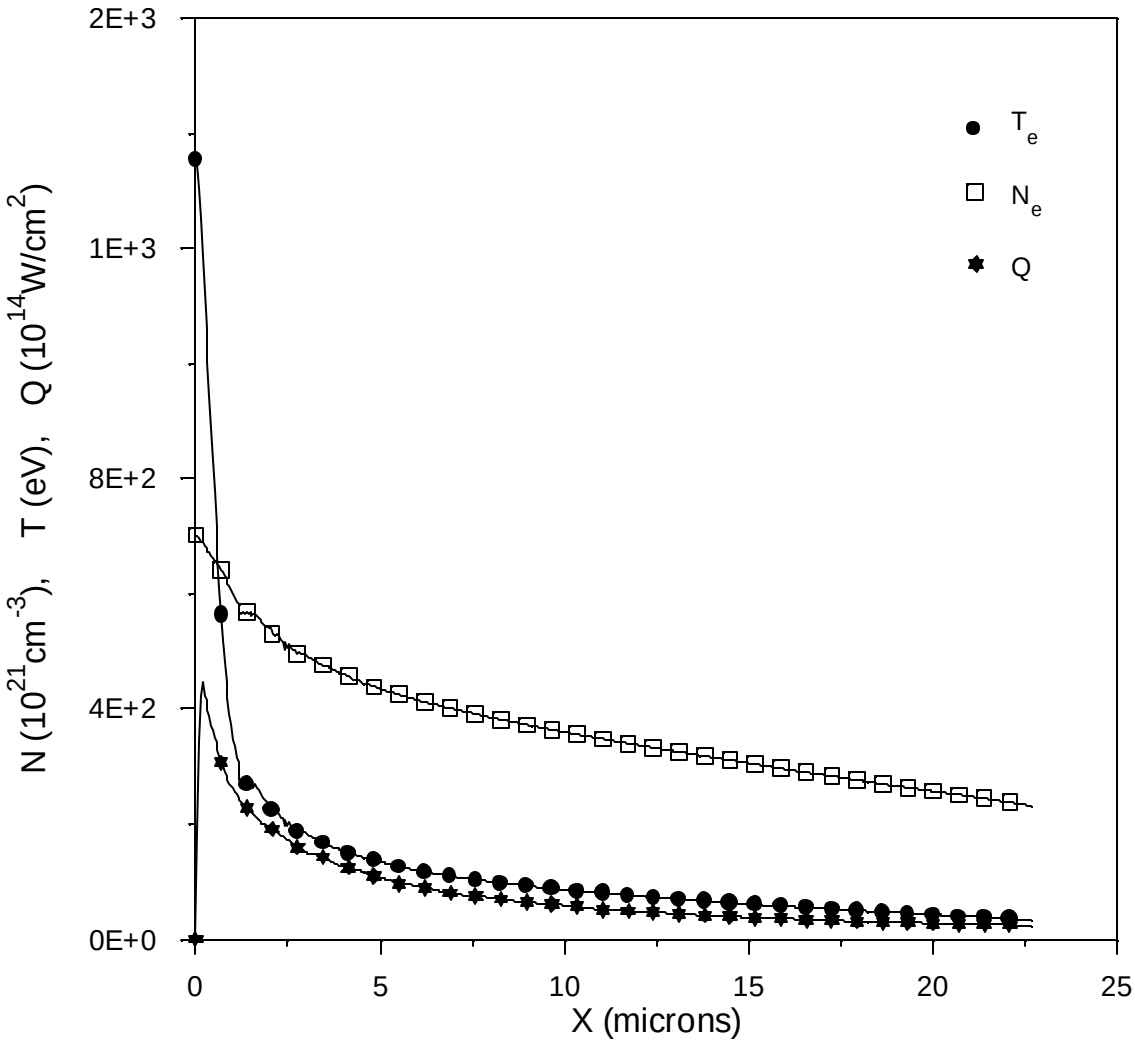

Stronger penetration of the heat front with beam-like hot electrons

Density , Temperature and Energy Flux.

3) $I_{0Hot} = 1\ \ 10^{18}$ W/cm^2, $T_{0Hot} = 40$ keV, n= 1/2, Beam-like

FWHM: 600 fs, t = peak

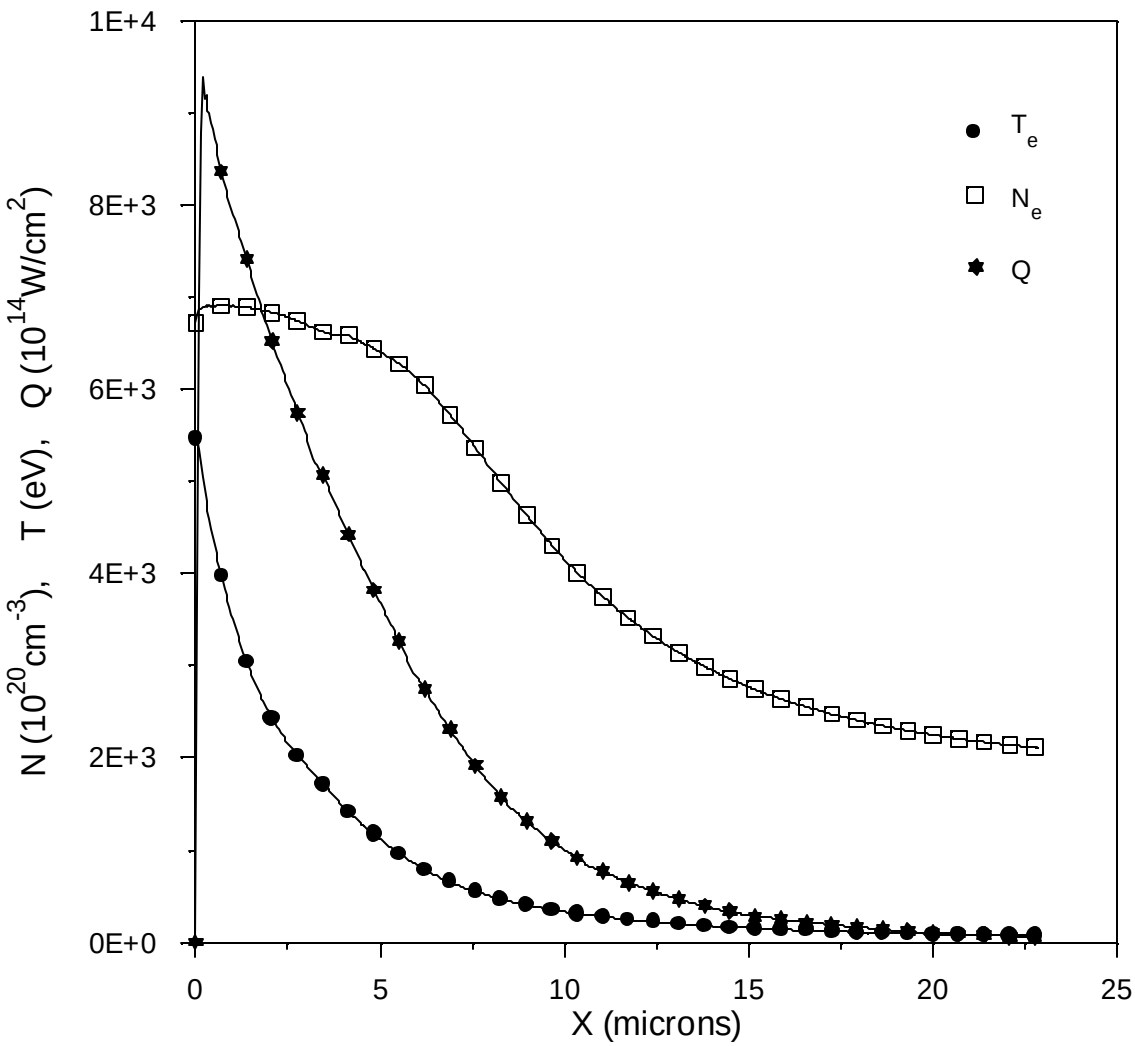

Stronger penetration of the heat front due to much higher I_{hot} and T_{hot}.

Density , Temperature and Energy Flux.

4) I_{0Hot} = 1 10^{18} W/cm^2, T_{0Hot} = 30 keV, n=-1/2, Beam-like

FWHM: 300 fs, t = peak of pulse

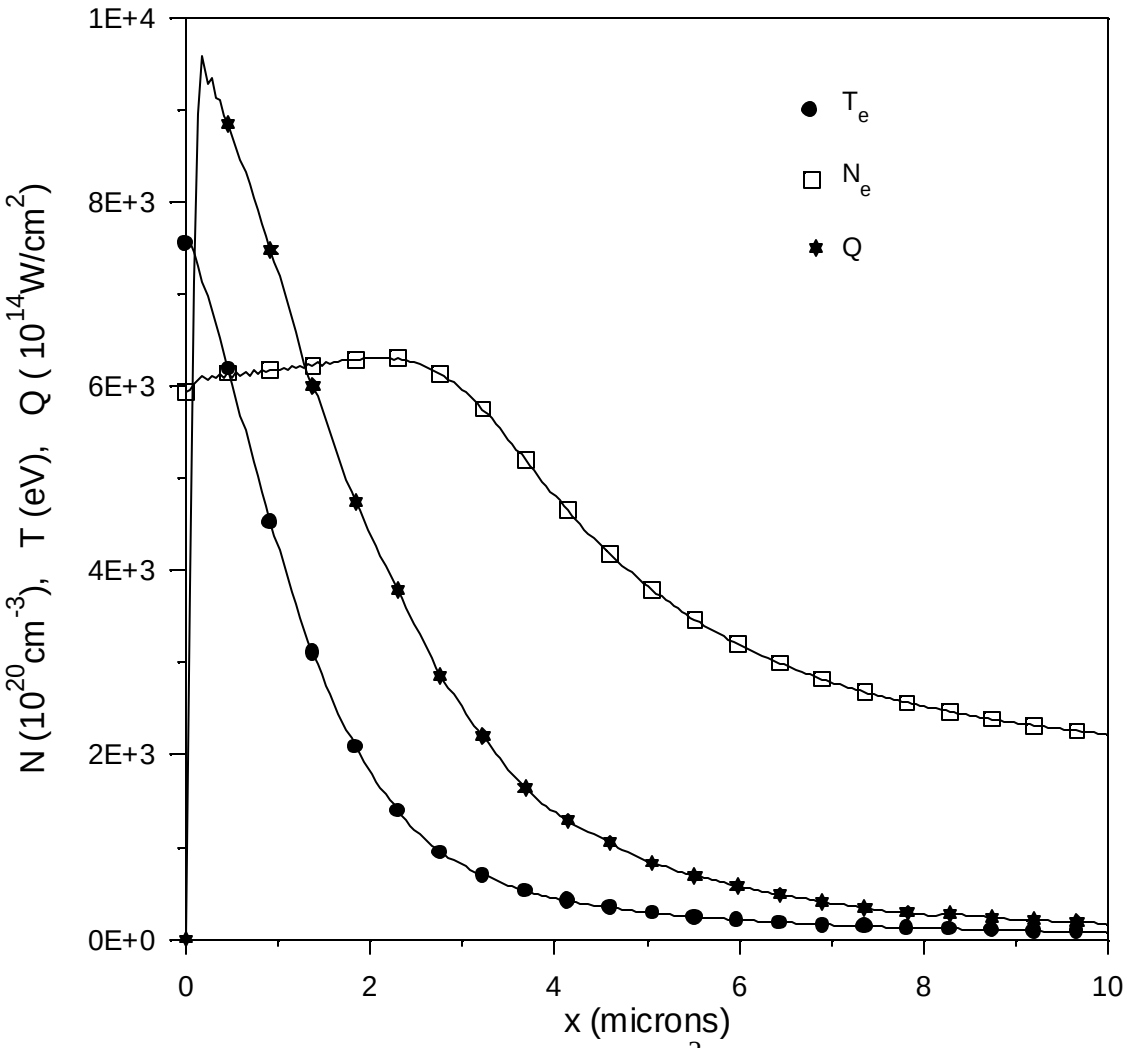

Comparison to case (3) (same I_{Hot}, lower $<V^2>_H$ and FWHM)

Lesser penetration of ionization front : Hot electrons penetrate less far.

Note maximum of <Z> and Ne at X=2.4 µm, not near X=0 :

Very hot electrons are less effective for ionization.

Two temperature fit

Find N_C, T_C, N_H, T_H to match 4 moments of $F_0(X,V,t)$ (C: cold, H: hot)

(Sum of two "3-D" Maxwellians (n=+1/2))

$<V^{-2}>$

$<1>$ $N_C + N_H = N_e$

$<V^2>$ $N_C T_C + N_H T_H = N_e T_e$

$<V^4>$

Two Maxwellians Fit.

1) $I_{0Hot} = 5\ \ 10^{16}$ W/cm^2, $T_{0Hot} = 20$ keV, n=-1/2, Isotropic

FWHM: 1.2 ps, t = peak + 100 fs

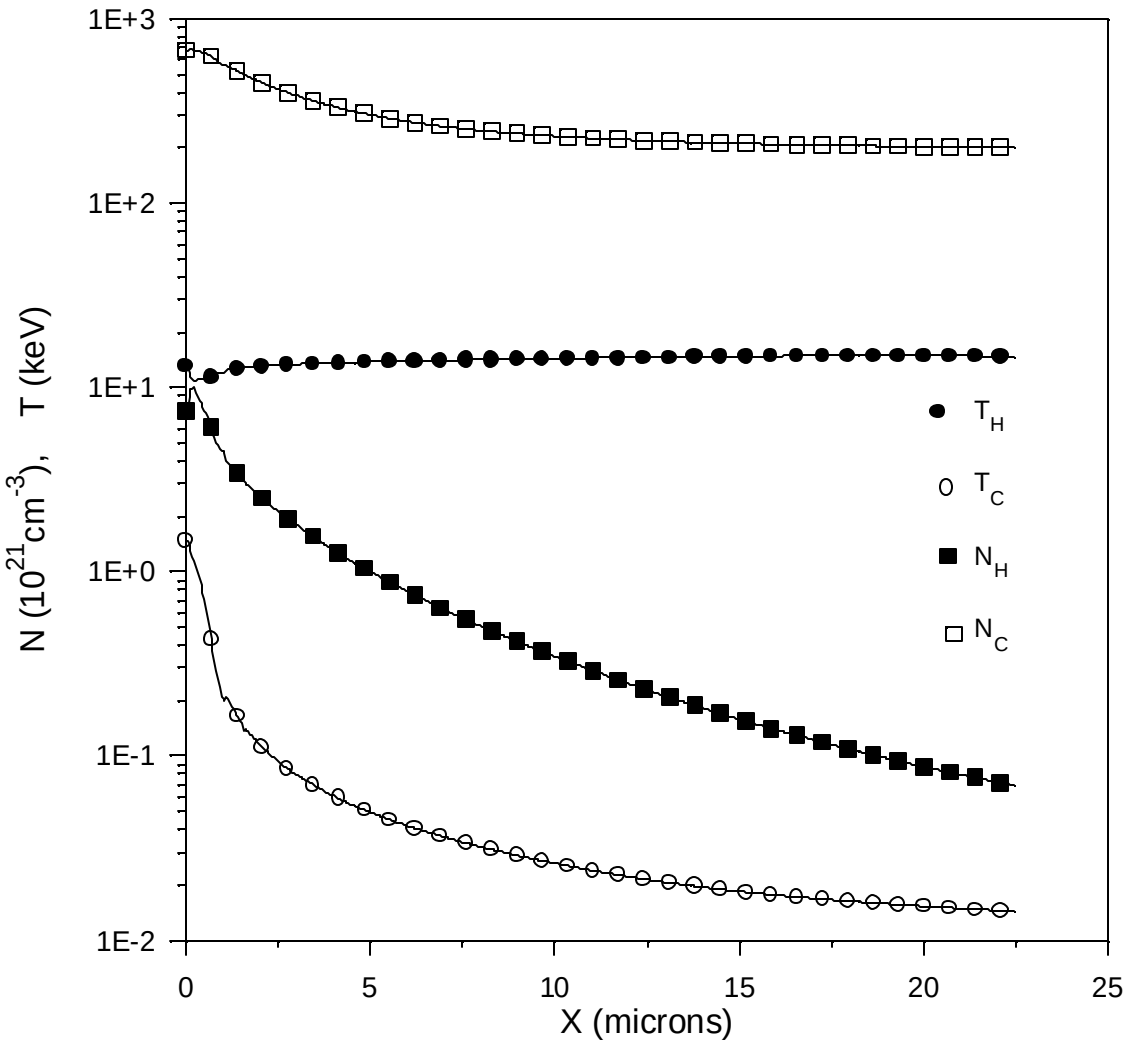

Two Maxwellians Fit.

2) $I_{0Hot} = 5\ \ 10^{16}$ W/cm^2, $T_{0Hot} = 20$ keV, n=-1/2, Beam-like

FWHM: 1.2 ps, t = peak + 100 fs

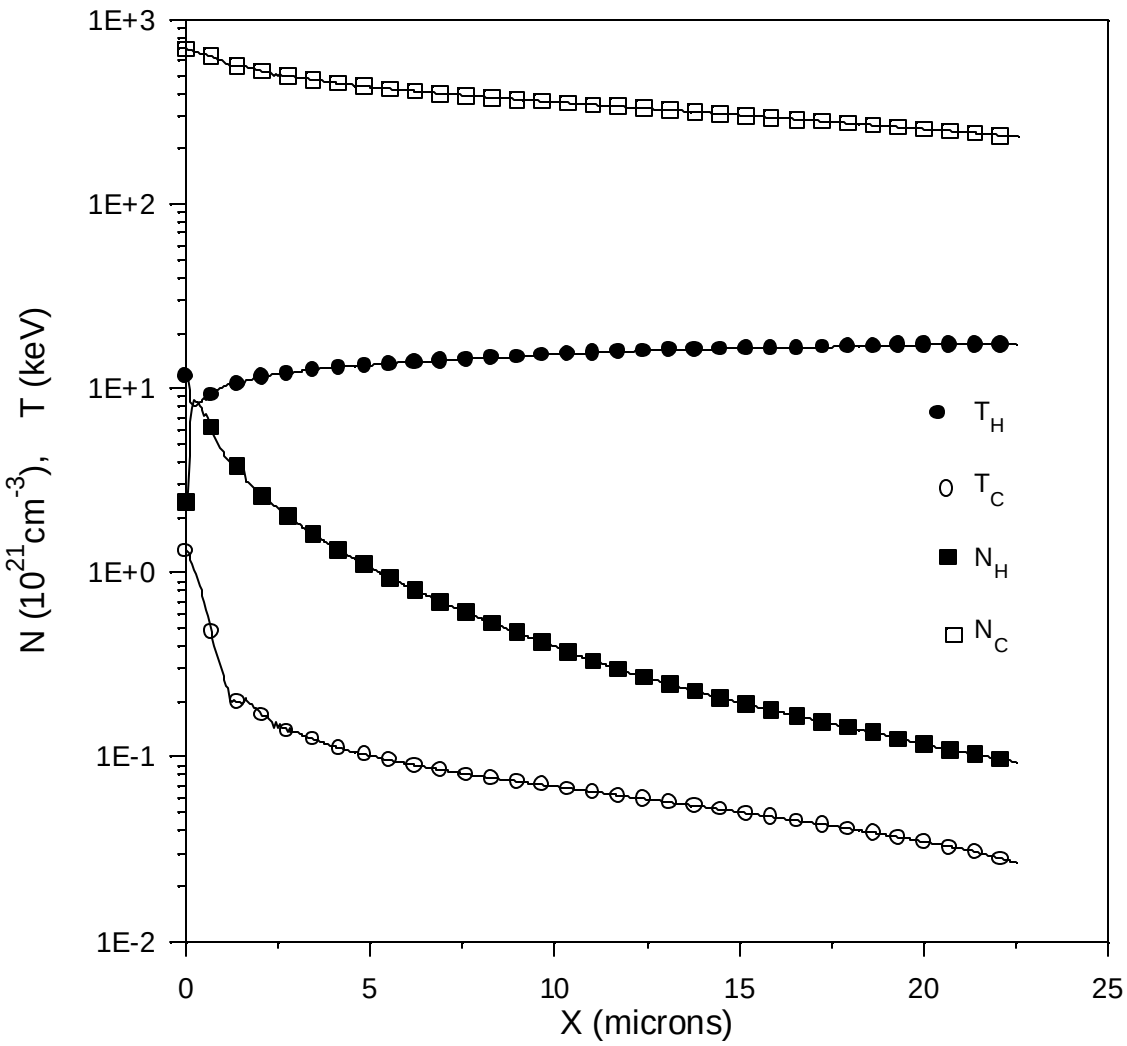

Note: Considerably higher T_C, in depth, with beam-like hots.
Slight increase of T_H with X: only more energetic electrons can stream inwards due to fewer collisions.

Two Maxwellians Fit.

3) $I_{0Hot} = 1 \ \ 10^{18}$ W/cm^2, $T_{0Hot} = 40$ keV, n= 1/2, Beam-like

FWHM: 600 fs, t = peak

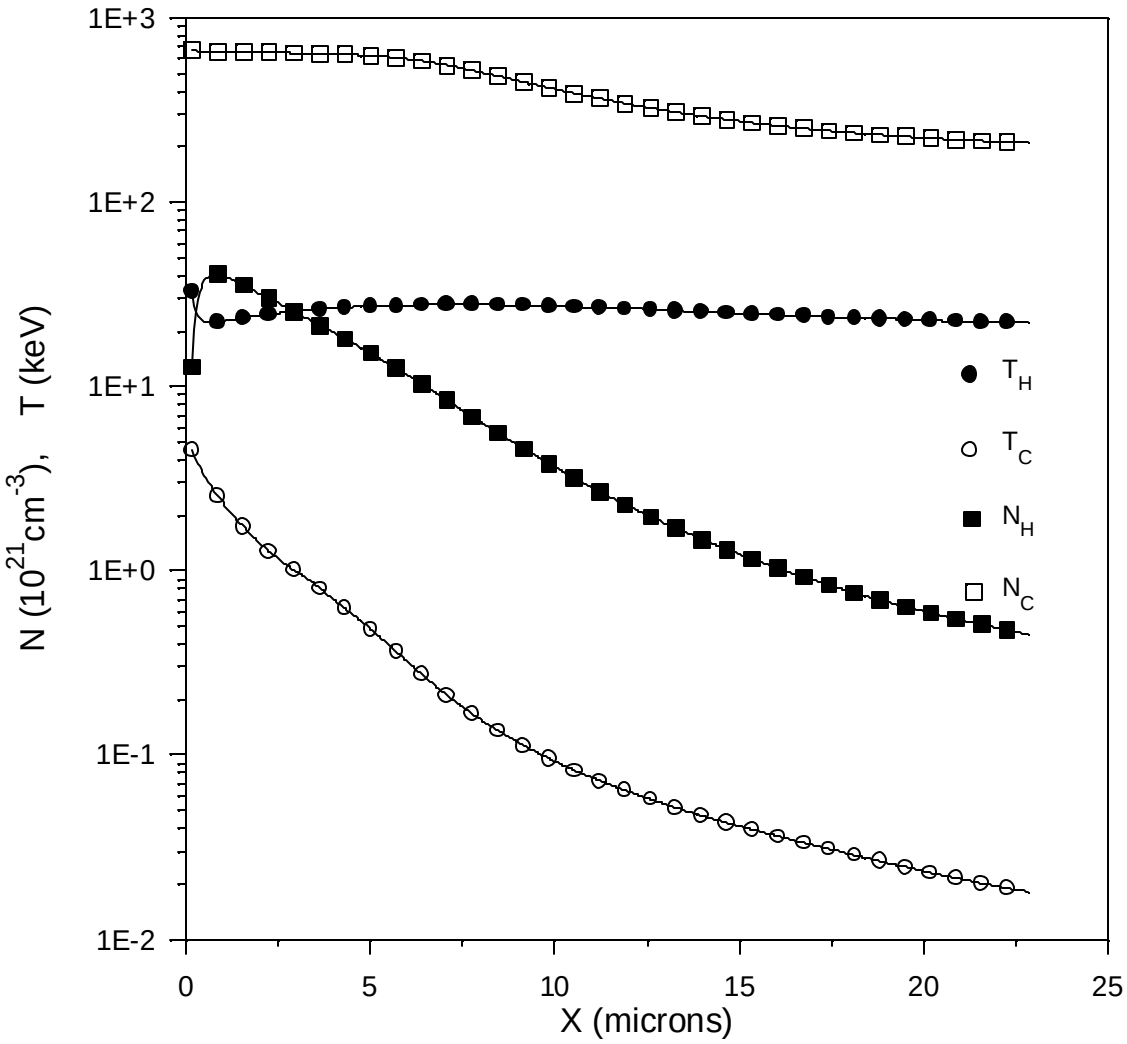

T_C higher than in case (2), up to 12µm. Effect of high power.
Beyond 12µm, T_C is lower. Reason unclear.
Very hot electrons may be less effective in transferring energy.

Two Maxwellians Fit

4) $I_{0Hot} = 1\ \ 10^{18}$ W/cm^2, $T_{0Hot} = 30$ keV, n=-1/2, Beam-like

FWHM: 300 fs, t = peak of pulse

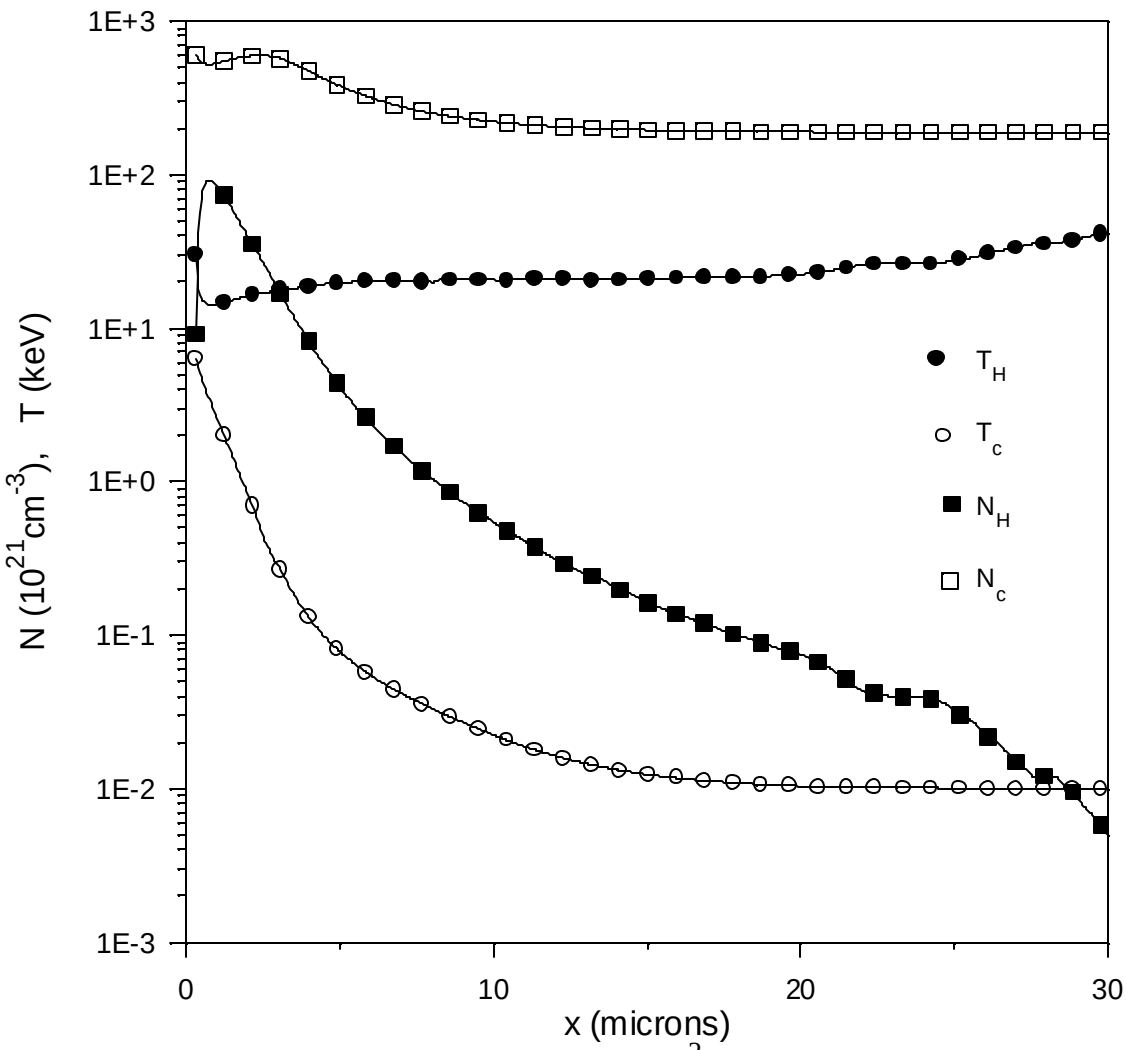

Comparison to case (3) (same I_{Hot}, lower $<V^2>_H$ and FWHM)

T_C higher up to X=1.2 µm, lower beyond.

Hot electrons deposit more energy at lesser depth, due to lower $<V^2>_H$.

Energy distribution function

1)I_{0Hot} = 5 10^{16} W/cm^2 , T_{0Hot} = 20 keV, n=-1/2, Isotropic

FWHM: 1.2 ps, t = peak + 100 fs

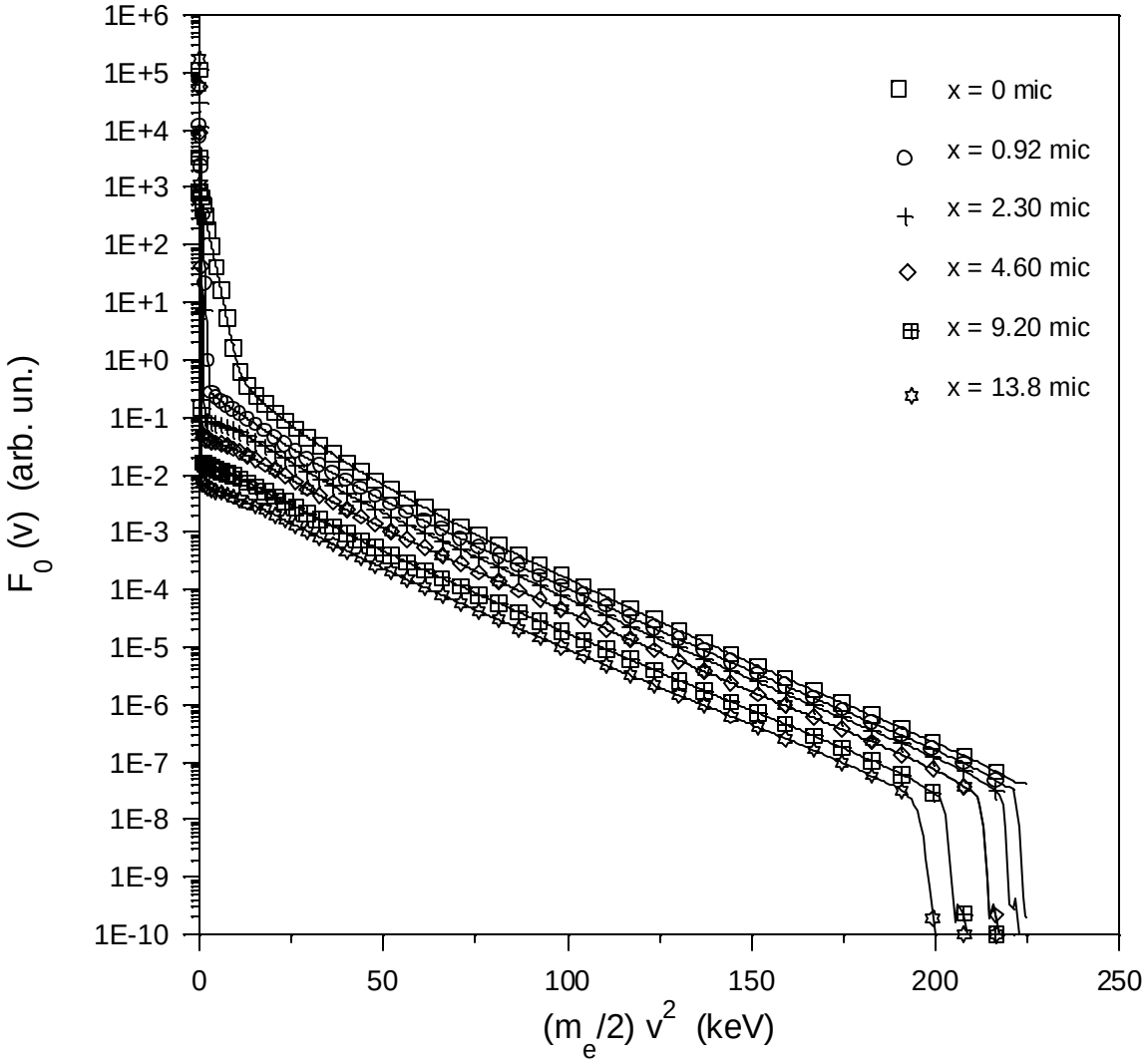

Energy distribution function

2) $I_{0Hot} = 5\ \ 10^{16}$ W/cm^2 , $T_{0Hot} = 20$ keV, n=-1/2, Beam-like

FWHM: 1.2 ps, t = peak + 100 fs

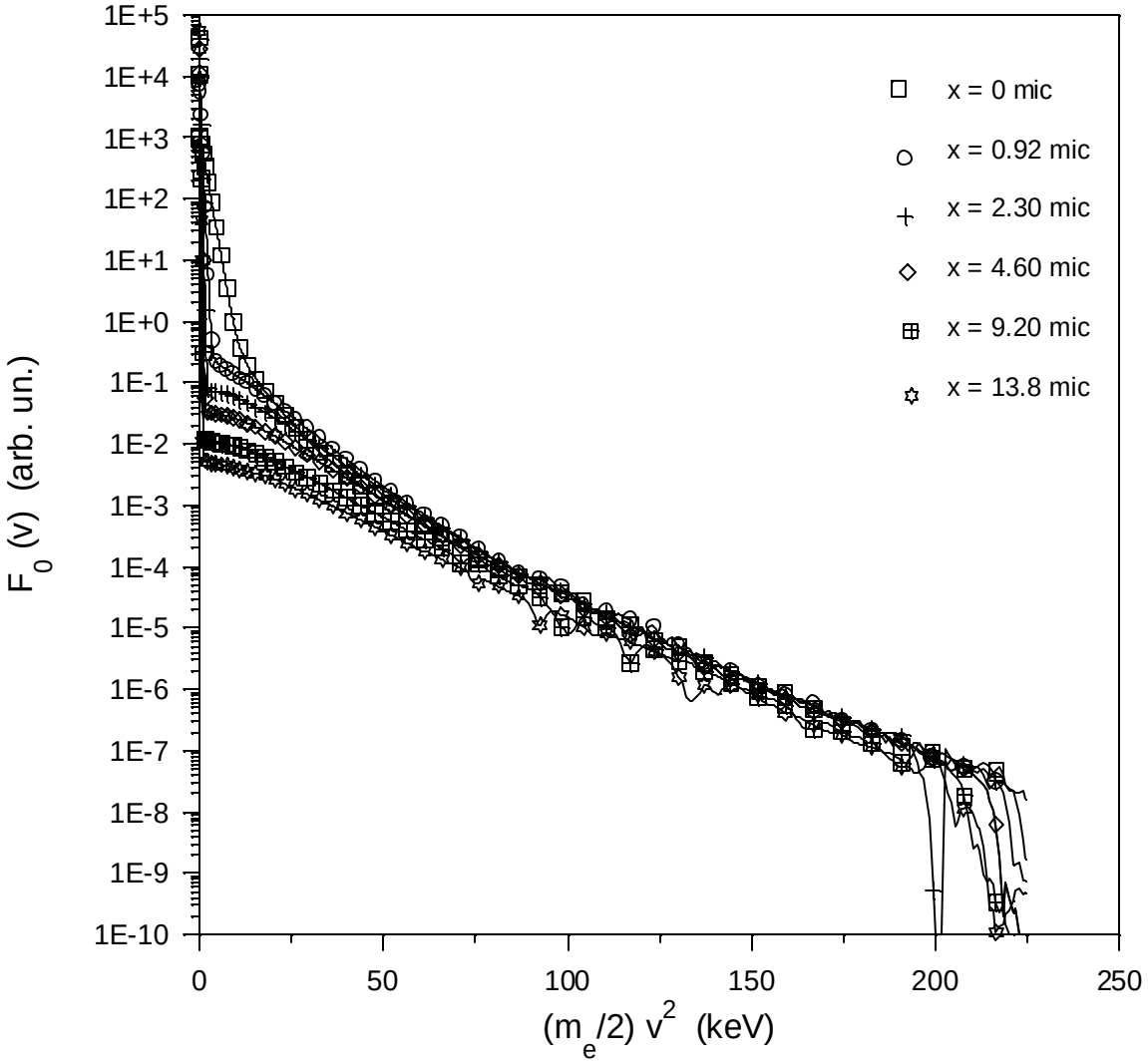

Stronger penetration of hot electrons in beam-like case.

Energy distribution function

3) $I_{0Hot} = 1\ \ 10^{18}$ W/cm^2 , $T_{0Hot} = 40$ keV, n= 1/2, Beam-like

FWHM: 600 fs, t = peak

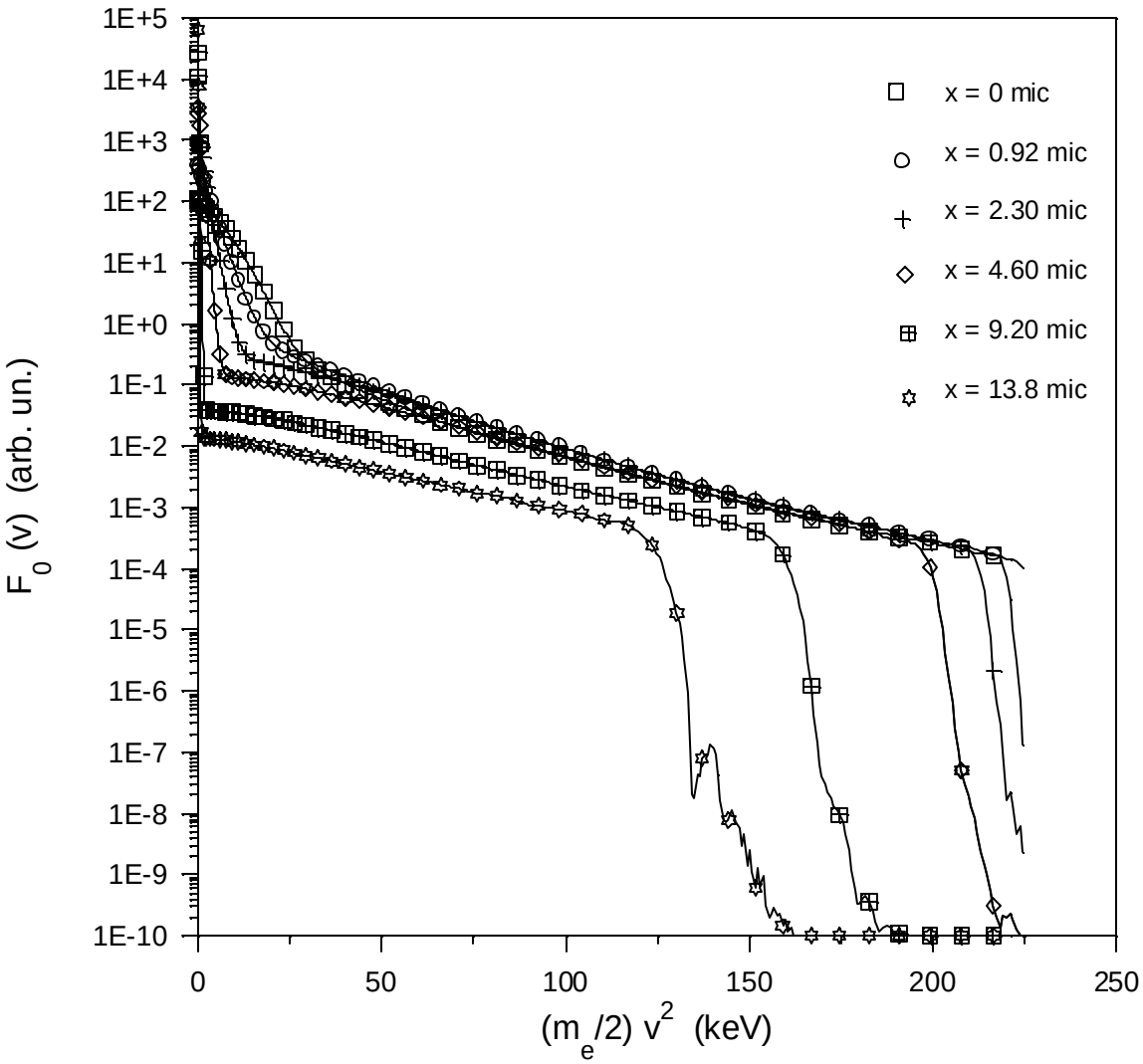

At high intensity: Strong braking of hots by the resistive electric field.
At X=0, truncation at 225 keV, max. energy.
At X=13.8 µm, this is shifted by about 70 keV.

Energy distribution function

4) $I_{0Hot} = 1\ \ 10^{18}$ W/cm^2, $T_{0Hot} = 30$ keV, n=-1/2, Beam-like

FWHM: 300 fs, t = peak of pulse

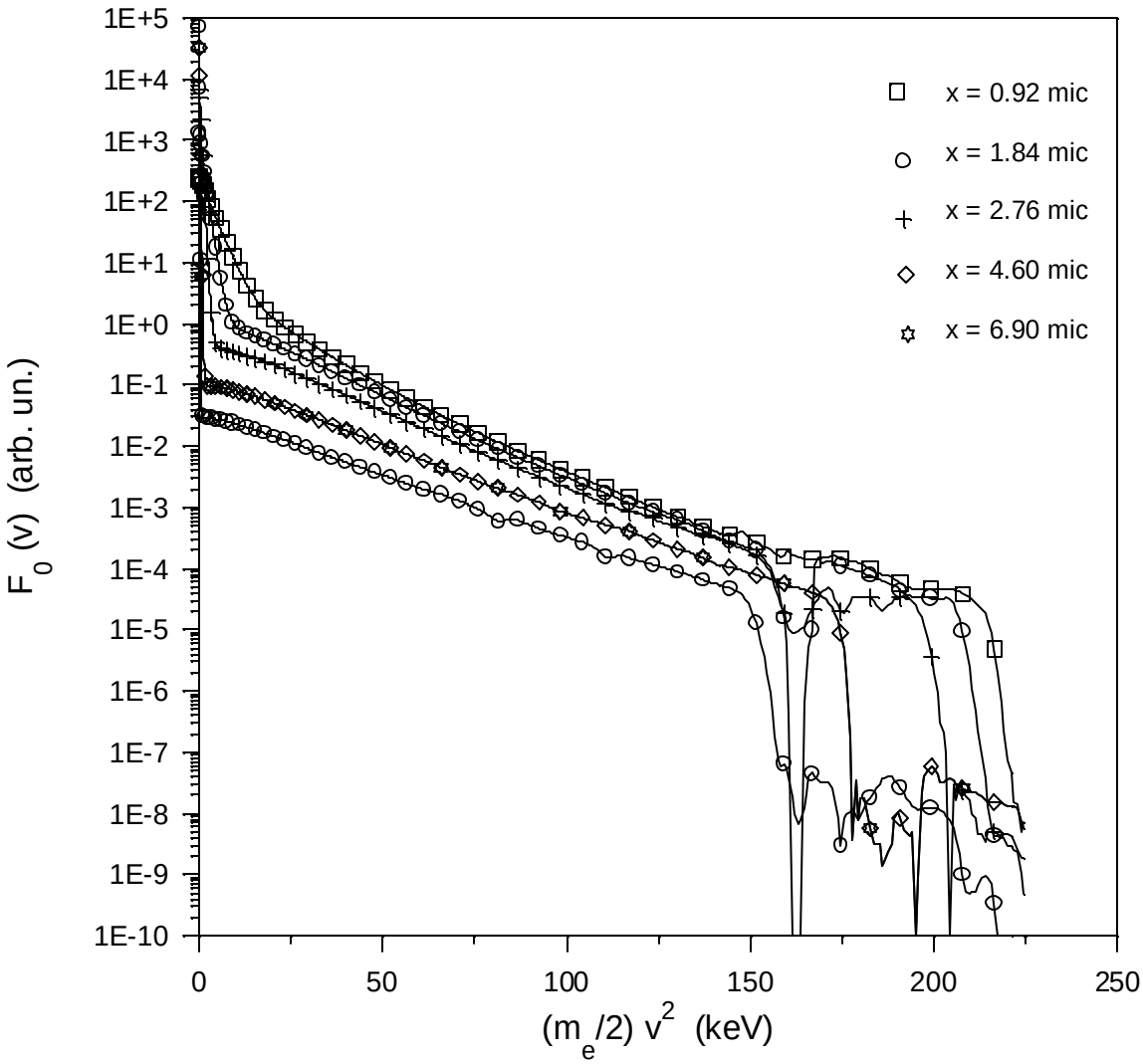

Compared to case 3, (same I_H), less penetration, due to lower T_H, $m\langle V^2\rangle_H$
But even stronger collisional braking, due to higher J_H (=2 I_H / $m\langle V^2\rangle_H$)

Differential energy flux

$F_1(x, v, t)\, v^5$, $\frac{m_e}{6} \int_0 F_1(x,v,t) v^5\, dv = Q_e(x,t)$

1) $I_{0Hot} = 5\ \ 10^{16}$ W/cm^2 , $T_{0Hot} = 20$ keV, n=-1/2, Isotropic

FWHM: 1.2 ps, t = peak + 100 fs

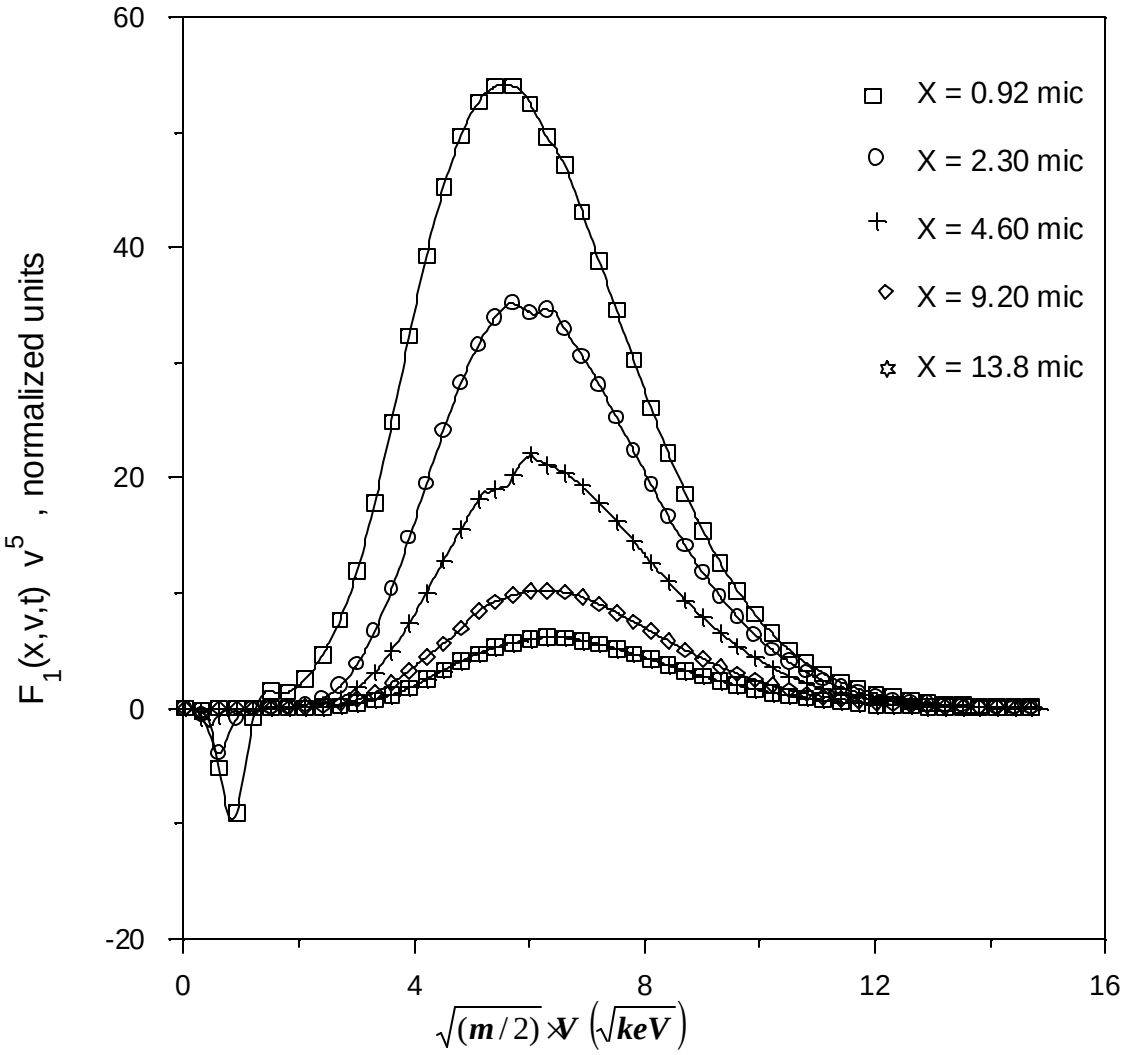

Differential energy flux

$F_1(x, v, t)\, v^5$, $\frac{m_e}{6} \int_0 F_1(x,v,t) v^5\, dv = Q_e(x,t)$

2) $I_{0Hot} = 5\ \ 10^{16}$ W/cm^2 , $T_{0Hot} = 20$ keV, n=-1/2, Beam-like

FWHM: 1.2 ps, t = peak + 100 fs

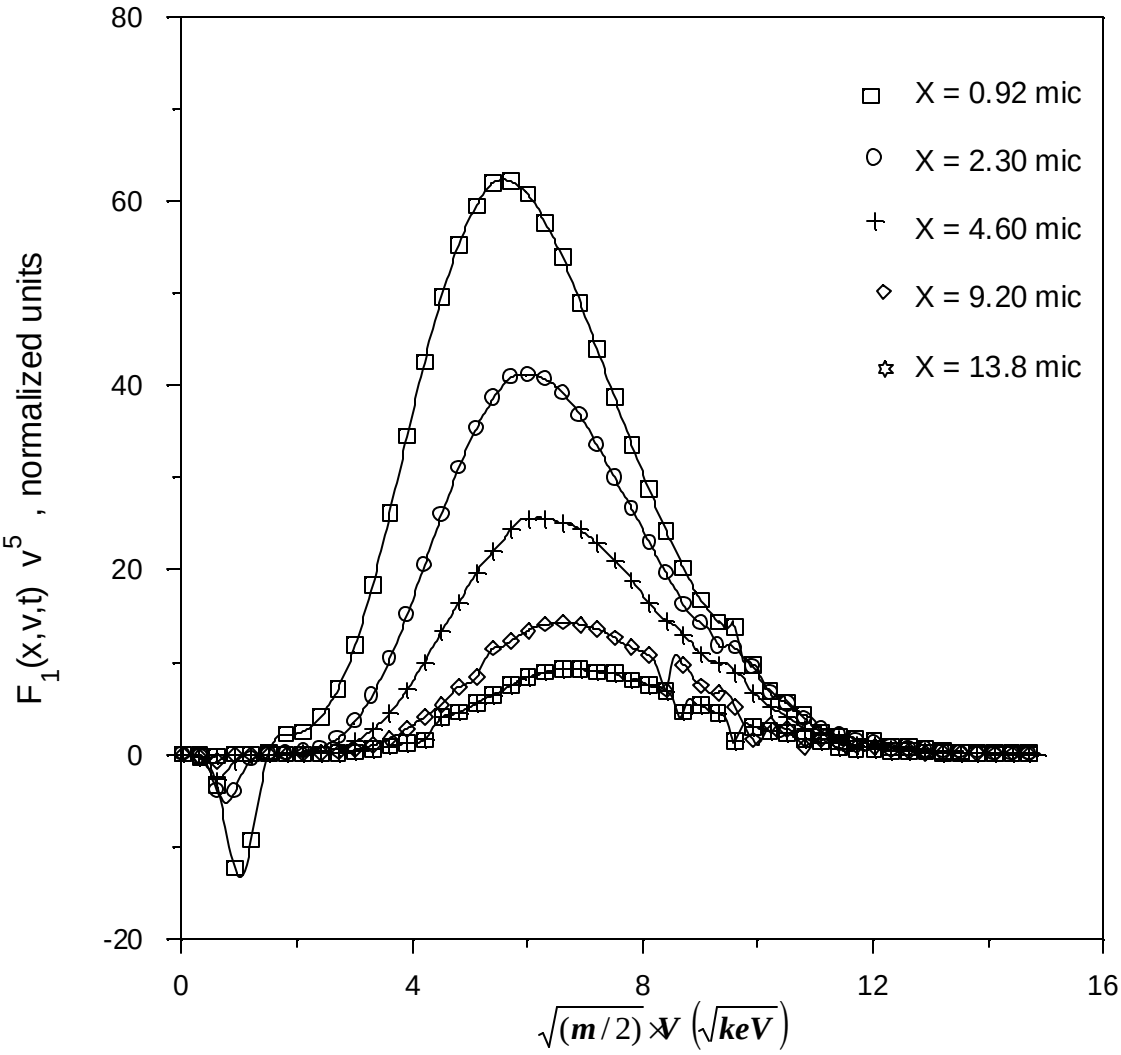

Note: Energy fluxes somewhat higher for beam-like hots.
Maximum shifts to higher energy in depth:
less collisional braking for faster electrons

Differential energy flux

$F_1(x, v, t)\, v^5$, $\frac{m_e}{6} \int_0 F_1(x,v,t) v^5\, dv = Q_e(x,t)$

3) $I_{0Hot} = 1\ \ 10^{18}$ W/cm^2 , $T_{0Hot} = 40$ keV, n= 1/2, Beam-like

FWHM: 600 fs, t = peak

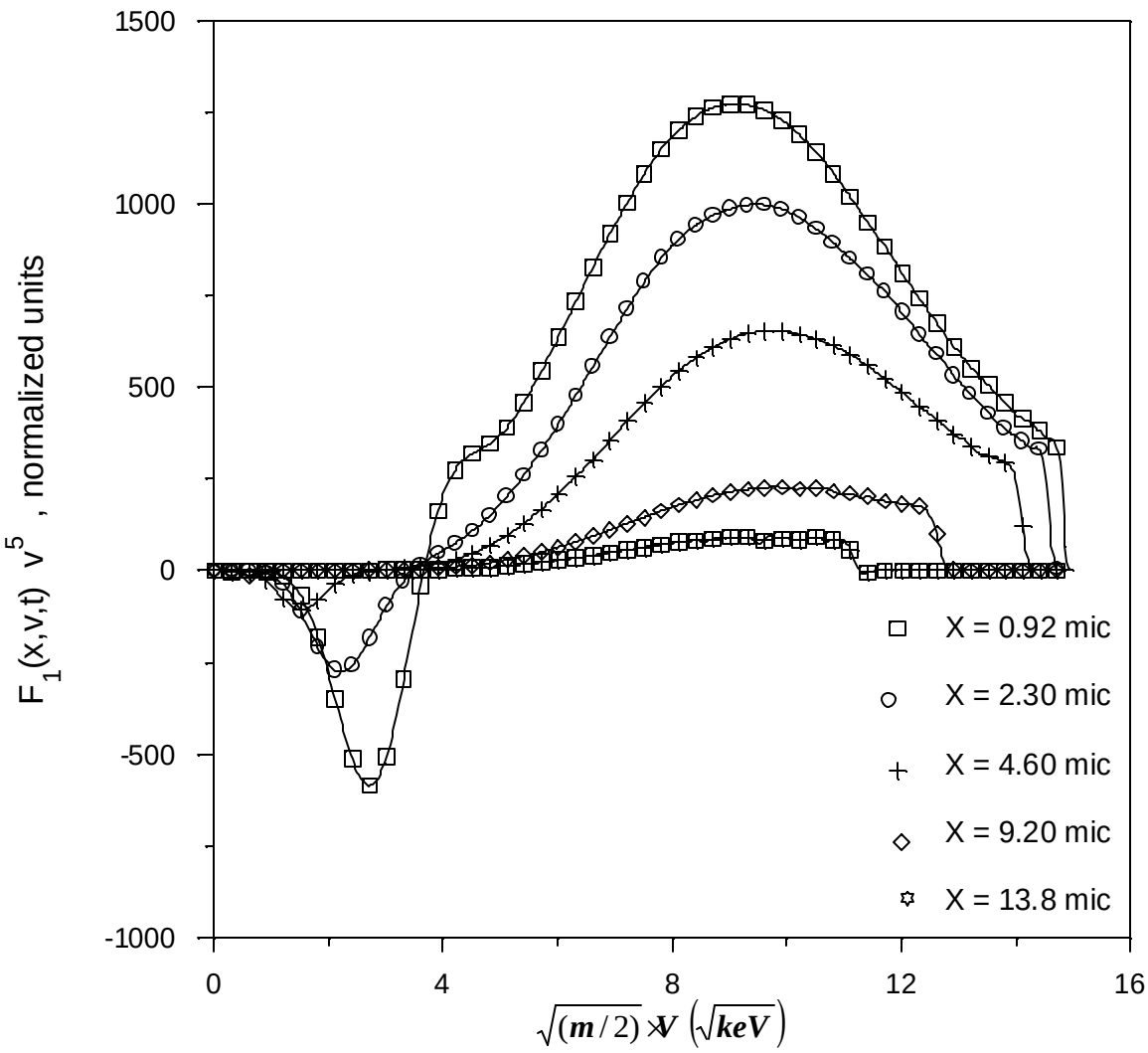

Note: Energy fluxes higher due to higher I_{0Hot} .

Maximum shifts to higher energy due to higher T_{0Hot} , $\langle V^2 \rangle_{Hot}$.

Differential energy flux

$F_1(x, v, t)\, v^5$, $\frac{m_e}{6} \int_0 F_1(x,v,t) v^5\, dv = Q_e(x,t)$

4) $I_{0Hot} = 1\ \ 10^{18}$ W/cm^2, $T_{0Hot} = 30$ keV, n=-1/2, Beam-like

FWHM: 300 fs, t = peak of pulse

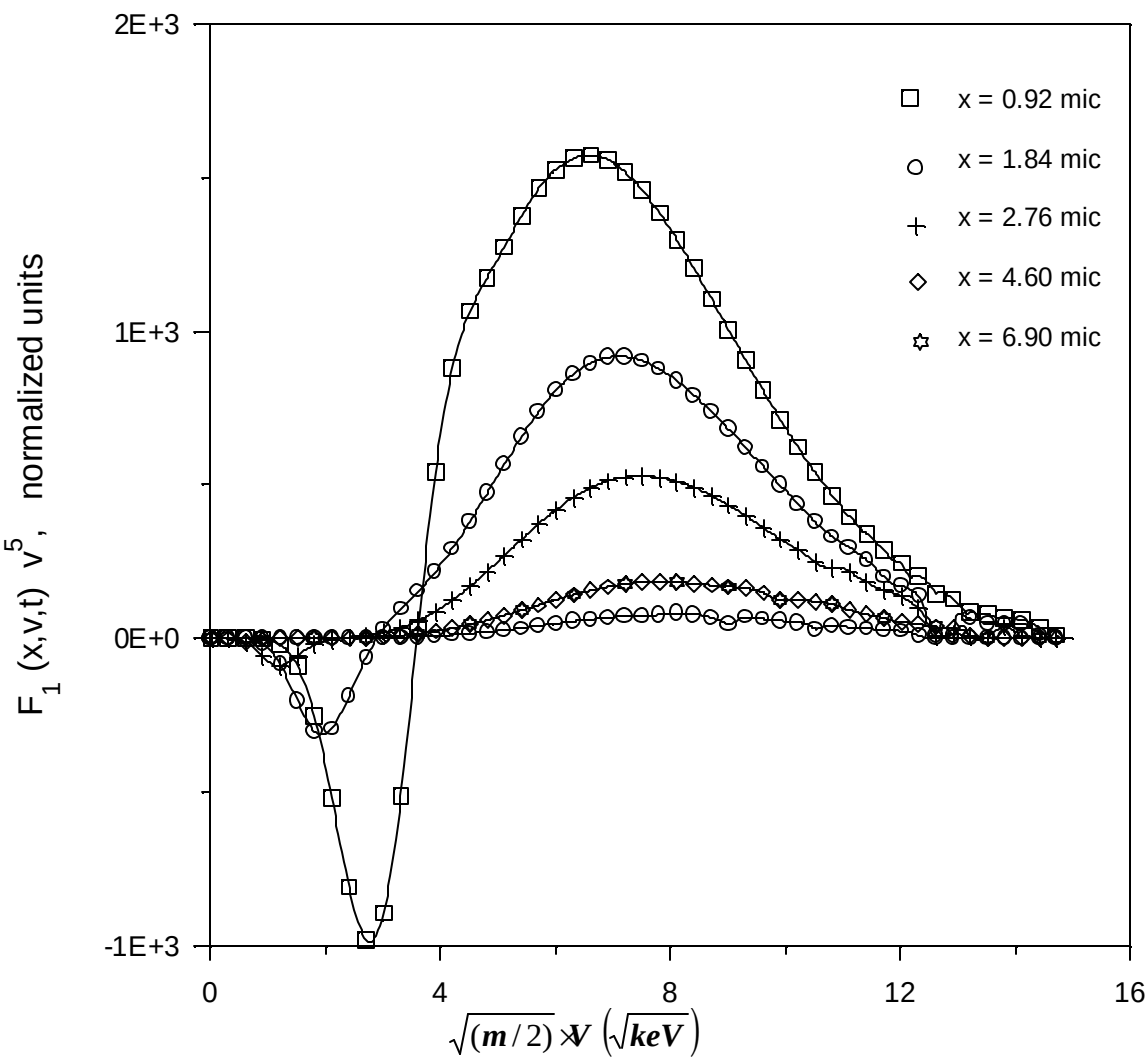

Compared to case 3, (same I_H), note maximum is at lower energy, due to lower $\langle V^2 \rangle_H$

Differential electron flux

$$F_1(x, v, t)\, v^3, \quad \frac{1}{3}\int_0 F_1(x,v,t)v^3\,dv = J_e(x,t) \quad 0$$

1) $I_{0Hot} = 5 \;\; 10^{16}$ W/cm^2 , T_{0Hot} = 20 keV, n=-1/2, Isotropic

FWHM: 1.2 ps, t = peak + 100 fs

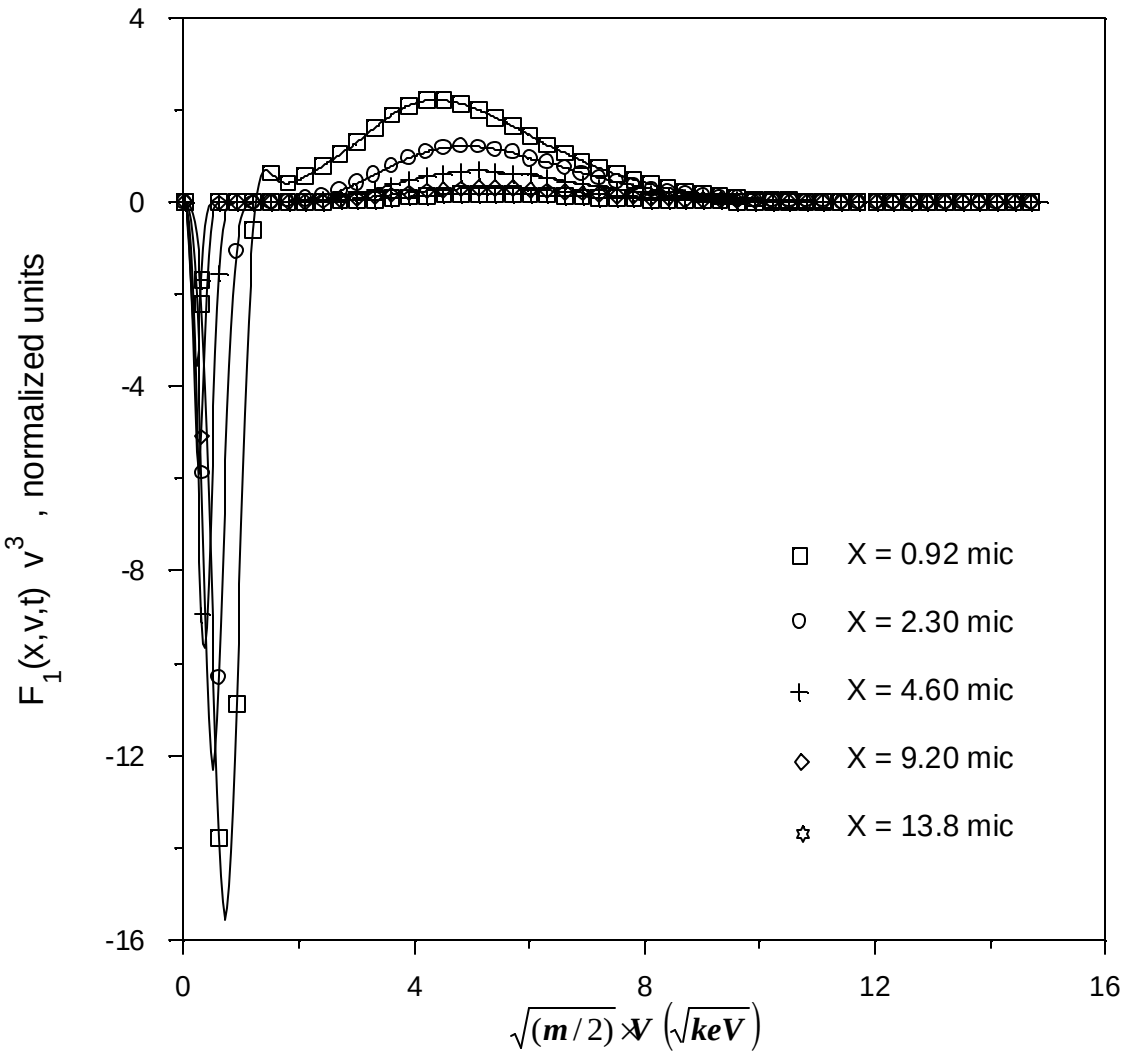

Differential electron flux

$$F_1(x, v, t)\, v^5, \quad \frac{1}{3}\int_0 F_1(x,v,t)\, v^3\, dv = J_e(x,t) \quad 0$$

2) $I_{0Hot} = 5 \;\; 10^{16}$ W/cm^2 , $T_{0Hot} = 20$ keV, n=-1/2, Beam-like

FWHM: 1.2 ps, t = peak + 100 fs

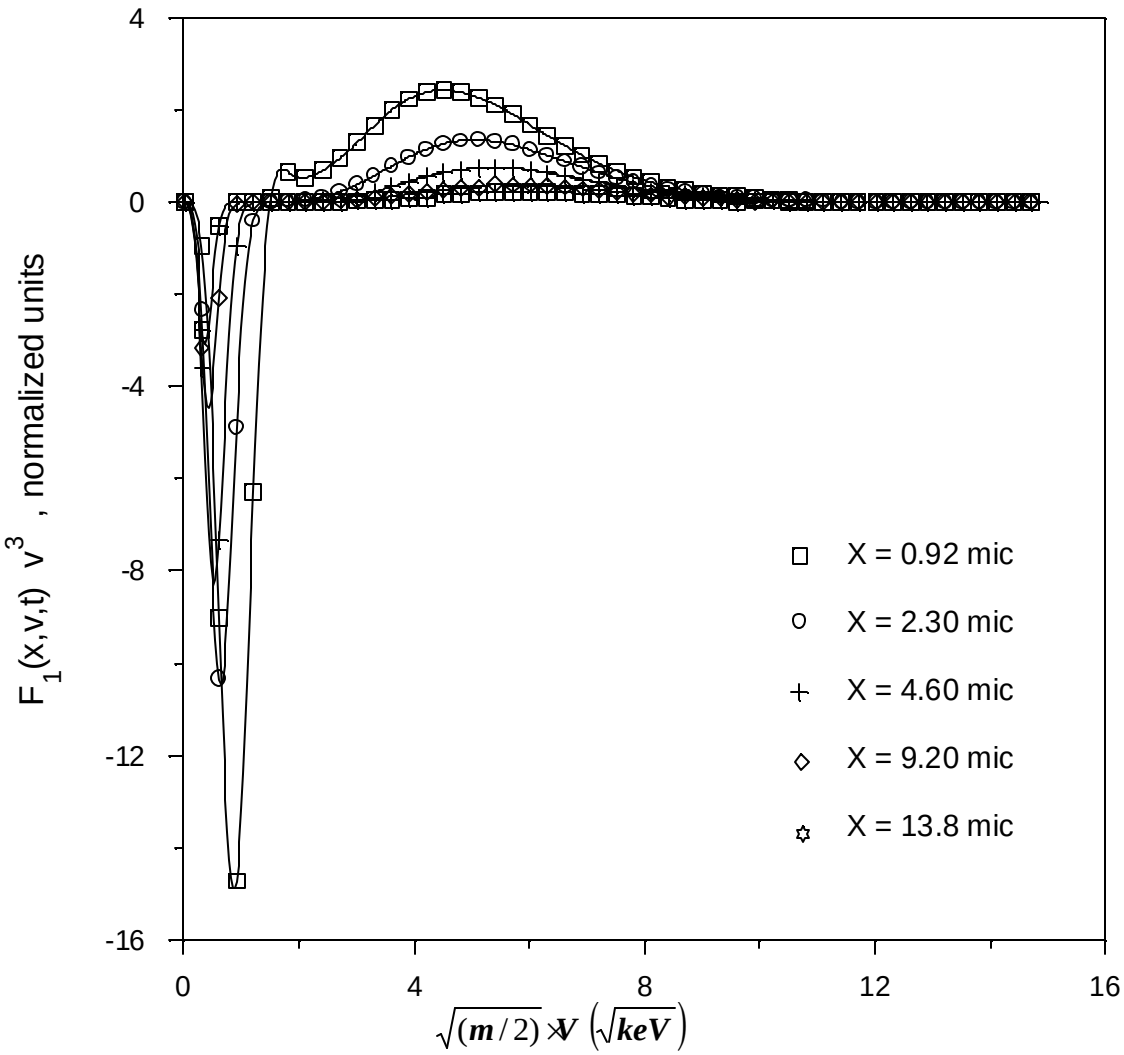

Note: The return current is carried by thermal electrons

Differential electron flux

$$F_1(x, v, t)\, v^3, \quad \frac{1}{3}\int_0 F_1(x,v,t)v^3\,dv = J_e(x,t) \quad 0$$

3) $I_{0Hot} = 1 \;\; 10^{18}$ W/cm^2 , $T_{0Hot} = 40$ keV, n= 1/2, Beam-like

FWHM: 600 fs, t = peak

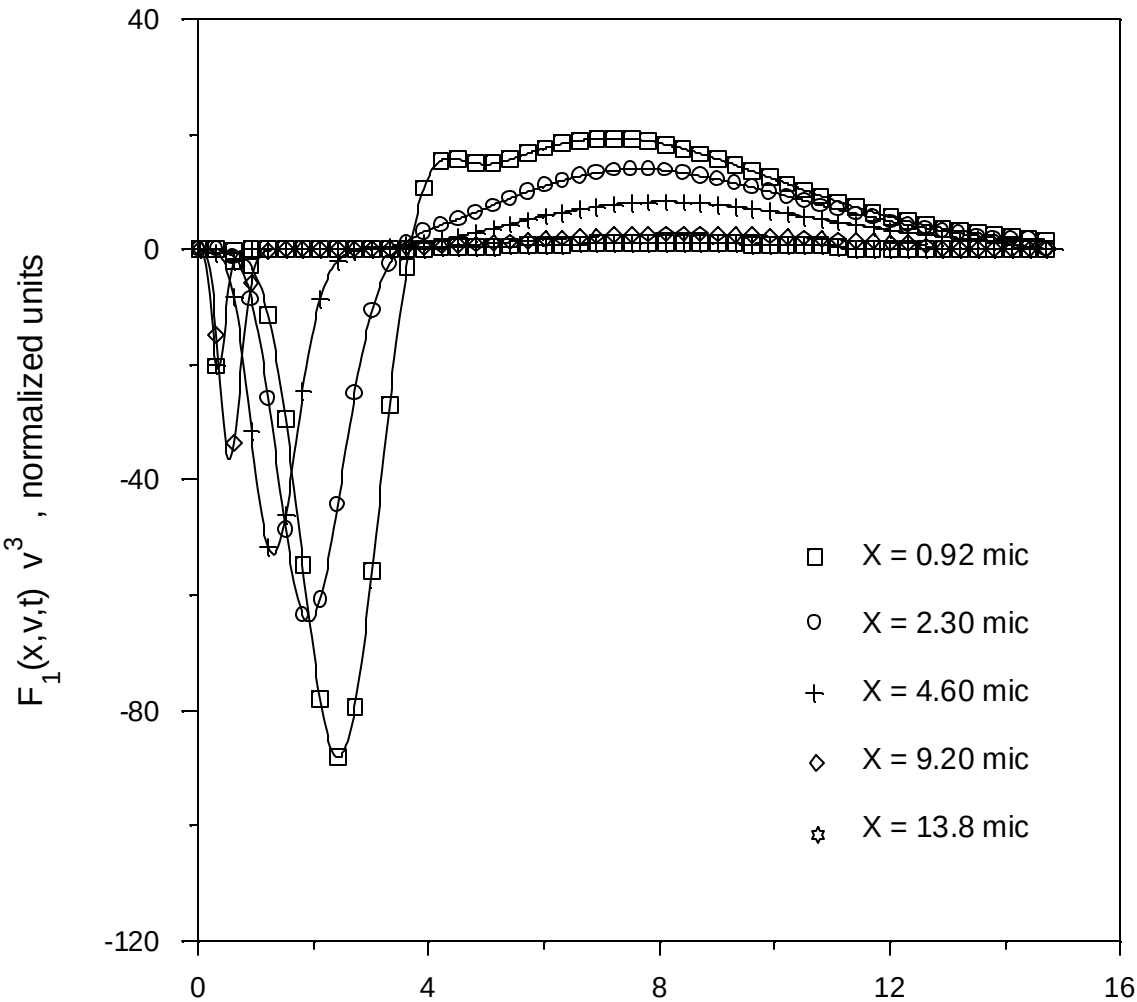

Return current is carried by thermal electrons.
Negative minimum at about 1.5 ($k_B T_C/m_e$) near the edge.
This ratio is somewhat higher deeper inside.

Differential electron flux

$$F_1(x, v, t)\, v^3, \quad \frac{1}{3}\int_0 F_1(x,v,t)v^3\,dv = J_e(x,t) \quad 0$$

4) $I_{0Hot} = 1 \;\; 10^{18}$ W/cm^2, $T_{0Hot} = 30$ keV, n=-1/2, Beam-like

FWHM: 300 fs, t = peak of pulse

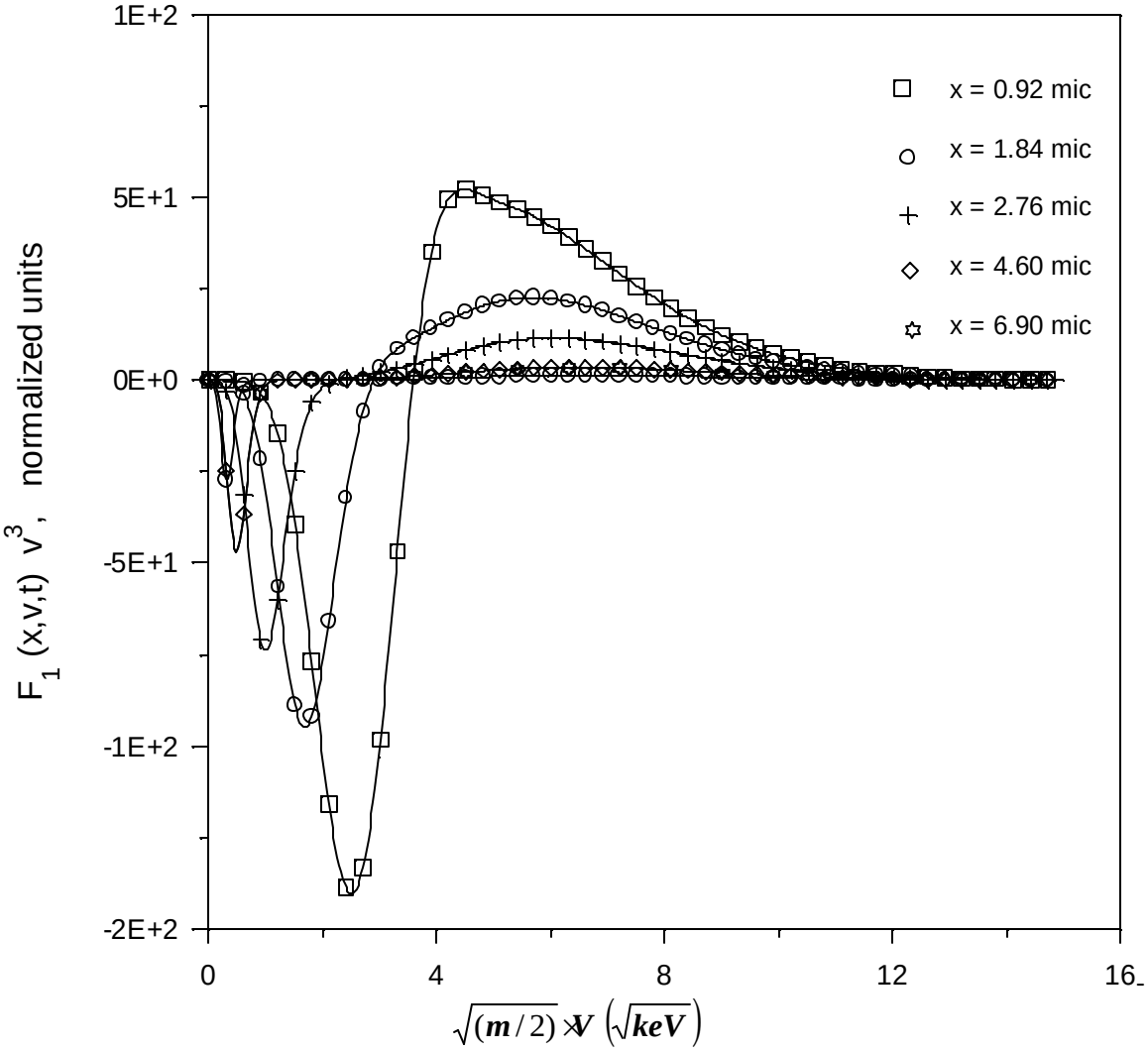

Same remarks as (3)

POST-PROCESSING FOR INSTABILITIES

2) **Ion-acoustic instability**

Preliminary analysis:

Instability if $|V_d| > C_s'$ *

($V_{"drift"} = V_d = V_{xm}$: V_x, at which ? $F(V_x, V_{perp})\, V_{perp}\, dV_{perp}$ is maximum)

* Define:

$C_s' = (k_B T_e'/M_i)^{1/2}$, where $k_B T_e' = m_e / \langle V^{-2} \rangle$

$C_s = (k_B T_e/M_i)^{1/2}$, where $k_B T_e = (2/3) m_e \langle V^2 \rangle$ (traditional sound speed)

C_s' is the correct sound speed, i.e. phase velocity for high k sound waves.

It is determined essentially by slow electrons.

For a single Maxwellian electron distribution, one would have $C_s' = C_s$.

We will plot both C_s' and C_s , for comparison to $-V_d$.

(minus sign omitted in plots)

Ion acoustic instability

1) $I_{0Hot} = 5\ \ 10^{16}$ W/cm^2 , $T_{0Hot} = 20$ keV, n=-1/2, Isotropic

FWHM: 1.2 ps, t = peak + 100 fs

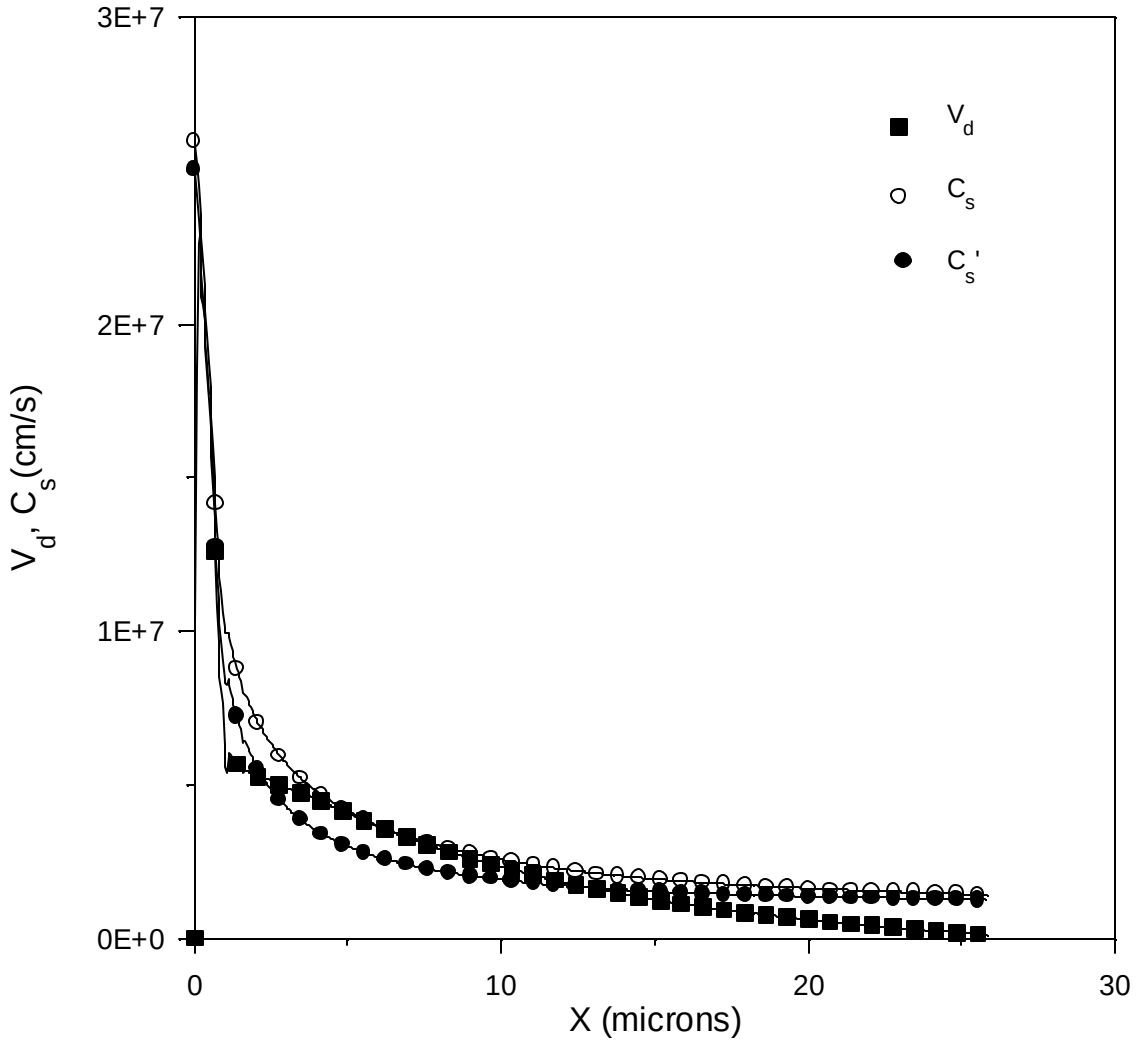

Ion acoustic instability

2) $I_{0Hot} = 5\ \ 10^{16}$ W/cm^2 , T_{0Hot} = 20 keV, n=-1/2, Beam-like

FWHM: 1.2 ps, t = peak + 100 fs

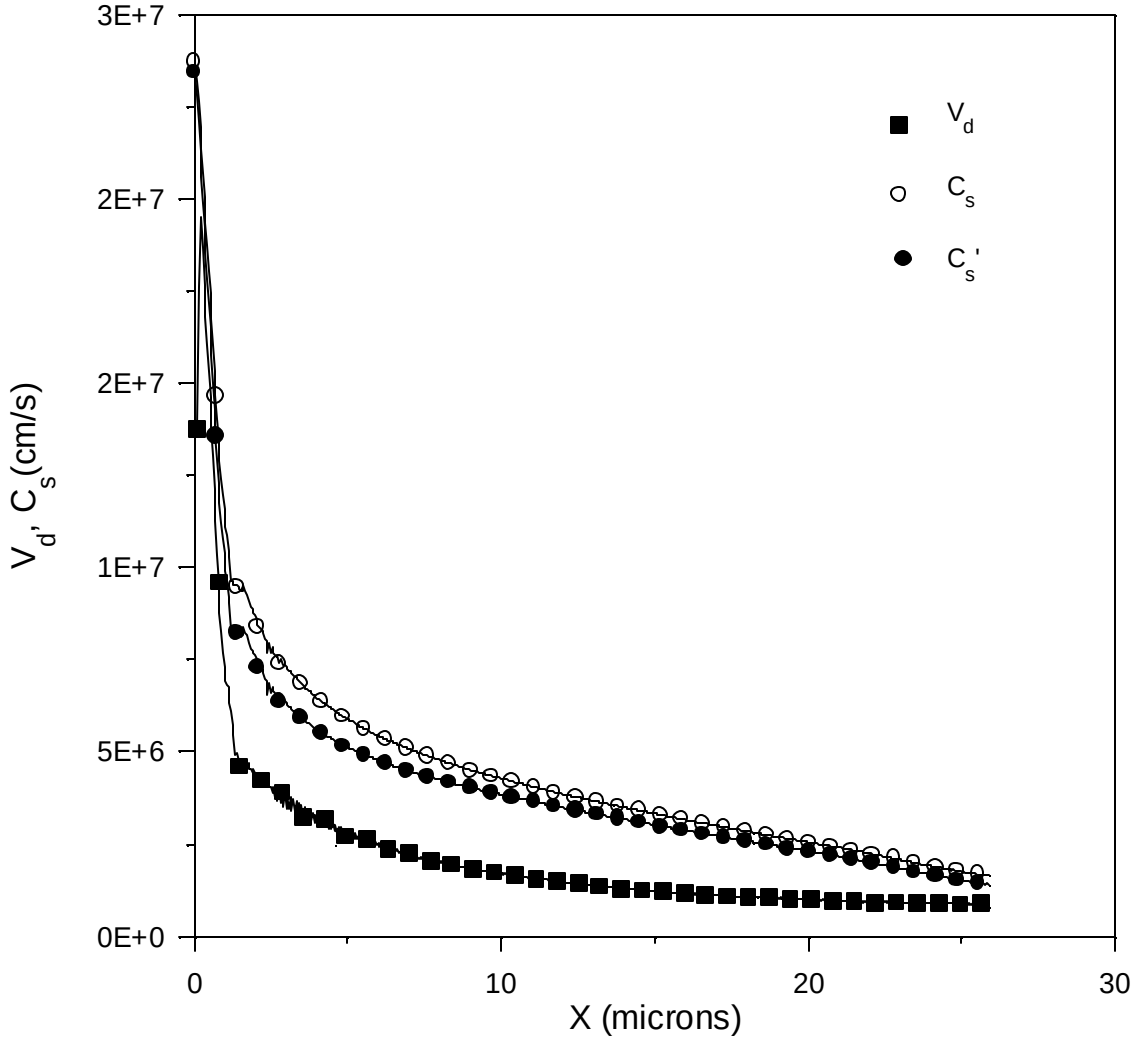

Drift velocity is lower than or near the sound velocity.

Instability will not grow at this low I_{Hot}

Ion acoustic instability

3) $I_{0Hot} = 1 \ \ 10^{18}$ W/cm^2 , $T_{0Hot} = 40$ keV, n= 1/2, Beam-like

FWHM: 600 fs, t = peak

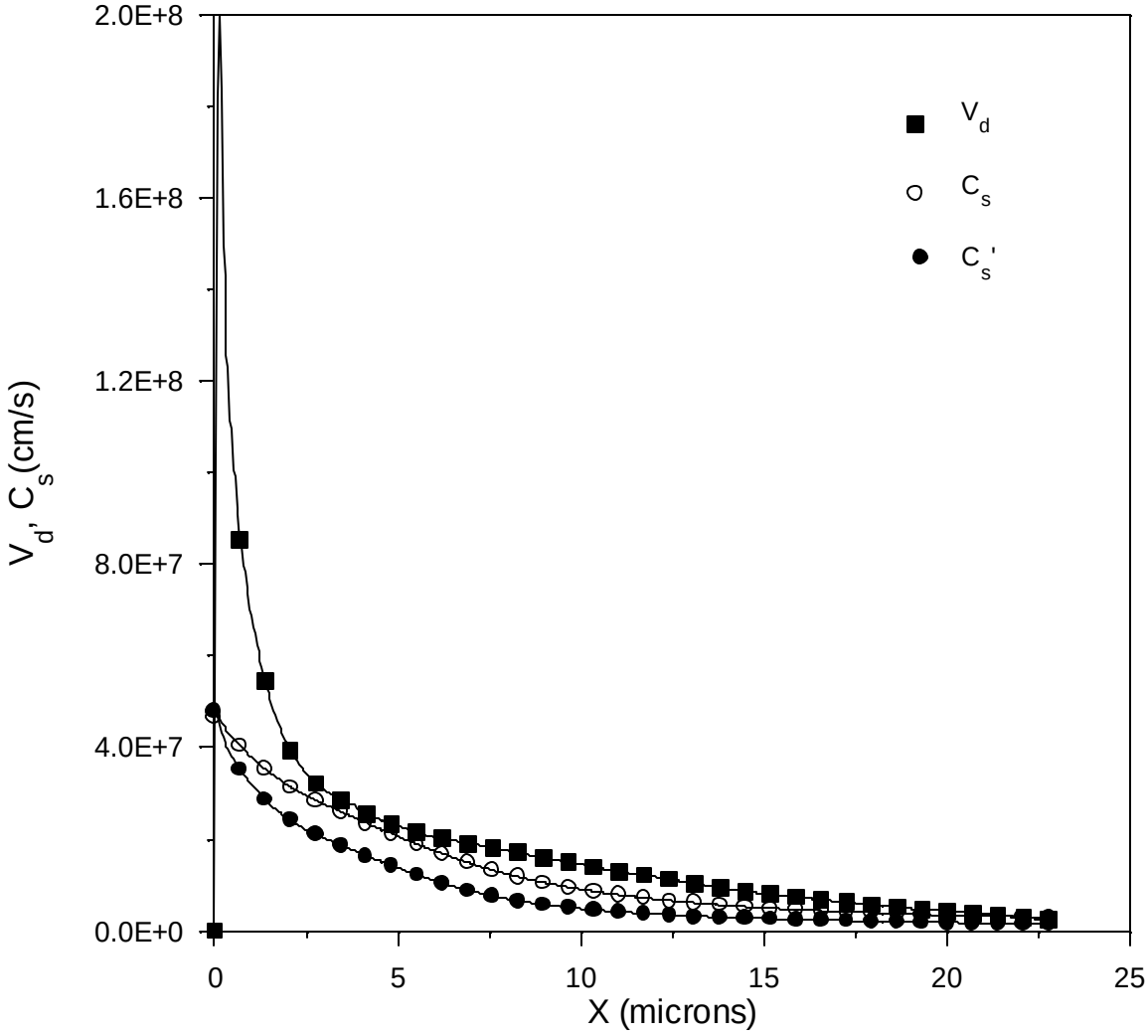

Drift velocity is higher than sound velocity.

Especially near edge.

Instability more likely to grow at this higher I_{Hot}.

Ion acoustic instability

4) $I_{0Hot} = 1\ \ 10^{18}$ W/cm^2, $T_{0Hot} = 30$ keV, n=-1/2, Beam-like

FWHM: 300 fs, t = peak of pulse

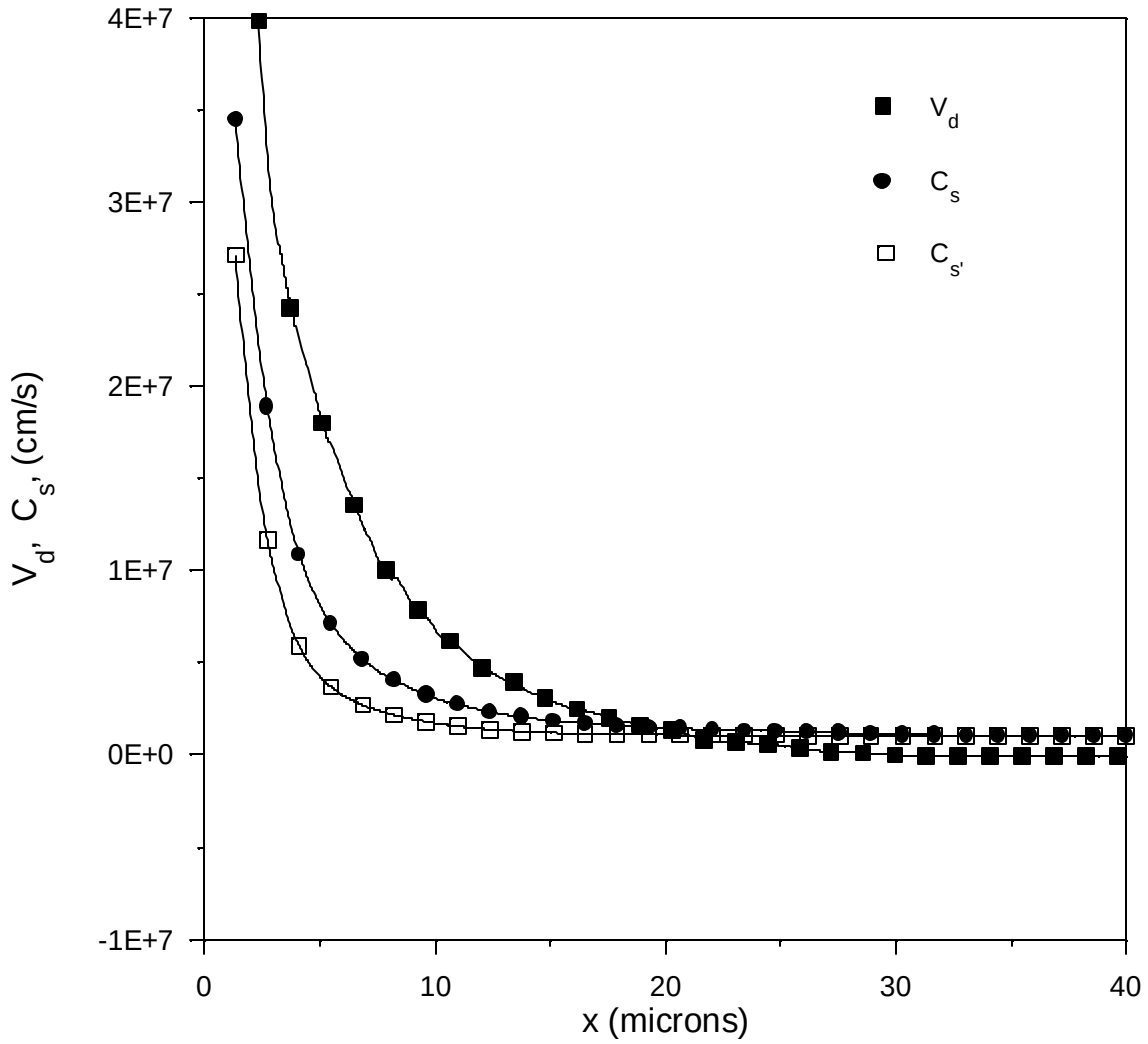

Here too, growth is likely to grow, as $V_d >> C'_s$ up to X ˜ 12 µm.

POST-PROCESSING FOR INSTABILITIES

Weibel instability (depends on F_2/F_0 at large V)

K_x mode: Excited if $F_2 < 0$

K_Y mode: Excited if $F_2 > 0$

Use: semi-collisional dispersion relations, from Bendib and Luciani (Phys. Fl. **30**, 1353 (1987)) ;

For beam-like hots:

Only the K_Y mode is unstable. ($F_2 > 0$)

For isotropic hot source:

Near source: K_x mode is unstable. ($F_2 < 0$)

(Transport effect: fast electrons with large $|V_x|$ spend less time near surface than those of same V, but larger V_{perp})

In depth: K_Y mode is weakly unstable. ($F_2 > 0$)

Similar to previous findings for collisional heating of thermals.

(Matte, Bendib, Luciani, PRL **58**, 2067 (1987))

Weibel Instability.

1) $I_{0Hot} = 5\ \ 10^{16}$ W/cm^2, $T_{0Hot} = 20$ keV, n=-1/2, Isotropic

FWHM: 1.2 ps, t = peak + 100 fs

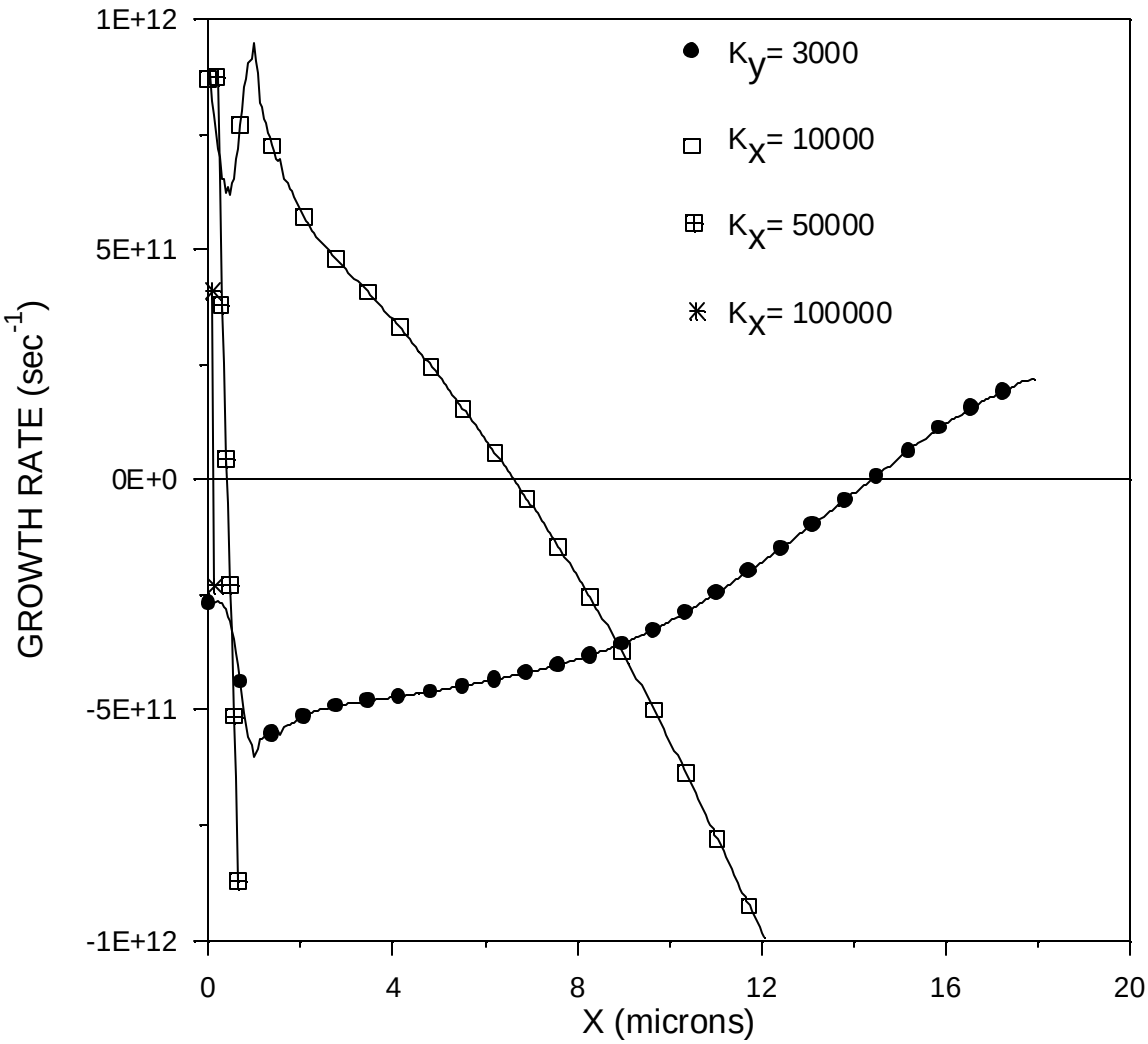

Both modes have weak growth rates, for this low I_{Hot}, and isotropic injection.

Weibel Instability.

2) $I_{0Hot} = 5\ \ 10^{16}$ W/cm^2, $T_{0Hot} = 20$ keV, n=-1/2, Beam-like

FWHM: 1.2 ps, t = peak + 100 fs

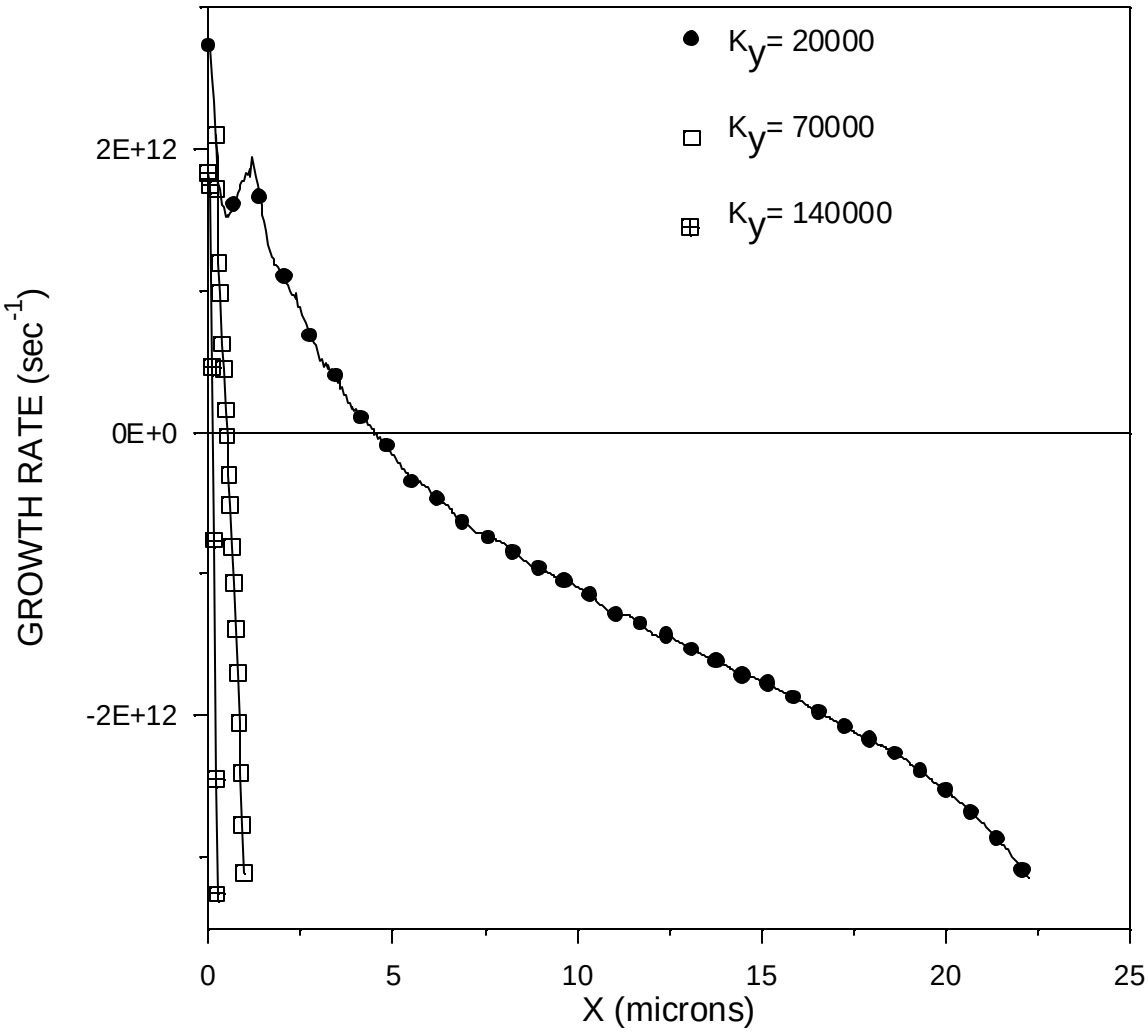

K_y mode has slightly less weak growth rate, for this low I_{Hot}, and beam-like injection.

Weibel Instability.

3) $I_{0Hot} = 1 \ \ 10^{18}$ W/cm^2, $T_{0Hot} = 40$ keV, n= 1/2, Beam-like

FWHM: 600 fs, t = peak

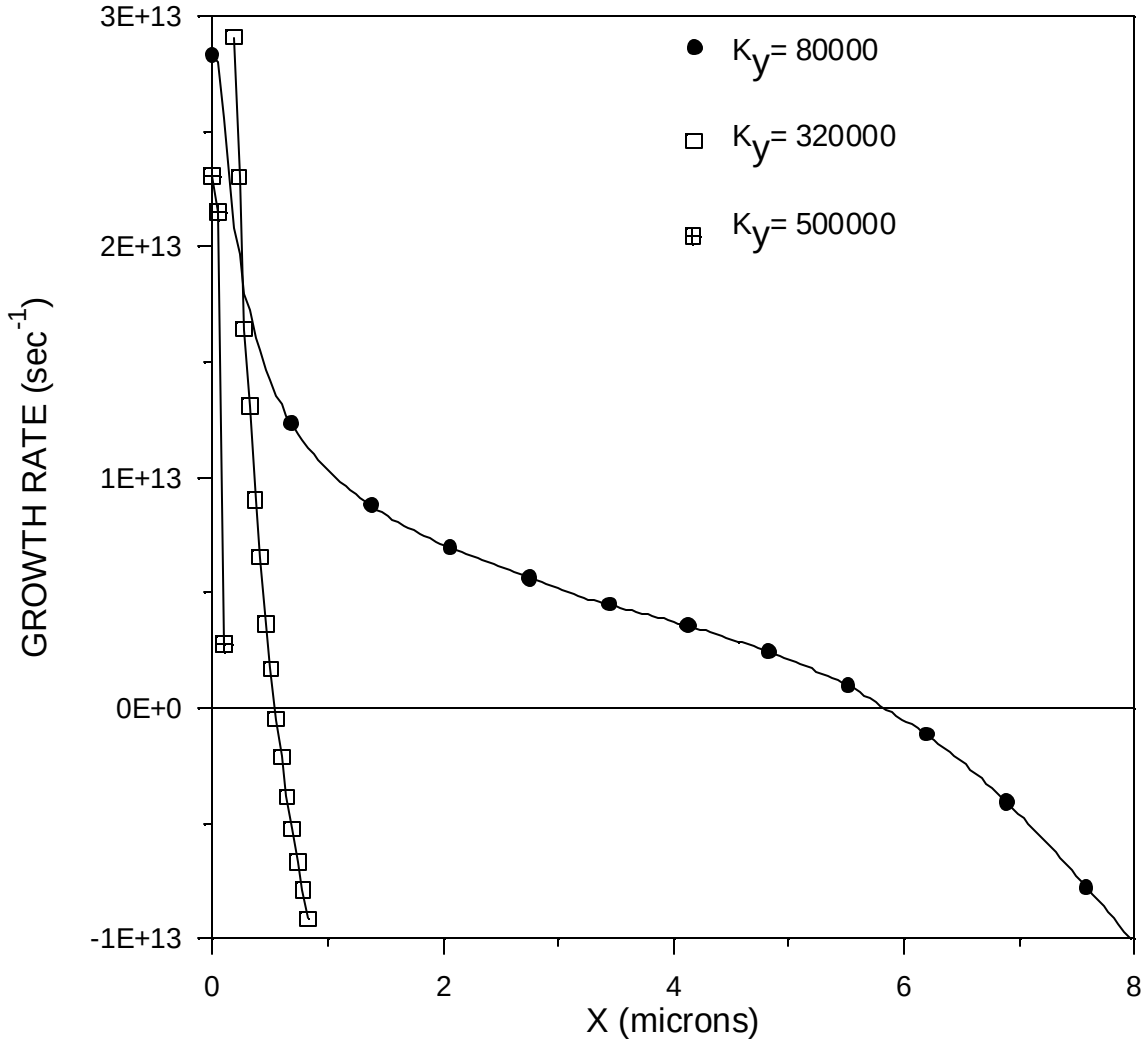

K_y mode has considerable growth rate,

for this higher I_{Hot}, and beam-like injection.

FWHM up to 20. (Near edge)

Weibel Instability

4) $I_{0Hot} = 1\ \ 10^{18}$ W/cm^2, $T_{0Hot} = 30$ keV, n=-1/2, Beam-like

FWHM: 300 fs, t = peak of pulse

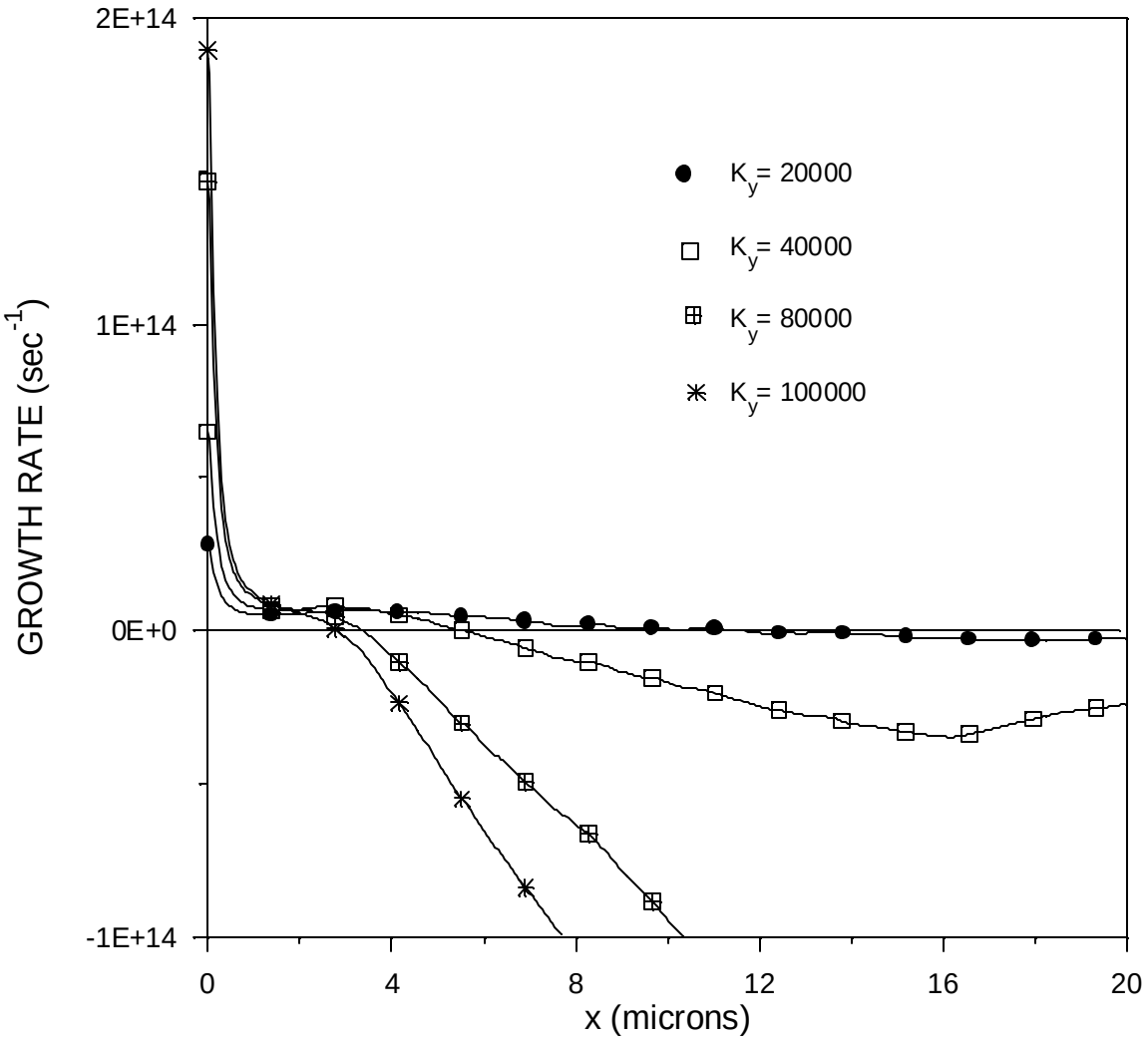

Very strong growth, but only very close to the edge

Electrical conductivity

? Classical electrical conductivity applicable for return current?

? Analysis of FPI runs: Get J_{ret}: $\frac{1}{3}\int_0^W F_1(x,v,t)v3dv=J_{ret}(x,t)$

s = E/ J_{ret}.

W: velocity v at which $F_1(x,v,t)$ changes sign.

? Classical conductivity.

Obtained, using T_{cold} from 2 temperature fit.

Electrical conductivity

3) $I_{0Hot} = 1 \ 10^{18}$ W/cm^2 , $T_{0Hot} = 40$ keV, n= 1/2, Beam-like

FWHM: 600 fs, t = peak of pulse

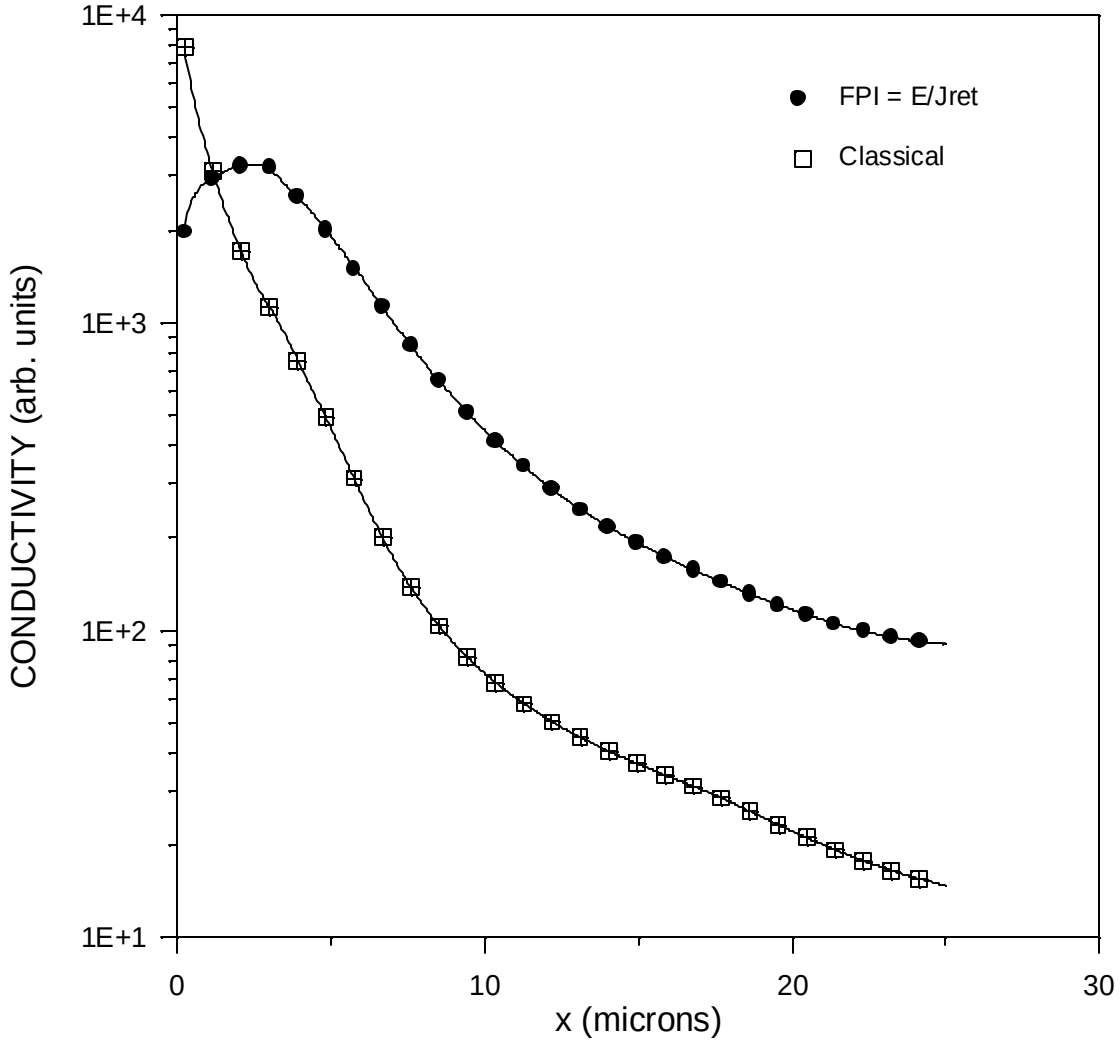

Conductivity considerably above classical, deep inside.

Non-local physical effects?

Electrical conductivity

4) $I_{0Hot} = 1\ \ 10^{18}$ W/cm^2, $T_{0Hot} = 30$ keV, n=-1/2, Beam-like

FWHM: 300 fs, t = peak of pulse

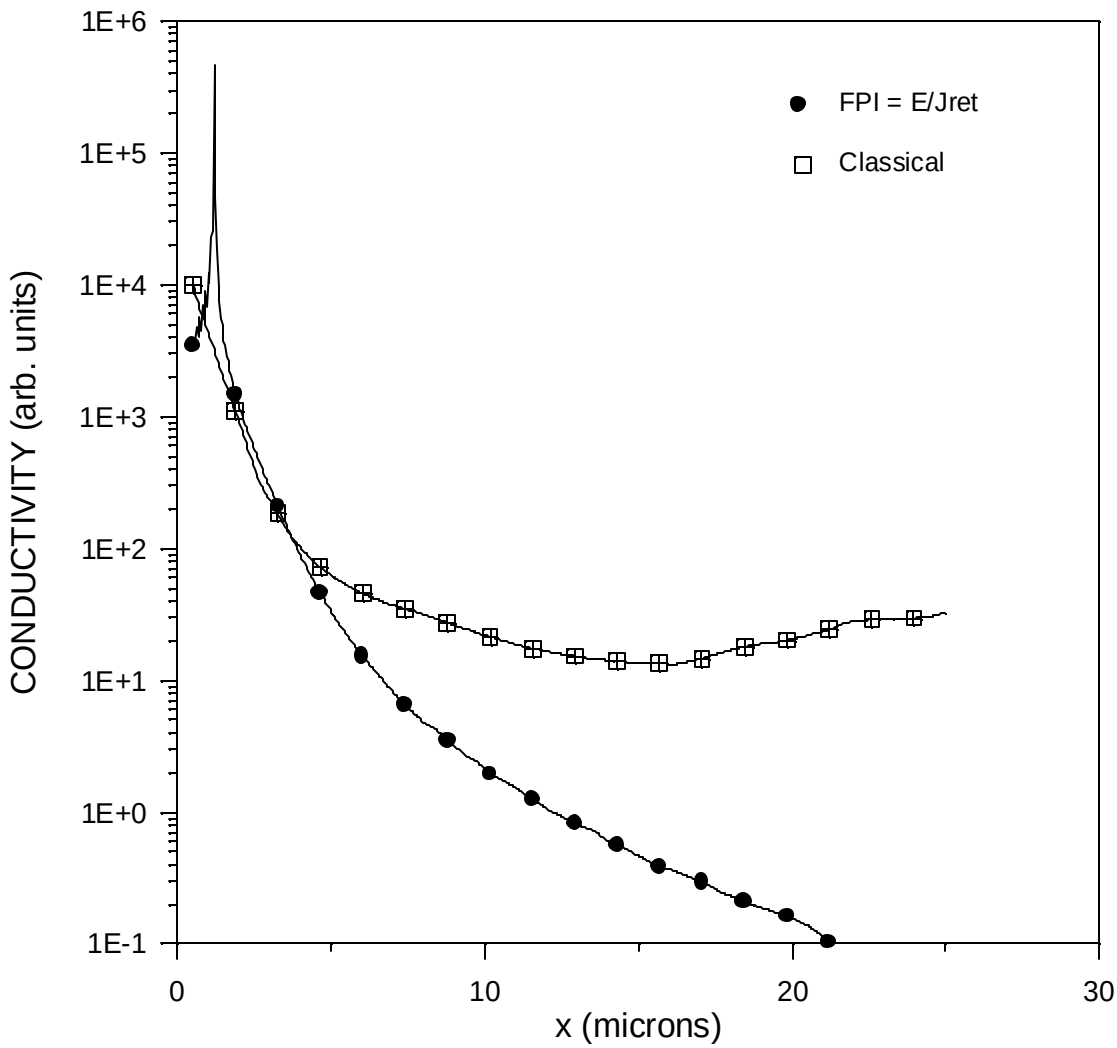

Opposite tendency: conductivity below classical. More study required

Note: Analysis is preliminary.

Difficulties: Getting the relevant T_{cold},

Separating J_{ret} from J_{Hot}

CONCLUSIONS

(preliminary)

The transport of hot electrons in solid density matter was simulated with an electron kinetic code.

Matter is heated and ionized in depth.

Hot and thermal components of the energy distribution are very distinct.

Energy flux is carried by the hots ; return current by the thermals.

Distributions unstable for both ion-acoustic and Weibel modes only for highest power, $I_{0Hot} = 10^{18}$ W/cm^2, not at $5\ 10^{16}$ W/cm^2.

- Beam-like injection is more favorable to the Weibel instability.

Electrical conductivity is non classical.

Next simulations and future work:

- Increase I_{Hot}.
- Vary other parameters of hot source: T_{Hot}, F_{0Hot} and anisotropy
- Do other materials. Results on Ta are too preliminary.
- Pursue and improve instability analyses.
- Add diagnostics, especially continuum X-ray spectrum and angular distribution.
- Improve electrical conductivity analysis.

  Seek formula for a future hybrid code (fluid colds, kinetic hots)

  (Should give a huge reduction in CPU time)

Propagation of petawatt laser-generated electron beams through solid density plasma

***R.B. Campbell*, T.A. Mehlhorn, S.A. Slutz, Sandia National Laboratories,**

D.R. Welch, Mission Research Corporation.

J.S. DeGroot and T.L. Marshall, U.C. Davis

Talk Outline

- Problem of laser-produced relativistic electron beam.
- The expansion of the REB
- LSP Code
- Effect of background bulk parameters, analytic estimate
- Possible method of improving beam collimation
- Conclusions and further work.

Problem of laser-produced REBs

- PW lasers interacting with solid material generate relativistic electron beams with currents that far exceed the Alfven current limit.

- These beams must propagate several hundred microns tightly collimated without deleterious instabilities:

- Beam must maintain a small footprint; on the order of the laser beam spot size.

- Experimental data indicates beam blows up to 100 micron diameter, this must be controlled.

GOALS:

- Understand the physics controlling the beam envelope evolution

2) Find ways to keep this blowup from happening

LSP Is Versatile in Its Ability to Treat Multiple Time and Spatial Scales

- Modified for this application under a MRC/Sandia agreement
- Uses a hybrid algorithm to address the issues concerning beam interaction with high plasma densities.
- Energy-conserving implicit and explicit algorithms including particle collisions.
- Plasma electrons are described with PIC methods using either fluid or kinetic equation
- The implicit algorithm useful for very dense plasmas where the details of electron plasma oscillations can be ignored.
- The explicit algorithm, requiring resolution of the plasma and cyclotron frequencies, includes a CIC (cloud in cell) method that greatly reduces numerical noise.
- Algorithm does not require that the Debye length be resolved to avoid grid heating.
- Coulomb scattering is modeled in Monte Carlo fashion. Spitzer collisions only; inelastic collisions with bound electrons are not yet included in these simulations.

Implicit E-beam Propagation

- 2-D, cylindrically symmetric, implicit hybrid mode.
- 200 micron thick foil comprised of an initially 5 eV pre-ionized CH plasma at solid density.
- foil electrons are treated as a PIC fluid at a density of 1.8×10^{23} cm^{-3}.
- beam electrons are treated as kinetic PIC particles and have a directed kinetic energy of 1MeV, 1MeV spread, and spot diameter of 30 microns, current density of 6×10^{12} A/cm^2.
- All heavy species are treated kinetically.
- The timestep used in the simulations was typically 0.8 fsec, several plasma periods.
- The cell side dimension is as small as 2.5 micron.
- With this problem setup, we can study large-scale filamentation, beam hollowing, beam dynamics, lose information associated with the fast temporal and fine spatial scales.

Without Intervention, Beam Collimates at 3-6x Injection Spot Size

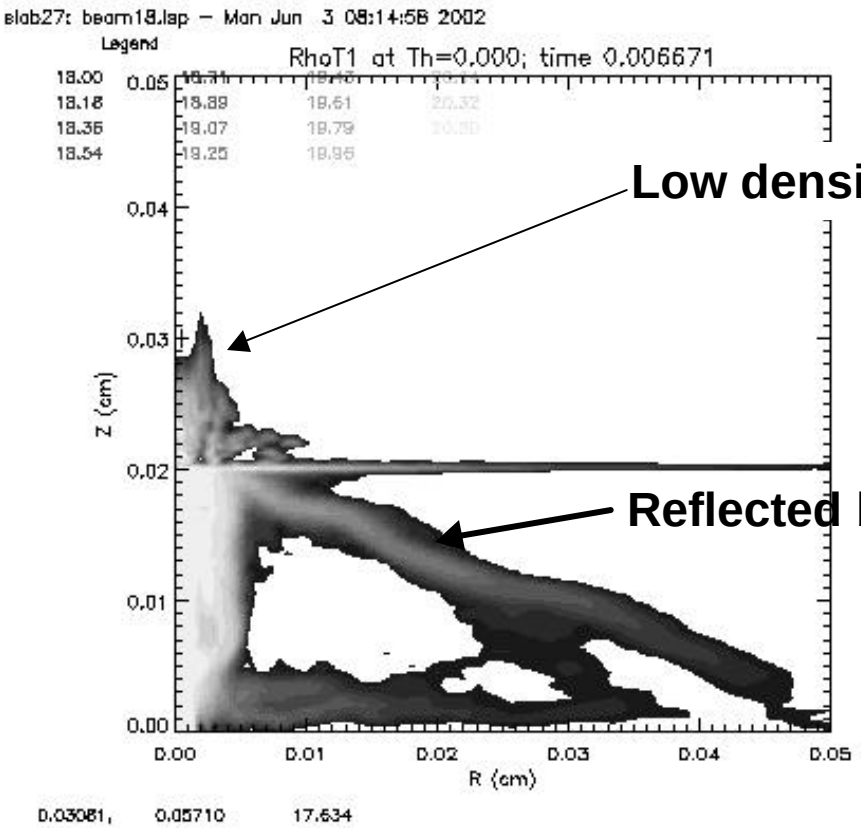

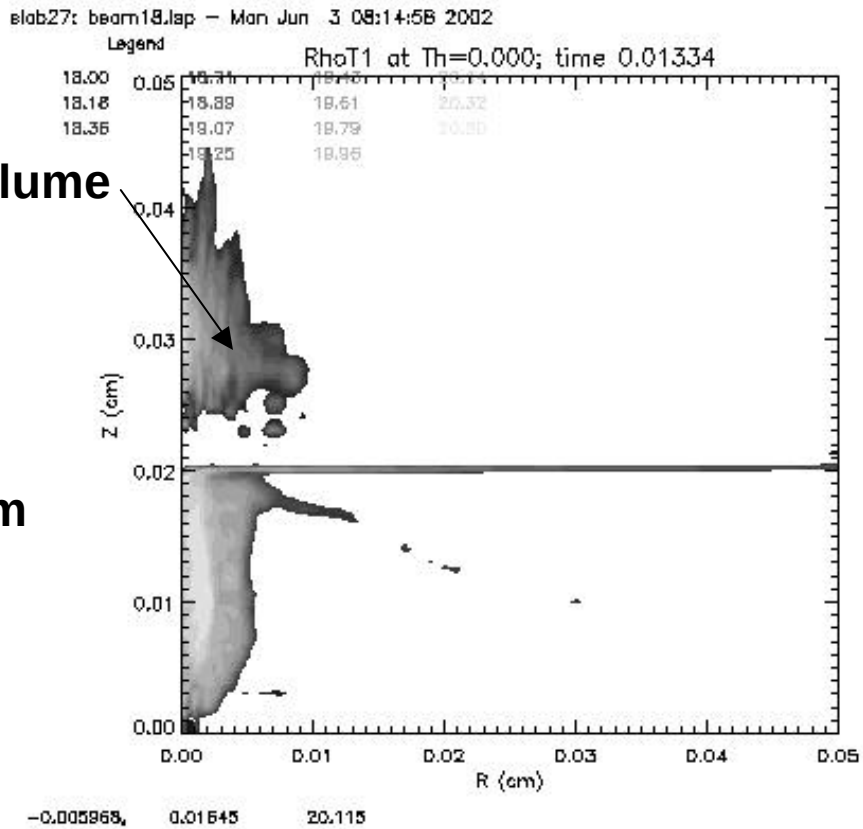

Low density plume

Reflected beam

Some large scale beam filamentation is evident

Controlling of the Beam Envelope Size and Shape Is Important

FI applications prefer beam spot size to be comparable to the laser spot

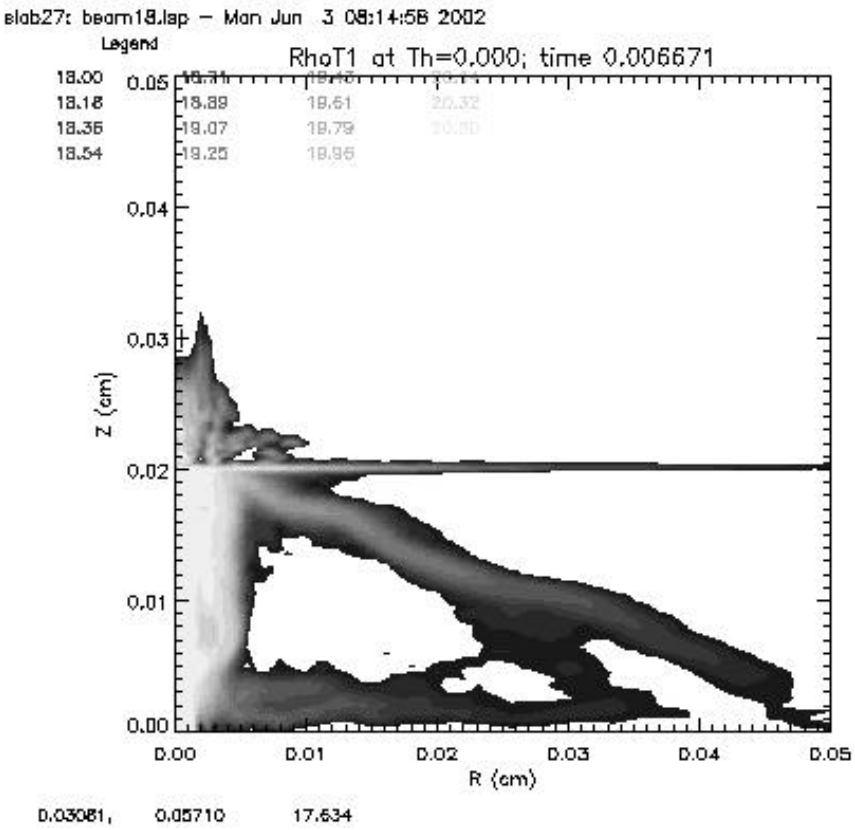

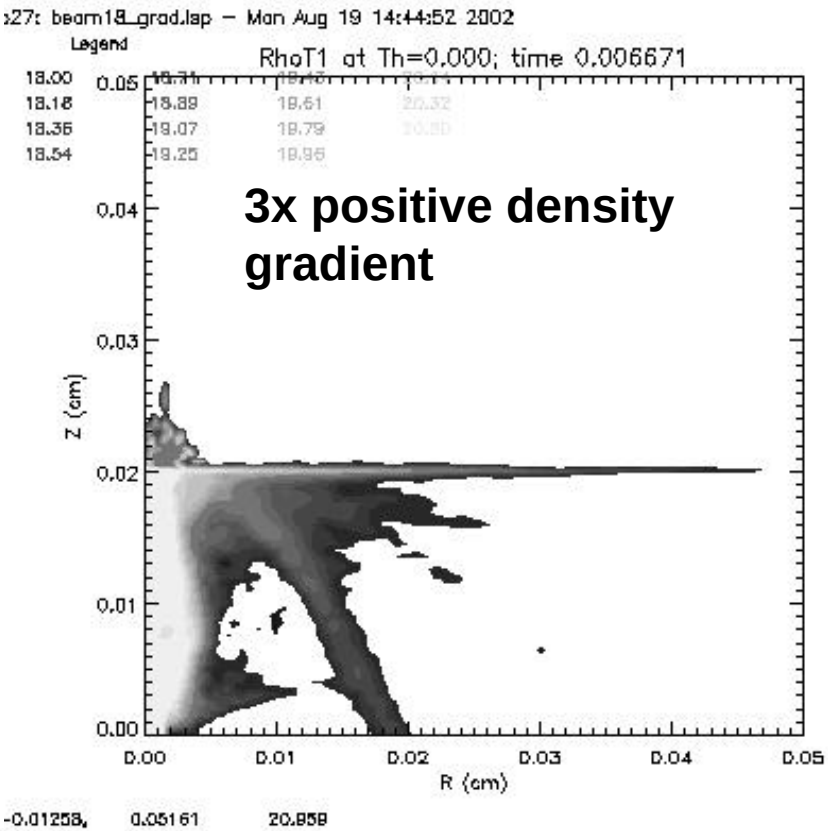

Background plasma bulk properties tend to have a noticeable effect on beam envelope dynamics.

Injection into higher density seems to keep the beam more tightly collimated

- At same beam power input, higher density implies lower plasma temperature, hence lower electrical conductivity.

- Lower conductivity implies faster current penetration into net current column, so beam envelope equilibrium occurs at a smaller radius.

- Analytic estimates of electron jet dynamics seem to support this view that radial magnetic field diffusion through the current channel is an important element of the physics.

Beam Envelope Leans on Hollow Magnetic Field Profile

Hot electron density

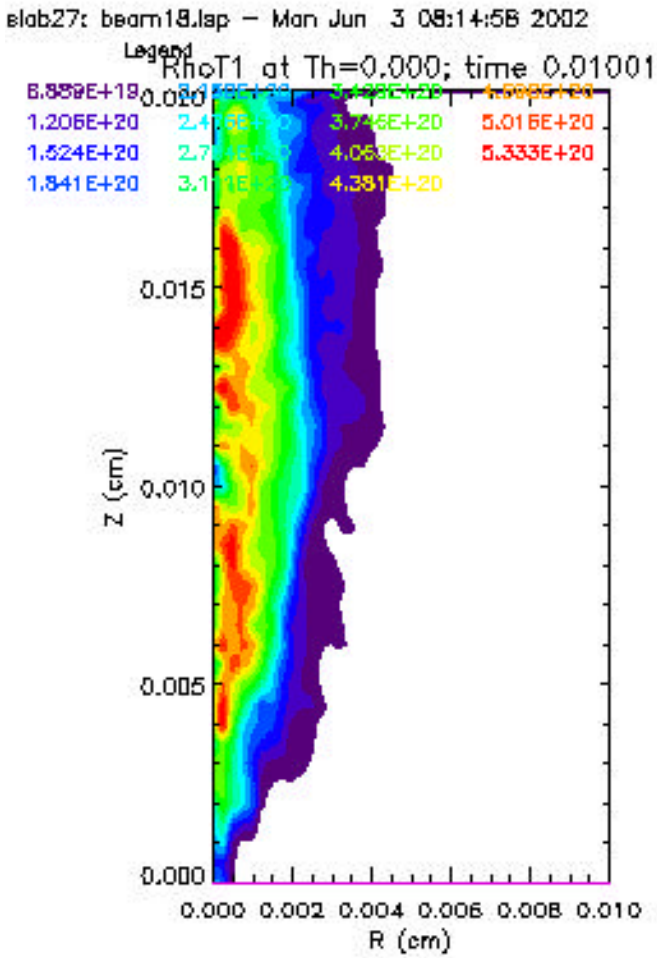

Mod-B contours

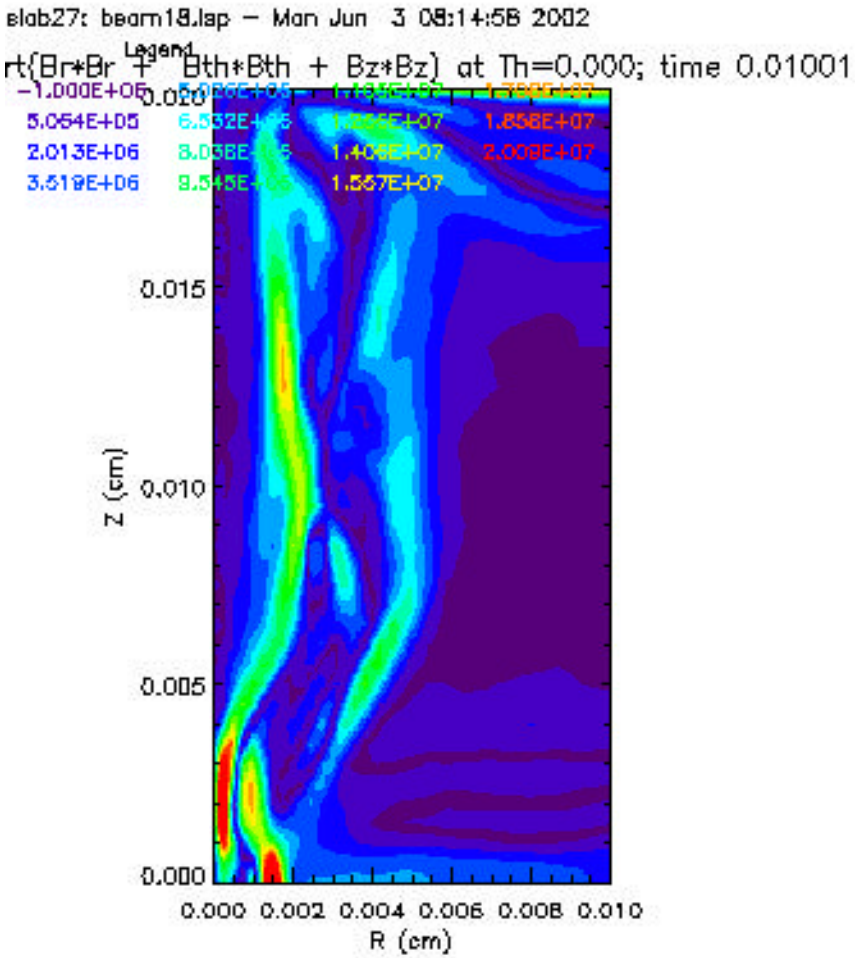

Current Neutralization Solution Shows a Hollow Magnetic Structure

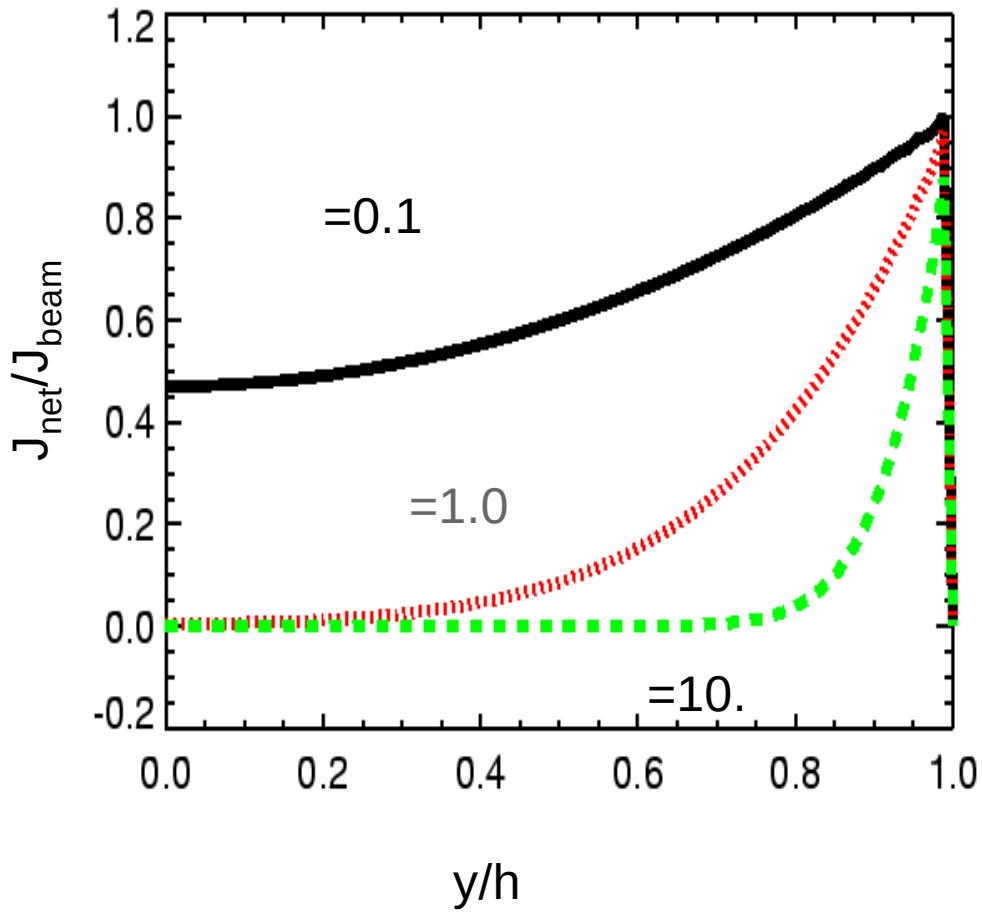

Analytic Fourier solution obtained with the simplifying assumptions

… Ohms law with constant conductivity

… charge neutrality

… Cartesian symmetry

Each mode has a diffusion time scale

…

$$t_n = m_0 s (2h/np)^2$$

Magnetic Trapping Determines the Radius of the Propagating Beam

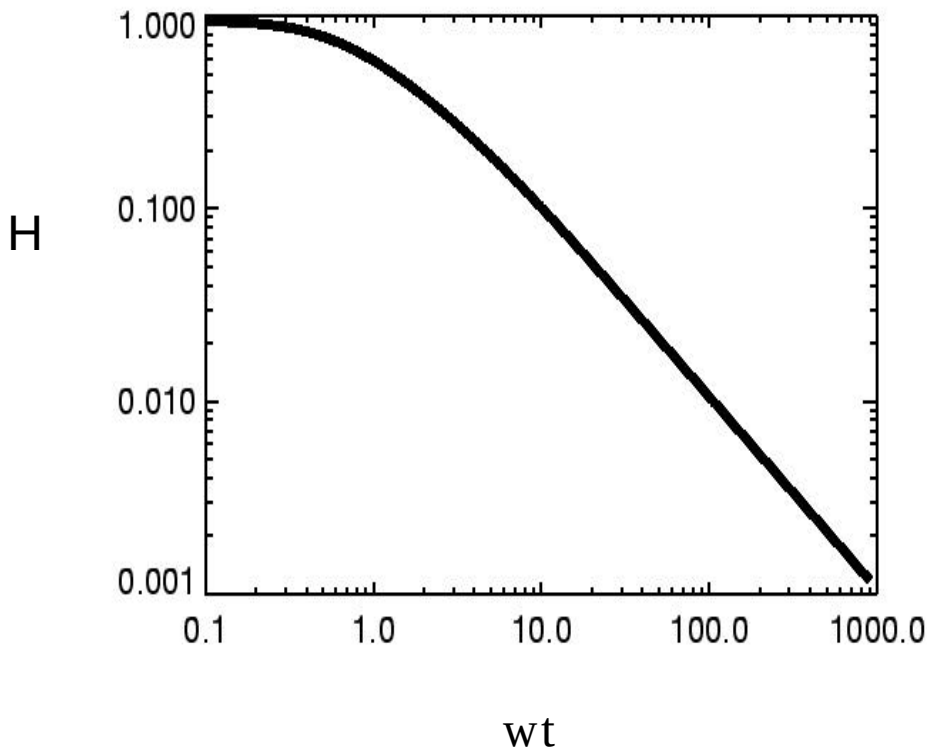

$$H = Bdr/(m_0 I_{beam}/4p)$$

The condition for trapping of the beam particles is

$$Bdr = 4mvg \sin^2(q/2)\cos(q/2)/q$$

The beam is hollow because particles spend more time at the outside where they are reflected

Beam heating raises the conductivity and decreases the trapping

Lowering the conductivity should decrease the beam size.

A Collimation Mechanism May Be Possible by Using Radial Zones of Dissimilar Materials

- **Observe that strong axial sheaths are formed on front and back when beam penetrates the foil, confining the hot electrons.**
- **The sheaths form where there is an axial electron density gradient.**
- ***Use this fact to achieve radial confinement by a radial electron density gradient*.**
- **By using dissimilar materials of varying Z, we might be able to tailor the electron density profile to suit our needs.**
- **Two examples:**

  Straight column plug

  Conical plug

Cartoon of Possible Collimation Mechanism

One material foil

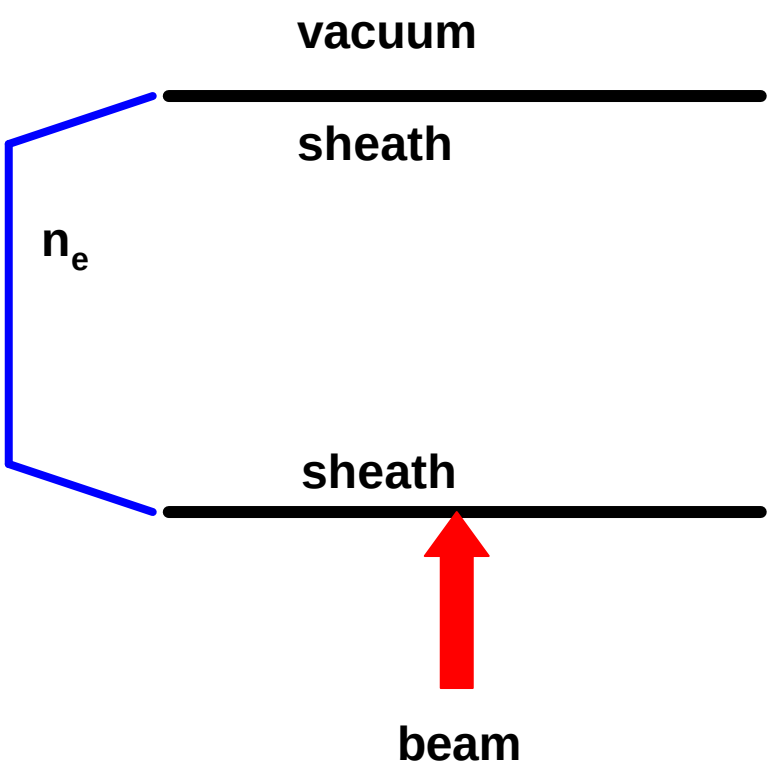

Multi-material foil

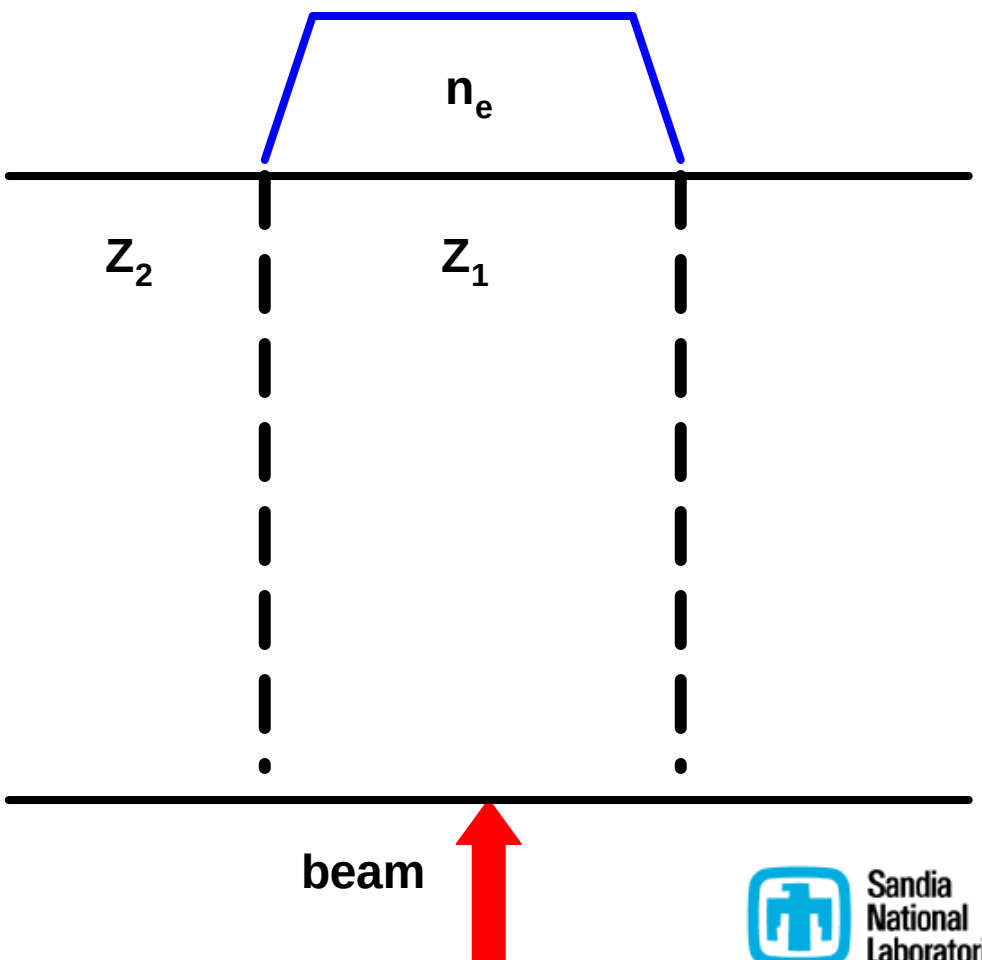

Two Examples of Collimation Geometries

Straight walled plug

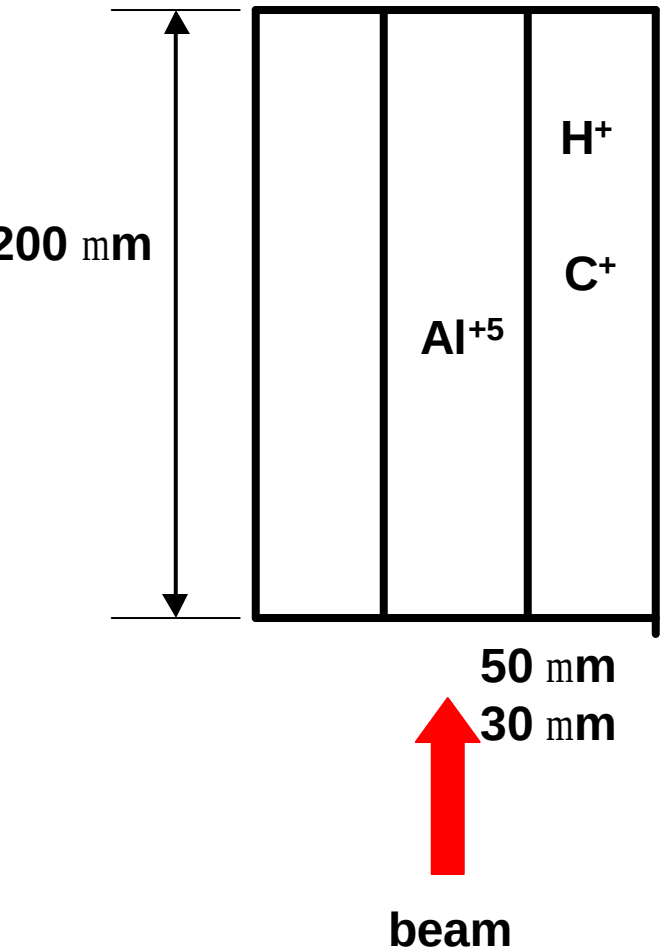

Conical plug

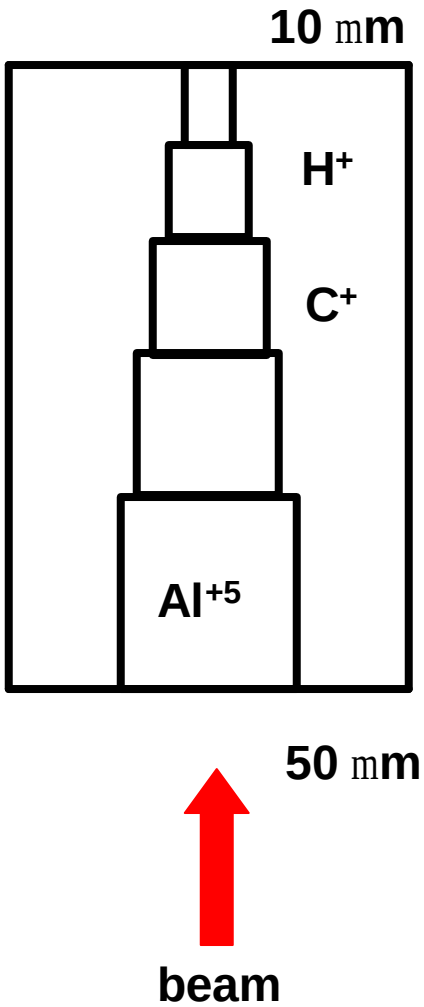

LSP uses rectangular meshes

One Material, Nominal Behavior, 6.67psec

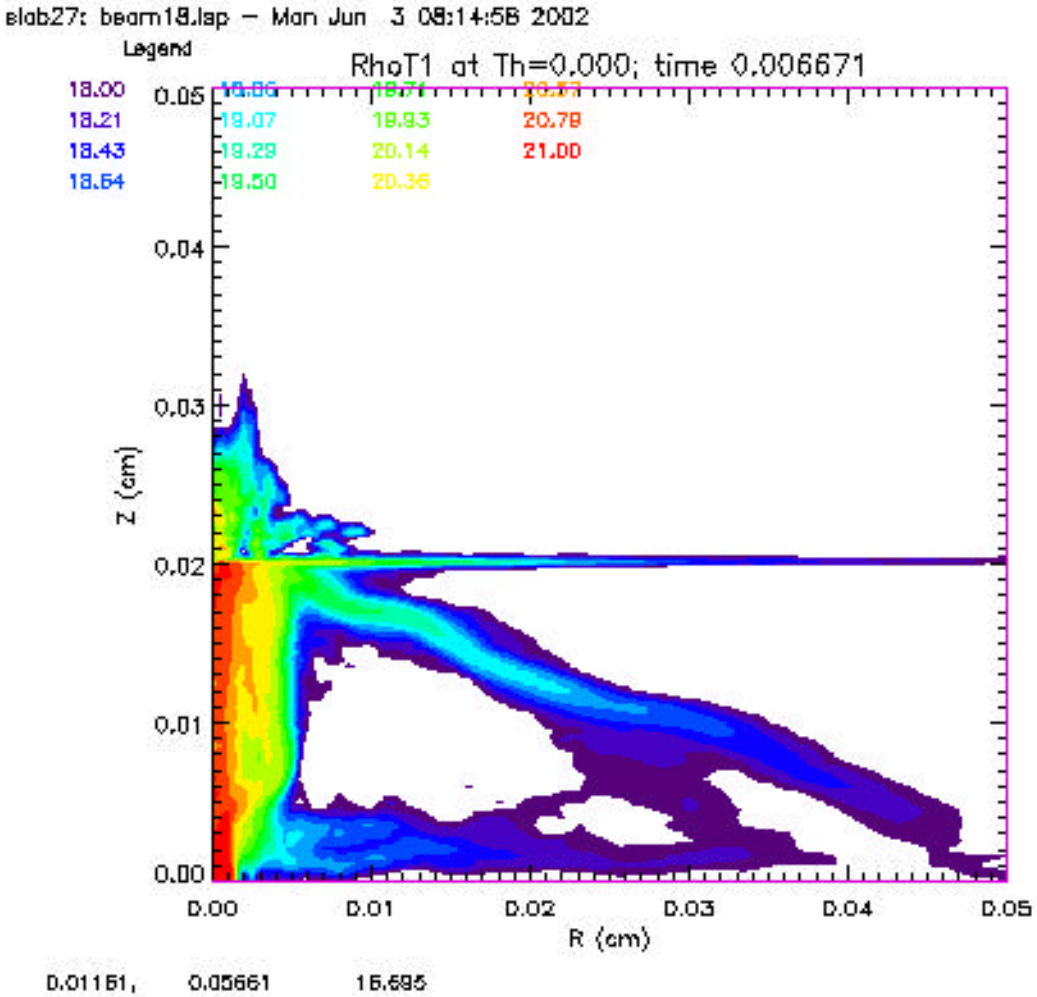

Nominal Beam Behavior, One Material

Straight Walled Plug 2 Material, 50 Micron Diameter, 6.67 psec

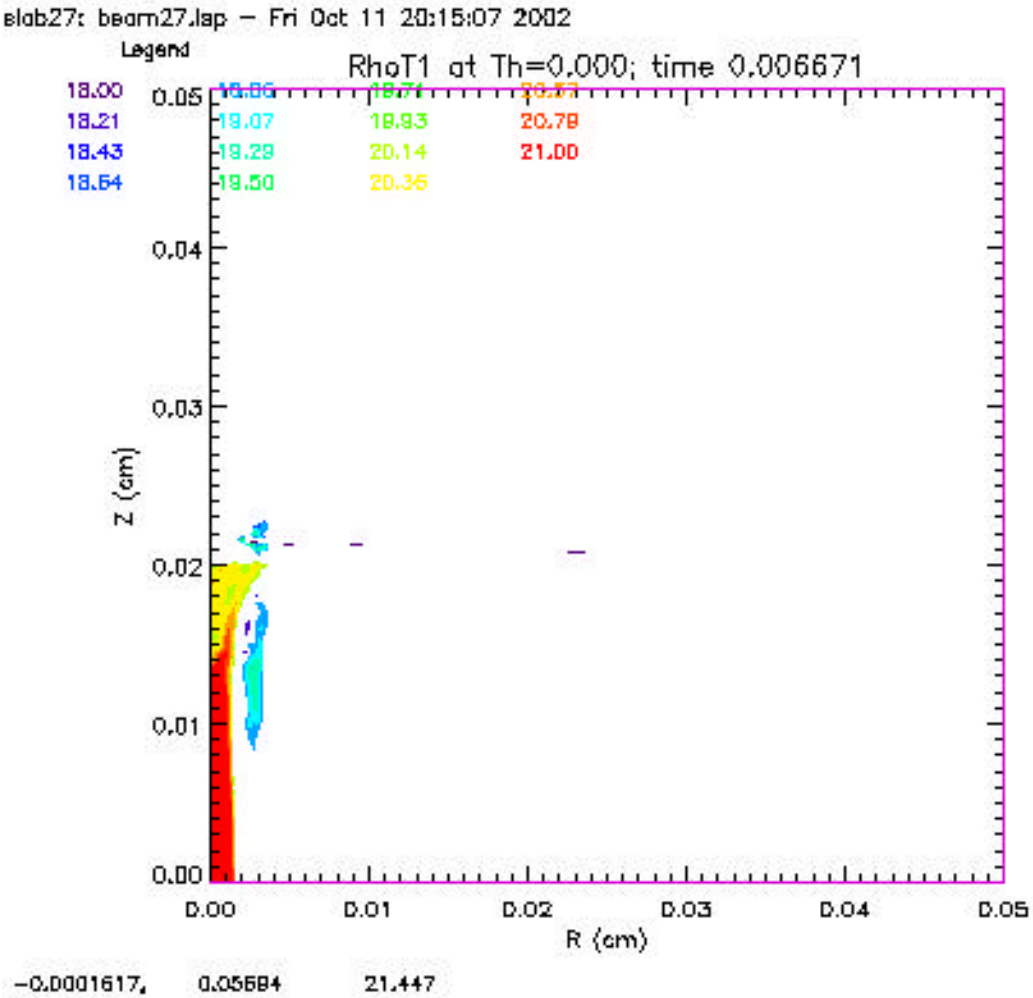

Straight Walled Plug 2 Material, 50 Micron Diameter

Conical Plug, 50 to 10 Micron Diameter, 6.67psec

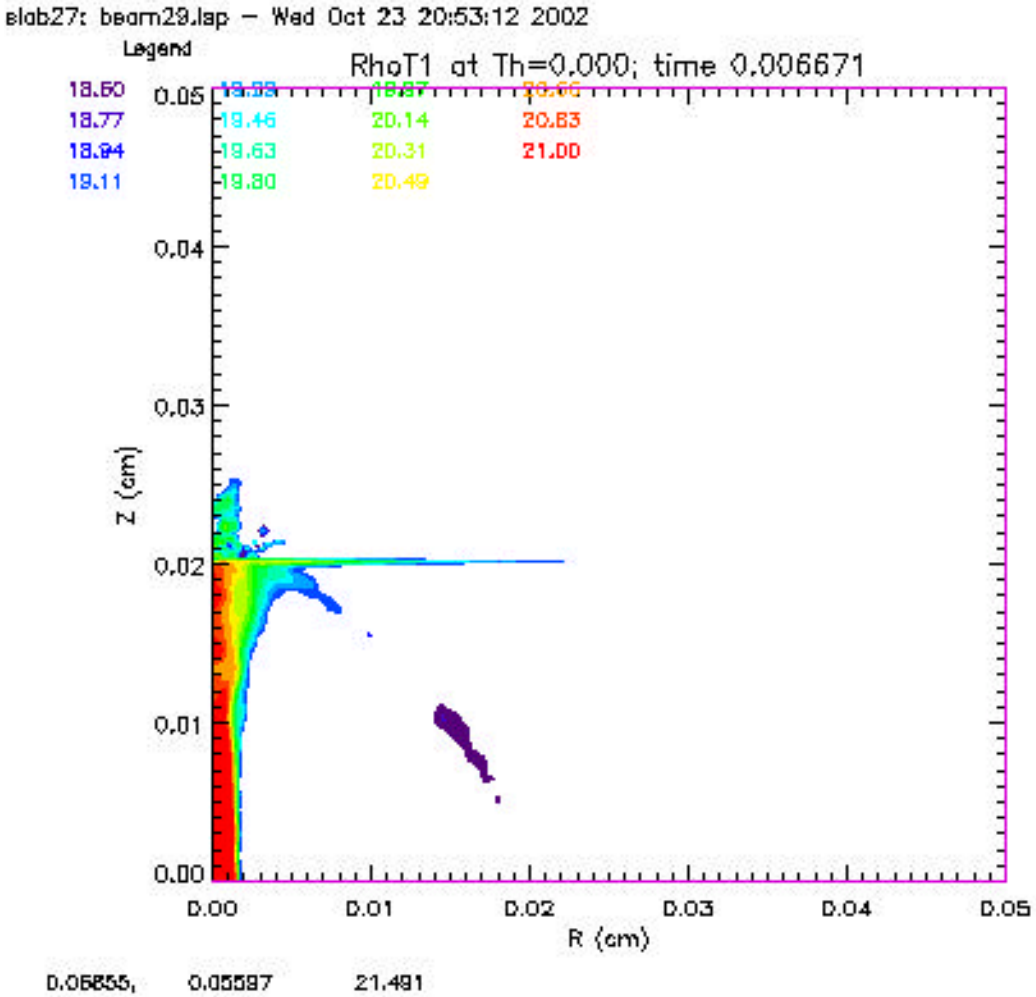

Conical Plug, 50 to 10 Micron Diameter

Conclusions

- The envelope of the beam self-consistently evolves to a diameter several times the incident laser spot, but there appears to be ways to influence this transverse size.

- The effect of bulk electrical conductivity seems consistent with analytic estimates, and is related to hot electrons interacting with the hollow self-consistent magnetic field structure.

- By considering layers of dissimilar materials, radial collimation seems possible, and would be an interesting subject of experimentation.

Imaging Ultra-High Current Electron Transport in Metals and Insulators by Laser-Accelerated Protons

T.E. Cowan, J. Fuchs, H. Ruhl, A. Kemp, P. Parks, Y. Sentoku, R. Stephens
(General Atomics-San Diego)

P. Audebert, J.C. Gauthier (*LULI, Ecole Polytechnique-Palaiseau)*

L. Gremillet *(CEA-Bruyeres le Chatel)*

A. Blazevic, M. Geissel, M. Roth *(GSI-Darmstadt)*

M. Hegelich, S. Karsch (*MPQ-Garching)*

GENERAL ATOMICS

FIW - 2002
St. Pete's, FL Nov. 18, 2002

Fast Ignition Challenge: coupling of relativistic laser to plasma and transport of high current, relativistic electron beam

Laser:
$??^2 \sim 10^{19}$ W/cm^2
~100 kJ in 10 ps

Energy deposition and heating in pre-compressed core

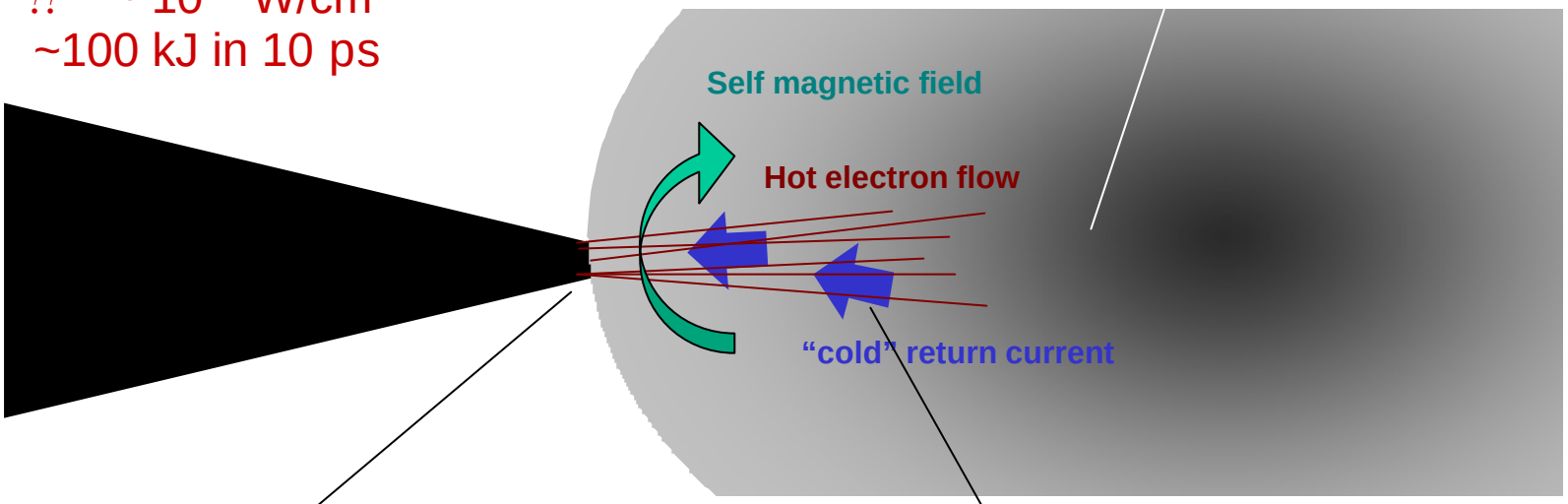

Absorption at critical density plasma surface (10^{21} cm^{-3})

Near perfect neutralization required by "cold" return current

>20 % coupling to electrons
>20 kJ in 10 ps
~1000 MA at ~2 MeV

Total current ($?_{hot} - ?_{cold}$) << Alfven limit [1] (~50 kA)

GENERAL ATOMICS

[1] Critical current where self magnetic field reverses particle direction, inhibiting transport

We are using sheath-accelerated protons from the rear surface to diagnose the hot electron sheath

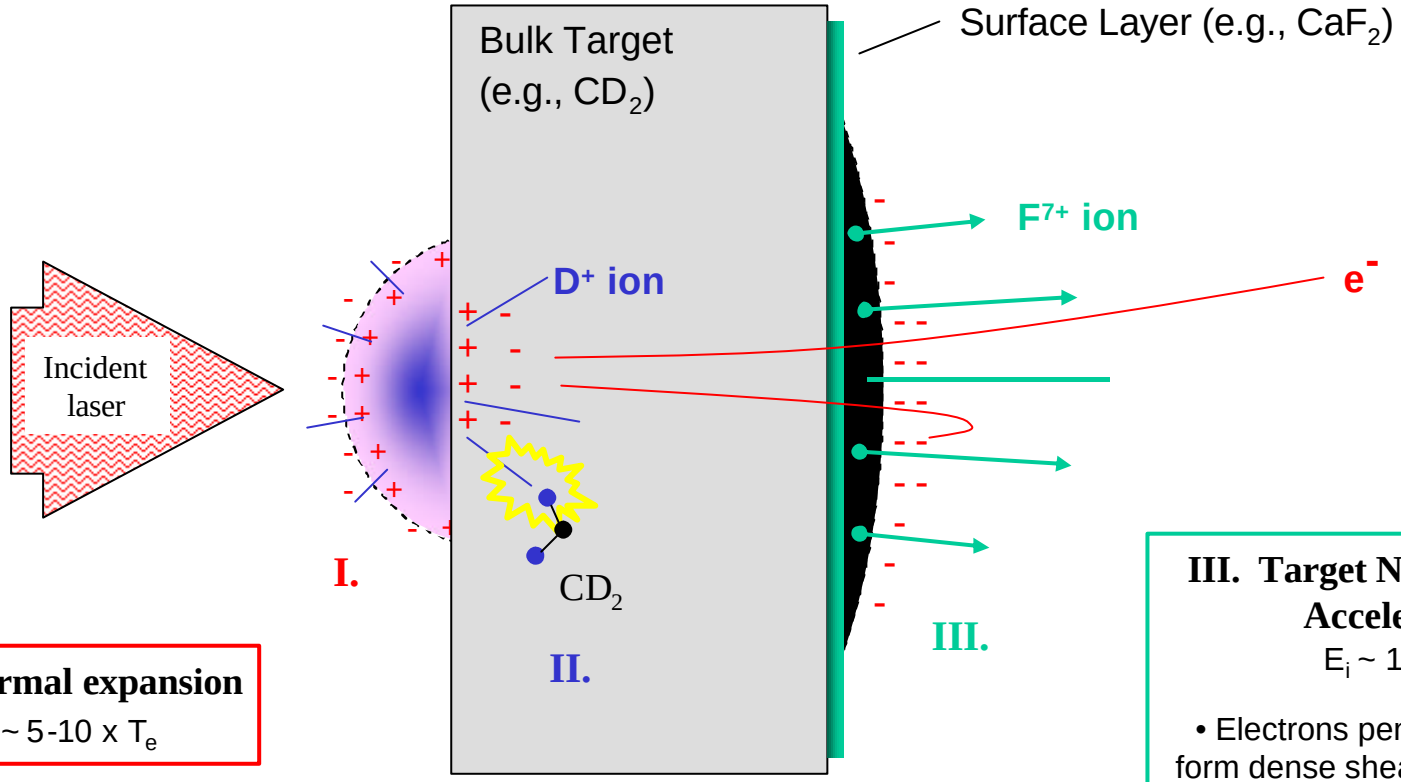

I. Thermal expansion

$T_i \sim 5\text{-}10 \times T_e$

II. Front-surface charge separation

Static limit: $T_i \sim T_e$

III. Target Normal Sheath Acceleration

$E_i \sim 10 \times T_e$

- Electrons penetrate target & form dense sheath on rear, non-irradiated surface
- Strong electrostatic sheath field ionizes surface layer ($E_o \sim kT / e?_d \sim MV/?m$)
- Rapid (~ps) acceleration in expanding sheath produces very laminar ion beam

GENERAL ATOMICS

Metallic targets produce a smoothly varying proton beam divergence, which decreases with proton energy

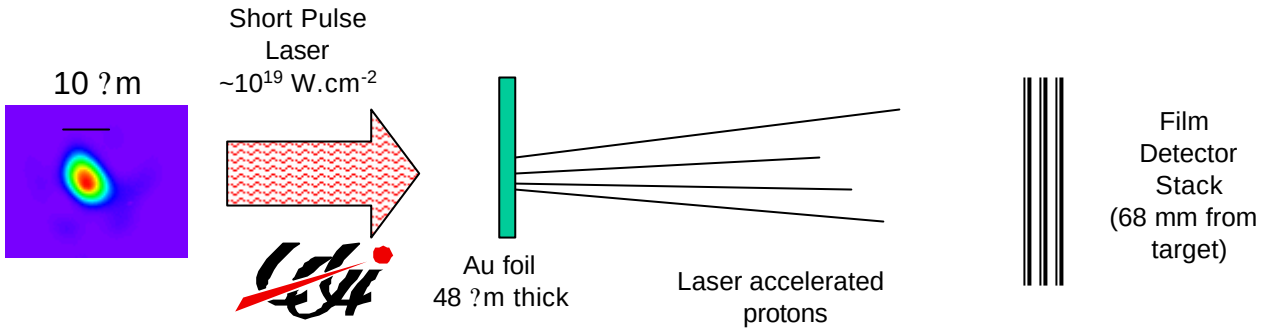

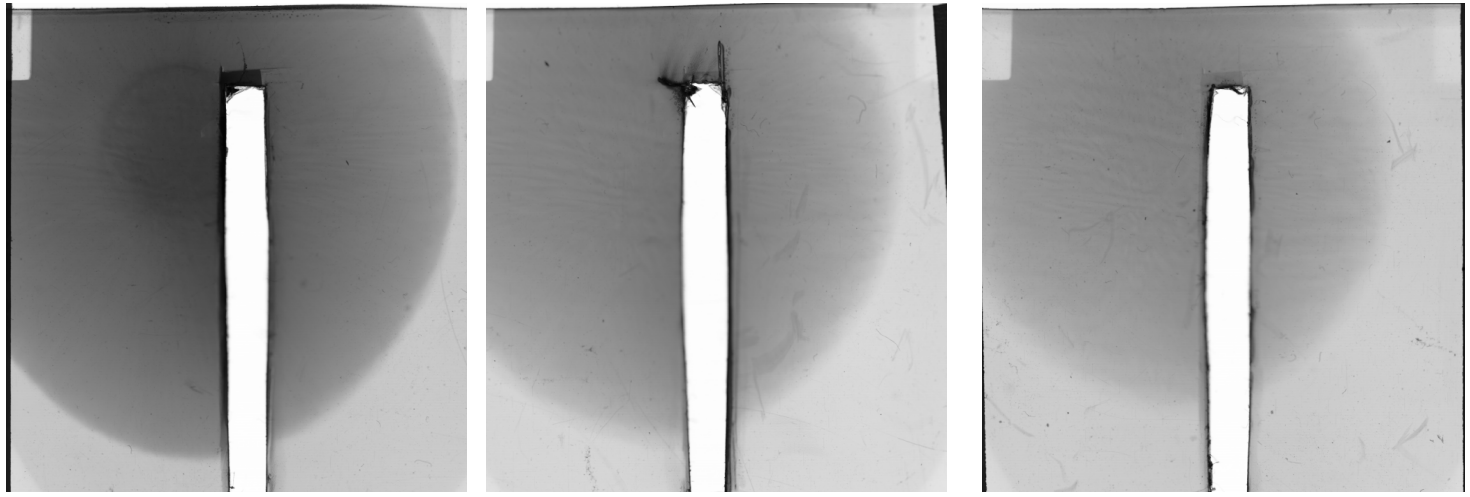

2 MeV 5 MeV 8 MeV

GENERAL ATOMICS

The angular divergence of cold, laminar ion beams can be understood in a simple, purely electrostatic pseudo-3D model

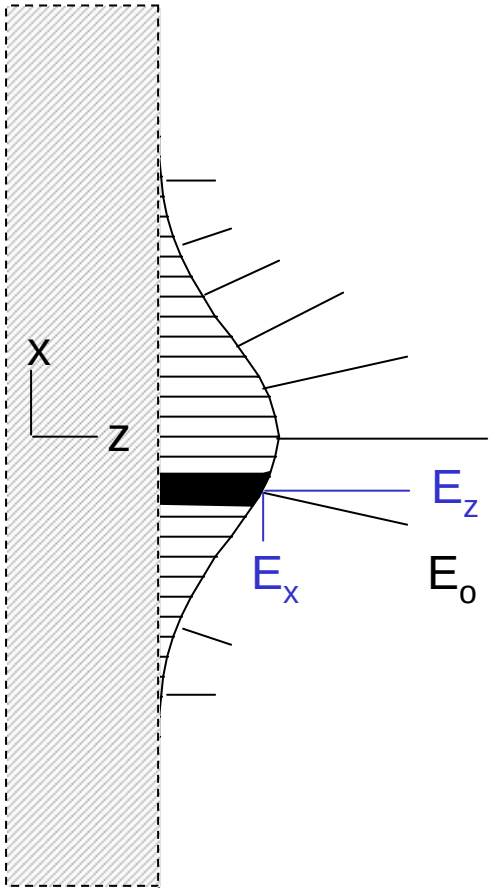

We model 3D expansion dynamics as laminar flow of 1D voxels

- Electric field proportional to charge enclosed in Gaussian pillbox

  $\mathbf{E_o} = 4? \; ? \sim n_{hot} \, ?_d \sim n_{hot}^{1/2} \, T_{hot}^{1/2}$

- Assume $T_{hot}(t)$ constant in space during acceleration
- Neglect radial hot electron transport during acceleration, $n_{hot}(x)$
- Neglect transverse spread of ion cloud during acceleration (typically, $?x \sim 0.1 \, ?m$, $?z \sim 20 \, ?m$)
- Radial electric field proportional to ion-front curvature

  $\mathbf{E_x} = (?z/?x) \, \mathbf{E_o}$

$$p(x,t) \; ? \; e?E_o dt \; ? \; n_{hot}^{1/2} ?T_{hot}^{1/2} dt$$

$$z(x,t) \; ? \; n_{hot}^{1/2} ?? \; T_{hot}^{1/2} dt\, dt' \; ? \; n_{hot}^{1/2} f(t)$$

$$p_x(x,t) \; ? \; e?E_x dt \; ? \; n_{hot}^{1/2} (?_x n_{hot}^{1/2}) ? \; T_{hot}^{1/2} f(t) dt$$

- Ion divergence is proportional to gradient of initial n_{hot}

$$?_x \; ? \; (p_x / p) \; ? \; (?_x n_{hot}^{1/2}) \; ?? T_{hot}^{1/2} f(t) dt \Big/ ?T_{hot}^{1/2} dt ?$$

GENERAL ATOMICS

The model suggests smooth transport through Gold

? ~ ?n_{hot}

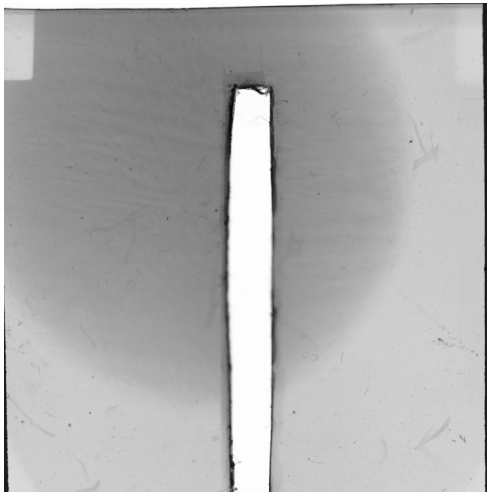

8 MeV

smooth sheath

+

smooth source (laser)
[assumption: laser imprinting]

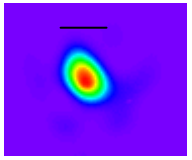

smooth transport

GENERAL ATOMICS

Model predicting laser imprinting of the ion beam and control of divergence tested with a line focus

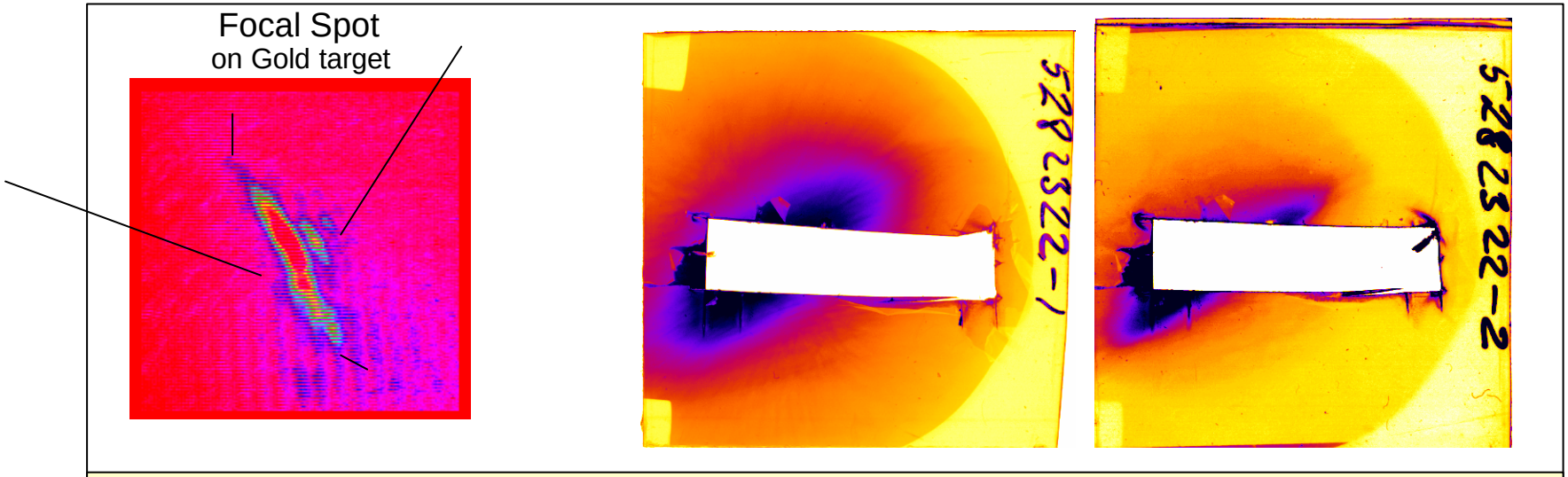

Measured laser focal spot and Laser-accelerated proton distributions

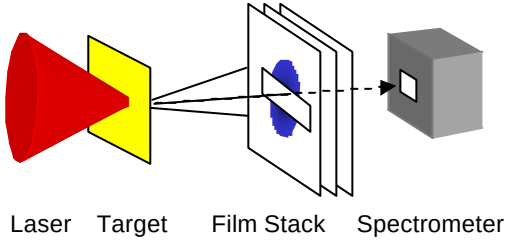

GENERAL ATOMICS

The quantitative comparison with the model allow to infer the PSF for transport through Gold

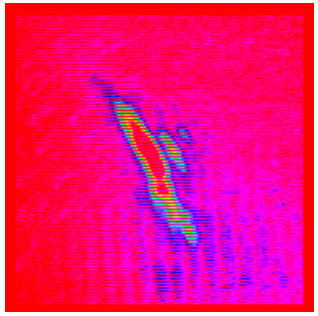

convolved with a Gaussian PSF ✍

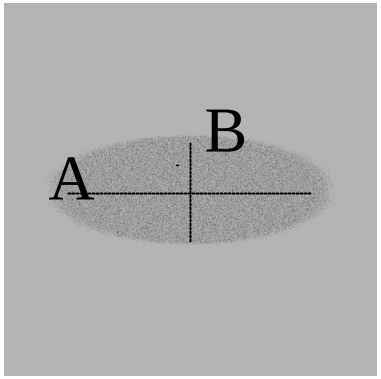

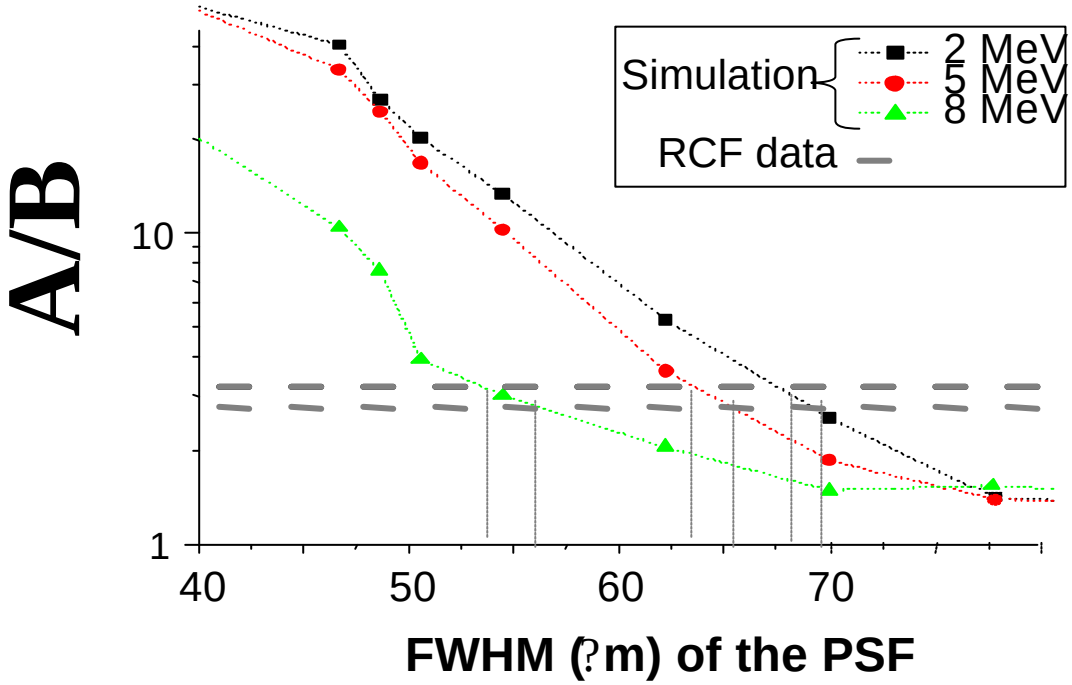

✍ sheath size at high energy ~ 60 ?m (?~30º)

good agreement with OTR

GENERAL ATOMICS

“Nano-beams” of ~10 MeV protons produced by short-pulse laser irradiation of a thin-foil optical grating

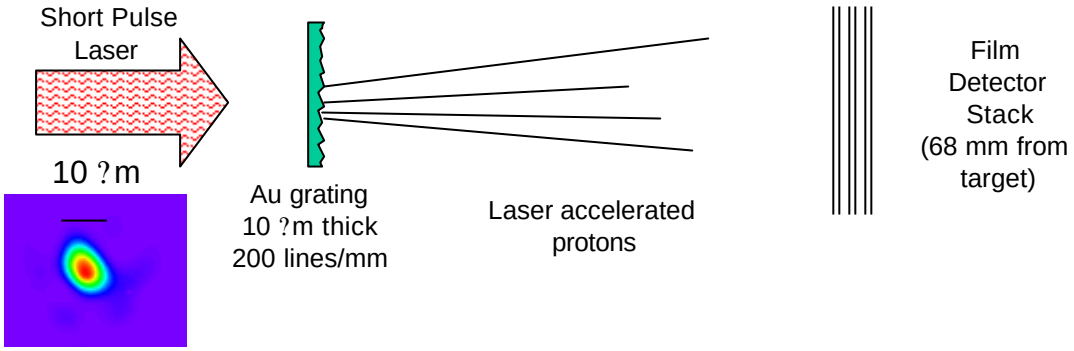

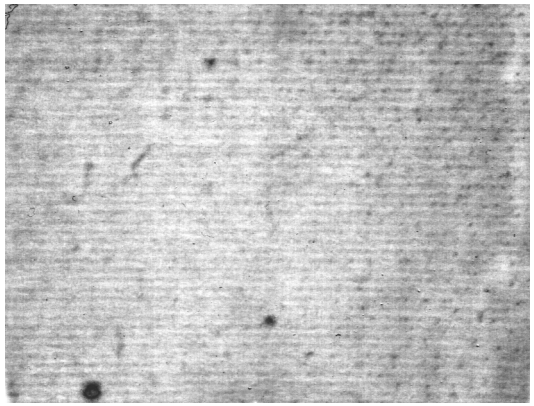

Photomicrograph of grating

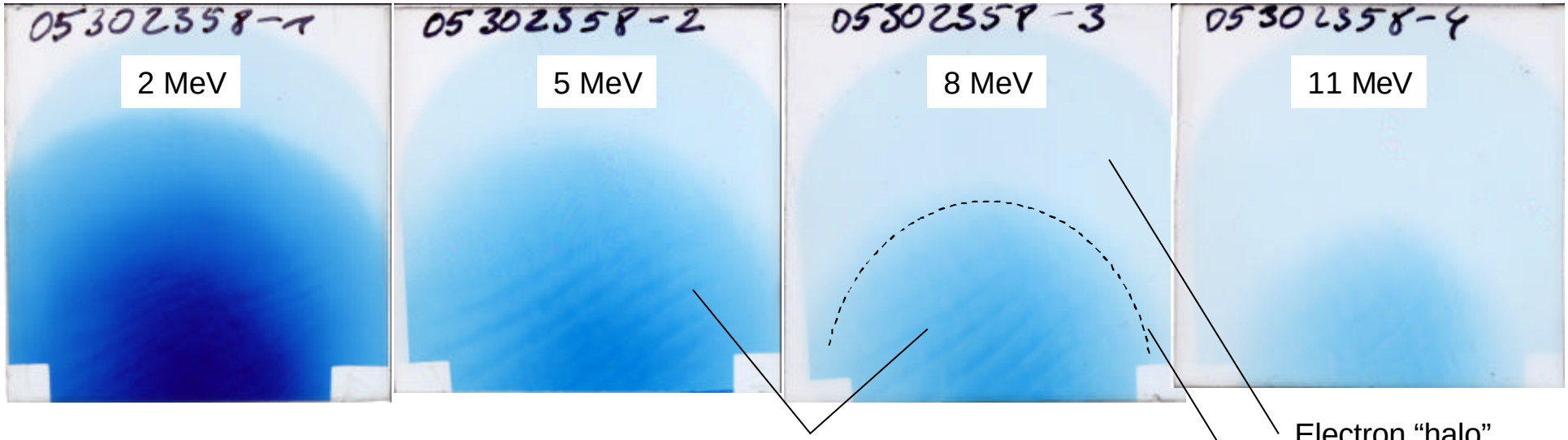

Proton micro-beams
(~200x magnified at film plane, 5 ?m spacing, <100 nm width at source)

Electron “halo”

Proton beam envelope

GENERAL ATOMICS

Nano-focusing is understood with help of PIC simulation of hydrogenous contaminant on a structured gold foil

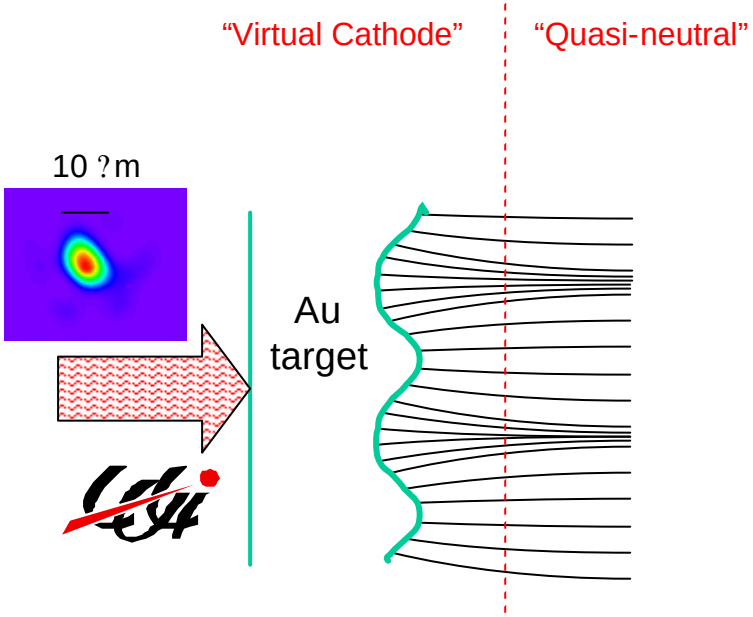

Proton beam-lets focused
to ~100 nm (rms)

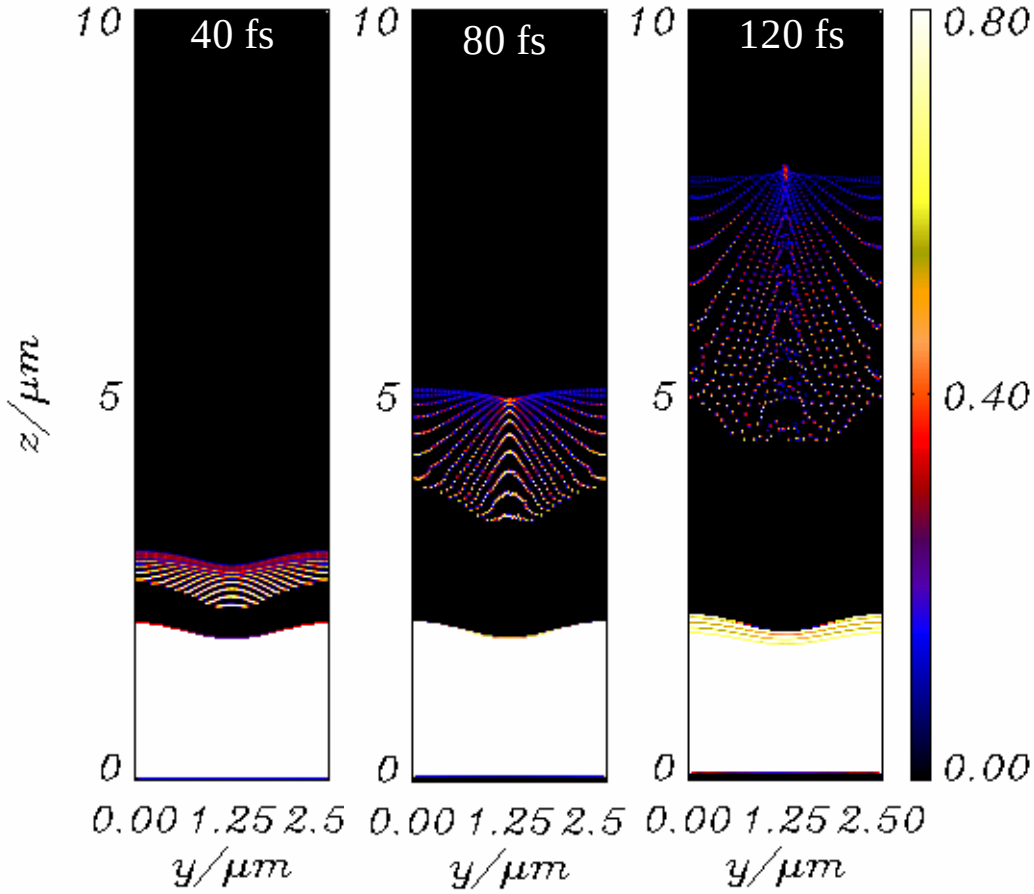

GENERAL ATOMICS

H. Ruhl

Using such beam fiducials allows to “image” the hot electron sheath profile, and hence relativistic electron transport

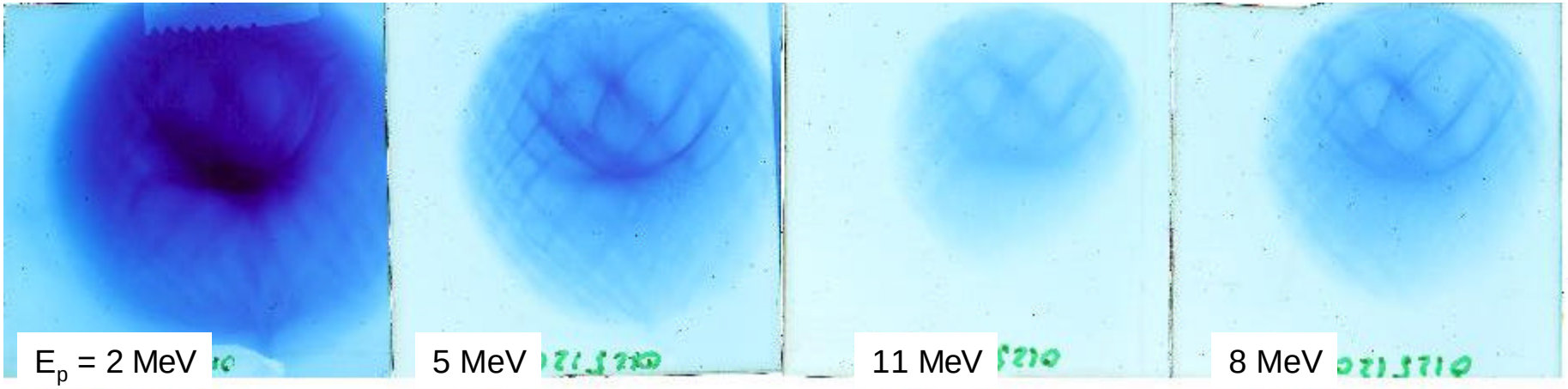

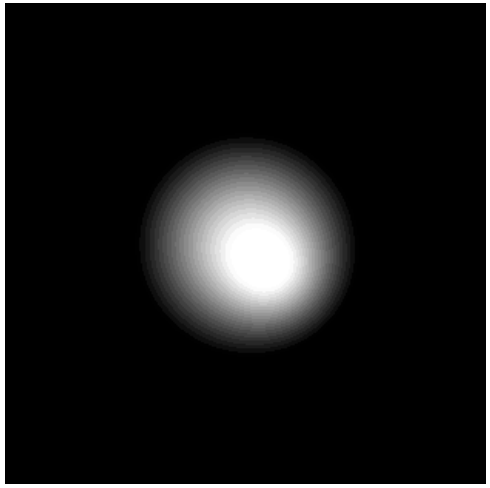

Simulated electron sheath density distribution (overlapping, off-center gaussians)

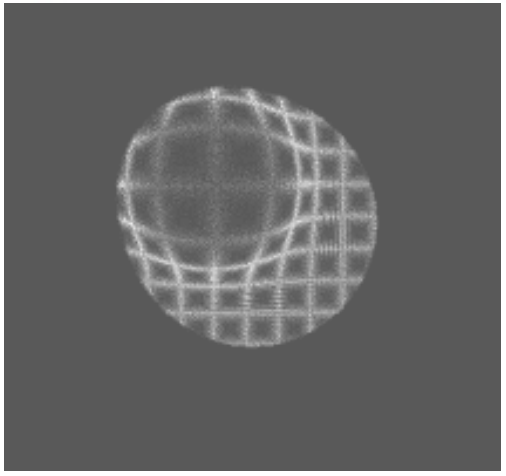

Simulated proton beam slice from structured target

Protons are extremely Sensitive to Filamentation of hot electron transport through solids (<1% density modulation)

GENERAL ATOMICS

Multiple hot-electron “filaments” should produce caustic-like patterns, as demonstrated with modulated laser focus

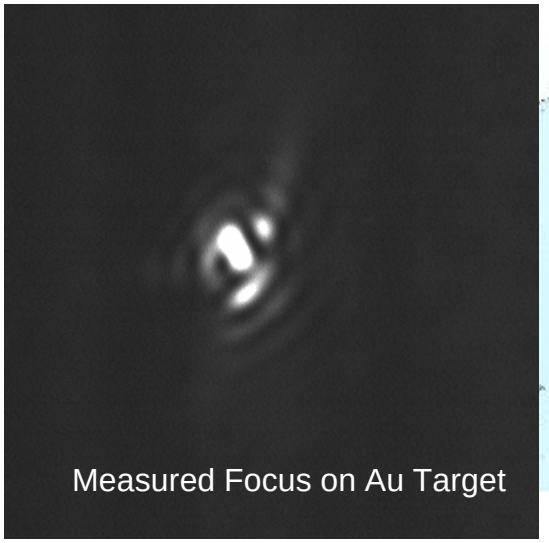

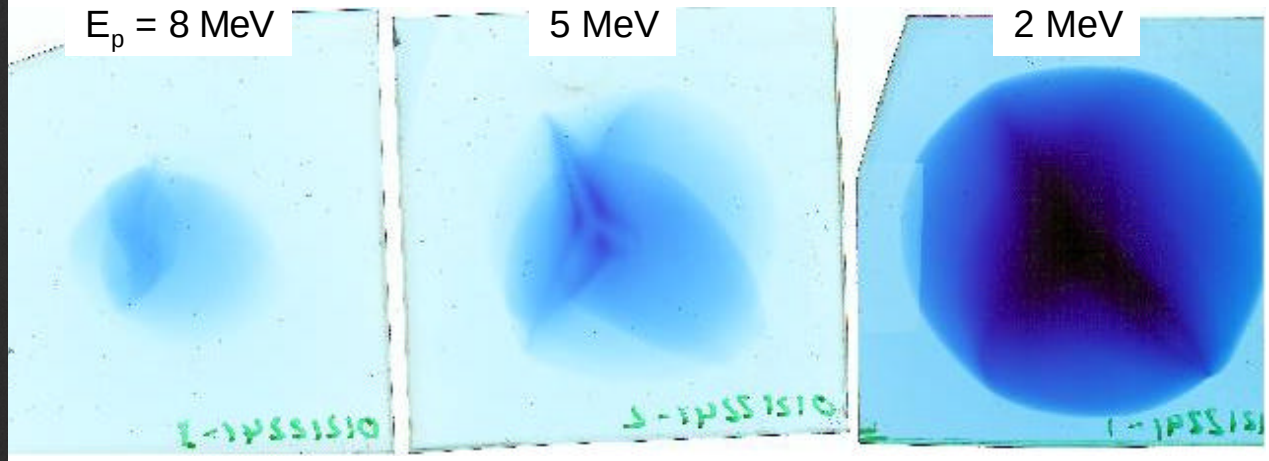

Measured Proton Distributions in RCF

Rear sheath profile

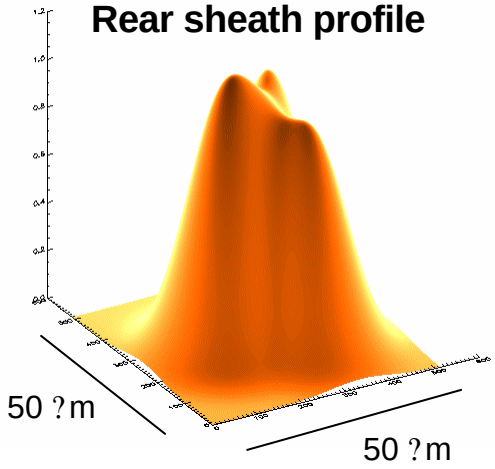

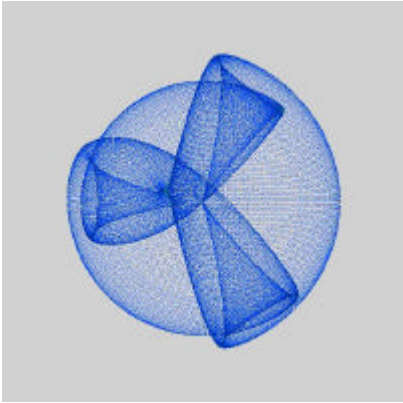

Simulation pattern

Again consistent with “smooth” electron transport in good conductors.

GENERAL ATOMICS

Rear sheath, as diagnosed by ion pattern, is strongly influenced by target materials and discontinuities

10 ?m

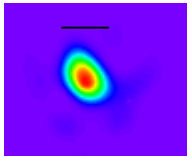

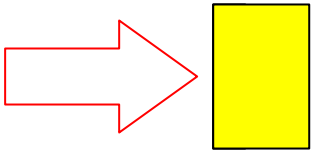

48 ?m Au

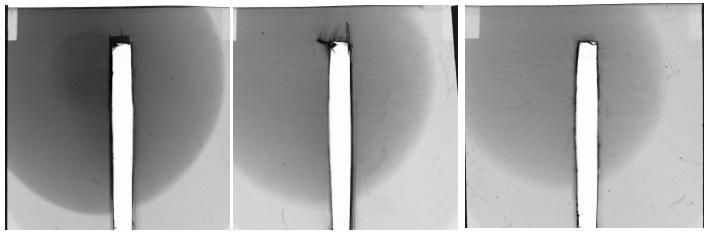

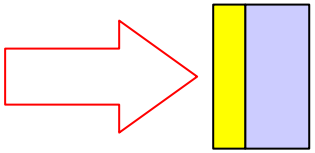

10 ?m Au
+ 50 ?m CH

(same in insulator alone)

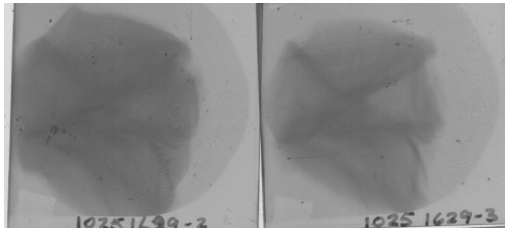

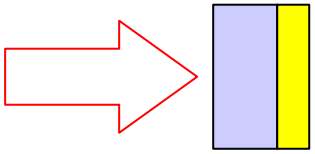

50 ?m CH
+ 10 ?m Au

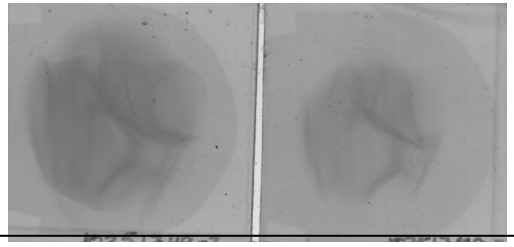

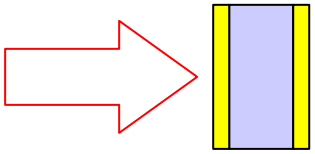

2 ?m Au
+ 80 ?m CH
+ 2 ?m Au

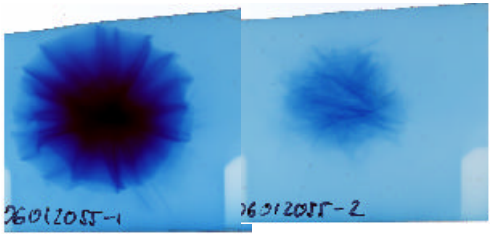

~2 MeV ~5 MeV ~8 MeV

GENERAL ATOMICS

3D Pâris simulations give a first hint at the importance of interface-induced beam disruption

1 J, 300 fs, 5 ?m radius, 20º, 500keV electron beam

Massive gold target

Au | Al (?×10) | Au

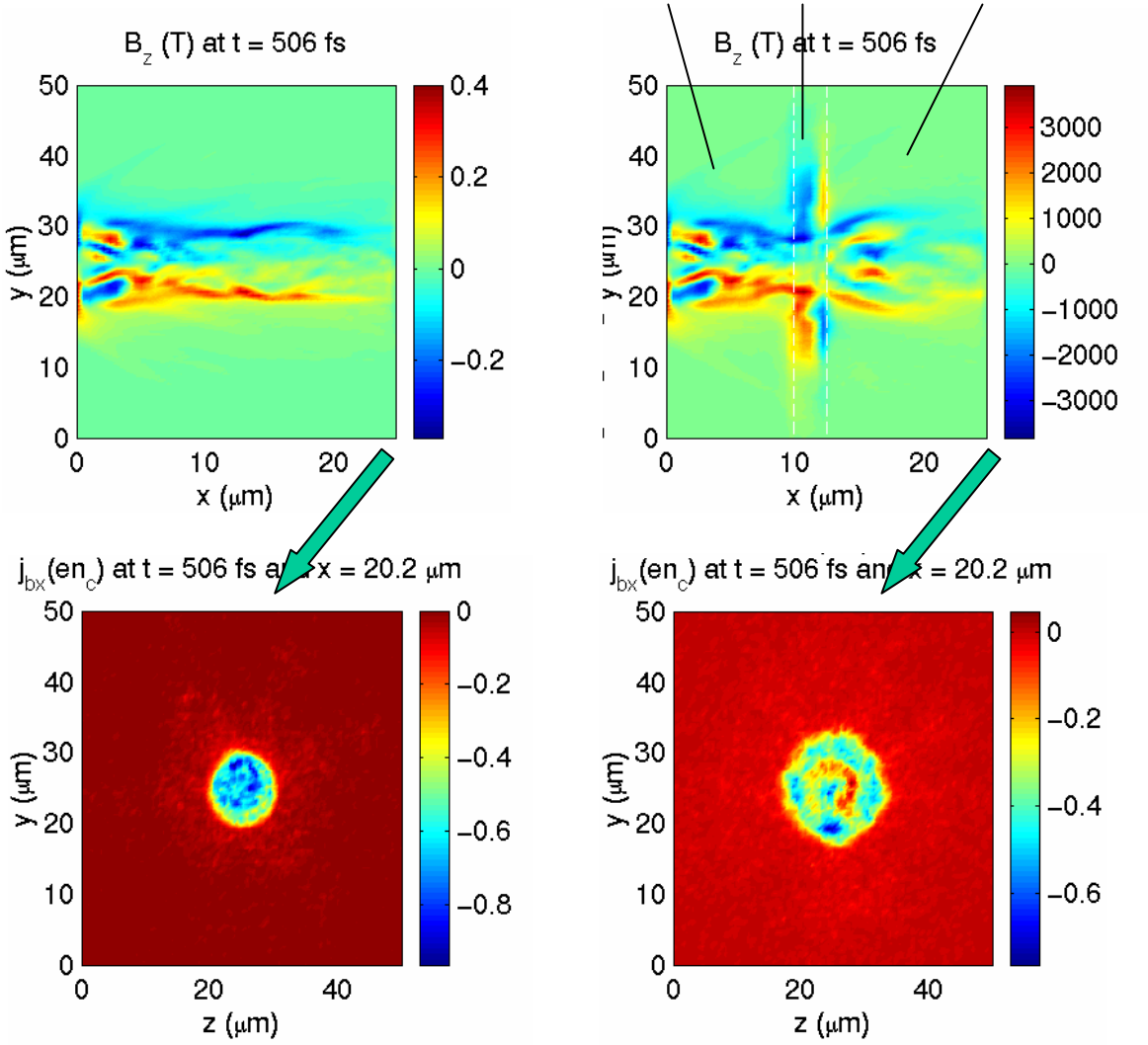

Pâris code: L. Gremillet, G. Bonnaud, and F. Amiranoff, Phys. Plasmas **9**, 941 (2002).

GENERAL ATOMICS

Summary and Conclusions

- Sheath-accelerated protons provide a powerful technique to image the hot electron transport through thin foils

- Laser imprinting and target shaping allow control of the proton beams

- Transport through metallic foils (Au & Al) appears to be very smooth

- Presence of insulating layers in multi-layered targets disrupts electron transport

- HOWEVER initially cold, solid target experiments may not be relevant for evaluating hot electron transport for Fast Ignition

Preliminary conceptual design for a z-pinch-fast-ignitor power plant

John S. De Groot
Sandia National Laboratories, USA
Plasma Research Group, UC Davis

E. Akli
Plasma Research Group, UC Davis

S. Slutz, C. L. Olson, G. E. Rochau
Sandia National Laboratories, USA

S. Hatchett
Lawrence Livermore National Laboratory, USA

Given at the Fast Ignition Workshop

November 19, 2002

St. Pete's Beach, Florida

Revised: November 25, 2002

Abstract*

We have performed a preliminary conceptual design of a z-pinch-fast ignitor driven (ZPFIM) IFE power plant. As in other z-pinch IFE power plant designs, a recyclable transmission line delivers electrical power to one or two wire arrays within a hohlraum. The wire array(s) implode and stagnate on axis resulting in x-rays that implode the capsule to high densities (ρ > 100 gm/cm^3). The fuel capsule is either a sphere with an inserted cone or a hemisphere to give assess to the fast ignitor laser. The advantages of the FI design are the much lower energy required to compress the capsule to high densities and the greatly relaxed capsule symmetry requirements. Since the target is fixed in space during the PW laser pulse, the laser pointing requirements are greatly relaxed over other IFE schemes. We find that the fast igniter design has the same cost of electricity as a conventional z-pinch design.

***Sandia is a multiprogram laboratory operated by Sandia Corporation, a Lockheed-Martin Company, for the United States Department of Energy Under Contract DE-AC04-94AL85000.**

Why fast ignition?

- In fast ignitor systems, a z pinch, laser or high ion beam compresses the plasma to high density (ρ > 100 gm/cm^3).
  - A PW laser heats and ignites the hot spot.
- The energy required to heat and ignite the hotspot is small compared to the energy required to create, heat, and ignite the central hotspot in the conventional central hot spot (CHS) ICF scheme.
  - The point is that the PW laser can be focussed to smaller hotspot diameters.
  - We can obtain high gain fusion with a much lower energy laser or z pinch that compresses the plasma.
    - Should be cheaper and more flexible.
- This is the first study to explore possible advantages of z-pinch driven FI power plant designs over CHS designs.

Conventional and FI Hotspot Ignition

- **Conventional central hot spot ICF scheme**
  - **Laser light (direct drive) or x-rays (indirect drive) heat a spherical plasma**
  - **The outer layers of the plasma expand and compresses the remaining plasma**
  - **A weak shock is driven in the plasma**
  - **When the shock is close to the center of the plasma, the drive power is increased, resulting in a hotspot**
  - **The hotspot radius is limited by the RT instability and the symmetry of the laser drive power**
- **Fast ignition**
  - **A PW laser heats a hotspot in the fuel.**
  - **A very small hotspot can be made since the laser light can be focused to a radius ~ 10μm.**
  - **For a 10μm hotspot, τ_{HS} ~ 10 ps, P ~10^{20} W/cm^2**
  - **At such high powers, laser-plasma interactions and electron energy transport are not known!**
  - **Electrons are driven relativistic by the laser field**

Isobaric and isochoric systems

- **Conventional central hot spot systems are isobaric systems.**
  - **The primary power source both compresses the fuel and ignites a hot spot (ZPMHD).**
  - **The fuel is compressed and the hotspot formed slowly so the hotspot and main fuel are in pressure equilibrium (isobaric).**
- **Fast ignitor systems are isochoric**
  - **The primary power source compresses the fuel (ZPFIM).**
  - **The hotspot is heated rapidly so the hotspot and main fuel have the same density (isochoric).**

Fast Ignition requires several key elements:

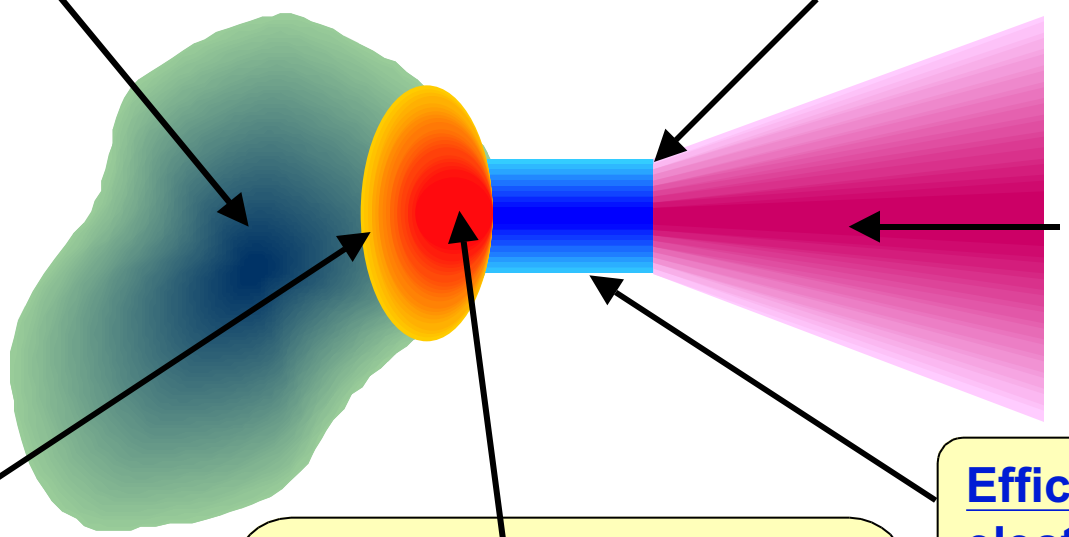

Implosion to high density blob

Efficient conversion: E_{laser} "beam" of ~ MeV electrons aimed at blob

Fast ignition requires several key elements:

Efficient transport of hot electron energy to blob

Propagation of burn throughout blob: (need ρR> ~ 1.8 g cm^{-2})

Efficient deposition of electron energy in region of ρR~0.5 g cm^{-2} (α range), heating it to 5-10 keV

Steve Hatchett LLNL

Cone-focussed scheme — Indirect drive:

A re-entrant tube and cone provide access for ignitor beam to the imploded, compressed core:

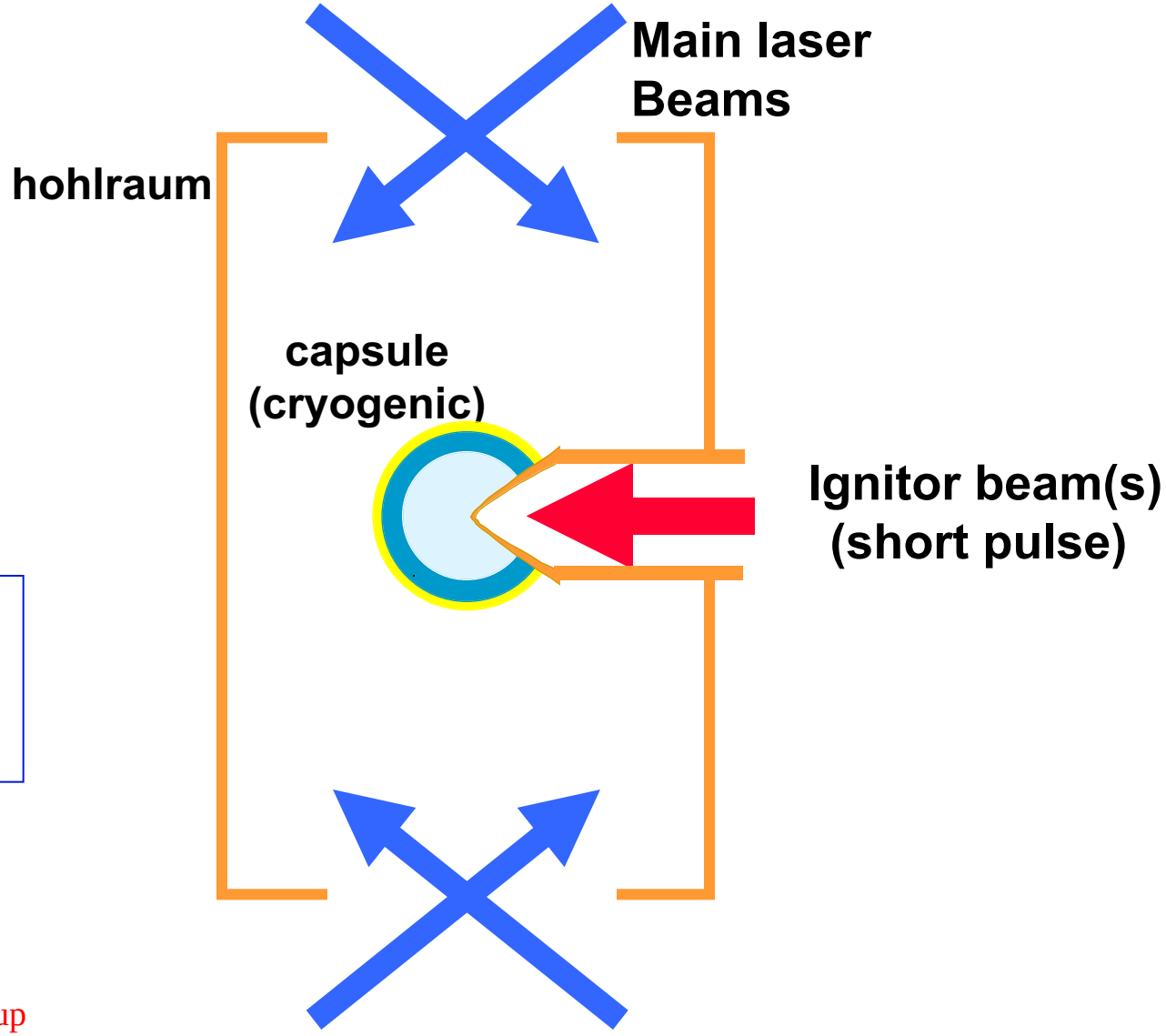

Direct Drive:

Same idea but no hohlraum

Steve Hatchett LLNL

Cone-focussed scheme immediately provides most of the key FI elements.

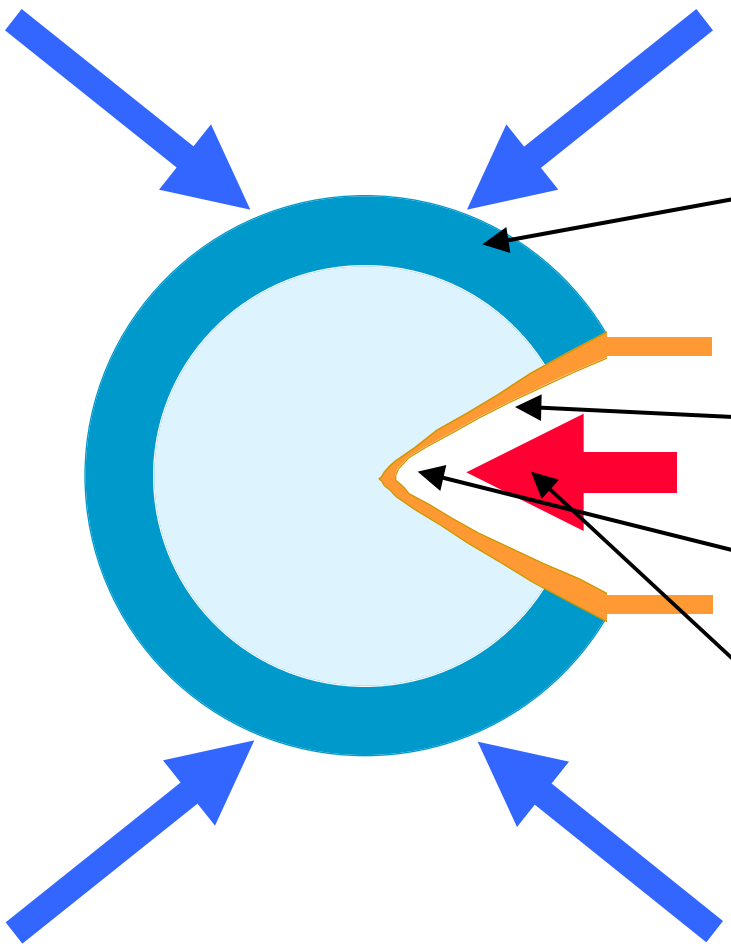

Steve Hatchett LLNL

Low aspect ratio capsule:
Get hi ρ blob with relatively low drive symmetry; no significant stability issues.

Cone provides pointing & puts deposition of laser close to hi _____ blob

E_{laser} to hots at surface, ~50% conversion (exp't)

Laser spot size & pulse length tuned to give hot e's with optimum range

A liquid DT cryo capsule concept is being developed which could significantly reduce cost

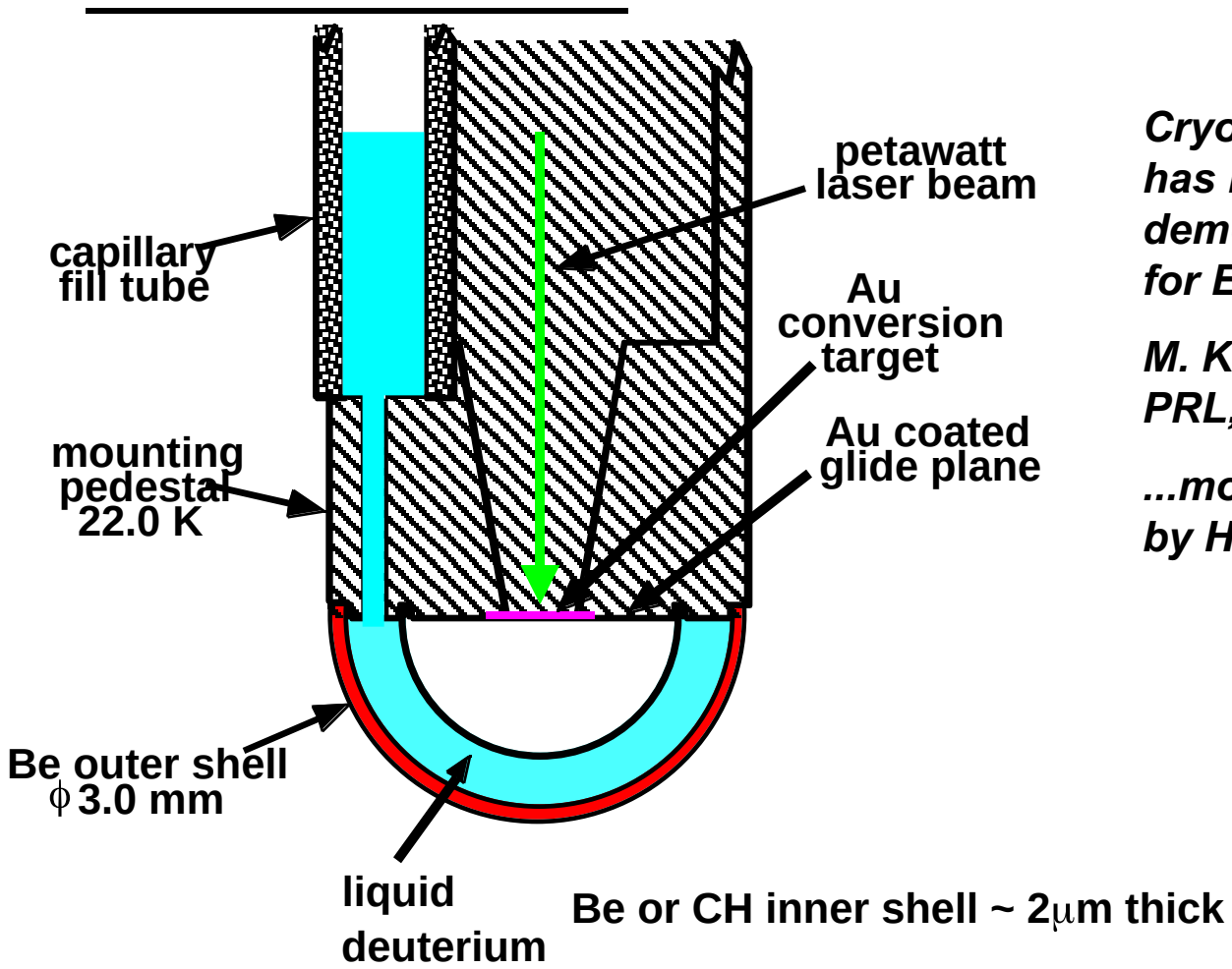

Cryogenic capability has been demonstrated at 22 K for EOS experiments

M. Knudson et al. PRL, 2002

...more details given by Hanson et. al.

Dave Hansen SNL

06/14/02

Simulations indicate a modest decrease in performance for a liquid fuel capsule

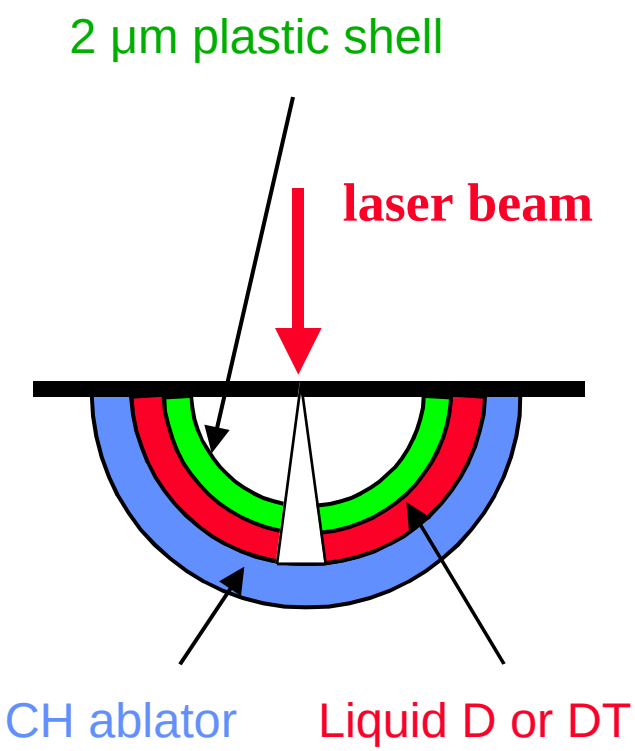

The plastic shell modestly reduces the fuel compression

This can be compensated by an increase in the capsule size

… more details given by Slutz, Vesey, and Hanson

Steve Slutz SNL

Cost of electricity

- **The cost of electricity is given by [B. G. Logan, "Inertial fusion reactors using Compact Fusion Advanced Rankine (CFARII) MHD conversion," Fusion Engineering and Design 22, 151 (1993)]:**

$$\mathrm{CoE} = \frac{114\,C_{direct}(G\$)\times \mathrm{IND}\times \mathrm{FCR}}{P_{net}(GWe)\times \mathrm{CF}} + \mathrm{Cop}$$

  - **IND = indirect cost = 1.73, FCR = fixed charge rate = 0.125, CF = plant capacity factor = 0.8, Cop = operating costs ≈ 1 ¢/kWh**
- **P_{net} is the net electrical power, $P_{net} = P_{fus}\,\eta_c$, P_{fus} is the average fusion power = Y/τ, η_c electrical plant efficiency, τ is the time between pulses.**
- **C_{direct} is the direct cost of the plant, G$**
  - **$C_{direct} = C_{drivers} + C_B$, $C_{drivers}$ = cost of the drivers, C_B is the cost of the balance of the power plant**
  - **$C_B = C_B(Y, \tau)$, Ref. 1**

Simple theory Z-Pinch-Fast-Ignitor Design(1)

- **We choose a 200kJ PW laser and an efficiency of conversion of laser energy to high energy electrons = 0.1.**
- **The energy required to ignite the the hot spot is (Atzeni, Phys. Plasmas, 6, 3316 (1999).**
  - $E_{HS} = 140\ (100/\rho)^{1.85}$, **kJ**
- **Assume that ρ = 300 gm/cm^3.**
- **The ignition energy = 20 kJ**
  - **This heats the alpha-range hot spot ($r_{HS}\ \rho$ = 0.9 g cm^{-2}, M_{HS}=3.1x10^{-5} g, r_{HS} = 29 µm) to the requisite 5 keV.**

Simple theory Z-Pinch-Fast-Ignitor Design(2)

- **Choose the outer fuel radius times the density, $\rho_{M} = 7$, so that the burn efficiency is high, $\phi = r_M \rho /(7 + r_M \rho) = 0.5$.**
- **This gives the outer radius of the compressed fuel, $r_M = 230$ µm and the mass of the fuel is $M_M = 0.016$ gm.**
- **Most of the fuel energy is the energy required to compress the fuel [(Lindl, "Inertial Fusion", (Springer-Verlag, 1998)).]:**
  - ➡ **$E_F = 0.35\ \rho^{2/3} M = 0.25$ MJ.**
- **The hohlraum efficiency is 0.15, the x-ray efficiency is 0.8, the rocket efficiency is 0.2.**
- **The required z-pinch drive is 10 MJ, and the fusion yield is 2.7 GJ!**

Comparison of ZPFIM and ZPMHD

- Estimates for the direct cost for the z-pinch driver (0.3 G$) and the PW laser (0.3 G$) are included in the ZPFIM design.
- 100M$ is included in C_B for the RTL processing plant.
- The latest estimates for ZPMHD have been included.

	ZPMHD	ZPFIM
1. Fusion yield/shot	3.2 GJ	2.7 GJ
2. Time between pulses	1.0 sec	1.0 sec
3. Fusion chamber minor radius	4 m	4 m
4. Tritium breeding ratio	1.1	1.1
5. Z-pinch energy delivered to the load	25 MJ	10 MJ
6. X-rays into hohlraum	20 MJ	8 MJ
7. Total driver cost	0.75 G$	0.6 GJ
8. Total plant direct cost	1.55 G$	1.4 G$
9. Total capital cost	2.8 G$	2.5 G$
10. Net electrical power	1.6 GWe	1.4 GWe
11. Net MHD electricity cycle efficiency	50 %	50 %
12. Cost of electricity	4.0 ¢/kWh	4.1¢/kWh

Summary

- **We have performed a preliminary conceptual study of a ZPFIM power plant with MHD conversion.**
  - **We also compared ZPFIM to the conventional center hot spot ZPMHD design.**
- **The initial results are very promising:**
  - **The ZPFIM design has several advantages:**
  - **The z-pinch energy delivered to the load is much lower for ZPFIM (10 MJ compared 25 MJ for ZPMHD).**
  - **The ZPFIM design is much more flexible**
    - **ZPFIM requires the z pinch to deliver about 8 MJ of x rays to the hohlraum.**
    - **ZR will deliver about 3.3 MJ of x-rays to the load.**
      - **<u>ZR can be used to show that the fuel can be compressed to close to the required final density and spatial profile for a power plant</u>.**

First results from simulations of a fast-ignitor electron beam on a OMEGA cryogenic target

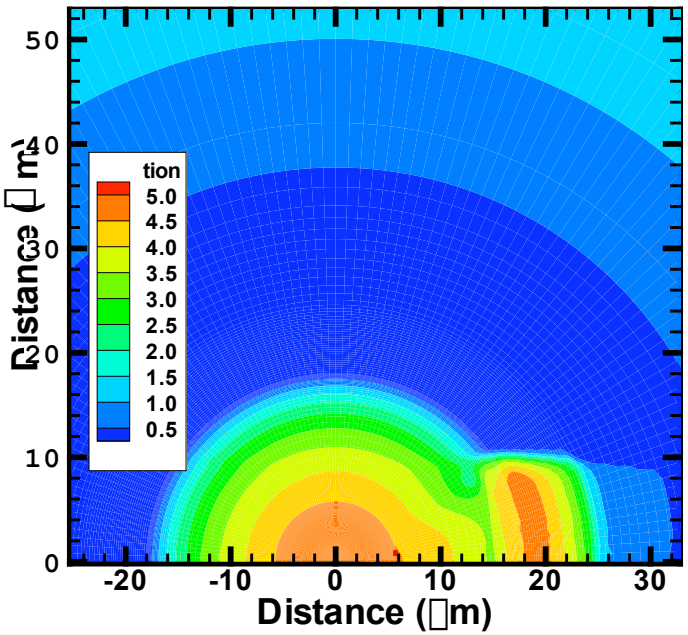

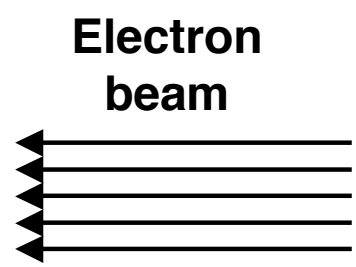

J. A Delettrez
University of Rochester
Laboratory for Laser Energetics

6th Workshop on Fast Ignition of Fusion Targets
St Pete's Beach, FL
16-19 November 2002

Contributors

S. Skupsky, C Stoeckl, and P. B. Radha

Laboratory for Laser Energetics
University of Rochester

Summary

Irradiation by the EP fast-ignitor beam of OMEGA-imploded cryogenic capsules provides sensitive observables

- The OMEGA EP laser will produce short-pulse (~20ps), high-intensity beams (>10^{19} W/cm^2) to study the physics of fast ignition.
- A relativistic electron model is being added to the multi-dimensional hydro code DRACO.
- In its first iteration, a simple penetration model is used to slow electrons from a mono-energetic beam source.
- The fast-ignitor beam lead to an increase in the neutron production rate of about an order of magnitude.
- A secondary implosion driven by the heated high density shell can be either “spherical” or one-sided depending on the electron source beam energy

A fast electron transport is being added to the 2D hydro code DRACO

- DRACO is an ALE multi-dimensional code designed to simulate the implosion of direct-drive ICF capsules.
- Work has started on a relativistic electron transport model:
  - Electrons enter at the pole as a cylindrically symmetric beam of a given radius.
  - In present work electrons are a mono-energetic beam produced as a square pulse in space and time.
  - They are instantaneously transported through the target
  - They give their energy to the background electrons using a penetration depth formulation applied in each zone.

The transport model has been compared with the result of Atzeni[1]

- Atzeni published a parameter study that used a similar transport model as the one presented here.
- He irradiated a sphere of 300 g/cm^3 sphere with varying electron beam radii, energies and penetration depths.
- He concluded that at least 13 kJ of fast electron energy was required to obtain ignition.
- Simulations with DRACO indicate that some boot strapping can be obtained down to about 7 kJ.

A direct-drive target was designed at OMEGA energy (25 kJ) to give > 300 g/cm^3 densities

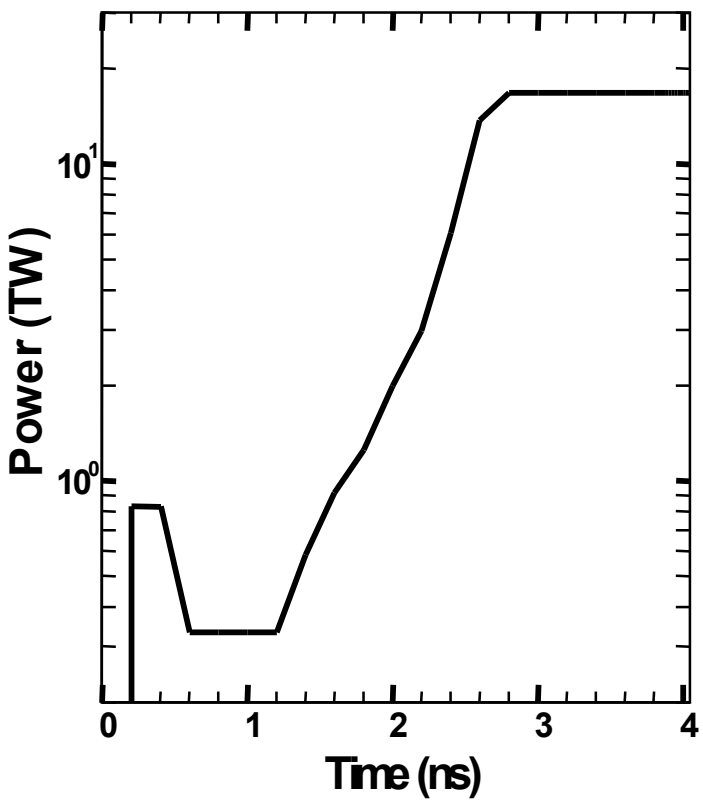

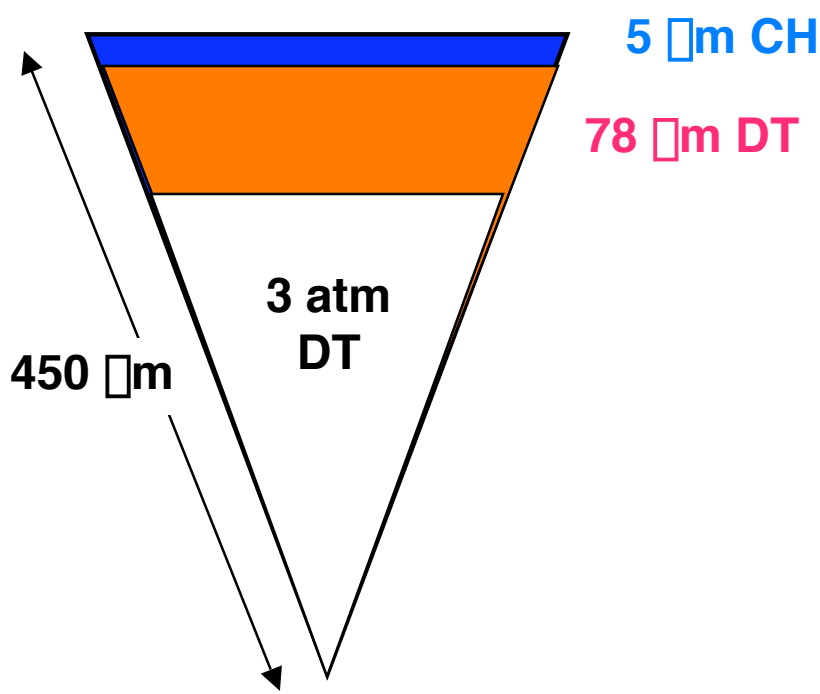

Fast-ignitor mass density are reached.

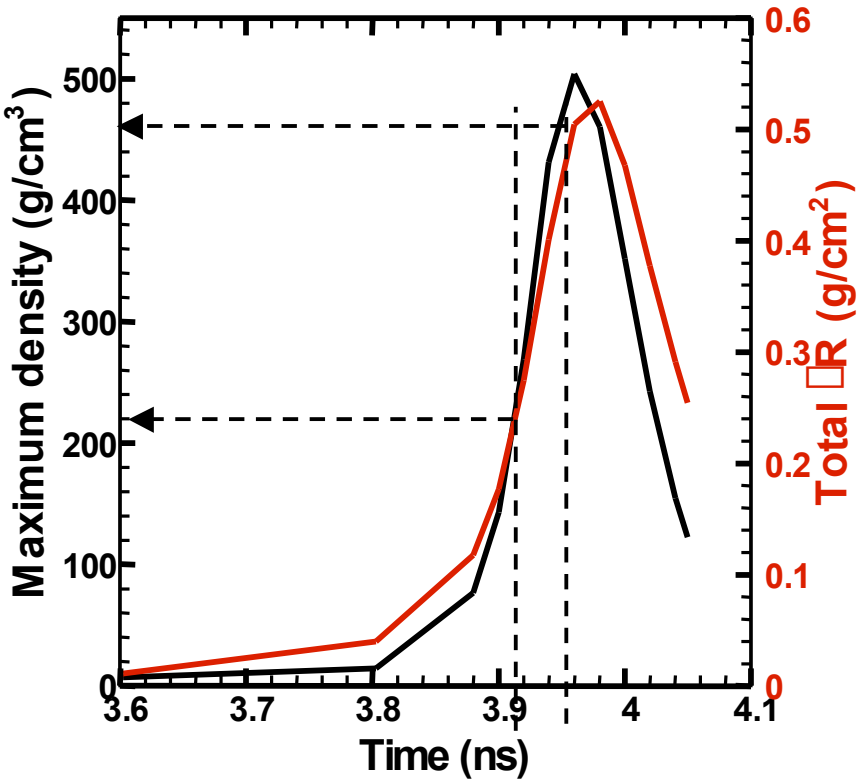

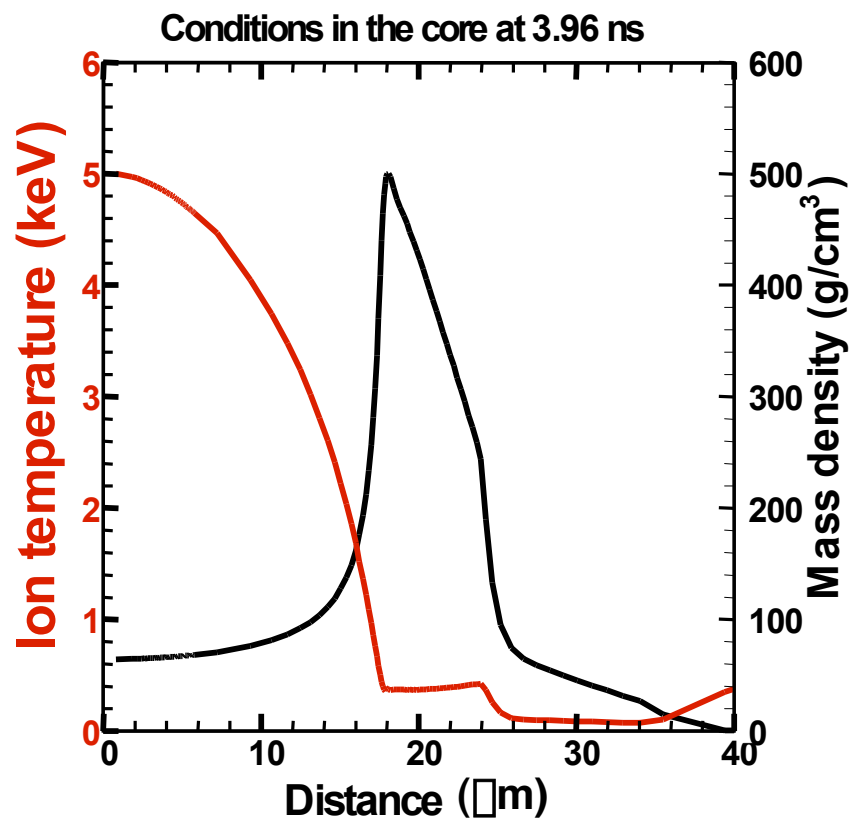

A 1-MeV electron has a range of about 0.4 g/cm^2

Simulations were carried out with a 20-ps, 1-MeV electron beam with energies of 400 J and 1 kJ

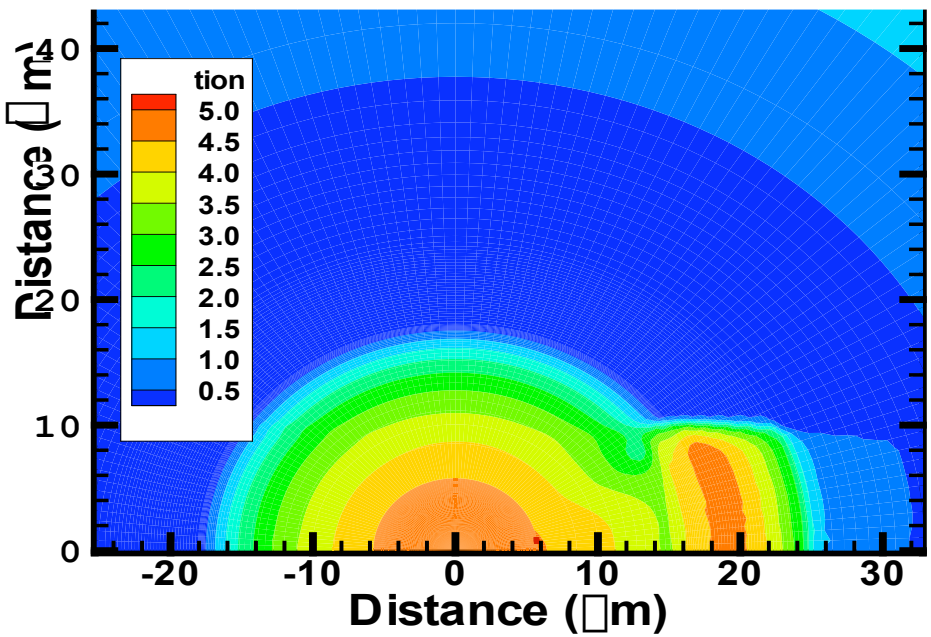

10- and 20-μm electron beam radii

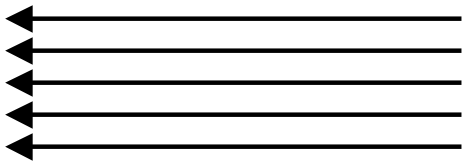

For low density (250 g/cm^3) the beam heats the two sides of the target and create colliding shocks at the center

UR LLE

9 ps into pulse

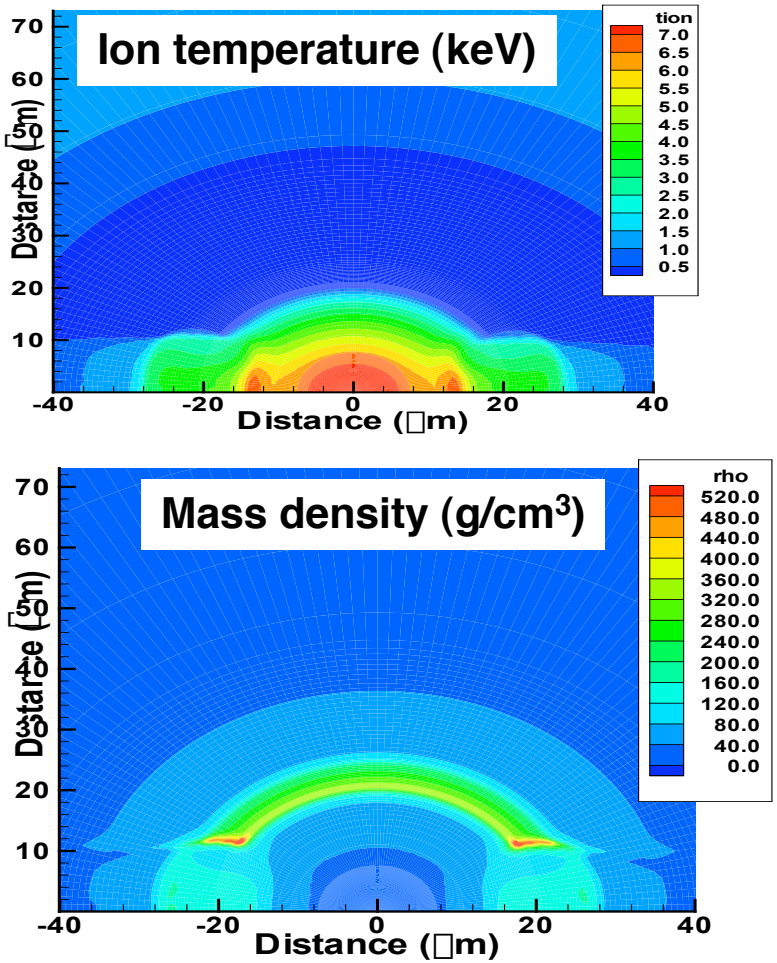

2 ps after end of the pulse

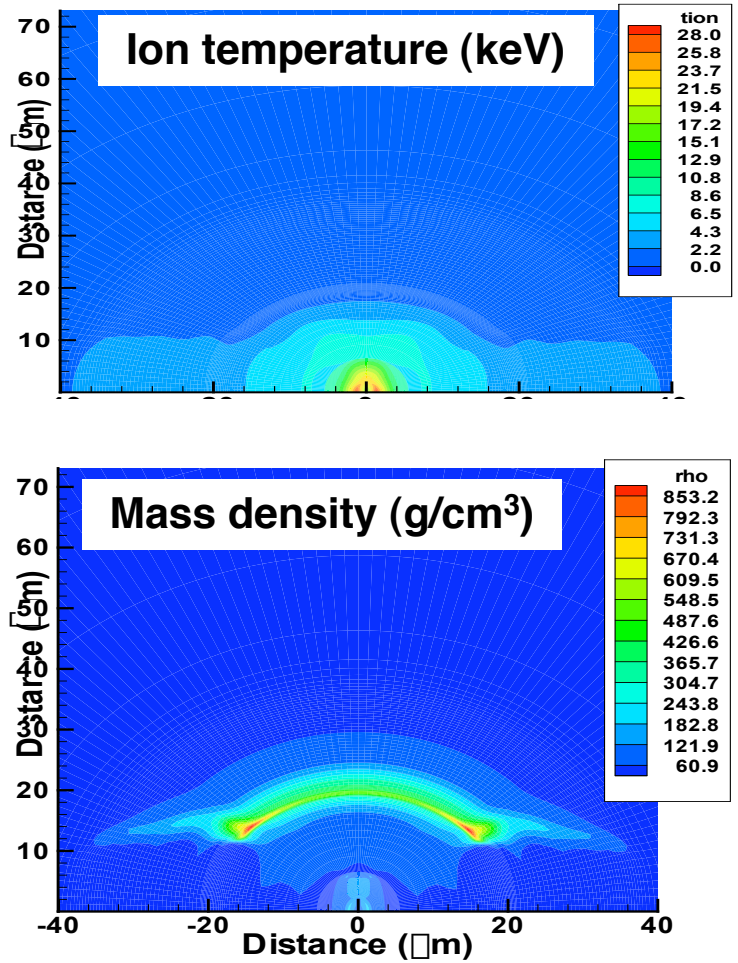

For high density (500 g/cm^3) the beam heats only one side of the target sending a shock through the center

UR LLE

4 ps into the pulse

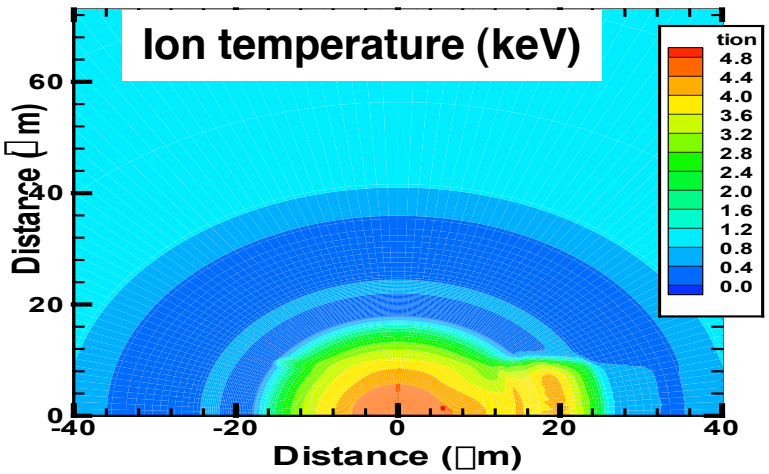

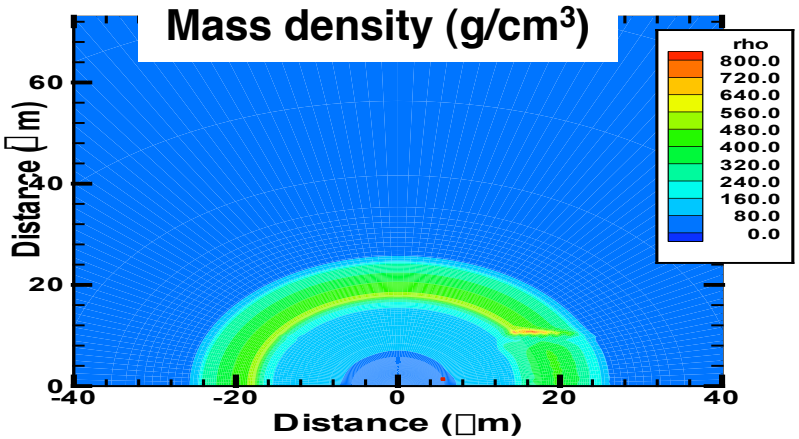

2 ps after the end of the pulse

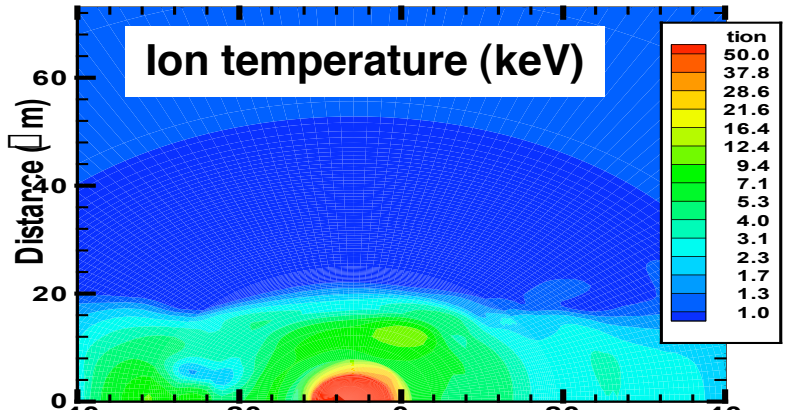

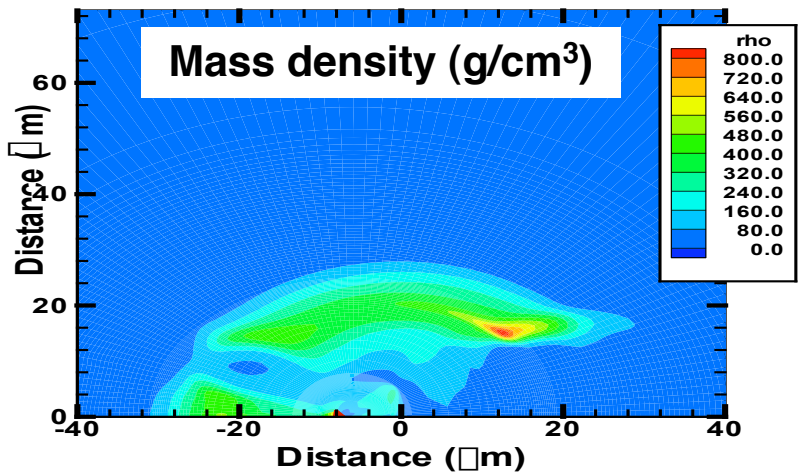

The fast-ignitor beam creates a burst of neutrons that can easily be diagnosed.

R = 500 g/cm^3, 10 μm radius

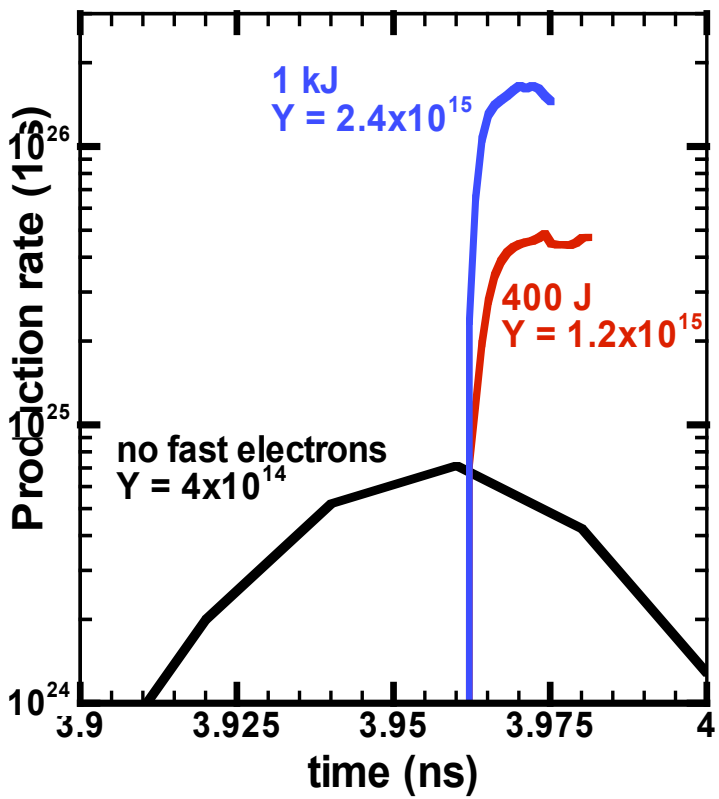

400 J pulse, 10 μm radius

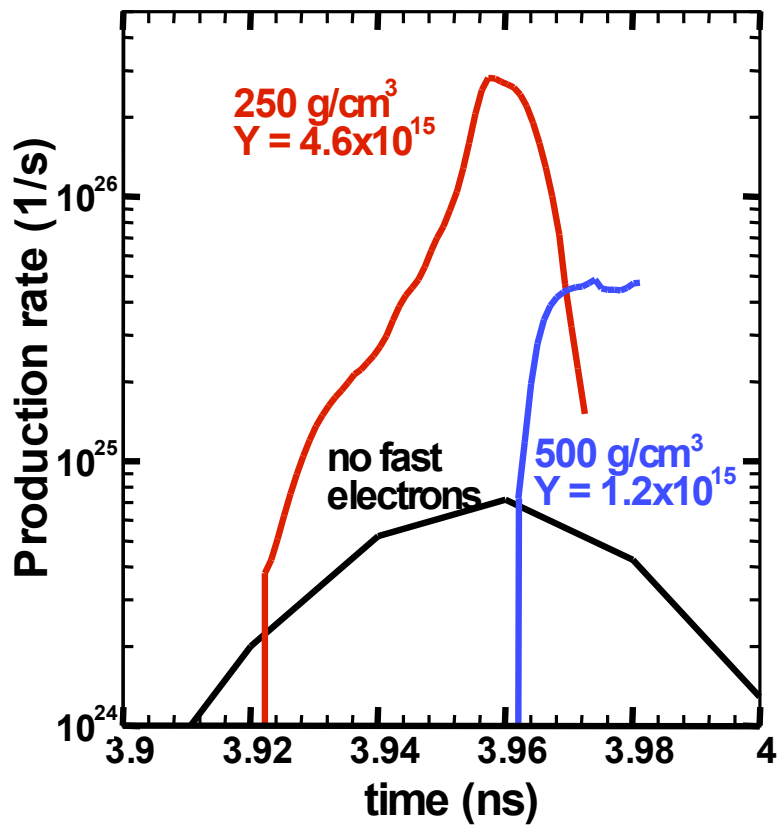

The yield is more sensitive to the beam radius for the 500 g/cm^3 case than for the 250 g/cm^3 case

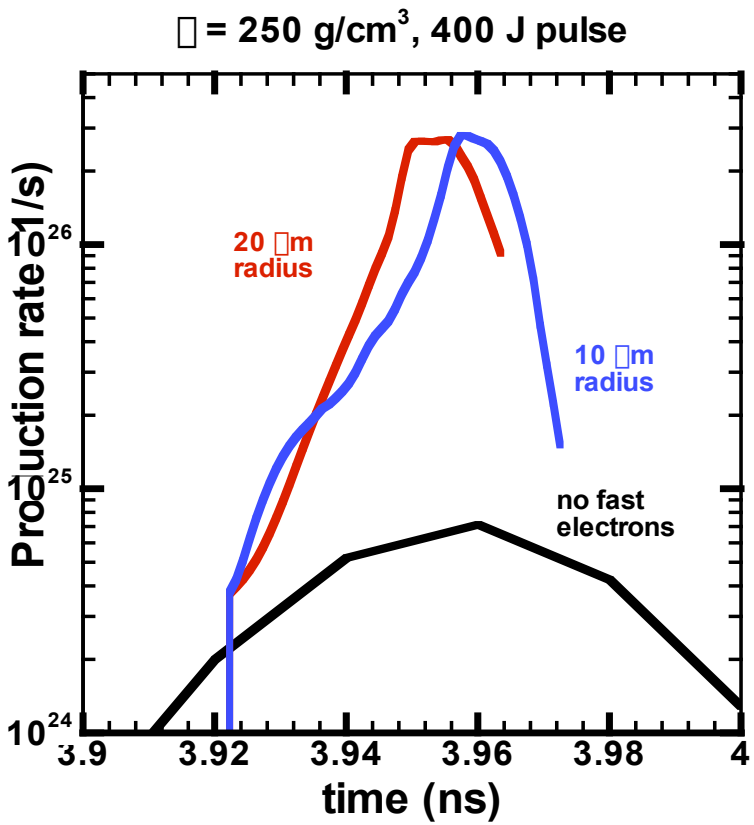

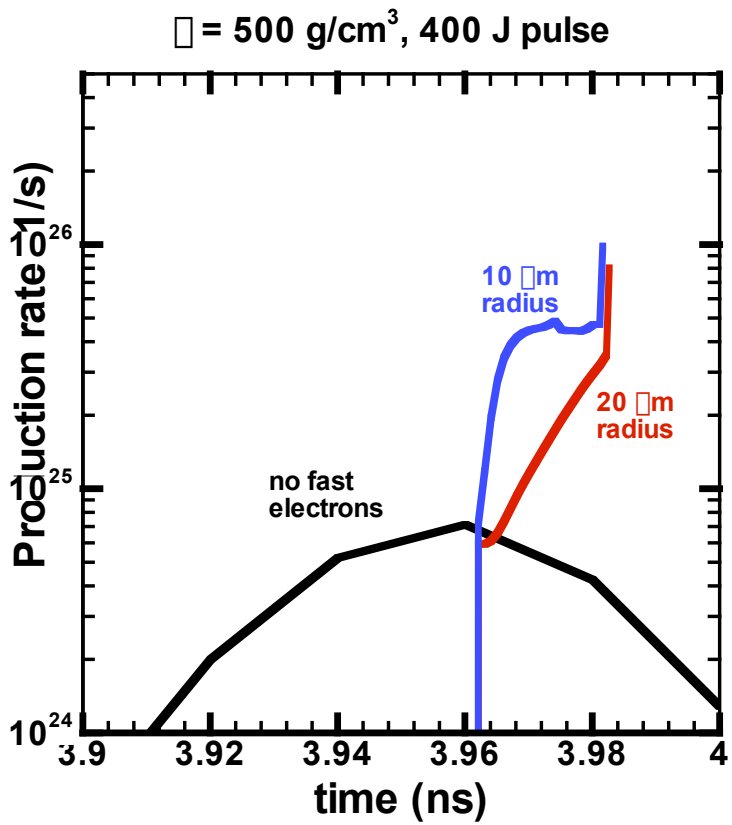

Future work includes improvements in the electron beam source and the transport

- Add a spectrum at a temperature given as a function of the fast-ignitor laser beam.
- Use a slowing down formula for the electron energy loss instead of a penetration depth model.
- Include beam spread.
- Add more realistic physics (return current, electric fields, magnetic fields) to the transport, either explicitly or

Conclusions

Irradiation by the EP fast-ignitor beam of OMEGA-imploded cryogenic capsules provides sensitive observables

- The OMEGA EP laser will produce short-pulse (~20ps), high-intensity beams (>10^{19} W/cm^2) to study the physics of fast ignition.
- A relativistic electron model is being added to the multi-dimensional hydro code DRACO.
- In its first iteration, a simple penetration model is used to slow electrons from a mono-energetic beam source.
- The fast-ignitor beam lead to an increase in the neutron production rate of about an order of magnitude.
- A secondary implosion driven by the heated high density shell can be either “spherical” or one-sided depending on the electron source beam energy
- Many improvements in the model are planned to make it more realistic.

400-J, 1-MeV electron beam of radius 10 μm started at 3.92 ns when ρ_{peak} = 250 g/cm^3

Ion temperature (keV)

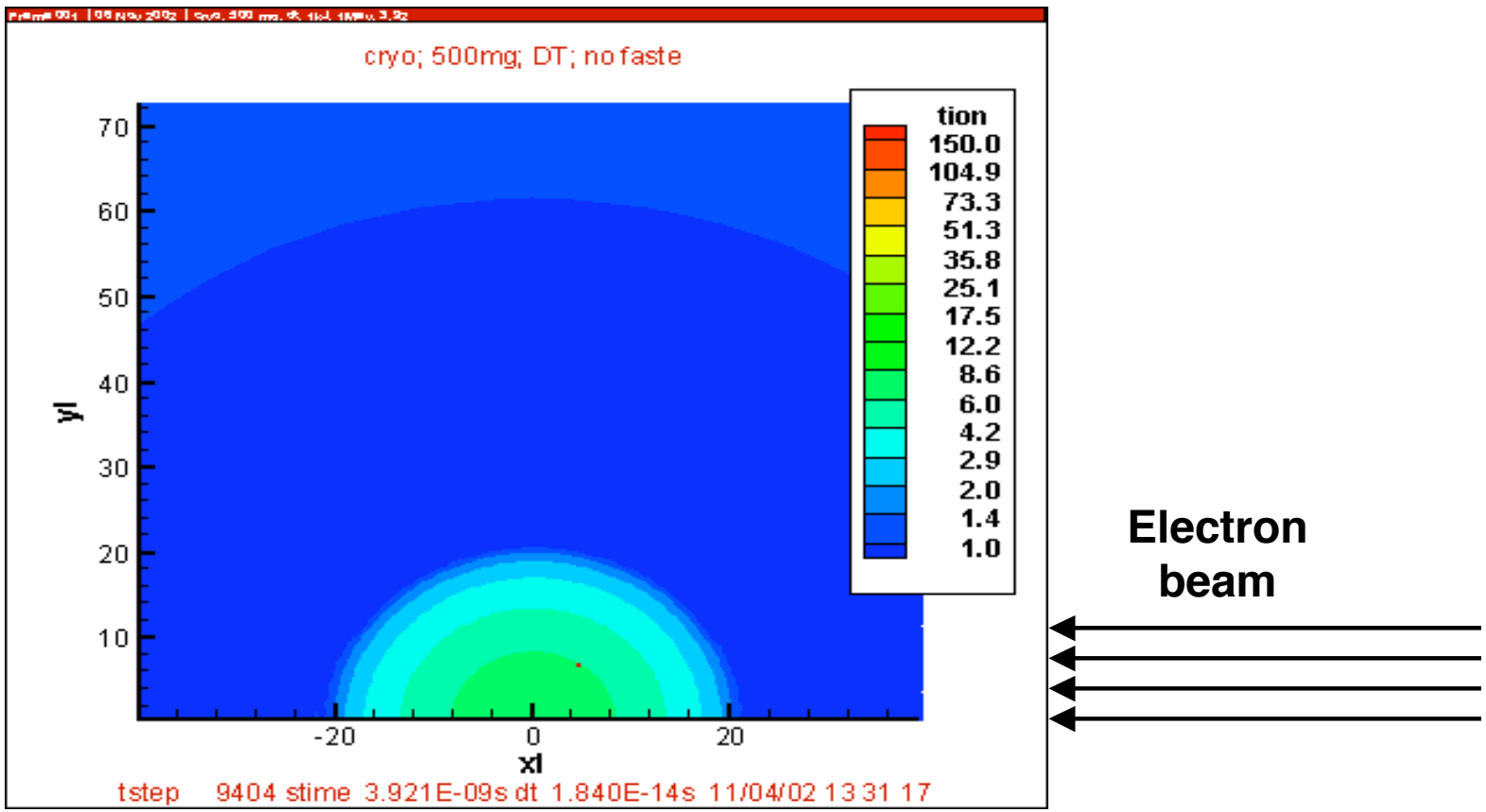

400-J, 1-MeV electron beam of radius 10 μm started at 3.92 ns when ρ_{peak} = 250 g/cm^3

Mass density (g/cm^3)

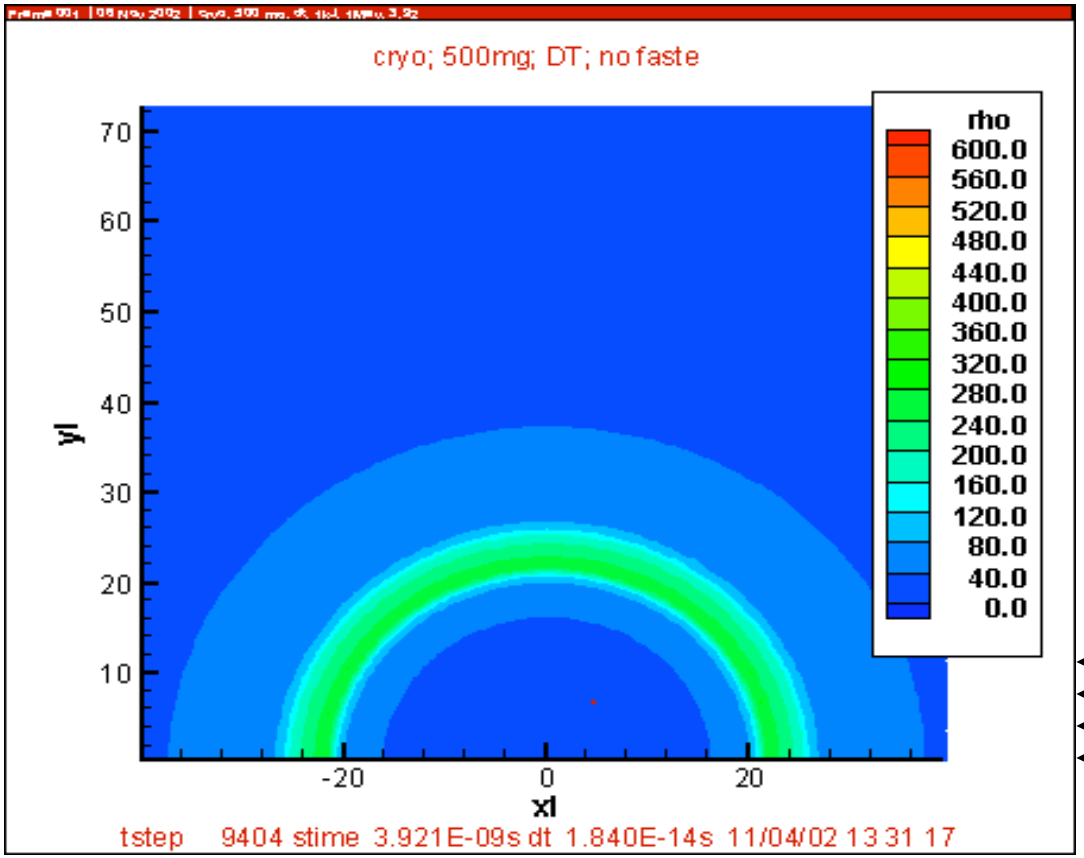

Electron beam

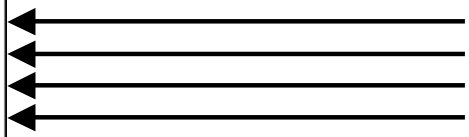

400-J, 1-MeV electron beam of radius 20 μm started at 3.92 ns when ρ_{peak} = 250 g/cm^3

Ion temperature (keV)

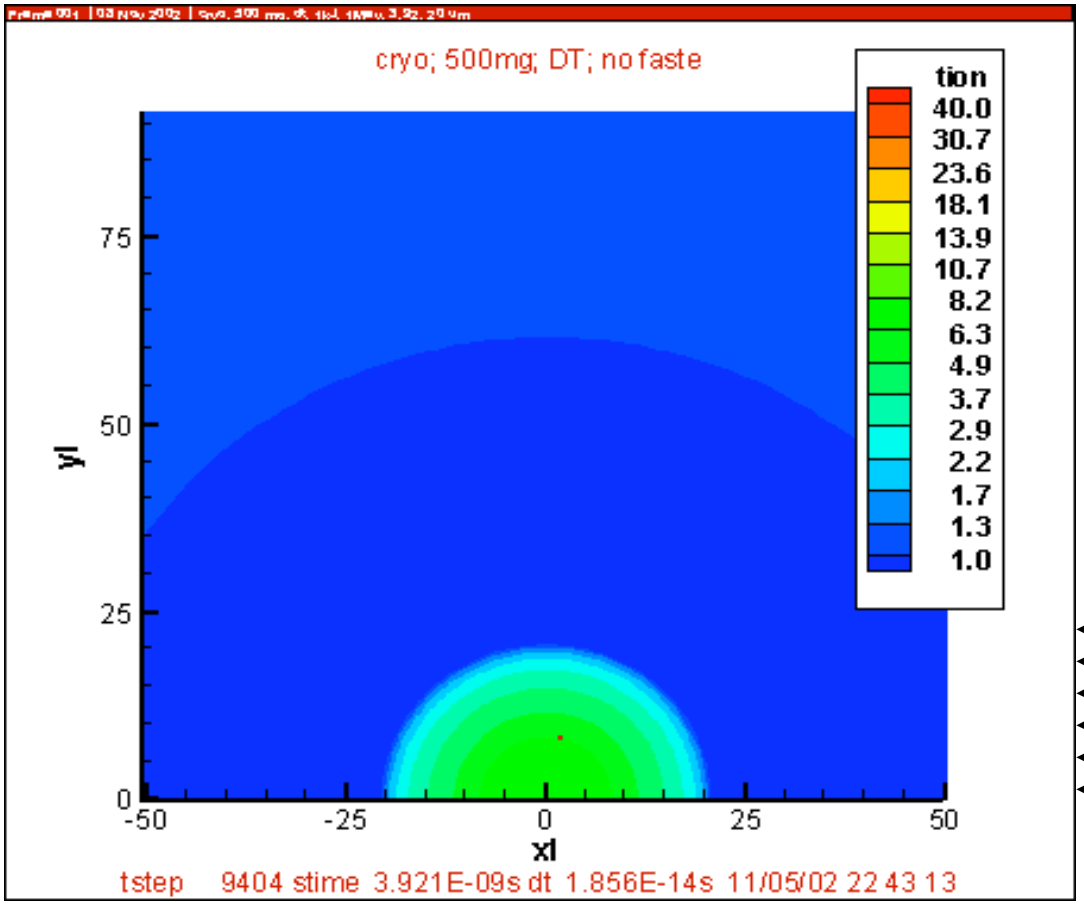

Electron beam

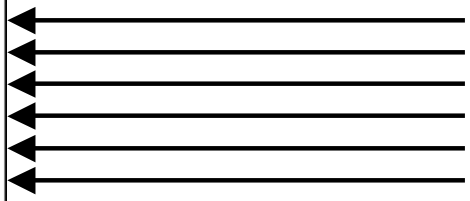

400-J, 1-MeV electron beam of radius 20 μm started at 3.92 ns when ρ_{peak} = 250 g/cm^3

Mass density (g/cm^3)

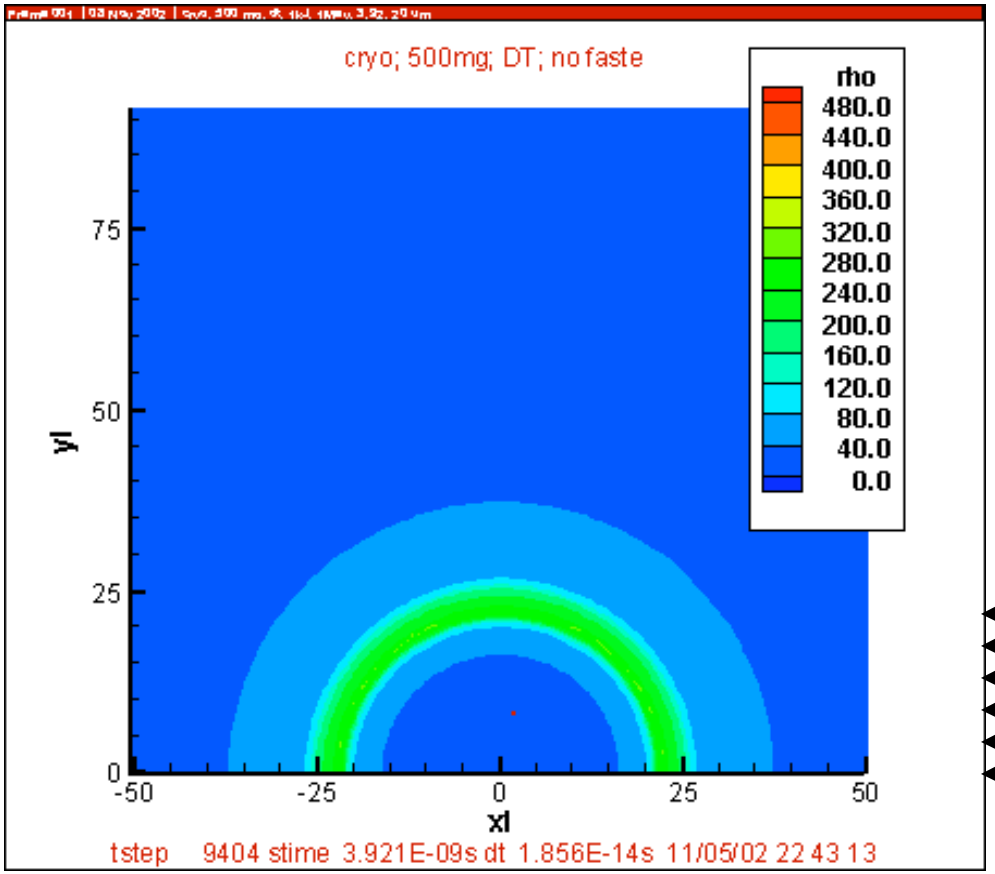

Electron beam

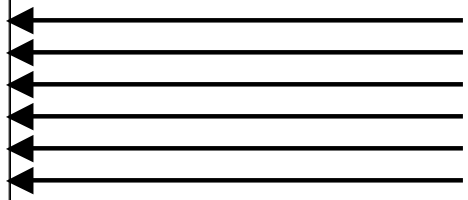

400-J, 1-MeV electron beam of radius 10 μm started at 3.96 ns when ρ_{peak} = 500 g/cm^3

Ion temperature (keV)

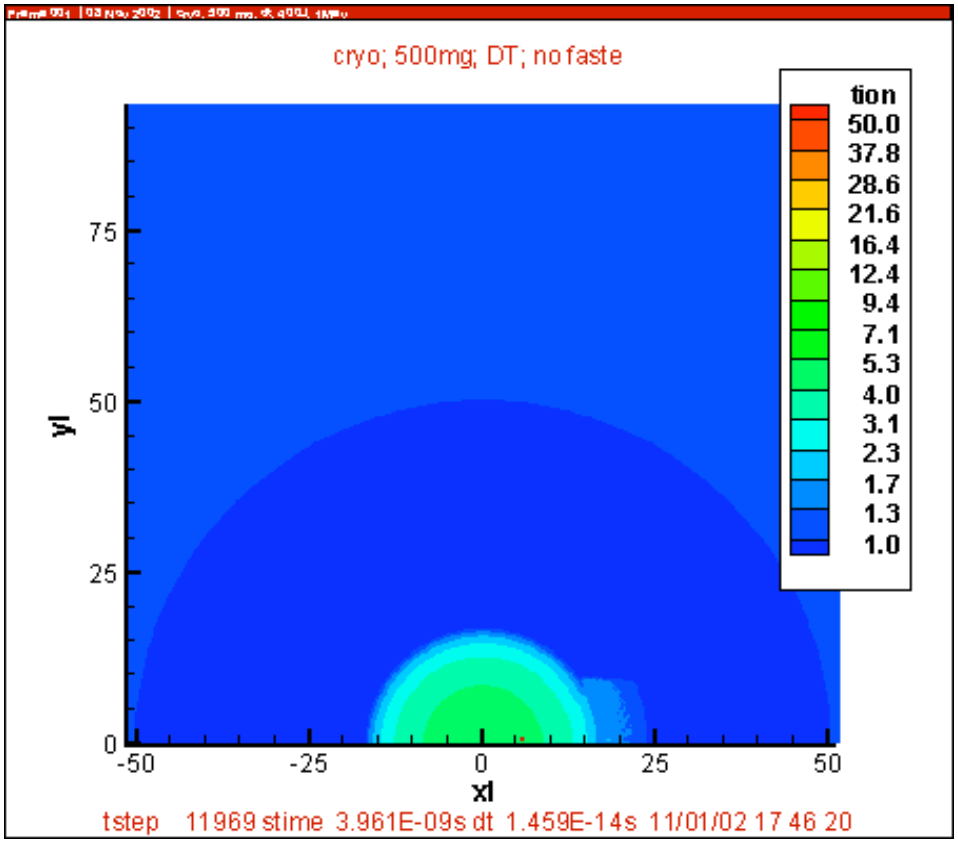

Electron beam

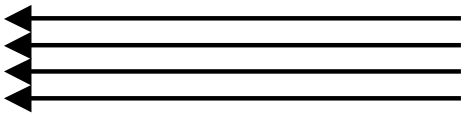

400-J, 1-MeV electron beam of radius 10 μm started at 3.96 ns when ρ_{peak} = 500 g/cm^3

Mass density (g/cm^3)

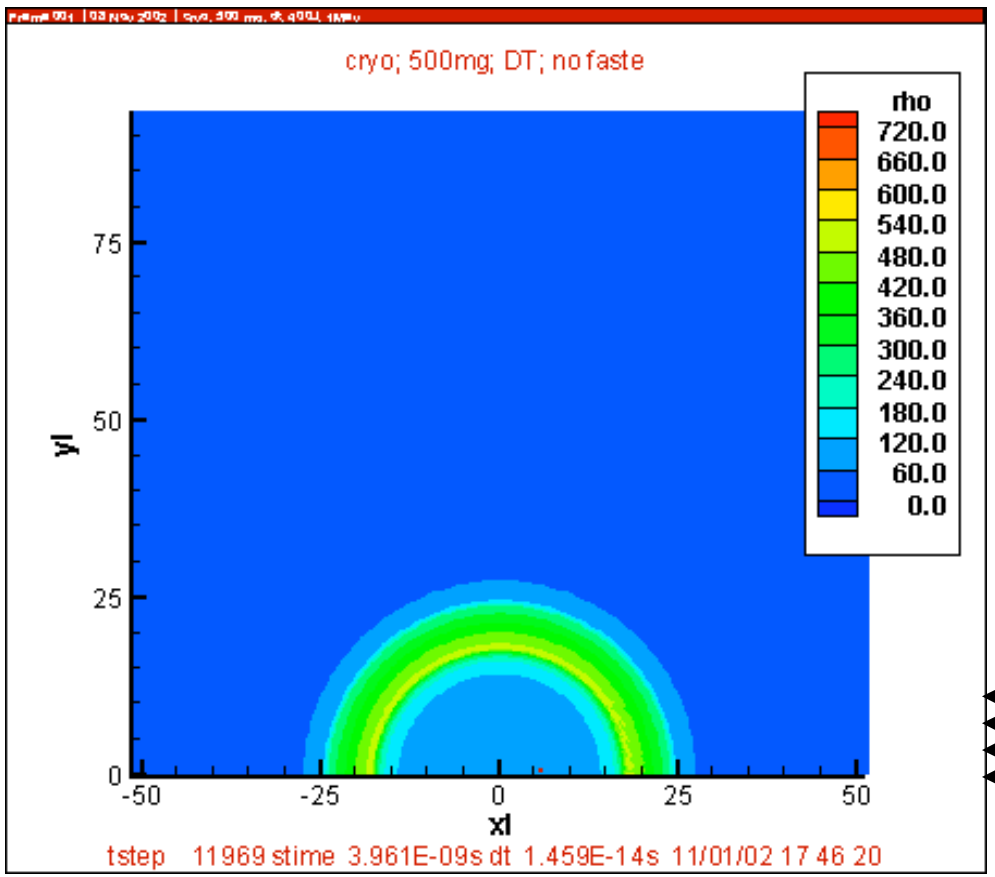

Electron beam

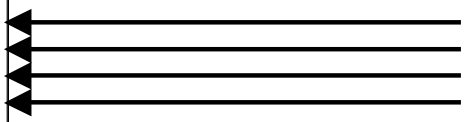

Propagation of charged intense particle beams in precompressed DT fuels

C. DEUTSCH
LPGP, UMR-CNRS 8578
Bât 210, Université Paris-Sud, Orsay, France

6th WKSP Fast Ignition of Fusion Target
16-19 November 2002, St Petes Beach, Florida

- Exponential growth of linear transverse weibel instability instability could be highly detriemental to the REB stopping in the outer layers of DT precompressed core.

- Linear stage plays a crucial role in initiating the transverse and deleterious further filamentation process which could divert a substantial amount of REB energy initially intended to be deposited in the precompressed DT target

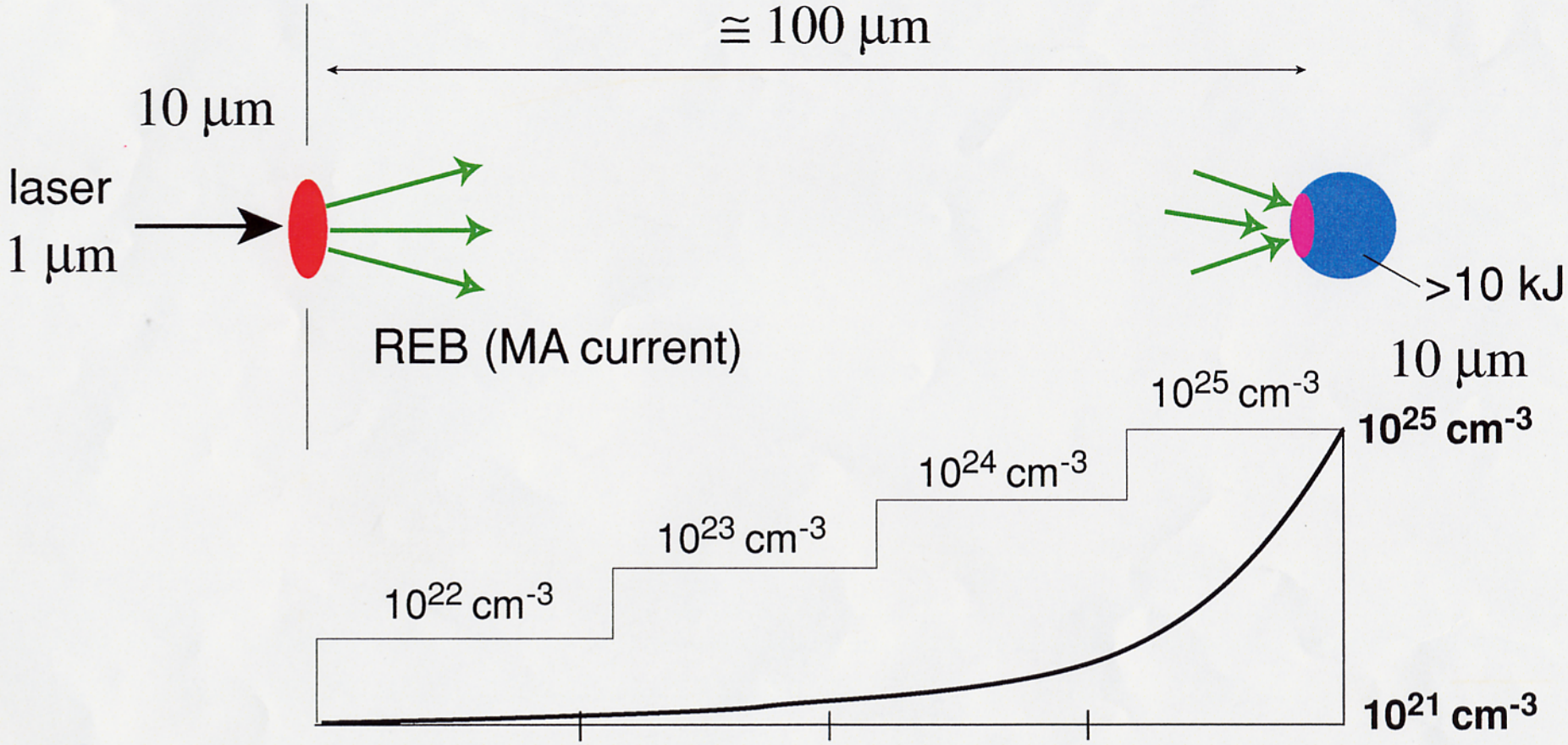
≅ 100 μm
10 μm
laser
1 μm
REB (MA current)
>10 kJ
10 μm
10^{25} cm^{-3}
10^{24} cm^{-3}
10^{23} cm^{-3}
10^{22} cm^{-3}
10^{25} cm^{-3}
10^{21} cm^{-3}

Fried-Conte Dielectric Function

$$W(z) = (2\pi)^{-\frac{1}{2}} \int_{-\infty}^{\infty} \frac{y}{y-z} \exp\left(-\frac{1}{2}y^2\right) dy$$

<u>high θ^p and high θ^b</u>

$$|\xi| < 1 \text{ and } |\eta| < 1$$

$$W(x) = i\left(\frac{1}{2}\pi\right)^{-\frac{1}{2}} \exp\left(-\frac{1}{2}x^2\right) + 1 - x^2 + \ldots.$$

$$1 - \frac{\omega_p^2}{\omega(\omega + i\nu)}\left[1 - A\left(1 + i\left(\frac{1}{2}\pi\right)^{\frac{1}{2}} \frac{\omega + i\nu}{kv_y^p}\right) + \frac{i\nu}{\omega}(1-A)\left(1 + i\left(\frac{1}{2}\pi\right)^{\frac{1}{2}} \frac{\omega + i\nu}{kv_{y'}^p}\right)\right]$$

$$- \frac{\omega_b^2}{\omega^2}\left[1 - B\left(1 + i\left(\frac{1}{2}\pi\right)^{\frac{1}{2}} \frac{\omega}{kv_y^b}\right)\right] = k^2c^2/\omega^2$$

where $v_y^p = \left(\theta_y^p / m\right)^{\frac{1}{2}}$ and $v = \left(\theta_y^b / m_1\gamma\right)^{\frac{1}{2}}$

Weibel-type electromagnetic instability

$$\omega = i\delta$$

δ is the growth rate of the instability

$$\delta, \nu \le \omega_p \text{ and } A \ge 1, B \ge 1$$

$$\delta \approx \delta_0 - (A-1)\nu\left(v_y^p\right)^{-1}\left[A / v_y^p + B\omega_b^2 / v_y^b \omega_p^2\right]^{-1}$$

$$\delta_0 = \left[(A-1)\omega_p^2 + (B-1)\omega_b^2 - k^2c^2\right]\left[\left(\frac{1}{2}\pi\right)^{\frac{1}{2}} A\omega_p^2 / kv_y^p + \left(\frac{1}{2}\pi\right)^{\frac{1}{2}} B\omega_b^2 / kv_y^b\right]^{-1}$$

high θ^p and θ^b

$$\overline{\text{high } \theta^p \text{ and low } \theta^b}$$

$$|\xi| < 1 \text{ and } |\eta| > 1 \text{ For } |y| > 1$$

$$W(y) = -\frac{1}{y^2} - \frac{3}{y^4} - \ldots.$$

$$1 - \frac{\omega_p^2}{\omega(\omega + i\nu)}\left[1 - A - \left(1 + i\left(\frac{1}{2}\pi\right)^{\frac{1}{2}} \frac{\omega + i\nu}{kv_y^p}\right)\right.$$

$$\left. - \frac{i\nu}{\omega}(A-1)\left(1 + i\left(\frac{1}{2}\pi\right)^{\frac{1}{2}} \frac{\omega + i\nu}{kv_y^p}\right)\right] - \frac{\omega_b^2}{\omega^2}\left[1 + B\frac{k^2 v_y^{b2}}{\omega^2}\right] - \frac{k^2c^2}{\omega^2} = 0$$

$$\delta \approx B^{\frac{1}{2}} k v_y^b \omega_b \left[\omega_b^2 + k^2c^2 - (A-1)\left(1 - \left(\frac{1}{2}\pi\right)^{\frac{1}{2}} \frac{\nu}{kv_y^p}\right)\omega_p^2\right]^{-\frac{1}{2}}$$

$$\frac{V_y^b}{c} \le \frac{\delta/\omega_p}{kc/\omega_p} \le \frac{V_y^p}{c}$$

From the dielectric tensor, we obtain the nonlinear dispersion relation for a purely transverse wave in the following form :

$$1+\chi^{NL}(k,\omega)=\frac{k^2c^2}{\omega^2},$$

$$\chi^{NL}(K,\omega)=-\frac{4\pi q^2}{\omega}i\int dp\tilde{G}(k,p,\omega)\left[\left(1-\frac{k\cdot v}{\omega}\right)v+\left(\frac{v^2}{\omega}-\frac{k\cdot v}{k^2}\right)k\right]\cdot\frac{\partial f(p)}{\partial p},$$

where $\chi^{NL}(k,\omega)$ denotes the nonlinear susceptibility

$$\tilde{G}(k,v,\omega)=\int_0^\infty dt\exp\left[i(\omega-k\cdot v)t-\frac{1}{3}\tilde{D}(v)k^2t^3\right],$$

where

$$\tilde{D}(v)=\frac{q^2}{(m\gamma)^2}\sum_{k_1}\int\frac{d\omega_1}{2\pi}\left|E(k_1,\omega_1)+\frac{v}{c}\times B(k_1,\omega_1)\right|^2$$
$$\times\int_0^\infty dt\exp\left[-i(\omega_1-k_1\cdot v)t-\frac{1}{3}\tilde{D}(v)k_1^2t^3\right]$$

Moreover, it is also useful to remark that the quasi-linear theory (Dupree-Weinstock) based on mode-mode coupling can provide even more accurate parameters, in the form

$$\boxed{A' = \frac{AT_p}{T_p + XD}\ ,\ B' = \frac{BT_p}{T_b + XD}}$$

with X, positive solution of ($u = (r\,v_b/\gamma_b)^2$)

$$\left(1+r^2\right)X^4 + \left[r^2\frac{T_p}{m} + \frac{T_b}{m\gamma}\left(1+r^2\right)\right]X^2 - u\left[\frac{T_p}{m} + \frac{T_b}{m\gamma}\left(u^2 - r^2\frac{T_p}{m}\right)\right] = 0$$

and $D = 511r\ (1-\gamma_b^{-1})$ in keV. Using respectively (A,B) and A',B') into the relevant linear dispersion relations, we obtain the WEI growth rates depicted on Figs. as linear and turbulent, respectively. We then emphasize moderately hot (T_p=100 eV) outer DT layers and 1 MeV REB with a thermal T_b=1 keV. Maximum LGR δ_{max} occurs close to the skin depth wavelength c/ω_p. δ_{max} is also shown steadily decaying with increasing N_p. Also, quasi-linear ('Turbulent') LGR profiles stand beneath linear ones.

$$\theta_y^p / m \rightarrow \theta_y^p / m + \frac{\omega_b^2}{\omega_p^2} \frac{p_d^{b2}}{m^2 \gamma^2}$$

$$\theta_y^b / m\gamma \rightarrow \theta_y^b / m\gamma + \frac{\omega_b^2}{\omega_p^2} \frac{p_d^{b2}}{m^2 \gamma^2}$$

$$p_d^b = mV_b$$

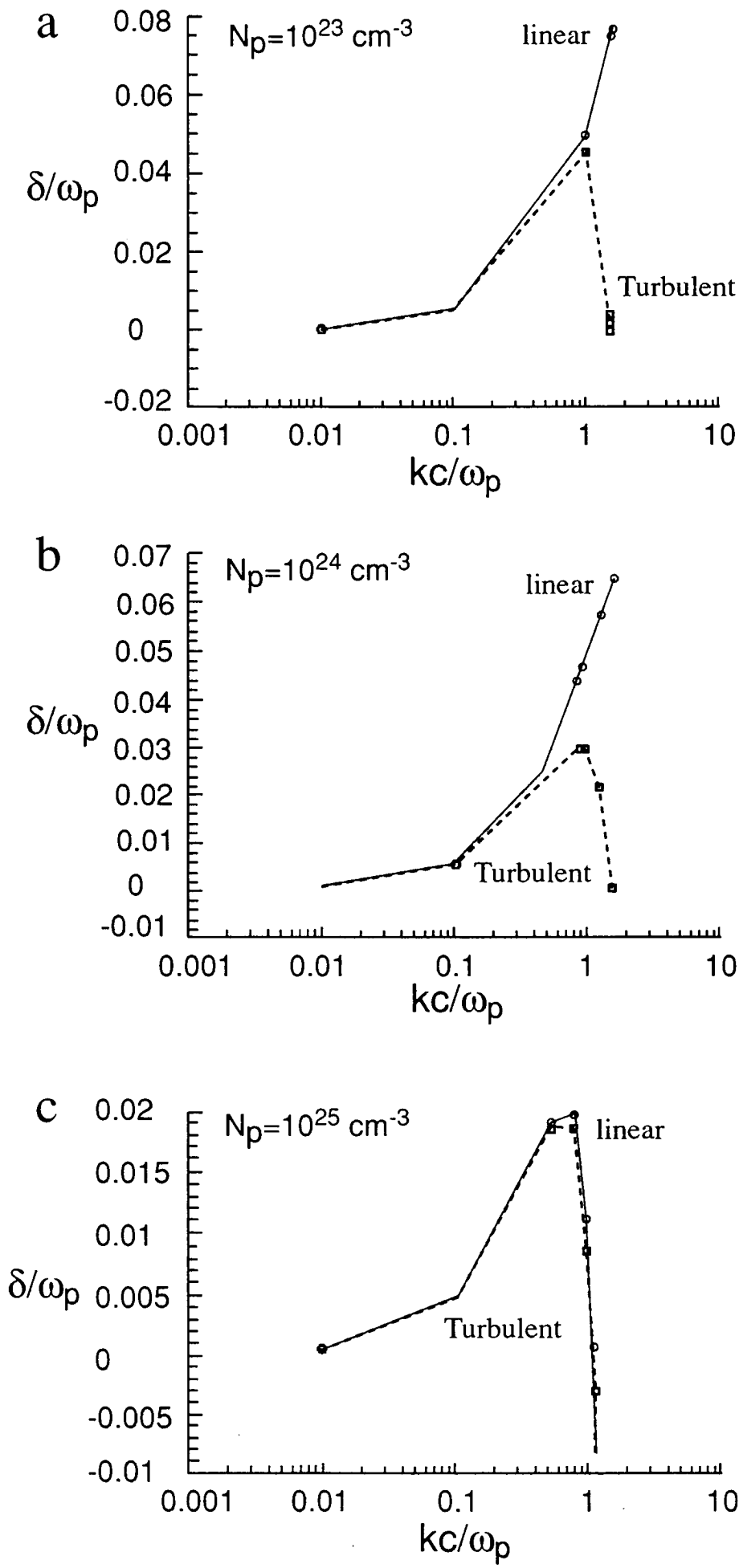
a
$N_p=10^{23}$ cm^{-3}
linear
Turbulent
δ/ω_p
0.08
0.06
0.04
0.02
0
-0.02
0.001
0.01
0.1
1
10
kc/ω_p
b
$N_p=10^{24}$ cm^{-3}
linear
Turbulent
δ/ω_p
0.07
0.06
0.05
0.04
0.03
0.02
0.01
0
-0.01
0.001
0.01
0.1
1
10
kc/ω_p
c
$N_p=10^{25}$ cm^{-3}
linear
Turbulent
δ/ω_p
0.02
0.015
0.01
0.005
0
-0.005
-0.01
0.001
0.01
0.1
1
10
kc/ω_p

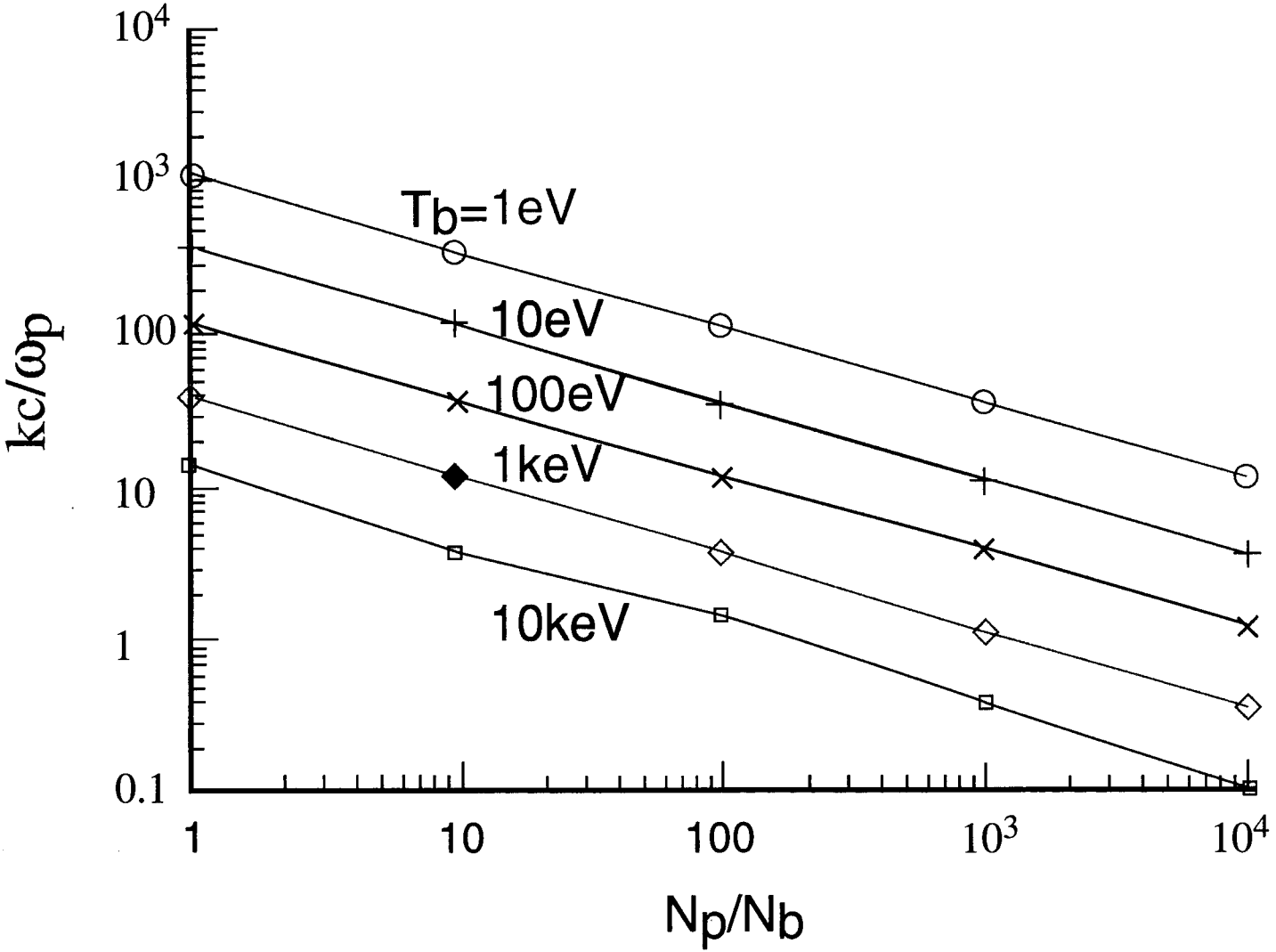
10^4
10^3
100
10
1
0.1
kc/ωp
Tb=1eV
10eV
100eV
1keV
10keV
1
10
100
10^3
10^4
Np/Nb

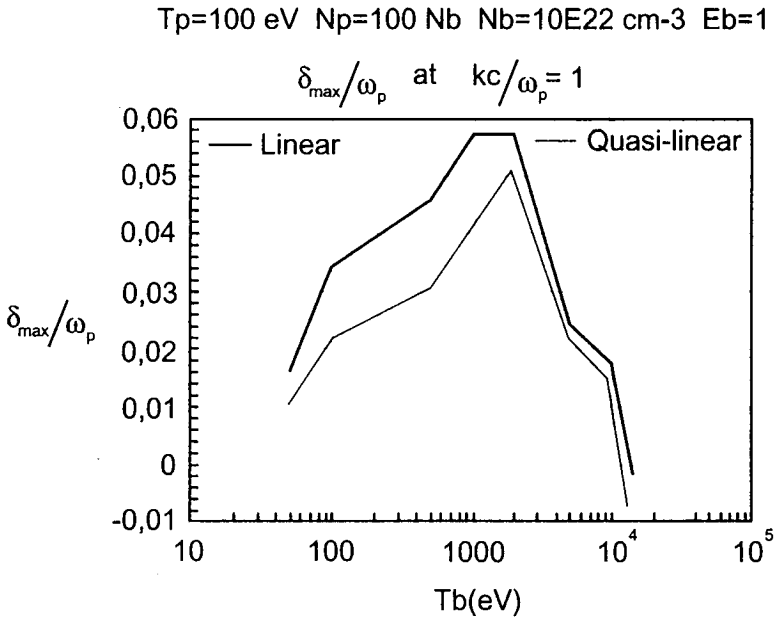
Tp=100 eV Np=100 Nb Nb=10E22 cm-3 Eb=1 MeV
δmax/ωp at kc/ωp= 1
Linear
Quasi-linear
δmax/ωp
0,06
0,05
0,04
0,03
0,02
0,01
0
-0,01
10
100
1000
10^4
10^5
Tb(eV)

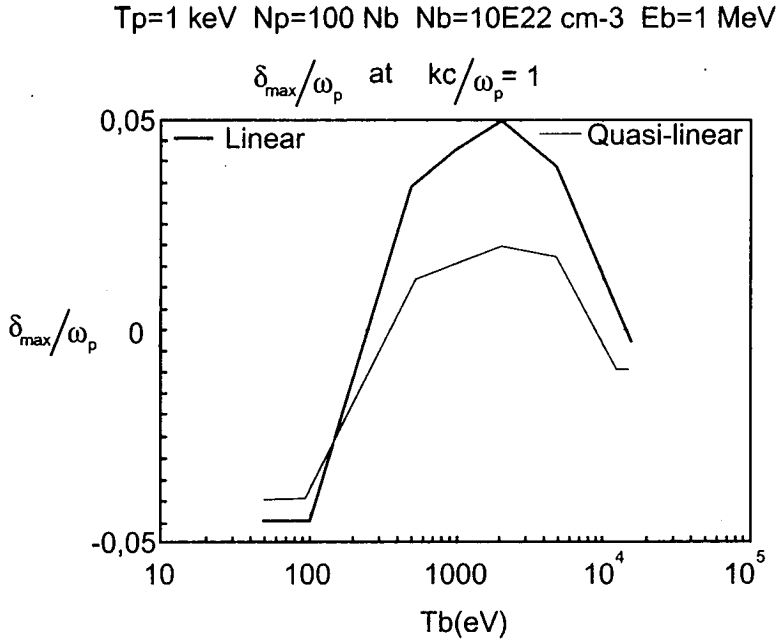
Tp=1 keV Np=100 Nb Nb=10E22 cm-3 Eb=1 MeV
δmax/ωp at kc/ωp= 1
Linear
Quasi-linear
δmax/ωp
0,05
0
-0,05
10
100
1000
10^4
10^5
Tb(eV)

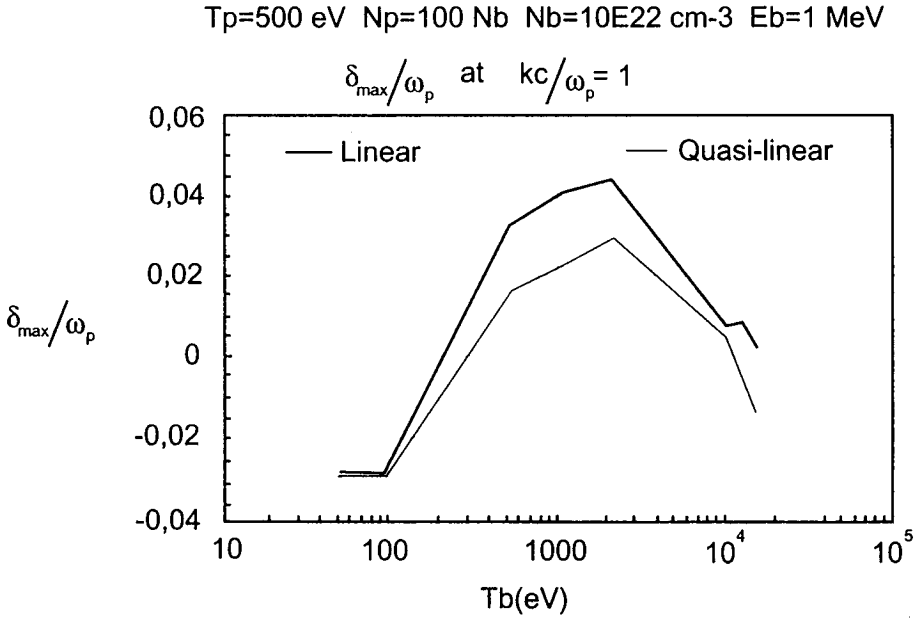
Tp=500 eV Np=100 Nb Nb=10E22 cm-3 Eb=1 MeV
δmax/ωp at kc/ωp= 1
Linear
Quasi-linear
δmax/ωp
0,06
0,04
0,02
0
-0,02
-0,04
10
100
1000
10^4
10^5
Tb(eV)

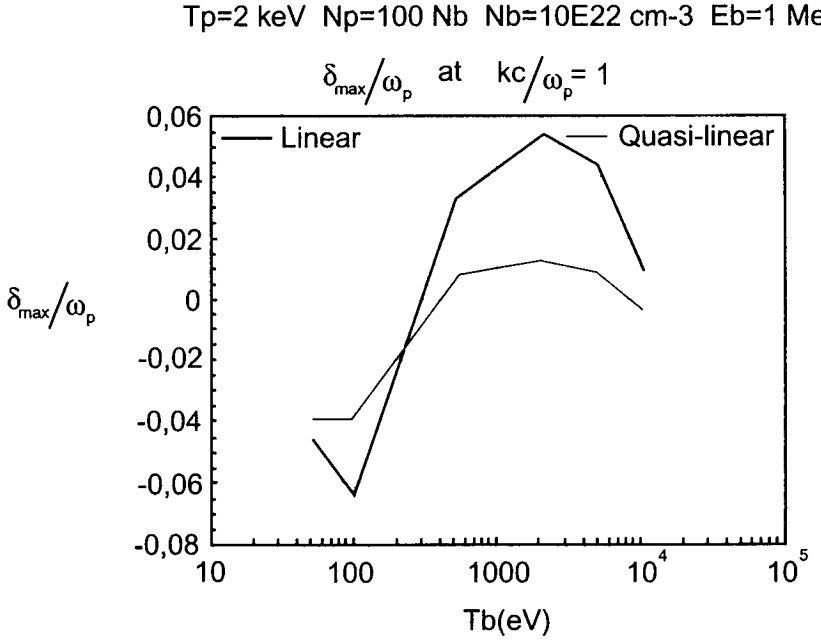
Tp=2 keV Np=100 Nb Nb=10E22 cm-3 Eb=1 MeV
δmax/ωp at kc/ωp= 1
Linear
Quasi-linear
δmax/ωp
0,06
0,04
0,02
0
-0,02
-0,04
-0,06
-0,08
10
100
1000
10^4
10^5
Tb(eV)

Tp=3 keV Np=100 Nb Nb=10E22 cm-3 Eb=1 MeV

δ_{max}/ω_p at $kc/\omega_p = 1$

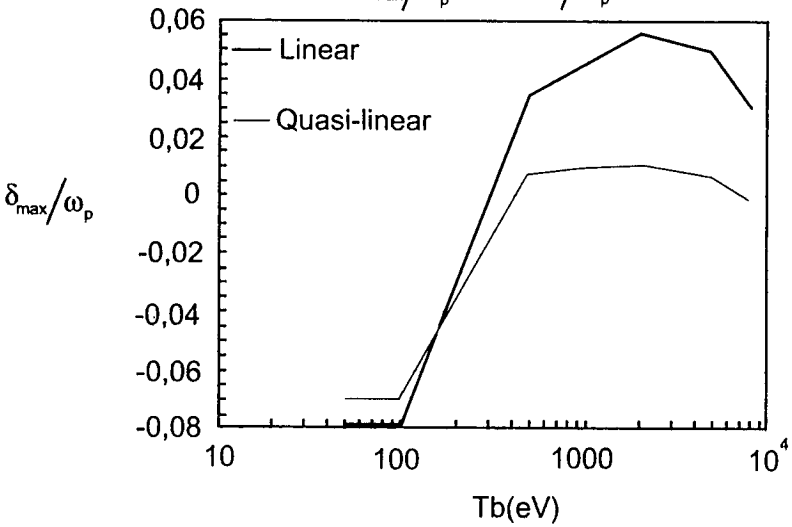

Tp=5 keV Np=100 Nb Nb=10E22 cm-3 Eb=1 MeV

δ_{max}/ω_p at $kc/\omega_p = 1$

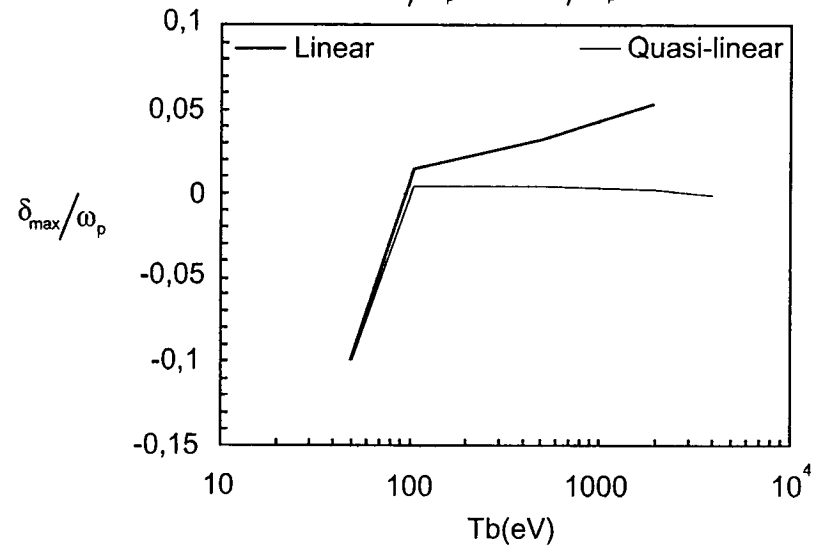

Tp=10 keV Np=100 Nb Nb=10E22 cm-3 Eb=1 MeV

δ_{max}/ω_p at $kc/\omega_p = 1$

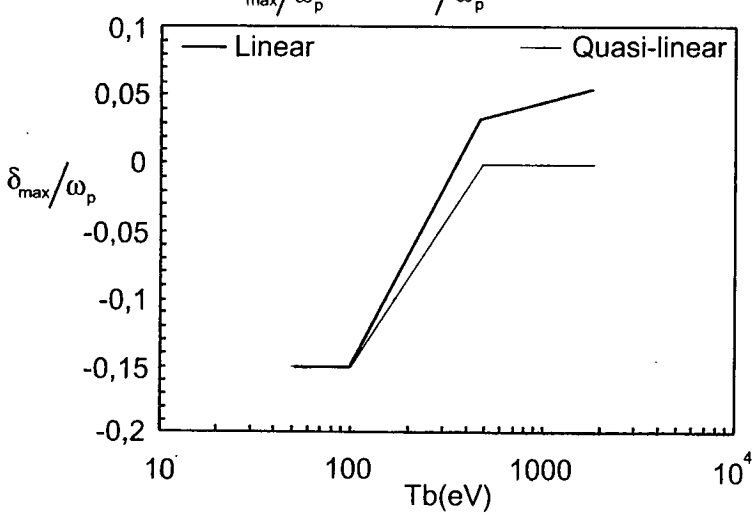

$$N_{efold} = \delta_{max} T_{stop}$$

$$T_{stop} = \frac{1}{c} \int_{E_b^{min}}^{E_b^{max}} \frac{1 + \frac{E_b}{m_e c^2}}{\left[\left(\frac{E_b}{m_e c^2}\right)\left(\frac{E_b}{m_e c^2 + 2}\right)\right]^{1/2}} \times \frac{dE_b}{\frac{dE_b}{dx}}$$

$$\cong \frac{100}{4} \times 10^{-4} \ \text{cm} \times \frac{1}{\beta_b c \ \text{cm/sec}}$$

$$\cong 10^{-13} \ \text{sec for 1 MeV REB}$$

- $\frac{\delta_{max}}{\omega_p}$ strongly dependent on $\frac{T_b}{T_p}$ and $\frac{N_b}{N_p}$

- Linear growth rates go negative for $T_b > 10$ keV

- $\frac{\delta_{max}}{\omega_p}$ # 0 for $T_p > 3$ keV

OPTIMAL REB TRANSPORT

$T_p > 3$ keV $T_b > 100$ eV $N_p > 100\ N_b$

Hole Boring thus Stands as a

Prerequisite to the Fast Ignition Scenario

for IFE

Tp= 100 eV Np = 100 Nb Nb = 10^22 CM-3 Eb = 25 MeV
Protons

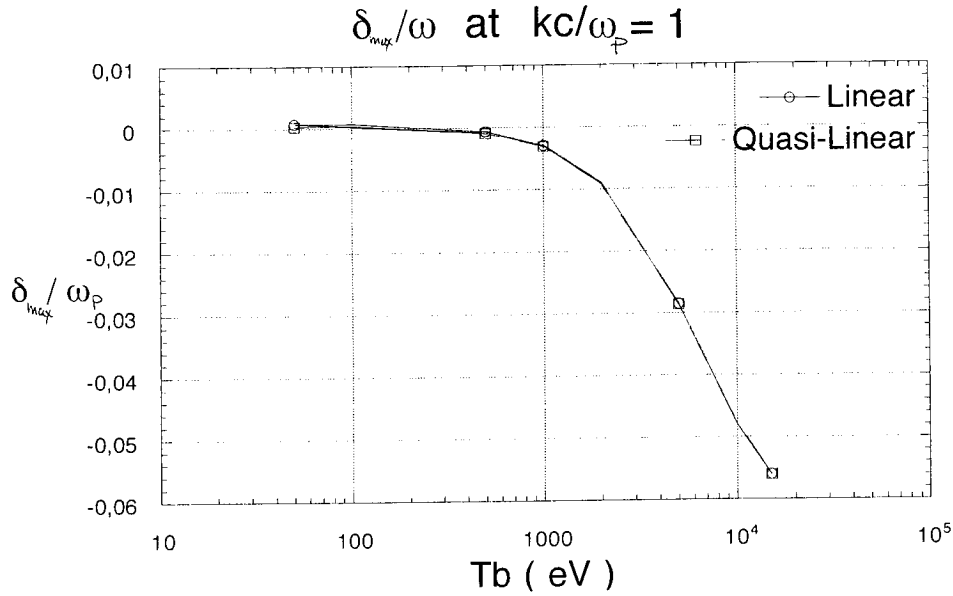

Tp = 500 eV Np/Nb = 100 Eb (Proton) = 25 MeV

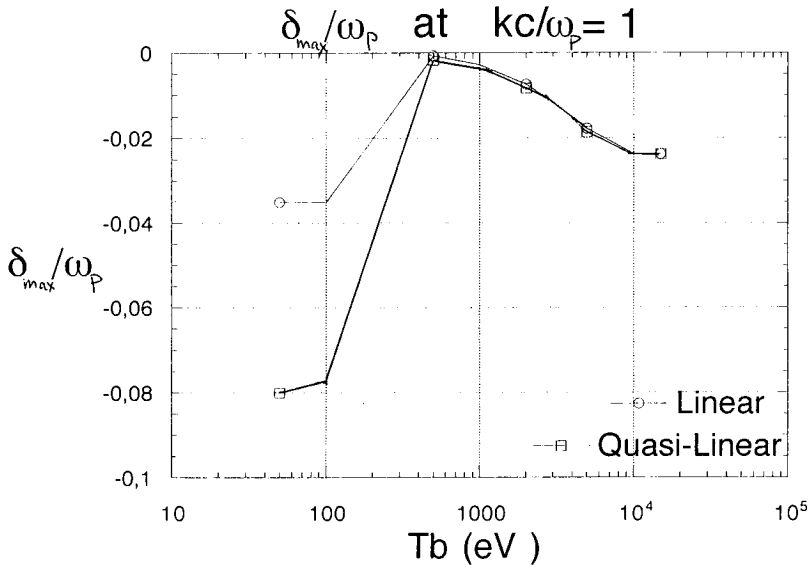

Tp = 1 keV Np/Nb = 100 Eb (Proton) = 25 MeV

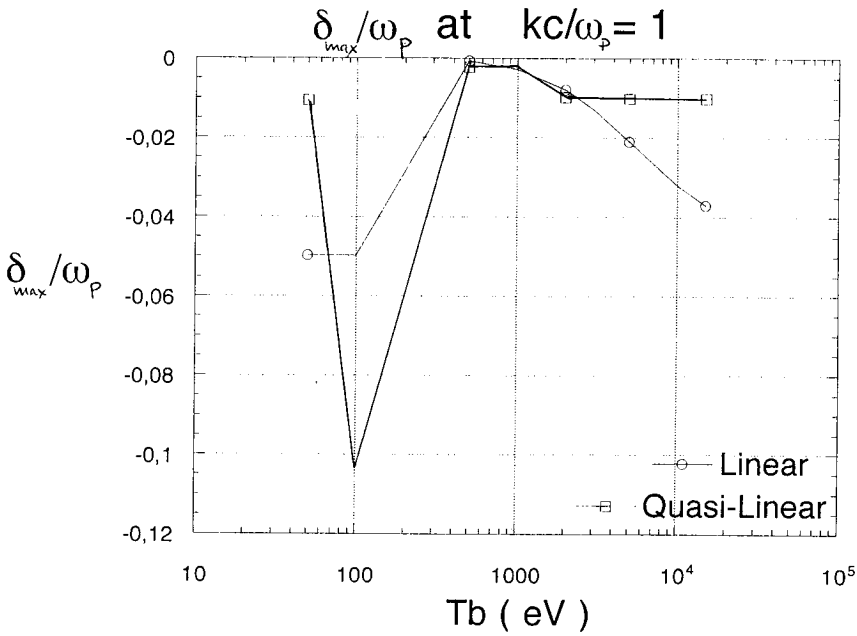

Tp = 3 keV Np/Nb = 100 Eb (Proton) = 25 MeV

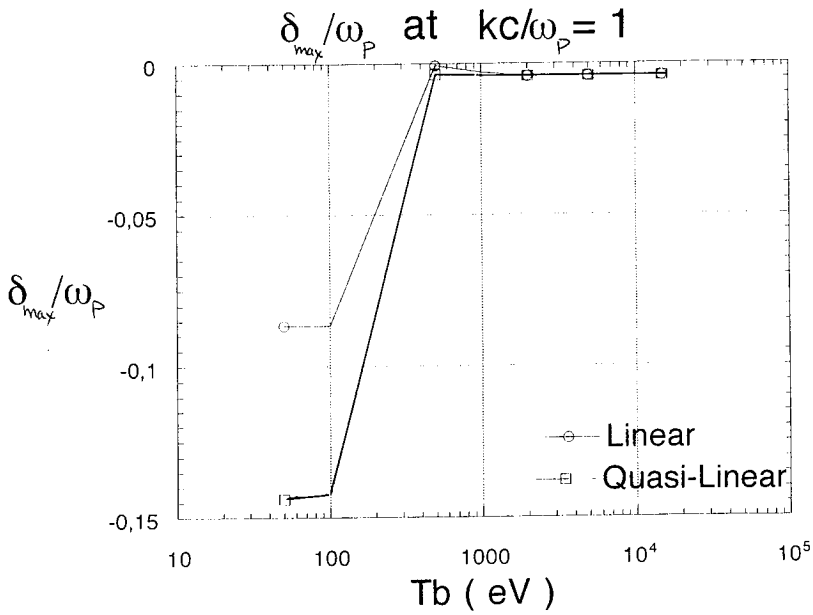

Tp = 5 keV Np / Nb =100 Eb (Proton) = 25 MeV

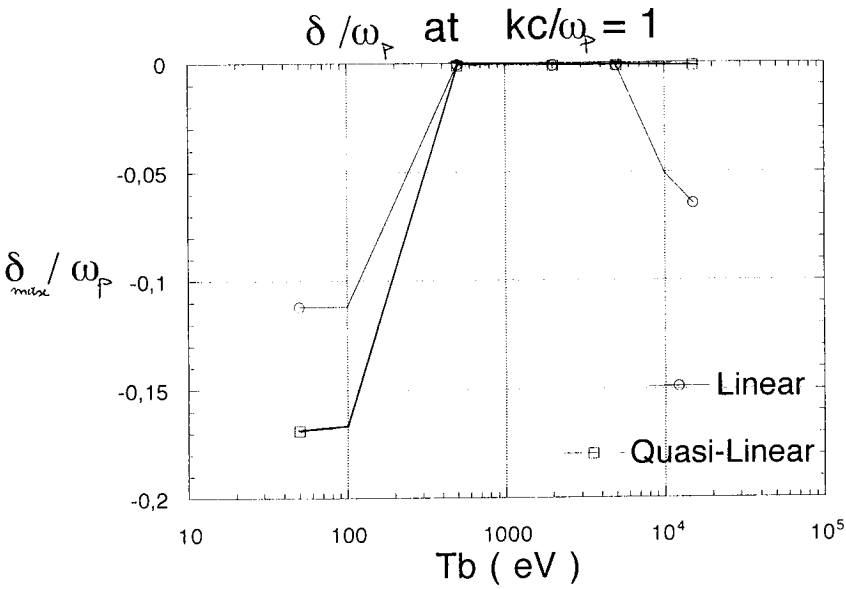

Tp = 10 keV Np/Nb = 100 Eb (Proton) = 25 MeV

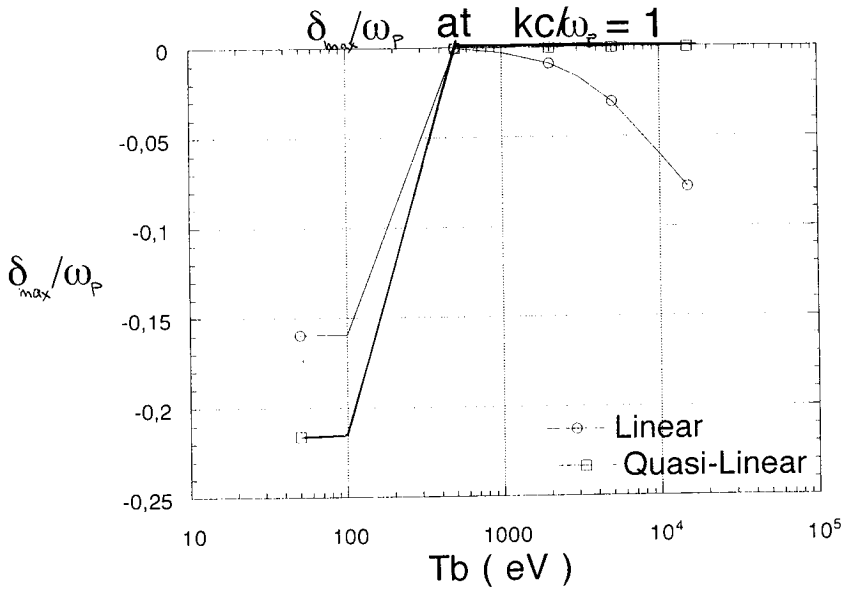

In summary, we have demonstrated through an efficient analytical modelling of the laser produced REB interacting with outer less dense layers of the supercompressed DT core that the initial in depth propagation phase of the REB within fast ignitor scenario could be effective on a time scale afforded by the linear growth of the electromagnetic instability, provided due account is given to temperature distributions in projectiles and target, respectively.

Those considerations are even more appropriate for nonrelativisitic proton beams which might offer the best option for driving fast ignition, provided their laser efficiency could be increased above 20 percent.

STRONG LANGMUIR TURBULENCE
(S L W)

cf. V.M. Malkin and N.J. Fish,, PRL **89**, 125004-1 (2002)

REB safely transported to the core provided density gradients are kept steep enough.

Inverse logarithmic slope of plasma density

$$L_n < L_{nc} = \frac{N_{ef}\ \omega_p}{2\int \Gamma(\vec{k})dk_{//}}$$

$$\Delta k_{//} \cong \frac{\Delta\theta\ \omega_p}{2c}$$

$$\swarrow$$

$$L_{nc} \approx \frac{N_{ef}\, c}{\Gamma\ \ \Delta\theta}$$

with $\Gamma \approx \omega_p \dfrac{n_b}{n_p}$ in kinetic regime

$$\max_{k//} \Gamma(\vec{k}) \sim \frac{2\omega_p}{\gamma_b \Delta\theta^2} \cdot \frac{n_b}{n_p}$$

with $k// \sim \frac{\omega_p}{c}$

Relevant quantity for REB collective stopping is beam relaxation length (BRL)

$$L_r \sim \frac{\gamma_b n_b m_e c^3}{\Gamma \; W_r}$$

W_r = LW energy density resonantly interacting with REB

$$L_r \sim \left(\frac{c}{2\omega_p}\right)\left(\frac{m_e c^2}{T_p}\right)^2 (\gamma\Delta\theta)^2 \left(\frac{W_{th}}{W_r}\right)$$

For modulational LW

$$W_{th} \cong \frac{n_p T_p^2}{m_e c^2}$$

If $W \geq W_{th}$ and $L_r \leq 50\ \mu m$

$np \sim 10^{26}$ e-cm^{-3} and $T_p \sim 1$ keV

$$\gamma_b \Delta \theta \leq 1$$

LW then tunes REB collective stopping just in the core.

CONCLUSION

Collective effects in the REB-target plasma interaction might prove helpful for achieving ICF fast ignition

ION ACCELERATION EXPERIMENTS WITH THE NEW SHORT-PULSE CAPABILITY ON TRIDENT

presented by:

Juan C. Fernández*

with contributions from:

B. Manuel Hegelich†, James A. Cobble*, Julien Fuchs‡[1], Thomas E. Cowan[1], Erik Brambrink†, Mathias Geissel†, Nathalie Renard-LeGalloudec[2], Samuel A. Letzring*, Randall P. Johnson*, Tsutomu Shimada*, Robert B. Gibson*, and Markus Roth†

†GSI, *Los Alamos, ‡LULI, [1]GA, [2]UNR

presented to:

6th Workshop on Fast Ignition of Fusion Targets

St. Pete's Beach, Florida on November 16--19, 2002

Outline:

- Laser system
  - Air compressor works fine!
- Ion-acceleration results:
  - Shaped foils
  - Deuterated-plastic
- Proton radiography
- Summary

Trident glass-laser system:

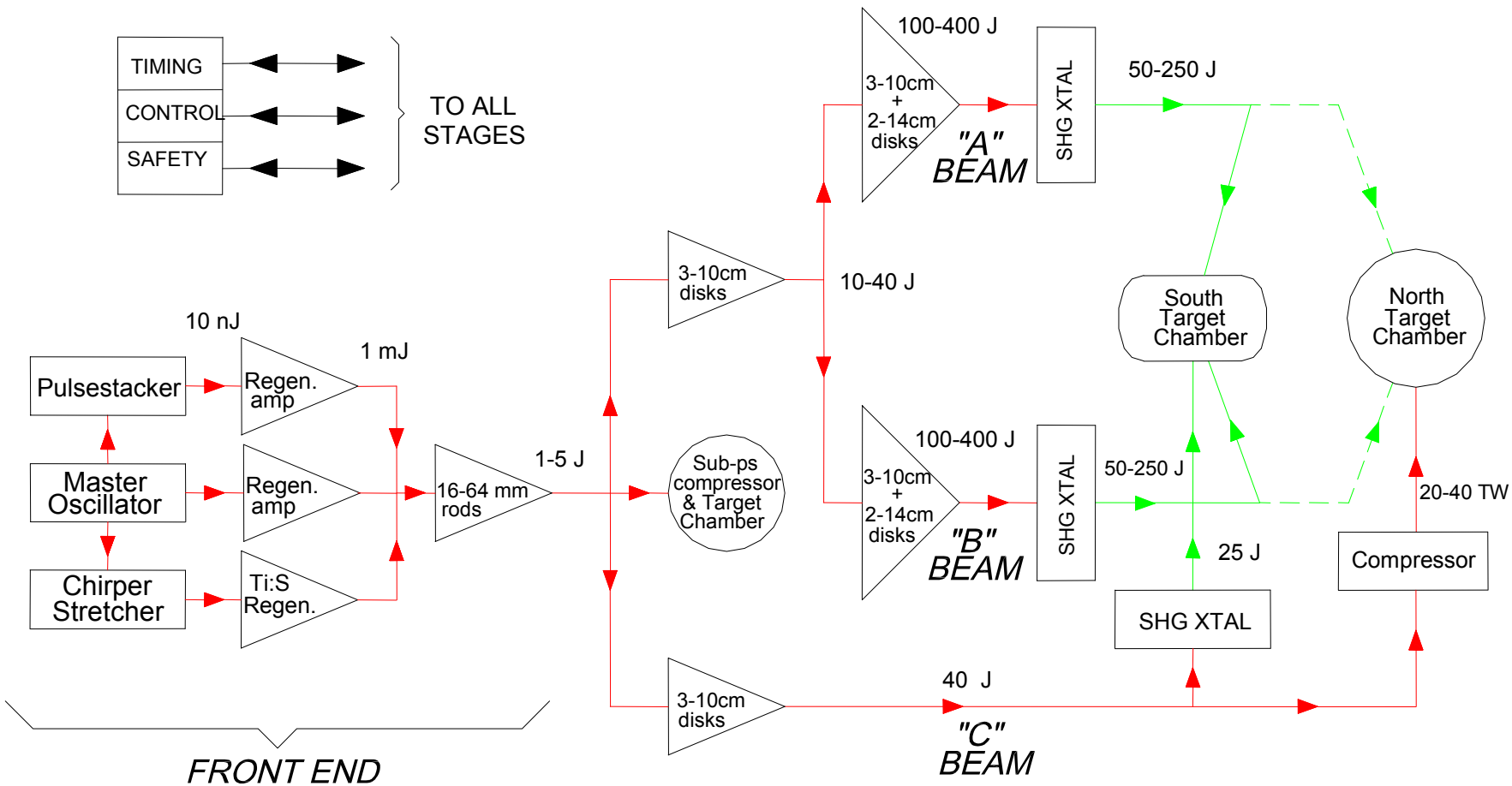

Energies shown are for pulse length range of .1-2 ns. C-beam could deliver 100 J Max.

Trident produces energetic pulses over 6.5 orders of magnitude in pulse length.

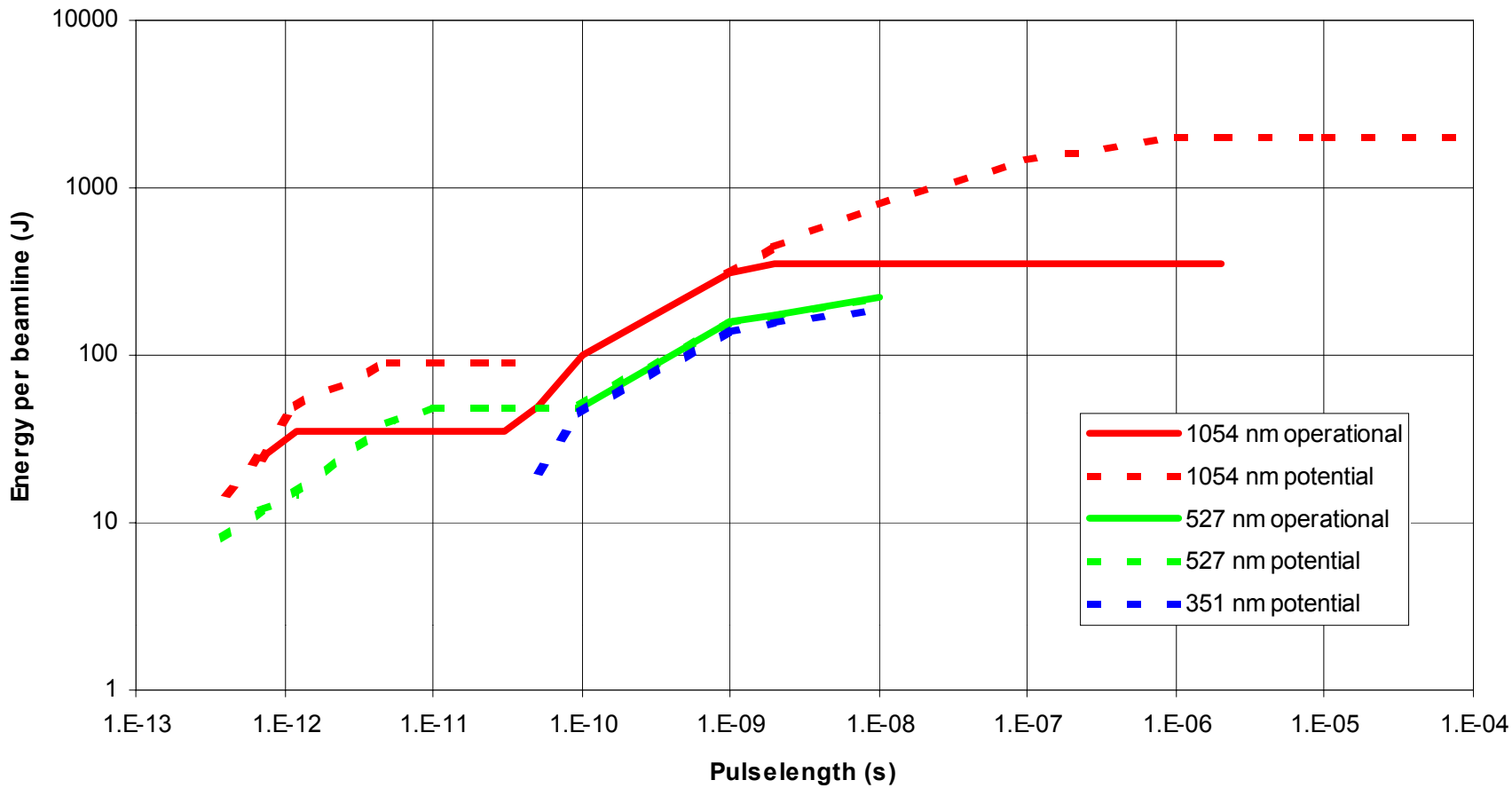

Trident C Beam delivers 30 TW sub-ps laser pulses.

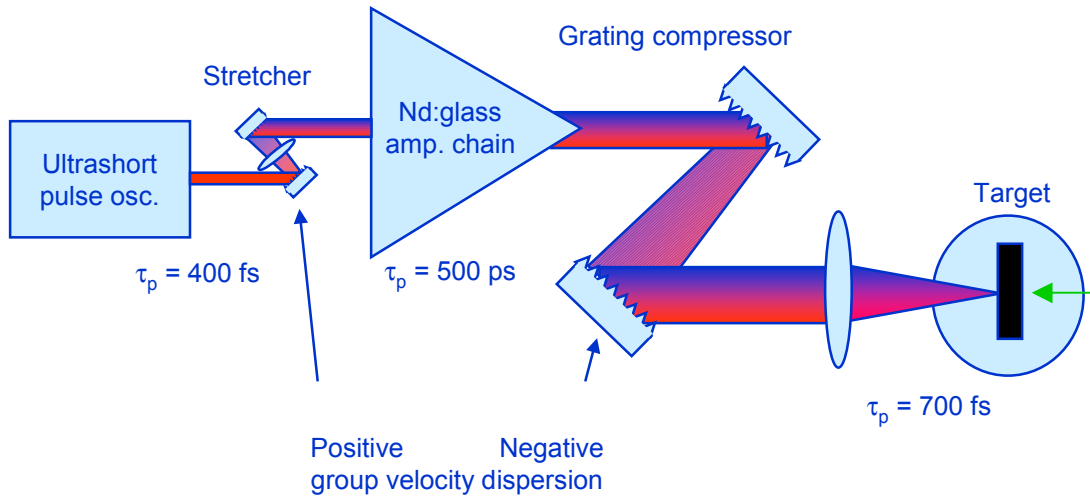

$E = 20\text{-}30$ J
$\tau_p = 0.6 - 1.0$ ps
$P = 30$ TW
$\lambda = 1053$ nm
$d_{spot} = 20\ \mu m$
$I > 10^{19}$ W cm^{-2}

- Conventional regenerative-amplifier oscillator stage → sub ps pulse
- Pulse is stretched to ~ 0.5 ns
- Pulse is amplified in standard Nd:glass amplifier
- Pulse is re-compressed in air (B-integral > 5) to ~ 0.6 – 0.7 ps with 40 cm Au gratings.
  - Serious beam breakup seen at > 30 TW.
- Pulse is focused with an f/2 parabola to 3 – 4 X diffraction-limit.
- Use 4 Pockels cells → contrast should be < 10^{-6}.

Trident C Beam compressor and North Target Chamber

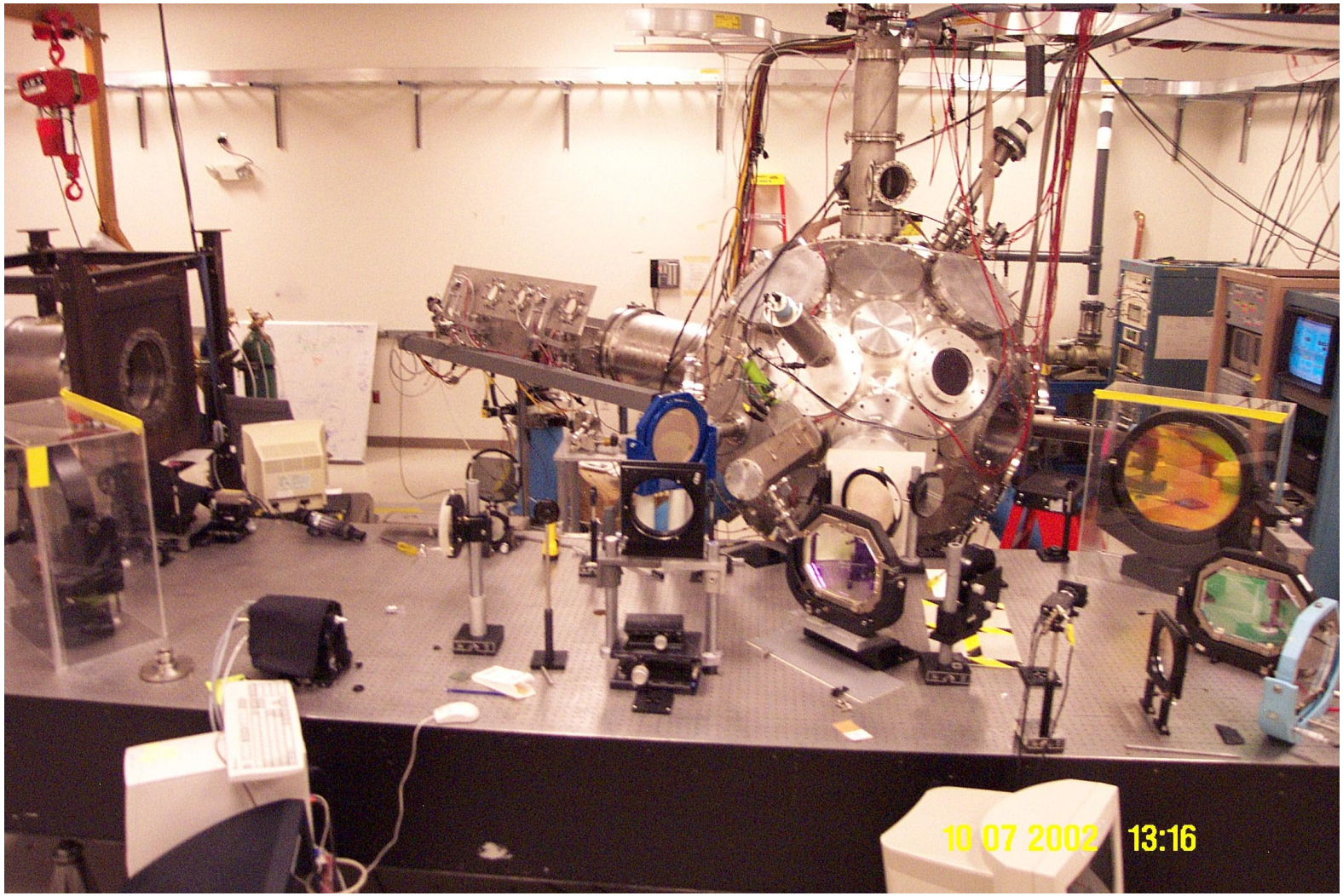

Initial data are consistent with ~ 20 μm focal spot (3 – 4 × DL).

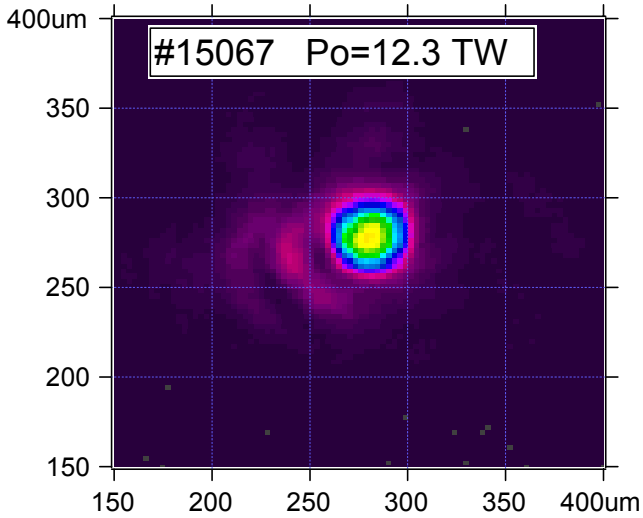

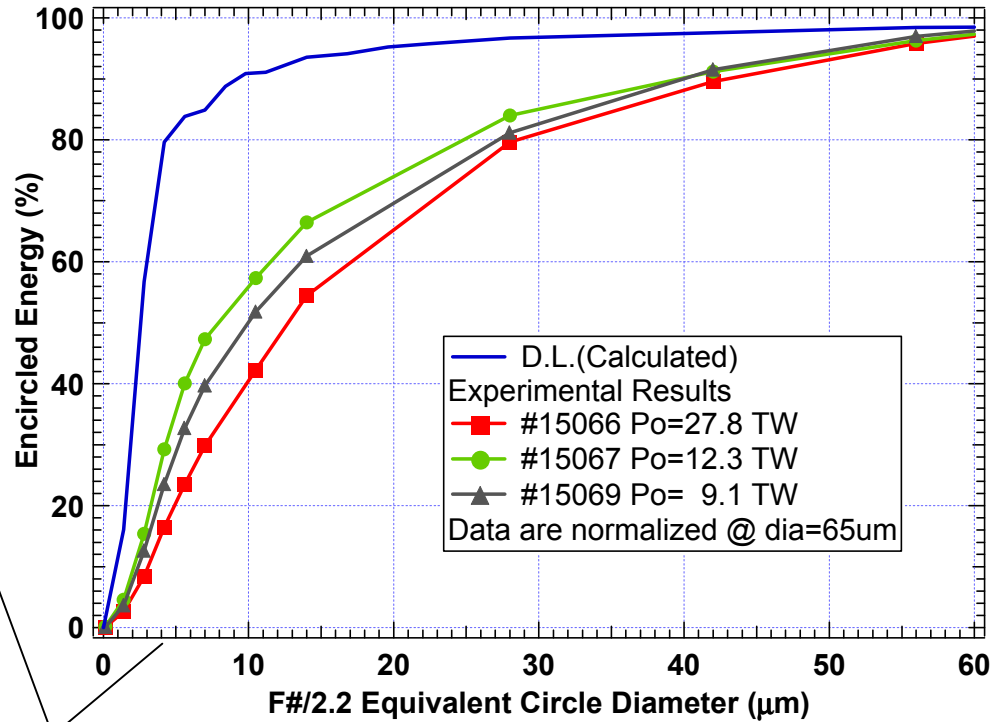

Equivalent focal-plane beam measurements (exclude parabola & blast shield)

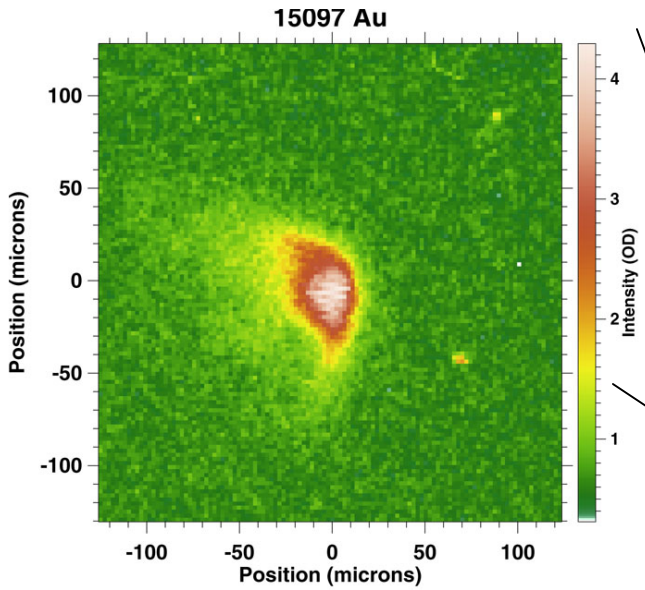

X-ray image of irradiated Au foil (> 2 keV photons)

A grooved Al target (courtesy of GA) was used to diagnose the laser-driven proton beam.

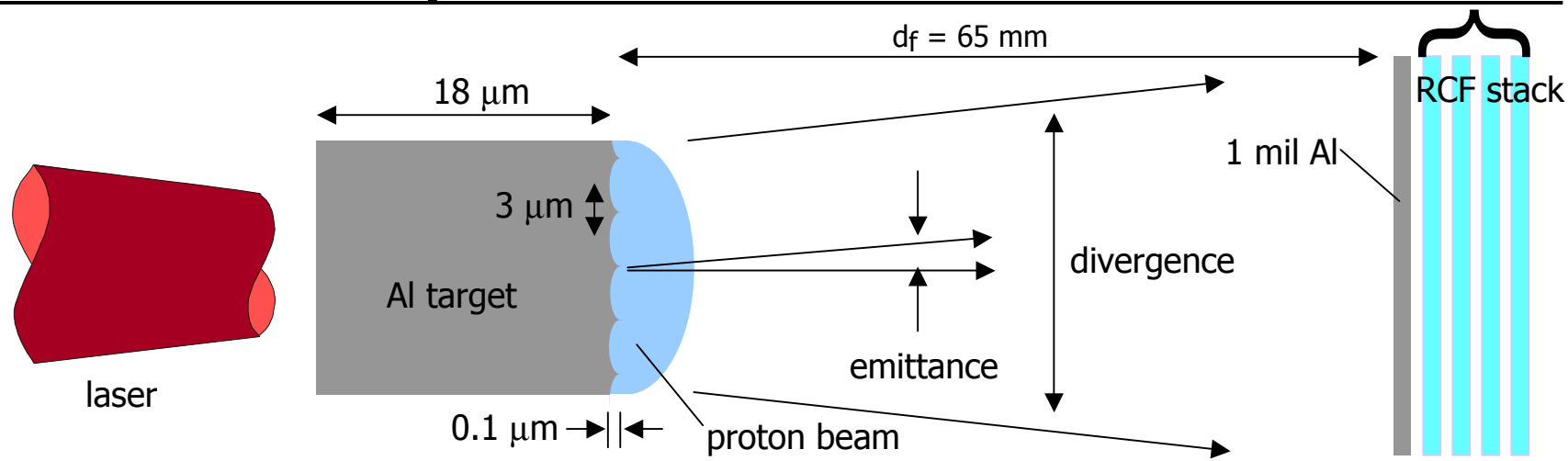

- Proton energies are > 2 MeV on the first radiochromic-film layer, > 5 MeV on the 2nd, > 8 MeV on the 3rd, and > 12 MeV on the 4th.
- Scheme relies on the groove pattern being imprinted in the RCF by the accelerated ions.
- Beam source size & divergence are determined from spot size on the RCF, source-film distance and number of grooves in the image.
- The emittance is deduced from the smeared groove size.

A grooved Al target was used to diagnose the laser-driven proton beam.

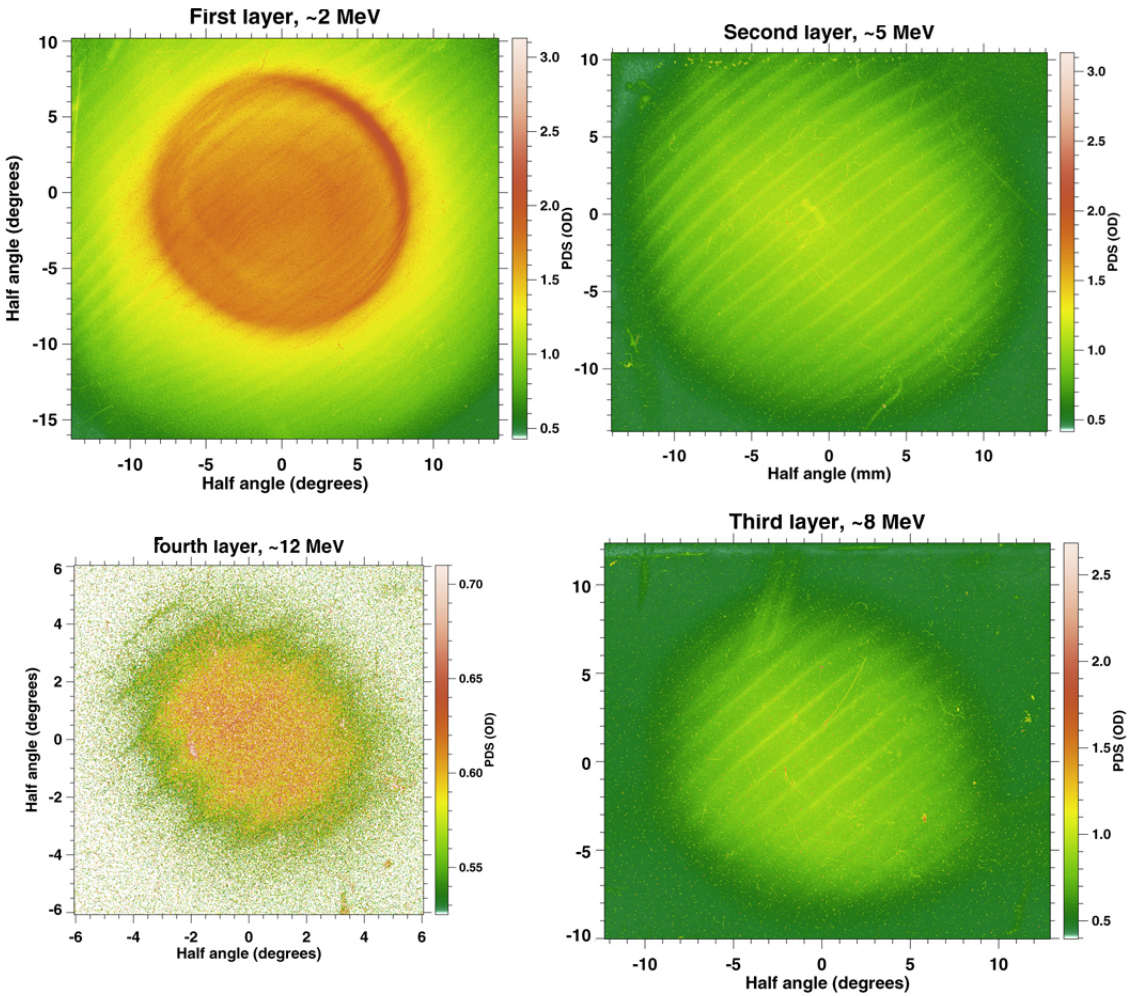

- Grooved pattern is not differential transmission of front-side beam (needed absorption coefficient is too high).
- Beam divergence decreases with energy: ~ 30° @ > 2 MeV to ~ 8° @ > 12 MeV.
- Proton source size decreases from ~ 78 μm @ > 2 MeV to ~ 15 μm @ > 12 MeV.
- Emittance: $(E_{trans}/E_b)^{1/2} \sim d_{smear}/d_f < 3.5 \times 10^{-3}$ @ 8MeV!

Nuclear activation was used to diagnose the location of accelerated ions (front Vs back surface).

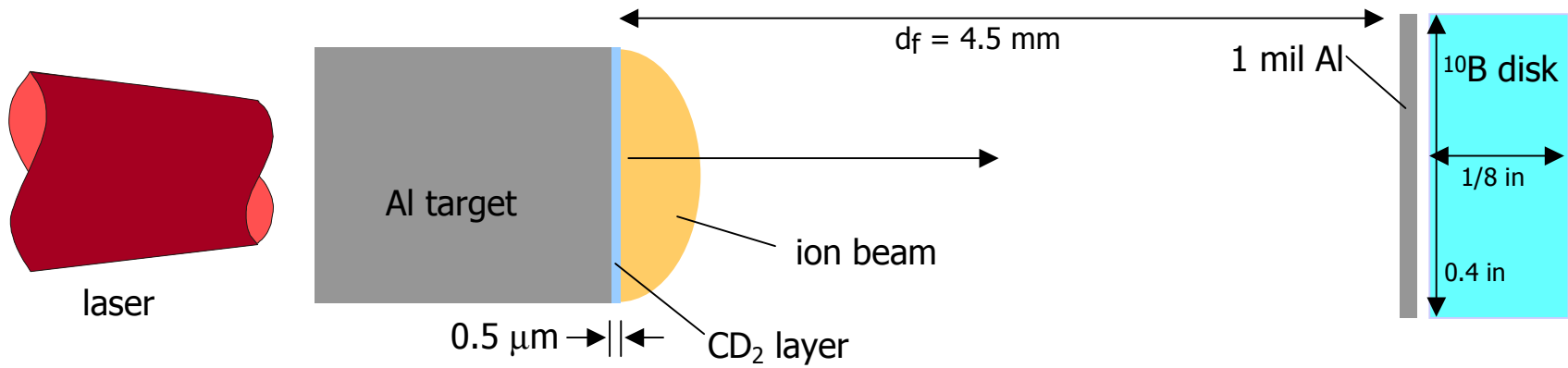

- The deuterated plastic coating was placed either at the front (illuminated) or back side of the target on different shots .
- Used nuclear activation of ^{10}B as a deuteron detector, ^{11}B as a proton detector as in Nemoto *et al.,* Appl. Phys. Lett. **78** (2001) 595.
- Shot with CH_2 coating did not activate the ^{10}B disk, *i.e.,* there was no significant ^{11}B contamination.
- The thickness of the Al substrate was varied.

For the given Trident energy, activation from back-side ions dominates as the target thickness is decreased.

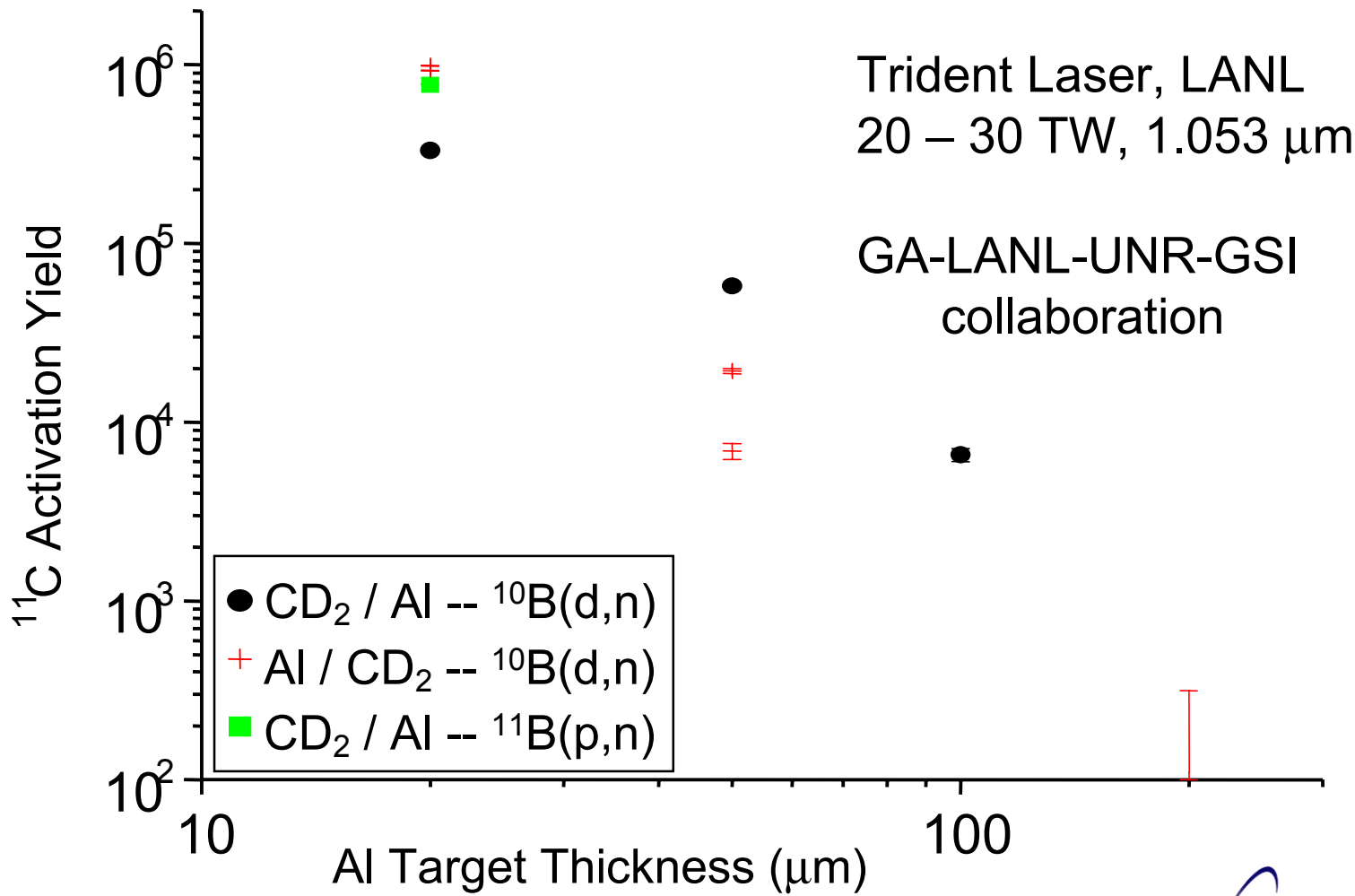

Laser-driven protons are useful for radiography of ICF capsules.

- Detector is radiochromic film.
- Protons making this particular image have energies > 2 MeV.
- Low beam emittance allows very high resolution, provided flux and energy are properly matched.
- Plastic capsule shown has an off-center cavity.

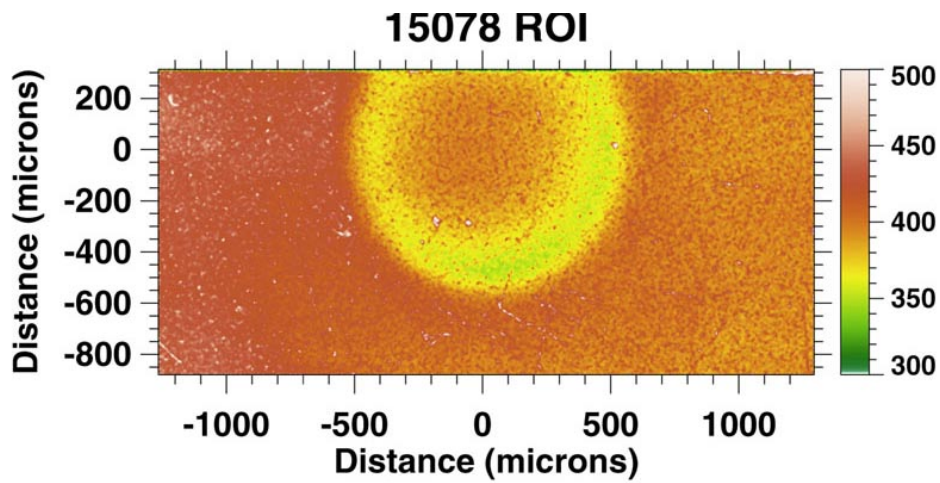

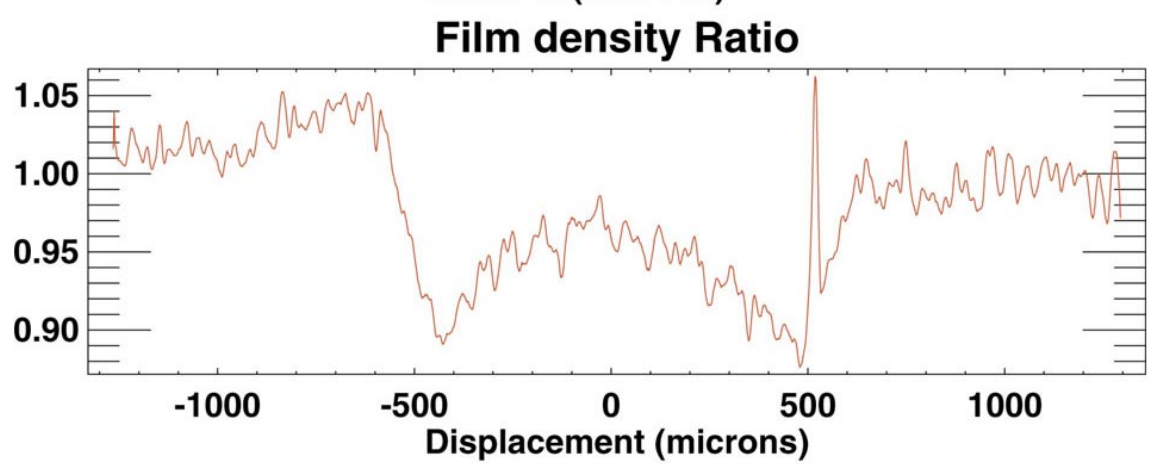

Electric fields can produce interesting (and confusing) effects in proton radiographs.

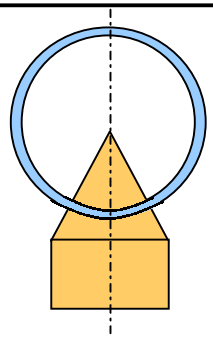

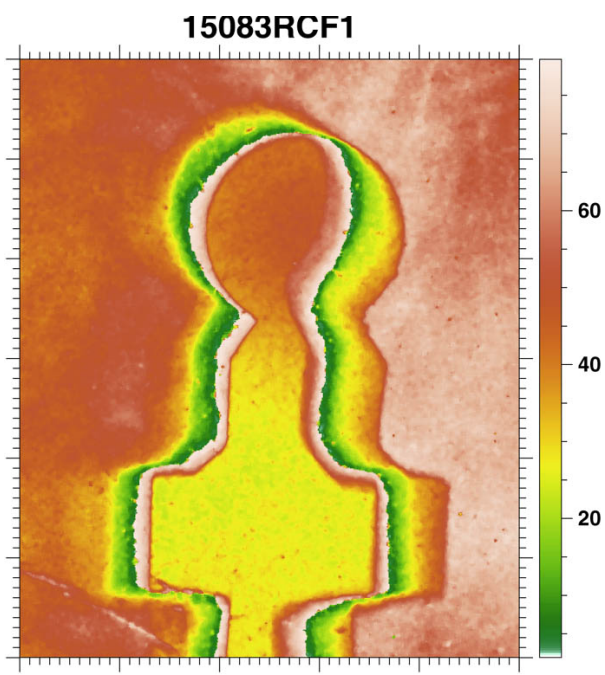

- Detector is radiochromic film.
- Protons making this particular image have energies > 2 MeV.
- Proton flux is very high in the image center → not a double exposure from a filamented beam.
- Appears that protons were bent around a vertical symmetry axis.
- This is the only target that shows this effect, and the only one mounted on a metallic stalk.

Conclusion:

- The main objective was achieved: to develop and demonstrate on Trident experiments a 30 TW short-pulse laser with good beam quality.
- Various new Trident systems had to be qualified at once:
  - Air compressor
  - New target positioner
  - New beam and alignment diagnostics and procedures.
- Based on our initial experience, the system will be improved.
- Investigated characteristics of laser-driven ions with the new system:
  - Determined the beam divergence Vs energy.
  - Deduced a very low beam emittance.
  - Perhaps observed transition from front Vs back-side acceleration.
- 30 TW Trident was used for proton radiography tests.
  - Interesting effects likely due to electrical charging of the target were observed.

Laser Produced Proton Beam Characteristics*

Kirk Flippo†, A. Maksimchuk, K. Nash, T. Lin, S. Banerjee, D. Umstadter

FOCUS Center / Center for Ultrafast Optical Science, University of Michigan, Ann Arbor, MI 48109-2099, USA

Y. Sentoku

General Atomics, San Diego, CA

V. Yu. Bychenkov

P. N. Lebedev Physics Institute, Russian Academy of Science, 117924 Moscow, Russia

*Supported by Division of High Energy Physics, Office of Energy Research, U. S. Department of Energy, award DE-FG02-98ER41071, with lasers supported by the National Science Foundation FOCUS Center and the UM Center for Ultrafast Optical Science

†email: kflippo@umich.edu

Material Effect on Proton Production

Conductor

Aluminum

- $\rho \sim 2.7\ g/cm^3$
- $\sigma = 10^4\ \Omega^{-1}m^{-1}$
- $Z = 13$

Insulator

Mylar (polyethylene terephthalate $C_{10}H_8O_4$)

- $\rho \sim 1.2\ g/cm^3$
- $\sigma = 10^{-11}\ \Omega^{-1}m^{-1}$
- $Z = 4.3$

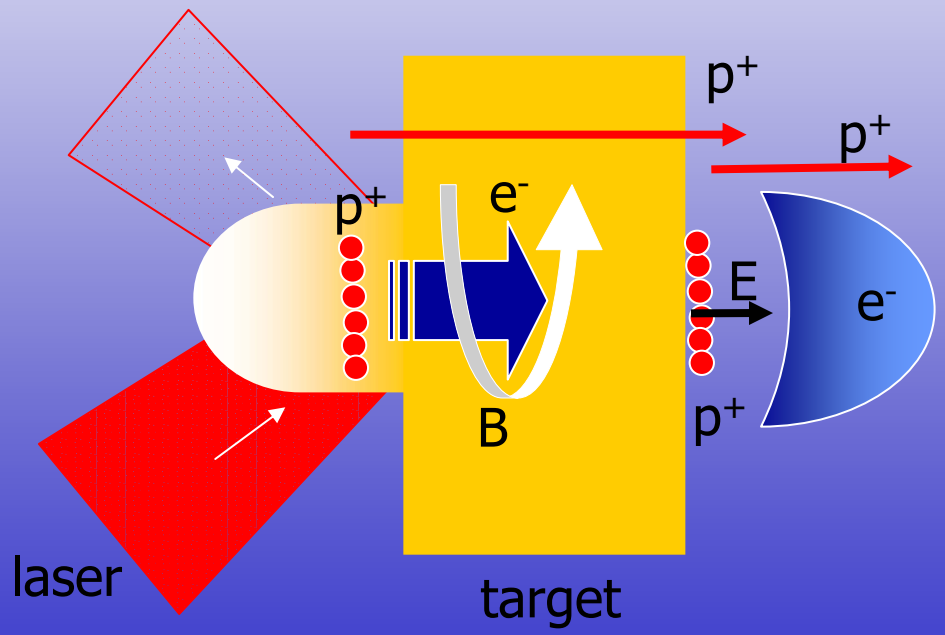

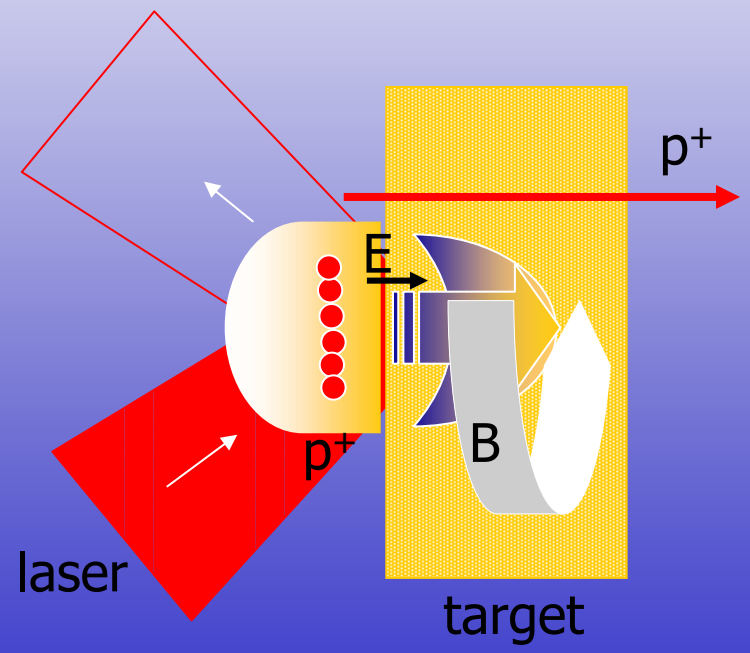

Accelerator Setup

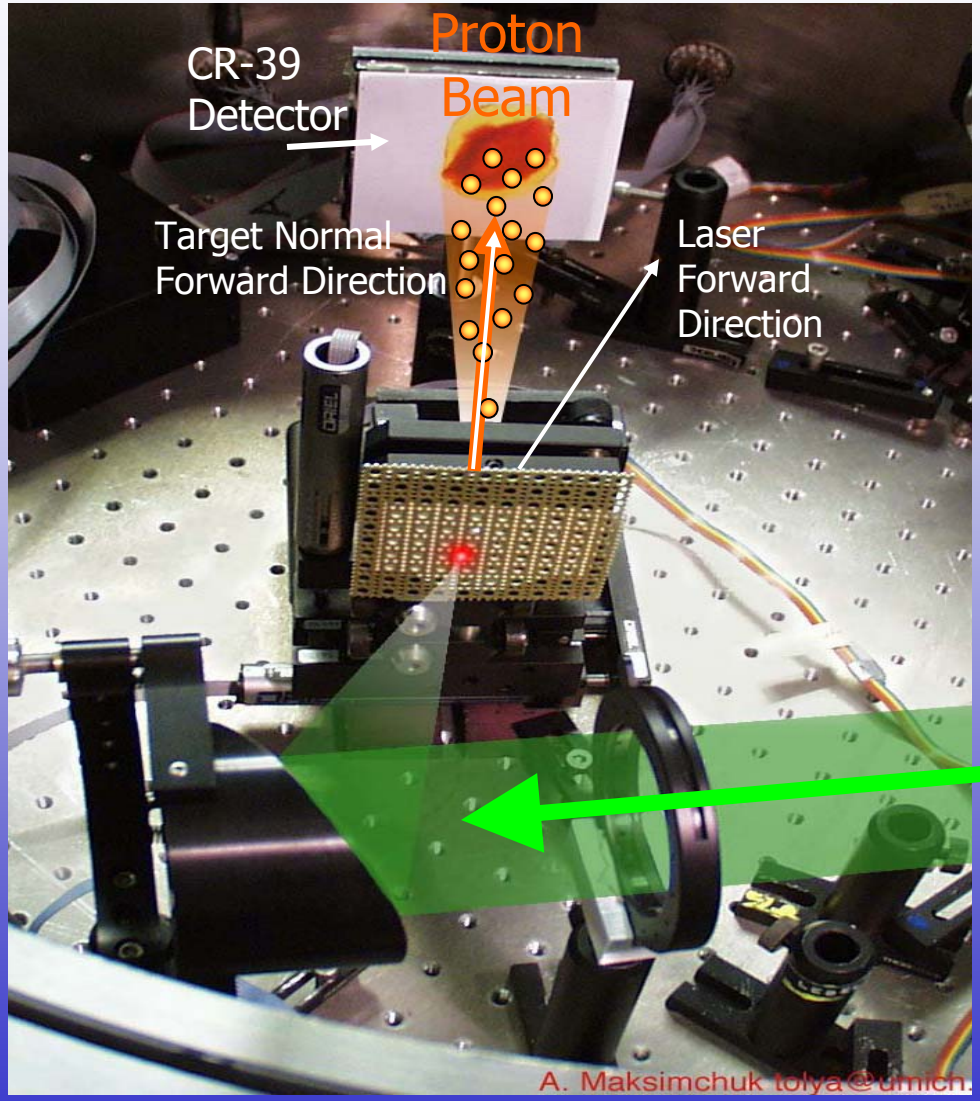

CUOS T^3 Laser Parameters:

- Ti:Sapphire / Nd:Glass
- 1.053 μm (ω_o), 527nm ($2\omega_o$)
- up to ~15 TW
- 6 J
- 400 fs
- Contrast: 10^{-5}:1 @ ω_o, 10^{-7}:1 @$2\omega_o$
- 2×10^{18} - 2×10^{19} W/cm^2

Incident Laser Spot

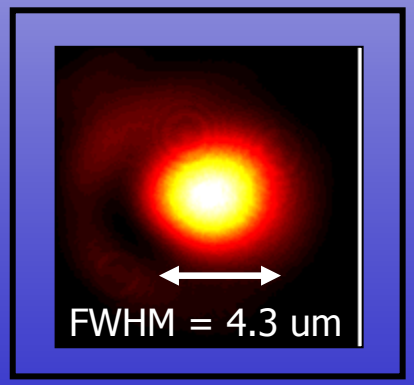

Front Surface Deuteron Acceleration

- Activation of ^{10}B to ^{11}C is achieved only by illuminating deuterons on the front surface.
- No activation when deuterons were on the back surface, or without deuterons (i.e. no production of ^{11}C detected from ^{11}B (p,n)^{11}C reaction).
- Deuterons have about ½ the E_{max} of the measured protons

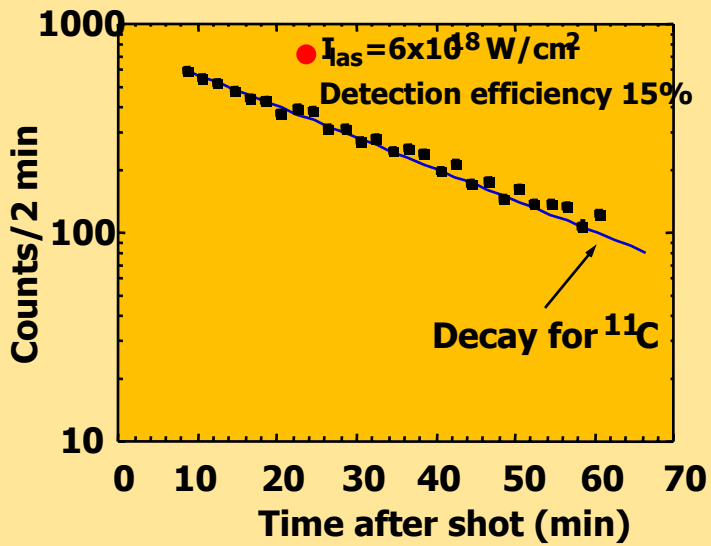

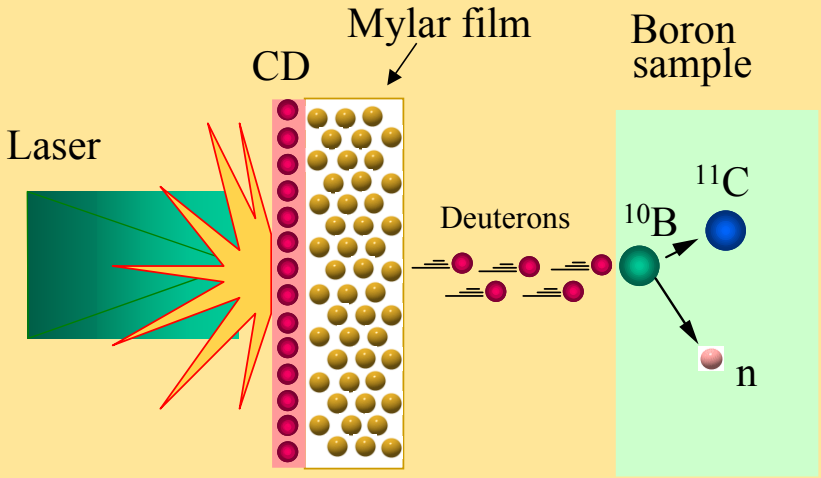

$^{10}B(d,n)^{11}C$ reaction

K. Nemoto, S. Banerjee, K. Flippo , A. Maksimchuk, D. Umstadter App. Phys. Lett, **78**, 595 (2001)

High energy protons accelerated from the front solid dense plasma's back side

Plasma Front-side → ← 40 n_c Back side of Plasma

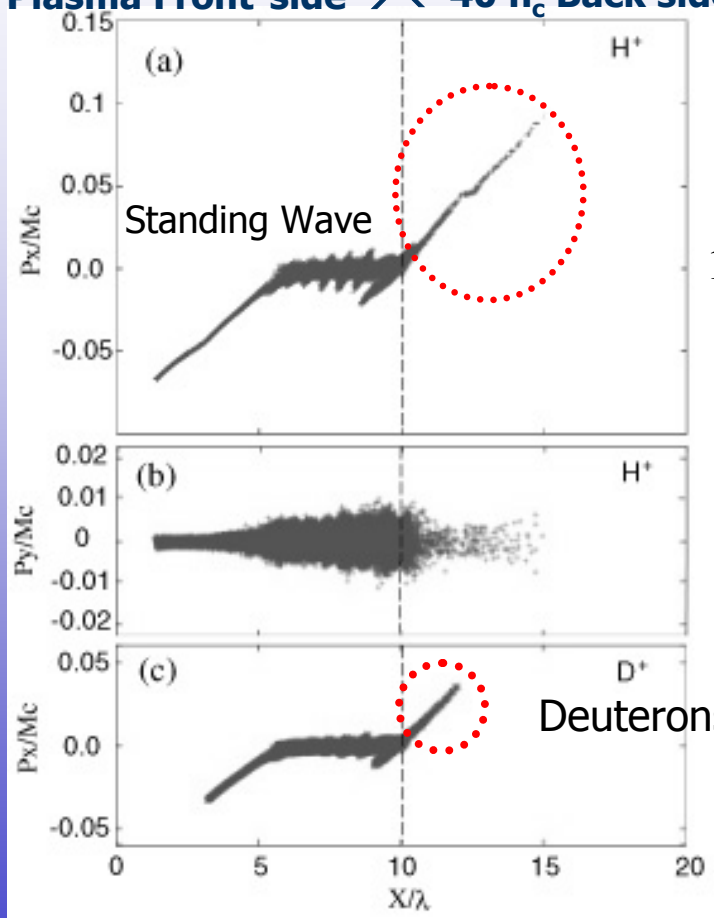

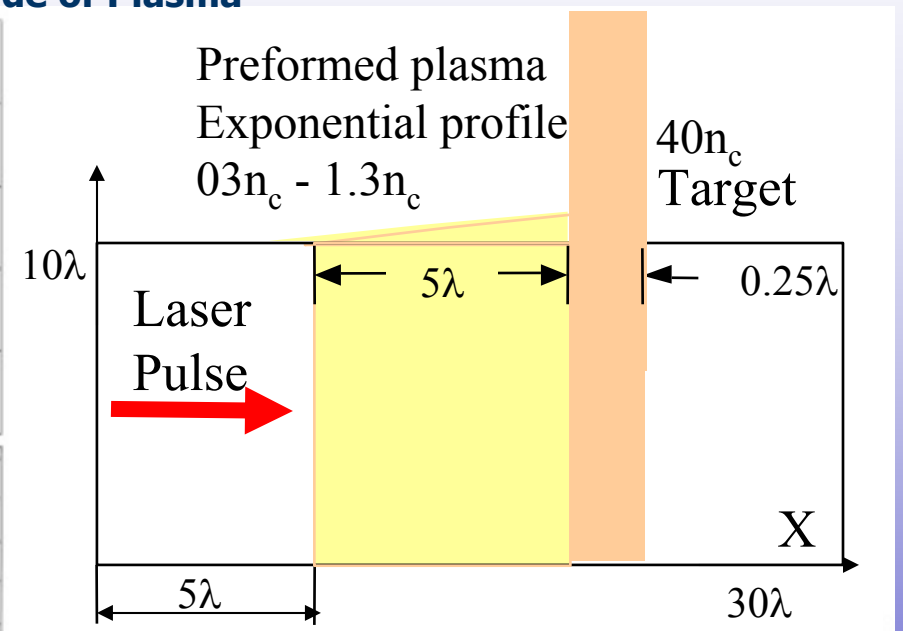

Deuterons have about ½ the Energy of the H^+

2D results (a=1)

Proton, (a) and (b), and deuteron, (c), phase plots at 330 fs.

Y. Sentoku, V. Yu Bychenkov, K. Flippo, A. Maksimchuk, K. Mima, G. Mourou, Z. M Sheng, and D. Umstadter (Appl. Phys. B. **74** p 207 (2002))

Electron orbits in two counter-propagating (incident and reflected) plane waves

$$E_{y0} = E_0(t)\cos(\omega t - kx) + rE_0(t)\cos(\omega t + kx)$$

$$B_{z0} = kE_0(t)\cos(\omega t - kx) - rkE_0(t)\cos(\omega t + kx)$$

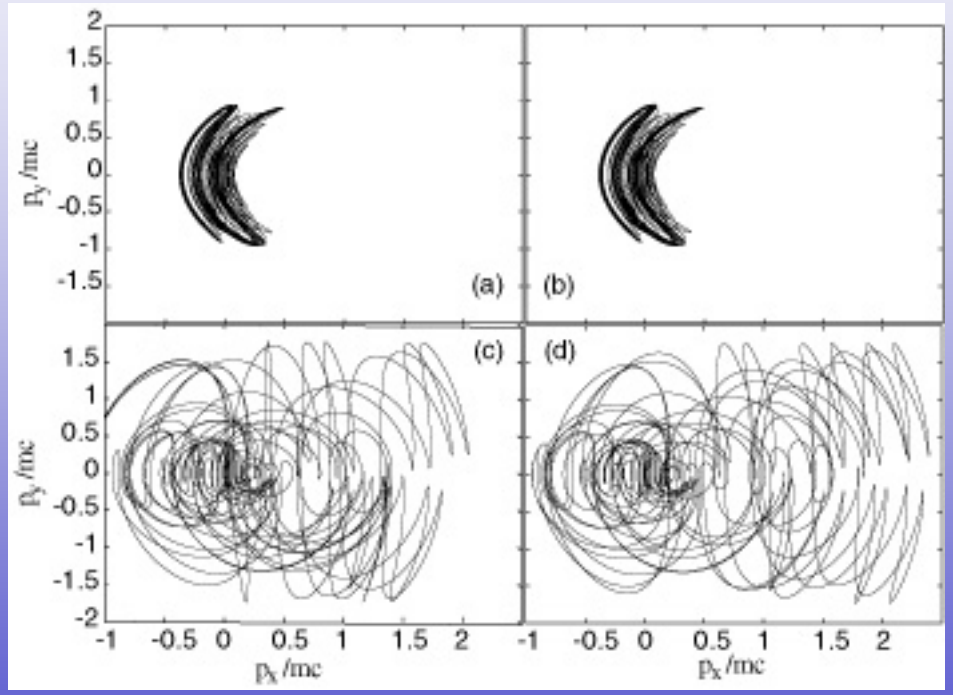

a=1, t=200τ

the reflection coefficient 0 < r <1

(a) r=0.1

(c) r=0.75

(a),(c) Perturbation **d**P_x=10^{-3} mc

(a),(b) ⇒ no difference between the cases with and without perturbation

Regular regime

(c),(d) ⇒ The particle orbits are different

Stochastic regime

τ - laser wave period

The wave amplitude E_0(t) had an exponential form as function of time till saturation at t=20τ .
Momentum perturbation **d**$P_x$was added at t=50τ

Crossed Beams in an Underdense Plasma

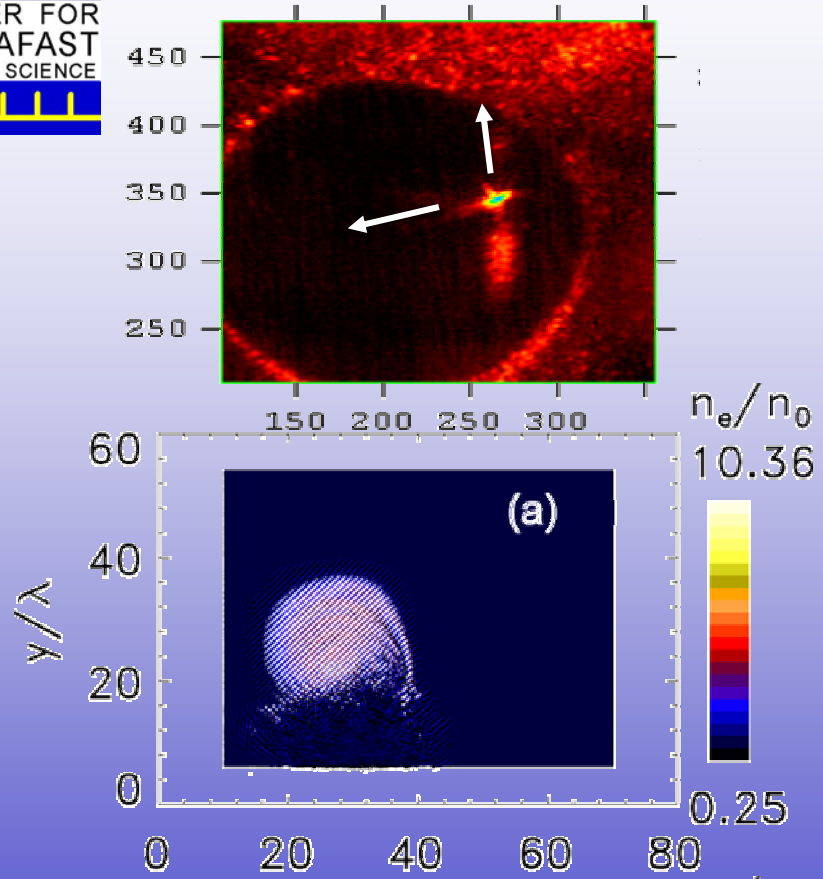

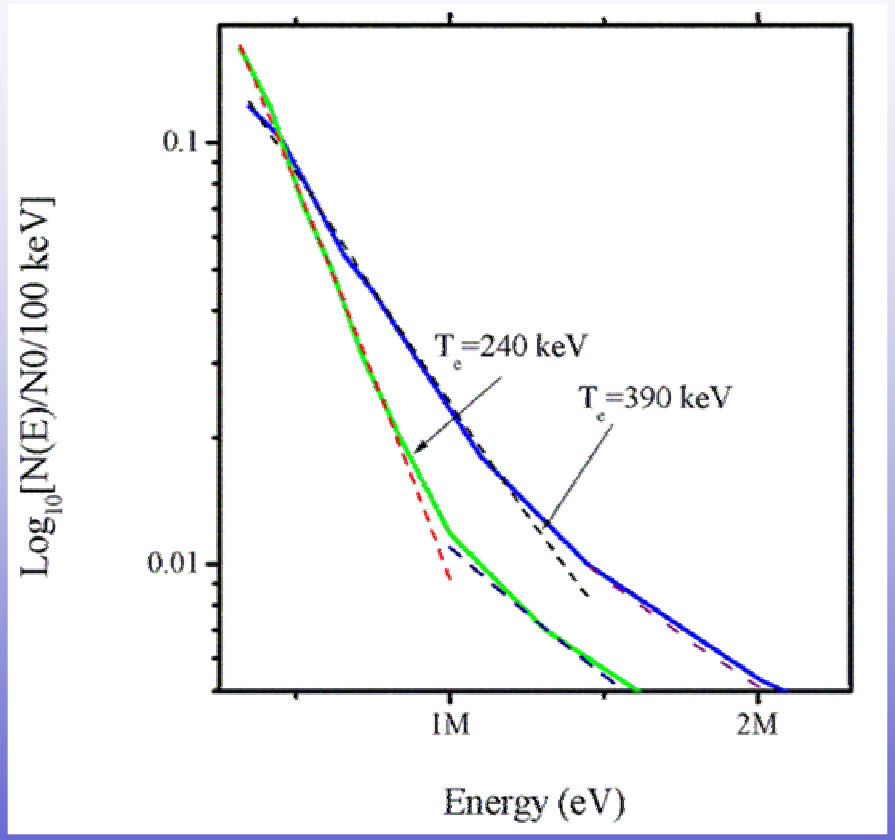

Bright spot (top left) in crossed beam geometry is Thomson scattered light from an electron density modulation in a standing EM wave. Density is shown in PIC simulation (bottom left) , and temperature increase is shown on the right, for one beam (green) and crossed beams (blue).

Courtesy P. Zhang and M. Sheng

Protons From Front Surface

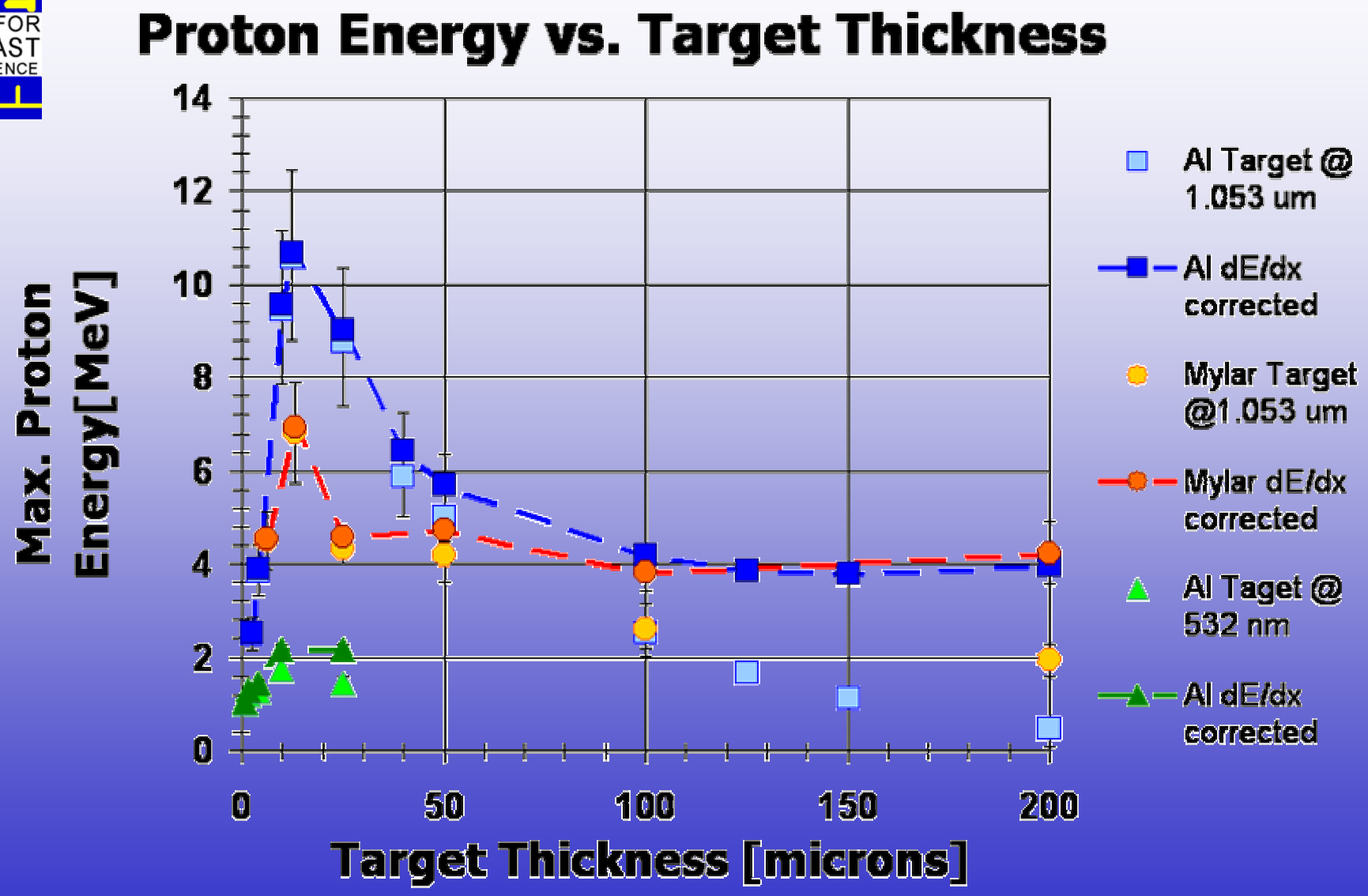

Electron Distribution From Al Target

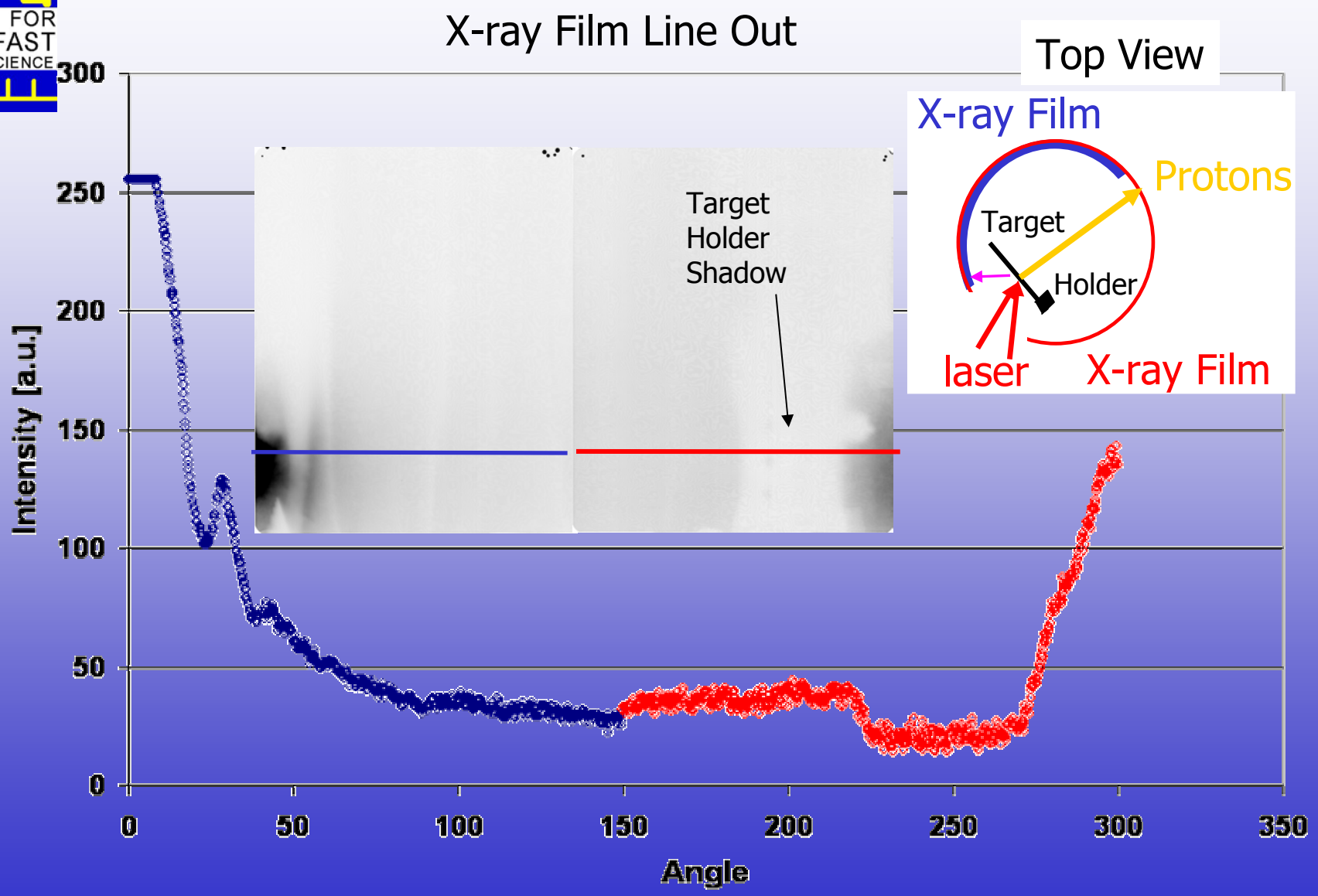

Initial Material Property Effects

Dielectric (Mylar)

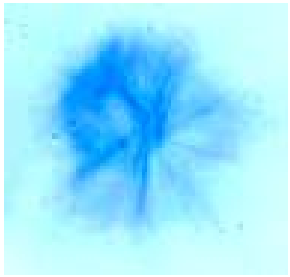

> 1.4 MeV
RCF

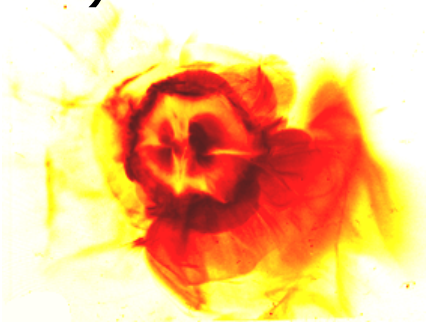

> 1.4 MeV
61º FWHM

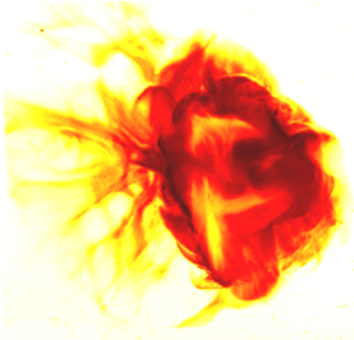

> 2 MeV
54º FWHM

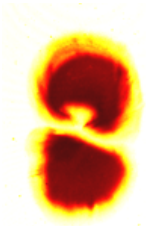

> 3 MeV
42º x 24º FWHM
53º X 33º Total

Spectra (x-ray film) showing structure

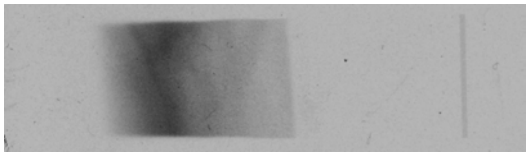

Mylar

2.5 MeV

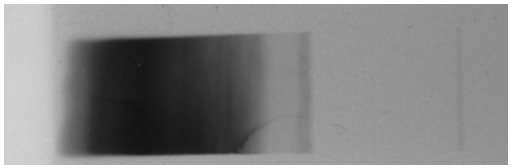

Aluminum

Conductor (Al)

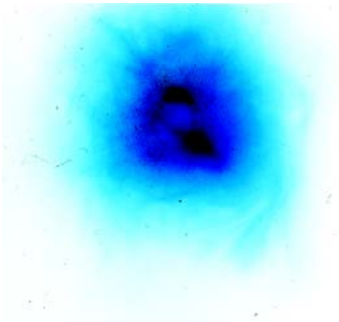

>1.4 MeV, RCF

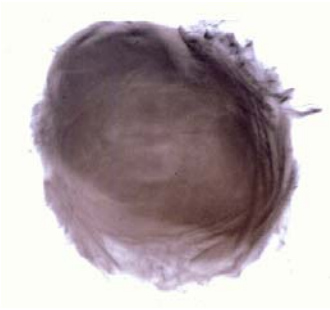

> 4 MeV
31º div.

Target Geometry

Radius of curvature ~ 0.2 mm

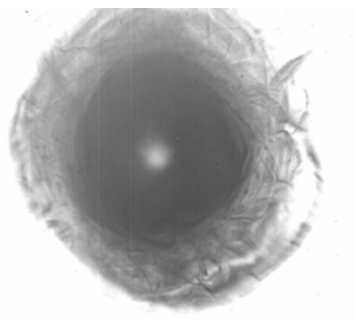

>1.4 MeV, 55º div. @ 1.5x10^{19} W/cm^2

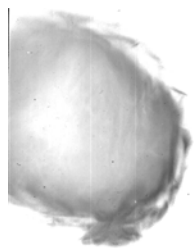

>2 MeV, 38º div. @ 1.2x10^{19} W/cm^2

Radius of curvature ~ 0.5 mm

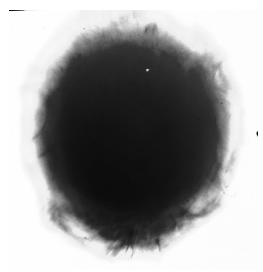

> 1.4 MeV, 44º div. @ 1.6x10^{19} W/cm^2

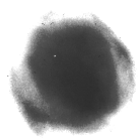

> 3 MeV, 28º div. @ 1.2x10^{19} W/cm^2

Curved Target Geometry 25 μm Al

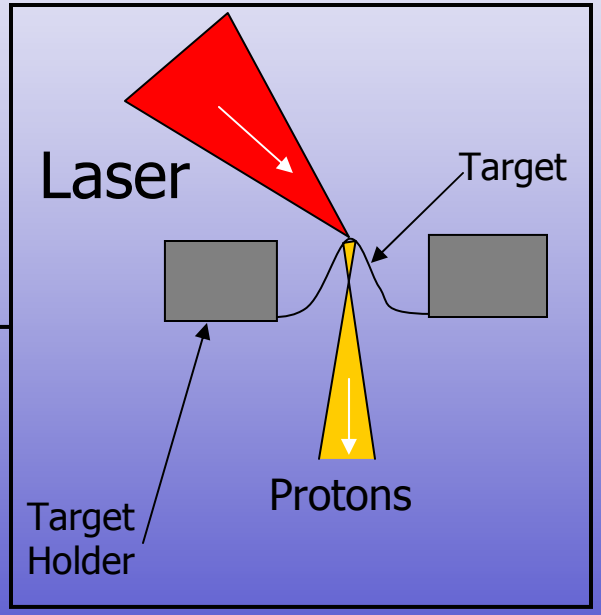

CR-39 Proton Spectrum

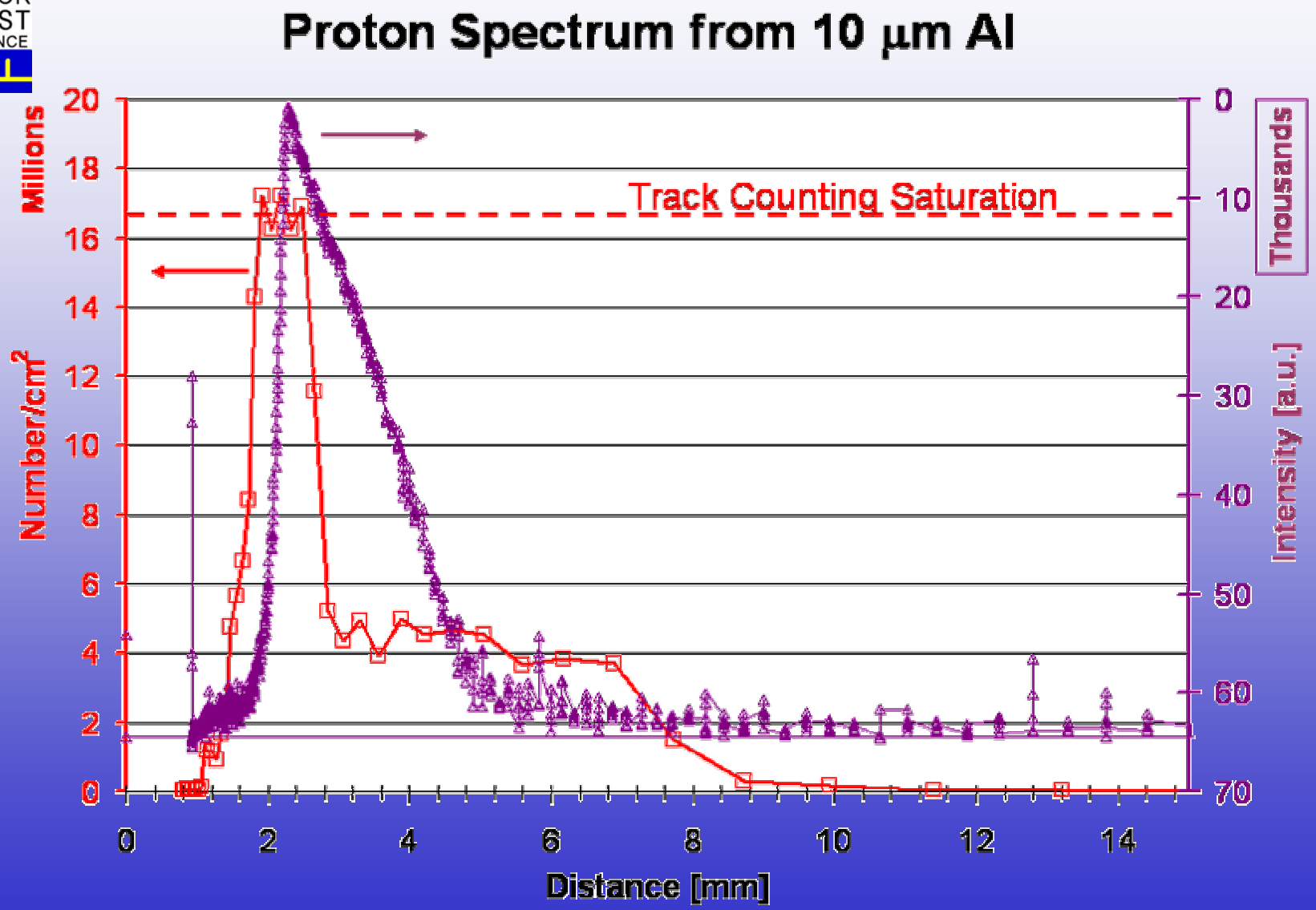

Target Geometry

~100 Micron Half Wire Cross-sections

Wire orientation:

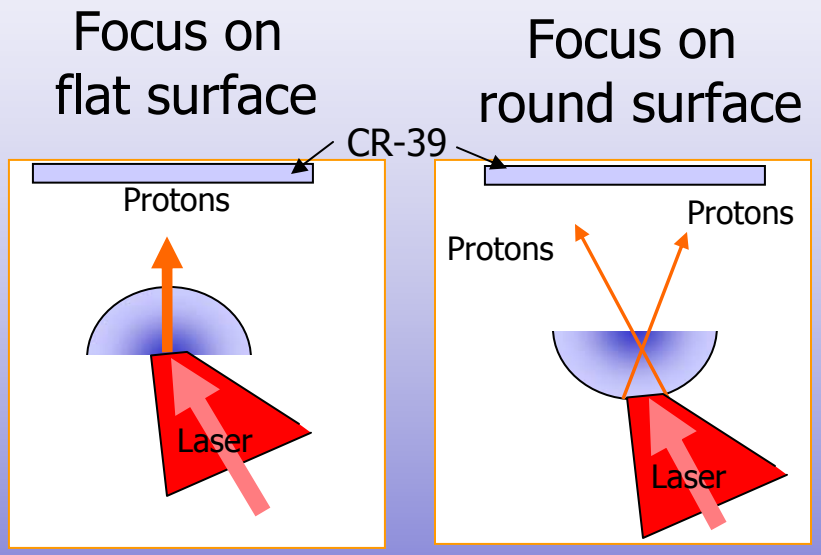

Beam Images:
Focusing on flat surface (840) creates an ion beam, while focusing on the round side produces a cylindrical-like spray

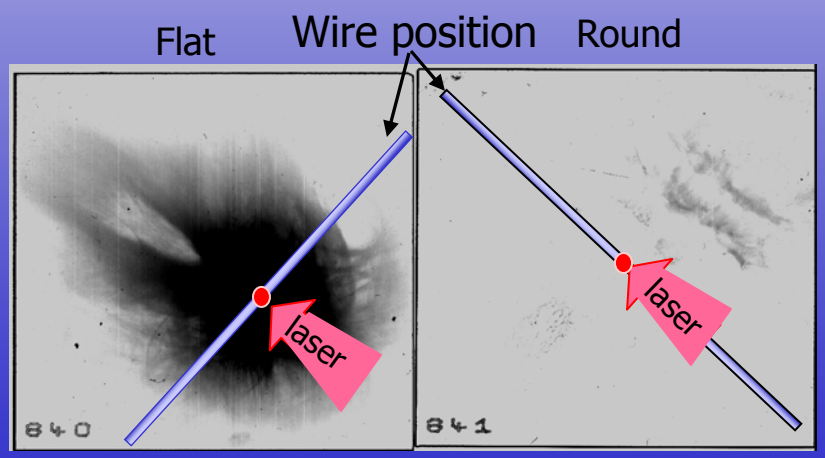

Target Surface Geometry

Use a material which will "trap" the laser light, to enhance the generation of hot electrons.

Electron Microscopy of LaserBlack™

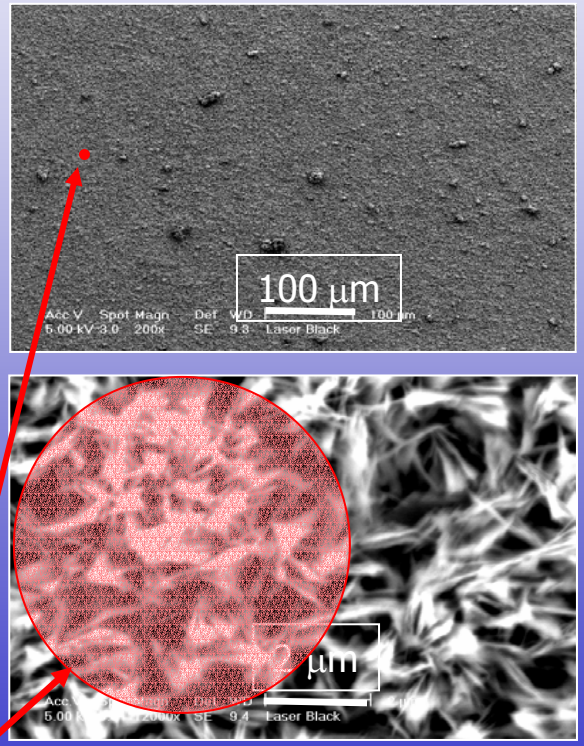

Laser Spot Size ~ 6 microns

Murnane et al. APL 62 (1993) used gratings and clusters, Kulcsar et al. PRL 84 (2000) used metallic "velvet".

Both showed enhanced X-ray yield from enhance electron heating from efficient coupling.

LaserBlack® is > 96% absorptive at 1 μm.

Results:

- 30 μm Laserblack target ~ 8.2 MeV max proton energy.
- Enhancement in the number of maximum energy protons.
- Beam profile does not suffer, regardless of which surface has been coated, and no imprinting of proton beam.

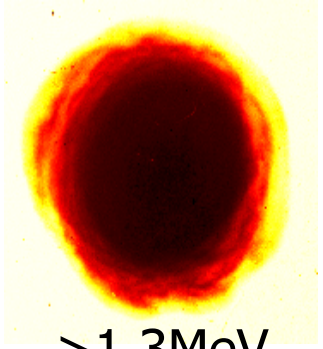

>1.3MeV
31º div.

Material Effects on Plume Profile

Proton Beam Images Using a CCD

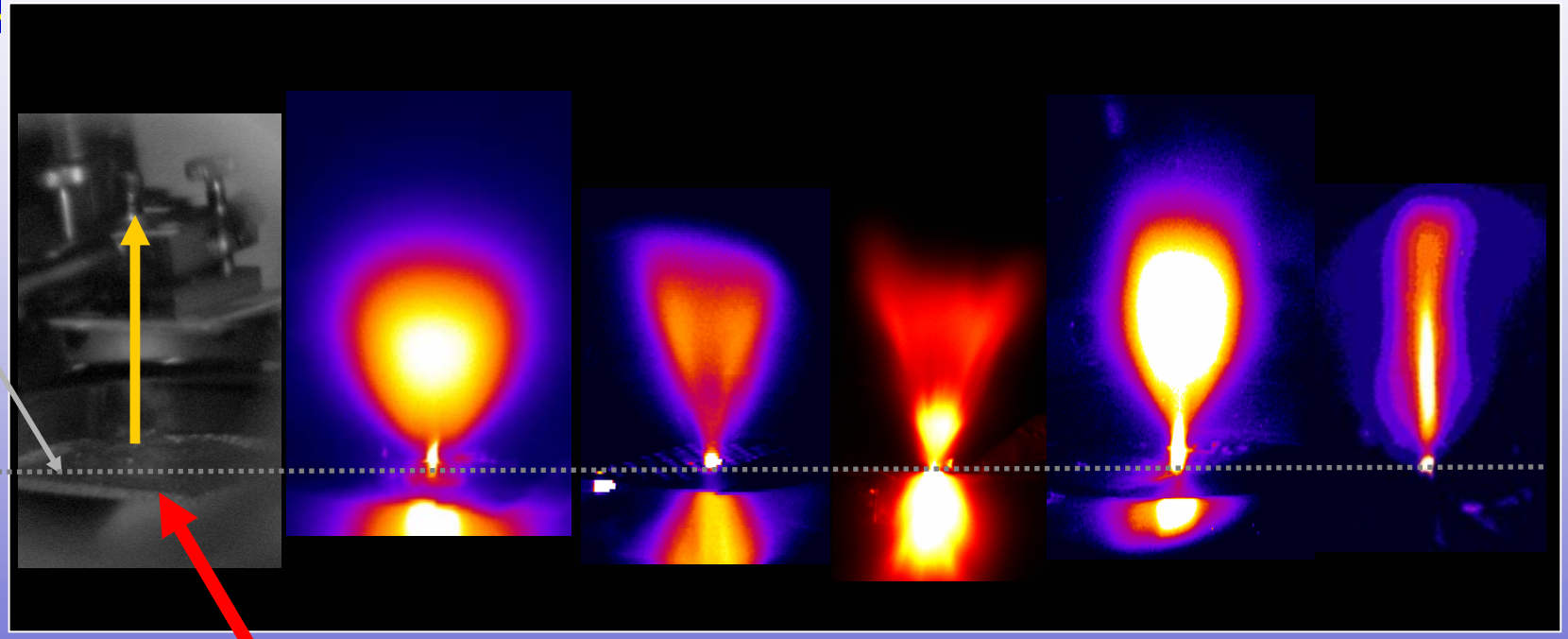

Target Plane

Dark Side

Illuminated Side

Laser Propagation Direction

Proton Beam is Emitted Normal to Target

25 um Al Target

25 um Mylar Target

25 um Mylar Target with 2.4 Torr He

4 Al Target, 4MeV beam No backfilled gas, 200 mTorr ambient

4 um Al Target with 2 Torr H_2

Plume Evolution in 1 Torr H_2 Ambient Backfill

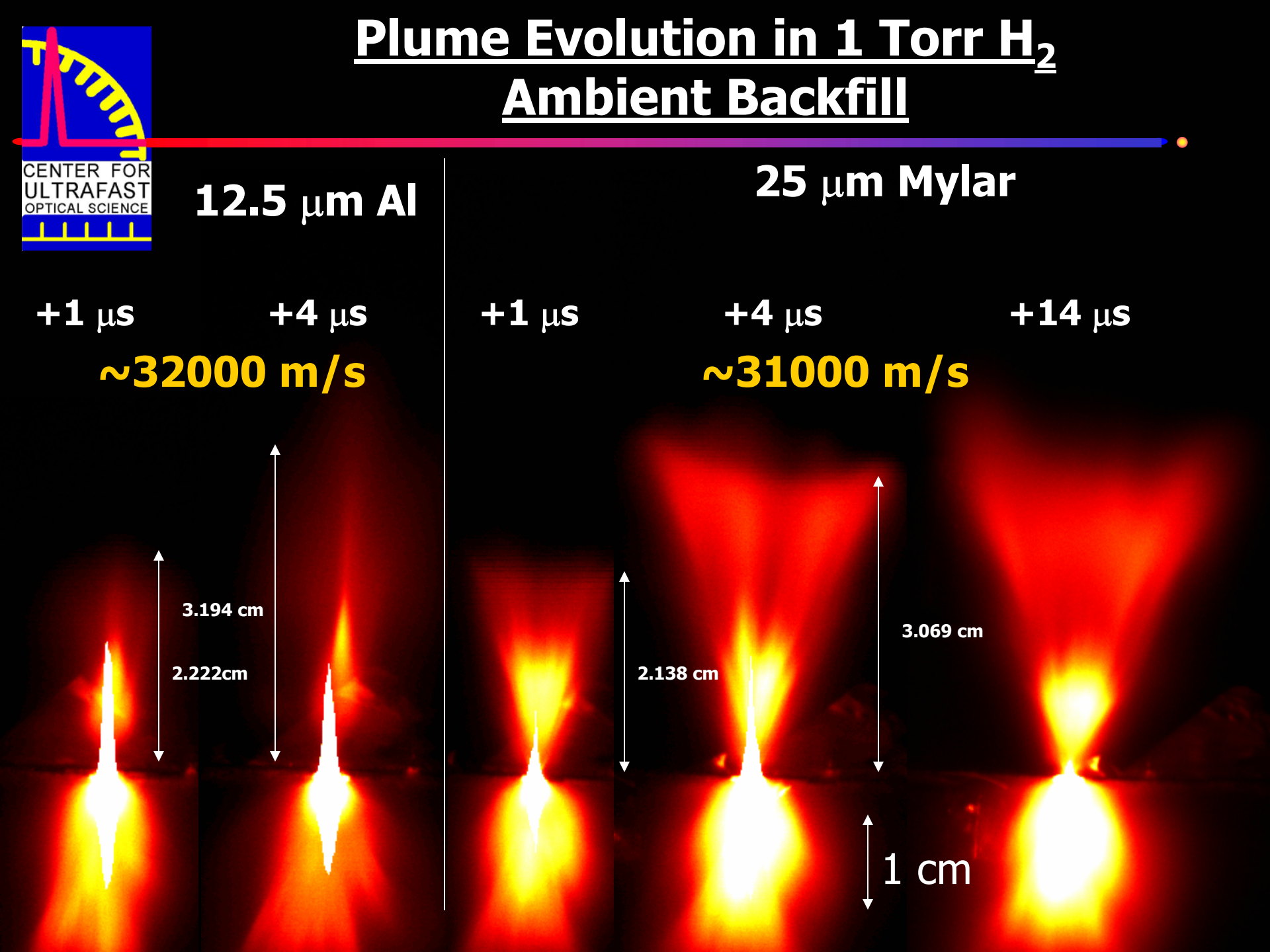

Proton Acceleration Summary

- Simulation and experiment support proton acceleration at the laser-irradiated side of the target, but on the back of the underdense plasma under these conditions
- CR-39 response is highly non-linear when scanned optically.
- Beam profile is a function of initial target conductivity, beam spectrum also has structure.
- Demonstrated beam profile modification with modest geometry, and enhancement of number at the maximum energy achieved by initial target geometry and surface conditions
- By using a highly absorptive material we have increased the number of maximum energy protons without sacrificing beam quality.

WHAT WE'VE LEARNED AND HAVEN'T LEARNED FROM RECENT ELECTRON TRANSPORT MEASUREMENTS

R.R. Freeman, C. Anderson, J.M. Hill,J. King, R. Snavely

University of California, Davis, CA, USA

S. Hatchett, M.Key, J. Koch, A. MacKinnon

University of California, Lawrence Livermore National Lab, Livermore,CA, USA

R. Stephens, T. Cowan

General Atomics, San Diego, CA, USA

This work was performed under the auspices of the U.S. Department of Energy, Contract No. DE-FG03-00SF2229, by the University of California, Lawrence Livermore National Laboratory under Contract No. W-7405-Eng-48, and with the additional support of the Hertz Foundation and General Atomics.

Ti and Cu Kα (10 μm res.)

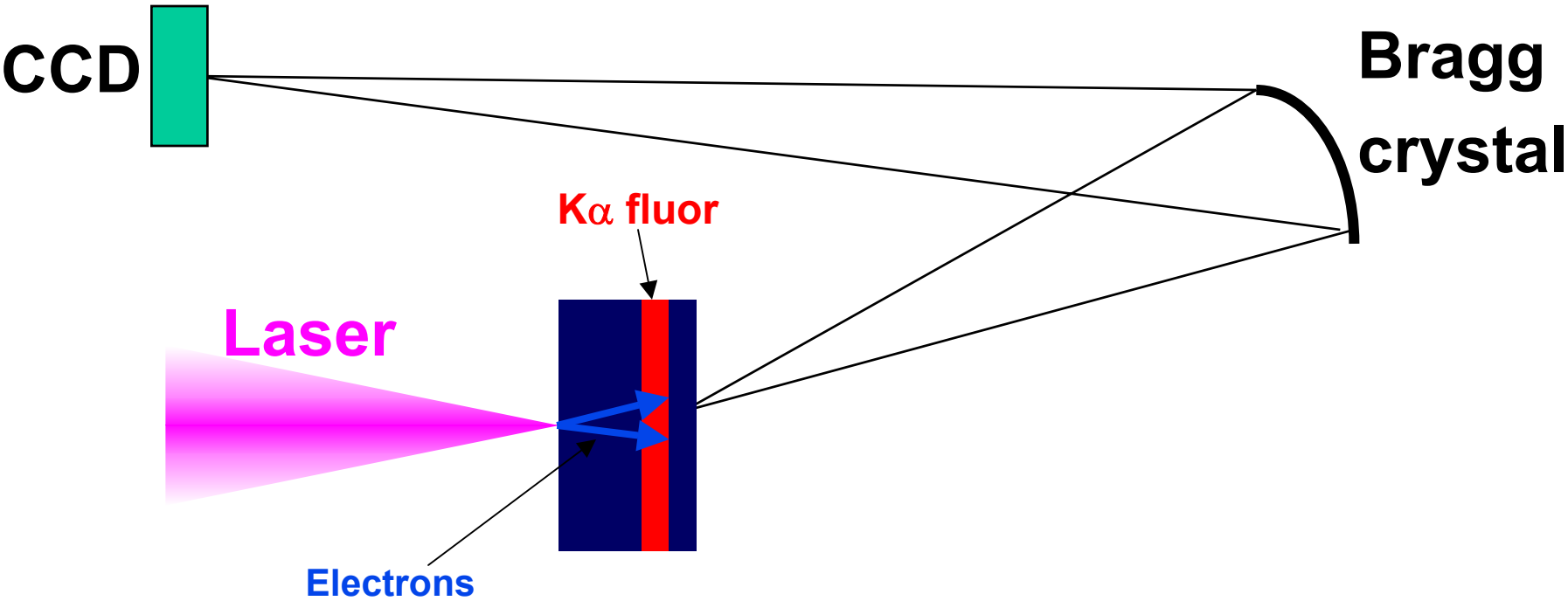

Our electron transport measurements record the image of the Kα emission spot at the Fluor as a function of its depth into the material (usually Al or CH)

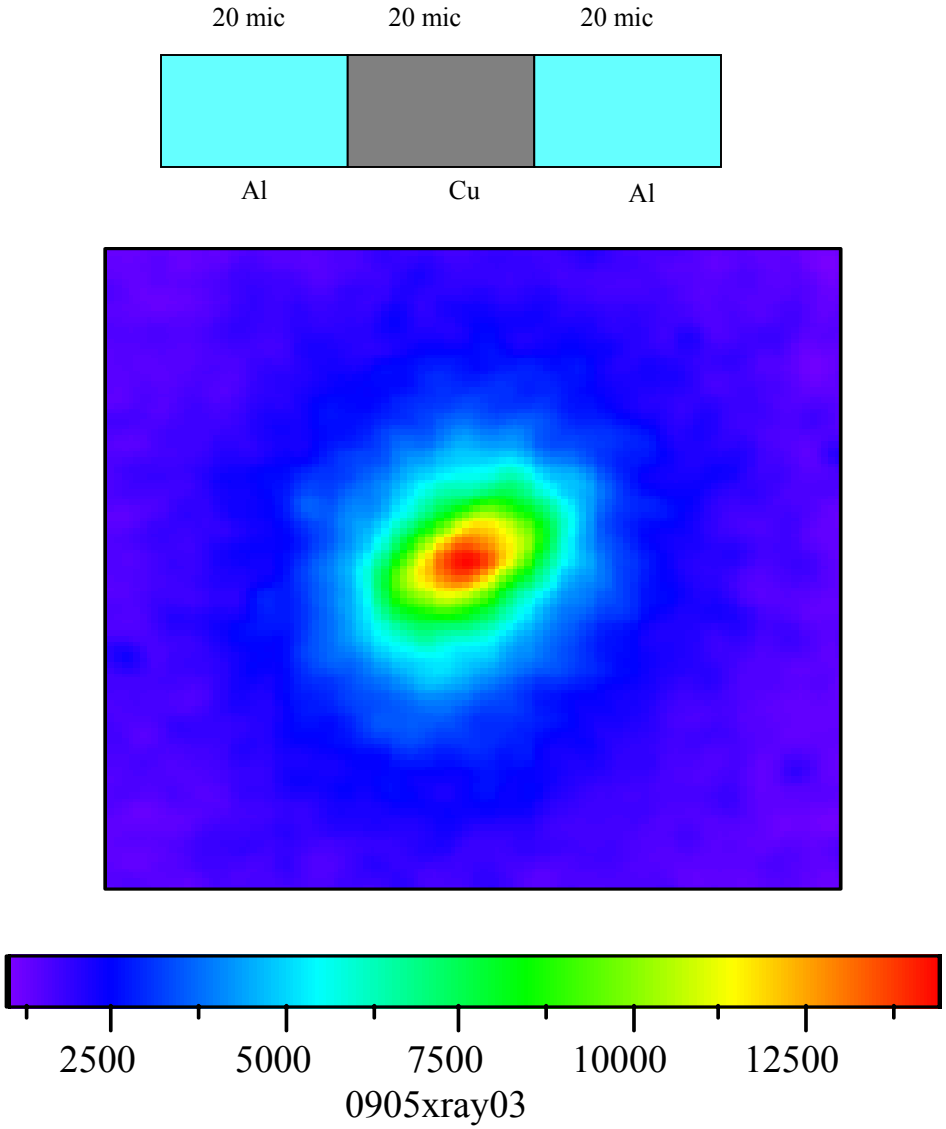
20 mic
20 mic
20 mic
Al
Cu
Al
2500
5000
7500
10000
12500
0905xray03

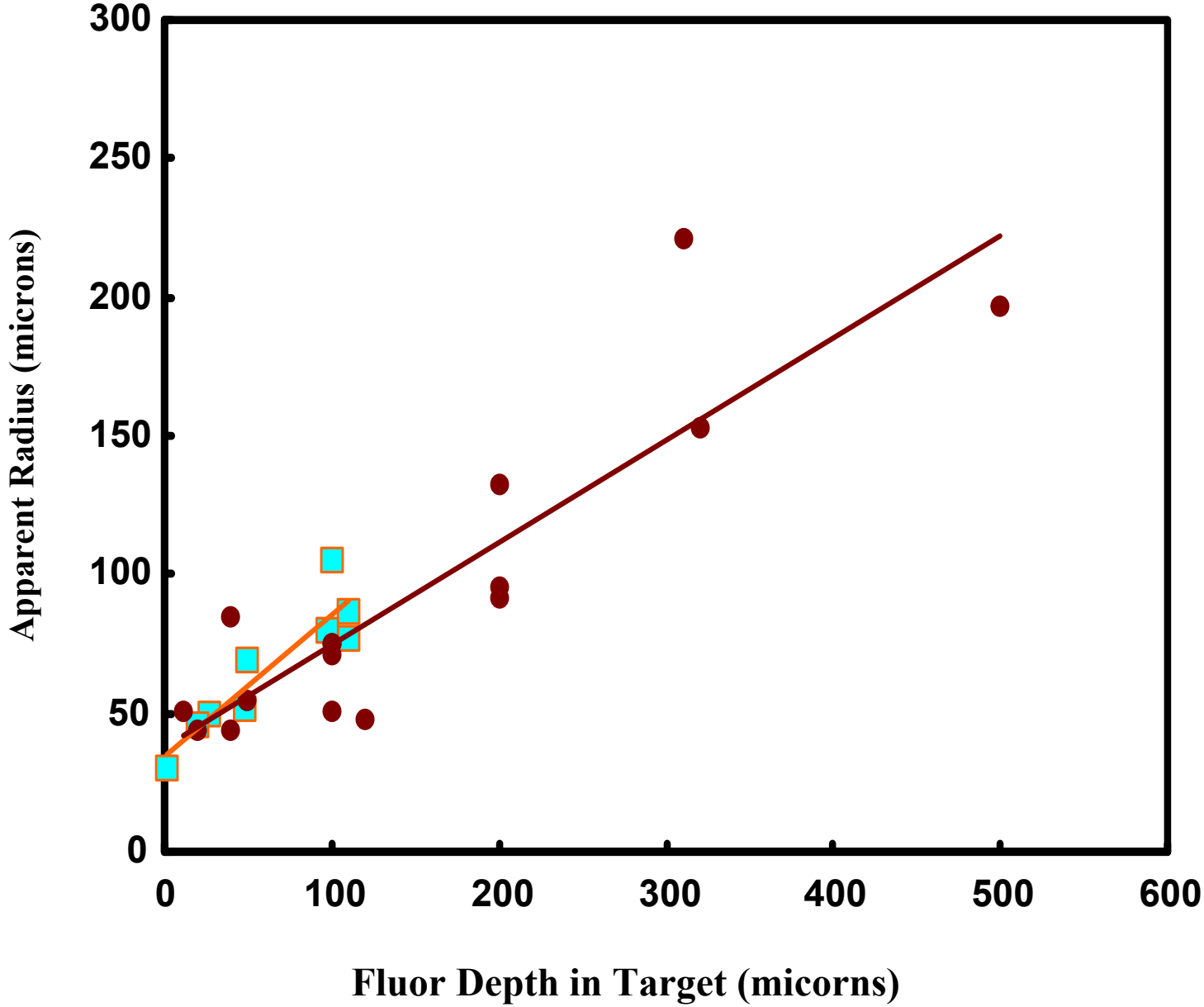
Apparent Radius (microns)
300
250
200
150
100
50
0
0
100
200
300
400
500
600
Fluor Depth in Target (micorns)

The physics of electron transport in dense plasma is complex - but central to many applications

Hybrid PIC model (Paris) (C Toupin et al. In Inertial Fusion Science and Applications 99 Publ. Elsevier p471 (2000)

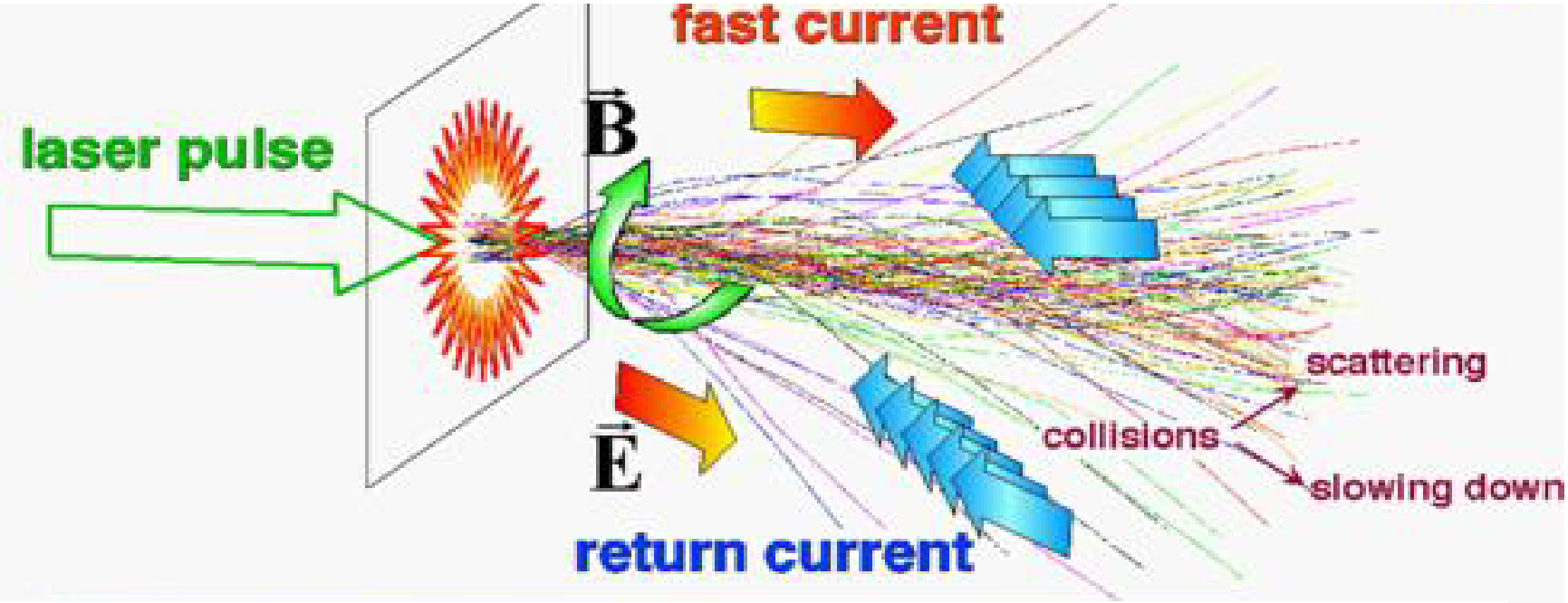

- **Relativistic current cancelled by cold return current**
- **Net current < Alfven limit (17$\beta\gamma$ kA)**
- **Strong magnetic guiding , resistive E field and Weibel instability**

Snap shots of beam particles, log n_b

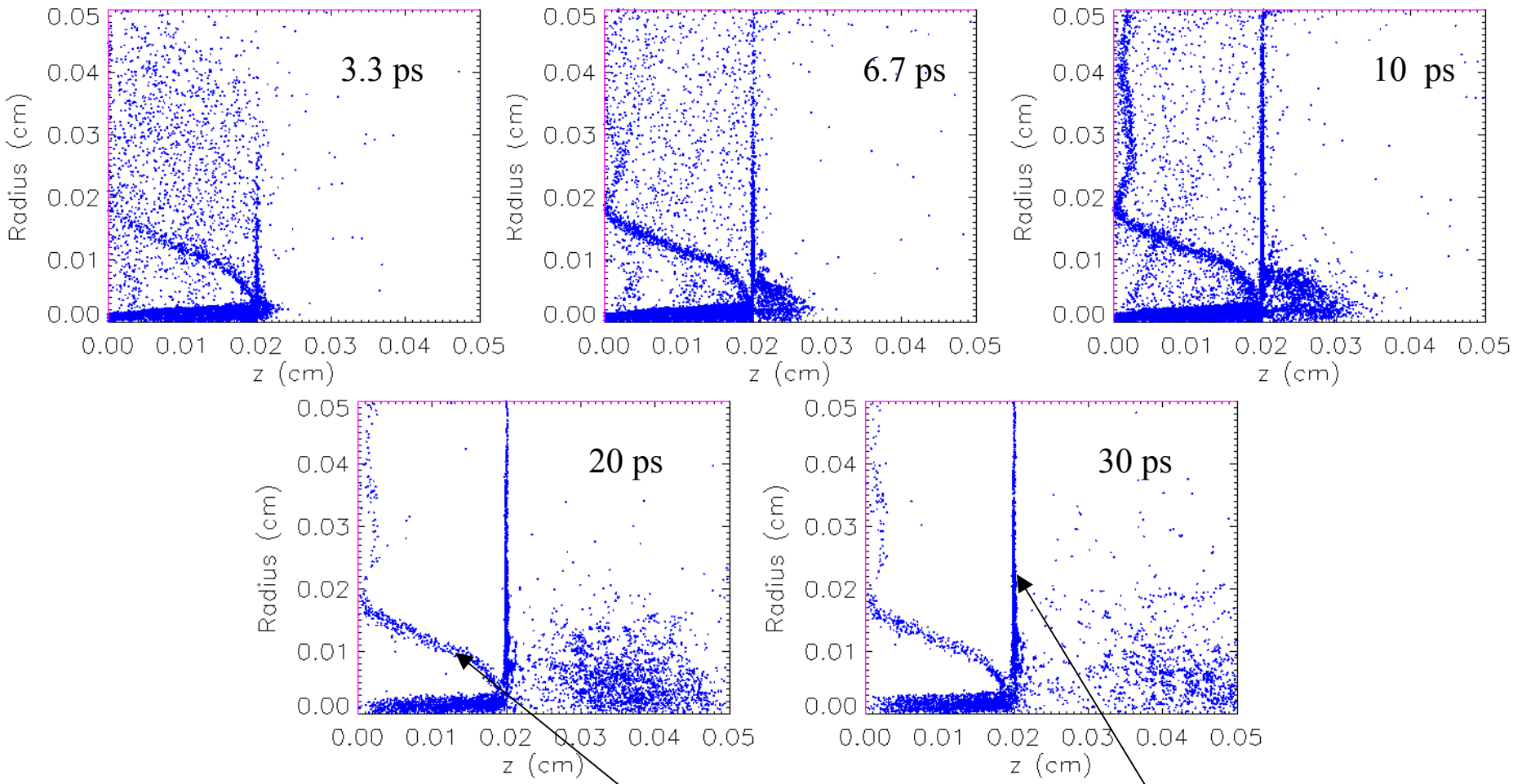

- Beam return current path back at 45 degrees and up the back interface

Weibel filamentation of hot electron flow is predicted by PIC simulations

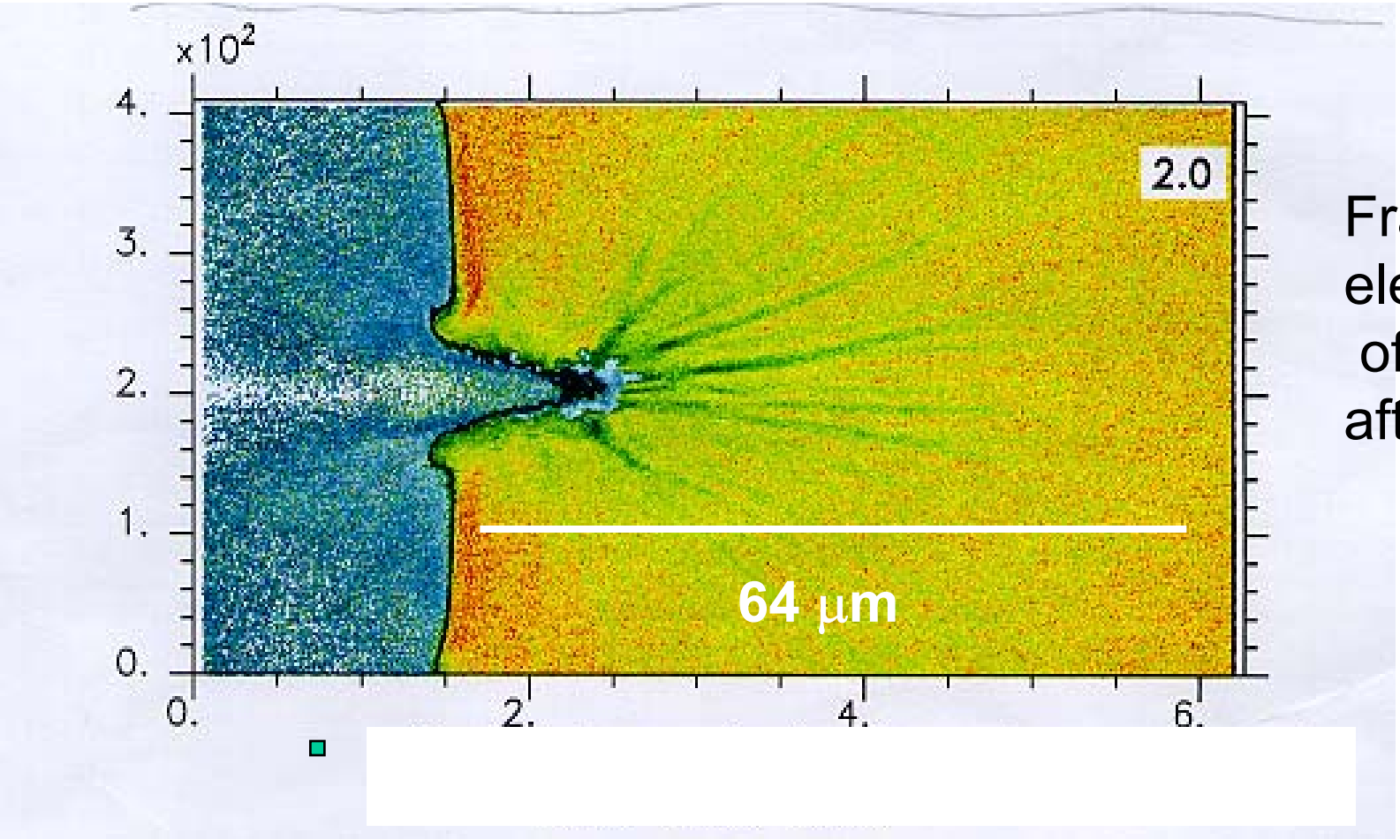

Fraction of electrons of 1-2 MeV after 1.2 ps

2D PIC calculation (JC Adam, S Heron) for 10^{20} Wcm^{-2}

The Petawatt laser has opened a new regime of high energy, ultra-relativistic laser/matter interaction.

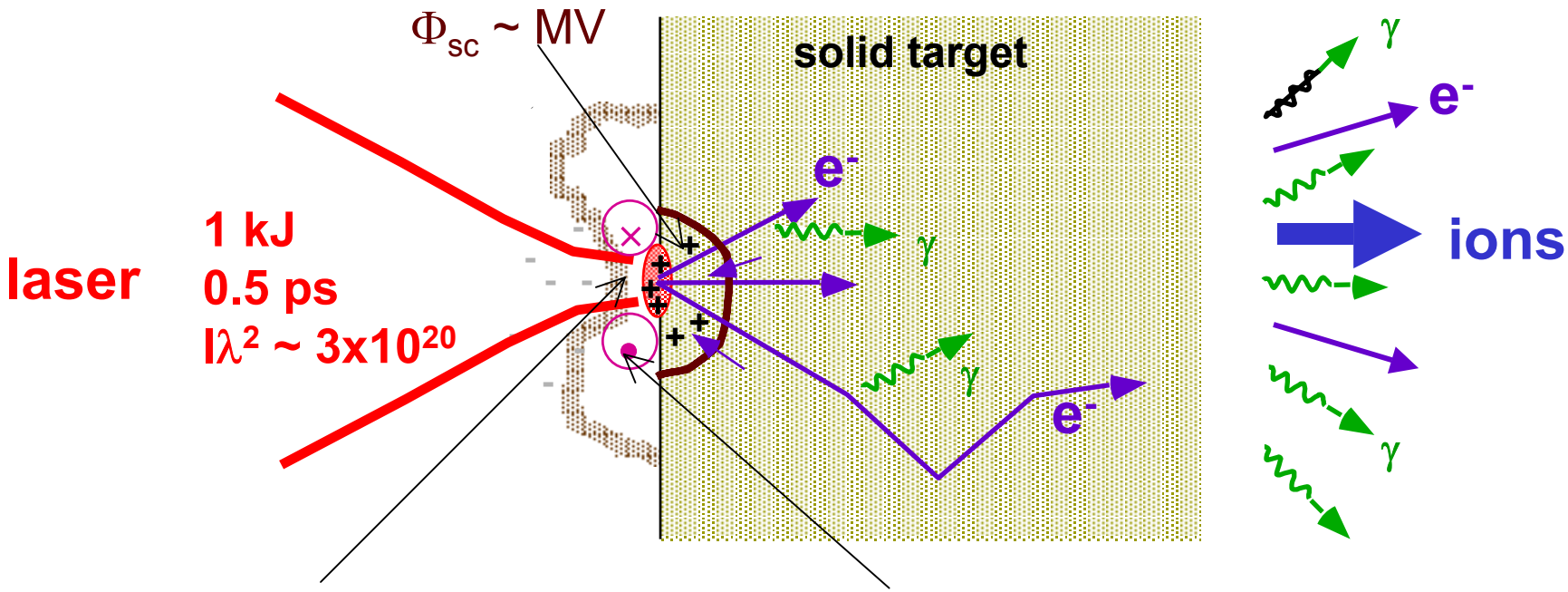

- **Cycle-averaged oscillation energy:** B > 10 MG

$$E_{avg} = mc^2[1+a_o^2/2]^{1/2} \underline{> 5\ \text{MeV}}$$

$$\sim U_{ponderomotive}$$

UNIVERSITY OF CALIFORNIA
Department of Applied Science, UCD

Ever-present prepulse creates plasma on front (laser side) of target, measured by interferometry.

Time = To-80ps

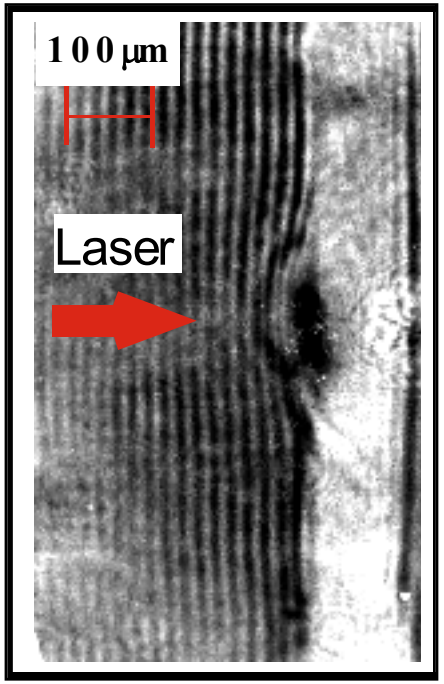

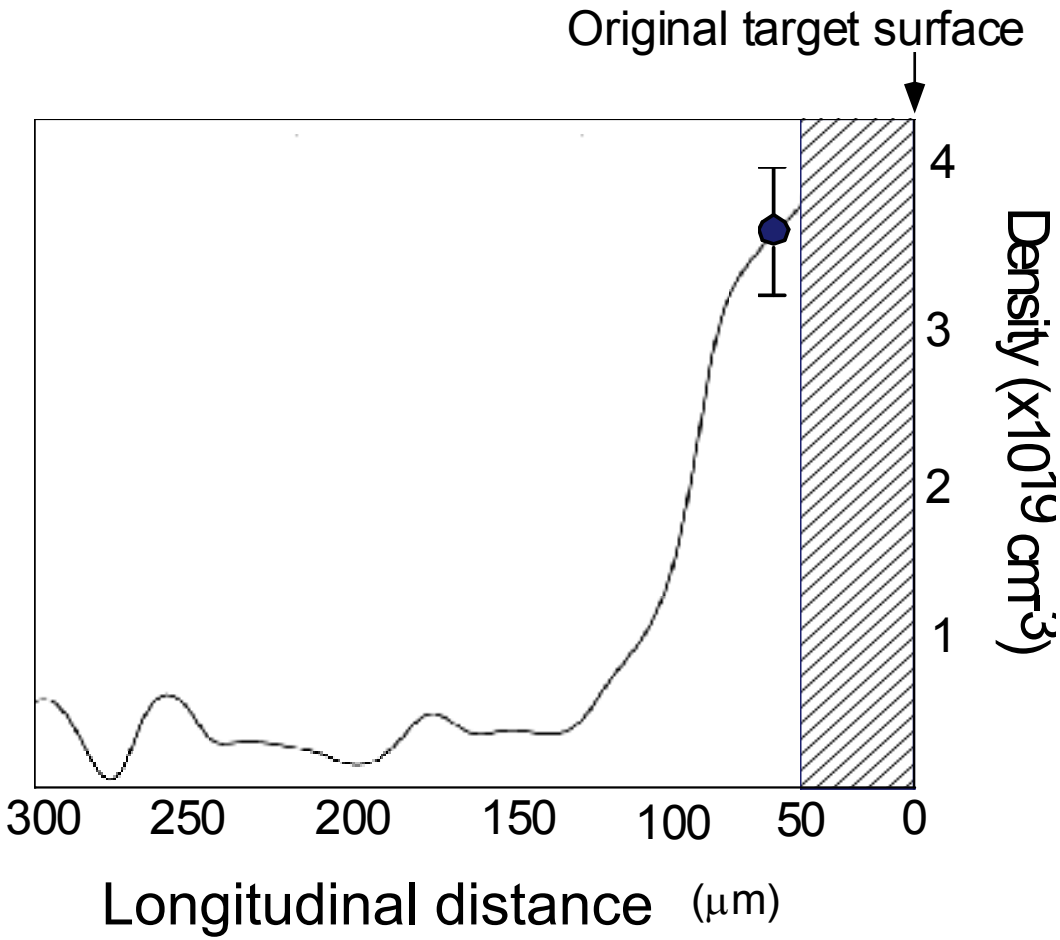

Target : 50μm CH

E ~ 600J

τ_p = 5ps; I ~ 5x10^{19} Wcm^{-2}

UNIVERSITY OF CALIFORNIA
Department of Applied Science, UCD

Resistivity dominates our current experiments but it should be negligible in the fast ignition DT fuel

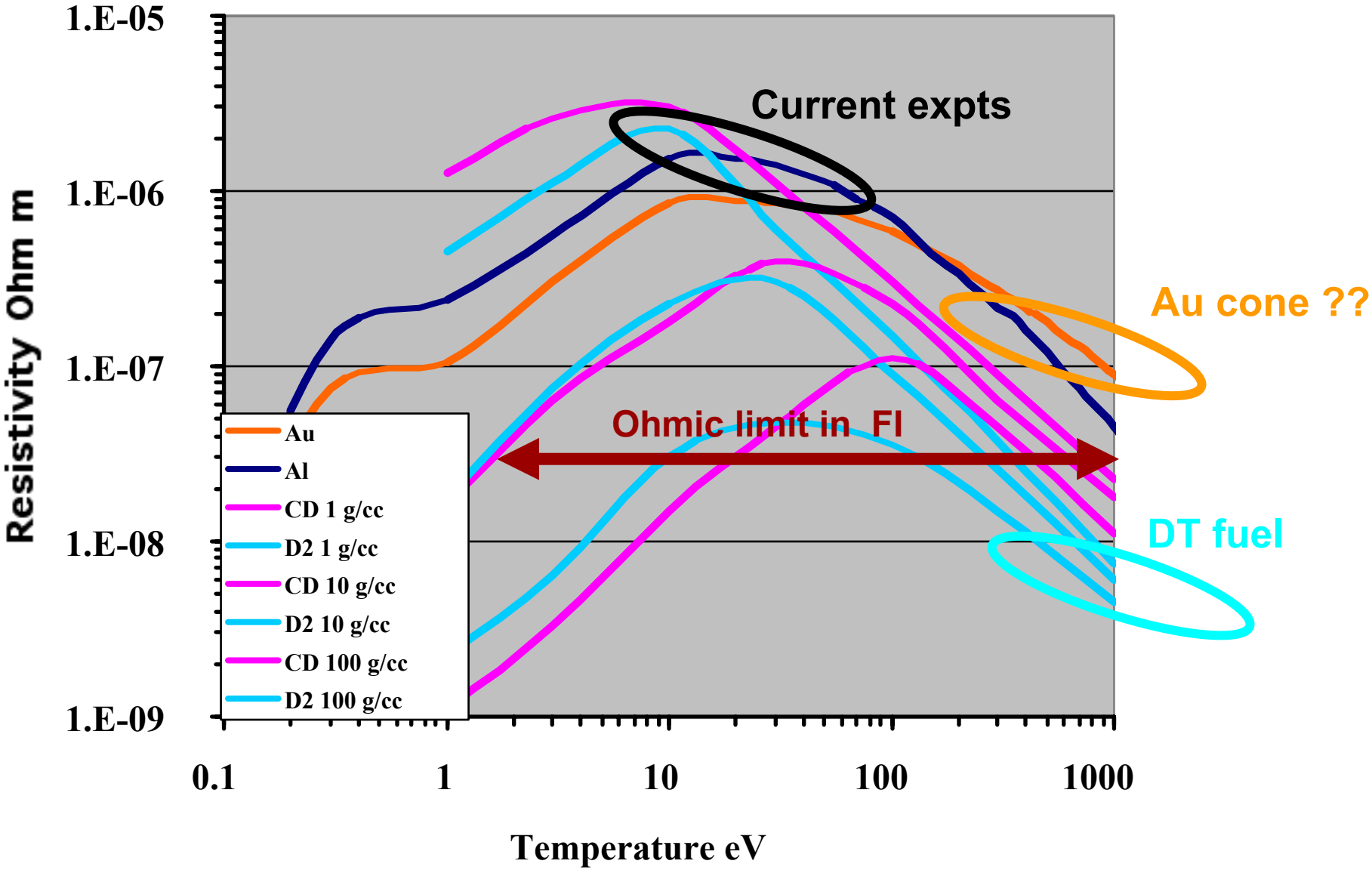

$B_\theta \sim 1/r$

$$B_\theta \sim \int \nabla n \times \nabla T$$

Cf: Forslund and Brackbill PRL 48 1614 (82)
J. Wallace, PRL 55 707 (85)
C.Ren et. al. POSTER 45 THIS CONFERENCE

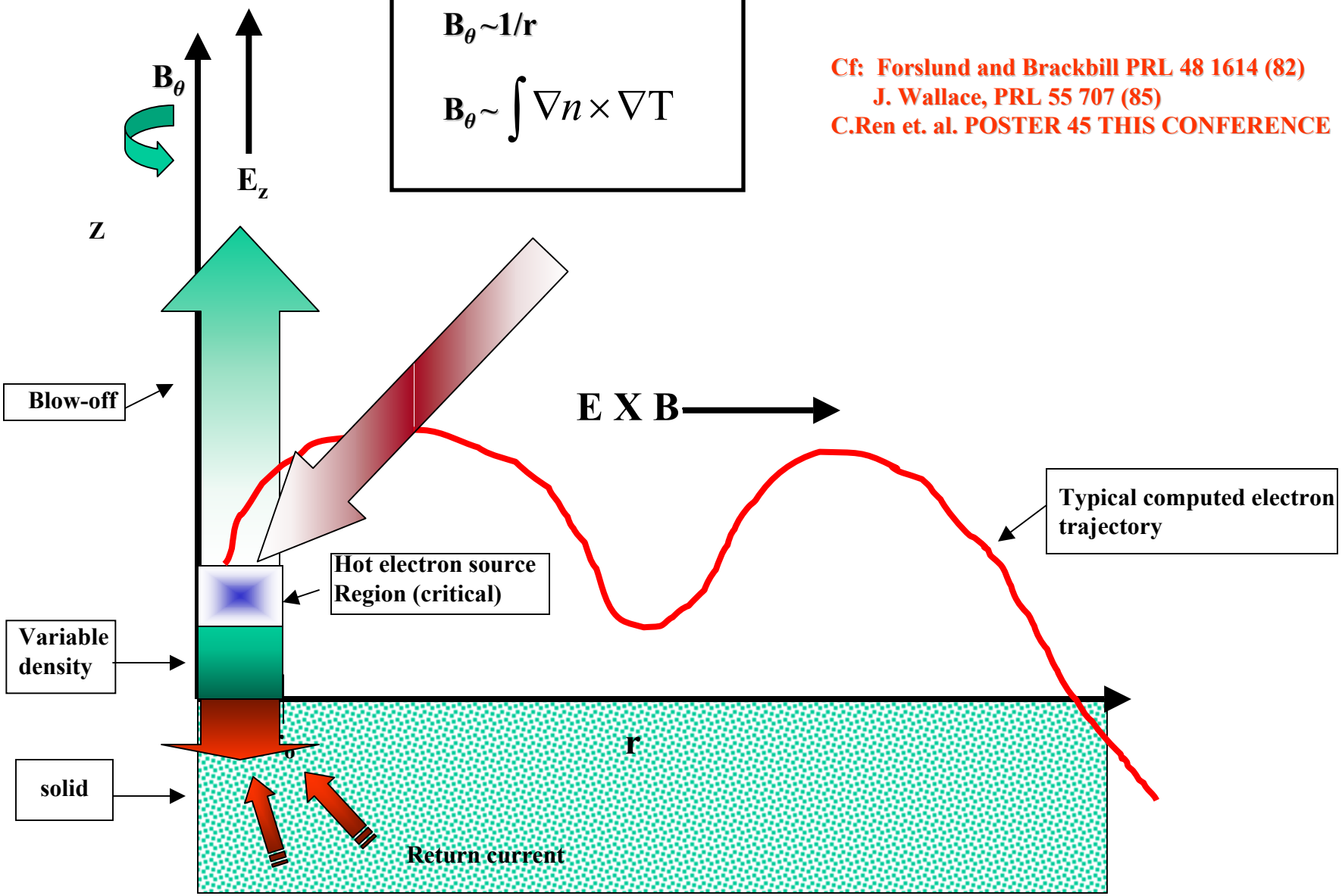

LLNL PETWATT
"HEATING" RINGS
(CF KOCH THIS WORKSHOP)

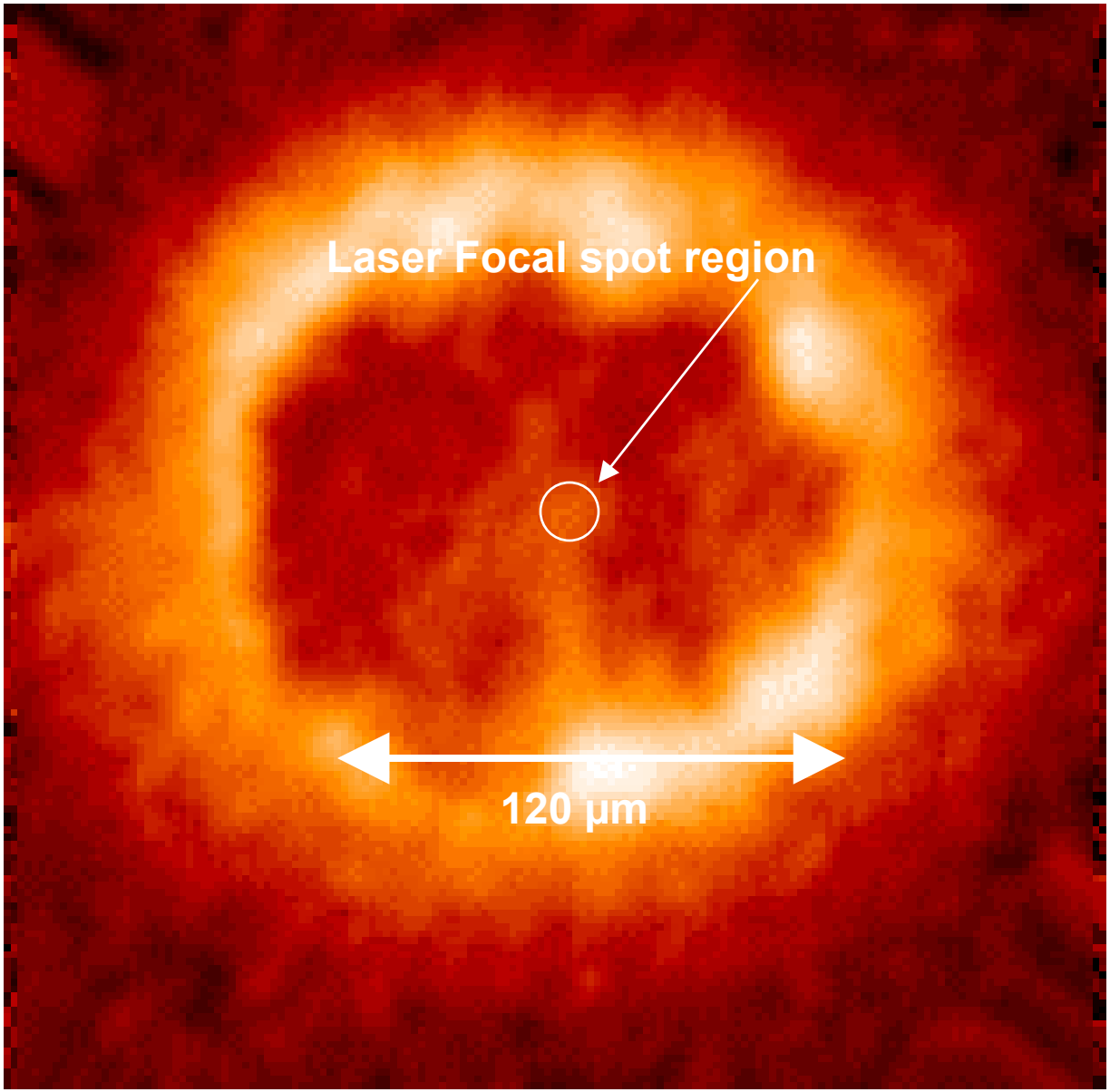

Short-pulse high-power laser propagation in hollow plasma channels

J. Fuchs[1,#], C. Labaune[1], H. Baculet[1], S. Depierreux[2]

[1] *LULI France*

[2] *CEA Bruyères-le-Chatel, France*

present adress: GENERAL ATOMICS

6th worshop on Fast Ignition of fusion targets
Florida, Nov. 16-19 2002

Motivation

- context : fast ignitor

M. Tabak et al., Phys. Plasmas **1**, 1626 (1994).

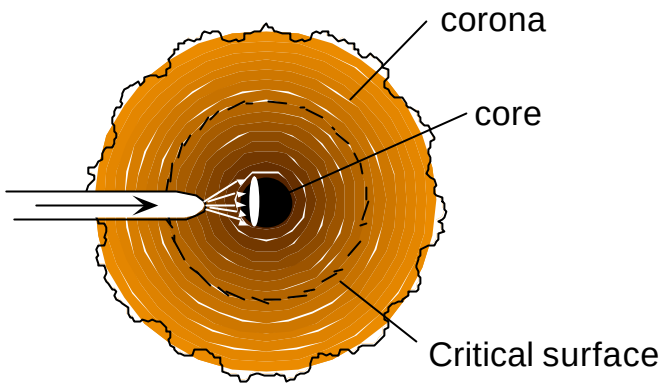

- Physics of short pulse channel drilling & self-guiding studied

P. Young et al., PRL **77**, 4556 (1996) ; M. Borghesi et al., PRL **78**, 879 (1997) ;
J. Cobble et al., Phys. Plasmas **4**, 3006 (1997) ; J. Fuchs et al., PRL **80**, 1658 (1998)

- Is there interest for propagation in channels ?

✍better guiding

✍reduction of parametric instabilities

T. Antonsen et P. Mora, PRL **74**, 4440 (1995) ; T.C. Chiou et al., Phys. Plasmas **2**, 310 (1995) ;
T.C. Chiou et al., Phys. Plasmas **3**, 1700 (1996) ; G. Shvets and X. Li, Phys. Plasmas **8**, 8 (2001)

✍a few studies in gas and/or at low intensities

K. Krushelnick et al., PRL **78**, 4047 (1997); A. Mackinnon et al., PRL **80**, 5349 (1998);
S. Chen et al., PRL **80,** 2610 (1998); J. Faure et al., Phys. Plasmas **7,** 3009 (2000)

Outline

Comparative study of guiding of a high intensity short-pulse $3\ 10^{18}$ W.cm^{-2} beam (P = 15 TW, $a_0 = 0.75$)

-in inhomegenous plasmas n_e^{top} ✍ $[10^{19}, 2\ 10^{20}]$ cm^{-3}
(Pc = [7 , 0.3] TW)

and

- the same with hollowed channels

- High energy gain in the mode
- High quality beam
- Reduced FSRS (but high quality FSRS beam)

Set-up / LULI TW facility

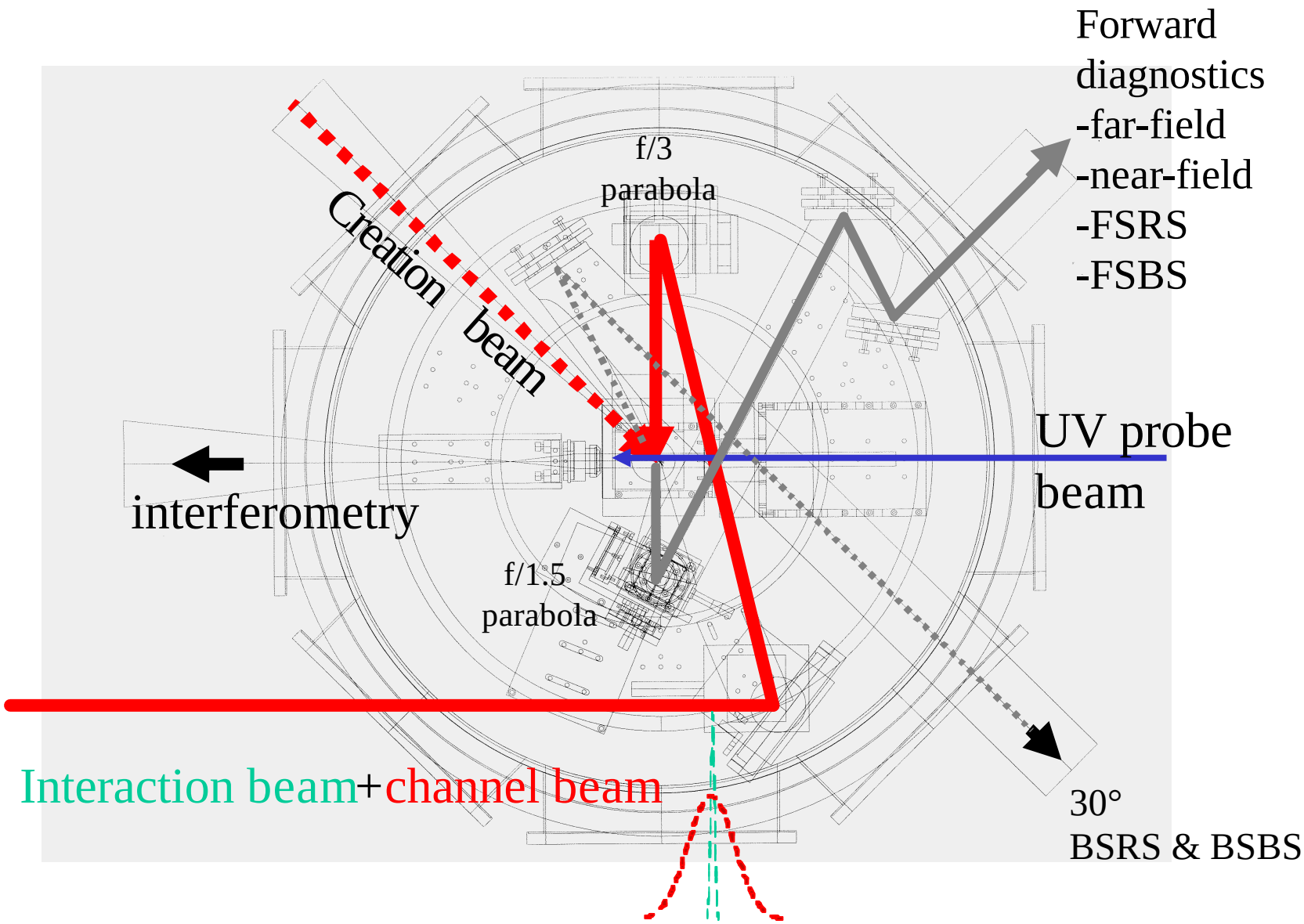

The long-pulse beam bores a channel all along the plasma

Target: 0.3 ? m CH ? $t=t_{channel}+50$ ps

Plasma-creation beam @ 45°

450 ps / 10^{13} W.cm^{-2}
1?

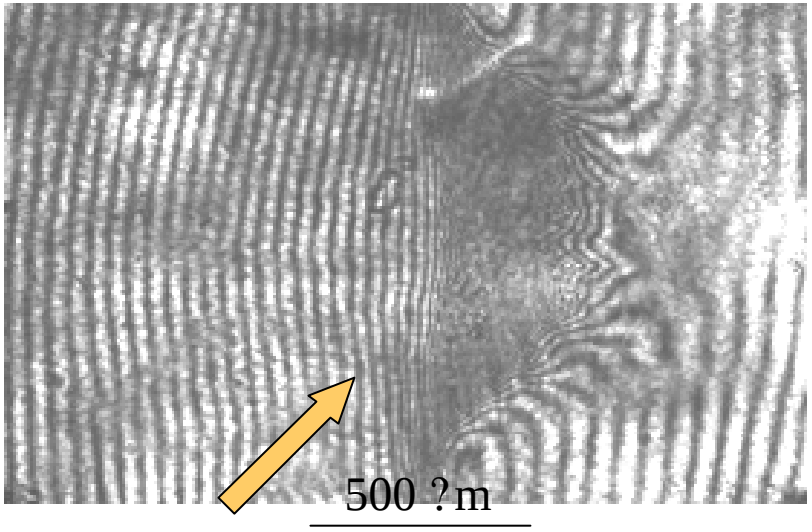

1.9 ns

Channel beam @ 0° focused 250 ? m in front

450 ps / 10^{16} W.cm^{-2}
1?

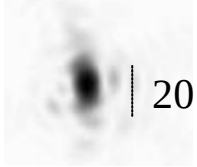

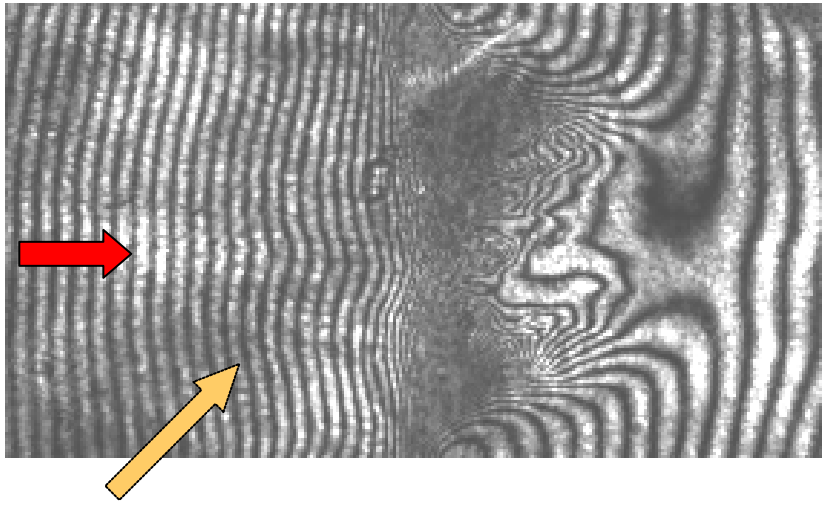

Hollow wide channel

Interaction beam

320 fs / 10 J
2?
FWHM~10 ?m

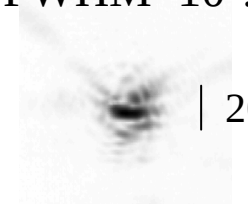

20 µm

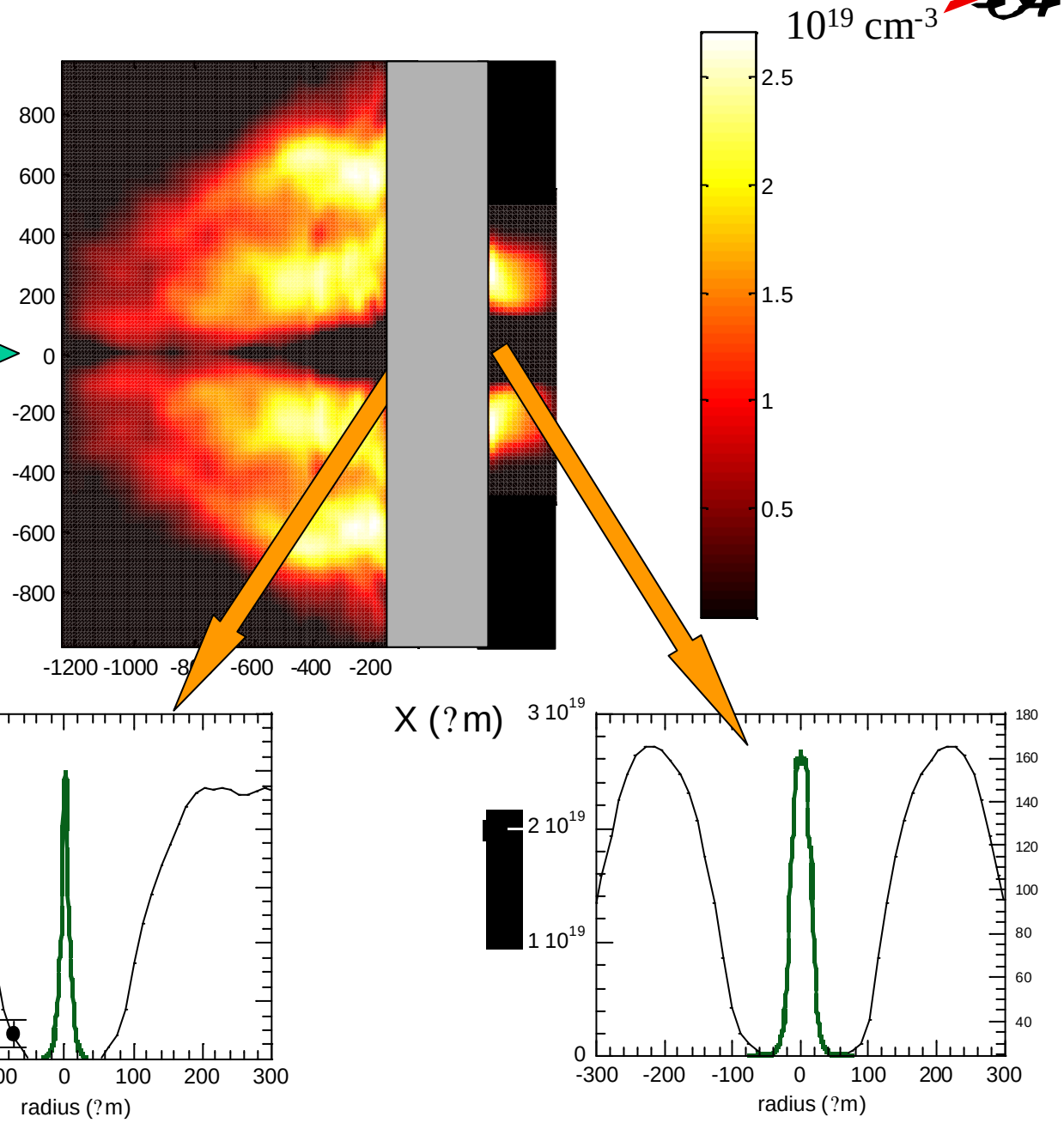

Transmitted 2? energy at high intensity (3 10^{18} W.cm^{-2})

- For 9-11 J of input energy of the interaction beam @ 2?
- Focusing in f/3, collecting in f/1.5

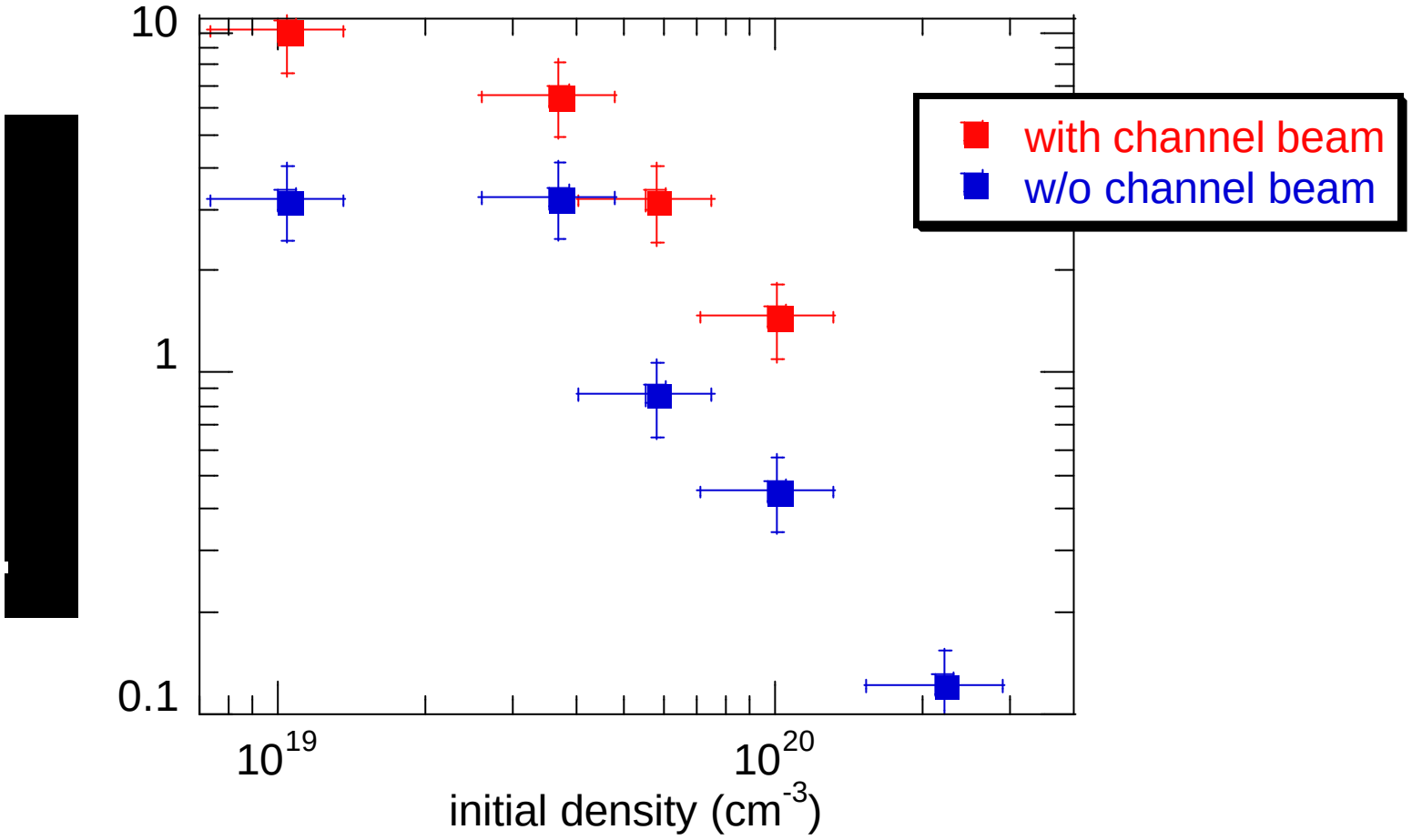

- Measurements show less than 0.1 % 2? conversion at 10^{18} W.cm^{-2}
  & similar density [Malka et al., Phys. Plasmas **4** 1127 (1997)]
- Tests made firing the channel beam only give
  an upper limit of 0.001 J of converted 2? **BUT** conversion may be higher in the channel dug by the fs pulse
- PIC simulations will help to evaluate the channel beam conversion at 2?

Near-field imaging in the output of the plasma to assess the beam structure

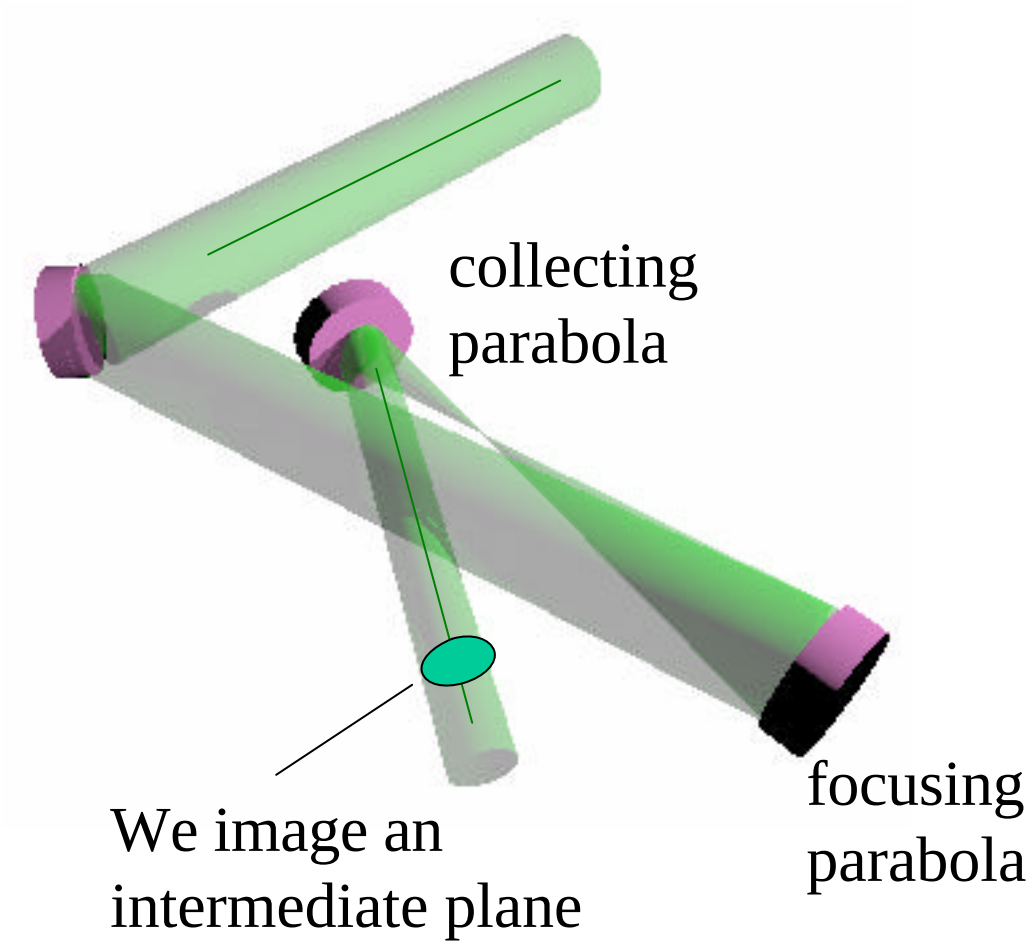

Image in vacuum
(size of laser near-field)

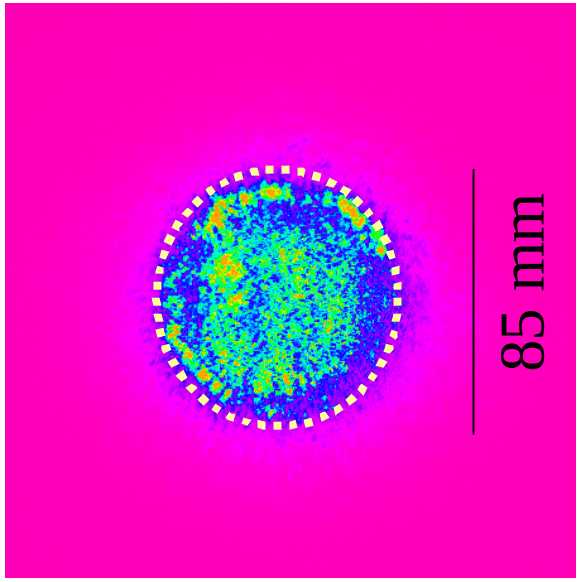

Obvious better guiding with the pre-channel applied

Near-field images of the interaction beam @ 3 10^{18} W.cm^{-2}
Plasma initial density ~ 4 10^{19} cm^{-3}

Interaction beam only

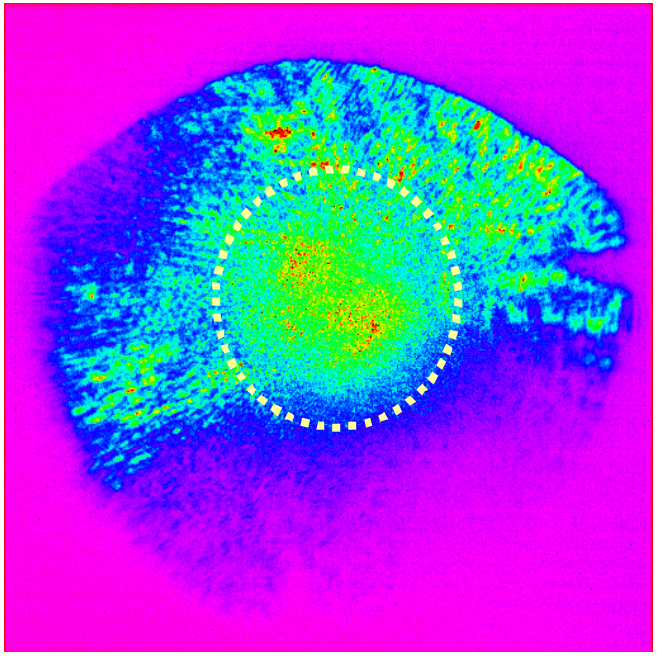

Interaction beam
+ channel beam

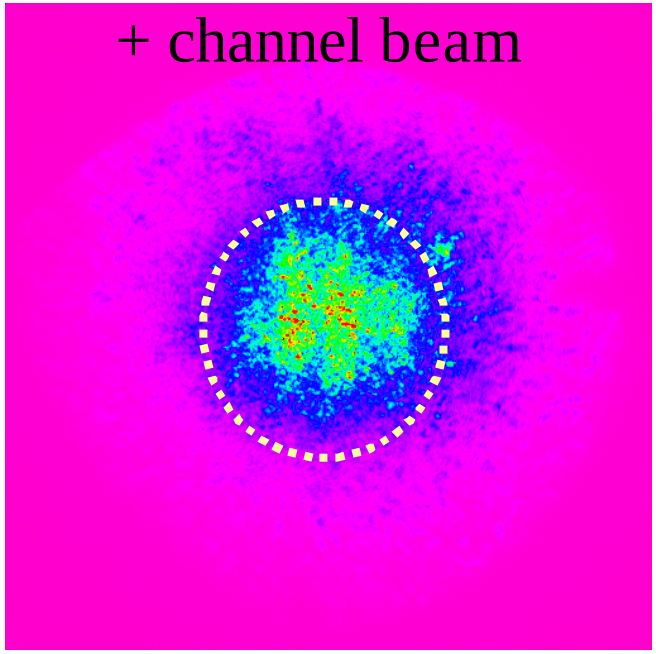

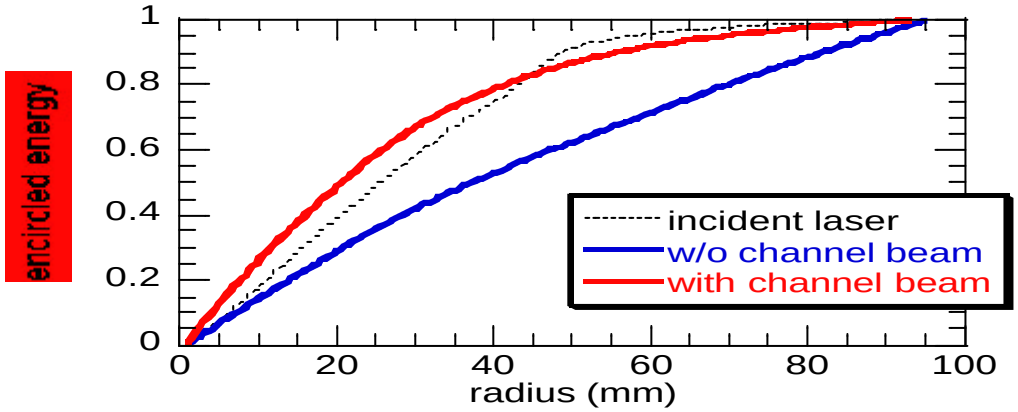

FSRS stabilized or reduced by the channel

- light between 0.5 ? m and 1 ? m
- interaction beam @ 3 10^{18} W.cm^{-2}
- Focusing in f/3, collecting in f/1.5

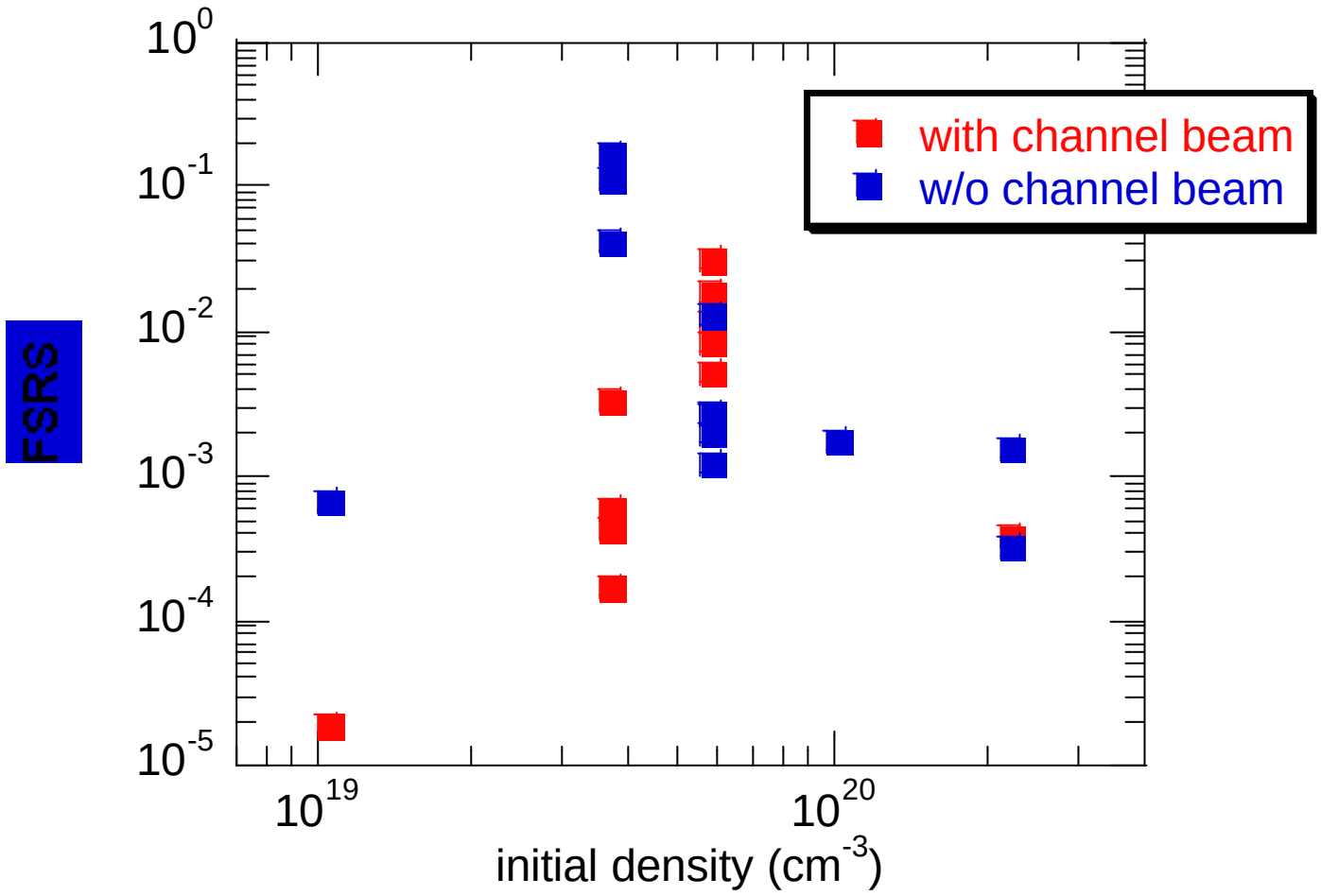

At low initial density the laser propagates well ✍ channel effect ?

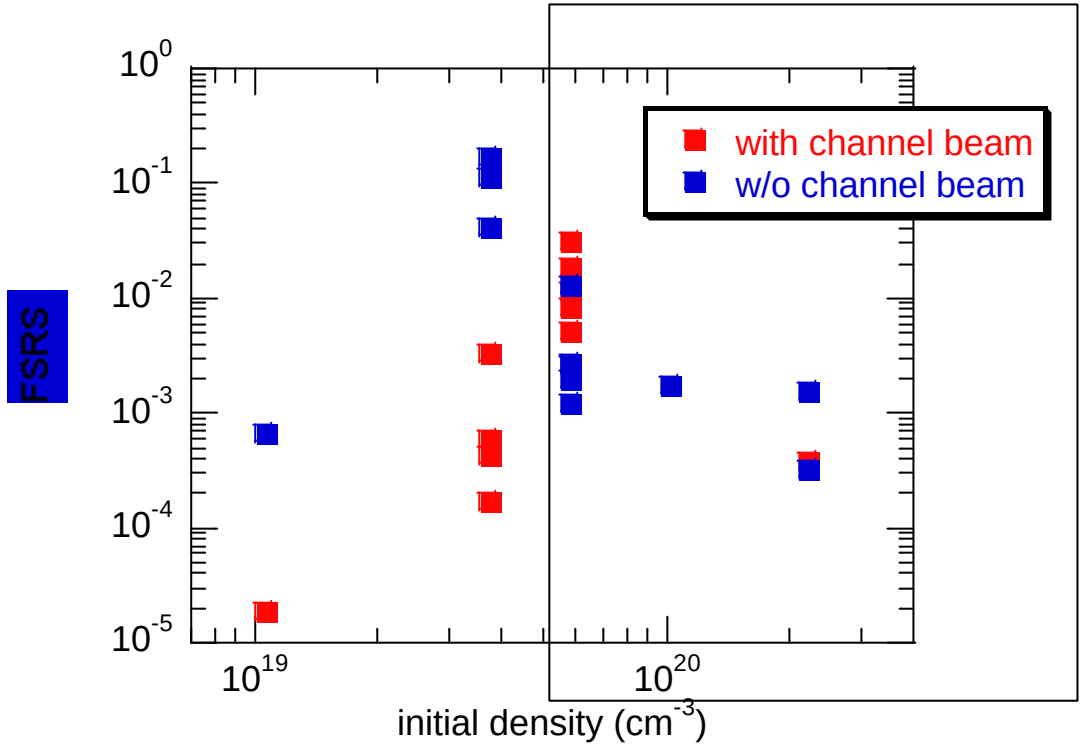

Interaction beam only

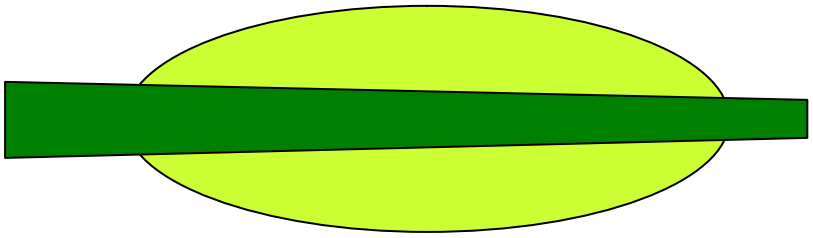

Interaction beam
+ channel beam

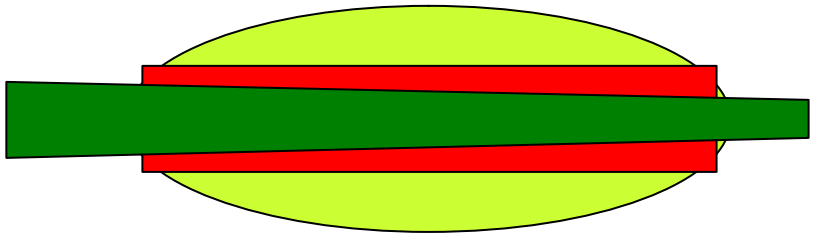

At higher density, balance between improved transmission and channel effect ?

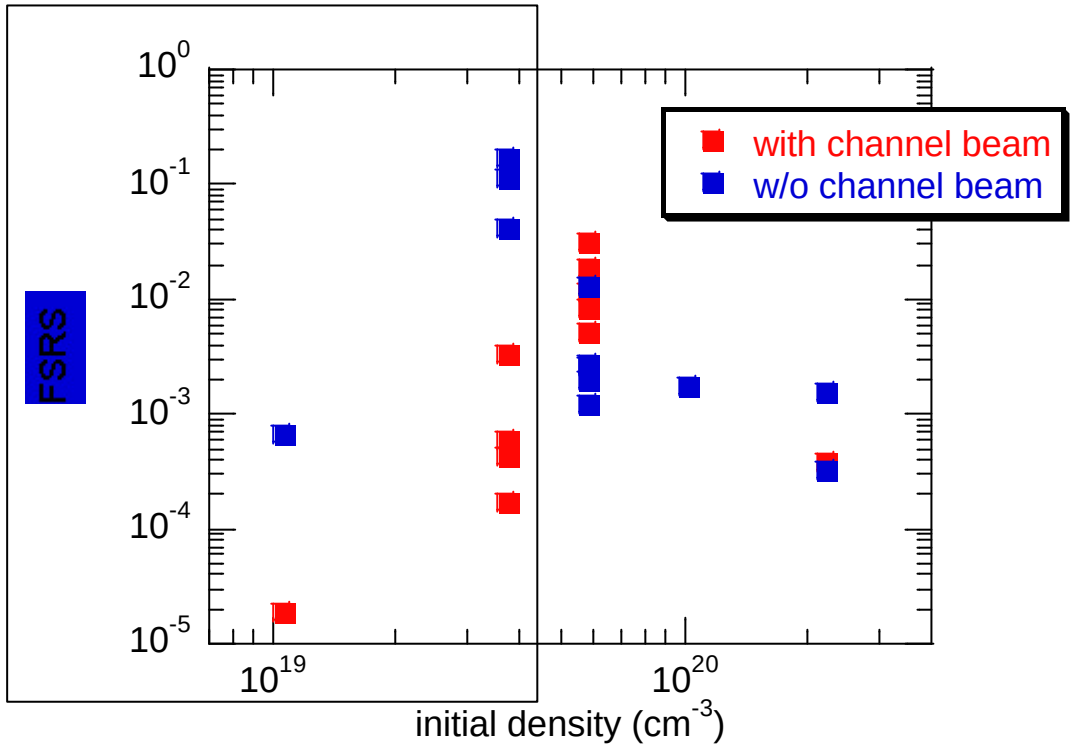

Interaction beam only

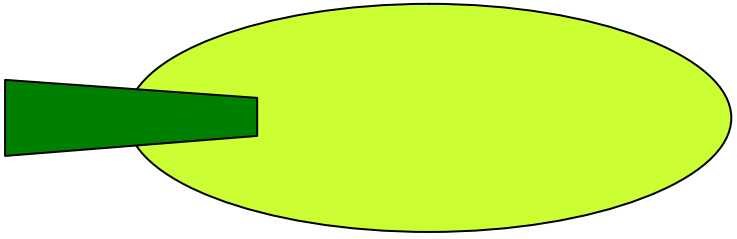

Interaction beam
+ channel beam

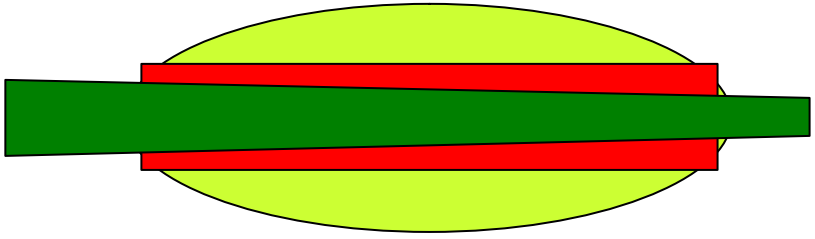

FSRS reduced but has an improved beam structure

Near-field images filtered [570-680 nm]
Plasma initial density ~ 4 10^{19} cm^{-3}

Interaction beam only

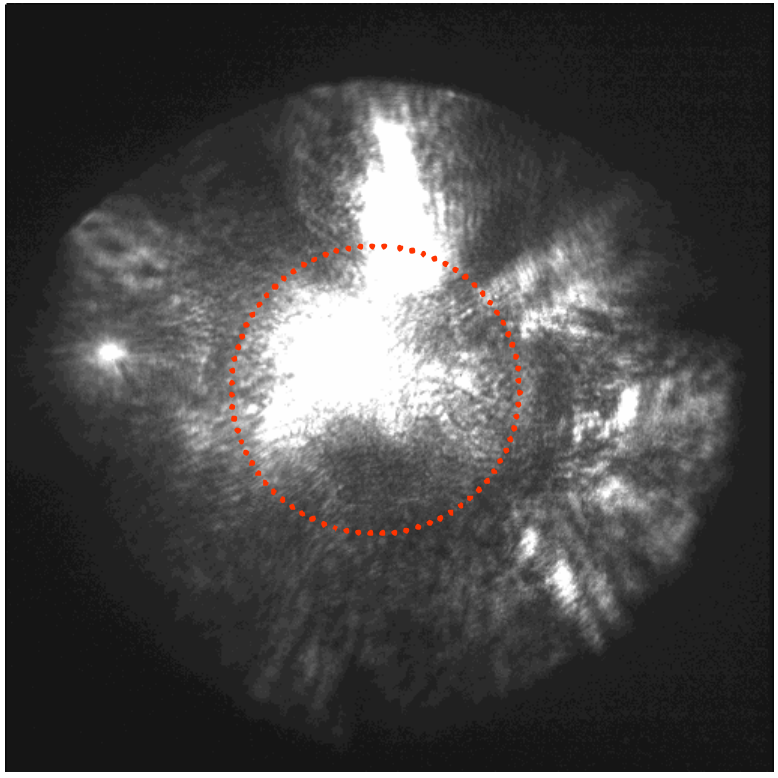

Interaction beam
+ channel beam

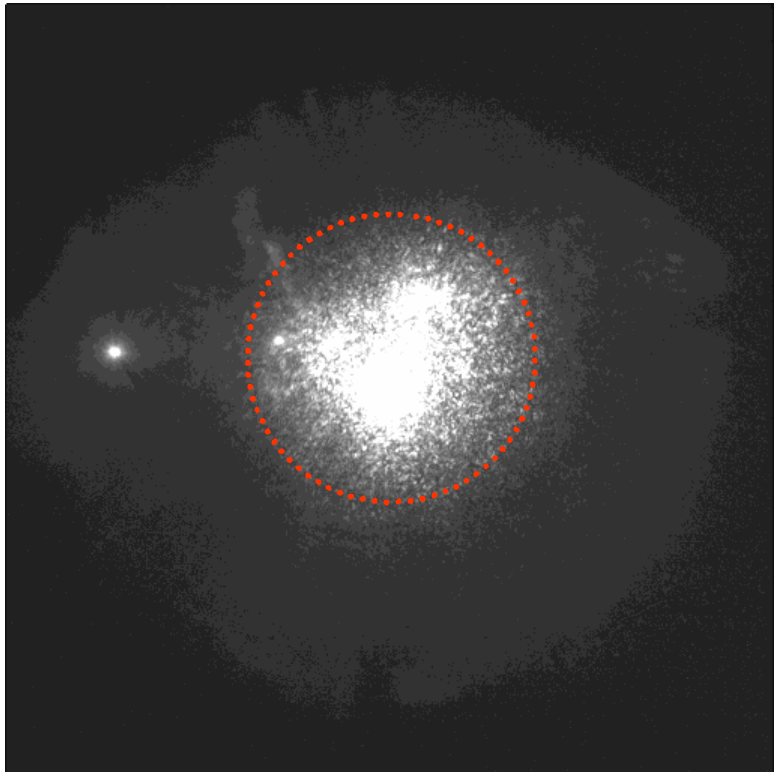

✍ correlation observed between FSRS beam & accelerated electron beam :
CO_2 experiments & short-pulse (Xiaofang Wang et al., PRL **84** 5324 (2000))

Conclusion

- Interest for propagation of high-intensity beams in channels

  → better beam, more energy & less coupling to FSRS

- Motivation for simulations

  Real influence of the channel structure over the density lowering ?

  Structure of the electron beam follows the forward SRS ?

  Confirm low contribution of the 2? converted channel beam to the fs transmission ?

Energy Deposition of Laser-Produced Ions in Fusion Plasmas

Dirk O. Gericke

Plasma Theory Group, Theoretical Division, Los Alamos National Laboratory

---

- Theoretical approaches for the stopping power
- Proton stopping in hot, dense fusion plasmas
- Energy deposition of multiply charged ions

Theoretical Approaches for the Energy Deposition

- Scattering theory for fast particles

$$\frac{\partial}{\partial x}\langle E\rangle = -\frac{Z^2 e^2 \omega_p^2}{v^2}\,\ln\left(\frac{mv^2}{\hbar\omega_{pl}}\right)$$

Bethe (1930)

- Extensions — Standard model for the stopping power

$$\frac{\partial}{\partial x}\langle E\rangle = -\frac{Z^2 e^2 \omega_p^2}{v^2}\left\{\ln\left(\frac{mv^2}{\hbar\omega_{pl}}\right) + f(\eta) + Z L_3\right\}$$

Bloch (1933), Deutsch et al. (1989)

- Dielectric theory — RPA approach

$$\frac{\partial}{\partial x}\langle E\rangle = -\frac{2Z^2 e^2}{\pi v^2}\int\limits_0^{k_{max}}\frac{dk}{k}\int\limits_{-kv}^{kv}\mathrm{d}\omega\,\omega\,\mathrm{Im}\;\varepsilon^{-1}(k,\omega)$$

Lindhard (1954)

- Fokker-Planck approach to the stopping power

$$\frac{\partial}{\partial x}\langle E\rangle = -\frac{Z_{\mathrm{b}}^2 e^2 \omega_{pl}^2}{v^2}\,G\left(\frac{v^2}{v_{th}^2}\right)\ln(\Lambda) + \Theta\left(\frac{v^2}{v_{th}^2}-1\right)\ln\left(1.123\frac{v}{v_{th}}\right)$$

Li & Petrasso (1993)

- Computer simulations — MD + PIC Zwicknagel et al. (1996 ++)

- Quantum kinetic approach

$$\frac{\partial}{\partial x}\langle E\rangle = \frac{\partial}{\partial x}\langle E\rangle_{\mathrm{RPA}} + \frac{\partial}{\partial x}\langle E\rangle_{\text{T-matrix}} - \frac{\partial}{\partial x}\langle E\rangle_{\mathrm{Born}}$$

Gericke et al. (1996), Gericke & Schlanges (1999)

- Dynamic T-matrix model for the stopping power

$$\frac{\partial}{\partial x}\langle E\rangle \sim \sum_c n_c\,\Lambda_c^3\,\frac{k_B T}{v}\int\limits_0^\infty dp\,p^3\,Q_{bc}^T(p,\lambda)\;\Phi\Big(f_e(p), f_e(\overline{p})\Big)$$

Gericke & Schlanges submitted

Results: Proton Stopping in Hot, Compressed Plasmas

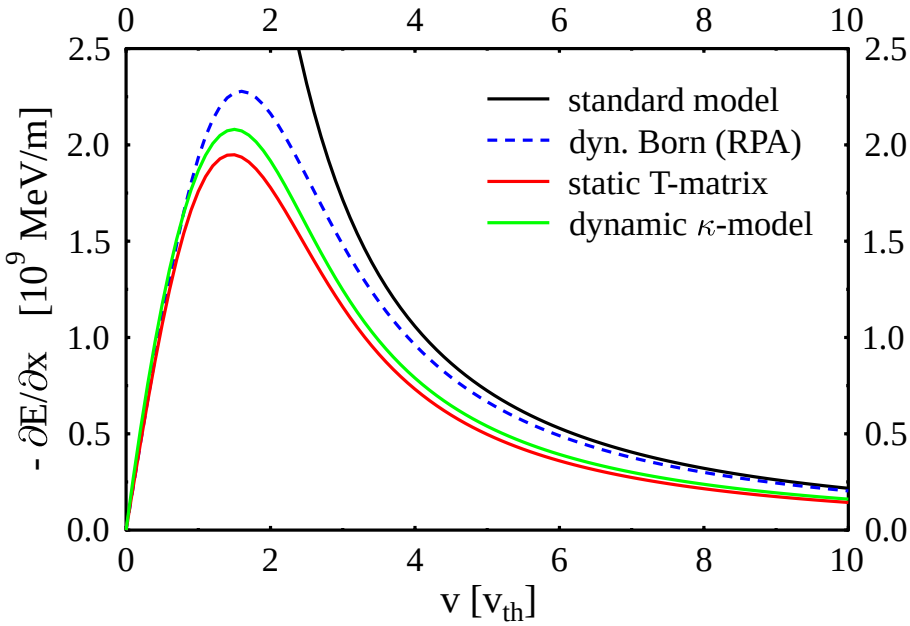

Energy loss of a proton in a fully ionized plasma with $n = 6 \times 10^{25}\,\mathrm{cm}^{-3}$ and $T = 7 \times 10^{7}\,\mathrm{K}$ versus particle velocity in different approximation schemes.

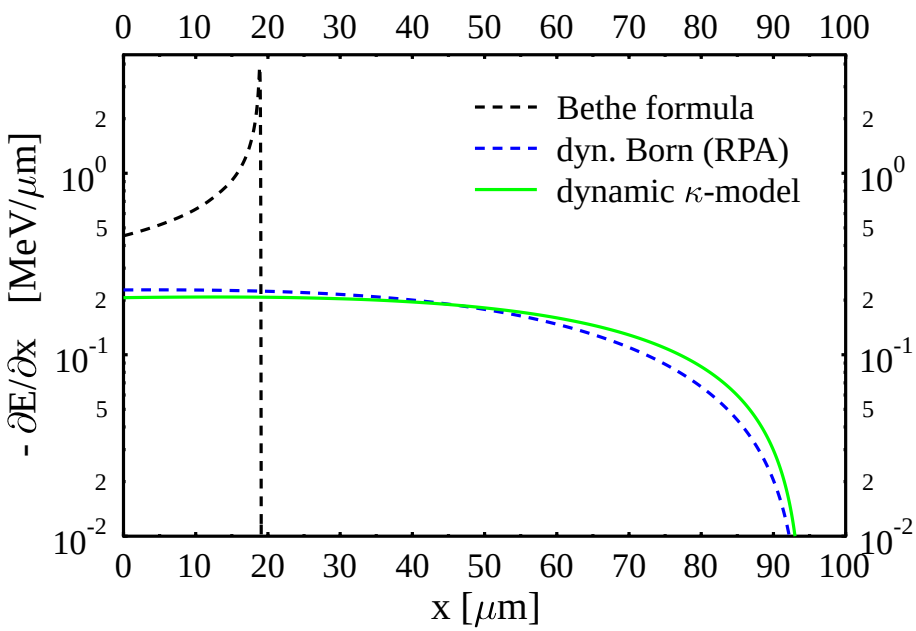

Energy loss of a proton in a fully ionized plasma (same plasma parameters as above) as a function of the position of the proton in different approximation schemes. The initial ion energy is $E(x=0) = 15\,\mathrm{MeV}$, which corresponds to an initial particle velocity of $v = 1.65\,v_{th}$.

Results: Proton Stopping in Hot, Compressed Plasmas

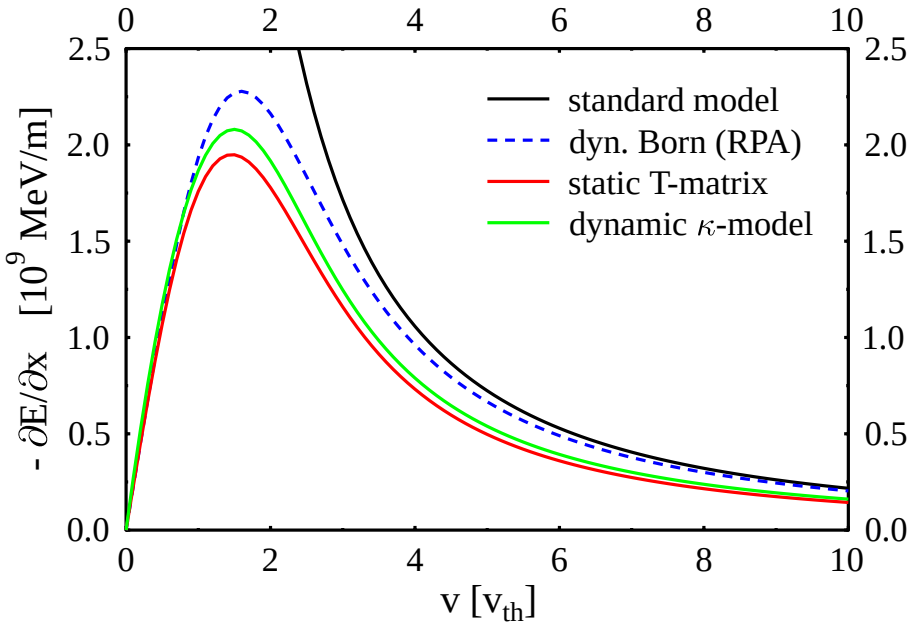

Energy loss of a proton in a fully ionized plasma with $n = 6 \times 10^{25}\,\mathrm{cm}^{-3}$ and $T = 7 \times 10^{7}\,\mathrm{K}$ versus particle velocity in different approximation schemes.

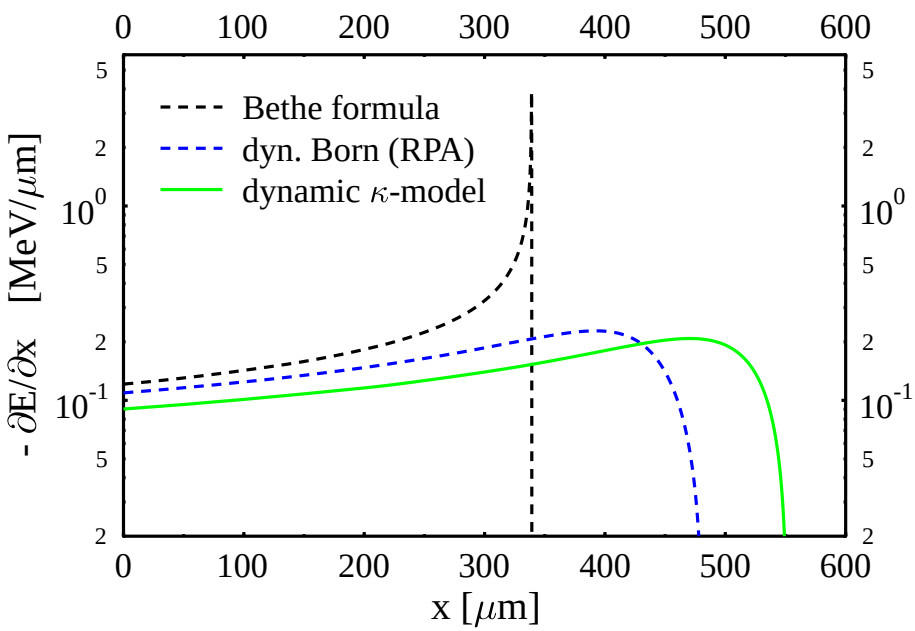

Energy loss of a proton in a fully ionized plasma (same plasma parameters as above) as a function of the position of the proton in different approximation schemes. The initial ion energy is $E(x=0) = 75\,\mathrm{MeV}$, which corresponds to an initial particle velocity of $v = 3.75\,v_{th}$.

Results: Proton Stopping for lower Plasma Temperature

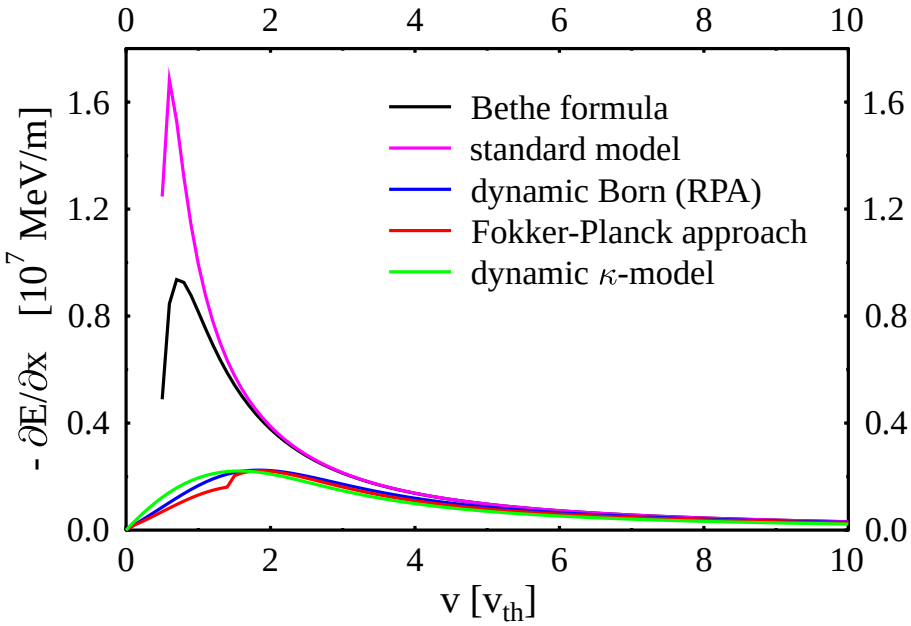

Energy loss of a proton in a fully ionized plasma with $n = 3.3 \times 10^{26}\,\mathrm{cm}^{-3}$ and $T = 2 \times 10^{7}\,\mathrm{K}$ versus particle velocity in different approximation schemes.

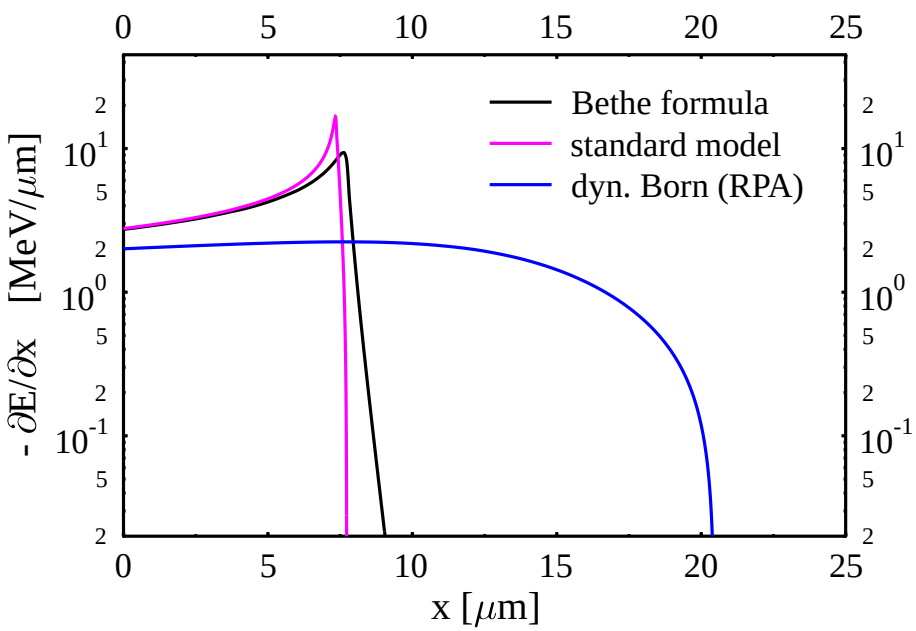

Energy loss of a proton in a fully ionized plasma (same plasma parameters as above) as a function of the position of the proton in different approximation schemes. The initial ion energy is $E(x=0) = 35\,\mathrm{MeV}$, which corresponds to an initial particle velocity of $v = 2.52\,v_{th}$.

Results: Stopping of Ions with Higher Charge Numbers

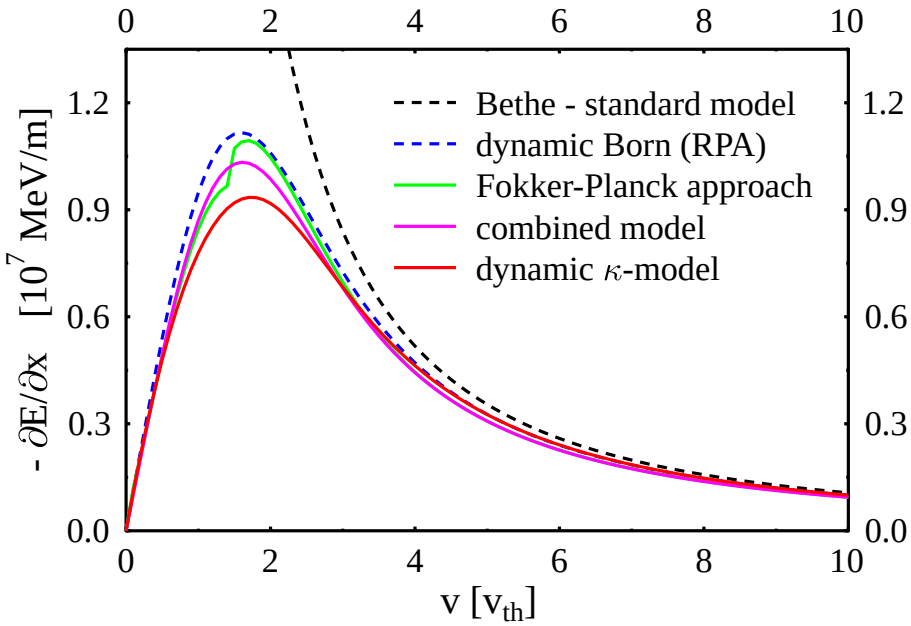

Energy loss of a fluorine F^{7+} ion in a fully ionized plasma with $n = 6.0 \times 10^{25}\,\mathrm{cm}^{-3}$ and $T = 7 \times 10^7\,\mathrm{K}$ versus particle velocity in different approximation schemes.

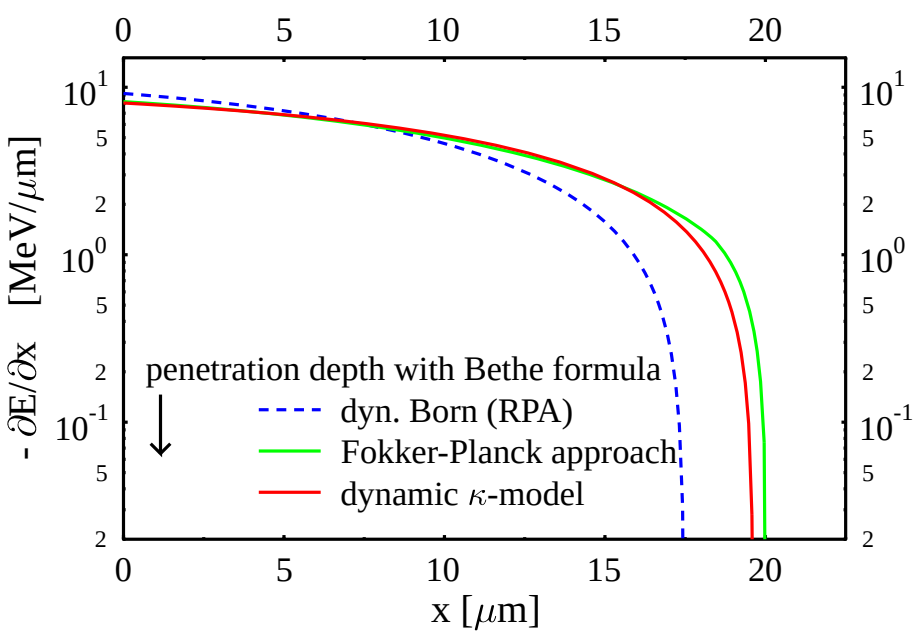

Energy loss of a fluorine F^{7+} ion in a fully ionized plasma (same plasma parameters as above) as a function of the position of the ion in different approximation schemes. The initial ion energy is $E(x=0) = 95\,\mathrm{MeV}$ ($5\,\mathrm{MeV/u}$), which corresponds to an initial particle velocity of $v = 0.95\,v_{th}$.

Conclusions

- In the important velocity range, all finite velocity theories for the stopping power predict a much smaller energy loss per distance than the Bethe formula and the standard model.
- In particular, the well-pronounced Bragg-peaks of the energy transfer predicted by the standard model are not present.
- Accordingly, the range of the protons is several times longer, and the energy transfer occurs more uniformly and to a larger volume.
- Higher charged ions (same beam energy) have much shorter ranges.
- Differences between Bethe theory and other approaches are larger than for protons since v/v_{th} smaller.
- For an exact prediction, strong coupling effects have to be included for lower target temperatures.

Neutron spectroscopy for plasma heating measurements in cone-guided shell implosion on VULCAN

6th Workshop on Fast Ignitor of Fusion Targets,
November 16, 2002,
Dolphin Beach Resort, Florida, USA

H Habara, K L Lancaster, and P A Norreys
CCLRC, Rutherford Appleton Laboratory

This work has been done in collaboration with the Lawrence Livermore National Laboratory, the Institute of Laser Engineering, Osaka University, Japan, the Gen Atomics Corp., the Queens University, Belfast, Imperial College, London, the University of Rochester and the University of Oxford.

Contents

Introduction - Cone-Guided Fast Ignitor Scheme

- Beam fusion reaction by ion acceleration

Large area Neutron Spectrometer Array (LaNSA)

- LaNSA system diagram
- LaNSA performance
- Operation software
- Spectrum Analyze using 3D Monte-Carlo simulation
- Calibration

Summary & Future Plan

Introduction - Cone-Guided Fast Ignitor Scheme

guiding the heating beam close to the compressed semi-hot core [1, 2].

(1) Compress the shell

(2) Shooting the core directory by Ultra Intense Laser Beam

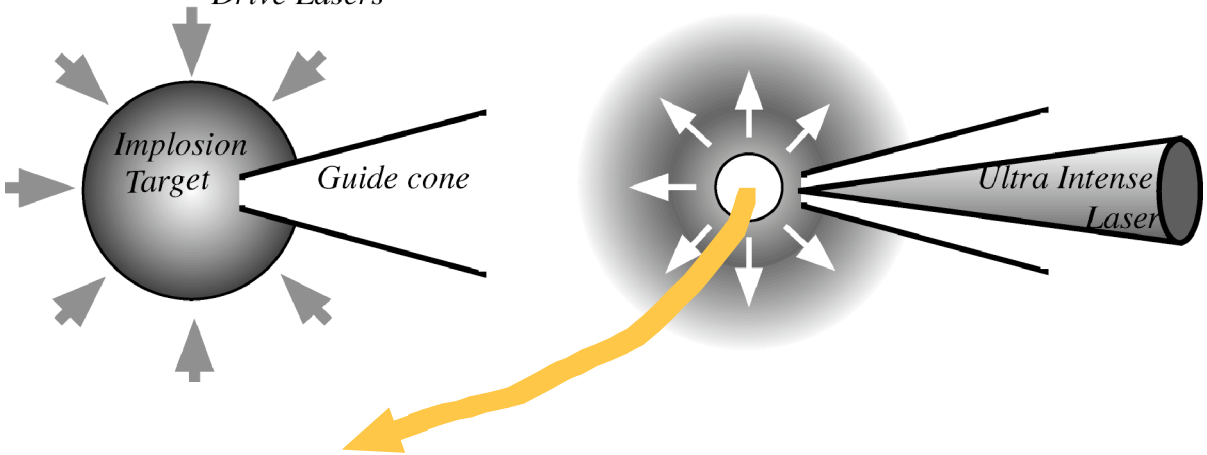

- Core temperature can be observed by neutron yield by D-D or D-T reaction - up to 0.8 keV [3]
- Corresponding neutron yield - approximately 3×10^7 - about 3-orders of magnitude without heating pulse

to measure the temperature more precisely...

High efficiency and high dynamics range neutron detector

[1] Norreys PA et al 2000 Phys. Plasmas 7, 3721
[2] R.Kodama et al 2001 Nature 412 798-802
[3] R.Kodama et al. 2002 Nature 418, 933

Ion diagnosis through fusion neutron spectrascopy
- Beam Fusion Reaction

Why do detection of fusion reaction neutron give imformation of accelerated ions?

Fusion reaction neutron is reflected for motion of accelerated ions.

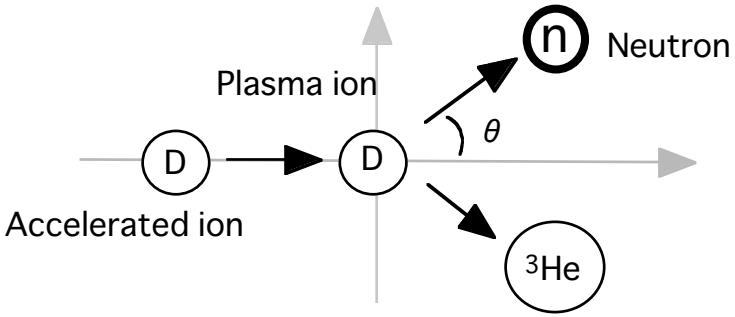

Momentum and energy between charged ions and neutron is conserved.

Neutron have an advantage of high permeability in overdense plasma compared with accelerated charged ions itself.

Neutron spectra at multi-directions can deduce momentum distribution of accelerated ions inside of plasma or solid

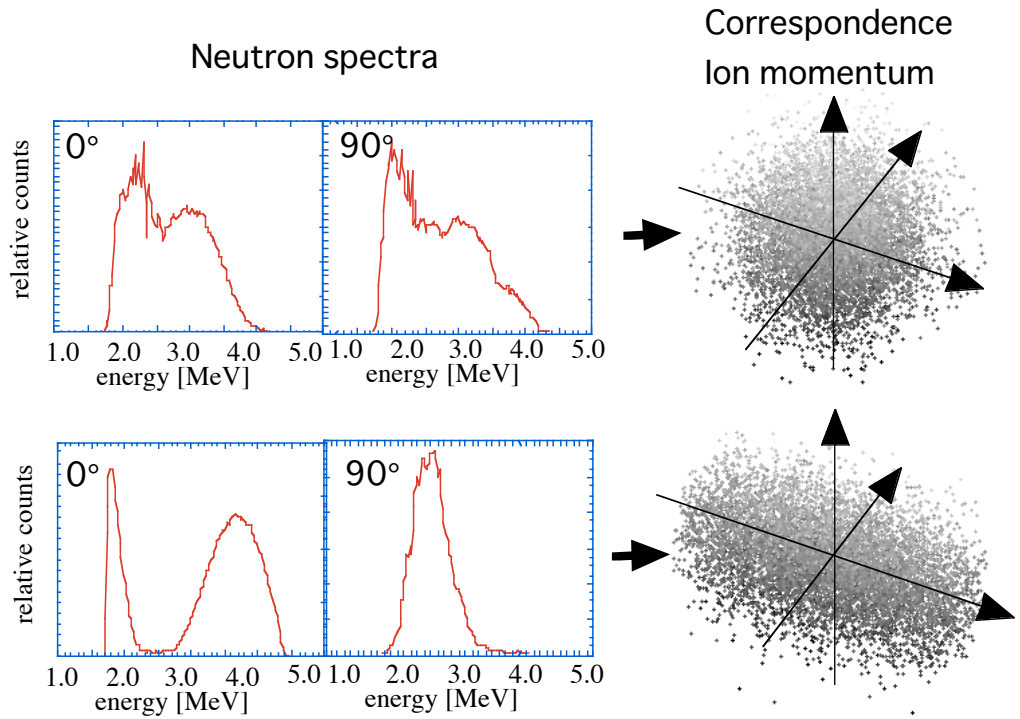

Large area Neutron Spectrometer Array (LaNSA)

- LaNSA is a multi-channel neutron detector based on Time-of-flight technique.
- LaNSA is a counting type (neutron yield is obtained by number of hit-detector, not output current from detector) array detector.
- LaNSA detector is a liquid scintillator which detect a neutron by knock-on proton scintillation combinined with photo-multi-amplifire tube.

LaNSA Array

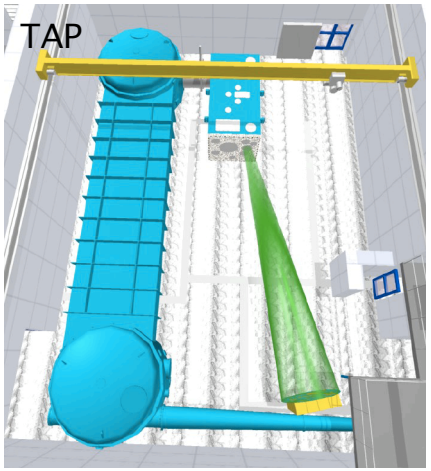

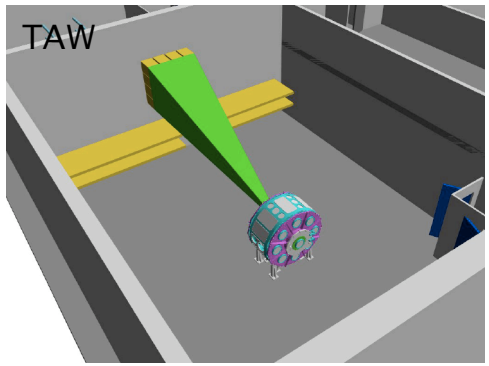

- LaNSA consists 3 arrays, one has 288 channel at TAW on VULCAN (100TW laser) and others are 256 channel at TAP (Petawatt laser)
- LaNSA control system consists CAMAC and Fastbus modules and it is operated by PC via TCP/IP protocol.

LaNSA system diagram

Signal Flow

(1) Neutron signals are detected at Detectors

(2) The signals are discriminated at Discriminator

(3) Then the signals are collected at TDC and ADC

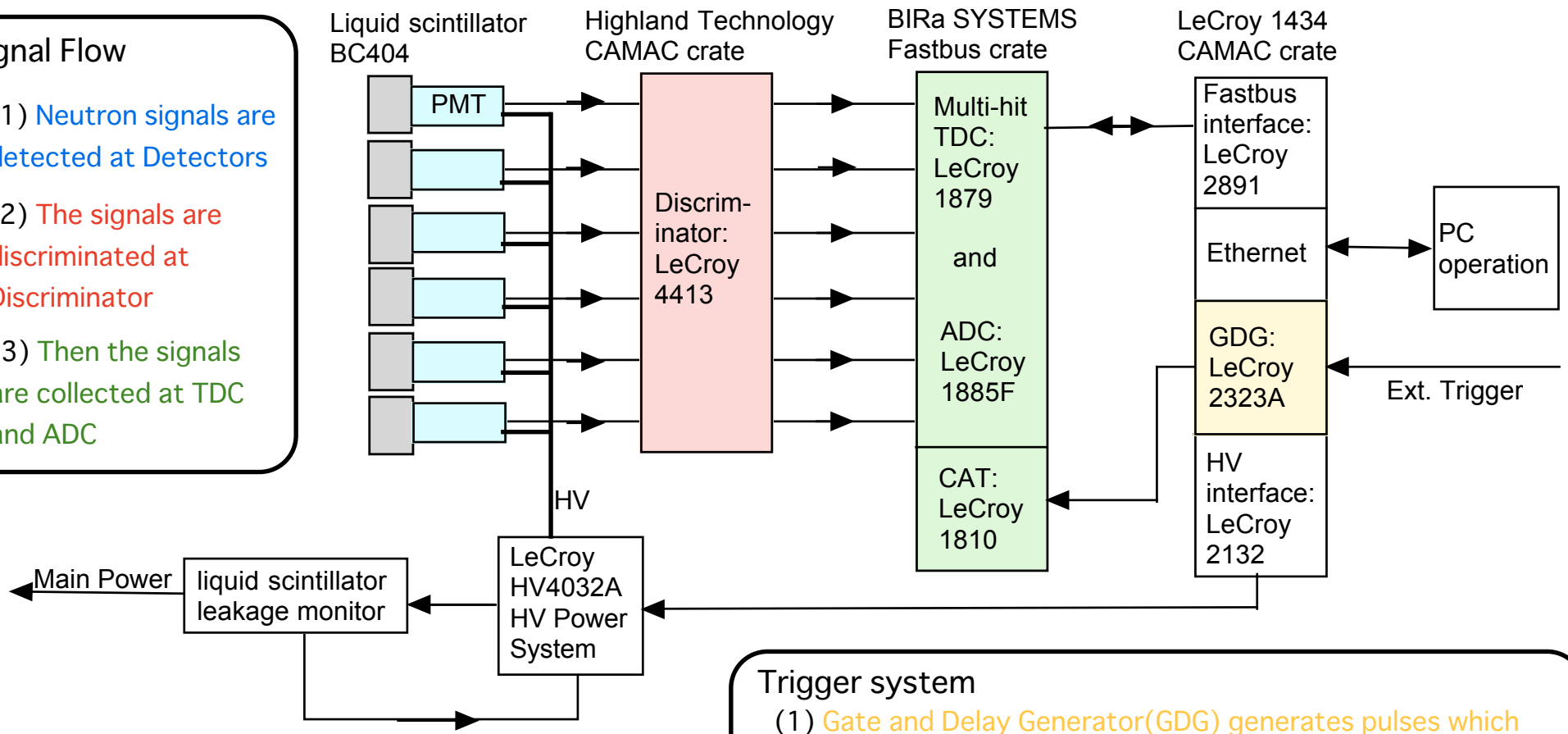

Trigger system

(1) Gate and Delay Generator(GDG) generates pulses which have a programmed width and delay.

(2) These pulses are introduced in CAT to drive TDC stop timing and ADC gate.

LaNSA performance

Energy resolutions

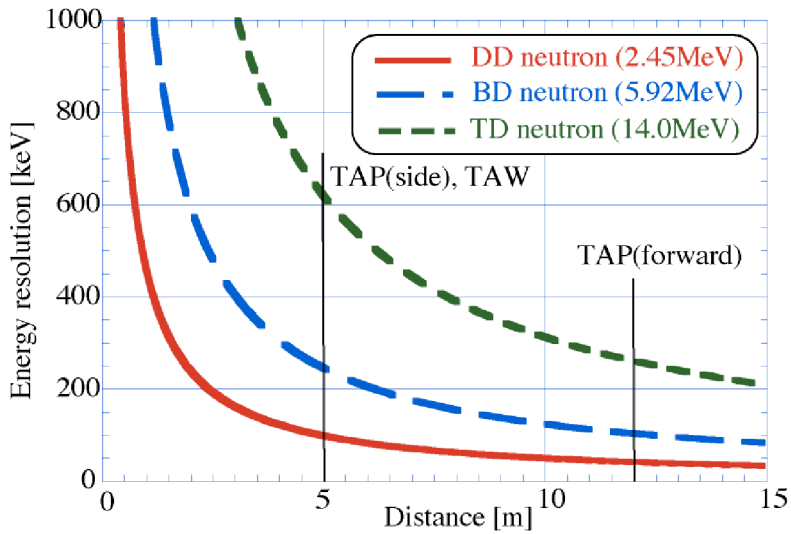

Dynamic range

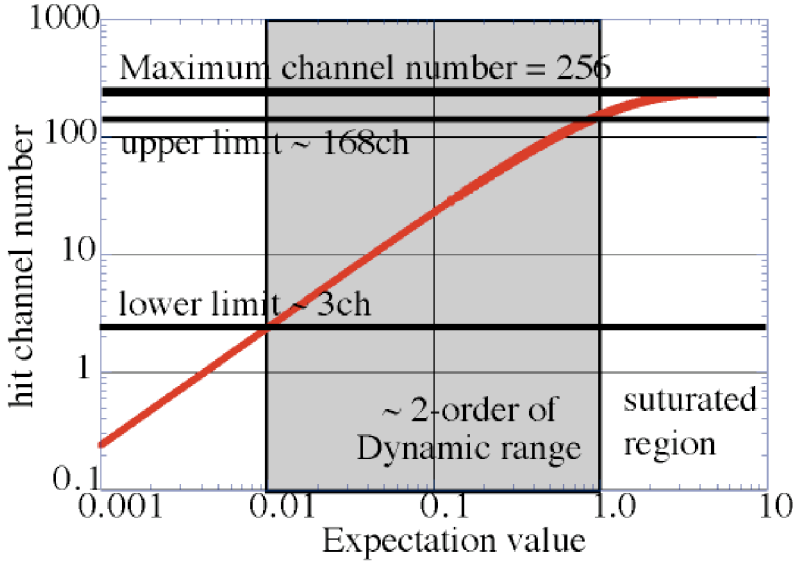

Energy resolution including the temporal resolution (about 4ns) of electronics

DD: 50keV - TAP (North)

100keV - TAW and TAP (West)

TD: 250keV - TAP (North)

600keV - TAW and TAP(West)

Dynamic range for TAW and TAP (West) Array

~ 2 order of magnitude

* Expectation value : Expectation number of neutron detectable at single detector

Expectation value $\mu = \mu_{sgl} Y_n$

Neutron hit number $\frac{N_{hit}}{N_{total}} = 1 - \exp(-\mu)$

Newly established operation software

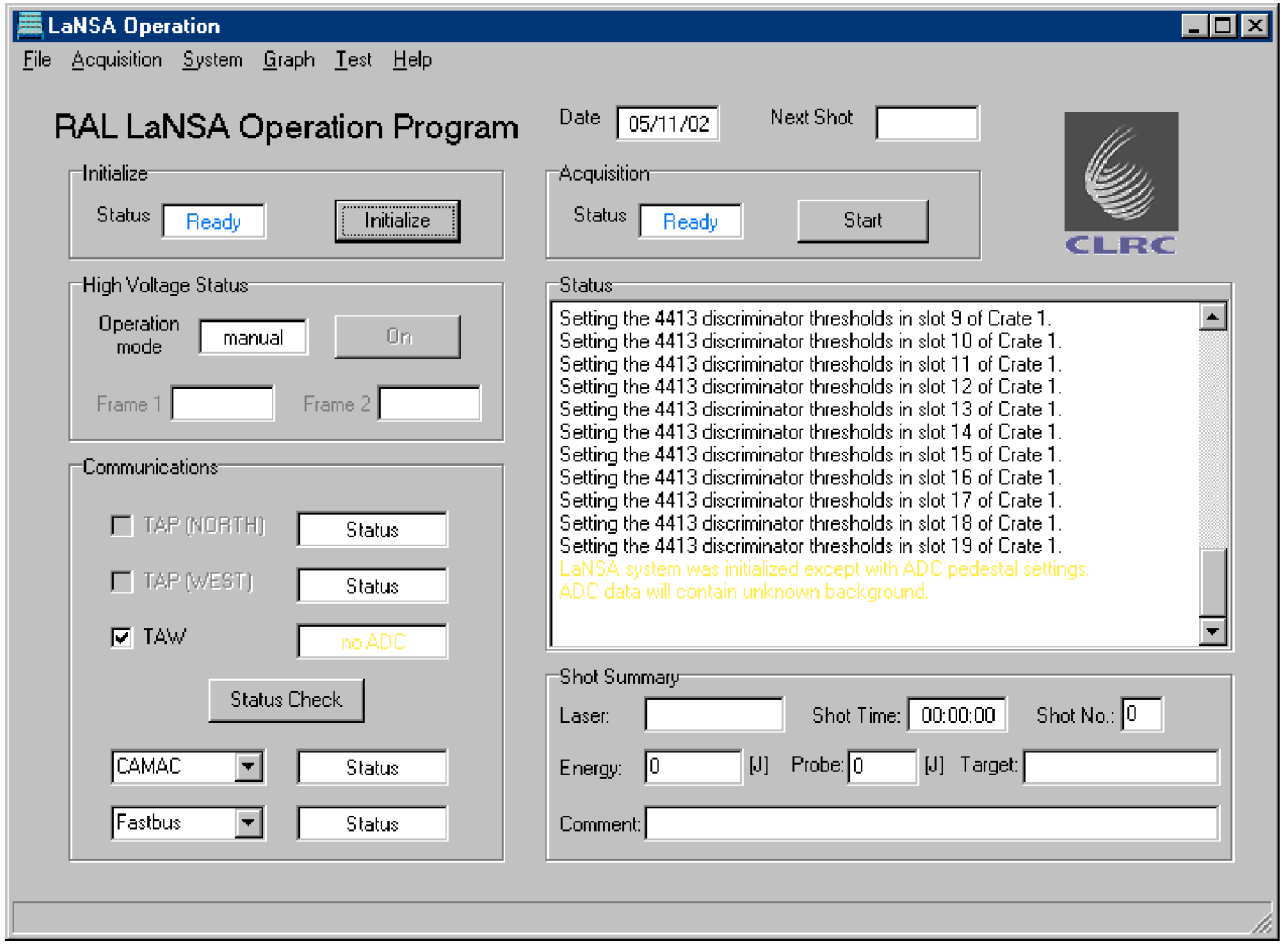

@ LaNSA Operation Program

- Written in Objective Pascal(Delphi) and Microcode for Fastbus operation
- Fully 32 bit Windows application
  - Objective Oriented Programming
  - Multi-Thread correspondence
  - Working on Windows NT4 or later

@ Easy to reinitialize of system and change CAMAC and Fastbus module parameters

@ Provide wide-range test mode to check the status of modules.

@ Any detected data are automatically saved

@ Check the HV status regularly on background

@ Report detailed status such as Initializing, Acquisition, Error and so on

3D monte-carlo simulation for neutron spectra analysis

Subject : To investigate neutron spectra giving different initial momentum distribution of accelerated ions

Initial momentum distribuion of ions are given to fit the simulation spectra to the experiments.

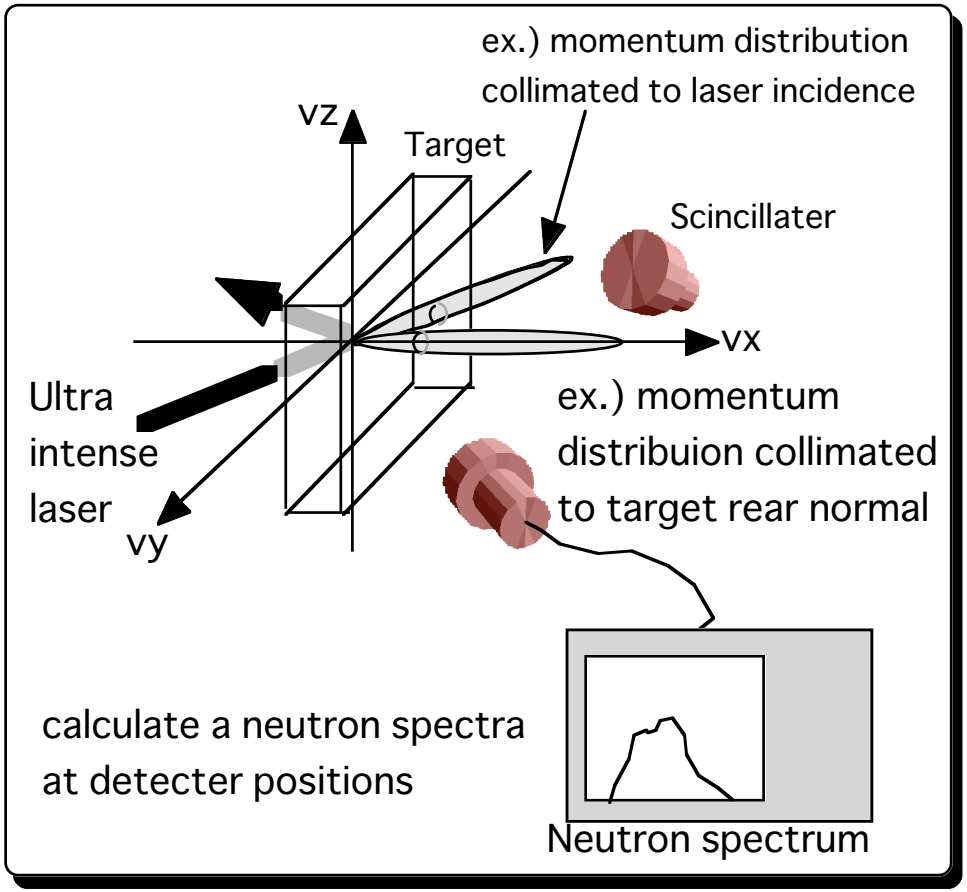

Taking account of two motions of acclerated ions in plasmas.

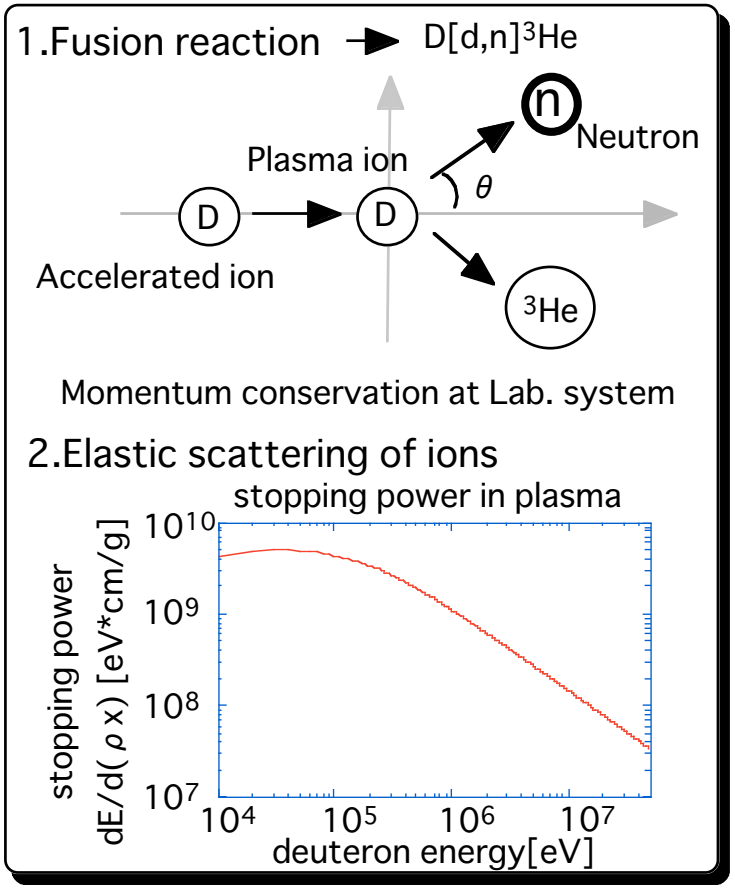

LaNSA Calibration

Voltage adjustment

- uniformalize output level of every channels

● Setup

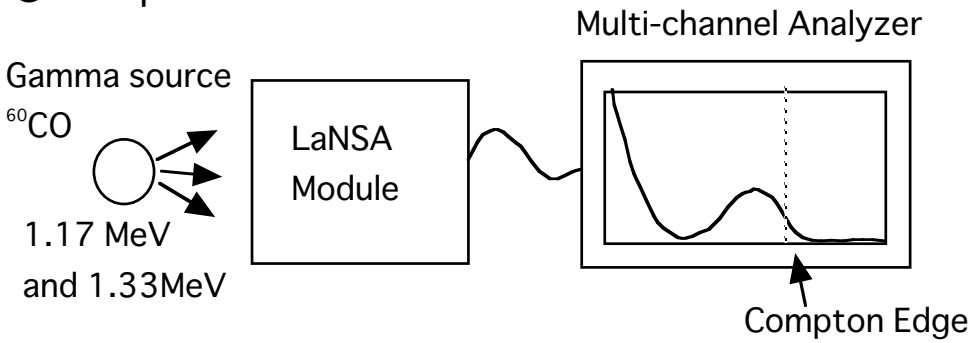

Check output of each channel of each module become same level of Compton edge of Gamma source.

typical output before the adjustment

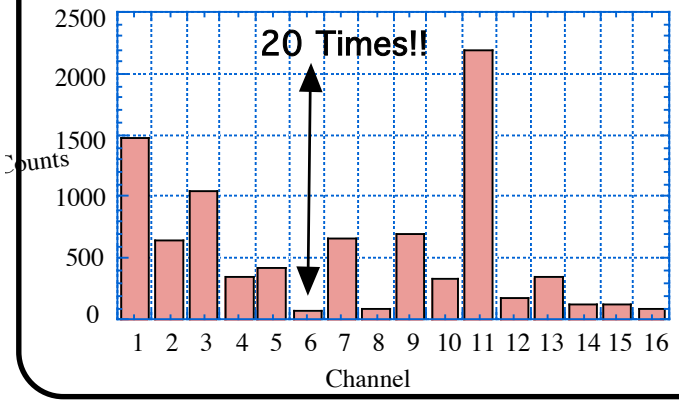

● Result

Every modules are set the same output level. The work takes about 2 weeks.

Timing calibration

- measure timing deviation among every channel and temporal resolution of electronics

● Setup

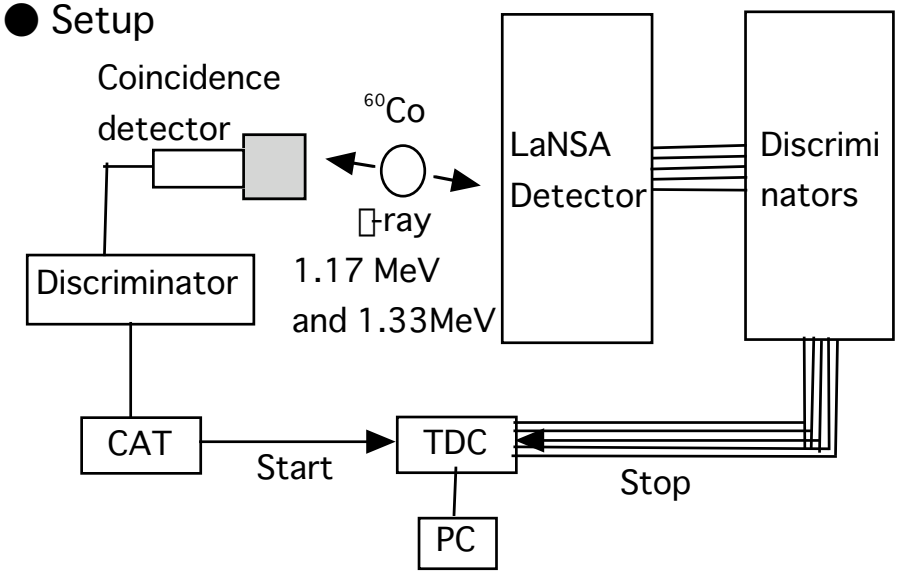

One of two gamma-ray from 60Co is used for start TDC and simultantly emitted other gamma is used for stop TDC. And the stop signals in one channel obey in Gamma distribution and its width indicates temporal resolution.

● Result Resolution < 4ns

Summary & Future Plan

- Large area Neutron Spectrometer Array (LaNSA) is re-constructed at RAL to measure plasma temperature and ion acceleration via neutron spectroscopy.
- LaNSA consists of 3 arrays, one for VULCAN (100TW CPA beam + 6 beam glass beam) experiment and others are for PW experiment.
- LaNSA has about 2-order of magnitude for dynamic range and about 50-100 keV energy resolution for D-D neutron.
- Newly establised operation software is developed
- We will have experiments for Cone-guided implosion experiment at VULCAN on Feb.-Mar./2003 and ion acceleration experiment at PW laser facility on Aug./2003 using LaNSA system

The experimental basis of fast ignition: a tutorial review

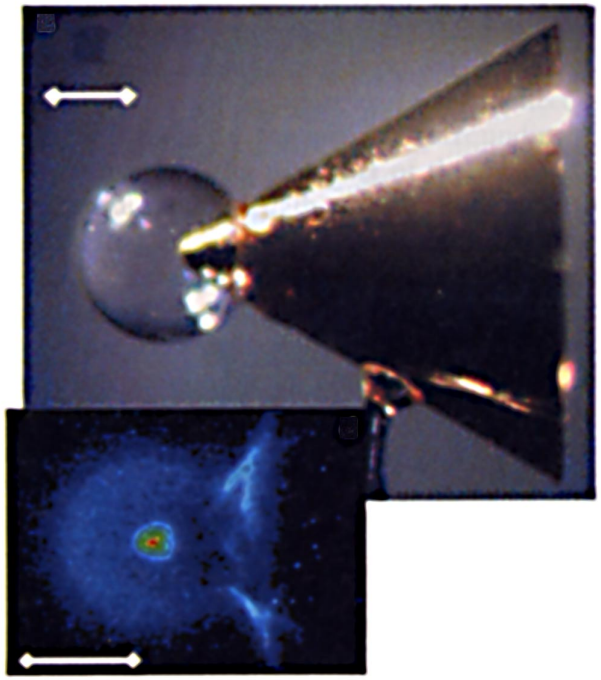

Michael H. Key

6th Workshop on Fast Ignition of Fusion Targets

Florida ,USA, Nov 17-19, 2002

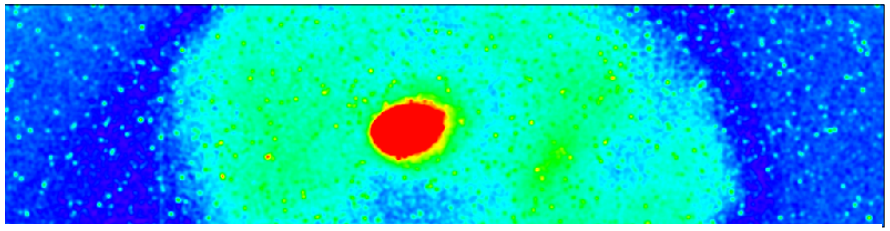

This work was performed under the auspices of the U.S. Department of Energy
by University of California Lawrence Livermore National Laboratory under contract No. W-7405-Eng-48

Experiments are the key to progress towards fast ignition

- Progressive development of CPA laser facilities is enabling more directly relevant experiments
- Innovative measurements are providing better experimental data
- There is a progression from scattered small scale physics experiments to more organized larger scale R&D directed to achieving fast ignition
- A mid term goal is to carry out integrated experiments which give a prediction of what is needed for full scale fast ignition through benchmarking of integrated models
- The major long term goals are ignition , high gain and inertial fusion energy

Fast ignition requires rapid isochoric heating of pre-compressed fuel - achieving that heating rate is the key problem

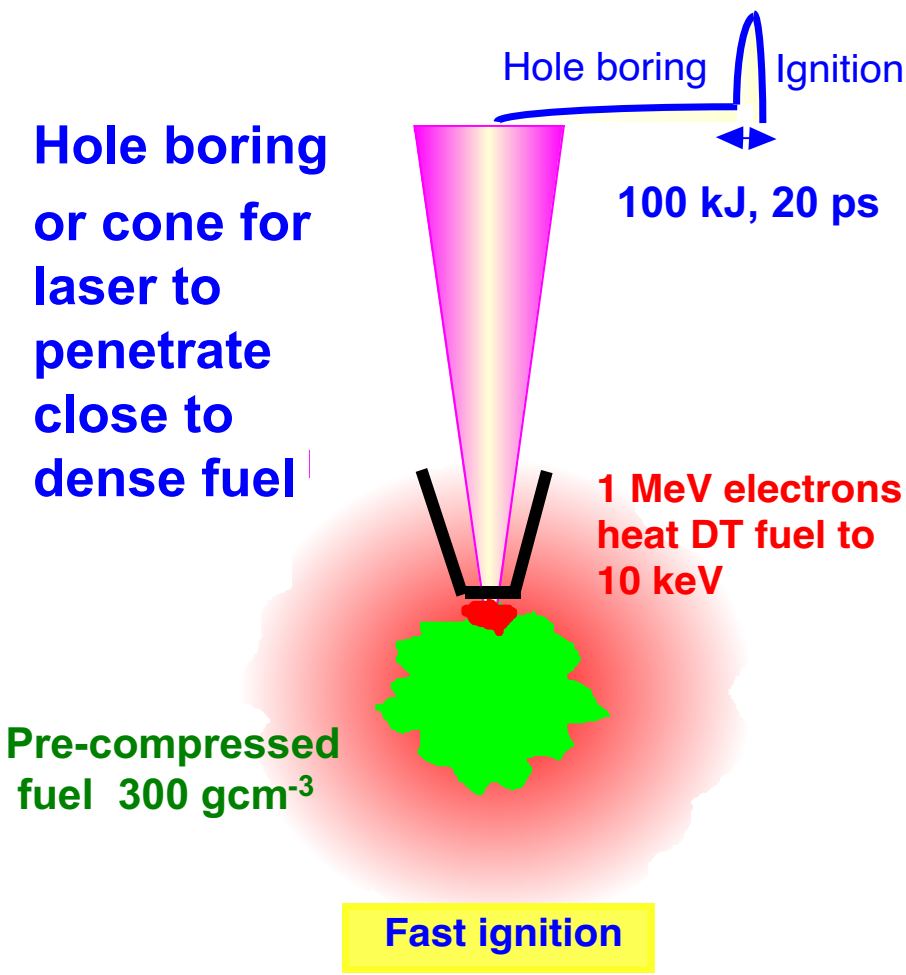

Ignition spot energy

$$E = 140\,(100/\rho)^{1.8}\ \text{kJ}$$

e.g. ρ=300 g cm^{-3}, E=17 kJ

in <20 ps

to r=19 μm hot spot

at 7x10^{19} Wcm^{-2}

Atzeni. Phys. Plas. 6 3316 (1999)

Tabak et al. Phys Plasmas 1,1626,(1994)

Cone target electron ignition is the most advanced approach - key results are from recent expts. at Gekko

•

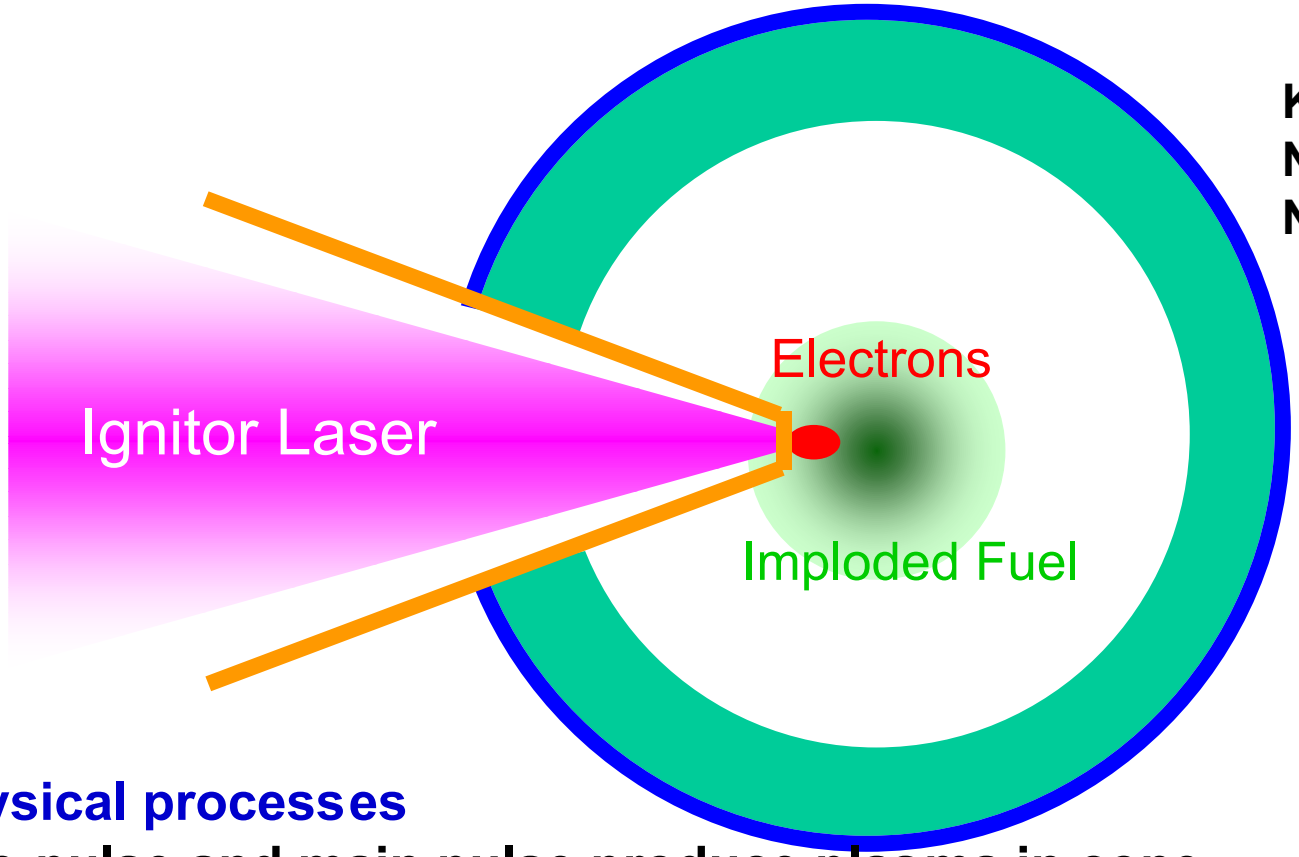

Kodama et al.
Nature 412 798 2001
Nature 418,934,2002

Physical processes

- Pre-pulse and main pulse produce plasma in cone
- Sub critical density and critical density interactions-absorption
- Electron sources at sub critical and critical density including side walls
- Electron transport in cone and beyond - heating beyond cone

We have encouraging but sparse data on interactions in a cone

Direct ‘super penetration ‘ or propagation via laser pre-formed hole uses a simpler target but has more complex interaction physics

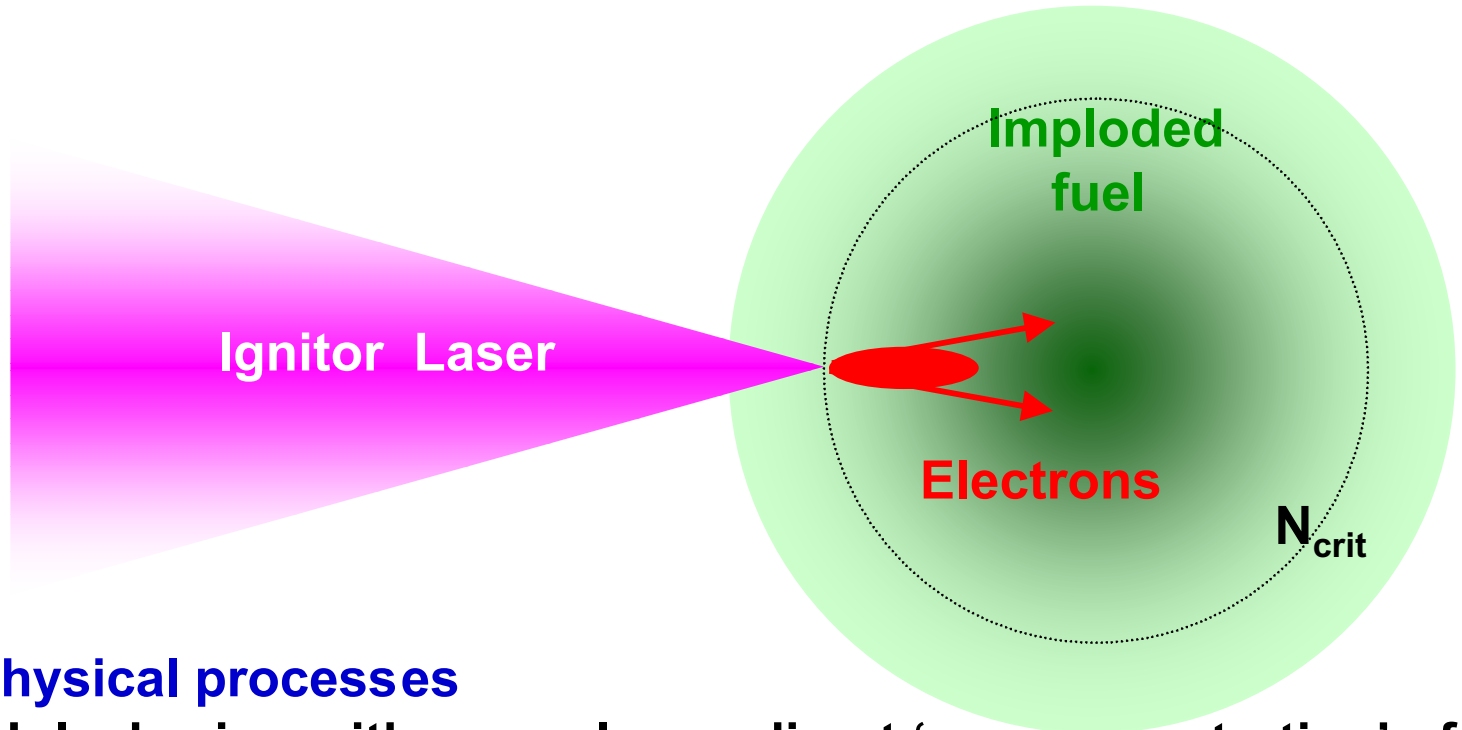

Physical processes

- Hole boring with pre-pulse or direct ‘super penetration’ of main pulse
- Sub critical density propagation and non linear interactions (Stimulated scattering , relativistic self focussing , electron acceleration)
- Electron source at critical density and ion acceleration

We have many small scale studies of the physics of this approach but limited success in first integrated experiments at Gekko

Proton ignition avoids the complexity of electron energy transport but introduces proton beam physics

- Same driver and fuel assembly options

- Novel physics of Debye sheath proton acceleration and focusing

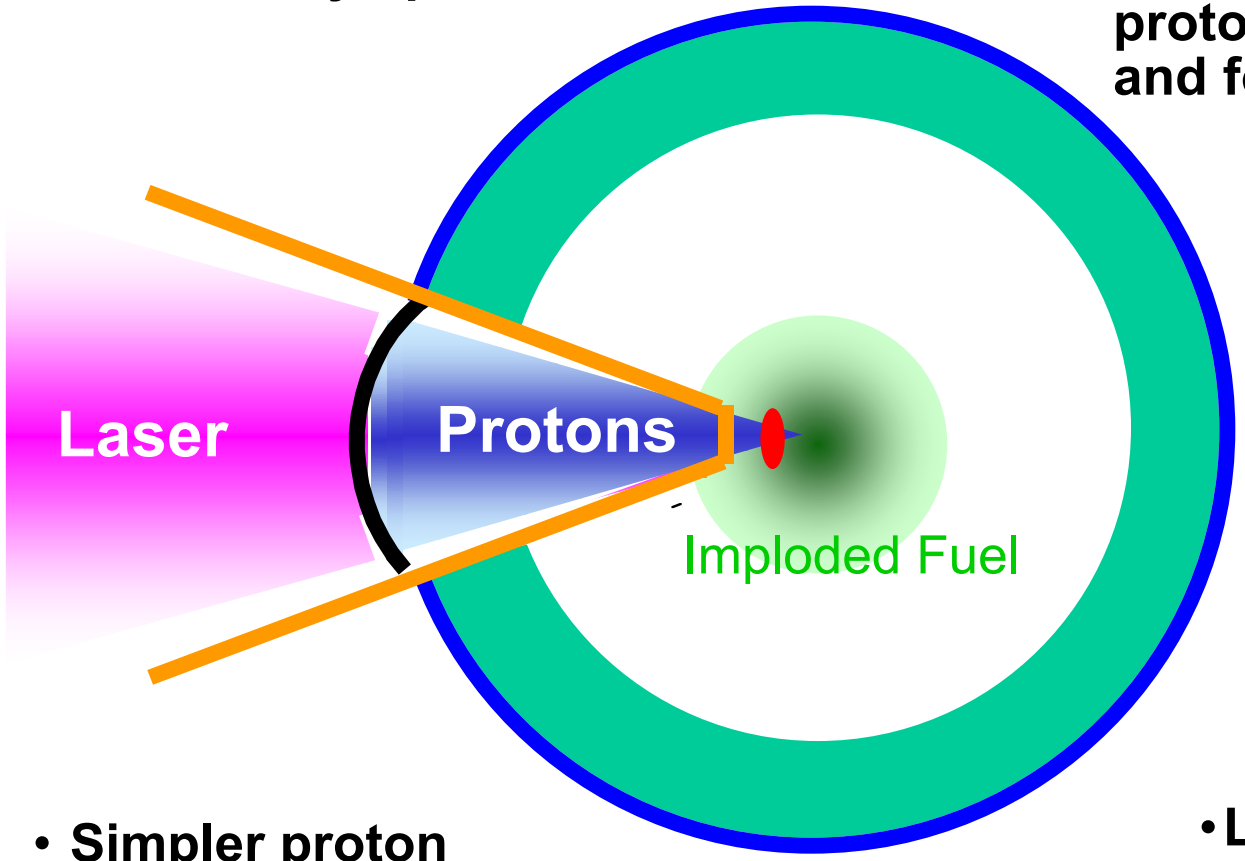

M. Roth *et.al.* Phys Rev. Lett 86,436 (2000).

Ruhl et al. Plas. Phys. Rep. 27,363,(2001)

Temporal, et al. Phys Plasmas 9, 3102, 2002

- Simpler proton energy transport

- Larger laser focal spot-easier to produce

Experimental basis is very sparse but interesting - new concept

Available lasers limit experimental options

- Early work :Table top 1TW ,100fs ,100mJ up to 40 TW ,20J, 0.5 ps
- Present and short term future 100TW to 1PW, <500J lasers with auxiliary long pulse/implosion (Gekko is outstanding)
- Longer term future work HEPW multi-kJ,10-20 ps lasers
- Pre pulse and focal spot characteristics are very variable and influence results
- Fraction of energy in central spot 30 to 40%
- ASE pre-pulse energy fraction 10^{-4}

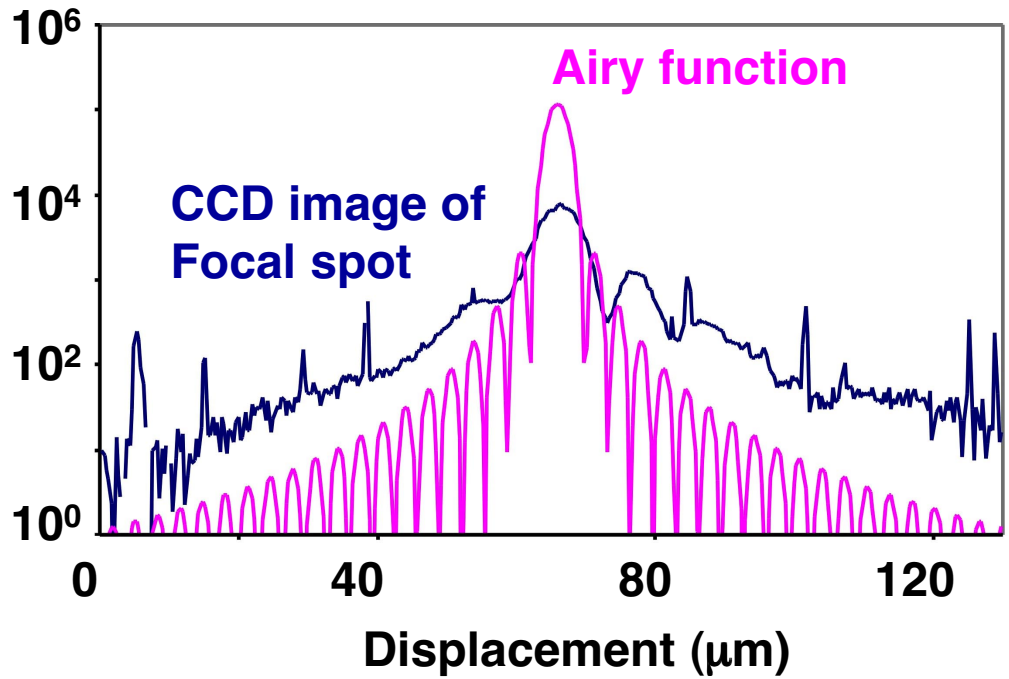

LLNL PW laser focal spot

Sub- critical density interactions and processes

- Ponderomotive self focusing/ hole boring has been studied by optical and x-ray laser probing using gas jet and ablated or exploded solid targets
- Relativistic self focusing observed in laser harmonic and x-ray images
- Thermo-electric magnetic fields observed by Faraday rotation of optical probe
- Stimulated scattering observed in spectra of forward and back scatter
- Sub critical electron acceleration observed as 'hot' component of energy spectrum - connects with extensive electron acceleration research

Most work to date has been small scale and physics oriented

Electron source energy spectrum (kT_{hot}) and beam angle

- **Bremsstrahlung hard x-ray spectra , fast ion energy limit**
  e.g. Beg et al kT_h= 100keV $(I\lambda^2/10^{17}Wcm^{-2}\mu m^2)^{1/3}$
  Phys. Plas. 4, 447, (1997)

- **magnetic electron spectrometer (electrons escaping Coulomb trap)**

- **Angular pattern of MeV Bremsstrahlung**

- **Angular pattern of nuclear activation (=10MeV Bremsstrahlung)**

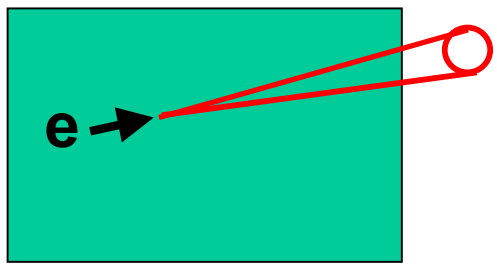

Bremsstrahlung radiation in cone angle 1/γ

Measured characteristics mostly on flat solid targets- not FI targets

Typical data on spectra and beam angle

10-40J, 1ps laser focused on
Al targets at 10^{18}-10^{19} W/cm^2
With p-polarization at 25° inc.angle.

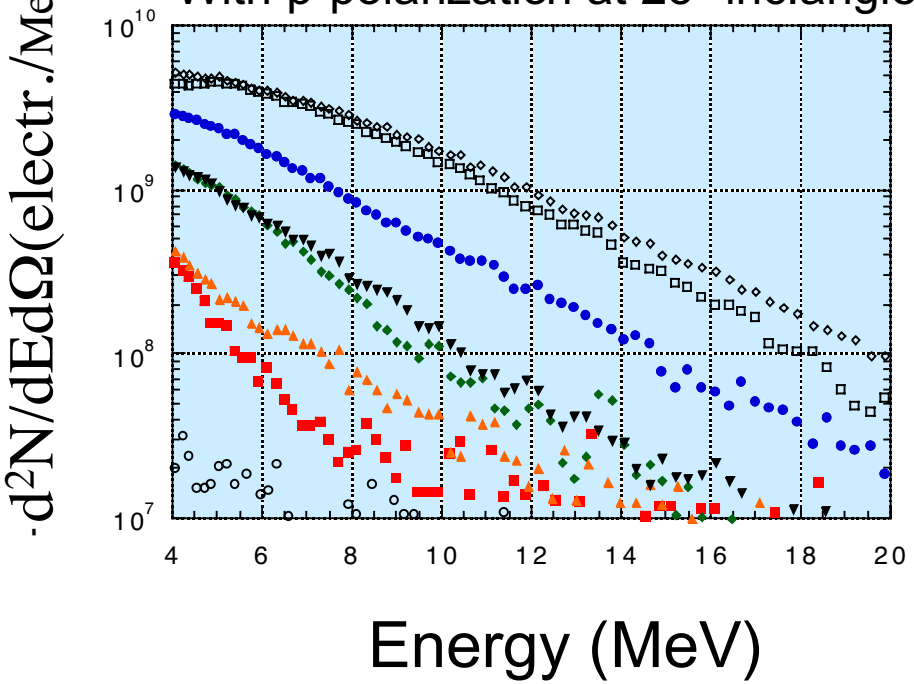

Typical electron spectrometer data (Gekko M2)

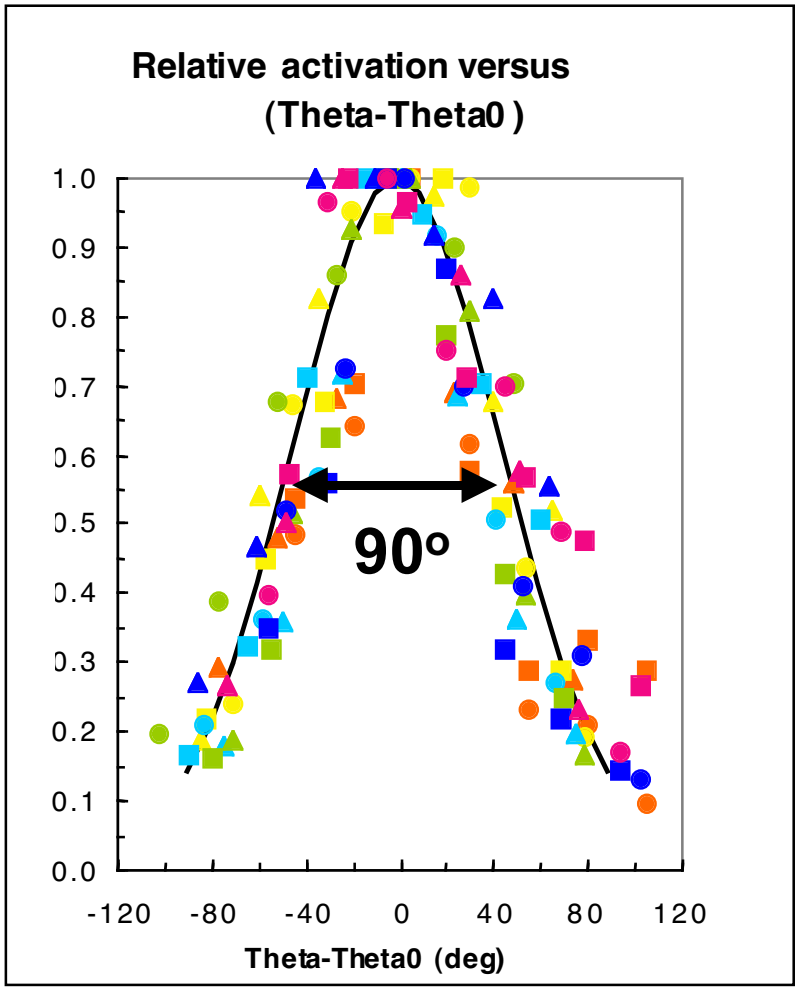

Angular pattern of nuclear activation (LLNL PW)

Conversion efficiency from laser energy to energy in electrons

- **Absorption fraction - measured only in low energy u.s.p. expts.**
- **K alpha yield - most commonly used - net conversion laser to electrons**
- **Bremsstrahlung yield - variant on Kalpha**

Some issues about interpretation due to Ohmic E field should be revisited for conditions closer to 'real' FI

Efficient conversion to electrons injected into solid matter has been measured from Kα emission by several teams

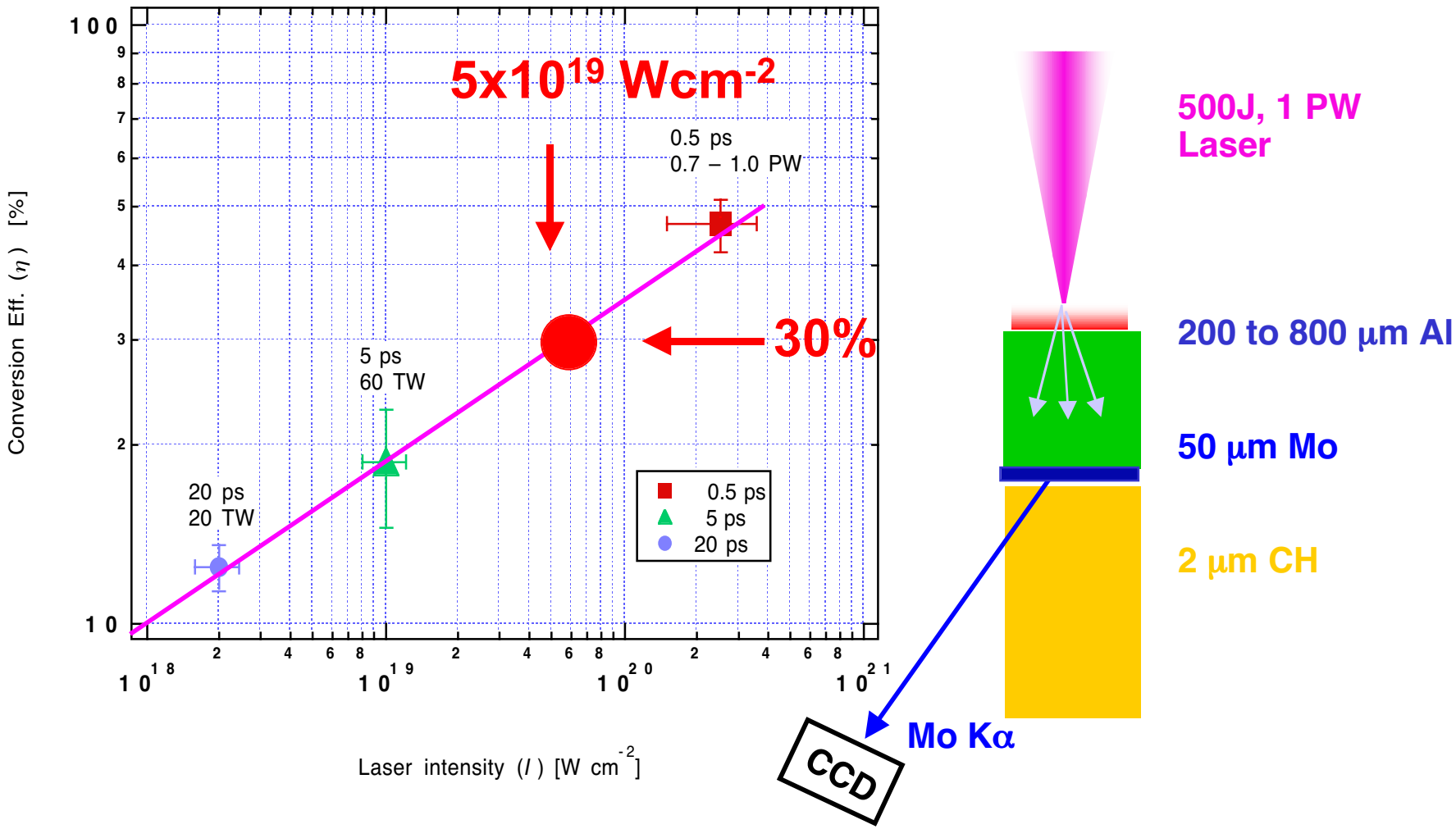

e.g. LLNL PW laser expts. K Yasuike et al. Rev Sci, Inst. 2001

Transport of electrons in solid targets has been studied by a variety of techniques

- Super critical B field observed in side emitted harmonic depolarization
- Planckian emission at rear surface (UV to XUV)
- Absorption of optical probe at rear surface
- OTR and ‘reflection trajectory ’ EM emission at rear surface
- K alpha yield/imaging of buried fluor layers
- Optical probing of electron induced opacity in dielectrics
- Spatial pattern of rear surface proton emission

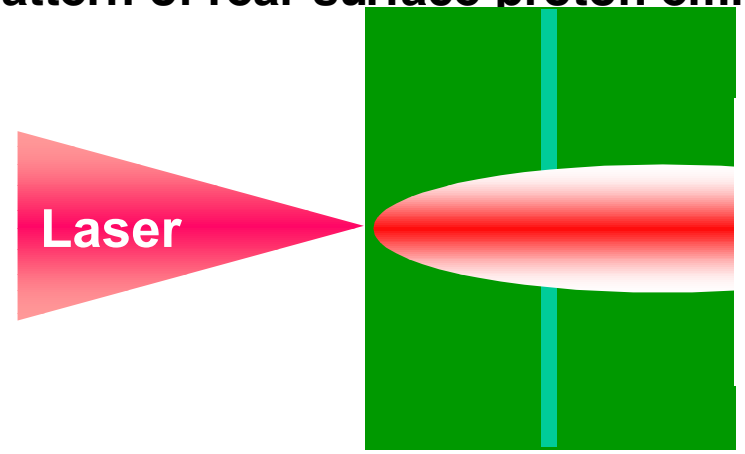

Measurements mostly in cold solids - some dominated by higher energy electrons-may show narrower beam angles
- beam direction may be unstable

Harmonic polarimetry used to measure strong B fields generated by electron beam (> 400 MGauss)

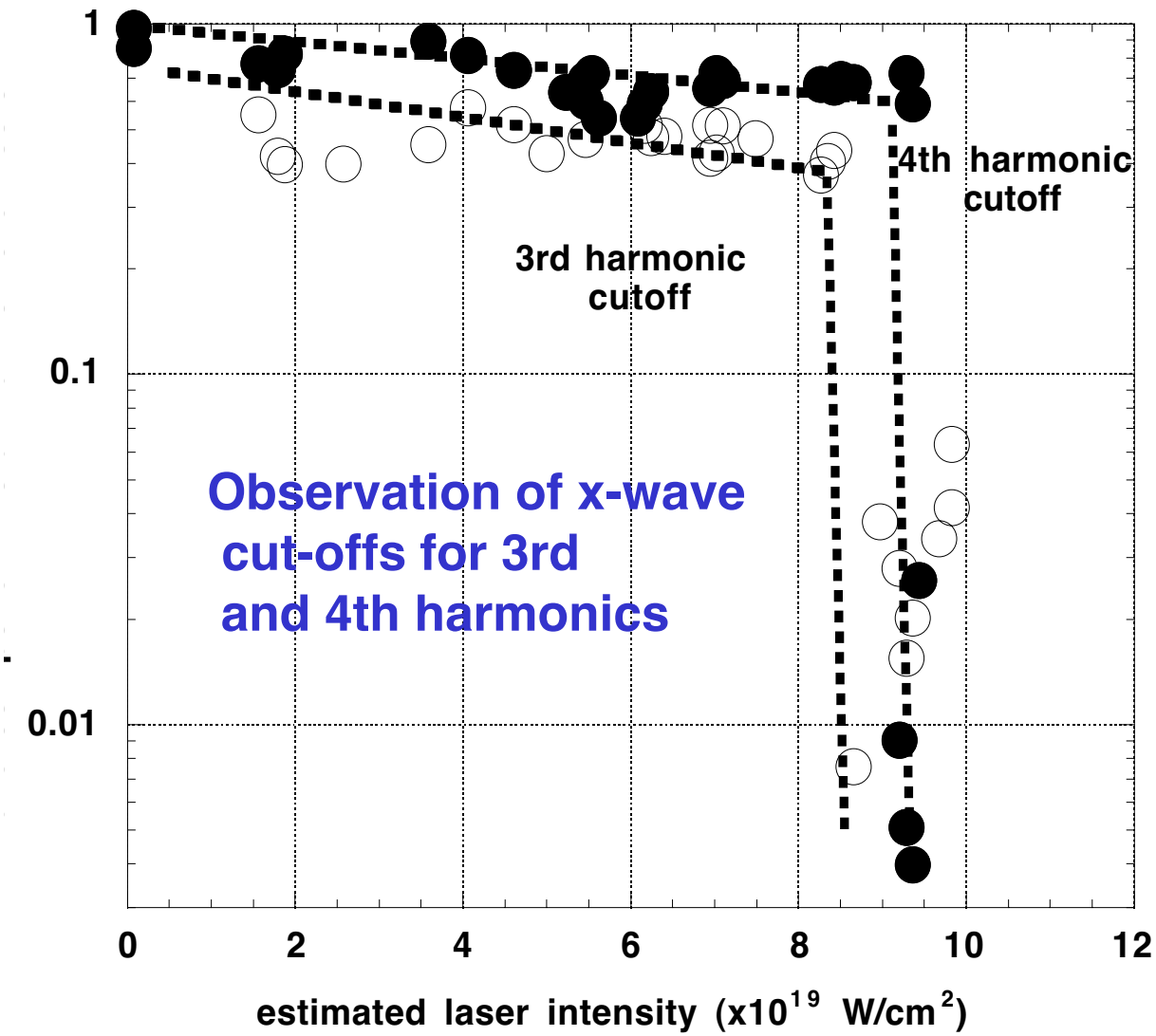

K. Krushelnick *et al.*

Imperial College, London

K_α image data show cone angle and minimum beam radius for electrons in Al

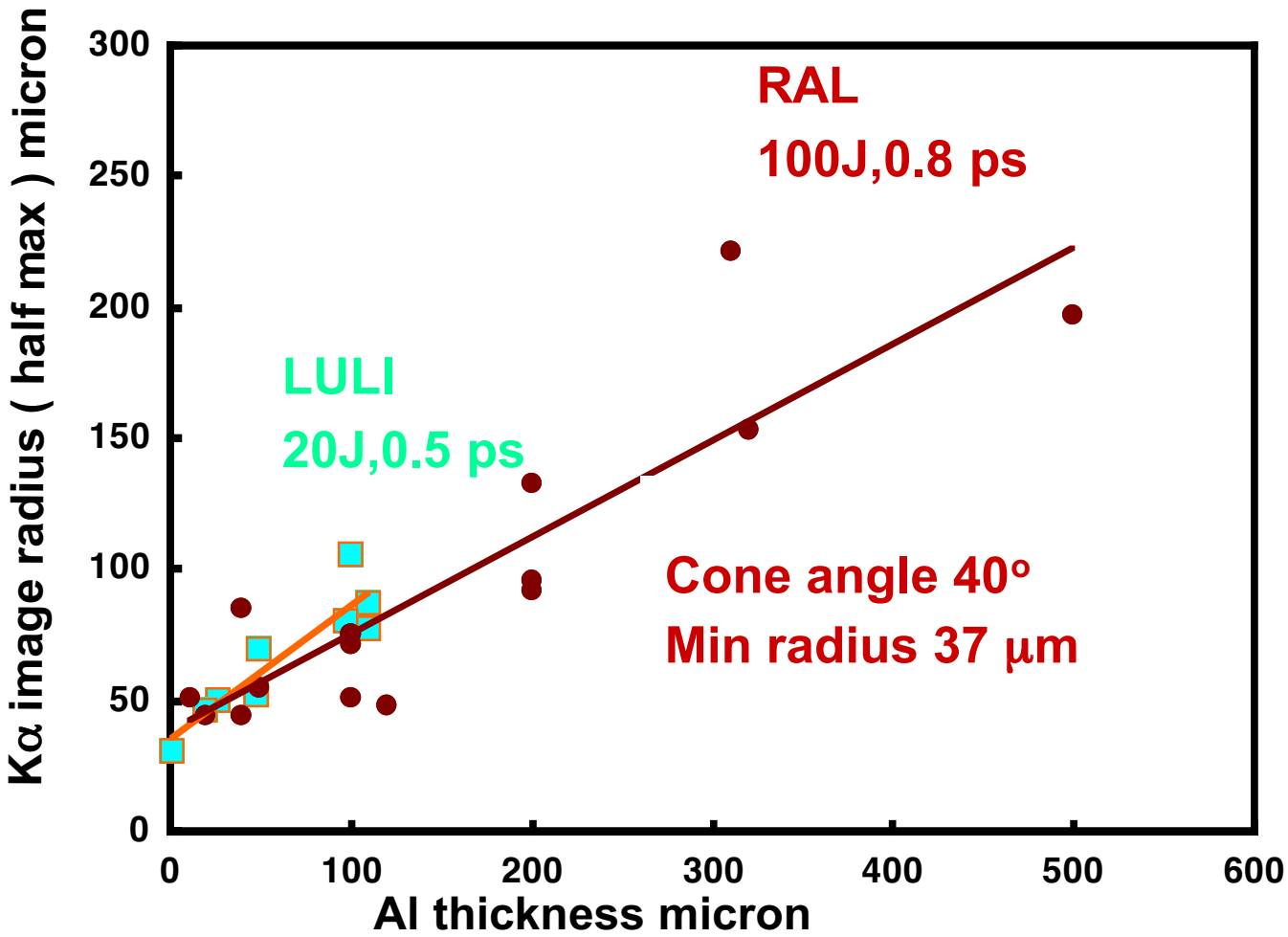

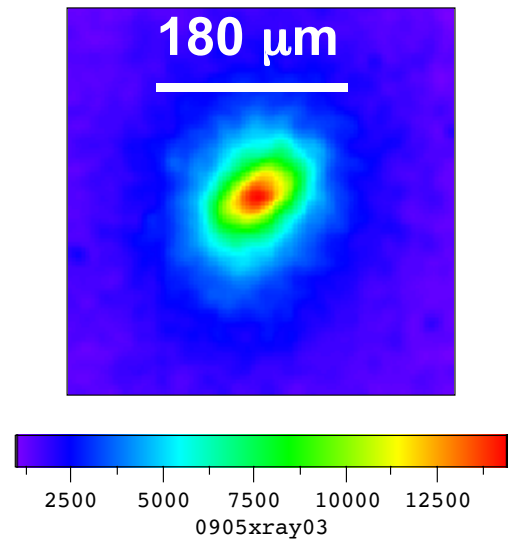

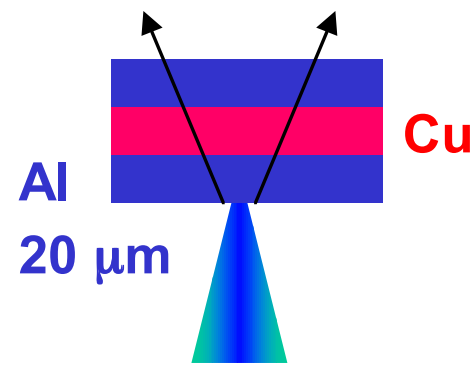

Stephens et al submitted to PRL --R Freeman & R. Snavely talks at this meeting

Rear surface optical Planckian emission characterizes electron heating patterns

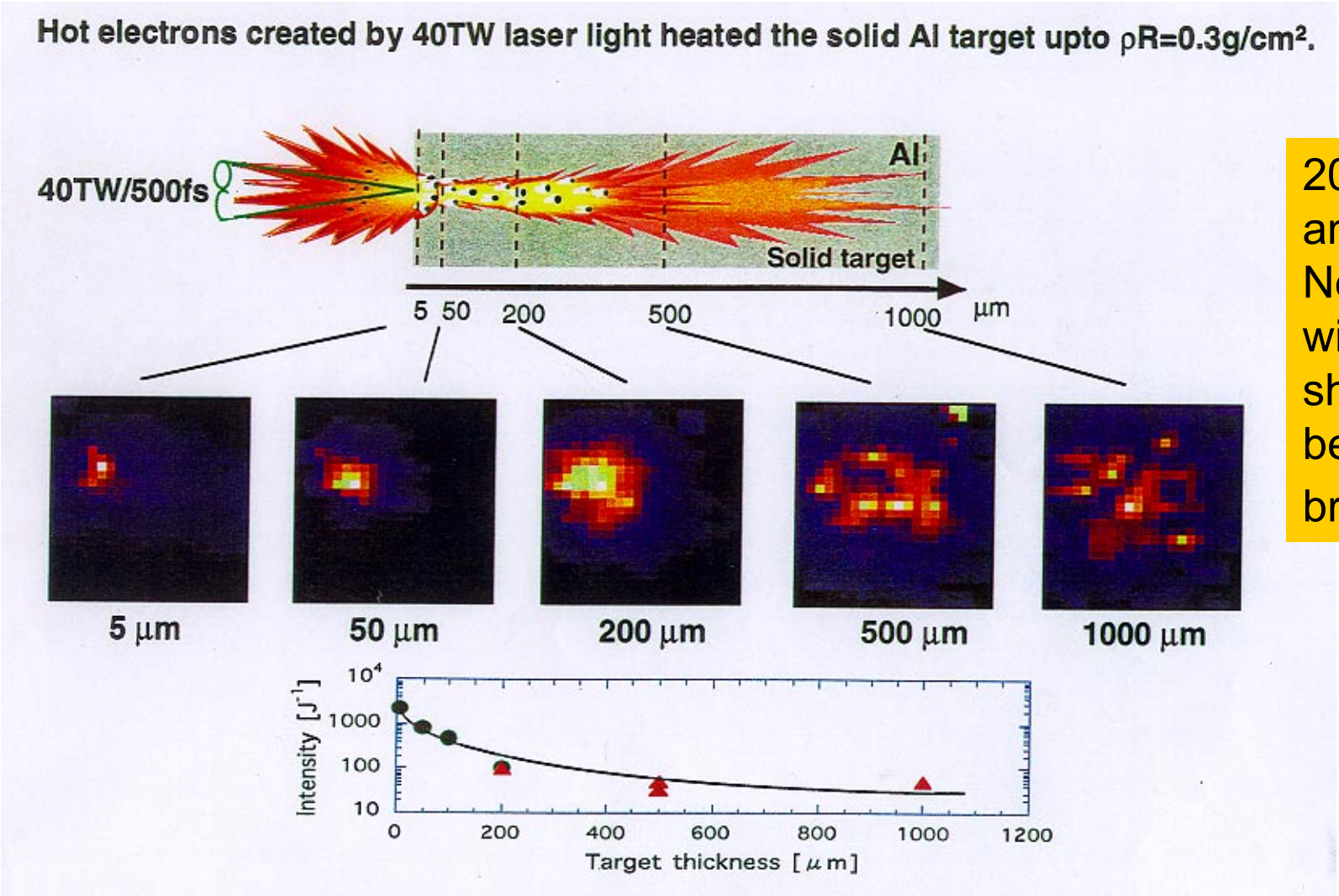

20°cone angle. New results with PW show less beam break up

R Kodama *et.al.* 4th International Workshop on Fast Ignition

Exit surface optical transition radiation was a surprising and useful discovery at LULI

Integrated diagnostics

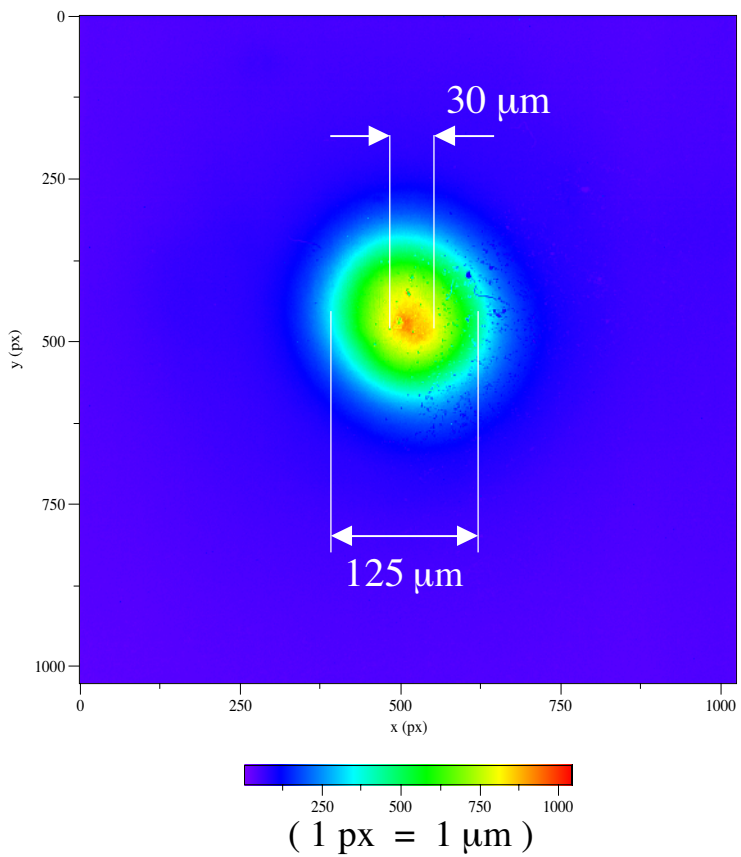

Time-resolved diagnostics

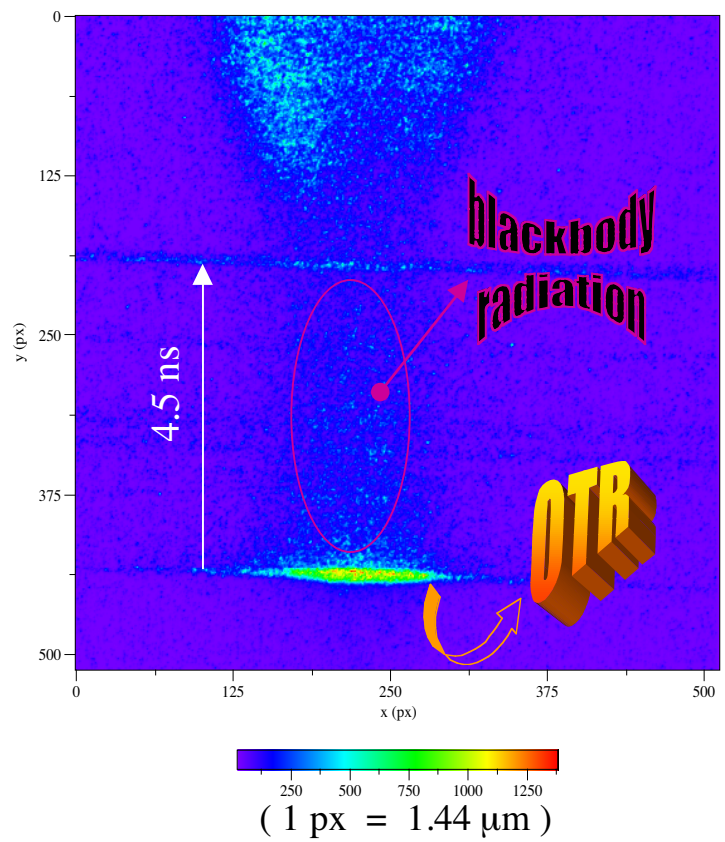

J Santos et al Phys Rev Lett 89, 025001-1(2002) and S Baton et al. - this meeting

Electron isochoric heating has been measured by several methods

- DD Neutron yield and energy spectrum kT >400eV
- H-like and He-like and continuum X-ray spectrum and x-ray images kT>200eV
- Planckian rear surface emission (XUV and X-ray) kT= 1 to 100eV
  Good spatial resolution
- Frequency shifted Kalpha kT =10 to300eV

D-D neutron yield and energy spectrum is a volume integrated heating diagnostic sensitive to region of highest temperature in CD and D_2 targets

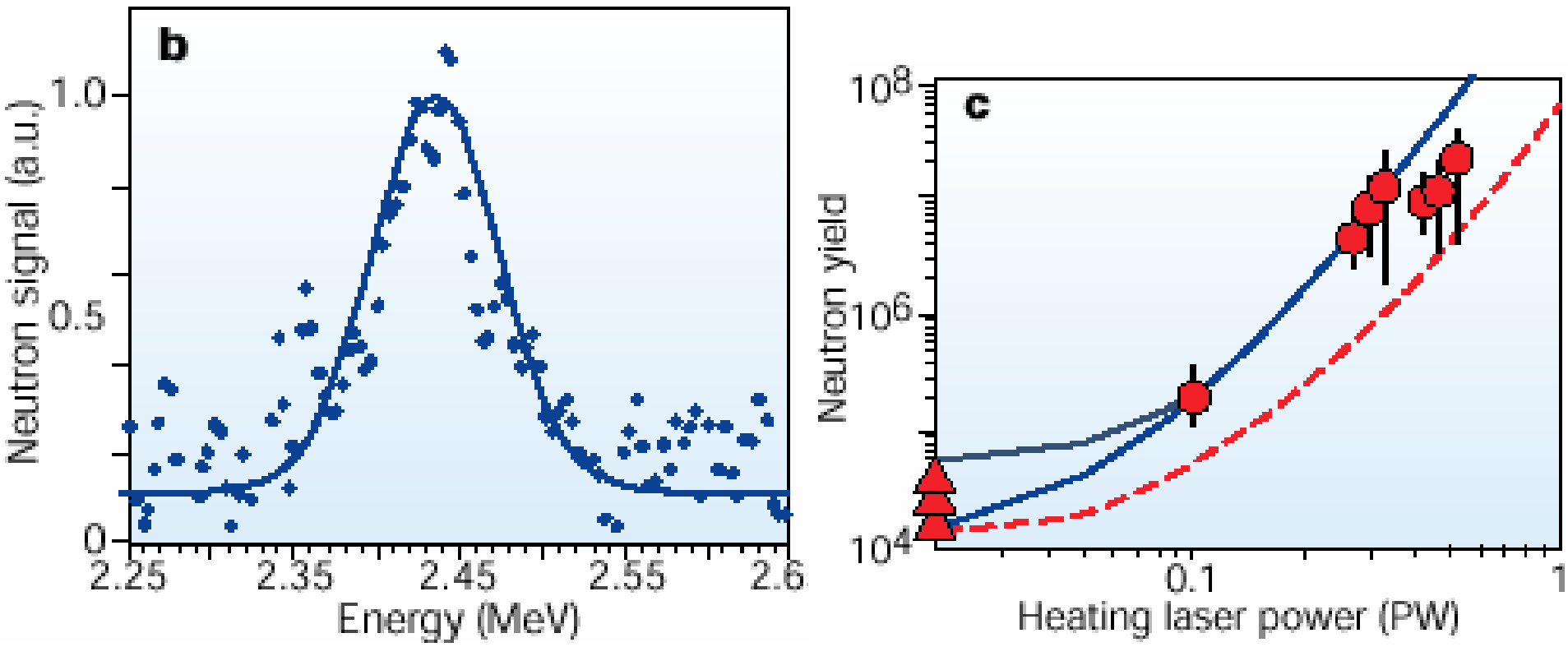

R Kodama et al Nature 418,934,2002

300eV isochoric heating by electrons is effectively measured by x-ray spectroscopy and x-ray imaging

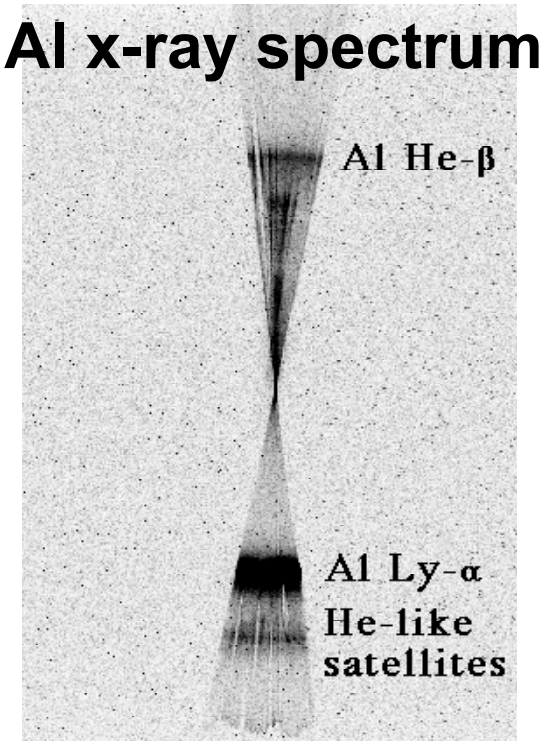

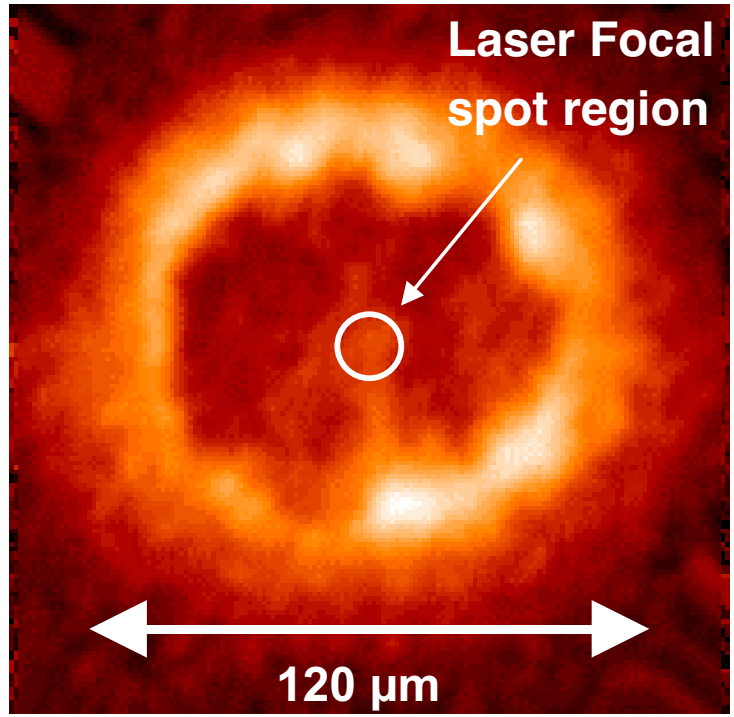

LLNL PW
J Koch et al .
Phys Rev. E
65,016410
(2002)

- 400J in 5 ps heats to 300eV
- Heated diameter >> focal spot
  -columnar over 100 μm depth

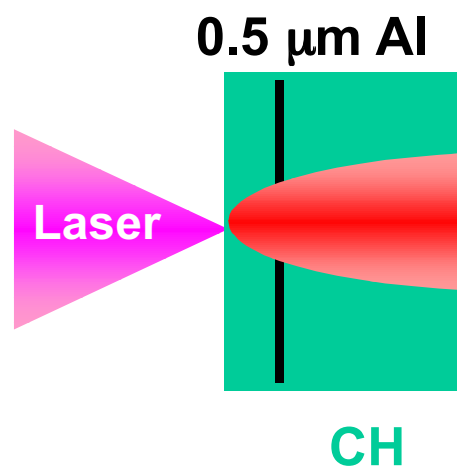

Planckian XUV emission shows 100 μm Al targets heated isochorically to 30 eV in a 120 μm hot spot at rear surface

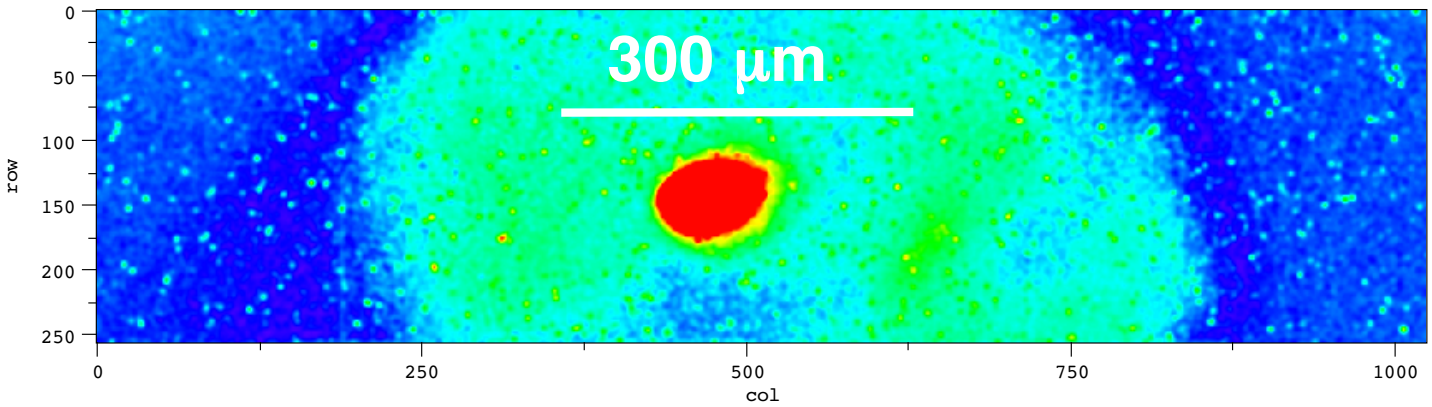

RAL 100J,1 ps expt.

Key et al Proc IFSA (2001)

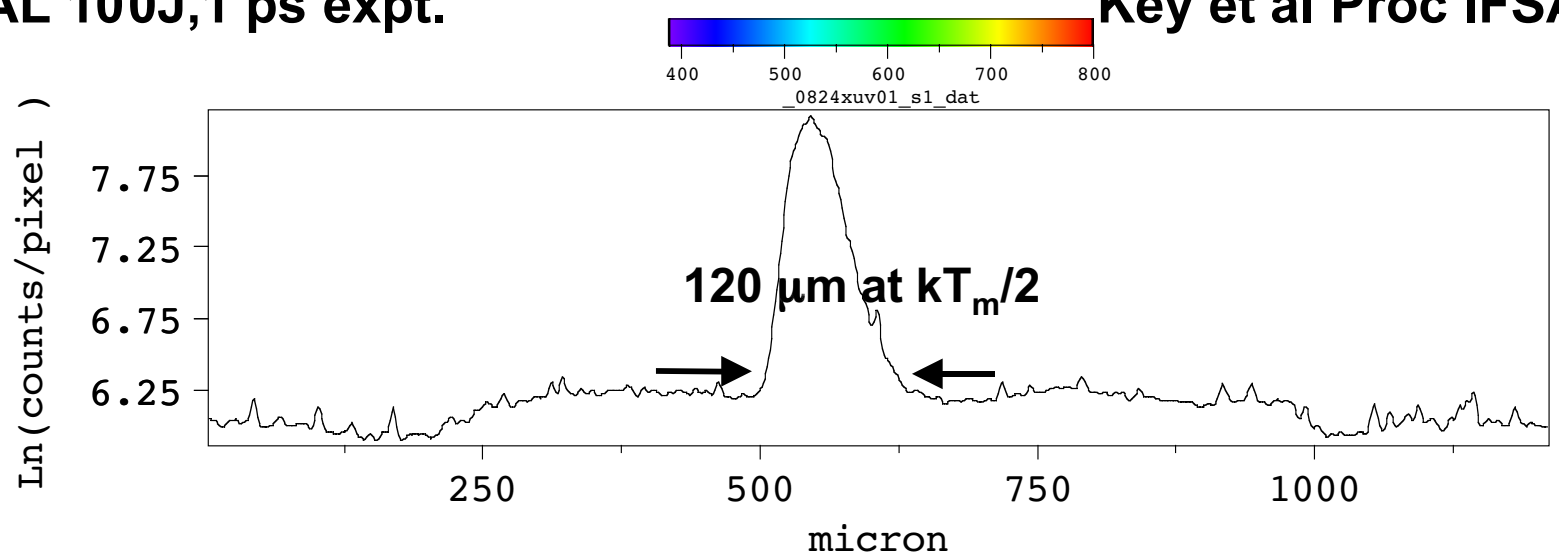

Results consistent with Kα data - heated region >> focal spot

Several observations suggest minimum electron beam size several times larger than optical focal spot

- We do not properly understand this
- It may be associated with the low intensity wings of the focal spot
- It may be irrelevant in cone geometry
- Radial ExB drift of magnetized electrons was studied extensively two decades ago - this may be happening in the surface plasma produced in the wings of the focal spot

Forslund and Brackbill
PRL,48,1614,(1982)

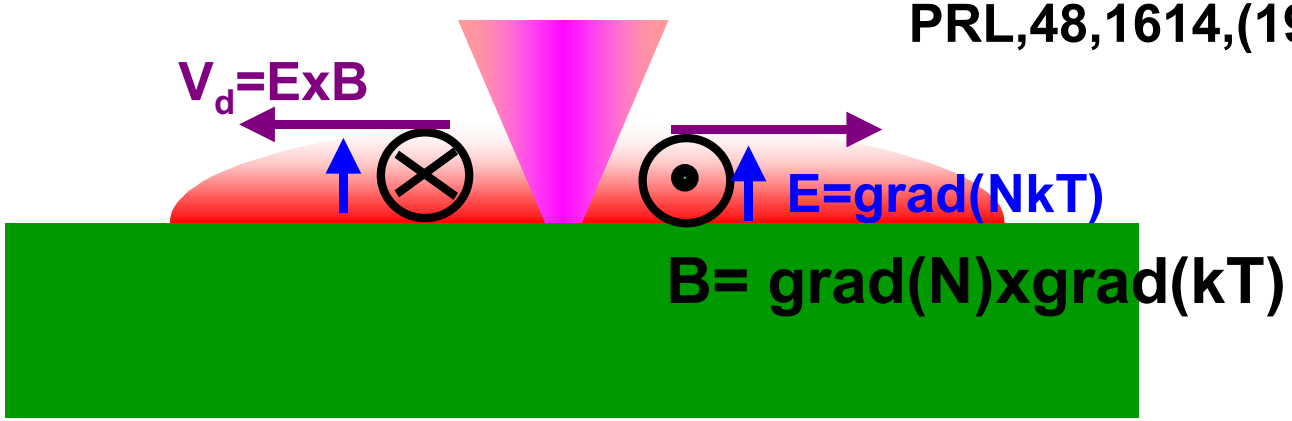

Resistivity dominates our current experiments but it should be negligible in the fast ignition DT fuel

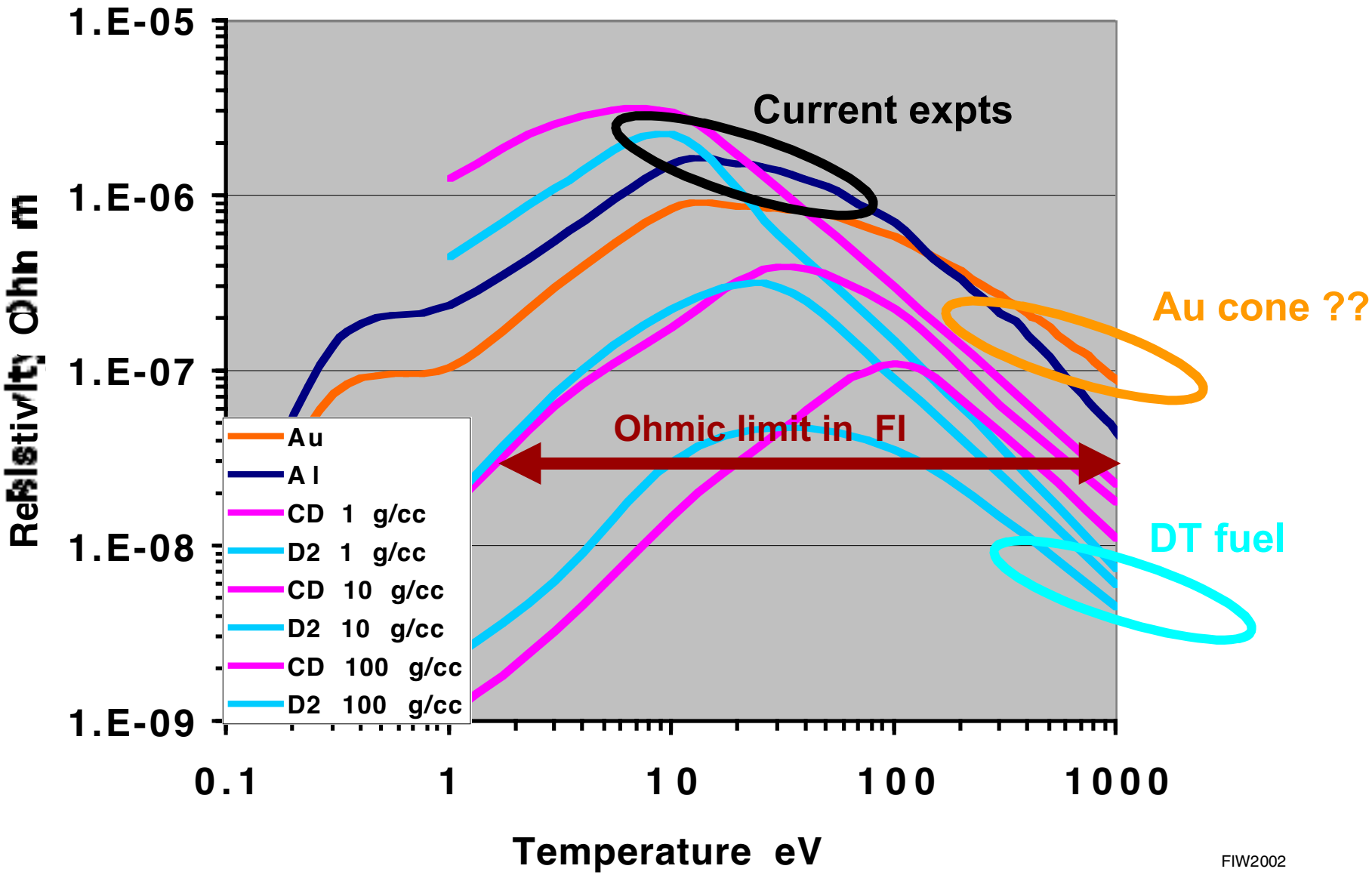

Laser generated proton beams- pattern , energy spectrum and conversion efficiency

- Radio chromic film dosimetry and tracks in CR39
- Magnetic spectrometer
- (p,n) nuclear activation
- Ions driven into target by light pressure: D-D beam target fusion - neutron energy spectra
- Spatial origin from imprinted rear surface perturbations
- Front /rear mechanisms

Collimated proton beams from the rear surface of thin targets were first observed in LLNL PW expts

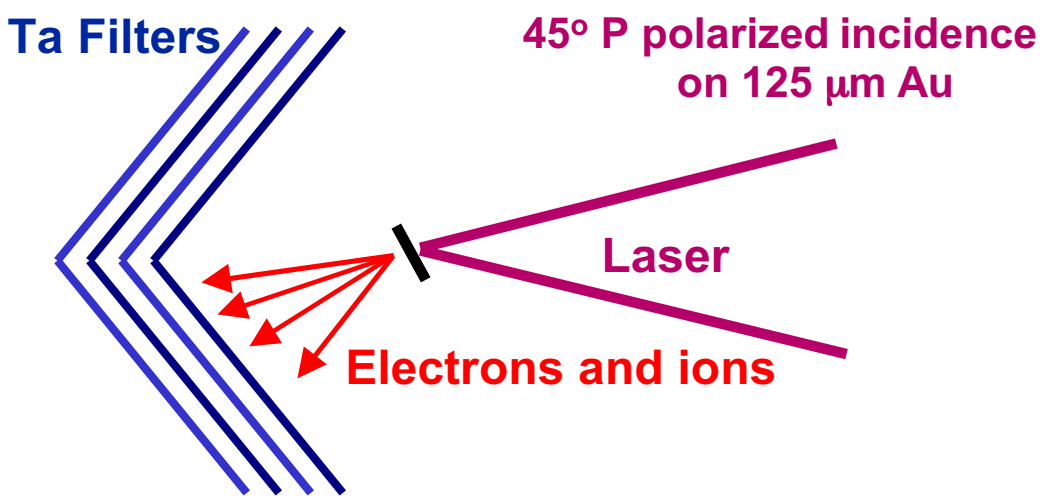

Up to 48J (12%) >10MeV and 58 MeV max

R Snavely et al. Phys. Rev. Lett. 85,2945 (2000)

First data from Oct 1998

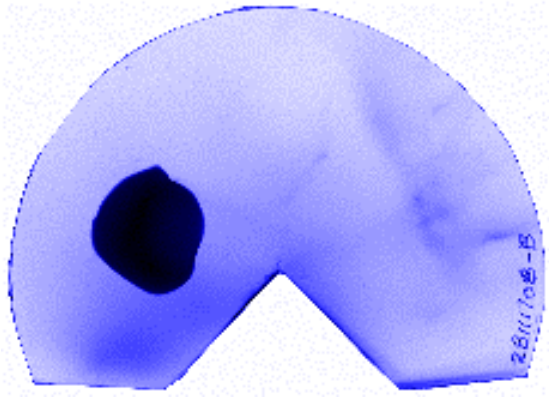

Image via 200μm Ta

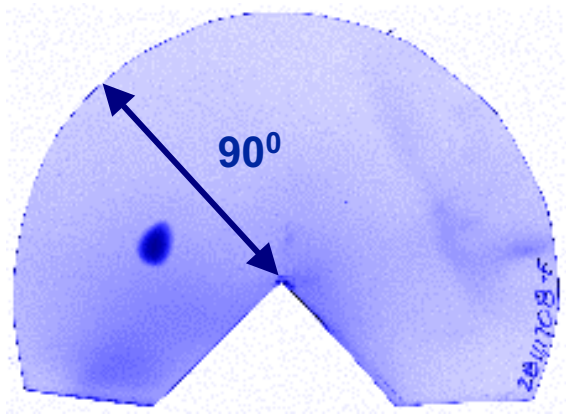

Image via 600μm Ta

Grooved targets have been used to measure the area on the rear surface emitting protons

Method due to Cowan et al .

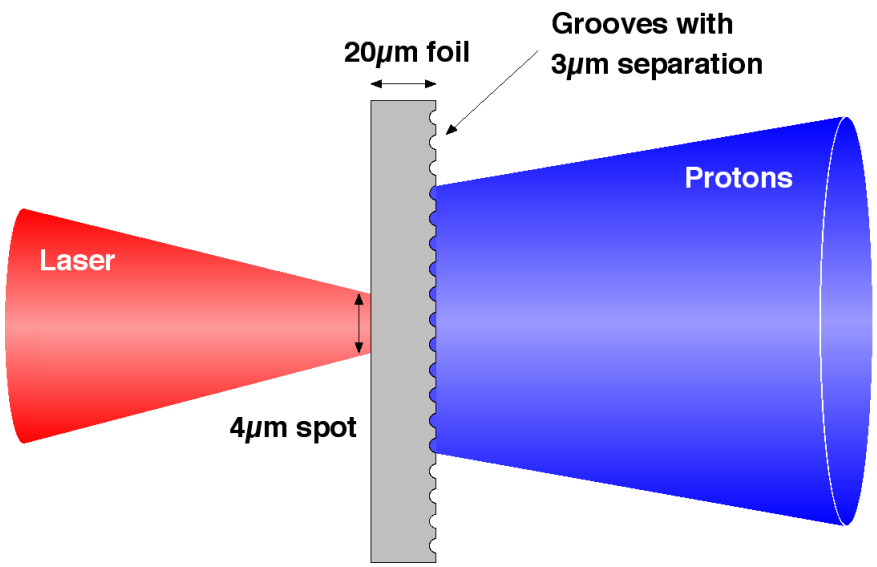

Proton image at 13.0MeV

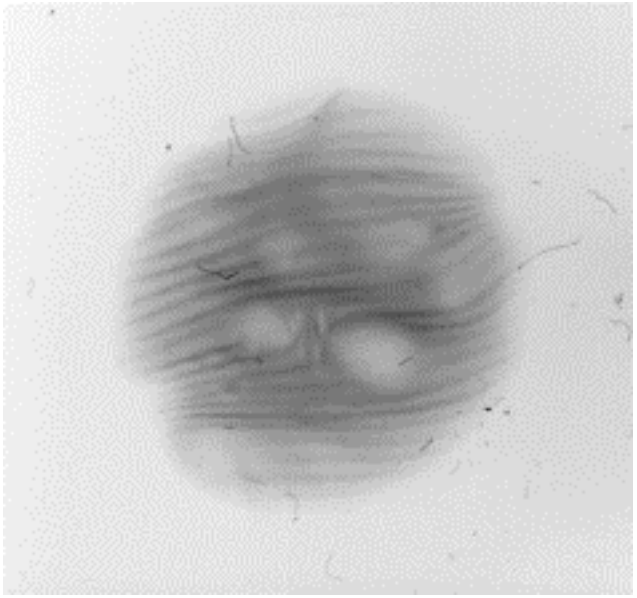

22 lines ⇒ 66μm surface area

Data from 100TW,100fs Janusp laser (P Patel et al - this meeting)

Proton beam quality /focussing/isochoric heating

- Edge penumbra
- Proton radiography
- Projection of grids
- Moire patterns
- Hemisphere focusing with Planckian emission from isochoric heating

Low emittance proton beam enables μm, ps probing measurement of E and B fields

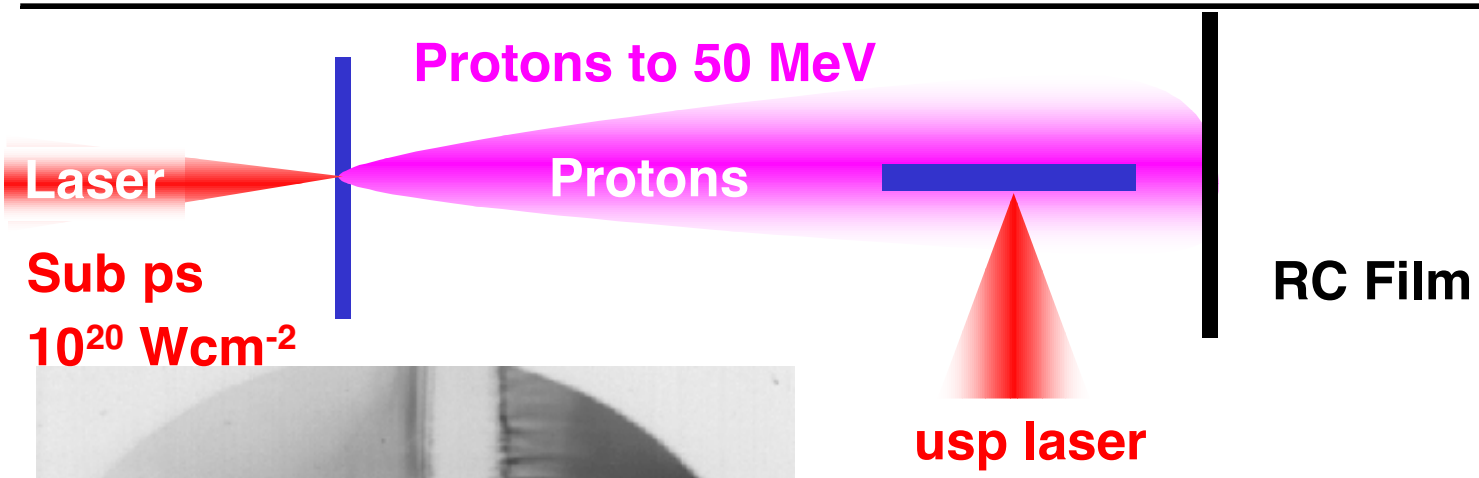

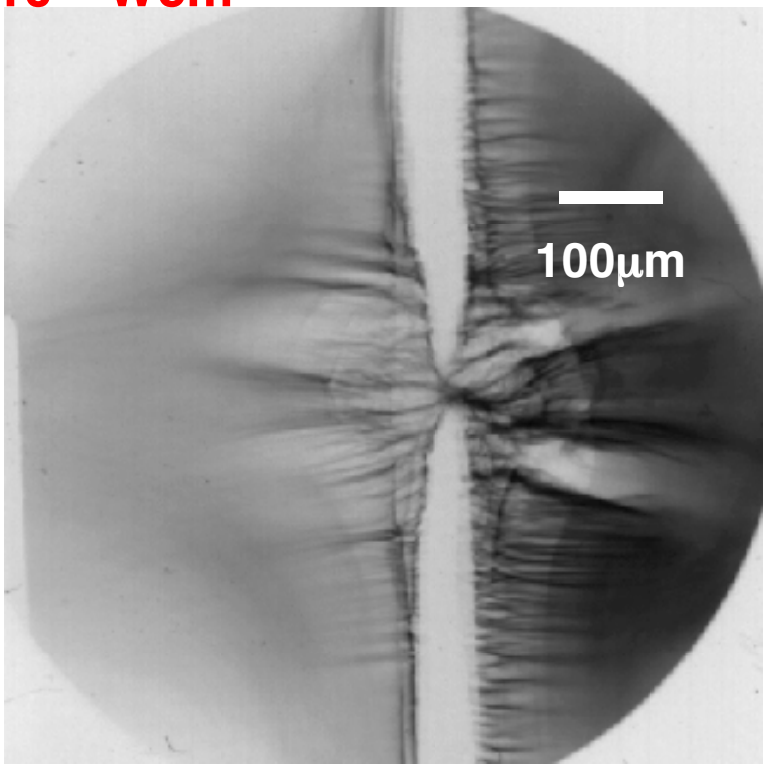

A Mackinnon - this meeting

Recent 100TW,100fs expt. shows evidence of ballistic proton focusing (to 50 μm) and enhanced isochoric heating

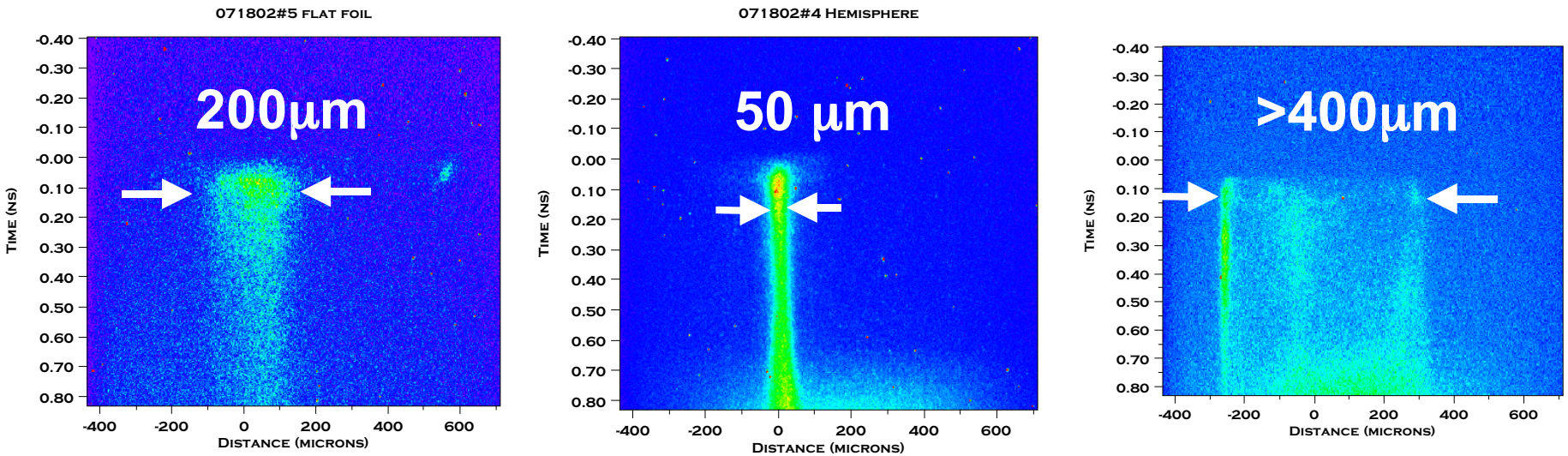

Streak images of Planckian emission

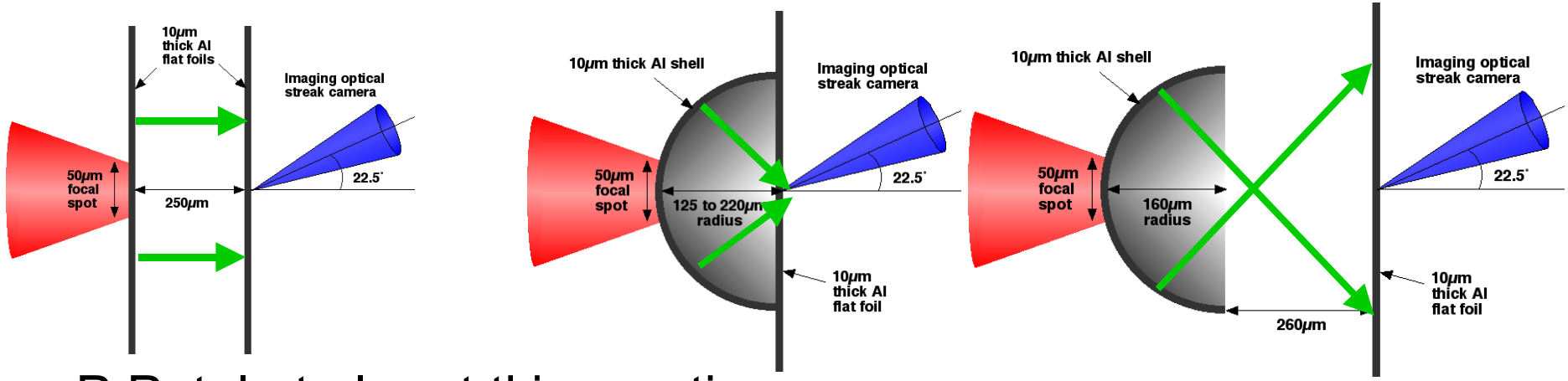

P Patel et al. - at this meeting

Fuel assembly

- Full range of ICF /facilities/diagnostics support this area BUT little has been done relative to conventional ICF
- Novel hydro -issues in cone targets
- Major challenges in fabrication of cryo -DT targets with cone insert
- Tolerance of laser wavelength / drive uniformity /target surface roughness all to be determined

Hydrodynamic issues for the cone target scheme

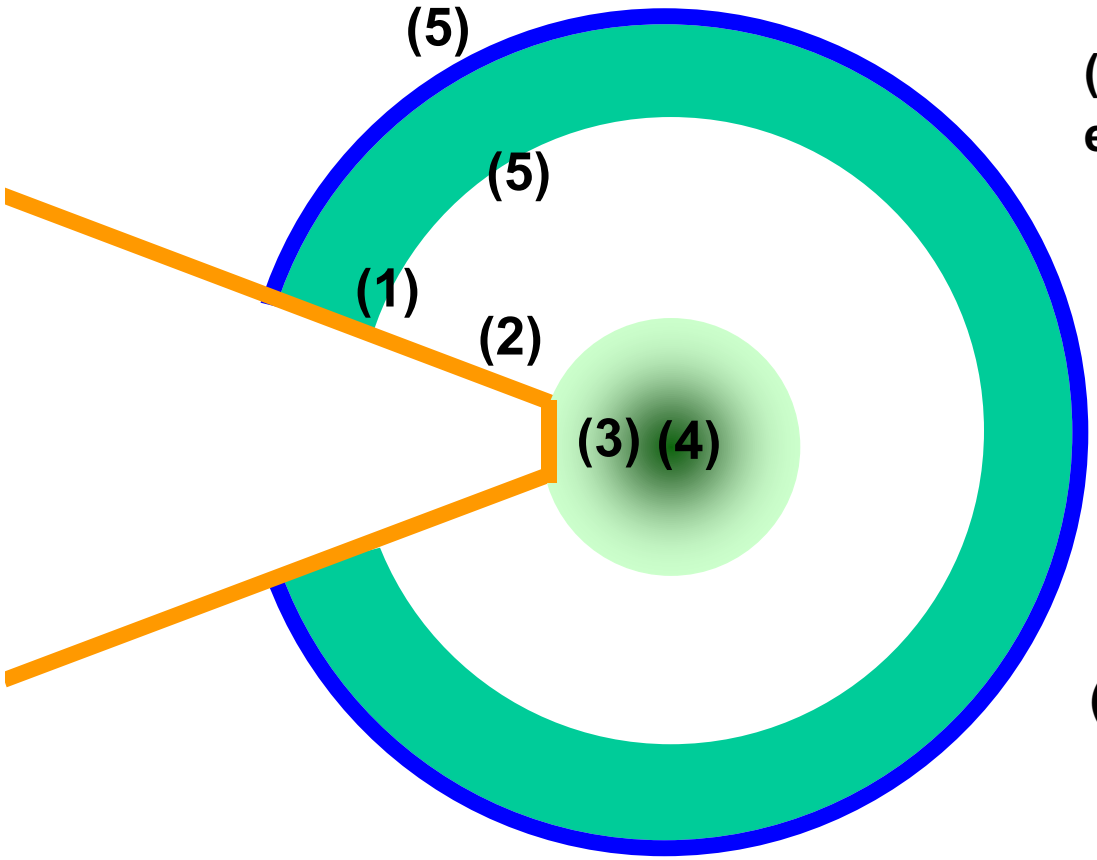

(1) Shell /cone interface hydro entrainment of cone material

(2) Preheat of cone ahead of imploding shell

(3) Cone tip-dense core transport distance

(4) Avoidance of 'hollow centre' in compressed core

(5) Drive symmetry and surface smoothness requirements

Hydro-dynamically equivalent CH shell targets are being studied at Omega by x- radiography

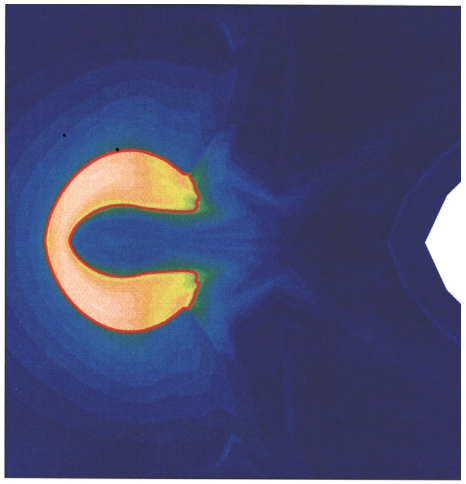

Lasnex model of Imploded density

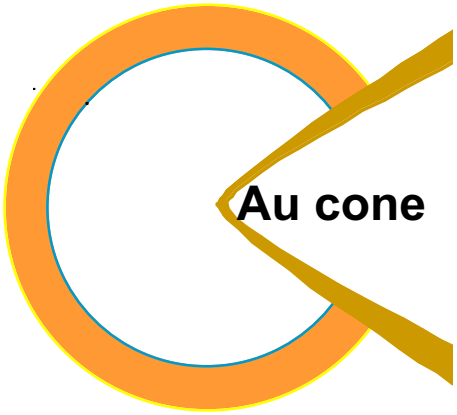

400 μm

Cone target at Omega

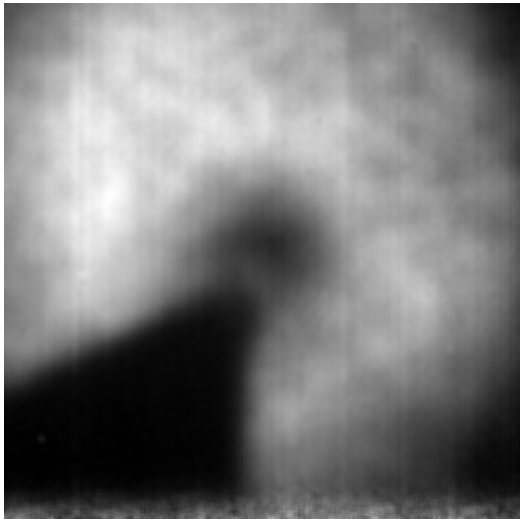

Radiograph

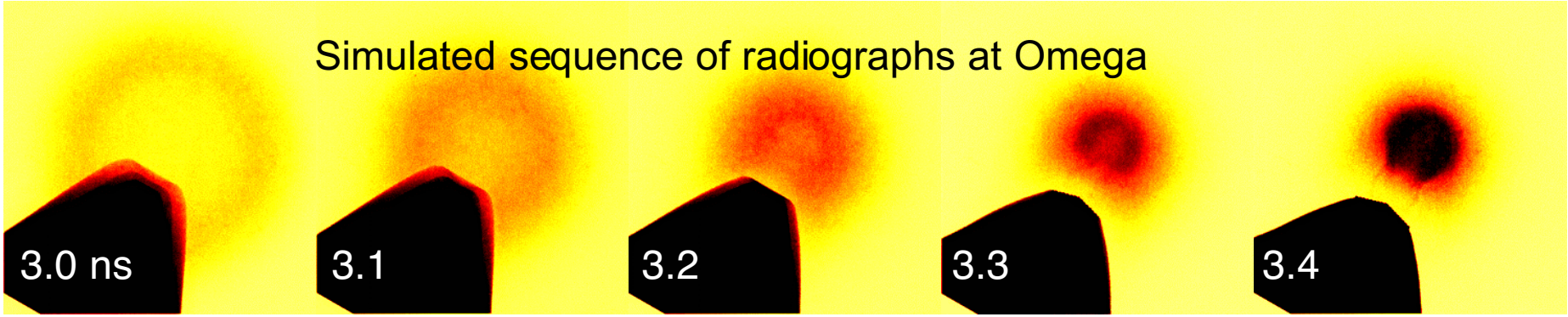

R Stephens et al. at this meeting

Z- pinch indirect drive is also being tested for FI fuel assembly at the Z facility

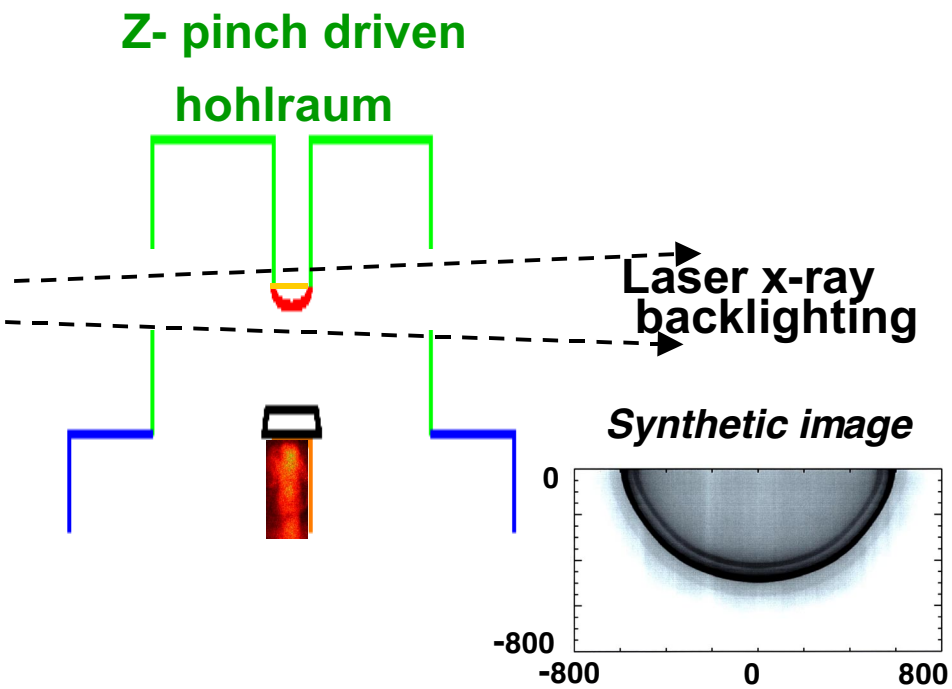

Radiograph of hemisphere implosion

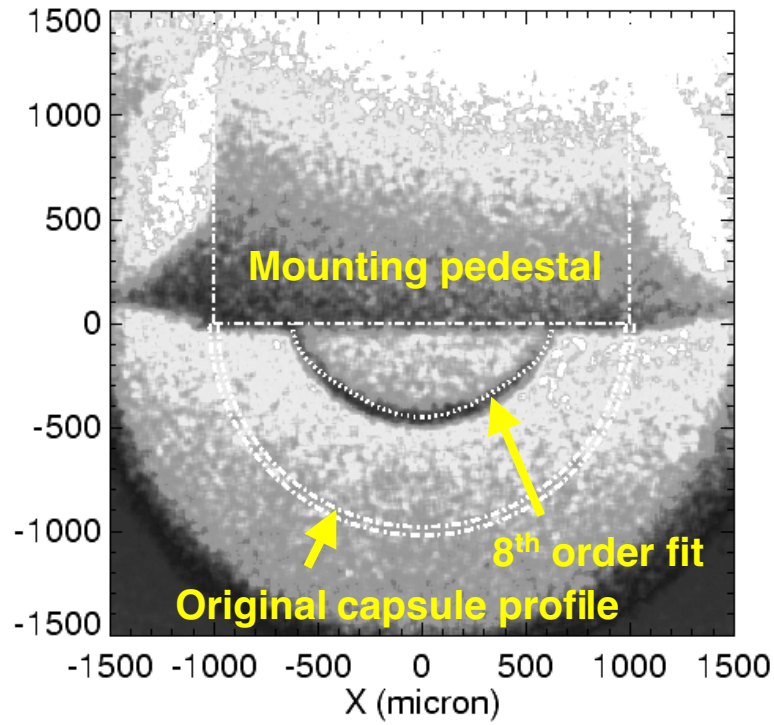

D Hanson et al. at this meeting

Trend to integrated long pulse /short pulse experiments was begun in Japan with 100 TW CPA beam focussed on implosion at 12 beam Gekko laser

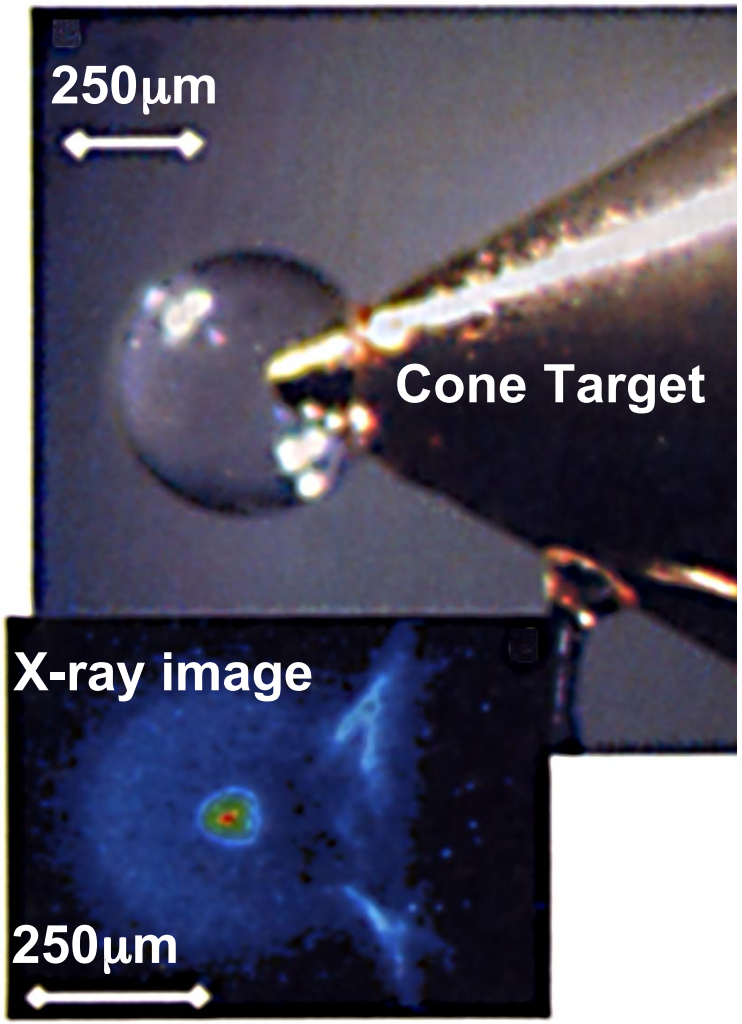

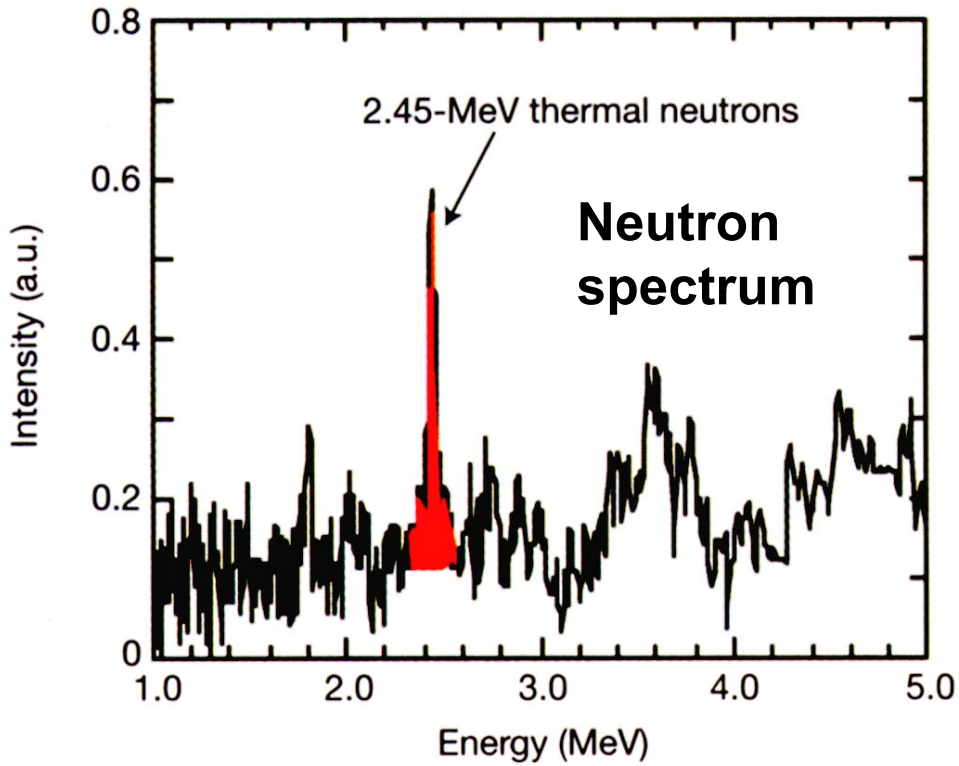

R Kodama et al .
Nature,412,798 (2001)

20% coupling efficiency MAJOR encouragement for FI

We can anticipate a next generation of higher energy PW experiments

- Firex project at ILE Osaka - 4 beam 10kJ, 10 ps
- US PW laser initiative (5kJ,20 ps beams at NIF , 2 beam HEPW 4kJ at Omega , 1 beam HEPW 2kJ at Z
- PW at LULI and HEPW at LIL in France
- PW at GSI Germany
- Long pulse coupled to PW at RAL

and new HEPW facility at AWE (UK)

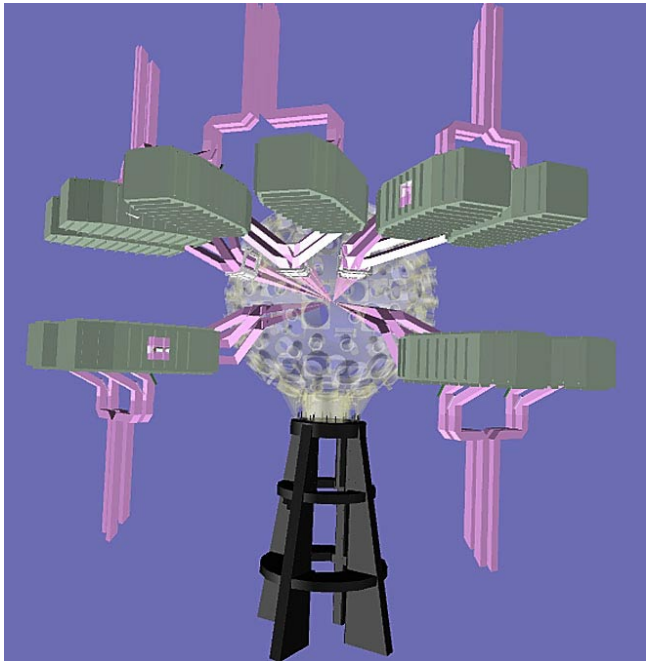

Important to have new expts which benchmark models enabling prediction of behaviors at full scale - also to have new expts closer to 'real' FI conditions

Status and issues for electron ignition

- Conversion to electrons measured and modeled - OK- but few data for cone or direct irradiation of implosion -none with FI relevant longer pulse and higher energy

- Transport partially understood - no fully consistent expts and models and no expts in 'non resistive' FI regime

- Gekko cone target HIGHLY successful in >20% gross heating efficiency. Physics not fully understood . Cone-less target OK ?

- Optimum electron energy depends on uncertain role of instability enhanced stopping in fuel

- Required ignition power fixes intensity at focal spot - electron energy may then be too high

Important to have new expts which benchmark models enabling prediction of behaviors at full scale - also to have new expts closer to 'real' FI conditions

Status and issues for proton ignition

- Conversion efficiency and emittance OK (but measured at <1 ps)
- Ballistic focusing and heating simple in principle - first expt only -but encouraging
- Large area of converter foil relaxes laser focusing and allows very long focal length - advantage
- Acceleration process requires cold rear surface - radiative preheat problem from compression ?
- Effects of longer pulses (20 ps cf. 1 ps) needs study
- 'Simple' energy transport not yet analyzed or studied in detail

Many issues remain unresolved pending further work but scheme is interesting because of potential transport simplification

Status and issues for FI fuel assembly

- First systematic fuel assembly experiments at Gekko, Omega and Z
- First results are on cone target scheme and show good results with some questions about entrained cone material - spherical implosions not studied
- Issues of cryo- targets and tolerance to drive and fabrication non- uniformity not yet addressed in experiments
- Optimum laser wavelength and alternative drivers beginning to be considered but little work done yet

No firm conclusion yet on best scheme

Overall Conclusions

- **FI experiments have advanced rapidly**

- **There is a transition in progress to more focussed larger scale activity**
  (Firex in Japan , HEPW initiative in US ,PW lasers in Europe at RAL, AWE, LULI, LIL and GSI)

- **No show stoppers have been found and FI is of increasing significance in IFE**

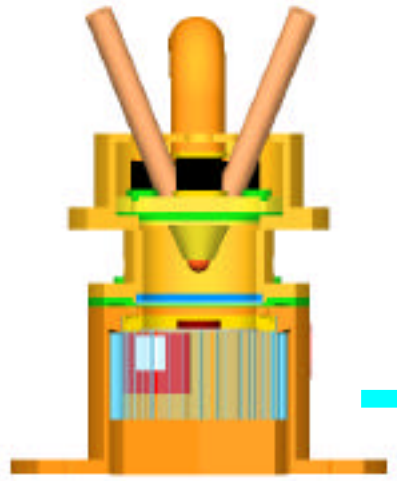

6th Workshop on Fast Ignition of Fusion Targets

St. Petersburg, Florida
November 16-19, 2002

Hemispherical Capsule Implosions in a Z-Pinch-Driven Fast Ignitor Fuel Compression Geometry

D. L. Hanson, R. A. Vesey, S. A. Slutz, M. E. Cuneo, J. L. Porter

Sandia National Laboratories*Albuquerque, NM 87185-1193

G. R. Bennett

K-tech Corp. Albuquerque, NM

***Sandia is a multiprogram laboratory operated by Sandia Corporation, a Lockheed Martin Company, for the United States Department of Energy under Contract AC04-94AL85000.**

We are exploring a hemispherical capsule FI compression geometry for single-sided z-pinch radiation drive

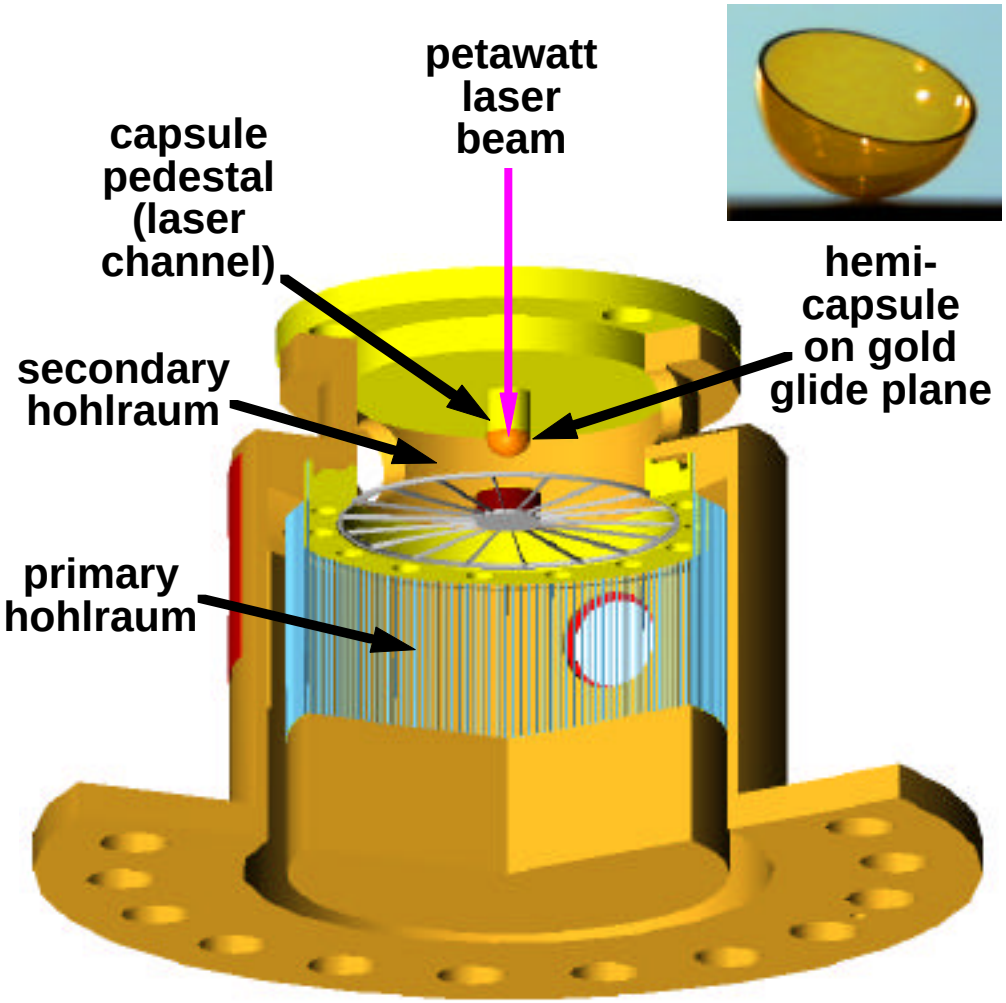

Hemispherical capsule fast ignitor compression geometry:

- **Hemispherical capsule mounted against flat high-Z glide plane on pedestal providing plasma-free short-pulse laser path**
- **Special case of 60° reentrant cone capsule geometry**

Advantages:

- **Hemispherical capsules can be imploded to high density with excellent equator-to-pole symmetry in single-sided drive configuration**
- **Hemispherical capsule geometry provides excellent access to both sides of glide plane for study of capsule-glide plane interactions during implosion**

Sandia National Laboratories

Hemispherical capsule implosion experiments performed on Sandia Z accelerator (20 MA, 120 TW pinch power, 90-100 eV seconday temperatures) using ZBL point projection backlighter

A capsule implosion image with high Bremsstrahlung background was recorded after peak compression

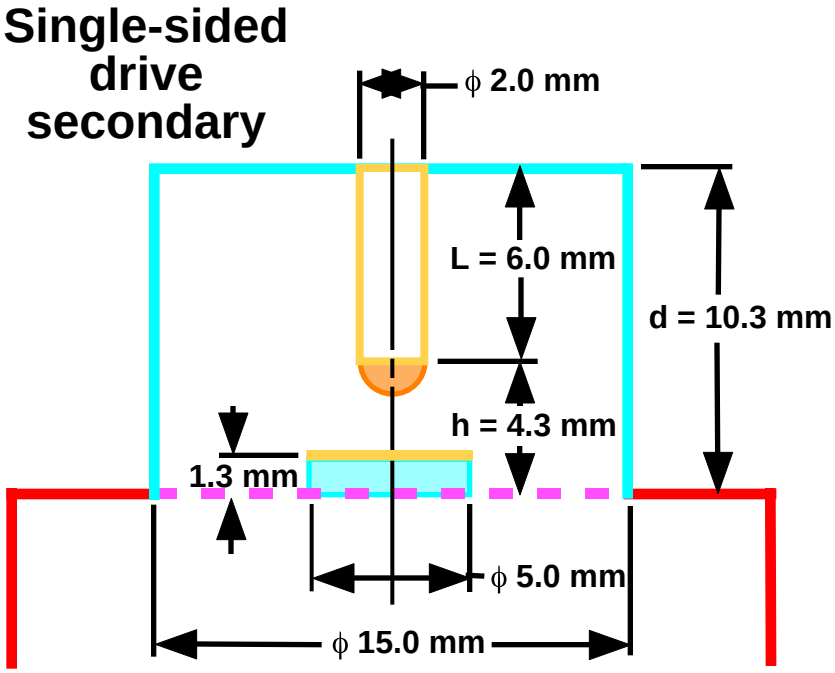

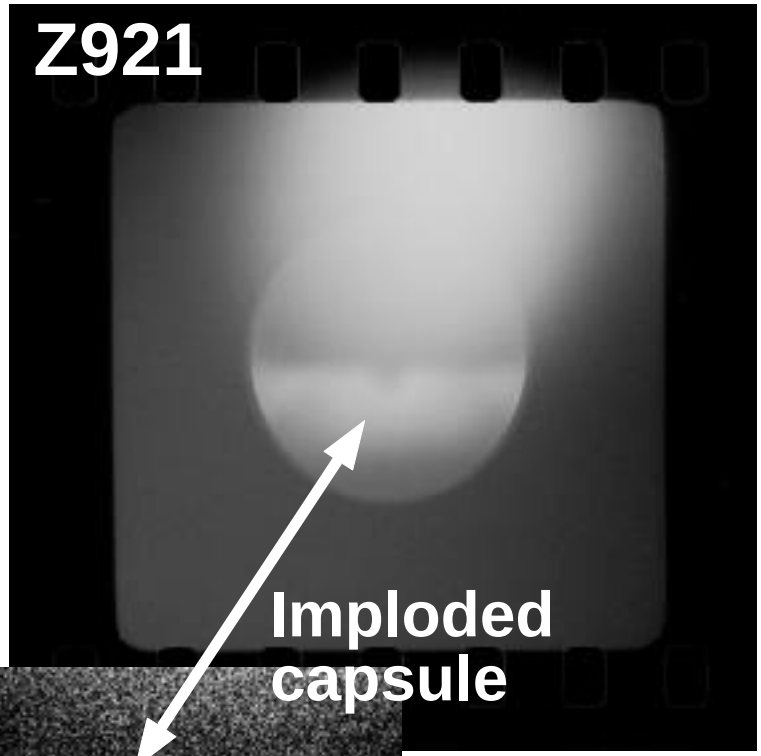

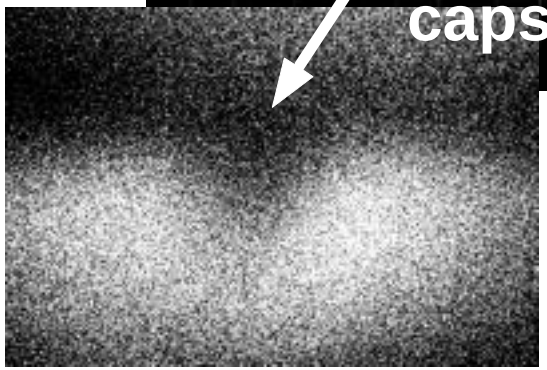

ZBL point projection backlit image at 6.7 keV with on-axis FOA recorded ~ 3.5 ns after hemi-capsule peak compression

$t_{pk\ cmp} - t_{pk} \sim 9$ ns

$t_{ZBL} - t_{pk} = 12.5$ ns

Sandia National Laboratories

A cleaner image was recorded before peak compression in a “diagnostic friendly” geometry

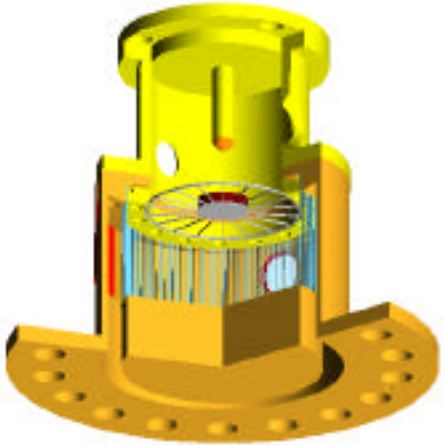

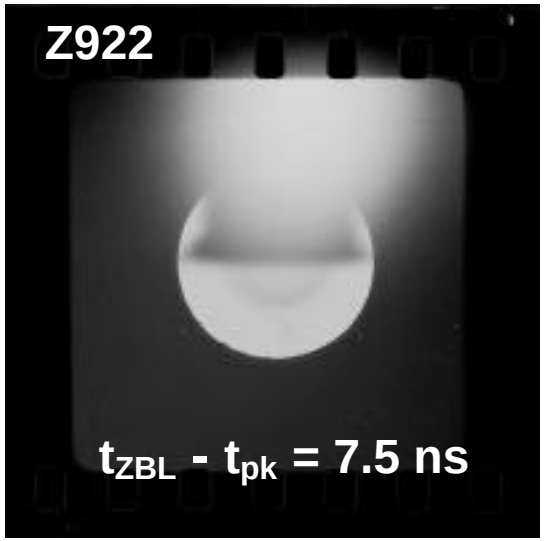

ZBL point projection backlit image at 6.7 keV with on-axis FOA (125 μm resolution)

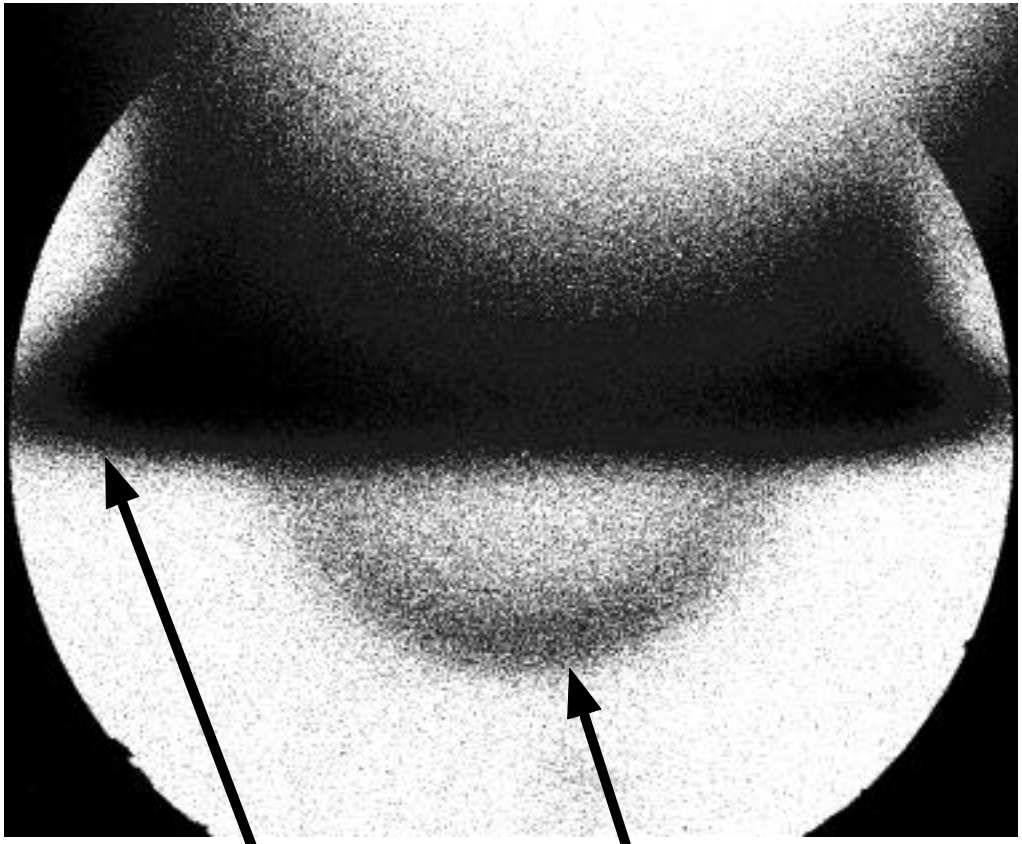

Gold edge expansion

Imploding shell

Sandia National Laboratories

On shot Z923, a clean, high-resolution capsule image was recorded using the ZBL off-axis FOA

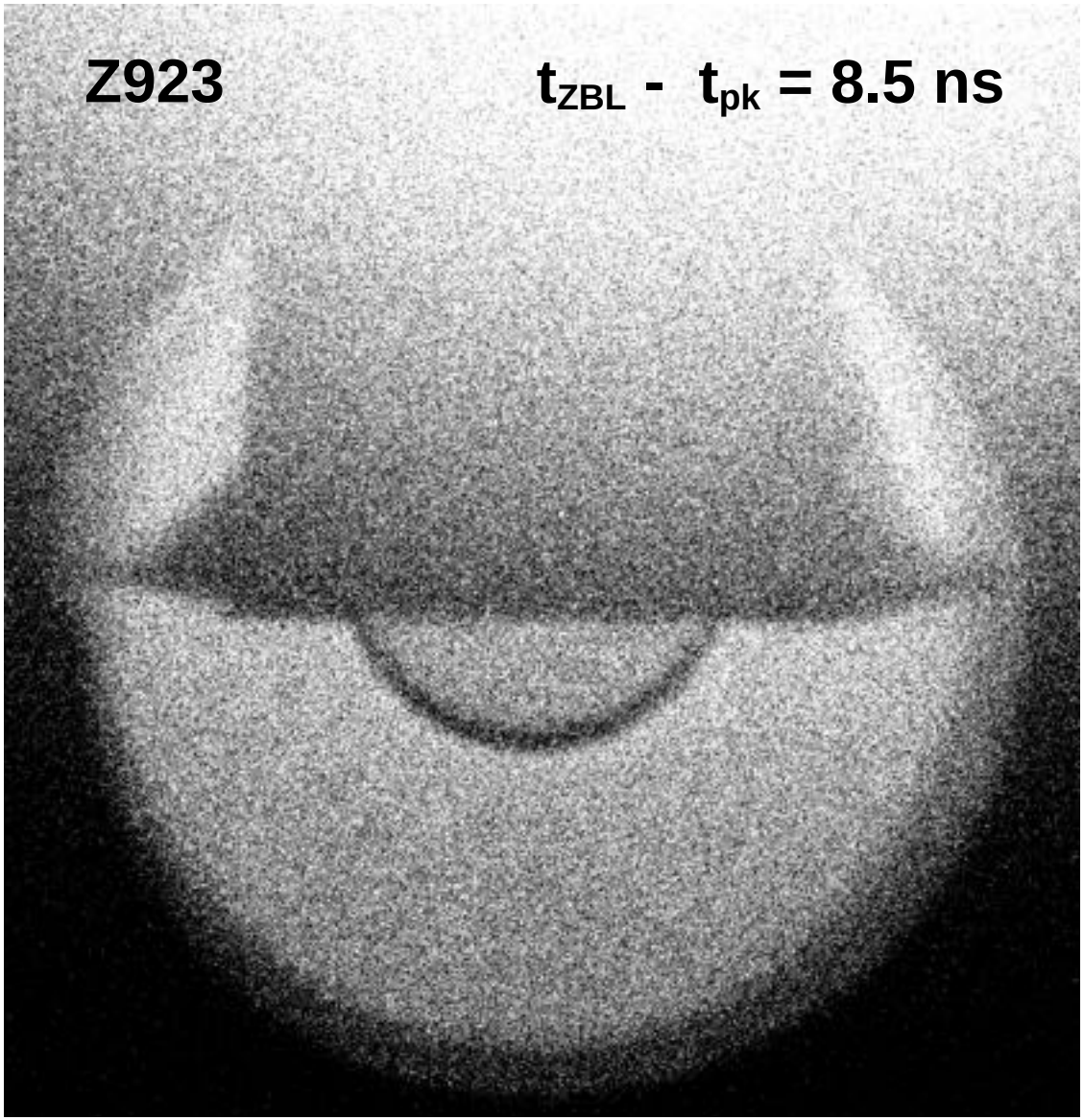

ZBL point projection backlit image at 6.7 keV with off-axis FOA (50 μm resolution)

Horizontal convergence ratio 1.9

Sandia National Laboratories

Asymmetric radiation flux distribution in this unoptimized geometry produces pole-hot drive

Assume no motion of capsule mounting surface:

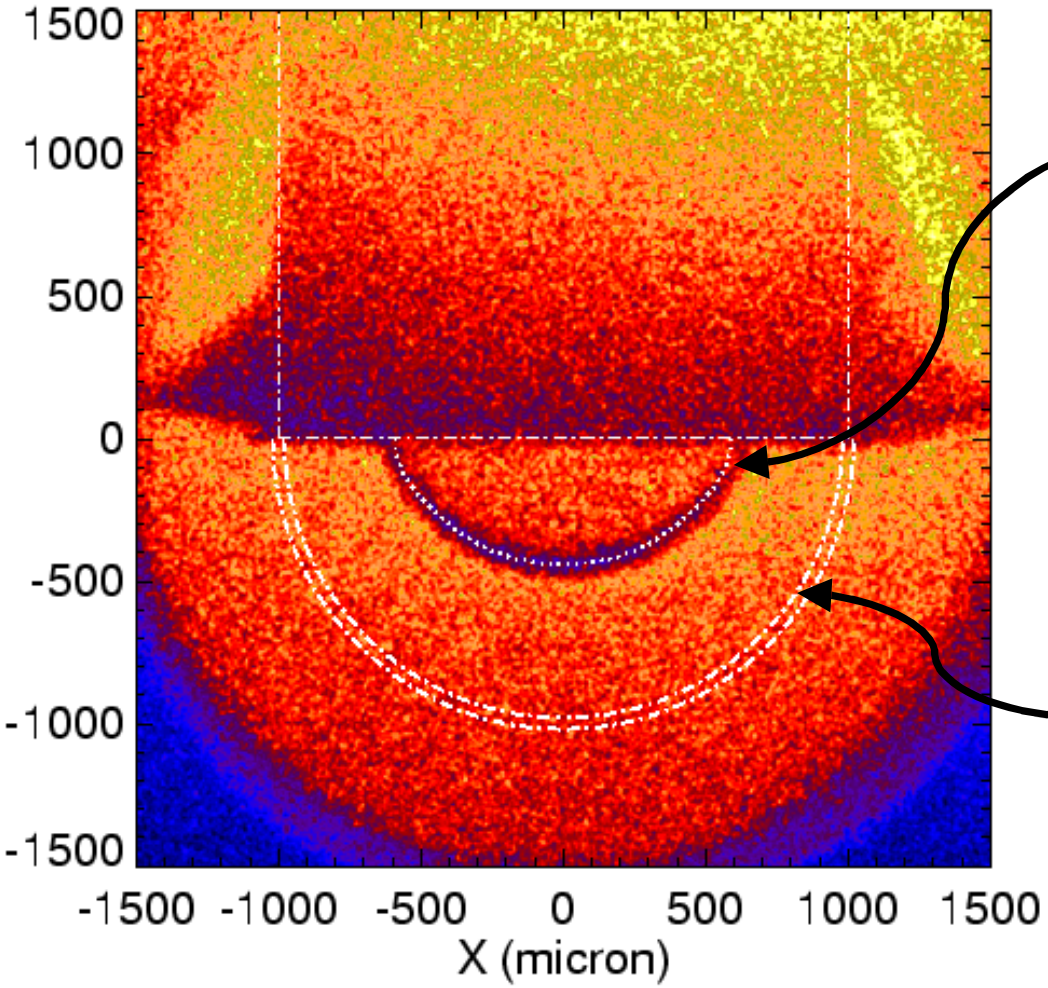

8th order fit:

a_0 = 520 μm
a_2 / a_0 = - 19.6%
a_4 / a_0 = + 6.8%
a_6 / a_0 = - 3.6%
a_8 / a_0 = +0.9%

Original capsule profile

OPTSEC predicts:

- **dominant P2 and P4 modes in fluence**
- **modes 2 thru 8 of correct sign to give observed shape**

Sandia National Laboratories

Lasnex simulations predict high compression densities for hemi-capsule implosions on ZR

OPTSEC viewfactor gives time-dependent asymmetry, input to 2D Lasnex capsule simulation as boundary condition

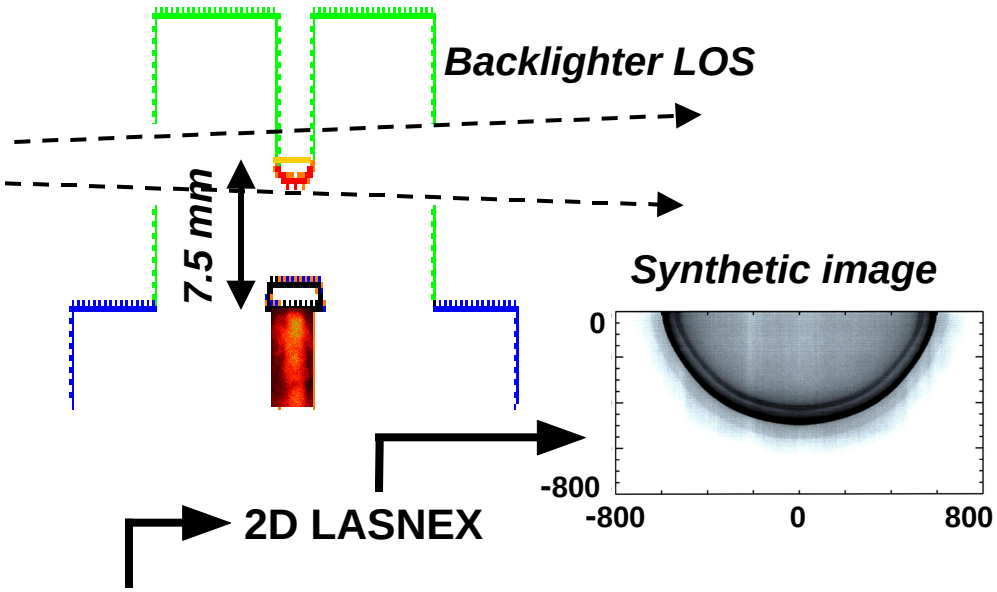

8th Order fit to limb shape:

Mode	Expt.	Sim.
a_2 / a_0	- 19.6%	- 11.8%
a_4 / a_0	+ 6.8%	+ 3.5%
a_6 / a_0	- 3.6%	- 2.4%
a_8 / a_0	+0.9%	+ 1.3%

2D simulations give polar-averaged peak ρ = 60 g/cc, ρr = 0.3 g/cm² for this case

More optimized Z hohlraum designs should allow ρ = 90-100 g/cc, ρr = 0.4 g/cm²

Simulations for ZR with cryo DT capsule give ρ = 160 g/cc, ρr = 0.65 g/cm²

Sandia National Laboratories

In the next shot series, a modified hemi-capsule mount will allow backlighting of the glide plane rear surface

Hemispherical shell geometry provides excellent access to the planar glide surface for interaction studies

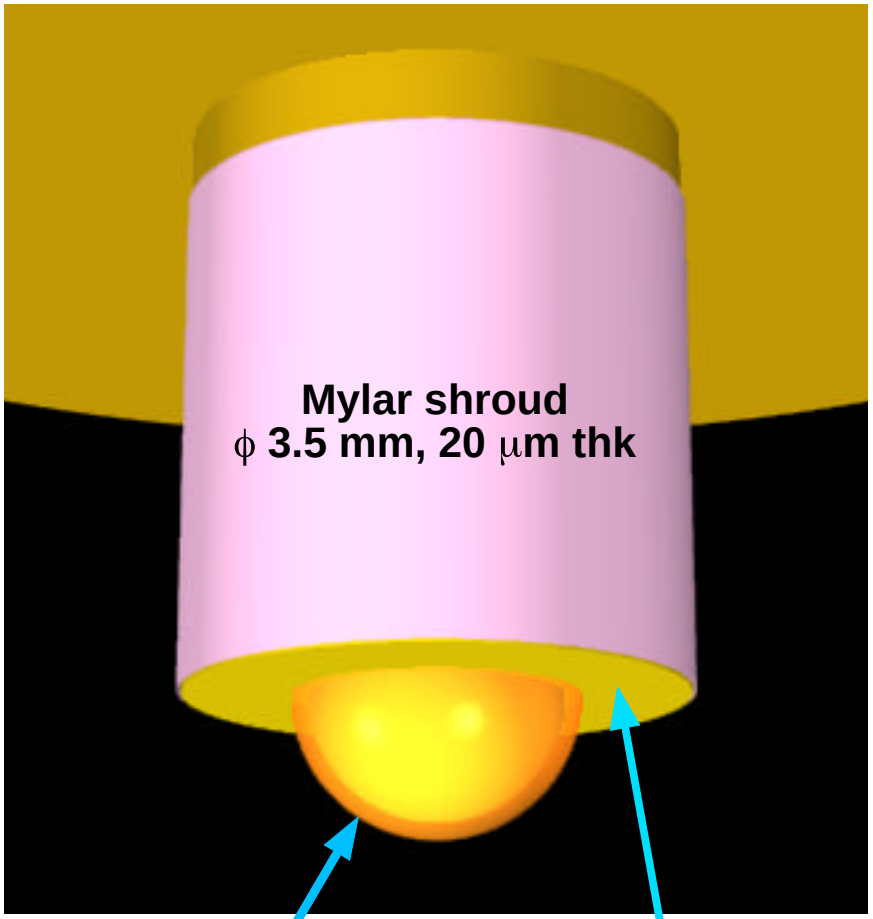

Au glide plane
ϕ 3.5 mm, 30 μm thick

GDP hemispherical shell
ϕ 2.0mm, 60 μm thick

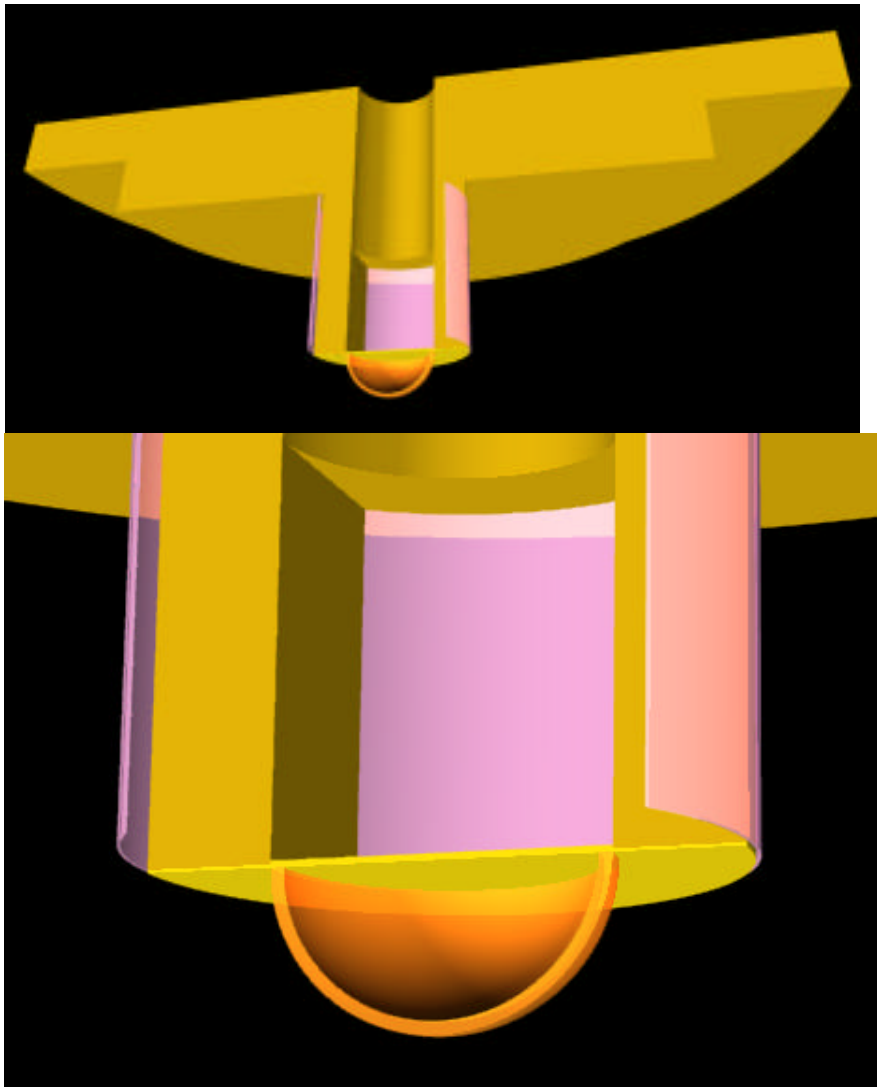

Sandia National Laboratories

We are beginning development of a cryogenic liquid fuel target for fast ignitor experiments on Z and ZR

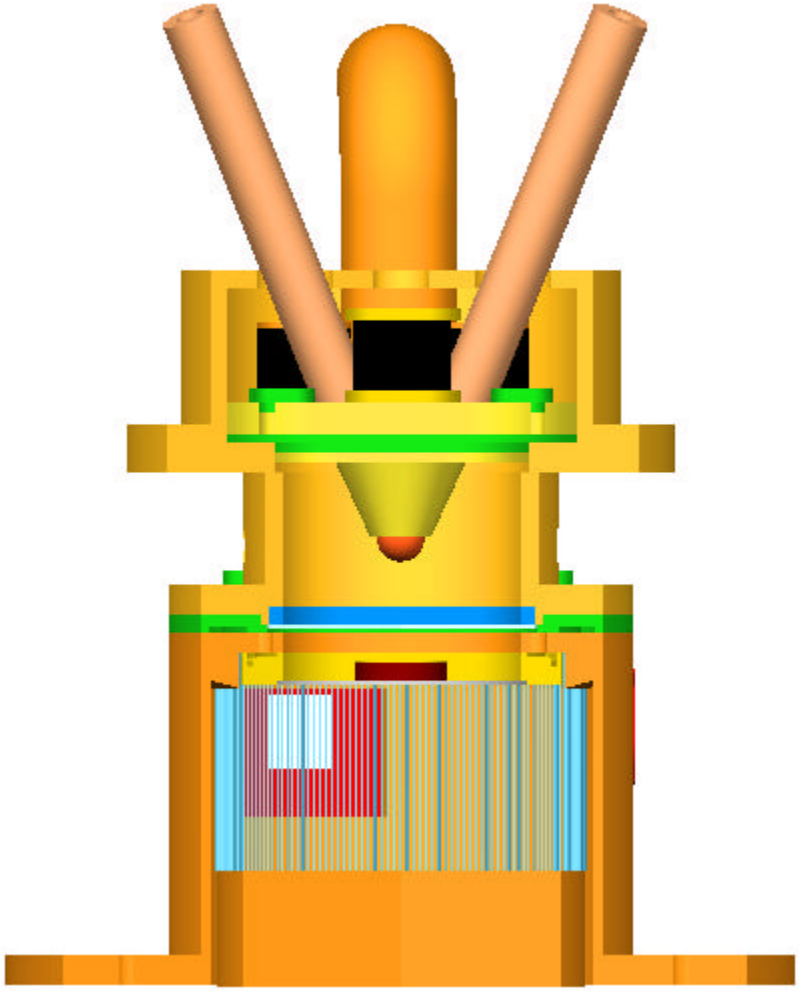

Motivation:

- drastically reduced cost compared to DT β-layering
- greatly reduced temperature control requirements
- surface quality of liquid fuel layer determined entirely by bounding shells
- well-adapted to hemispherical capsule configuration in single-sided drive
- suitable for fusion energy applications
- infrastructure for fielding liquid fuel cryogenic targets already exits on Z

Sandia National Laboratories

Related poster: Steve Slutz, "Fast Ignition Capsules Using Liquid Cryogenic Fuel"

ICF target of choice for standard central spark ignition is a uniform β-layered DT-ice capsule

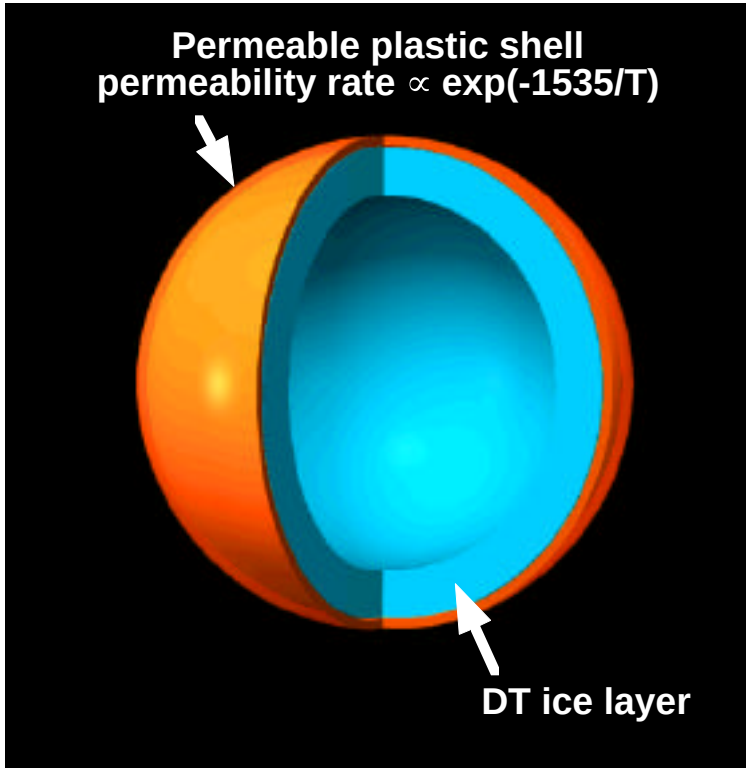

- Must get enough gas inside capsule to condense ice shell
- Spherical plastic capsules are slowly filled to 1200 atm by room temperature diffusion through shell
- Slow pressure ramp required to maintain P differential of ≤ 0.2 atm
- Gas in capsule and pressure chamber then simultaneously frozen out, eliminating pressure on shell
- Capsules with DT ice layer must be stored and transported at very low temperature (19 K)

This procedure would be compatible with fast ignitor spherical/reentrant cone or hemispherical capsule geometry, but is very expensive

Sandia National Laboratories

It may not be possible to generate spherical isotherms required for uniform DT β-layering in a cone geometry

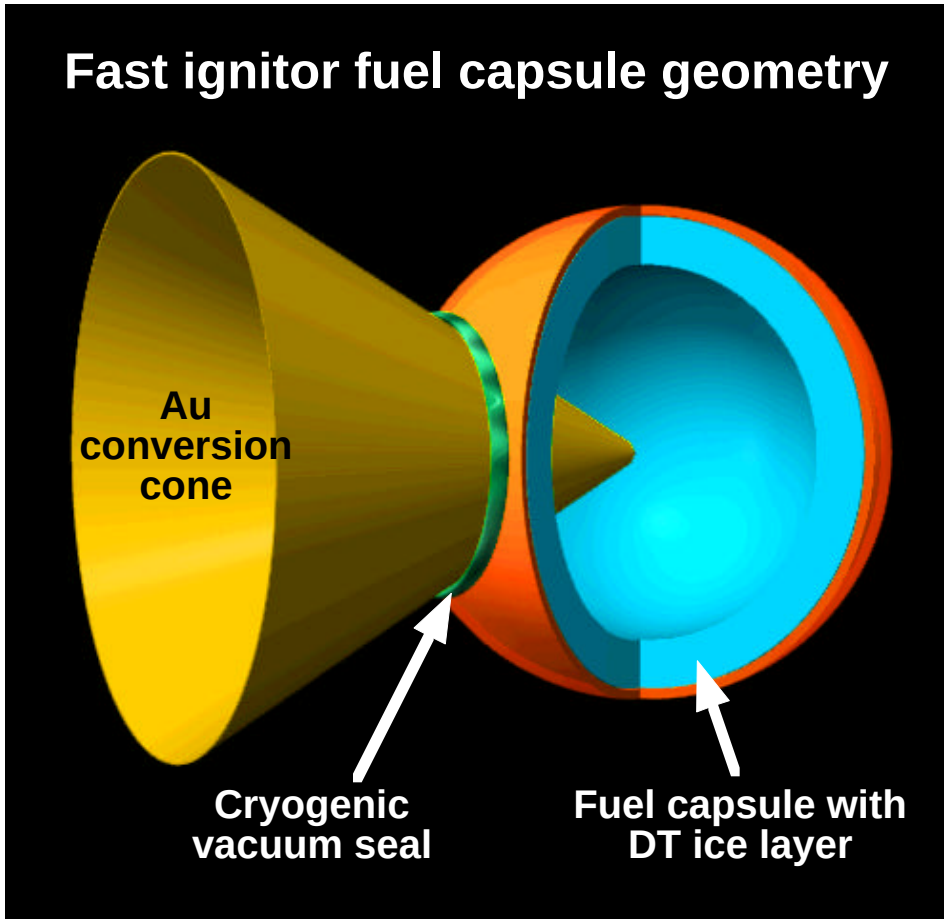

- DT ice thickness uniformity conforms to the temperature isotherms at the capsule surface
- Hohlraum surface geometry (and gas fill convection) must control the temperature profile and thermal gradients to produce virtually spherical isotherms at the capsule surface for uniform DT ice layer

Reentrant cone disrupts symmetry of thermal environment and will be coated with DT ice inside the capsule

Sandia National Laboratories

We have designed a cryogenic liquid target for the Z-pinch fast ignitor driver configuration

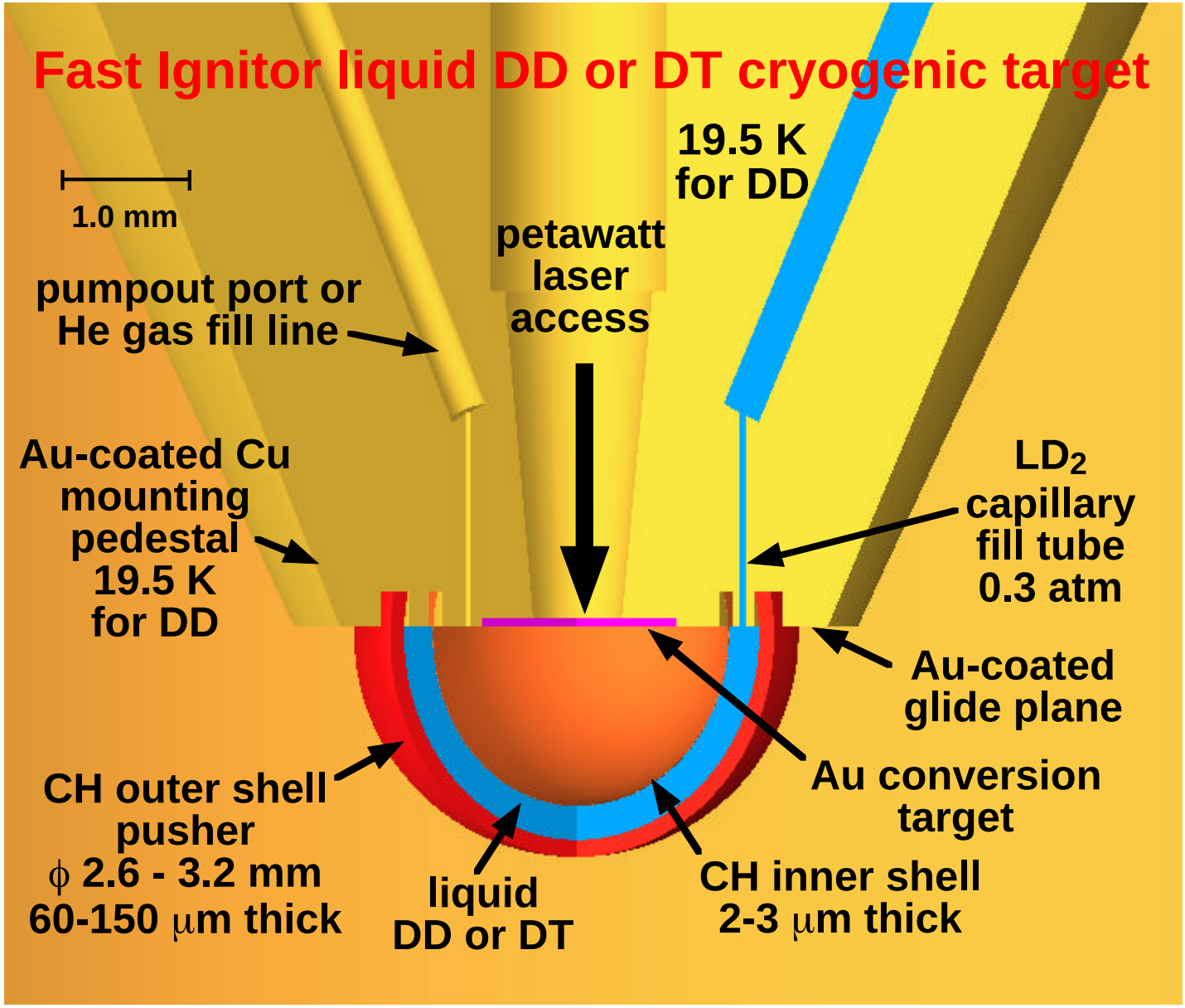

Sandia National Laboratories

The secondary hohlraum forms a stable thermal environment for the cryogenic liquid target

Fast Ignitor liquid deuterium cryogenic target

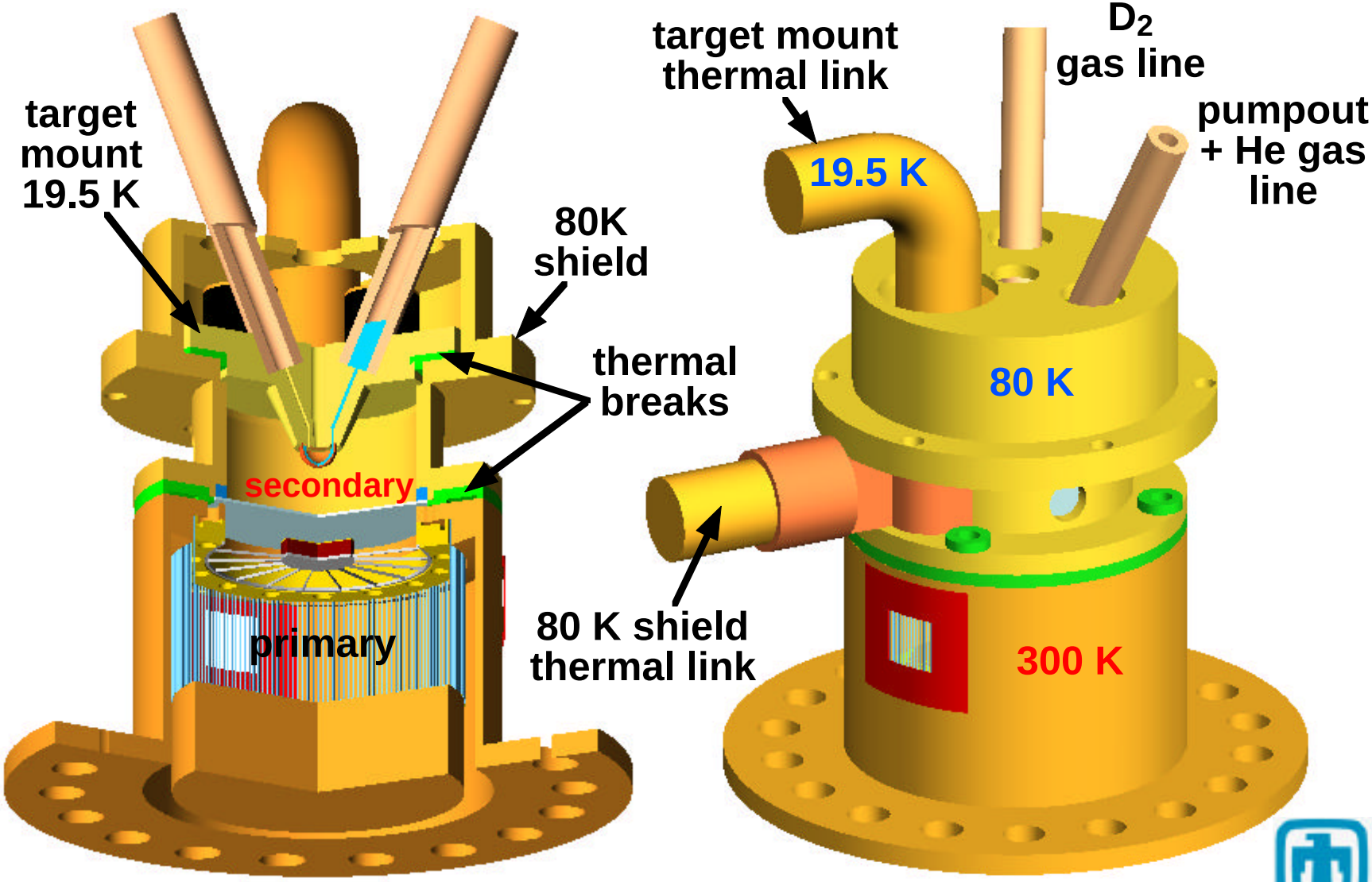

Sandia National Laboratories

Cryogenic liquid fuel targets have some important advantages over DT-ice capsules

To supply the required number of hydrogen molecules to form a solid density fuel layer, we have replaced a very small volume gas capsule filled to extremely high pressure (400-1200 atm) before cooling with a very large gas reservoir operating at ~ 0.3 atm pressure.
This is facilitated in the 180°-cone fast ignitor compression geometry by the ability to construct the target on a flat, solid platform capable of supporting external gas lines.

- **Liquid in a gravitational field precisely fills the available space, so the dimensions, thickness, uniformity, and surface finish of the liquid fuel layer are determined entirely by the properties of the shells bounding the liquid - these shell parameters can be accurately measured off-line and checked in-situ**
- **Both DD and DT can be shot in a cryogenic liquid fuel target, which does not depend on energy from tritium β-decay or an external source to redistribute solid fuel by sublimation into a uniform layer**
- **There is no advantage for solid over liquid hydrogen in initial fuel density - DD ice density is only about 14% greater than liquid D_2 density at 19.5 K**

Much of the infrastructure for cryogenic liquid deuterium targets already exists on Z

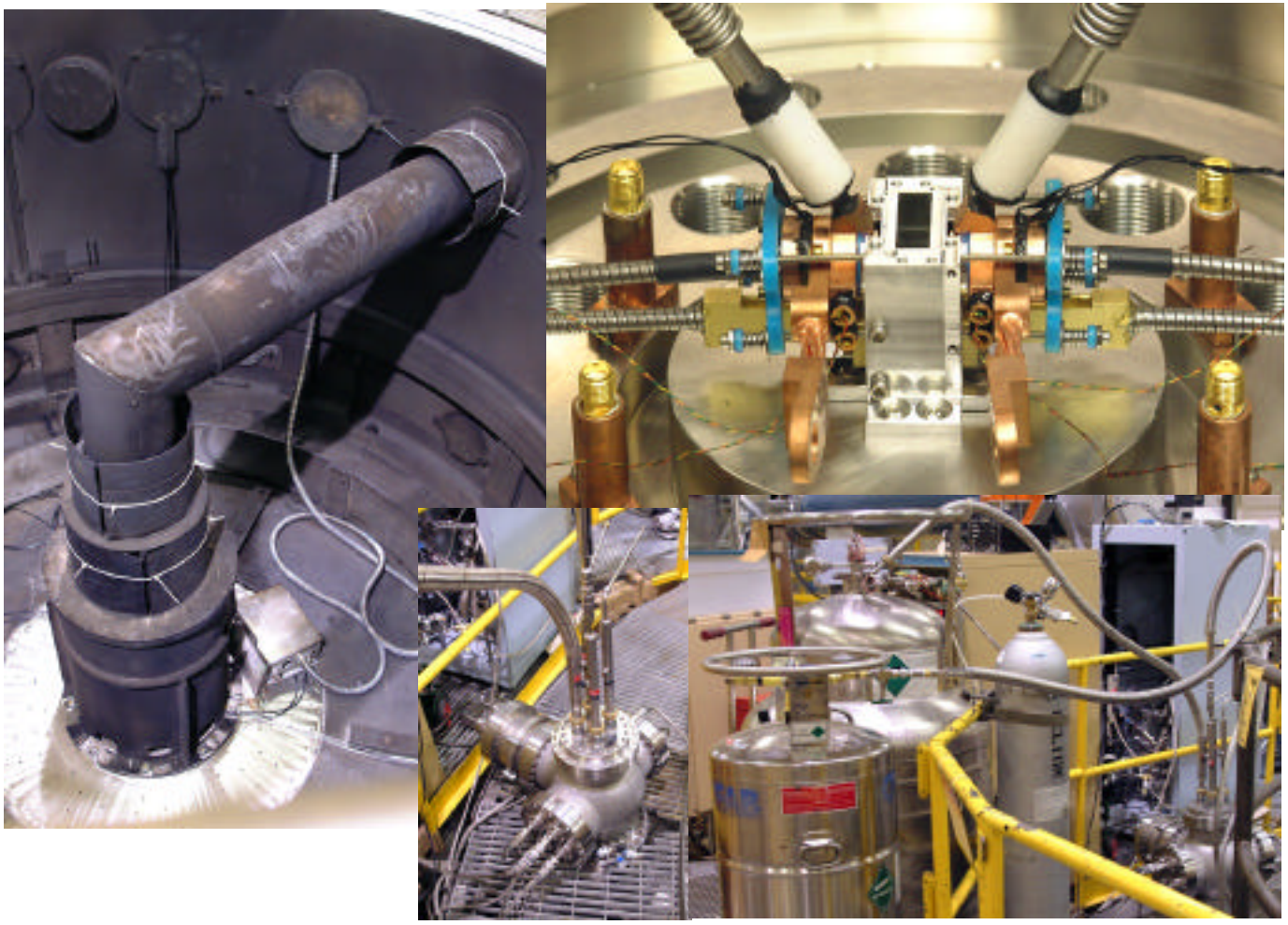

We have been condensing liquid deuterium samples for D_2 EOS measurements on Z for 4 years

Ref: M. D. Knudson, D. L. Hanson *et al.*, PRL 87, 225501 (2001)

Sandia National Laboratories

It is important to minimize the thickness of the inner plastic shell

External collapsing pressure for polystyrene spherical shell
E = 3.4 GPa ν = 0.33

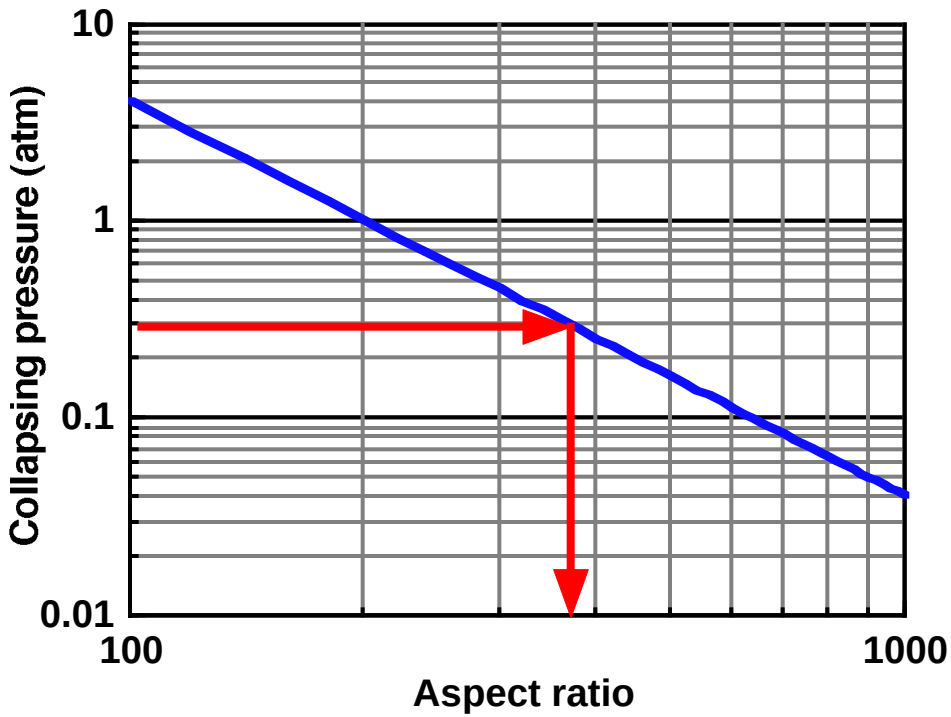

The minimum shell thickness for a plastic capsule of 1.0 mm radius is about 3 μm

He internal pressure could support a thinner shell but would limit capsule convergence

Because the density of the inner shell is about 4 times the density of liquid DT, the fuel-shell interface is unstable and the materials could mix, resulting in a reduction in capsule performance

It is important to minimize the mass of the inner plastic shell, but quite thin shells are possible at operating pressures of 0.3 atm

Critical buckling pressure for complete thin spherical shell:

$$P_c = 2E/((3(1-\nu^2))^{1/2} R_a^2)$$

where: R_a = aspect ratio = r/t
E = Young's modulus
ν = Poisson's ratio

Ref: W. Flugge, Stresses in Shells (Berlin: Springer-Verlag, 1960) pp. 472-8.

Sandia National Laboratories

The most difficult problem will be fabrication and mounting of the large, thin-wall inner shells

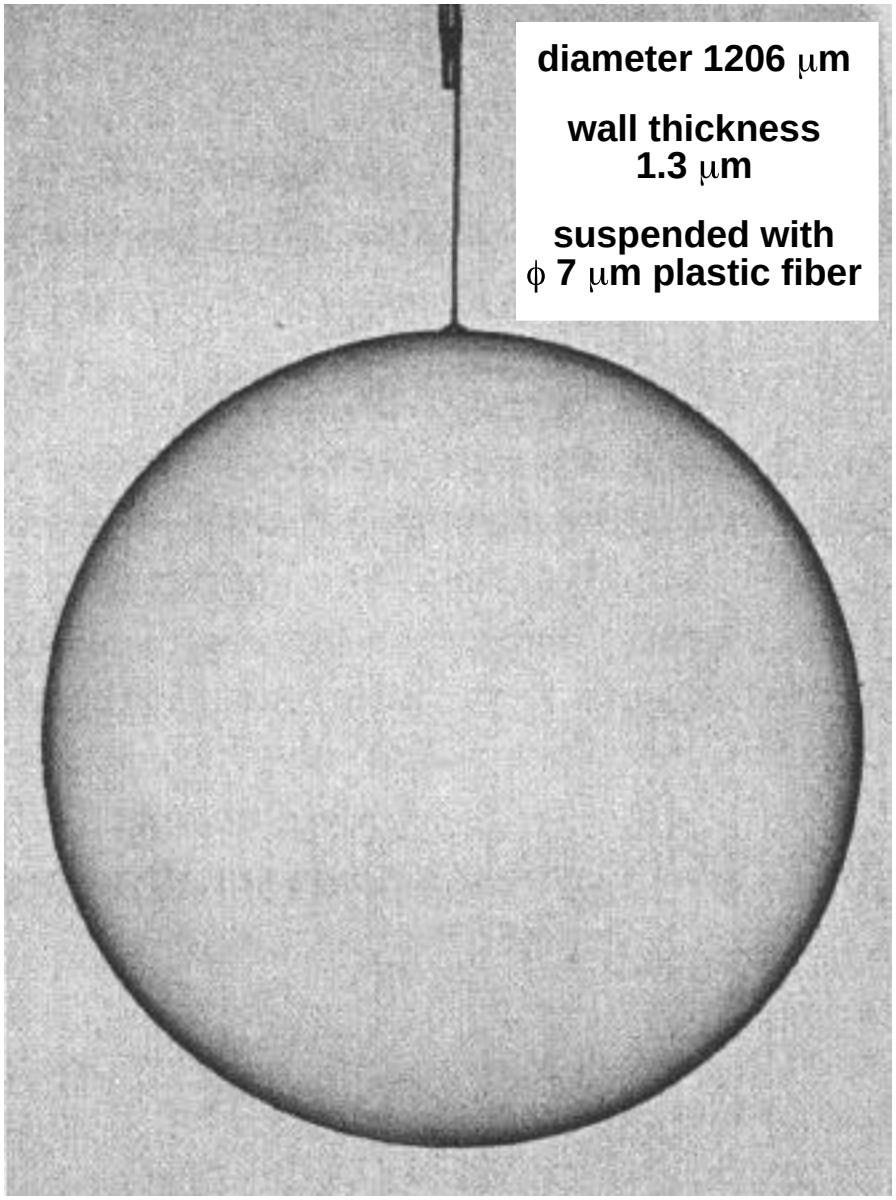

Large, high-aspect-ratio glass microballon targets have been fabricated for direct-drive laser fusion experiments

Ref.: T. Norimatsu *et al.*, "Fabrication of large-diameter, high aspect-ratio glass microballon targets for laser fusion research", J. Vac. Sci. Technol. A6, 2552 (1988)

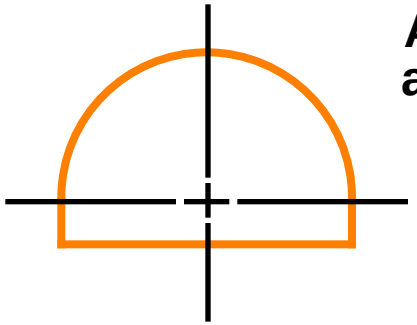

An effort is underway at General Atomics to fabricate ϕ 2.0 mm, 2-5 μm thick CH hemi-shells on a mandrel

Sandia National Laboratories

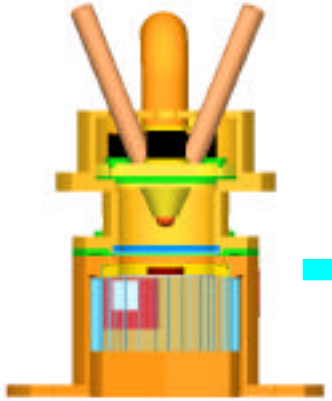

Summary

- Initial Z experiments have demonstrated the feasibility of recording high resolution ZBL point projection backlit images of hemi-capsule implosions in single-pinch Brems environment

- The hemispherical capsule geometry provides access to the region behind the glide plane for investigation of the complex hydrodynamics of the capsule/glide plane interaction during implosion

- A hemispherical cryogenic liquid fuel target system is being developed for future fast ignitor neutron production experiments on ZR with a petawatt laser

Sandia National Laboratories

Cone-Focussed Fast Ignition: Sub-Ignition, Proof-of-Principle Experiments

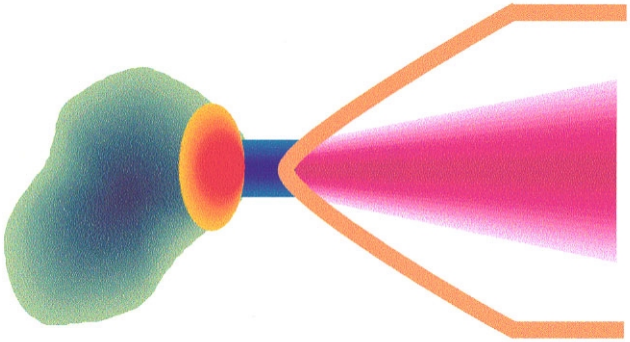

S. P. Hatchett
O. S. Jones
M. Tabak
R. E. Turner
LLNL

R. B. Stephens
GA

6th Workshop on Fast Ignition of Fusion Targets

November 16-19, 2002
St. Petes Beach, Florida USA

This work was performed under the auspices of the U.S. Department of Energy by the University of California, Lawrence Livermore National Laboratory under Contract No. W-7405-Eng-48.

Fast Ignition requires several key elements:

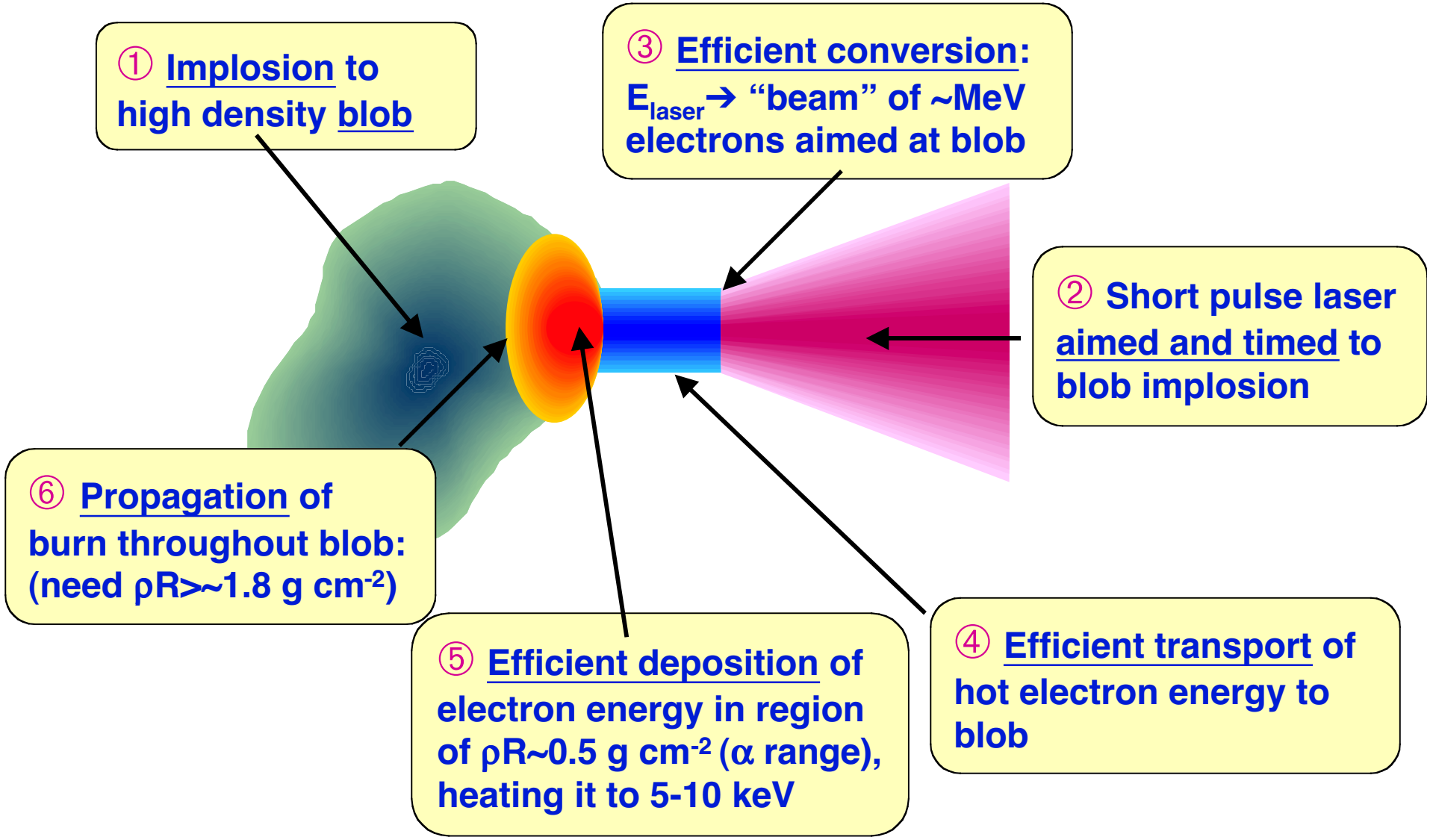

Cone-focussed scheme — Indirect drive:

A re-entrant tube and cone provide access for ignitor beam to the imploded, compressed core:

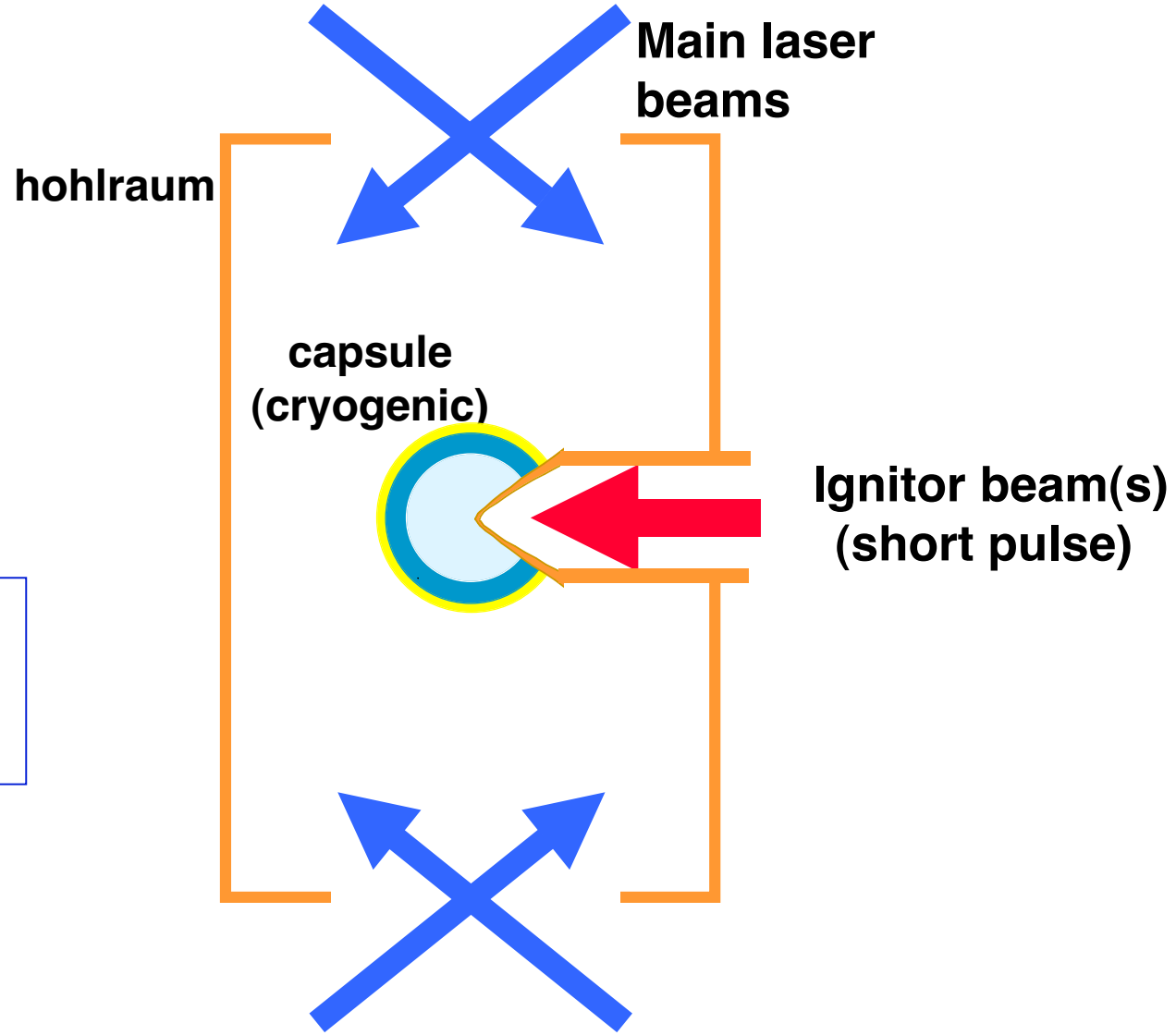

Direct Drive:

Same idea but no hohlraum

Cone-focussed scheme immediately provides most of the key FI elements.

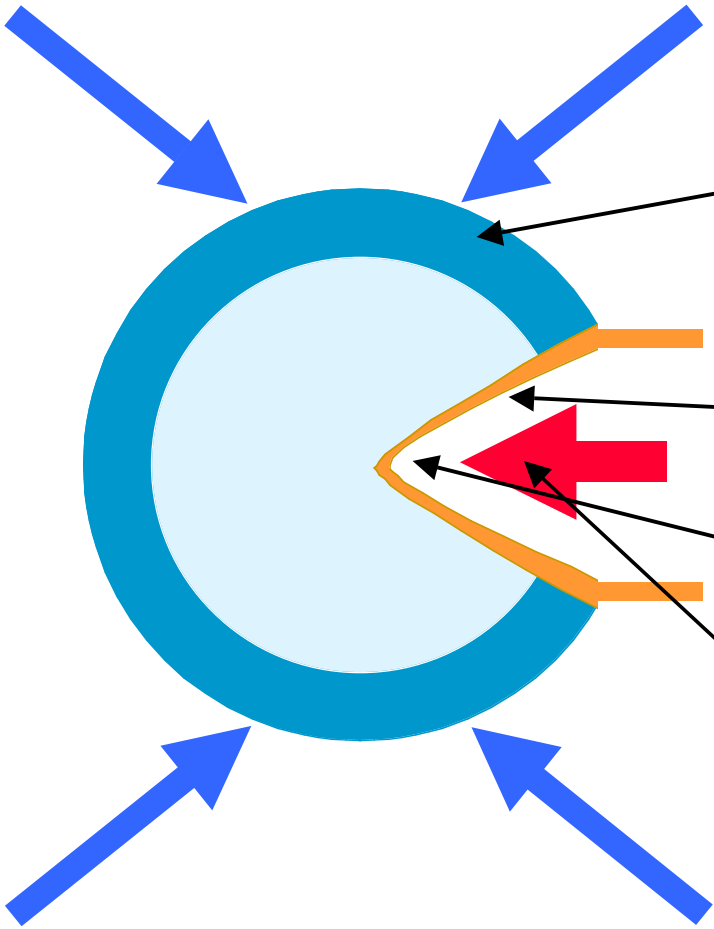

① Low aspect ratio capsule: Get hi ρ blob with relatively low drive symmetry; no significant stability issues.

②④ Cone provides pointing & puts deposition of laser v. close to hi ρ blob

③ E_{laser} → hots at surface, ~50% conversion (exp't)

⑤ Laser spot size & pulse length tuned to give hot e's with optimum range

NIF ignition scale capsule (absorbs ~150kJ) can be imploded to $\langle\rho R\rangle_{DT}$=2.18 g cm^{-2}.

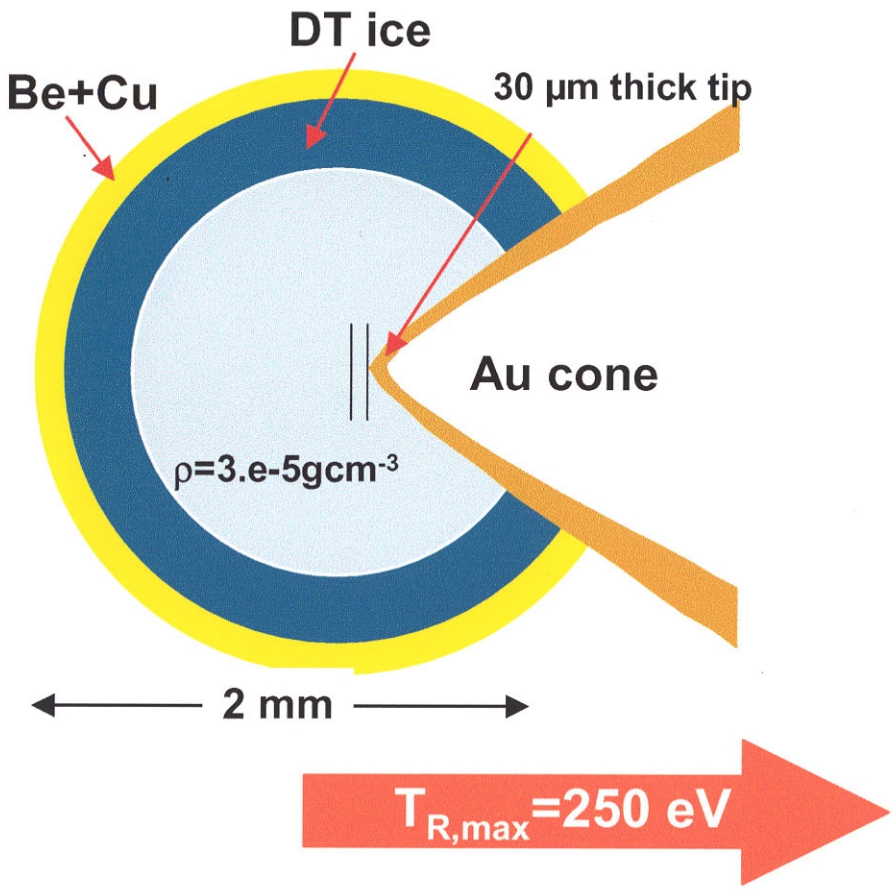

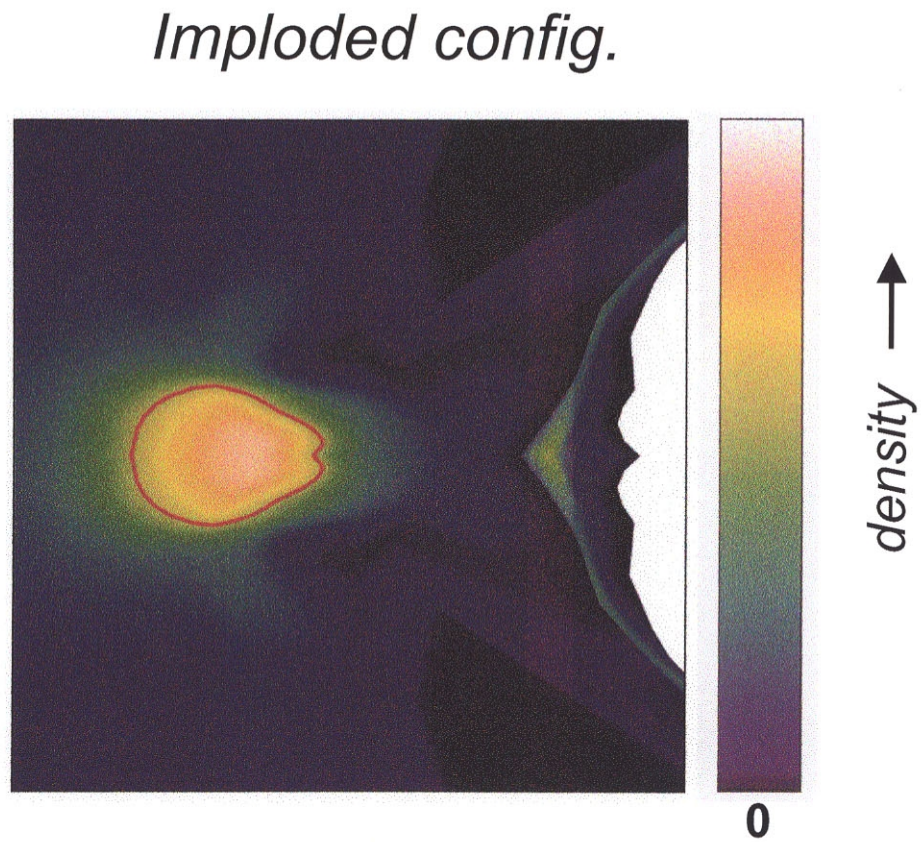

Minimum total electron beam energy required for ignition depends strongly on beam geometry:

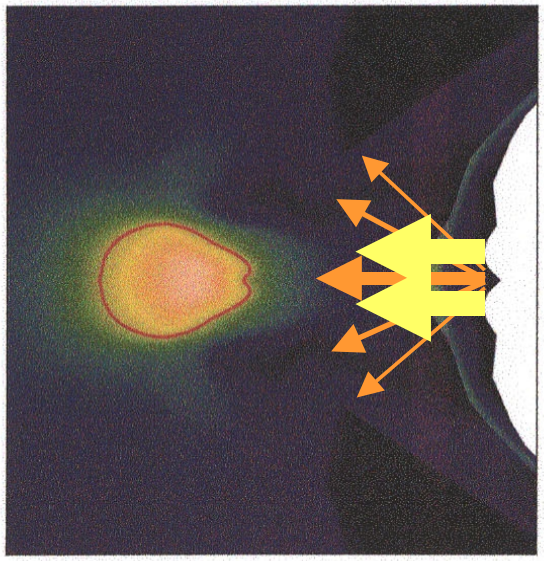

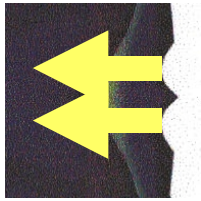

Collimated beam
diam.= 40 µm

- $E_{beam,\ min}$ ~ 30 kJ
  ⇔ 8 NIF quads
- Yield = 27 MJ

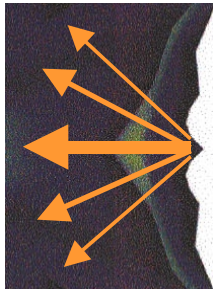

Divergent beam
50° fwhm

NO GO

- $E_{beam,\ min}$ ~ 150 kJ
  ⇔ 36 quads
- Yield = 24 MJ

Early experiments need to show whether beam is collimated or divergent.

Purpose:

Cone-focussed, sub-ignition experiments on NIF and/or OMEGA-EP could provide the evidence for the transport and coupling required for FI — in highly FI relevant conditions.

- **Cone-focussed hydrodynamics has been successfully demonstrated**
- **Cone-focussed, OmegaEP or NIF implosions can produce highly relevant, hot, high density, high electrical conductivity beam path conditions (without cryogenics).**
- **X-ray and neutron images should show where and by how much the hot electrons (or protons?) have heated the plasma.**

Cone focussing works, but more experiments will fill in important details:

Radiographs from indirect drive Omega experiment

Original cone was blunt hyperboloid

Shadow shows sharp point - broadening with time

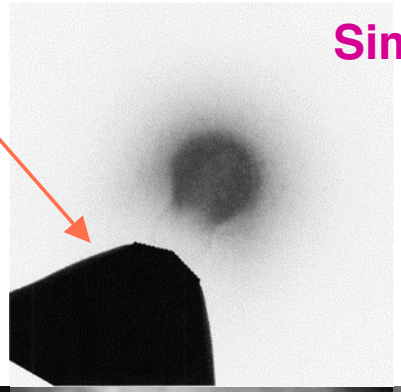

Simulated radiograph

140 ps interval

Experiment

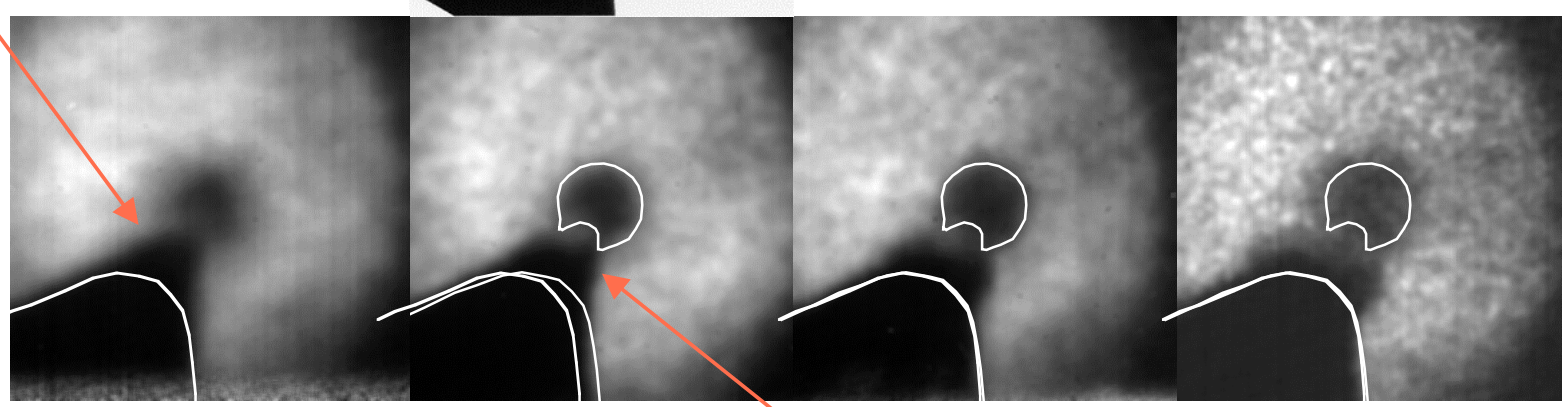

Gold plasma?

The NIF deployment strategy would allow proof-of-principle experiments in FY07.

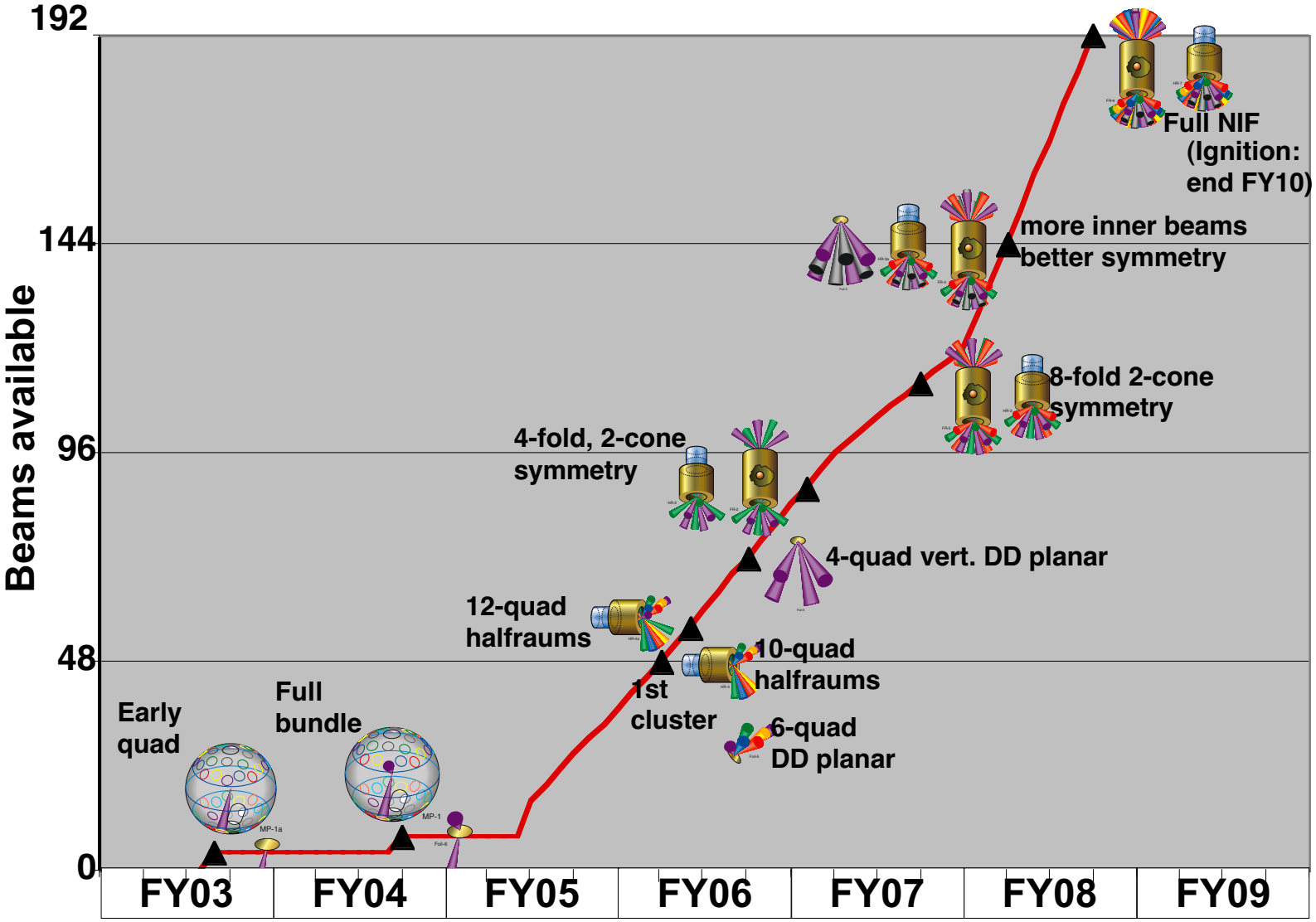

Early NIF "proof of principle" experiments can demonstrate FI implosion and ignitor beam collimation & heating:

Implosion drive=250 kJ (16 quads); case/capsule ~2.1

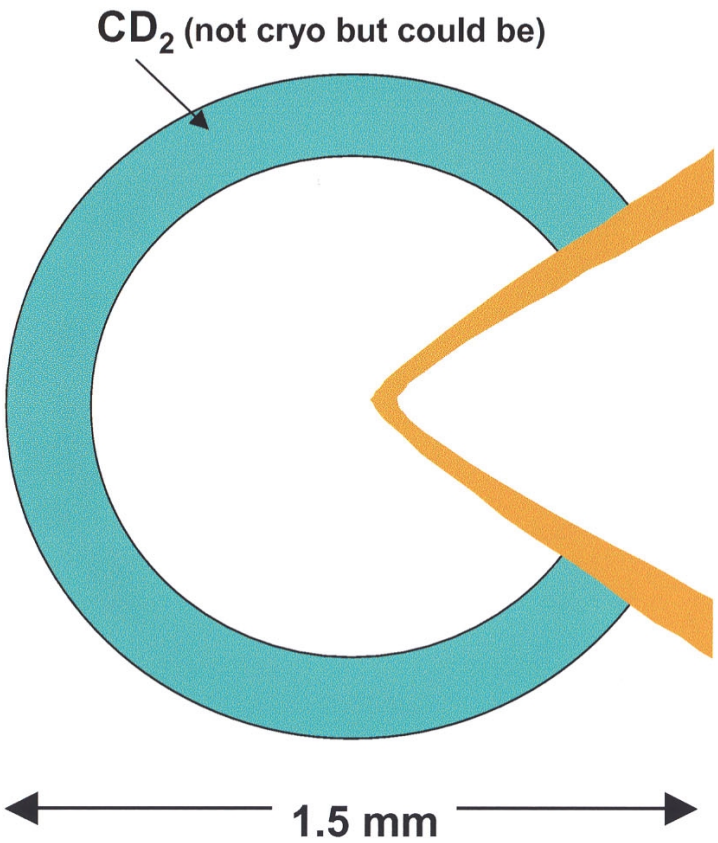

Imploded Config.

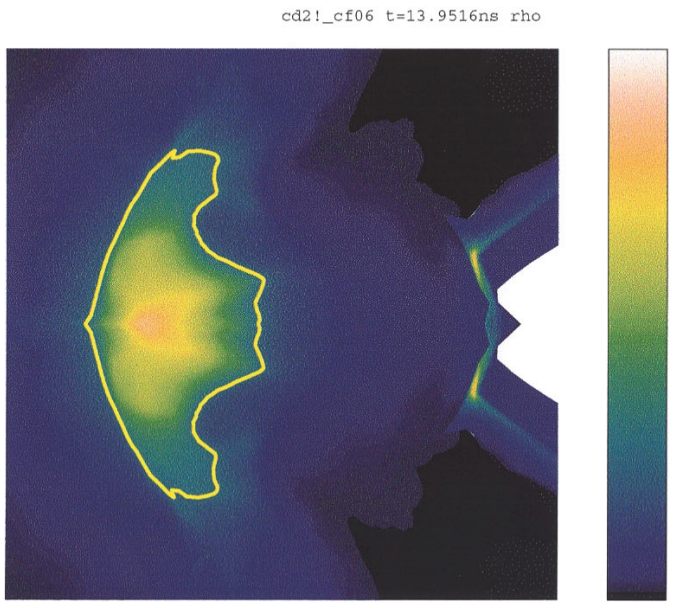

ρR=1.0 g cm^{-2} ; $Yield_{implosion}$=1.5e4 neutrons

$Energy_{blob}$ ~ 2 kJ

Implosion is “cold”, but backlighter shows a dense blob:

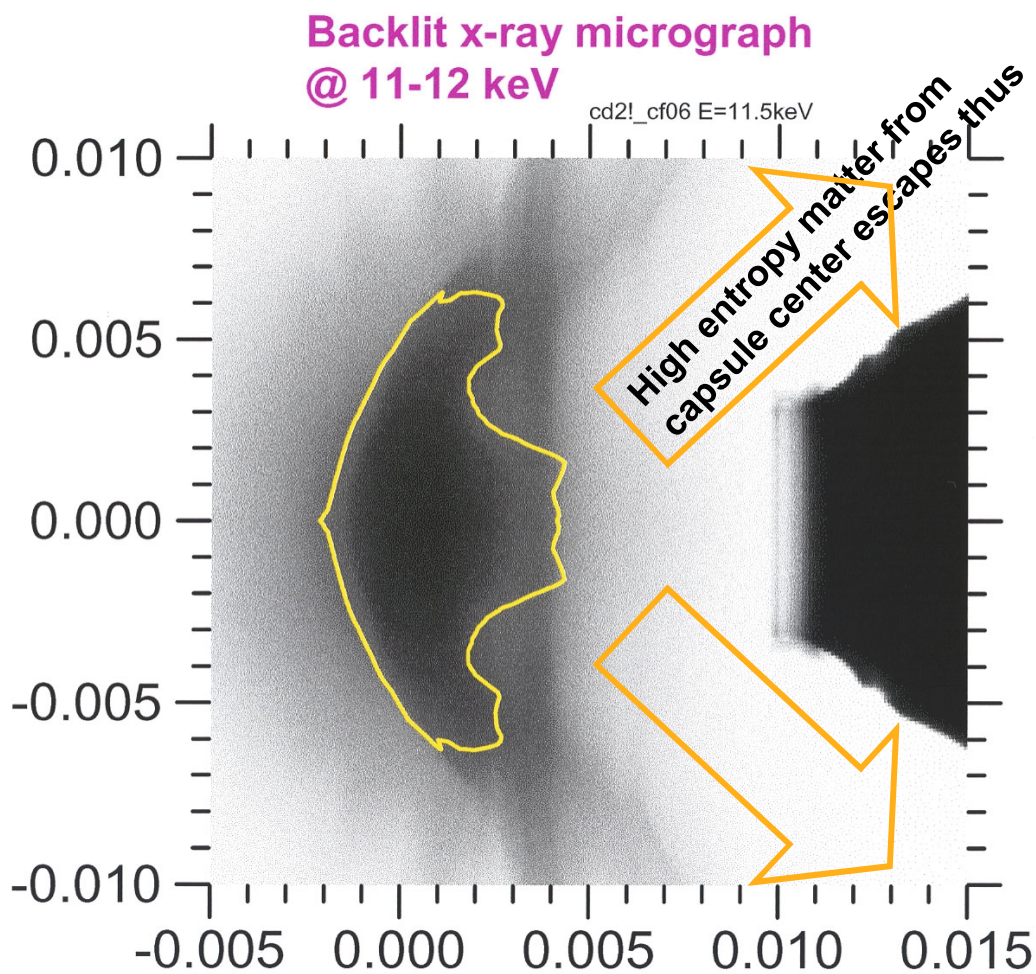

Short pulse should hit early-NIF scale target within a wide, ~100 ps, window of peak implosion <ρR>:

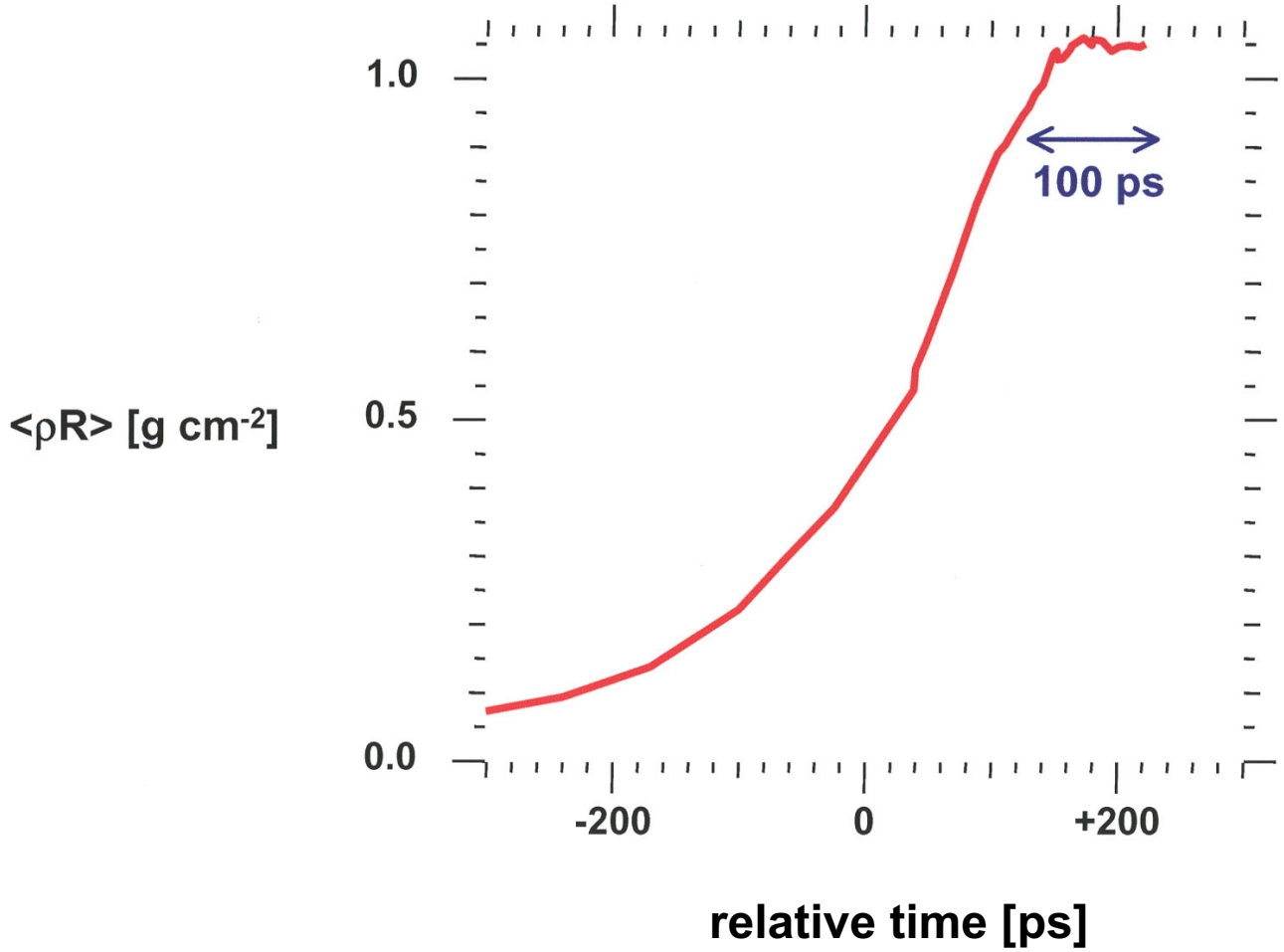

Cone is main source of drive asymmetry: Imperfect symmetry from close-coupled hohlraum and only 16 quads is not a problem.

Simulated backlit radiographs illustrate one of FI's advantages — much less drive symmetry sensitivity.

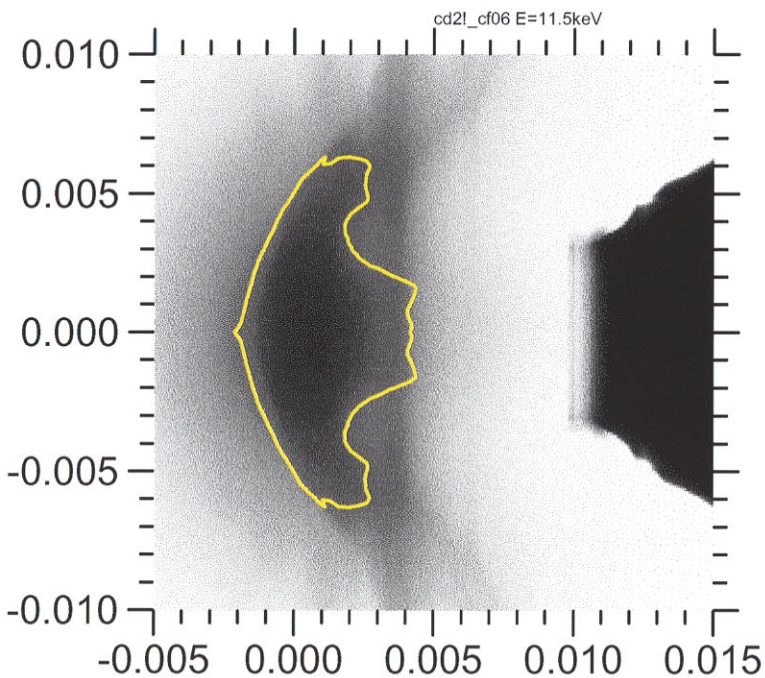

Cone-focussed

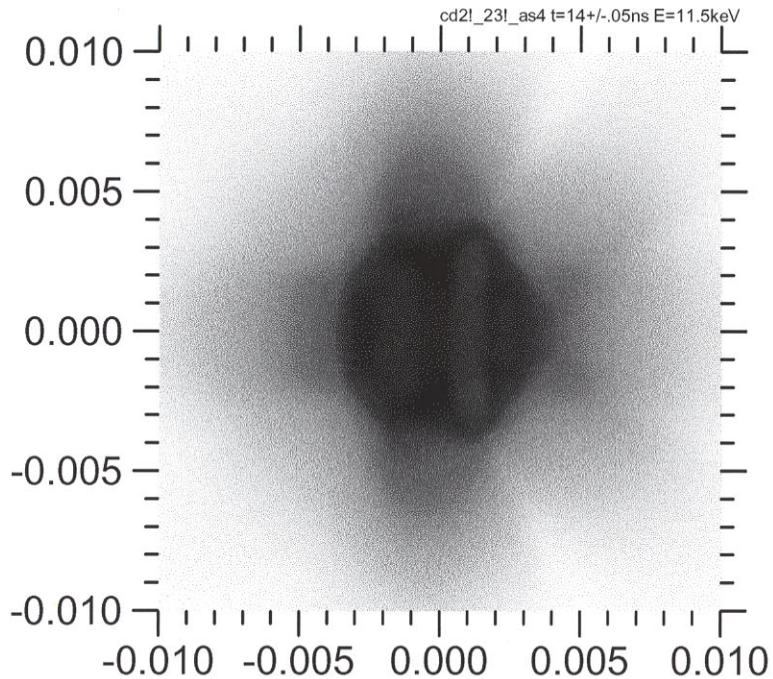

Full sphere, 2-D with same spectrum of ℓ-modes in drive as calculated by 3-D view-factor code

Short pulse energetics:

1 NIF beamlet, converted to short-pulse and focussed on an isolated spot, should produce about 0.52 kJ of hot electrons with $\langle E_e \rangle \sim 3$ MeV (tunable).

- **2.6 kJ @ 1 PW (0.1% damage probability)**
- **Focus 40% of energy into an area of (25 micron)^2**
- **$I = 6.4 \times 10^{19}$ watts cm^{-2} $\Rightarrow$ $U_{pond} = 3$ MeV $\sim \langle E_e \rangle$**
- **Convert ~ 50% of the 40% high intensity light to hot electrons.**

  (2.6 x 40% x 50% = 0.52 kJ)

(Overlap of wings from many spots, or better spot quality, would allow much more than 40% of total energy to be at high intensity.)

With 4 NIF beamlets of short-pulse (2.1 kJ of hot e⁻'s)

Hot electrons collimated or divergent? Changes in heating pattern are obvious:

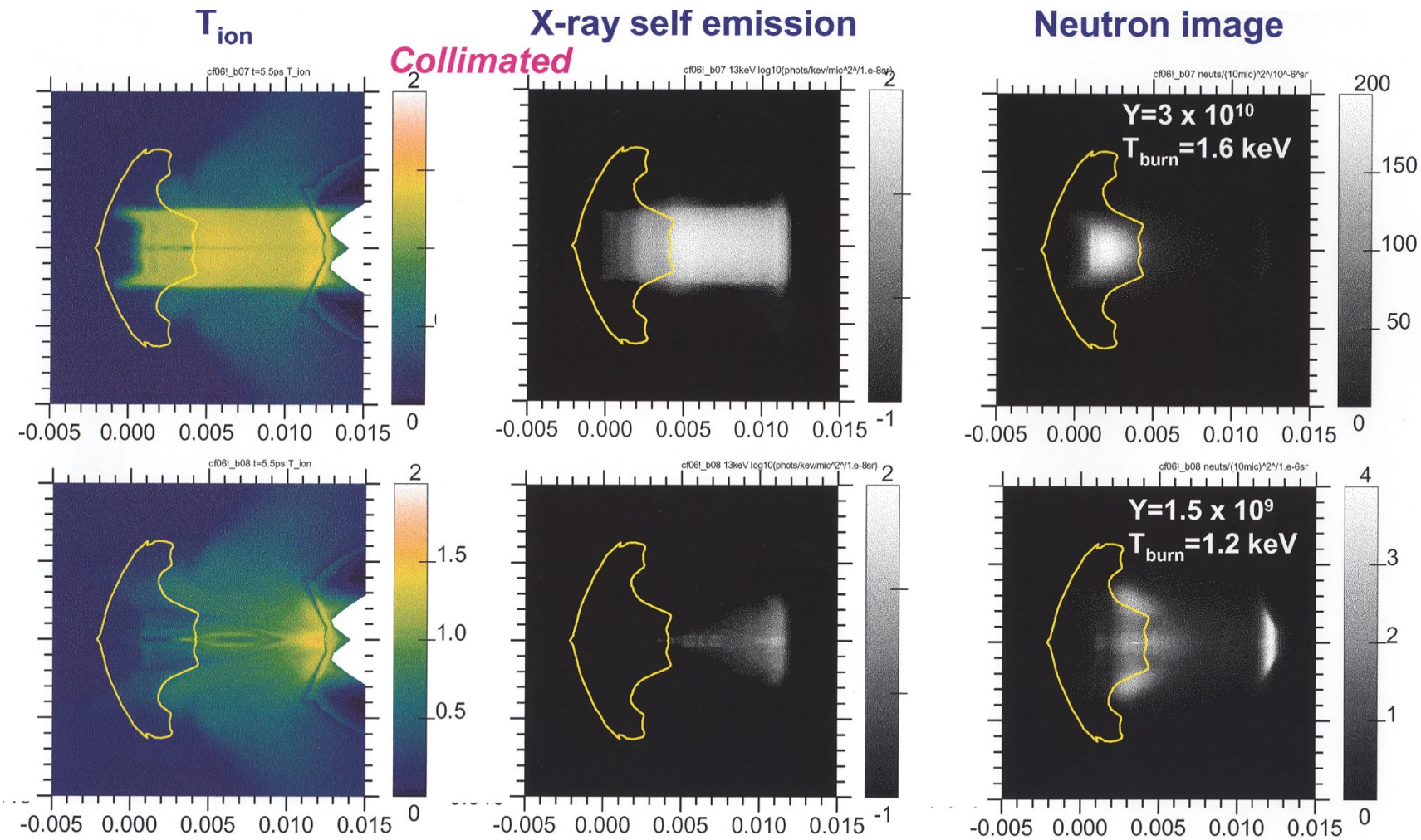

Divergent (40° fwhm)

Protons? Ion acceleration & focussing studies are at early stage. A rough experimental calculation:

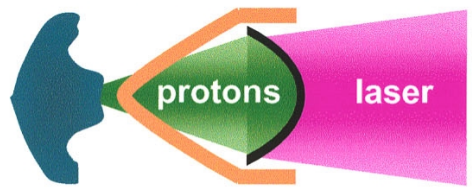

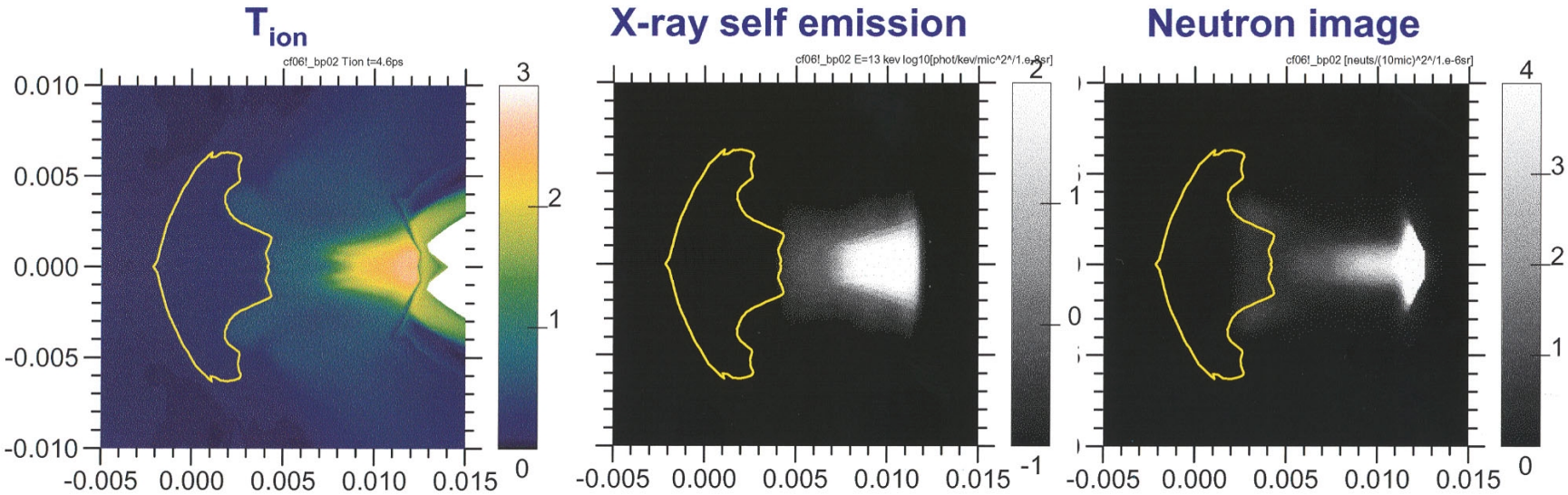

Input: 1.25 kJ p's (~12% conv. from laser)
$\langle E_p \rangle$= 3 MeV (~ $\langle E_e \rangle$)
focussed onto 50 mic diam. spot
from cone with $\theta_{1/2}$=20°.

Focussing is apparent; range is insufficient to reach hi ρ

(But see new ideas on range lengthening and velocity dispersion effects [Temporal et al PoP 9,3098])

Ion ranges may be effectively lengthened by ion spectra/velocity dispersion effects: [*Temporal et al PoP 9, 3098]:*

- Sheath acceleration model naturally produces an ion spectrum, $N_{ion}(E) \sim \exp(-E/\langle E_{ion}\rangle)$, with $\langle E_{ion}\rangle \sim$ few x U_{pond}.

- Standoff distance between ion source and target blob means fastest ions with longest ranges arrive first.

- Energy deposition by early arriving ions heats the path — allowing the later arriving bulk of ions to penetrate more deeply.

Effective range lengthening from $N_{ion}(E) \sim e^{-E/\langle E \rangle}$ and standoff distance of 1mm has substantial effect at this "early NIF" scale.

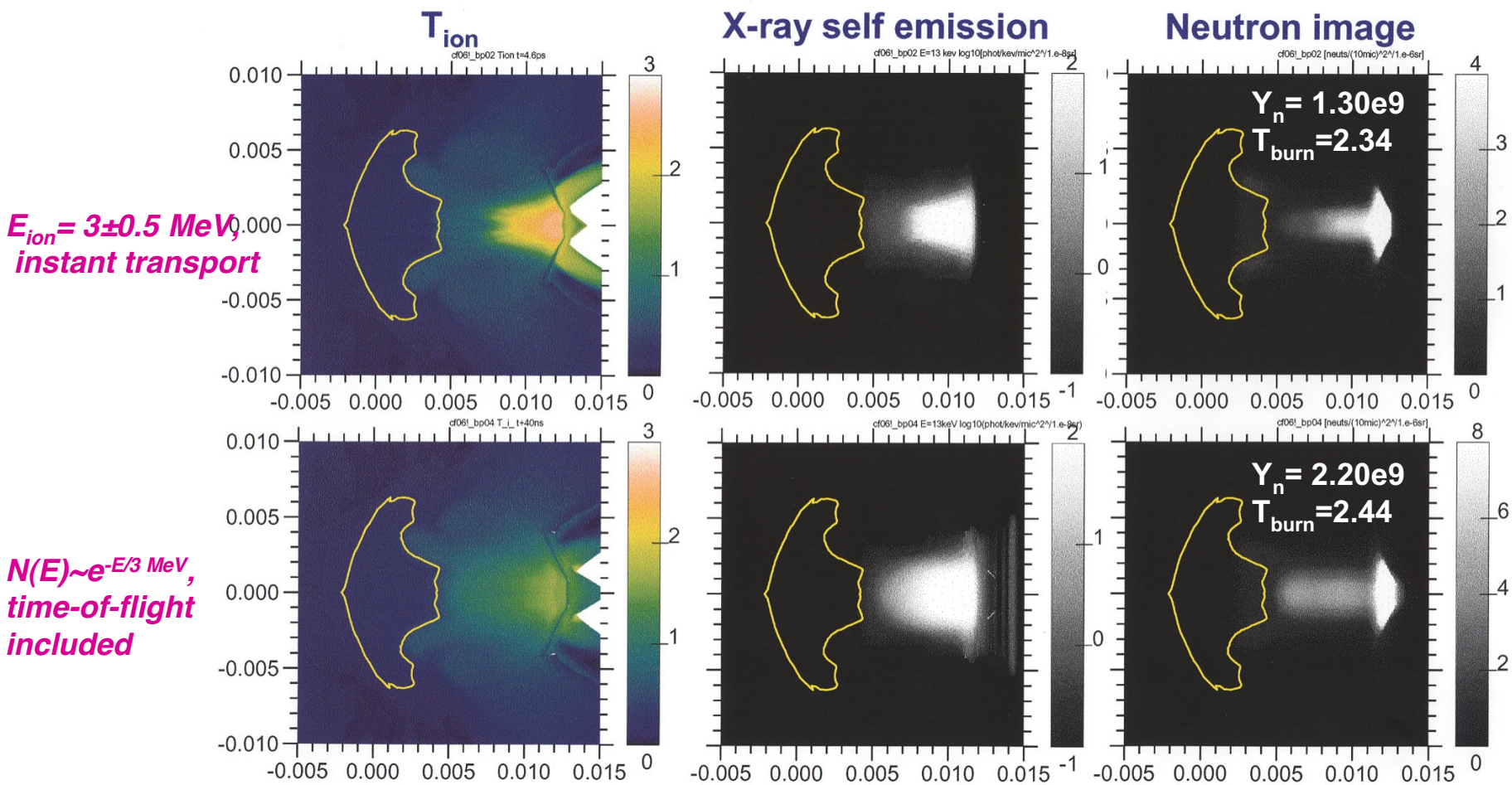

This is a sensitive result: at 2mm the longer time-of-flight dispersion, ~ 100 ps, allows cooling, and yield drops.

A cone-focussed, directly driven OMEGA implosion can also set the stage for a highly FI-relevant transport/coupling experiment:

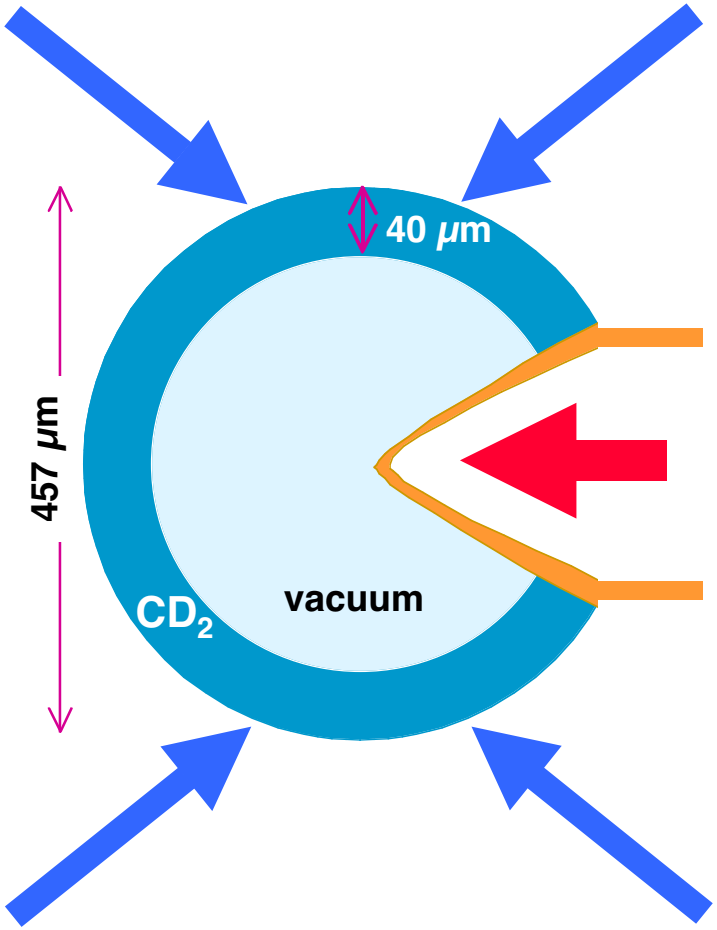

55* beams (uniform) PS 26

Backlit radiograph (8 keV) at max ρR

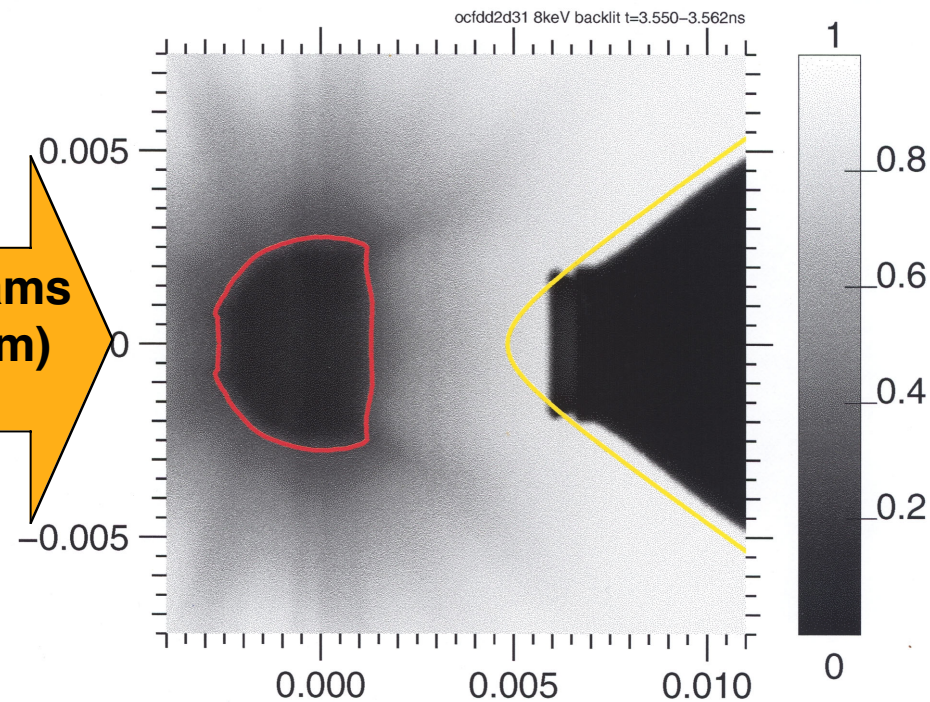

Blob ρR ~ 0.44 g cm^{-2}
<ρ> ~ 120 g cm^{-3}
<T> ~ 0.4 keV
Total Energy in blob ~ 0.6 kJ

* Omit 5 beams from solid angle subtended by cone.

Coupling/burn calculation:

Link imploded core and cone to a new lagrangian simulation; drive with mock e^-'s (ions with A=1/1822)

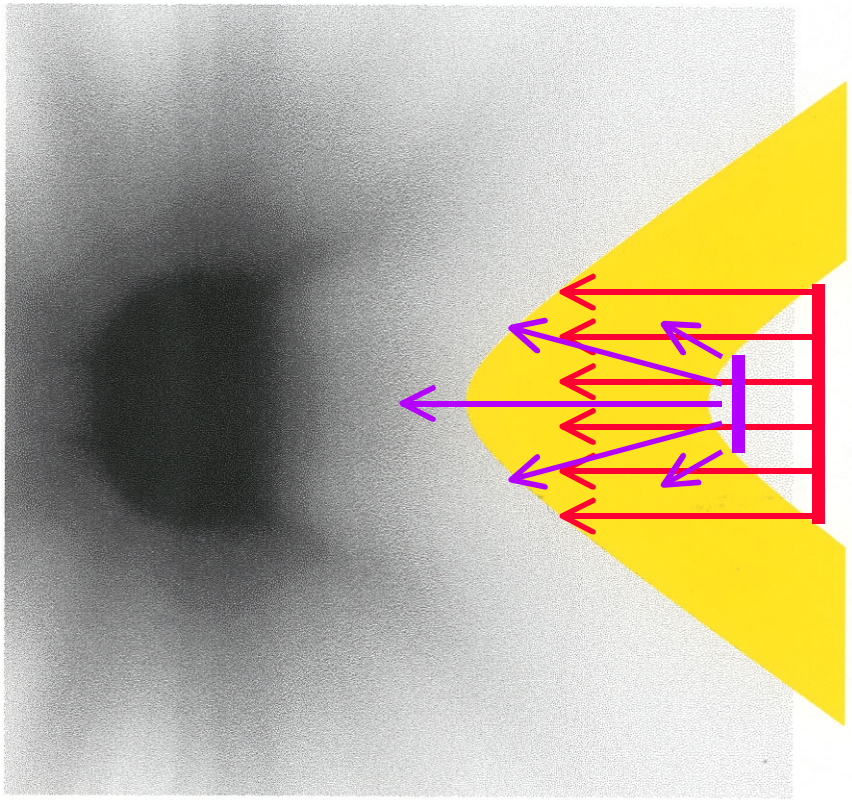

Launch mock e^-'s from some disk with some angular distribution. (collimated, or divergent)

Assume pulse duration of 10 ps.

Optimize e^- energy for best coupling to blob. Here optimum was 0.8 MeV for mock e^-'s corresponding to ~1.6 MeV for real e^-'s

Look at effects of varying total e^- energy (varying total short-pulse laser energy, assuming 50% conversion.)

CAVEAT: Mock e^-'s travel in straight paths, so all transport that changes paths is "modelled" by the initial disk/angle distribution.

Heating is the clear signature of laser conversion, beam transport, and coupling. For FI, we have to heat the blob.

The experimental objective should be spatially resolved measures of the heating — x-ray and (possibly) neutron images.

Baseline is image set with no short pulse laser:

X-rays
[$\log_{10}$ photons/keV/μm^2/10^{-8}sr @ 6 keV]

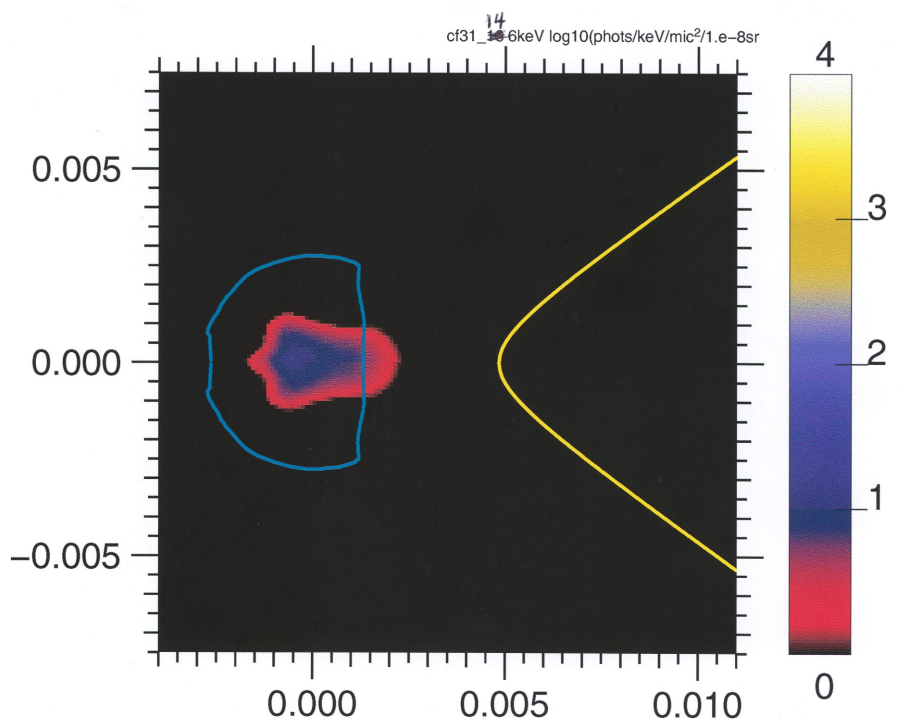

Neutrons
[neutrons/(10 μm)^2/10^{-6}sr]

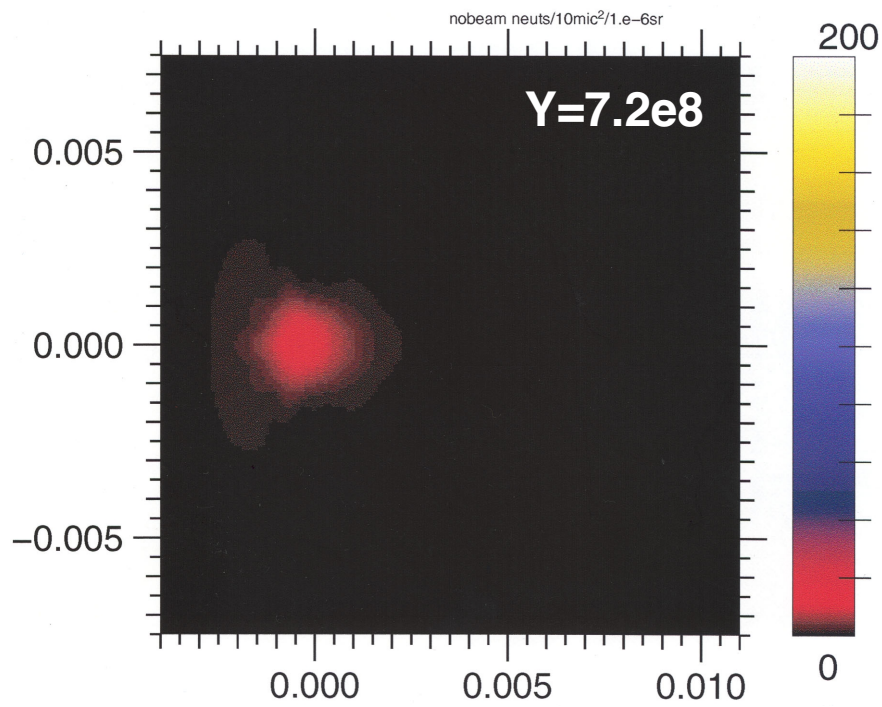

$E_{short\ pulse}$~2.6 kJ ($E_{e\ beam}$ ~0.5 kJ) would allow heating diagnosis on OMEGA implosions

T_{ion} [keV] | **X-rays - 6 KeV [$\log_{10}$ photons/keV/μm^2/10^{-8}sr]** | **Neutrons [neutrons/(10 μm)^2/10^{-6}sr]**

Collimated transport
50 μm diam. beam

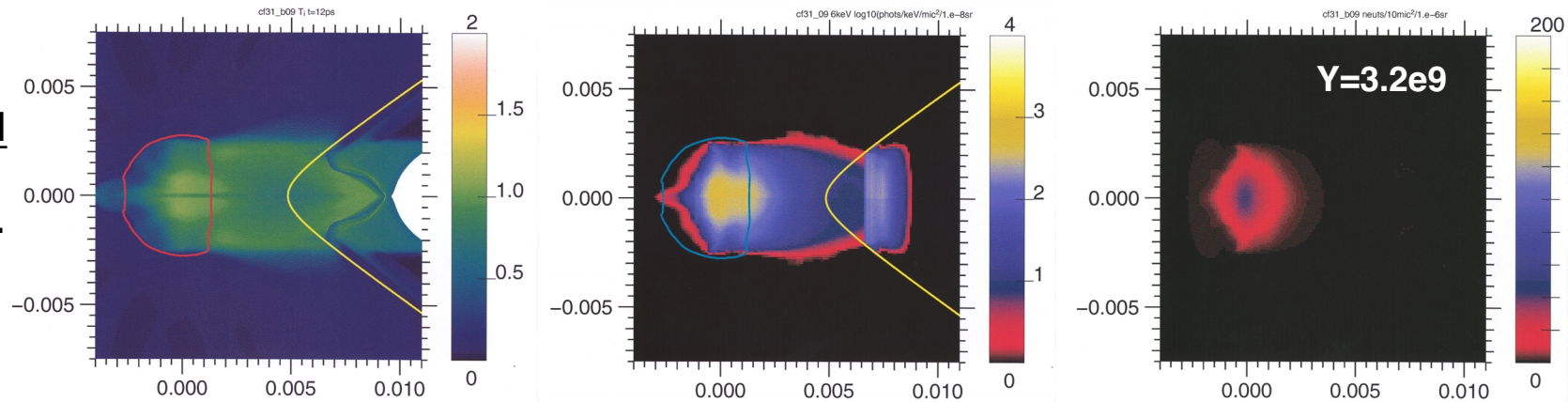

Divergent transport
40° FWHM

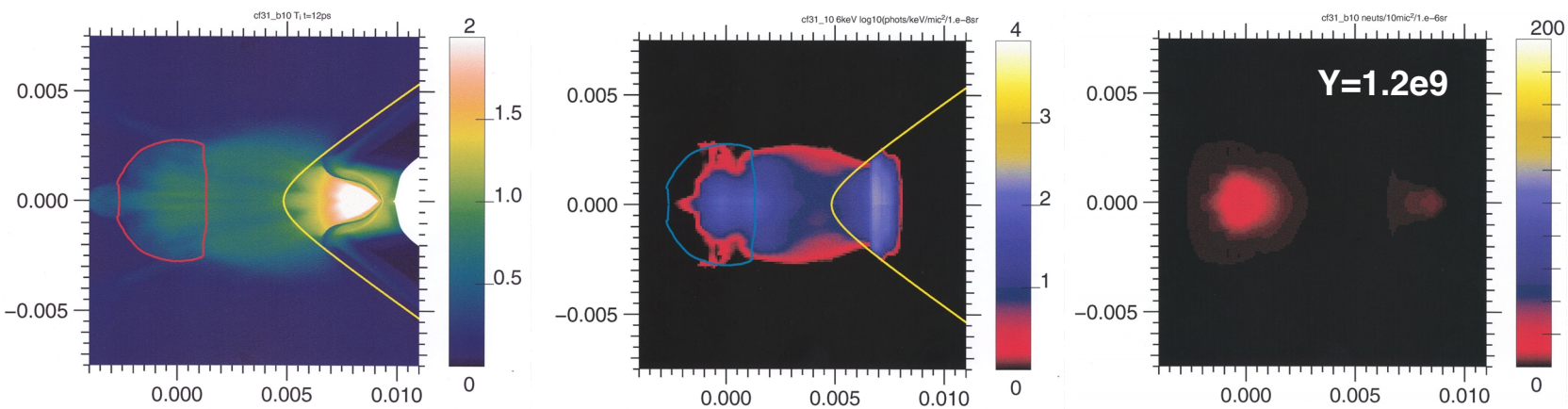

Better spot quality ($E_{e\ beam}$ ~1.3 kJ) could give dramatic data.

T_{ion} [keV]

X-rays - 6 KeV [$\log_{10}$ photons/keV/μm^2/10^{-8}sr]

Neutrons [neutrons/(10 μm)^2/10^{-6}sr]

Collimated transport 50 μm diam. beam

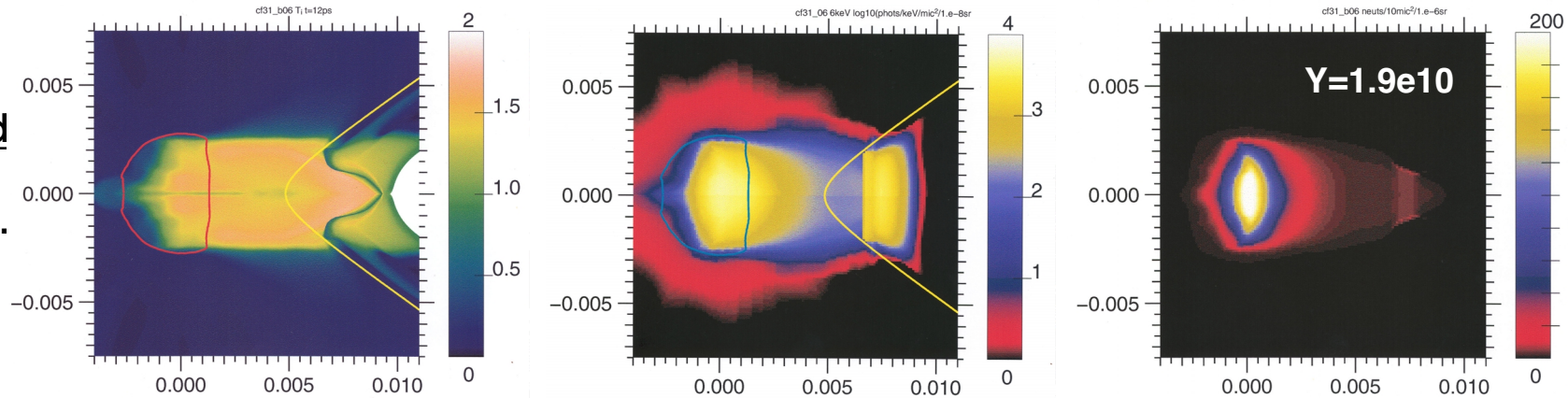

Divergent transport 40° FWHM

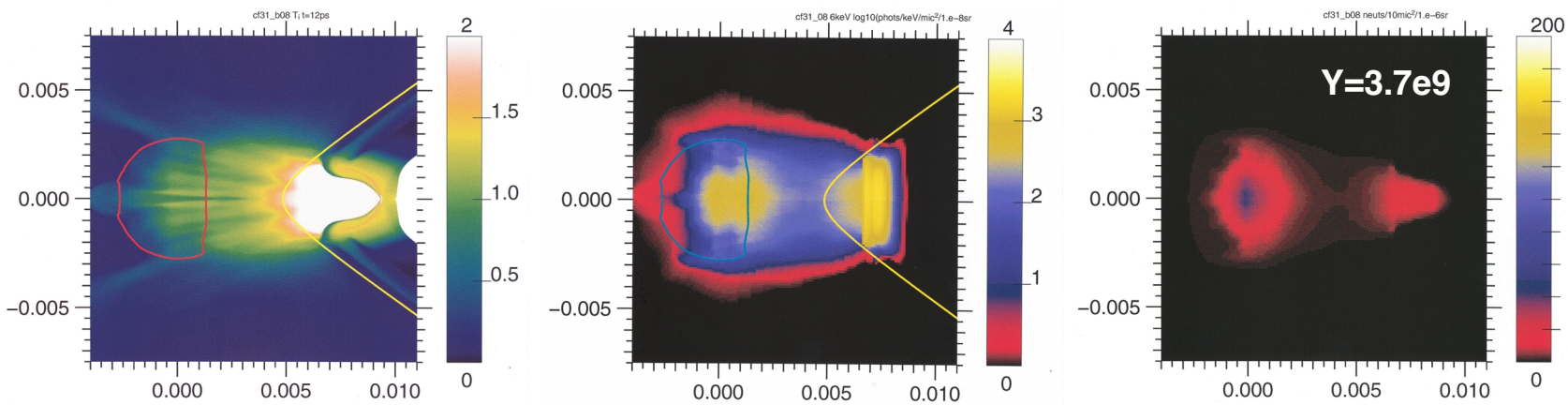

Neutron imaging may help to fully interpret neutron data:

Neutrons
[neutrons/(10 μm)^2/10^{-6}sr]

No short pulse

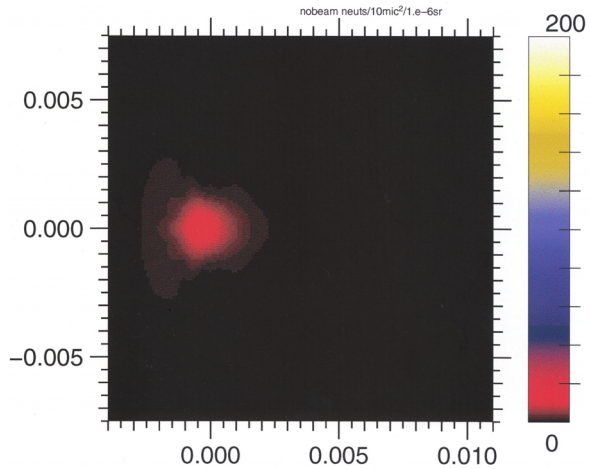

Y_n = 7.2 x 10^8

$E_{e\ beam}$ ~1.3 kJ
<u>Divergent</u> transport
40° FWHM

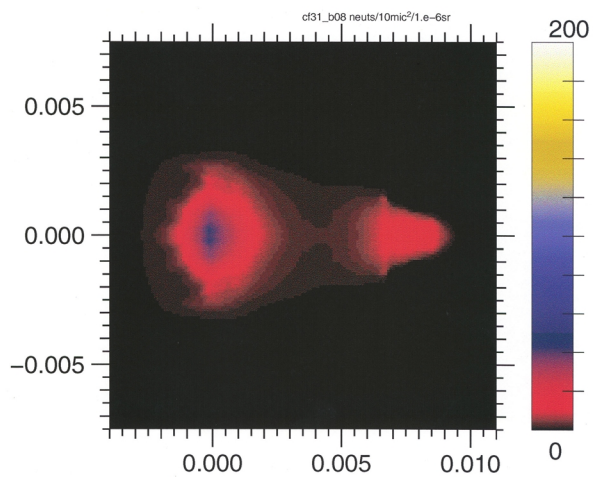

Y_n = 3.7 x 10^9 [~5X]
(much from near cone)

Sub-ignition implosion density and temperature conditions are highly relevant to full-scale FI.

- **Dense blob and intervening matter are hot**, T~several x 10^2 eV, *before* short pulse; elec. conductivity is well into Spitzer regime. CD_2 conductivity ~ 1/3 D_2 conductivity.

- **Electrical conductivity is high enough** that hot-e beam does not have to expand to support an equal return current.

- **Magnetic and scattering effects on hots are comparable**, assuming $I_{net} \sim I_{Alfvén,}$: Hots scatter through ~1- few radians (rms) while traversing ~1 beam radius.

“Highly relevant to full-scale FI” , in more detail, means:

$I_{hot} >> I_{Alfven}$ (where hot e$^-$ gyroradius ~ hot e$^-$ beam radius)

so $I_{hot} \approx I_{cold,return}$

Ohm’s Law : $I_{cold} \approx E\,\sigma\,\pi r_{beam}^2$

$eEL_{beam} << T_{hot}$?

NO in current experiments with PW lasers on solid targets

YES in these proposed NIFand OMEGA experiments.

Electrical conductivity between cone and blob (Lee and More) is in "Spitzer" regime, and high enough that the hot e^- transport is not dominated by resistive effects:

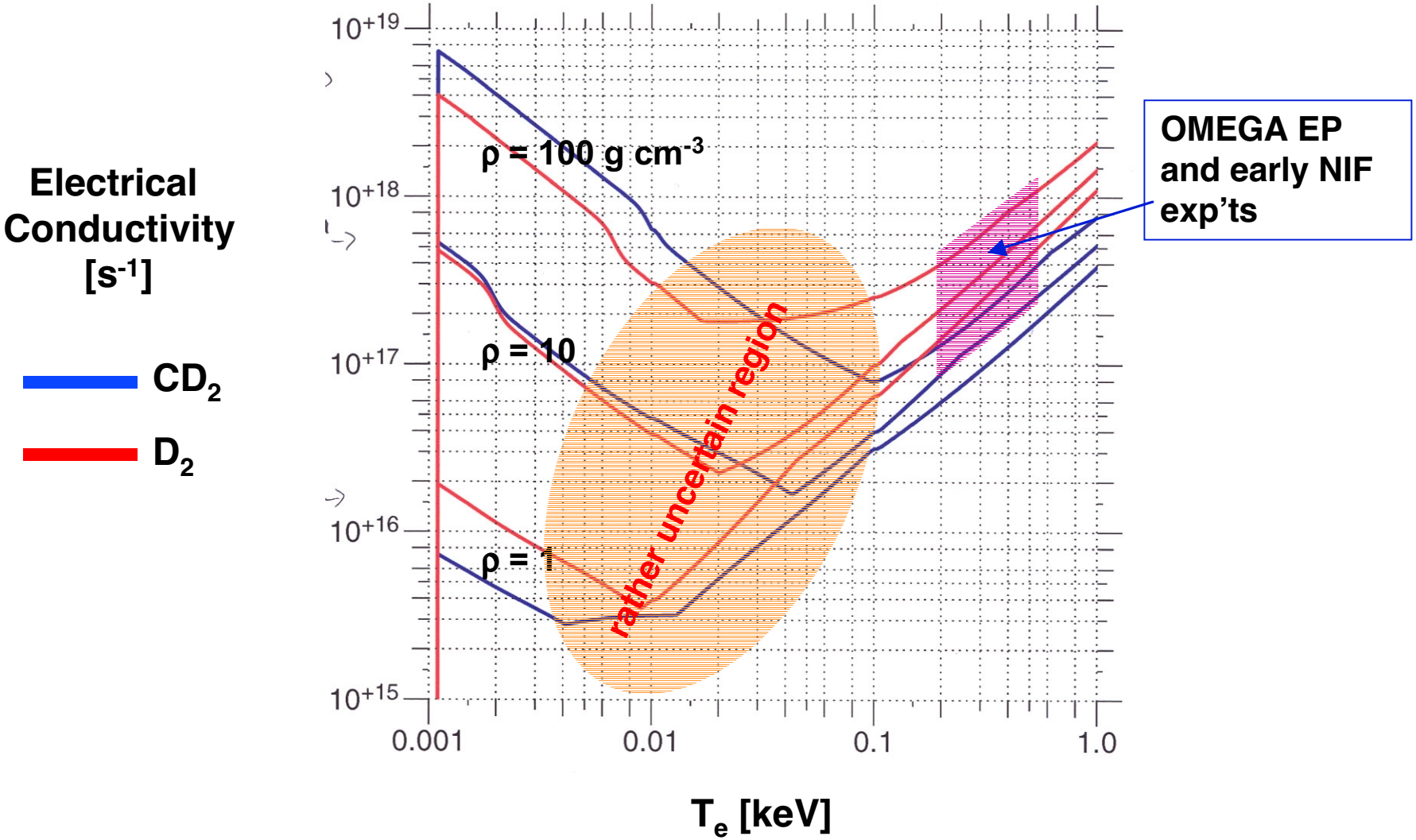

Cryogenic targets introduce significant fabrication difficulties, but would be a test of the real thing.

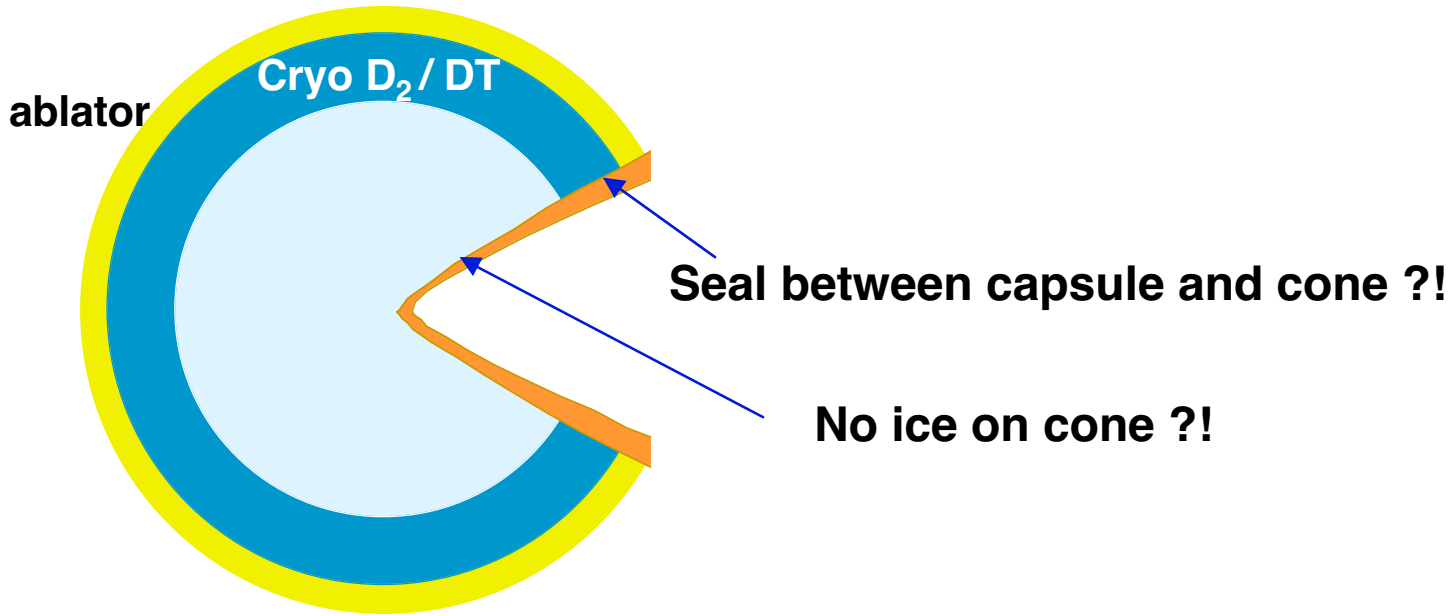

- D_2 elect. conductivity is (only) ~3x CD_2
- Experiments with different materials might give insight into transport and coupling.
- Collisionless deposition (to Langmuir turbulence) may be different in hydrogen.

Summary:

Cone-focussed, sub-ignition experiments on NIF and/or Omega EP could provide the evidence for the transport and coupling required for FI — in highly FI relevant conditions.

- **Cone-focussed, NIF and/or OMEGA-EP implosions can produce highly relevant, hot, high density, high electrical conductivity beam path conditions (without cryogenics).**
- **Short pulse energy requirement: must increase internal energy of the imploded blob by >~ 50%**
- **X-ray and neutron images should then show where and by how much the hot electrons have heated the plasma —demonstrate geometry and efficiency of transport and coupling**
- ***Proton* FI transport and heating efficiency can also be demonstrated.**
- **Early cryo experiments may be difficult; added value is, for now, hard to judge.**

CLRC

The Vulcan Petawatt Interaction Facility

MHR Hutchinson, JL Collier, CN Danson, CB Edwards,
D Neely and B Wyborn

Central Laser Facility,

CLRC Rutherford Appleton Laboratory
Chilton, Didcot, Oxfordshire, U.K. OX11 0QX
h.hutchinson@ rl.ac.uk

Outline

- Specification
- Technical Approach
- Current Status

Technical approach: 1PW; 10^{21} W.cm^{-2}

3 x 208mm aperture disc amplifiers to boost energy with low B - integral; 600mm output to avoid grating damage

$$\text{Irradiance on target} \sim \frac{\text{Beam energy}}{\text{Pulse duration} \times \text{Spot size}}$$

enhanced bandwidth using OPCPA front end

adaptive optics for ~ diffraction limited performance

Upgrade schematic

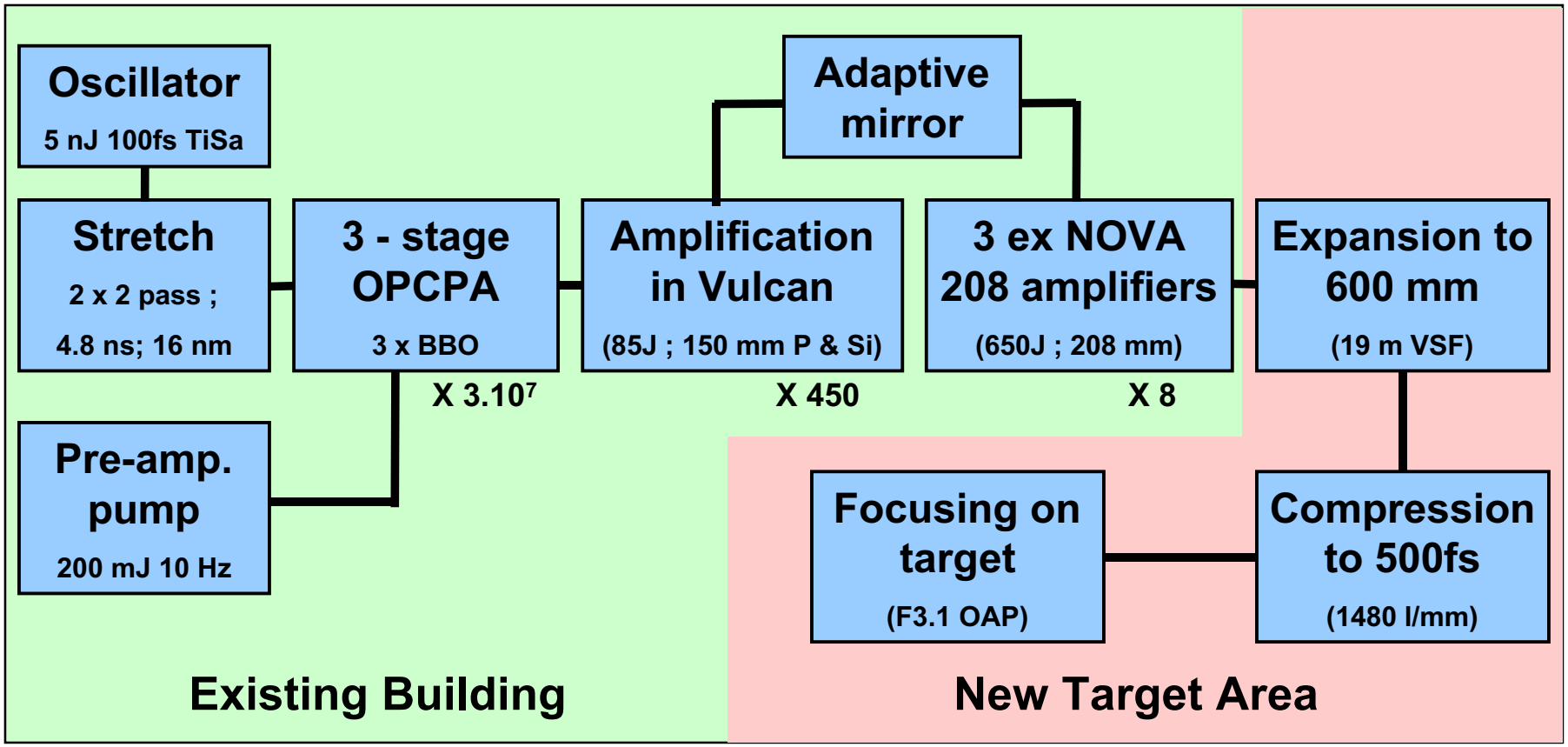

Vulcan PW Specification

- Output Energy 670 J
- Energy on Target 500 J
- Pulse Duration on Target 500 fs
- Output beam diameter 600 mm
- Flux on Compressor Gratings 170 mJ. cm^{-2}
- **OPCPA** front end preserves bandwidth & contrast
- **Adaptive optics** to give beam quality close to d.l.

The OPCPA scheme

OPCPA uses the pump laser efficiently:

long pulse
narrow bandwidth
non-diffraction limited
B-integral ~3

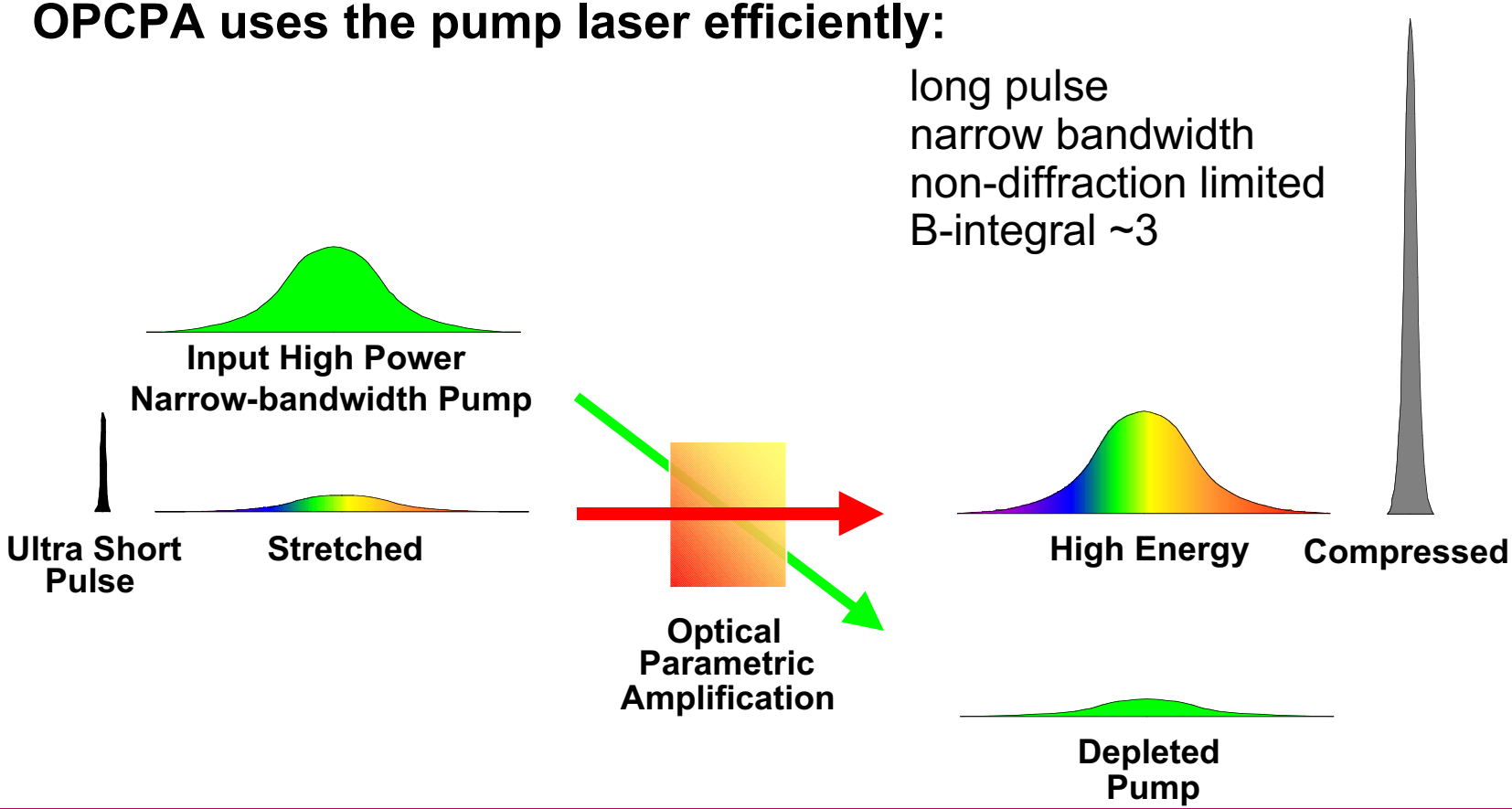

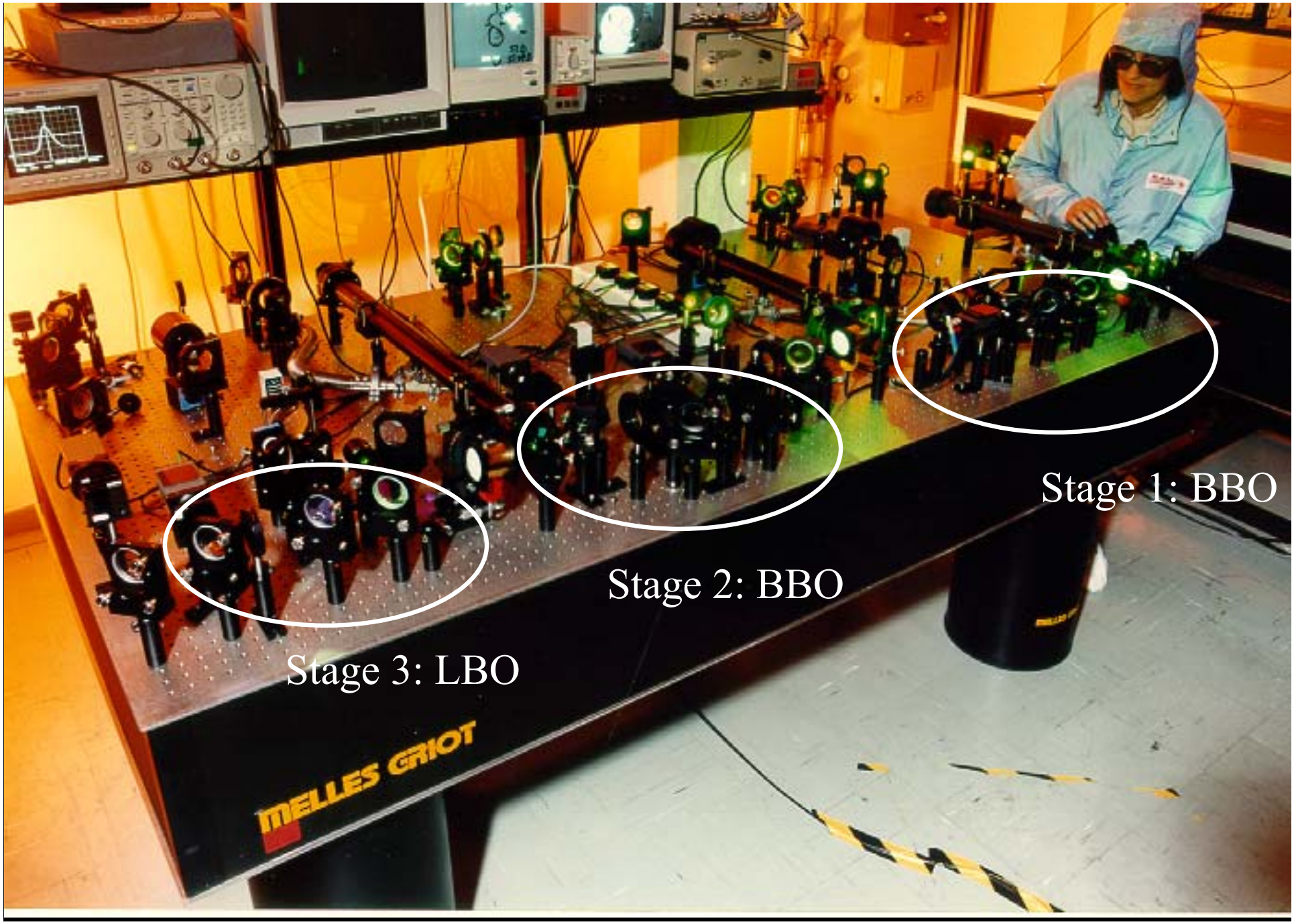
Stage 1: BBO
Stage 2: BBO
Stage 3: LBO
MELLES GRIOT

Bandwidth delivery for PW power

OPCPA pre-amp to 10 mJ:

Input bandwidth	16 nm
Input stretched pulse	4.8 ns

Nd:glass amp to 500 J:

Output bandwidth	4 nm
Output stretched pulse	1.2 ns
$\tau_{compressed}$	500 fs

achieved using mixed glass

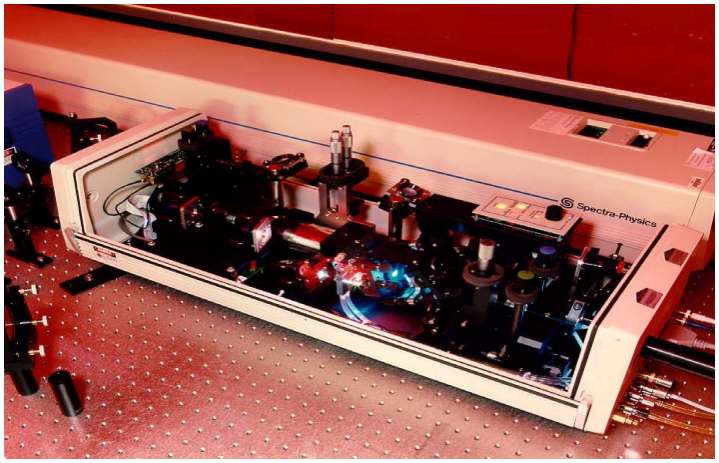

Energy diagnostics

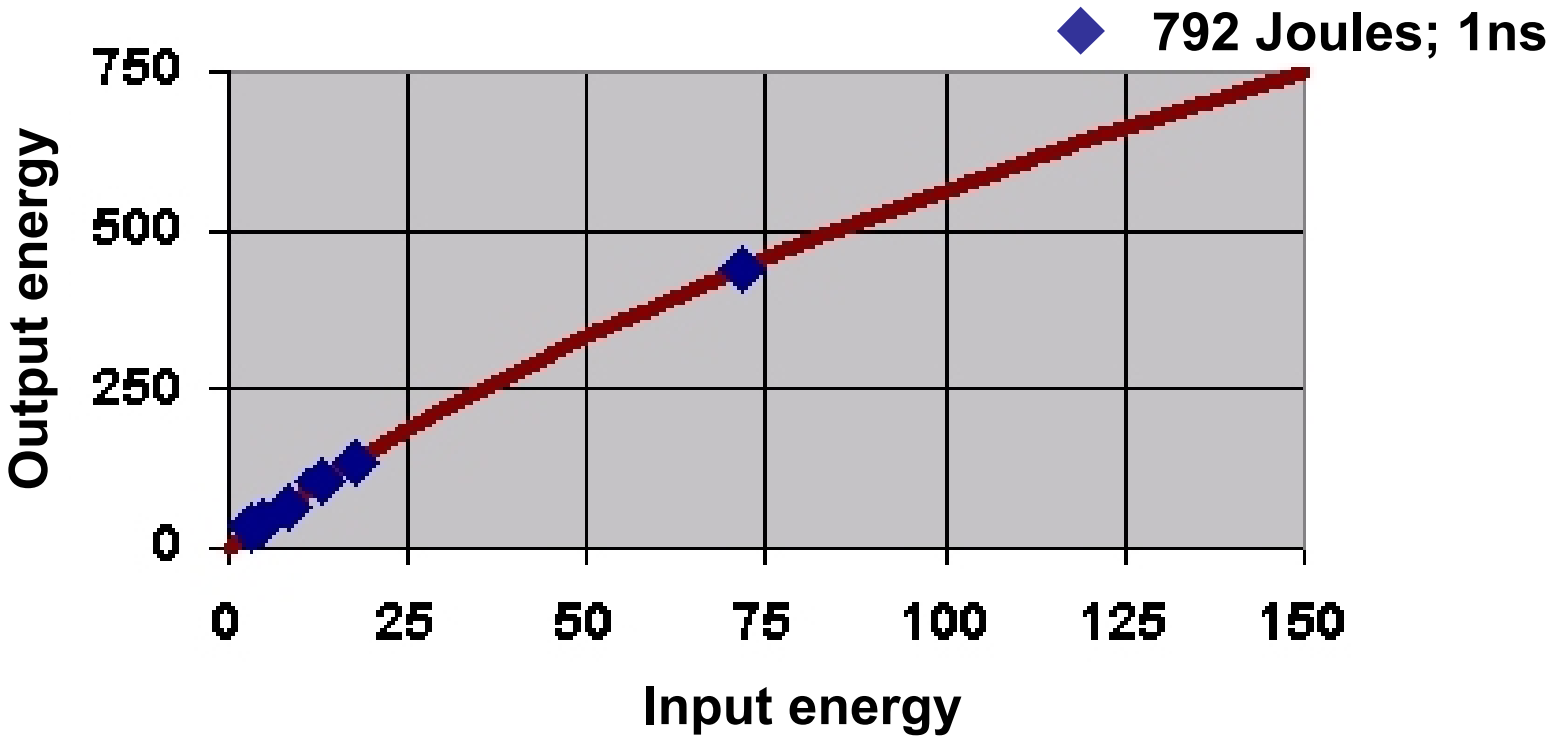

Compressor chamber

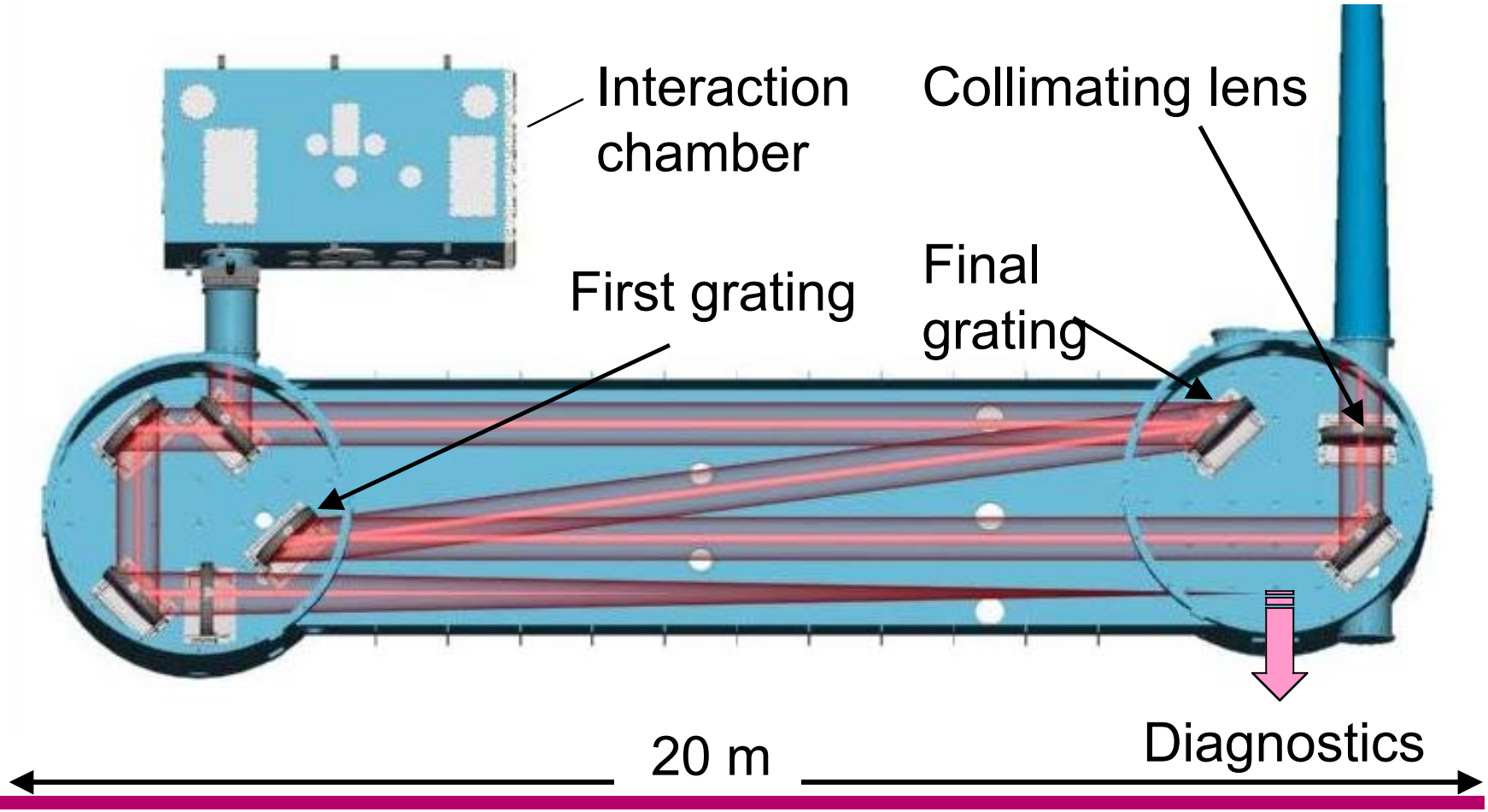

Petawatt Target Area

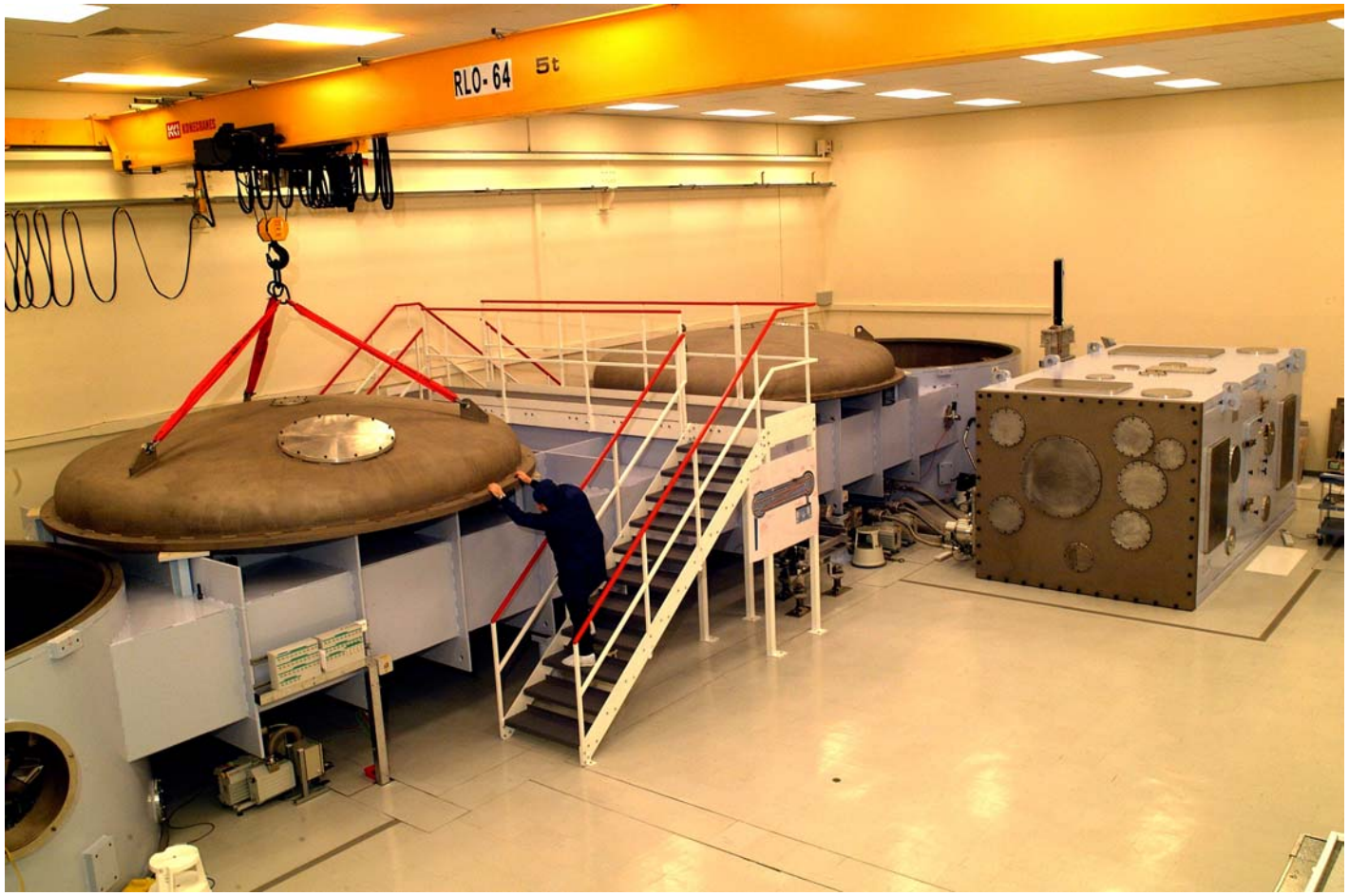

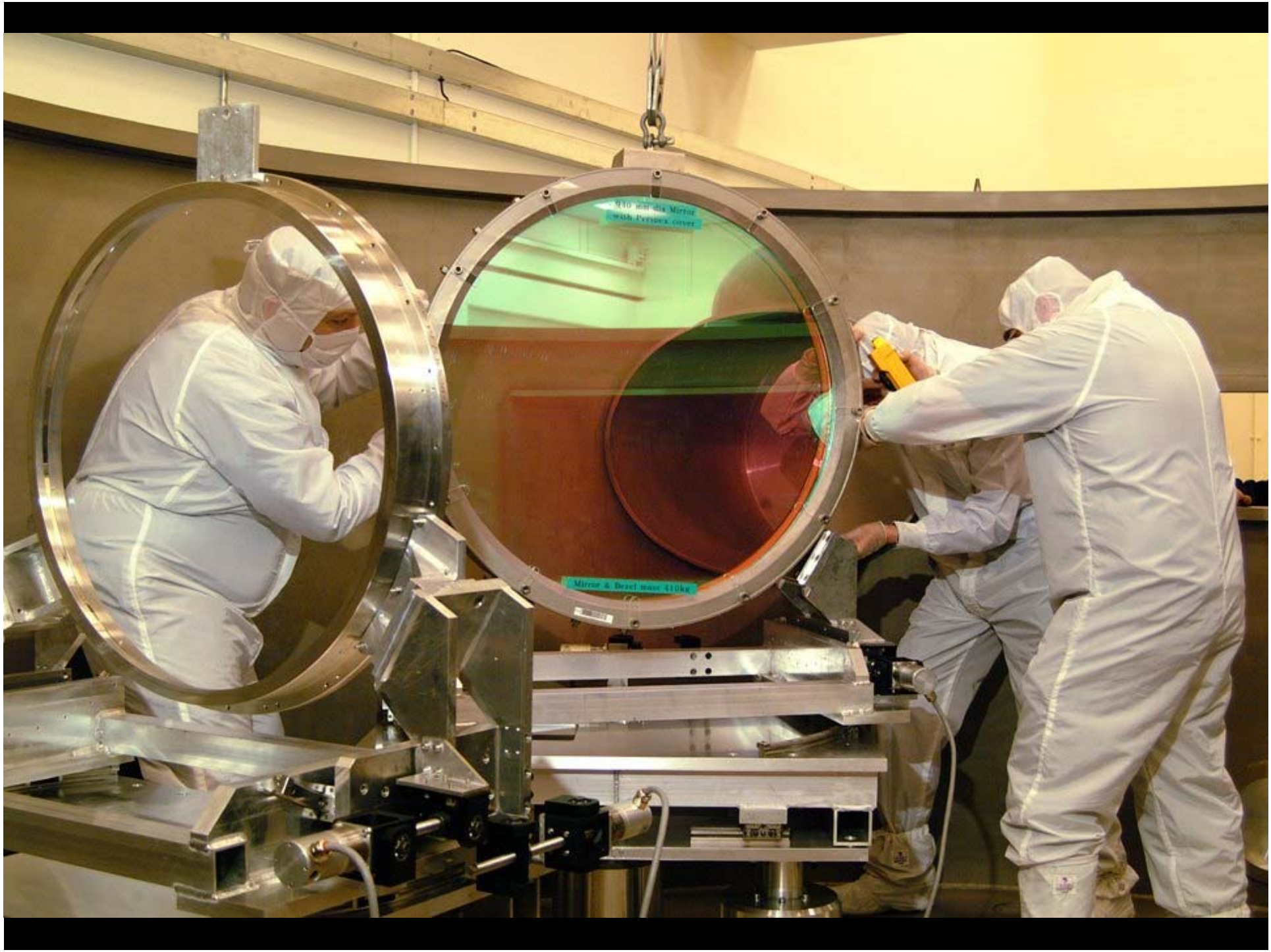
Mirror & Bezel max 410kg

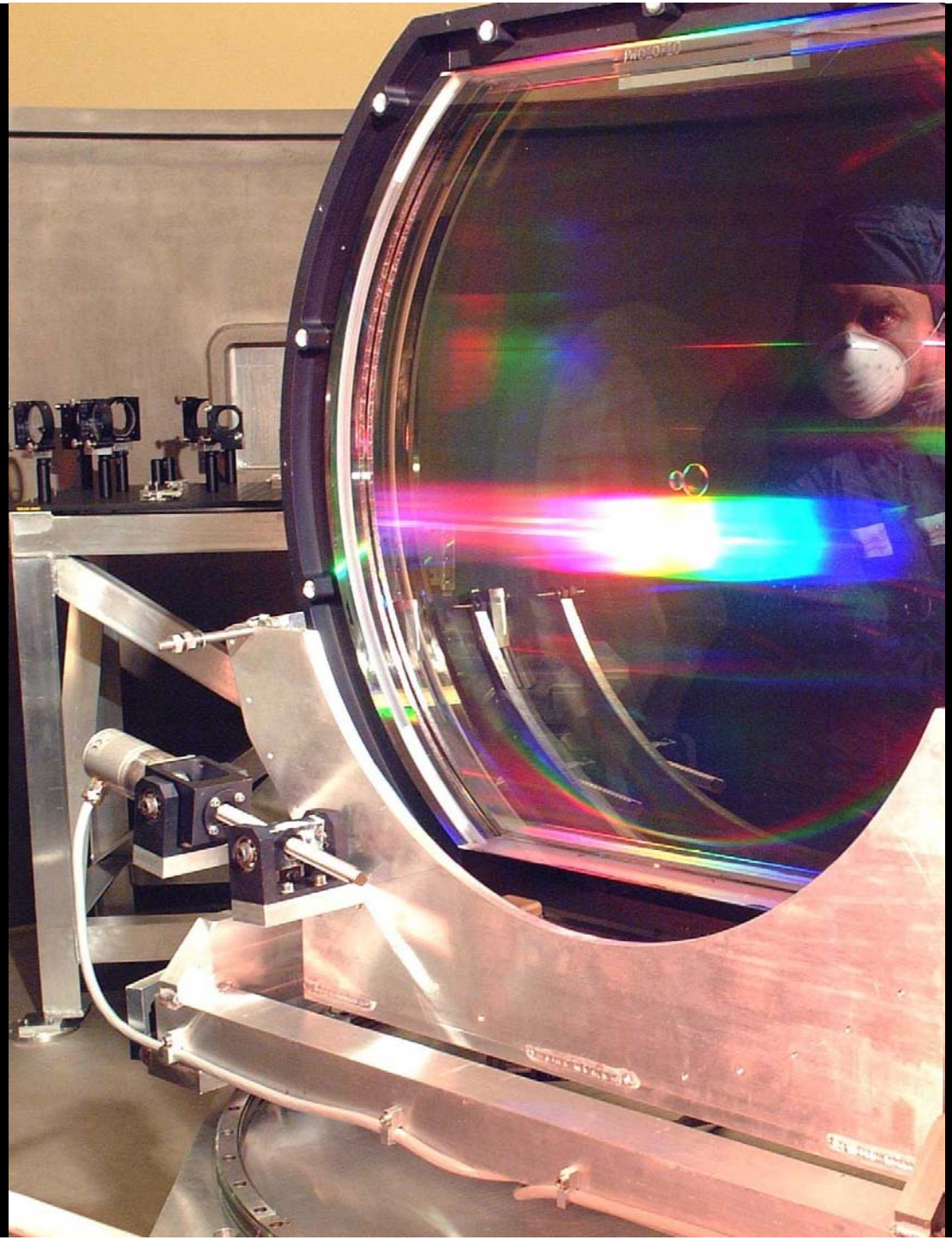

OPCPA Vacuum Compression

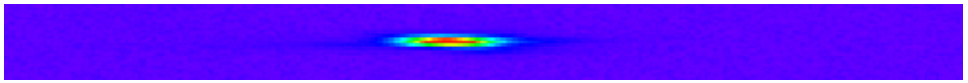

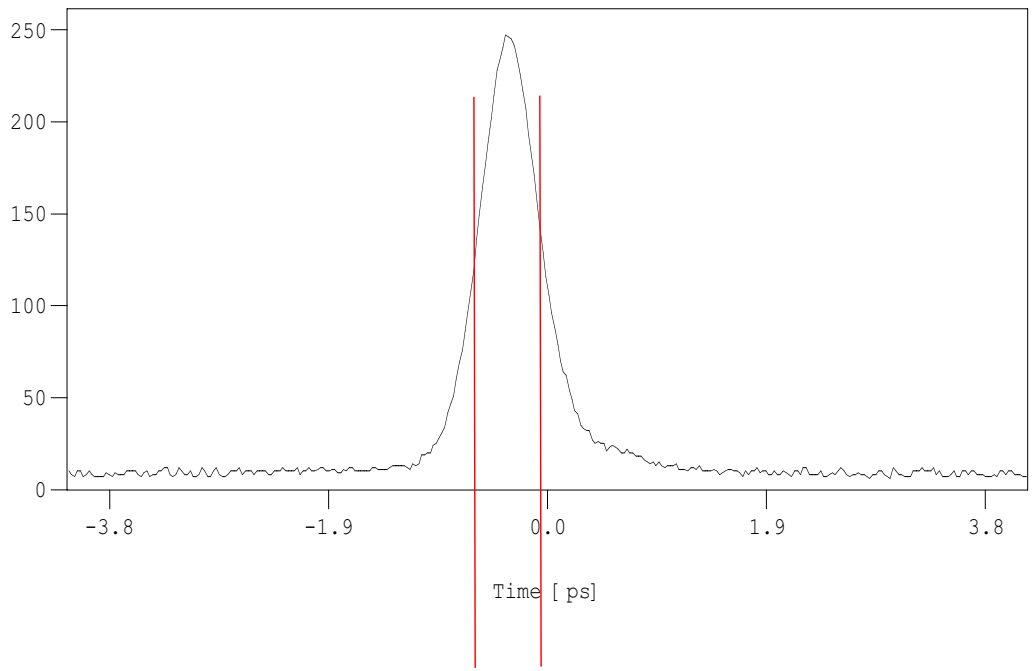

Duration 400 fs FWHM

10 mJ OPCPA 10Hz

Propagation through the Vulcan chain

Compression under Vacuum

Dispersion plane autocorrelator

Transform limited duration

Beamline Configuration for A.O. tests

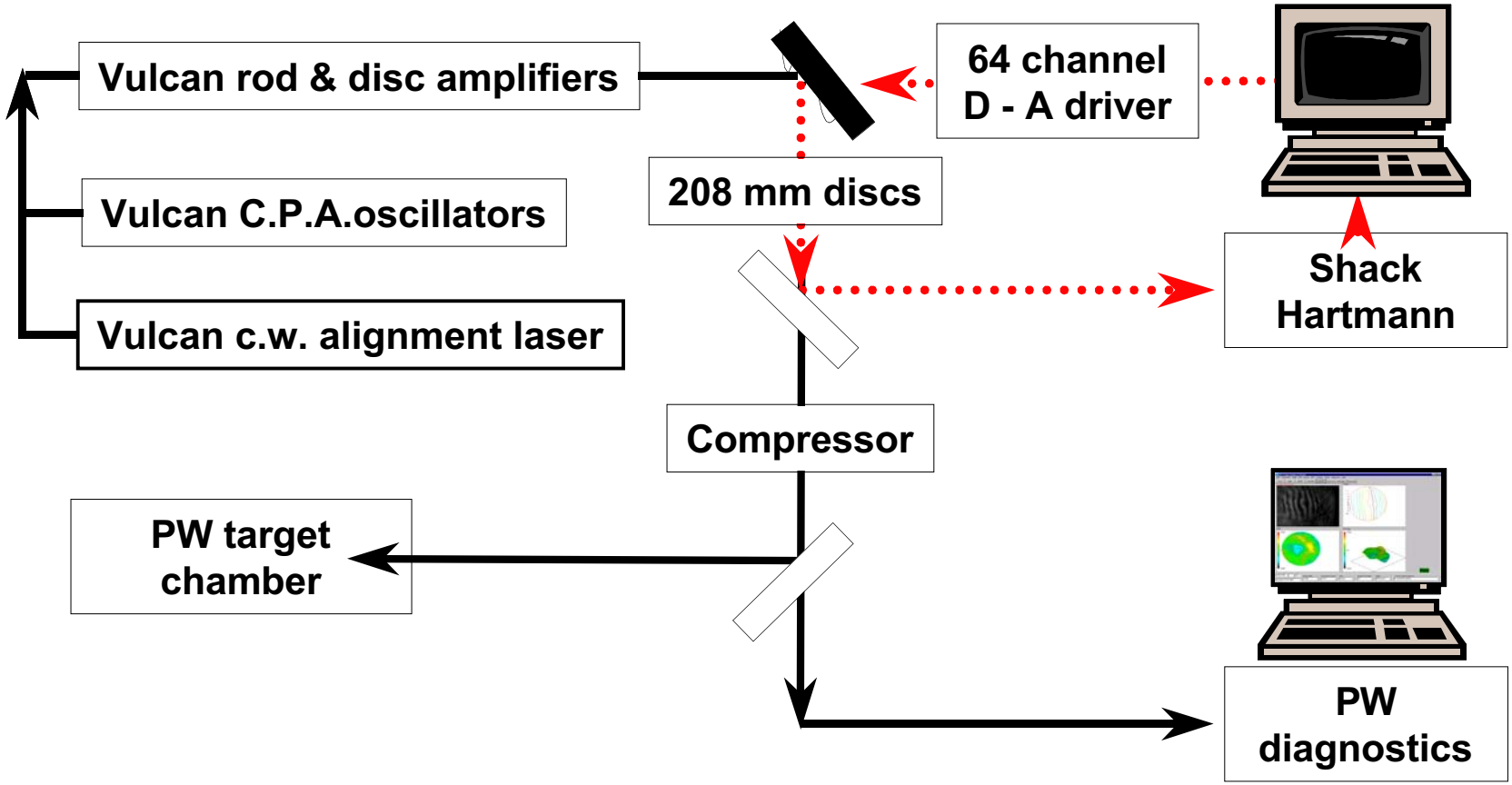

Adaptive Mirror

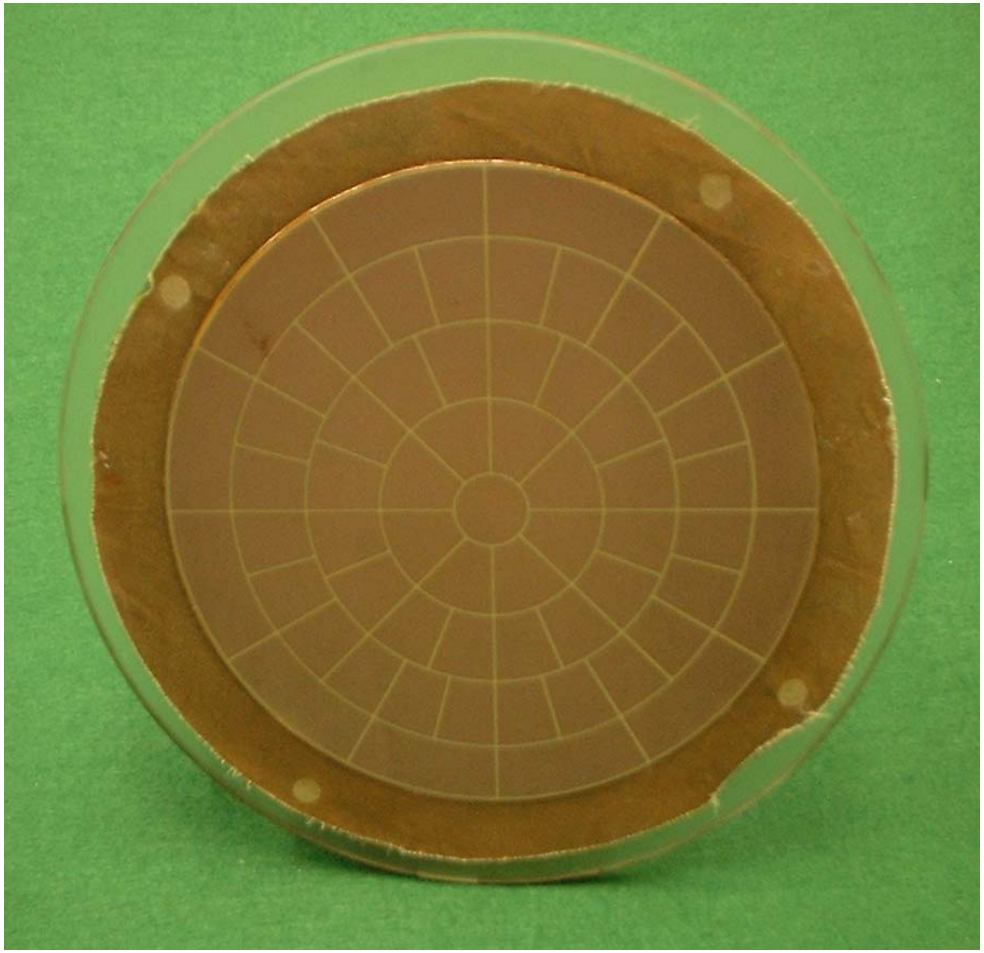

- 61 actuators; 49 within beam area
- Areas of central 49 are equal in area
- Mirror mount handles tip / tilt

AO sampling follows the 208 mm disc amplifiers

Adaptive optics makes a dramatic improvement to the focal spot

Pre - correction

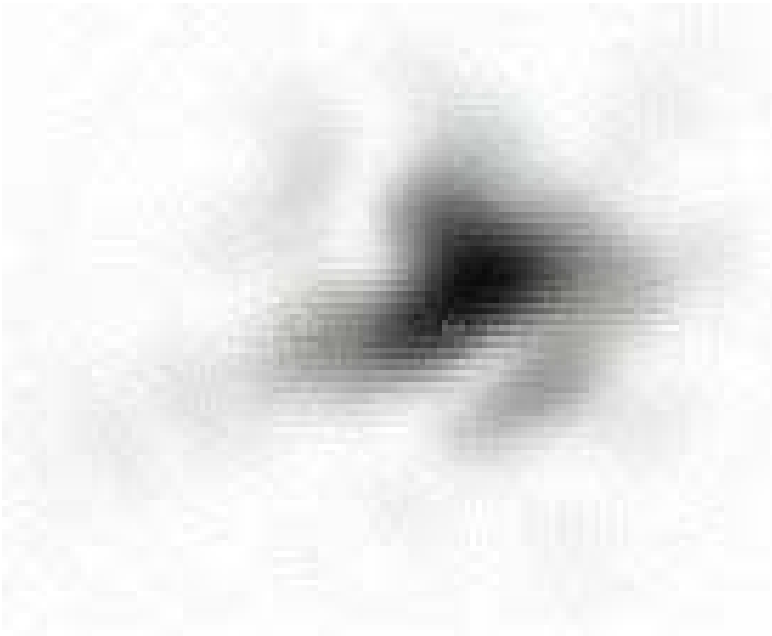

With correction

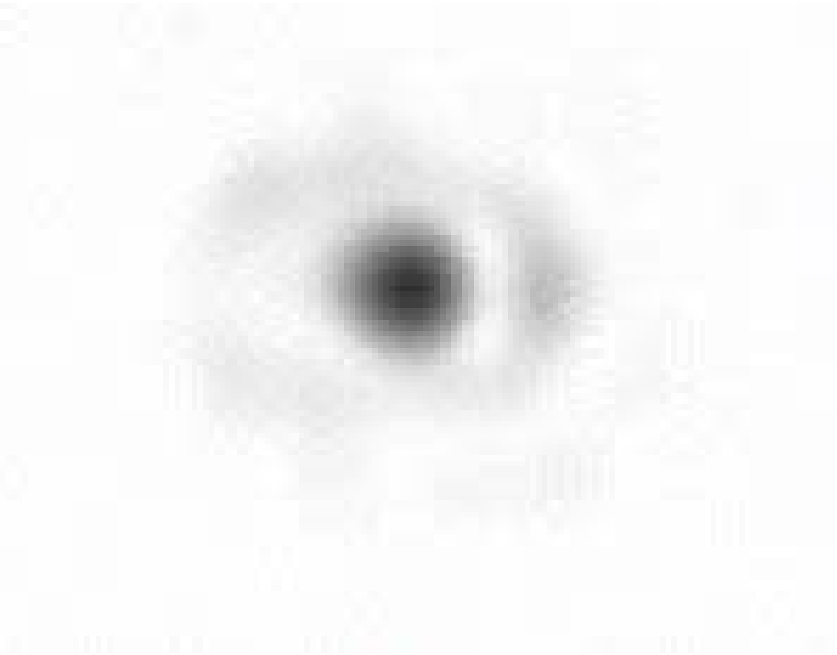

F#3.1 Off Axis Parabola

- XZ $\phi\theta$R distributed loading
- 5 μm reproducibility
- Dampening ~ 4 seconds

- f =1.8m, OAD =0.45 m
- ϕ =0.65 m
- λ/4 @ 632 nm
- λ/4 per cm

Point spread function

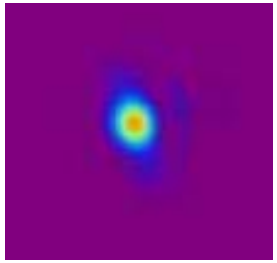

5 microns

Focal spots in focal plane of 600 mm F#3 OAP after vacuum compressor

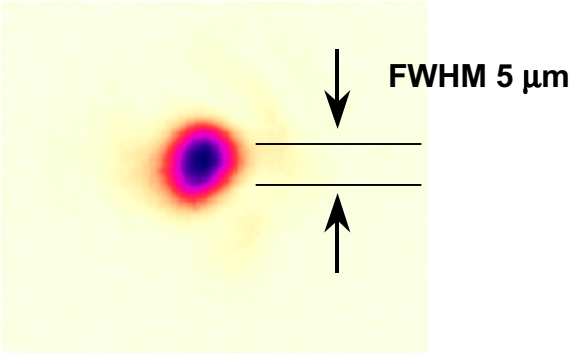

Narrowband CW Reference Beam

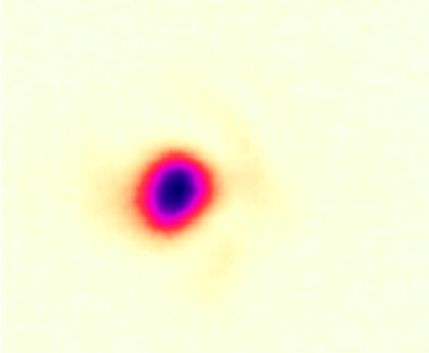

Vulcan Corrected Narrowband CW Beam

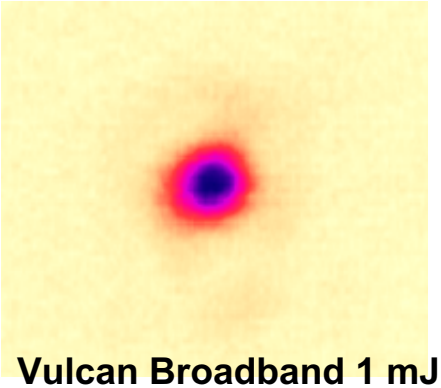

Vulcan Broadband 1 mJ Shot (9 sec cycle)

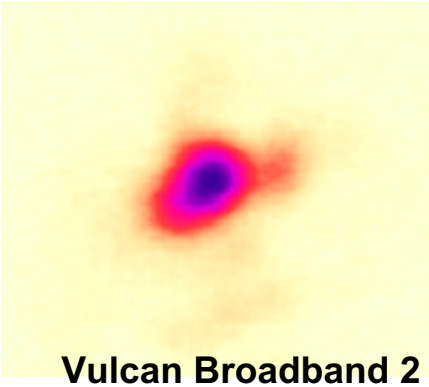

Vulcan Broadband 2 J Shot (Rods)

Interaction chamber

2.5 m

- 20 m^3 Interaction volume
- Finite element analysis stress calculations

Maximum side wall deflection <1 mm

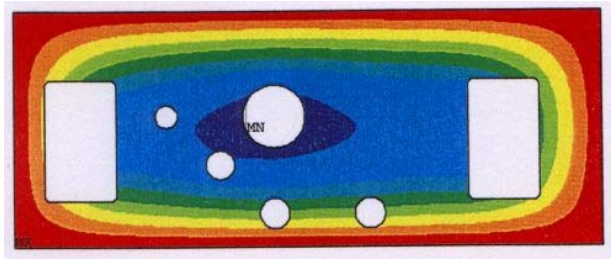

- Walls are 120 mm thick steel
- Floor is 120 mm thick steel and secured by array of 32 pre-tensioned bolts: *Maximum floor deflection <5 μ*

γ Shielding

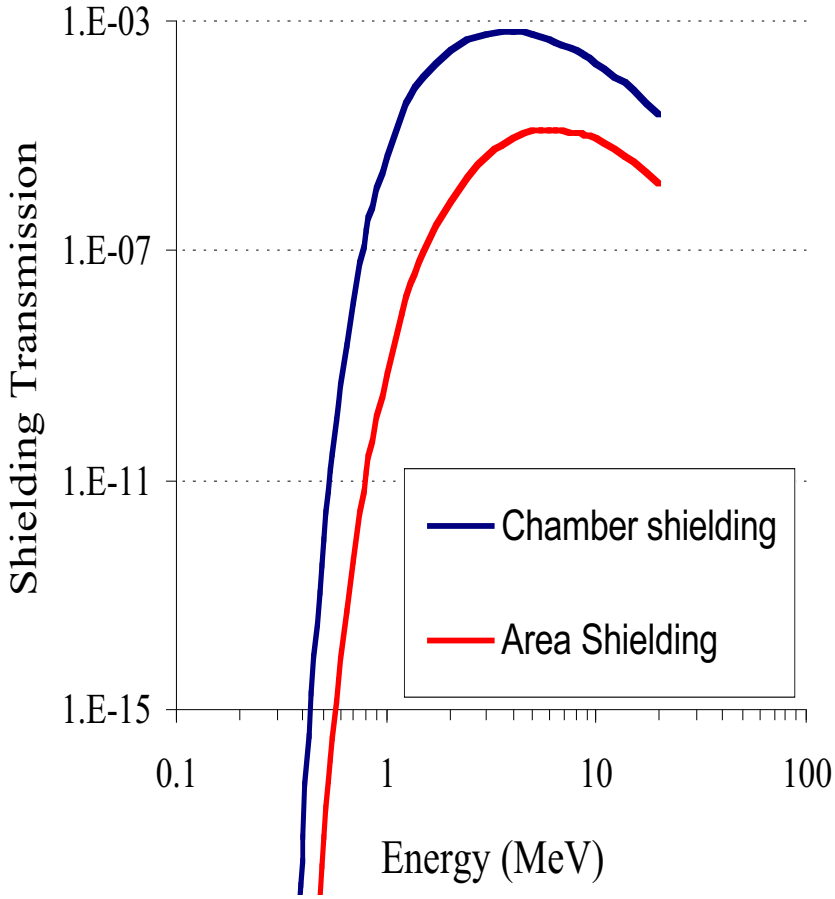

Chamber shielding	X 1000 @	4 MeV
Area shielding	X 50,000 @	6 MeV

Shielding Design

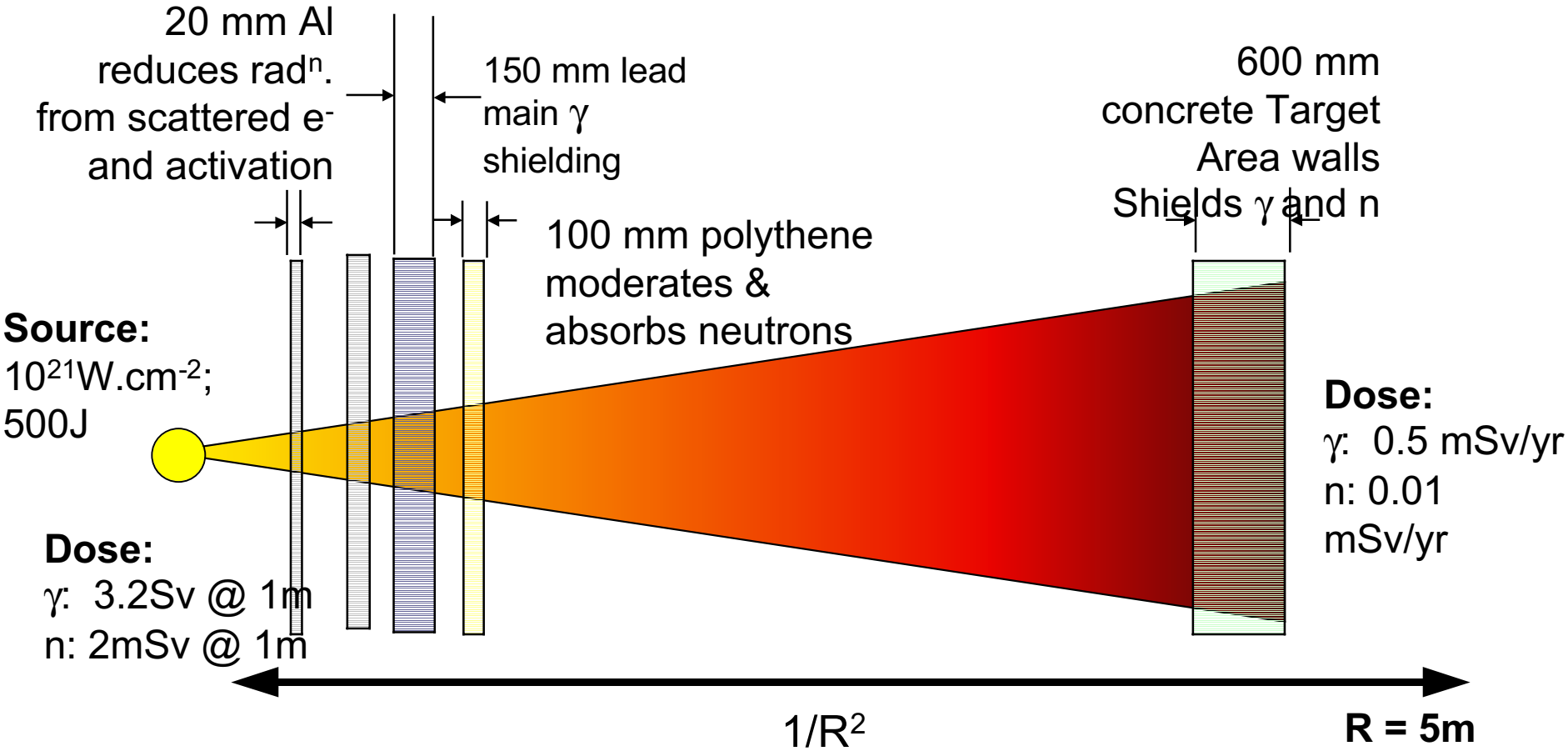

Neutron Shielding

- 600 mm concrete walls
- 5% Borated plastic on roof
- 100 mm high density polyethylene

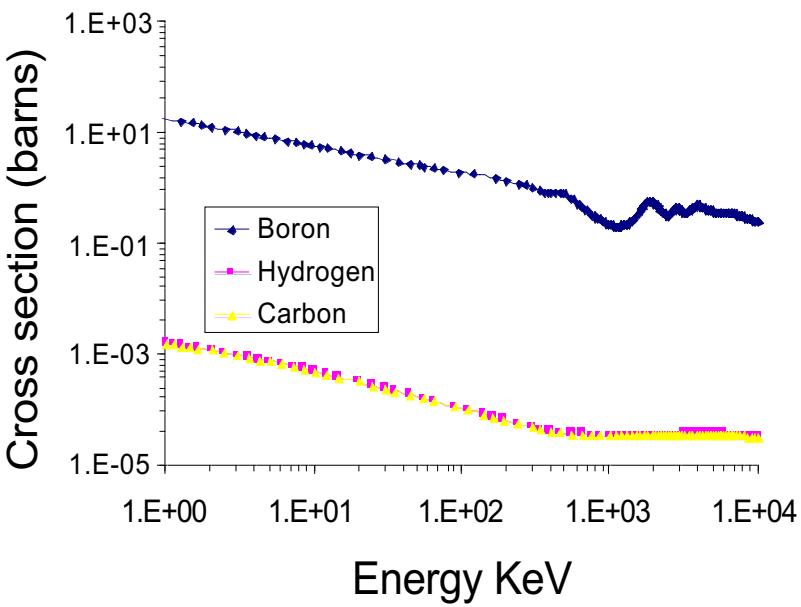

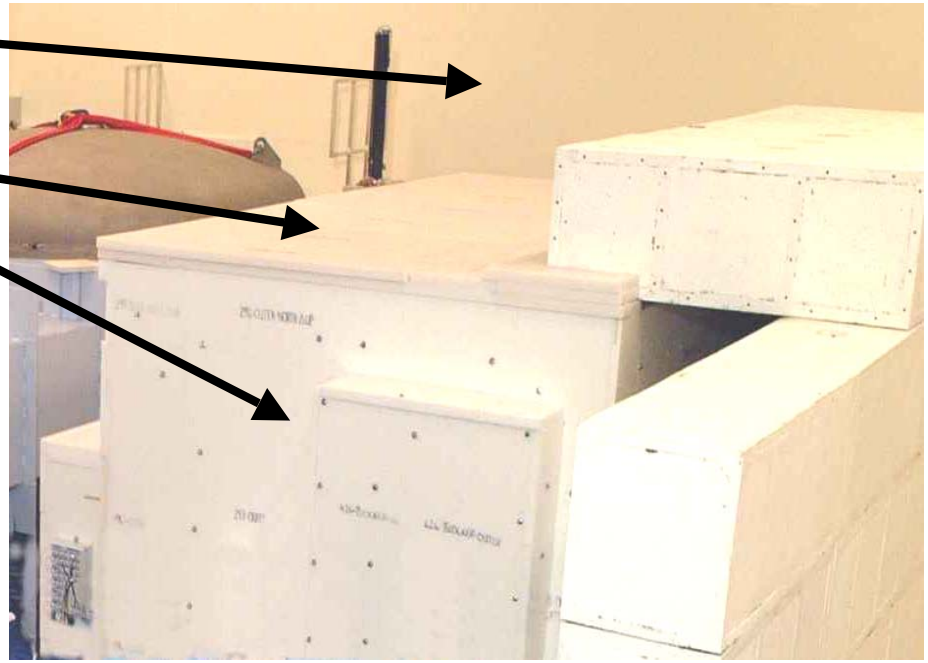

- 2 mSv / shot @ 1 m
- 0.01 mSv per year outside area

Commissioning

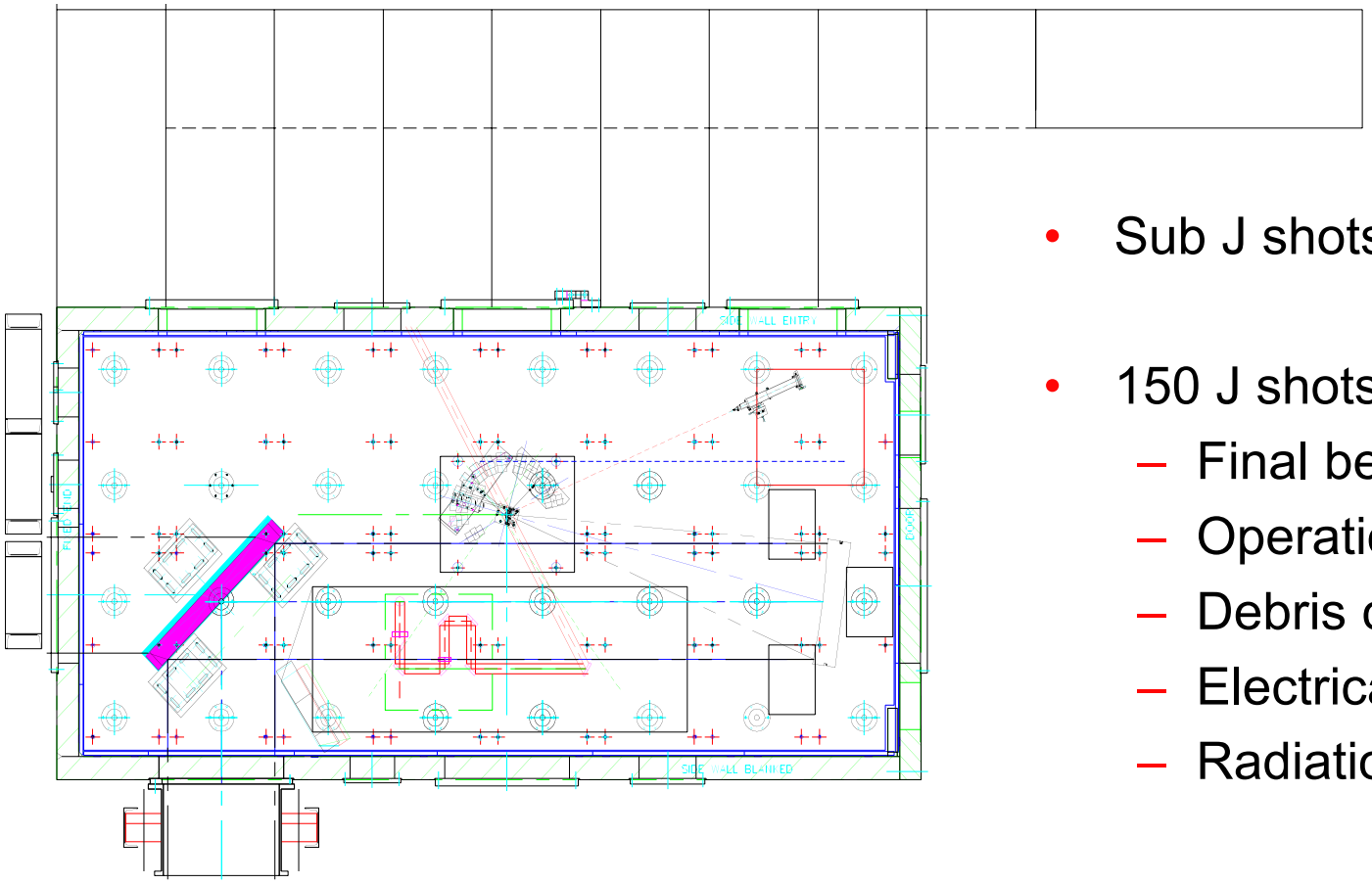

- Sub J shots June 2002
- 150 J shots Sep/Oct 2002
  - Final beam quality
  - Operational experience
  - Debris characterisation
  - Electrical noise
  - Radiation shielding

γ Distribution

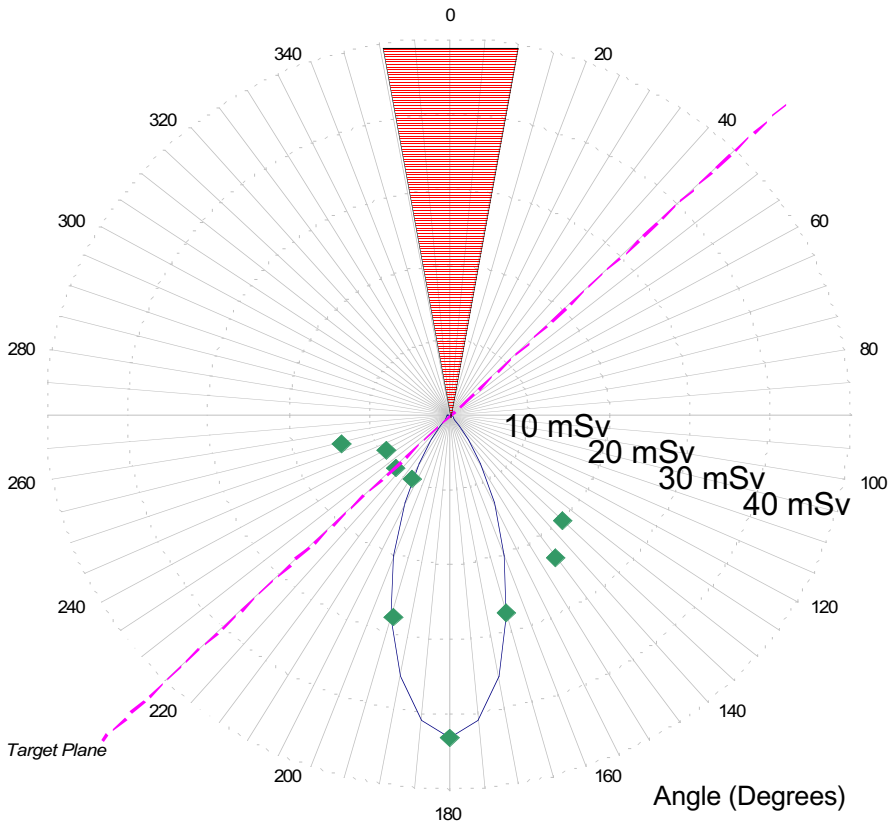

- 1mm Gold Target @ 45º
- 400TW on Target
- 4×10^{20} W/cm^2
- 43 mSv peak forward dose

Intensity on Target

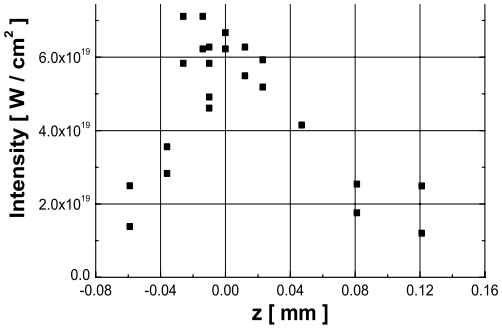

0.5 mm wide crater produced by 60 J shot on gold

45deg angle of incidence, 30% of energy contained in FWHM of focal spot, 65% throughput @ 1.4 ps

•Debris shielding ?

Status of Commissioning

- The full energy specification is now available from the laser
- Shielding has been verified at 400TW using a gold target; 43 mSv @ 1 metre (γ) in the chamber; insignificant dose detected outside
- The energy will be increased to 0.5 PW on target during November, with a user experiment in December, 2002.
- The energy will be increased gradually to give PW performance early in 2003

Acknowledgements

Petawatt Laser Heating of High-Density Plasmas

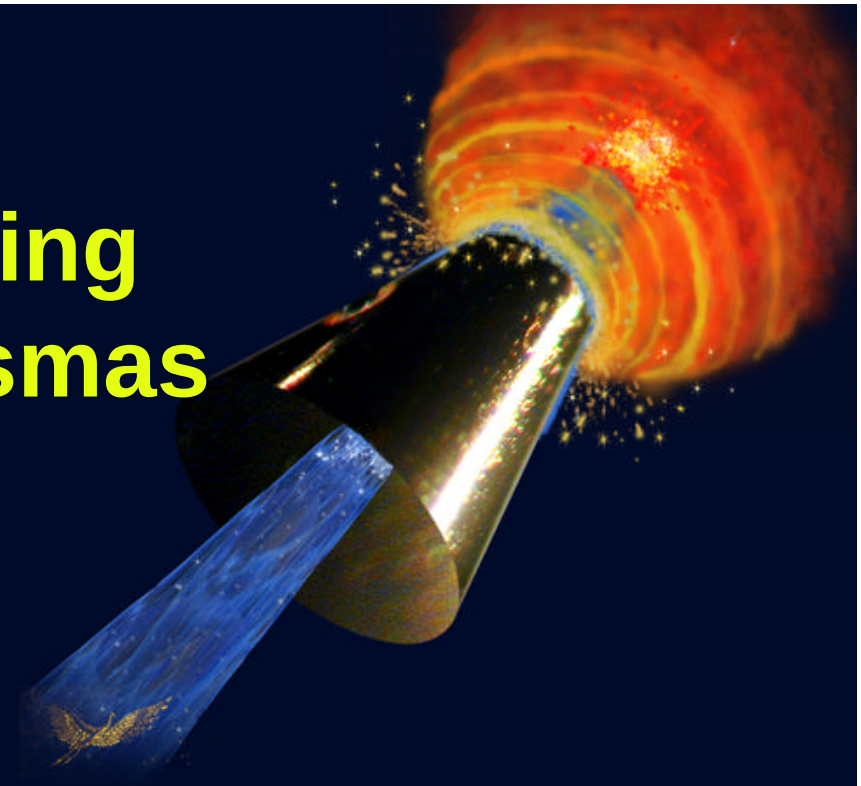

- contents
  - summary of FI research at ILE Osaka
  - demonstration of enforced heating
  - heating physics
  - summary and toward ignition and burning

Ryosuke Kodama

Institute of Laser Engineerign, Osaka Univ.

6th workshop on FT of Fusion target
2002. 11.17
At St. Petes Beach Florida

Co-authors

ILE Osaka Univ.

K. A. Tanaka, Y. Kitagawa, K. Mima,
H. Azechi, H. Nishimura, H. Shiraga, M. Nakai K. Shigemori,
H. Fujita,H. T. Jitsuno,
T. Norimatsu, K. Nagai, S. Sakabe, N. Miyanaga, Y. Izawa
T.Yamanaka,
Y. Toyama, T. Miyakoshi, M. Tampo, H. Fujioka, A. Ahamed
H. Yoshida, K. Sawai, Y. Kimura T. Kawasaki,
O. Maegawa, K. Suzuki, S. Matsuo

P. A. Norreys(RAL), H. Habara (RAL), K. Lancaster (RAL),
M. Zepf(QB), K. Krushelnic(IC),R. G.Evanse (YU),
T Hall (ESSEX) , Dangor (IC)

Fast Ignitor Research at ILE Osaka (1983-2002)

ILE Osaka Univ.

1983 Proposal of Enforced Heating of Core Plasmas with ps Lasers

(T. Yamanaka, Kongo project internal report 1983)

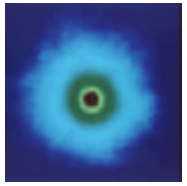

1991 Demonstration of High-Density Compression (x1000 solid)

(H. Azechi at al., Laser Part. Beams 69,1383 (1992)

1994 Proposal of FI (M. Tabak et al., Phys. Plasmas1, 1626 (1994))

Laser Hole Boring Exp. : start the FI exp. with GEKKO XII

1. (R. Kodama et al., Phys. Rev. Lett. 77, 4906 (1996);R. Kodama et al.,Plasma Phys. Contl. Fusion 41, 419 (1999); K. Takahashi et al., Phys. Rev. Lett. 84,2405(2000))

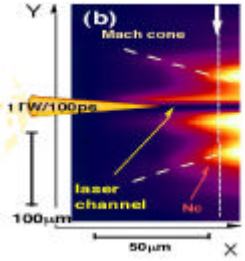

1997 100TW Laser Interaction exp.

Propagation into Overdense Regions (super-penetration mode)

2. (K. A. Tanaka et al., Phys. Plasmas 7, 2014 (2000))

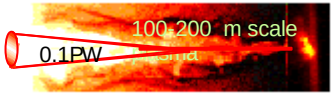

Efficient Generation of Energetic Electron and its Heating

3. (R. Kodama et al., Phys. Plasmas 8, 2268 (2001))

30-40% for the solid target interaction and 20% for the long scale plasmas at super penetration mode. (laser to forward directed electrons)

Jet-like electron propagation (20-30 deg. divergence beam) and Efficient heating

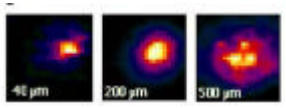

Start the imploded plasma heating exp. with 3 different approaches

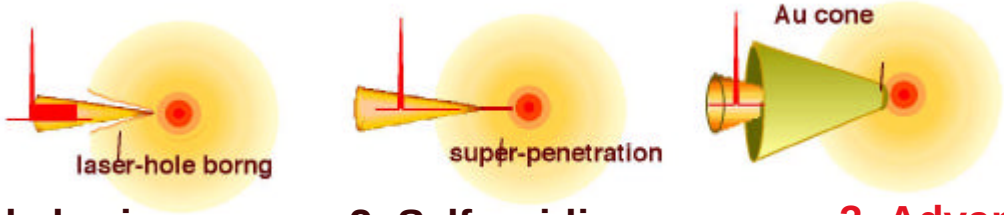

1. Hole boring **2. Self-guiding** **3. Advanced FI Targets**

Progress of Fast Ignitor Research at Osaka

1997 Advanced Target:
Fabrication of Hemisphere shell with plane targets
Osaka (R Kodama and T. Norimatsu)

1998 Adv. Target proposal with RAL:
Conical implosion and Cone-shell target
(P. Norreys, S. Rose and R. Kodama)

1999 Exp of conical implosion with Vulcan in RAL
(P. Norreys et al, Phys. Plasma 7, 3721(2000))

2000 Exp of cone-shell target with 100TW laser heating with GEKKO XII in Osaka
(R. Kodama et al., Nature 412, 798 (2001))

2002 Exp of PW heating with cone-shell targets
(R. Kodama et al., Nature 418, 933 (2002))

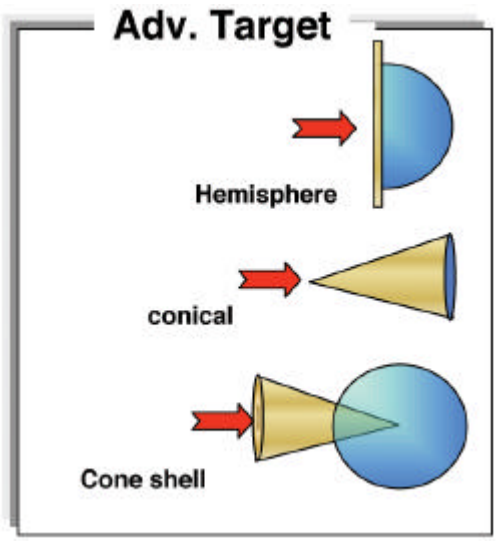

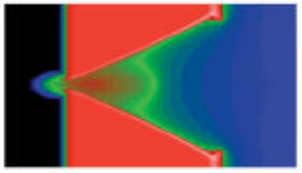

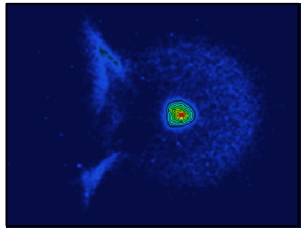

Toward ignition and burning

Demonstration of Cone Shell Implosion Shows Well Compression

ILE Osaka Univ.

The experiments was carried out with a Au-cone CD shell(500μmf/7μmt).
The CD shell was imploded with 9 beams of the GEKKOXII green laser.
50-70 times solid density was obtained as an average core density, which was well consistent with the 2-D hydrodynamic simulation (average core density: 100g/cc).

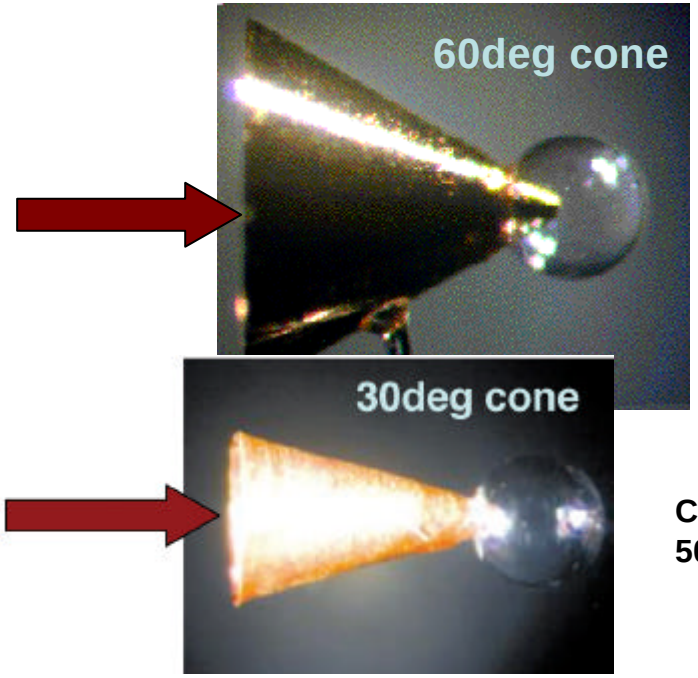

CD shell
500μmf/6-7μmt

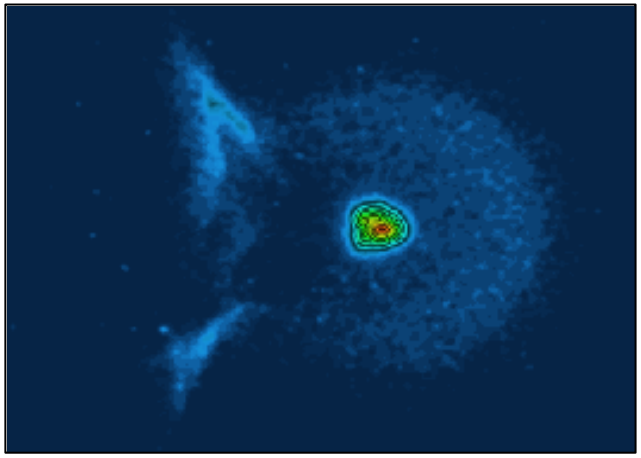

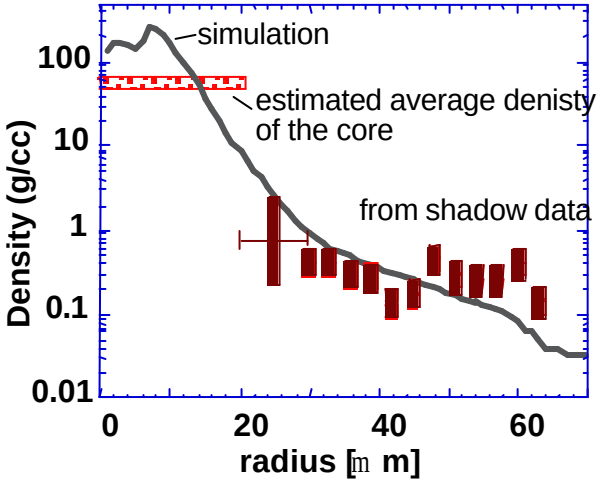

heating
1 beam / 1.053 μm / 0.5-1ps/0.1-1PW

GXII for implosion
9 beams / 1.2-2.5kJ/0.53 μm/ 1ns- Gaussian or 1.2 flat top / with RPP

Evidence of Enforced Heating on X-ray Images

X-ray framing images clearly shows the enforced heating of the core plasma. Enhancement of of the thermal neutrons was proved only when the heating pulse was injected at the maximum compression.

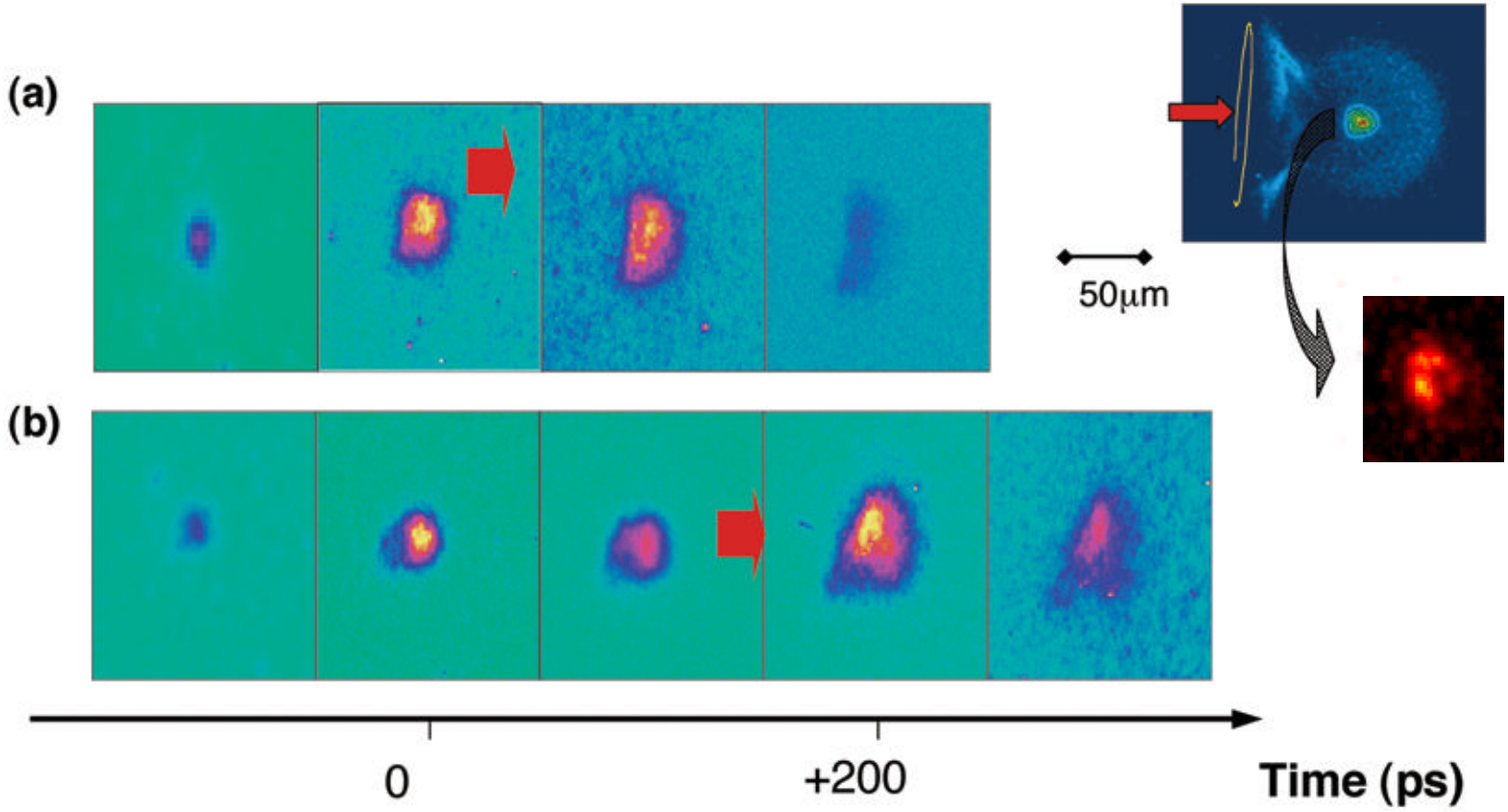

R. Kodama et al., Nature 412,798,(2001)

Evidence of Enforced Heating of the Core Plasma on the Neutron Yield

Thermal neutron yields were enhanced with injection of 100TW laser light by one order of magnitude. The result implies the first evidence of enforced heating of the stagnated higher density core plasmas.

Neutron Spectra from the implosion plasmas

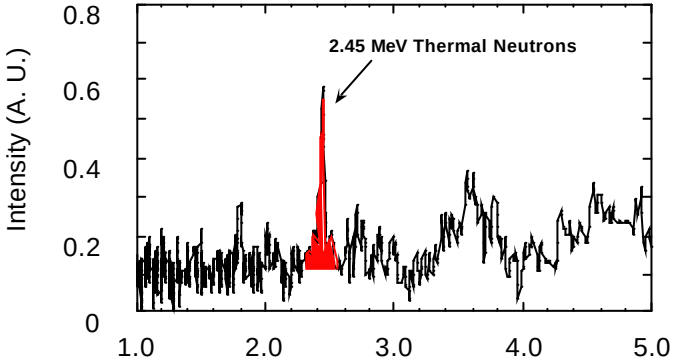

Ny:1-3x10 5

at the max. compression

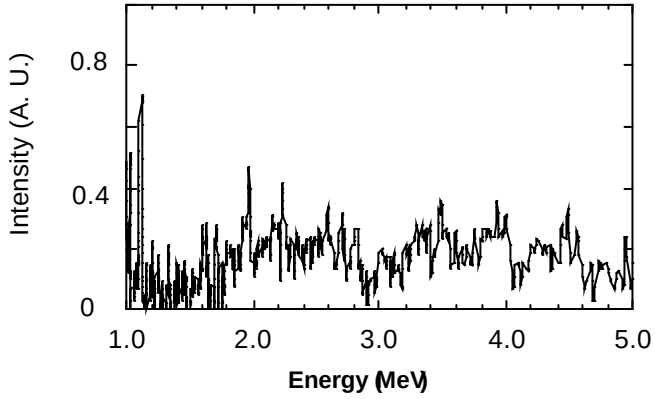

Ny:<1x10 4

200ps before the max. compression

R. Kodama et al., Nature 412,798,(2001)

PWM Laser

100TW

The first demonstration of fast heating.

PW Laser

The compressed fuel is efficiently heated by a short pulse laser with a power near equivalent to the ignition laser?

PW Laser System Performance

ILE Osaka Univ.

The PW laser is perfectly synchronized with the GXII system. The maximum output laser energy is 1.1kJ with FF of 62%. The compressed pulse duration is 0.47- 0.8 ps and focusing spot size is about 30mmf through a deformable mirror. PW was realized on targets with 420J and 0.5-0.8ps.

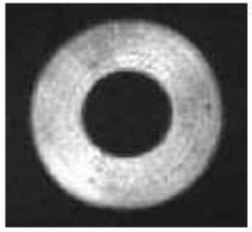

#1774 FF=62%
with a serrated aperture

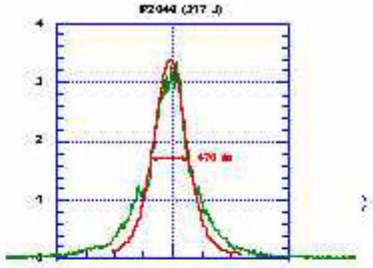

#2045 τ_L = 470 fs

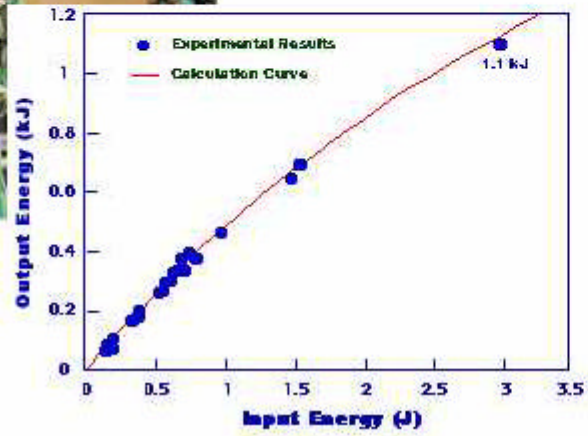

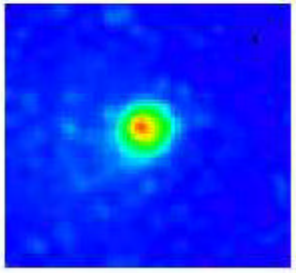

Spot size is 30μmϕ

Fast Heating is Possible during the Stagnation Time from Enhancement of the Neutron Yield

Heating was realized in the time duration of less than 100ps at near the maximum compression.

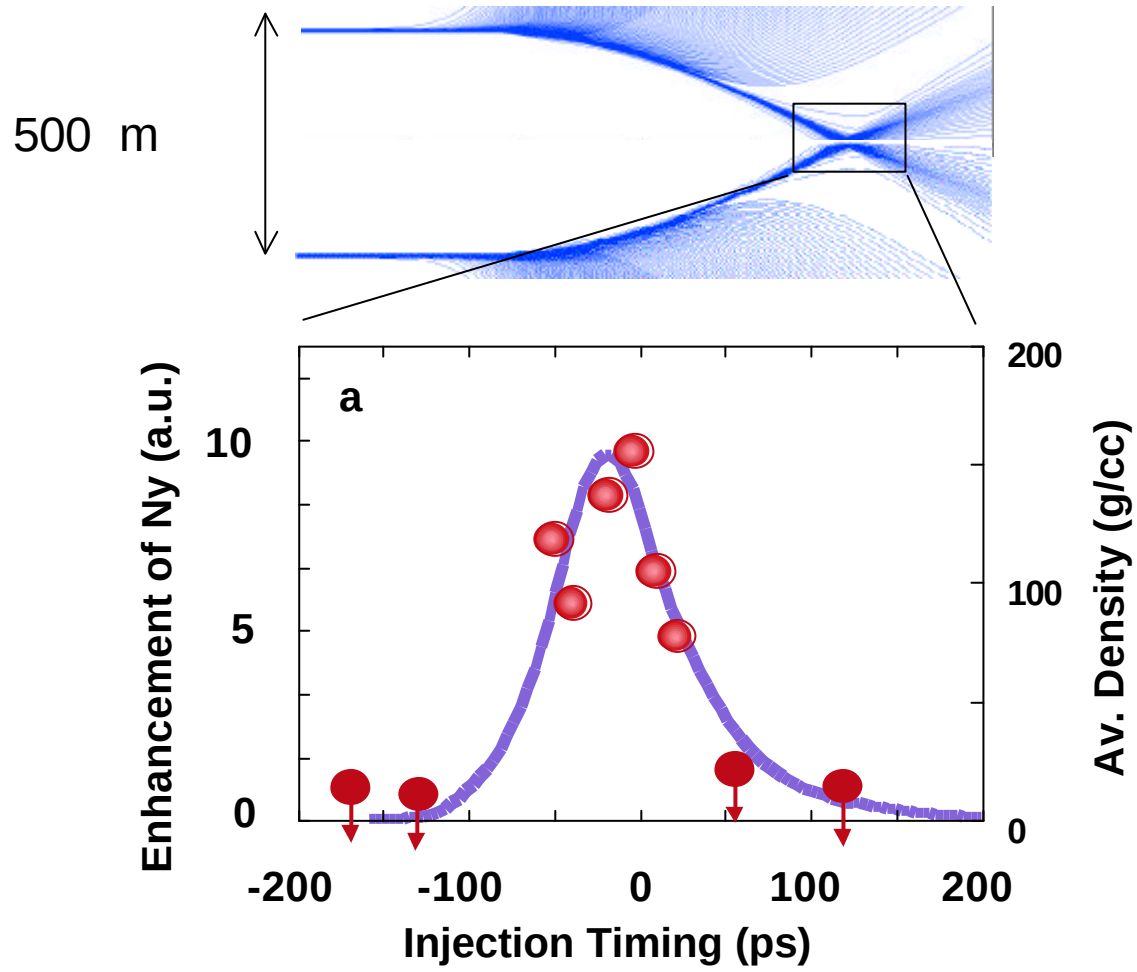

R. Kodama et al., Nature 418,933,(2002)

Thermal Neutrons Increases with the Laser Power

ILE Osaka Univ.

Enforced heating is realized at a heating power equivalent to the ignition condition on the current.

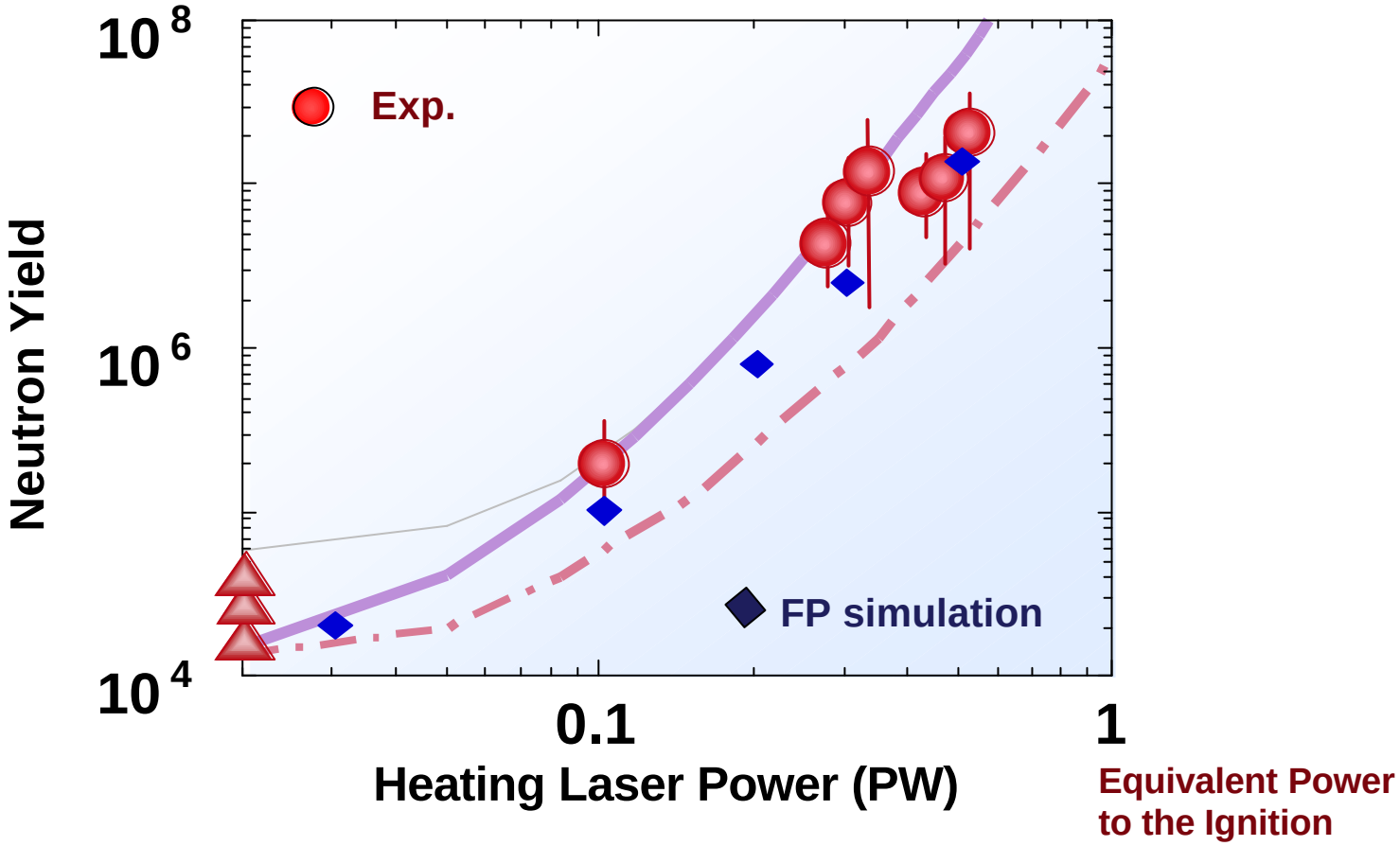

R. Kodama et al., Nature 418,933,(2002)

Fast Heating of the Compressed Core Plasmas upto 1keV

Neutron spectrum indicates a heated plasma temperature of about 0.9 keV, which is consistent with the temperature increase from the neutron yield enhancement. This heated ion temperature is also close to the electron temperature of 1keV estimated from a continuum slope of the x-ray spectra (3keV - 4keV) .

Coincidence of the neutron detectors signals

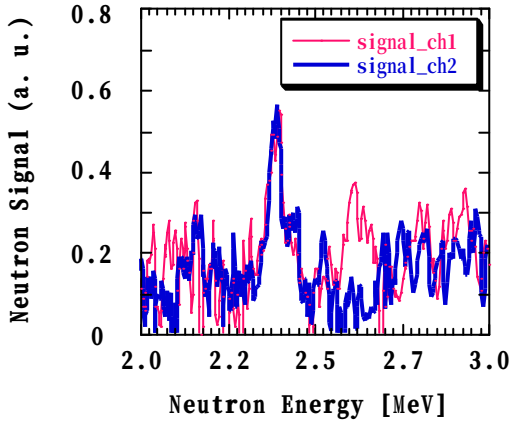

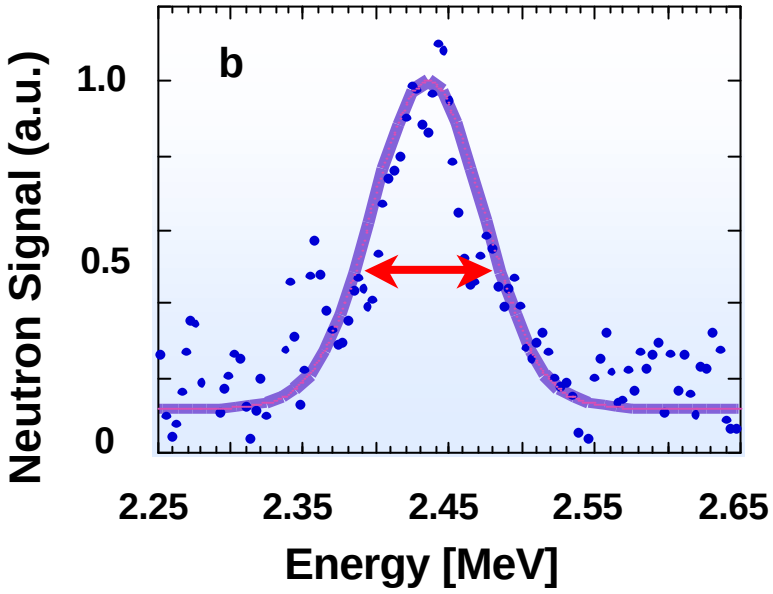

FWHM: 90±5keV keV
Resolution:50 keV

0.86 ±0.1 keV

R. Kodama et al., Nature 418,933,(2002)

Heating Physics with High-Density Energetic Electrons

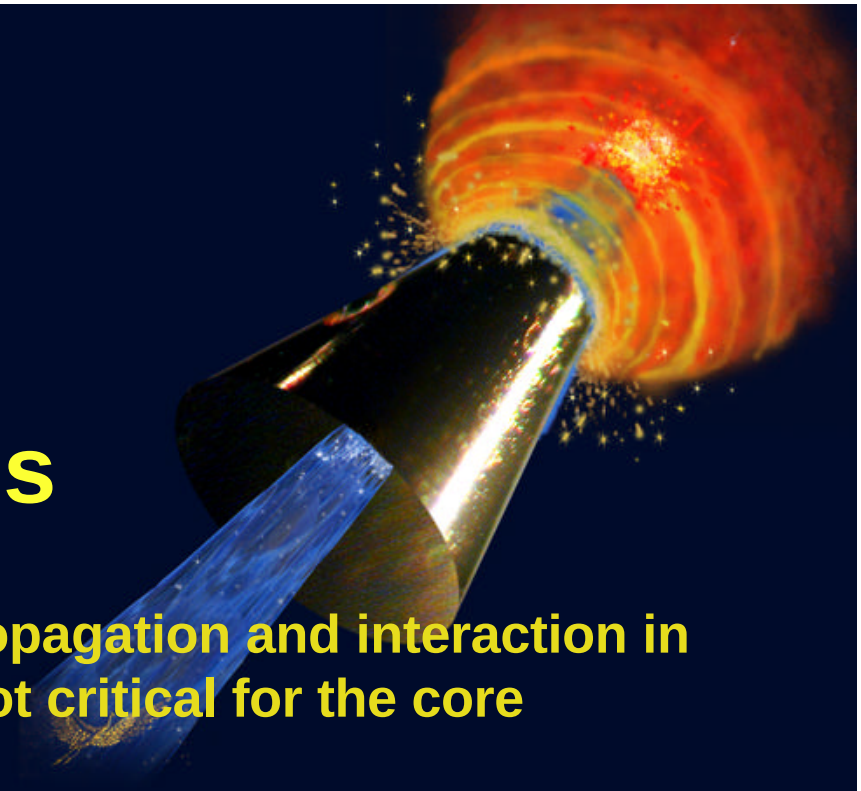

In the cone shell target, laser propagation and interaction in long scale-length plasmas are not critical for the core heating.

The critical issues in the cone shell target are heating physics or energy transport as well as the implosion of the cone-attached shell.

To study more detail of the heating physics, we have investigated the energetic electron transport in solid targets.

High-Density Electron Jet Created with Ultra-Intense Laser Light Heats the Solid Target

ILE Osaka Univ.

Rear side emission due to the energetic electrons in the solid target was observed with an UV high speed sampling camera, indicating a jet-like propagation. The divergence of the propagation is 20-30deg from the exp.

PIC simulation shows the electron jet

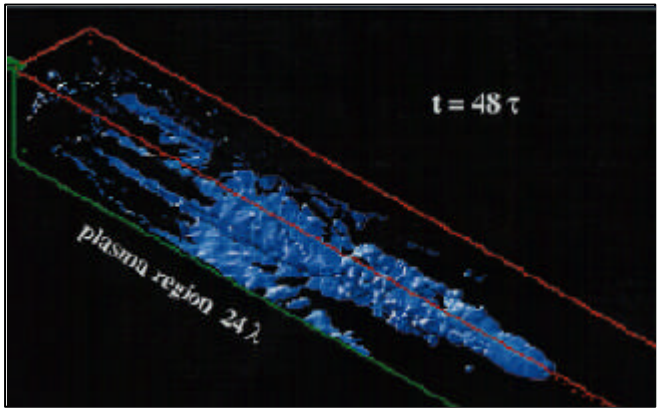

Heating of solid Al targets with the electron jet

Hot electrons created by 30-40TW laser light heated the solid Al target upto rR=0.3g/cm².

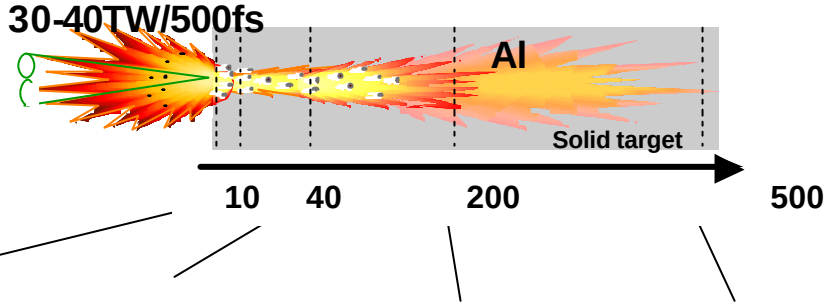

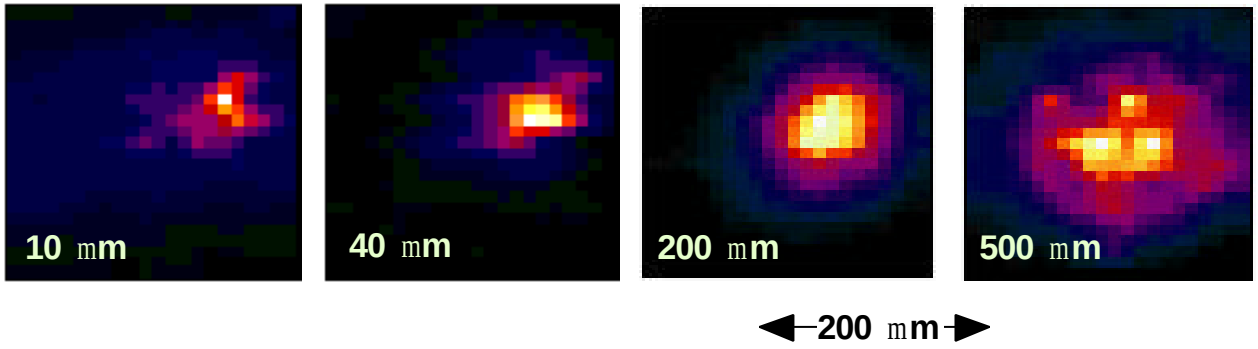

Angular Distribution of g-Ray or Electron Beam Detected with the Imaging Plate

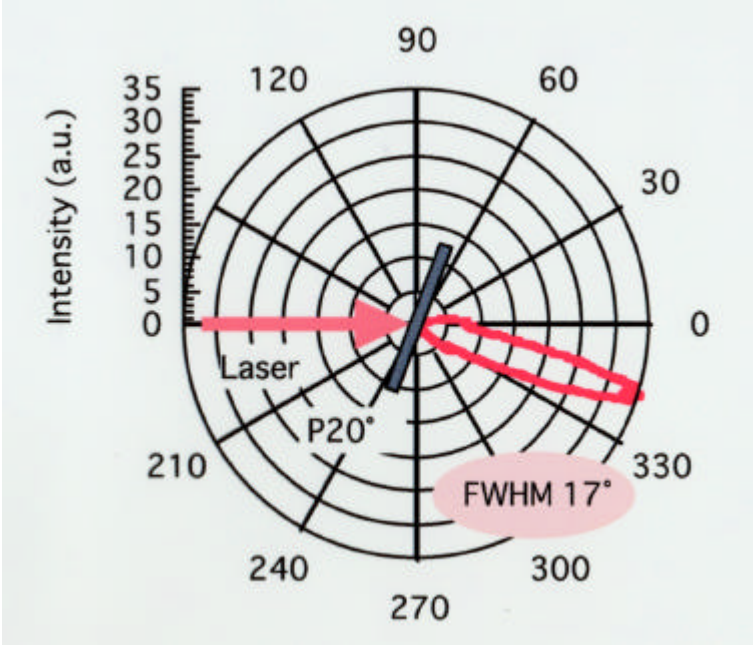

Angular distribution

Laser polarization

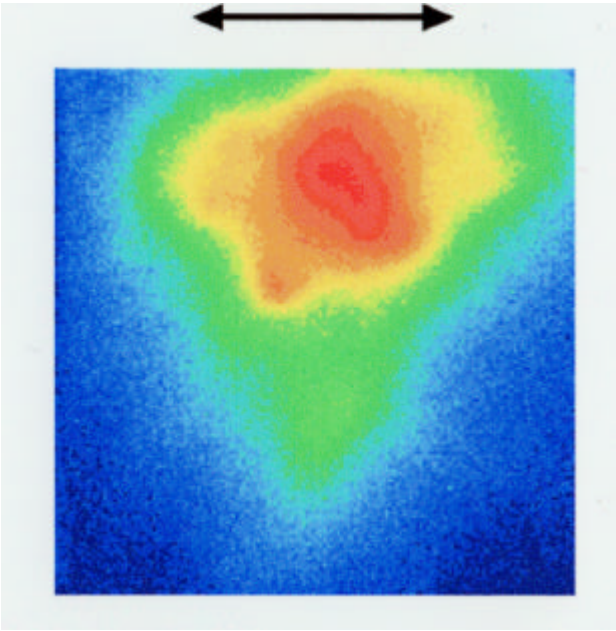

Image detected with the IP

Energetic Electron Beam was Created at the Tip of the Cone

ILE Osaka Univ.

Energetic electrons from the the tip of the cone propagate into the solid Al block(200㎜m). The propagation pattern is consistent with that of the laser absorption, indicating 20-30 deg divergence beam.

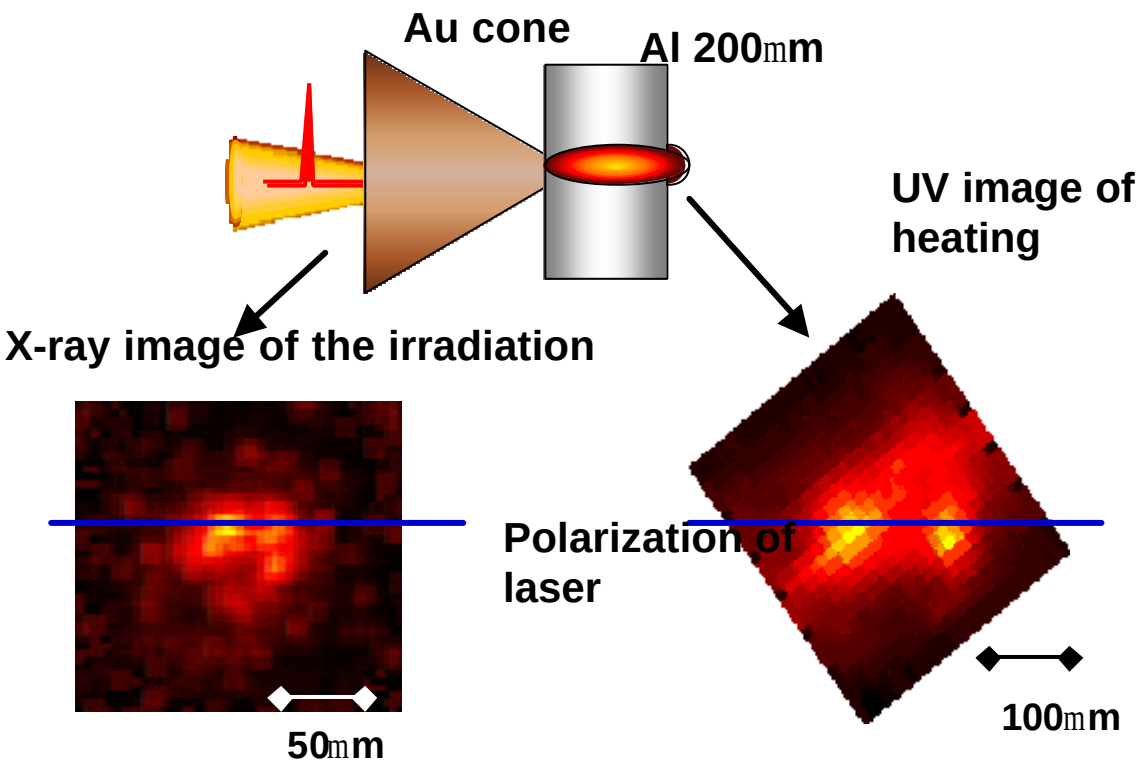

Electron Angular Distribution

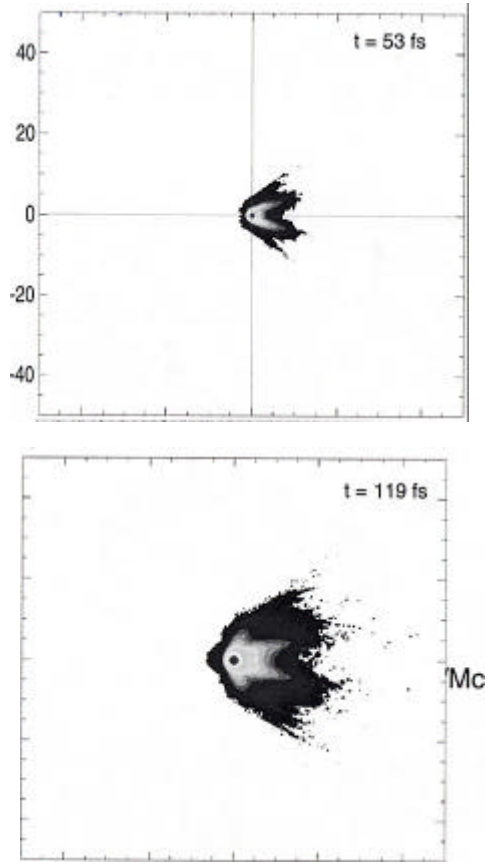

The Number of the Filament Decreases with the Intensity of the Rear Emission as well as with the Decrease in the Target Thickness

Higher power irradiation generates energetic electrons with higher current, resulting in more collimation of the electron channel due to the higher magnetic field.

	15TW	30TW
Al 500 μm	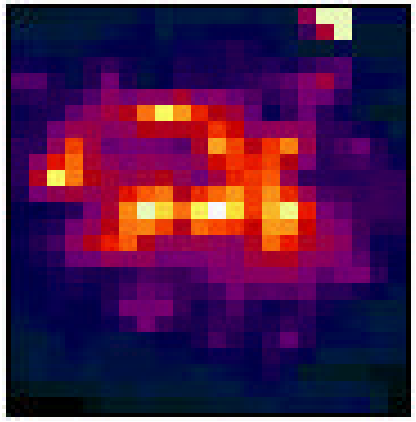	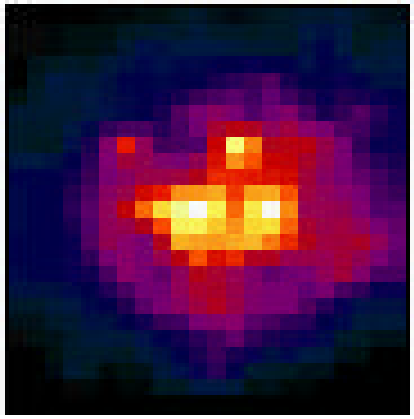
Al 200 μm	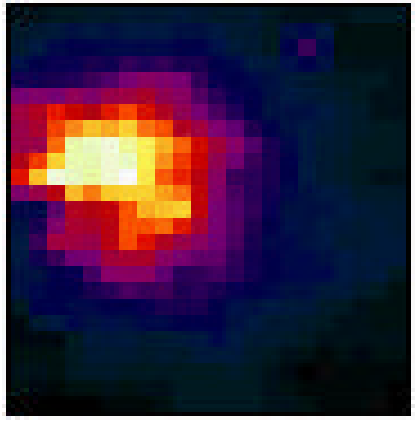	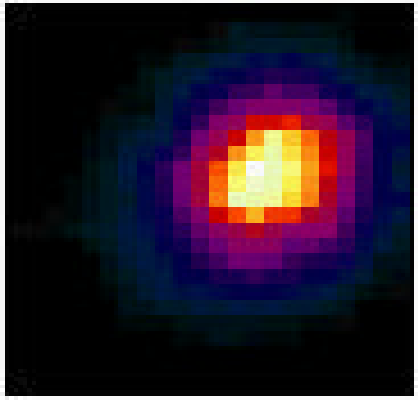

Filament Propagation and Strongly Nonlinear Heating Disappear at Higher Power Irradiation up to PW

ILE Osaka Univ.

Filament number and peak intensity of the rear emission were measured in 200 m Al targets changing the laser power up to near PW.
The filament could merge due to a magnetic field generated by inhomogeneous conductivity, which depended on the heated temperature and/or heating power.

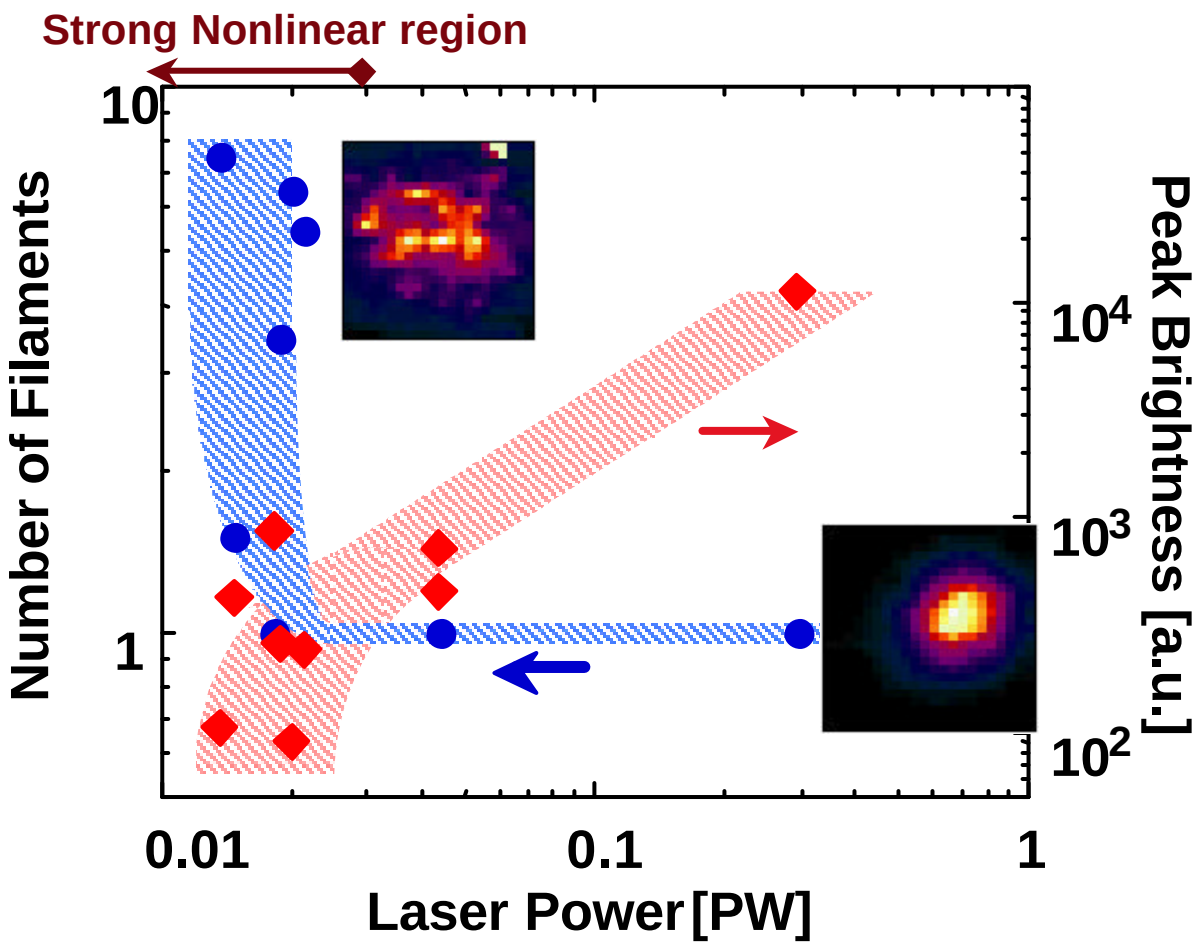

Number of the Beam Filaments Decreases with the Peak Intensity of the Rear Emission

ILE Osaka Univ.

Filamentation was investigated changing the target thickness, material and laser energy. The filament number decrease with the peak intensity, indicating the stabilization of filament propagation at higher current or temperature.

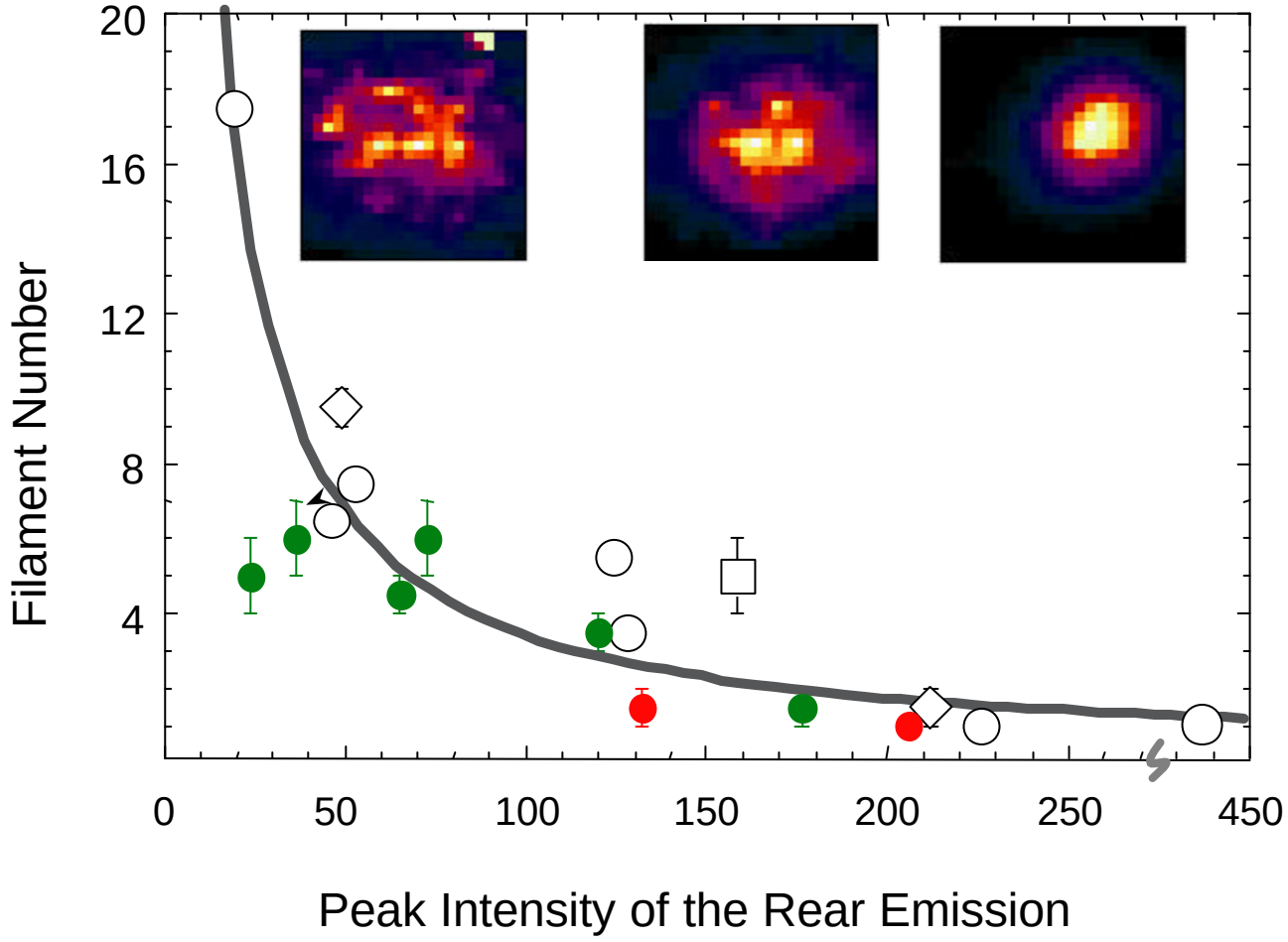

Summary

We have demonstrated enforced heating of imploded plasmas using cone-shell targets.

PW heating experiments indicate efficient heating of the core plasmas:

- neutron yield was enhanced by 3 order of magnitude by 0.5PW heating.
- The heated temperature was about 1 keV.
- 15-30% coupling efficiency could be expected.

Single stream of the electron propagation was observed at higher laser irradiation whereas more filaments appeared at lower irradiation.

Filament propagation might be stabilized by a magnetic field due to inhomogeneous conductivity dependent on the self-heated temperature.

All the experimental results with the PW laser is hopeful for a relatively compact ignition facility.

Principle of Fast Ignition must be Proved with FIREX Project

ILE Osaka Univ.

Investigation of heating physics and implosion performance of cone shell targets

Detail of the heating physics is being studied with a PW laser. Cone shell implosion is being investigated with the GEKKO XII and the integrated code.

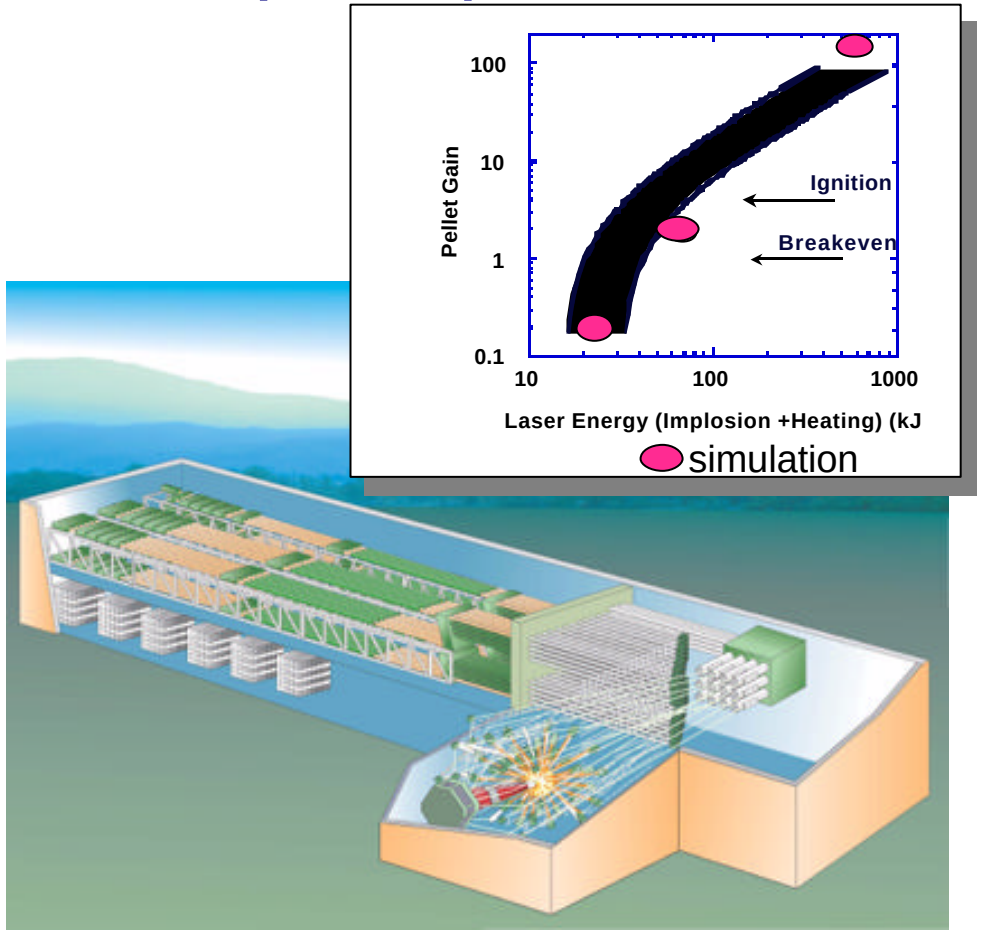

FIREX project

Laser Energy:

30 - 50kJ ($E_{implosion}$) +

10 - 30kJ($E_{heating}$)

If the fuel density= 300g/cm^3 (r=15mm, h=22%, rR=0.5g/cm^2), Near ignition and burning

The new laser system will be set in the GEKKO XII laser building.

Laboratory measurements of magnetic fields from intense laser interactions with solid targets

Karl Krushelnick

The Blackett Laboratory,
Imperial College of Science, Technology and Medicine,
University of London,
London UK

Collaborators

A. Gopal[1], F. N. Beg[1], E. L. Clark[1,3], A. E. Dangor[1], M. Tatarakis[1], M. Zepf[1] ,
P. A. Norreys[2], M. S. Wei[1], R. Evans[2,3], U. Wagner[2],

1. Blackett Laboratory, Imperial College of Science, Technology and Medicine, London UK
2. Rutherford Appleton Laboratory, Chilton, Oxon, UK
3. AWE plc, Aldermaston, Reading, UK

Summary

- Ultra high magnetic fields (~ 1GGauss) are produced during high intensity ($>10^{19}$W/cm^2) laser plasma interaction.

- These fields are localised near the critical density surface, last for very short times and extremely difficult to measure using external probing methods.

- We have developed two techniques which have allow field measurements using harmonic polarimetry
  i. The cut-off method has measured ~400 MG (1)
  ii. Measuring the harmonic depolarisation due to Cotton- Mouton effect suggests a field of ~0.7 GGauss near the critical density surface.

- Initial measurements of the spatial distribution of these ultra high magnetic fields are reported.

- The temporal evolution of the magnetic field is observed using a longer incident pulse (this suggests that the field grows in time ~ $B_{laser} \sim I^{1/2}$)

(1) M. Tatarakis et al., Nature, ***415****, 280 (2002).*

Outline

- VULCAN laser system
- Magnetic field measurements using harmonics
- Cutoff measurements
- Cotton-Mouton effect with XUV harmonics
- Spatial resolution
- Temporal behavior

High intensity lasers

- Recent developments in laser technology have enabled intensities ~ 10^{21} W/cm^2 and PetaWatt (10^{15} Watt) lasers (VULCAN upgrade at RAL)

- Can produce plasmas with relativistic electron temperatures - leading to fundamentally new physics

- Magnetic field can be 100's of MegaGauss - approaching that found in astrophysical situations such as neutron stars

- Experiments begin to become complicated because of fast particle production and chamber/target activation

VULCAN laser system

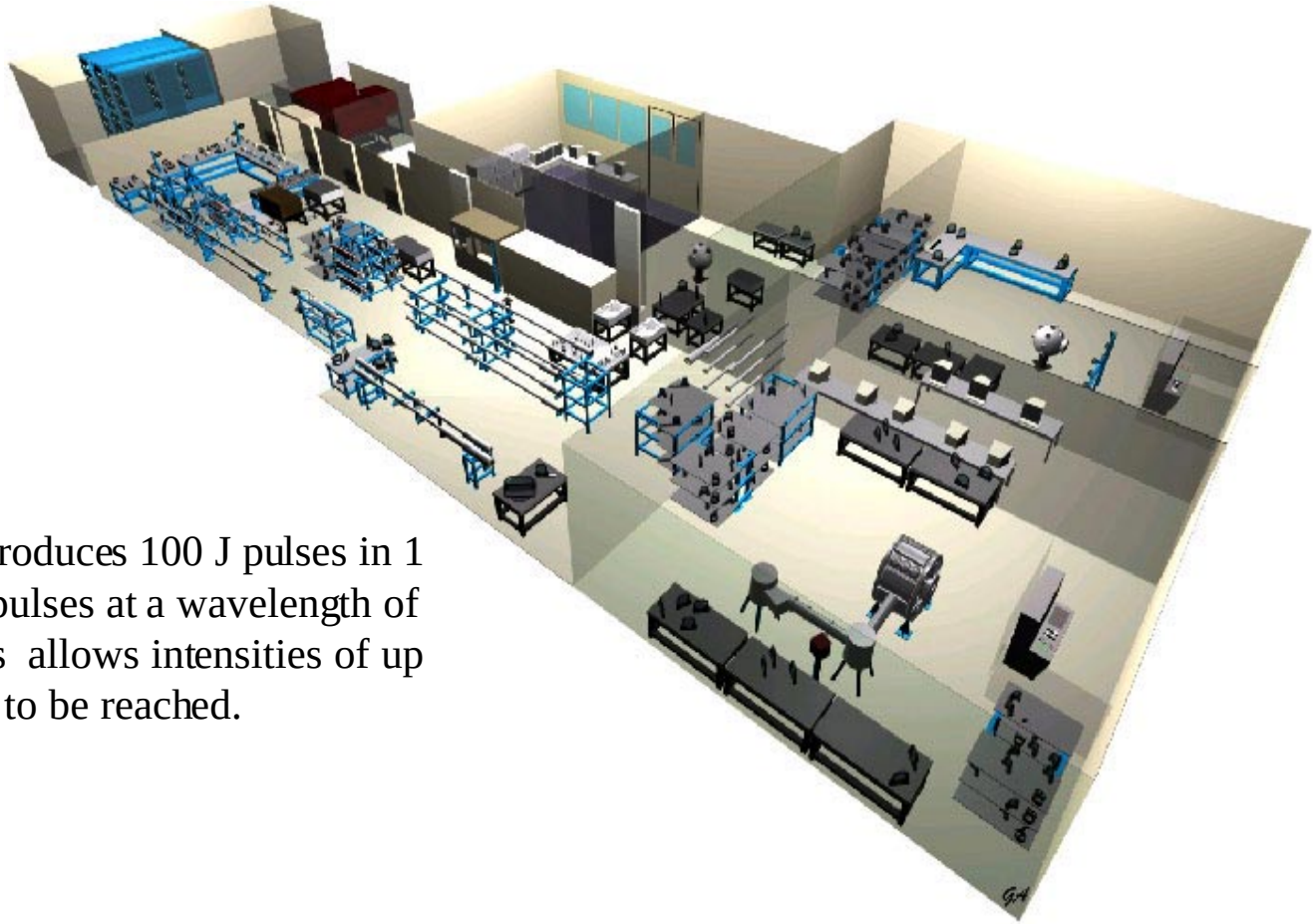

Vulcan CPA produces 100 J pulses in 1 psec duration pulses at a wavelength of 1053 nm. This allows intensities of up to 10^{20} W/cm^2 to be reached.

Short Pulse Laser -- Solid Interactions

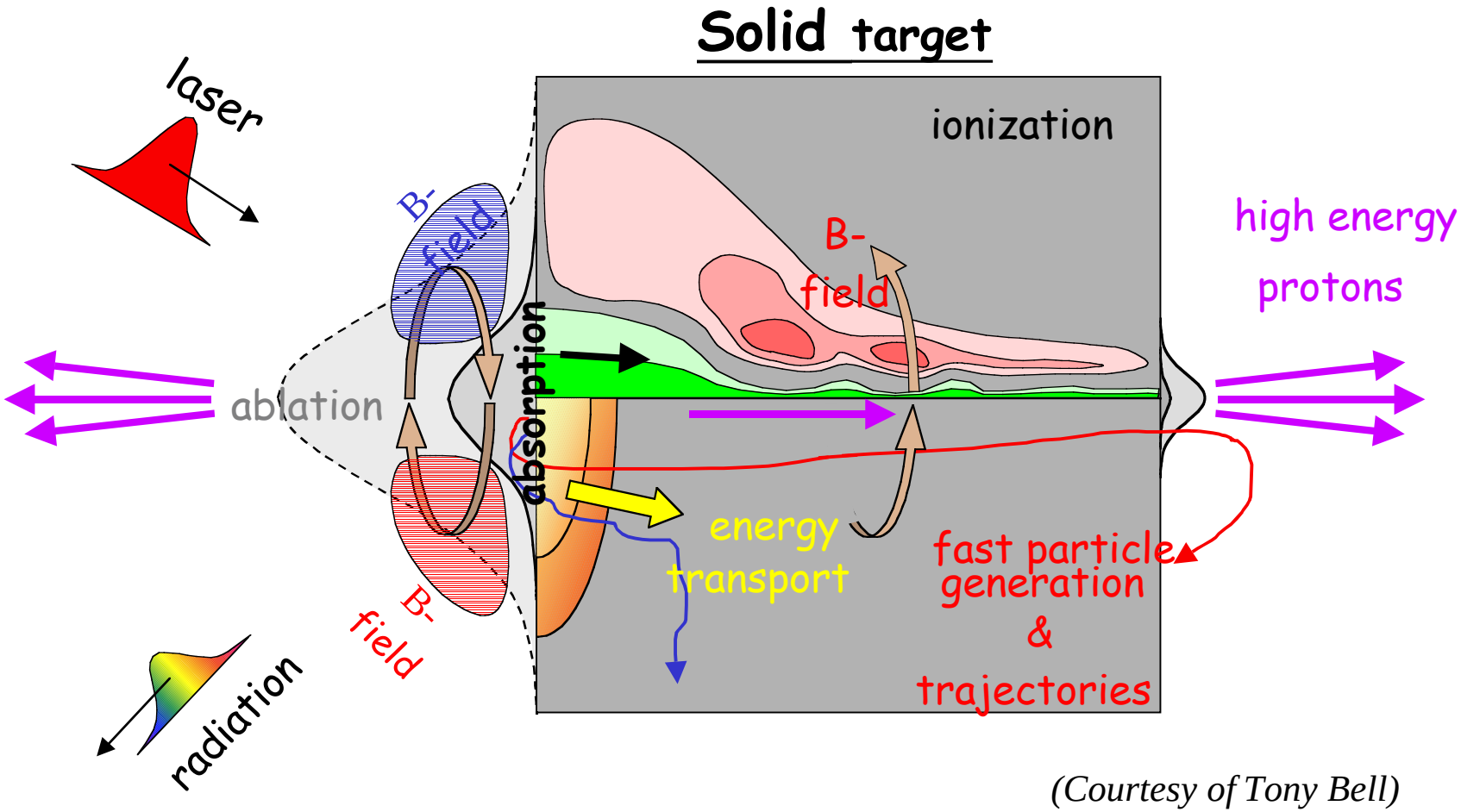

(Courtesy of Tony Bell)

Importance of magnetic fields in high intensity laser produced plasmas

In inertial confinement fusion (Fast Ignition)

- **can affect the direction and energy deposition of hot electrons**
- **can affect the equation of state**
- **can reduce the heat flow in the interaction region**
- **can affect the the atomic structure of plasma ions**

In astrophysics

- **very high magnetic fields exist in astrophysical objects such as neutron stars and white dwarfs. Laboratory generation of magnetic fields similar to these may help our understanding of such objects.**

Such fields approach those observable in astrophysical phenomena

In the center of the Crab nebula a pulsar (neutron star) rotates with a speed of 30 times per second. The blue color shows the area where electrons spin in the huge magnetic field.

Mechanisms of magnetic field generation

1. Non zero vector product of temperature and density gradient.

Faraday's law, $\frac{\partial \mathbf{B}}{\partial t} = -\nabla x \mathbf{E}$

$$\frac{\partial \mathbf{B}}{\partial t} = \nabla x \left(\frac{\nabla p_e}{n_e e} \right) = \frac{k_e \nabla T_e x \nabla n_e}{n_e e}$$

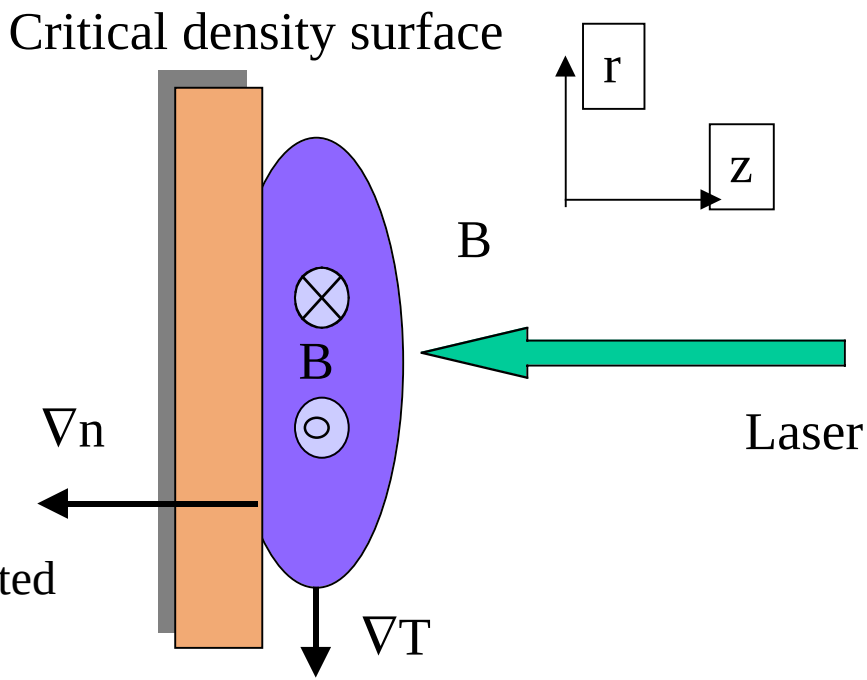

2. Current due to fast electrons generated during the interaction

3. DC currents generated by the spatial and temporal variation of the ponderomotive force of the incident laser pulse $B_{dc} \sim B_{laser}$*

* *R.N.Sudan, Phys. Rev. Letts.,* ***70,*** *3075 (1993)*

Existing experimental techniques

- External probes - magnetic tapes, induction coils etc. (low temporal response)

- Faraday rotation - maximum measured field ~ 10 MG*

  An external linearly polarised probe beam is used and the induced rotation of the polarisation resulting from the magnetic field is measured.

Electromagnetic waves propagating parallel to the direction of the magnetic field experience rotation of the direction of polarisation.

For an external probe laser to propagate through plasma

$\omega_{laser} > \omega_{p,}$ for e.g. for a solid plasma $\omega_p=10^{15}$ rad/sec, so the external laser frequency required lies in the x-ray range.

Experimental schematic

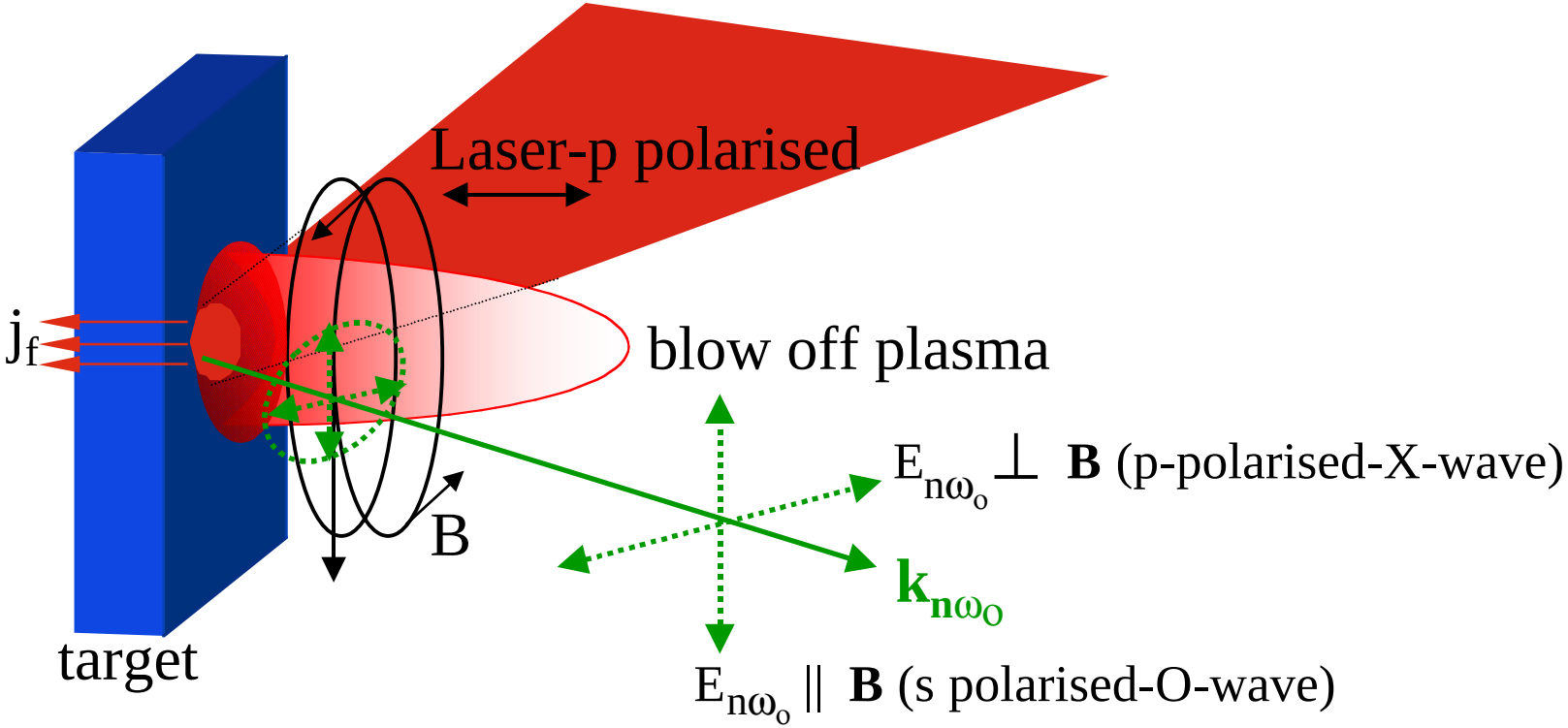

X-Wave cutoffs

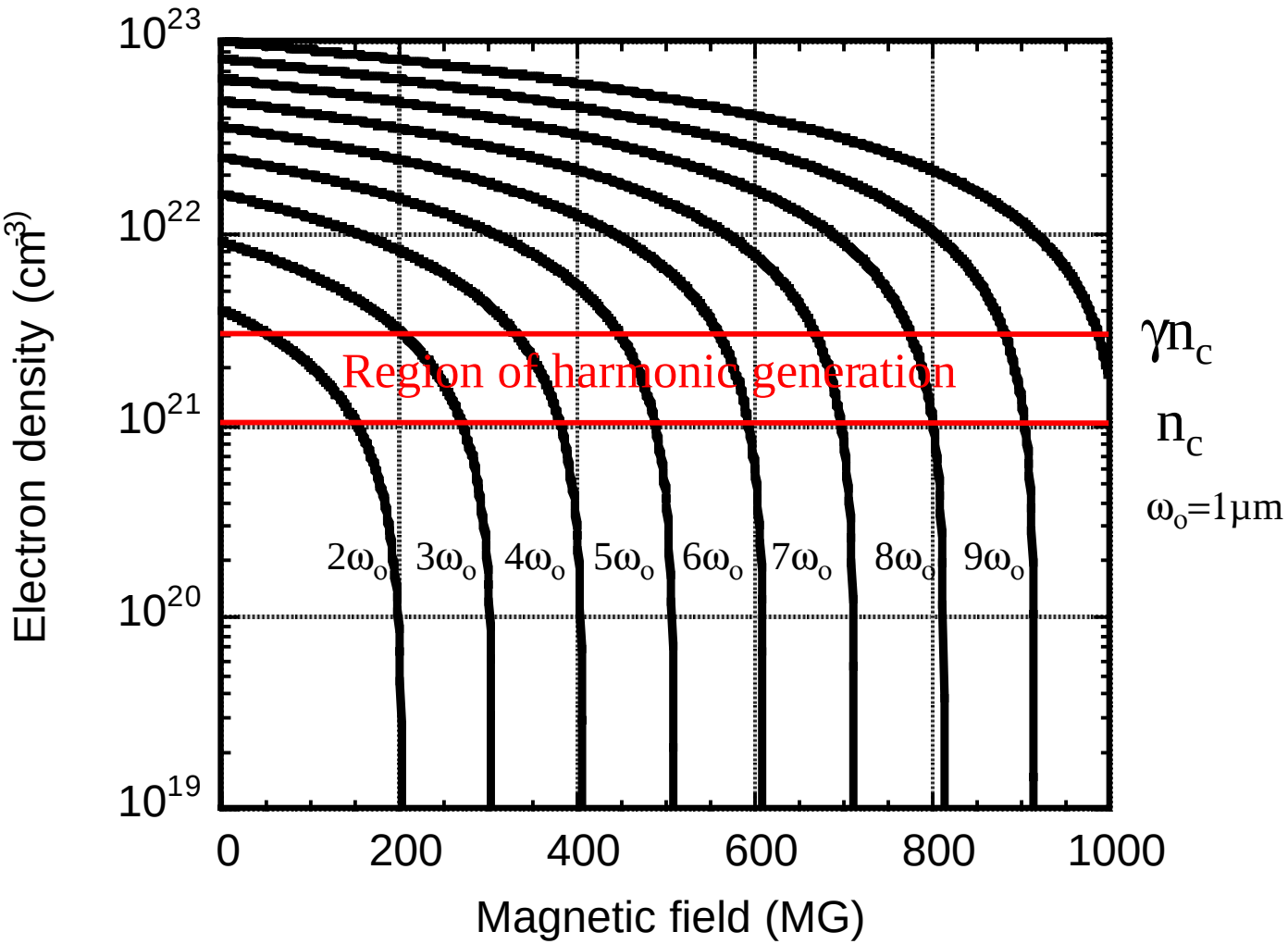

Observation of cutoffs

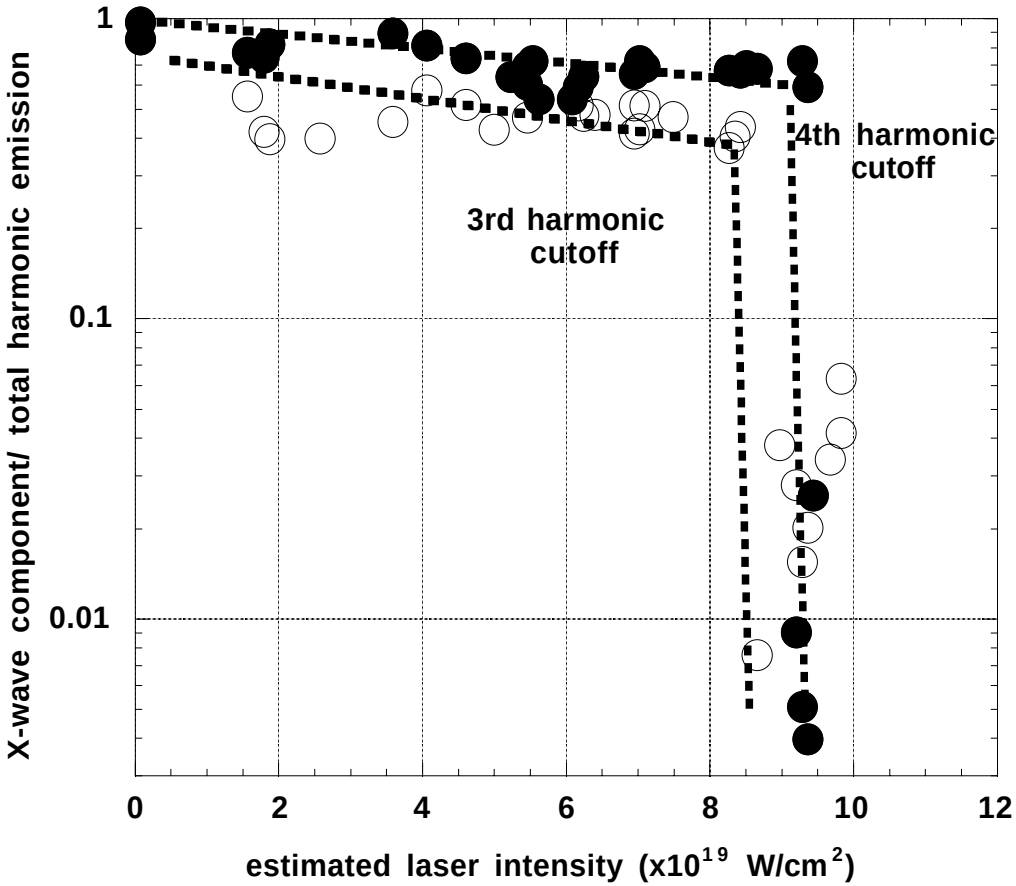

Cotton-Mouton effect

The plasma acts as a birefringent medium in the presence of a magnetic field which introduces ellipticity on the self-generated harmonics produced at the critical density surface. This assumes that the harmonics are generated at the same time as the magnetic field.

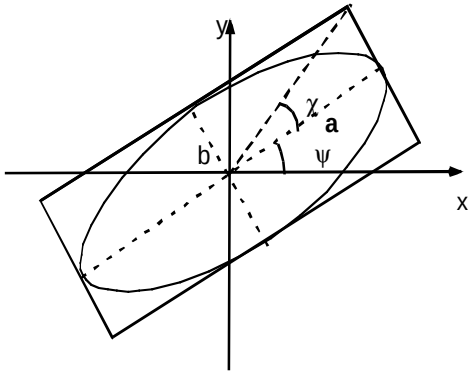

$$s_1 = \cos 2\chi \cos 2\psi$$
$$s_2 = \cos 2\chi \sin 2\psi$$
$$s_3 = \sin 2\chi$$

Stokes Vector S= $\begin{pmatrix} s_0 \\ s_1 \\ s_2 \\ s_3 \end{pmatrix} = I \begin{pmatrix} 1 \\ s_1 \\ s_2 \\ s_3 \end{pmatrix}$

i.The induced ellipticity is calculated by measuring the initial and final Stokes parameters of the harmonics.

ii. Stokes vectors define the polarisation properties of an electro-magnetic wave.

The final polarisation of the harmonics detected $S_{out}(z)=M.S_{in}(0)$

M is the transition matrix, which can be obtained from

$$\frac{ds}{dz} = \Omega(z) \times s(z) \quad \text{where,} \quad |\Omega| = \frac{\omega}{c}(\mu_1 - \mu_2)$$

and

$$\mu_1^2 = 1 - \frac{\omega_p^2}{\omega^2}(O - wave)$$

$$\mu_2^2 = 1 - \frac{\omega_p^2}{\omega^2}\frac{\omega^2 - \omega_p^2}{\omega^2 - \omega_p^2 - \omega_c^2}(X - wave)$$

Experimental Setup

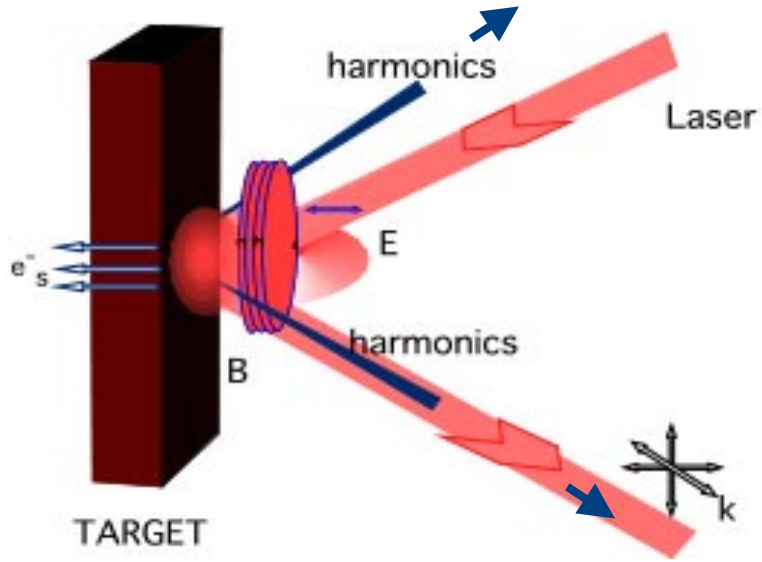

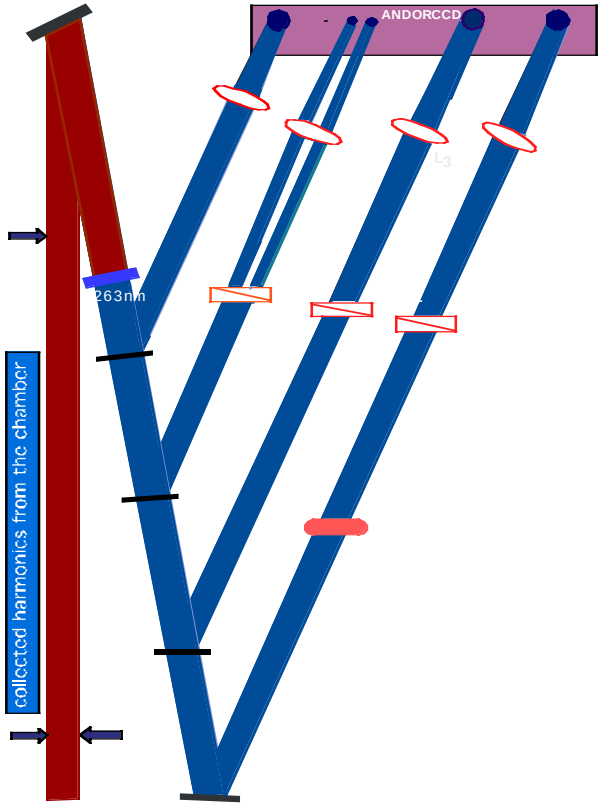

Laser Parameters :

Energy - up to 120 J
Pulse duration-1ps
Spot size - 10 microns
Electric field vector -p polarised

Target :

optically polished glass (10x10 mm^2)

POLARIMETRY SET UP

Cotton Mouton results

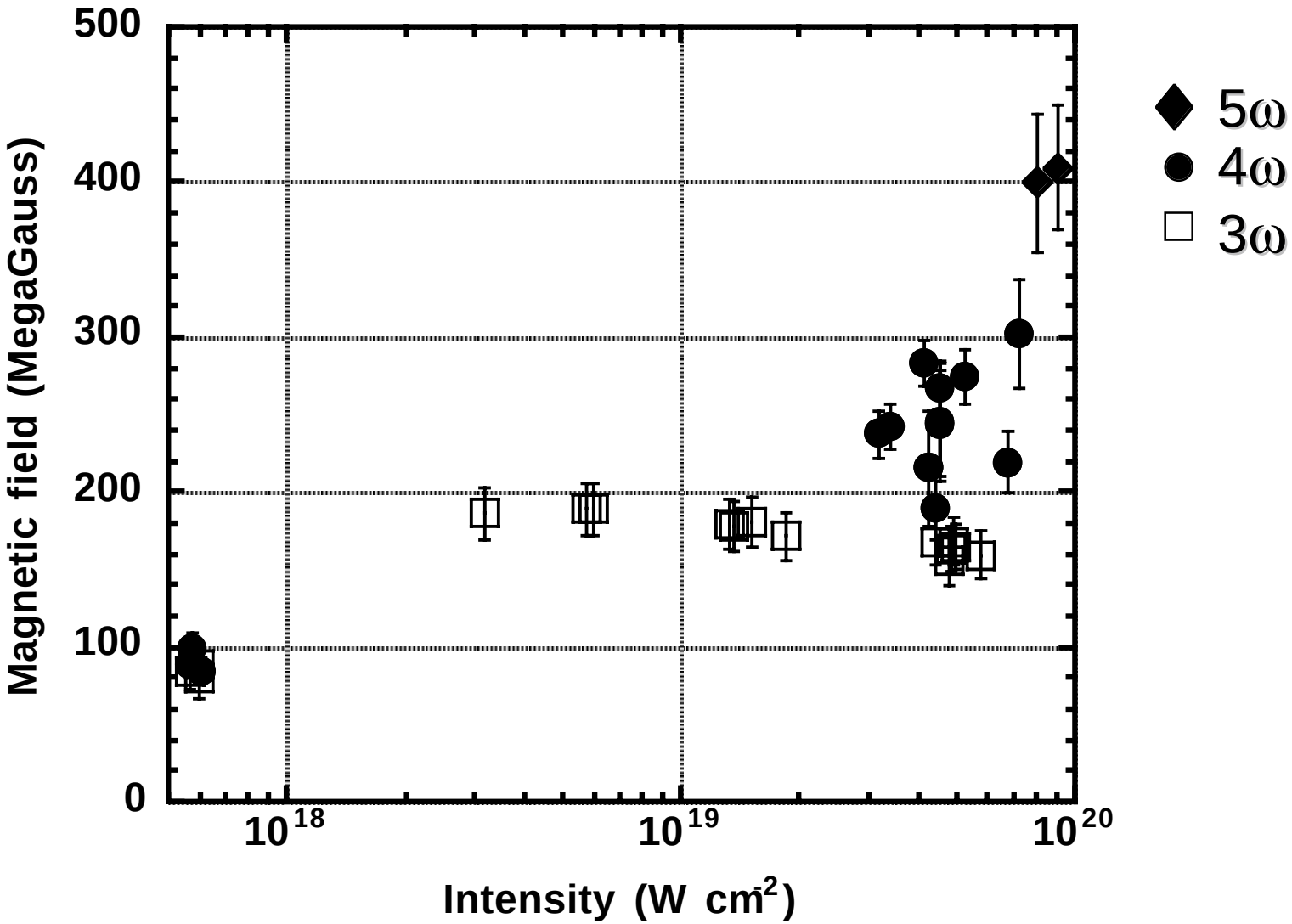

X-Wave cutoffs

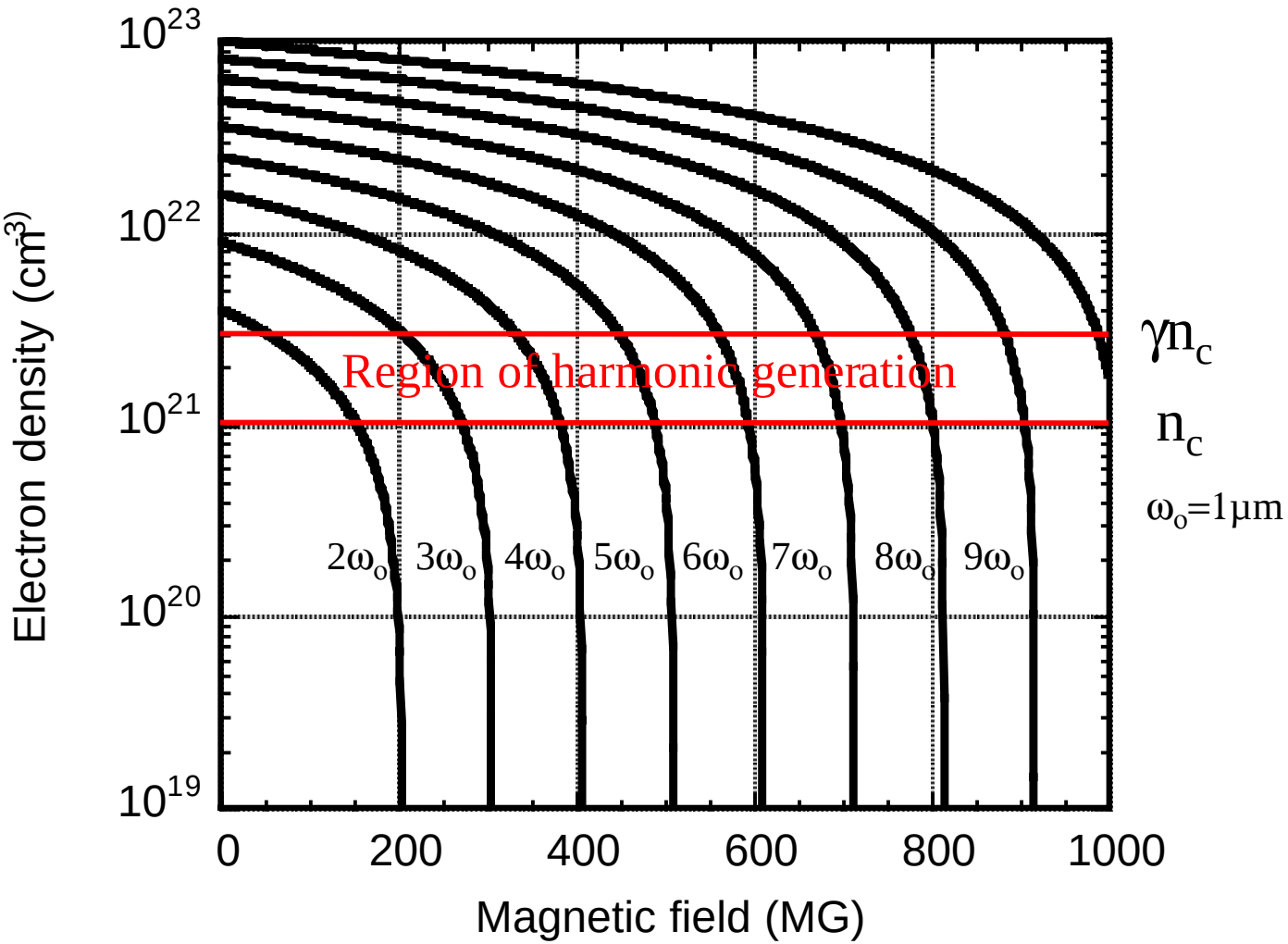

Harmonics of the laser frequency are emitted to very high orders (up to 75th)

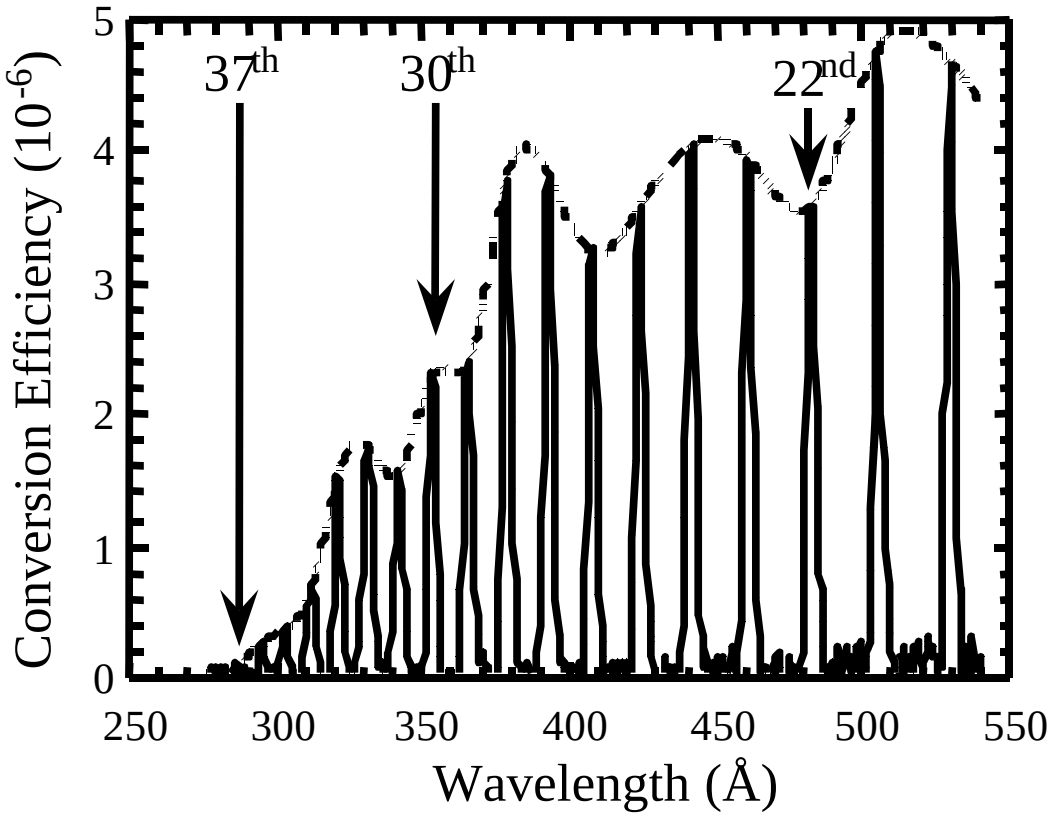

I. Watts *et al.*, Phys. Rev. Lett. **88**, 155001 (2002)

XUV-Polarimetry of High Harmonics

Measured Polarisation of the Harmonics:

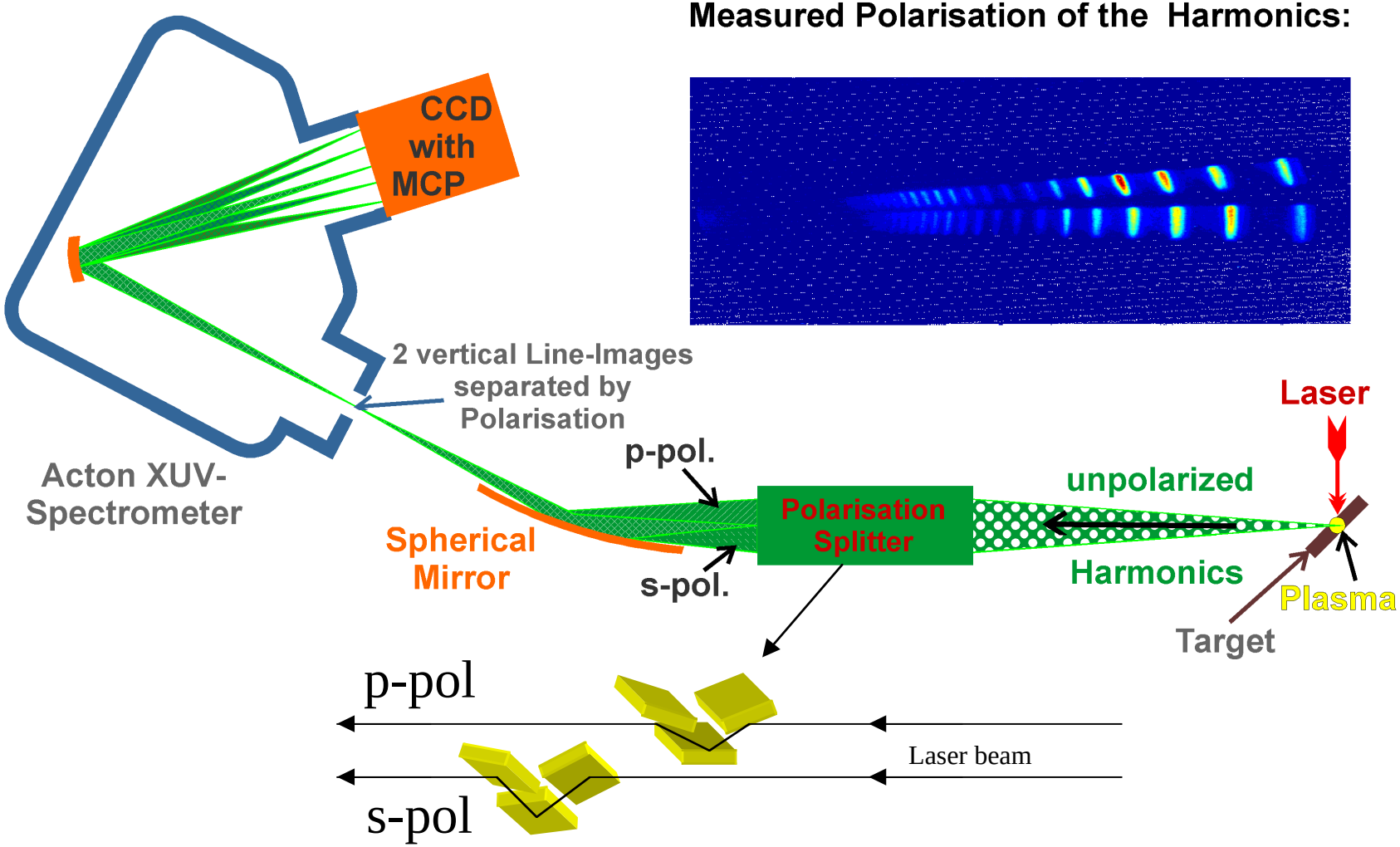

Harmonic depolarization follows λ^3 scaling

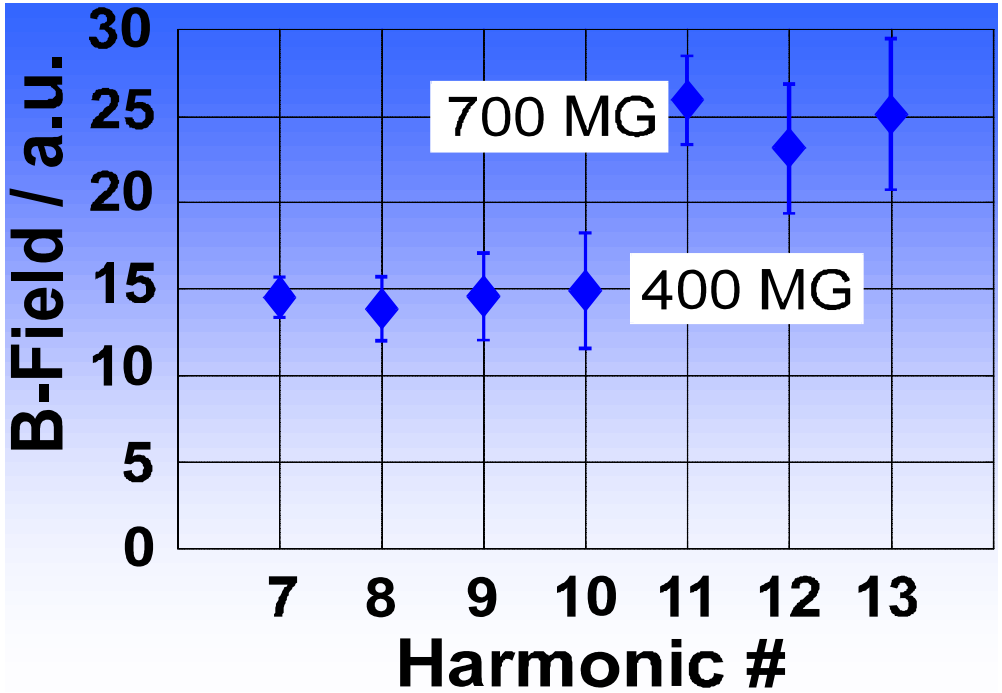

$$\frac{b}{a} = 2.49 \text{ x } 10^{-21} \lambda_{\mu m}^{3} \int n B_{MG}^{2} dl$$

b/a is the induced ellipticity

- this suggests that fields in the higher density regions of plasma are up to 0.7 ± 0.1 Gigagauss

2D PIC simulation results (OSIRIS - courtesy W. Mori UCLA)

Laser Incidence direction

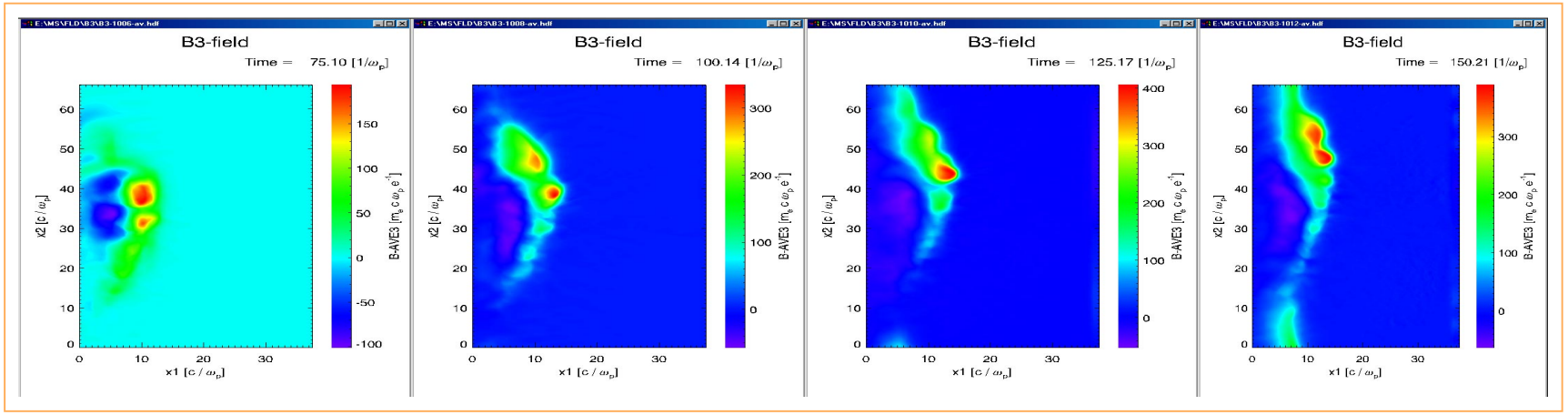

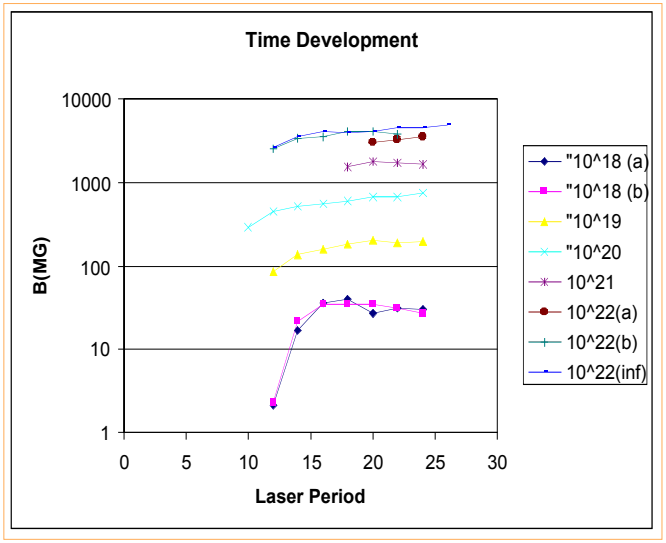

Osiris 2-1/2 D
Simulations at 45 degree incidence

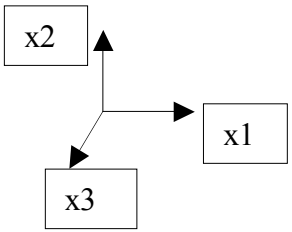

Intensity 10^{19}W/cm^2

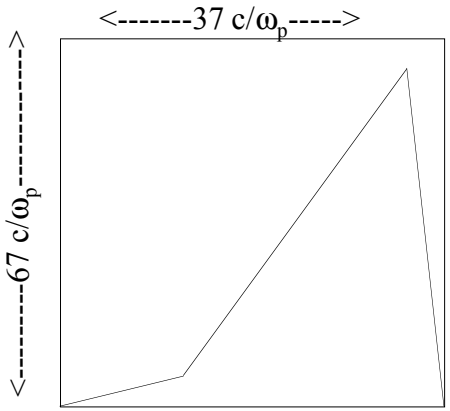

Spatially resolved measurements

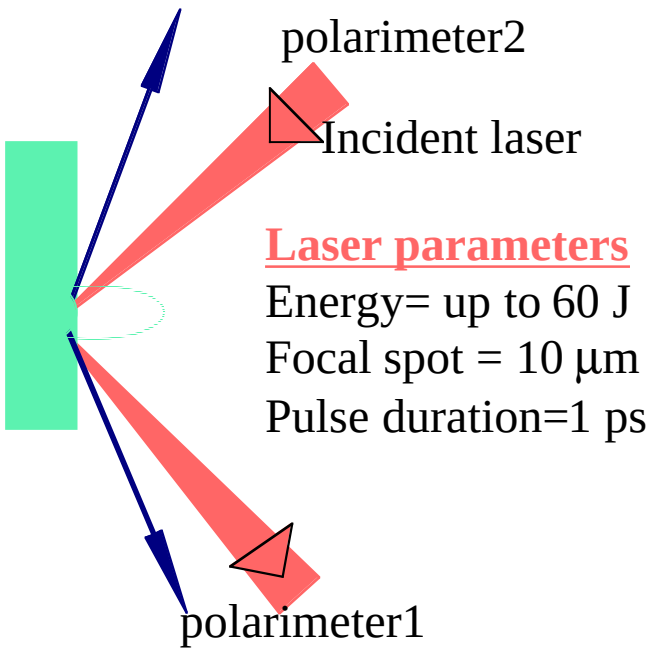

Laser parameters

Energy= up to 60 J
Focal spot = 10 µm
Pulse duration=1 ps

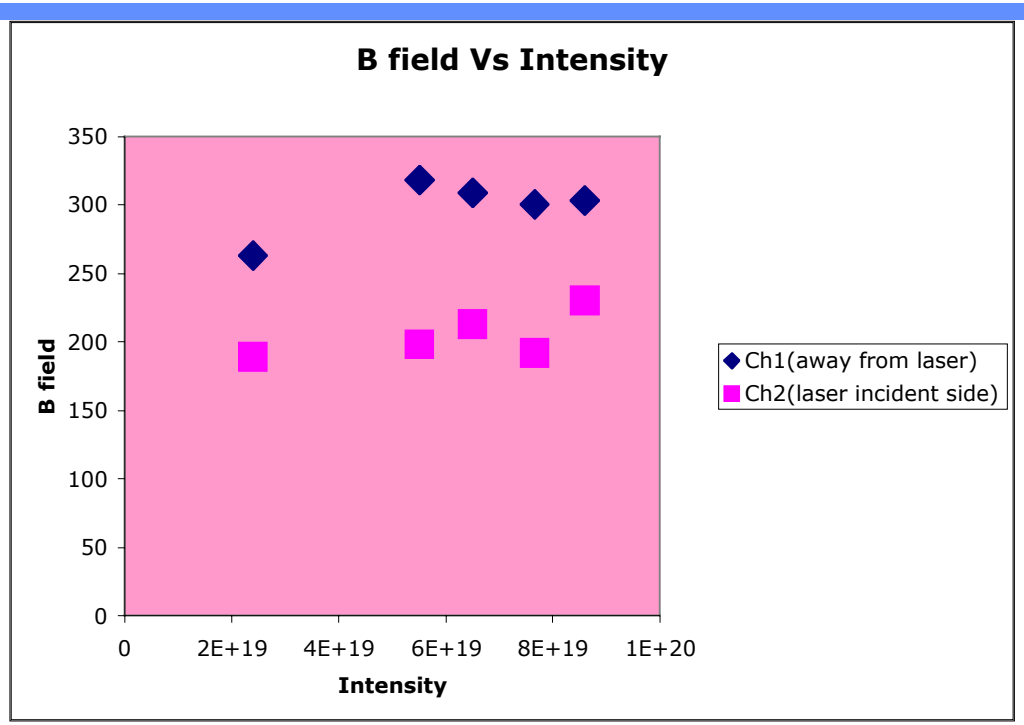

- under the assumption that the density profiles on both sides are similar there is a marked assymetry in the magnetic field
- calculations using more accurate density and field profiles are underway.

2D PIC simulations

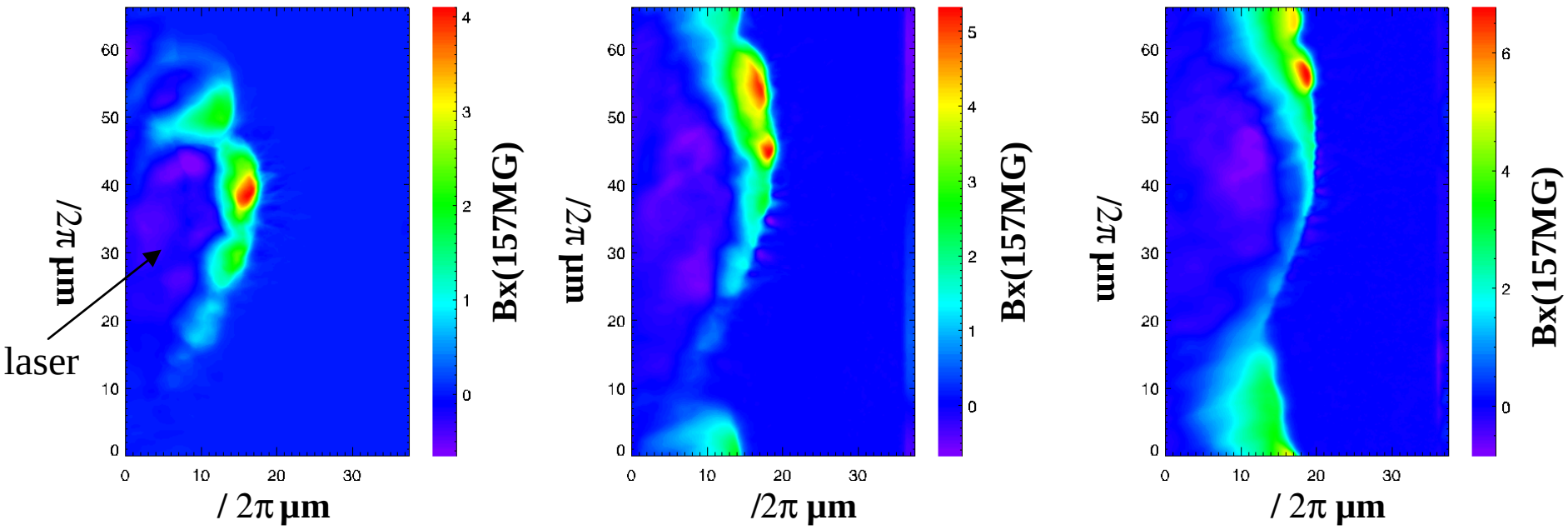

27 fs 40 fs 55 fs

Experimental setup for time-resolved measurements

Incident laser pulse ~ 10 psec

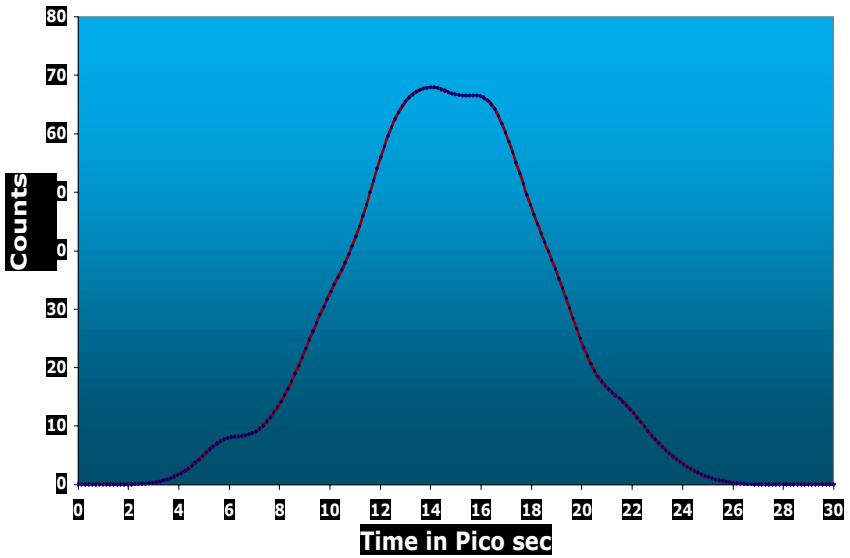

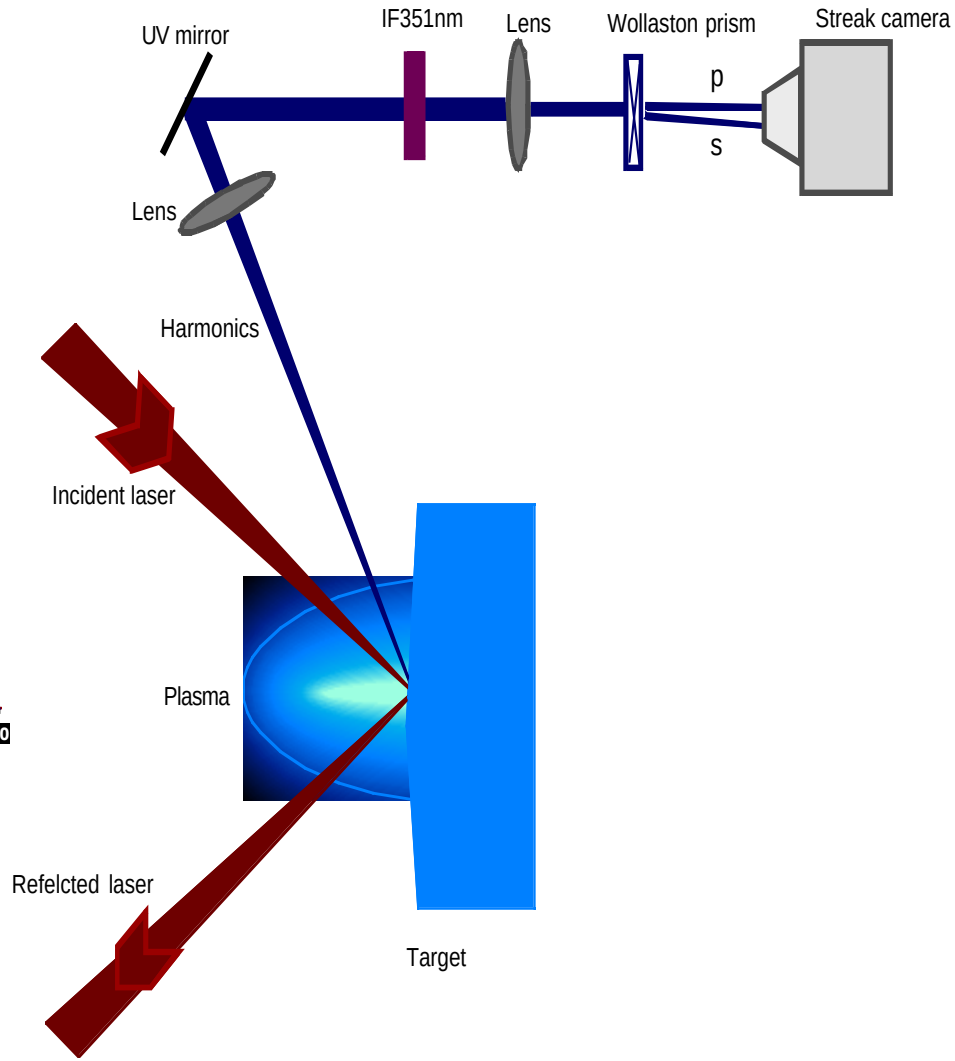

2D PIC simulations

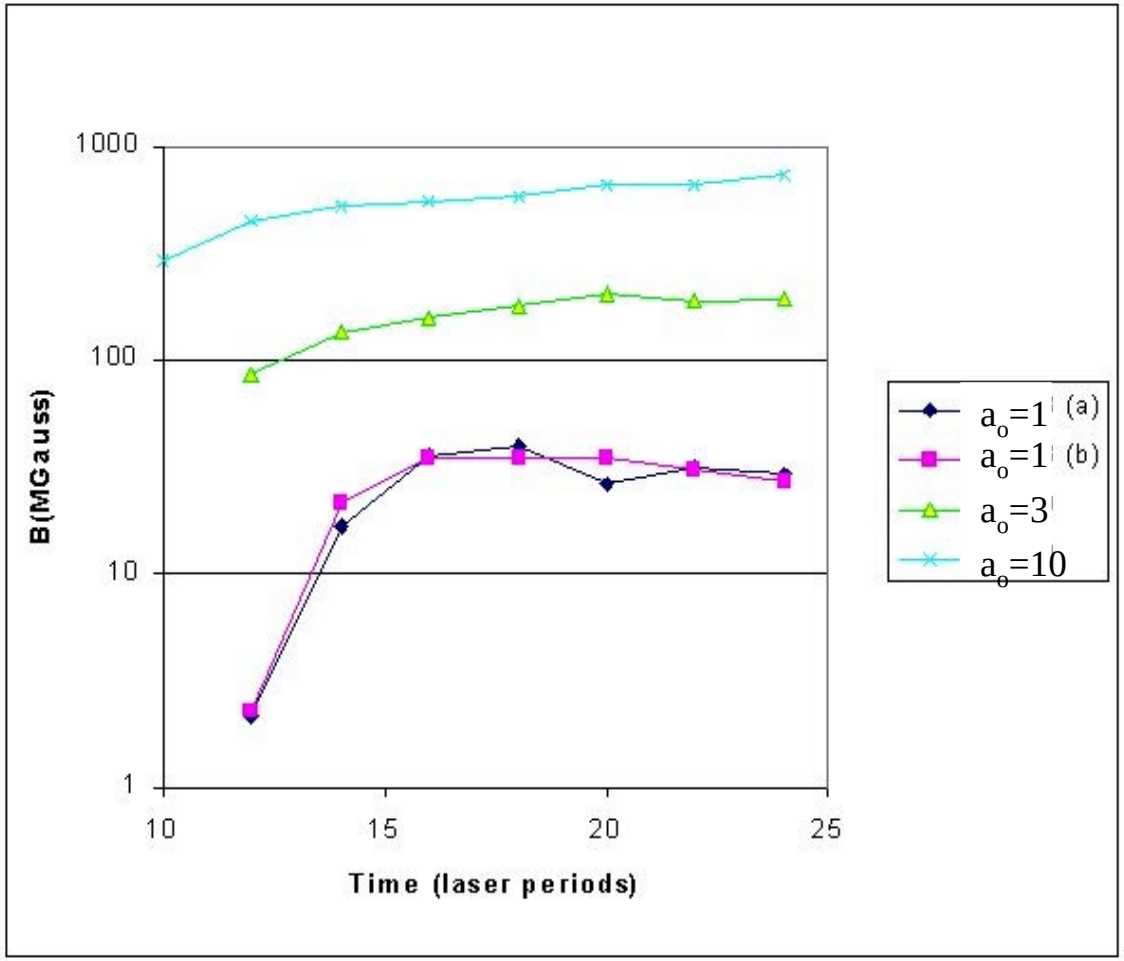

Experimental Observations

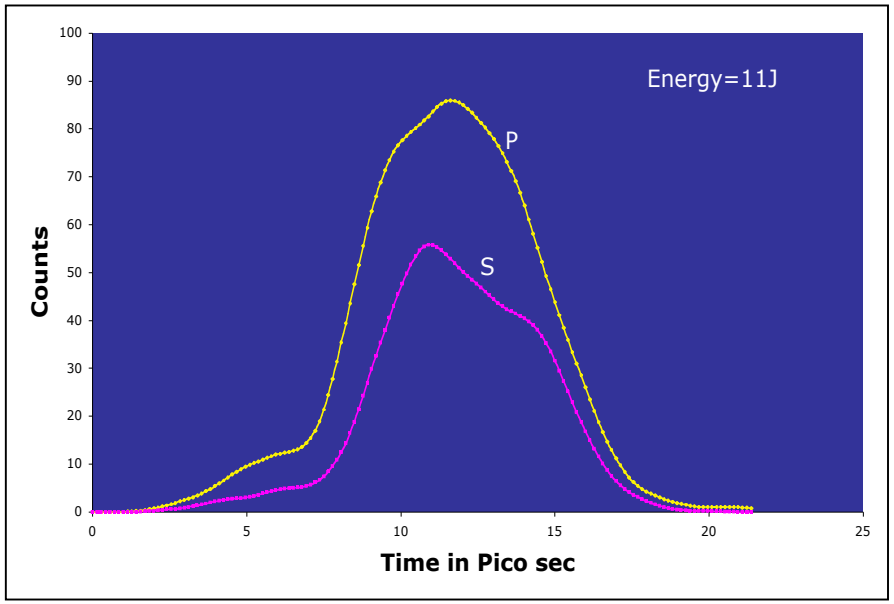

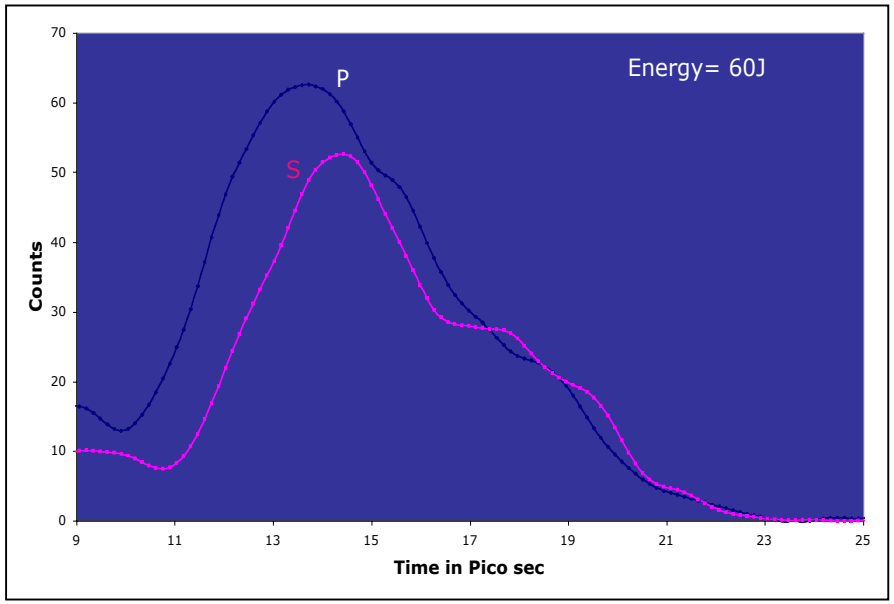

Summary of temporally resolved measurements of the 3rd harmonic

Temporally resolved measurements show :

• The ratio of 'S/P' increases as the intensity increases.

• The gradient of 'S/P' plot is greater for higher intensities and is slower than the rise time of the intensity .

• The duration of the magnetic field is at least as long as the incident laser pulse (no information about convection and diffusion of field after the interaction).

•The third harmonic is initially primarily p-polarised. During the interaction the amount of s-polarisation increases dramatically - likely due to an increase in the magnetic field. At later times the harmonic is unpolarised (perhaps because of a change in the mechanism of 3rd harmonic generation - Langmuir wave collapse?)

Summary

- measurements of high order harmonics can provide useful information about the physics of high intensity laser interactions with high density plasmas

- polarimetry measurements of harmonic emission imply the generation of magnetic fields approaching ~ 1 GigaGauss

- spatially resolved measurements agree with simulations that magnetic field assymetries are produced from 45 degree angles of incidence

- temporally resolved measurements suggest that the growth rate of the magnetic field is ~ $I^{1/2}$ suggesting theponderomotive force is the principal field generation mechanism

Ion Beams in Short Pulse, High Intensity Laser Matter Interactions.

B. F. Lasinski, A. B. Langdon, C. H. Still, M. Tabak, R. P. J. Town, W. L. Kruer, and S. C. Wilks

Lawrence Livermore National Laboratory

D. R. Welch

Mission Research Corporation

for the

Fast Ignitor Workshop

November, 2002.

This work was performed under the auspices of the US Department of Energy by the University of California Lawrence Livermore National Laboratory under contract No. W-7405-ENG-48

We are beginning a new effort to model the production of ion beams in short-pulse, high intensity laser matter interactions.

- We are building on our previous work in this area: S. Wilks *et al*, PoP, **8**, 542 (2001) and S. P. Hatchett *et al*, PoP, **7**, 2076 (2000).
- Parameters are motivated by earlier Petawatt experiments [R. A. Snavely *et al*, PRL, 85, 2945 (2000)] and more recent experiments on JanUSP as reported in A. J. MacKinnon *et al*, PRL, **88**, 215006 (2002) and Hui Chen *et al*, Poster CP1.133 (this conference).
- We are in the early stages of using these 2 modeling tools for these studies:
  - Z3, our modern massively parallel explicit particle-in-cell code
    - PIC codes simulate the production of energetic charged particles in the laser matter interaction.
  - LSP, a direct implicit code developed at Mission Research
    - Code reference: D. R. Welch *et al*, Nucl. Inst. Meth. Phys. Res. **A 242**, 134 (2001).
    - LSP models the transport of energetic charged particles through high-density matter. Please also see: CP1.113 by M. Tabak *et al* and C. P. 1.114 by R. P. J. Town *et al*.

Earlier PIC modeling and experiments have elucidated the role of density gradients in energetic ion production

- Basic idea is that sheath electric fields formed by the hot electrons at the rear surface of the target accelerate ions.

- This mechanism at the front surface is not as effective due to the shallower density gradients expected there.

- Our goal is to build on these efforts to be able to specify in detail how to focus these energetic ions with the required energy spectrum for the many proposed detector and fast ignition scenarios.

Our 1D simulations are a prelude to more complex 2D and 3D modeling

In 1D, model overdense plasma slabs with steep gradient at the back and shallower gradient at the front surface.

Sample density profile:

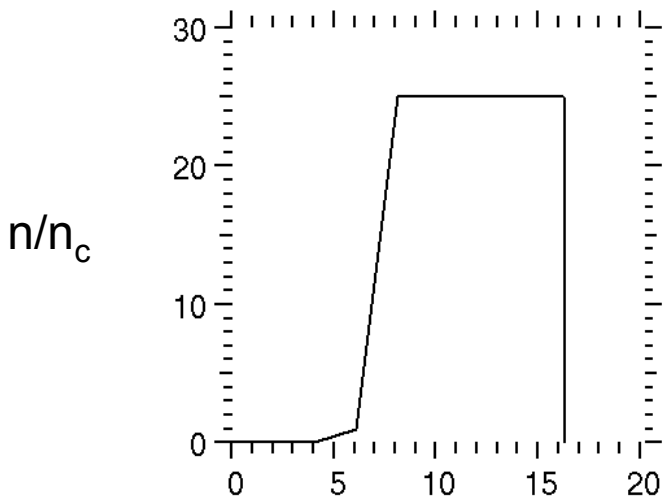

z = laser propagation direction in μm

Several families of simulations: peak density $10n_c$, $25\ n_c$ with laser intensities 1×10^{18} to 1×10^{20} W/cm^2 for 1 μm light and T_e = 3, 5 keV

In 1-D, explore the zoning and computational requirements needed to study this ion acceleration process.

We monitor the Poynting flux to ascertain how far the laser has penetrated the relativistically overdense plasma slab.

As part of the Z3 diagnostics suite, we apply a low pass temporal filter, $[\sin(\pi\omega/\omega_0)/(\pi\omega/\omega_0)]^2$, to fields and fluxes to separate the laser and the low frequency fields and fluxes. We identify these quantities with the subscript s

Example: Laser at 2 x 10^{19} W/cm^2 for 1 μm light onto a 25 n_c, 3 keV plasma slab.

Plot $(\overline{\text{Poynting flux}})_s$ at 60(-) 120(-) 180(-) 240(-) 300(-) fs:

$(P)_s$

Normalized to incident flux for 2 x 10^{19} W/cm^2

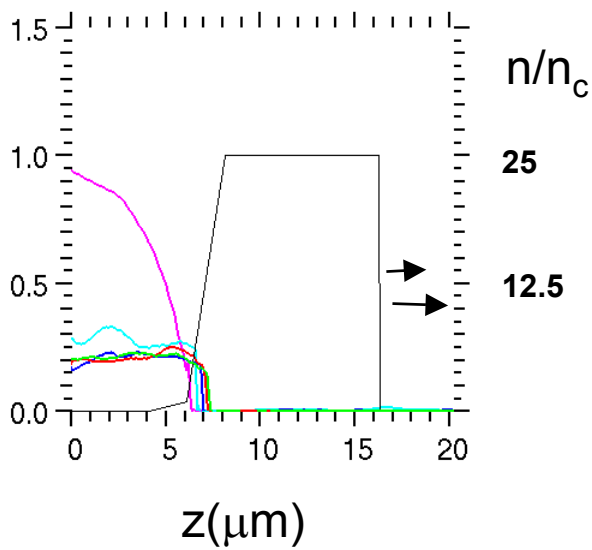

Laser rises to full value in 50 fs

There is considerable reflection once laser hits the overdense plasma.

The heated electrons rapidly traverse the plasma slab.

Electrons: uz vs z

Ions: uz vs z

t = 75 fs

uz

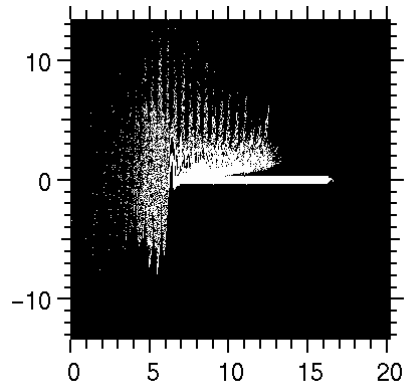

Heated ions emerge from the steep back surface at early times due to the finite $(vth)_e$.

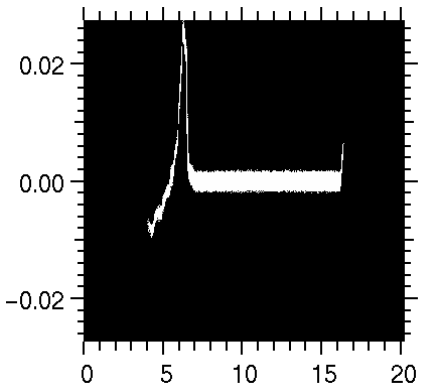

t = 90 fs

uz

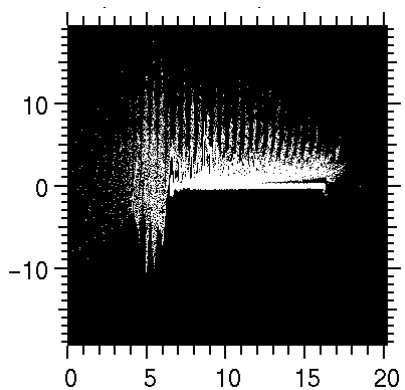

At 90 fs, heated electrons just reach the back surface of the slab which is 25 n_c for 8 μm.

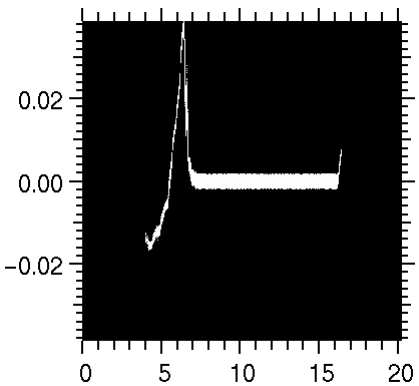

z(μm)

z(μm)

Ions: $m_i = 1836\ m_e$; $ZT_e/T_i = 14$

Ions at the back have increased acceleration once heated electrons reach that surface.

Electrons: uz vs z

Ions: uz vs z

t = 105 fs

uz

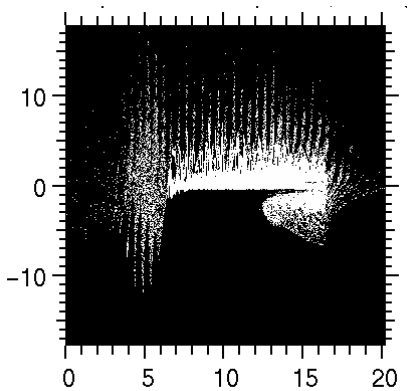

For these parameters hole boring initially produces the hottest ions, but these will take a long time to reach the rear surface.

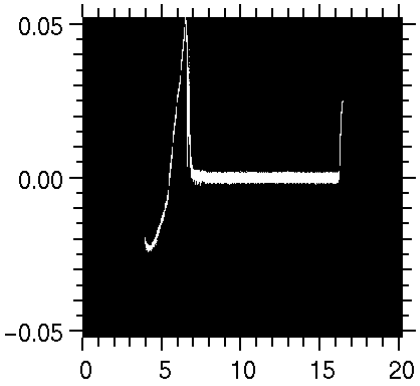

t = 120 fs

uz

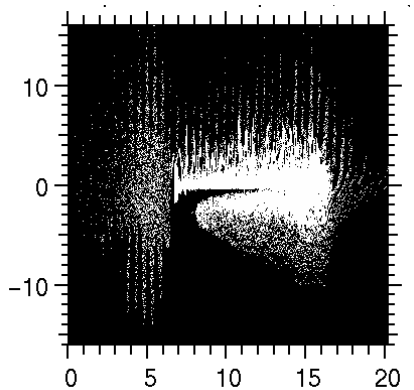

z(μm)

Heated electrons have been turned around and have almost gotten back to the front surface at 120 fs.

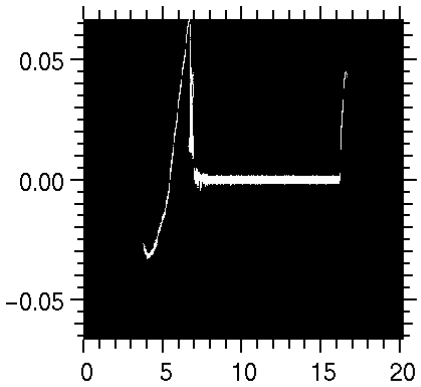

z(μm)

At later times, the most energetic ions are at the back surface

Electrons: uz vs z

Ions: uz vs z

t = 195 fs

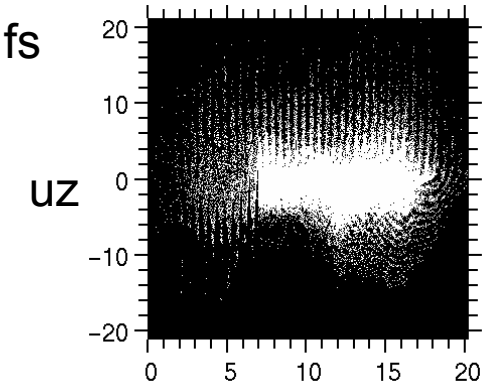

In this simulation, there are copious amounts of hot electrons throughout the plasma slab by ~ 200 fs

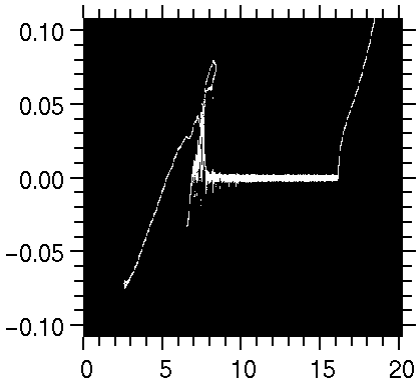

t = 210 fs

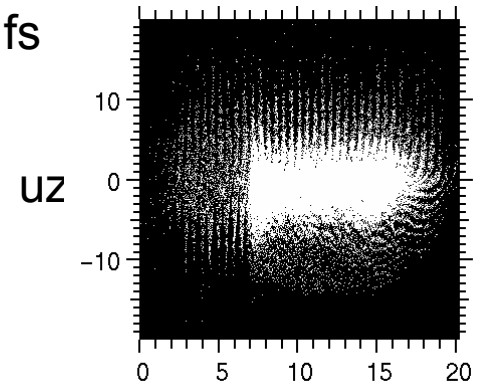

Recall that the laser has not yet penetrated appreciably into the overdense plasma slab at this time.

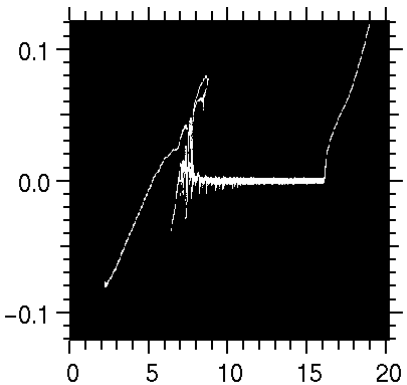

z(μm)

z(μm)

We monitor the distribution functions and find the expected energetic electrons.

Number vs kinetic energy

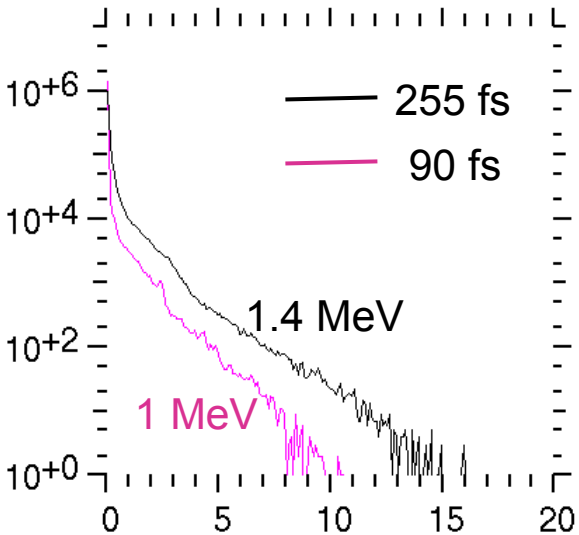

kinetic energy (MeV)

At 90 fs, the energetic electrons have just reached the back surface.

There has been significant slab heating at 255 fs

Electron kinetic energy vs time

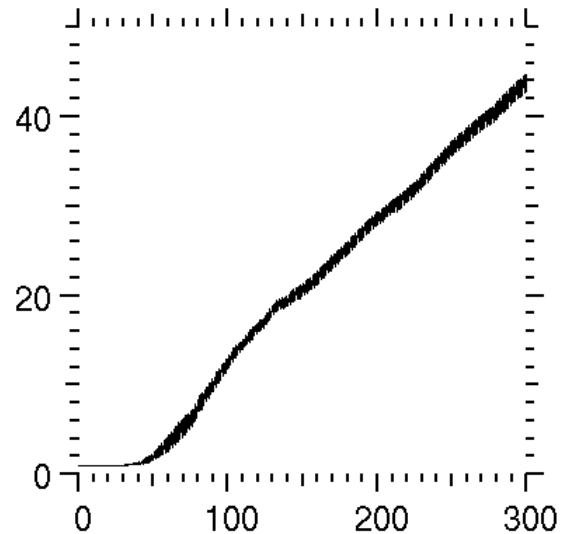

time (fs)

Here, the kinetic energy is normalized to the initial electron kinetic energy

We observe significant ion heating

Number vs kinetic energy

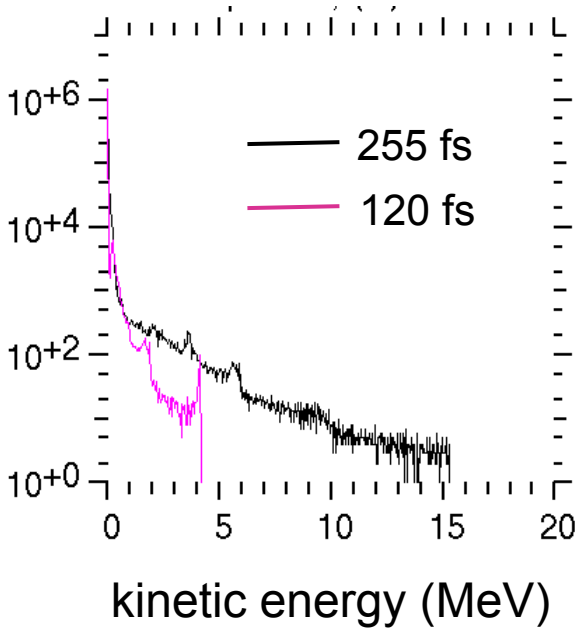

Ion kinetic energy vs time

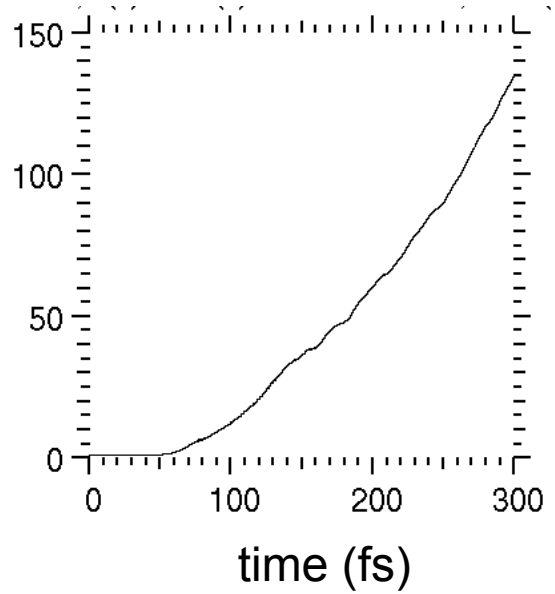

Here, the kinetic energy is normalized to the initial ion kinetic energy

As expected, we find profile steepening due to the laser penetration.

Plot of ion density, n/n_c, at t=180 fs.

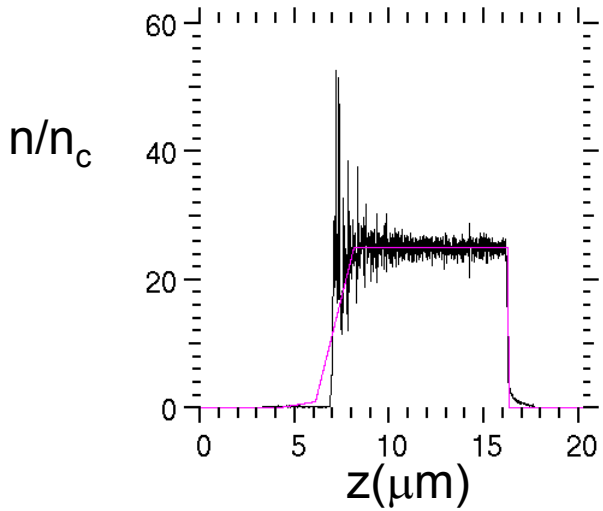

The initial density profile is shown by the magenta curve

- These 1D simulations contain the essential physics of energetic proton generation
- They are well resolved with 2.5 λ_{de} per dz and approximately 60 cells per vacuum laser wavelength and 1.5 x 10^6 particles per species.
- These 1D simulations serve as comparison points for modeling in which these criteria are relaxed as needed for 2D and 3D studies.

Use LSP to monitor protons which come off the back of a CH plasma slab 200 microns thick.

Monitor protons at 16.67 ps. Incident beam of electrons is on for 10 ps.

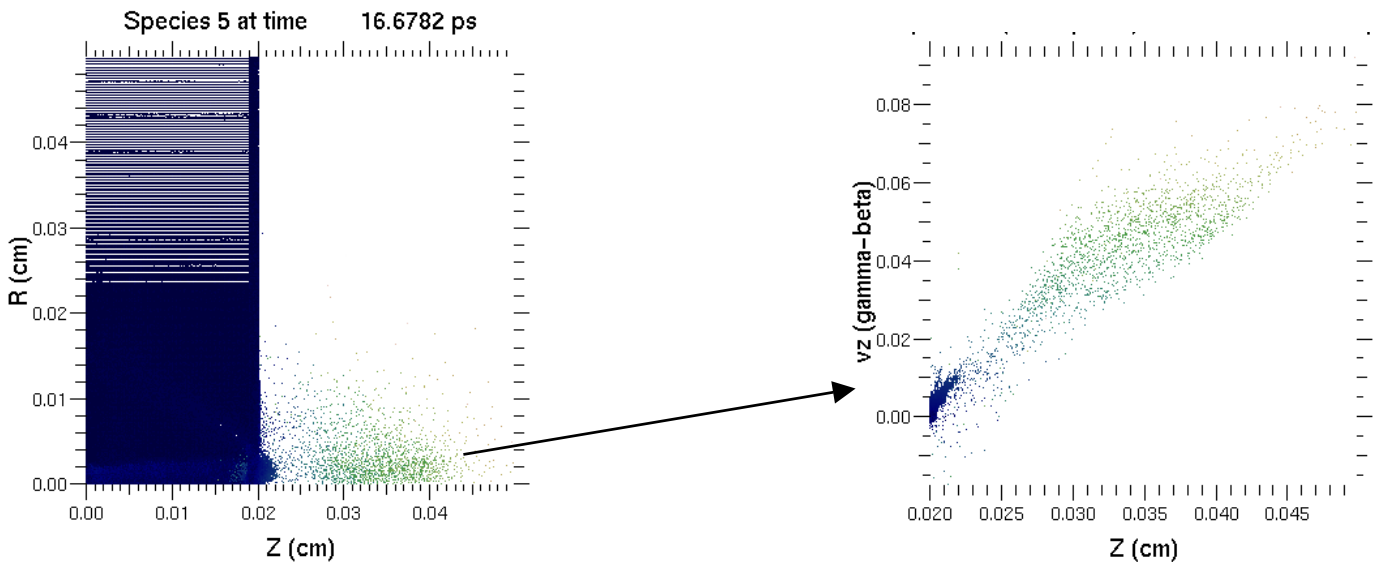

Incident beam of electrons at γ = 2.79 is injected at left hand edge of plasma slab

We have a strategy mapped out for further LSP studies.

- Check how proton spectra off the back depend on initial electron beam energy. (Preliminary results suggest that proton spectra in LSP for electron beams thru thick slabs are relatively insensitive to electron beam directed energy).
- Specialize to slabs with only a thin layer of hydrogen at the back end.
- Investigate sensitivity to zoning at the rear of the plasma slab.
- Then model the transport of protons through various plasma slabs.

We are beginning a new effort to model the production of ion beams in short-pulse, high intensity laser matter interactions.

- We are building on our previous work in this area: S. Wilks *et al*, PoP, **8**, 542 (2001) and S. P. Hatchett *et al*, PoP, **7**, 2076 (2000).
- Parameters are motivated by earlier Petawatt experiments [R. A. Snavely *et al*, PRL, 85, 2945 (2000)] and more recent experiments on JanUSP as reported in A. J. MacKinnon *et al*, PRL, **88**, 215006 (2002) and Hui Chen *et al*, Poster CP1.133 (this conference).
- We are in the early stages of using these 2 modeling tools for these studies:
  - Z3, our modern massively parallel explicit particle-in-cell code
    - PIC codes simulate the production of energetic charged particles in the laser matter interaction.
  - LSP, a direct implicit code developed at Mission Research
    - Code reference: D. R. Welch *et al*, Nucl. Inst. Meth. Phys. Res. **A 242**, 134 (2001).
    - LSP models the transport of energetic charged particles through high-density matter. Please also see: CP1.113 by M. Tabak *et al* and C. P. 1.114 by R. P. J. Town *et al*.

Application of fast ignition to heavy-ion fusion *

B. Grant Logan, LBNL
Debra Callahan LLNL

6th International Workshop on Fast Ignition of Fusion Targets
Dolphin Beach, Florida
November 17-19, 2002

- **Fast ignition target requirements for fuel compression using heavy-ion beam indirect drive (results on an analytic model by Debra Callahan, LLNL)**
- **Impacts of fast ignition on HIF target chambers**
- **Dielectric wall accelerators for fast ignition with heavy-ions**

*This work was performed under the auspices of the U.S. Department of Energy by the University of California, Lawrence Berkeley and Lawrence Livermore National Laboratories under Contract Numbers DE-AC03-76SF00098 and W-7405-Eng-48, and by the Princeton Plasma Physics Laboratory under Contract Number DE-AC02-76CH03073

Fast ignition was one of the original ideas for heavy-ion fusion

- The original idea for driving fusion targets using heavy-ion beams by Al Maschke in the 1970's was based on direct-drive compression with heavy ion beams of 10 ns duration, followed by ignition with a short pulse (100 ps) of high energy heavy ions-although it was not referred to then as fast ignition.

- Ion deposition peaks near the end of the ion range→ near 100% coupling efficiency→ fuel "tamping" extends ion ignition pulse up to 100 to 200 ns

- Today, electron-cooling, pulse compression and focusing of heavy-ion bunches from storage rings at GSI Germany, (similar plans at ITEP in Russia and in RIKEN in Japan) have made significant progress to the point that the next GSI ring upgrade should be able to deliver 40 kJ of 100 GeV Uranium ions to a few hundred micron focal spot within a 40 ns pulse. This terawatt ion beam peak power would, however, still be too low for fast ignition by a factor of 10^3 to 10^4, even allowing for longer pulses.

- More advanced accelerator, pulse compression and target schemes might be considered to close this gap [Logan PPPL ICC conference, April, 1999, Sharkov/Basko, et.al at the HIF2002 Symposium in Moscow], and recent discovery of conversion of short-pulse laser light to few-ps light ion beams [Nova Petawatt experiments on rear-foil proton acceleration]

The National Ignition Facility (NIF) will prove the scientific feasibility of ignition and energy gain in the laboratory for Inertial Fusion Energy (IFE)

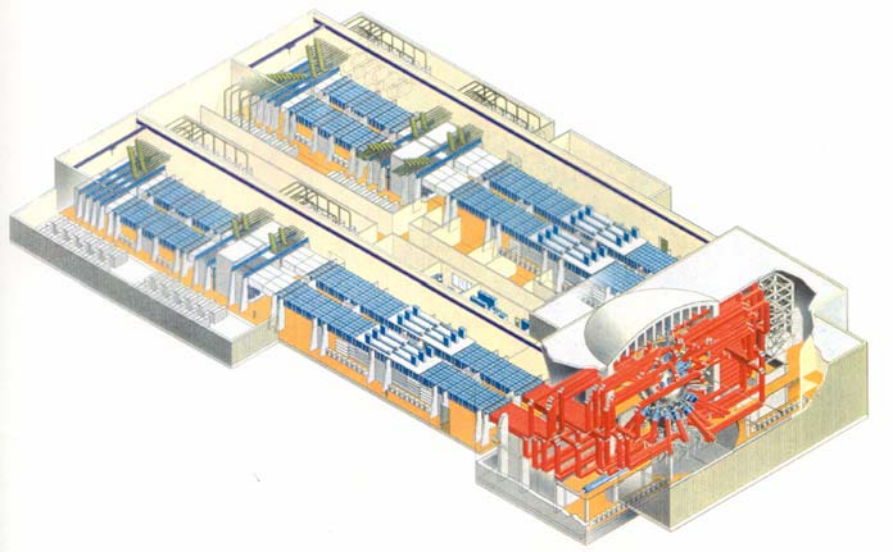

LLNL Associate Director George Miller (Dec. 2001) "The facility is really coming together and we are pointing to first light to the target chamber in about 18 mo and real experimental data." For further information, see the NIF web site: http://www.llnl.gov/nif/

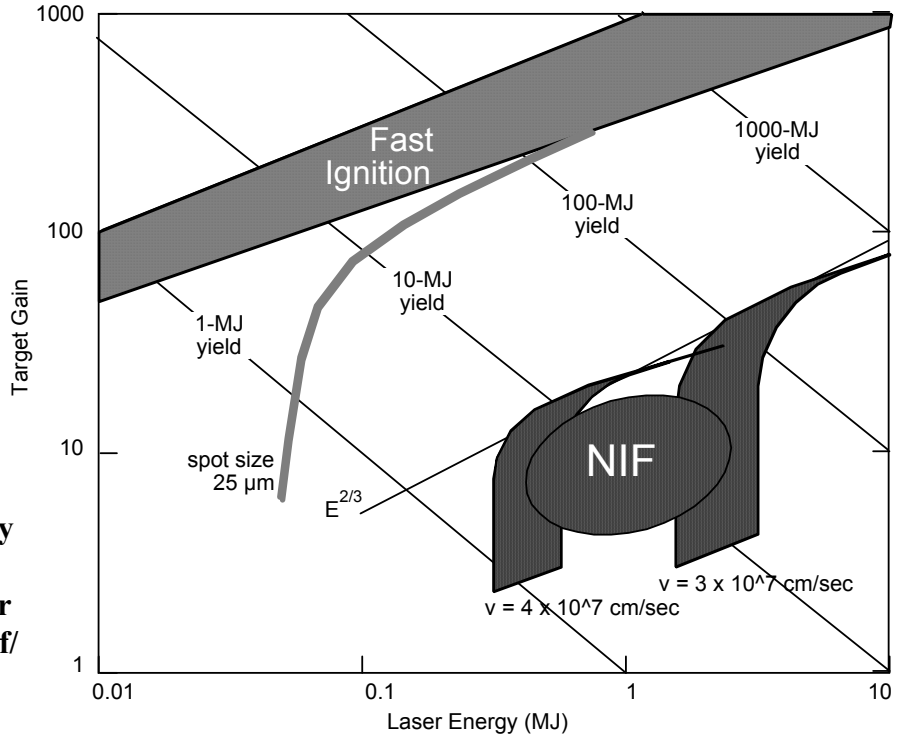

NIF will provide important data for heavy-ion fusion:

- **Achievable target gain →affects total ion beam energy/accelerator efficiency/cost**
- **Required capsule precision, smoothness →affects HIF target fabrication costs**

Why Heavy Ions?

→ High energy accelerators with MJ class beam energies exhibit efficiency, pulse rate and durability needed for IFE

→Clear bore magnets used to focus the beams can tolerate target debris and radiation.

→ Same motivations apply to using heavy-ions vs lasers for fast igniters

Need for high power + need to minimize current (for focusability) → High ion kinetic energy

↓

High Z ions for dE/dx (or else range too long)

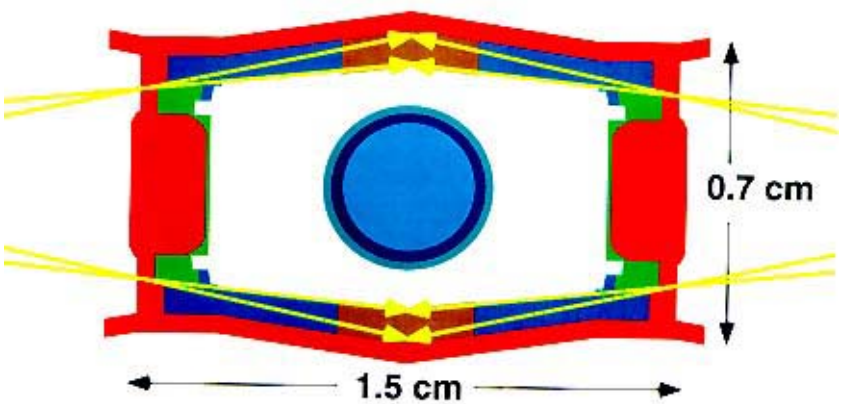

For fast igniter focusability we might use high Z, 50-200 GeV heavy ions together with close-in micro plasma lens or local magnetic self pinching

HIF target designs will also set HIF accelerator beam requirements. Advances in HIF target design have much leverage to reduce or mitigate accelerator requirements

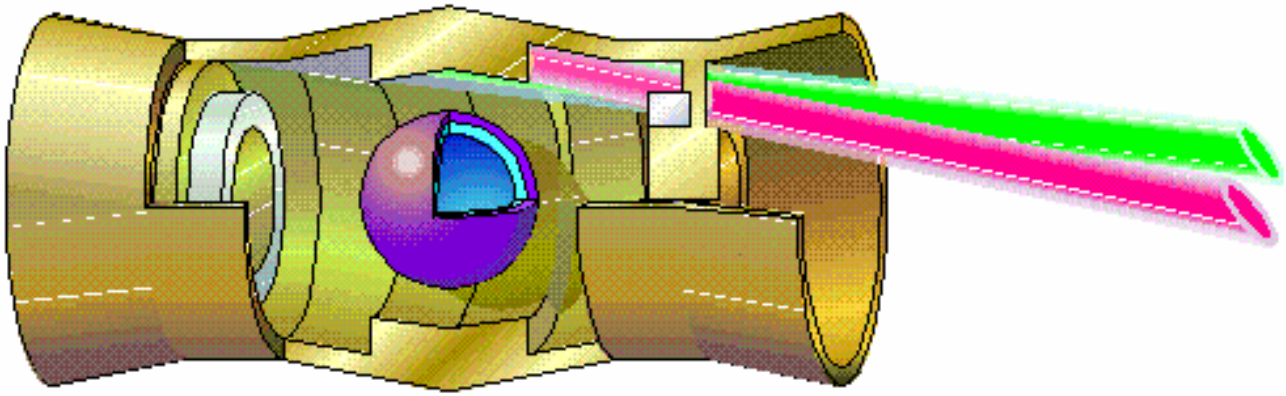

- Decrease ion range →reduce accelerator voltage and cost
- Increase spot size →allow higher beam emittance or smaller number of beams
- Increase pulse width →reduce ion bunch compression needed

→ Fast ignition may reduce HIF indirect drive requirements for fuel compression even more in these same ways

Increasing target array illumination cone angle allows more room for shielding between final focus magnets

(From Jeff Latkowski, LLNL)

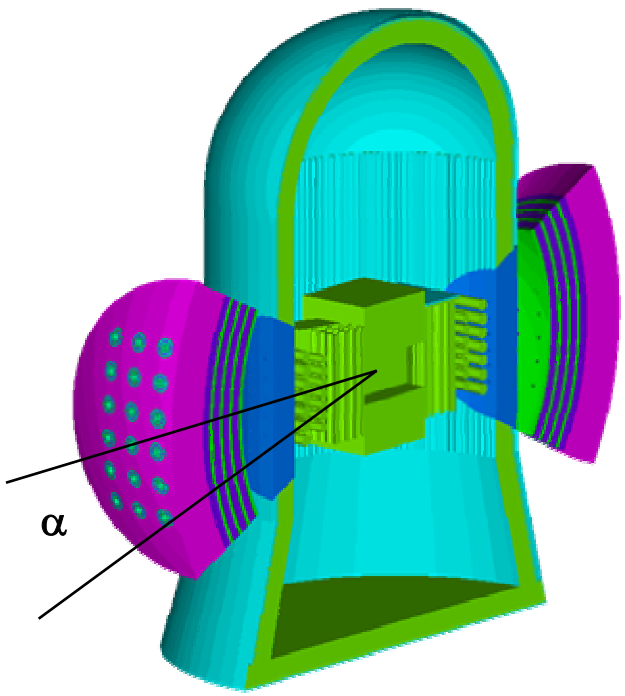

α = final focus magnet array half-angle

Increasing the array half-angle by 50% gives most of the benefits of doubling the array.

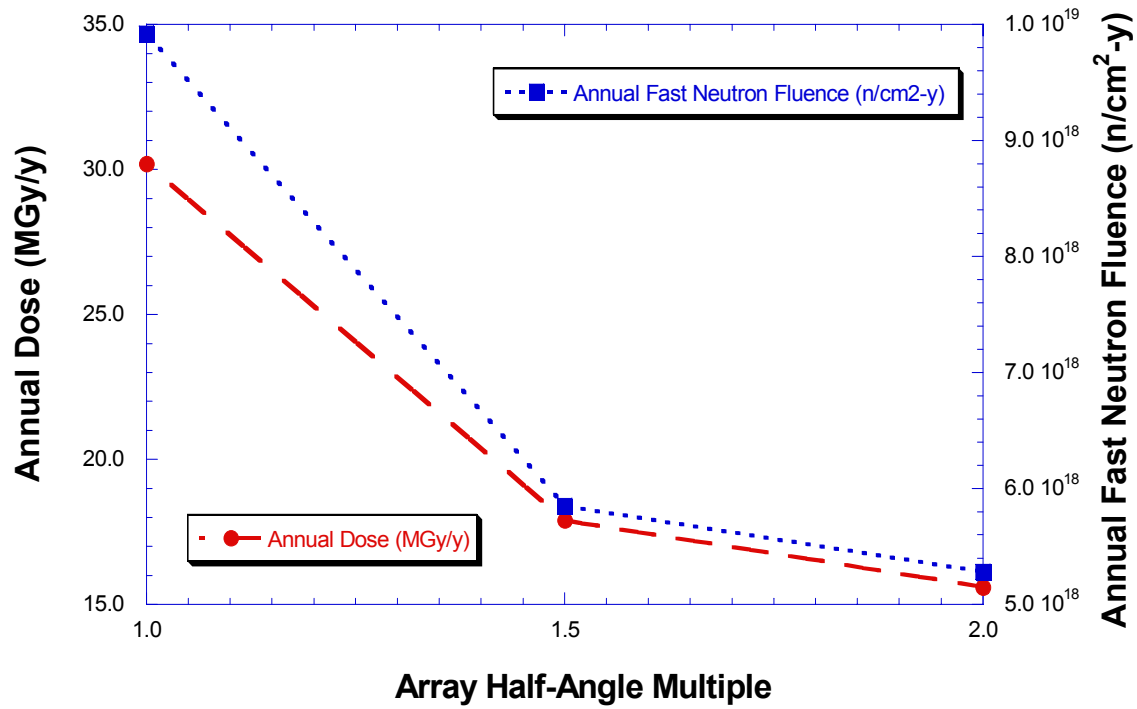

Scalings predict that using a 26% smaller hohlraum will reduce the energy to 3.5 MJ

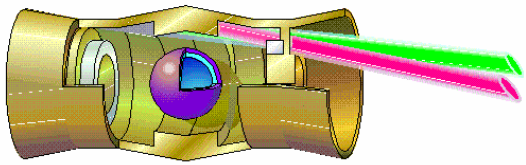

Energy distribution in conventional case to capsule ratio target

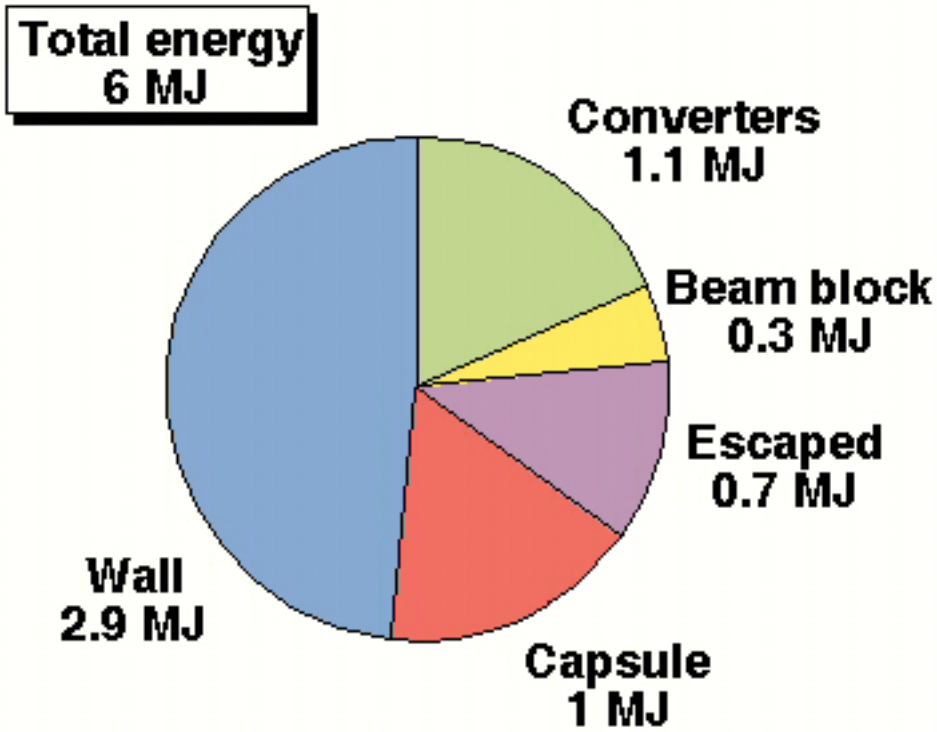

Energy scaling:

- Wall ~ area ~ L^2
- Converters ~ volume ~ L^3
- Beam block ~ area ~ L^2
- Escaped ~ area ~ L^2
- Capsule unchanged

This predicts a 3/4 scale hohlraum (L = 0.74) will require 3.5 MJ

Fast ignition *might* benefit heavy ion fusion in a variety of ways: higher gain or lower drive energy, lower peak ion power (for fuel compression), less required ion bunch longitudinal compression and bigger spots (allow higher longitudinal and transverse emittance), and more room for shielding final focus magnet arrays.

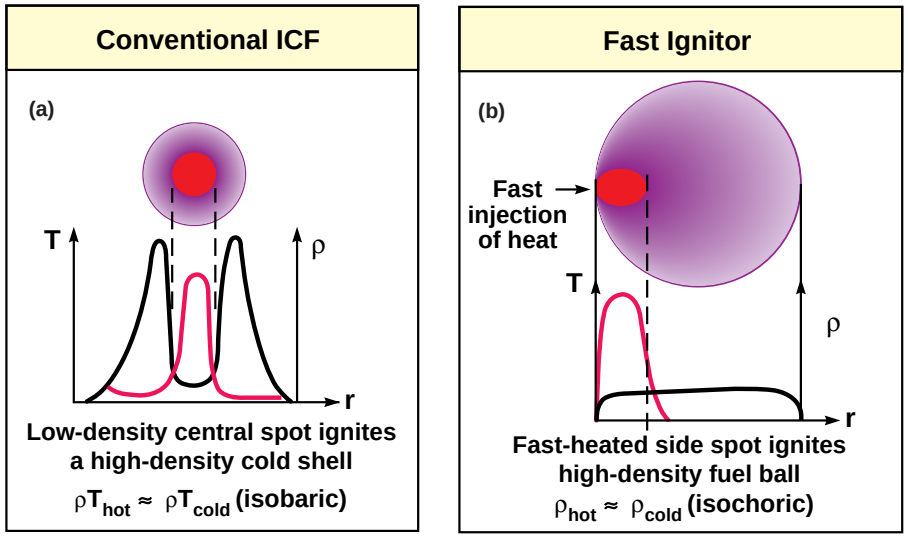

50-00-0397-0426Bbp01

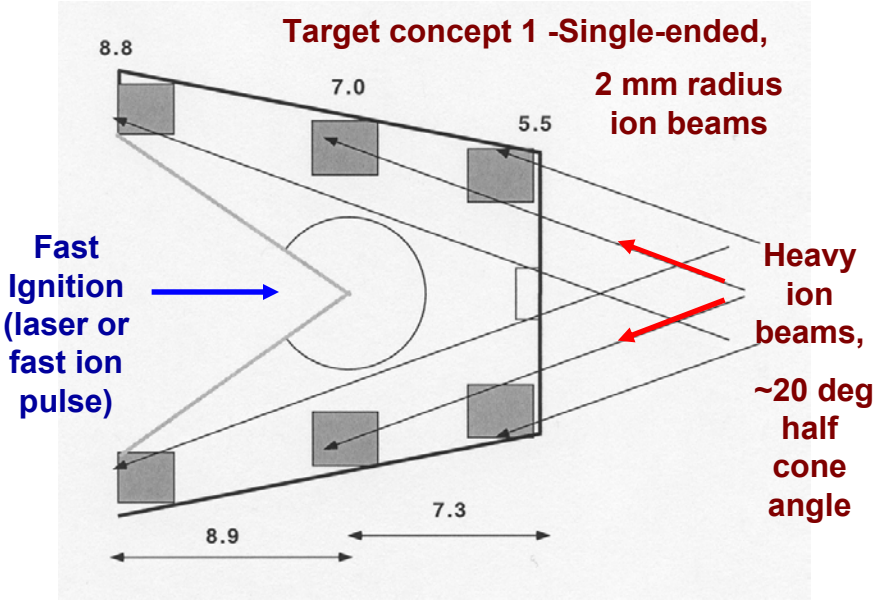

In principle, fast ignition can reduce total drive energy for any driver used to supply the dominate energy for fuel compression (as long as the igniter beam energy < 1 MJ)

This talk summarizes recent work of Debra Callahan (LLNL), who used analytic target models to estimate ion beam requirements to drive three hohlraum geometries at 150 and 120 eV

Two other heavy-ion driven hohlraum geometries were studied to explore the possibility of larger beam spots

Target Concept # 2 Single ended ion driven hohlraum with 4 mm radius ion beams

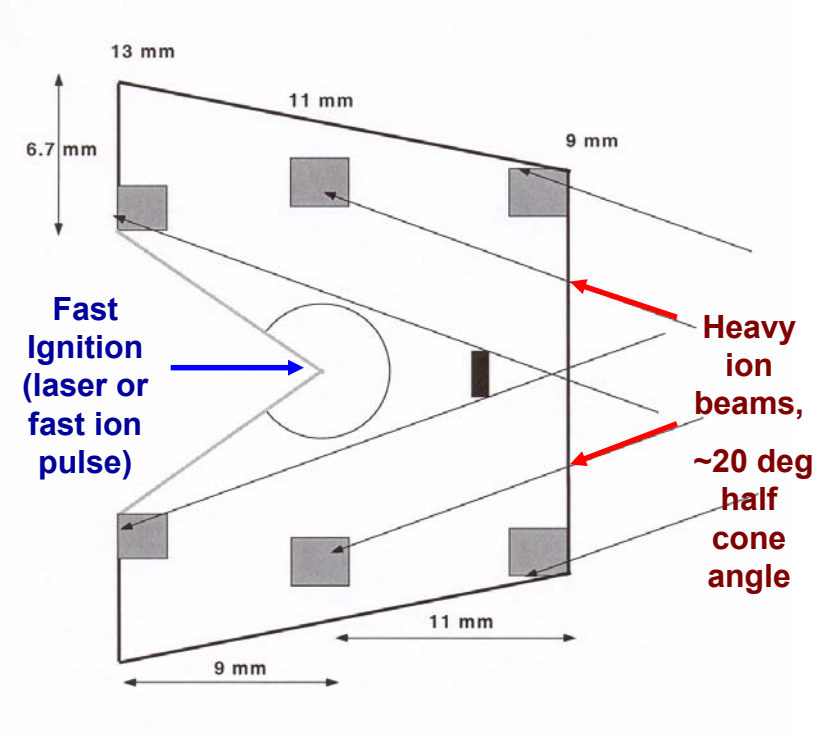

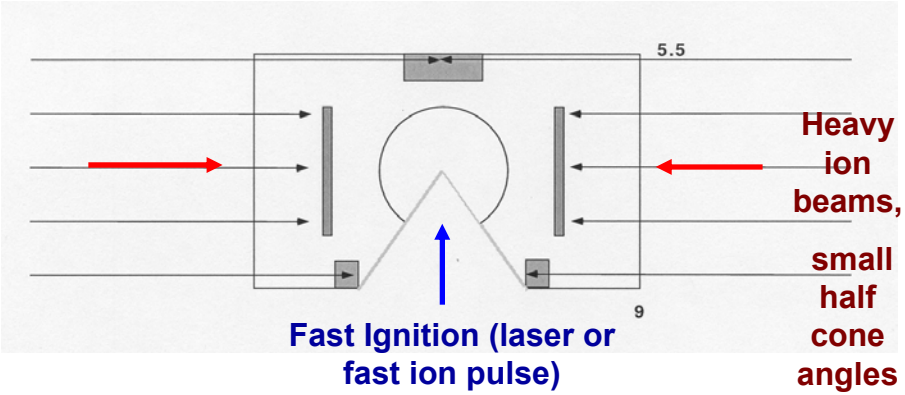

Target Concept # 3 Double-ended ion driven hohlraum with 5 mm radius ion beams

Summary of results of Debra Callahan's analytic model

Target Concept	Hohlraum T_{rad} (eV)	Target Yield in MJ [Gain]	Ion energy (MJ)	Incident Igniter E_b (MJ @30%)	Ion power (TW)	Ion Pulse width (ns)	Spot radius (mm)	Drive1/2 Angle* (deg)
Conv. close coupled	240	430 [130]	3.3	NA	330	8	1.0	12
FI #1	150	460 [160]	2.7	0.15	160	17	2.0	20
FI #1	120	350 [140]	1.9	0.6	68	28	2.0	20
FI #2	120	350 [76]	4.0	0.6	150	28	4.0	20
FI # 3	150	460 [150]	2.9	0.15	170	17	5.0	<10
FI # 3	120	350 [120]	2.3	0.6	82	28	5.0	<10

→Preliminary conclusions: Fast ignition with heavy-ion driven compression in hohlraums may not increase target gain much because of radiator enthalpy.

→ May significantly reduce longitudinal beam compression, allow larger spot sizes and beam array angles (relaxes driver brightness, more room for focus magnets).

→Much more analysis needed on target symmetry, stability, and fabrication!

Monochromatic "fast proton" beam (from surface contaminants) exhibits accelerator-quality emittance (<0.5 mm-mrad) and bunch charge (~1 nC)

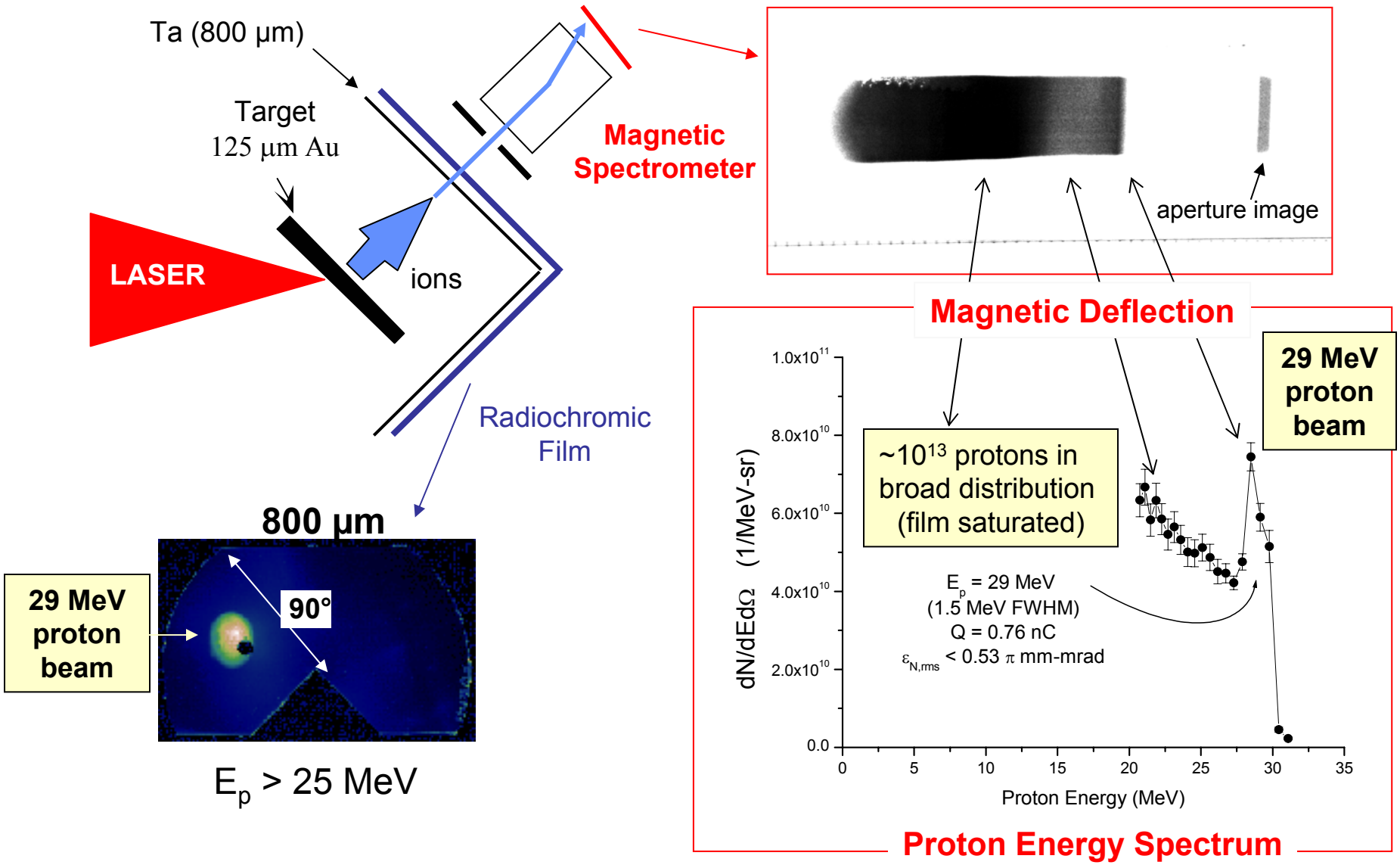

GENERAL ATOMICS

(From T.E. Cowan, M. Roth, J. Johnson, M. Perry, *et al.* (LLNL,GSI, MSFC, UA-Huntsville)

Protons and ions are accelerated in relativistic laser-solid interactions by three principal mechanisms

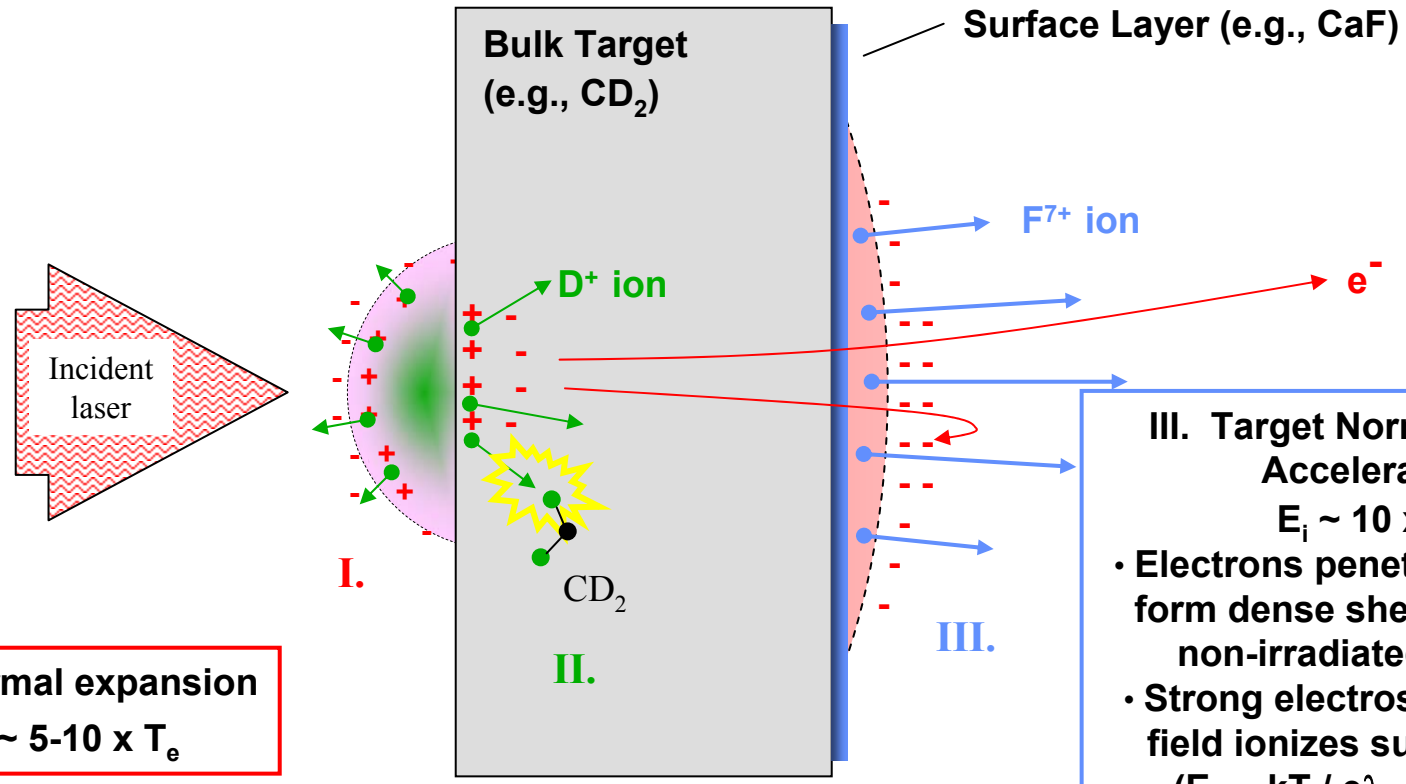

I. Thermal expansion
$T_i \sim 5\text{-}10 \times T_e$

II. Front-surface charge separation
Static limit: $T_i \sim T_e$

III. Target Normal Sheath Acceleration
$E_i \sim 10 \times T_e$

- Electrons penetrate target & form dense sheath on rear, non-irradiated surface
- Strong electrostatic sheath field ionizes surface layer ($E_o \sim kT / e\lambda_d \sim$ MV/μm)
- Rapid (~ps) acceleration in expanding sheath produces very laminar ion beam

GENERAL ATOMICS

(From Tom Cowan, GA)

Compact Dielectric Wall Accelerator with laser-ion injection for HIF ion-target interaction research

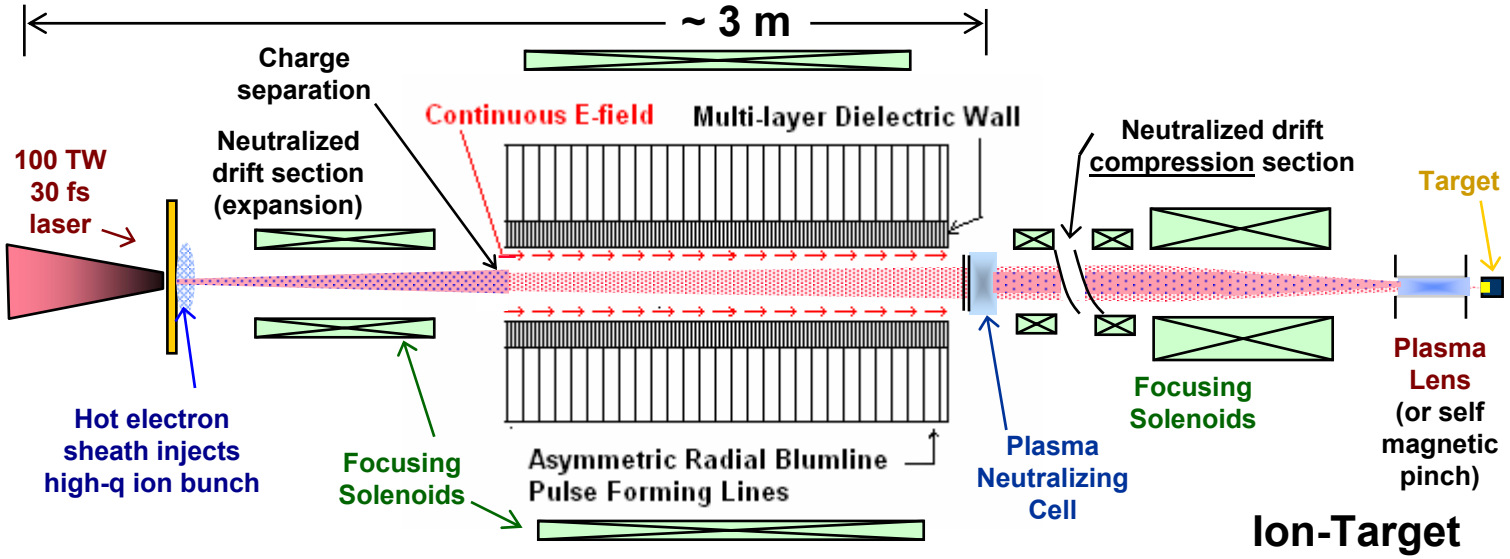

Laser-Ion Injector
10-20 MeV, q ~8-9 ions

Dielectric Wall Accelerator
~20-30 MV/m

Ion-Target Interaction @ 200 to 400 MeV

Development of advanced proton diagnostics for probing plasmas and shocked materials

The National Ignition Facility

Andrew Mackinnon

P.K.Patel, D.F. Price, M. Allen, M.H. Key, P.T. Springer

Lawrence Livermore National Laboratory

M. Borghesi,L. Romagnani

University of Belfast, U.K.

O.Willi, G. Pretzler

University of Dussledorf, Germany

Y. Sentoku, T. Cowan, R. Stevens, H. Ruhl

General Atomic, San Diego,CA

R. Snavely, J. King, R.R. Freeman,

University of California, Davis

J.C.Gauthier P. Audebert,

Ecole Polytechnique, Paris

P. Norreys, K.Lancaster, R.C.Clarke,R. Heathcote

Rutherford Appleton Laboratory, UK

GENERAL ATOMICS

LULI

UC DAVIS,

University of Dussledorf,

Rutherford Appleton Laboratory

*Work performed under the auspices of the U.S. Department of Energy by Lawrence Livermore National Laboratory under contract No. W-7405-ENG-48.

Recent experiments have detected an intense beam of protons emitted from the rear of the foil

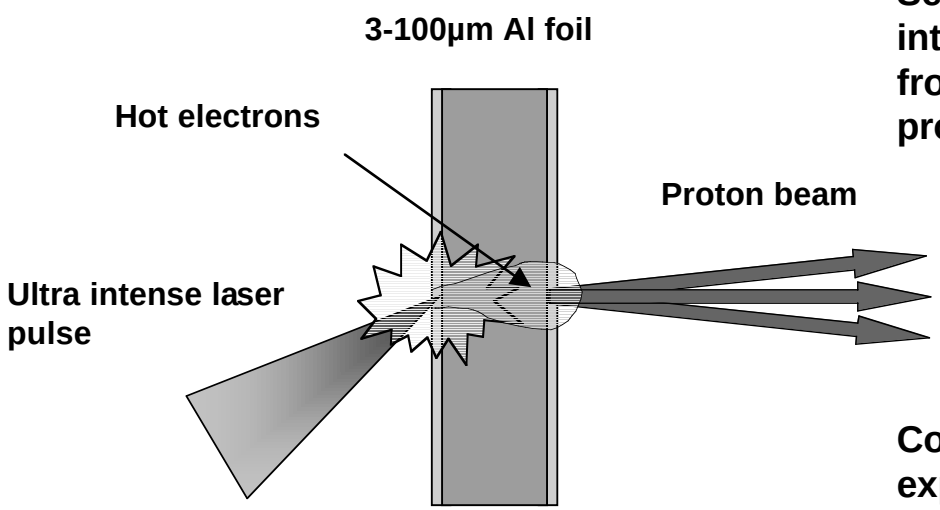

Several groups reported observations of an intense collimated beam of protons emitted from the rear of laser-irradiated foils. The protons are:

Highly collimated
Normal to rear surface
Intense
Energetic

Conflicting theories have been proposed to explain the origin of the protons, the acceleration mechanism, and the beam characteristics

Radiochromic film images of proton beam

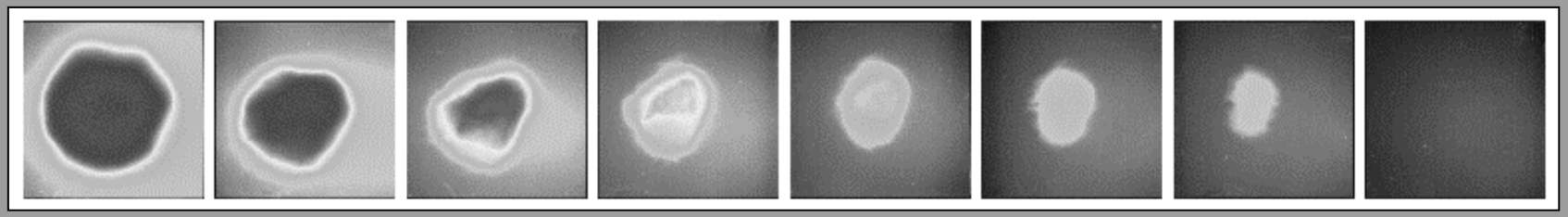

5.7 MeV | 8.9 MeV | 11.3 MeV | 13.4 MeV | 15.3 MeV | 17.0 MeV | 18.5 MeV | 23.4 MeV

In the last two years many groups have carried out experiments on laser driven proton beams

Michigan
Maxsimchuk, Nemeto, Umstadter et al.,

Osaka (GEKKO)
Murakami et al.,

RAL(VULCAN)
Clark, Zepf, Krushelnick, Norreys et al.,

LLNL(PW)
Snavely,Hatchett, Key et al.,

- **1-10% conversion of incident laser energy into protons with E >4MeV**
- **E_{max} ~ 50MeV**
- **highly directional (1-15°)**
- **Small emittance**

RAL(VULCAN)
Borghesi,Willi, Mackinnon et al.,

LLNL(JanUSP)
Patel,Mackinnon et al.,

LULI
Cowan,Audebert,Gautier,Pretzler,Roth et al.,

The laminar nature of the beam allows structures of order of 1μm to be resolved

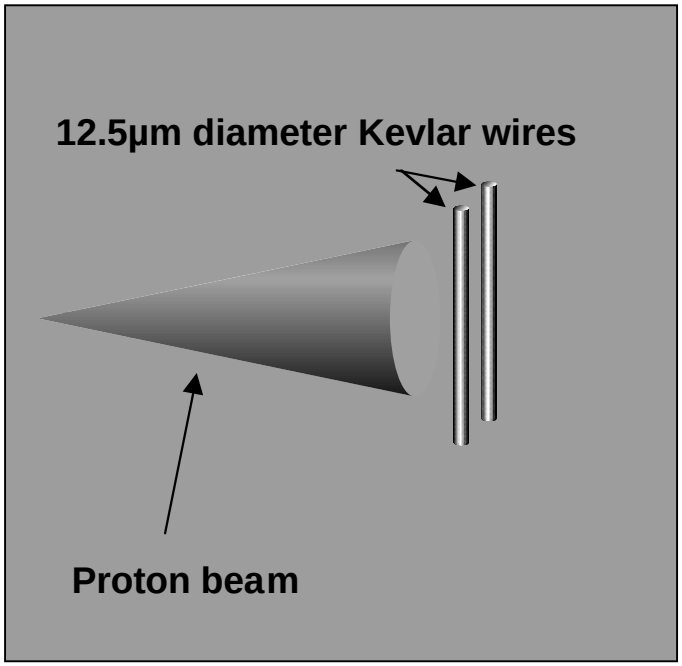

Optical Image

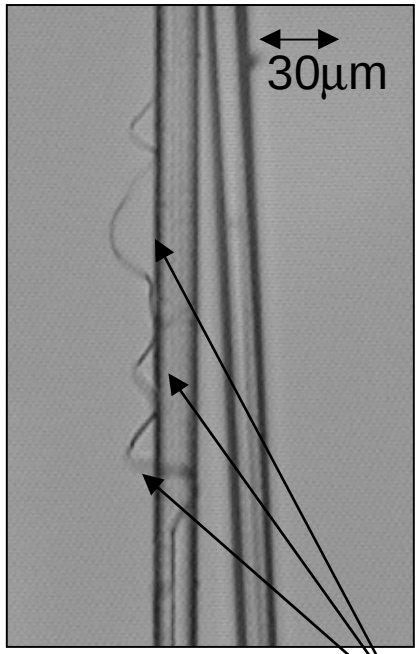

7MeV protons

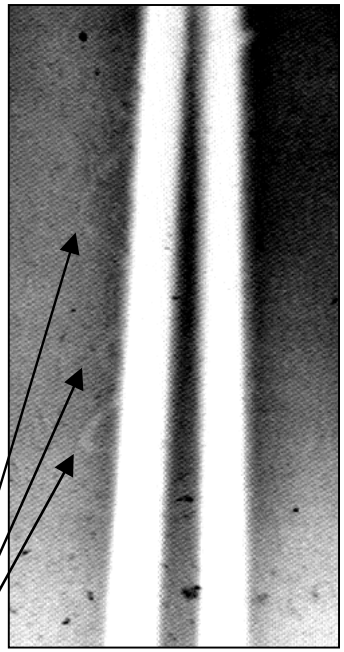

1μm wide Kevlar strands

• For thin objects resolution is a few μm but is limited in larger,thicker objects by the multiple scattering effect within the target and detector

Monte-Carlo proton transport shows that multiple scattering can account for the image formation

Proton transport through a wire

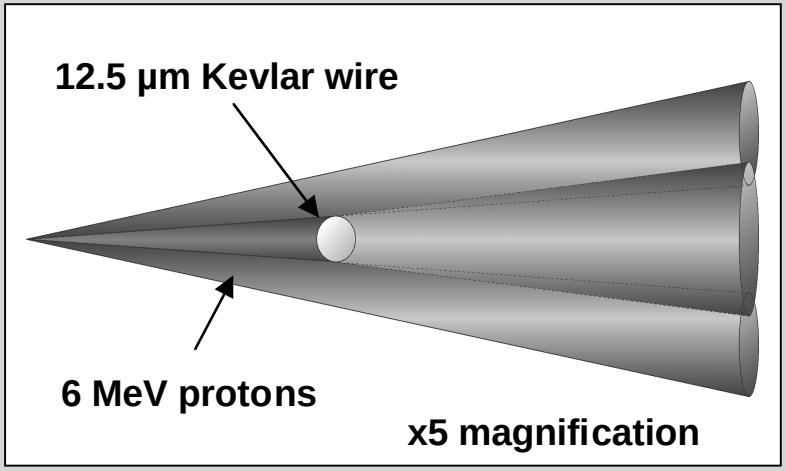

Code includes source size, multiple scattering, and detector response

Calculated lineout across wire

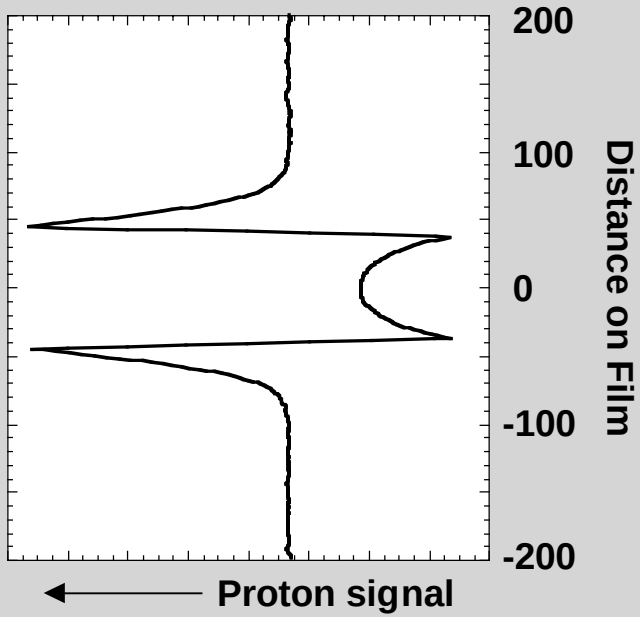

DATA
Lineout from 6MeV proton image of Kevlar wire

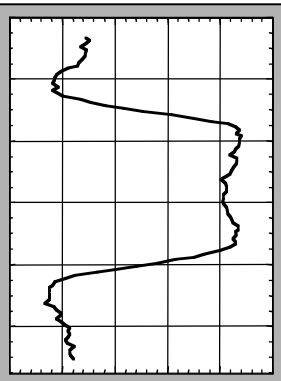

Proton radiographs of thick wires and rippled foils also show few micron spatial resolution

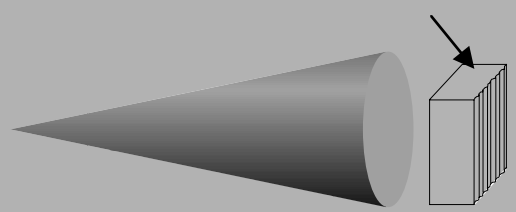

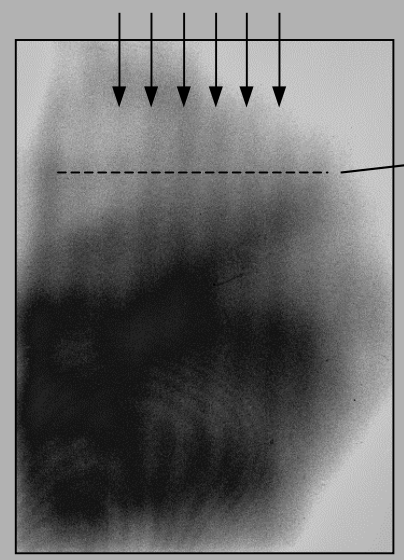

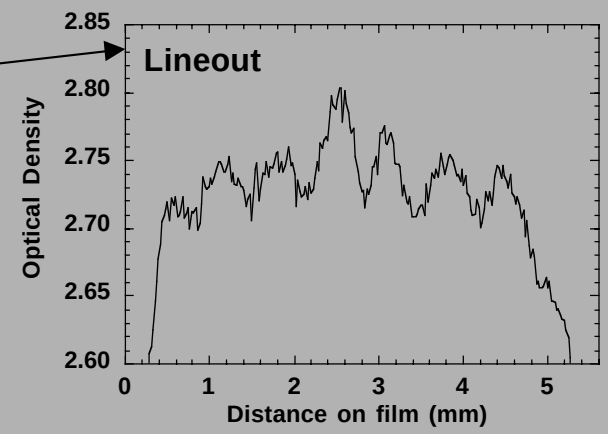

- We can develop this technique to obtain micron spatial resolution and picosecond time resolution of thick, high-Z objects
- This should allow proton radiography of RT growth to be diagnosed in 10-20µm tantalum - requires 5-10µm resolution
- Experiments on JanUSP and SRIM modeling is being carried out to test resolution limits in these conditions

Deflectometry techniques such as Moire can be used to precisely measure small deflection angles

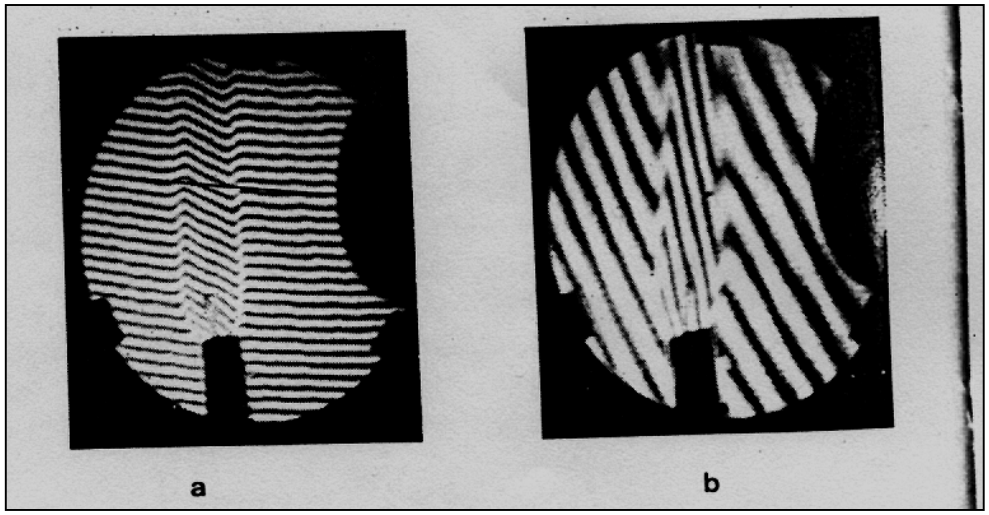

• Refractive index of flames - fringe shifts are quantitatively related to refractive index gradient
(Kafri&Glatt, The physics of Moiré Metrology)

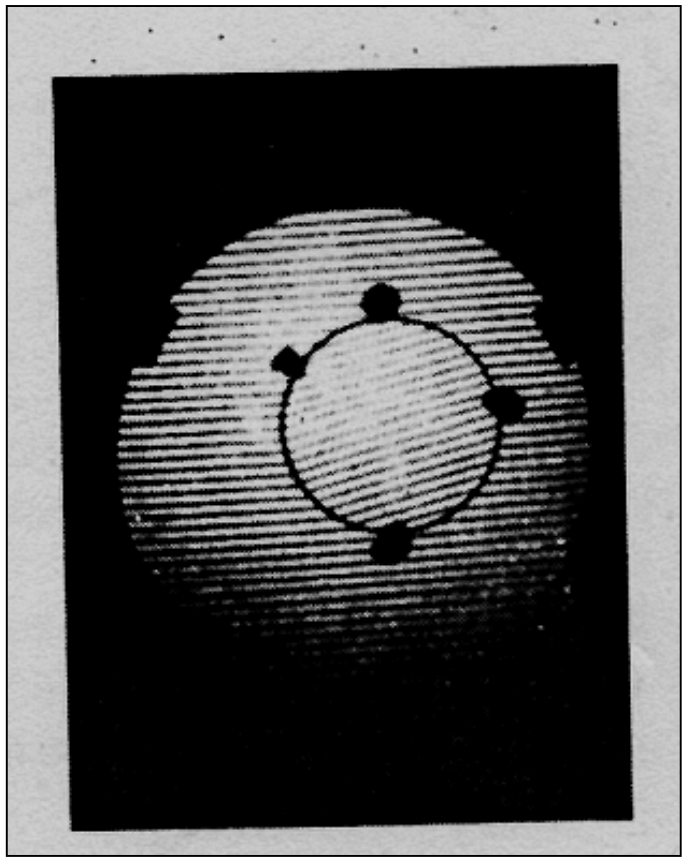

• Focal length of lenses (diverging lens)

The Moiré effect can be used to measure field gradients via proton deflections

Moiré effect occurs when light or particles passes between two crossed gratings

- Two identical gratings rotated at angle to each other produce Moiré fringes

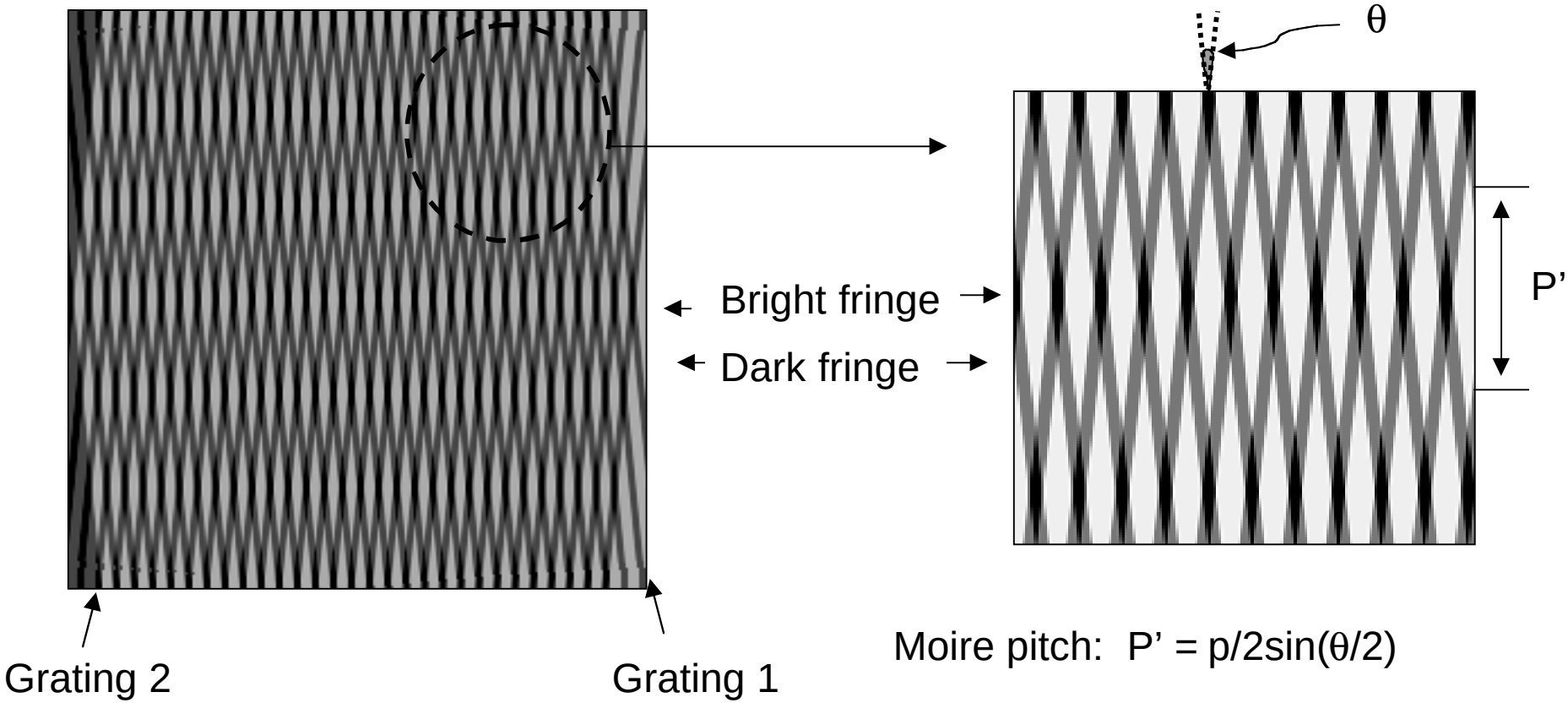

Moire pitch: $P' = p/2\sin(\theta/2)$

Fringe shifts are directly proportional to beam deflections

High contrast Proton Moiré fringes have been obtained with 1D gratings

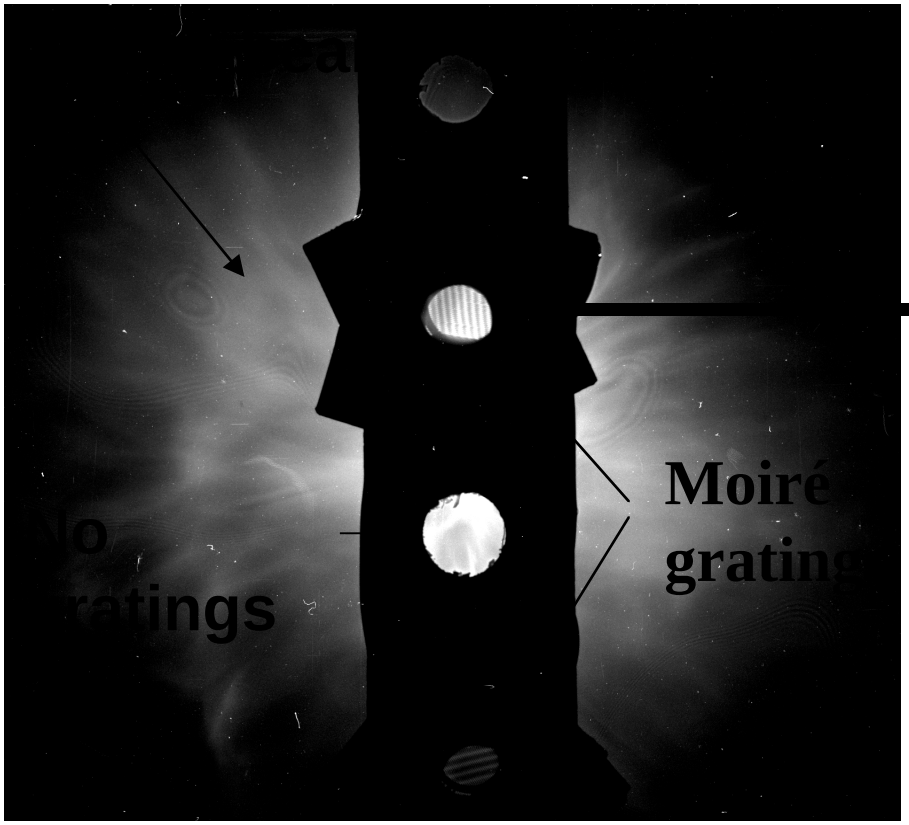

Moiré Fringes

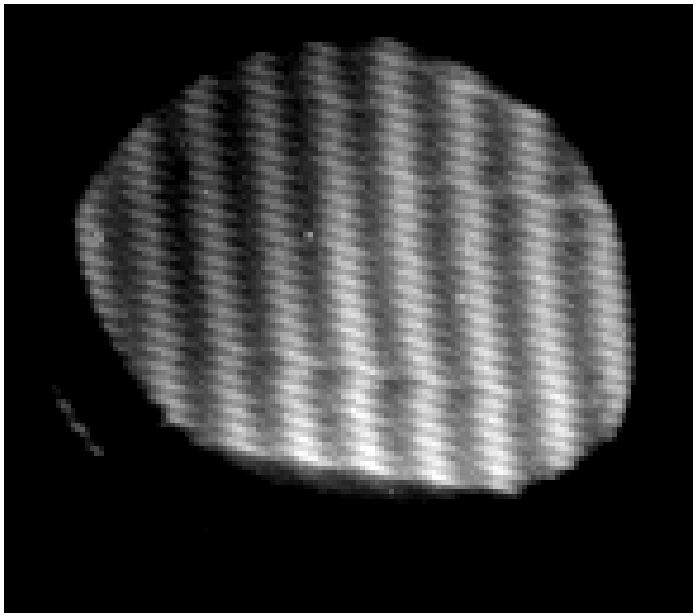

Fringes are rotated w.r.t. optical pattern

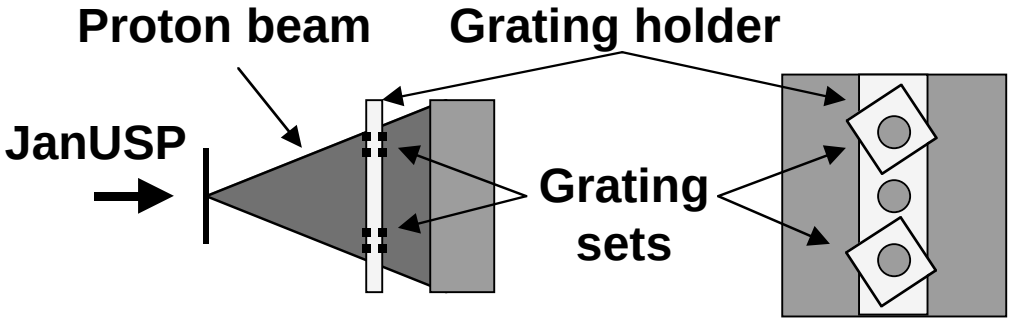

Shifts in the fringes can be mapped to deflections in the proton beam as it passes through a plasma

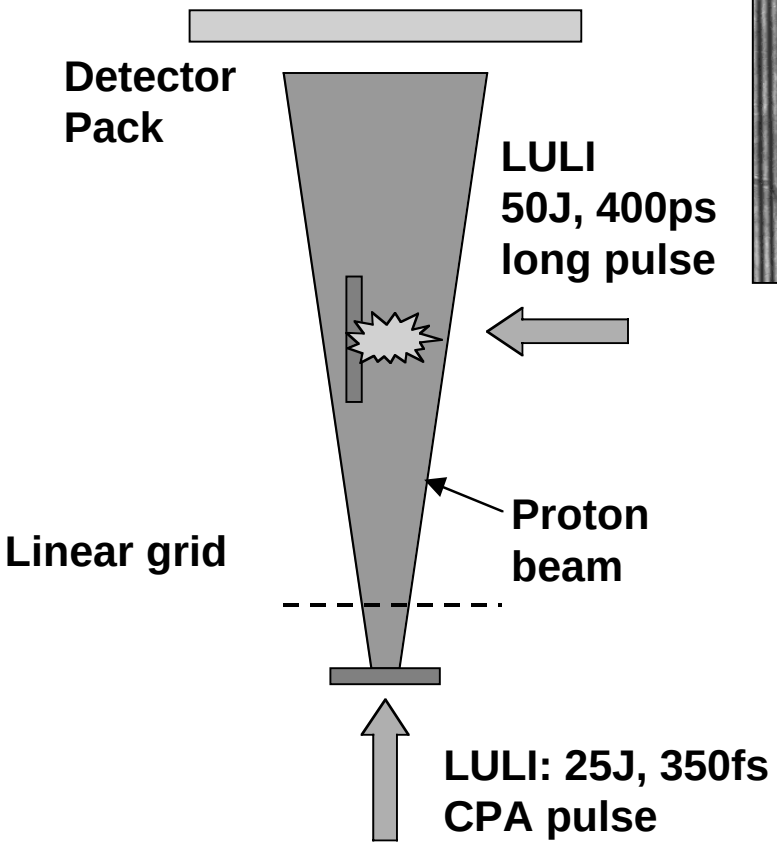

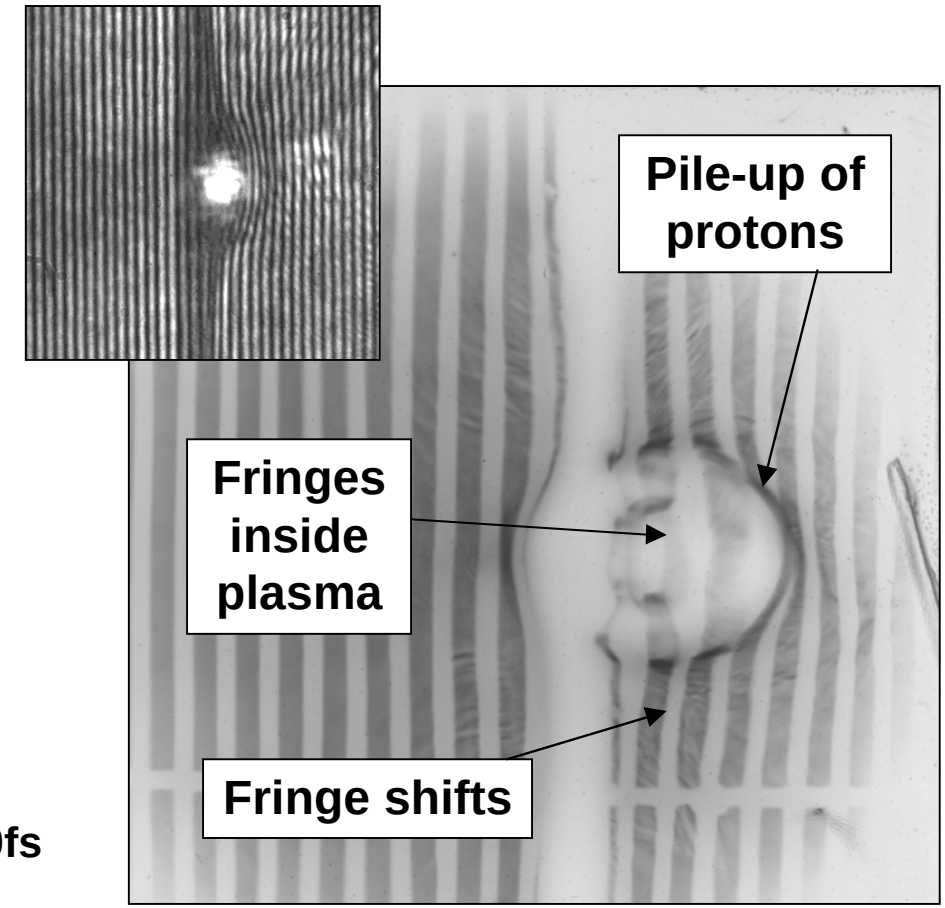

Shifts from the undisturbed fringe position give a 2D map of the proton beam deflections - similar to interferometric techniques

2D information can also be extracted by using a square mesh instead of linear grid

RCF Image: 8MeV protons

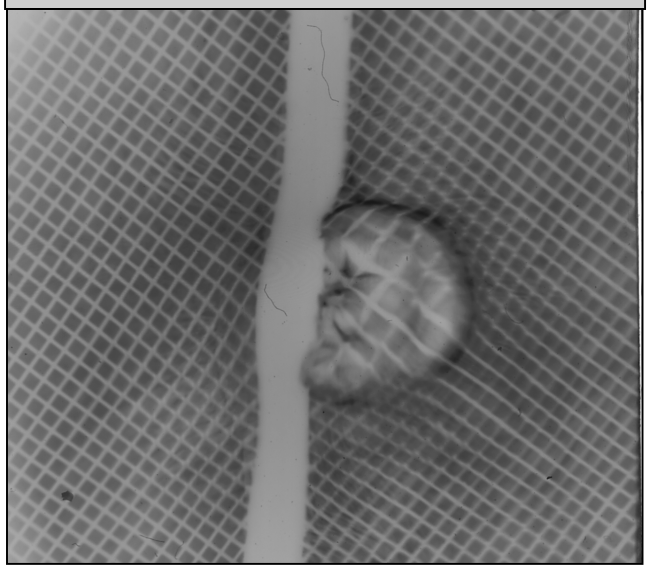

LULI Laser
λ = 1μm
τ = 700ps
I = 3×10^{15} Wcm^{-2}

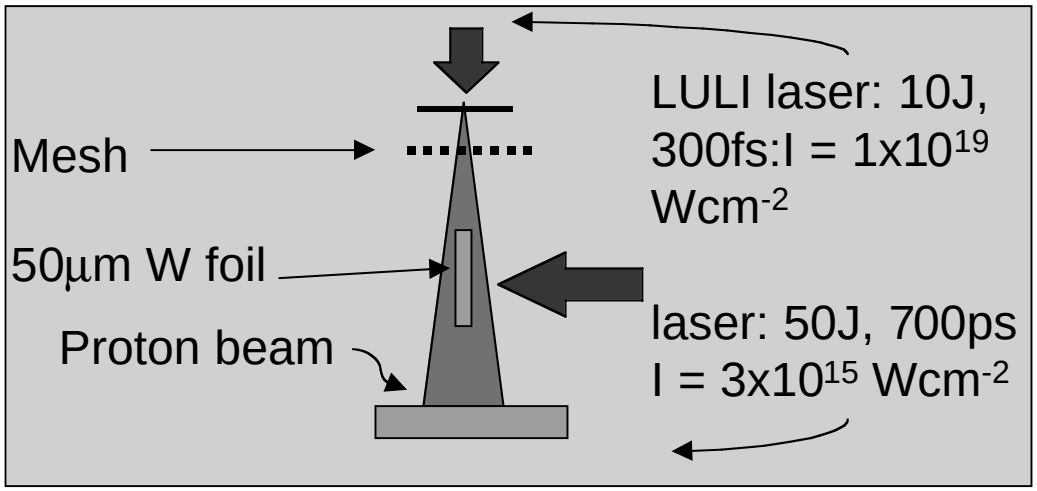

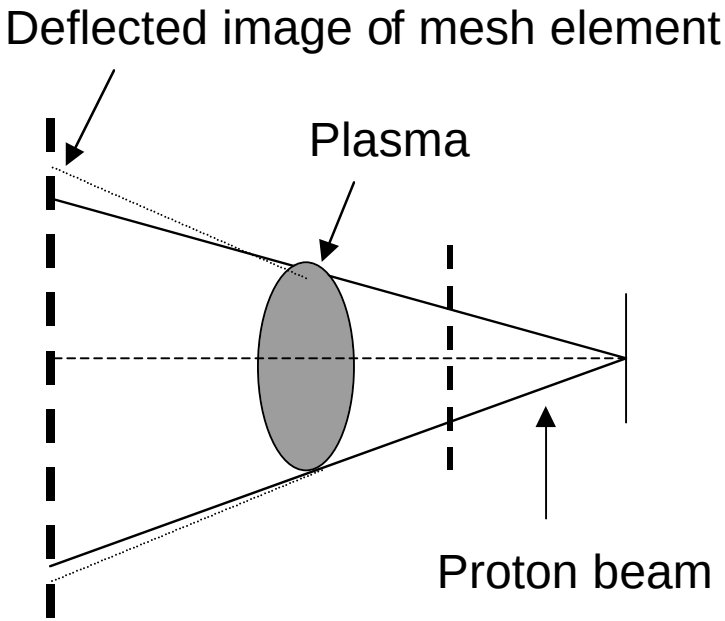

The technique may be used to characterize hohlraum magnetic fields

- **Deflections obtained by observing shifts in Moiré fringes**

Proton Moiré

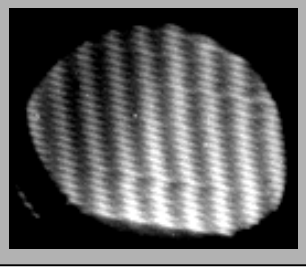

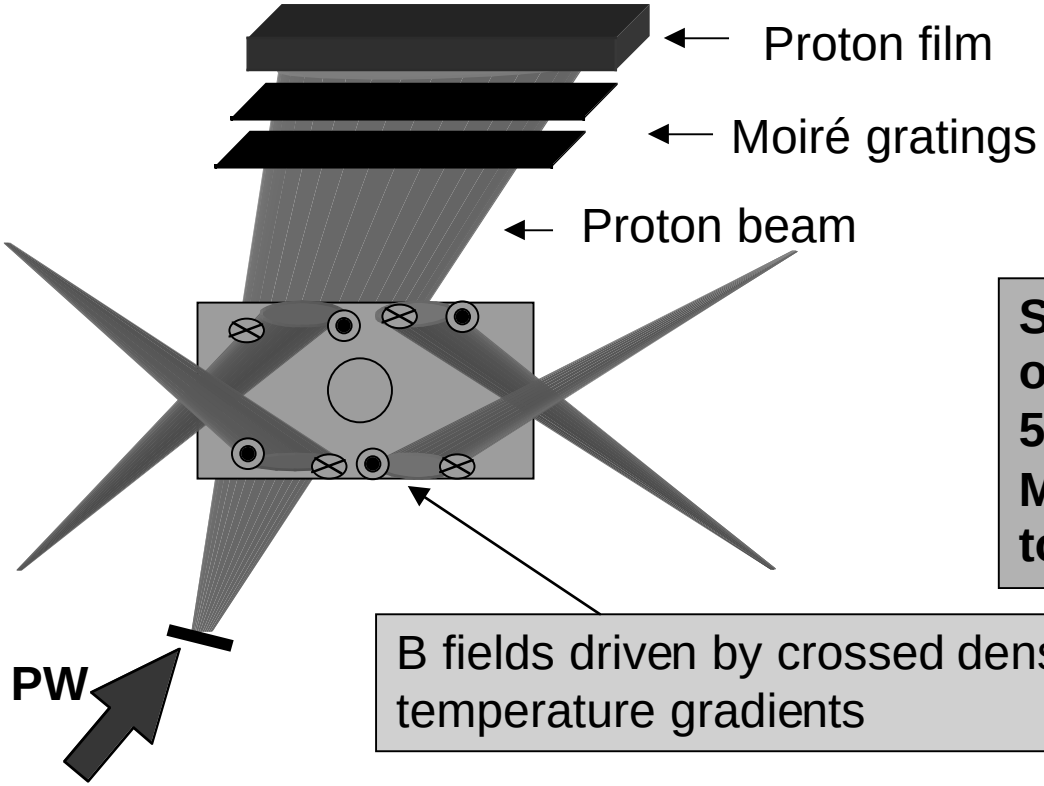

B fields driven by crossed density and temperature gradients

Simulations predict 1MG B fields over 500μm -> rotation angles of ~ 5-10° for 6MeV protons: Proton Moiré can measure angles down to < 0.1°

1ps at 3kJ; I = 1×10^{19}Wcm^{-2}; T_p = 1MeV; CE~1% of protons 6MeV => 5×10^{13} protons.

Proton radiographs of imploding cores have been recently obtained on the Vulcan laser

Cold target

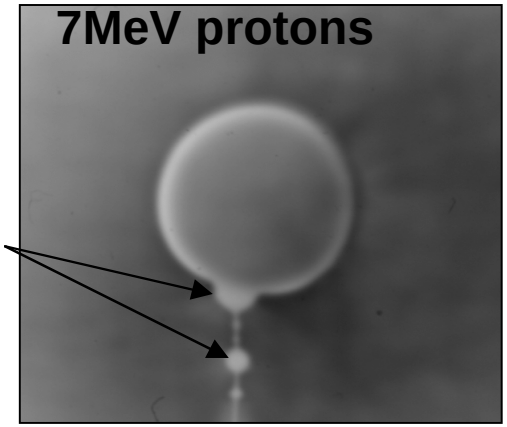

Symmetric drive

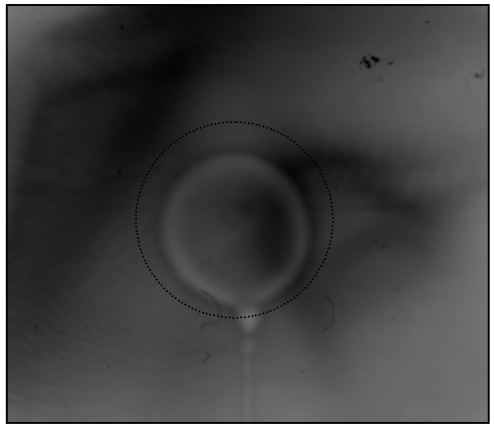

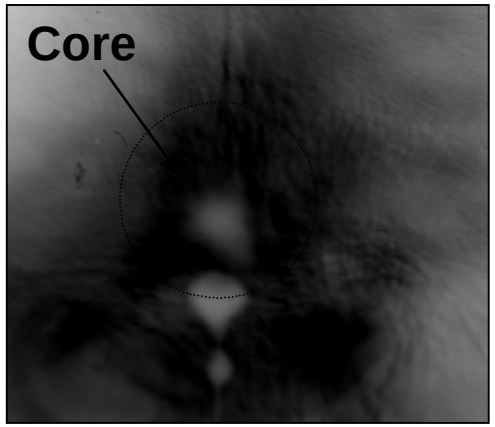

To + 2.0ns **To + 3.0ns**

Heaters: 6x50J @ 1ns
Targets: 500µm 7µm and 3µm wall

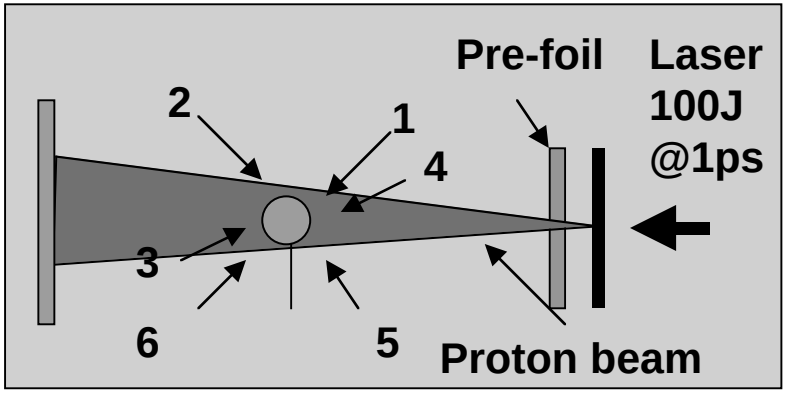

Asymmetric drive

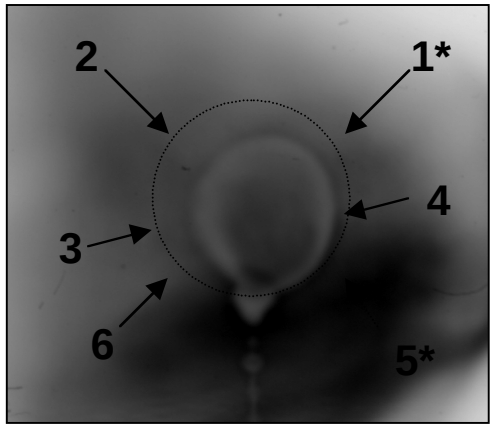

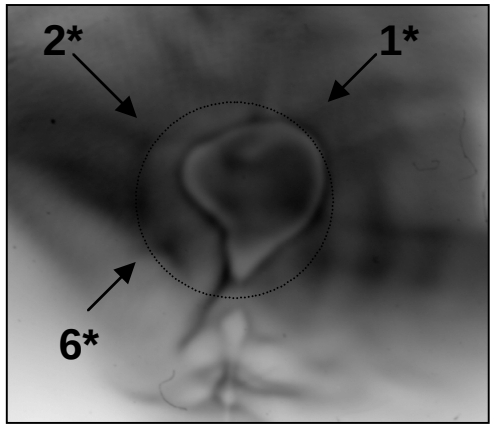

To + 2.0ns
(*B5 and B1 off)

To + 1-5ns*
(*B2; 5ns early,B1&B6:2ns early)

Summary

Proton beams produced by laser have some unique properties:

- **They are highly laminar**
  - **micron scale resolution**
- **Very short duration ~modeling suggests few 100fs to few ps**
  - **experiments show at least <few ps (Borghesi et al., Phys. Plasmas 2002)**
- **Highly penetrating**
  - **up to few mm of solid density material for ~20MeV protons**
- **Can apply optical deflectometry techniques to improve precision of measurements**

Applications

- **Electromagnetic field diagnostic**
- **A density perturbation diagnostic**
- **Density diagnostic in implosions (- small scale/NIF scale ?)**
- **Measurement of the location and/or density of shock fronts in laser and x-ray driven experiments**
- **Proton/Heavy ion focusing for isochroic heating**

Electromagnetic Emission from Short-Laser Pulse Interaction with High Density Plasmas

A. Maksimchuk, K. Flippo, D. Umstadter

University of Michigan, Ann Arbor

V. Yu. Bychenkov

P. N. Lebedev Physics Institute, Moscow, Russia

V. T. Tikhonchuk

Institute of Fundamental Physics, University of Bordeaux, France

G. I. Dudnikova

Institute of Computational Technologies, Novosibirsk, Russia

FIW 2002

Motivation

- Experiments on ion acceleration have shown that the amplitude of charge separation field could be as high as 1 TV/m
- Relativistic electrons traversing these fields due to acceleration/deceleration may be efficient emitters
- Earlier experiments by Santos et. al, PRL (2002) showed the conversion efficiencies of $\sim 10^{-13 \div 14}$ in visible.
- Directional compact source in XUV.
- Examine mechanisms of EME

Experimental setup

No target

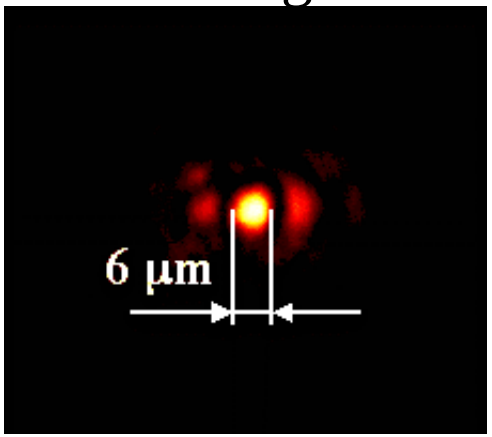

ND=7

10 TW Nd:glass laser
λ=1.053 μm K_I~10^5
F/3 focusing optics
I=10^{19} W/cm^2

Spectrograph

CCD

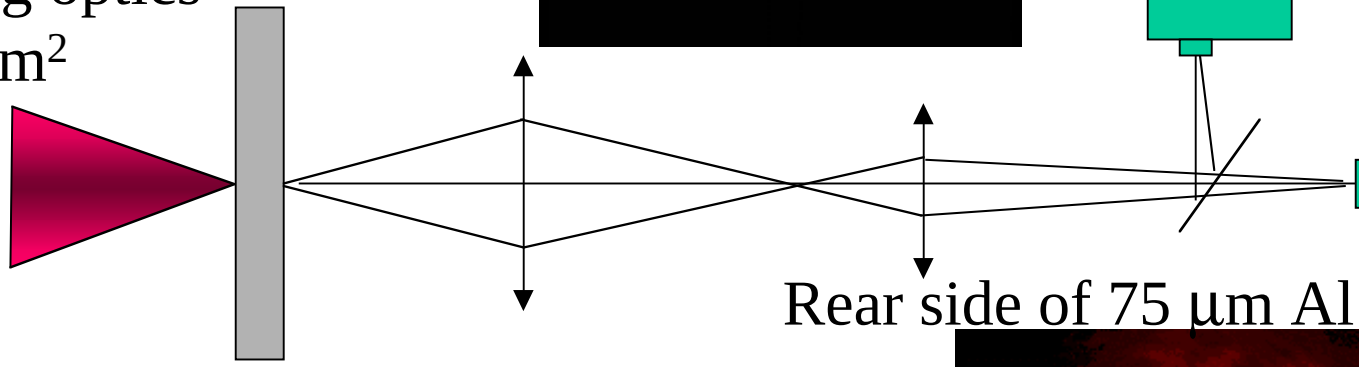

Rear side of 75 μm Al target

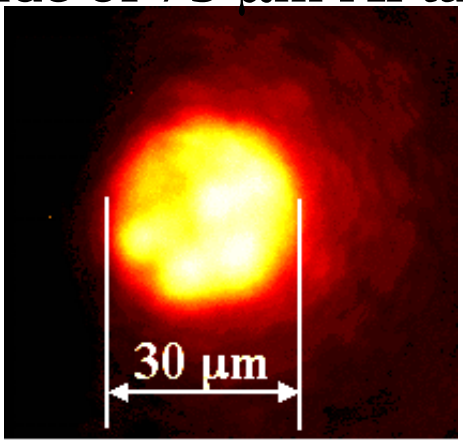

thin film metallic targets
L=12 ÷ 500 μm

Experimental results

Transmission of the fundamental

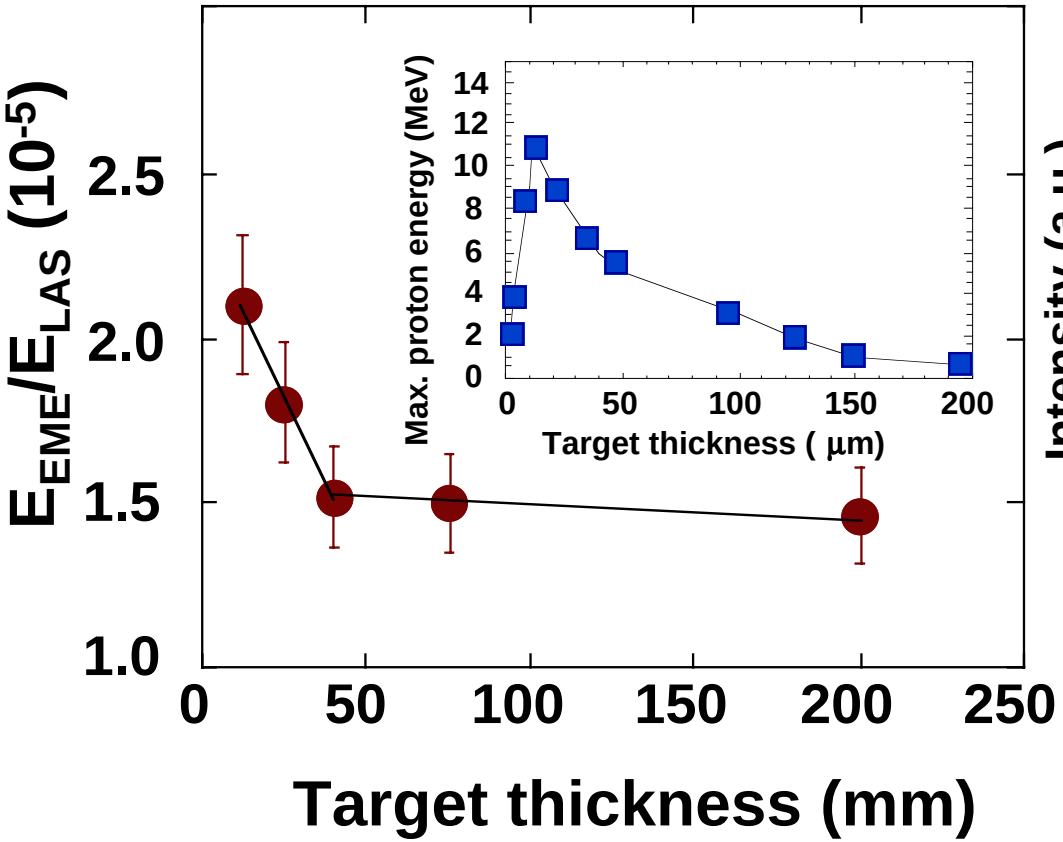

Transmitted spectrum in visible

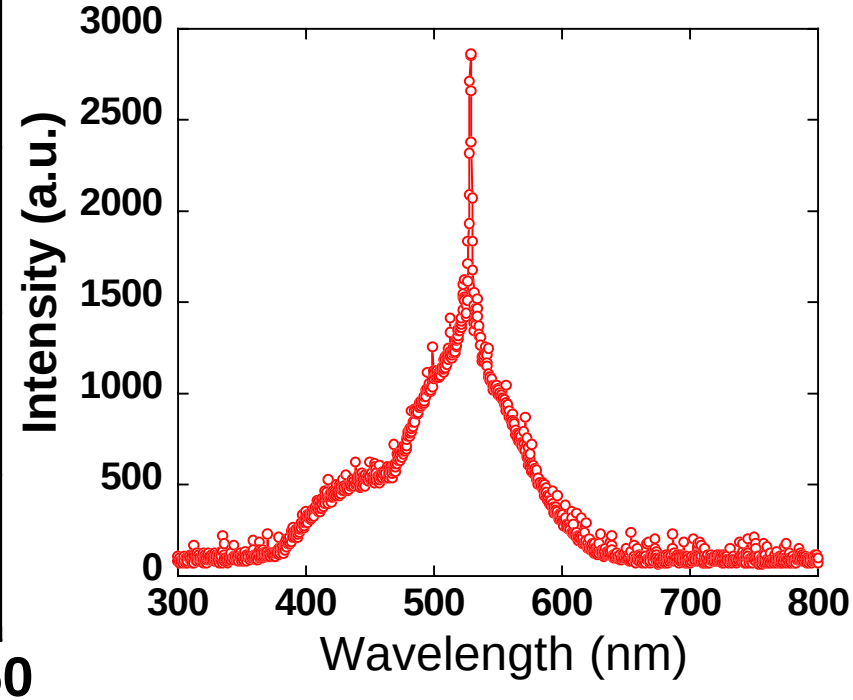

Scheme of EME in laser-target interaction

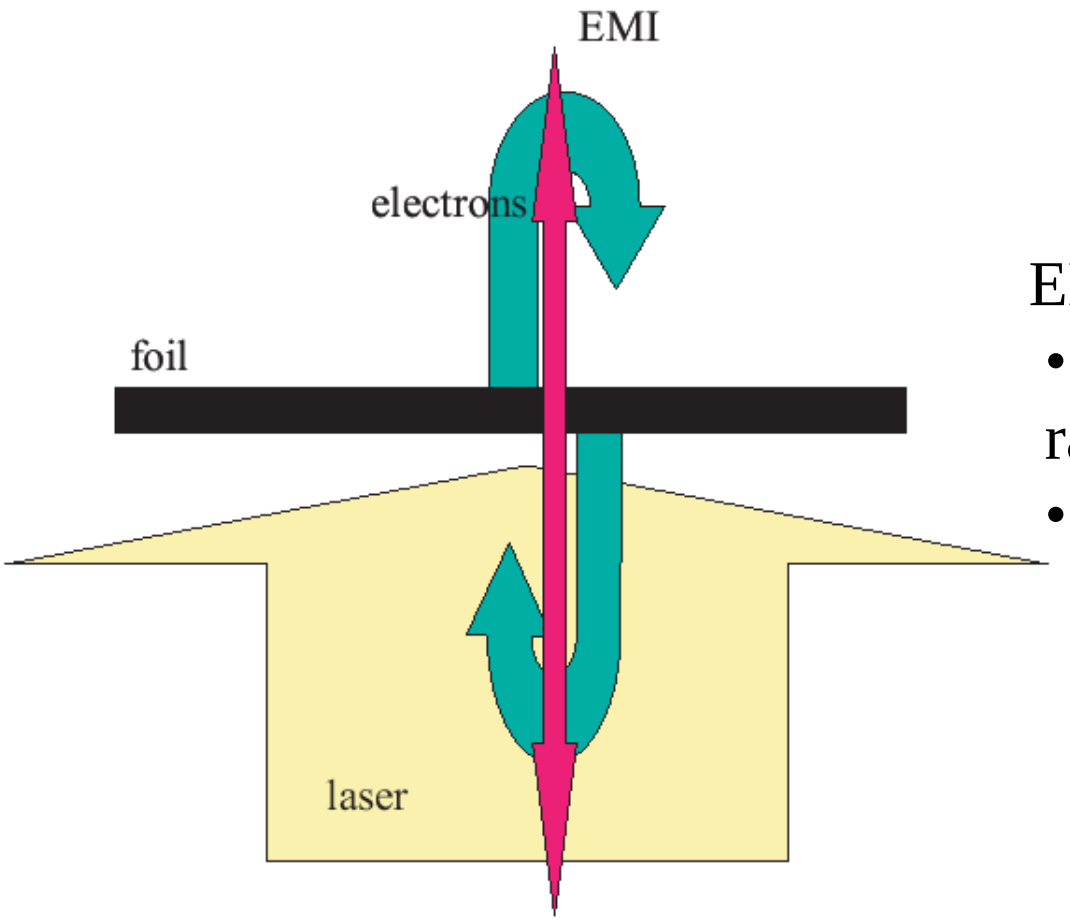

EME mechanisms:

- bremsstrahlung/synchrotron radiation
- transition radiation

Power of EME

Power of EME radiation defined by the Larmor formula:

$$W = \left(2r_e / 3mc\right)\left|\dot{\mathbf{p}}\right|^2 \gamma^6 \approx \left(\gamma - 1\right)\gamma^6 \varepsilon r_e c / l^2 \quad (1)$$

Describes two types of radiation:
(i) bremsstrahlung radiation,
when $\mathbf{p}$ changes in magnitude;
(ii) synchrotron radiation,
when $\mathbf{p}$ changes in direction

Deceleration length- electron beam Debye length

$$l \approx c\sqrt{\gamma_b} \big/ \omega_{pb},$$

where $\omega_{pb} = \left(4\pi e^2 n_b / m\right)^{1/2}$ e$^-$ beam plasma frequency

$\varepsilon = \left(\gamma_b - 1\right)mc^2$ e$^-$ beam kinet. energy

Bremsstrahlung radiation

Deceleration time $\tau_e = l/c,$

Energy emitted by a single electron $E_b \approx \gamma^{13/2} \varepsilon r_e \omega_{pb} / c$ (2)

Maximum is at frequency and corresponds to visible or infrared spectral regions $\omega \sim c/l = \omega_{pb} / \sqrt{\gamma_b}$

This is the main difference between collisionless “vacuum” bremsstrahlung radiation due to electron interaction with collective plasma field and conventional one originated from particles collisions, requires hot dense plasma and occurs at short distances

Transition radiation

Transition energy loss emitted by an electron traversing vacuum-plasma boundary (fully ionized or metal targets)

$$E_t \approx \frac{1}{3}\varepsilon r_e \omega_{pe} / c \qquad (3)$$

because $\omega_{pe} >> \omega_{pb} \Rightarrow E_t > E_b$

The spectrum of transition radiation corresponds to the frequencies

$$\omega \sim \gamma \omega_{pe}$$

and lies in UV and XUV spectral region

Integrated characteristics of EME (I)

The total number of accelerated electrons:

$$N_b = \alpha E_L / K_b$$

where α is absorption coeffecient,

E_L is the laser pulse energy

Energy emitted by all decelerated electrons due charge separation

$$E_{total}^{b} \approx \alpha \gamma^{13/2} E_L r_e \omega_{pb} / c \qquad (4)$$

Accounting for multiple electron passes, the energy conversion coefficient of laser light into optical emission reads:

$$\boxed{\eta_b \approx \alpha \gamma^{6} \sqrt{M/Zm} r_e \omega_{pb} / c} \qquad (5)$$

Integrated characteristics of EME (II)

Transition radiation to be effective has occur at quite sharp plasma-vacuum boundary and is formed in the finite zone of the length $L_t \sim \left(c/\omega_{pe}\right)\gamma_b^{*}$

*V. L. Ginzburg and V. N. Tsytovich, IPP, New York, 1991

If the width of transient layer $L>L_t$ then intensity of transient radiation decreases exponentially $\propto \exp\left(-L/L_t\right)$

$$\eta_t \leq \alpha r_e \omega_{pe}/c \qquad (6)$$

EME is highly anisotropic due to relativistic electron motion. It is concentrated within a cone of $\theta \approx 1/\gamma_b$ in the direction of the laser beam.

For $I=10^{20}$ W/cm^2 $\qquad \theta \leq 10^{\circ}$

$\eta \sim 10^{-4}$ due to charge separation

$\eta \sim 10^{-6}$ due to transition radiation

Spectrum of bremsstrahlung emission I

We assume that accelerated electrons have an exponential energy distribution $dn_b/d\varepsilon \propto \exp\left(-\varepsilon/K_b\right)$

If target thickness δ is smaller than the Debye length of fast electrons, $\delta \le l$,the electrostatic field due to the charge separation can be approximated as following:

$$E \approx K_b\, x/el^2, |x| \le l$$

$$E \approx K_b/ex, |x| > l$$

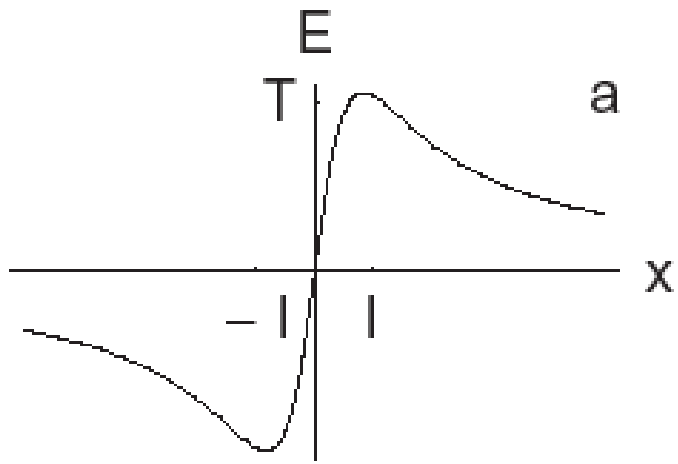

Spectrum of bremsstrahlung emission II

Accelerated electron is trapped in this electrostatic potential and involved in periodic motion around the target. The period and amplitude, x_0, of the oscillation depend on the electron energy. For a relativistic electron its orbit has a saw-tooth shape.

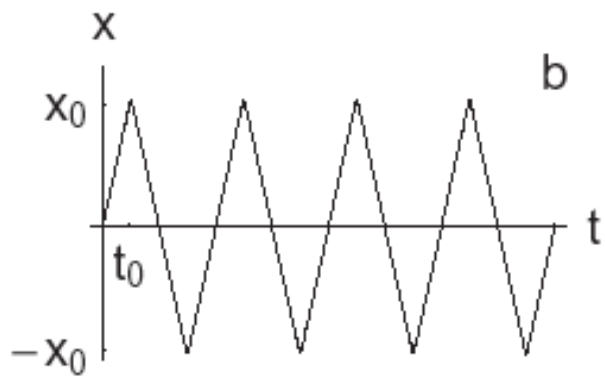

Low energy electrons, $\varepsilon \le K_b$, are trapped within the Debye sheath and amplitude of their oscillation is proportional to the energy:

$$x_0 \sim l\sqrt{\varepsilon / K_b} \qquad (7)$$

Spectrum of bremsstrahlung emission III

For high-energy electrons, $\varepsilon > K_b$, the excursion length is much longer

$$x_0 \sim l \exp\left(\varepsilon / K_b\right) \qquad (8)$$

Because x_0 defines the frequency of electromagnetic emission, $\omega \sim c/x_0$, Eqs. (7) and (8) allow to define the spectrum of emission:

$$P_\omega \propto \dot{p}^2 \, dn_b / d\varepsilon \qquad (9)$$

The acceleration/deceleration rate decrease with the electron energy, and the emission spectrum has the shape

$$I_\omega \propto \left(\omega l / c\right)^3, \omega \le c / l;$$

$$I_\omega \propto \left(c / \omega l\right)^2, \omega \ge c / l$$

with the maximum at $\omega \sim c / l = \omega_{pb} / \sqrt{\gamma_b}$

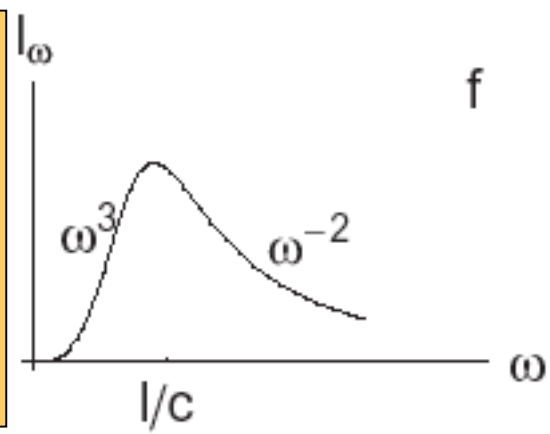

Second harmonic generation I

vxB electron acceleration is responsible for $2\omega_L$ modulation of current of relativistic electrons.

We will estimate emission efficiency at $2\omega_L$ by modeling the source as disk with diameter - d , thickness l and electric current $j_2 = \alpha_2 e n_b c$, where α_2 is the depth of the current modulation at $2\omega_L$

The radiation field at distance R from the source is defined as

vector potential $$\mathbf{A}_2 = -\frac{1}{cR}\int d\mathbf{r}\mathbf{j}_2(r, t - R/c + \mathbf{rn}/c) \quad (10)$$

Where **n** is the unit vector in the direction of observation.

Second harmonic generation II

The emission maximizes at the surface of the cone with apex angle $\sim c/\omega_L d$ and along the direction of electron propagation

The electric field can be estimated as $\alpha_2 e n_b (ld/R)$, and the emission power is proportional to the laser intensity:

$$\boxed{P_2 \sim 10^{-2} \alpha_2^2 \gamma_2^2 mc^2 \omega_L d/r_e} \qquad (11)$$

where $\gamma_b \sim a$.

For the modulation depth α_2~10% and
electron spot diameter ~ 10 μm, conversion efficiency ~10^{-6}

Parameters for 2D3V PIC simulation

Linear polarization (P)
Full ionized plasma H
Simulation box:40λ x 40 λ
10^6 particles
32 particle in cell

Laser pulse duration 10λ
Focal spot 10λ

$$a = \frac{eE}{mc\omega} = 3,$$

$$I\lambda^2 = 9\times10^{18}\ \mathrm{Wcm^{-2}}\mu\mathrm{m}^2$$

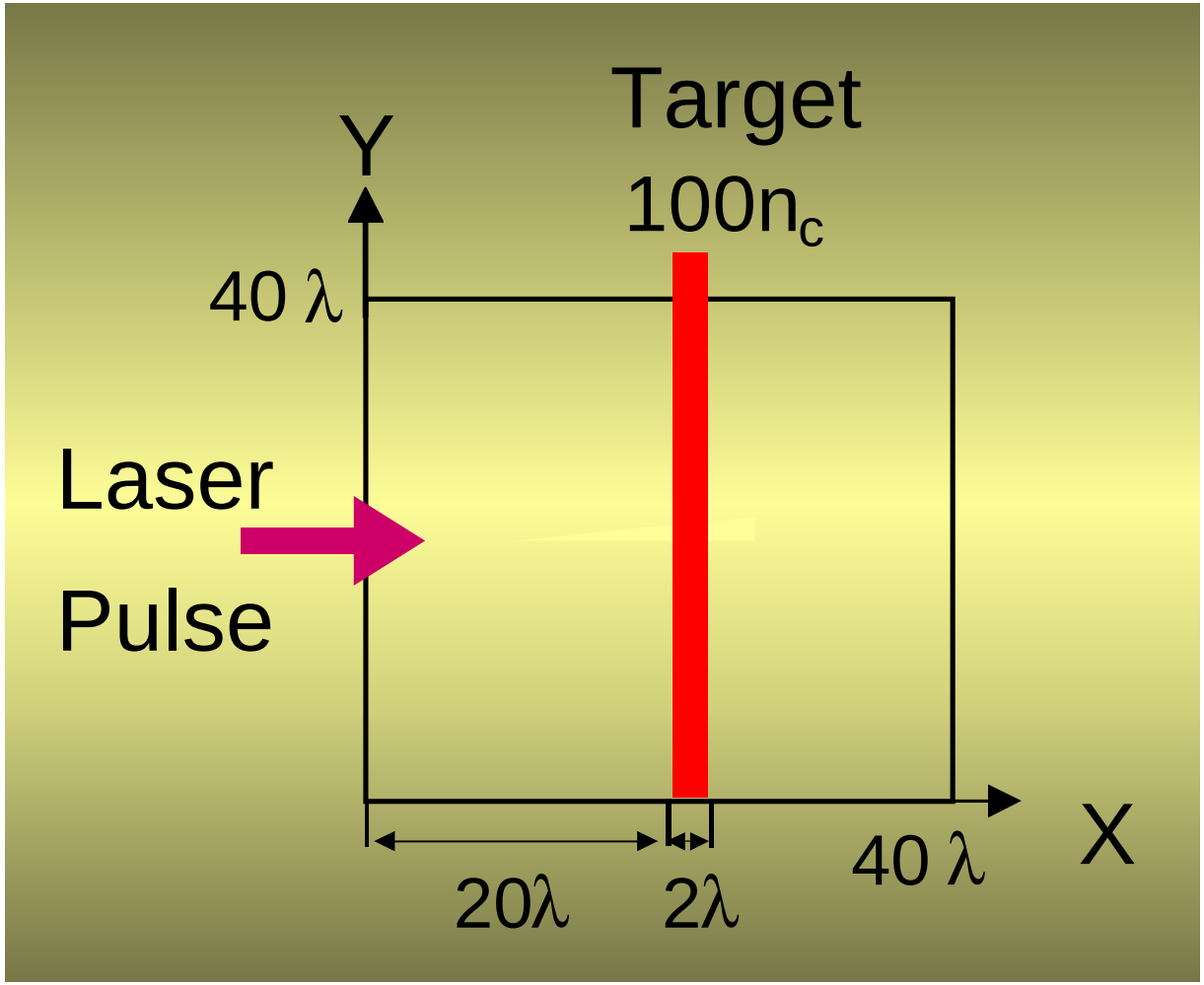

The vector Poynting field behind the target

a=3

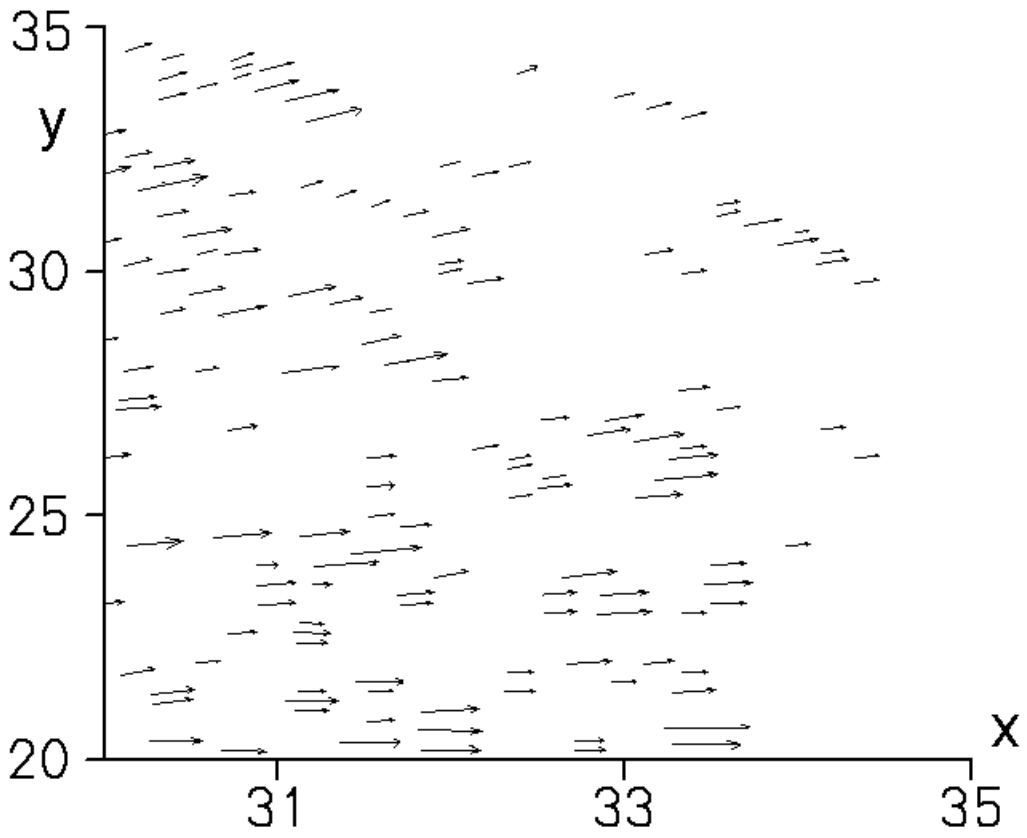

Spectrum of EME behind the target

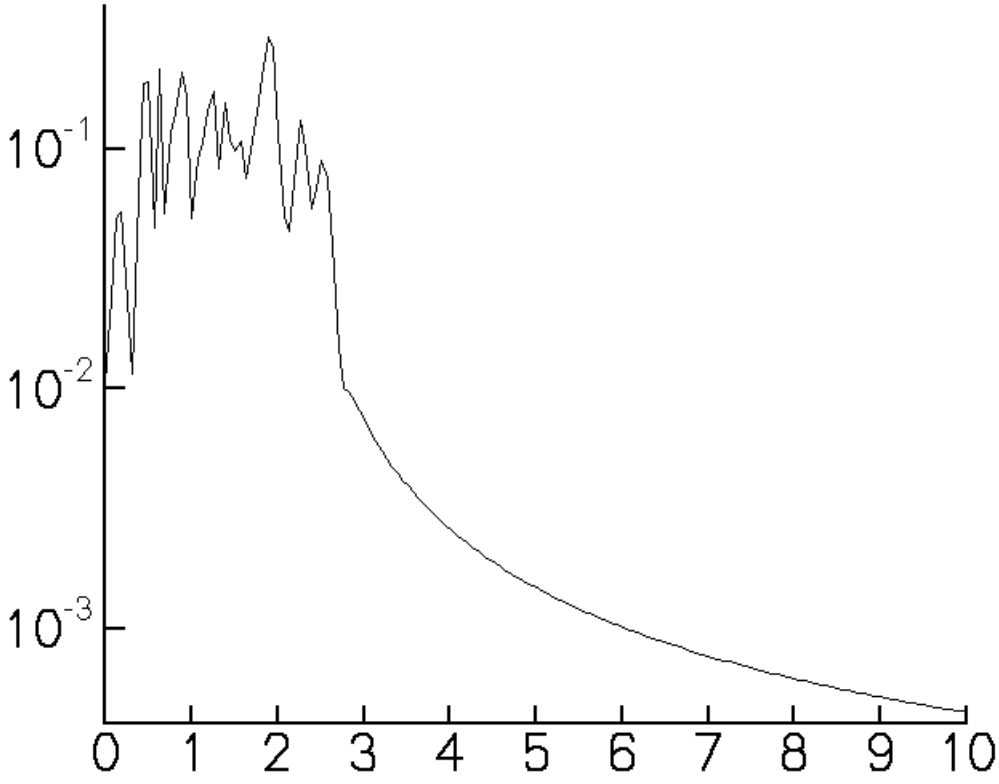

Summary

- We have observed radiation at fundamental frequency behind thin film targets with energy ~ $10^{-5}E_L$
- This radiation was attributed to emission of relativistic electrons accelerated/decelerated in charge separation electrostatic fields
- We analytically examined the mechanisms of EME
- EME might be useful diagnostics of the transport of high current electron beams in solid dense matter

Ultra-relativistic laser modification of the fast igniter scenario of inertial fusion

V. M. Malkin and N. J. Fisch

Princeton University

Fast ignition delivers high gain at low driver energy

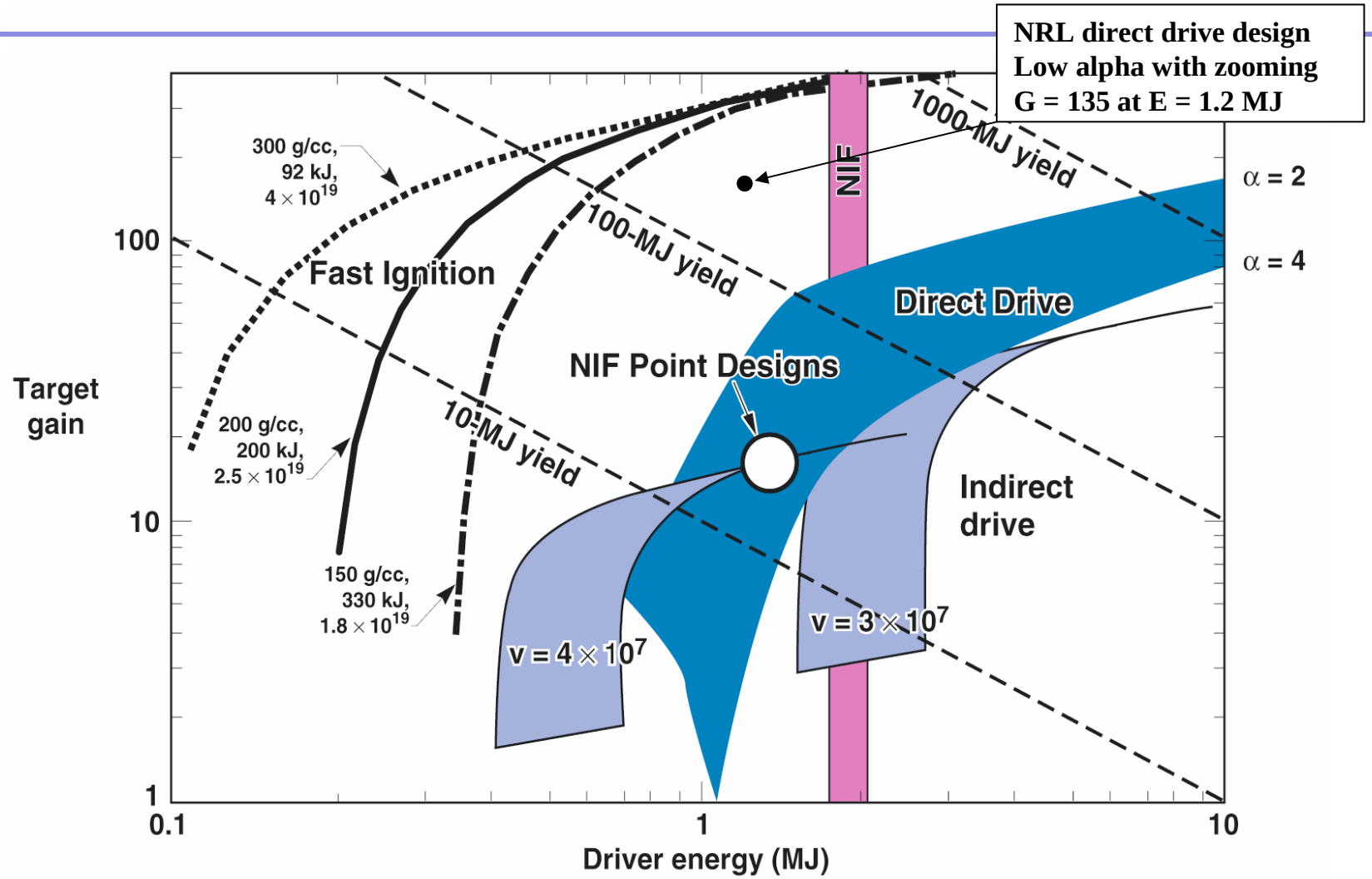

The two viable fast-ignition concepts share fundamental issues: hot-electron production and transport to the core

UR LLE

Channeling

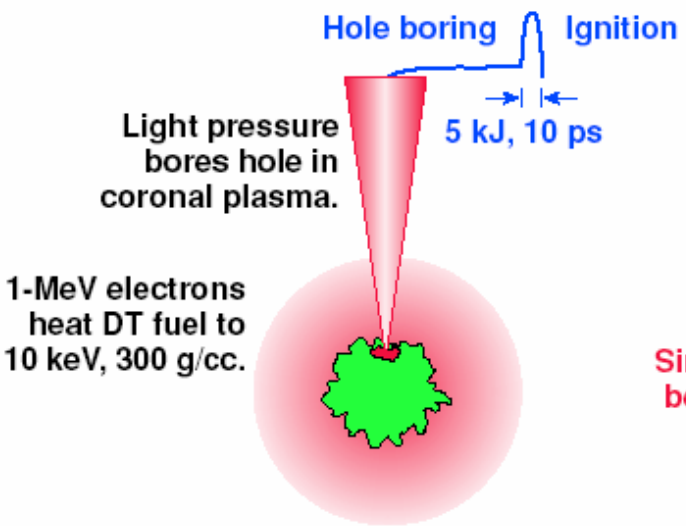

OMEGA EP would validate this concept with existing shperical cryo capsules.

Cone-focused ignition

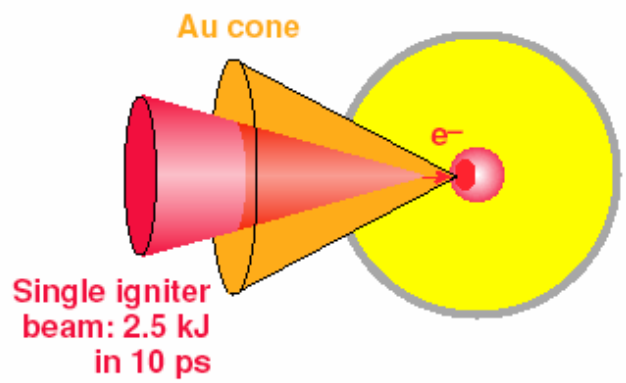

LLE has the cryogenic infrastructure to develop and shoot cryogenic cone-focused capsules.

Which electrons can efficiently heat the core?

Conventional paradigm:

Just electrons of energy not much higher than 1 MeV can be stopped in the core.

We challenge this paradigm by suggesting a mechanism of decelerating substantially even ultra-relativistic electrons in the core.

Potential advantages of ultra-relativistic regimes:

- Fast-igniter concept gains flexibility;
- More intense lasers can be used;
- More energy can be deposited within smaller areas and shorter times;
- More energy can be transported at less current, which tends to reduce transport instabilities.

Stopping mechanism

Conventional paradigm:

Fast electrons are stopped primarily by their Coulomb collisions with the core particles.

We show that Langmuir wave turbulence is excited by the beam in the core for a broad parameter range of practical interest.

Turbulence dramatically reduces the beam relaxation length in the core.

Collisinal threshold for the turbulence excitation

Collisions between the core electrons and ions cause strong damping of Langmuir waves.

To overcome it, the collisionless instability growth rate must exceed the damping rate:

$$\boxed{\Gamma > \nu .}$$

For the D-core concentration $n_e = 10^{26}\ \mathrm{cm}^{-3}$

and electron temperature $T_e \sim 5$ KeV ,

the Langmuir wave damping rate is

$$\boxed{\nu \approx 5\times 10^{14}\ \mathrm{sec}^{-1}}$$

Collisionless instability growth rate

In the kinetic instability regime, the maximized over Langmuir wavevectors collisionless growth rate is

$$\boxed{\Gamma \sim \frac{2\omega_e n_b}{\gamma_b \Delta\vartheta^2 n_e},}$$

where $\omega_e = 5.64\times10^4\sqrt{n_e \times \mathrm{cm}^3}\ \mathrm{sec}^{-1}$ – is electron plasma frequency; n_b, γ_b and $\Delta\vartheta$ are the beam concentration, relativistic factor and angular spread, respectively.

Numerical example :

$n_e = 10^{26}\ \mathrm{cm}^{-3}$, $n_b = 5\times10^{22}\ \mathrm{cm}^{-3}$, $\Delta\vartheta = 0.1$ and $\gamma_b = 50$,

gives $$\boxed{\Gamma \sim 10^{15}\mathrm{sec}^{-1}}$$

Core turbulence

- Thus the collisional threshold for Langmuir turbulence excitation in the core is easily exceeded even for ultra-relativistic beams.

- The saturated level of the turbulence depends on specific regime of nonlinear stabilization, and there are quite a few different regimes.

Strong Langmuir turbulence threshold regime

In this regime, taking place in a broad parameter range, the average energy density of the turbulence is close to the threshold of Langmuir wave modulational instability and collapse,

$$W_{th} \sim \frac{n_e T_e^2}{m_e c^2}$$

The beam relaxation length

Under conditions when a noticeable part of the turbulence energy is located in the resonant domain of Langmuir wave-vector space, the electron beam relaxation length in the core can be evaluated for the above listed parameters as

$$L_r \sim 50\ \mu\text{m}.$$

For beams of smaller relativistic factors ($\gamma_b < 50$), the relaxation length quickly decreases (assuming the same relaxation regime and other conditions)

$$L_r \propto \gamma_b^{\ 2}$$

Beam transport near the core

$$\Gamma \propto \omega_e \frac{n_b}{n_e} \propto n_e^{-1/2}, \quad \nu \propto n_e T_e^{-3/2} \quad \text{(up to a logarithm)}$$

$$\Downarrow$$

$$\Gamma / \nu \propto (T_e / n_e)^{3/2}.$$

- If T_e/n_e decreases outside, the core instability can coexist with the stable transport near the core.
- If T_e/n_e increases outside, another effect is needed to stabilize the transport near the unstable core.

Convective stabilization of the beam transport near the core

The longitudinal wavenumber of a Langmuir wave evolves as

$$\frac{dk_{\|}}{dt} = -\frac{\omega_e}{2}\frac{\partial \ln n_e}{\partial z} \equiv -\frac{\omega_e}{2L_n}.$$

While crossing the resonant interval $\Delta k_{\|}$ (located near $k_{\|} \approx \omega_e / c$), the wave amplitude undergoes

$$\Lambda \approx 2L_n \int_{\Gamma(\vec{k})>\nu} [\Gamma(\vec{k}) - \nu]\, dk_{\|} / \omega_e$$

exponentiations. If Λ_0 exponentiations can be tolerated, the stabilization condition is

$$L_n \le \Lambda_0 \omega_e / 2 \int_{\Gamma(\vec{k})>\nu} [\Gamma(\vec{k}) - \nu]\, dk_{\|} \equiv L_{nc}.$$

Numerical example of the transport stability condition near the core

For $\Lambda_0 = 7$ and the above other parameters, corresponding to

$$\max_{\vec{k}} \Gamma(\vec{k}) \equiv \Gamma \approx 2\nu \approx 10^{15}\ \mathrm{sec}^{-1},$$

the condition for the convective stabilization of the beam transport at nearly core concentration is

$$L_n \leq L_{nc} \sim 50\ \mu\mathrm{m}\,.$$

Conclusions

- For realistic fast igniter parameters, ultra-relativistic electron beams can excite in the core Langmuir turbulence potentially capable of significant decelerating these beams within the core.
- Moreover, transport the beams near the core can be convectively stabilized by natural density gradients.

Open issues

- It is necessary to identify regimes where ultra-relativistic beam relaxation consists primarily in the electron deceleration rather than angular scattering.
- Note:

There are experiments reporting 40% collective deceleration of moderately relativistic beams in plasma, but an extrapolation to ultra-relativistic beams require scrutiny.

Models for intense laser-matter interaction studies

R. J. Mason
Los Alamos National Laboratory

6th Workshop on Fast Ignition of Fusion Targets
St. Pete Beach, FL
Nov. 16-19, 2002

Full-particle implicit plasma simulation grew from the need to model ICF electron transport driven by CO_2 lasers

- Suprathermal electrons were driven by lasers into the surface of a pellet.

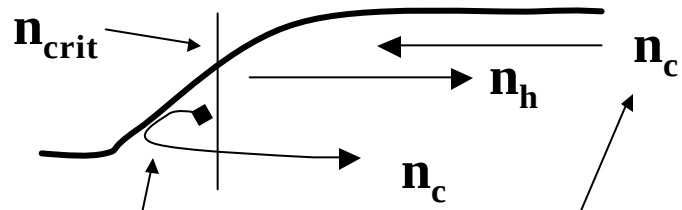

- Resistive E-fields drew a cold return current.

- Pressure driven E-fields held the hot electrons near in the high density regions and forced fast ion blow-off.

A very early treatment used counter-streaming hot and cold diffusing electrons

VOLUME 42, NUMBER 4 PHYSICAL REVIEW LETTERS 22 JANUARY 1979

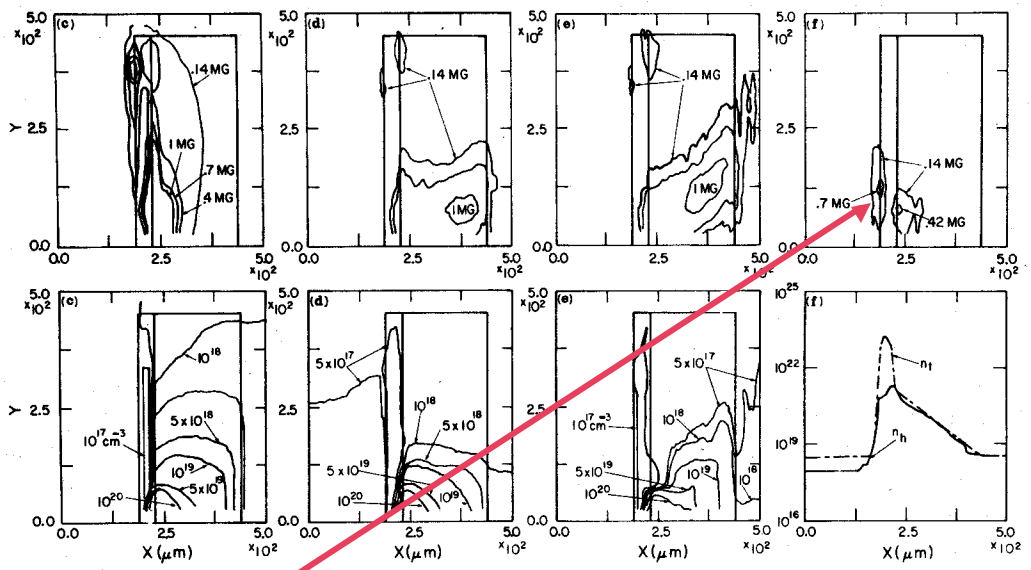

FIG. 2. Results at 20 psec with $B \neq 0$. Upper frames, B-field contours; lower frames, n_h contours for runs (c)–(e), and axial densities run (f). Run (c), with $\omega\tau_{h,c} = 0$; run (d), with $\omega\tau_{h,c} \neq 0$, but transverse $\nabla P \times \vec{B}$ currents neglected; run (e), full model solution; run (f), results for a plastic foil at $t = 2.5$ psec, showing the prompt rear surface B field from hot electrons.

B-fields were predicted for the back side of the foil, following the arrival of hot electrons

We tried to use the E-fields from Ohm's law in the background to govern hot particle transport

$$0 = n_c e\vec{E} \quad u_{ci} n_c (\vec{v}_c \quad \vec{v}_i); \quad n_c v_c = n_h v_h$$

- Later we realized that an E-field balancing the hot electron pressure was needed to hold the suprathermals in the corona.

$$0 = P_h \quad en_h \vec{E}$$

- Adding these gave a momentum-like equation that with a finite E-field unless n_e 0; introduction of the electron inertial terms and Ampere's law avoided this singularity.

This first moment method neglected electron inertia but allowed particle hot electrons

Phys. Fluids **23**, 2204 (1980)

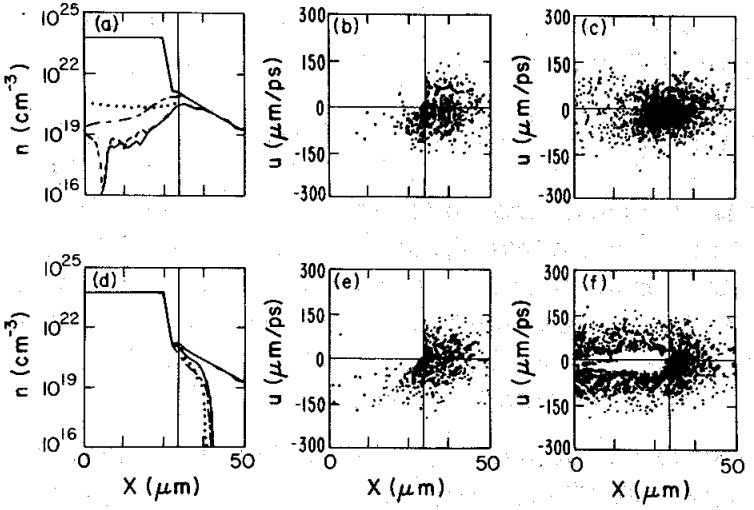

FIG. 4. Collisional effects in SiO_2 at 2 psec under standard illumination: (a) hot density profiles with all on ——, scattering off ----, drag off ——, scattering and draf off ···; (d) corresponding cold density profiles; hot electron phase space with (b) all on, (e) scattering off, (c) drag off, and (f) scattering and drag off.

E-fields could also be calculated by a successful charge dilation technique

Hot particle electrons underwent Rutherford scattering

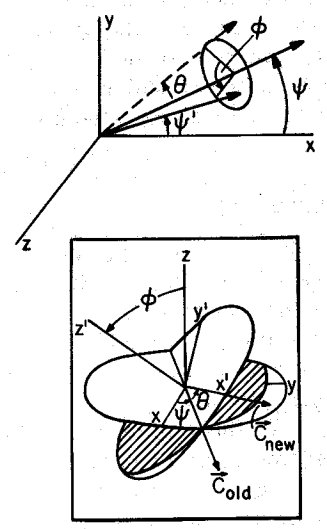

FIG. 1. Relation between the angles involved in a scattering event as **c** goes to **c'** and $\psi \rightarrow \psi'$.

Implicit Moment codes can be thought of as "Super-Hybrid" models

- The electron density from a Boltzmann factor, $n_e = n_o e^{ef/kT_e}$, which can yield $\vec{E} = P_e / en_e$, and which can be singular as $n_e \to 0$, is replaced by a full set of fluid equations to provide $\mathbf{j}^{(m+1)}$, $n_e^{(m+1)}$ and most importantly, $\mathbf{E}^{(m+1)}$ and $\mathbf{B}^{(m+1)}$ at the next time step.
- Numerous Refs. in the paper explored these models in the 1981-89 time frame

Implicit Moment codes avoid singularities in the velocities at low densities

- The electron velocities are obtained from the updated currents, rather than, say, an Ampere's law, e.g.,

$$\vec{v}_e = \frac{j_e}{en_e} = \frac{c}{4pen_e} \quad \vec{B}$$

- That is, we use:

$$m_e \frac{n_e \vec{v}_e}{t} = \quad \overline{P} \quad en_e(\vec{E} + v_e \quad \vec{B}/c) \quad u_{ei} n_e(\vec{v}_e \quad \vec{v}_i)$$

New currents are combined with Maxwell's equations to produce the field predictions

We must solve:

$$\frac{\vec{E}}{t} = \quad 4pe(Zn_i\vec{v}_i \quad n_e\vec{v}_e) + c \qquad \vec{B}$$

with

$$\frac{\vec{B}}{t} = \quad c \qquad \vec{E}$$

For plasma motion in the x-y plane this approach leads to a complex elliptic system for E_x, E_y and B_z

The implicit currents

$$\mathbf{j}_\alpha^{(m+1)} = \mathbf{j}_\alpha^{(m)''} + n_\alpha^{(m)} \varepsilon_\alpha^{(m)} \frac{[\mathbf{E}^{(m+1)} + \mathbf{E}^{(m+1)} \times \mathbf{\Omega}_\alpha + (\mathbf{E}^{(m+1)} \cdot \mathbf{\Omega}_\alpha)\, \mathbf{\Omega}_\alpha]}{(1 + \Omega_\alpha^2)}$$

Combine with Ampere's Law to yield the E- field components

$$E_x^{(m+1)} = \left(E_x^{(m)''} - \beta E_y^{(m)''} + \gamma \frac{\partial B_z^{(m+1)}}{\partial y} + \gamma\beta \frac{\partial B_z^{(m+1)}}{\partial x} \right) \Big/ (1 + \beta^2)$$

$$E_y^{(m+1)} = \left(E_y^{(m)''} + \beta E_x^{(m)''} - \gamma \frac{\partial B_z^{(m+1)}}{\partial x} + \gamma\beta \frac{\partial B_z^{(m+1)}}{\partial y} \right) \Big/ (1 + \beta^2).$$

Which combine with Faraday's Law to give the elliptic equation for B_z

$$B_z^{(m+1)} = B_z^{(m)} - c\, \Delta t \left[\frac{\partial E_y^{(m+1)}}{\partial x} - \frac{\partial E_x^{(m+1)}}{\partial y} \right]$$

Once the fields are known, we can update the plasma components, and particularly the electrons as particles

- If the electron moments -- n_e $\mathbf{j}_e$, and the pressure tensor $\mathbf{P}_e$ are simply updated from the fluid data, <u>we have a hybrid code</u> -- *probably with a small Dt, if* $\mathbf{P}_e$ *is left explicit.*

- If *instead* electron particles are moved each cycle to update the moments, we have a full-particle implicit plasma code.

The Moment Method moves particle or fluids through these implicit E- and B-fields

- Particles can use conventional centered differencing.
- Fluid can avoid excessive diffusion using Van Leer methods.
- A “current correction” must be added to the Ampere’s Law to account for the difference between the predicted current and the true currents registered when the plasma components move in the fields.
- In theory, the difference between these two currents can be iterated to zero.

Performance Issues

- Relativistic corrections are needed for practical applications. (*Direct Implicit particles preferred?*)
- Fast particles set the time step -- slow electrons can encounter finite grid instability.
  - Cure this with a fluid background component, or "local times stepping".
- The Hall term effects (from $\mathbf{v}^{(m+1/2)}$ x $\mathbf{B}$) can be diffusive
  - Need careful differencing to assure that Ñ x ($\mathbf{v}$ x $\mathbf{B}$) = 0 in uniform density regions.

Unique Implicit Capabilities

- Conductors can be treated as dense collisionless plasmas for the modeling of complex Pulse Power plasma switches.
- A mixed particle-fluid (hybrid) capability permits the accurate modeling of suprathermal electron transport in dense target plasmas for the ICF Fast Ignitor.

Our implicit approach allows for the use of either fluids or particles as may prove optimal

With both particle ions and particle emission electrons, for example, we see the Plasma Opening switch evolving as:

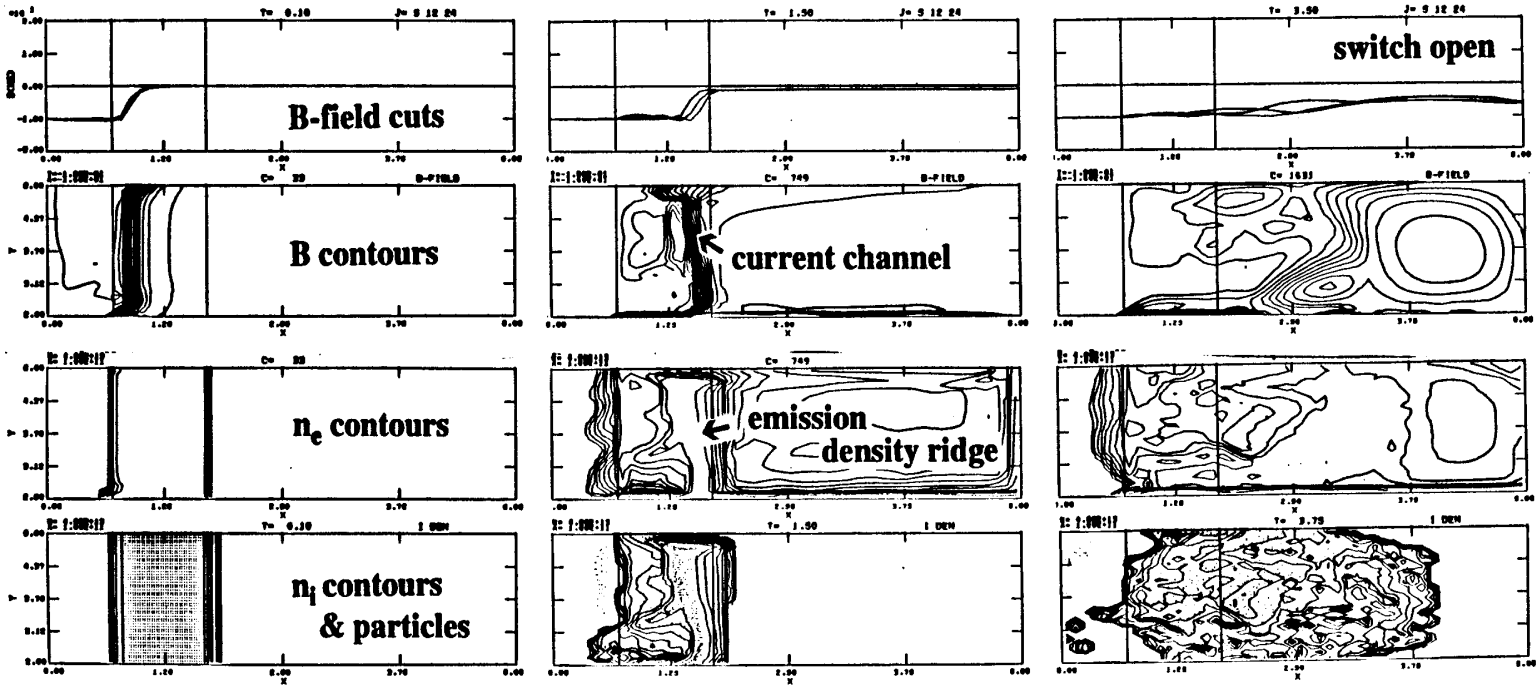

ANTHEM in its full-fluid mode has helped to understand and design new pulse power switches

- The multi-gap POS can open to a high impedance

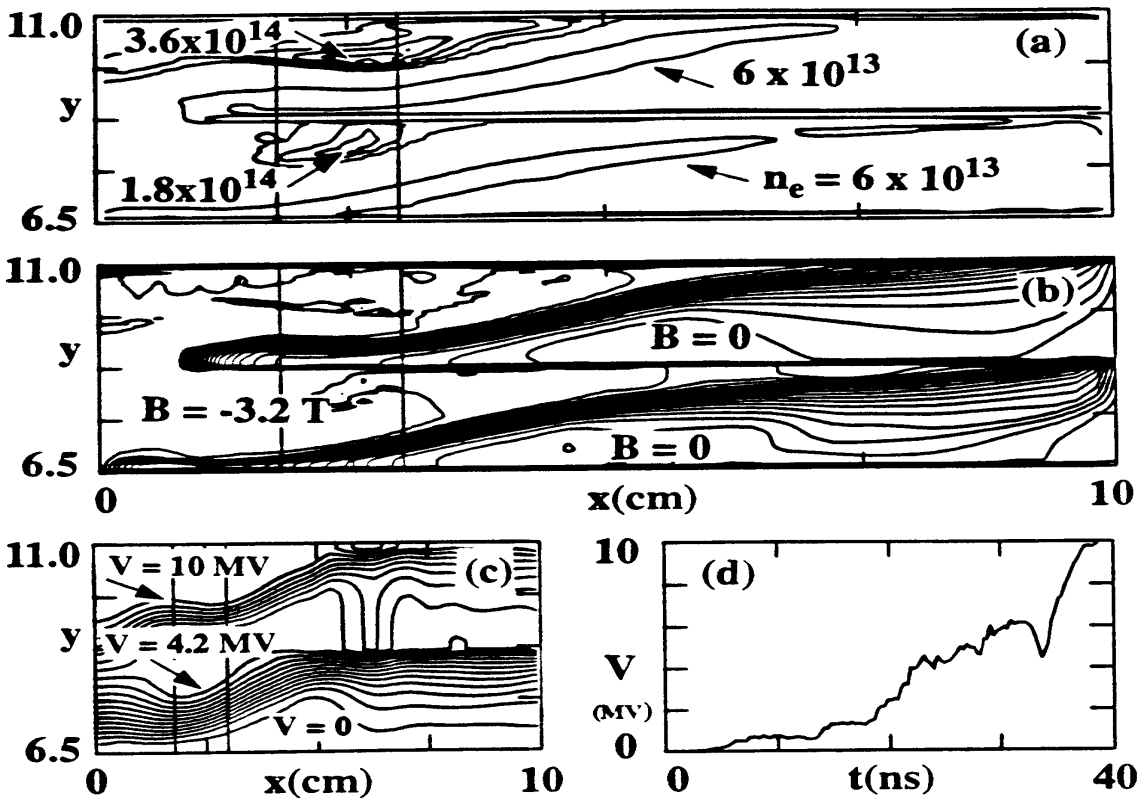

Intense Short Pulse Laser-Matter interaction research is a hot topic of world-wide interest

- **Petawatt facilities are under construction or planned in Japan, Germany, Britain, France, and at Rochester, and Sandia.**

- **Smaller facilities are operational at LLNL, LANL, and many universities.**

- **Applications are to the Fast Ignitor (FI) , radiography, materials and EOS studies.**

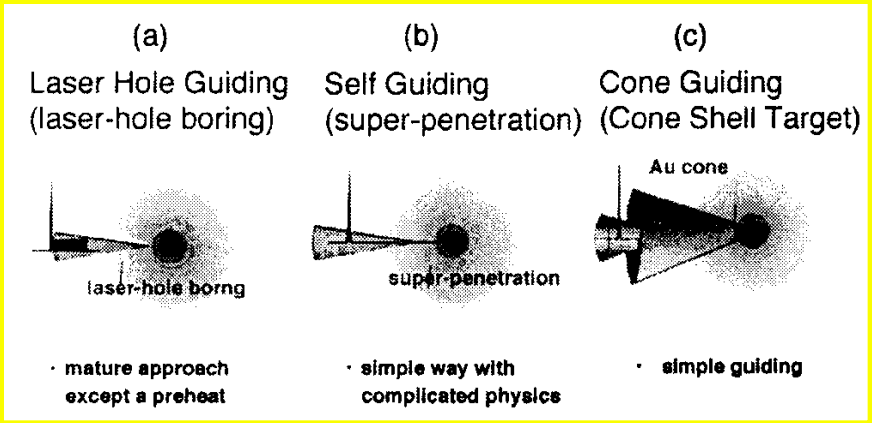

The Fast Ignitor uses hole-boring, and self-focusing thru coronal plasmas and intense magnetic fields to heat the surface of a pre-compressed DT target, possibly via a fast ions, to initiate thermonuclear burn.

AMOPP_02_2

Features engaged for the Fast Ignitor

- Fluid “cold” background and “hot” emission electrons, fluid ions.
- “Hots” emitted isotropically at critical and over a skin depth.
- Momentum equations advance relativistic momentum p, v = p/ .
- Hot e^- drag against the background electrons - absorption at back bd.
- Specular boundaries top and bottom.
- Grid-following light deposition algorithm with inverse-bremsstrahlung.
- Hot e^- scatter against the ions -- introduces resistivity.
- Flux-limited thermal conduction in the hot and cold electron fluids.

In application to the Fast Ignitor we add ponderomotive terms to the electron momentum equations

- **These are of the form $F_{h,c} = -(w^2_{ph,c}/2w^2)\,\tilde{N}I$, in which I is the laser intensity and $w_p^2 = 4pe^2n/(m_o g)$ with m_o the electron rest mass.**

- **They give rise to the predicted E-field:**

$$\boldsymbol{E}^{(m+1)} = \frac{\boldsymbol{E}^{(m)} \quad [4pe\boldsymbol{f}^{(m)} + c \quad x\boldsymbol{B}^{(m+1)}] \quad t + [\frac{\boldsymbol{P}}{en} \quad \frac{\boldsymbol{v}^{(m+1)} x\boldsymbol{B}^{(m)}}{c} \quad \frac{4p \quad e}{2mcw^2} \quad I](w_p \quad t)^2}{1 + (w_P \quad t)^2}$$

which has a curl, yielding a B-field, i.e.,

$$\boldsymbol{B}^{(m+1)} = \boldsymbol{B}^{(m)} - c \quad x\, \boldsymbol{E}^{(m+1)} \quad t.$$

For a 4 x ncrit plasma driven at 5.6 x 10^{18} W/cm^2 we calculate a supercritical 16 MG B-field

- The slab accelerates at a velocity consistent with $nM_pu^2 = I/c$

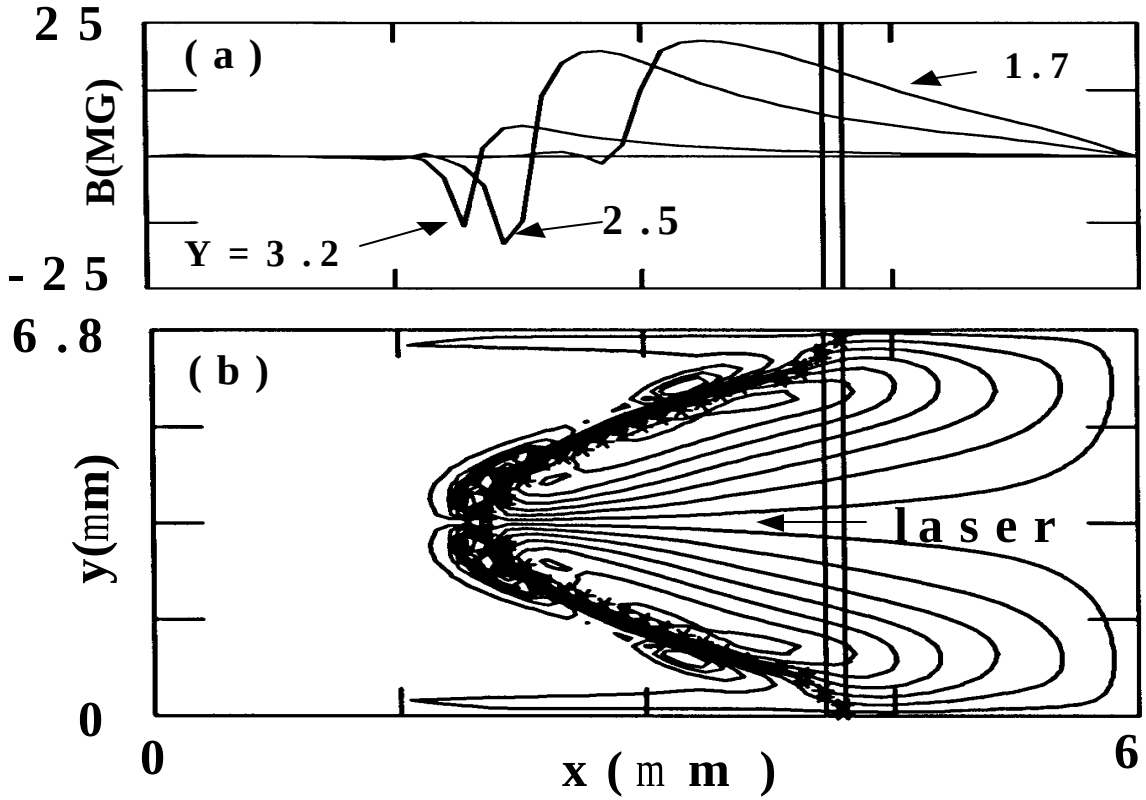

Mason/Tabak
PRL-1998

* marks the critical surface

The internal magnetic fields are consistent with a laser push driving the net electron flow axially into the target

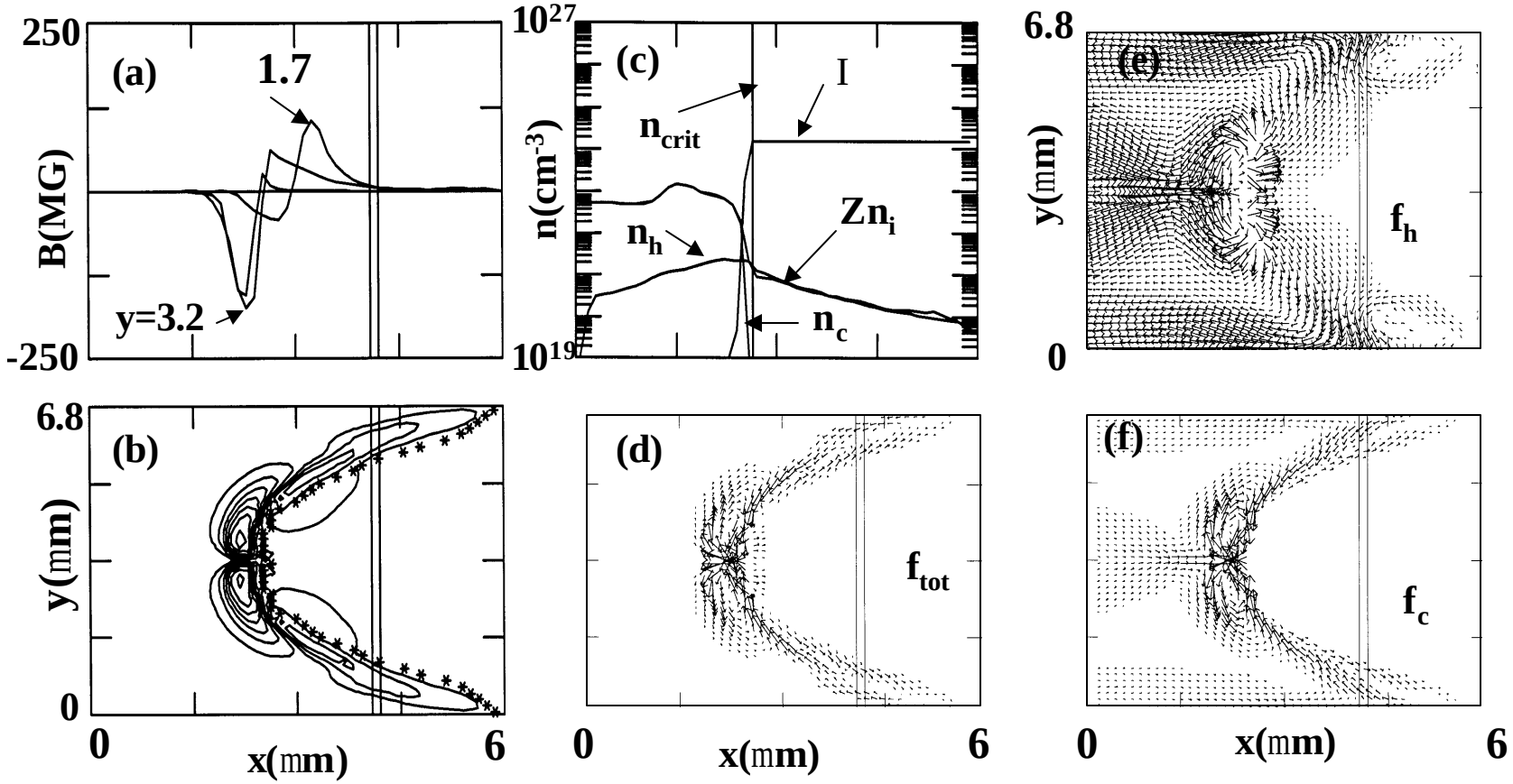

The illumination of a 200 x n_{crit} plasma with a 1.3 x 10^{19} W/cm^2 driver gives 250 MG internal B-fields, but only 65 MG thermoelectric (external) B-fields when the ponderomotive force is suppressed.

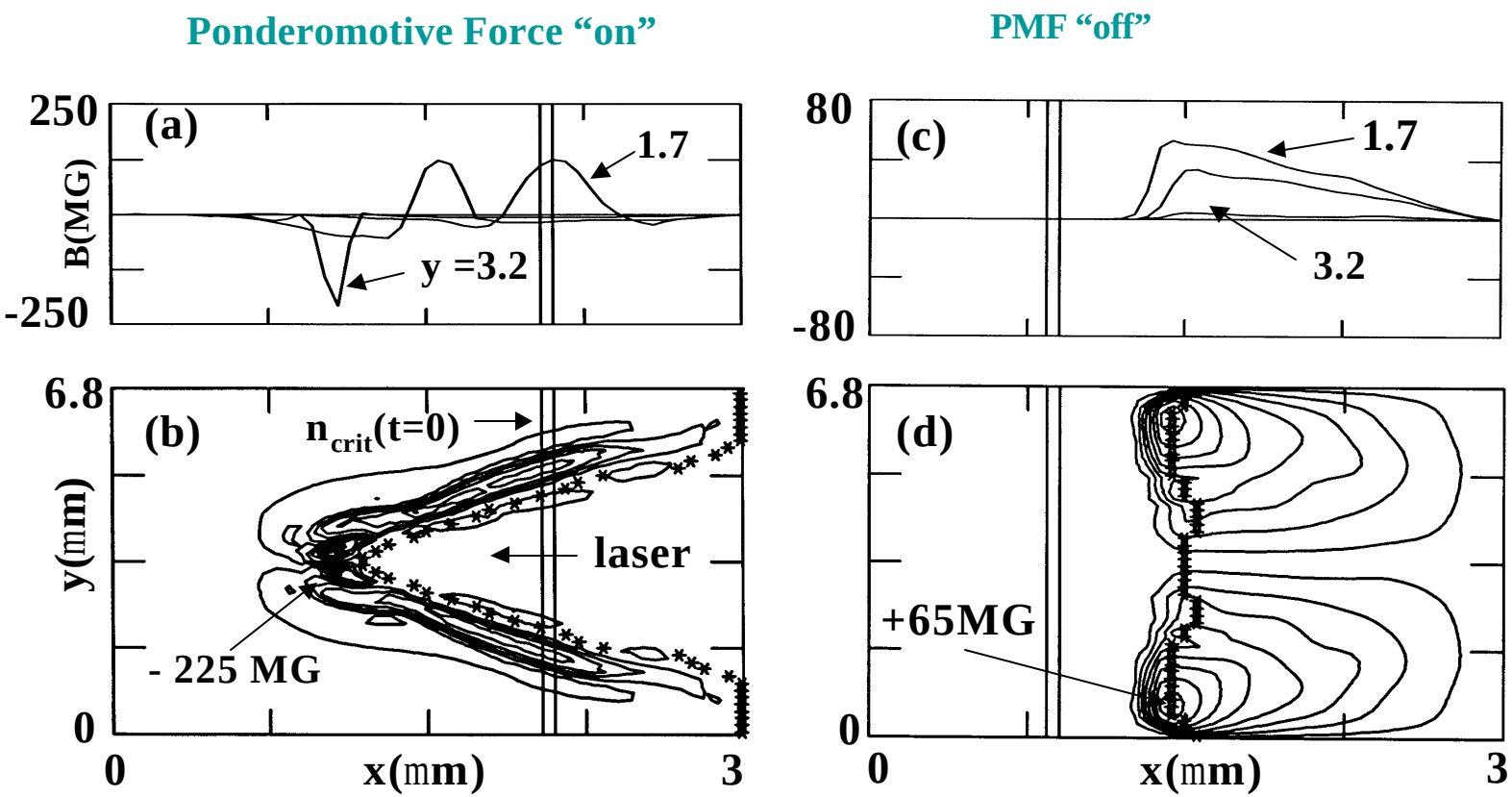

At 1.6 x n_{crit} the 3.2 x 10^{18} W/cm^2 laser burns through the background by relativistic lowering of w_p

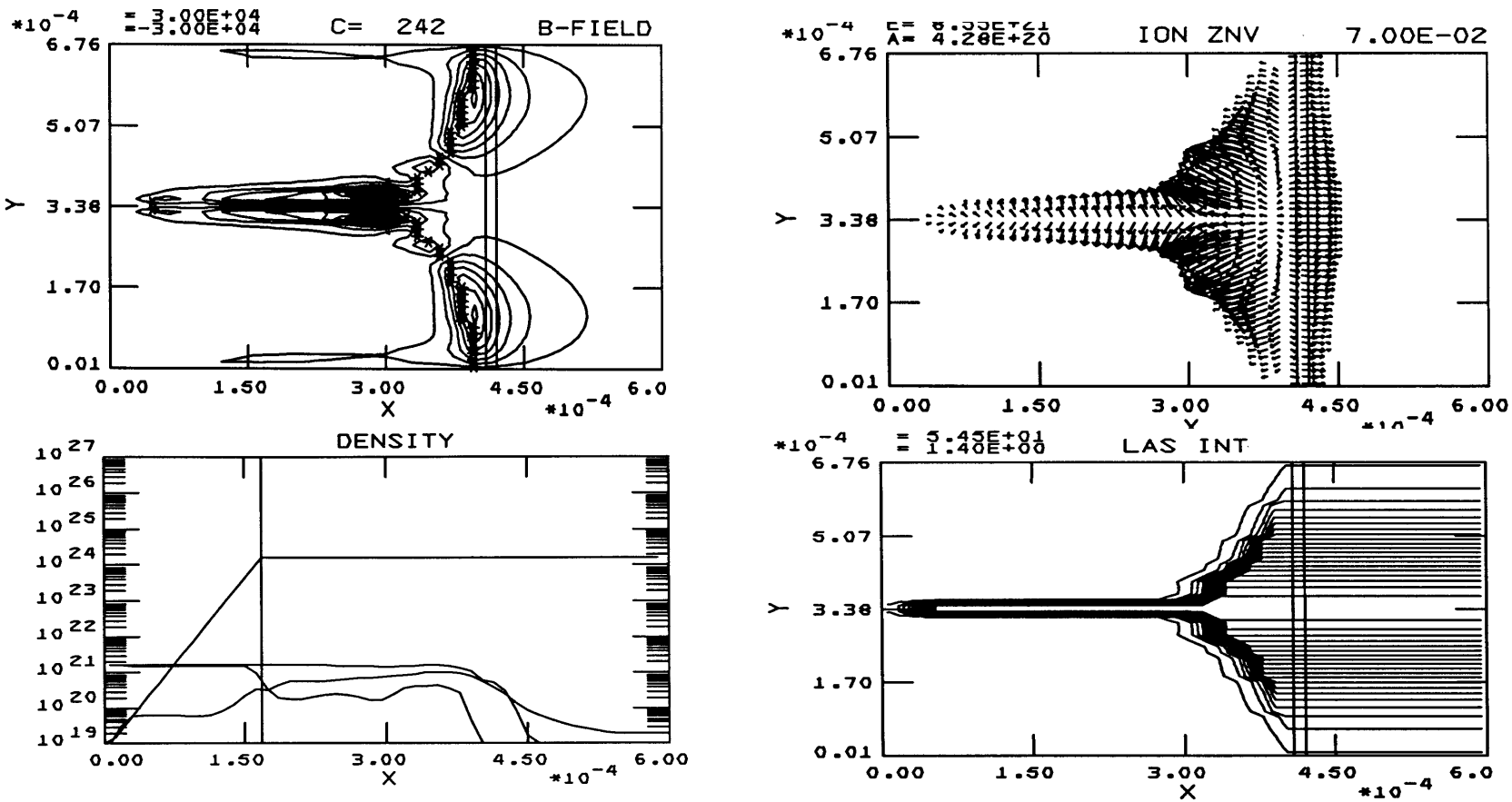

At 0.35 x ncrit with 40% anomalous absorption over 40 mm the laser creates a channel down to 0.2 n_{crit} and a ~10 MG B-field with electrons following the beam

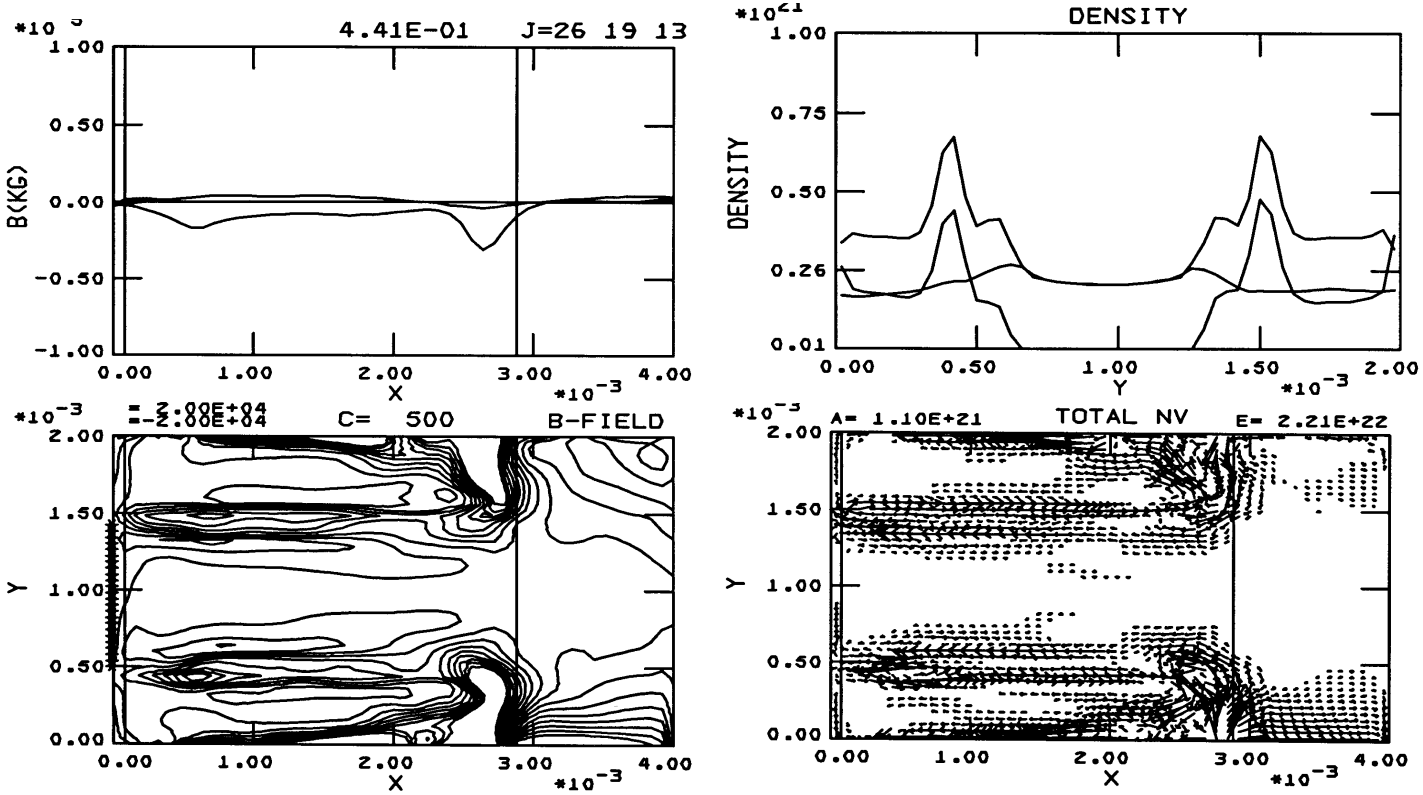

Our research objectives include pressing applications

- **We need to calculate the hot electron transport through 10^3 x n_{crit} plasmas (explicit PIC has been limited to 50 x n_{crit}) + coronal and channel plasmas**

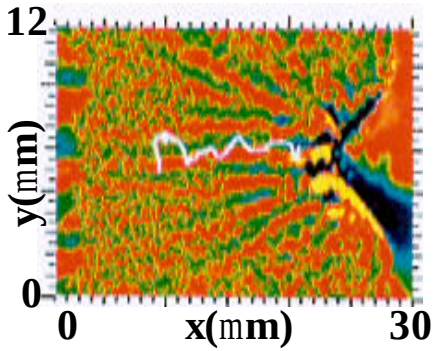

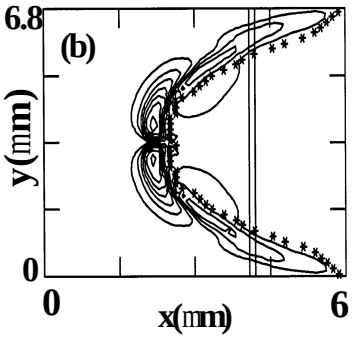

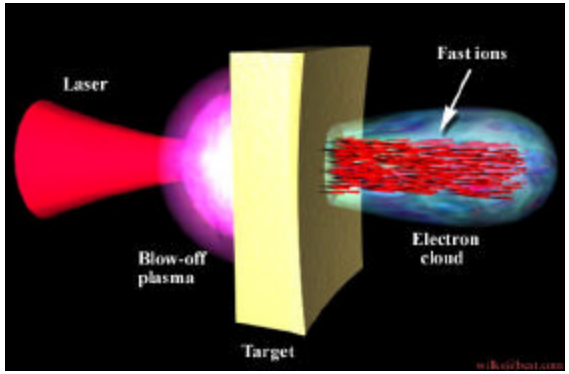

- **We need to model fast ion emission From the rear side of curved dense foils with related back-side B-fields and focusing**

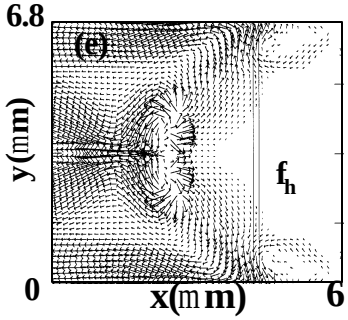

Laser

- **We need to determine the e^- emission Spectrum with resistance and B-fields controlling the return current**

Observations

- **B-fields exceeding 250 MG have been calculated for I > 10^{19}W/cm^2 and sharp profiles with peak densities exceeding 200 n_{crit}.**
- **Electron trapping near critical may derive from the PMF B-fields**
  - **This could localize the electron coupling to ions and aid fast ignition.**
- **Such trapping can give rise to fast ion blow-off.**
- **Intense propagation into 0.35 n_{crit} channels ejects ions laterally and yields a PMF-sourced 10 MG B-field at the channel edge, corresponding to hot electron flow in the laser direction.**
- **If refraction were added to ANTHEM, a central focusing of the light and dependent B-field are anticipated.**

Conclusions

- **Implicit models such as ANTHEM can provide new insights concerning short-pulse laser-matter interactions.**

- **Hybrid capabilities permit the study of dense target plasmas collisionally restricting the flow of return current electrons, at vanishing Debye lengths, while following the details of relativisitic incident electron streams.**

- **Weibel instability, as modified by collisions, can be examined, as can the pinching of incident electron streams by self-consistent B-fields.**

- **Surface and internal sources for fast ion generation can be explored, permitting a study of Fast Ignition by a converted short-pulse ion driver.**

Simulations on Implosion of Hydrodynamics and Electron Transport in Cone Target

K.Mima, Y.Sentoku, T.Johzaki, H.Sakagami*, H.Nagatomo, and F.I. Research Group of Osaka University

Institute of Laser Engineering, Osaka University

*** Himeji Institute of Technology, Faculty of Engineering**

Outline

ILE OSAKA

- Summary of the recent cone target F.I. experimental results
- Hydrodynamics of non-spherical cone target implosion
- Laser and electron energy transport in cone-laser interaction
- Toward integrated F.I. Code development
- Conclusion and summary

Peta watt laser heating experimental results of cone guide target

ILE OSAKA

Injection Timing is estimated by X-ray streak camera images, and it agrees with a maximum compression time of simulations.

Required timing accuracy is ±50ps which is longer than 1D implosion core plasma life time.

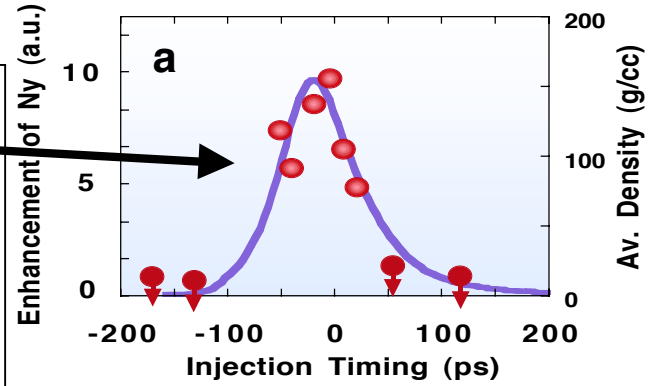

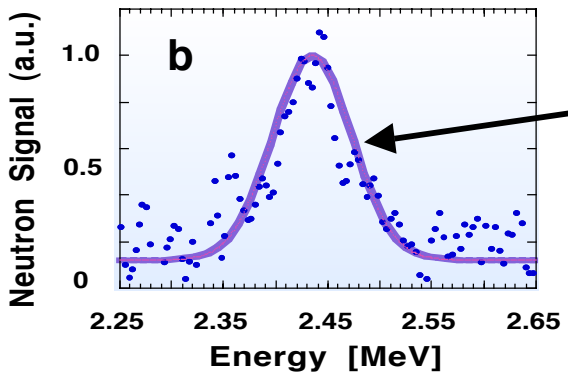

800eV

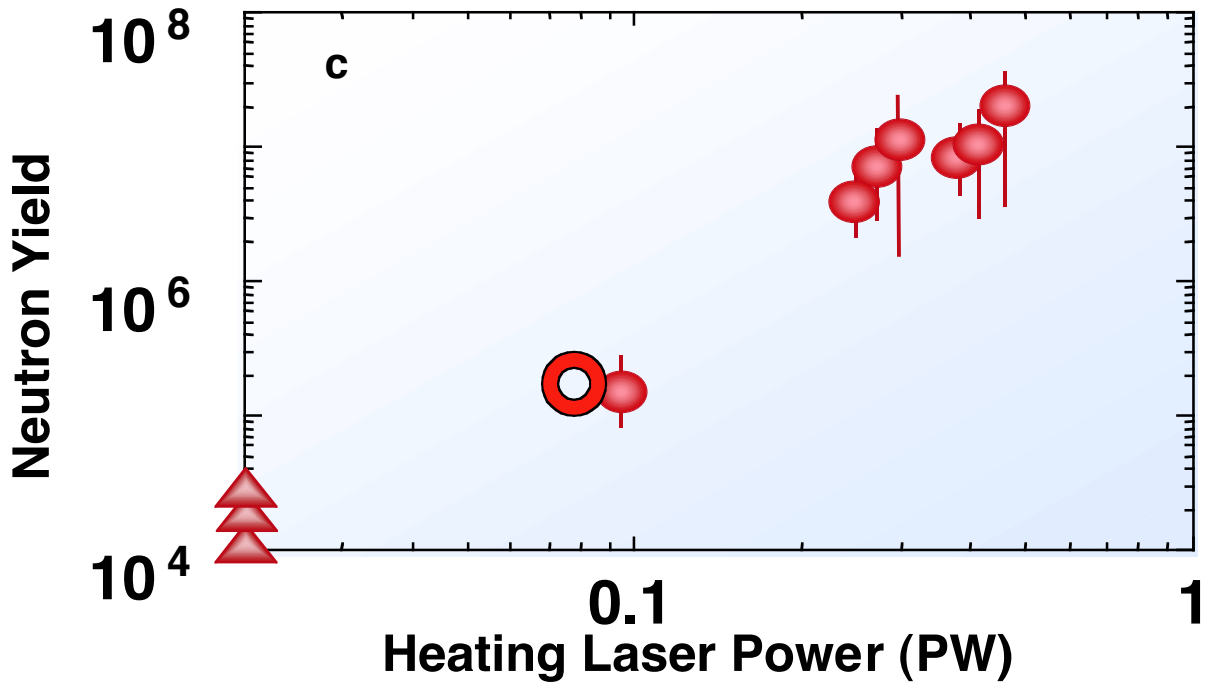

The rise time and the decay time of plasma temperature are longer than expected.

Electron temperatures are critically dependent on the injection time of PW laser with respect to the maximum compression time. This result is consistent with that of neutron yields. c.f.:$T_{i,n}$ ~950 eV

ILE OSAKA

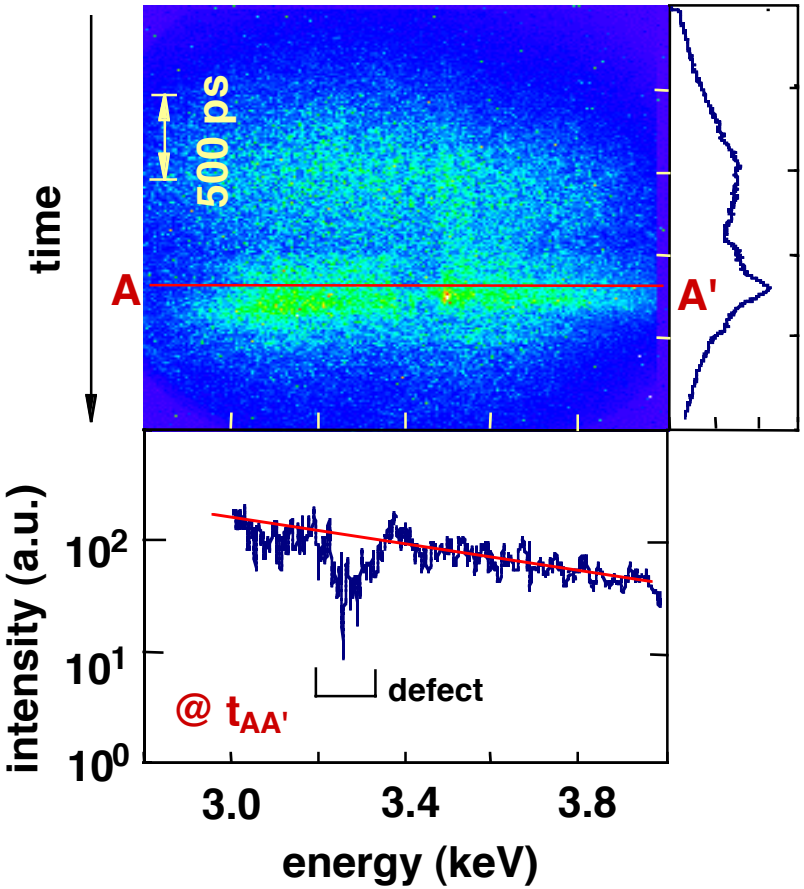

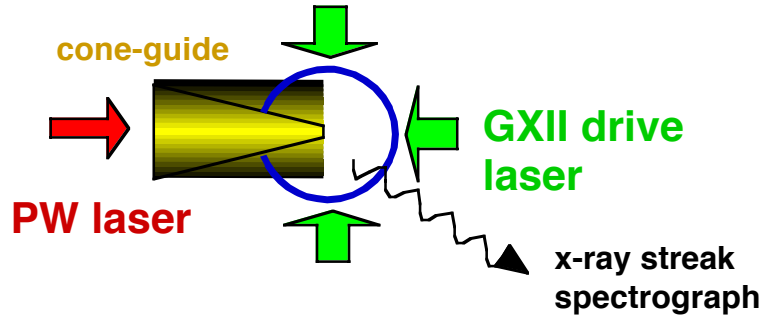

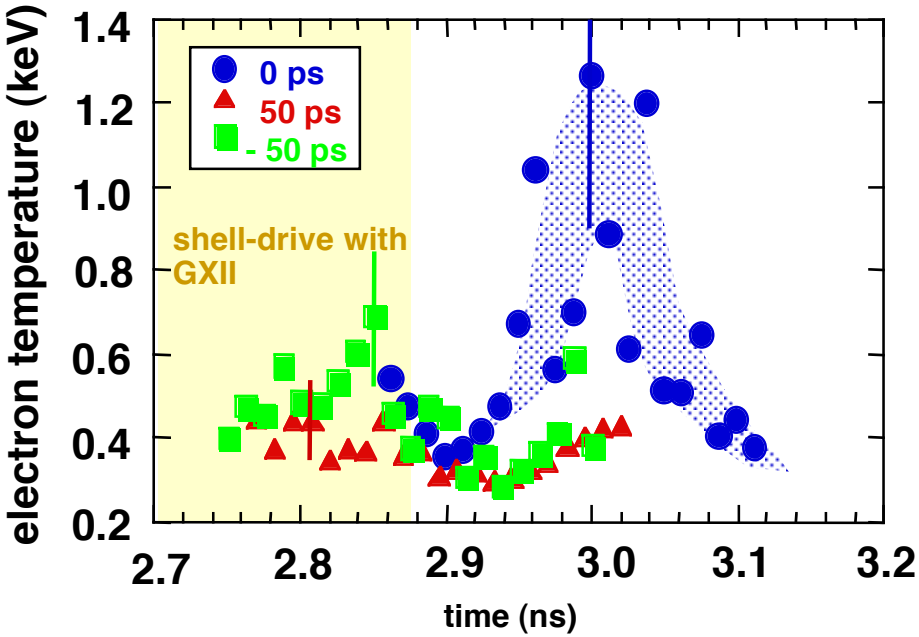

Analysis of non-spherical implosion

ILE Osaka

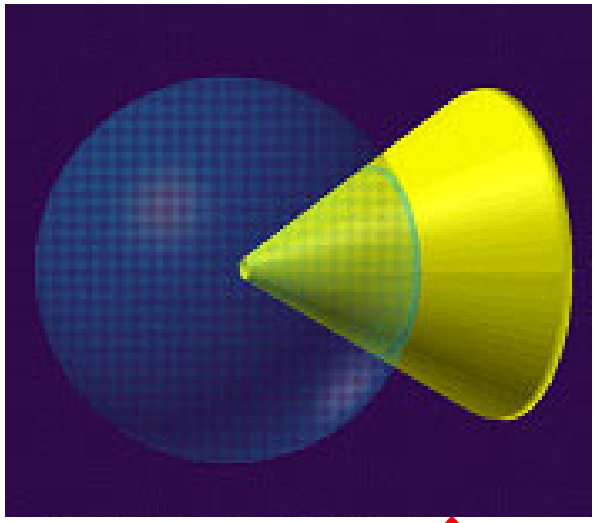

Wavelength : 0.53μm

Intensity : 2×10^{13} W/cm^2 (t<0.4 ns)
1×10^{14} W/cm^2 (t>0.4 ns)

on the initial shell surface
(little smaller than the values of GEKKO XII experiments)

Ray-trace : 1 - D (radial direction)

For the gold cone, CH, of which mass is the same as gold, was substituted.

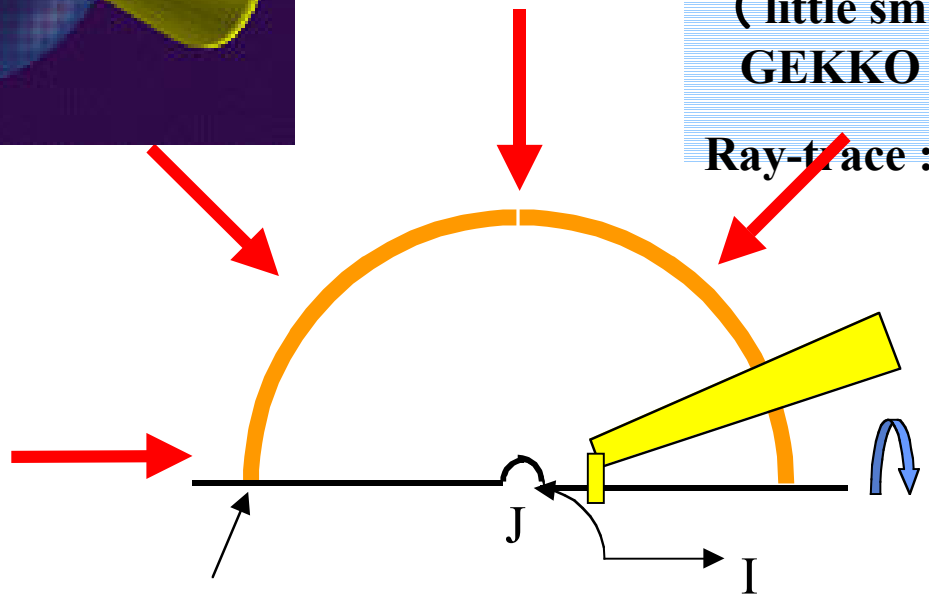

Axial symmetry

Shell Target : CH 8μm

Grid Number :

250 (r- direction) x 242 (θ - direction)

Density Contours in logarithmic scale (cone open angle = 30)

High density core plasma can be produced in non-spherical implosion.
The life time of high density core is longer by 3 times than that of spherical implosion case.

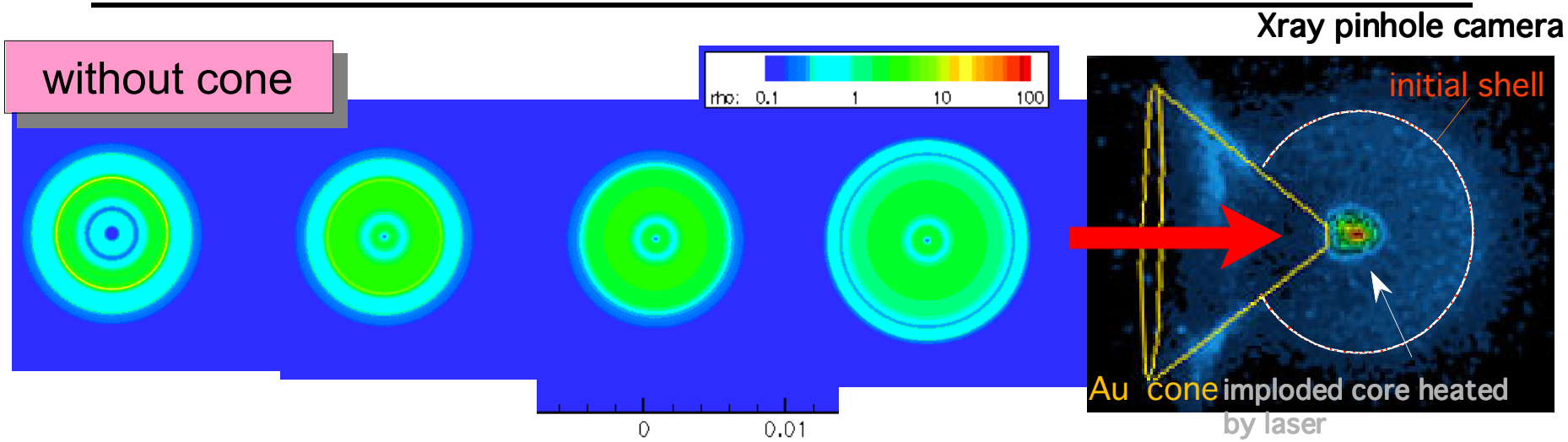

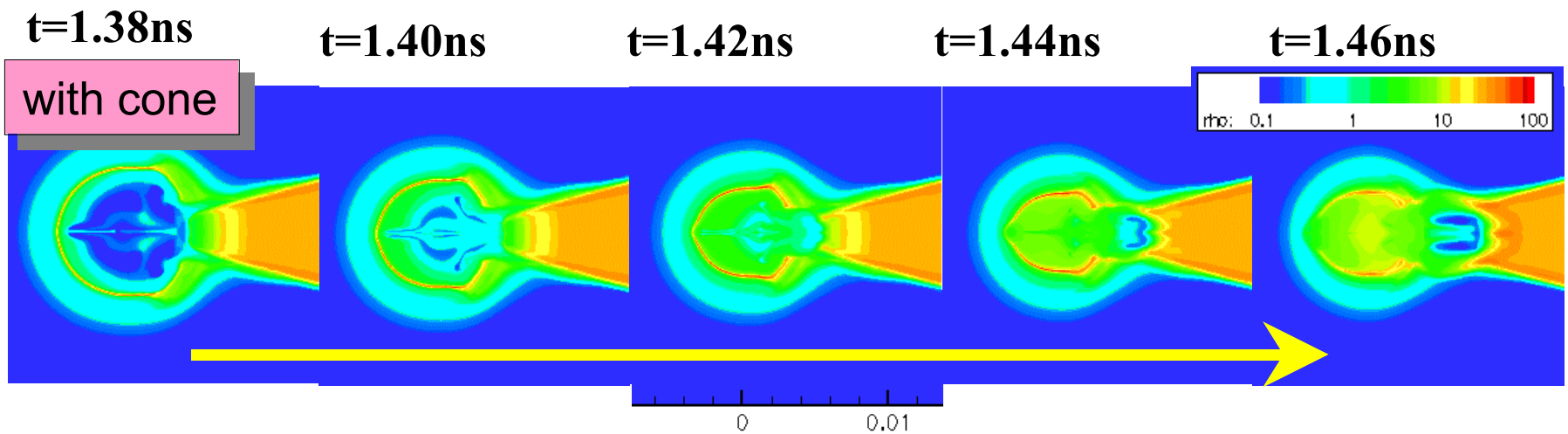

IF/P-07 Nagatomo

ILE Osaka

Pressure Contours in logarithmic scale (cone open angle = 30)

The center of the hot spark and the center of mass density are shifted to the right-hand side of the mass center toward the cone tip.

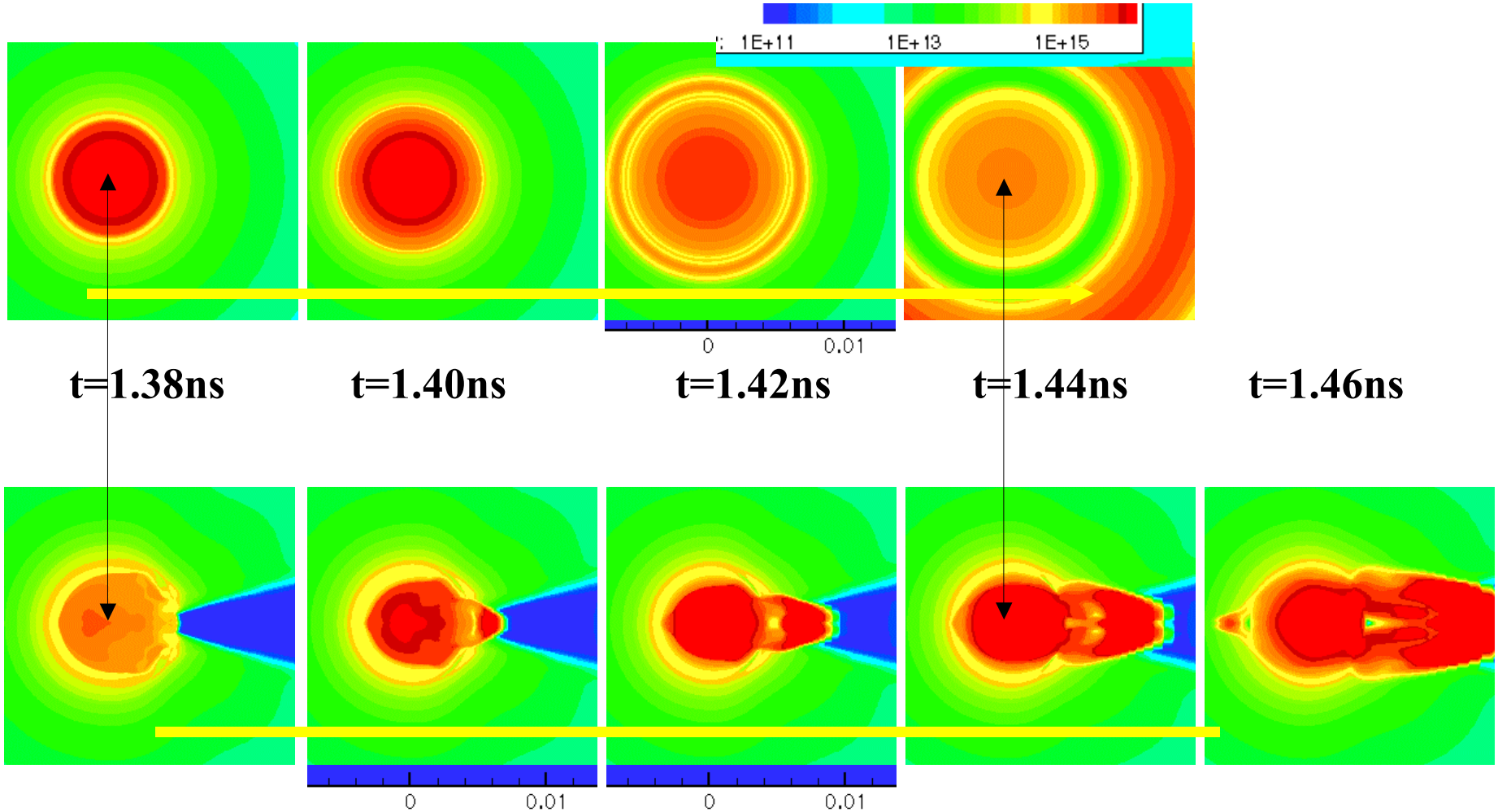

Why Cone target ?

ILE OSAKA

Focusing the laser light to high intensity without fine optical tuning.

- **Laser energy in the wing of the focus spot can be collected**
- **Focus position and direction is controlled better than the Self-Focusing in a Coronal Plasma**
- **Higher conversion efficiency and focusing of electron energy flow are expected.**

The interaction of laser light with conical target is studied by E-M 3D-PIC simulation.

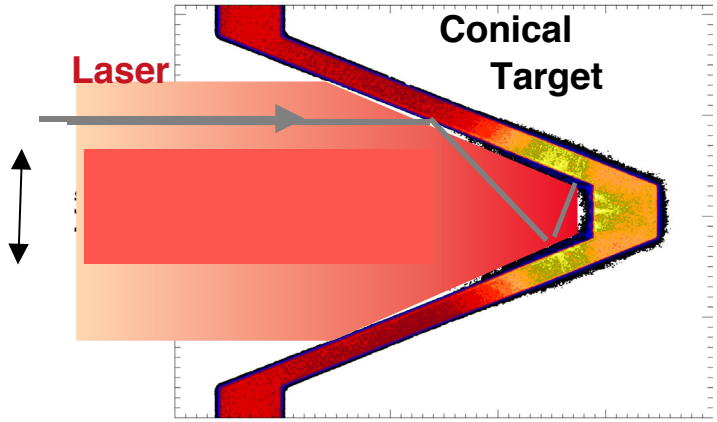

Energetic Electron Beam was Created at the Top of the Cone

Energetic electrons from the cone heated the solid Al (200μm). The heating pattern is consistent with that of the laser absorption, indicating 20-30 deg divergence beam.

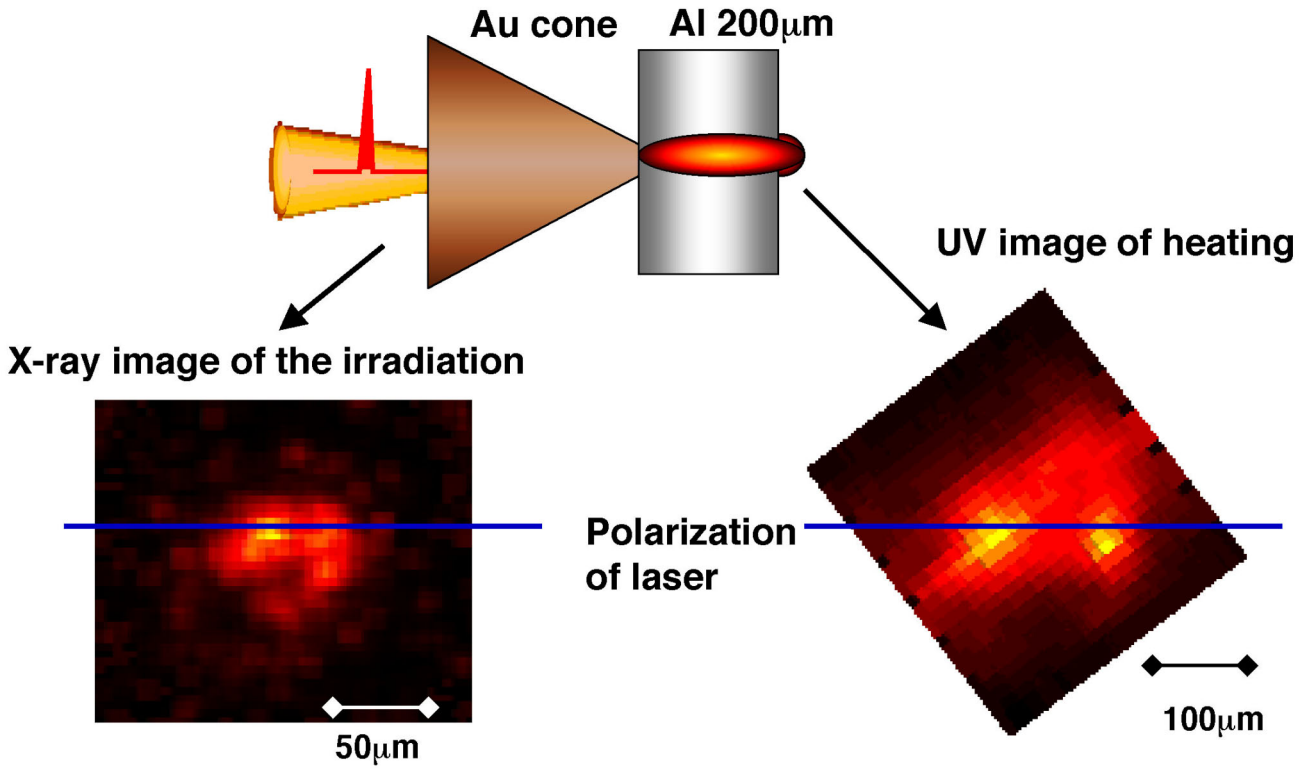

As a electron beam divergence is estimated to 60 deg, this indicates that the magnetic field confines the electron beam.

Laser beam is guided and focused by cone and relativistic electrons are also confined

ILE OSAKA

Laser field intensity distribution

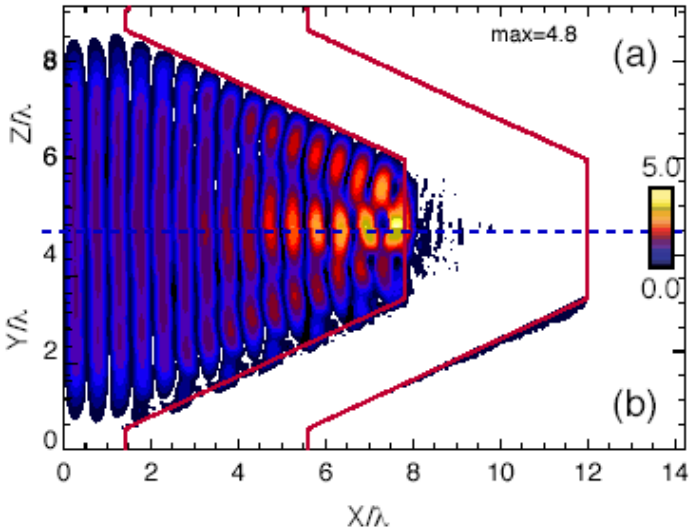

Magnetic field and electron energy density profile

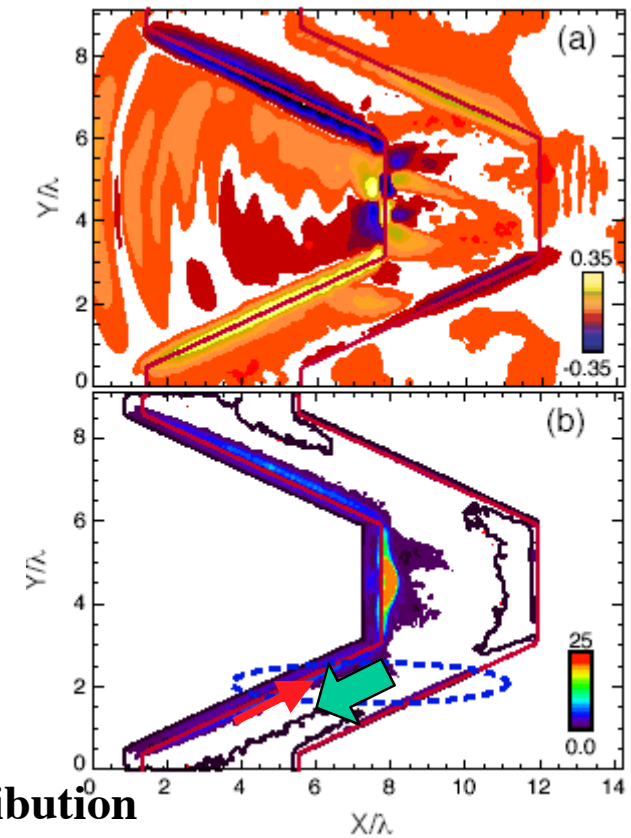

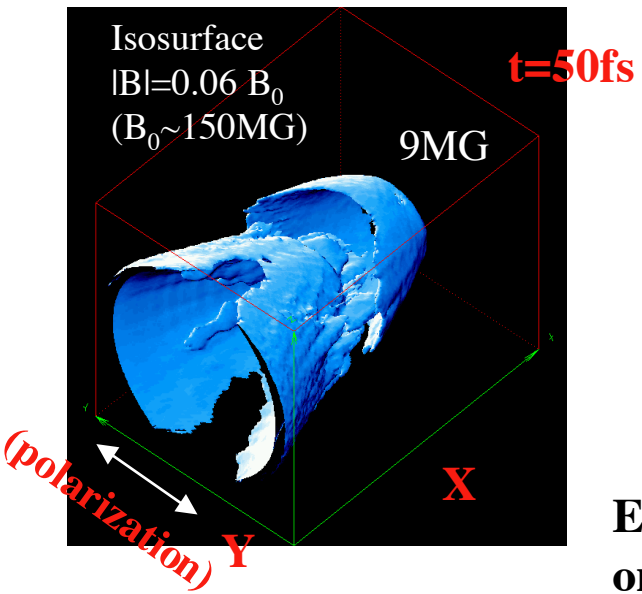

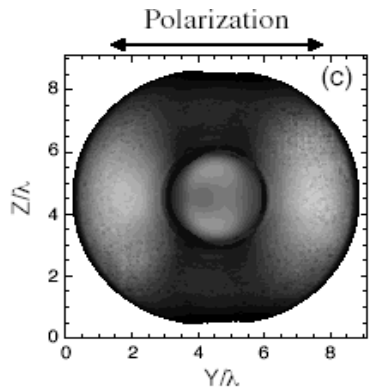

Electron Energy distribution on the cross section of cone

Rev. Electron Energy and Momentum Characteristics in Cone Target

ILE OSAKA

Electron Energy Density $(\gamma-1)n_e/n_c$ at $t=16\tau$

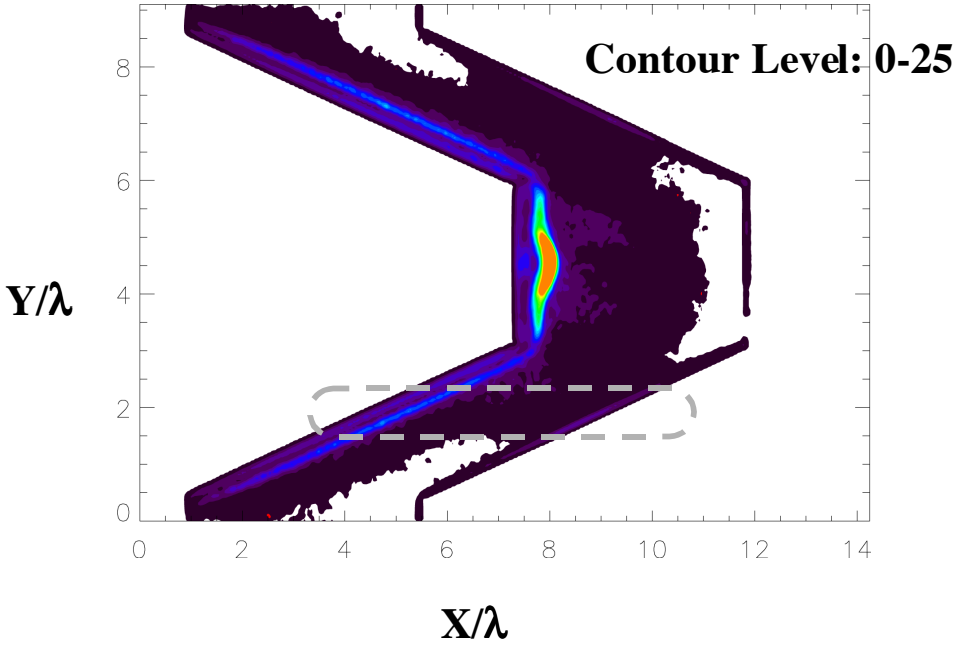

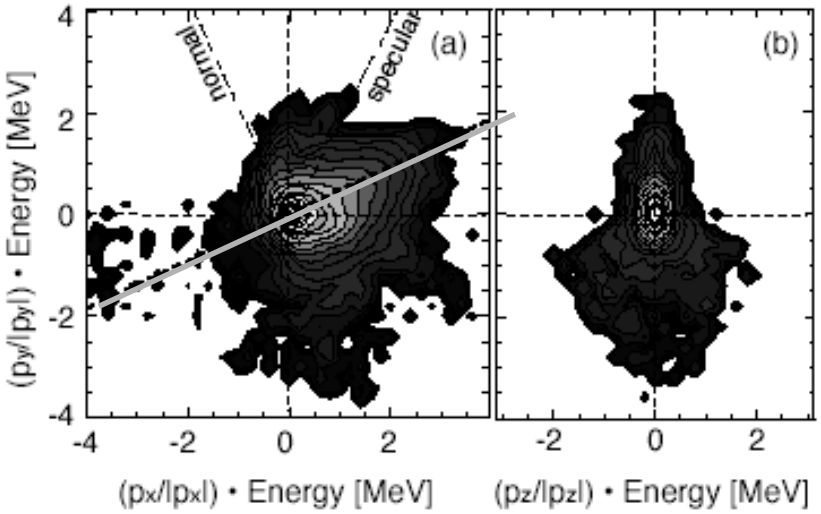

The reason for the long life time of high plasma temperature is due to electrons which travel along the cone and heat the core lately.

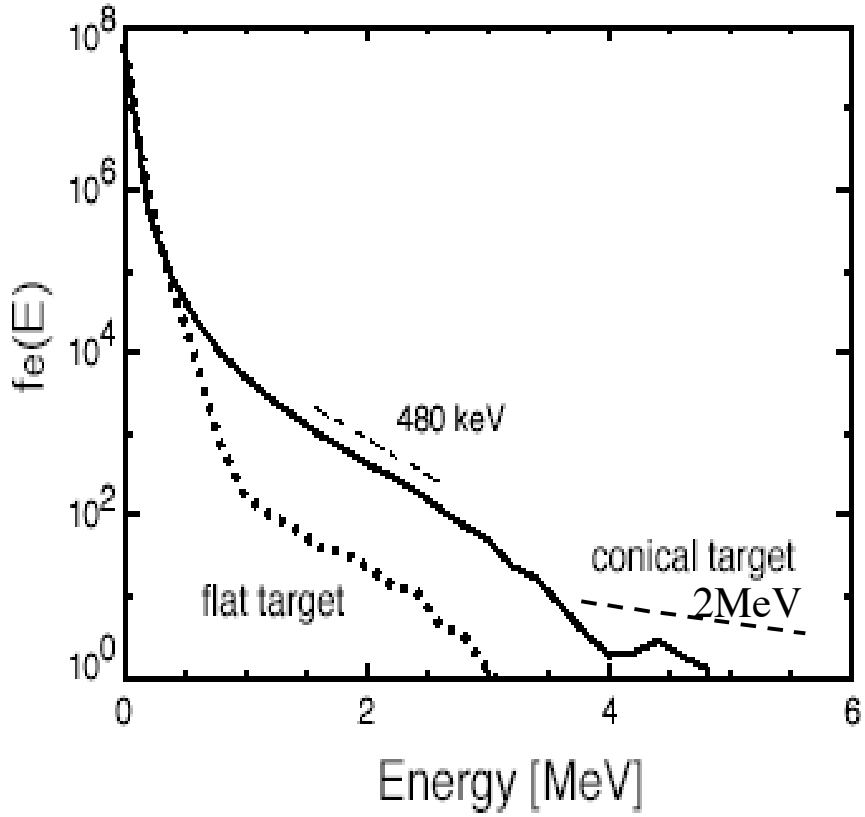

Why cone guiding is necessary ?

Far Field Pattern & Encircled Energy

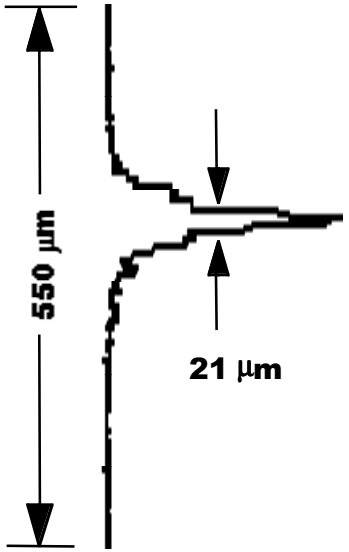

FFP (Far Field Pattern)

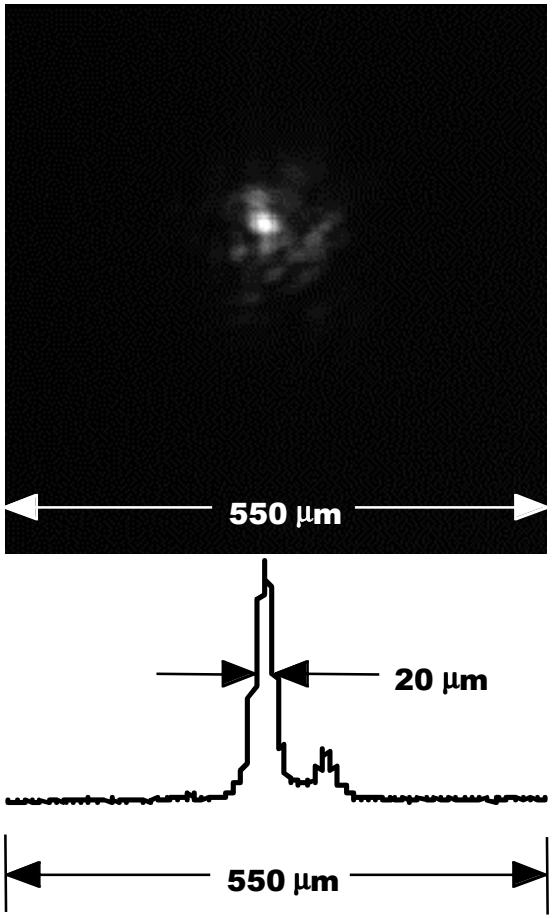

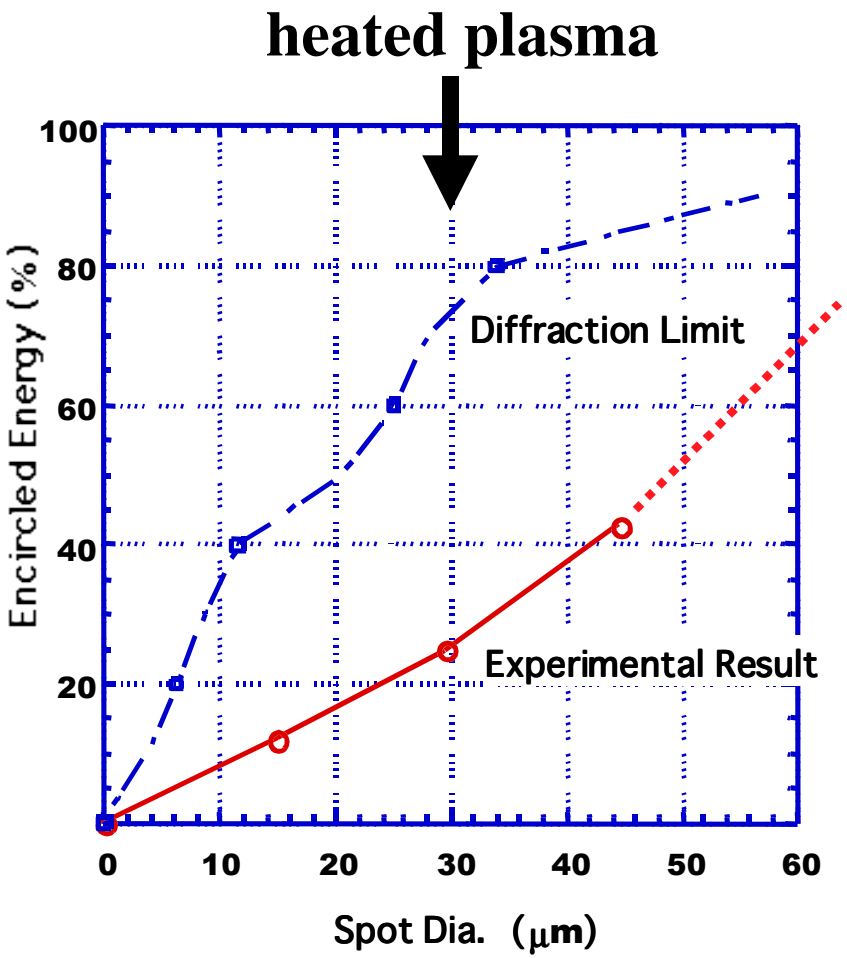

IF/P-04,Izawa

Simulation model for Analysis of Experimental Results and Prediction for the FIREX

ILE OSAKA

$T \cdot \rho \cdot Z \cdot A_i$

ILESTA1-D

Hydoro. : 1-fluid / 2-temp. model

+

Radiation : Multi-group diffusion

Fast Electron spectrum and transport by PIC and Relativistic Fokker-Planck simulations

•Heating rate

System : 1D Slab

Initial plasma profiles

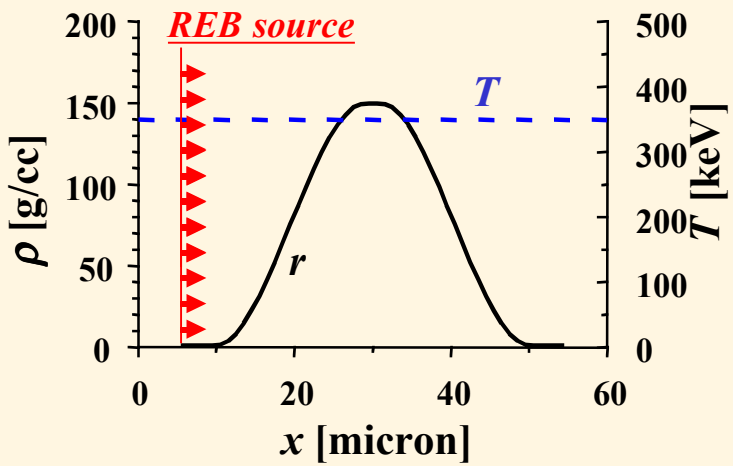

Stationary CD plasma : $\rho X = 0.32$ g/cm^2

Relativistic Electron Beam (REB)

$I_{REB}^{MAX} = 10^{18} \sim 10^{20}$ W/cm^2

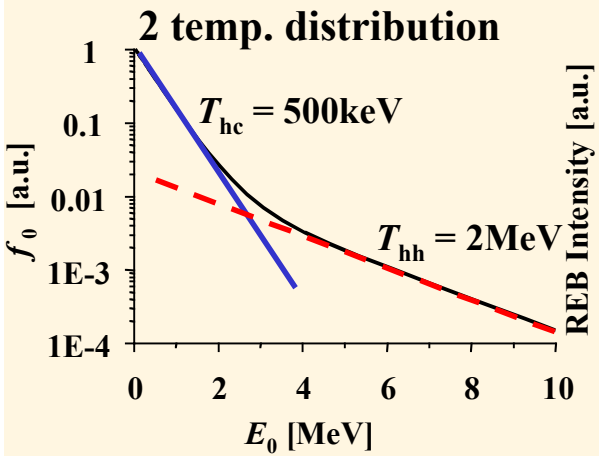

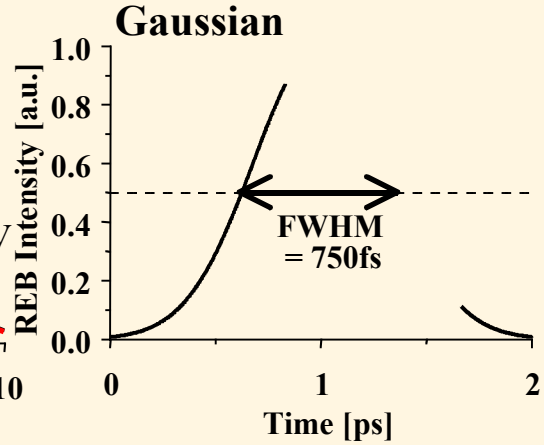

Simulation for PW experiments

ILE OSAKA

By assuming 30μmϕ beam spot and 40% energy coupling efficiency from laser to REB

Heating Laser power, $P_L = I_{REB} \times \pi r_b^2 / \eta_h = 1.77E\text{-}5 \times I_{REB}$

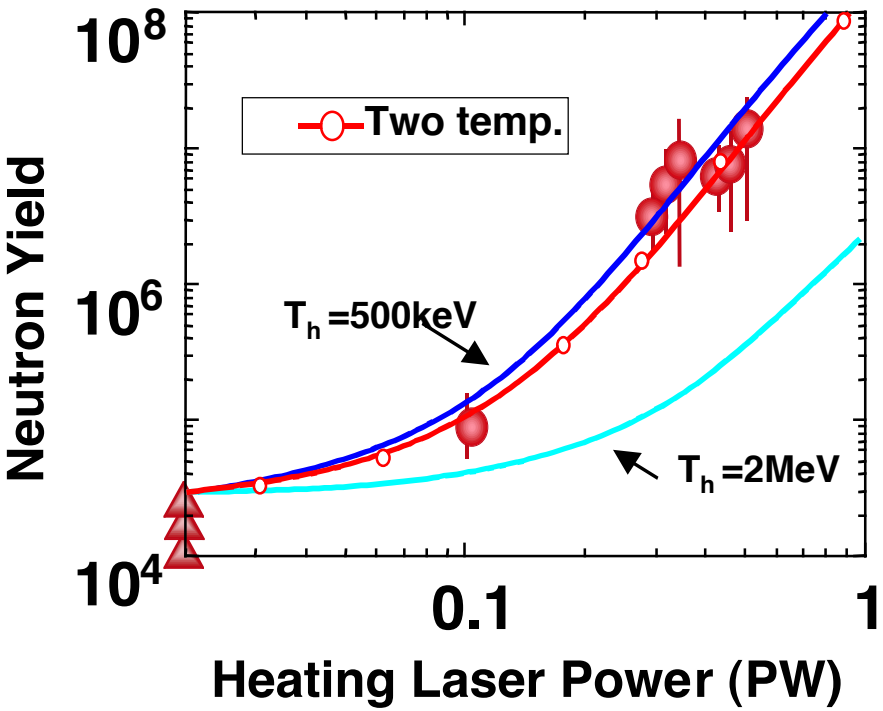

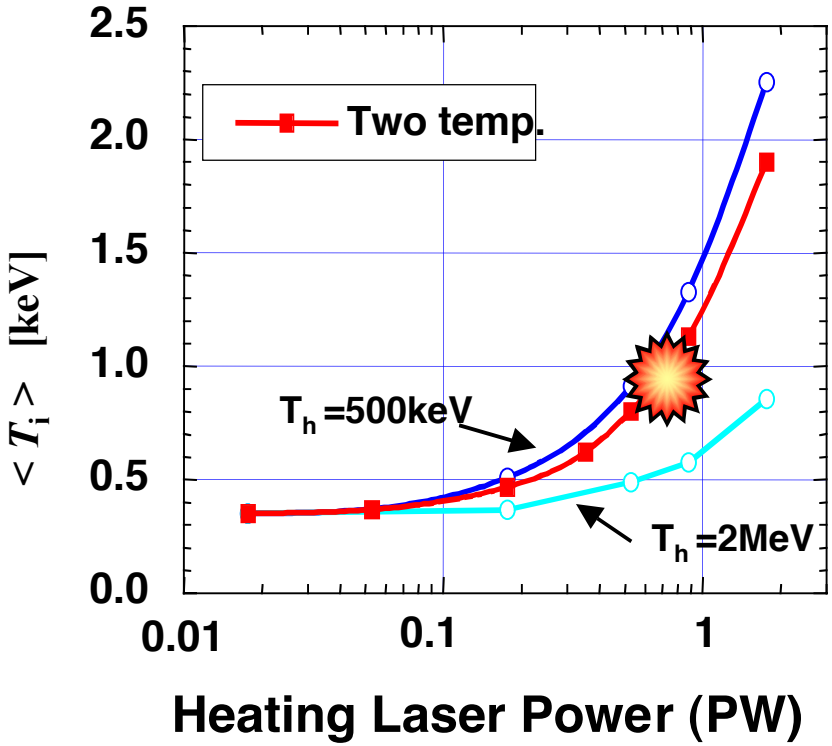

◎ Sub – MeV electrons play important roles in core heating.

◎ Simulation results are in good agreement with experimental results.

Simulation for FIREX-I

ILE OSAKA

✓Beam electron energy spectrum : slope temperature (1comp. or 2comp.)

✓ REB duration = 10ps

⇒ By assuming 30μmϕ beam spot and 40% coupling efficiency from laser to REB

Heating Laser power, $P_{Lh} = I_{REB} \times \pi r_b^2 / \eta_h$

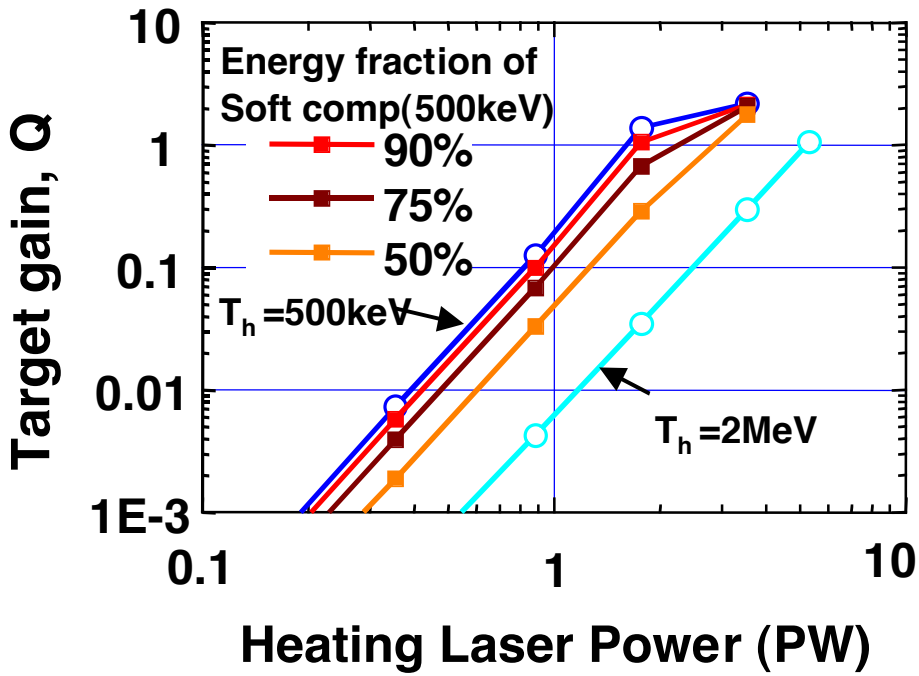

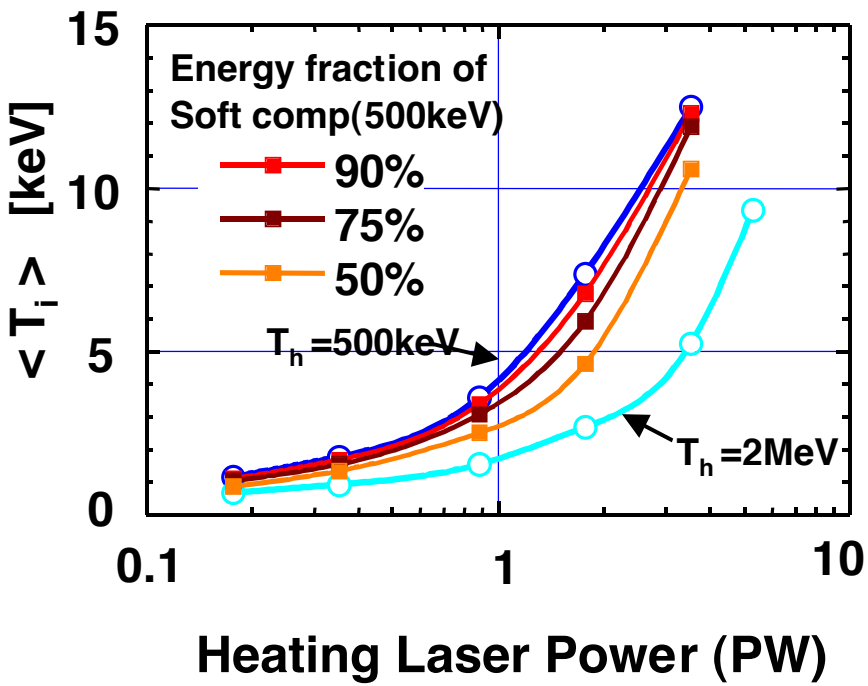

FI^3 Project

- Fast Ignition Integrated Interconnecting code

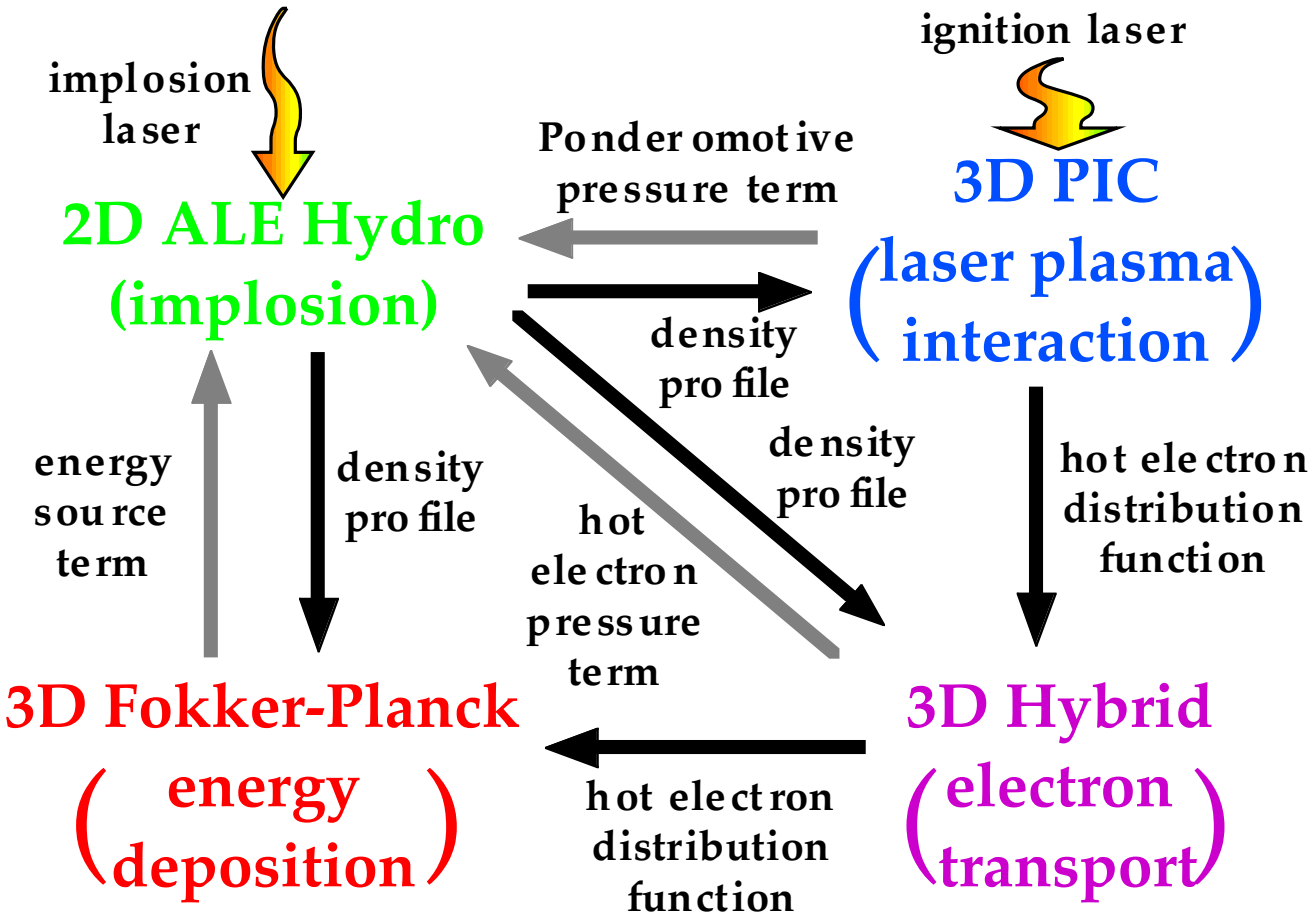

Summary and Conclusions

ILE OSAKA

- By completion of Peta Watt laser / GEKKO XII system ,Fast Ignition integrated experiments have advanced significantly.

- The cone shell target is found to be effective not only for injecting short pulse laser closer to the core plasma but also guiding relativistic electrons generated on the side wall of the cone toward the core plasma.

- In the experiments , it is found that the dense plasma of 60g/cc was heated up to 1 keV. The plasma temperatures of 80J and 300J(0.6PW) heating indicate that coupling efficiency of the heating is constant 25% in the power range of PW.

- The neutron yield enhancement factor and its laser power dependence of experiments are predicted by the combined simulations with PIC, Fokker Planck and hydro simulation codes.

- The above simulation results predict that the significant fusion burn Q~0.2 can be achieved with 10kJ/10ps laser ,GEKKO XII and DT cryogenic target. This leads to the F.I. Ignition and burn projects ;FIREX-I and -II.

Plasma expansion into a vacuum

Patrick Mora

Centre de Physique Théorique

Ecole Polytechnique, Palaiseau

Introduction

- Plasma expansion into a vacuum: an old problem relevant to recent experiments on ion acceleration
  - Krushelnick *et al.*, Phys Plasmas **7**, 2055 (2000)
  - S. P. Hatchett *et al.*, Phys. Plasmas **7**, 2076 (2000)
  - E. L. Clark *et al.*, Phys. Rev. Lett. **84**, 670 (2000)
  - A. Maksimchuk *et al.*, Phys. Rev. Lett. **84**, 4108 (2000)
  - E. L. Clark *et al.*, Phys. Rev. Lett. **85**, 1654 (2000)
  - R. A. Snavely *et al.*, Phys. Rev. Lett. **85**, 2945 (2000)
  - A. J. Mackinnon *et al.*, Phys. Rev. Lett. **86**, 1769 (2001)
  - J. Badziak *et al.*, Phys. Rev. Lett. **87**, 215001 (2001)
  - A. J. Mackinnon *et al.*, Phys. Rev. Lett. **88**, 215006 (2002)
  - M. Hegelich *et al.*, Phys. Rev. Lett. **89**, 085002 (2002)
  - M. Roth *et al.*, Phys. Rev. ST Accel. and Beams **5**, 061301 (2002)

Motivations

- Importance of a correct theoretical/numerical prediction of the ion energy spectrum and of its cut-off at high energy (in relation with the structure of the ion front)
- Most previous works on plasma expansion into a vacuum did not address the structure of the ion front and the ion energy spectrum
- Among the works which did address these items, no clear picture comes out and contradictory results are given.

Previous description of the ion front

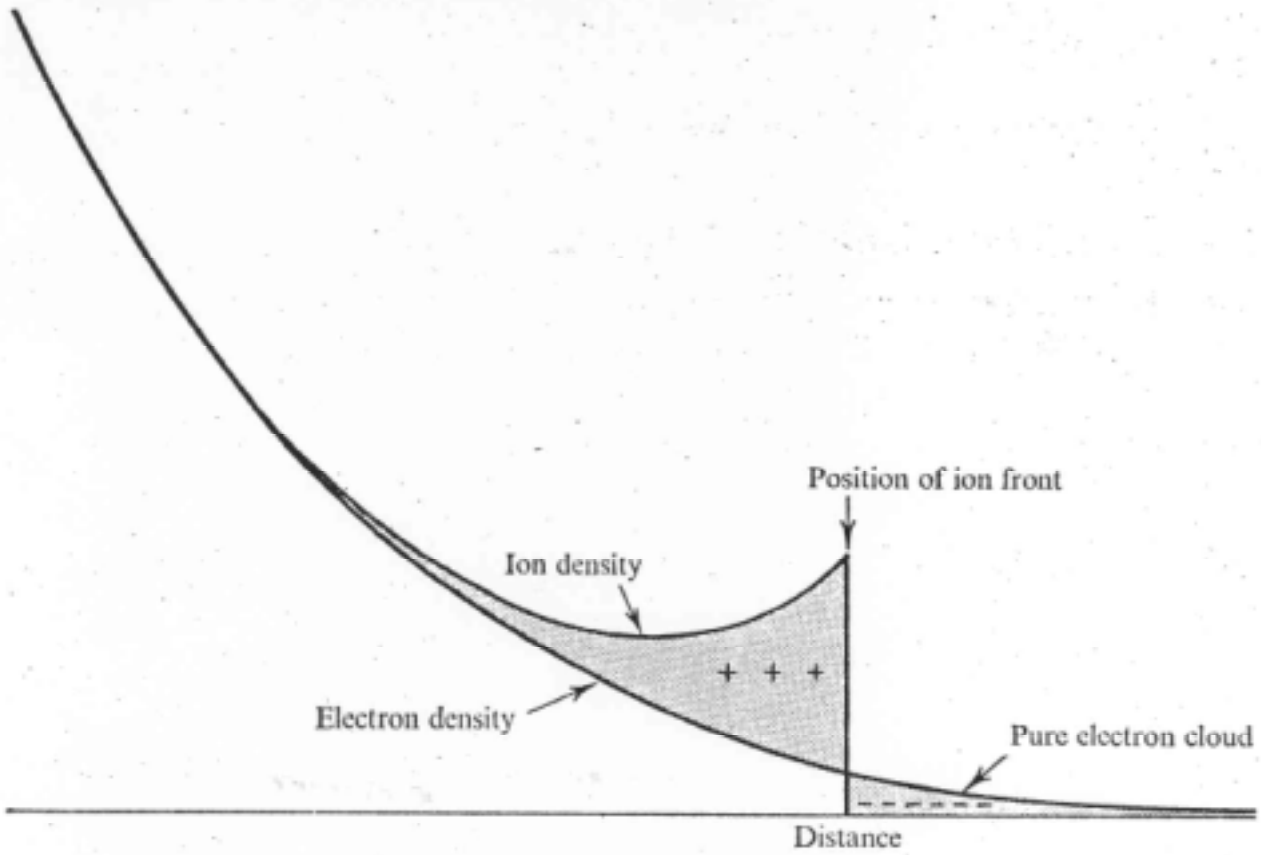

FIGURE 2. Variation of ion and electron densities at the front.

J. E. Crow, *et al.*, Plasma Physics **14**, 65 (1975)

Previous numerical results

Widner *et al.*, Phys. Fluids **14**, 795 (1971)

Crow *et al.*, Plasma Physics **14**, 65 (1975)

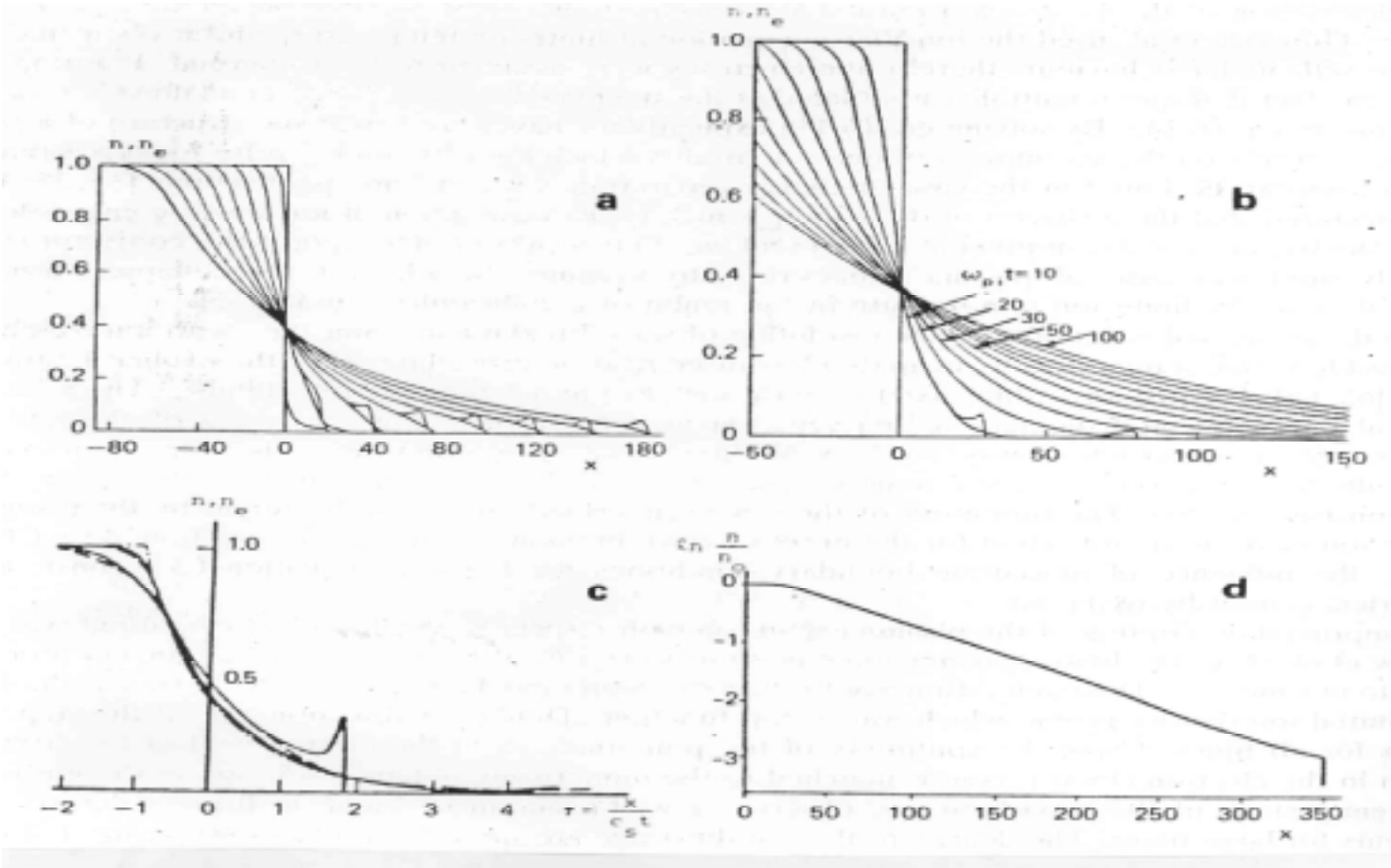

Gurevich *et al.*, Sov. Phys JETP **53**, 937 (1981)

True *et al.*, Phys. Fluids **24**, 1885 (1981)

Theoretical model: initial condition

At time t=0 a plasma occupies the half space x<0 and begins to expand into a vacuum.

$$n_e = n_{e0} \exp(e\Phi / k_B T_e)$$

$$\varepsilon_0 \frac{\partial^2 \Phi}{\partial x^2} = e(n_e - Zn_i)$$

$$E_{front} = \sqrt{\frac{2}{e}} E_0$$

$$E_0 = \left(\frac{n_{e0} k_B T_e}{\varepsilon_0} \right)^{1/2} = \frac{k_B T_e}{e \lambda_{D0}}$$

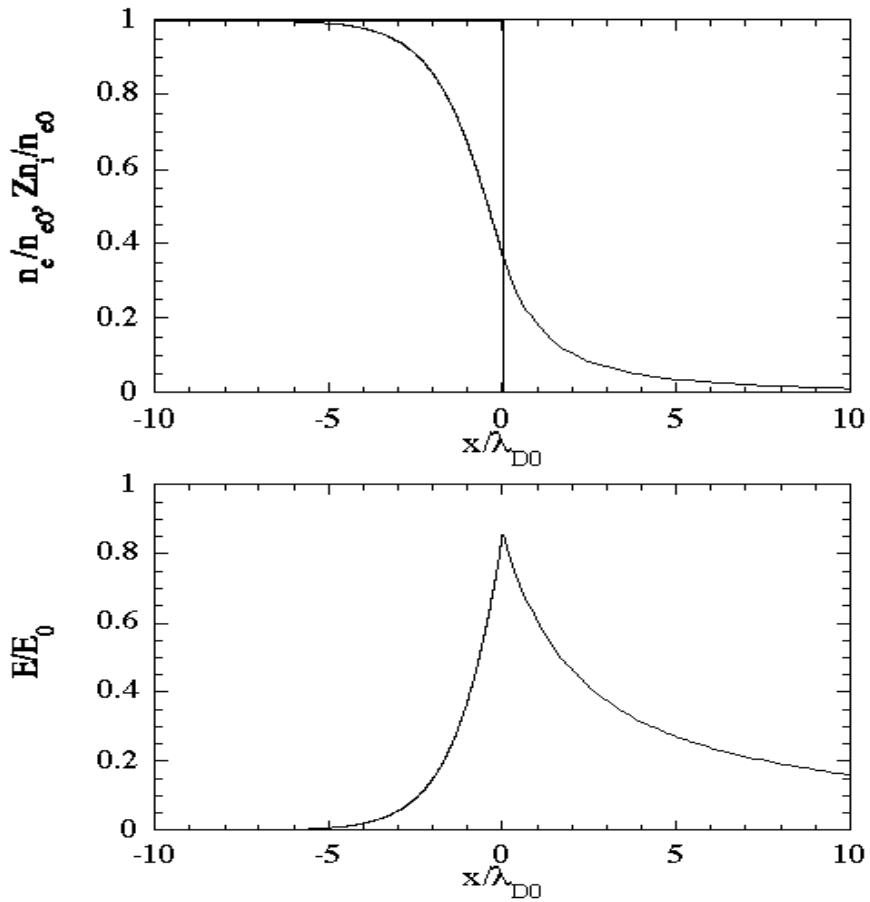

Equations of the model for t>0

$$\left(\frac{\partial}{\partial t} + v\frac{\partial}{\partial x}\right)n_i = -n_i\frac{\partial v}{\partial x}$$

$$\left(\frac{\partial}{\partial t} + v\frac{\partial}{\partial x}\right)v = -\frac{Ze}{m_i}\frac{\partial \Phi}{\partial x}$$

$$n_e = n_{e0}\exp(e\Phi / k_B T_e)$$

$$\varepsilon_0\frac{\partial^2 \Phi}{\partial x^2} = e\left(n_e - Zn_i\right)$$

Self similar solution for t>0 and $x+c_s t>0$

$$\boxed{v = c_s + x/t}$$

$$\boxed{n_e = Zn_i = n_{e0}\exp(-x/c_s t - 1)}$$

$$\boxed{E_{ss} = \frac{k_B T_e}{e c_s t} = \frac{E_0}{\omega_{pi} t}}$$

Validity : $\boxed{c_s t > \lambda_D}$ or $\begin{cases} \boxed{\omega_{pi} t > 1} \\ \boxed{2\ln(\omega_{pi} t) > 1 + x/c_s t} \end{cases}$

Ion front position and velocity

If one declares that the ion front coincides with the point where the self-similar solution breaks down, i. e., where $c_s t \approx \lambda_D$, one gets

$$\boxed{x_{front} / c_s t \approx 2 \ln\left(\omega_{pi} t\right) - 1}$$

$$\boxed{v_{front} \approx 2 c_s \ln\left(\omega_{pi} t\right)}$$

Note that this implies

$$\boxed{E_{front} \approx 2 E_{ss} = 2 E_0 / \omega_{pi} t}$$

Numerical solution

Lagrangian code solving fluid eqs. + Poisson eq., using « standard » methods:

- leap-frog for ion motion,
- nonlinear Poisson Eq. is linearized with respect to small variation from previous time-step solution with a fast converging iterative method:

$$\exp\left(\frac{e\Phi}{k_B T_e}\right) \approx \exp\left(\frac{e\Phi_{old}}{k_B T_e}\right) \times \left(1 - \frac{e\Phi_{old}}{k_B T_e} + \frac{e\Phi}{k_B T_e}\right)$$

Boundary condition : $E_{front} = \sqrt{2}\,\frac{k_B T_e}{e\lambda_D}$

Charge density and electric field at $\omega_{pi}t=50$

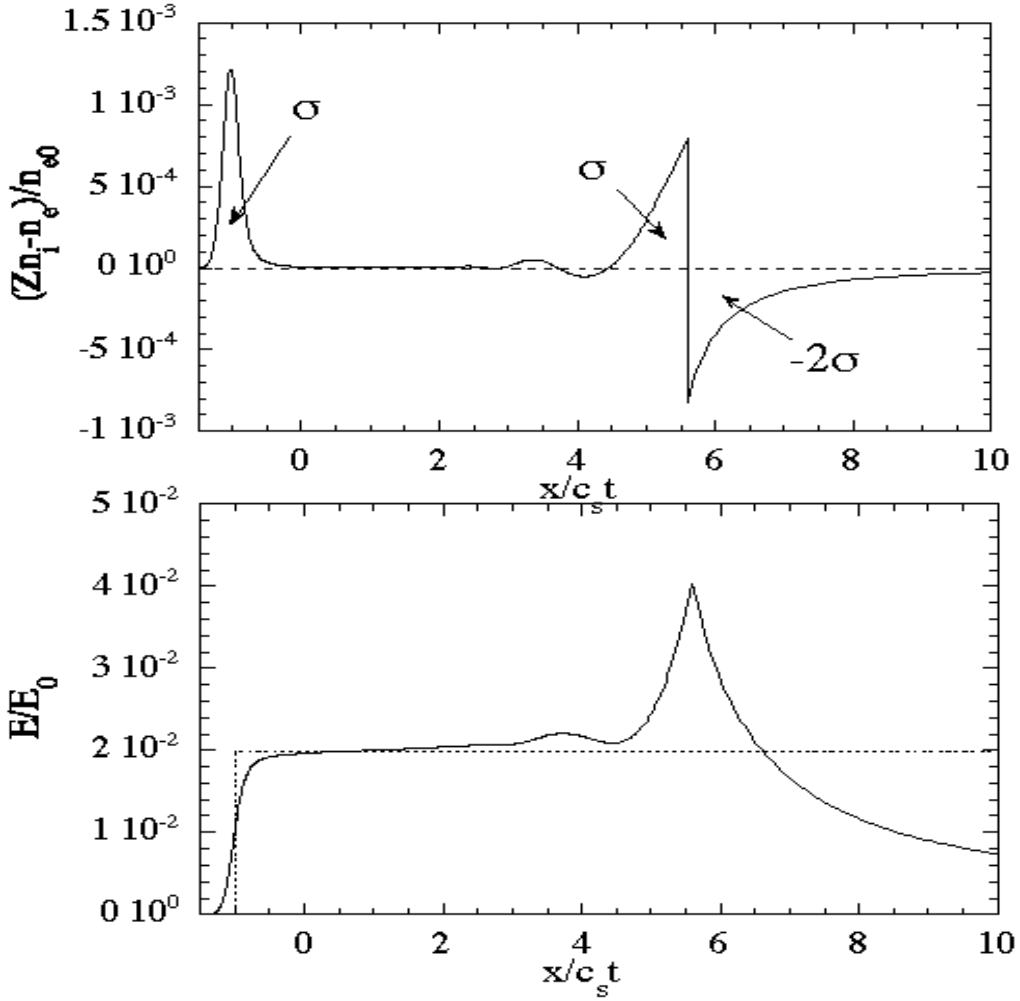

$$\sigma = \varepsilon_0 E_{ss}$$

Time evolution of E_{front} and v_{front}

$$E_{front} \approx \frac{2E_0}{\sqrt{2e + \omega_{pi}^2 t^2}}$$

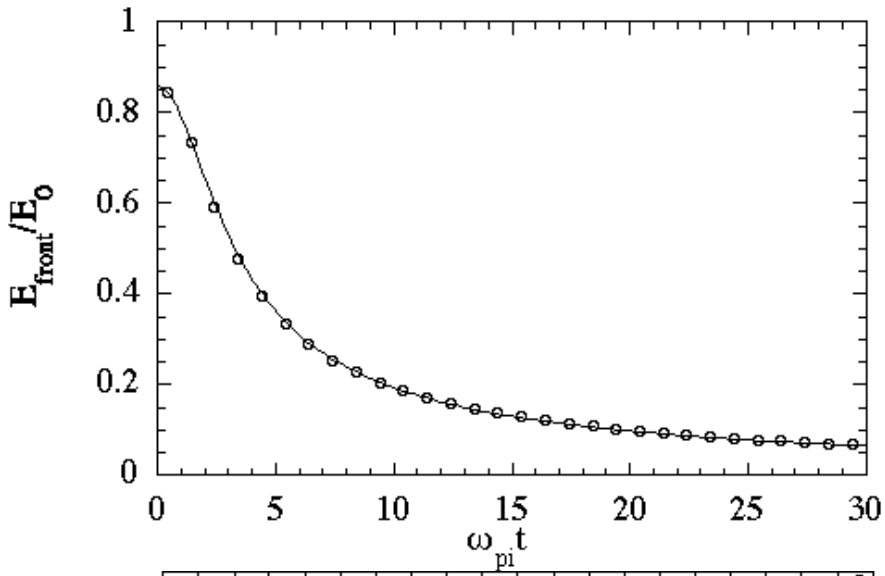

$$v_{front} \approx 2c_s \ln\left(\tau + \sqrt{\tau^2 + 1}\right)$$

where $\tau = \omega_{pi} t / \sqrt{2e}$

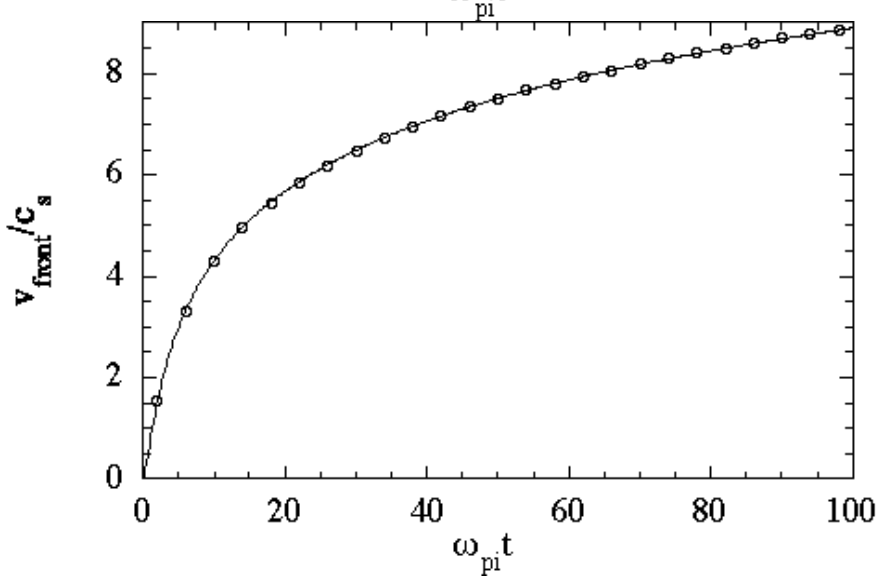

Structure of the ion front

$$n_{e,\ front} \approx \frac{2n_{e0}}{\omega_{pi}^2 t^2}$$

$$n_{i,\ front} \approx \frac{4n_{i0}}{\omega_{pi}^2 t^2}$$

$$\left(\frac{\partial}{\partial x}\ln n_e\right)_{front} \approx -\frac{2}{c_s t}$$

$$\left(\frac{\partial}{\partial x}\ln n_i\right)_{front} \approx -\frac{1}{2c_s t}$$

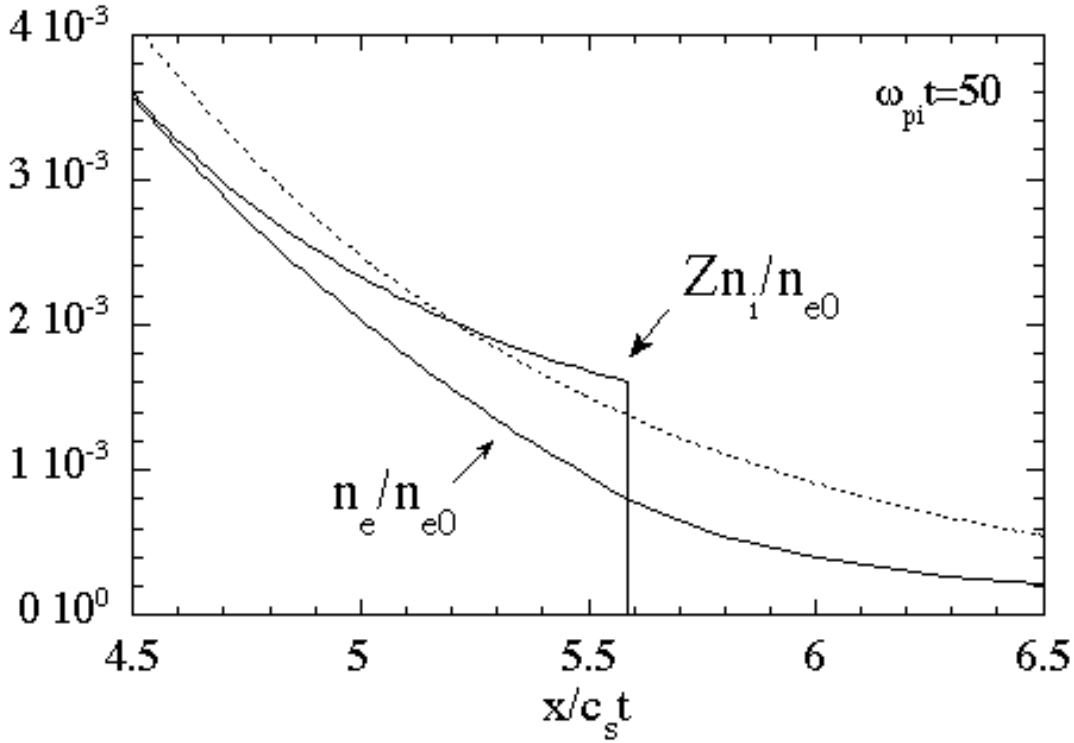

No ion bump !

Energy spectrum

$$\frac{dN}{dE} = \frac{n_{i0} c_s t}{\sqrt{2EE_0}} \exp\left(-\sqrt{\frac{2E}{E_0}}\right)$$

where

$$E_0 = Zk_B T_e$$

$$E_{max} \approx 2E_0 [\ln(2\tau)]^2$$

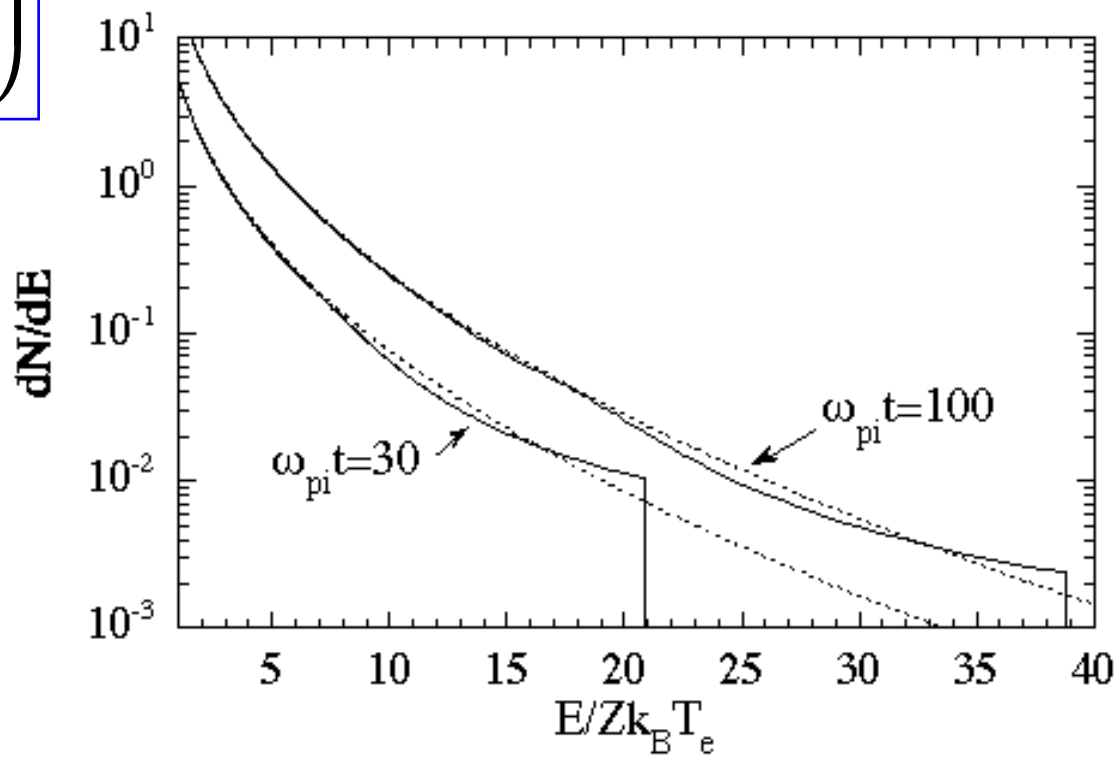

Conclusion

- Controversy about the existence of an ion bump solved

- Maximum ion energy

$$E_{\max} \approx \frac{1}{2} Z k_B T_e \left[2 \ln(\omega_{pi} t) + \ln 2 - 1 \right]^2$$

- In the interpretation of a real experiment additional effects have to be taken into account

Relativistic laser-plasma interactions relevant to advanced fast ignition

Peter Norreys

Physics Group Leader,
CCLRC Rutherford Appleton Laboratory
Chilton, Didcot,
Oxfordshire,
OX11 0QX
United Kingdom.

Acknowledgements

R Clarke, J Collier, H Habara, K Lancaster, S Hawkes, D Neely
and all the staff of the Central Laser Facility, CCLRC Rutherford Appleton Laboratory

A MacKinnon, P Patel R Snavely and Mike Key,
Lawrence Livermore National Laboratory

C Stoeckl and C Sangster
University of Rochester

R Stephens, T Cowan
General Atomics

R King R Freeman
Univ. California Davis

R. Kodama, K. Mima, H. Fujita, Y. Kitagawa, T. Miyakoshi, N. Miyanaga, T. Norimatsu, T. Shozaki, K. Shigemori, A.Sunahara, M. Tampo, K. A. Tanaka, Y. Toyama, T Yabuuchi and T. Yamanaka
Institute of Laser Engineering, Osaka University, Japan

C.Murphy, K Krushelnick and B Dangor
Imperial College, London

L.Romagnani, M Borghesi and M Zepf
Queens University of Belfast

Steve Rose
University of Oxford

Roger Evans, Nigel Woolsey
University of York

Thanks to the Royal Society, JSPS, EPSRC, NSF, DoE and the MoD.

Outline of presentation

¥ Very brief review of progress in advanced fast ignition using guided compression

¥ Design philosophy behind the experimental campaign using the Vulcan laser

¥ Current status

¥ Future outlook

Cone guided compression

- **A British - Japanese team have made rapid progress in the past three years in advanced fast ignition studies**

¥ first proof of concept cone-guided experiments (type b) performed at RAL in 1999

¥Good agreementshape of guided foils with 2D hydro simulations & first indications of short pulse heating of compressed matter

¥Gave greater confidence to undertake (type a) experiments at Osaka, especially given the encouraging numerical simulations of Steve Hatchett & Max Tabak

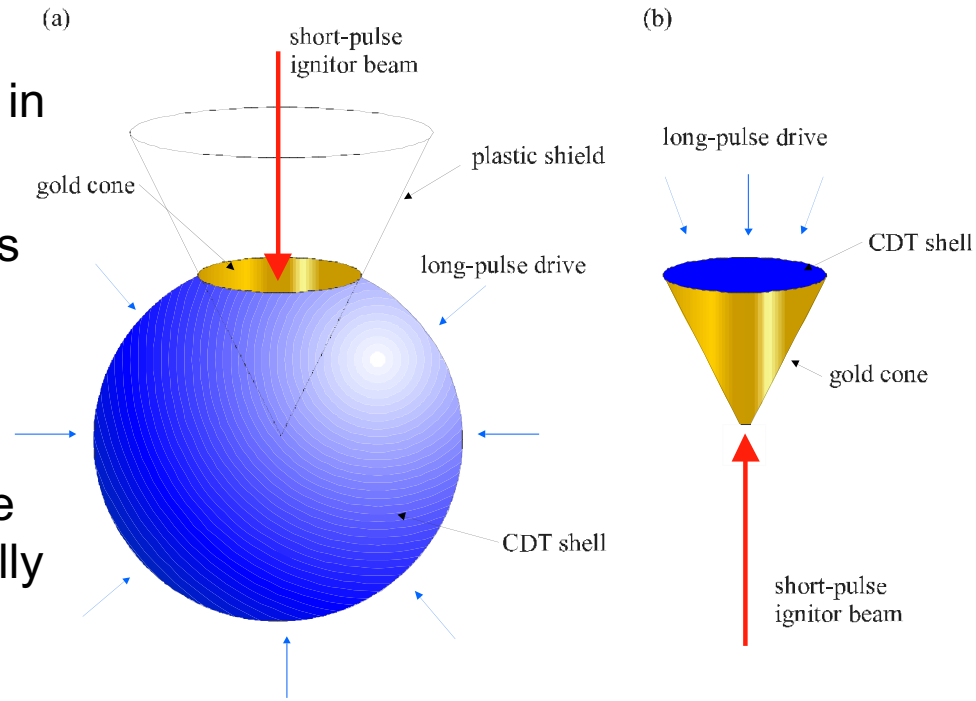

P.A.Norreys et al., Physics of Plasmas 7, 3721 (2000)

Time integrated and time resolved x-ray images confirm implosion symmetry & short pulse heating

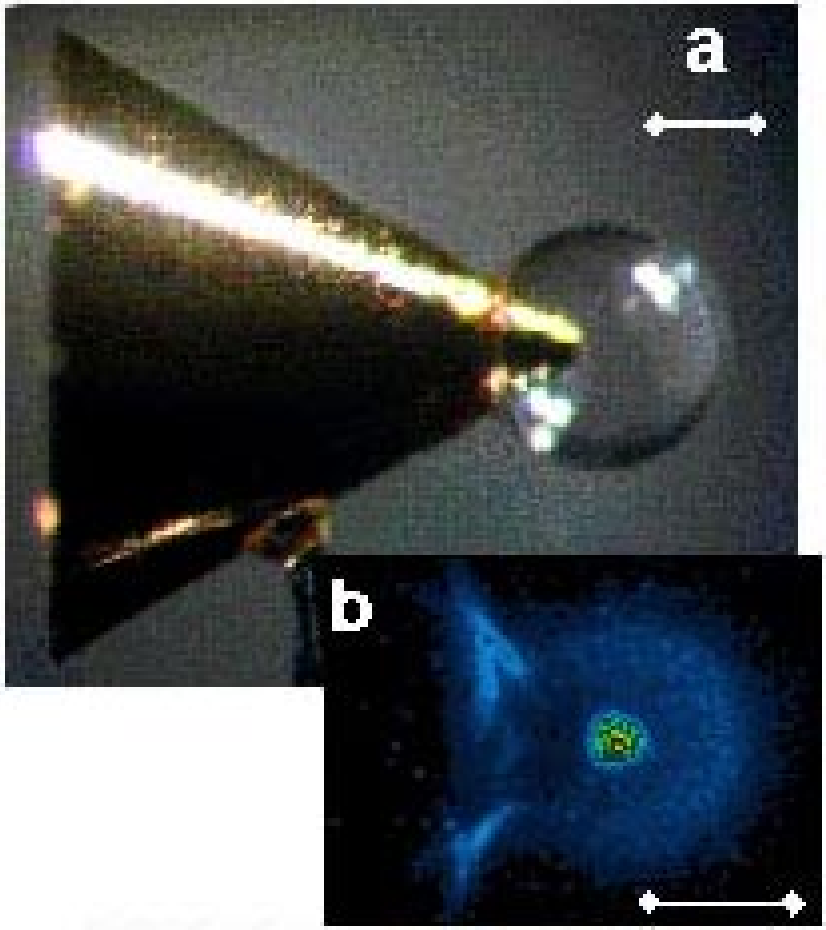

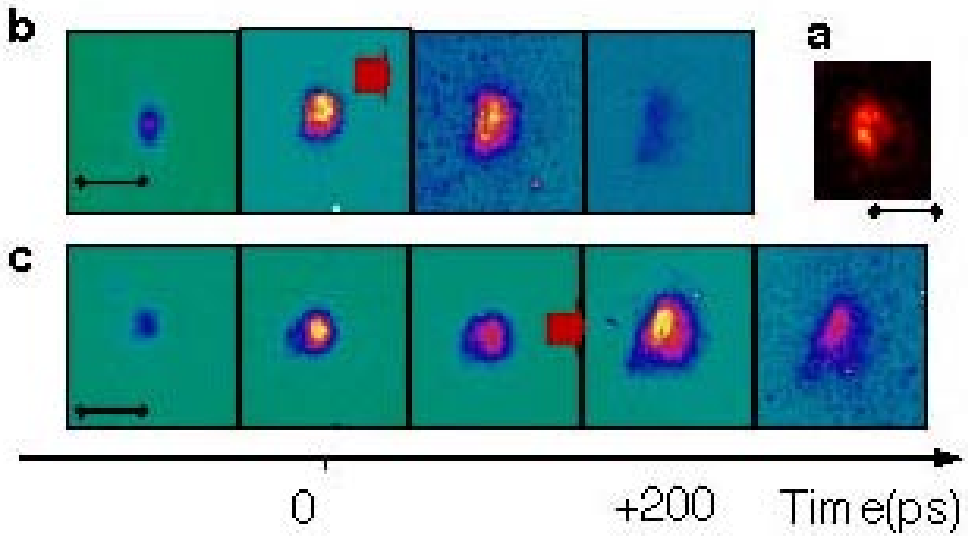

R.Kodama, P.A.Norreys, K.Mima *et al.* Nature **412,** 798-802 (2001).

X-ray radiographic measurements indicates that densities of 50-70gcm^{-3} were achieved.

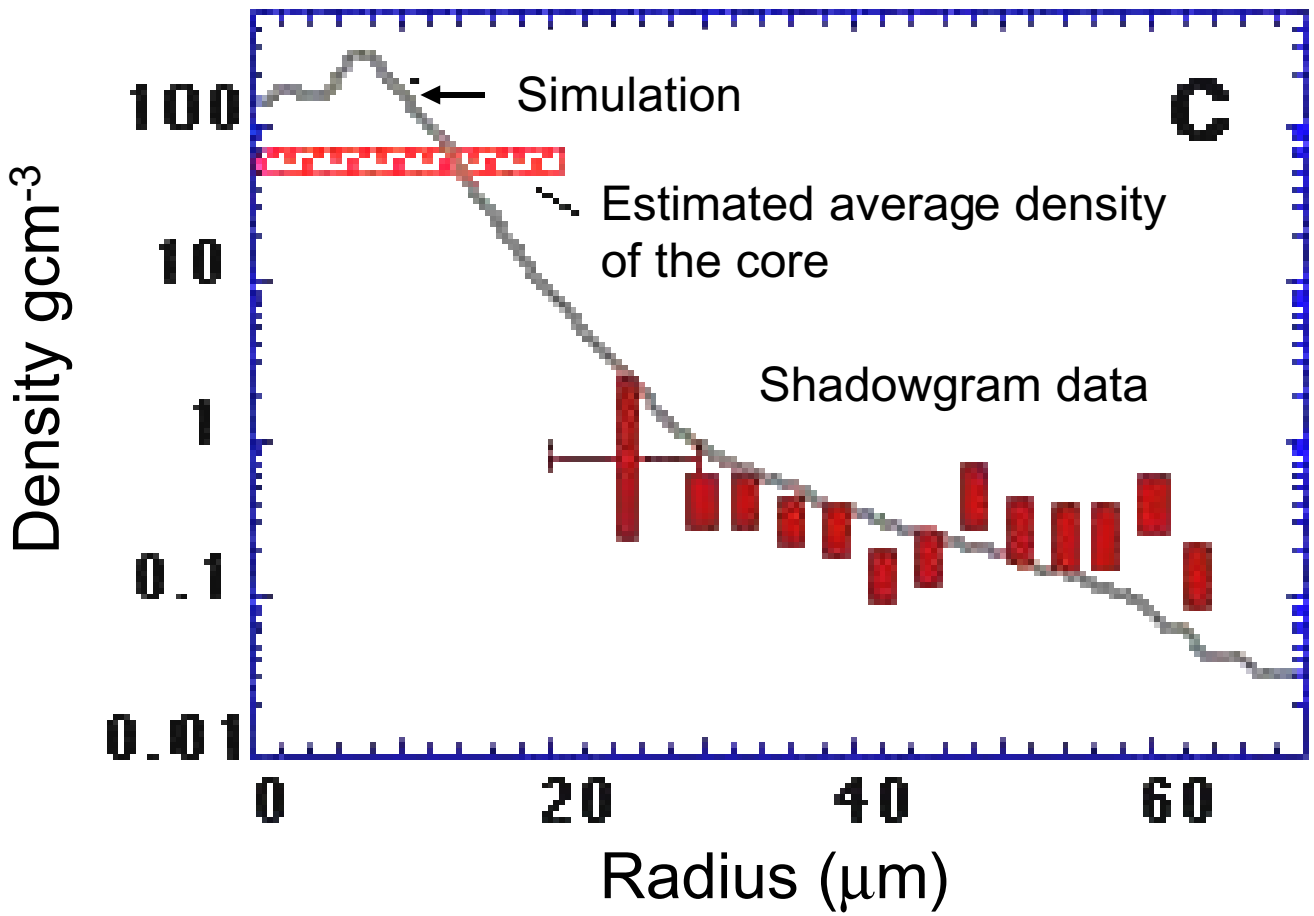

Experiments this year have demonstrated

- ¥ **X1000 enhancement of fusion products**
- ¥ **Confirmation of 20% conversion efficiency**
- ¥ **Ion temperature of 800 eV from neutron energy width**
- ¥ **heating as a function of stagnation timing**

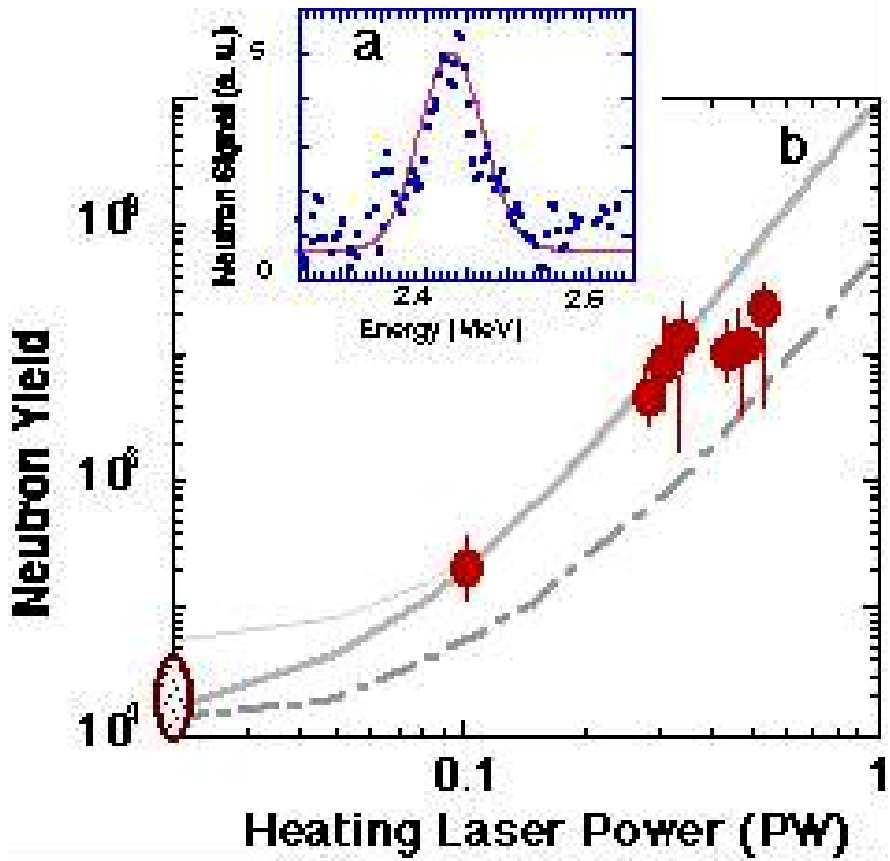

R.Kodama *et al.* Nature **418**, 933 (2002)

Design philosophy behind the Vulcan campaign

The option of using lower intensity may also re-open the possibility of using longer wavelength light (1/2 and 1 micron instead of 1/3 and 1/4). This could reduce the requirement for frequency conversion of Nd glass or more complex solid state lasers with the attendent cost, complexity and inefficiency

Max Tabak, James Hammer, Michael Glinsky, William Kruer, Scott Wilks, John Woodworth, Michael Campbell, Michael Perry and Rodney Mason
Physics of Plasmas **1**(5), 1626 (1994).

¥ The GEKKO XII laser delivered 1.2kJ, 2ω, 1 nsec to target

¥ The Vulcan VI beamlaser can deliver 1.0kJ, ω, 1 nsec to target

Chamber Layout - Sept / Oct 2002
LLNL/RAL/ILE Collaboration

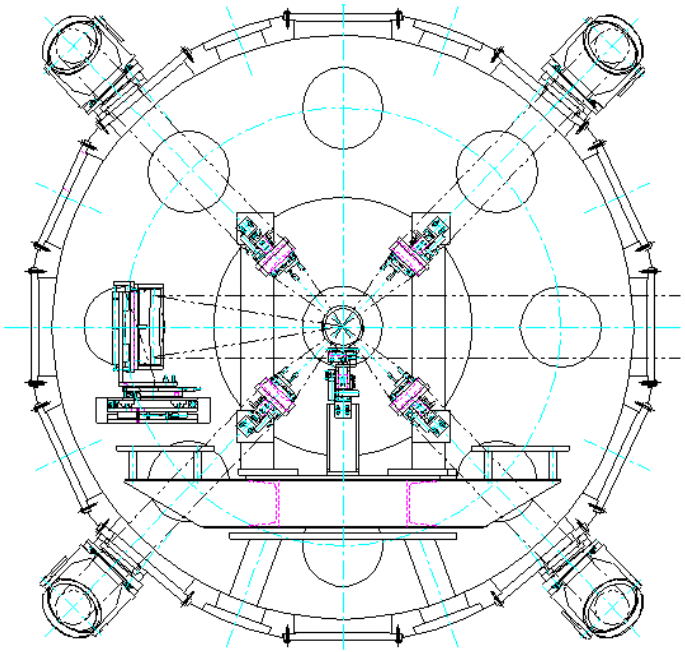

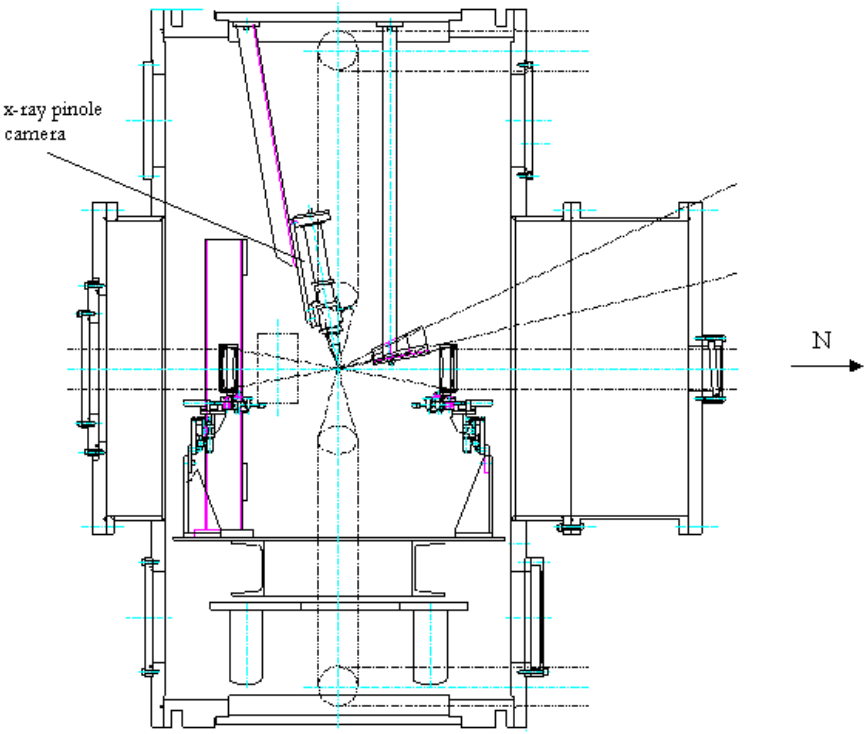

Neutron detector configuration - Sept / Oct 2002 LLNL/RAL/ILE Collaboration

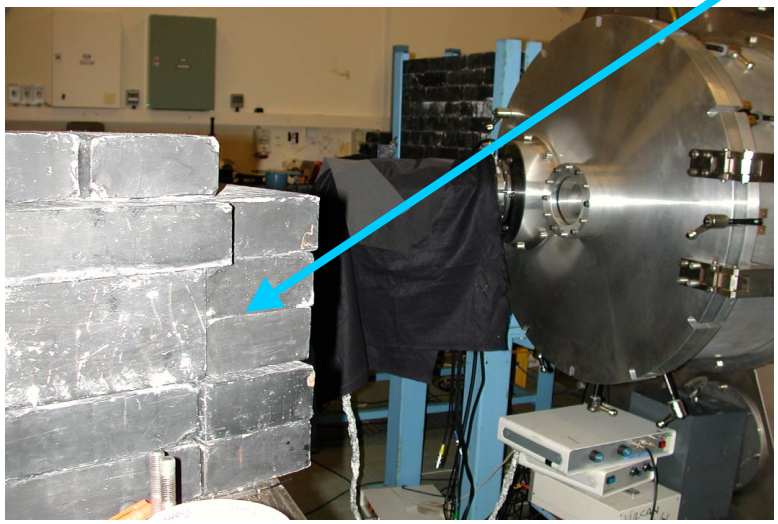

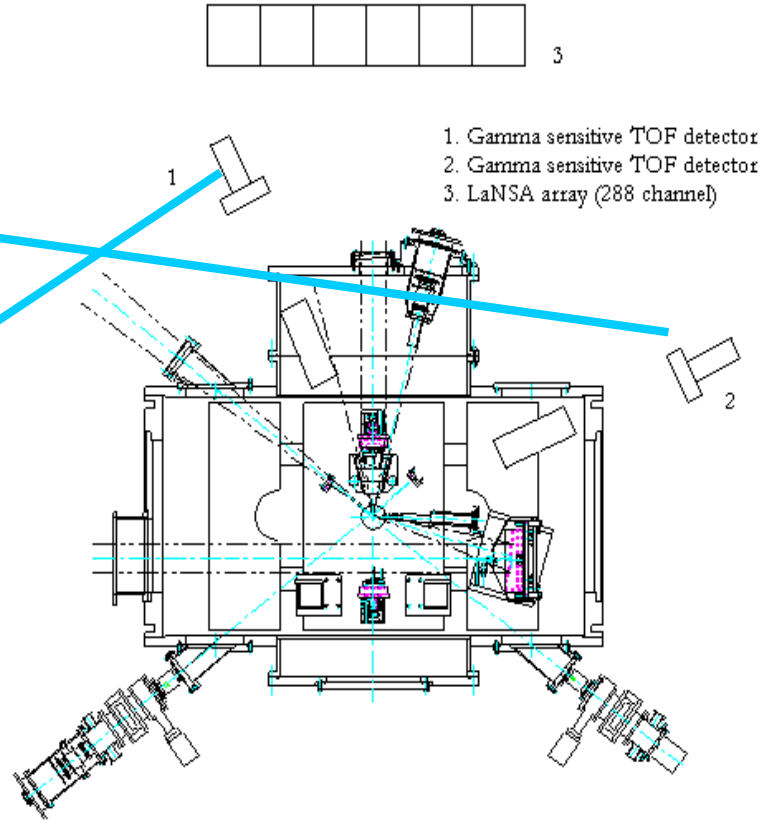

Calculated performance before the Sept/Oct 2002 experiment

¥Medusa simulations with intensity on target of 10^{14}Wcm^{-2} and 500 micron diameter (blue) and 350 micron diameter CH shells (green).

¥Indicate thatthe implosion time of a 7 micron diameter shell should be 1.4 nsec after peak of drive pulse for 60% absorption of ω_0 light.

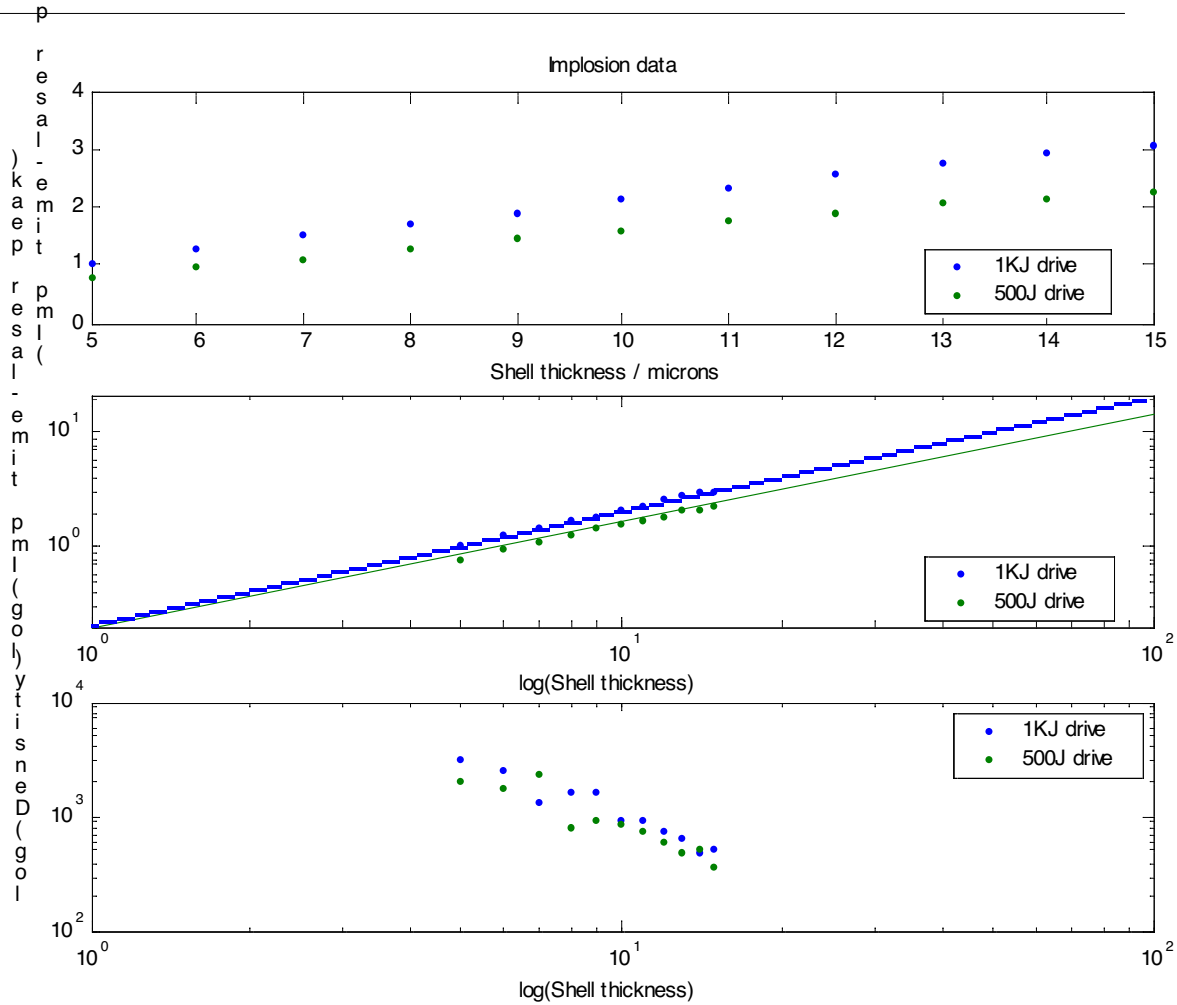

Medusa simulation data - time resolved density plots

¥Proton imagingdata indicates a stagnation time 3 nsec after the peak of the pulse for 3-micron diameter shells - longer than expecte

¥Need to reduceabsorption fraction to 30% to match implosion time with Medusa

¥Similar stagnation times anticipated when the laser drive energy from 300J to 900J and thicker targets are used

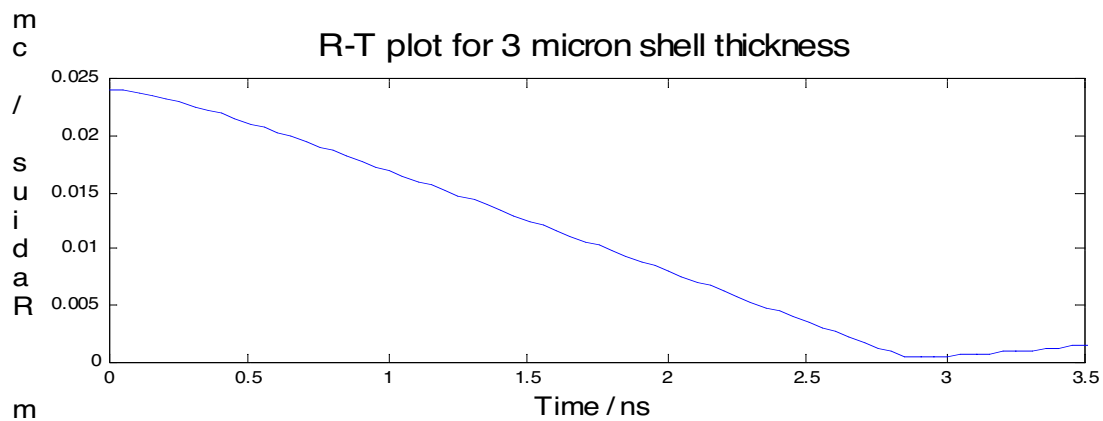

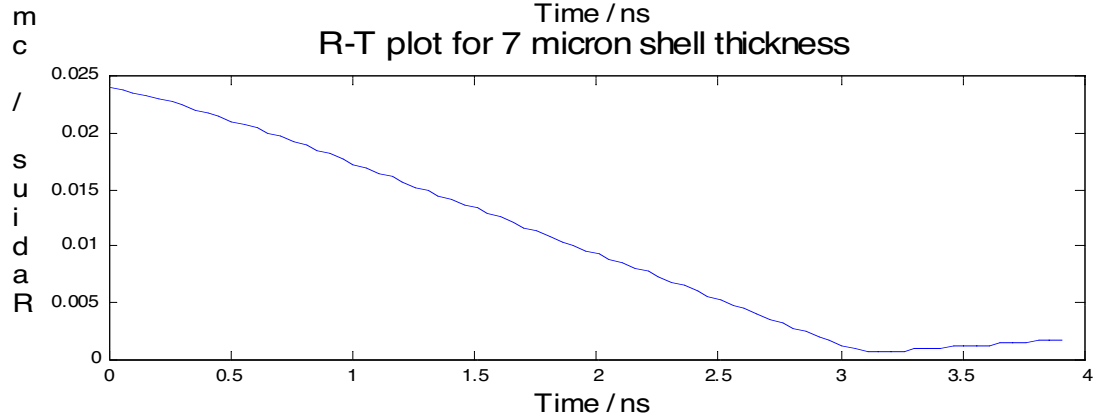

Medusa simulation data - Time resolved capsule radius plots

¥ Medusa simulations overestimate compressed density - but indicate a relatively long stagnation time with 7-micron diameter shells

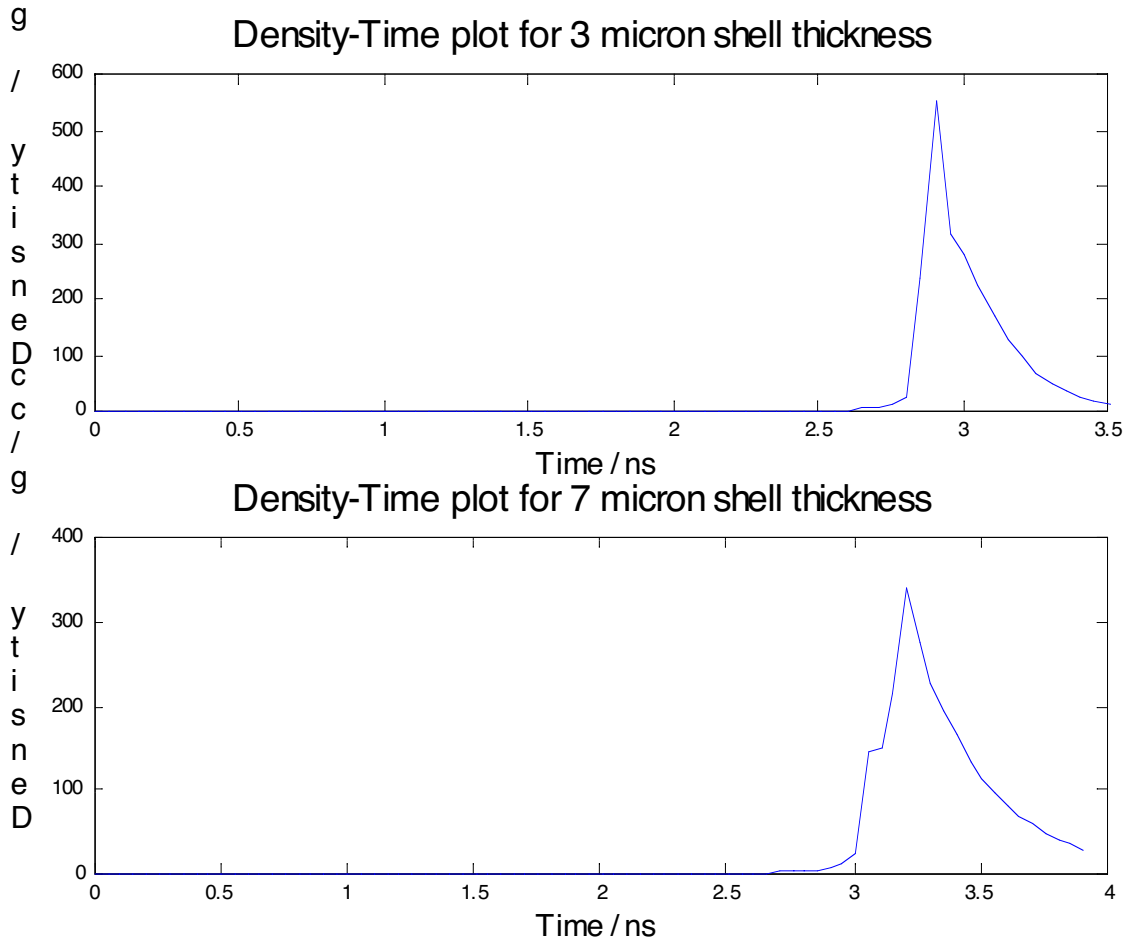

Results - Sept / Oct 2002 LLNL / RAL / ILE Collaboration

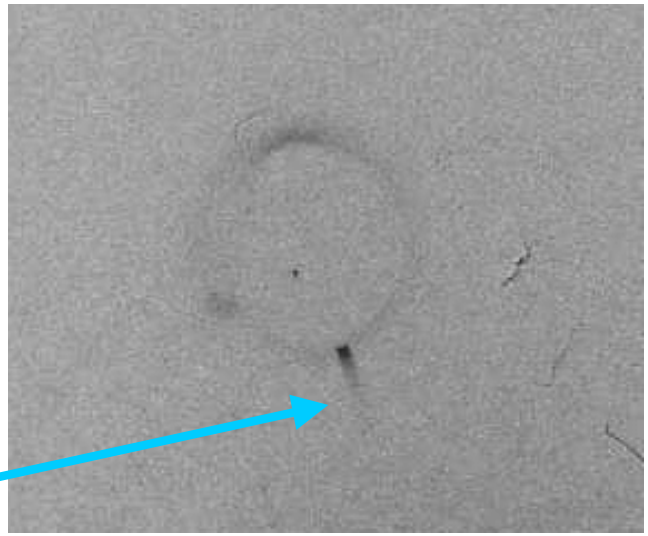

X-ray pinhole image

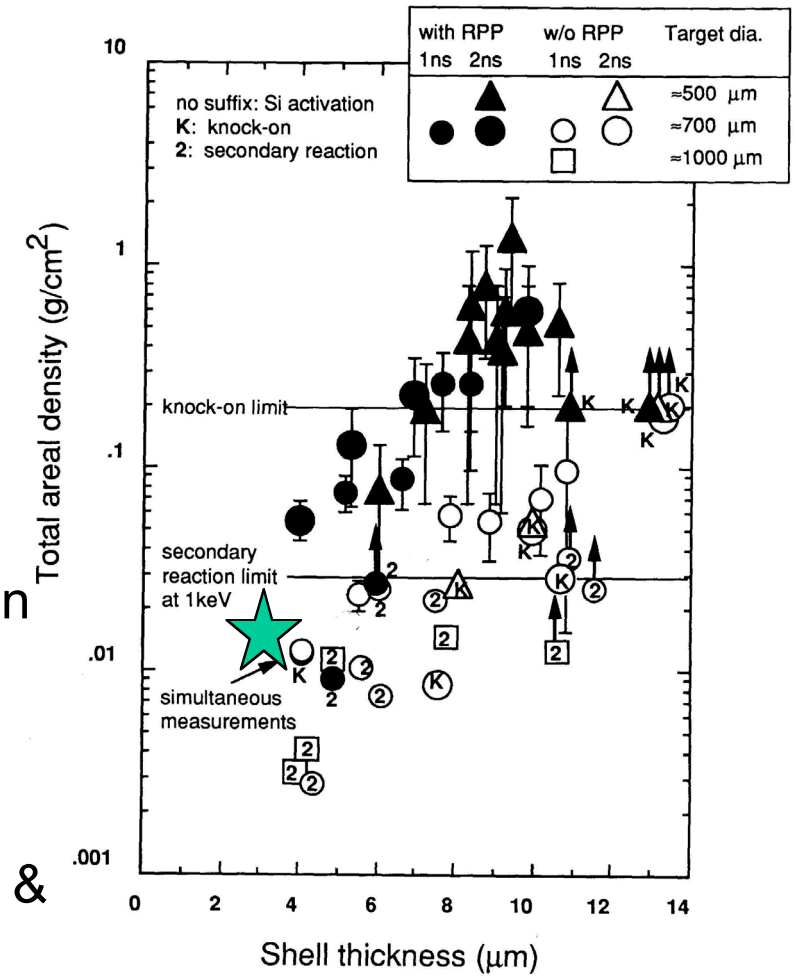

From proton data and Medusa simulation ($\Delta m/m$= 0.6, Δm= 1.6μg) Inferred ρR ~ 0.015 g/cm^2

Larger ρR (upto 0.2g/cm^2) may be achieved with 7μm wall thickness shells & phase plates - needs experimental test

H.Azechi et al. Laser & Particle Beams **9,** 2 (1991)

Large area Neutron Spectrometer Array (LaNSA)

Å LaNSA is a multi-channel neutron detector based on the Time-of-Flight technique.

Å LaNSA is a counting type array detector where the neutron yield is obtained by number of neutron hits recorded in the detector, rather than by the output current from the detector.

Å Each element in the array consist of a liquid scintillator which detect a neutron by knock-on proton scintillation combined with light amplification photo-multiplier tube.

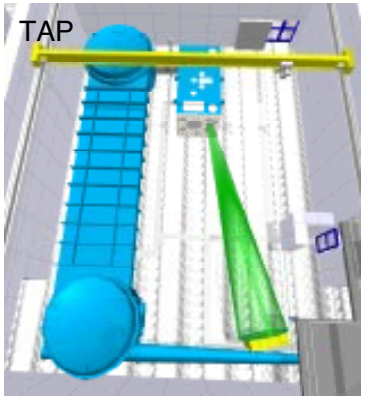

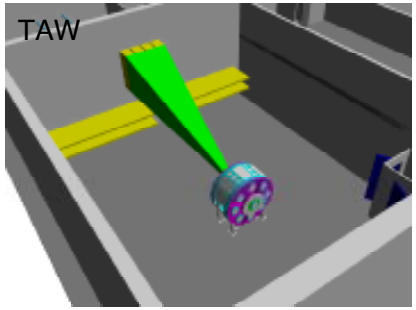

LaNSA Array

Å LaNSA consists 3 arrays, one has 288 channels in TAW - the VULCAN 100TW laser target area and others are 256 channels in the PetaWatt target area

Å LaNSA control system consists CAMAC and Fastbus modules and it is operated by PC via TCP/IP protcol.

LaNSA system diagram

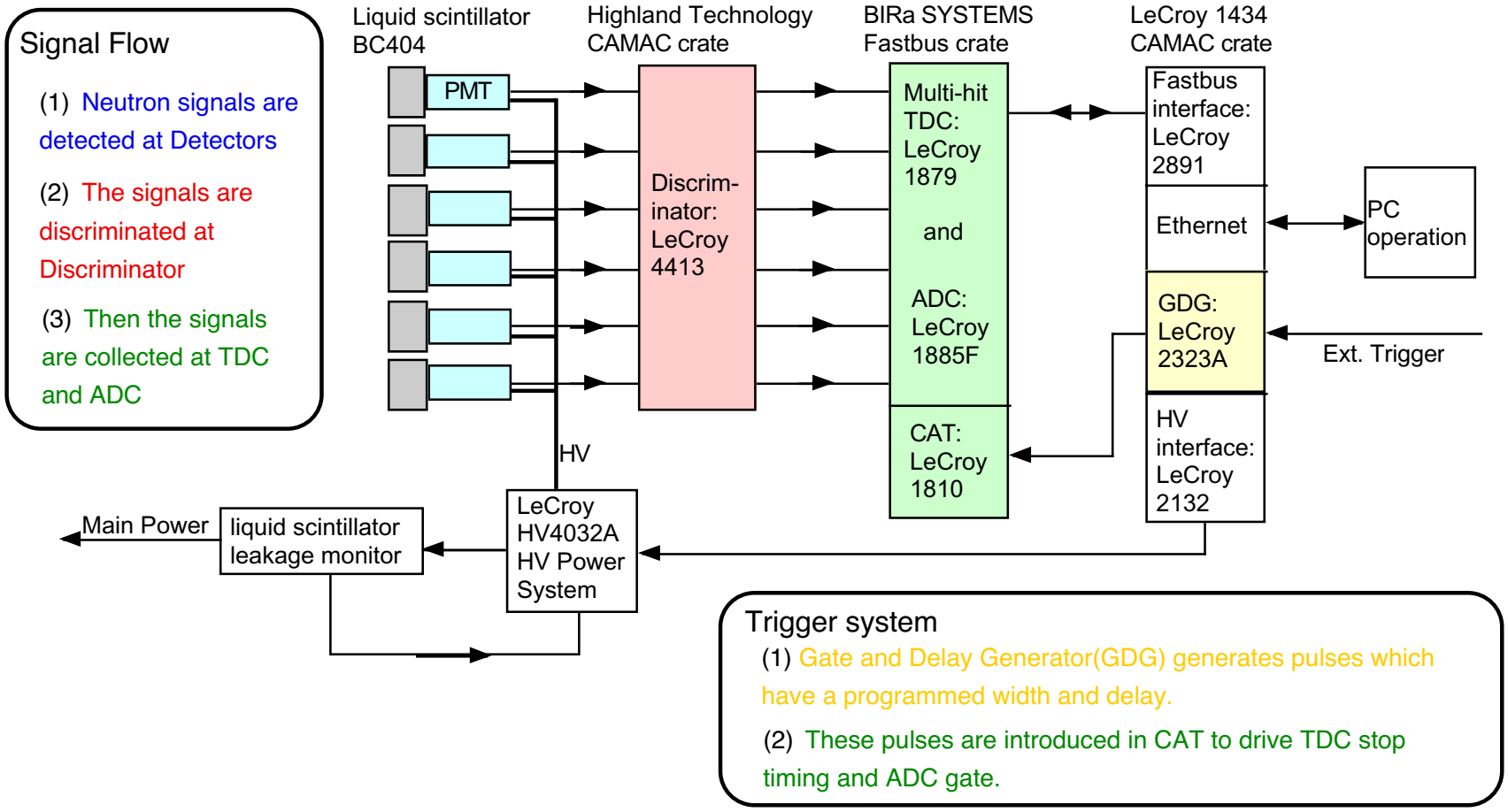

LaNSA Performance

Energy Resolutions

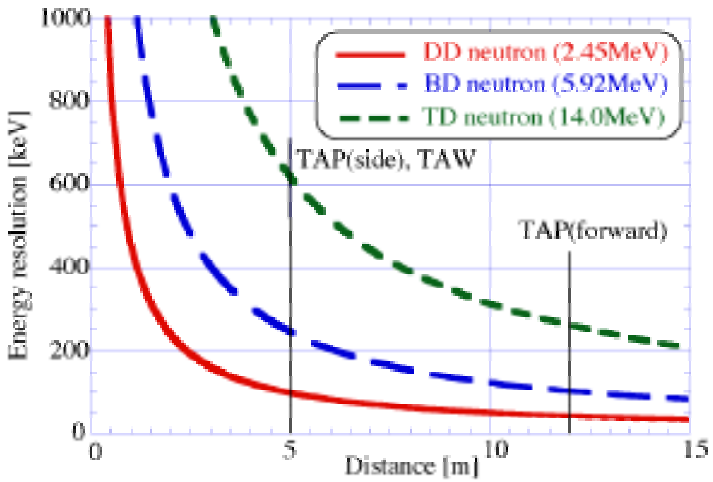

Energy resolution including the temporal resolution of electronics
DD: 50keV - TAP (North)
100keV - TAW and TAP (West)
TD: 250keV - TAP (North)
600keV - TAW and TAP(West)

Dynamic range

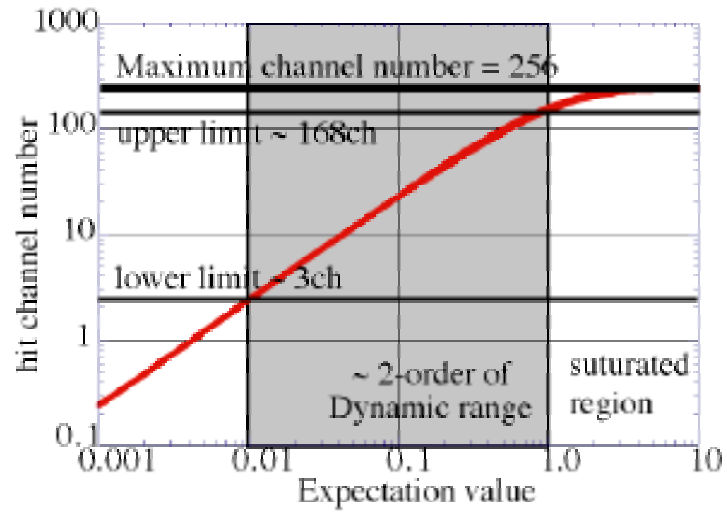

Dynamic range for TAW and TAP (West) Array ~ 2 order of magnitude

* Expectation value : Expectation number of neutron detectable at single detector

Expectation value $\alpha = \eta_{sgl} Y_n$

Neutron hit number $\frac{N_{hit}}{N_{total}} \approx 1 - \exp(-\alpha)$

Newly established Operational Software

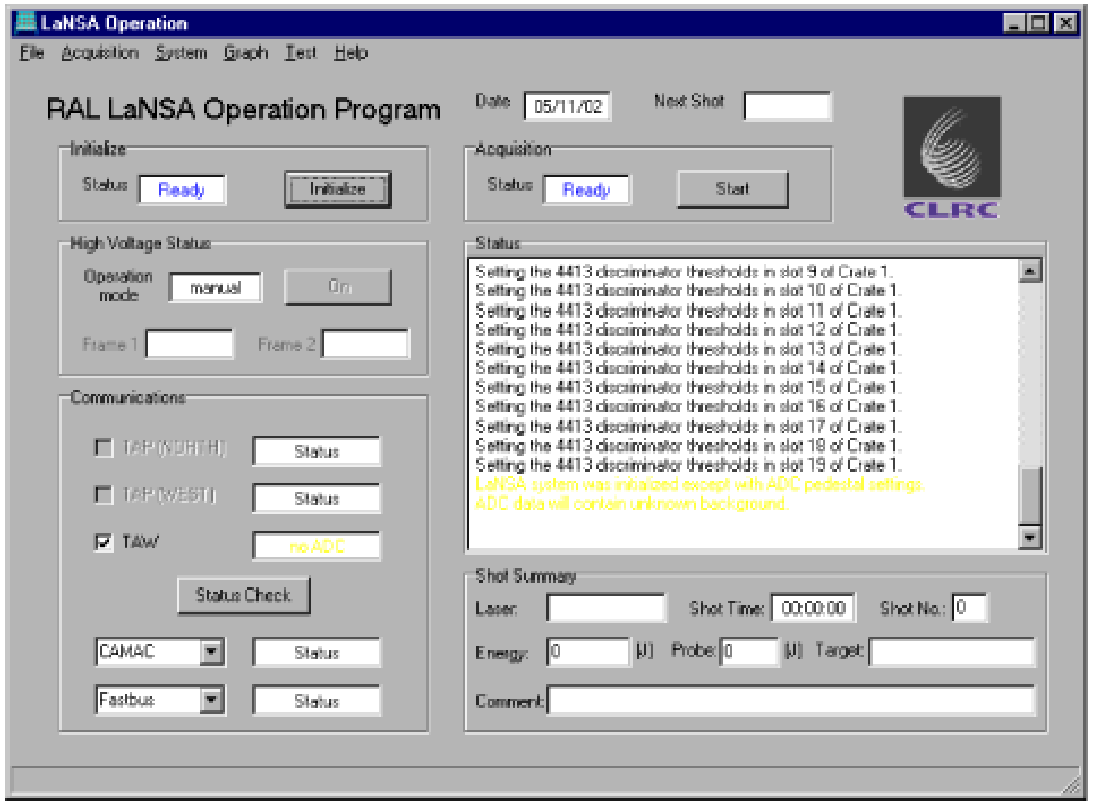

@ LaNSA Operation Programme

Written in Objective Pascal(Delphi) and Microcode for Fastbus operation

Fully 32bit Windows application
Main Feature
- Objective Oriented Programming
- Multi-Thread correspondance
- Working on Windows NT4 or later

@ Easy to re-initialize of system and change CAMAC and Fastbus module parameters

@ Provide wide-range test mode to check the status of modules.

@ Check the HV status regularly on background

@ Report detailed status such as Initializing, Acquisition, Error and so on

Calibration - voltage adjustment

normalise output level of every channels using gamma source

Setup

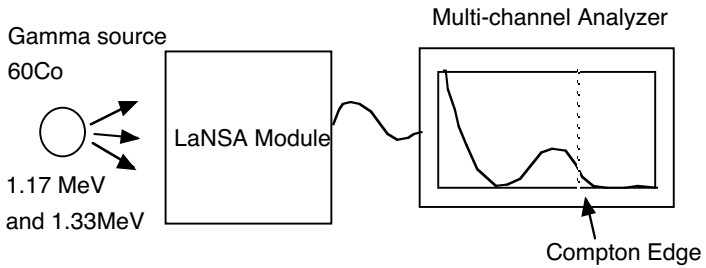

Check output of each channel of each module become same level of Compton edge of gamma source.

typical output before the adjustment

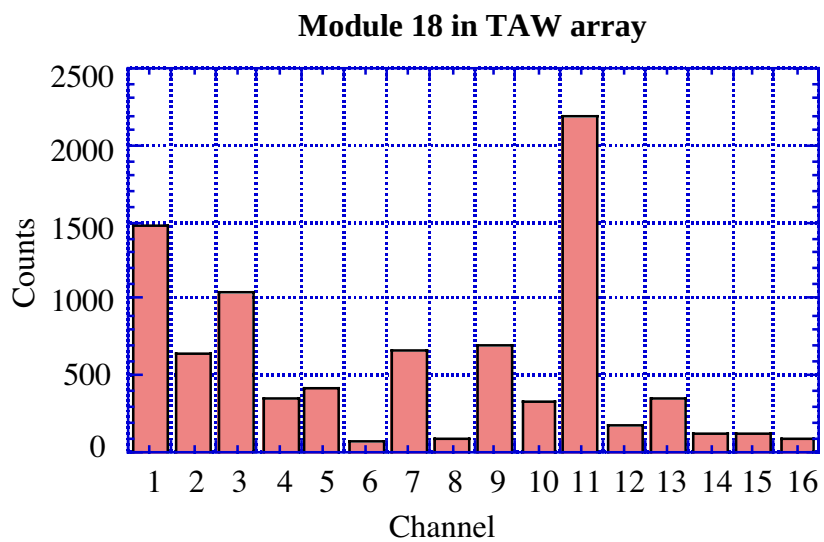

Result Every modules are set the same output level.
The work takes about 2 weeks.

Future outlook

Possible developments in the UK in near/medium term:

¥ Routing additional beams in the Vulcan PW

¥10-20 psec operation: are there any MHD instabilities preventing energy transport?
¥Heating of compressed matter with ion beams?
¥Performance of new target designs more relevant to IFE

¥ Multiple PW beam interactions on the Helen Upgrade laser

Summary

¥ The absorption of laser energy is somewhat lower than anticipated - longer implosion times

¥ Compressed densities of 3gcm^{-3} and core diameter of 100μm indicates ρR of 15 mg cm^{-2} - in line with expectations from 12 beam implosions with GEKKO XII of hollow shell targets of 500 μm diameter and 3μm wall thickness

¥ The laser energy will beincreased to 900J on target and CD shell diameters of 500 μm with 7μm wall thickness will be used. ρR of 200mgcm^{-2} may be expected with random phase plates

¥ High sensitivity neutron detectors have been re-commissioned for the experiment - and will be calibrated by exploding pushers.

¥ Everything is set for interesting physics in Feb/March 2003.

MEASUREMENT OF ULTRA-HIGH MAGNETIC FIELDS IN PETAWATT LASER EXPERIMENTS

A.A. Offenberger[1], N.J. Peacock[2], A.J. Mackinnon[3],
M. Tsukamoto[4], M.H. Key[3]

[1]University of Alberta, [2]UKAEA Culham Laboratory,
[3]Lawrence Livermore National Laboratory, [4]Osaka University

Fast Ignitor Workshop – St. Petersburg (2002)

OUTLINE OF TALK

- Motivation – to use non-thermal cyclotron emission to measure magnetic fields generated in targets irradiated at relativistic laser intensities

- Present harmonic emission measurements (concentrating on 2ω)
- (have also measured 3ω, 4ω, $3\omega/2$ for 100TW and $3\omega/2$ for PW)

- - experiments with 100TW: $I \cong 5\times10^{19}$ W/cm^2
- - weakly modulated sub-structure in 2ω harmonics

- - experiments with PW: $I \cong 4\times10^{20}$ W/cm^2
- - strongly modulated sub-structure in 2ω harmonics
-
- Discuss model for interpreting spectra that yields

- - ponderomotively enhanced intensity
- - relativistic parameter γ
- - B-field in over-dense region

MOTIVATION – MEASUREMENT OF LARGE MAGNETIC FIELDS

- Vacuum B-fields of 2,900 MGauss accompany focused laser intensities of 10^{21} W/cm^2; in turn, azimuthal magnetic fields of several hundred MGauss are predicted when electron jets are generated and transported into the target

- Such high fields are interesting in their own right and are particularly important in the "fast ignitor" concept for ICF, since they may dominate laser energy deposition by influencing electron transport

- Direct measurement of B-fields are intrinsically difficult since they are generated in over-dense plasma ($n_e > n_c$), not normally visible to optical probing (note that cyclotron emission has a wavelength > 10μm for parameters of these experiments)

- With a large relativistic parameter $\gamma = (1 + I\lambda^2/2.74\text{x}10^{18})^{0.5}$, however, harmonic emission from higher densities may be generated and detected

- By this means, the observation of sub-harmonic structure superimposed on $2\omega_o$ generated in PW laser irradiated targets has been interpreted to provide the first evidence for large B-fields in over-dense plasma at relativistic laser intensities (Proc. Of 2nd Symposium on Advanced Photon Research, Nara 2000)

PARAMETERS OF THE EXPERIMENT

- 100 TW laser parameters
- - energy $\leq$ 40 J
- - pulse width $\approx$ 400 fs
- - focal spot d =15μm
- - intensity $I_L \cong 5x10^{19}$ W/cm^2 ; $\gamma = [1+1/2(eE_o/m\omega_o c)^2]^{1/2} \cong 4.4$

- PW laser parameters
- - energy $\leq$ 500 J
- - pulse width $\approx$ 500 fs
- - focal spot d =18μm
- - intensity $I_L \cong 4x10^{20}$ W/cm^2 ; $\gamma = [1+1/2(eE_o/m\omega_o c)^2]^{1/2} \cong 12.1$

- Targets
- - CH for 100 TW
- - Au for PW

- Diagnostics
- - monochromator/16 bit CCD camera for harmonic light spectroscopy

HARMONIC MEASUREMENTS – 100 TW

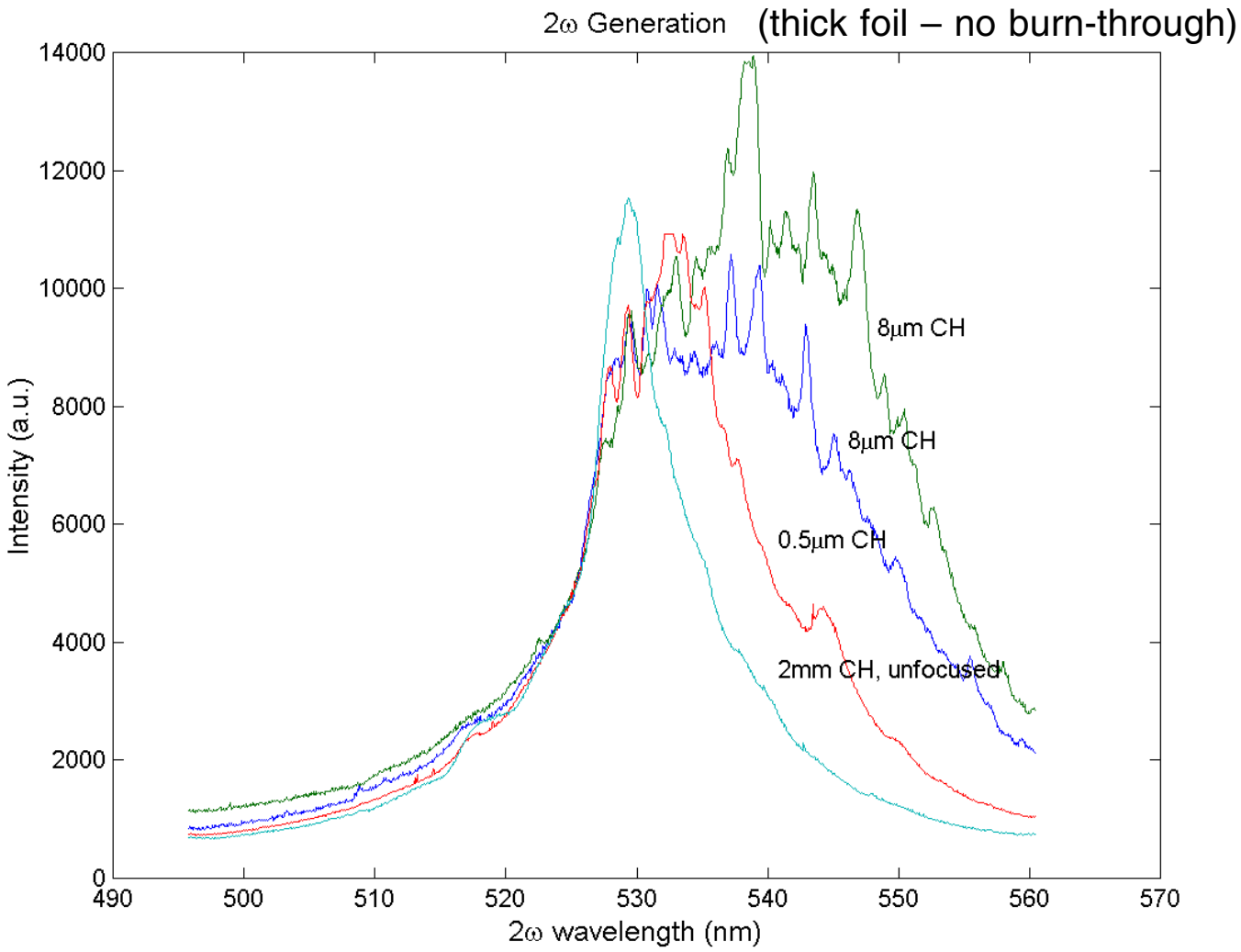

ANALYSIS OF HARMONIC MEASUREMENTS – 100 TW

- Recession velocity from Doppler shift (CH target)
- - determined from relative shift of $2\omega_o$ radiation
- - measured red-shift (of 8 μm foil) is $\Delta\lambda \cong 19$ nm

- Then for $\Delta\omega/2\omega_o = \Delta\lambda/\lambda$ and $\omega_{refl} = 2\omega_o\,(1-u/c)/(1+u/c)$
- experiment gives $u/c \cong _\ \Delta\lambda/\lambda \cong 0.018$

- From simple momentum balance $\rho u^2 = I_{abs}/c$; $u/c = [(n_c\, m_e/\rho)\,(I\lambda^2/2.7\text{x}10^{18}\,]^{1/2}$
- For $I\lambda^2 = 5\text{x}10^{19}$ W/cm^2 μm^2, $\rho = 1$ gm/cm^3; predict $u/c = 0.0041 << (u/c)_{expt}$
- (requires $I=19.3 \times I_{vac}$; implies $\gamma = 18.8$)

- Alternatively, if ω_o radiation penetrates to $\gamma\, n_c$ (where momentum is deposited)
- with $\gamma = [1+ I\lambda^2/2.7\text{x}10^{18}\,]^{1/2} > 1$, a self-consistent solution of
- $u/c = [(\gamma\, n_c\, m_e/\rho)\,(I\lambda^2/2.7\text{x}10^{18})]^{1/2}$ (a cubic equation), yields
- - $I_{abs}\lambda^2 = 1.4\text{x}10^{20}$ W μm^2 /cm^2 ($\cong$ 2.7x the incident vacuum level) and,
- - effective $\gamma = 7.1$

- Note: the inward motion of the front during the pulse is $\Delta z = u\,\Delta t = 2.7$ μm;
- therefore emission localized (but space-time integrated)

OPTICAL SETUP FOR PETAWATT EXPERIMENT

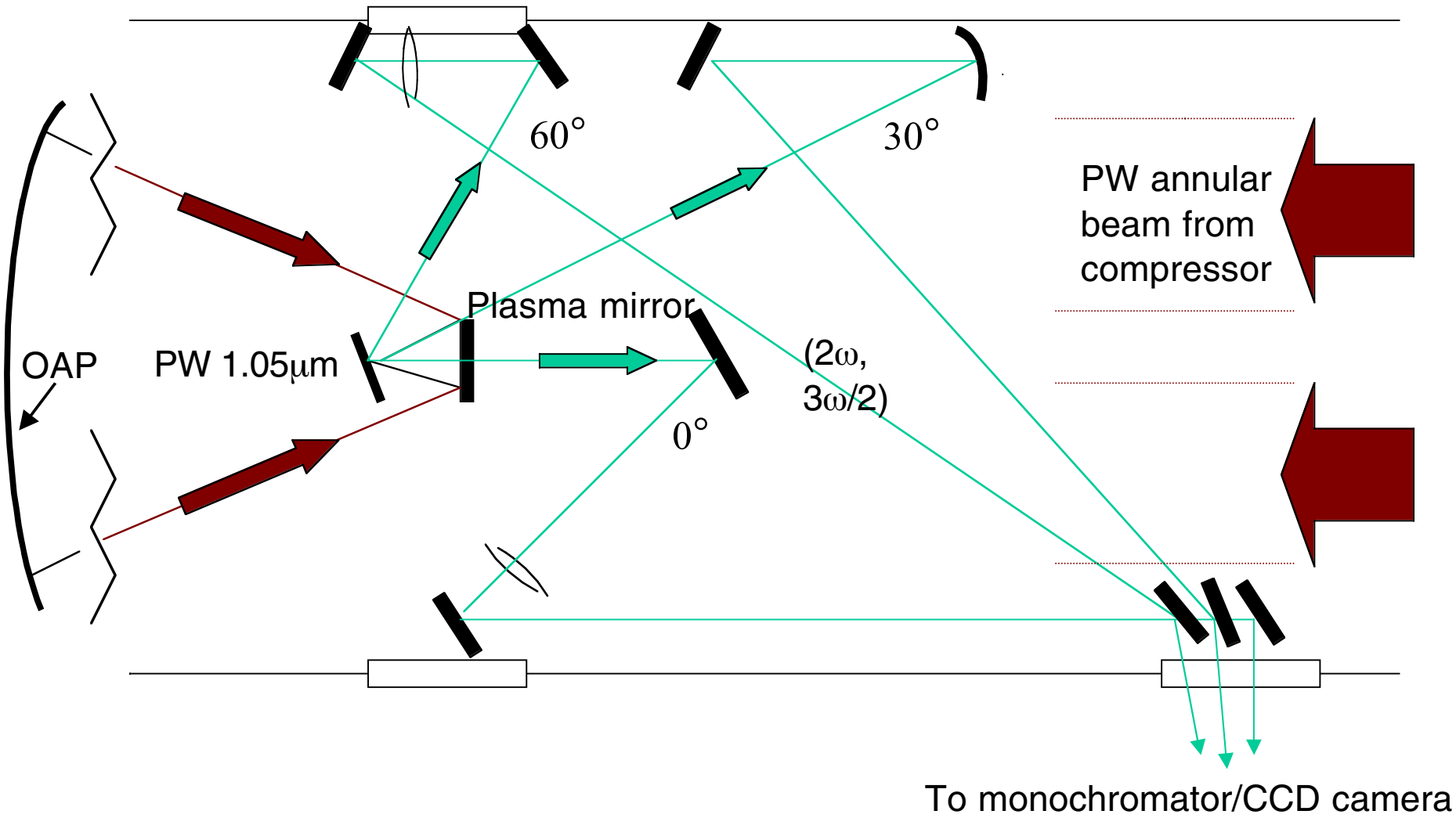

HARMONIC MEASUREMENTS – PW

¬ Low dispersion of 2ω spectrum (with large attenuation)

¬

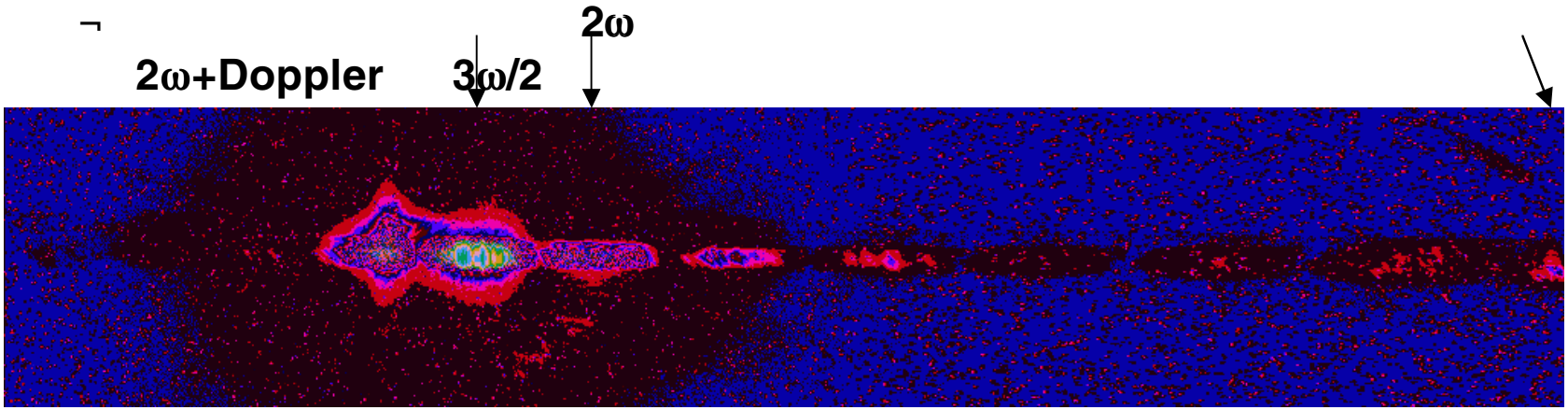

HARMONIC MEASUREMENTS – PW

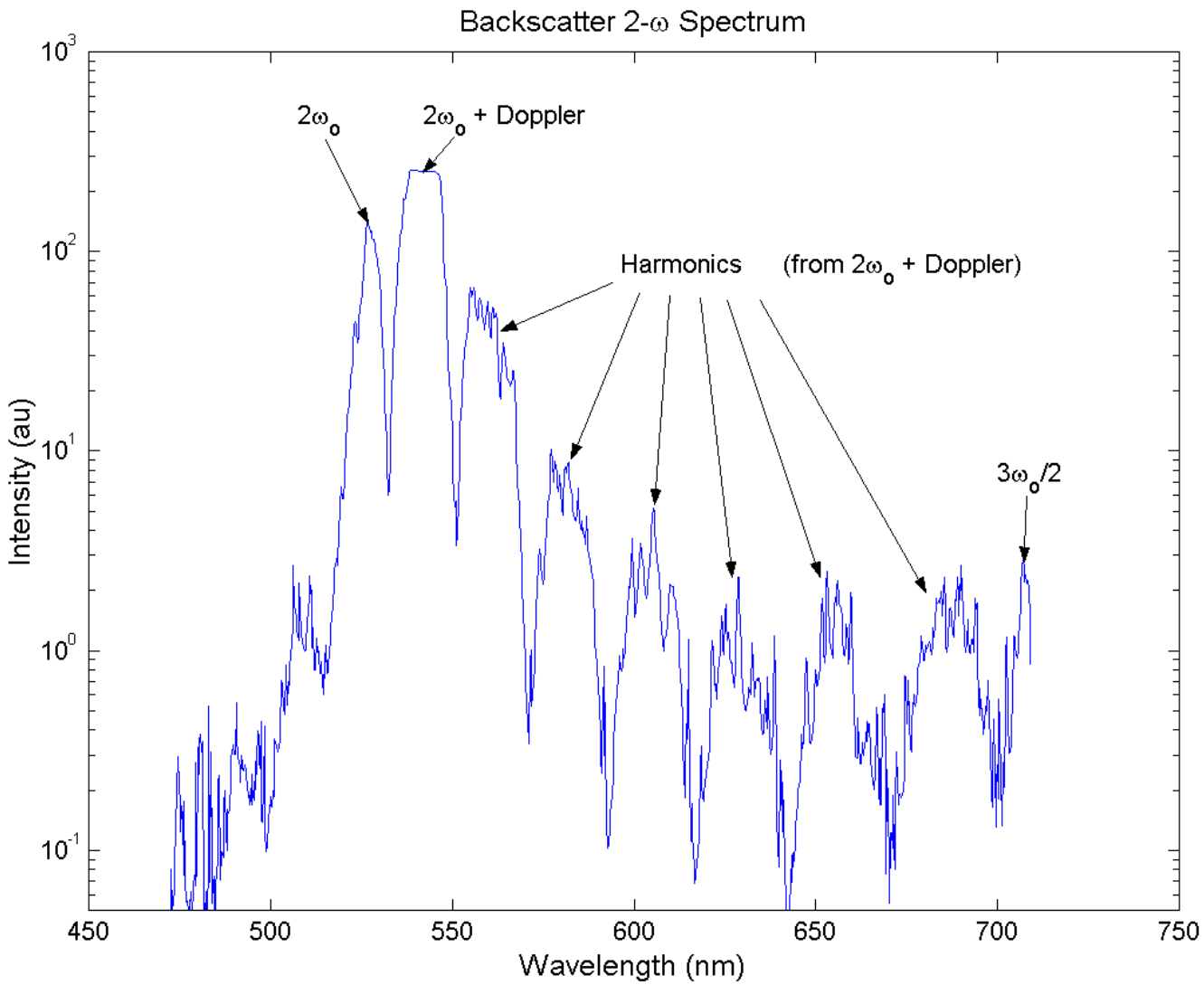

ANALYSIS OF HARMONIC MEASUREMENTS – PW

¬ Recession velocity from Doppler shift (Au target)
¬ - determined from relative shift of $2\omega_o$ radiation
¬ - measured red-shift (of massive Au target) is $\Delta\lambda \cong 15$ nm

¬ Then for $\Delta\omega/2\omega_o = \Delta\lambda/\lambda$ and $\omega_{refl} = 2\omega_o\ (1-u/c)/(1+u/c)$
¬ experiment gives $u/c \cong _\ \Delta\lambda/\lambda \cong 0.0142$

¬ From simple momentum balance $\rho u^2 = I_{abs}/c$; $u/c = [(n_c\ m_e/\rho)\ (I\lambda^2/2.7\text{x}10^{18}\ ]^{1/2}$
¬ For $I\lambda^2 = 4\text{x}10^{20}$ W/cm^2 μm^2, $\rho = 18.8$ gm/cm^3; predict $u/c = 0.0027 << (u/c)_{expt}$
¬ (requires $I=22.4 \text{ x } I_{vac}$; implies $\gamma = 57.2$)

¬ Alternatively, if ω_o radiation penetrates to $\gamma\ n_c$ (where momentum is deposited)
¬ with $\gamma = [1+ I\lambda^2/2.7\text{x}10^{18}\ ]^{1/2} >> 1$, a self-consistent solution of
¬ $u/c = [(\gamma\ n_c\ m_e/\rho)\ (I\lambda^2/2.7\text{x}10^{18}\ ]^{1/2}$ (a cubic equation), yields
¬ - $I_{abs}\lambda^2 = 7.1\text{x}10^{20}$ W μm^2 /cm^2 (~ 1.8x the incident vacuum level) and,
¬ - effective $\gamma = 16.1$

¬ Note: the inward motion of the front during the pulse is $\Delta z = u\ \Delta t = 2.1\ \mu$m;
¬ therefore emission localized (but space-time integrated)

ANALYSIS OF HARMONIC MEASUREMENTS – PW

- Consider the sub-harmonic spectrum (under relativistic conditions)
- - with $I = W/cm^2$, the incident vacuum wave fields are given by
- $E_o = 27.5\ I^{1/2}$ V/cm and $B_o = 0.0915\ I^{1/2}$ Gauss
- - for $I = 4\times10^{20}$ W/cm^2, $E_o \cong 5.5\times10^{11}$ V/cm and $B_o \cong 1800$ MGauss

- Electron & ion plasma frequencies cannot account for observed modulation
- $\Delta\omega/2\omega_o = \omega_{pe}/2\omega_o = \Delta\lambda/\lambda$ requires $n_e \cong 6\times10^{18}$ cm^{-3} (too low)
- $\Delta\omega/2\omega_o = \omega_{pi}/2\omega_o = \Delta\lambda/\lambda$ requires $Z/A \cong 12$ (too high)

- Note that for $\gamma > 1$ and harmonic number >1, the incident wave can penetrate the over-dense plasma from which the harmonic emission can readily emerge

HARMONIC GENERATION & EMISSION IN STATIC B-FIELD

For current $I = (e\, n_c\, c)\, \pi\, r^2$; sheath edge $B = _\, \mu_o\, e\, n_c\, c\, r \cong 600$ MGauss ($r=2\ \mu m$)

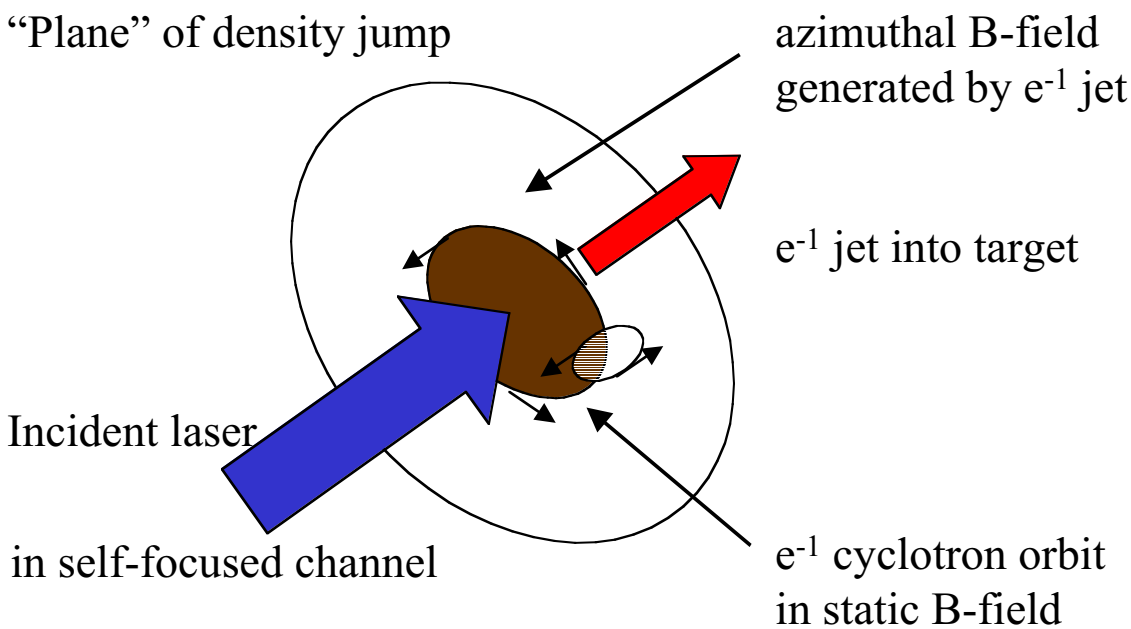

Model

– in the presence of large static azimuthal B-field (generated by the axial electron jet), electron motion due to additional Lorentz force superimposes cyclotron sub-harmonic structure on the $2\omega_o$ spectrum

– recent calculations for intensity $I>10^{19}$ W/cm^2 confirm emission features (Phys. Plasmas **9** 3193 (2002))

CALCULATED REFLECTED SPECTRUM

- From: J. Zheng et al, Phys. Plasmas **9** 3193 (2002)

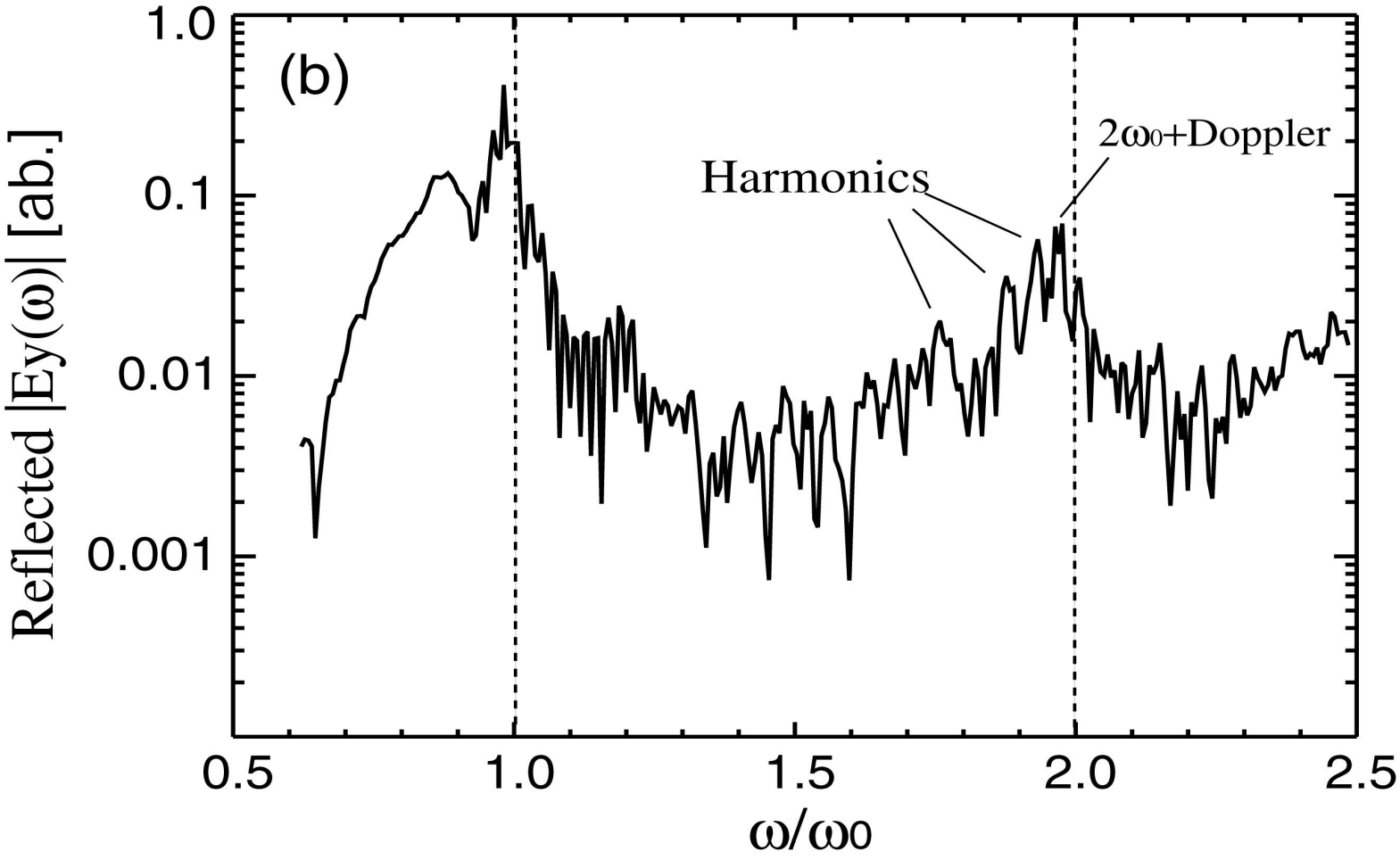

B-FIELDS DERIVED FROM HARMONIC MEASUREMENTS

- Now $\omega_{ce} = eB/\gamma mc = 1.76\text{x}10^7\ B/\gamma$ (B = Gauss) and $2\omega_o = 3.58\text{x}10^{15}\ s^{-1}$

- For PW: $\Delta\omega/2\omega_o = \omega_{ce}/2\omega_o = \Delta\lambda/\lambda \cong 21/527$; $B/\gamma = 8.1$ MGauss
- Using the self-consistent value for $\gamma \cong 16.1$, we obtain **B ≅ 130 MGauss**
- Even larger periods have been observed ($\Delta\lambda \cong 40$ nm) for which **B ≅ 260 MGauss**

- Note: the electron cyclotron orbit radius $r_{ce} = c/\omega_{ce} = 2.1\ \mu m$ for 130 MGauss; emission localized (but measured spectra are space & time integrated)

- Though less clear, if interpret modulations in 100 TW case as cyclotron harmonics
- For 100 TW: $\Delta\omega/2\omega_o = \omega_{ce}/2\omega_o = \Delta\lambda/\lambda \cong 3.1/527$; $B/\gamma = 1.2$ MGauss
- Using the self-consistent value for $\gamma \cong 7.1$, we obtain **B ≅ 8.5 MGauss**

- Note: if larger γ's are valid, B-fields of 462 and 23 MGauss would be inferred for the PW and 100 TW experiments

SUMMARY OF 100 TW & PW EXPERIMENTS – HARMONICS & B-FIELDS

- Ultra-high laser intensities ($I \cong 4x10^{20}$ W/cm^2) generate different harmonic spectra to that observed at lower intensity ($I \cong 5x10^{19}$ W/cm^2)
- - pronounced modulations and sidebands in the harmonics
- - asymmetric sub-harmonic emission – red-shift more prominent

- From spectra, obtain recession velocity & estimate of ponderomotive self-focusing:
- - for 100 TW, CH target: $I_{pond} \approx 2.7x\ I_{inc}$
- - for PW, Au target: $I_{pond} \approx 1.8x\ I_{inc}$

- From spectra, obtain lower limit on relativistic parameter:
- - for 100 TW, CH target: $\gamma = 7.1$
- - for PW, Au target: $\gamma = 16.1$

- From spectra, estimate induced B-field from sub-harmonic structure:
- - for 100 TW: $B/B_o \cong 0.013$
- - for PW: $B/B_o \cong 0.072$

- Higher harmonics ($3\omega_o$, $4\omega_o$, etc.) would allow probing of even higher densities
- ($9\ n_c$, $16\ n_c$, etc., limited by magnetic field)

Fast Electron Penetration and Return Current into Plasma Pellets with and without a Hollow Wedge

C.Ren, F.S.Tsung, and W.B.Mori

Department of Physics & Astronomy, UCLA, USA

S. Amorini, R.A.Fonseca, and L.O.Silva

GoLP/Centro de Fisica dos Plasmas, IST, Portugal

J.C.Adam

Ecole Polytechnique, France

Motivation

- Fast electron transport is critical to fast ignitor concept.
- Full size PIC simulation impossible at the moment
- Model problem simulation results depend on **plasma density, boundary conditions** and **pellet geometry** used.
  - Need to fully study these effects before extrapolating results
- Key question; will the deposited laser energy be carried **forward** by fast electrons or go **around** the target surface?

Computational Challenge

- The dense core region ($n>10^4 n_c$, r~20 μm) beyond reach of PIC
  - lack of physics knowledge
  - may need 2M node-hours
- The $n=40\ n_c$ (r~40 μm) region within reach
  - 160M particles and 3000 node-hours.
- Laser can reach this region either through hole-boring or attached cone.

Compressed Pellet

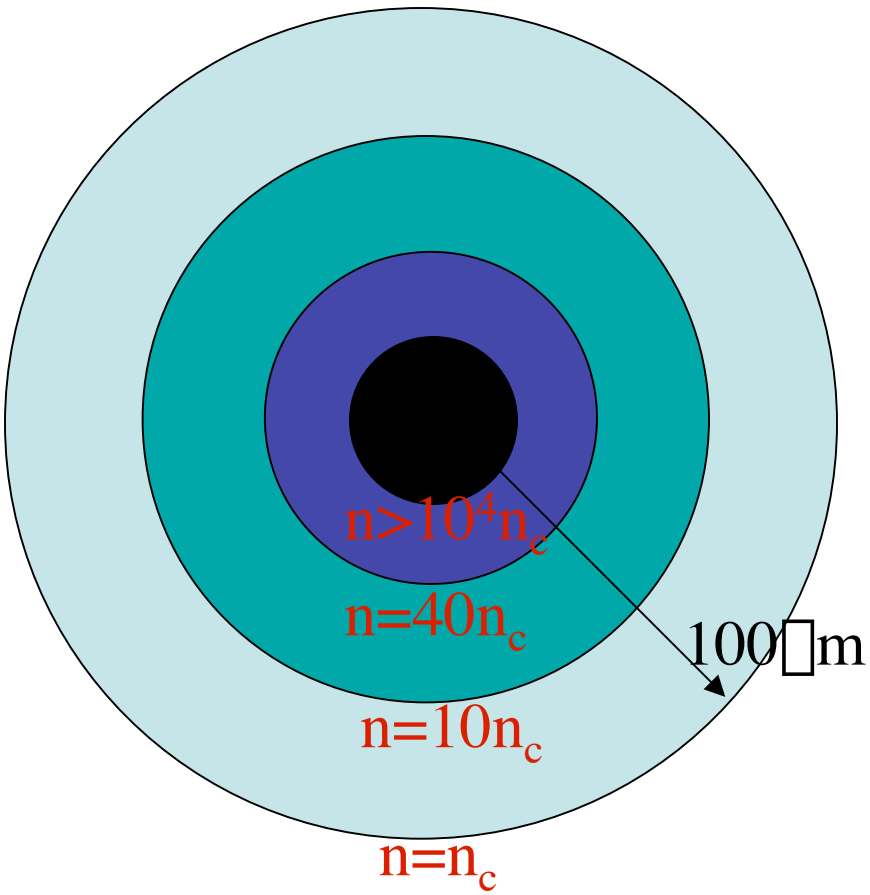

Parameters for Simulation Set I:
High Density (Low Resolution)

- Vacuum region between target and boundary to reduce boundary effects
- Round targets with and without hollow wedge
- **3600□3600** grids, **4** particle/cell
- **1□m**-laser from left wall antenna, **I=10^{20} w/cm^2**, spot size **6.4 □m, 1 ps** long, **s**-polarized.
- Initial **Te=20keV** and **Ti=40eV**
- Periodic boundary in transverse and absorbing boundary in longitudinal directions.
- Higher resolution runs for n=40n$_c$ underway

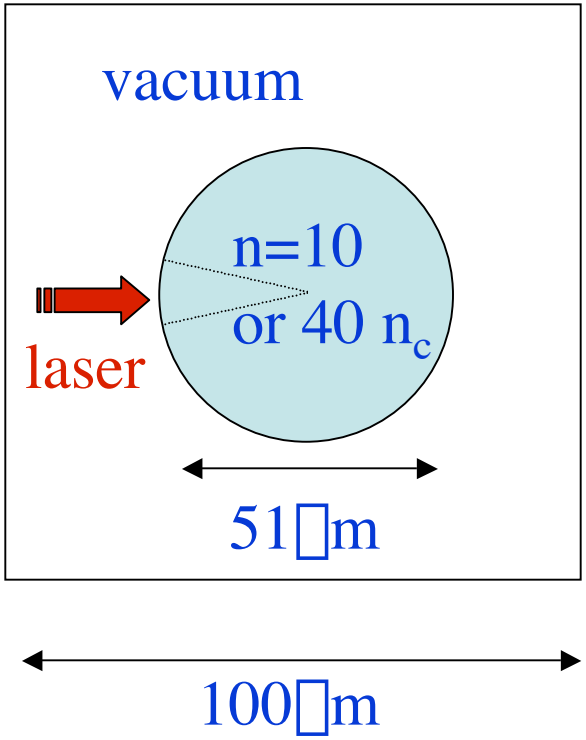

Parameters for Simulation Set II:
Low Density (High Resolution)

- Core density $n=5n_c$
- Linear density gradient to target edge ($n=1\ n_c$)
- $\Delta x=\Delta y=$**0.3 c/ω_p**, **16** particle/cell
- **1 μm**-laser from left wall antenna, **I=10^{19} w/cm^2**, spot size **7 μm, 80 fs** long, **s**-polarized.
- Cold plasma
- Periodic boundary in transverse and absorbing boundary in longitudinal directions.

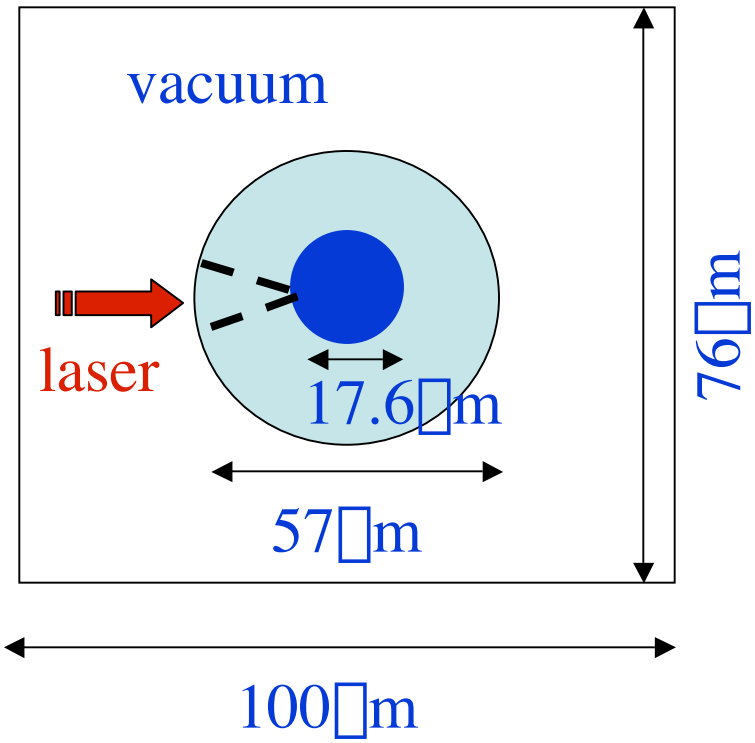

Laser Filamentation in Low Plasma Density (Set II)

no wedge

wedge

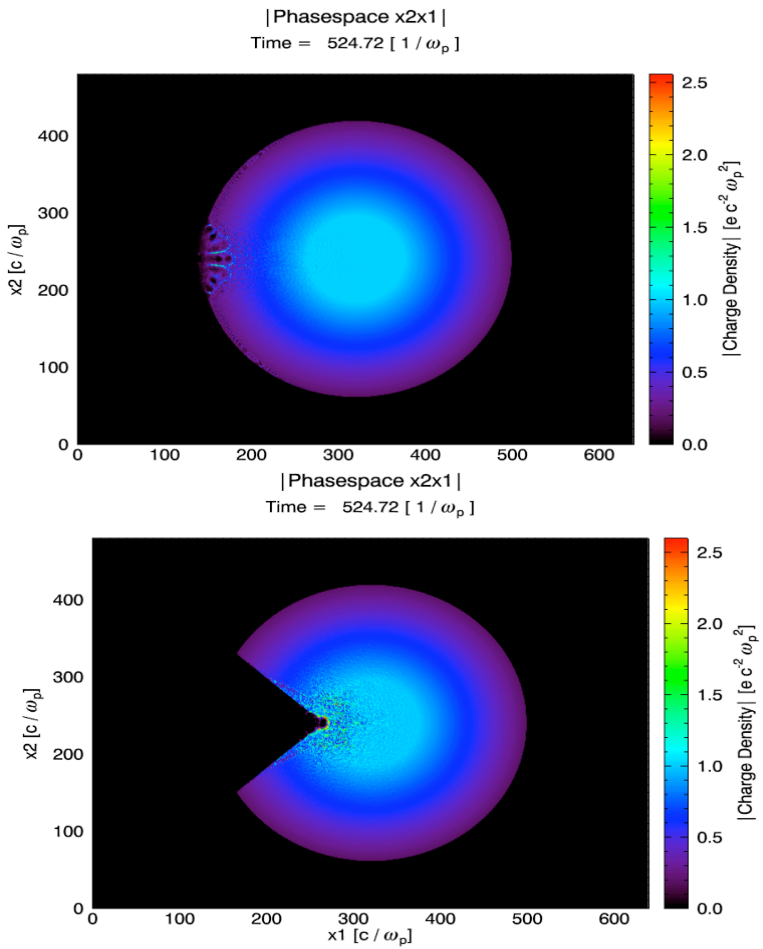

T=616 fs

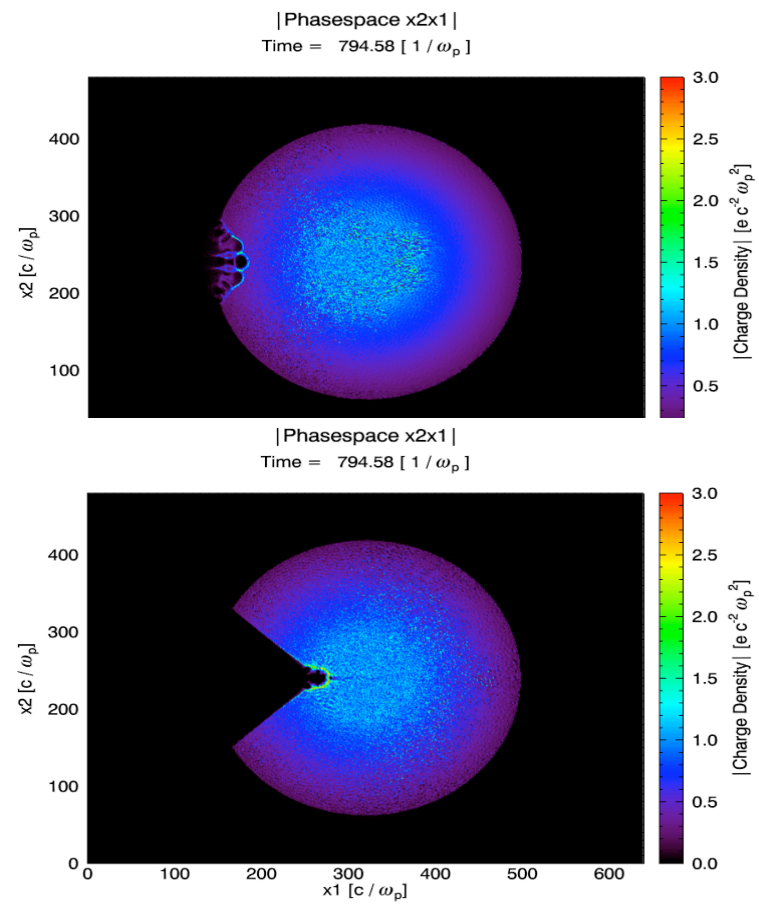

T=933 fs

Hole-boring Seen from High Intensity Laser (10^{20}W/cm^2 at n=10 n_c)for Both Geometries

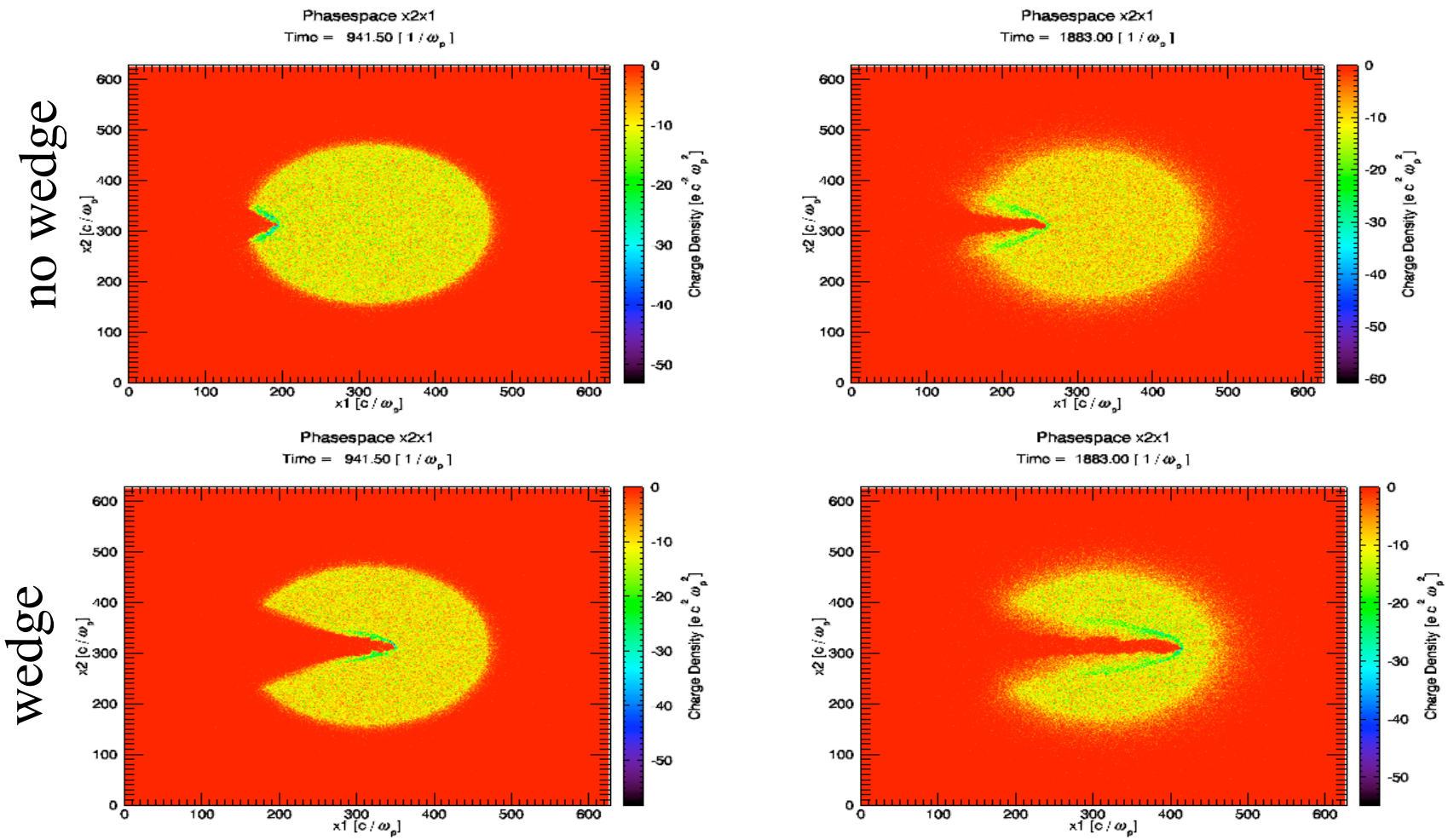

T=500 fs

Set I

T=1000 fs

Details of the Channel

no wedge

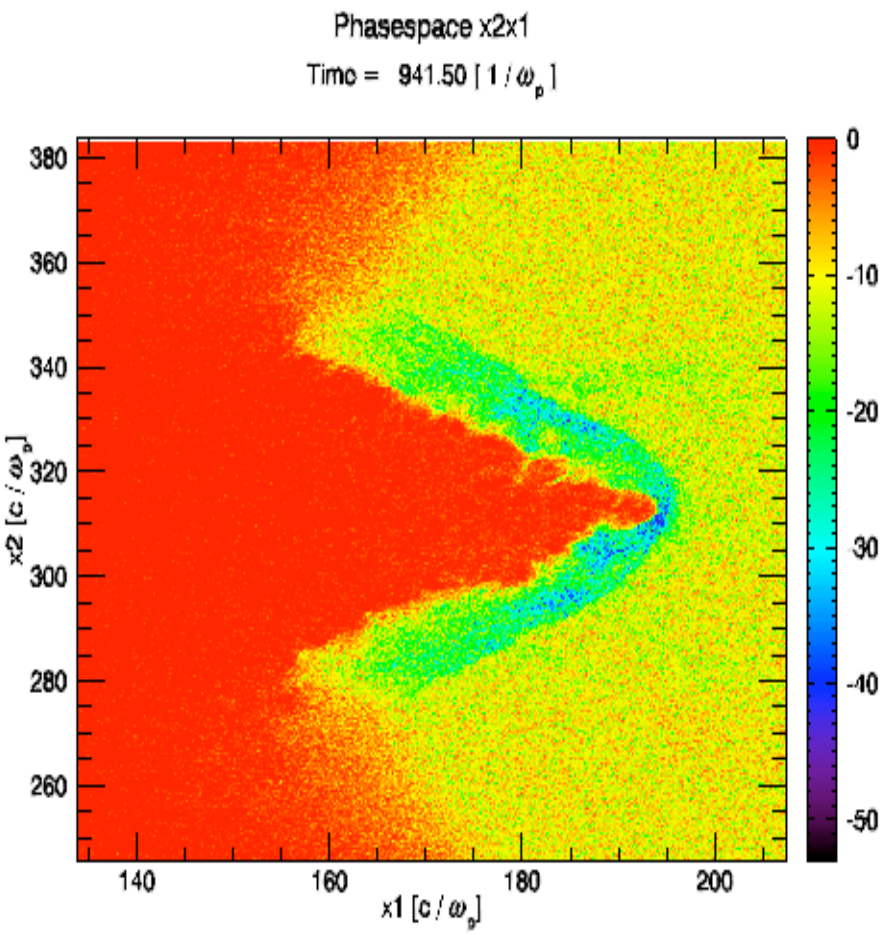

T=500 fs

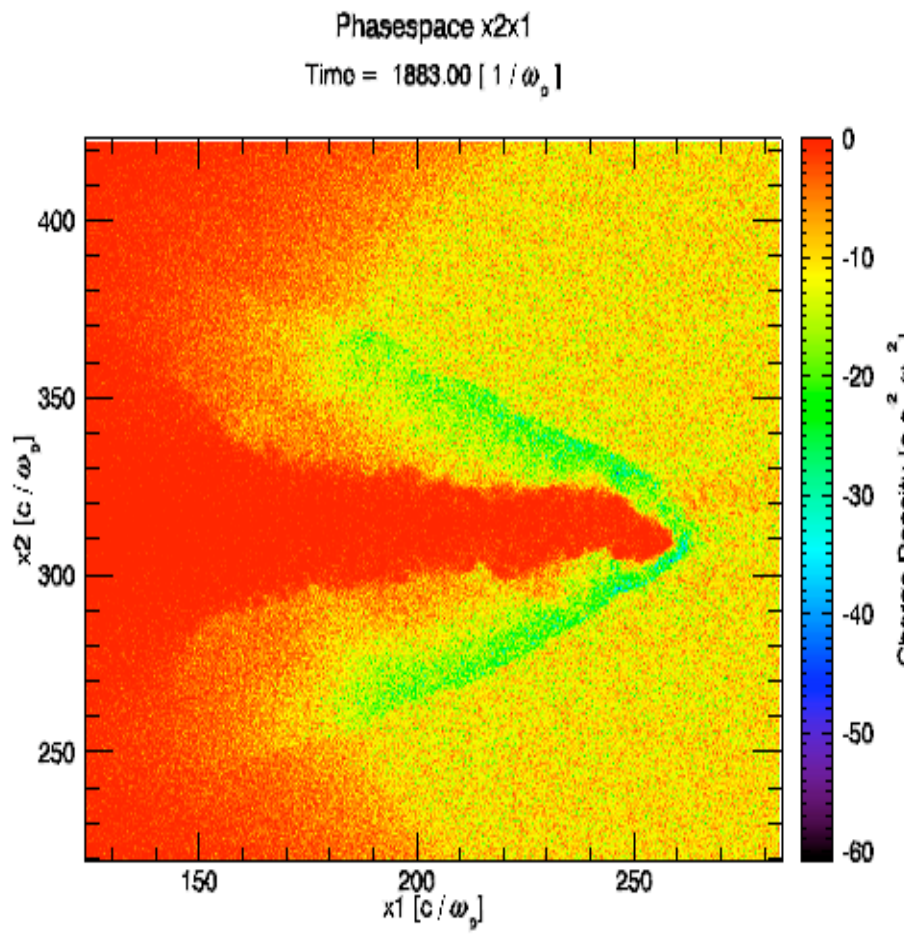

T=1000 fs

Much Less Hole-boring Seen into $n=40n_c$

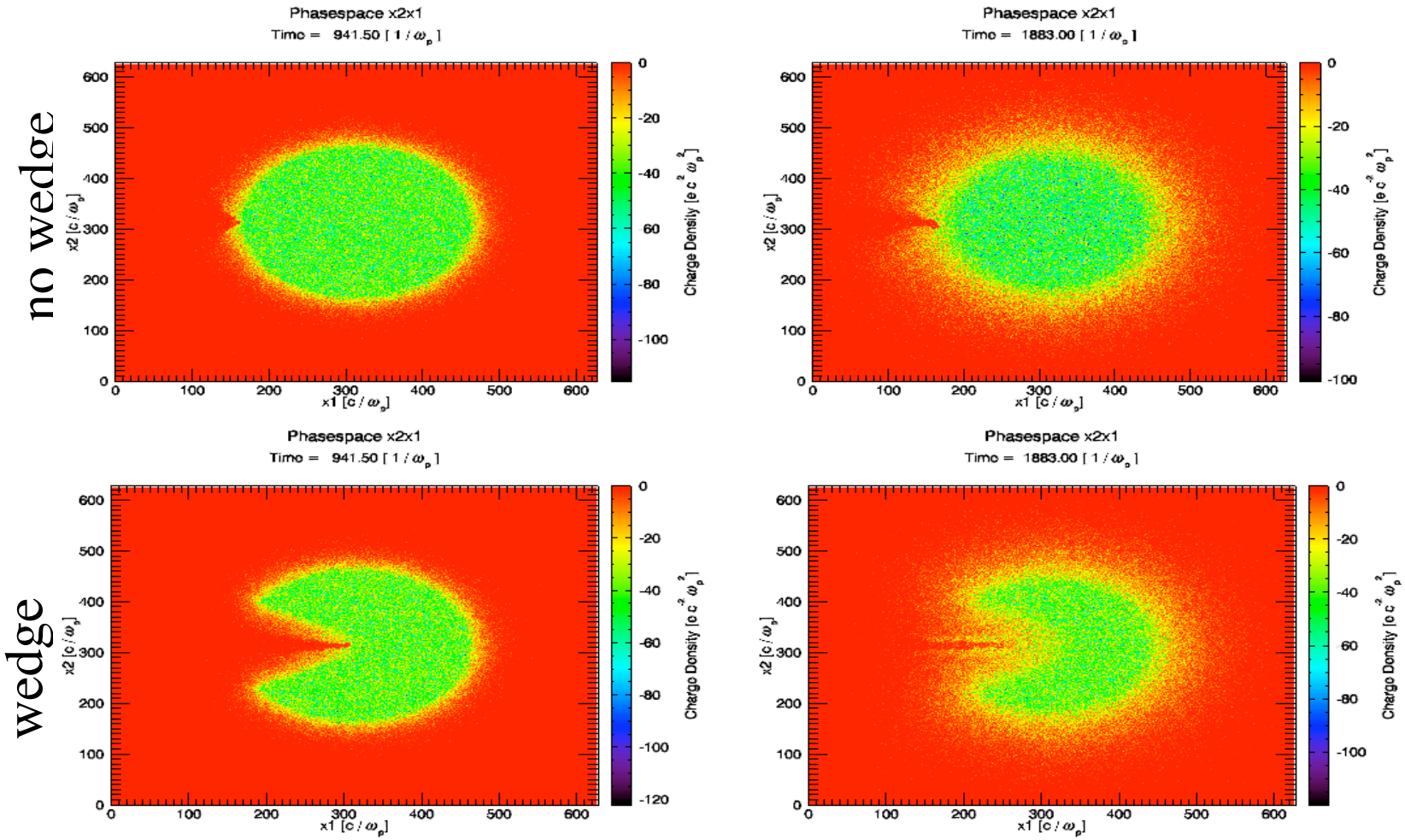

T=500 fs

T=1000 fs

Part of Fast Electrons Go Around Target

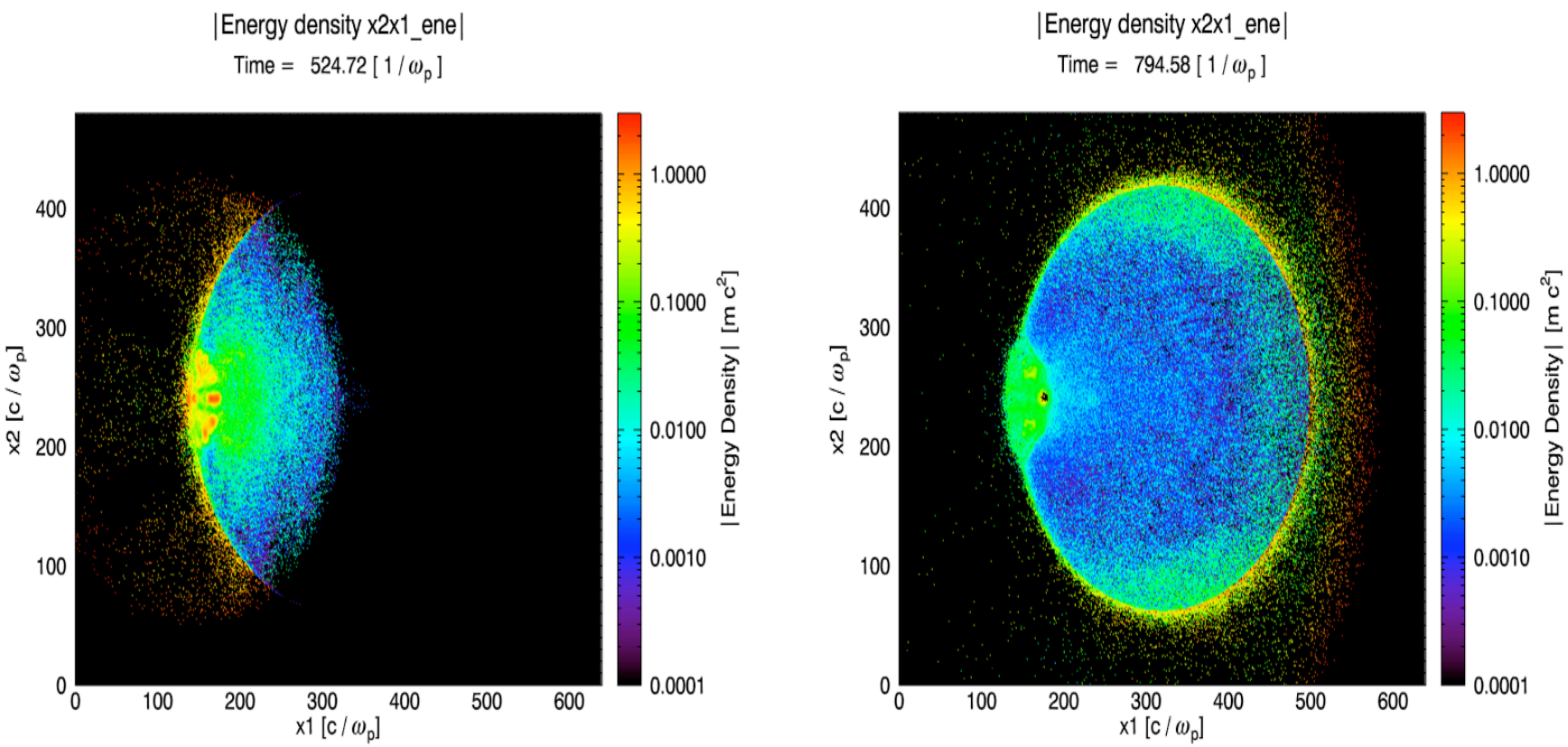

Set II, no wedge

Wedge Help Fast Electron Go Forward

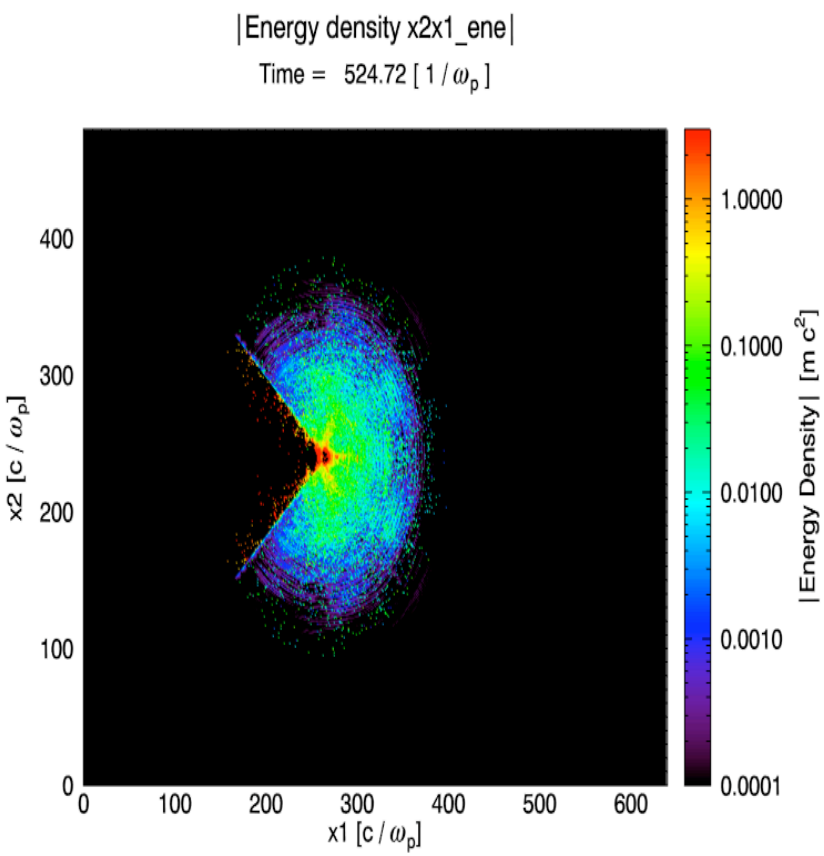

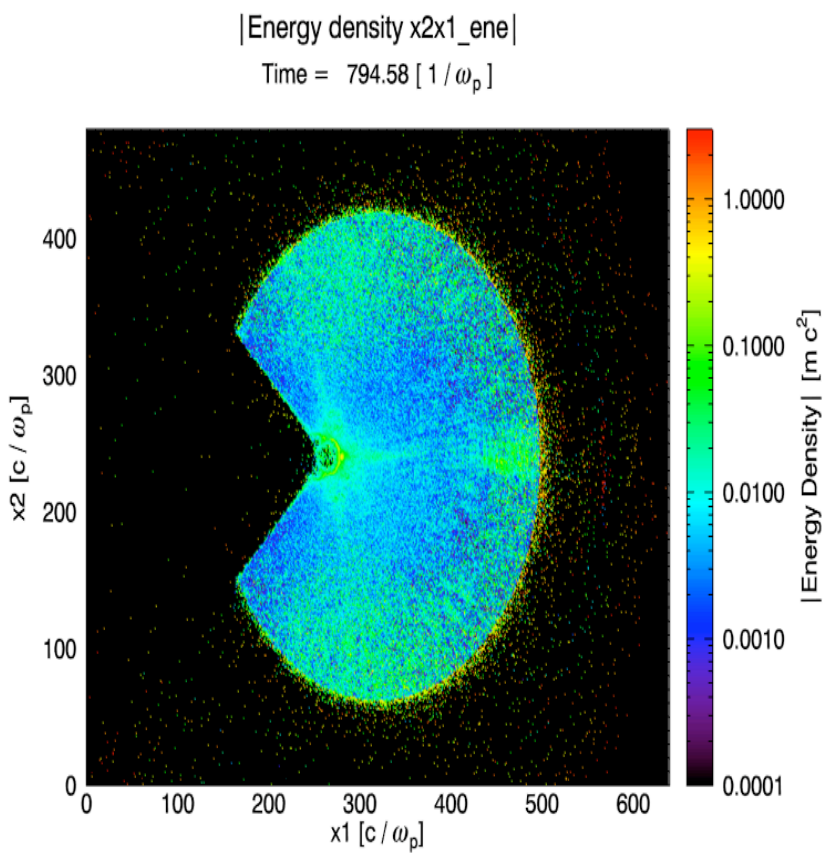

Set II, with wedge

Laser Energy Transport along Surfaces and in the Channel

Poynting flux

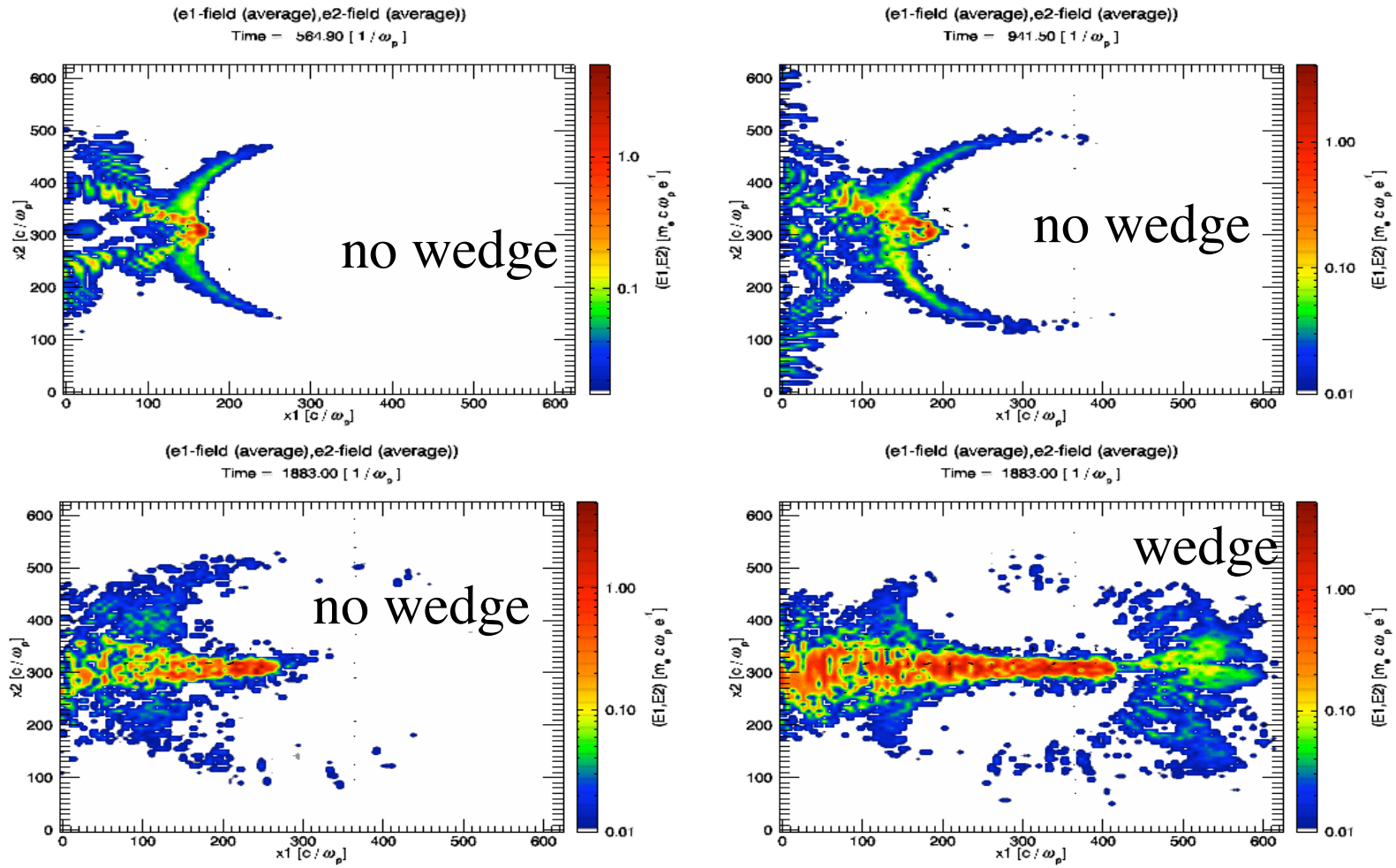

n=10 n_c

Magnetic Polarity Suggests □T□□n Origin

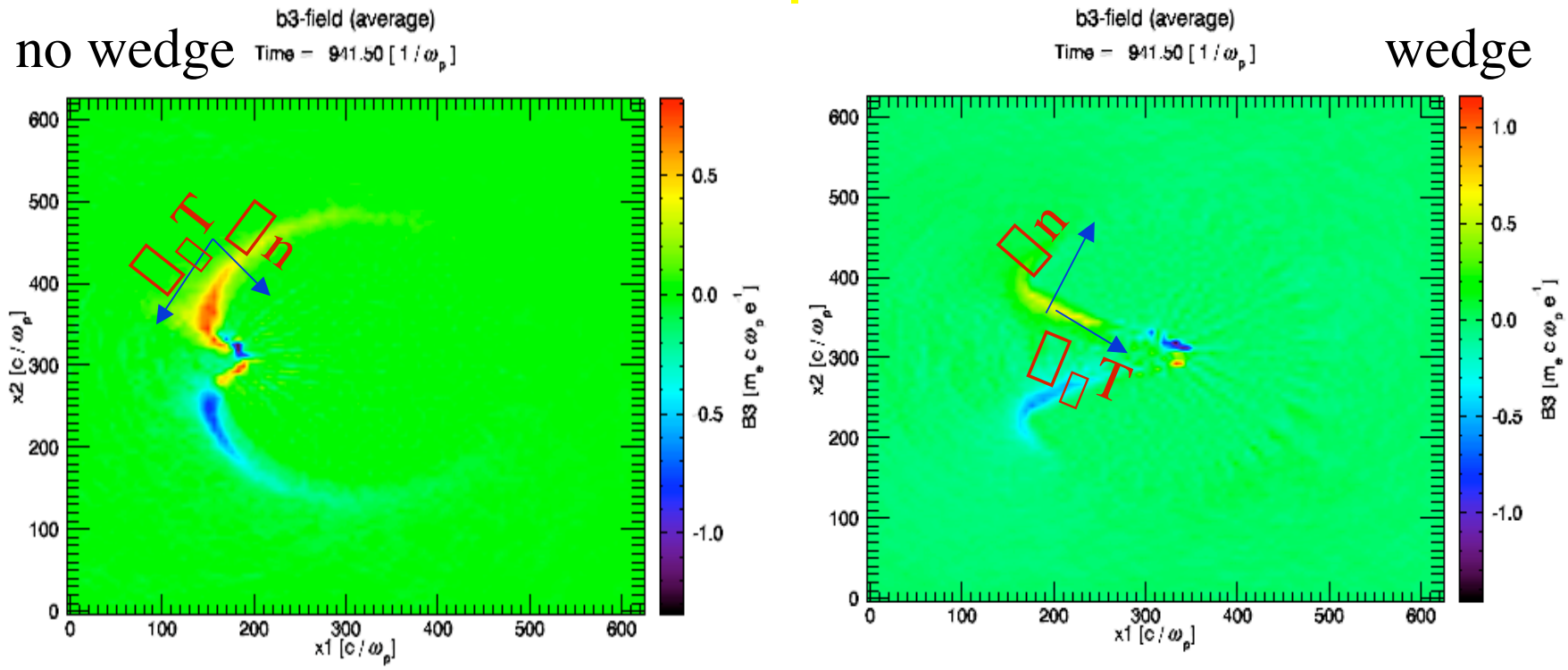

- Polarity consistent with □T□□n direction
- Magnetic field strongest on edge where □n largest
- (See Forslund & Brackbill, ‘82)

Current Penetration Seen at $n=10n_c$ but <u>not</u> at $n=40n_c$

- B3 spatially averaged over laser wavelength
- Current penetration beyond channel at $n=10n_c$ (Pukhov'97)
- Penetration not totally forward
- Penetration not seen at $n=40n_c$
- Return current filament seen near edge

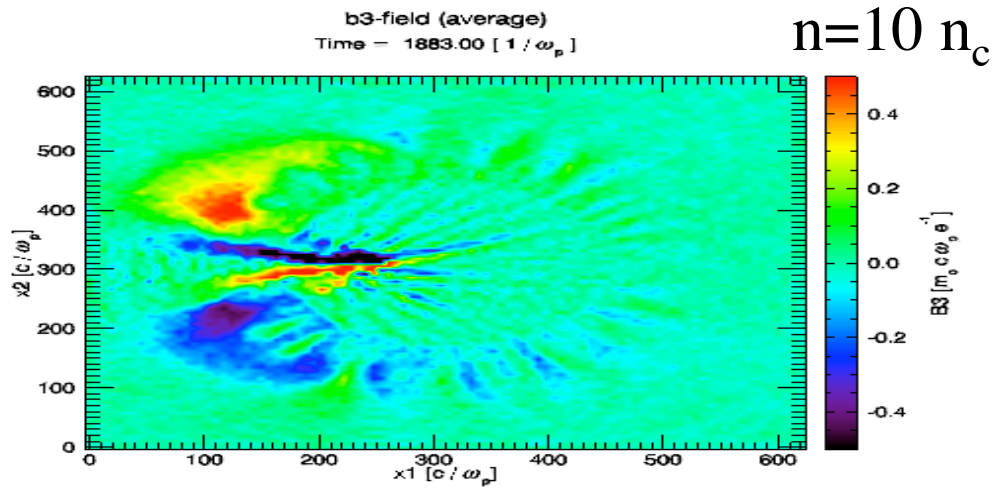

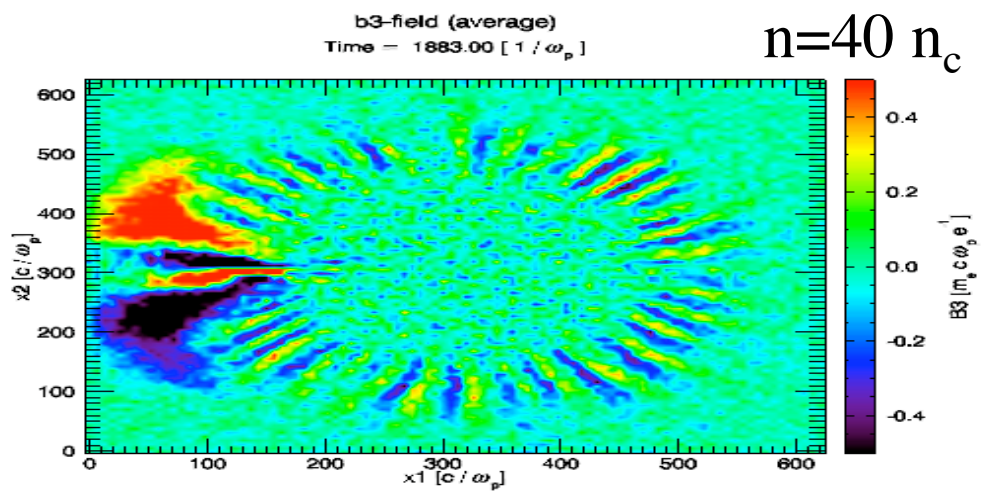

Summary

- Key parameter is ponderomotive potential/plasma pressure~**a/n**, if assuming constant temperature.
- Hole-boring only occurs in large a/n.
- Magnetic field generated by □T□□n mechanism
- Part of laser energy transports along target surfaces.
  - Fast electron
  - Poynting flux
- Higher resolution simulations for n=40 n_c and wider density variation with more detailed diagnostics are underway.

6th Workshop on Fast Ignition of Fusion Targets

November 2002

Laser accelerated ions for fusion research

Markus Roth

Outline

Experiments

Proton beam quality

^{a}Heavy Ion acceleration

Simulation

Target stability in proton fast ignition

Construction

Status of PHELIX

Experimental Setup

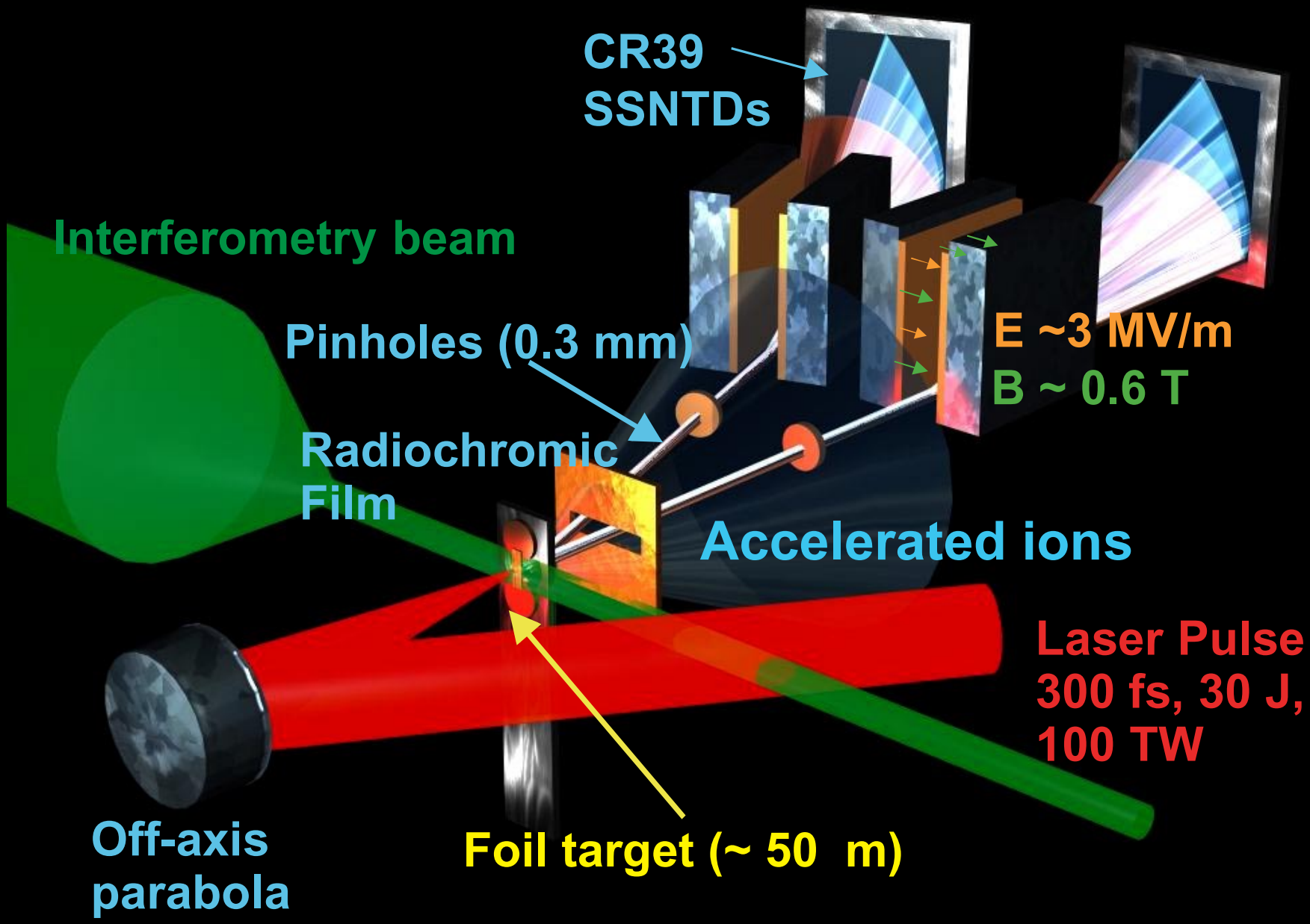

Slit-emittance measurement of beam core at spectrometer aperture

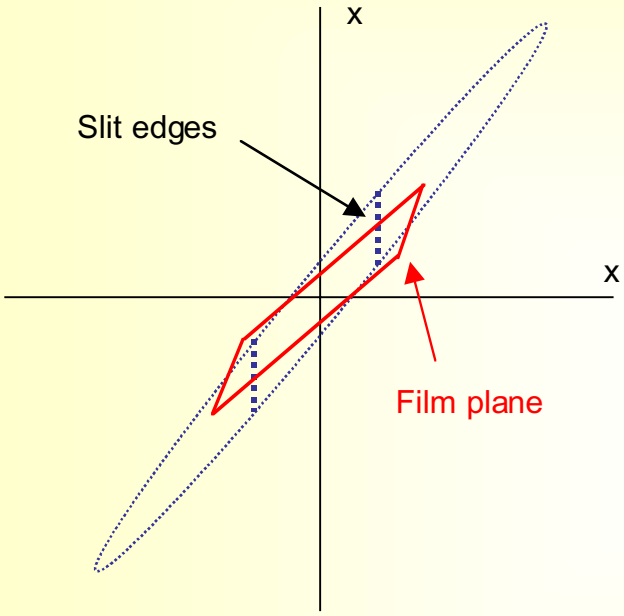

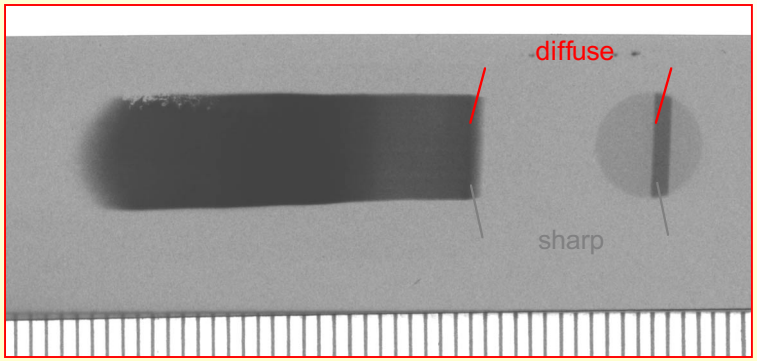

Preliminary Fit Results:
at film $\Delta x < 9\ \mu m$
at aperture $\Delta x < 2.5e\text{-}5$
(at x = 2.68 mm, x = 2.2e-3)

Effective Source Size:
$\Delta x < 31\ \mu m$

RMS emittance:
$\varepsilon < 2.2\ \pi$ mm-mrad at 29 MeV
ε-norm < 0.53 π mm-mrad
(PETAWATT results)
new:
ε-norm ~ 0.06 π mm-mrad
(LULI results with improved diagnostics)
Corresponds to a temperature of less than 40 eV !

CERN proton linac: ε-n = 1.7 π mm-mrad

The longitudinal emittance is also small
$\Delta E \Delta t$ ~ MeV-ps ~ keV-ns

Quality of laser accelerated ion beams

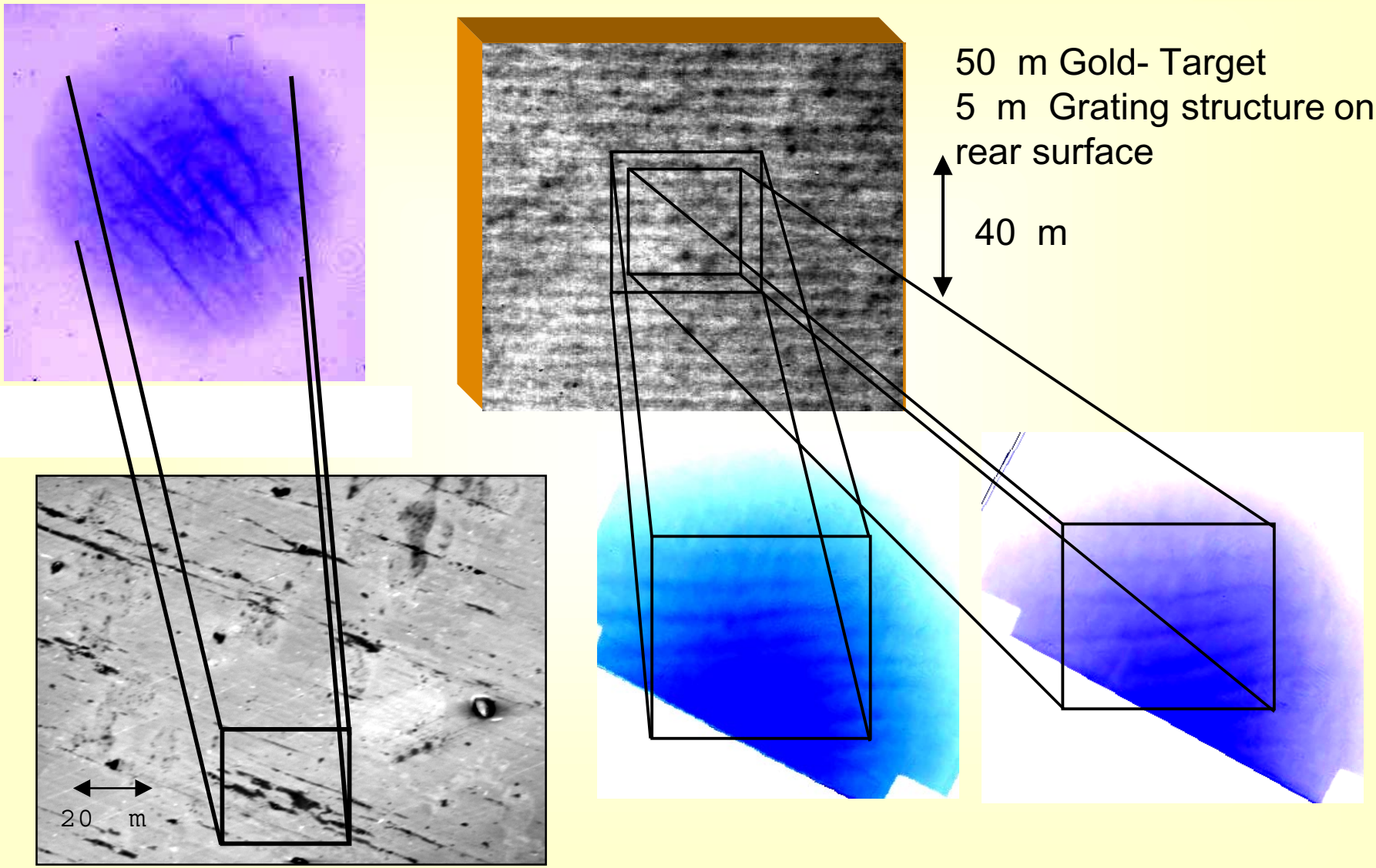

Similar to microscopic structures at target rear surface

Sub-structures below one micrometer have been observed

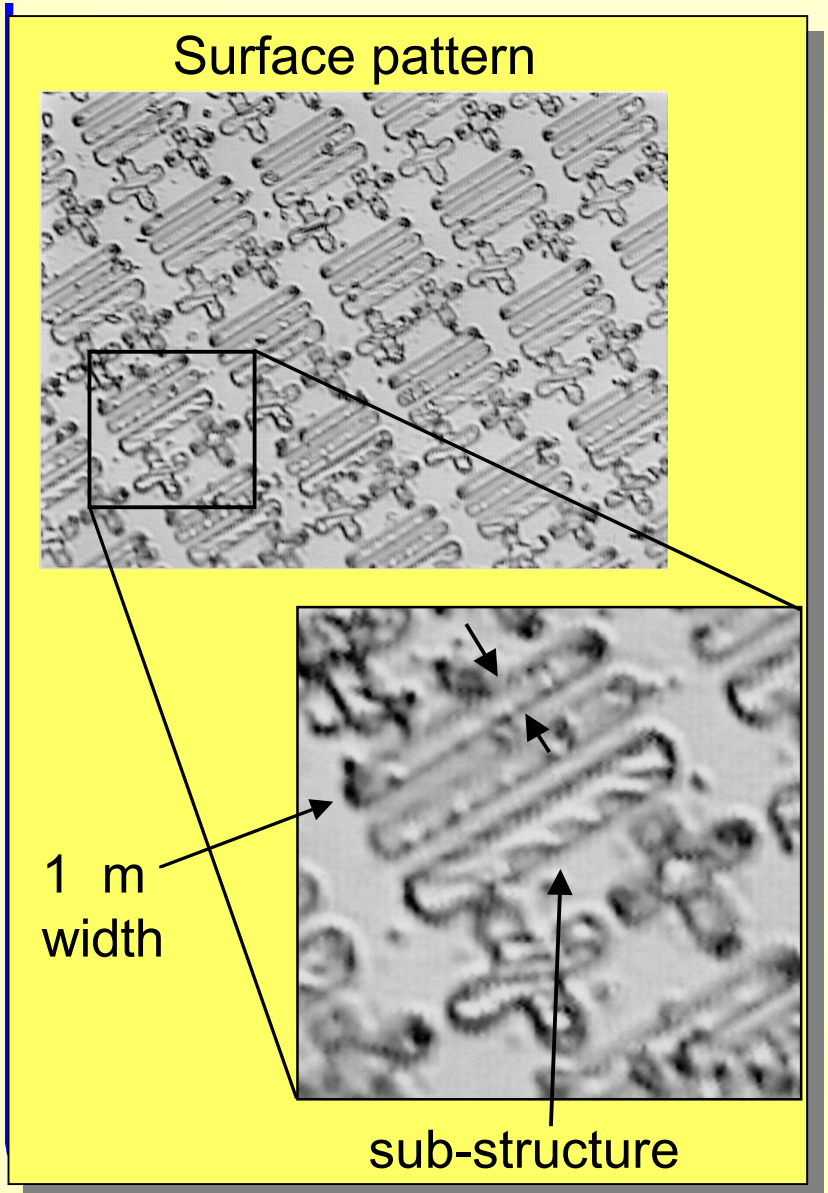

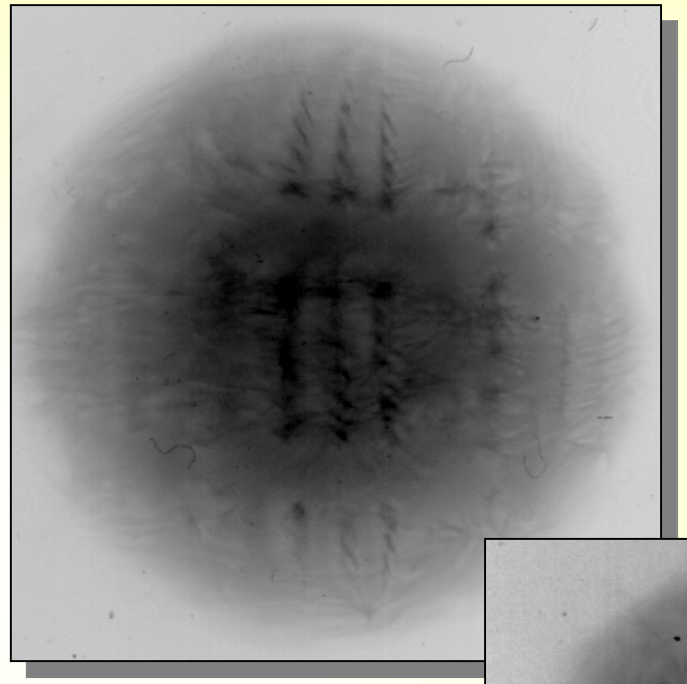

5 MeV

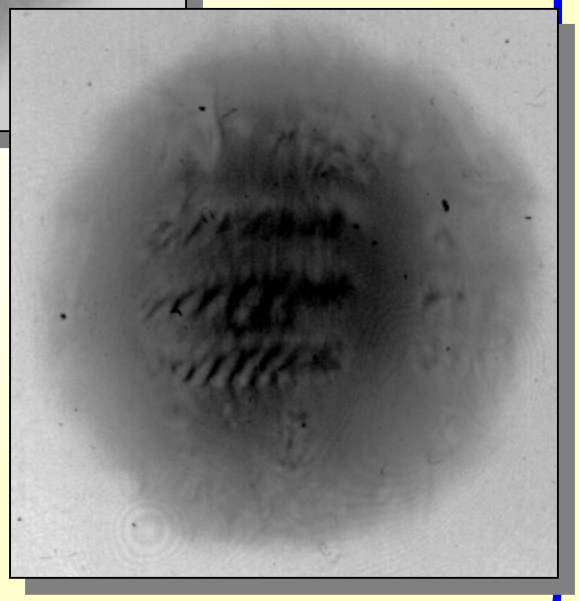

11 MeV

Real source size of protons is strongly energy dependent

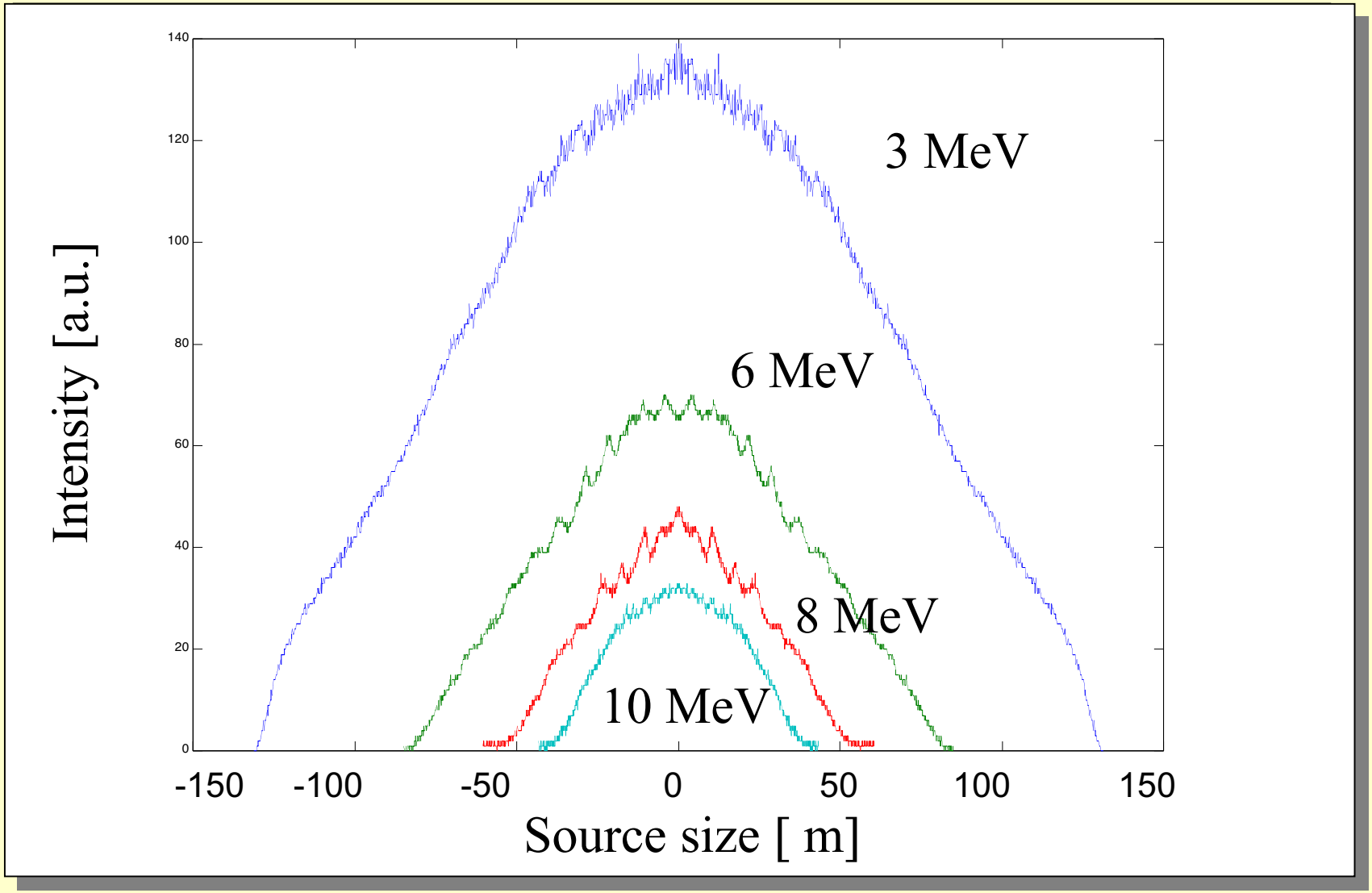

Target rear surface imprint in ion beam

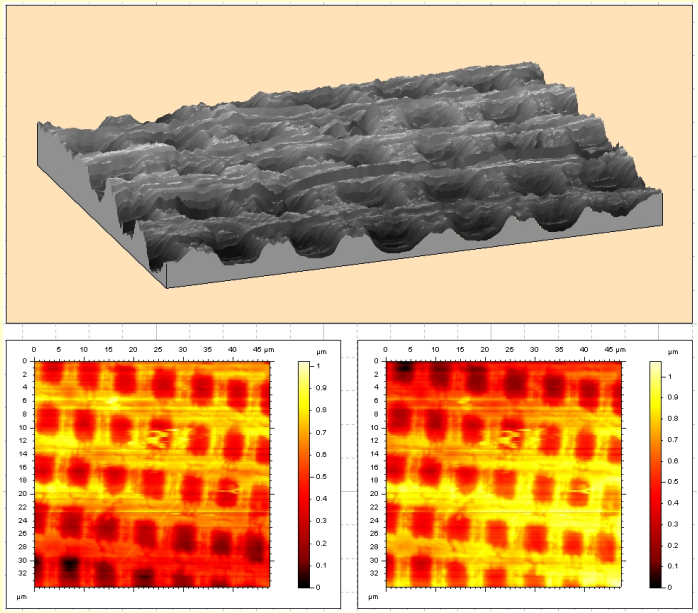

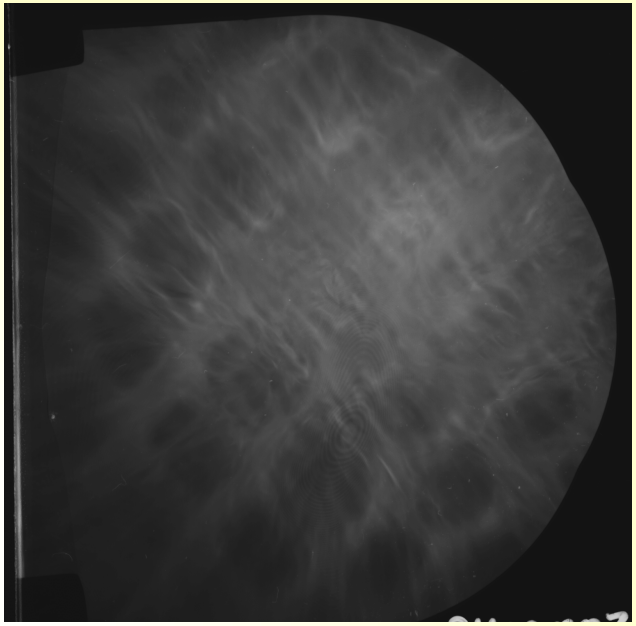

LANL Trident-Laser shot E_{laser} = 26 J, I = 7 x 10^{18}W/cm^2

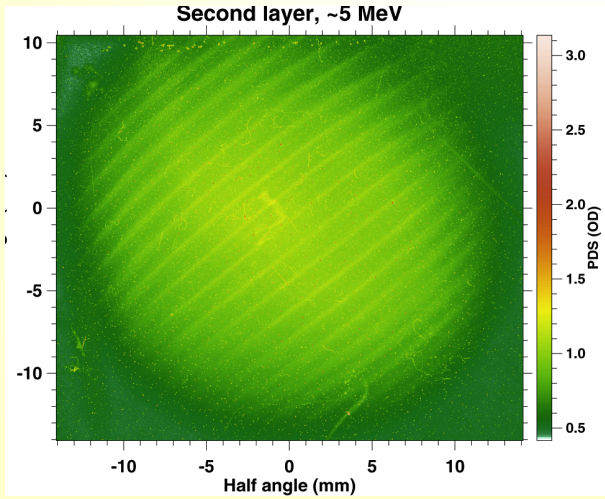

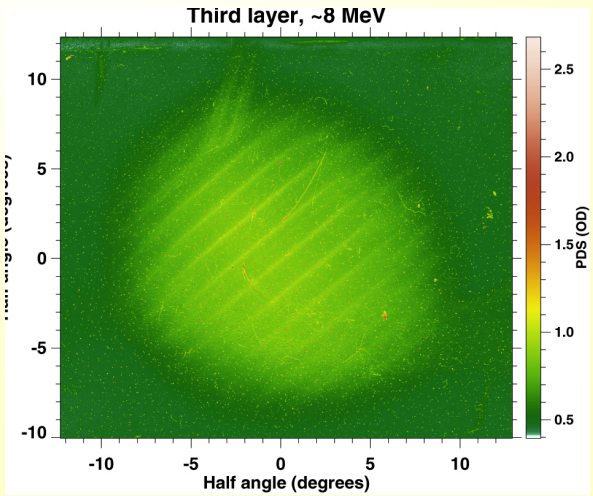

CaF_2 target

Target W 50m backside coated
with 0.3 m CaF_2

not heated

resivetively he

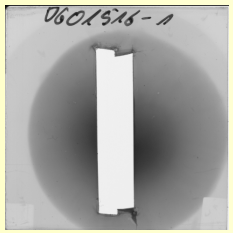

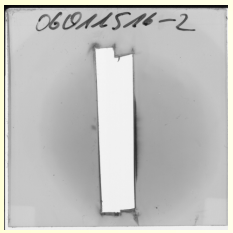

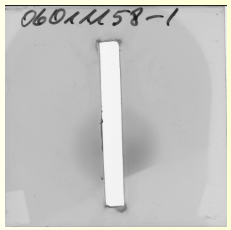

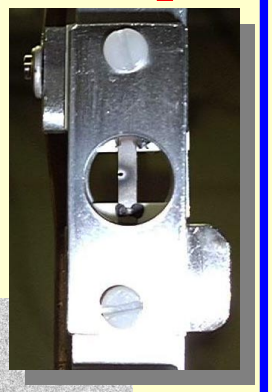

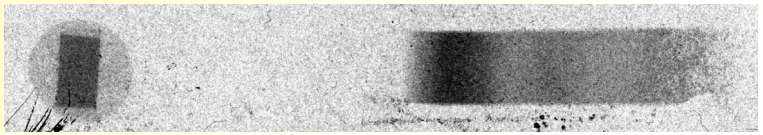

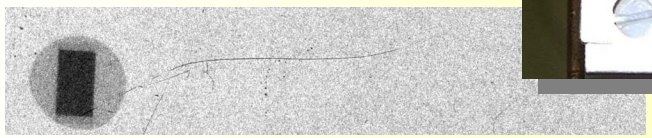

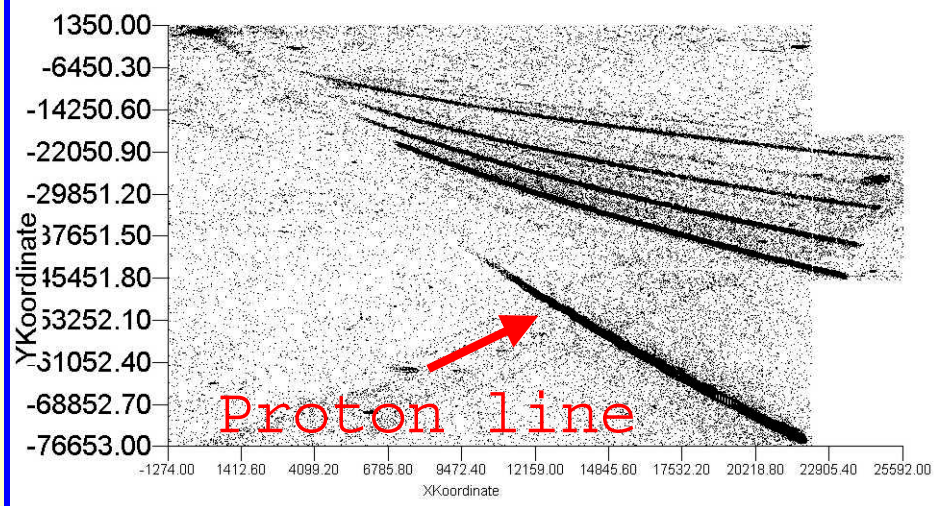

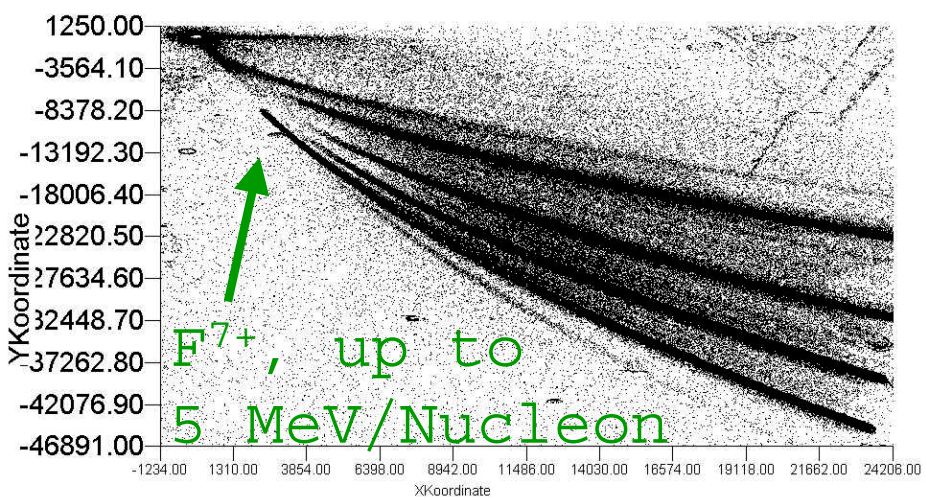

F^{7+} spectra

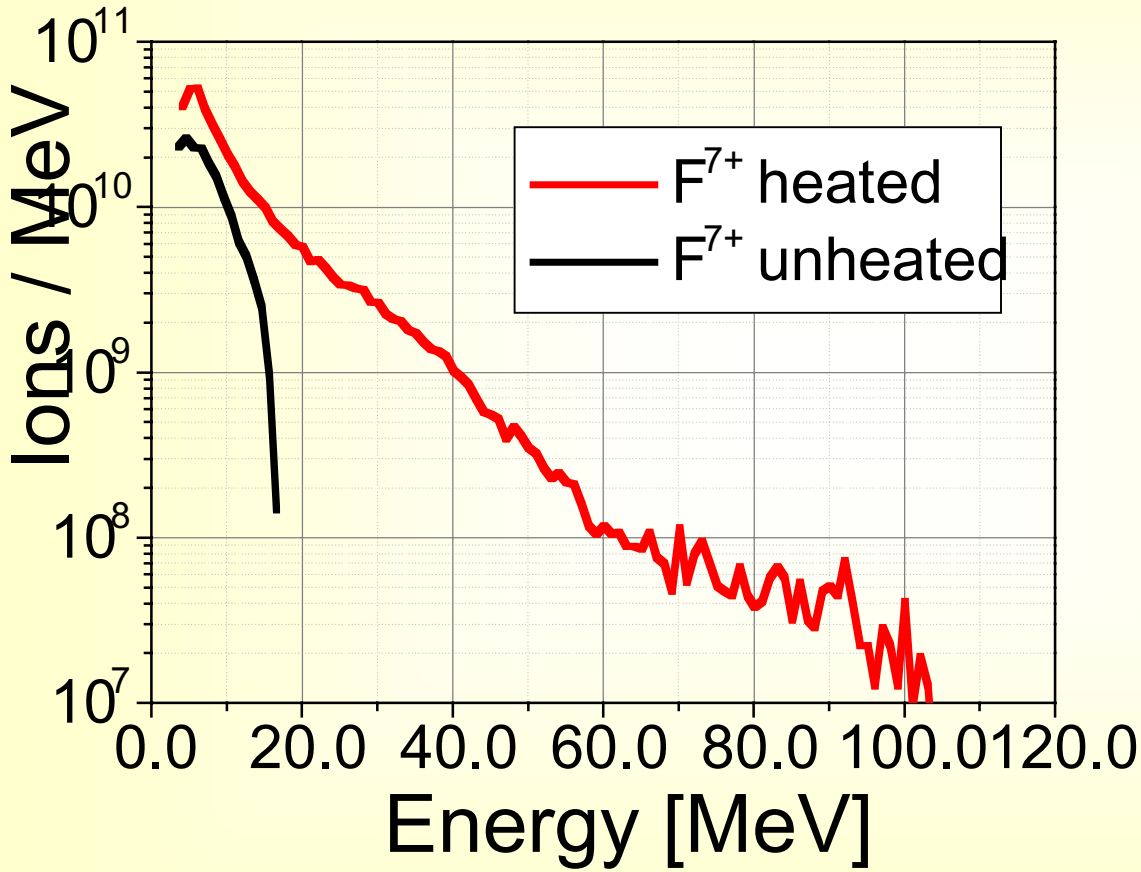

E_{max} > 5MeV/nucleon

~ 5% of laser energy in heavy ions

corresponds to ~ 23 MeV protons

(backside!)

Energy and angular Dependence

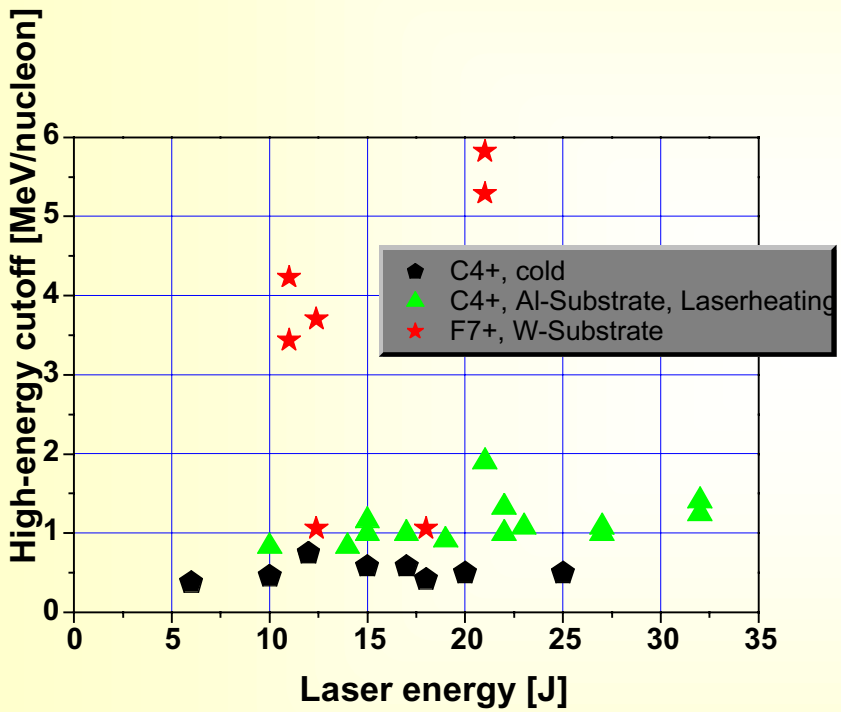

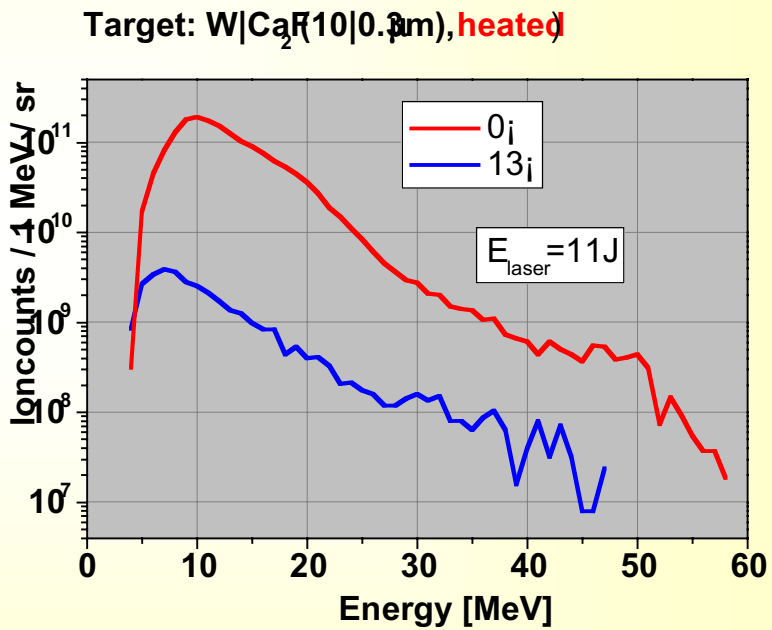

Accelerating Fields

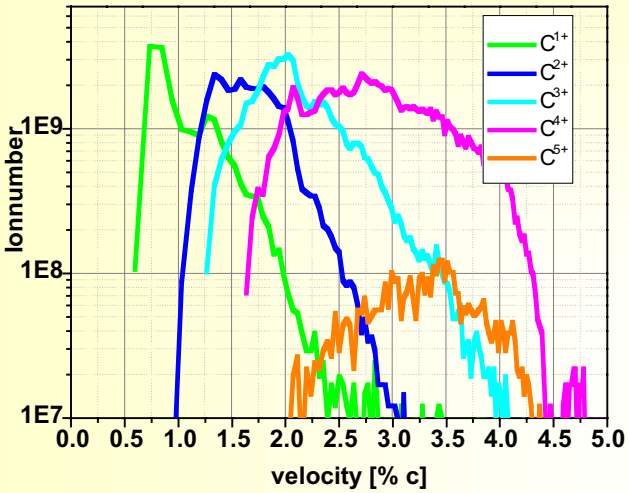

From C^{2+} spectra:

¥ E_{max}: 1 x 10^{11} V/m (just below C^{3+})

¥ t ~ 10ps (highest velocity/energy)

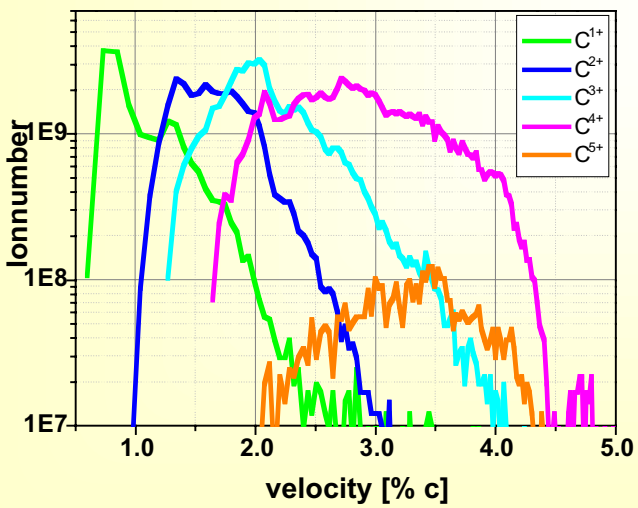

C4+:

E_{max}: 5.3 TV/m (< U_{C5+})

E_{min}: 0.2 TV/m (> U_{C4+})

$E(\tau_{laser})$: ~ 2 TV/m

t ~ a few hundred fs

Proton Fast ignition - target stability (1)

Target under consideration: **1-D 3-T code DEIRA**

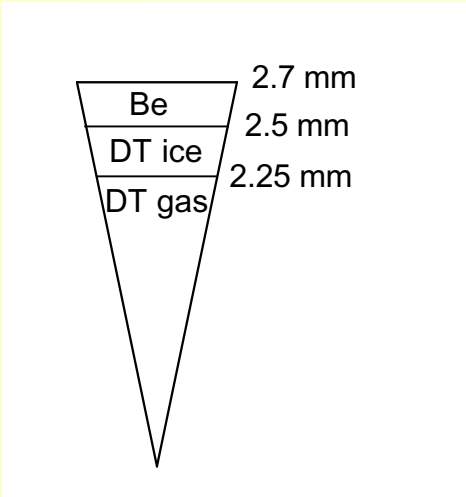

High yield target:
4.4 mg fuel mass, yield 500 MJ

Driving X-ray pulse:

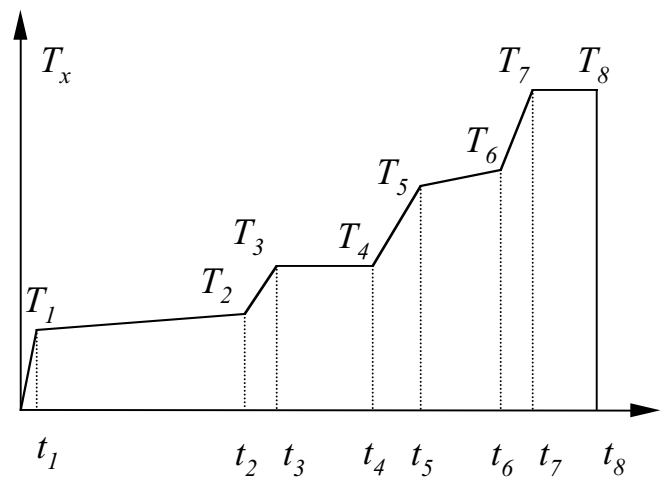

t_1 = 2.0 ns, T_1 = 90 eV;
t_2 = 24.0 ns, T_2 = 95 eV;
t_3 = 26.0 ns, T_3 = 110 eV;
t_4 = 32.0 ns, T_4 = 110 eV;
t_5 = 34.5 ns, T_5 = 130 eV;
t_6 = 39.0 ns, T_6 = 145 eV;
t_7 = 44.0 ns, T_7 = 240 eV;
t_8 = 46.0 ns, T_8 = 240 eV;

Driving pulse for optimum compression without ignition

Absorbed X-ray energy: $E_{caps} \approx 1$ **MJ;**

Implosion velocity: $v_{im} = 2.40\times10^7$ **cm/s;**

Maximum compression: $\langle\rho r\rangle_m = 3.53$ **g/cm²** **at** $t_m = 47.76$ **ns,**

$R_{DT} = 0.180$ **mm,** $r_{DT} = 180 — 260$ **g/cm³,**

$T_{DT} = 0.80 — 0.38$ **keV;**

Proton fast ignition - target stability (2)

Problems: 1) Proton production target rear surface has to remain cold
2) A vacuum gap for acceleration is required
3) distance between proton target and capsule should be small

→ Proton target is closely attached to the target or hohlraum therefore subject to the soft-x-rays driving the capsule

→ A shield is required to protect the production target

Requirements for the shield:

as thin as possible to avoid energy loss/straggling

thick enough to protect the target

Proton fast ignition - target stability (3)

A 15µm (30µm, 50µm) thick planar gold wall after the radiation pul

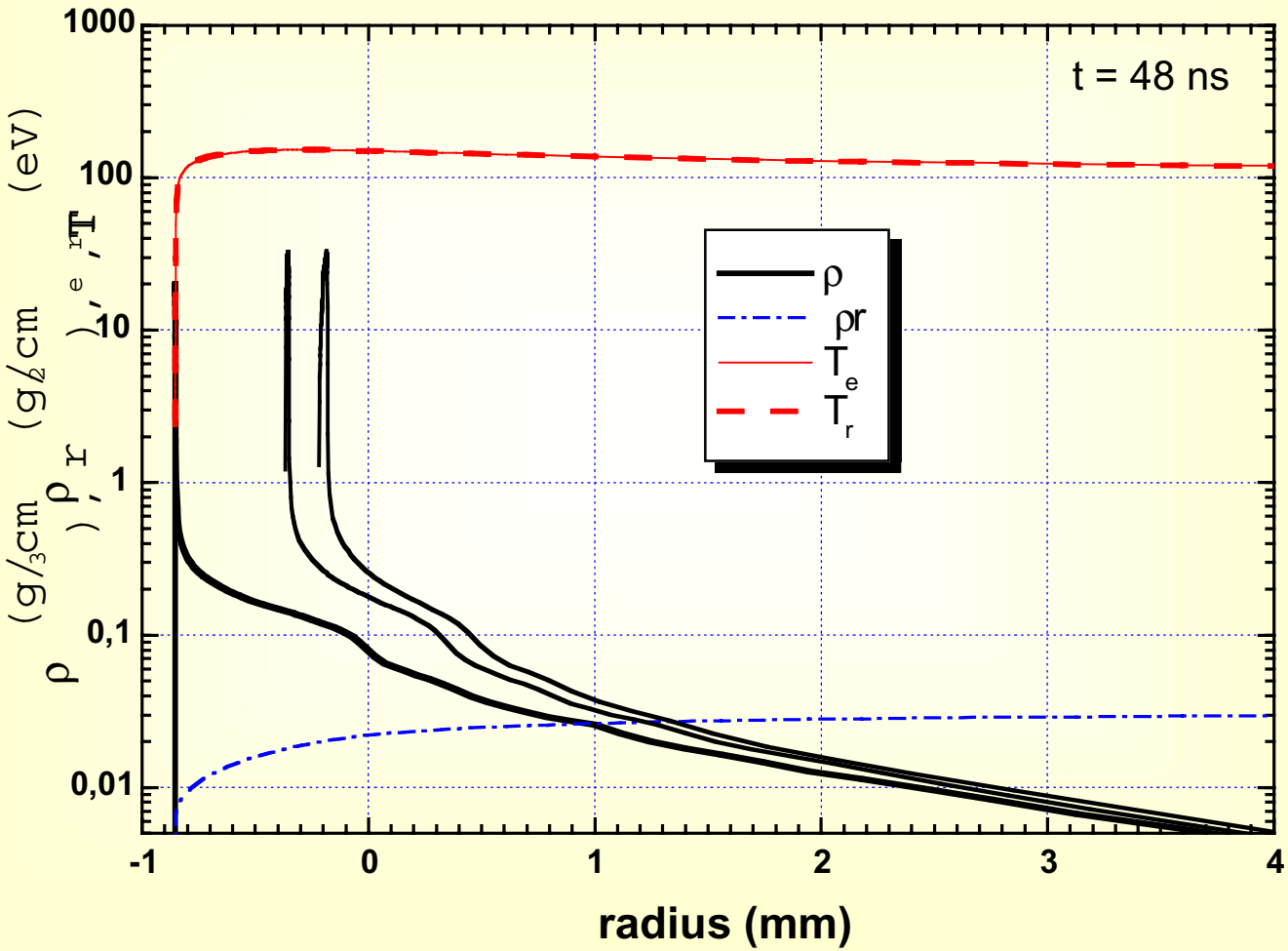

Proton fast ignition - target stability (4)

Rear-side history of a 15 (30µm, 50µm) thick planar gold wall

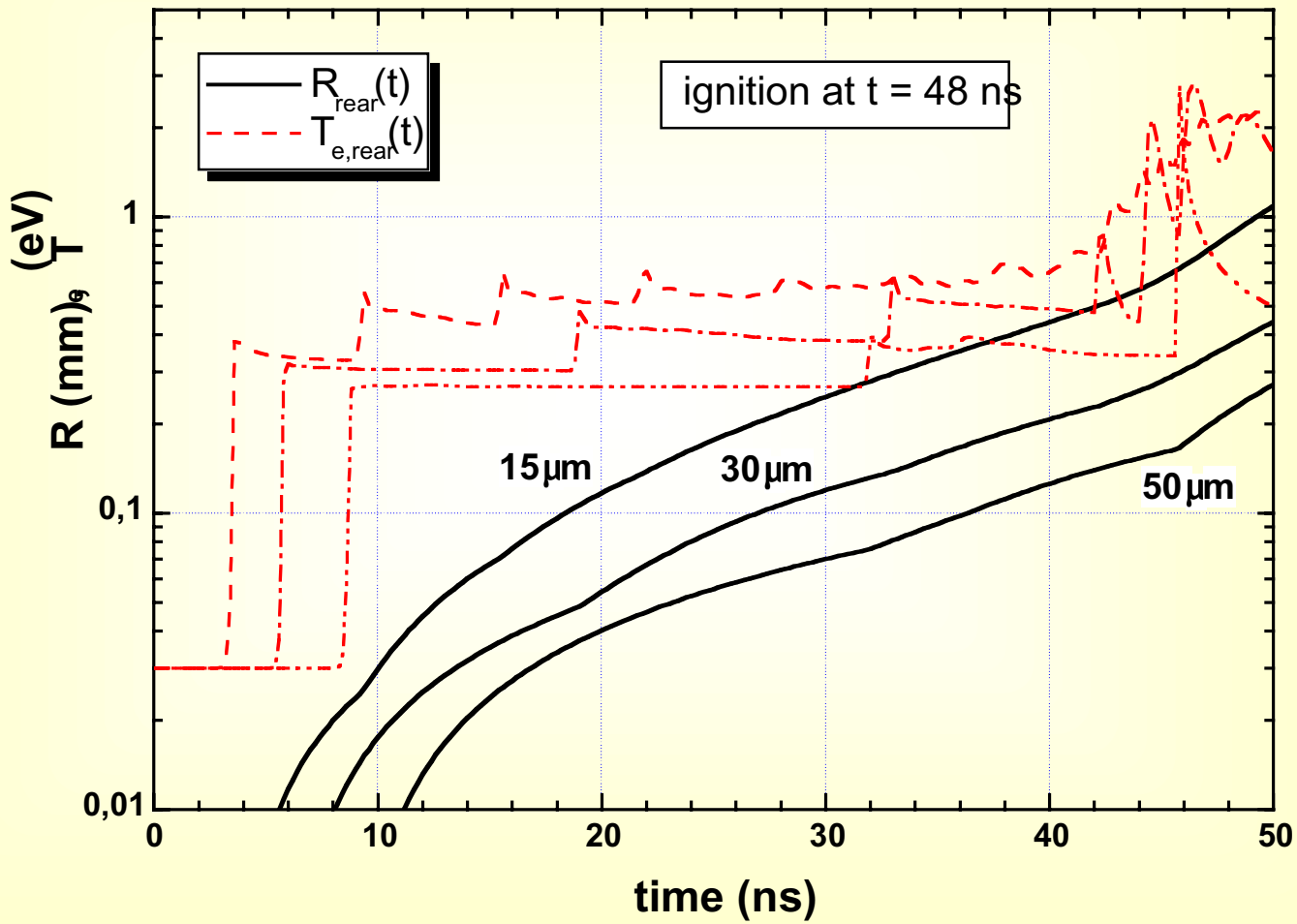

Proton fast ignition - target stability (5)

Conclusion:

a 50 m shield is displaced by 280 m at the time of igniti on (maximum compression)

the shield is heated up to 2-3 eV at the time of ignition

temperature of the production target closely coupled to the shield (a problem ? Evaporation of proton layers)

a second (thin) shield could further reduce the thermal load on the target

PHELIX

Petawatt High Energy Laser for Heavy Ion Experiments°°°°

Graphical overview

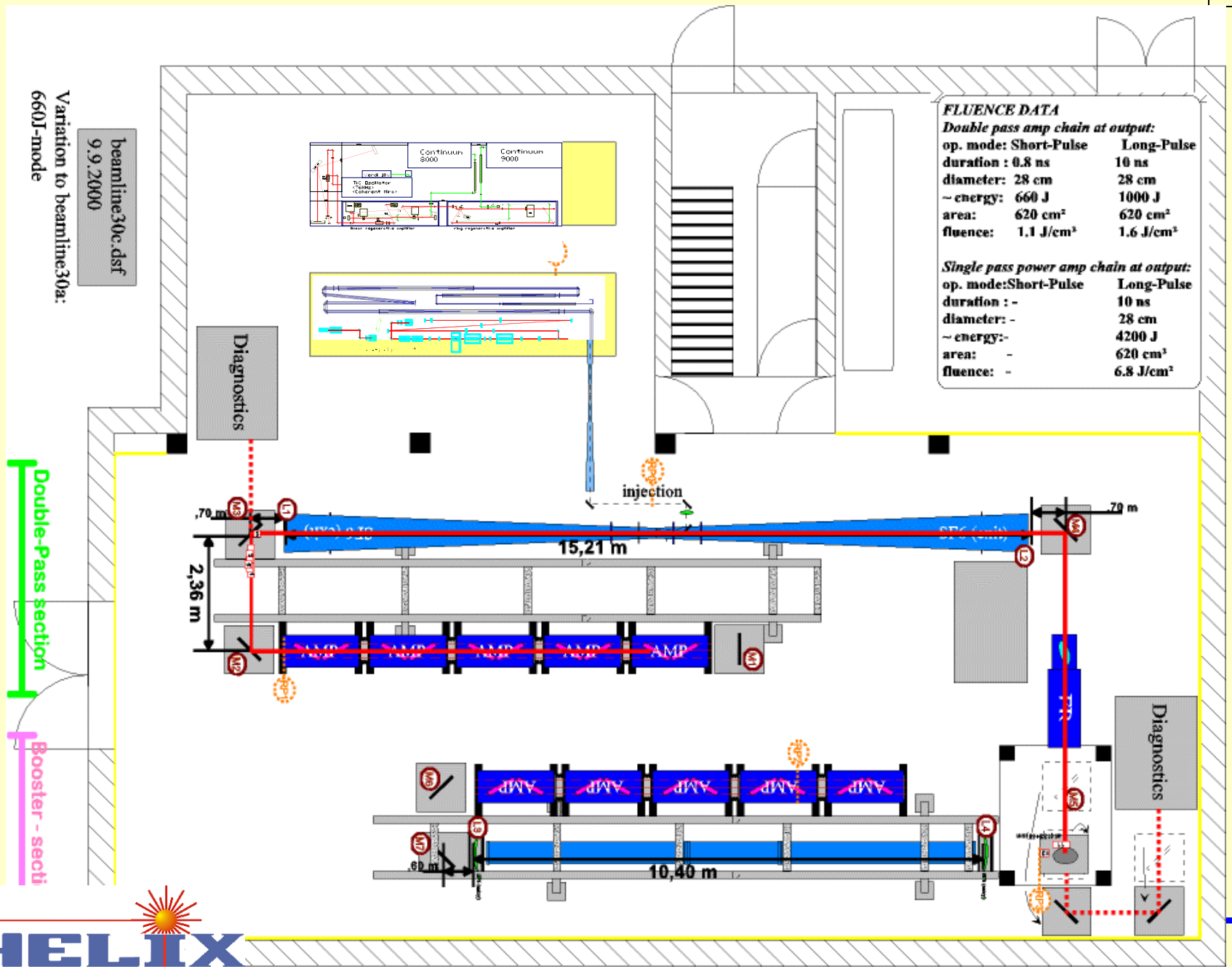

Femtosecond Frontend

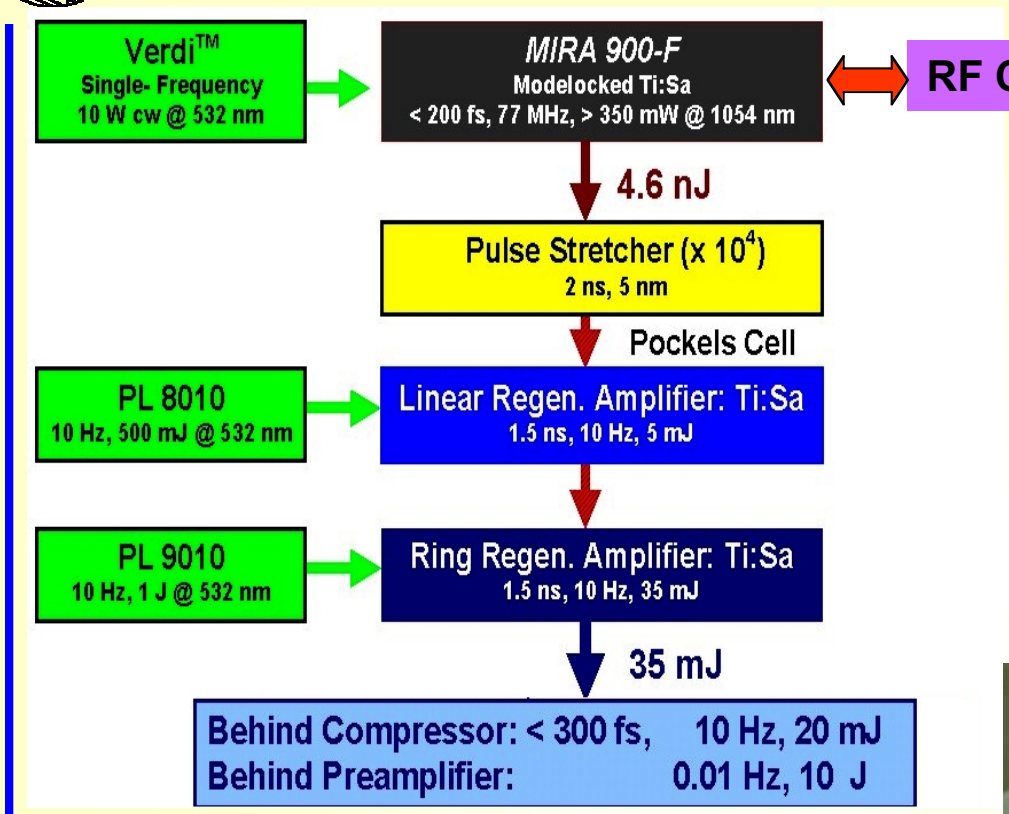

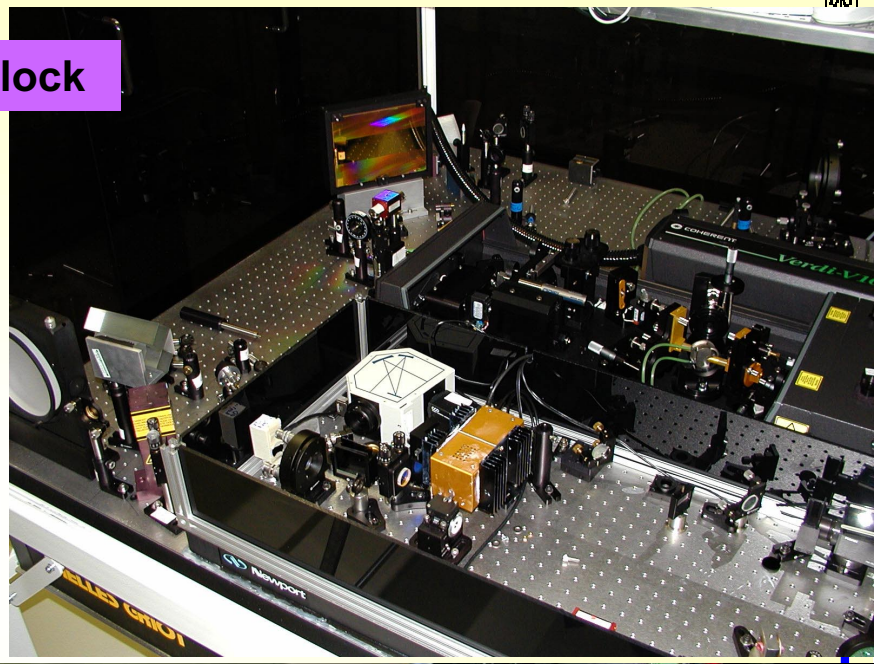

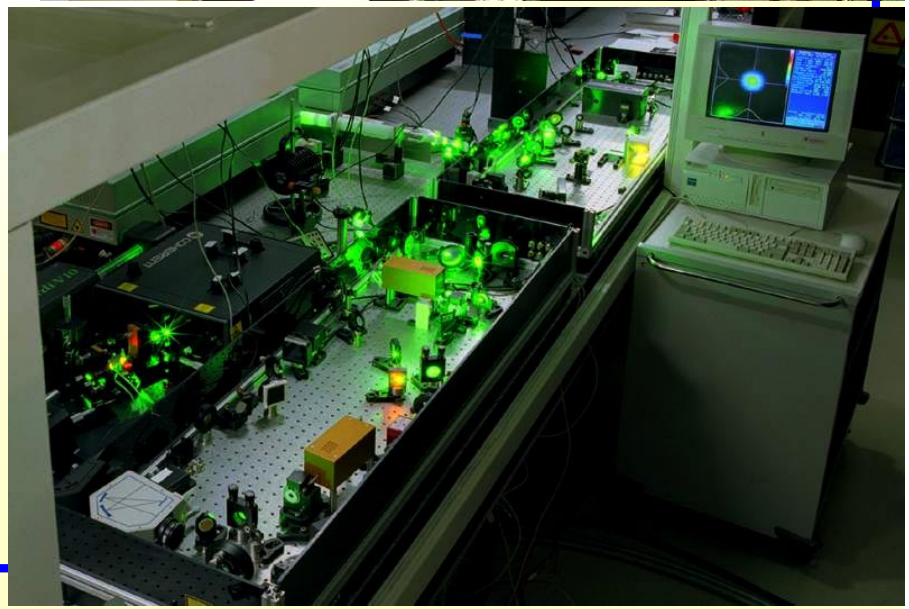

- ✓ > 40 mJ output out of regenerative amplifier
- ✓ synchonization operating
- ✓ mode quality and stability up to specification

Nanosecond Frontend

Diode Pumped
Single Frequency Yb:Silica
Fiber Ring Master Oscillator
300 ns. 960 Hz

↓

Pulse Slicer: 30 ns

↓

Phase Modulator

↓

Fiber Amplifier

↓

Amplitude Modulator with
TEK Arbitrary Waveform Generator

↓

Nd:glass Regen. Amplifier → 50 mJ Selectable ns Time Structure

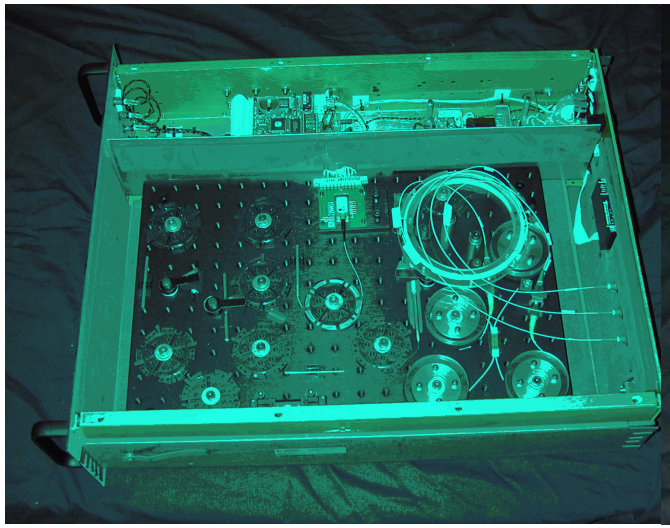

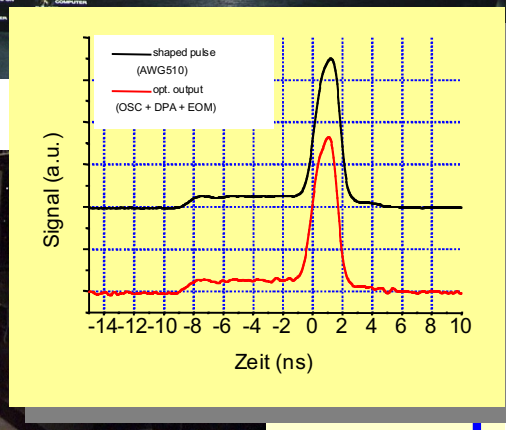

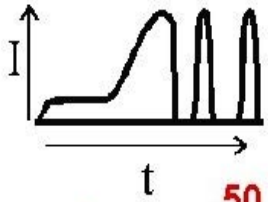

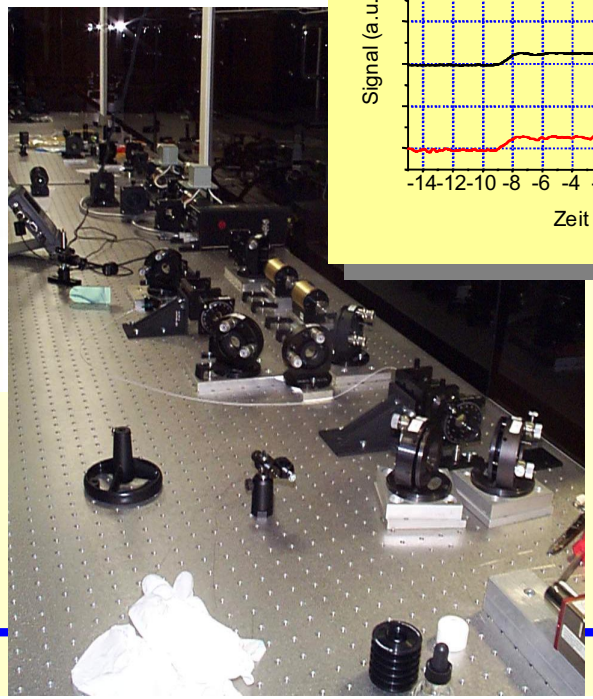

✔
- ¥ 40 mJ output out of regenerative amplifier
- ¥ pulse shaping tested
- ¥ fail/safe system tested at LLNL (M. Roth)

Beamtransport

There are different experiment regions:

Z6:
ns 1-5kJ pulses
HHT:
ns 1-5kJ pulses
Petawatt
ESR:
fs 10 J

✓ ¥ contract for construction of beamline to Z6

➡ ¥ setup of beamline towers to Z6 (october 2002)
¥ setup of beamline
¥ install mirror mounts, optics, vacuum, nitrogen, and controls

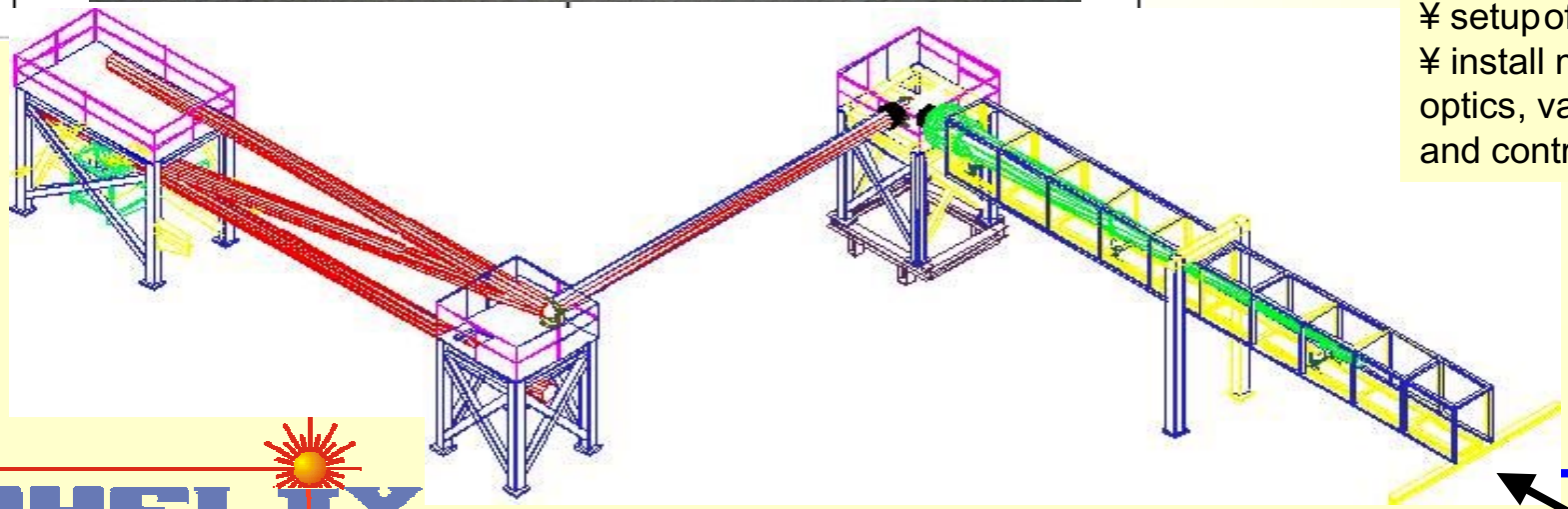

Special thanks to:

GSI: *A. Blazevic, E. Brambrink, M. Geissel,*
Plasma Physics *M. Basko*

GA: *T. E. Cowan, H. Ruhl, M. Allen, A. Kemp,*

LULI: *P. Audebert, J. Fuchs, J. C. Gauthier*

MPQ/LMU: *M. Hegelich, S. Karsch, K. J. Witte, D. Habs,*

LANL: *J. Cobble, R. Johnson, S. Letzring, J. Fernandez*

and the PHELIX -Crew

Fast Ignition Integrated Interconnecting Code Project

H. Sakagami and K. Mima*

Comp. Eng., Himeji Institute of Technology

*ILE, Osaka University

FI^3 Project

- Fast Ignition Integrated Interconnecting code

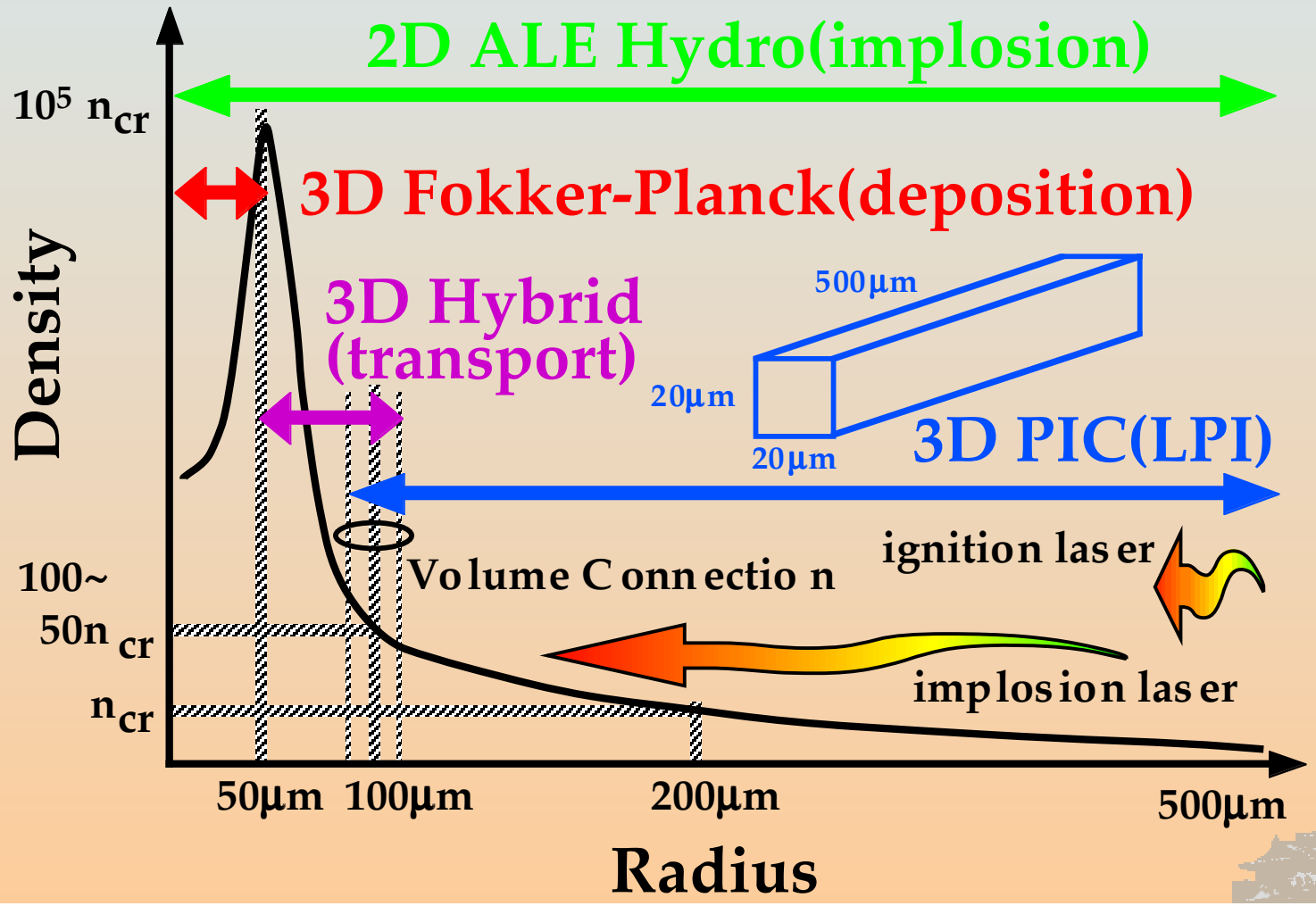

Code Integration Diagram

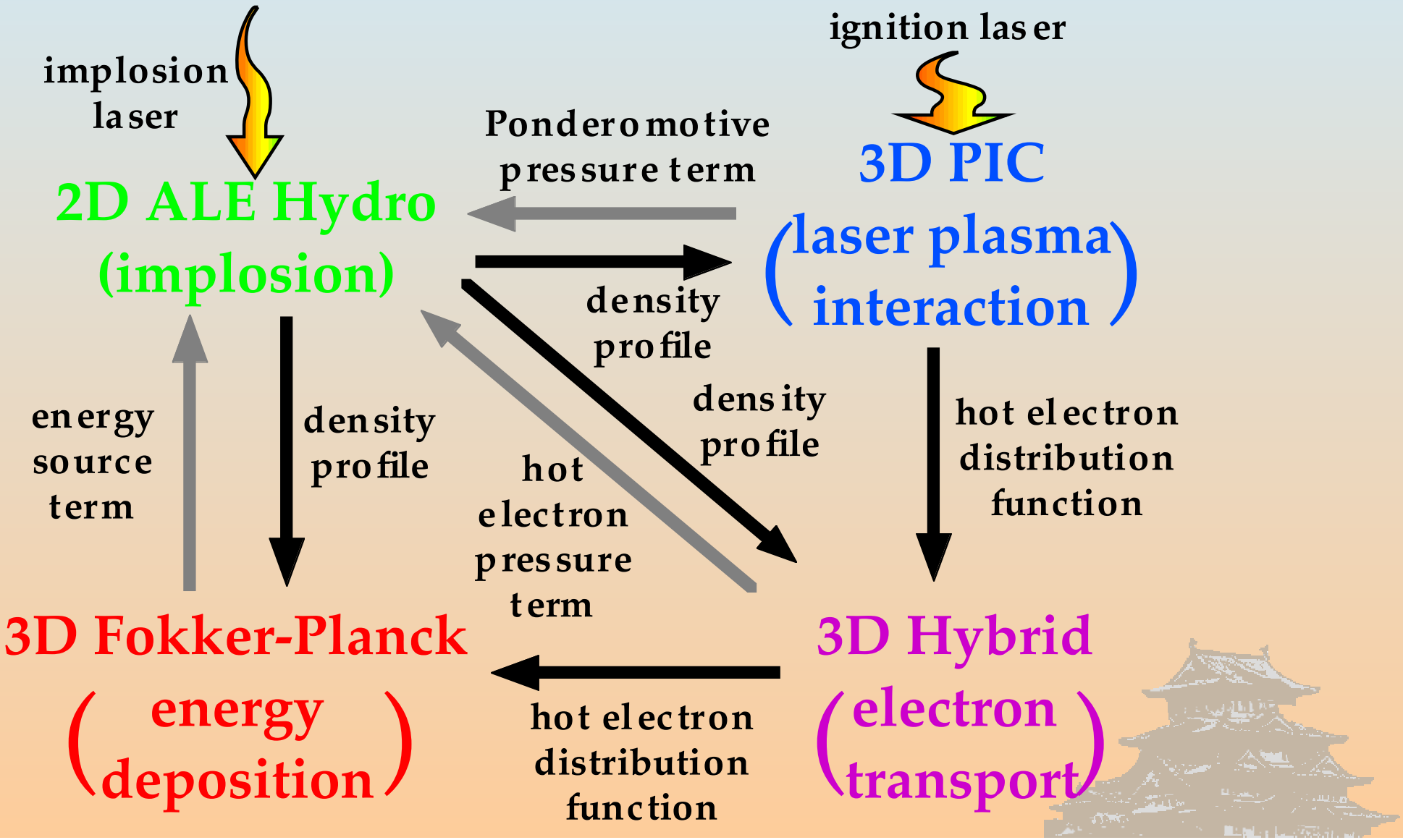

Interconnecting Protocol

- standard protocol is too heavy!
  - Globus, CORBA, SOAP
  - not easy to program
- TCP/IP based lightweight protocol
  - LAN, dedicated line and the Internet
  - procedure-free communication system
  - proxy routing system
- Distributed Computing Collaboration Protocol
  - simple and easy for computational users
  - asynchronous communication

Implementation of DCCP

- Arbitrator
  - manage/control communicators
- Communicator
  - transfer data instead of user's code
- Code
  - user's simulation program

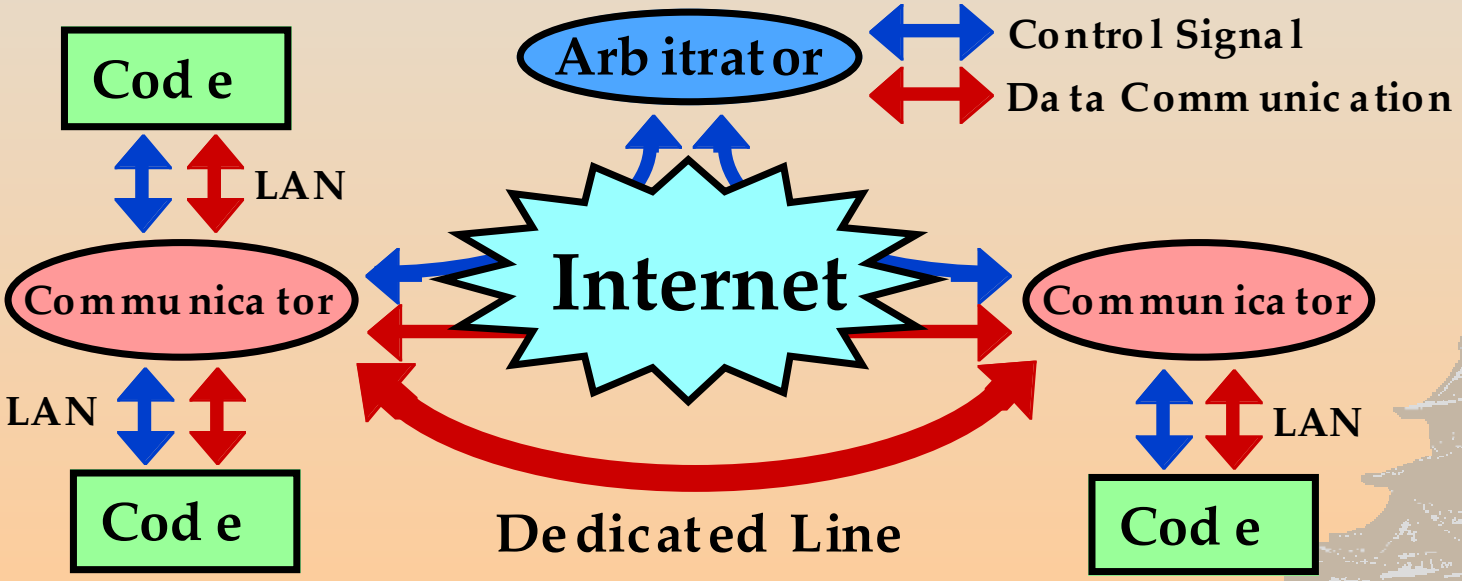

Summary of DCCP

- Code
  - dccp_initialize : initialize and advertise to Comm.
  - dccp_send : send data to another Code
  - dccp_receive : receive data from another Code
  - dccp_finalize : finalize and advertise to Comm.
- Communicator
  - dccp_invoke : invoke and advertise to Arb.
  - dccp_inform : inform something to Arb.
  - dccp_inquire : inquire about Code to Arb.
  - dccp_transfer : transfer data between Comms
  - dccp_terminate : terminate and advertise to Arb.
- Arbitrator
  - dccp_notify : notify Code info to Comm.

Collaboration

- easy to develop codes individually
  - efficiently run each code on appropriate architecture machine such as VEC, VP, SMP, MSP
- 2D ALE Hydro : Osaka University
- 3D PIC : Himeji Tech. & Osaka University
- 3D Hybrid : Setsunan University
- 3D Fokker-Planck : Kyushu University
- Communication Protocol : Himeji Tech.

Collective Particle Approach

- FISCOF
  - Fast Ignition Simulation code with COllective and Flexible particles
- statically get together many particles into one representative particle
- dynamically split collective particle into many normal particles under appropriate conditions (future plan)

ALE Hydro and Collective PIC Codes

2D ALE Hydro (implosion) → density profile → **3D PIC (laser plasma interaction)**

- ALE hydro code computes implosion dynamics and snapshots a density profile at maximum compression.
- Collective PIC code obtains the density profile and introduces initial plasmas corresponding to the profile.
- The profile is passed through a file at this moment.

Density Profile from ALE Hydro Code

- cut the profile between (a) $0.1n_{cr}$ or (b) $0.05\ n_{cr}$ and $100\ n_{cr}$

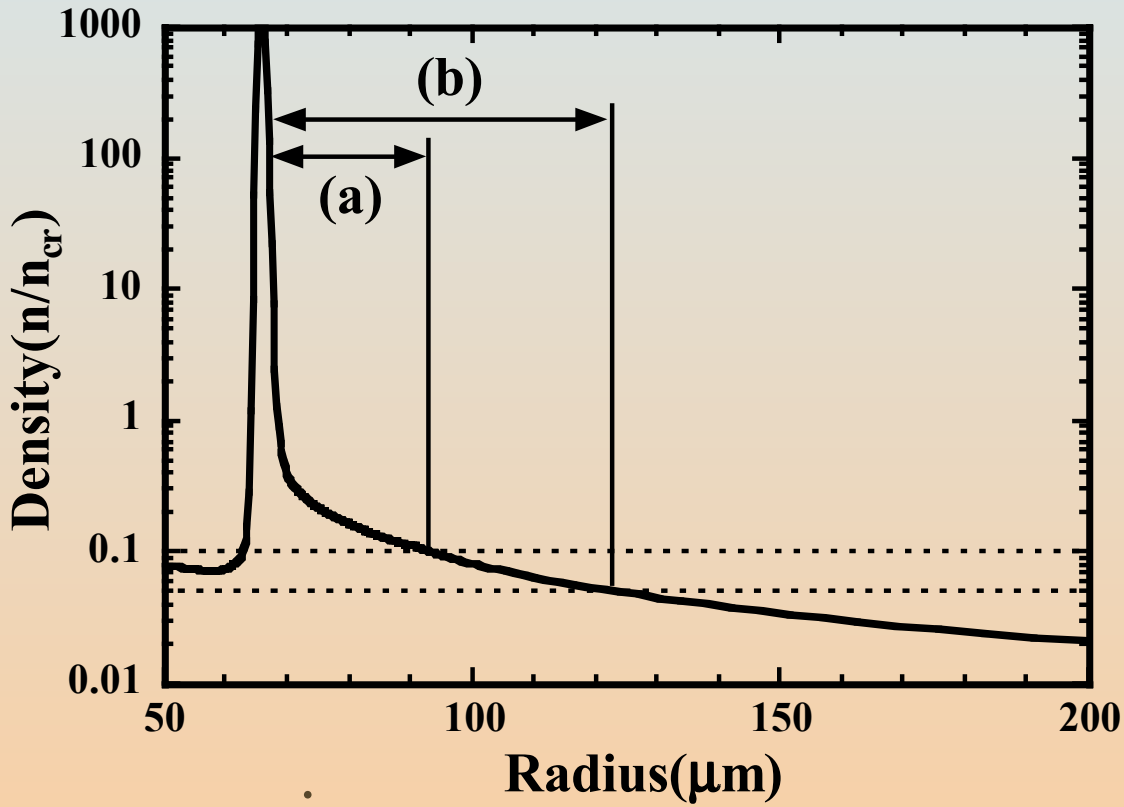

- profiles for comparison
  - (c) linear profile (0-100 n_{cr}/ 25μm)
  - (d) flattop profile (100 n_{cr}/ 20μm)

Simulation Parameters

- ignition laser
  - Gaussian pulse, λ=1.06 [μm]
  - $I\lambda^2 = 1\text{x}10^{20}$ [W/cm^2-μm^2], HWHM = 4λ (50[fsec])
- $n_{max} = 100\ n_{cr}$
  - vary number of electrons per mesh to fit the profile
  - 200 electrons per mesh at $n > 2\ n_{cr}$
  - flattop region of 100 n_{cr} behind the profile (10μm)
- immobile ions
- simulation time
  - 100 ~ 400 [fsec]

Electron Phase Space

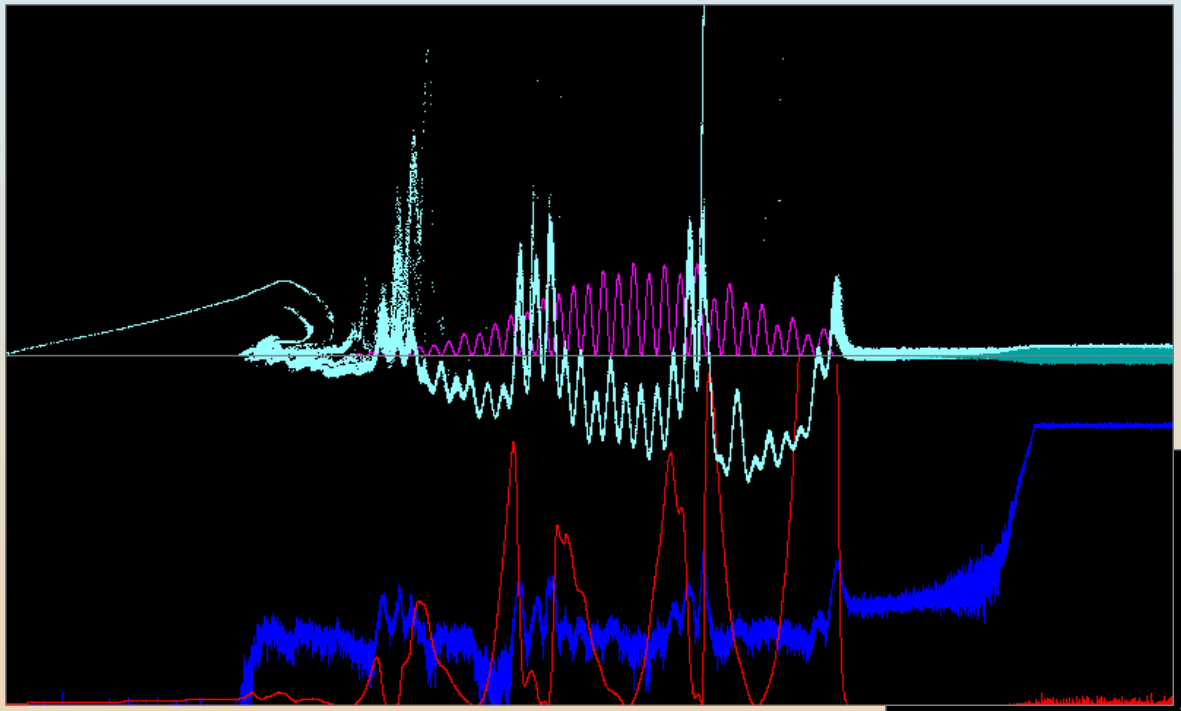

time = 80 [fsec]

- (a) ALE profile cut at 0.1 n_{cr}

time = 120 [fsec]

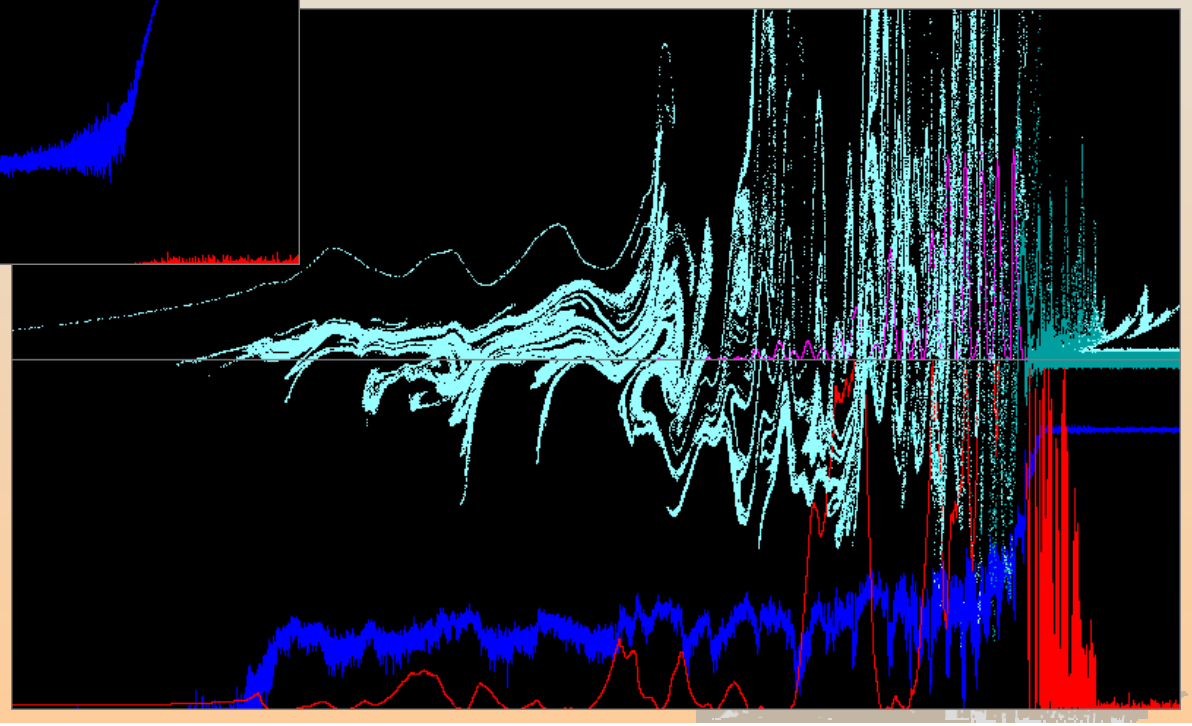

Super Hot Electron Current

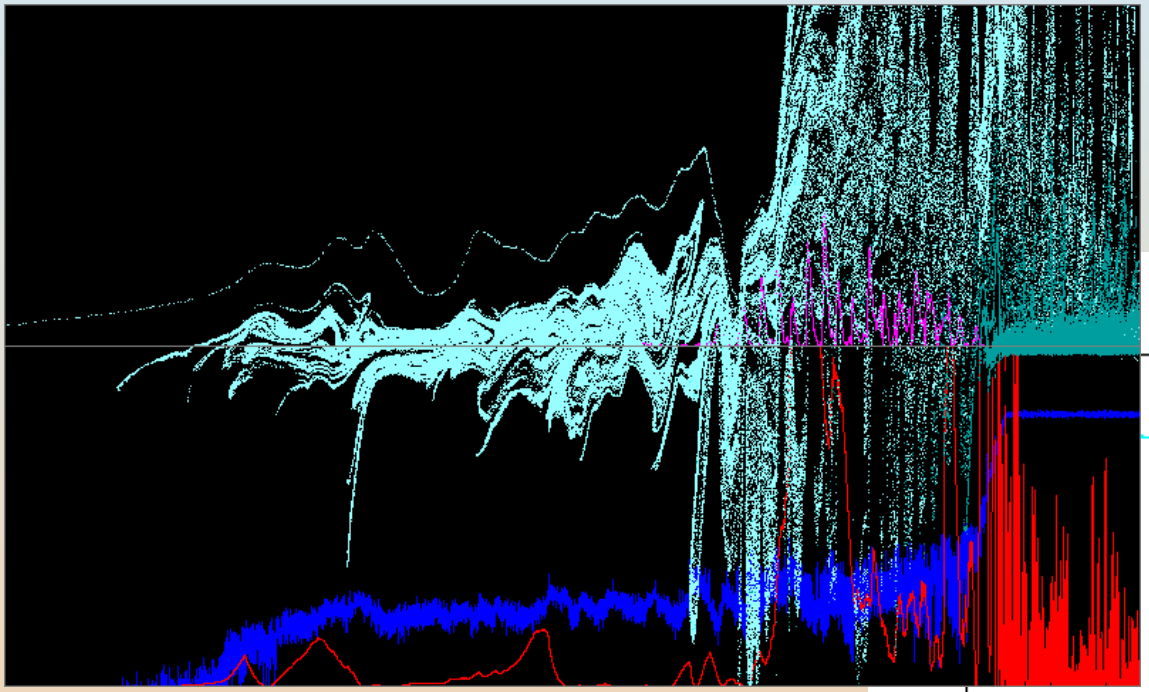

- (a) ALE profile cut at 0.1 n_{cr}

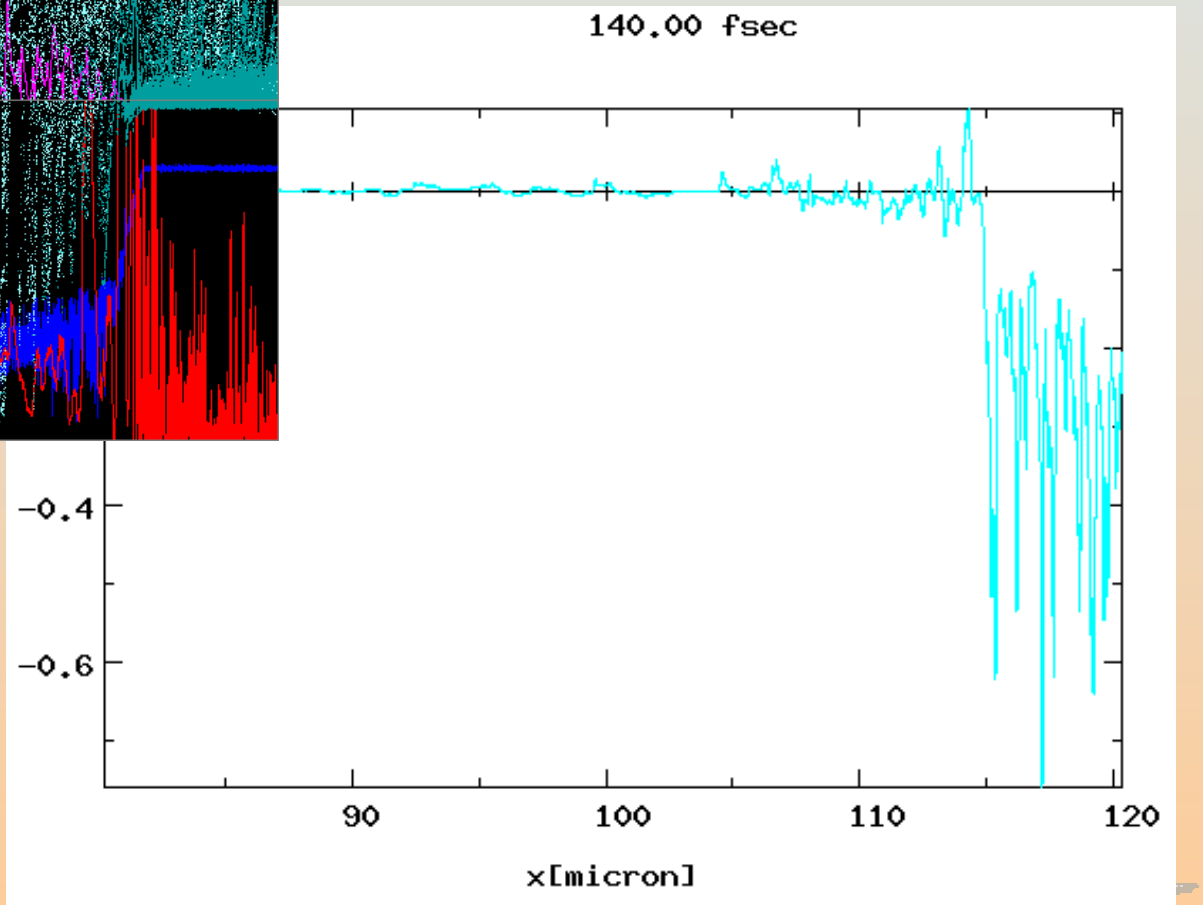

time = 140 [fsec]

Absorption Rate of Ignition Laser

- As the ignition laser can interact with long underdense plasma in ALE profiles, more than 40 % of the energy of the ignition laser can be converted to super hot electrons.

(a) ALE profile cut at 0.1 n_{cr}	40%
(b) ALE profile cut at 0.05 n_{cr}	47%
(c) linear profile	16%
(d) flattop profile	2%

Electron Energy Distributions

- More super hot electrons are generated in ALE profiles.

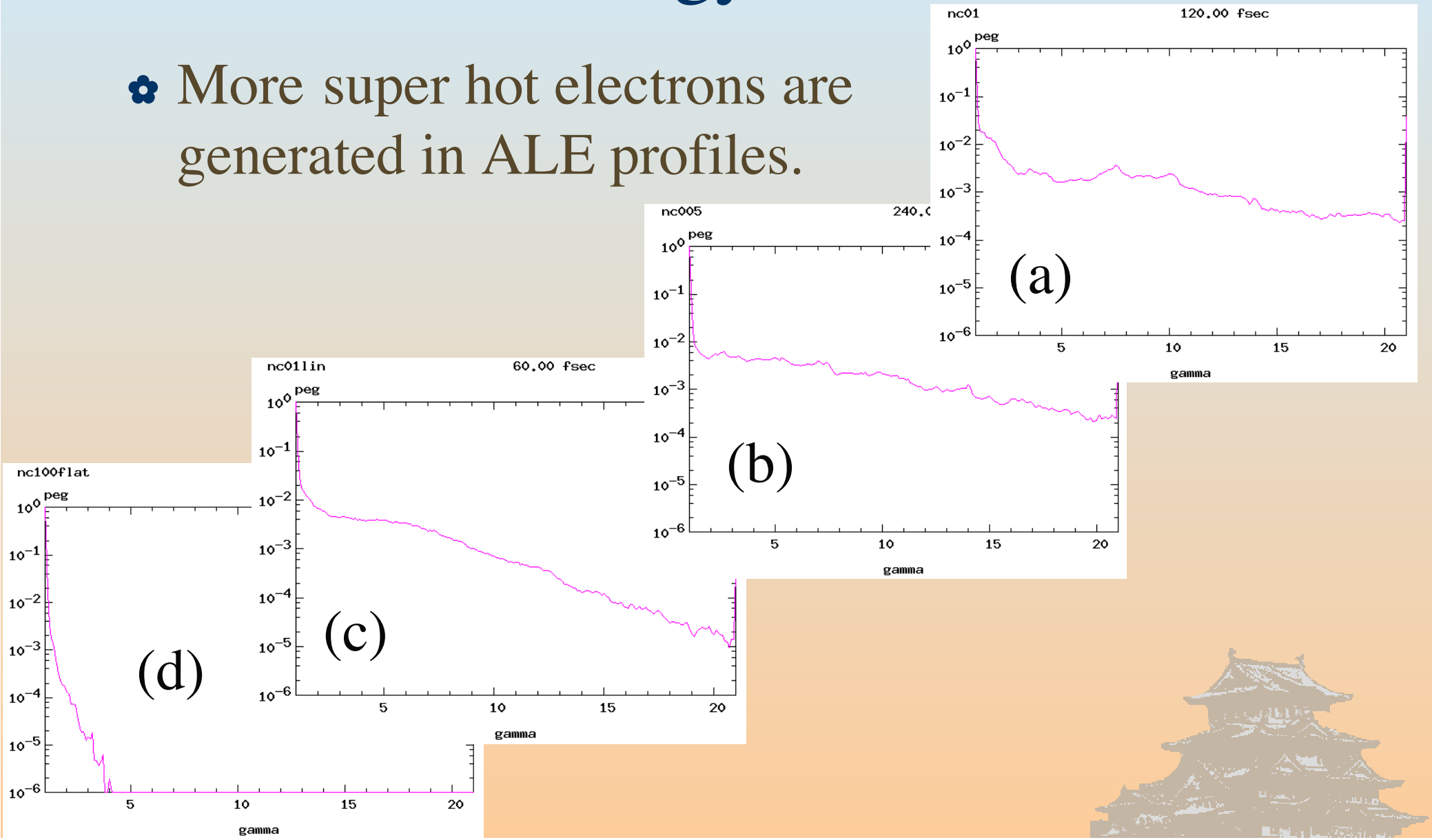

Spectrums of Reflected Laser

- The parametric instabilities in the underdense region can produce spectrum below the laser frequency with ALE profiles

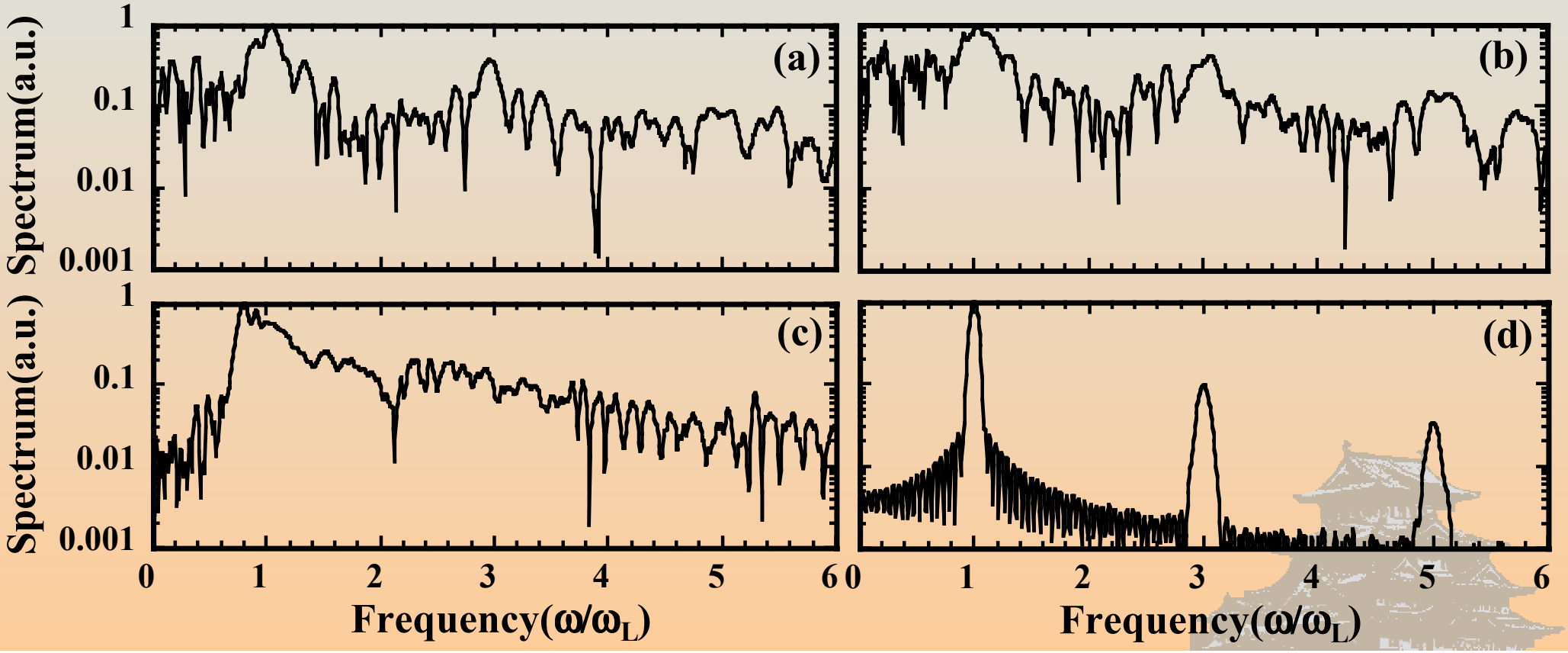

Electron Momentum Space

- Even normal incident and 1-D simulation, twin electron jets were observed only in the dense flattop plasma profile.

$n_{max} = 10\ n_{cr}$

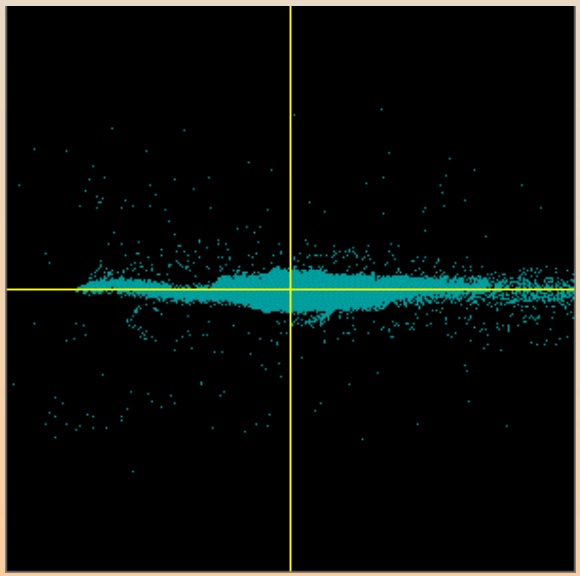

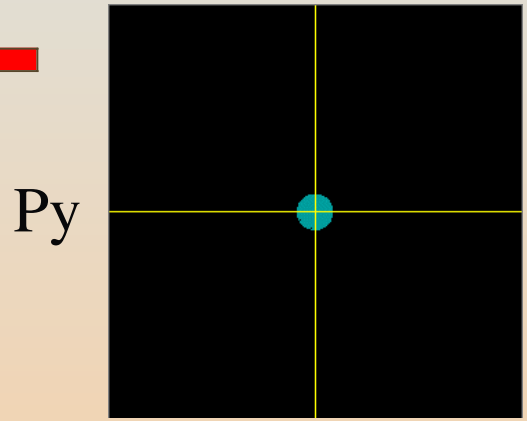

initial

$n_{max} = 100\ n_{cr}$

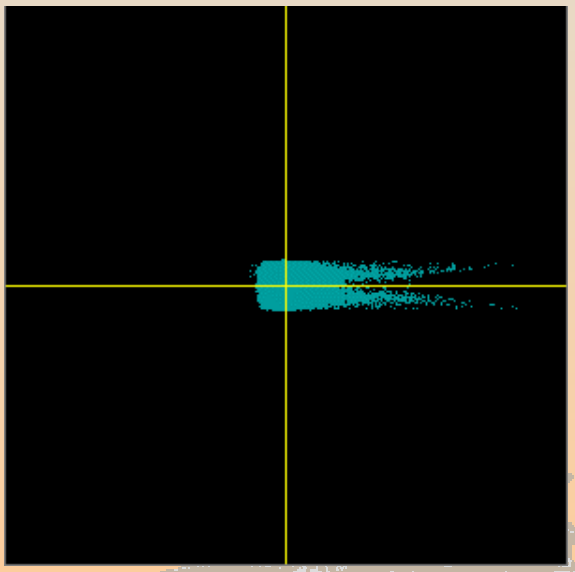

Summary

- We have just started the Fast Ignition Integrated Interconnecting code project.
- The collective PIC code obtains density profile at maximum compression from the ALE hydro code, and we can simulate laser-plasma interactions in a realistic situation.
- We have evaluated absorption rate and reflected laser spectrum and found mush differences between the realistic plasma profile and the conventional plasma profile in PIC simulations.

Direct drive implosion experiments of plastic shell targets with gold cone for fast ignition research

K. Shigemori, R. Kodama, H. Shiraga, K.A. Tanaka, S. Fujioka, T. Muranaka, M. Tanaka, Y. Toyama, K. Mima, H. Nishimura, H. Nagatomo, A. Sunahara, and T. Yamanaka

Institute of Laser Engineering, Osaka University, Osaka, Japan

We report a series of experiments on the implosion of plastic shell targets with gold cone. From previous experiments, the cone-guided shell target indicates excellent performance for efficient heating with additional ultraintense laser [1]. The experiments were done on the GEKKO-XII laser facility at the ILE, Osaka Univ. Nine beams of the twelve beams of the GEKKO-XII drove the CD shell targets with gold cone. We observed implosion dynamics (shell dynamics) with an x-ray streak camera. Also we employed x-ray backlighting with x-ray framing camera to estimate the density of the compressed core. The dynamics of imploded shell were well reproduced by the one-dimensional simulation ILESTA-1D code. Also, the density at the maximum compression timing is 60~70% of the density from the ILESTA-1D.

[1] R. Kodama *et al*., Natute **412**, 798 (2001); R. Kodama *et al*., Nature **418**, 933 (2002).

Collisionless electron transport and ion acceleration in laser-solid interactions

Luís O. Silva

S. Amorini, M. Marti, J. R. Davies, R. A. Fonseca
IST, Lisbon, Portugal

C. Ren, F. Tsung, W. B. Mori
UCLA

J.-C. Adam, A. Héron
École Polytechnique

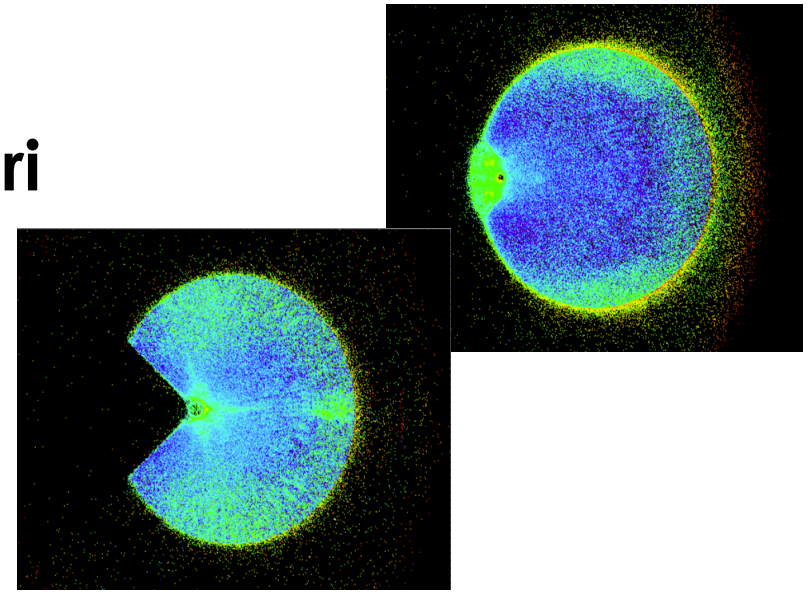

This work was partially supported by FCT (Portugal) and DOE

presented at the FIW2002, St. Pete's Beach, Florida, USA, November 19, 2002

Outline

- Collisionless instabilities of beams
- The Weibel instability of finite width beams
- Coupling between the purely transverse and the purely longitudinal unstable modes (filament tilting)
- Ion acceleration beyond the 10^{20} W/cm^2: shock acceleration
- PacMan/cone/wedge targets vs cylinder

  preliminary 2D PIC simulations
- Conclusions

Collisionless instabilities of beams

- General theory: Watson, Bludman, Rosenbluth (1960)
- Weibel/filamentation instability:

  $\gamma \sim (n_b/n_0)^{1/2}$

  $k_\perp \sim \omega_{pe0}/c$ ($T \neq 0$)

  Pinching/filamentation

- Two-stream instability:

  $\gamma \sim (n_b/n_0)^{1/3}$

  $k_\parallel \sim \omega_{pe0}/v_b$

  Longitudinal bunching

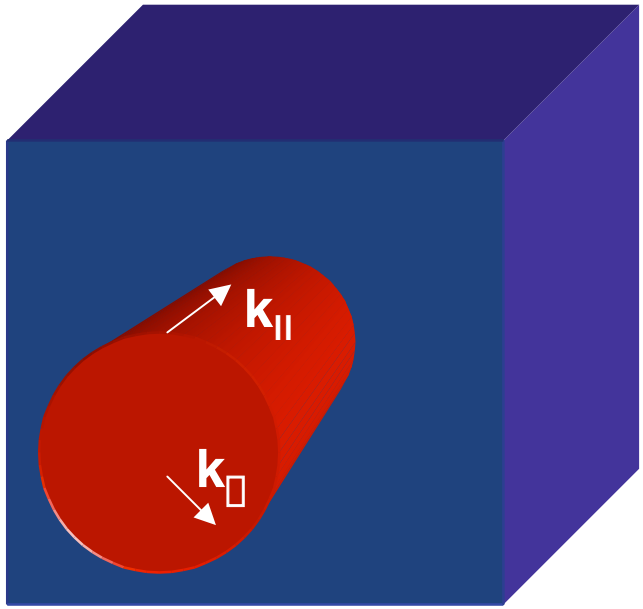

- In general, multidimensional electromagnetic beam-plasma instability will be a combination of transverse and longitudinal unstable modes

The Weibel instability of finite width beams

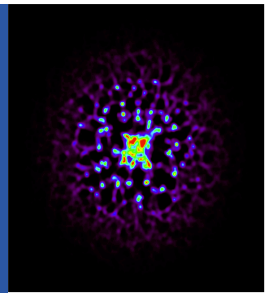

Luís O. Silva @ Fast Ignitor Workshop 2002, Florida, USA, November 19, 2002

Finite width beams with $I > I_{Alfven}$

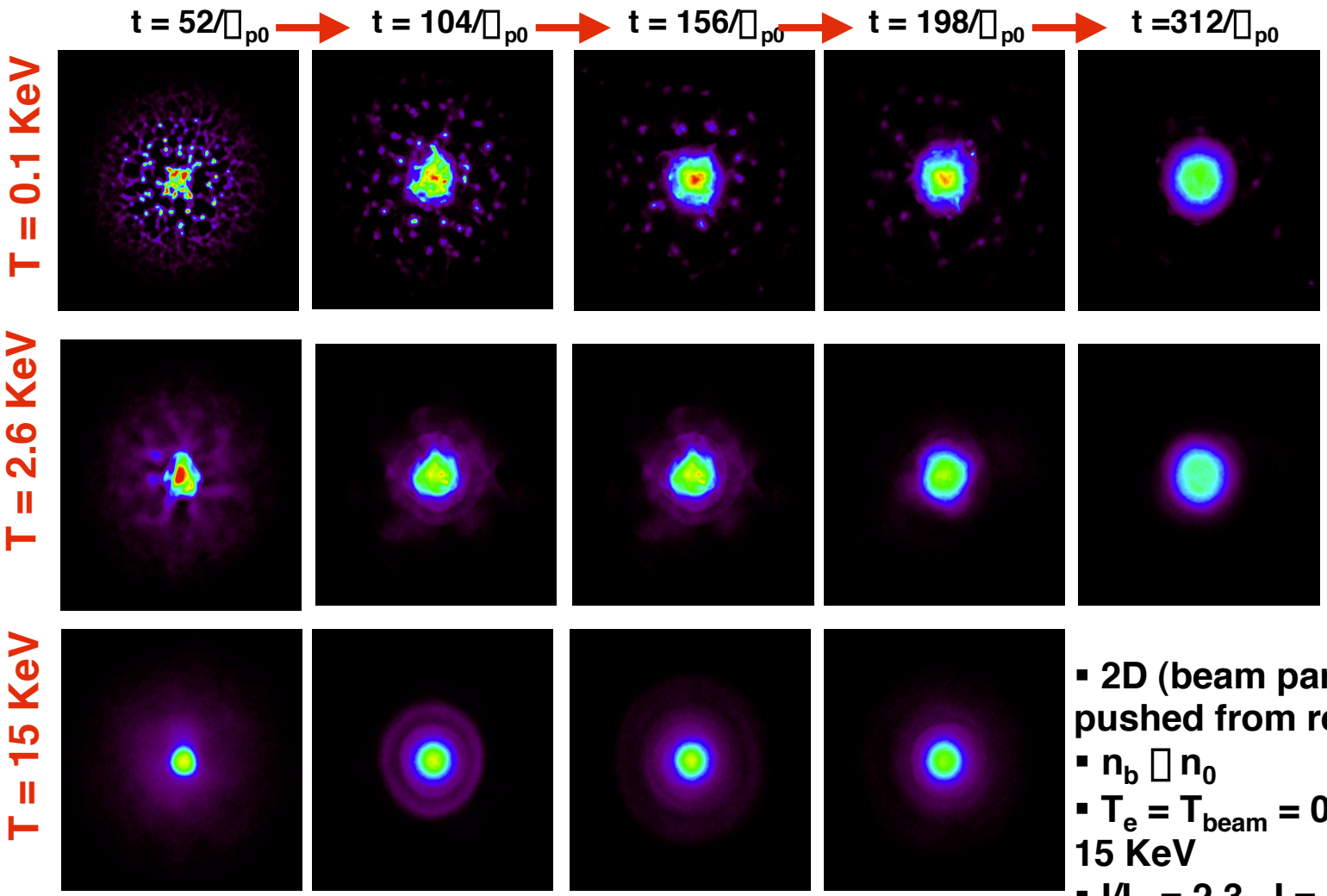

- 2D (beam particles are pushed from rest to $\gamma_{beam} \sim 7$)
- $n_b \sim n_0$
- $T_e = T_{beam}$ = 0.1 KeV, 2.6 KeV, 15 KeV
- $I/I_A = 2.3$, I = 270 KA @ Intensity ~ 5×10^{19} W/cm^2 and $n_0 = 10^{22}$ cm^{-3}

Beam hosing

- Ion channel is formed due to total evacuation of the background plasma electrons from the beam region

Plasma electrons **Plasma ions**

T = 0.1 KeV

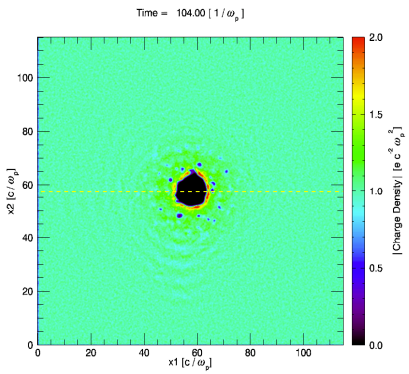

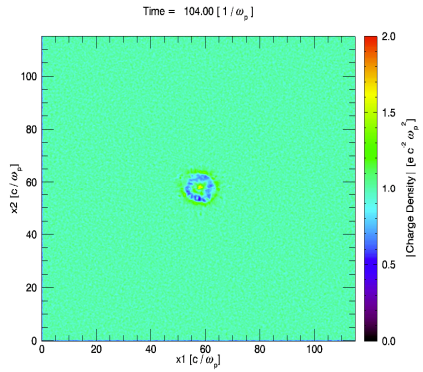

T = 15 KeV

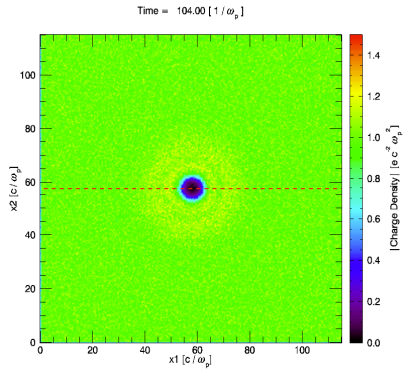

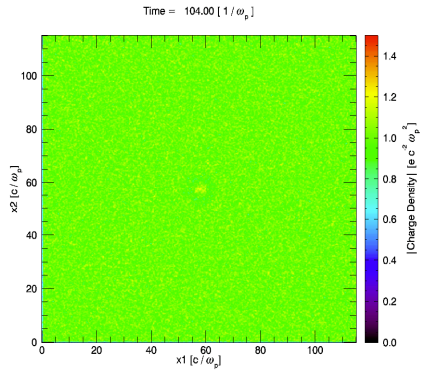

- Conditions for beam hosing are set up before ion motion becomes important

Filament tilting

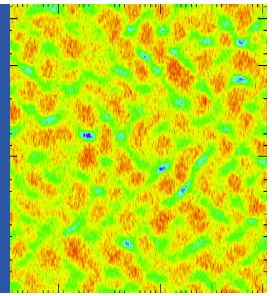

Three-dimensional PIC simulations I

- **Osiris***

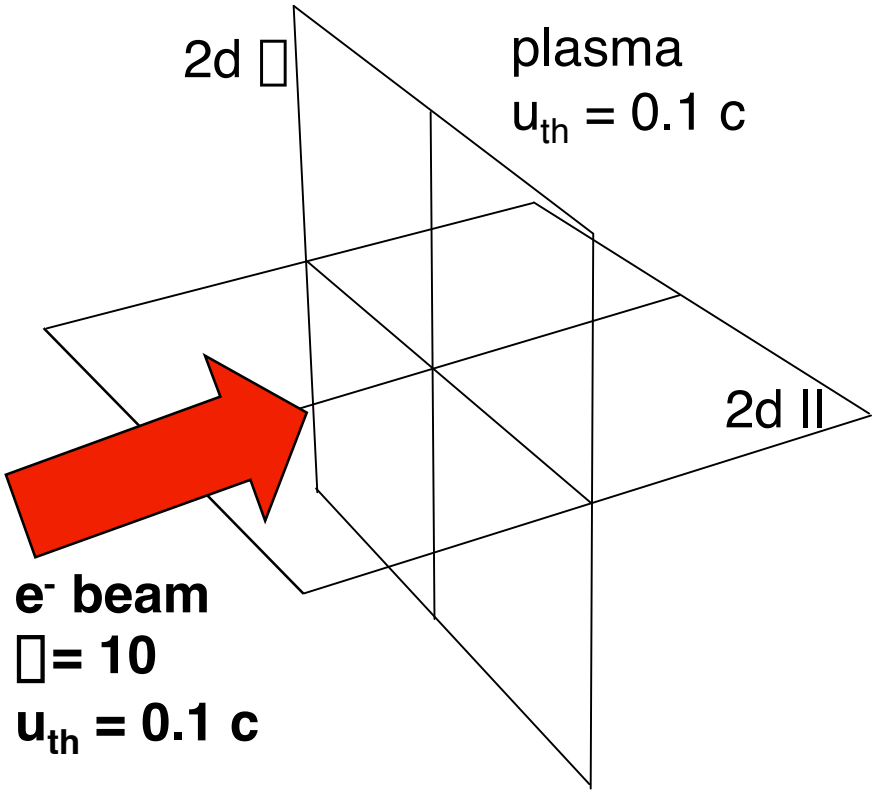

e^- beam
γ = 10
u_{th} = 0.1 c
n_b/n_0 = 0.1

Periodic system
Current and charge neutral
Moving ions

- 3D runs
  - $(128)^3$ cells
  - $(12.8\ c/\omega_{p0})^3$
  - $\omega_{p0} t_{max} = 500$
  - 16 particles/(species·cell)

- 2D runs (∥ and ⊥)
  - (512 × 128) cells
  - $(51.2 \times 12.8)\ (c/\omega_{p0})^2$
  - $\omega_{p0} t_{max} = 500$
  - 16 particles/(species·cell)

*R. G. Hemker, UCLA PhD Thesis, 2000; R.A. Fonseca et al, LCNS 2002

Three-dimensional PIC simulations II

Beam density @ $t = 62.4/\omega_{pe0} = 7.5\ \tau_{weibel}$

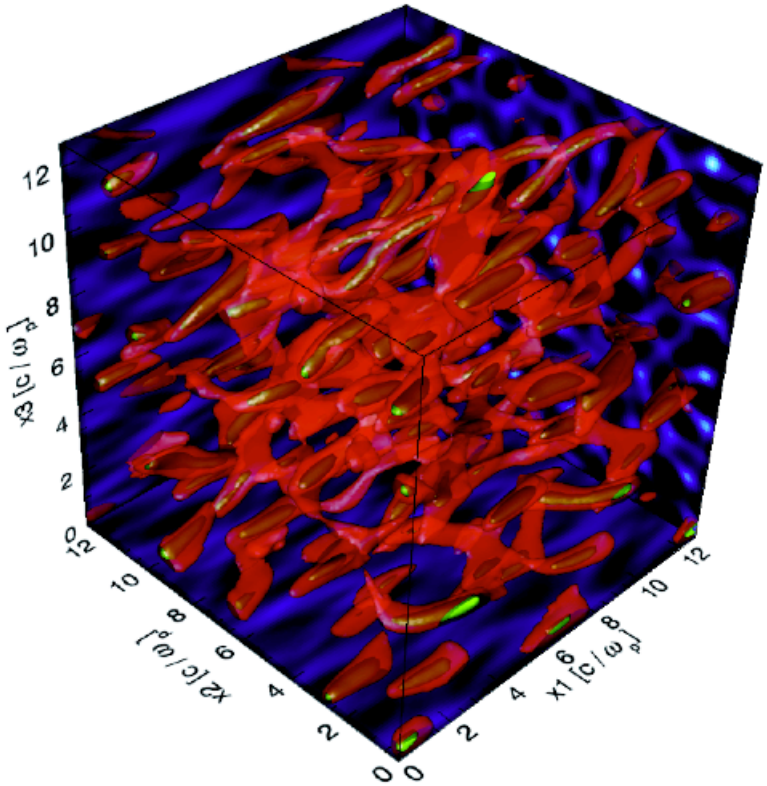

Green = 1.15 n_{e0}; Red = 0.53 n_{e0}

FFT

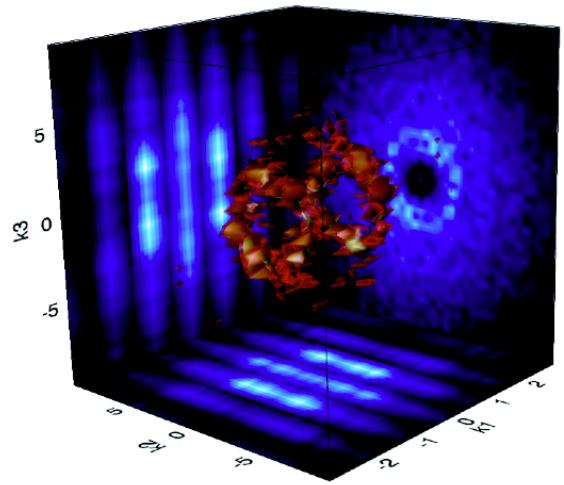

Green = 40%; Red = 27.5%

Fastest growing mode

$k_1 \sim 1$ $k_\perp \sim 3$

$\theta_{tilt} \sim 18.4°$

Covariant fluid theory I

$$\frac{\partial T_i^{\alpha\beta}}{\partial x^\beta} = m_i \bar{n}_i F^\alpha$$ **Covariant fluid equations** $F^\alpha \equiv$ Lorentz 4-force

$$T^{\alpha\beta} = p\,\eta^{\alpha\beta} + (p+\rho)U^\alpha U^\beta$$ **Energy-momentum stress tensor**

3D representation

$$(\partial_t + \mathbf{v}\cdot\nabla)\mathbf{v} = \frac{qnc^2}{\gamma^2(p+\rho)}\left[\mathbf{E} + \frac{\mathbf{v}}{c}\times\mathbf{B}\right] - \frac{qn}{\gamma^2(p+\rho)}(\mathbf{v}\cdot\mathbf{E})\mathbf{v} - \frac{c^2}{\gamma^2(p+\rho)}\left[\nabla p + \frac{\mathbf{v}}{c^2}\partial_t p\right]$$

+ Maxwell's equations

Key issue: relativistic equation of state $p(T,n)$ **and** $\rho(T,n)$

Covariant fluid theory II

$$U^{\alpha} = \int u^{\alpha} \frac{f(u)}{(1+\mathbf{u}\cdot\mathbf{u})^{1/2}} d\mathbf{u}$$ **Fluid proper velocity**

$$T^{\alpha\beta} = mc^2 \int u^{\alpha} u^{\beta} \frac{f(u)}{(1+\mathbf{u}\cdot\mathbf{u})^{1/2}} d\mathbf{u}$$ **Energy-momentum stress tensor**

In the rest frame of the fluid: $T^{11} = p \qquad T^{00} = \rho$

For a waterbag $f(u)$ **:**

$$\frac{p}{n_0 mc^2} = \frac{1}{8u_0^3}\left\{u_0\tilde{n}\left(1+u_0^2\tilde{n}^2\right)^{1/2}\left(2u_0^2\tilde{n}^2-3\right)+3\,\mathrm{arcsinh}\left(u_0\tilde{n}\right)\right\} \qquad \tilde{n} = \left(\bar{n}/n_0\right)^{1/3}$$

$$\rho = n_0 mc^2\left[\tilde{n} + \frac{1}{2}u_0^2\tilde{n}^{5/3}\right] - p$$

Tilted filamentation of relativistic electron beams I

Multidimensional (2D) electromagnetic beam-plasma instability ($T_b \neq 0$)

$u_b = 10$
$u_0 = 0.22$
$n_b = 0.1\ n_0$

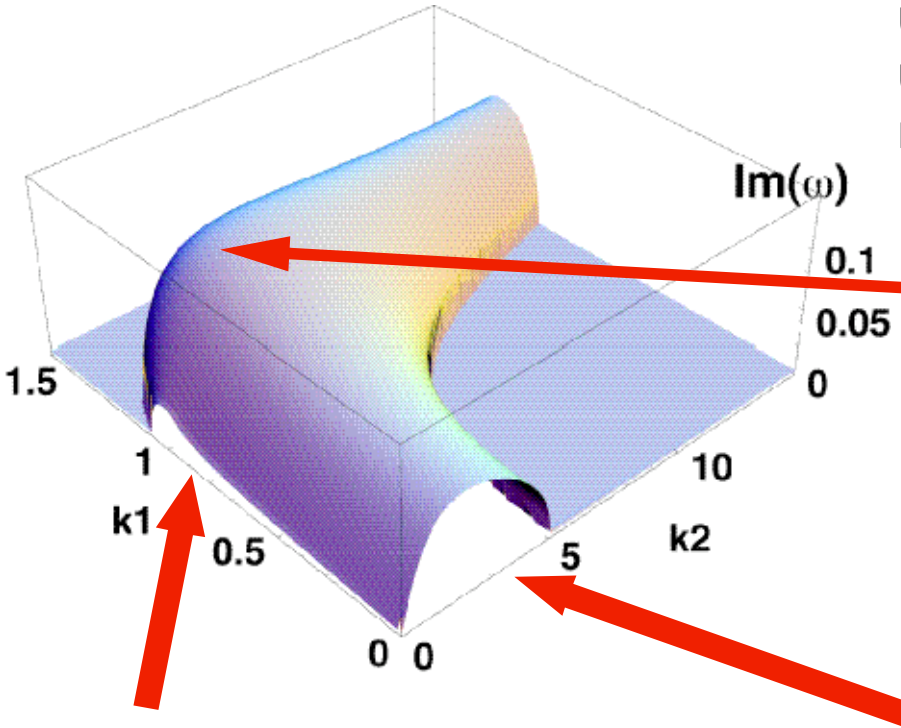

Fastest growing mode
$k_{1mx} \sim 1 \quad k_{2mx} \sim 3$

$\theta_{tilt} = \arctan(k_{1mx}/k_{2mx})$
$\theta_{tilt} \sim 18.4°$

two-stream instability
(similar to fluid theory)

Weibel instability
(similar to waterbag kinetic)

Tilted filamentation of relativistic electron beams II

Maximum growth rate

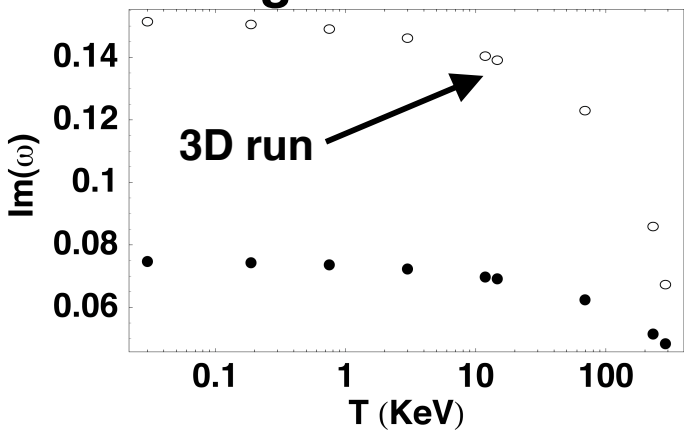

$$\frac{T}{mc^2} = \int \mathbf{u}\cdot\mathbf{u}\,\frac{f(u)}{(1+\mathbf{u}\cdot\mathbf{u})^{1/2}}\,d\mathbf{u}$$

Tilting angle

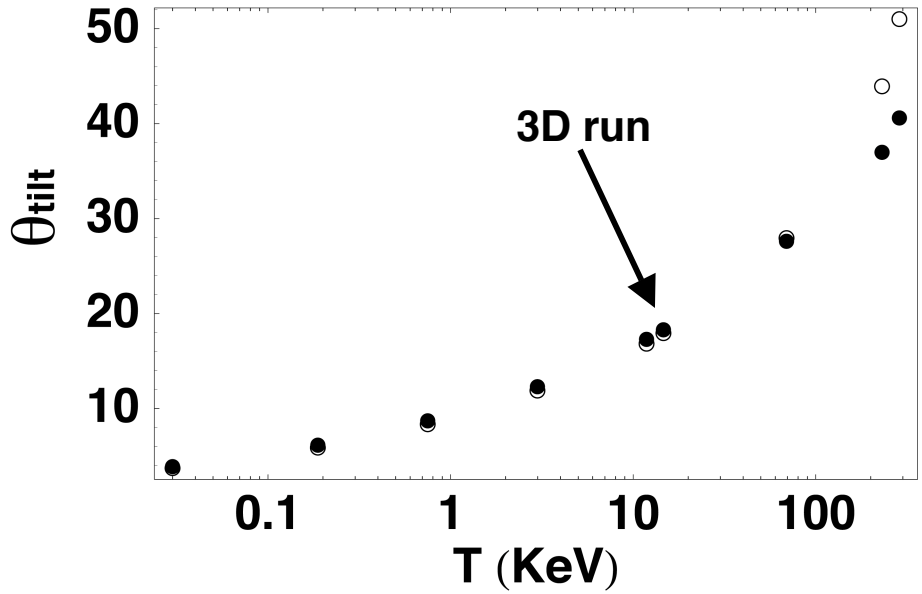

$u_b = 10$
$n_b = 0.1\ n_0$ o
$n_b = 0.0125\ n_0$ •
Cold plasma

$k_1 \sim \omega_{pe0}/c$ & $k_2 \sim$ as $T\uparrow \Rightarrow \theta_{tilt}\uparrow$

Comparison theory-simulation I

Electron beam spatial structure

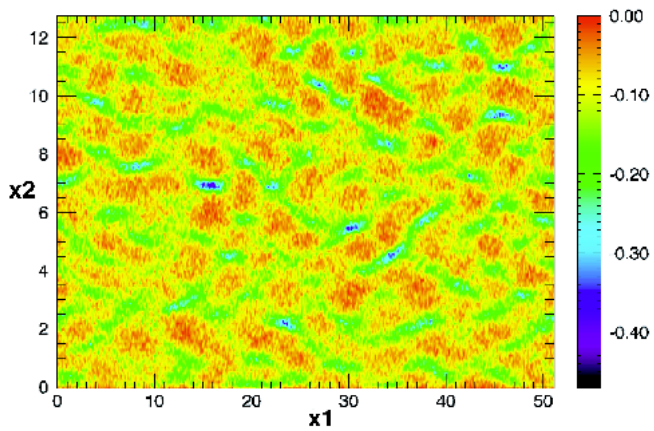

Beam

FFT

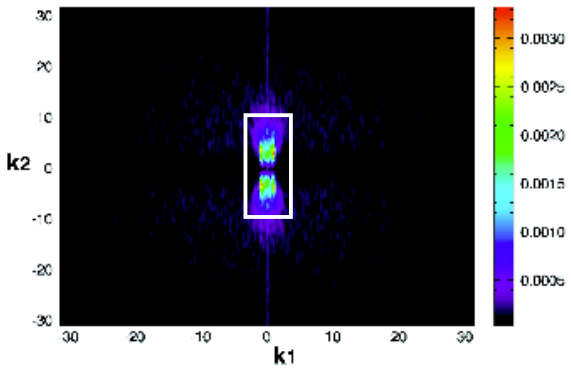

FFT (zoom)

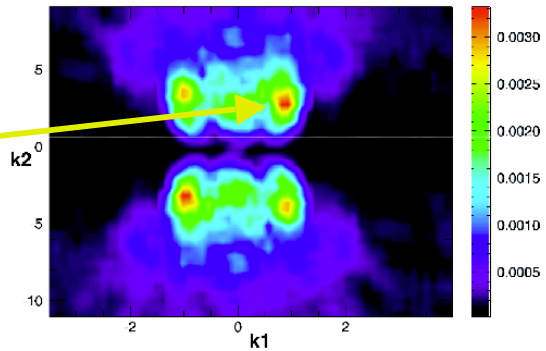

$k_{1mx} \sim 1$, $k_{2mx} \sim 3.0$

Typical spraying angle ~ 18°

2D II runs
(512 □ 128) cells
(51.2 □ 12.8) $(c/\square_{p0})^2$
$\square_{p0} t_{max} = 500$
16 particles/(species□cell)

Comparison theory-simulation II

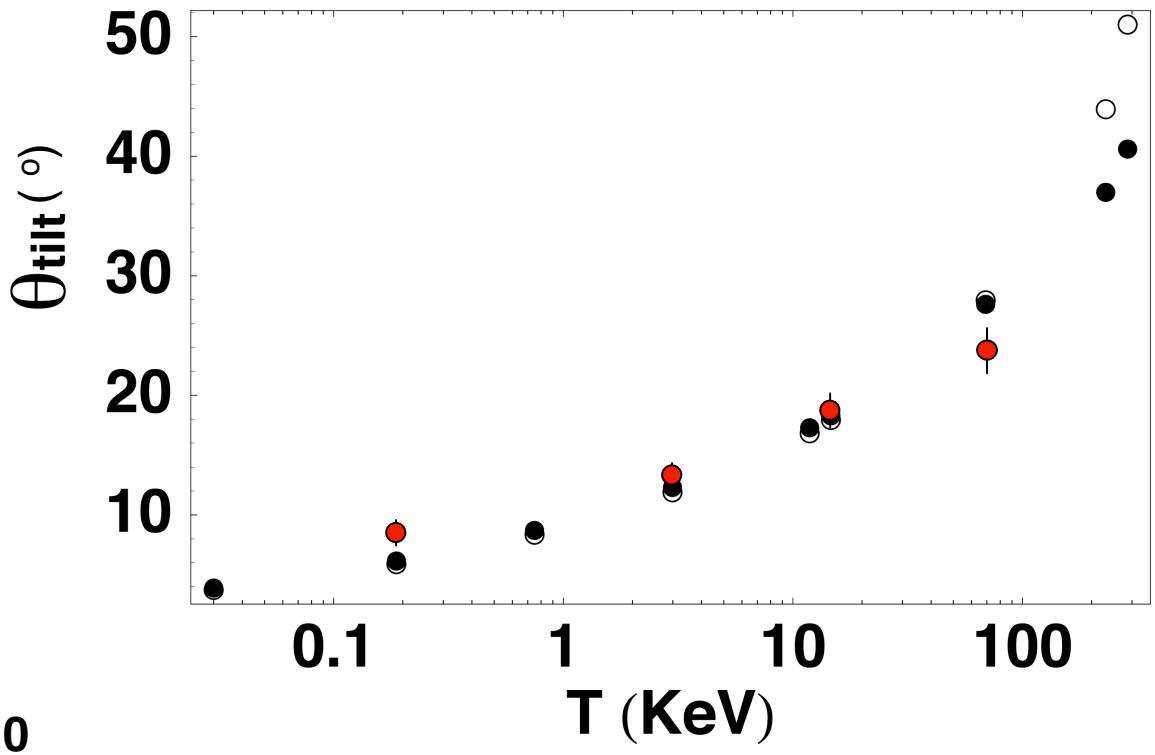

$u_b = 10$

$n_b = 0.1\ n_0$ ○

$n_b = 0.0125\ n_0$ •

Simulation $n_b = 0.1\ n_0$ ●

2D II runs

(512 □ 128) cells

(51.2 □ 12.8) $(c/\square_{p0})^2$

$\square_{p0} t_{max} = 500$

16 particles/(species□cell)

Proton shock acceleration in thin targets

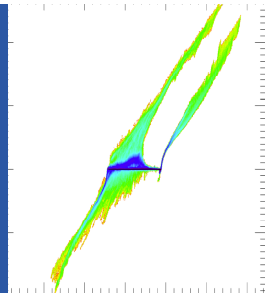

Simulation Details

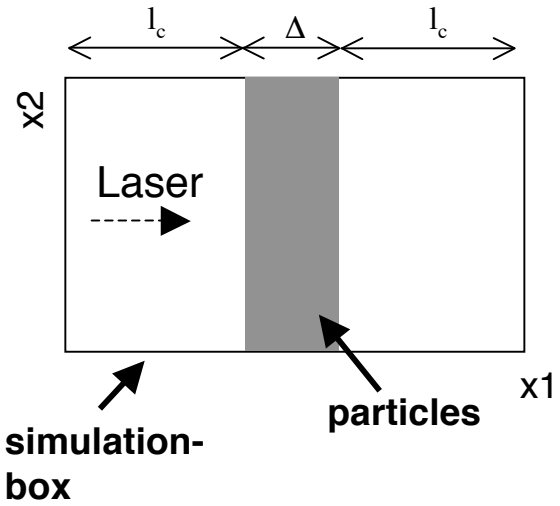

Δ: 1 - 40 μm
l_c: 20-80 μm
n_0 / n_{cr}: 10 - 90

a_0: 0.25 - 20
λ_{laser}: 1 μm
L_{pulse}: 100 fs (FWHM)
Laser spot size: 6 μm

1D (typical values)
- 36000 x 3 Cells
- 32 particles / cell

2D (typical values)
- 3000 x 2000 Cells
- 4 x 4 particles / cell

Proton shock acceleration

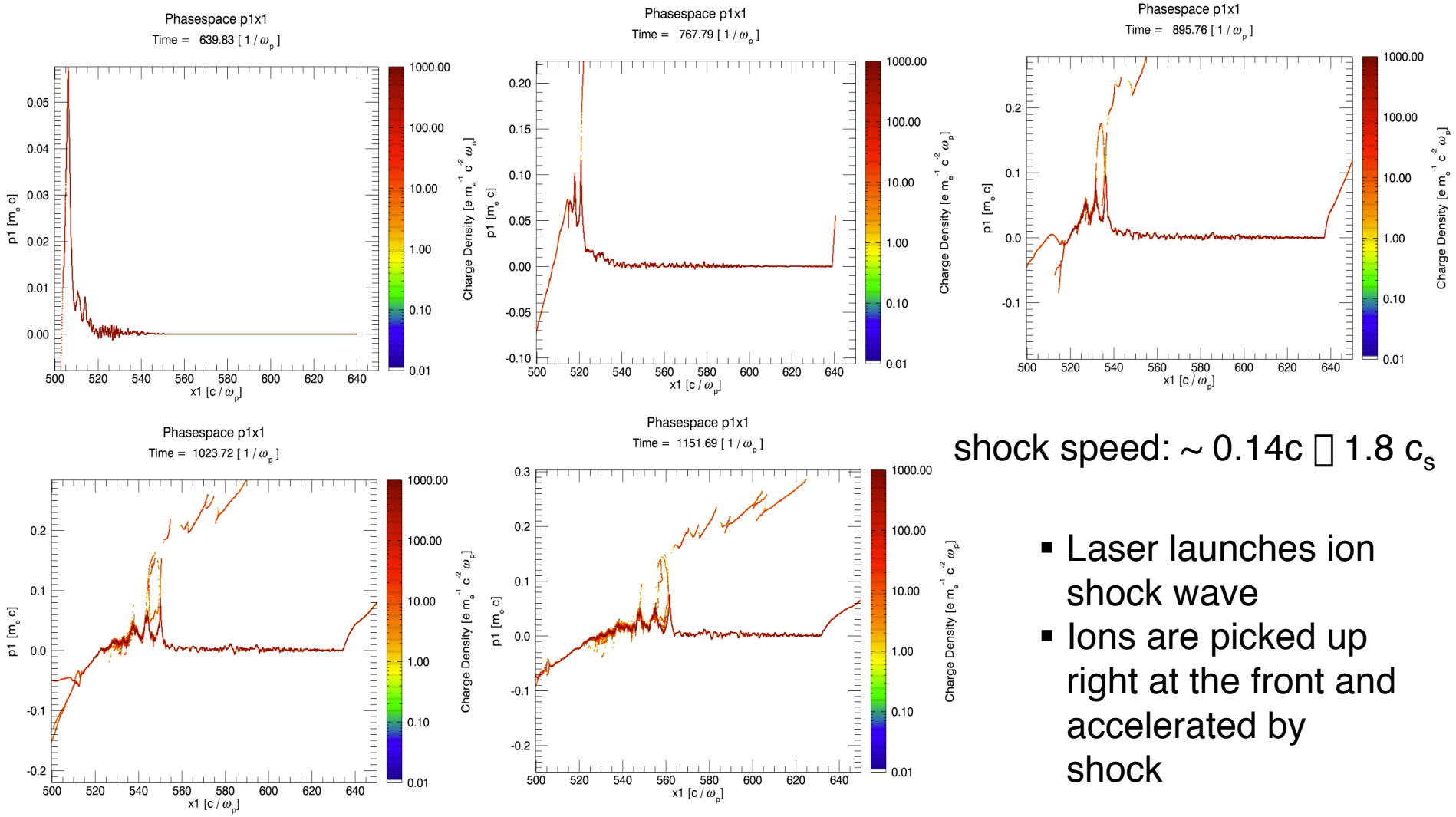

shock speed: ~ 0.14c □ 1.8 c_s

- Laser launches ion shock wave
- Ions are picked up right at the front and accelerated by shock

ion phase space p1x1

Maximum energy of protons

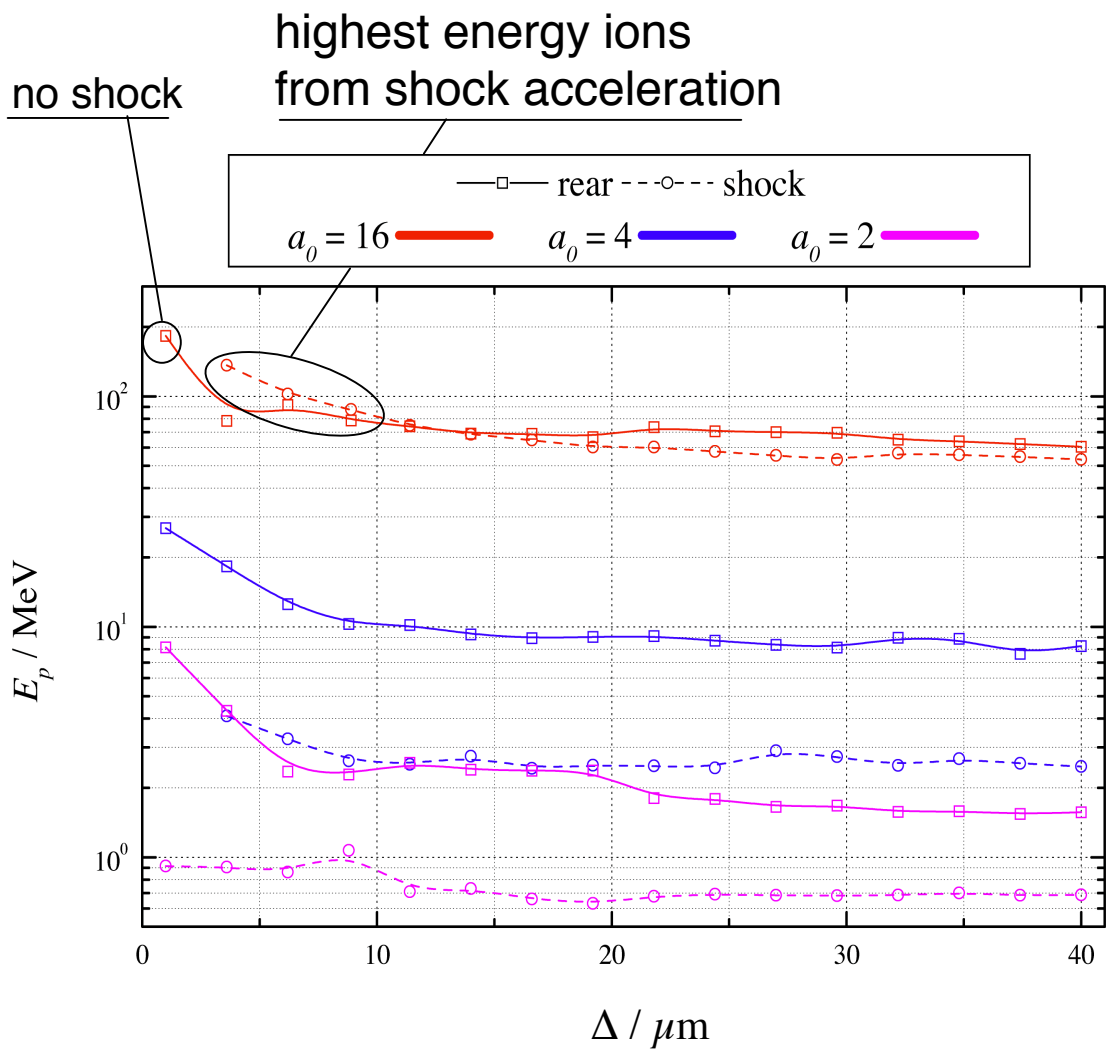

- highest energy in forward direction
- energy measured at 80 μm from target

Acceleration mechanisms

No shock

Shock with higher energy than rear

Shock with lower energy than rear

Diffusive/sheath acceleration

Ion phase space p1x1

shock acceleration

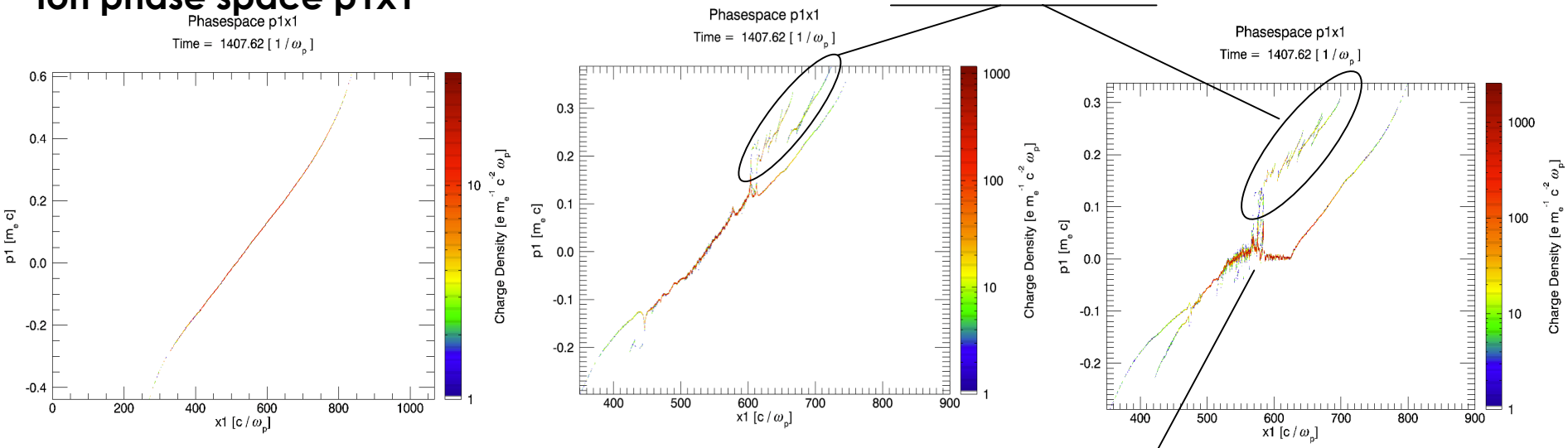

a0 = 16
Δ = 1 μm

a0 = 16
Δ = 6.2 μm

a0 = 16
Δ = 8.8 μm

As seen recently in
B. Lasinski et al, this meeting
Y. Sentoku et al (2001,2002)

Shock acceleration vs sheath acceleration

No shock

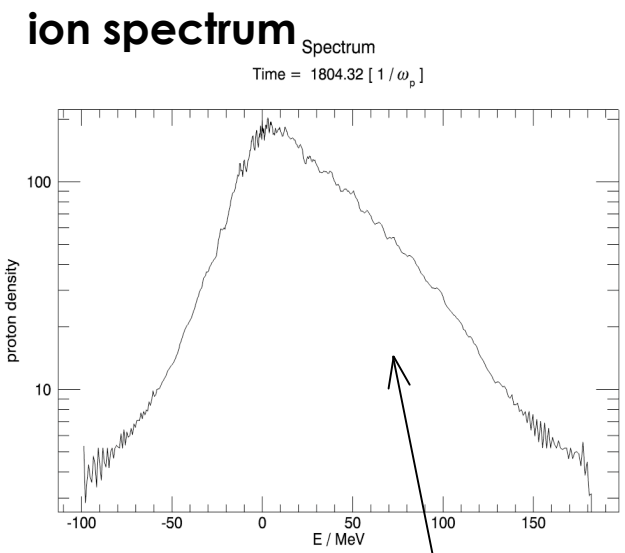

a0 = 16
Δ = 1□m

Shock with higher energy than rear

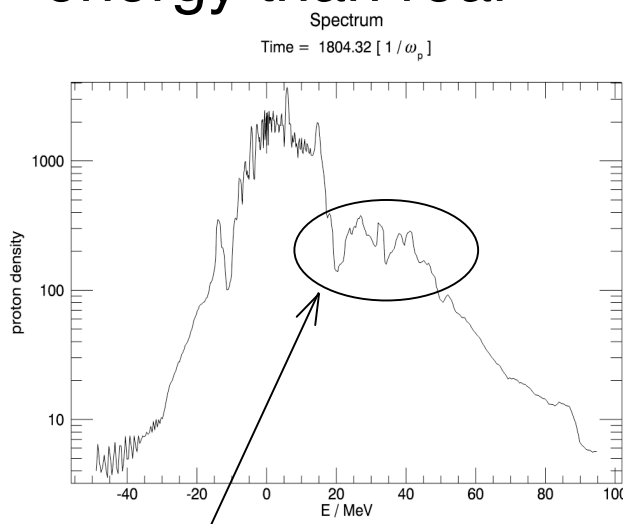

a0 = 16
Δ = 6.2 □m

Shock with lower energy than rear

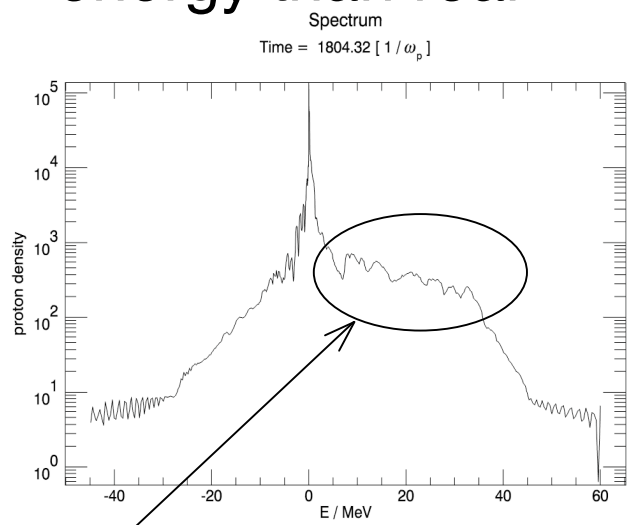

a0 = 16
Δ = 8.8 □m

- with shock, plateau on spectrum is observed
- without shock, spectrum close to symmetric

Signature for proton shock acceleration in ion spectrum

absence of shock

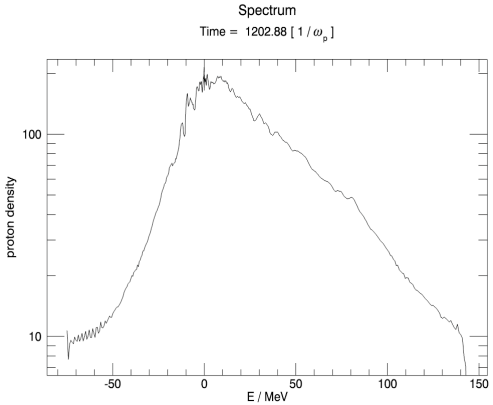

Ion spectrum

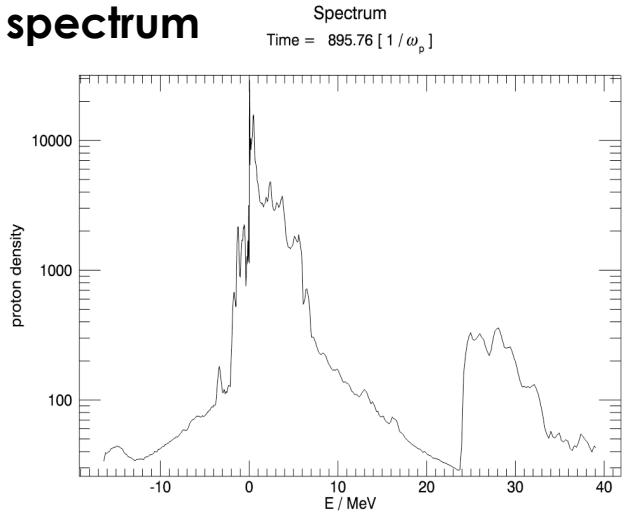

Plateau on fast ions

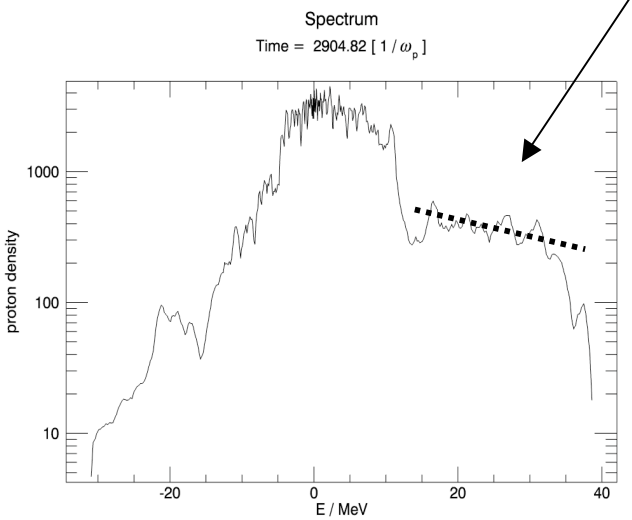

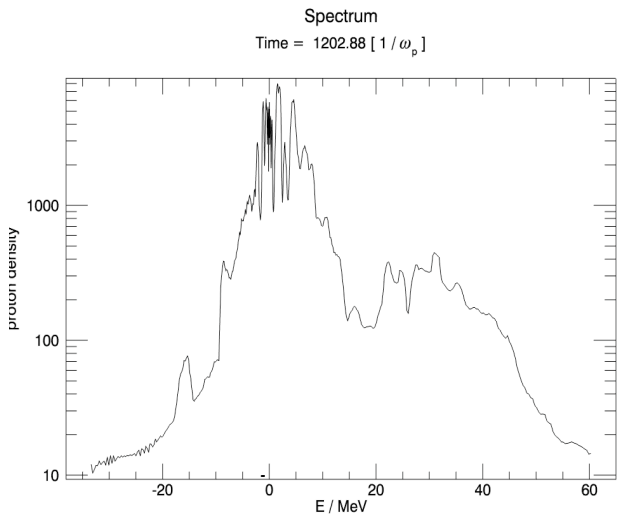

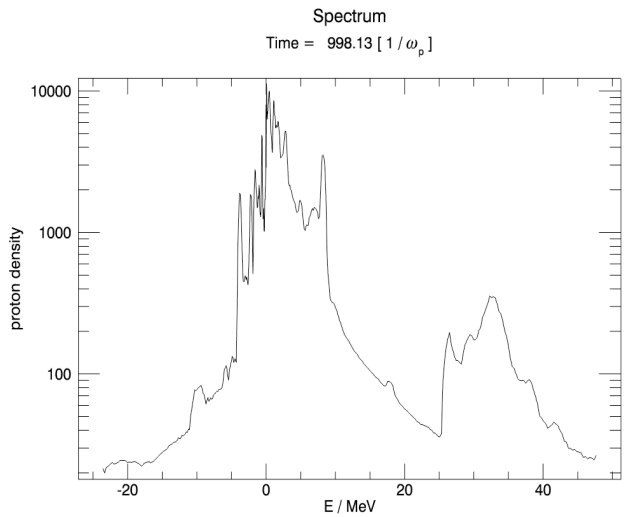

time

2D evidence for strong shock acceleration

Electric field |E|

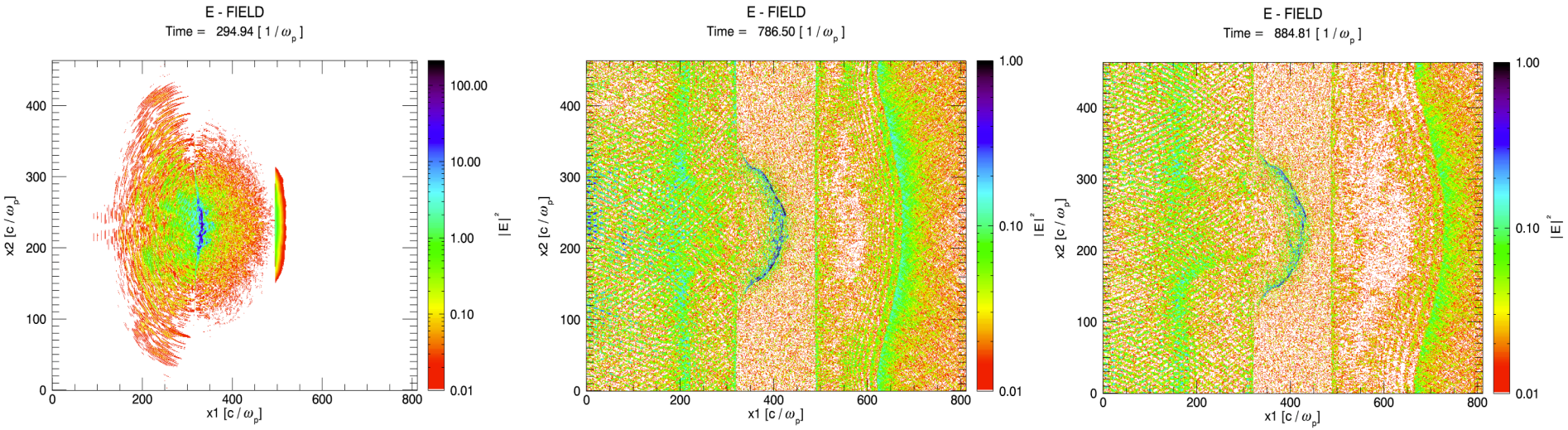

ion phase space p1x1

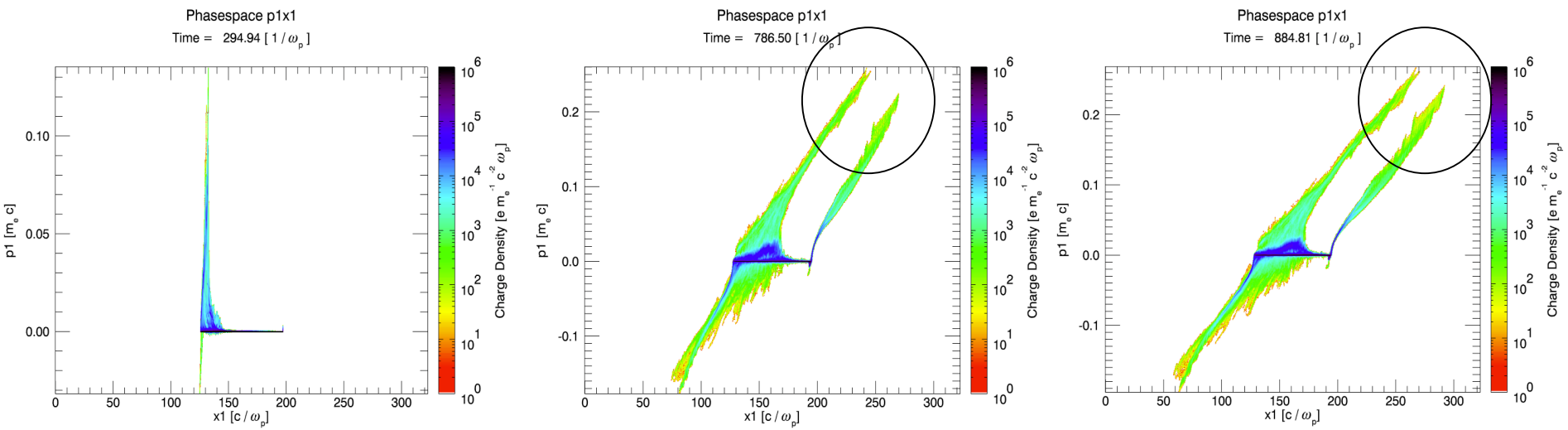

time

PacMan vs Cylinder

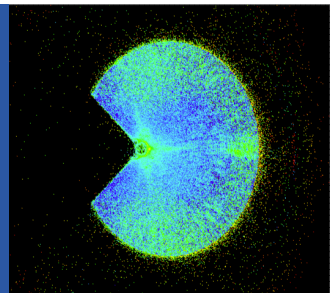

Simulation details

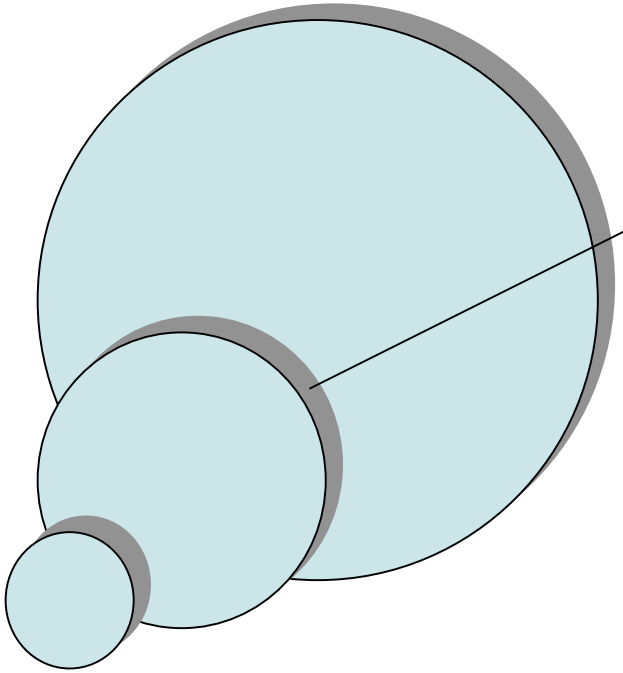

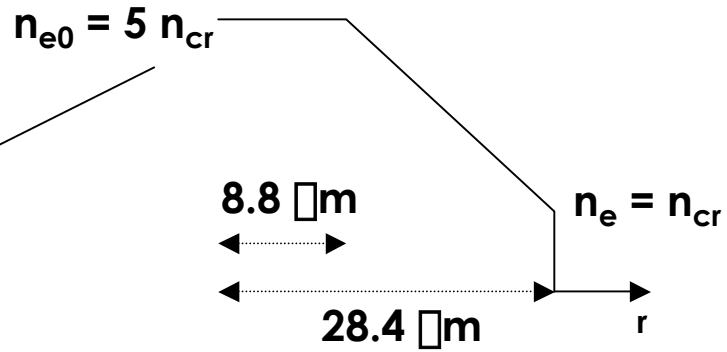

(J.-C. Adam, A. Héron, 2001)

$I_{laser} = 10^{19}$ W/cm^2

τ_{laser} ~ 80 fs (FWHM)

σ_{laser} = 1 μm

Length of run ~ 500 fs

Cone angle = 60°

Tip of cone at 5 n_{cr} surface

Box size 100 μm × 76 μm

$\Delta x = \Delta y = 0.3\ c/\omega_{pe0}$

16 particles/(cell × species)

Moving ions

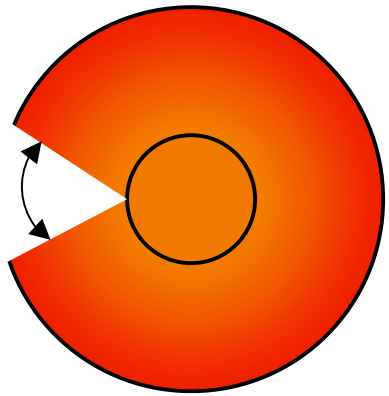

Energy evolution

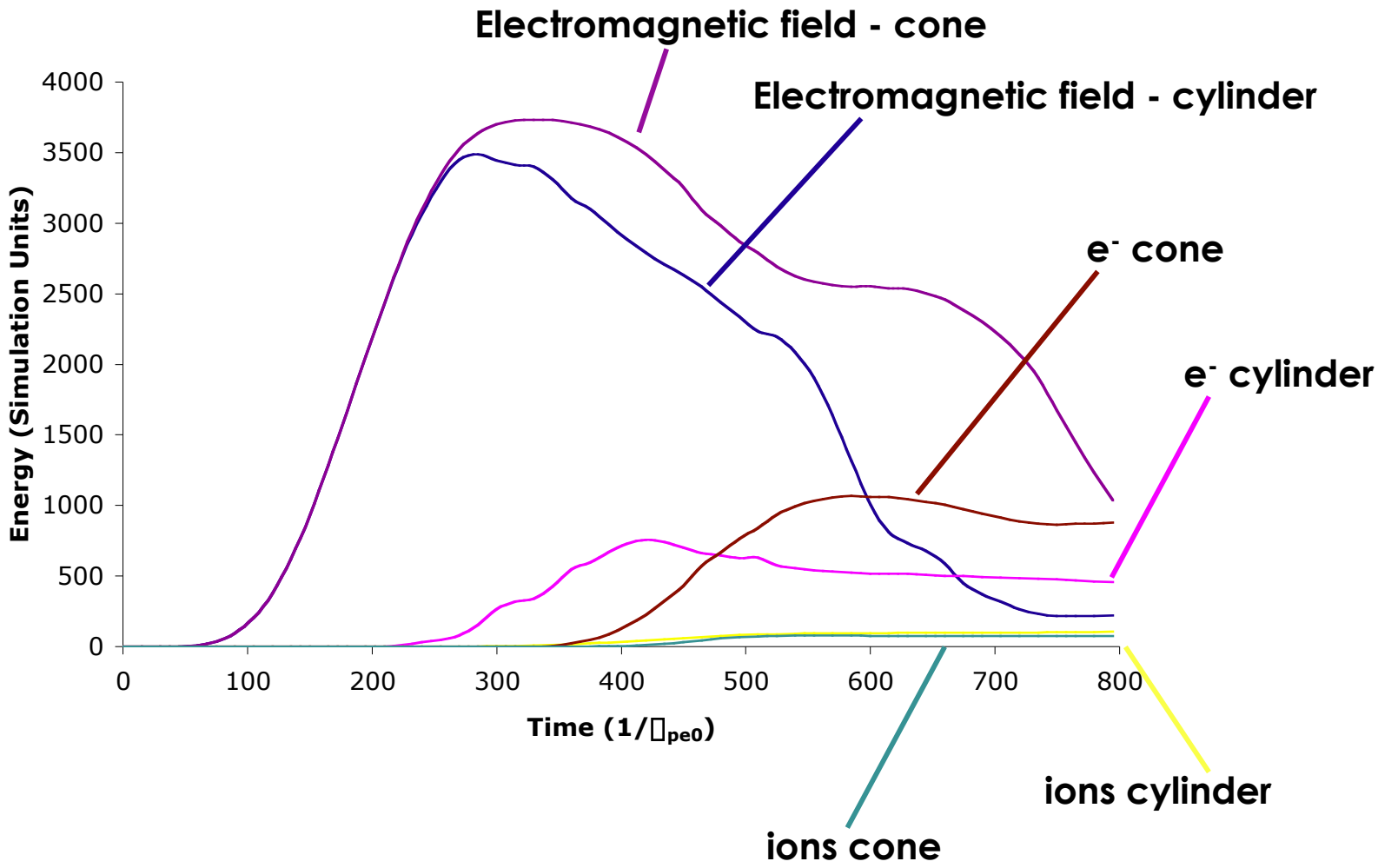

Conclusions

- Tilted filamentation observed in experiments (K. Krushelnick et al, this meeting) and simulations (J.-C. Adam et al, this meeting) is seeded at the collisionless time scale by the coupling of transverse and longitudinal unstable modes of electromagnetic beam-plasma instability
- At high intensities (~ 10^{20} W/cm^2) proton shock acceleration plays a significant role
- Very preliminary results PacMan seems to help:
  - Twice the energy in e^-
  - More clear evidence for e^- beaming
  - But still lots of energy in the boundary of target

  … more work needs to be done to understand the physics

Fast Ignition Capsules using liquid cryogenic fuel

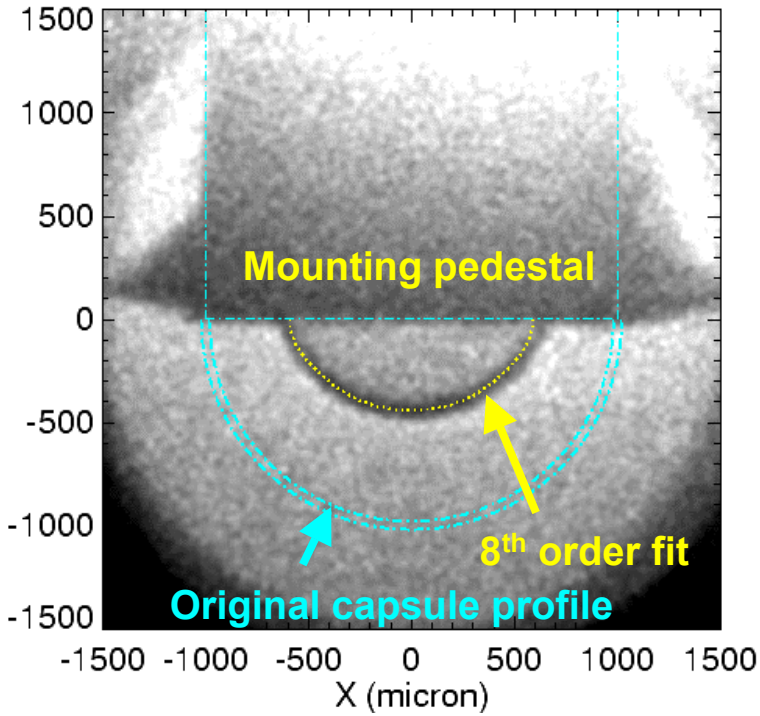

S.A. Slutz, R.A. Vesey, and D.L. Hanson,

Sandia National Laboratories

6th Workshop on Fast Ignition of Fusion Targets

16-19 November, 2002, Florida

Sandia is a multiprogram laboratory operated by Sandia Corporation, al Lockheed Martin company, for the United States Department of Energy under contract DE-AC04-94AL85000

Sandia National Laboratories

Short pulse laser deposition needs to be studied at the conditions appropriate for fast ignition

Particle propagation depends strongly on the plasma state and density
….degree of current neutralization
…level of filamentation instabilities

High densities required, since the ignition energy decreases strongly with density, $E_{ignition}=140(\rho/100)^{-1.85}$ KJ

Cryogenic capsules are required with fuel $\rho r \sim 0.6\text{-}1.0$ g/cm^2

Liquid cryogenic capsules would not need the accurate temperature control required by β layering

… drastically reduced the cost of the system

… simplified fusion energy applications

Sandia National Laboratories

Conservative hohlraum design yielded images of imploding CH hemi shell on Z

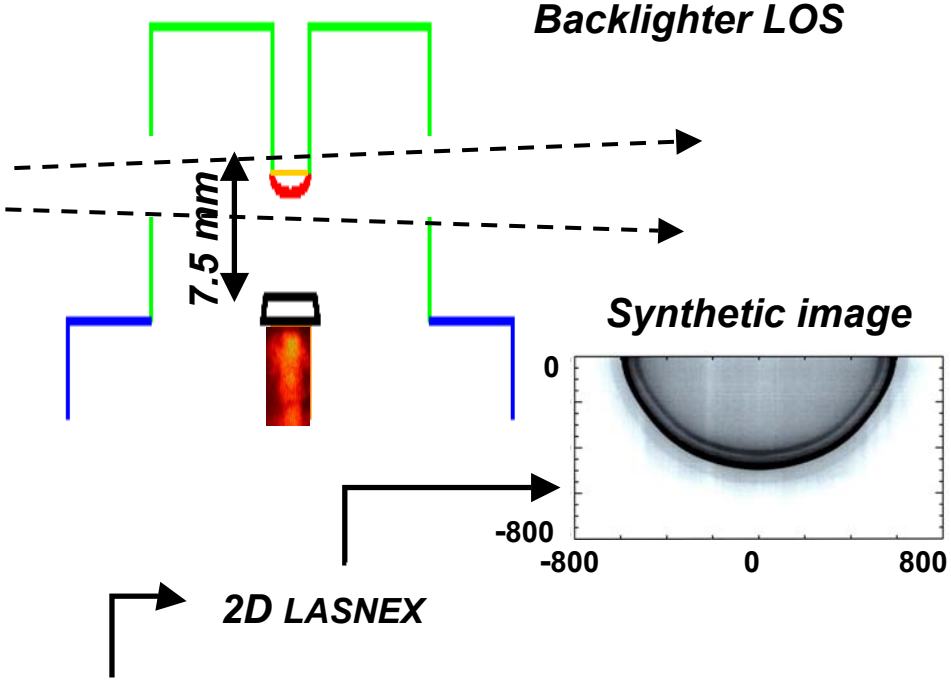

2D time-dependent viewfactor

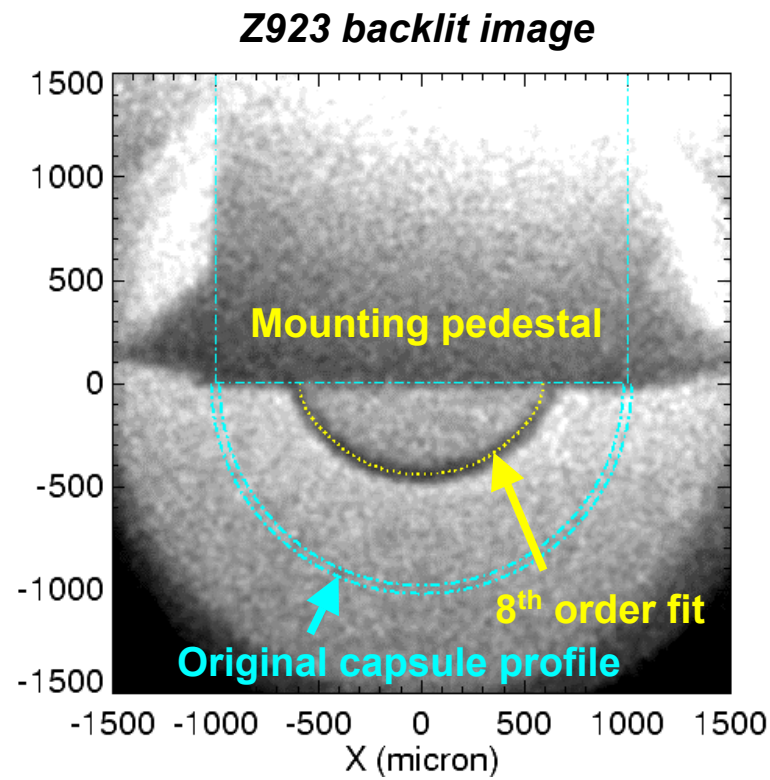

2D simulations give polar-averaged peak ρ = 60 g/cc, ρr = 0.3 g/cm^2 for this case

More optimized Z hohlraum designs should allow ρ = 90-100 g/cc, ρr = 0.4 g/cm^2

Simulations for ZR with cryo DT capsule give ρ = 160 g/cc, ρr = 0.65 g/cm^2

Sandia National Laboratories

Inexpensive cryo capsule using liquid DT

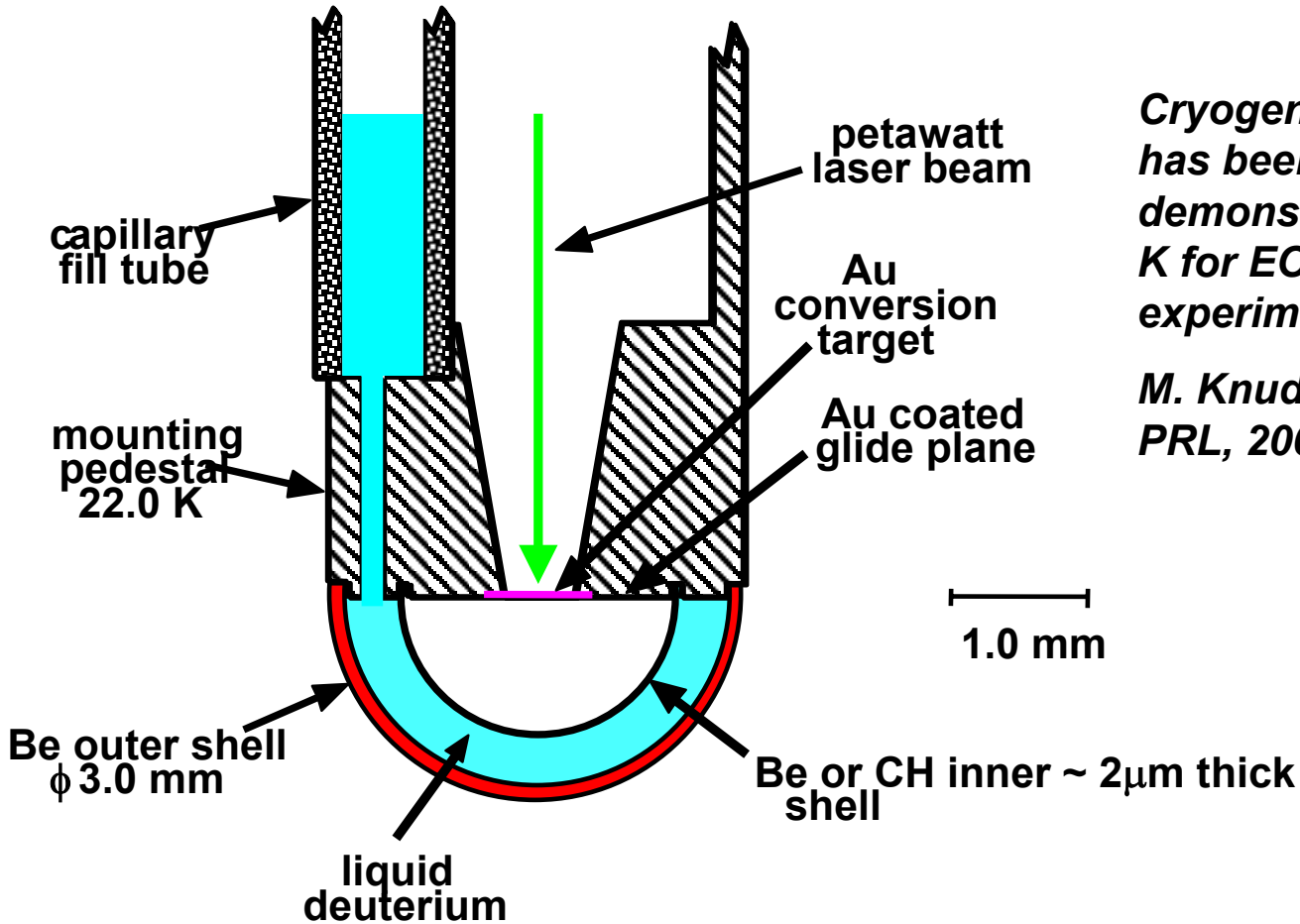

Cryogenic capability has been demonstrated at 19.5 K for EOS experiments

M. Knudson et al. PRL, 2002

The inner plastic shell can be quite thin

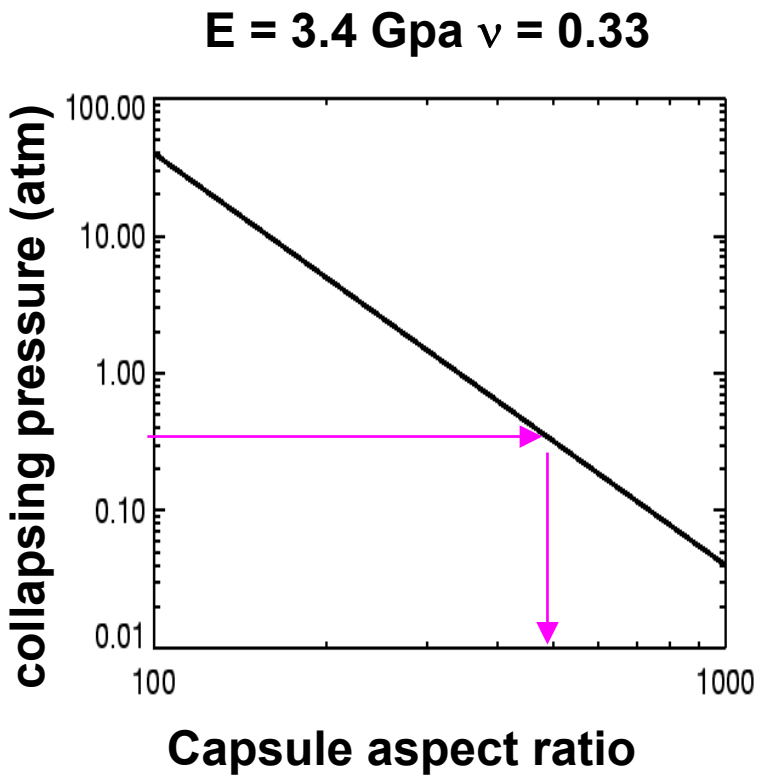

The liquid DT or DD can be provided at a pressure of approximately 0.3 atmospheres and a temperature of about 19.5 K

Calculations show that an aspect ratio of ~ 500 can withstand 0.3 atm.

A 1 mm capsule requires a shell thickness of ~ 2 μm

Sandia National Laboratories

A sequence of capsules was previously designed for fast ignition*

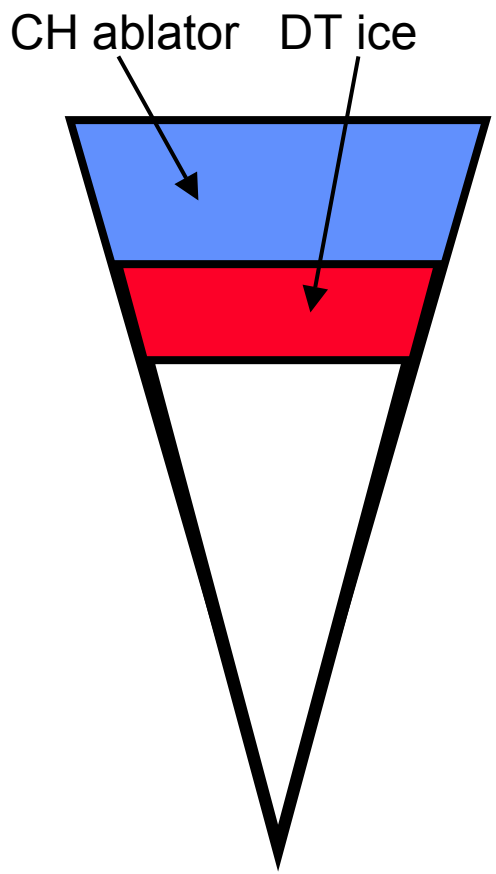

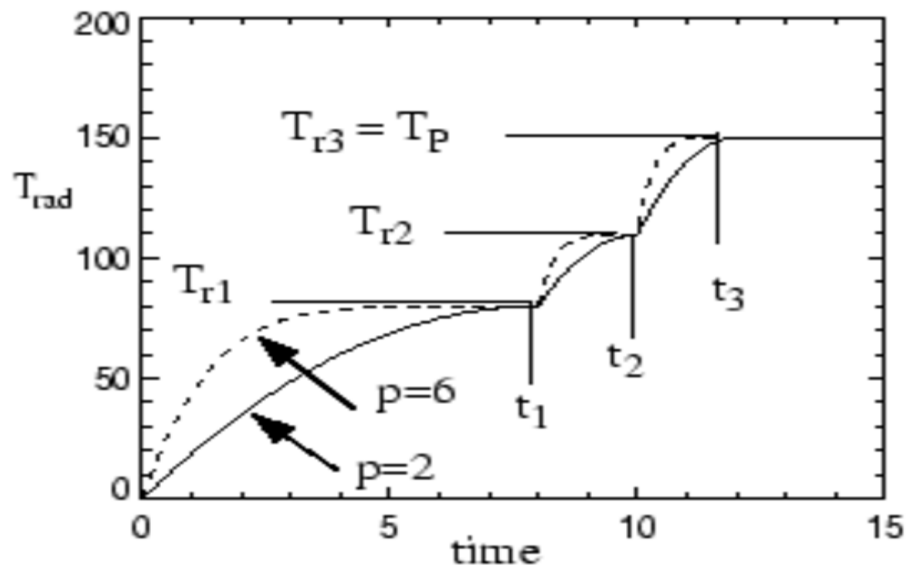

A three step temperature profile produces an essentially isentropic implosion

* S.A.Slutz and M.L. Herrmann accepted Phys. Plasmas

Sandia National Laboratories

Fuel density is a strong function of the peak drive temperature

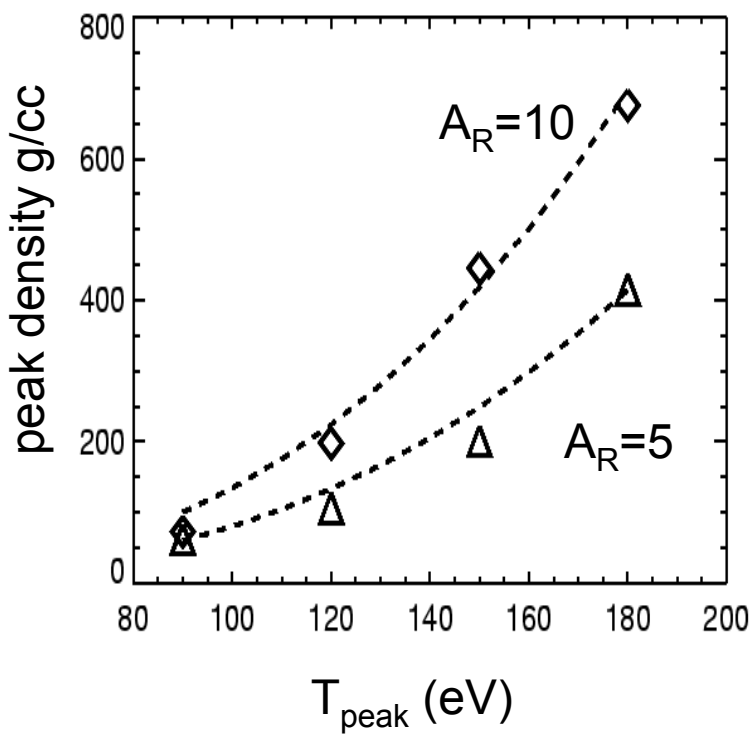

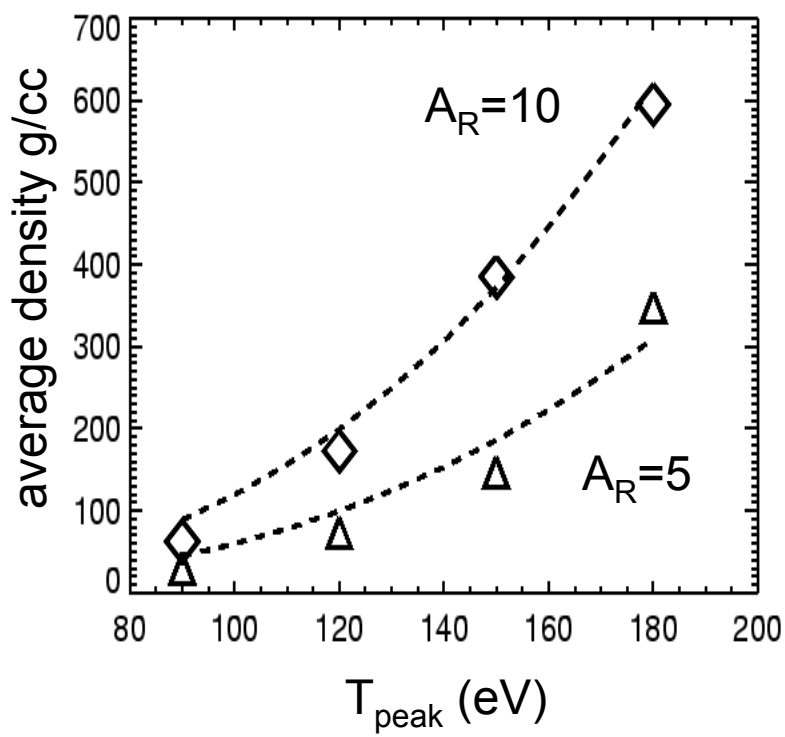

Sandia National Laboratories

The 180 eV drive capsule design has been modified for liquid fuel

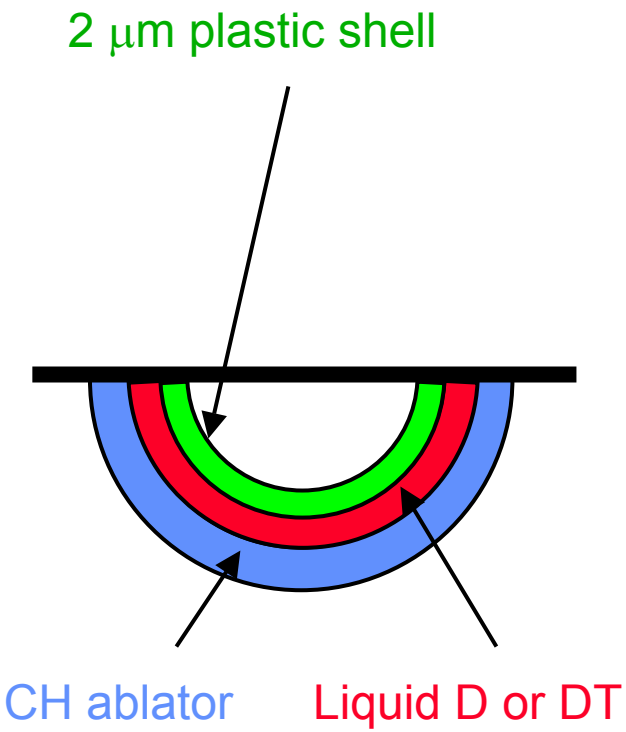

A DT ice capsule with a radius of 0.75 mm yields a final fuel ρr = 1.0 g/cm^2 which is the threshold required for ignition

Adding a 2 μm plastic shell to hold in the liquid fuel reduces the final ρr to 0.7 g/cm^2

Increasing the capsule radius to 1.1 mm and lengthening the pulse shape results in a final ρr = 1.07

Increasing the capsule radius to 1.3 mm results in a final ρr = 1.24, which should provide a higher burn fraction

1-D results at peak density used to set up a 2-D hemispherical simulation

Ignition threshold and burn fractions were determined for each capsule

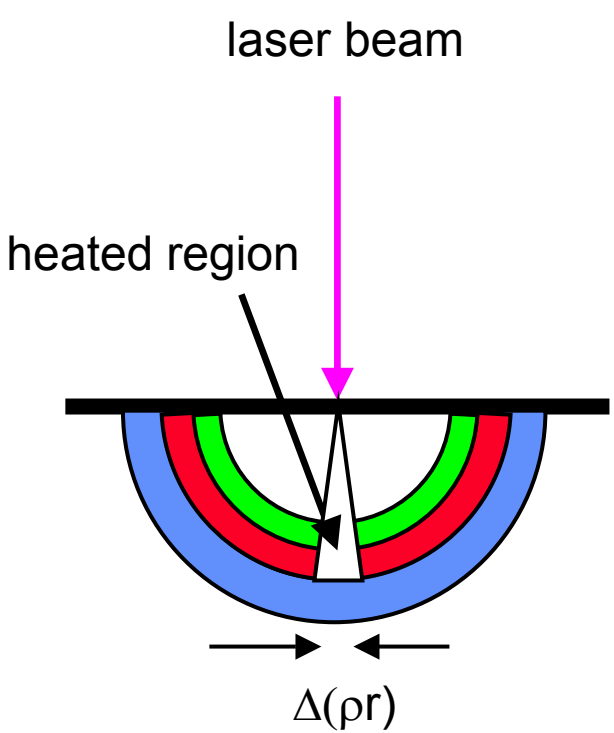

A conical region was heated at constant power for a time t_{pulse}

The optimum heating pulse length was ~10 ps

The cone angle and power were adjusted

DT ice capsule: ρ_{max} ~ 380 g/cc

$E_{ignition}$ ~ 37 kJ, Yield ~ 3 MJ and 10% burnup

The 1.1 mm capsule: ρ_{max} ~ 340 g/cc

$E_{ignition}$ ~ 60 kJ

Yield ~ 5 MJ and ~ 10% burnup

The 1.3 mm capsule: ρ_{max} ~ 300 g/cc

$E_{ignition}$ ~ 70 kJ

Yield ~ 15 MJ and ~ 15% burnup

Sandia National Laboratories

Inner plastic shell could be subject to the Rayleigh-Taylor instability

The density of the plastic shell is about 4 times the density of liquid DT

The stability could be improved by timing the shocks so that a rarefaction wave travels outward through the plastic shell before the arrival of the subsequent shocks

The mass of the plastic shell is so small that it can mix with the fuel and still burn

… complete mixing of the plastic shell of the 1.1 mm capsule

into the fuel reduced the burn efficiency from 11% to 8%.

Relativistic Electron Beam Transport And Characteristics In Solid Density Plasmas

Richard A. Snavely
LLNL/UC DAVIS

C. Andersen, J. Hill, J. King, R. Freeman	UC DAVIS
T. Barbee, S. Hatchett, M. H. Key, J. Koch, A. MacKinnon	LLNL
T. Cowan, R. Stephens	G.A.
Y. Aglitskiy	NRL

Presented at:

6th Workshop on Fast Ignition of Fusion Targets

November 19, 2002

St. Petes Beach, Fl. USA

This work conducted under the auspices of the U.S. Department of Energy by the Lawrence Livermore National Laboratory under contract No. W-7405-ENF-48.

OFES Collaborative Efforts - World Wide

F. Amiranoff	**LULI**
D. Batani	
S.D. Baton	
L.Gremillet	
M. Koenig	
E. Martinolli	
E.Perelli-Cippo	
J.J. Santos	
F. Scianitti	
N. Fisch	**Princeton**
T. Hall	**Univ Essex**
P. Norreys	**RAL**
Rabec Le Gloahec	**CEA-FR**
C. Rousseaux	

P.K.Patel, D. Hicks
Lawrence Livermore National Laboratory
Y. Sentoku
University of Osaka
M. Borghesi
Queens University, Belfast, UK
O. Willi, *University of Dusseldorf, Germany*
H. Ruhl, *General Atomics, USA*
C. Stoeckl *UR LLE*

have experiment,
will travel .

LLNL / GA / UC Davis
OFES Program Highlights

- ¥ Review some interesting electron related observations made from the LLNL Petawatt Laser and more recent experiments at slightly lower power.
- ¥ Very preliminary look at our 3 week old data from RAL. Our attempt at better understanding of electron transport at solid density via x-ray fluorescence. In particular the first transverse imaging of the entire relativistic electron beam path.
- ¥ These experiments were performed at:

  LULI Laser 20J, 0.5 ps @ Ecole Polytechnique

  Vulcan laser 100 J, 0.8 ps @ RAL

  and of course the *Nova Petawatt Laser System*

- * Part of an ongoing effort to better develop theory and experimental capability suitable for understanding relativistic laser plasma physics on the road to Fast Ignition.

Why Are We Studying This??

the trouble with f_e ...

the Electron Distribution Function

$$f_e\,[E,q,t] = f_u + f_b + f_{pond} + f_{other} + f_{ret} + f_{ds} + f_{esc}$$

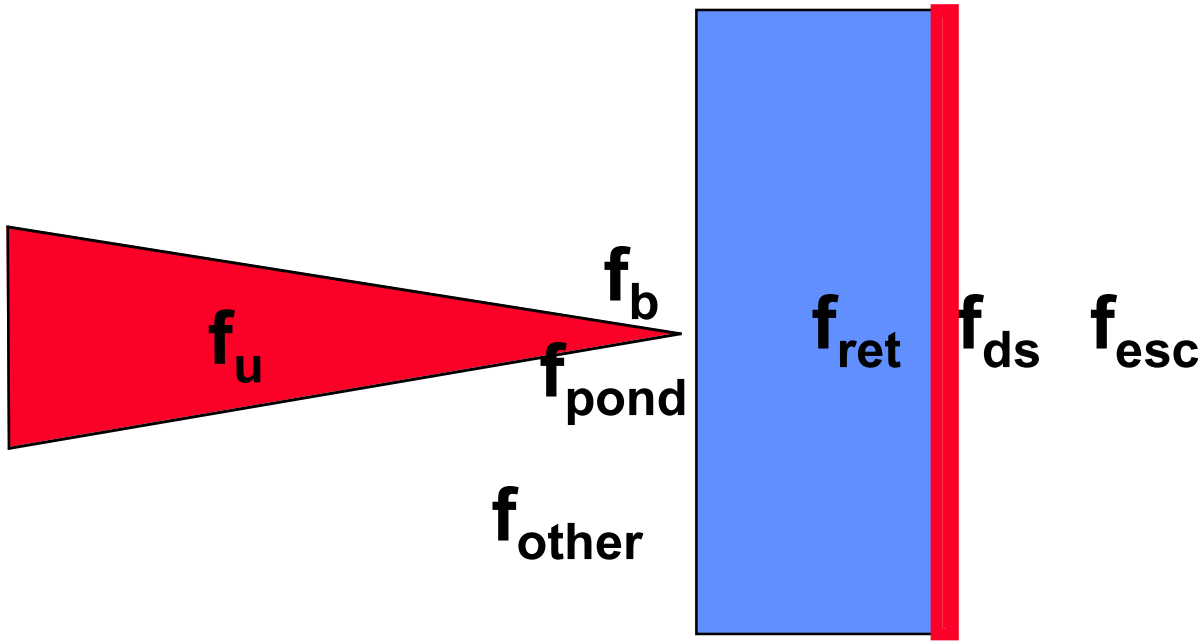

In the beginning (97) PW-Laser Radiography ruled the earth ...

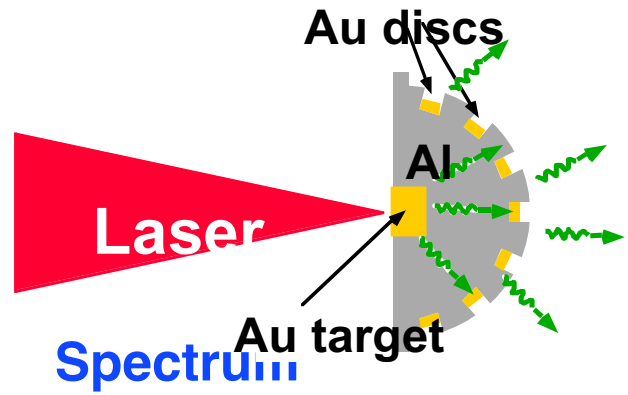

^{197}Au(γ,xn) cross sections

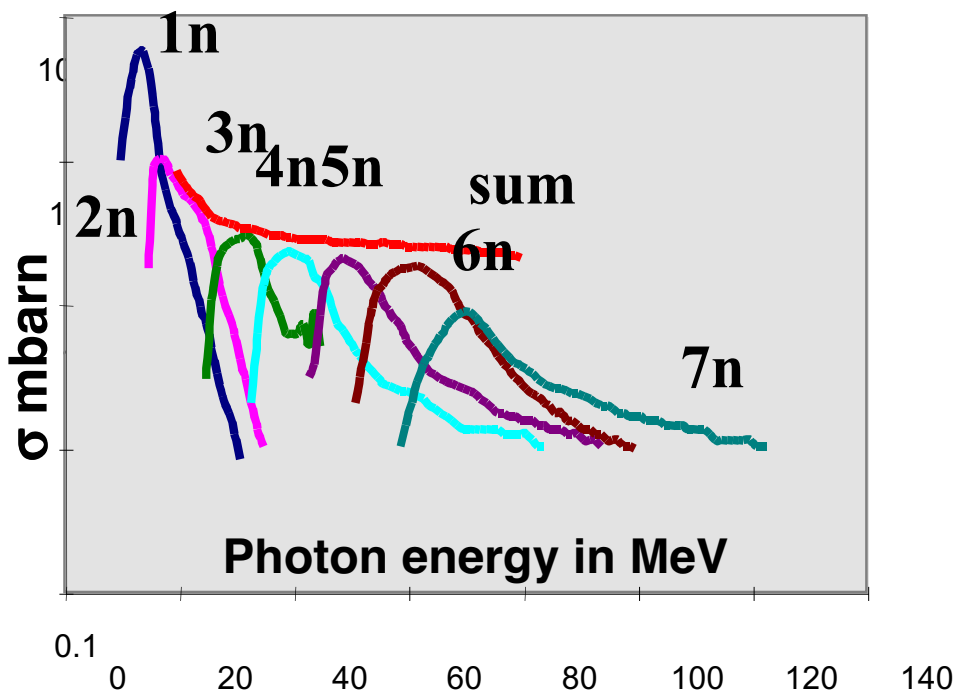

Spectrum

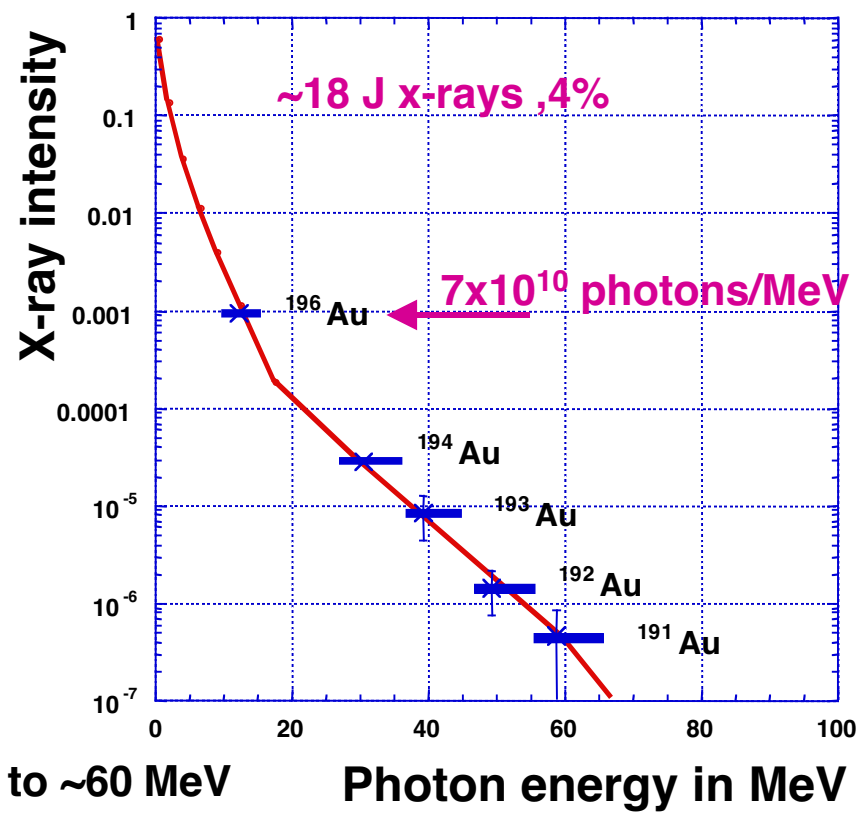

Gold activation has given the spectrum from ~8 to ~60 MeV
And above Ponderomotive scaling
Consistent with underdense process.

Shot 28061708 ,432J

Photons > ~8 MeV activated (γ,xn) a hemispherical array of gold discs; total x-ray dose > 0.2 MeV was measured by a shielded, conical array of TLD's.

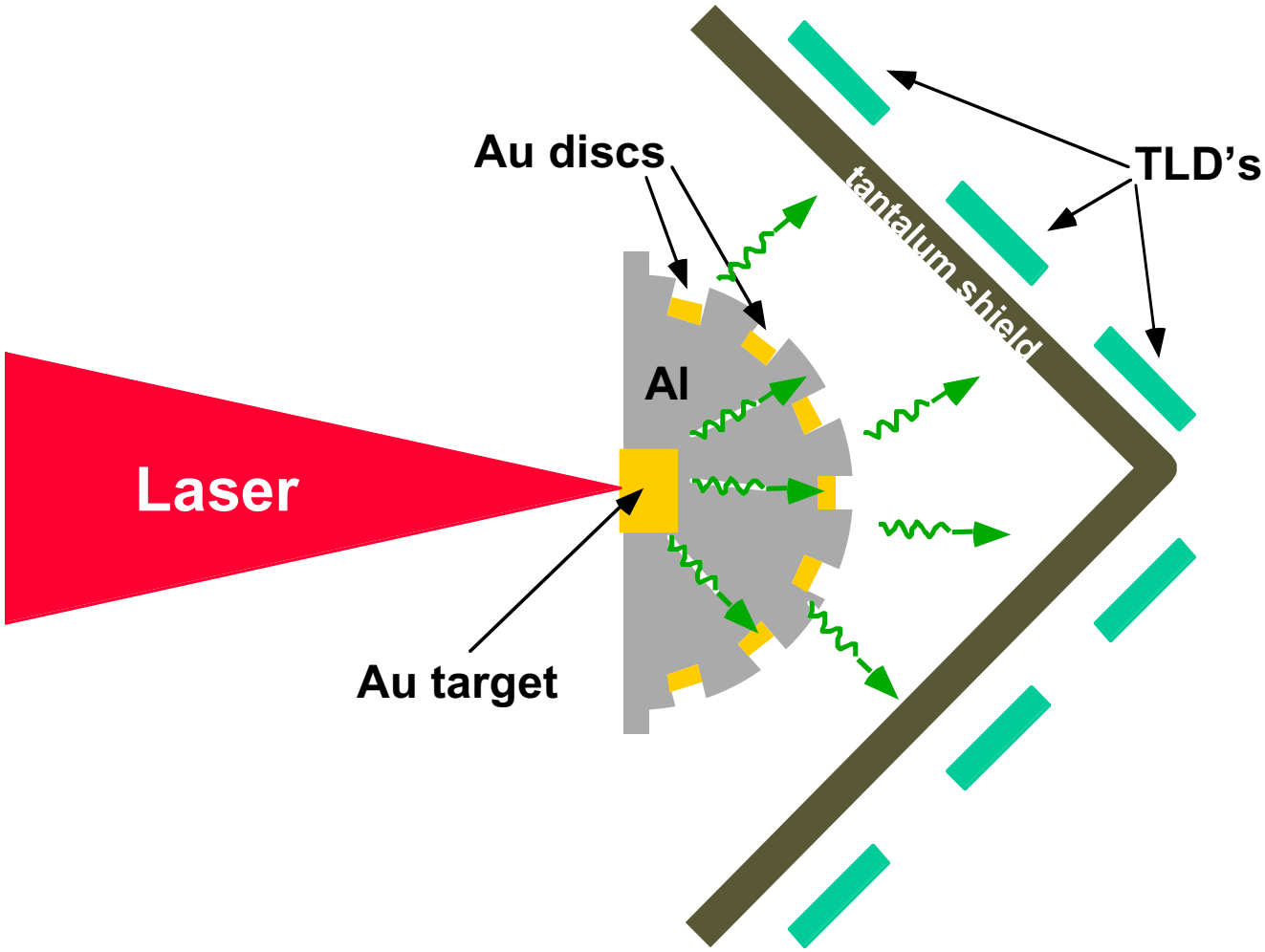

Photons:

2π pattern of Au activation (~10-16 MeV) has similar direction but sharper peak than integrated x-rays

(γ,n) photo-nuclear activation of Au

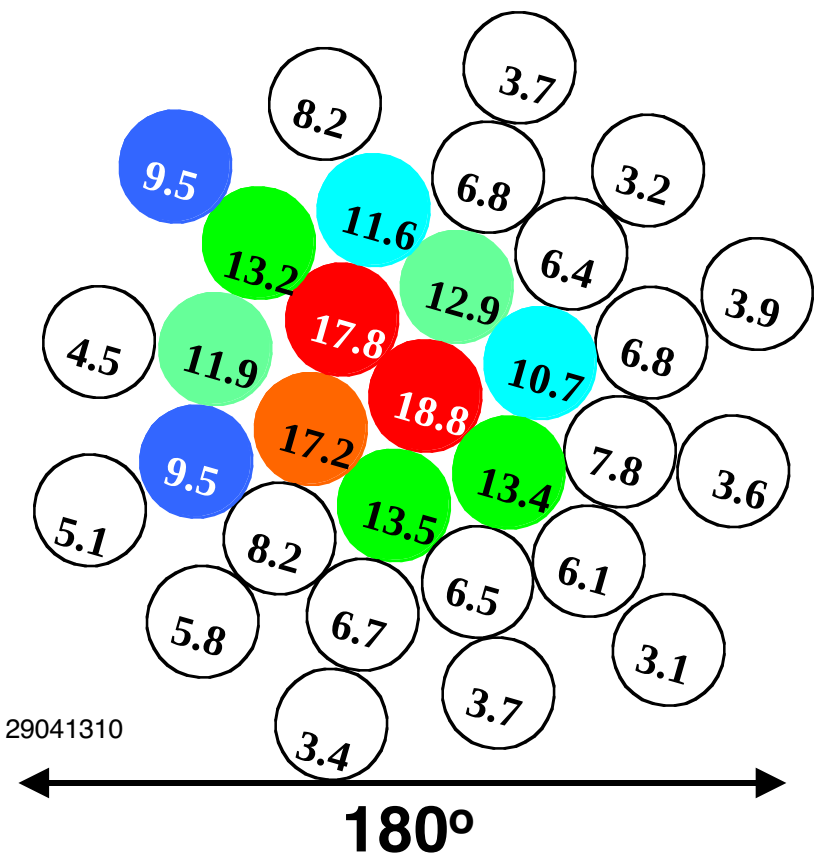

Fraction of activated atoms x10^{15}

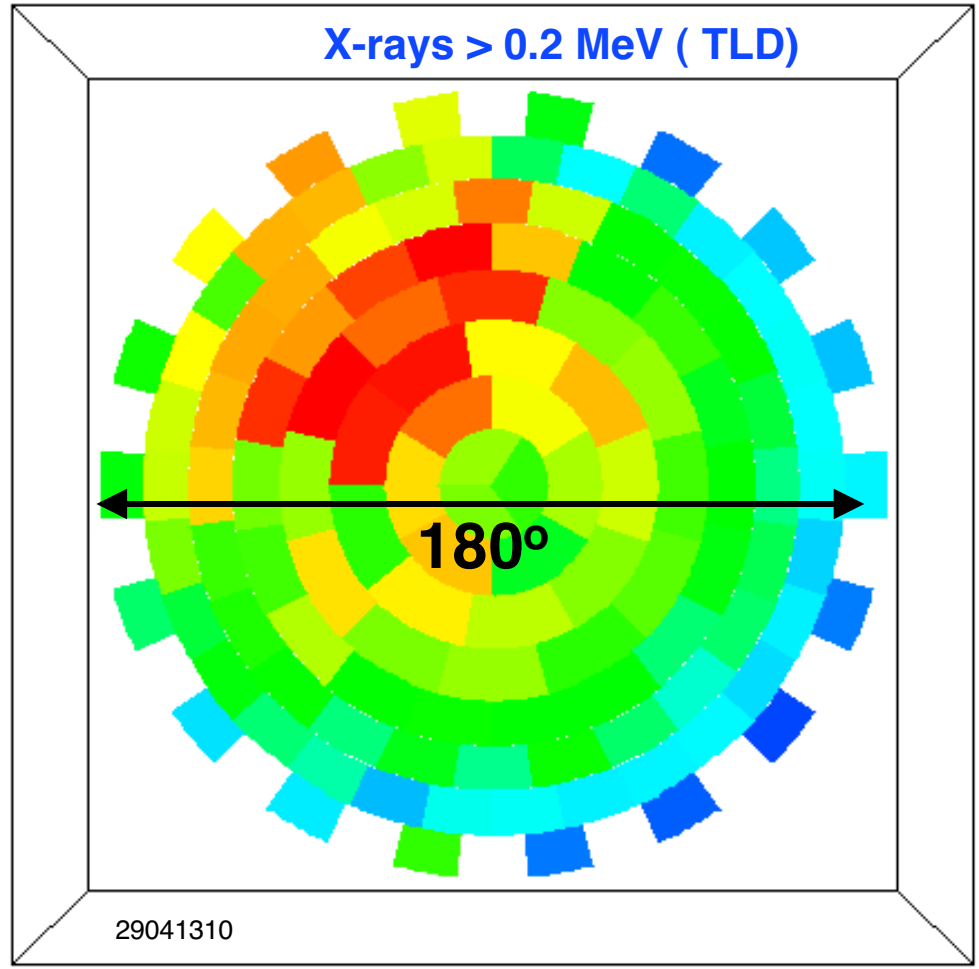

0.52 | 0.36 | 0.2 Rads at 1m

Hemisphere angular pattern of activation has reproducible ± 50° fwhm but softer x-rays sometimes exhibit filaments in the electrons

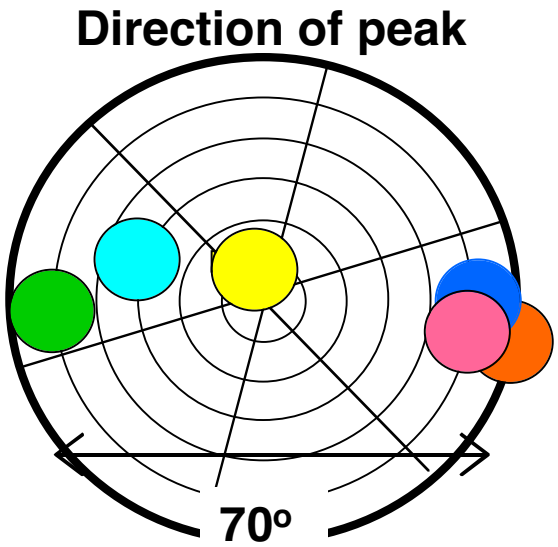

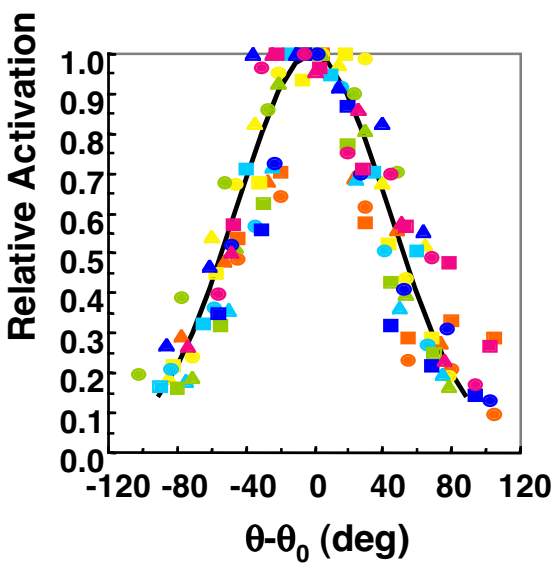

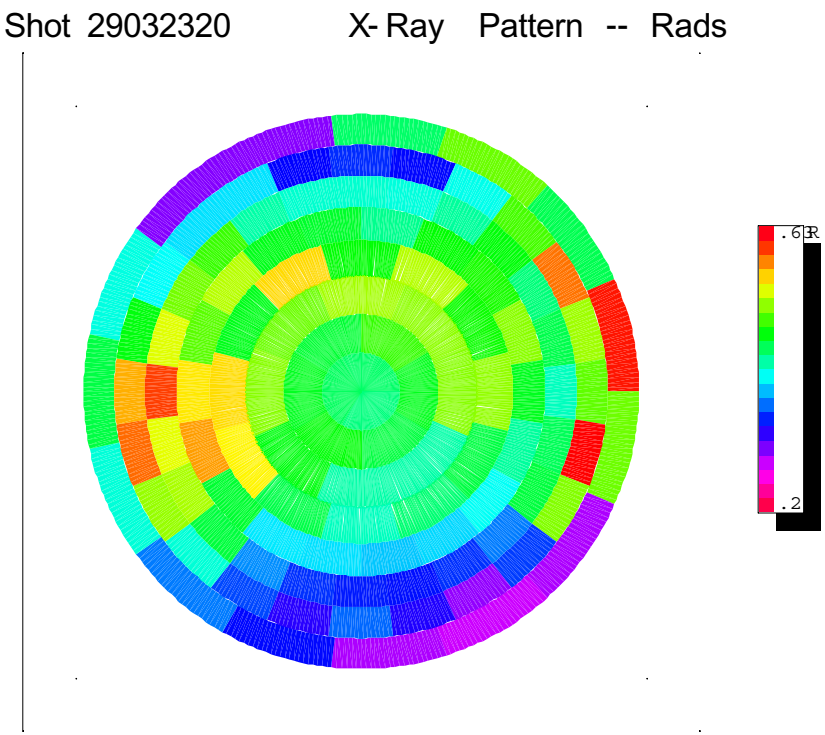

120 TLD array pattern has broader wings and even filaments at times...

Buried tracer layers show annular heating
Same as for the escaped electrons into RCF

0.5 μm Au foils buried in CH emit x-rays when heated to $T_e \approx 300$ eV

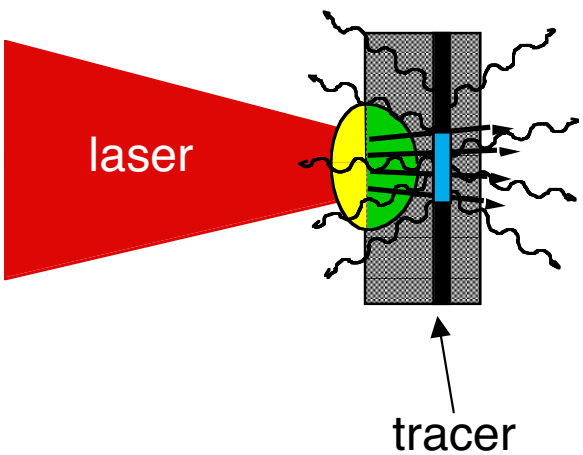

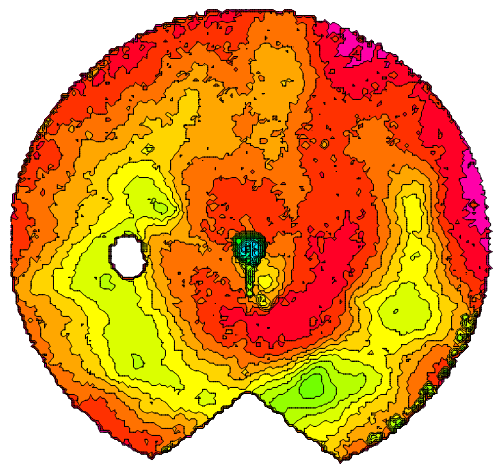

Escaped electron pattern @~2MeV

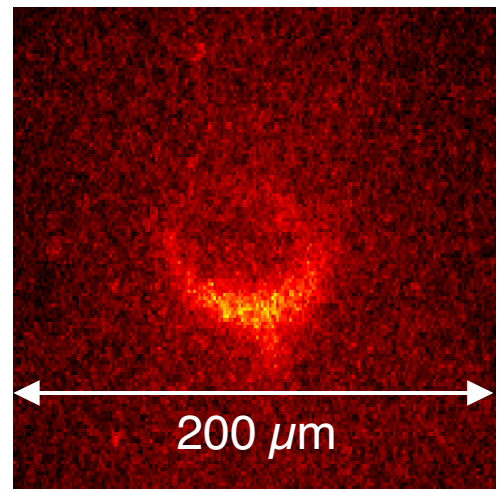

100 μm depth

Are these artifacts of underdense interactions or are they related to transport issues…….?

Electron transport questions evidenced from features in the proton Petawatt Data….

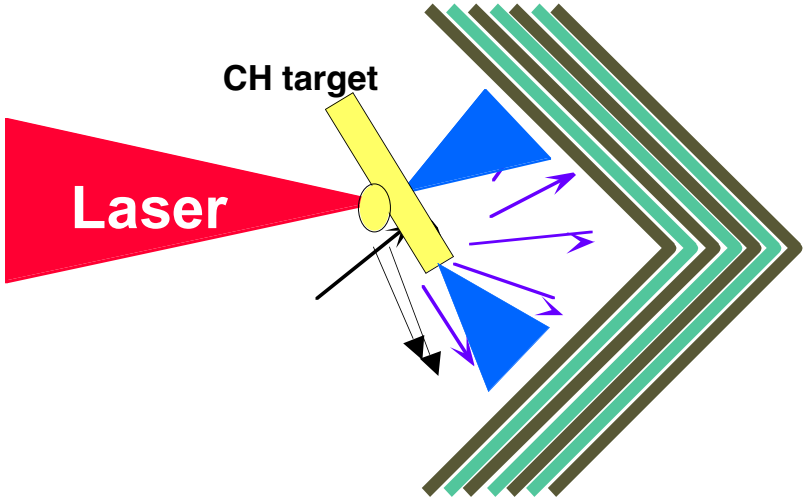

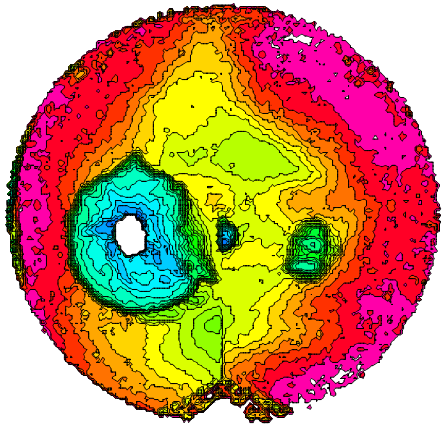

Au target
electron shadow

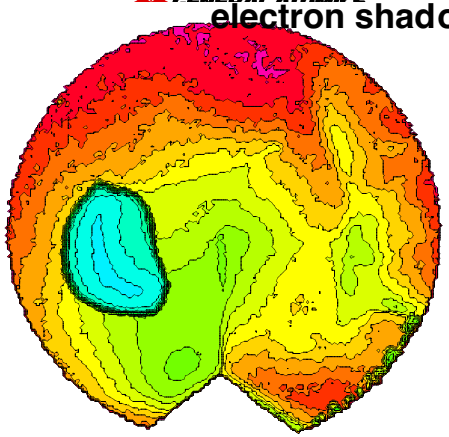

CH target
electron filaments

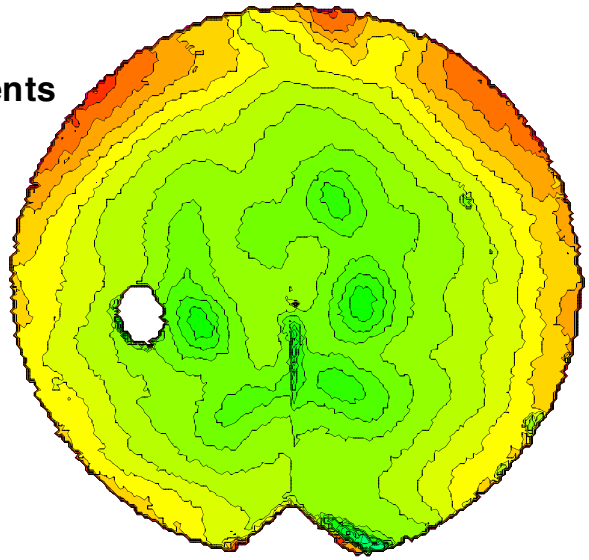

CH target
electrons flood
entire target
"Proton Diode"
with edge emission

Reminiscent of
"Reflex Triode"
20 years ago!

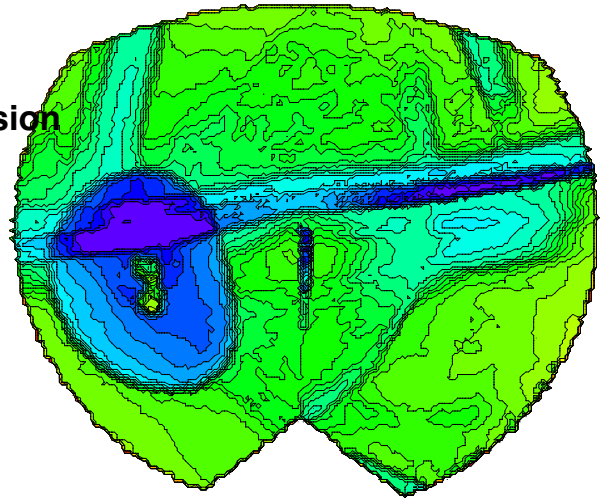

Here's Our Experiment: New Diagnostics Offer Simultaneous Imaging of Cu or Ti Kα and 180 Å XUV Planckian Emission

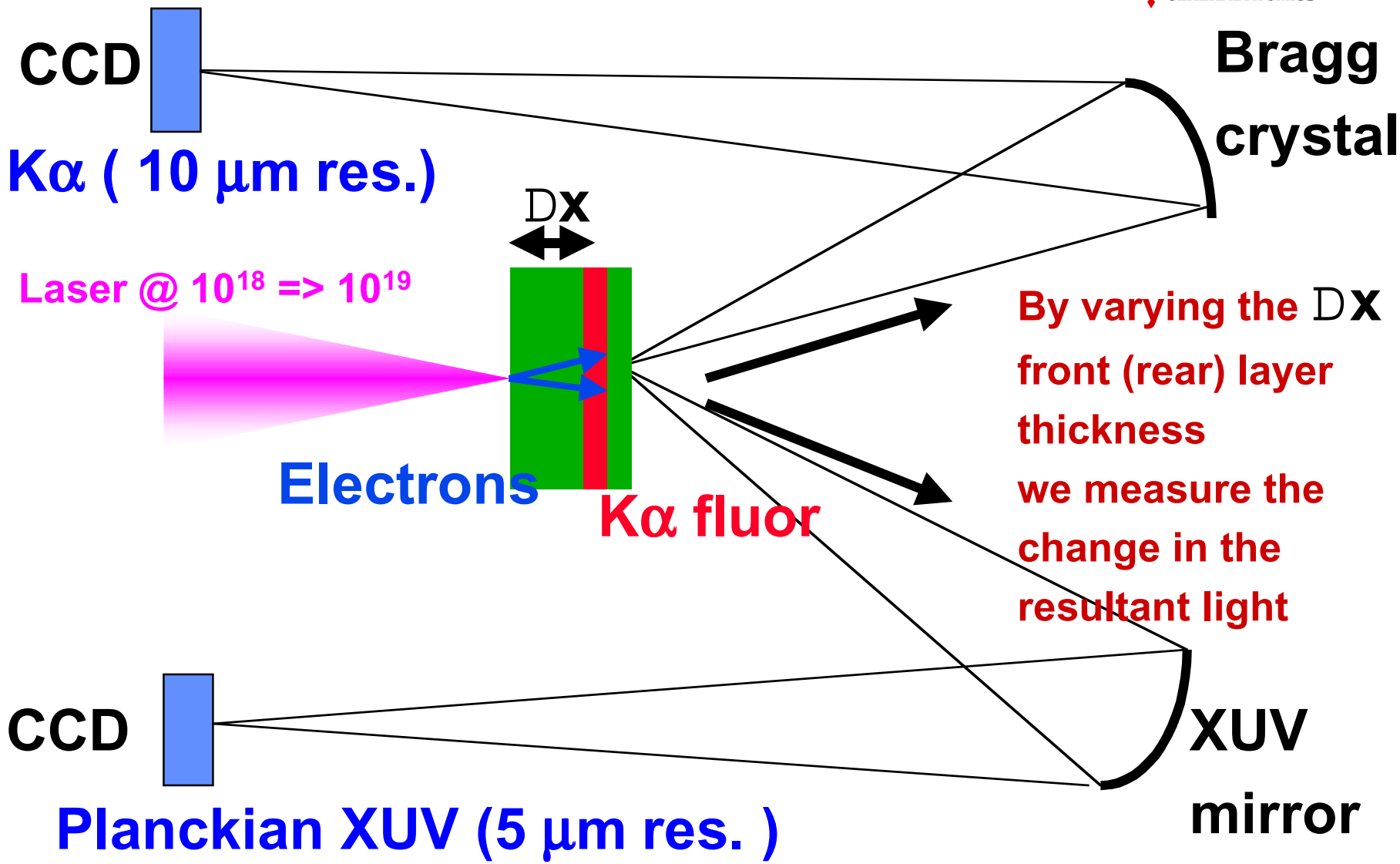

A picture is worth a thousand words…….

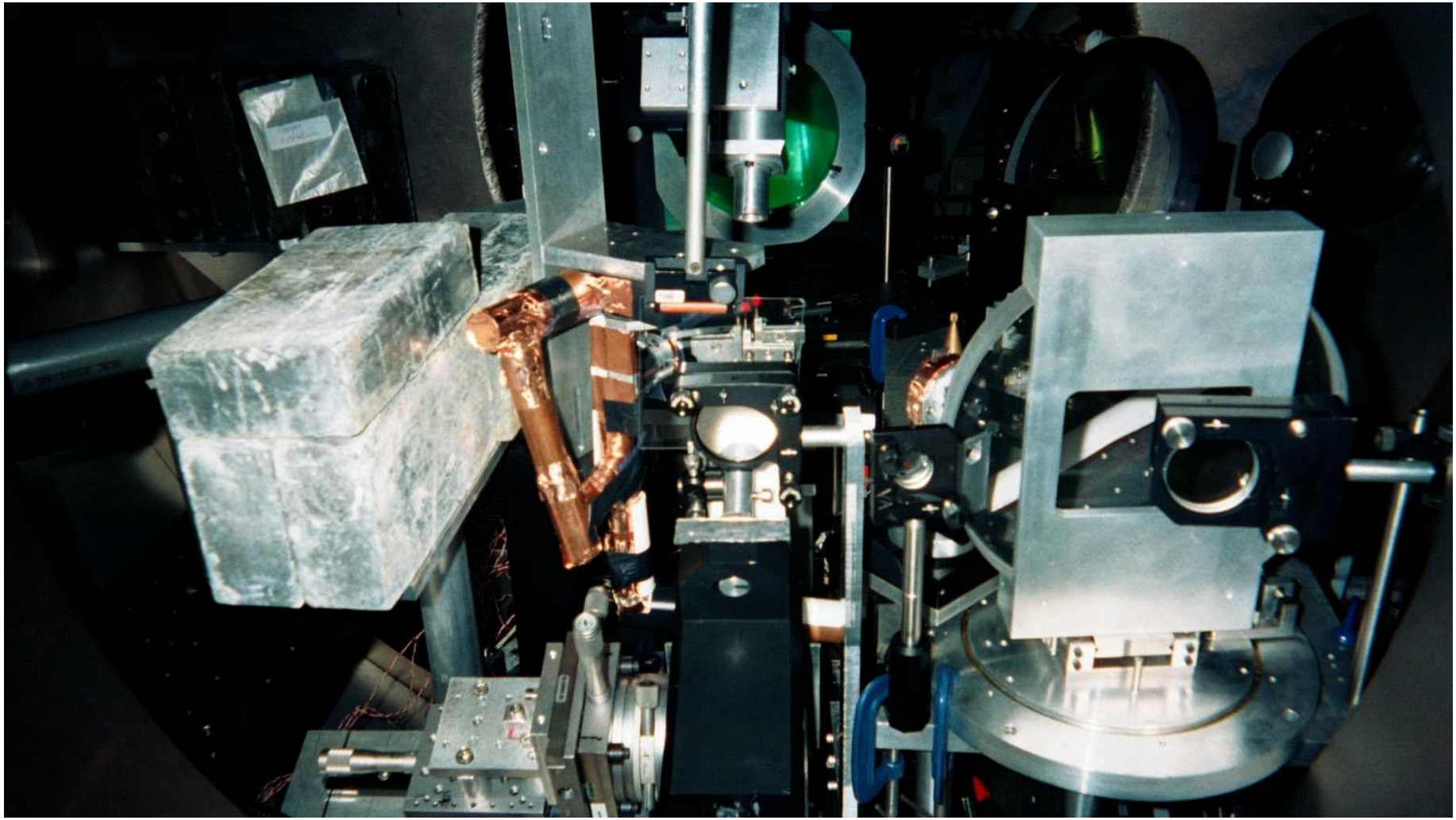

The Electron Beam Evidenced In the X-Ray is Structured after 300 μm Propagation through CH But structure not seen in Aluminum

Plastic (s15)

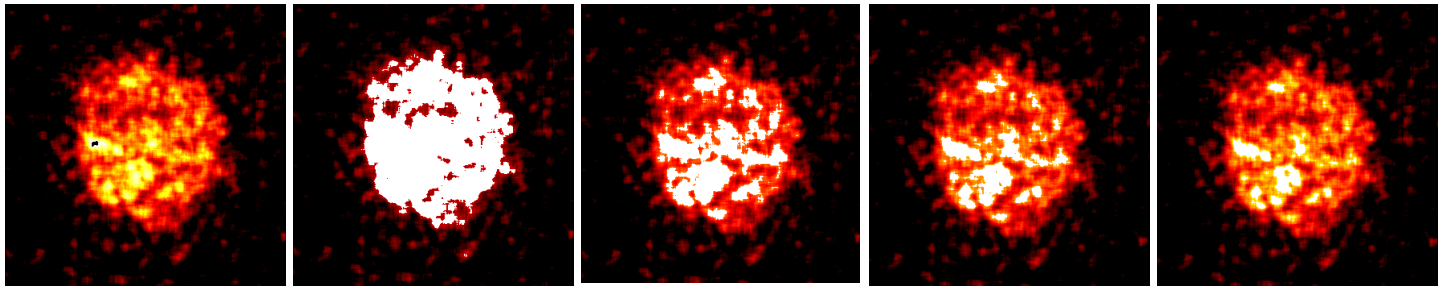

Fr = 0.67 Fr = 0.33 Fr = 0.20 Fr = 0.10

Aluminum (s21)

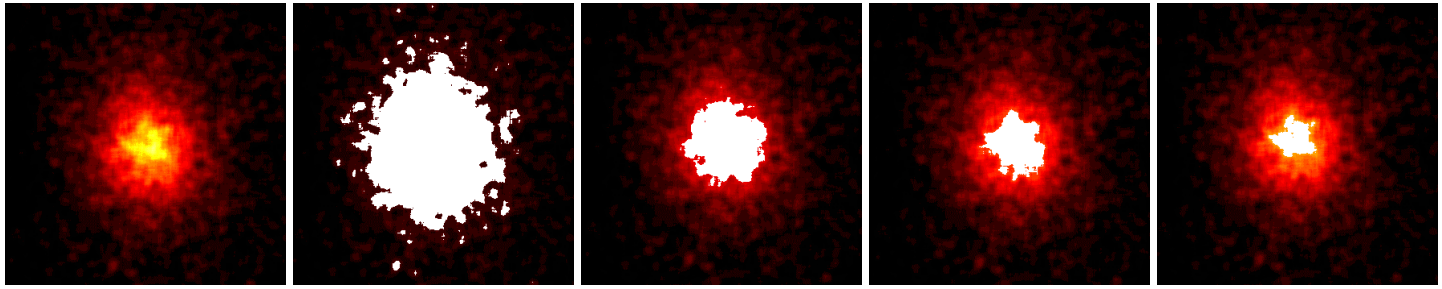

1000 μm

White shows area of pulse containing specified fraction of pulse energy

Does this Indicate Ionization Front Propagation or Could it Be Magnetic Skin Depth Effects of the Hots vs Colds?

Electron transport in CH target shows beam break up with 80° divergence (RAL)

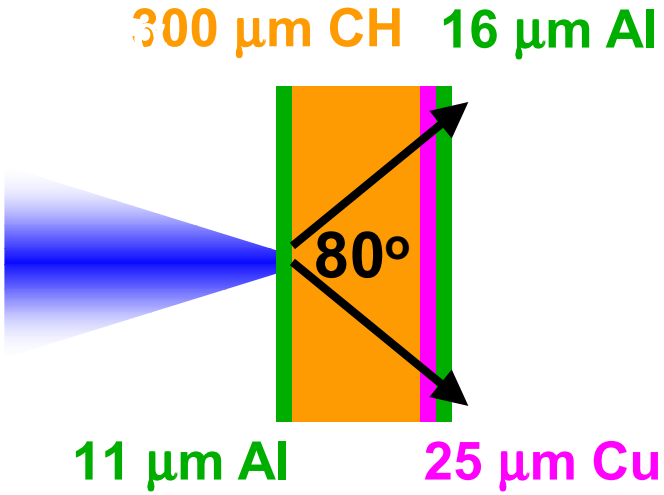

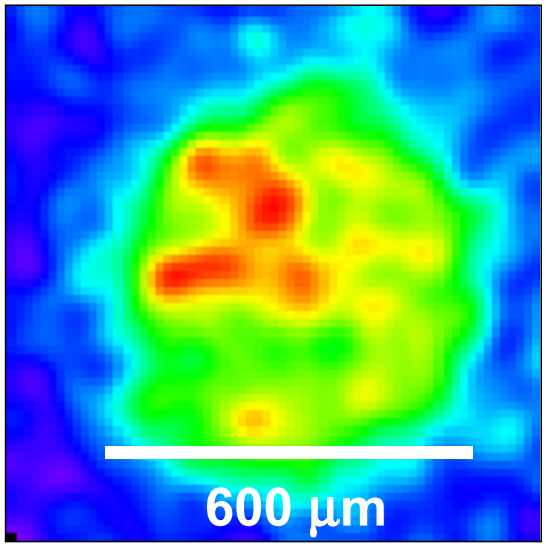

Hot spots of electron filaments over broadly divergent electron beam

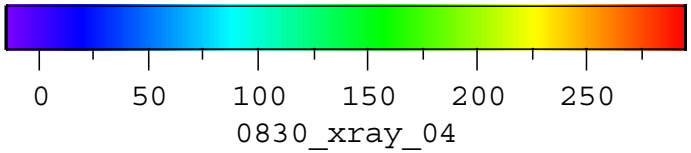

Image of 8 keV Cu Kα

Due to CH being initially an insulator?
Is this an indication of Role of Return Current in Transport of the HOTS?

Al Bremsstrahlung and Ti Kα images Demonstrate the Stochastic Behavior of the Electron Beam Angle Relative to Laser Axis (LULI)

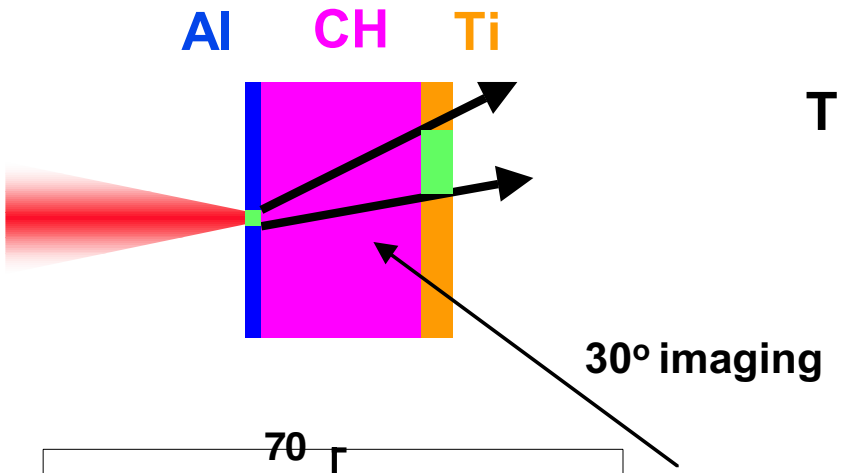

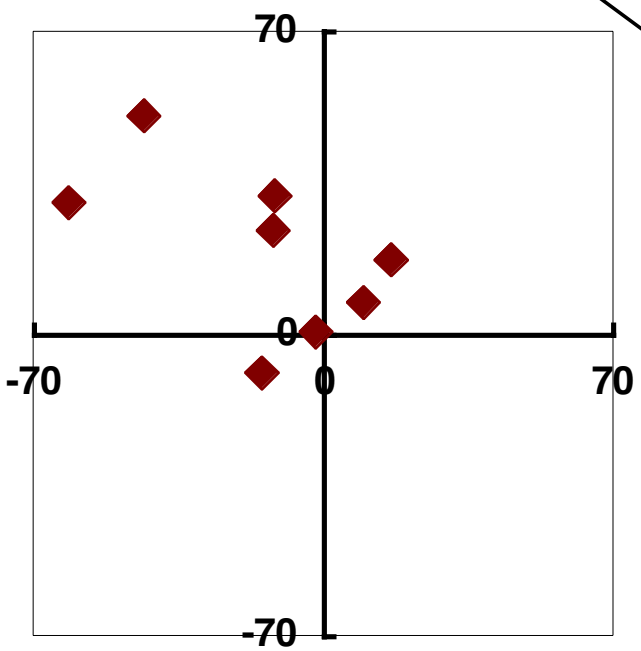

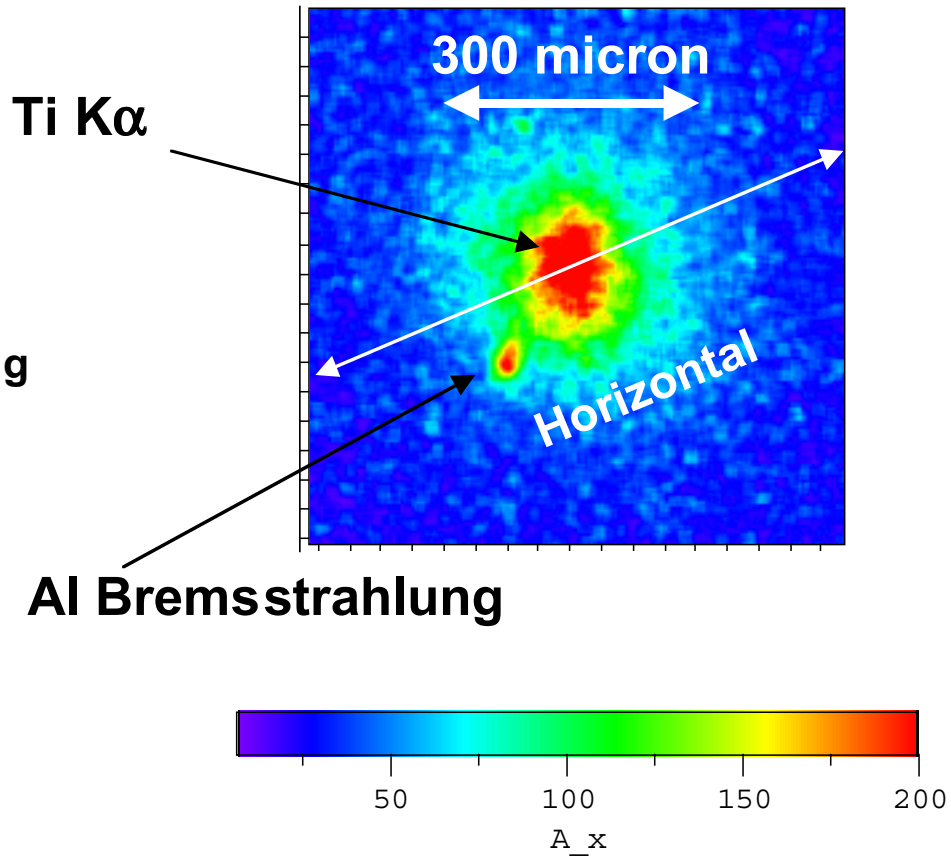

Electron beam is *Typically* off Laser Axis

Is this a feature of J X B ?

LULI and RAL Kα data show similar cone angle and minimum radius via Al layer

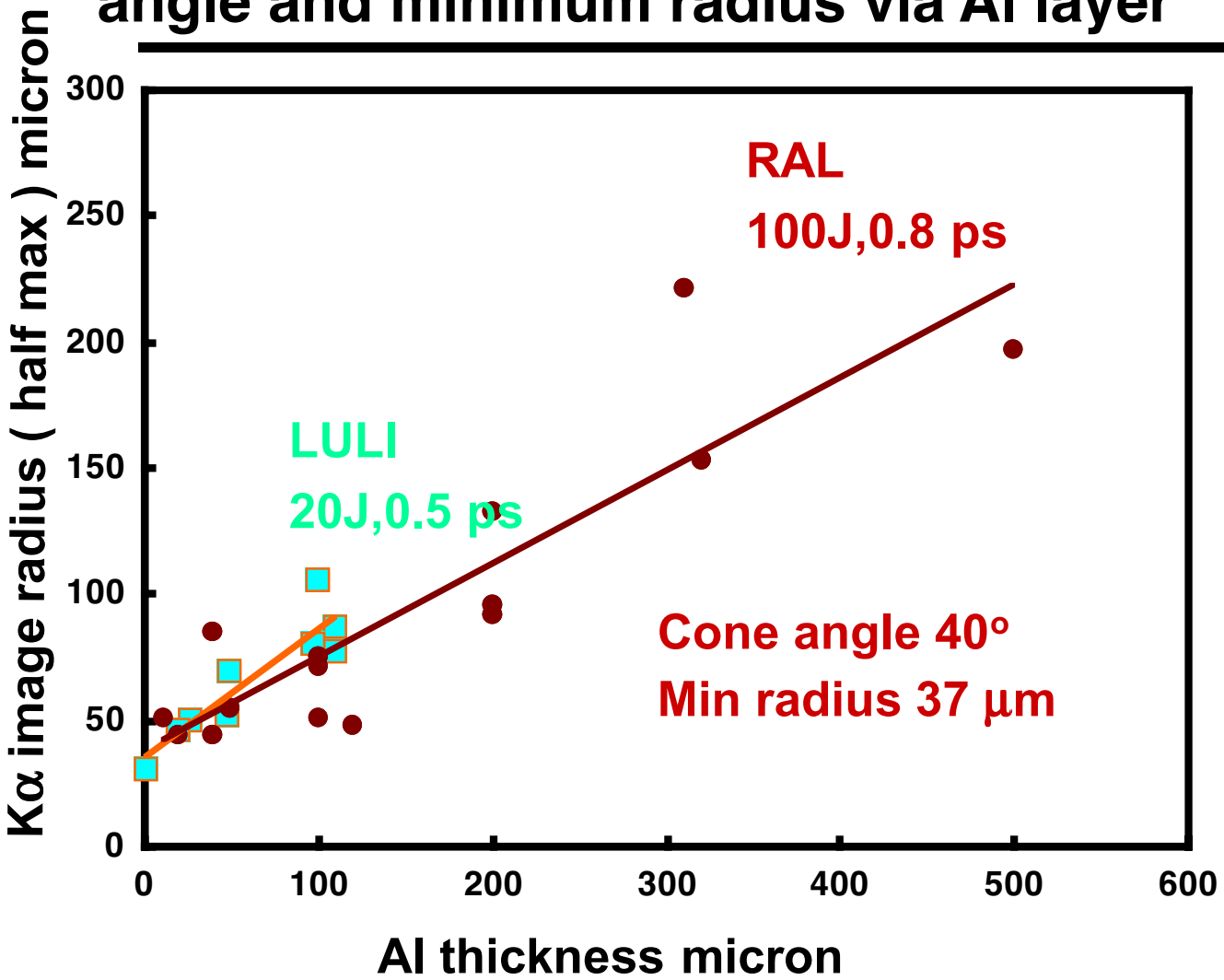

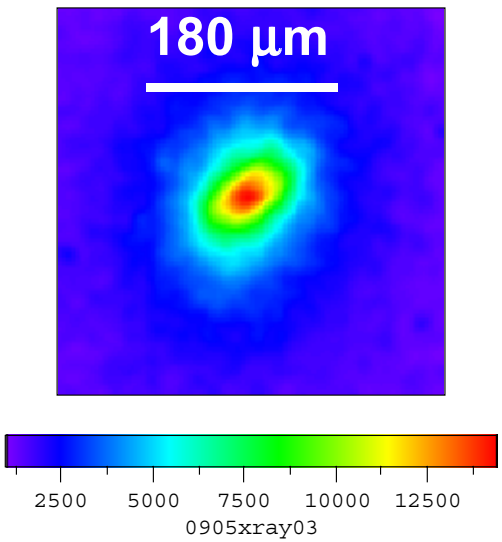

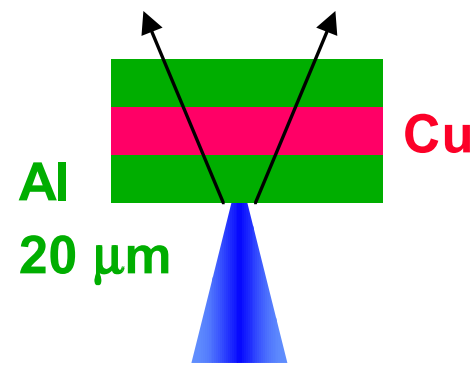

Refluxing Electrons Reflecting Off Rear Debye Sheath May Effect Images Analyzed by Monte Carlo Model

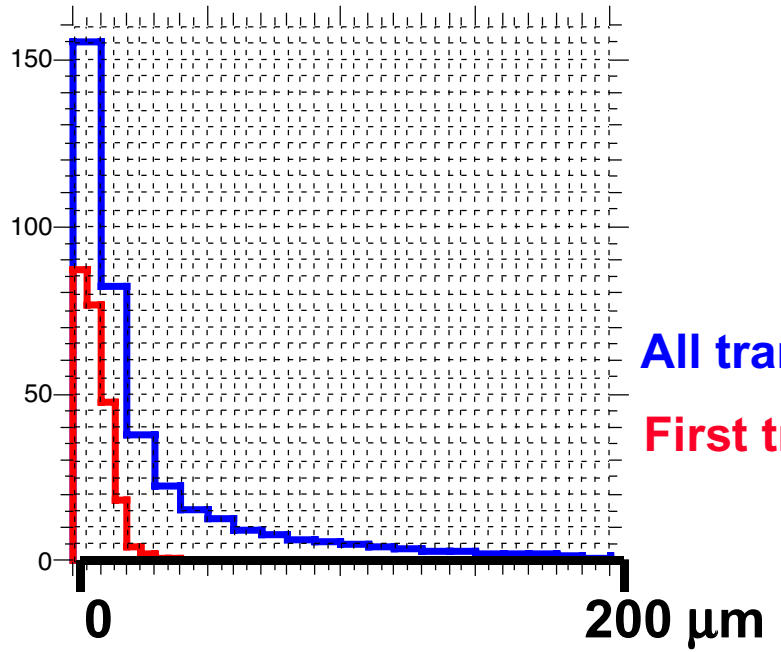

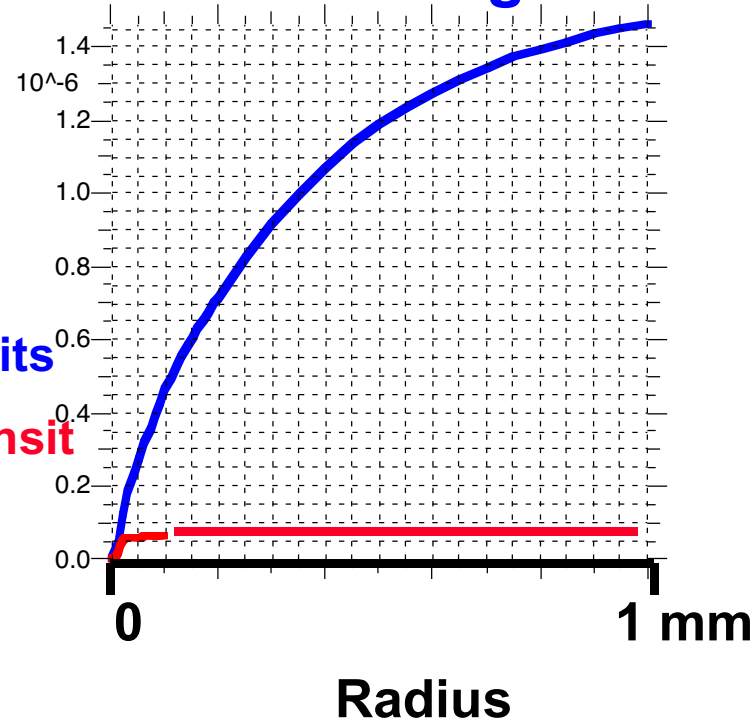

All transits

First transit

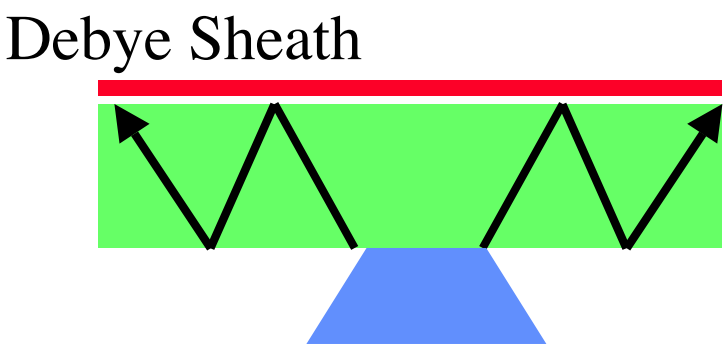

20 µm T foil

27 µm source

52 ° cone

600 keV =kT $_{hot}$

Central image spot size not much changed by refluxing-possible increase in energy in wings

Here's Our Experimental Variant: Image Cu-Kα transversely so both lateral and longitudinal temperatures maybe measured

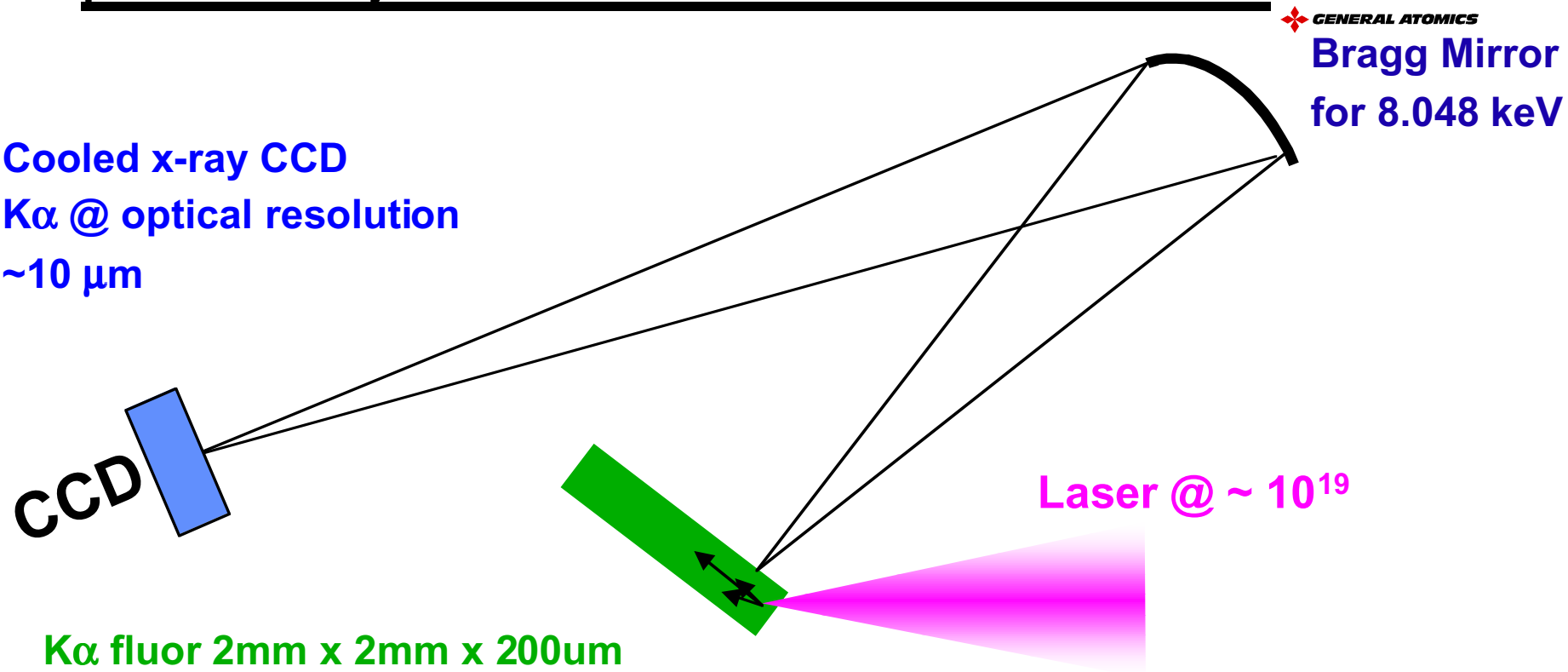

Kα fluor 2mm x 2mm x 200um
Solid-solution of 50% Cu 50% Al
via RST (Rapid Solidification Technology)

Technique reduces influence of refluxing on image signal.
Can study interface physics

Image resolution test on 20 um Cu triangle is coupled with x-ray CCD in single photon counting mode to provide spectrum and yield of k-alpha. See Christian Stoeckl (UR LLE) for details

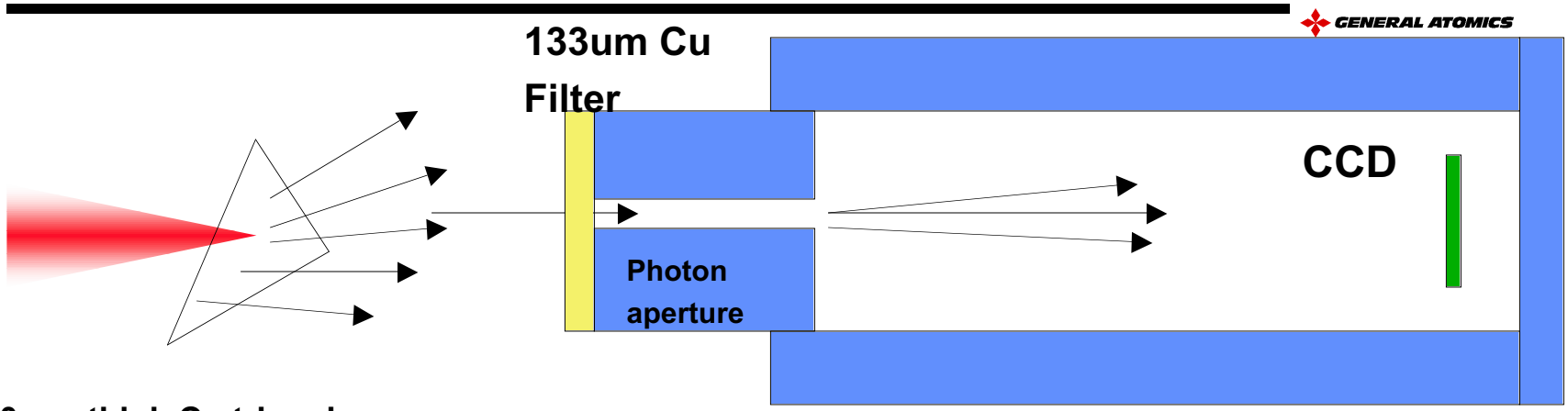

20 um thick Cu triangle
apex to base - 80 um
apparent res. ~9-12 um

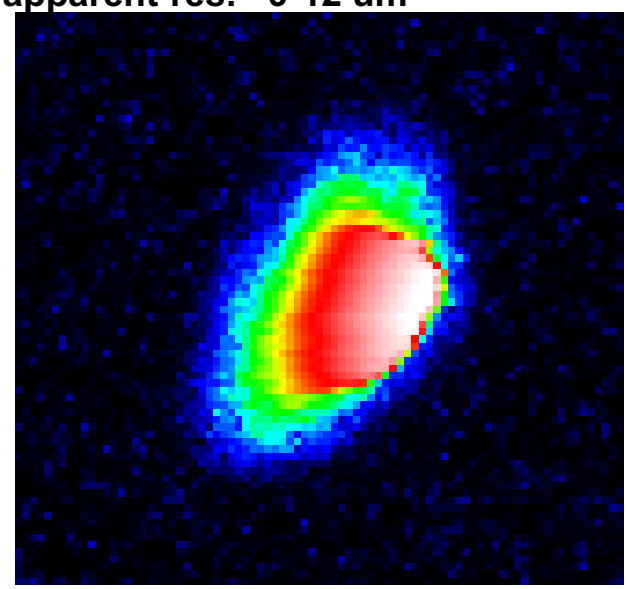

~9 10^10 Cu k-alpha photons/steradian ie.
~.015 Joules of ka light or .015% efficient

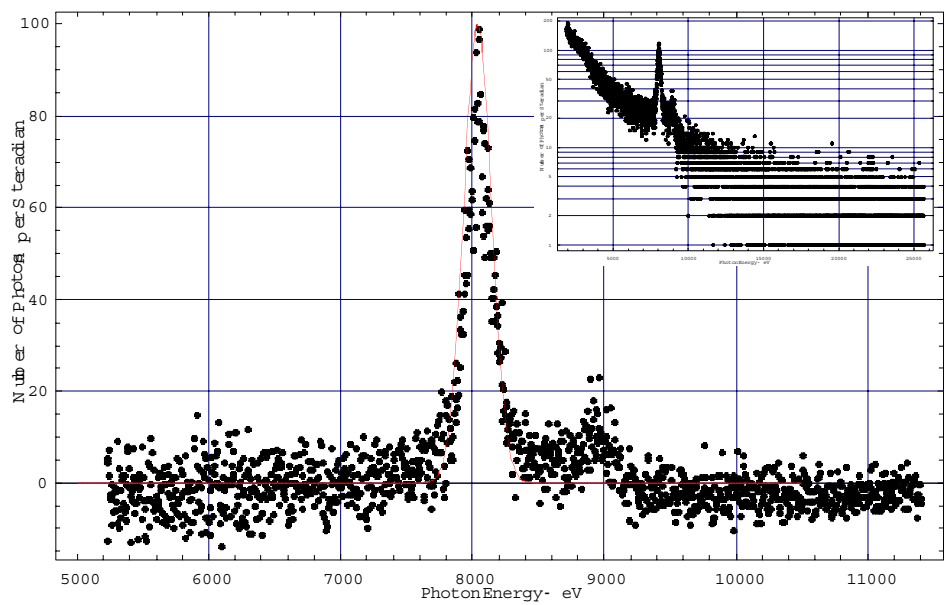

So what to we see? Too much x-ray noise!

Effect is to modulate 'smooth' kα on top of a bumpy mountain of noise….still several features are seen

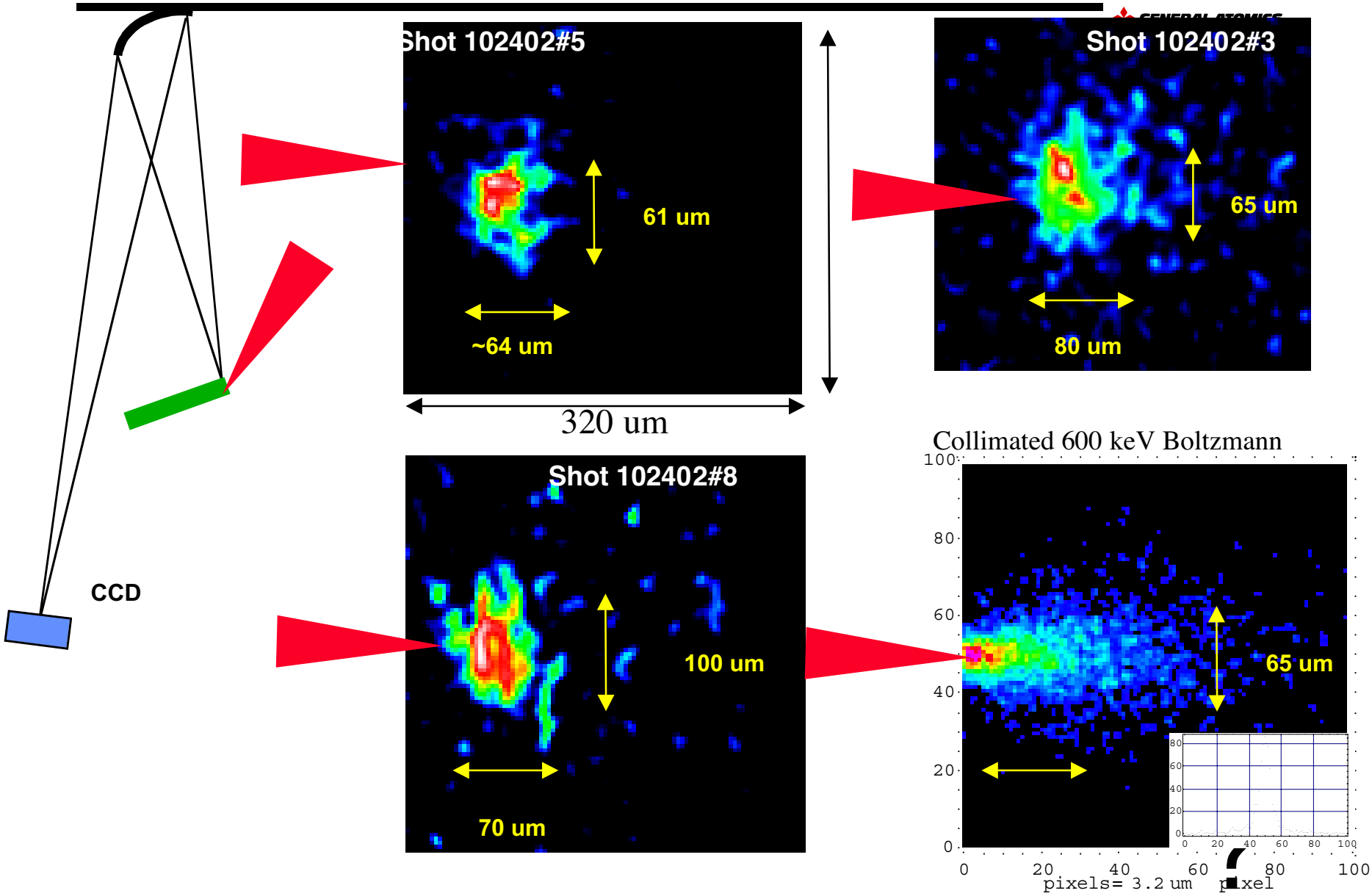

A modest model just how wrong is realistic collisional transport?

F(E) is by choice Gaussian spot intensity profile with 30% energy in central 11 um, balance into wings.
Two temperature profiles-
low energy/isotropic + high energy/directed
(600 KeV Boltzmann + 600 KeV Relativistic Maxwellian)

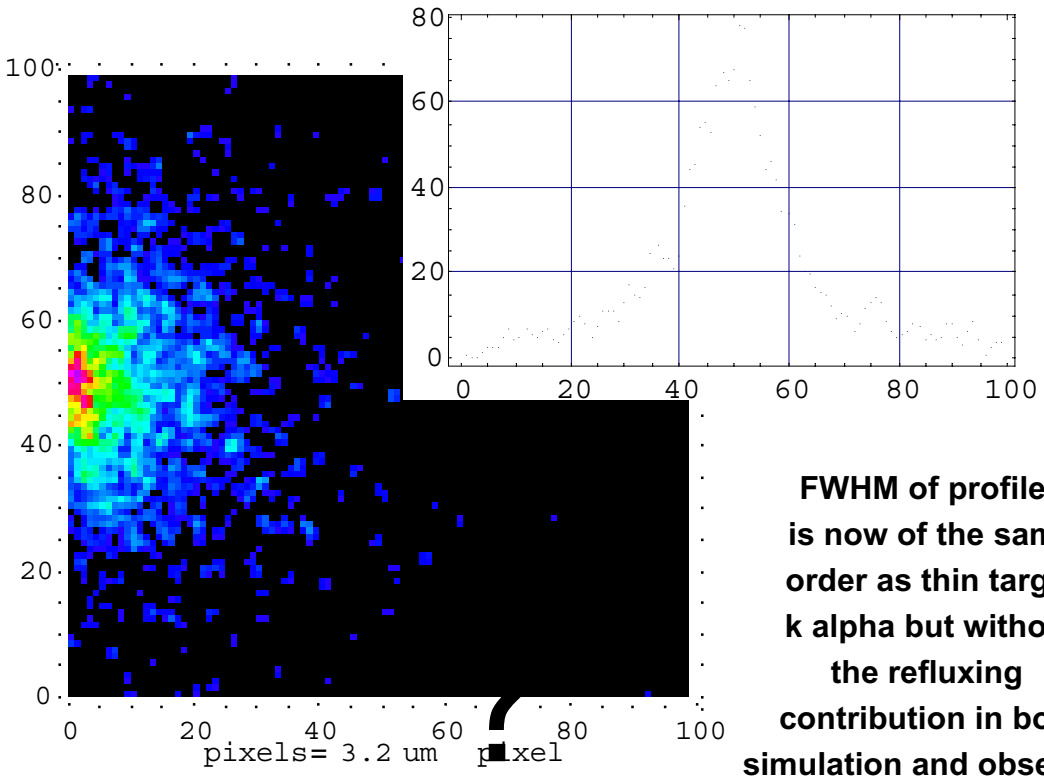

FWHM of profiles is now of the same order as thin target k alpha but without the refluxing contribution in both simulation and observed

Egs4 Monte Carlo Code
-time independent-condescended history electron transport
-full photon and photo-electron cascades down to 1keV
-entire phase space description E(x,k,T)
-benchmarked k-alpha fluorescence

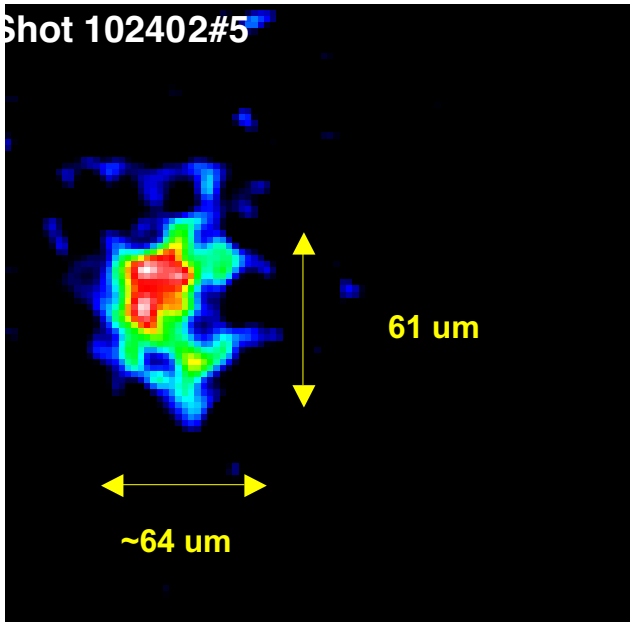

Conclusions

- Extraordinarily complicated electron generation and transport exists for laser intensities normally incident at 10^{18} 10^{20} W/cm^2 (but that really isn t news)

- Transport data from LULI (20J,0.5 ps) and RAL (100J, 0.8 ps) :
- - Different transport for CH verses Al media
  -Wide variability in electron beaming direction similar to PW.
  - agrees with LULI on electron flux patterns (<40° divergent)

- *Very* preliminary results of transverse imaging of relativistic electron transport via Cu k-alpha appear promising. Required photon flux at depths of interest is sufficient. Rough qualitative agreement with Monte Carlo calculations provides useful initial straw-man models of transport for comparison to more more advanced codes.

GENERAL ATOMICS
AND AFFILIATED COMPANIES

Compression Dynamics of an Indirect Drive Fast Ignition Target

R.B. Stephens

General Atomics

S.P. Hatchett, R.E. Turner

Lawrence Livermore National Laboratory

K.A. Tanaka, R. Kodama

Institute for Laser Engineering

This work was performed under the auspices of the U.S. Department of Energy under Contract No. DE-FG03-00SF2229, by the University of California, Lawrence Livermore National Laboratory under Contract No. W-7405-Eng-48, and with the additional corporate support of General Atomics.

Is a reentrant cone shell a feasible approach?

- **Questions for this study:**
  - Can one assemble a usable core?
  - Is the anisotropic implosion properly described with existing hydro models?
- **Results:**

  Target hydro is well modeled by standard codes

  The fuel is assembled in a reasonably compact form.

  Indirect drive x-rays generate Au vapor from the surface of the gold cone and that vapor is mixed into the low density core.

  Minimizing that contamination source is important

Experimental setup - Shell

- Target was scaled from the NIF ignition target and driven in a scale 1 hohlraum with 14 kJ from Omega.
- Shell is 510 μm od with a 57 μm thick plasma polymer wall.
- Cone is ~ 50 μm thick Au with a hyperboloidal tip (focii separation 40 μm) and a 35° half angle; the intersection of the asymptotes are 12 μm from the center of the shell.

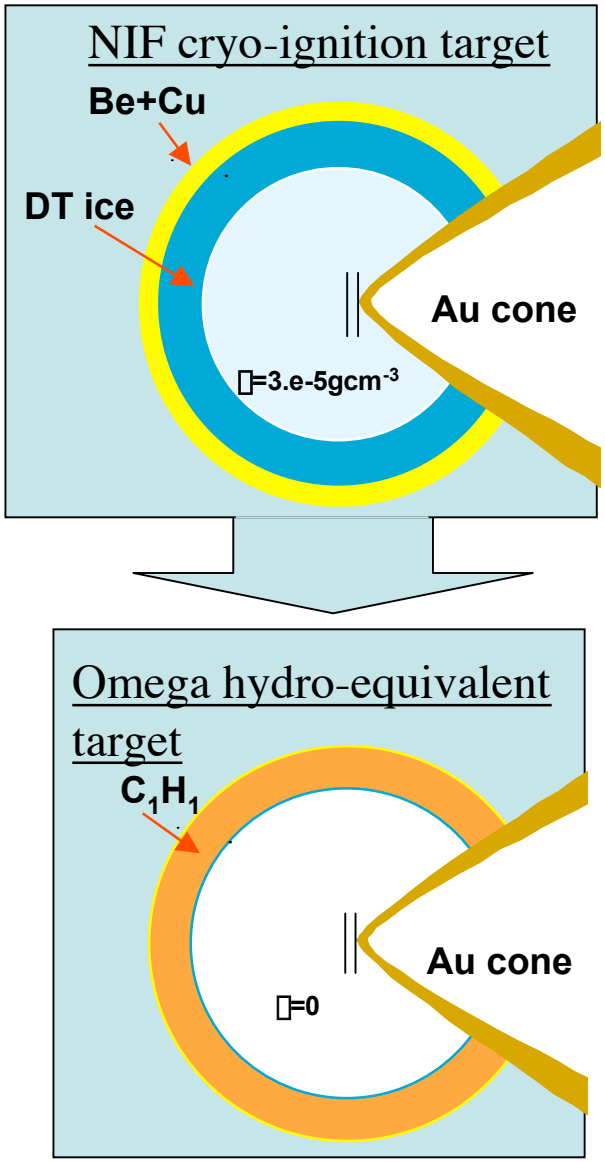

Experimental setup - Hohlraum

- Backlighter windows orthogonal to hohlraum and cone axes; Fe (6.7 keV) radiation.
- Gold cone stepped outside the shell to avoid the high angle laser beams and to avoid creating hot spots on the cone surface close to the shell.

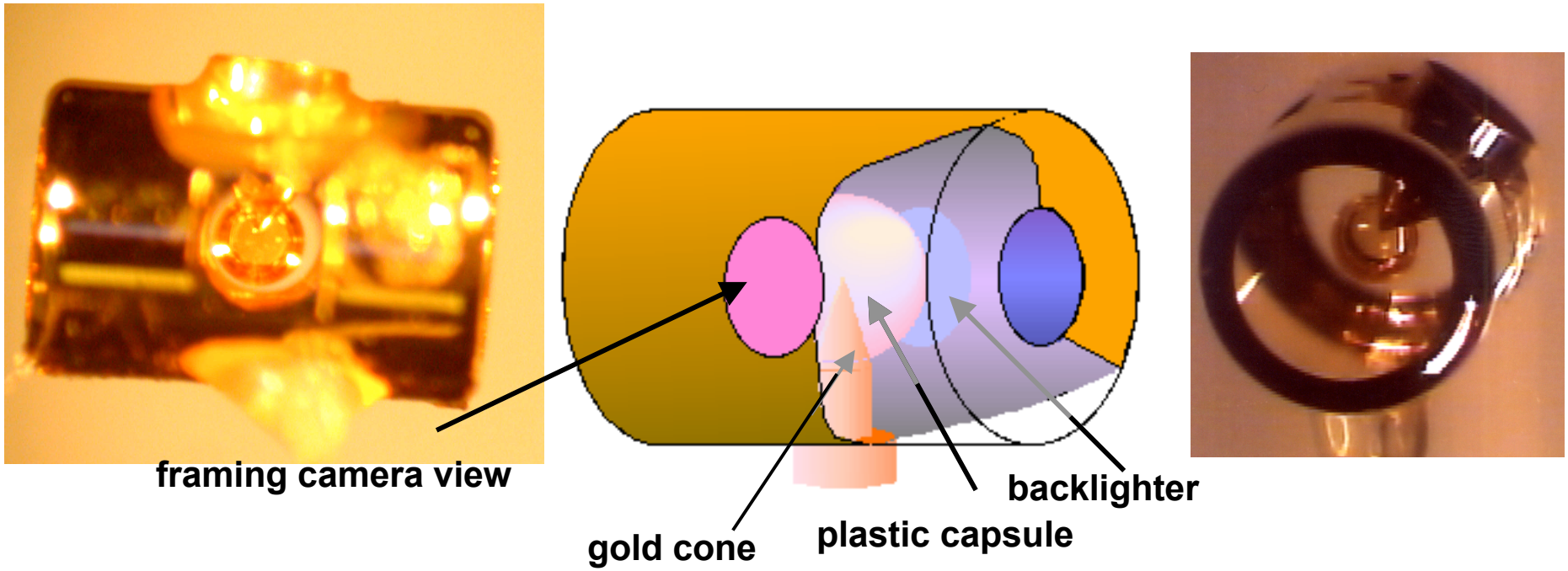

Image sequence shows symmetry and size

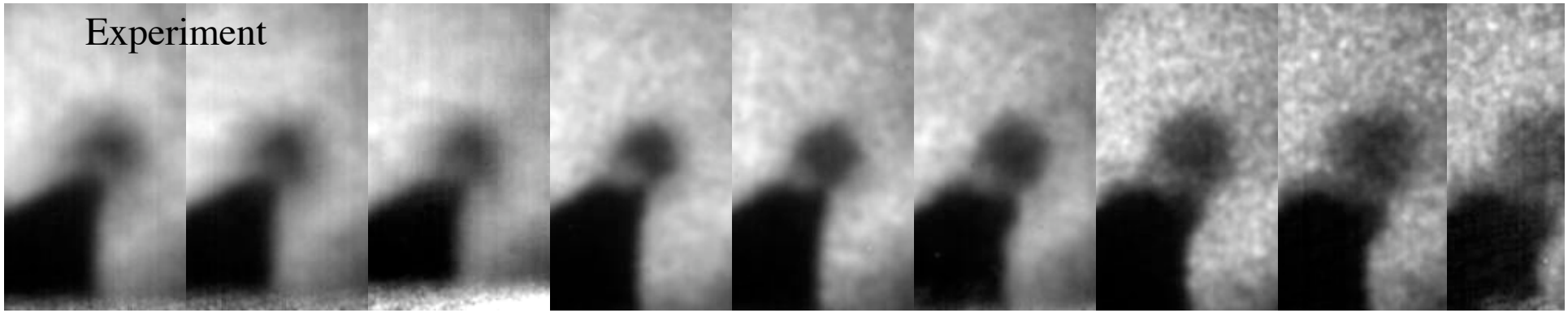

Stagnation

Time (ns) 3.2 3.3 3.4 3.5 3.6

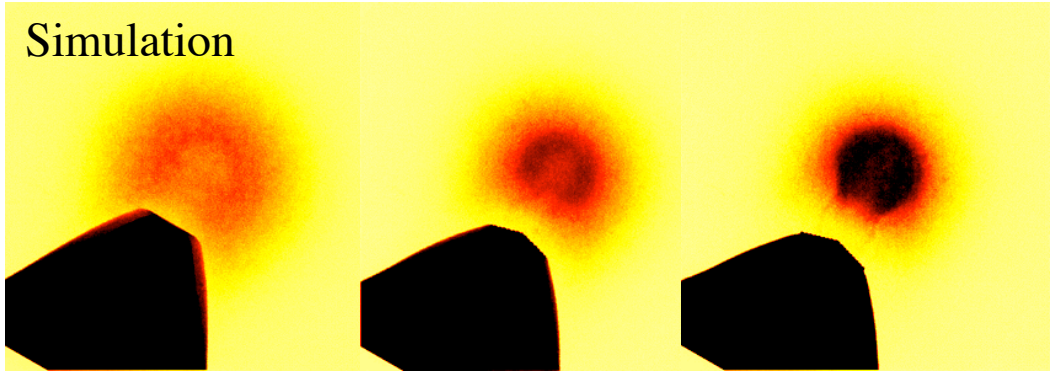

100 μm

- Shell images are very similar to previously calculated simulation
- Cone images are initially too pointed, then blow apart

Lineouts are used to quantify plasma evolution

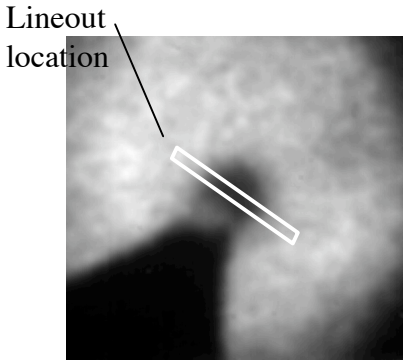

- Background descibed w/ parabola fit at edges away from shell obscuration
- Dark count estimated from unexposed regions of image
- Profiles smoothed w/ 30 μm boxcar average

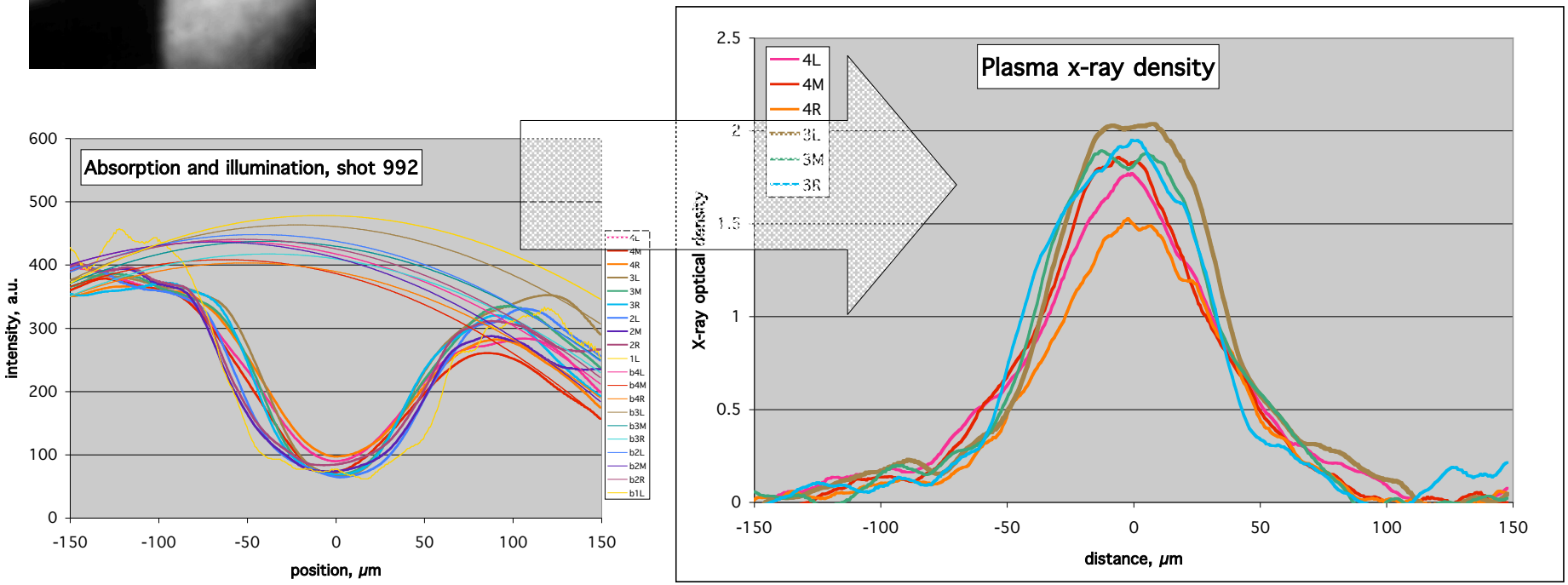

Compressed shell to a compact mass

- m/m_o~30%
- ρ_{st}~20g/cc
- ρR~0.07g/cm^2

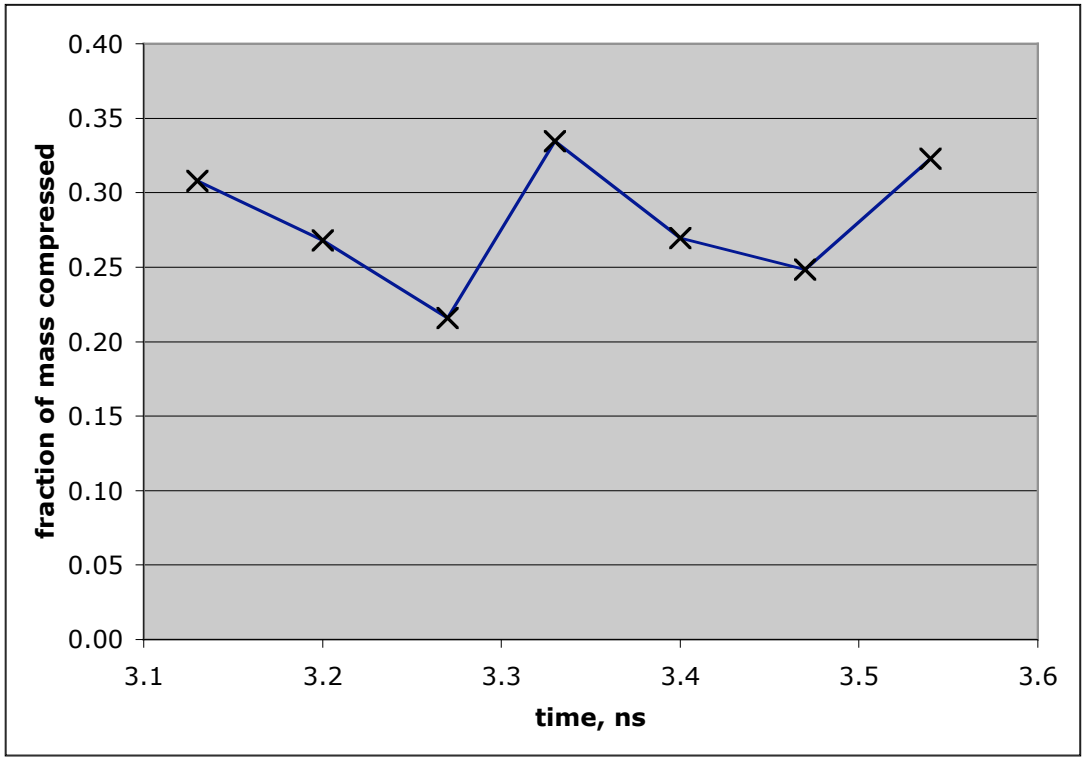

Exptl profiles don't match simulations

- Pre-stagnation, profiles have strong central absorption
  - fwhm and maximum density don't change much
- Stagnation profile like homogenous sphere

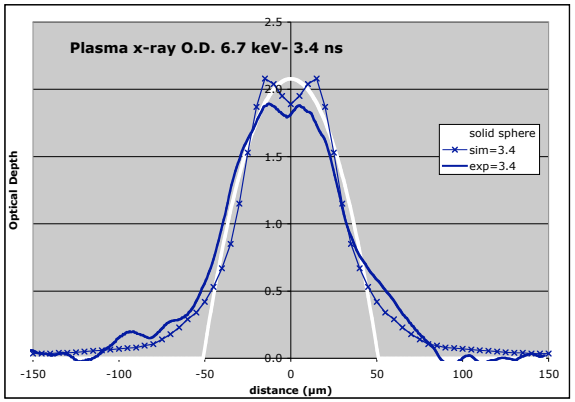

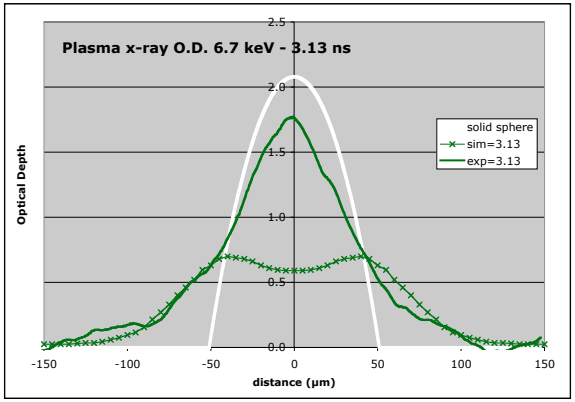

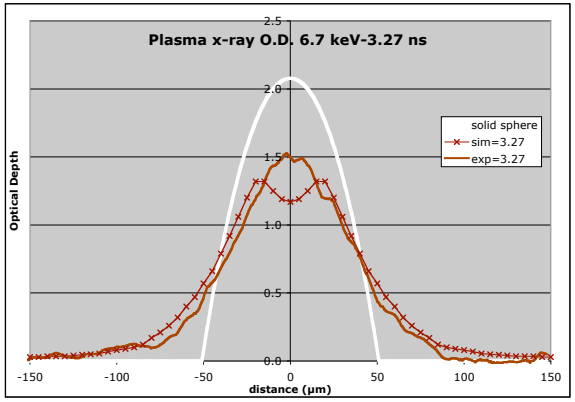

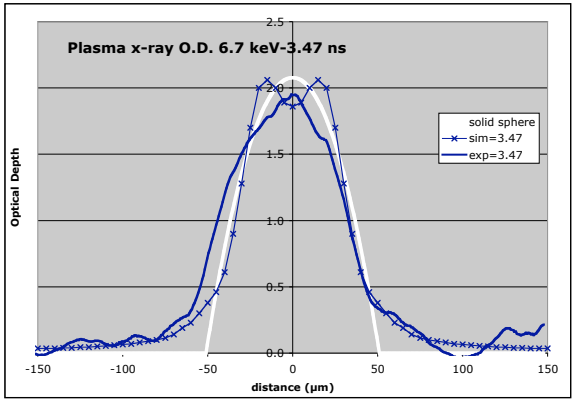

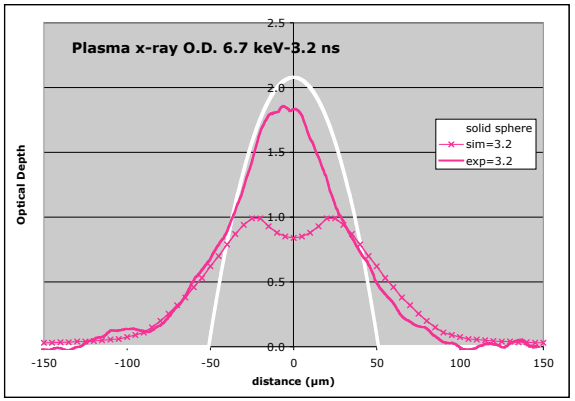

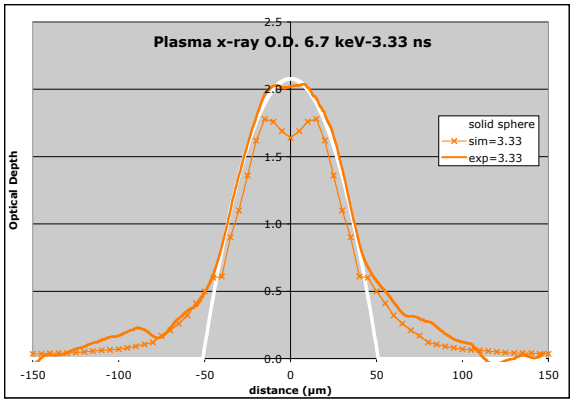

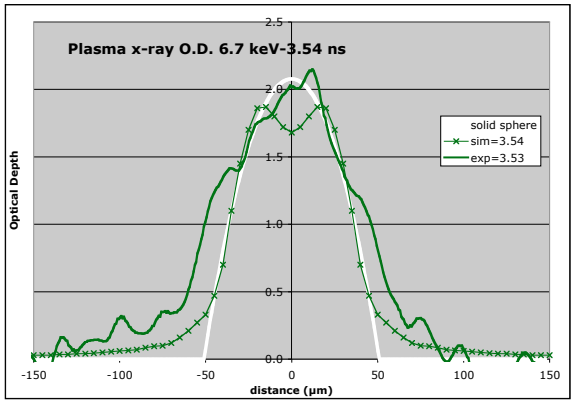

Before stagnation

Near stagnation

After stagnation

RBS:

And cone is vaporizing!

- The pointed shadow is not that of the hyperboloidal cone
- Log grey scale shows transmission through vapor
- Au m-lines (~2.5keV) penetrated shell and heated the cone

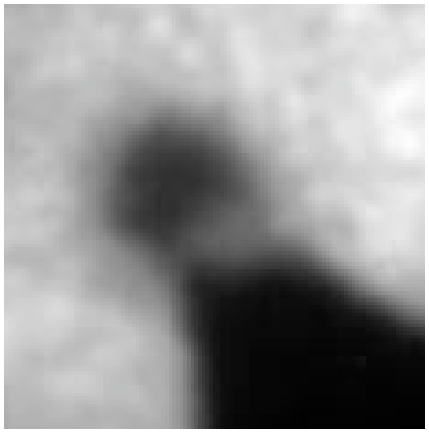

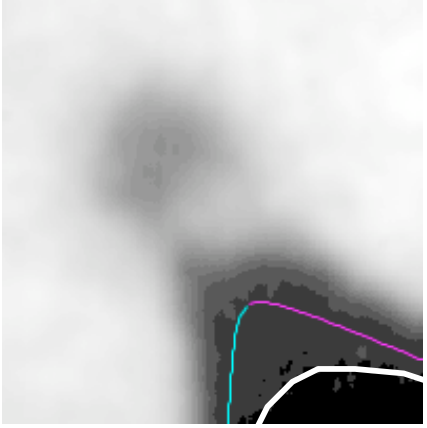

(log grey scale)

Gold getting into central cavity

- Simulation shows gold vapor coming off
  - In absence of collapsing shell, would extend to position of low density core
- Collapsing shell pushes gold back
  - dense gold vapor should not be R-T stable against CH vapor

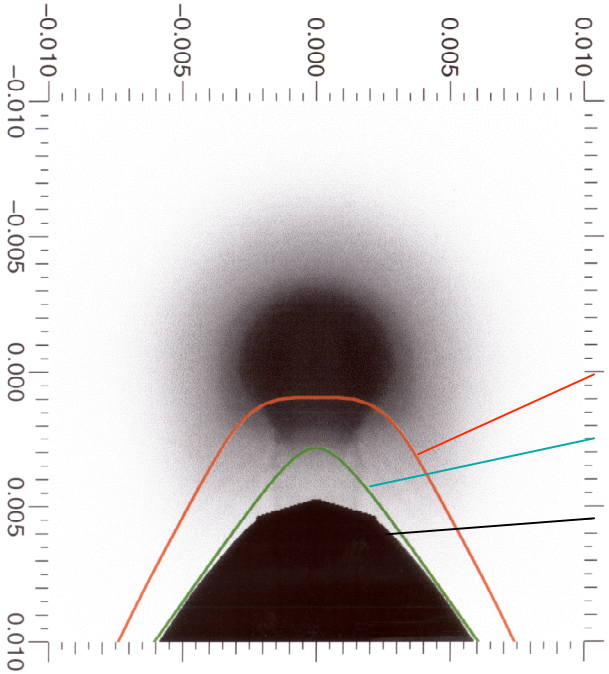

Detailed calculation done w/o Au vapor

Gold vapor limit

Original cone

Deformed cone

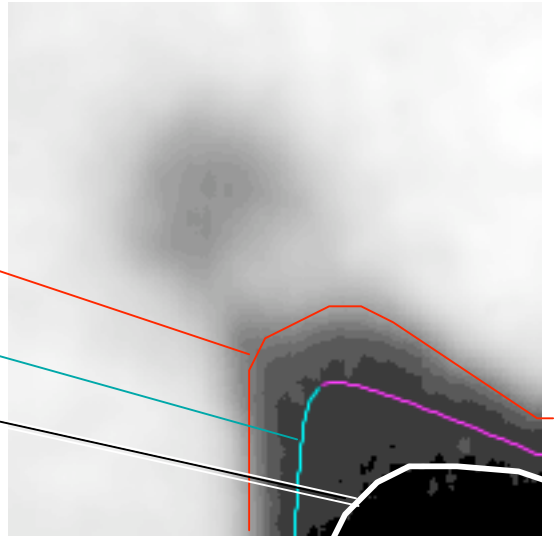

Log grey scale

Gold getting into central cavity

- Simulation shows gold vapor coming off
  - In absence of collapsing shell, would extend to position of low density core
- Collapsing shell pushes gold back
  - dense gold vapor should not be R-T stable against CH vapor

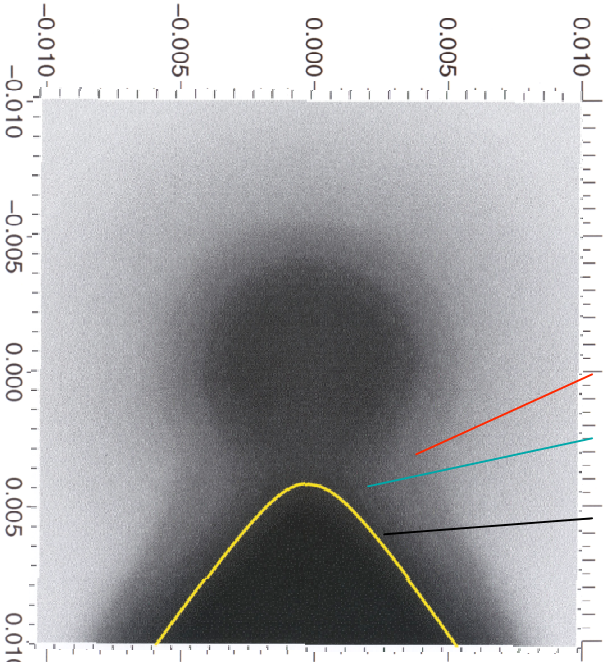

Calculation done w/ Au vapor added

Gold vapor limit

Original cone

Deformed cone

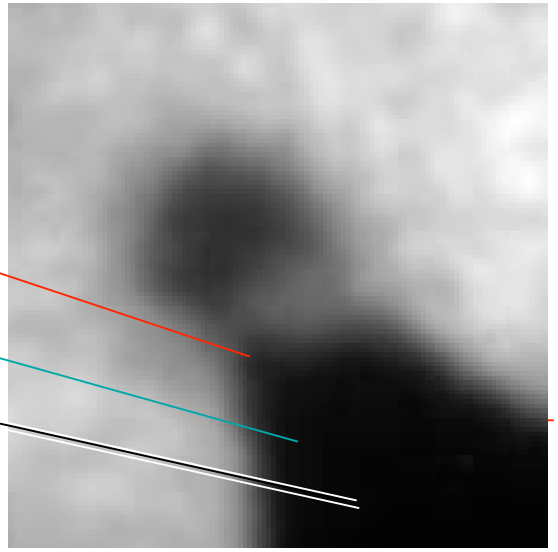

Lin grey scale

Gold absorption disappears at stagnation??

- 20% of pre-stagnation absorption in sharp central peak
  - Causes anomalously narrow half width
  - Attribute to gold in low density core
- Central peak disappears at stagnation
  - Mix into dense shell?? - unlikely
  - Squirted toward cone?? - $v_{core} \sim 300 \mu m/ns$
- Gold amounts to ~0.4 wt% of total mass
  - Fatal in dense shell (~0.1wt% is limit)
  - Irrelevant if confined to low density core

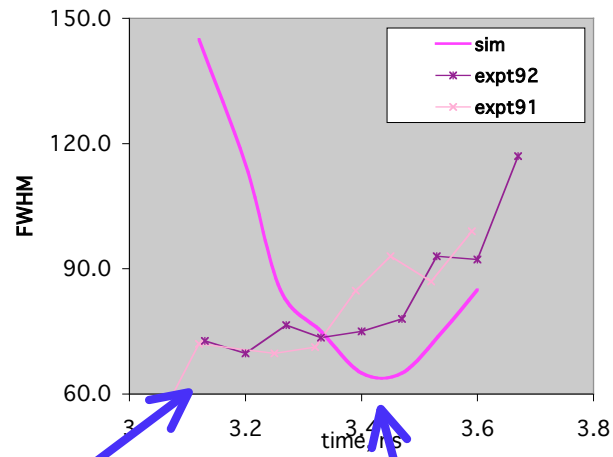

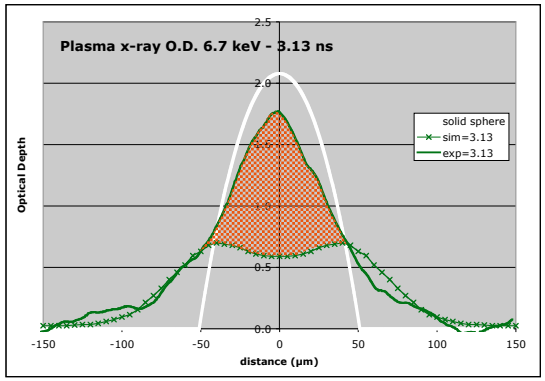

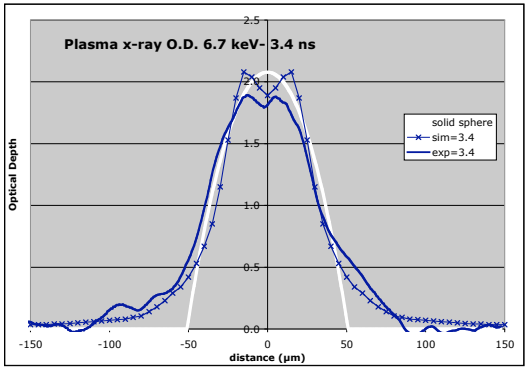

Design target to minimize contamination?

- Penetrating radiation comes from non-thermal m-line radiation
- Not easily avoided - all cocktail elements have similar lines
- How does problem scale in going to ignition scale?
  - Hohlraum intensity larger
  - Thicker shell wall absorbs better (abs length at 2 keV ~100 μm for C, Be)
  - Can't model transfer efficiency of Au to dense shell.
- Can restructure target
  - Low Z coating on cone
  - Shine through barrier (for keV x-rays)
  - Direct drive target

Cocktail Elements m-lines
41Nb ~2.7 keV(L)
57La ~1 keV
60Nd ~1.5 keV
64Gd ~1.5 keV
73Ta ~2 keV
74W ~ 2 keV
79Au ~2.5 keV
82Pb ~ 2.8 keV
83Bi ~ 3 keV
92U ~ 4 keV

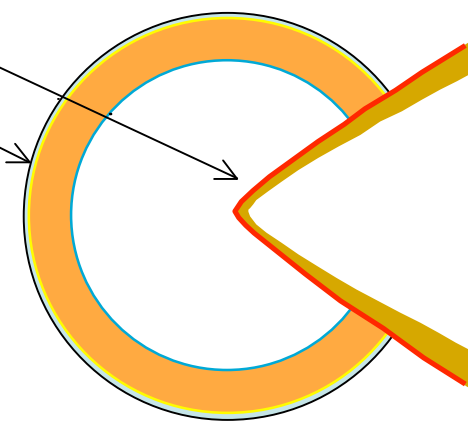

Summary

- Target hydro is well modeled by Lasnex
  - Max density, size, topology
- The fuel is assembled in a reasonably compact form
  - 0.3 of the total mass is compressed, density~20 g/cc, rR~ 0.07 g/cm^2
- Indirect drive x-rays generate Au vapor from the surface of the gold cone and that vapor is mixed into the low density core.
  - ~0.4wt% of the mass of the target
  - ? Vapor possibly not mixed in with the dense fuel
- Minimizing that contamination source is important
  - low z cone coating
  - a shine through barrier (for keV x-rays
  - **direct drive.**

29219 Framing Camera image

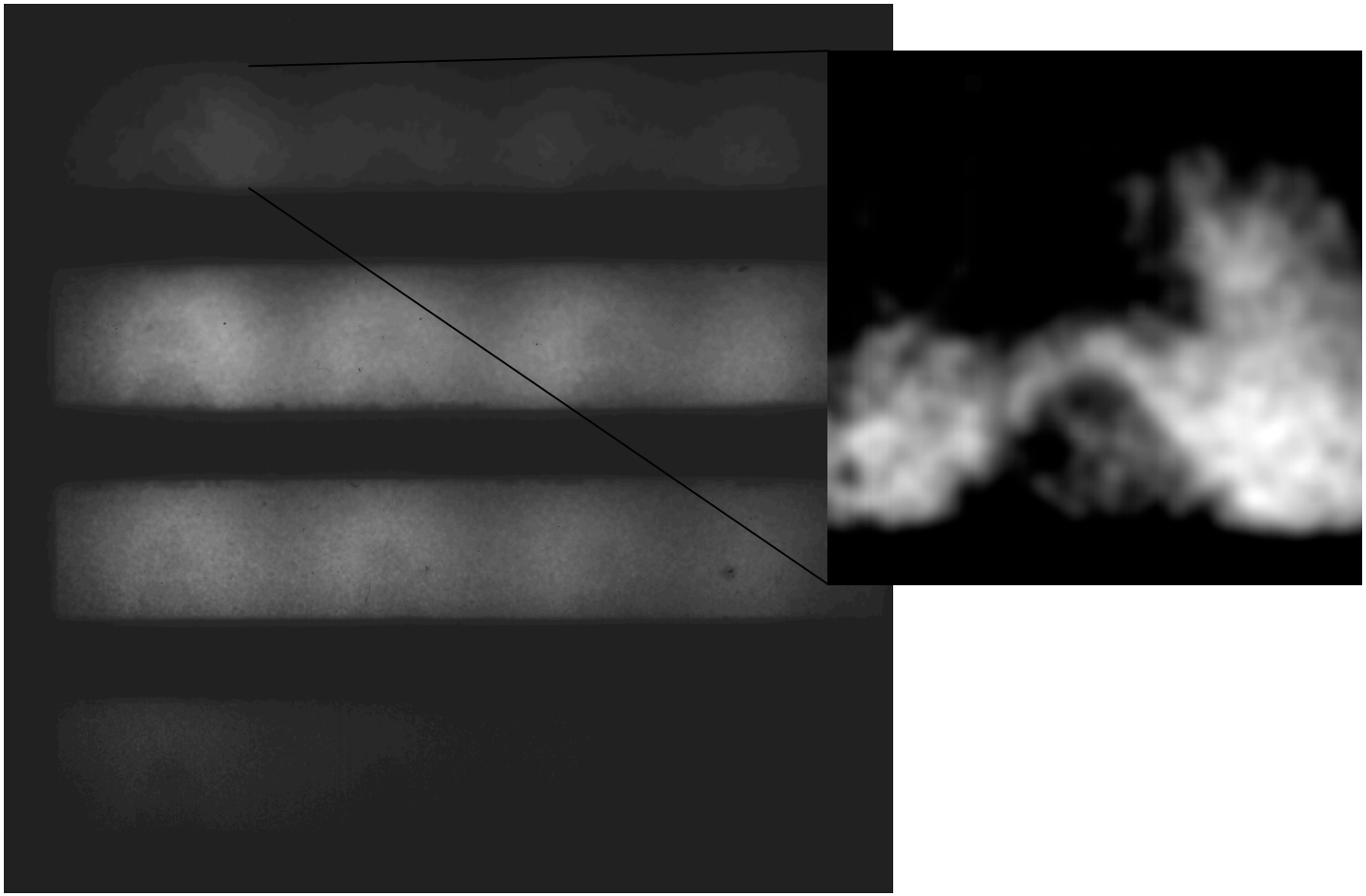

RBS:11/19/02

29219 Individual images

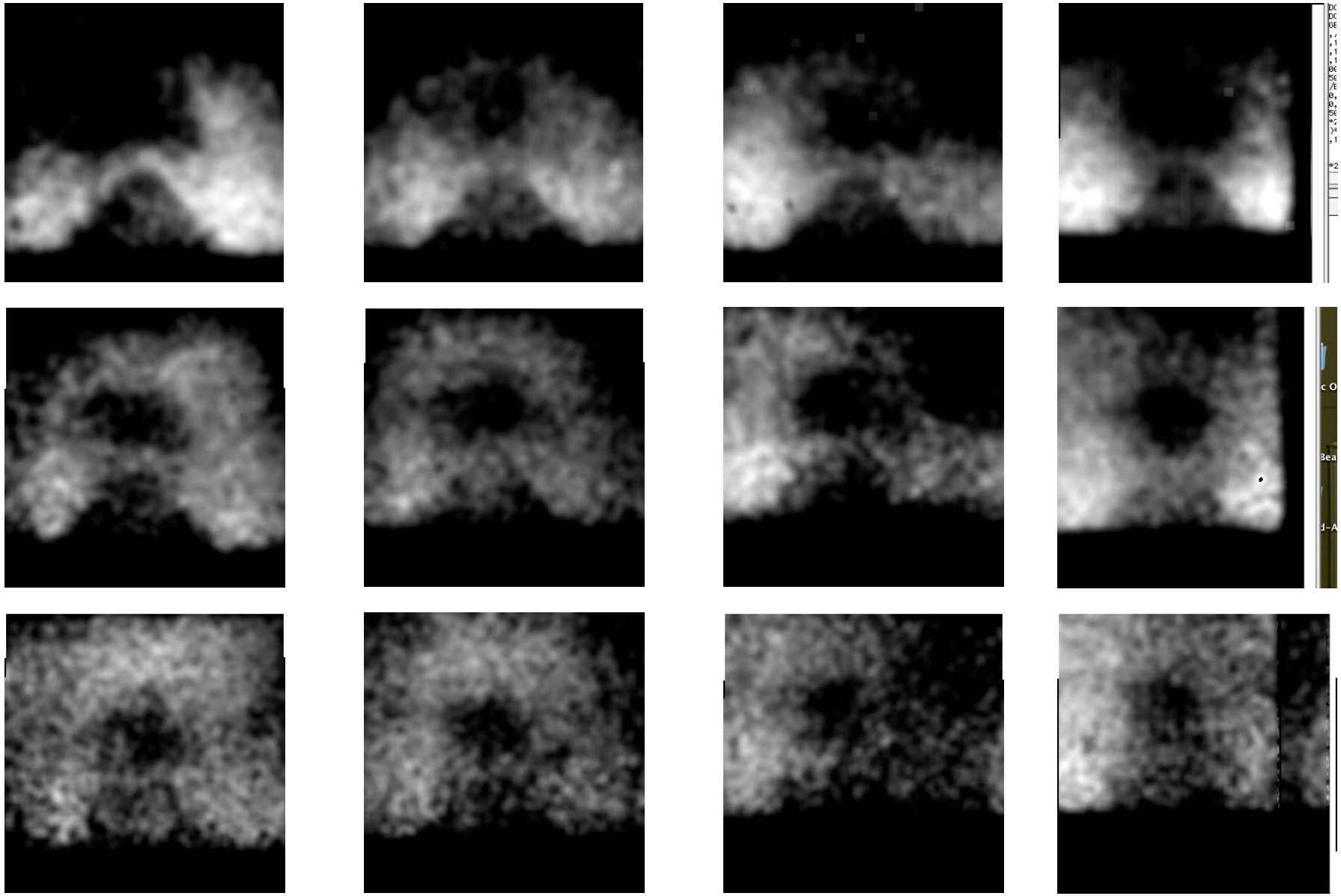

RBS:11/19/02

Fast ignition targets for fusion energy

Rich Stephens
General Atomics

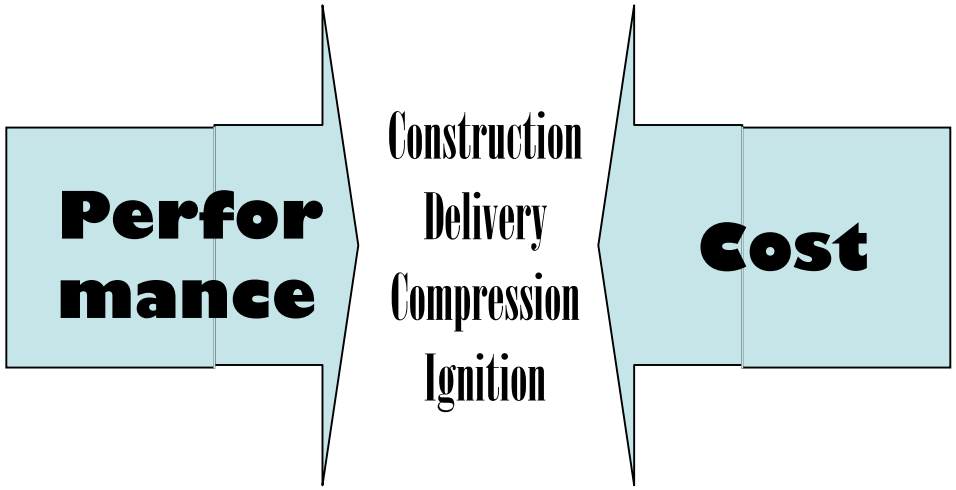

Fast Ignition Workshop 2002
St Pete's Beach, 16-19 Nov '02

FI targets must meet multiple constraints

- Construction - cost
  - Fast throughput - reduces tritium inventory
- Deliver to TCC - robust
  - Survive heating by radiation, uneven gas conduction
- Compress - performance
  - Produce compact mass (minimize hot spot)
- Ignite - gain
  - Efficient delivery of short-pulse energy

Target factories for central hot spot targets seem feasible

- Chemical engineering approach to Target Fabrication Facility (TFF)
- Costing is done for an “nth-of-a-kind” plant
- Results guide process development

Major Parameters

- 500,000 targets per day
- 2-3 weeks on “assembly line”
- Installed capital of $97M
- Annual operating cost of $19M
- Cost per injected target estimated at 16.6 cents

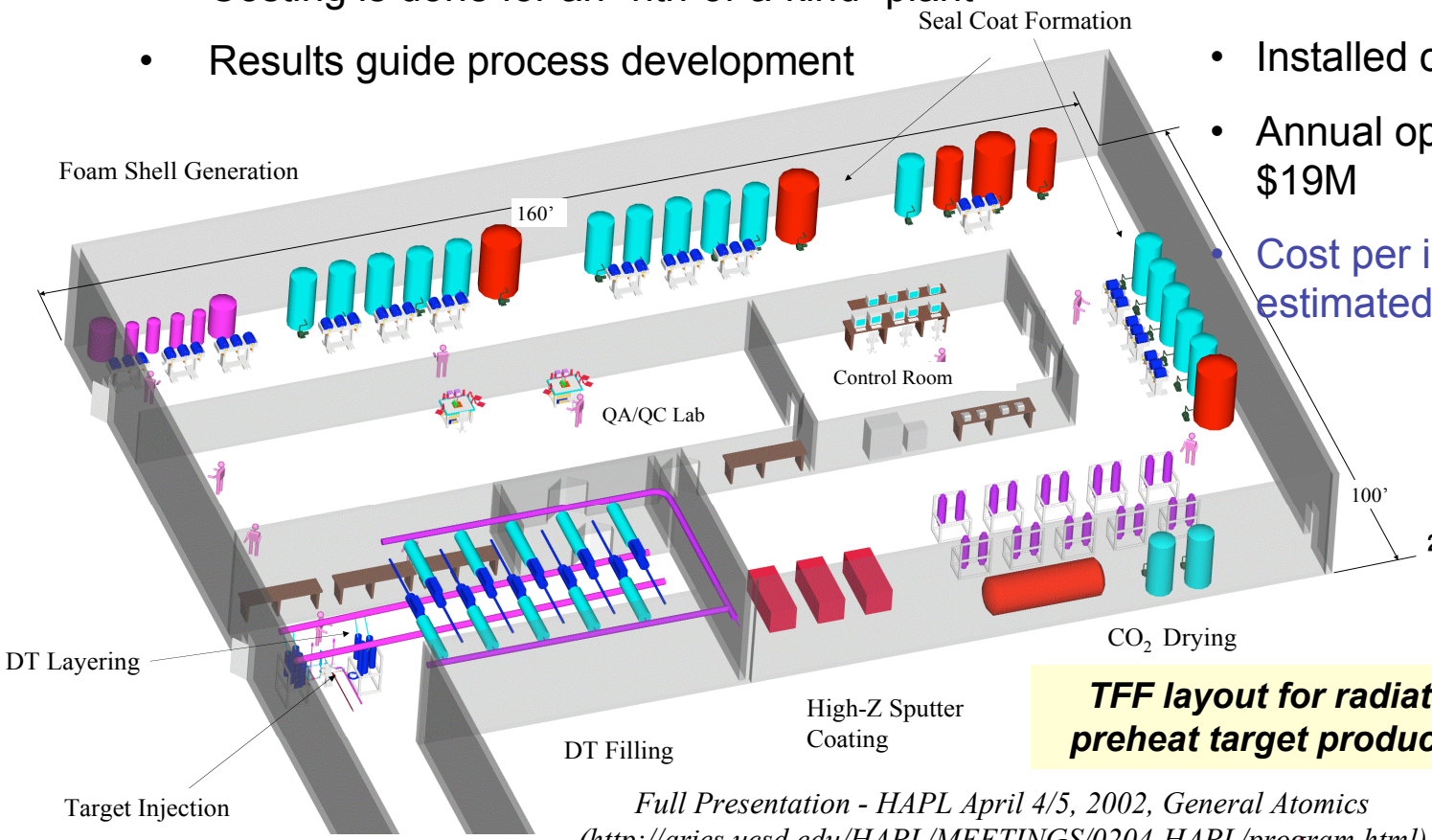

NRL radiation preheat target

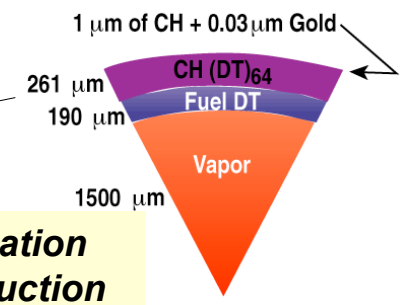

TFF layout for radiation preheat target production

Full Presentation - HAPL April 4/5, 2002, General Atomics (http://aries.ucsd.edu/HAPL/MEETINGS/0204-HAPL/program.html)

Direct capsule fabrication by microencapsulation

Schematic of microencapsulation

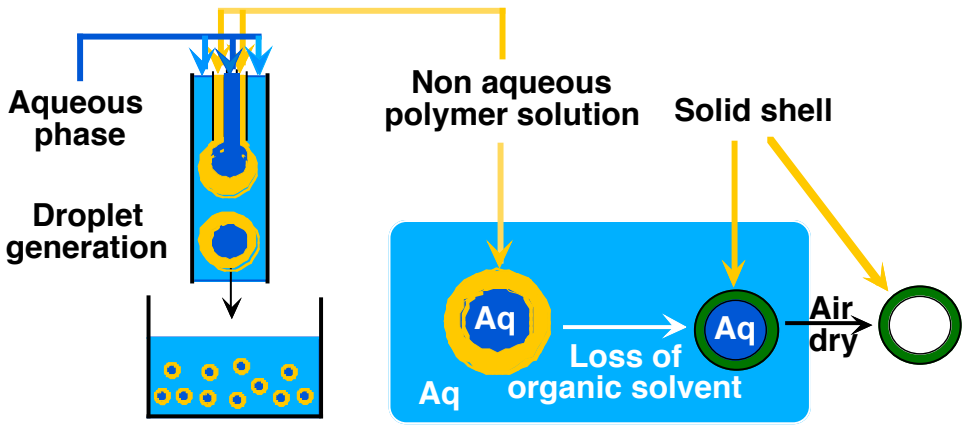

Power spectrum of 4.6mm CH capsule, 45 μm wall, OOR <1% of radius, NC <3% of wall, rate 36/minute (M. Takagi)

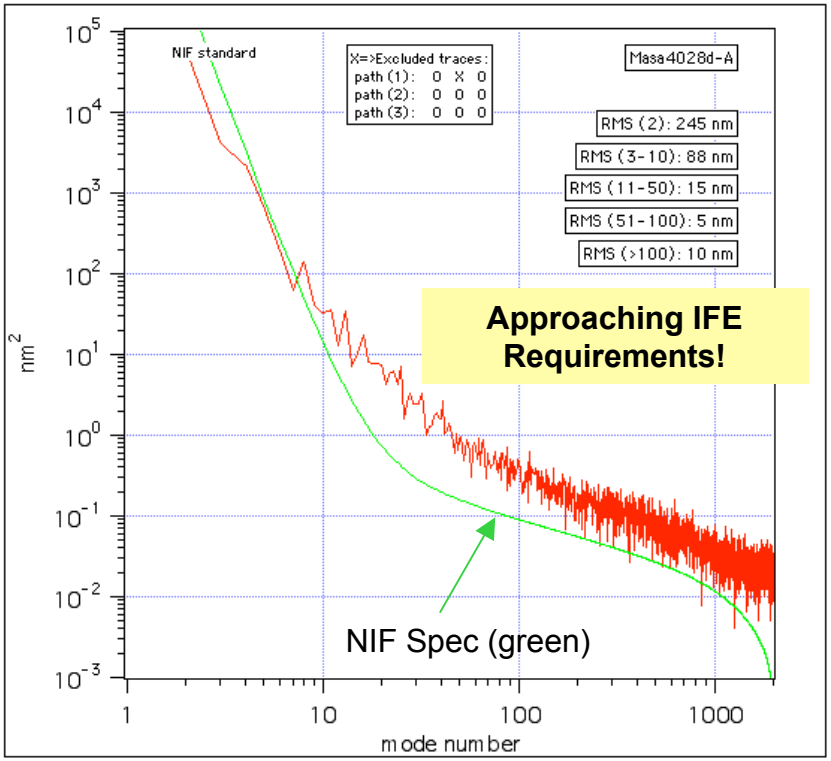

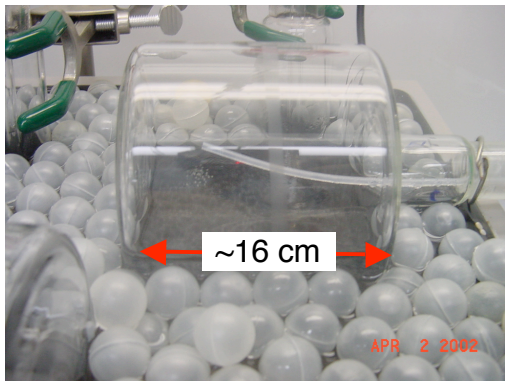

Laboratory scale rotary contactor

Microencapsulation may be most cost-effective pathway...

GENERAL ATOMICS

But FI targets are problematical

- Asymmetry causes construction complexities
  - Must make robust joint between reentrant cone and shell
  - Must set up uniform ice layers
- High Z cone causes contamination worries
  - Must minimize cone heating
  - Must limit mixing in collapsing shell

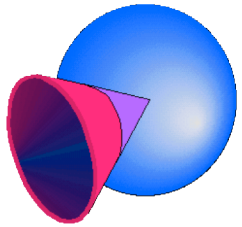

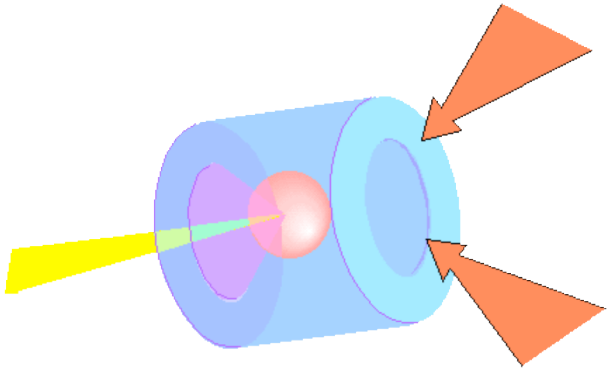

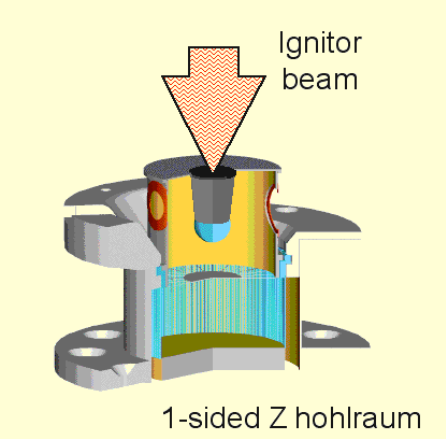

There are much faster ways to make targets

- Stamp out and join hemishells

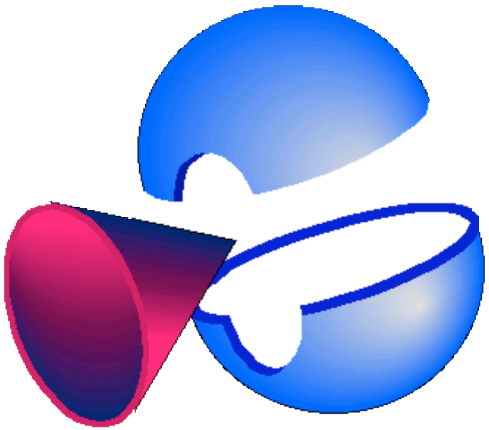

- Injection mold and freeze in place (use foam for opacity adjustment)

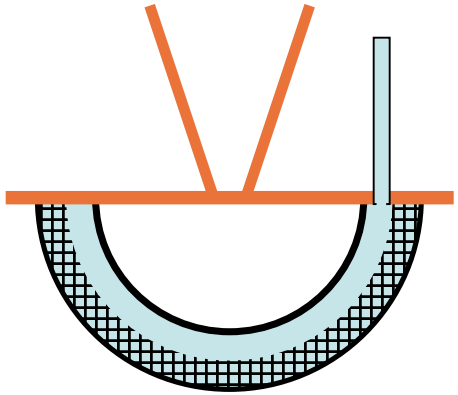

Ref S.A. Slutz "Fast Ignition capsules using liquid fuel"

There are advantages in direct molding of targets

- Avoids stresses from cooling
- Avoids diffusive fill and beta-layering
- Avoids vapor transport (unsuitable for asymmetric FI targets
- Avoids tight temp controls
- Allows longer heatup time on injectio
- Pure DT Allows lower absorption for Dir Drive(but that interferes with compression)

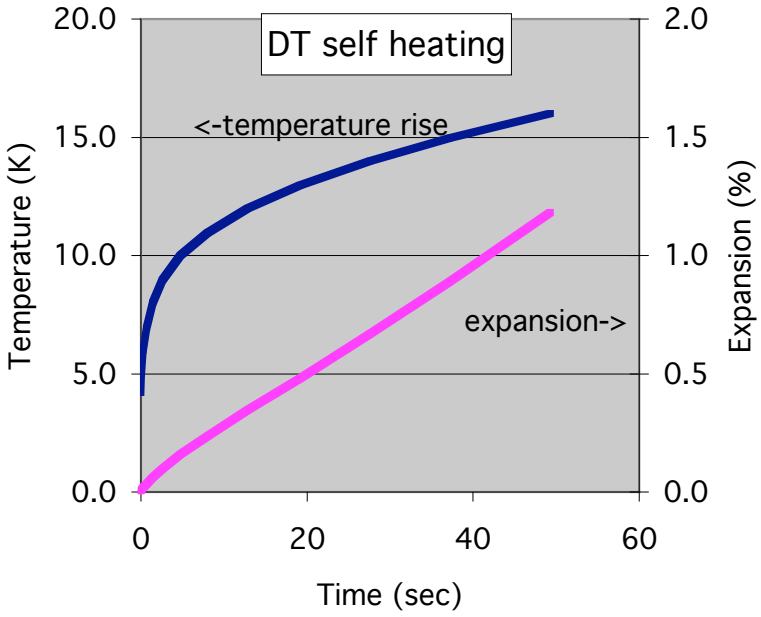

†This make a significant difference in target fab economics

GENERAL ATOMICS

Mold contamination might be tolerable?

- Low density core will contain debris from initial structure
  - Inner wall partially vaporizes when shock wave crosses
  - Cone surface vaporizes from high energy hohlraum spectrum
- That contamination is largely irrelevant
  - Reentrant cone geometry ejects such debris (inner mold surface might be a problem)
  - Fast Ignition doesn't burn low density volume
- Must worry about mixing of low density core with dense shell
  - Thin RT unstable shells used to eliminate low density core would be sensitive to these impurities

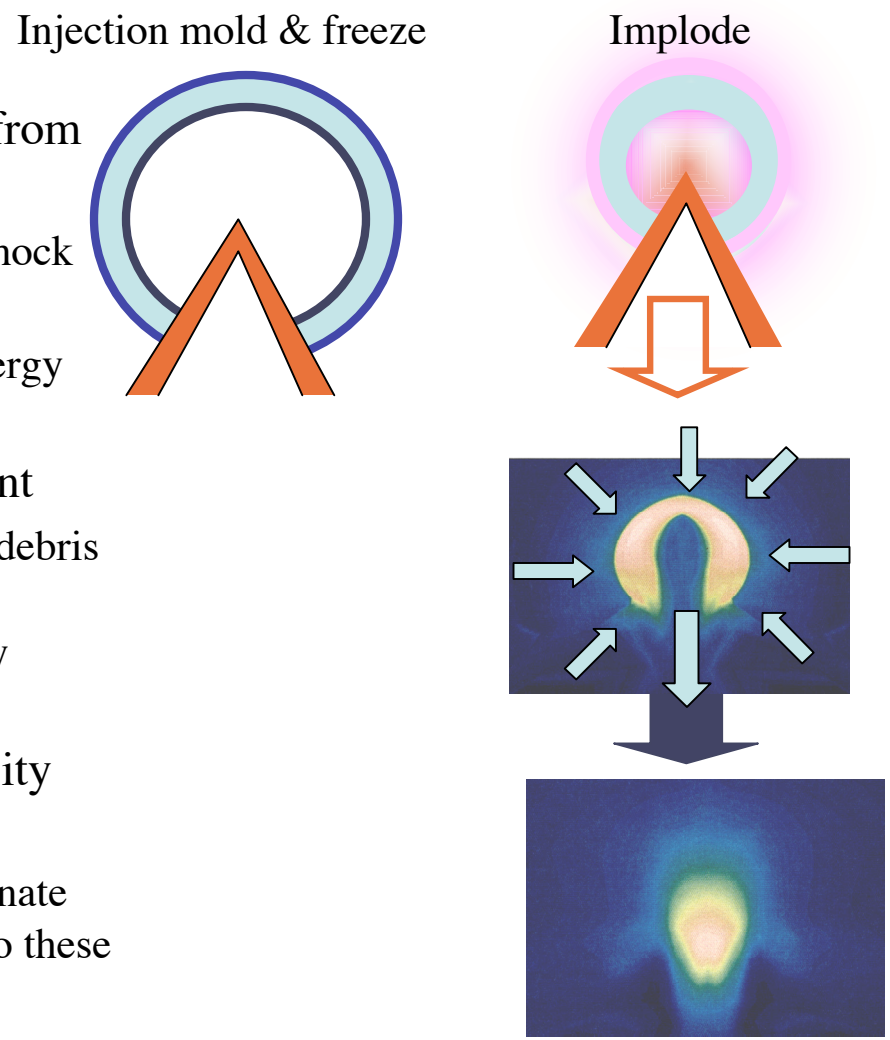

Important to minimize high mode instability growth

- Minimize gas in central core with high aspect ratio shell -
  - Allows compact fuel mass
  - But such shells are unstableand require much smoother surfaces
- Minimize inner wall mixing
  - But mixing could quench hot spot and allow more compact mass

Direct drive targets - an unprotected target will not survive with high chamber gas pressure

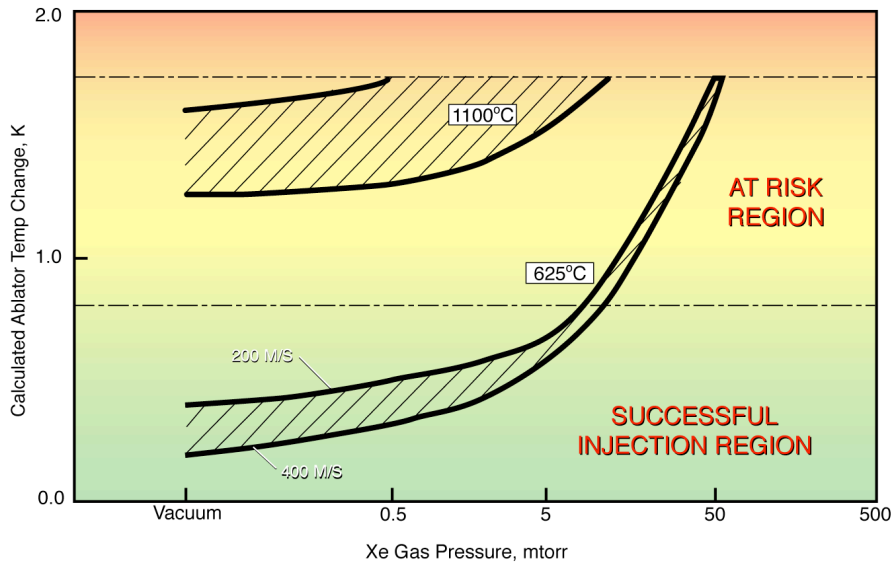

The chart above was "optimistic"

- Assumes 98% reflectivity (300 A gold is about 96% reflective, palladium is less)
- Uses average convection heat flux (peak flux up to 3 times higher)
- Does not include condensation
- Gas may be much hotter than chamber wall (with significant plasma heating)

GENERAL ATOMICS

A cone shields its shell from asymmetric heat flux

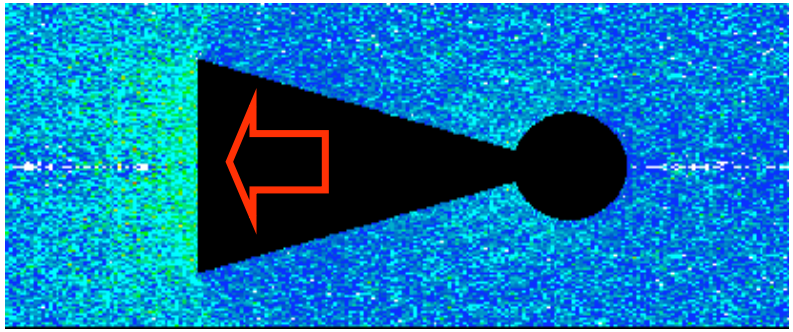

The cone provides a 3-fold decrease in the max heat flux as compared with the unprotected target. Improvement over flat shield is due to gas reflection off lateral surfaces.

Radius of the shield - 4mm
Radius of the target - 2 mm
Temperature -1773 K
Density STD - 50 mtorr
Speed - 400 m/s

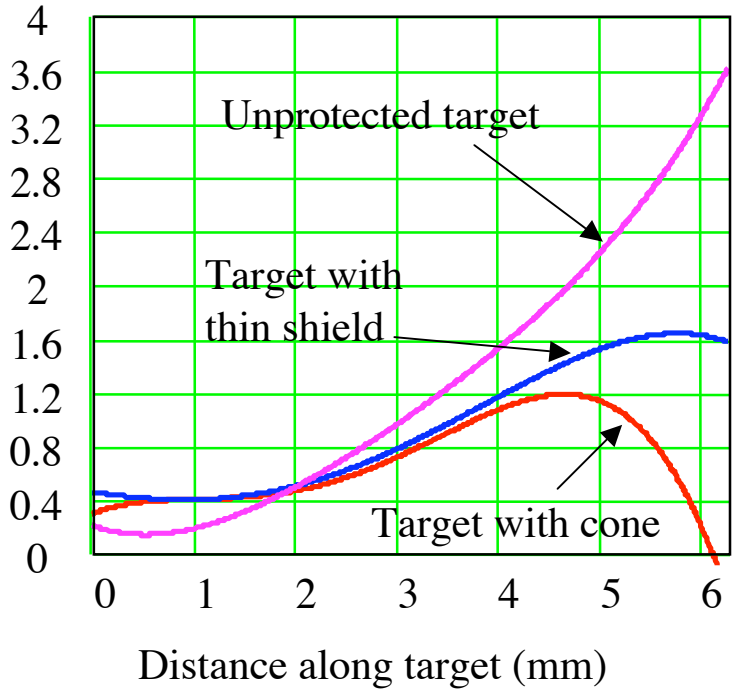

GENERAL ATOMICS

Also have to be careful of radiation load

- Must maintain proper coupling to laser drive
  - NRL target uses metal surface for radiation preheat, W, Au, Pd,…
- Require reflection >~98%
  - AuPd is acceptable
  - Can't disperse metal into ablator
- Or transmission >~98%
  - Is that possible?

NRL radiation preheat target

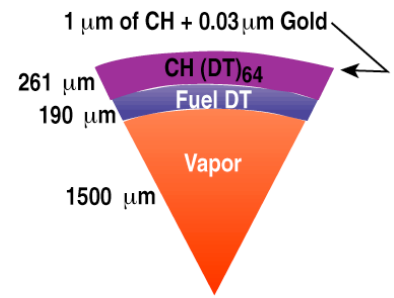

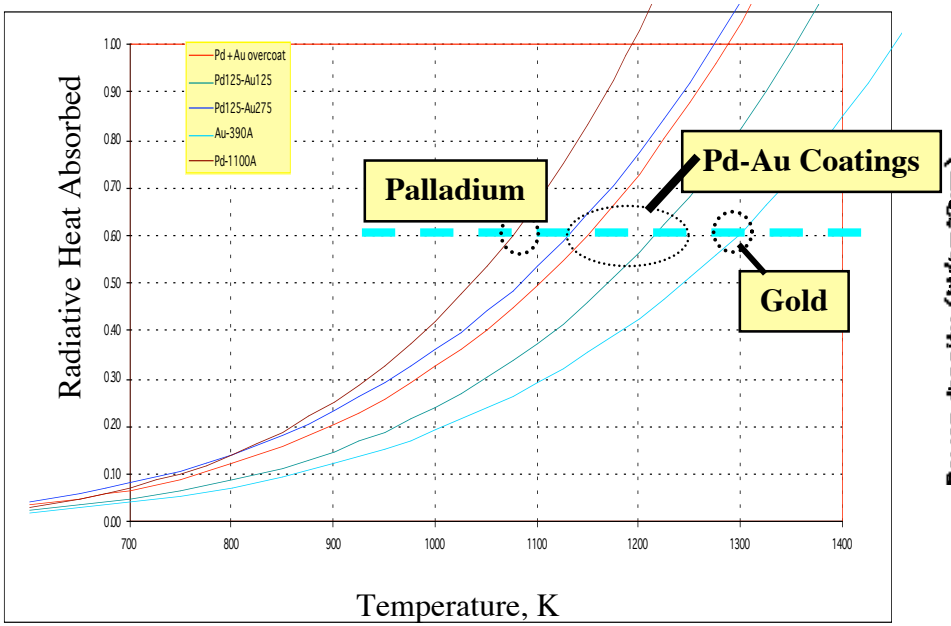

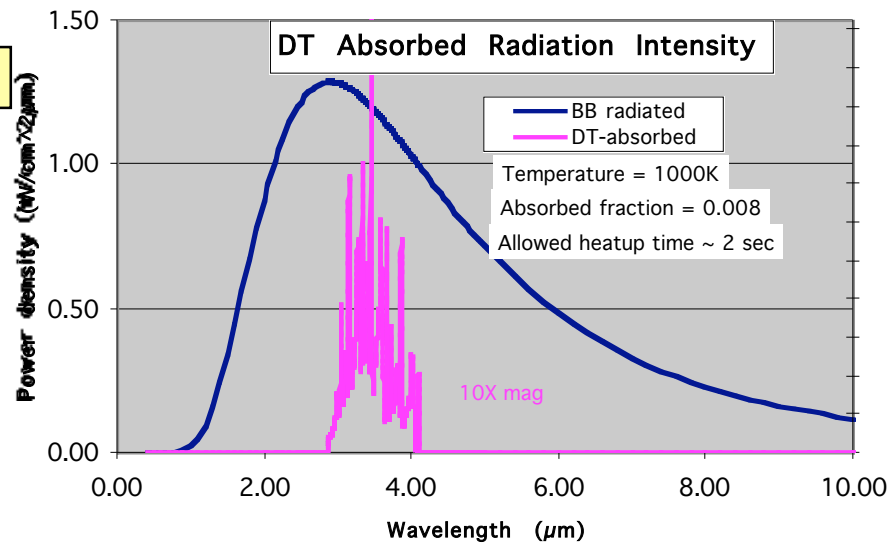

GENERAL ATOMICS

Cone serves several purposes

- Thermal layering?
  - Perhaps mold or inject
- Mechanical integrity and maintain shape
  - Foam shell would be compliant
  - Must not allow shell distortion on cooling
- Efficient collapse
  - Minimize PdV work on gas

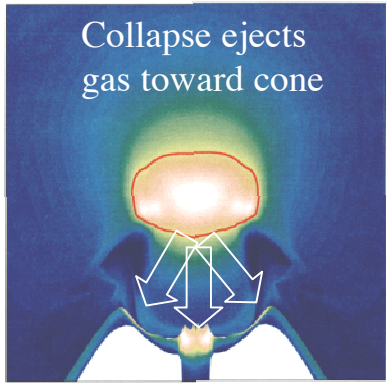

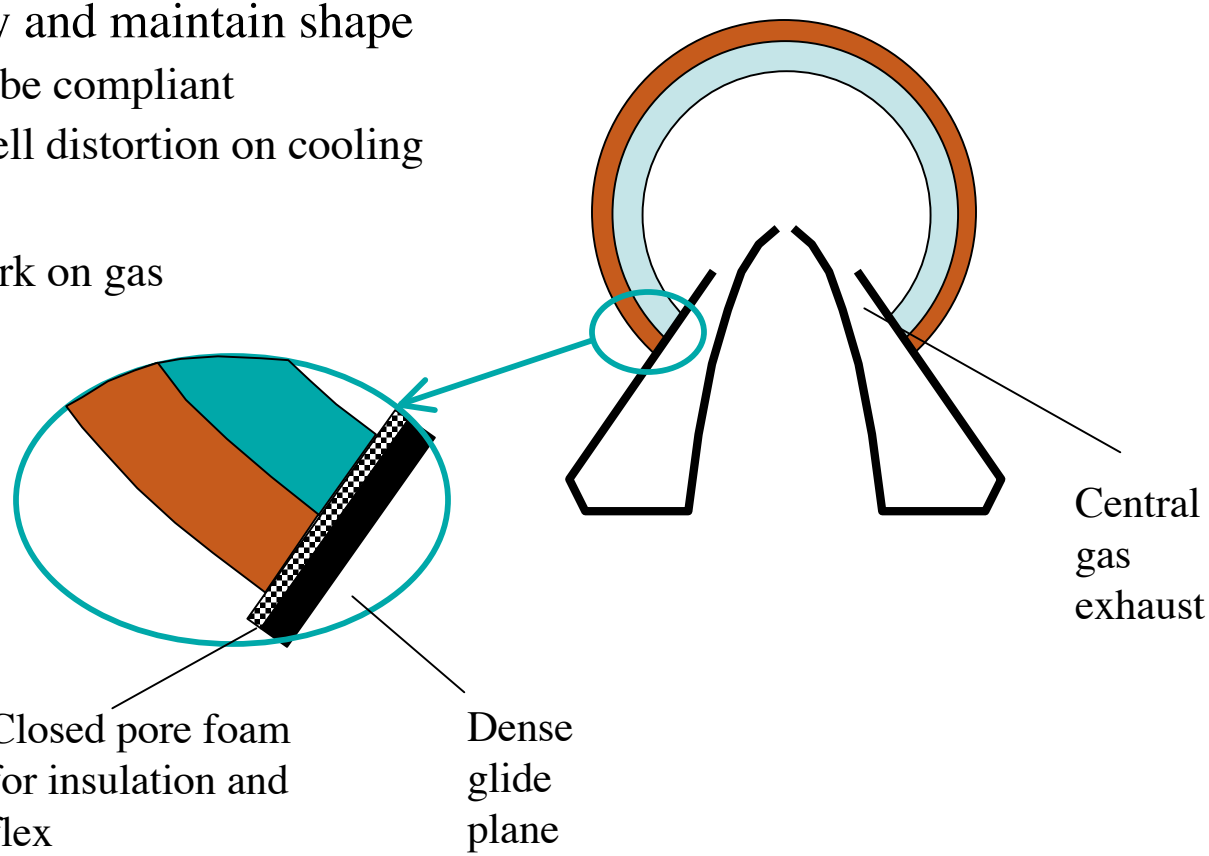

Cone purposes (cont.)

- Exclude plasma
  - Need high density only near outside
  - Longer than blow-off distance
- Focus laser? (outer region of cone)
  - Winston concentrator is most efficient optics
  - Must remain effective for ~30 ps
- Produce electrons (inner region of cone)
  - Gold is efficient
  - What thickness? (survive ~30 ps)

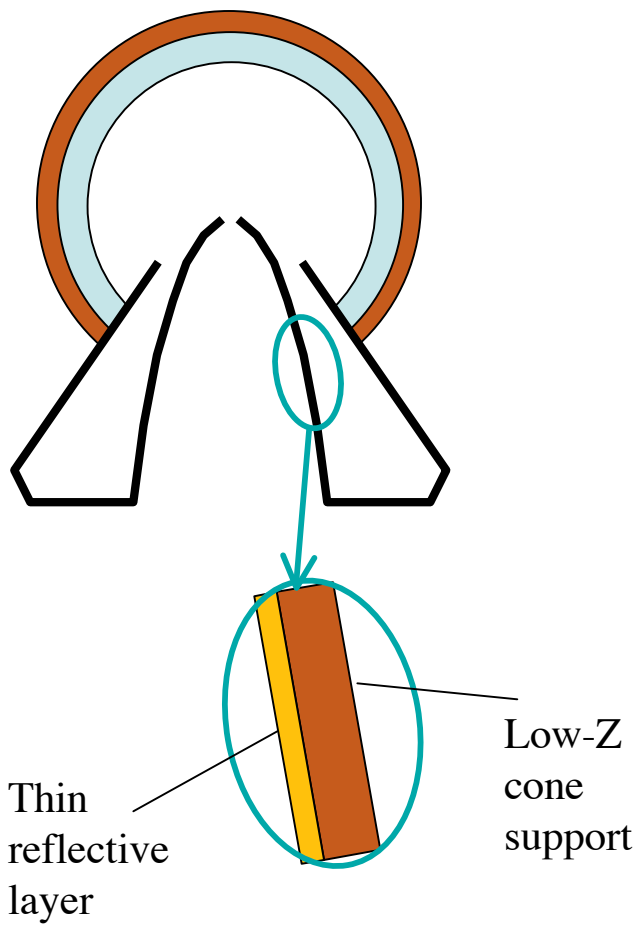

Cone purposes (cont.)

- Guide electrons to shell
  - Is side wall shape important?”
  - Hollow tip cone eliminates interfacial problems?

    (but that puts a jet of gas down the center of the cone)

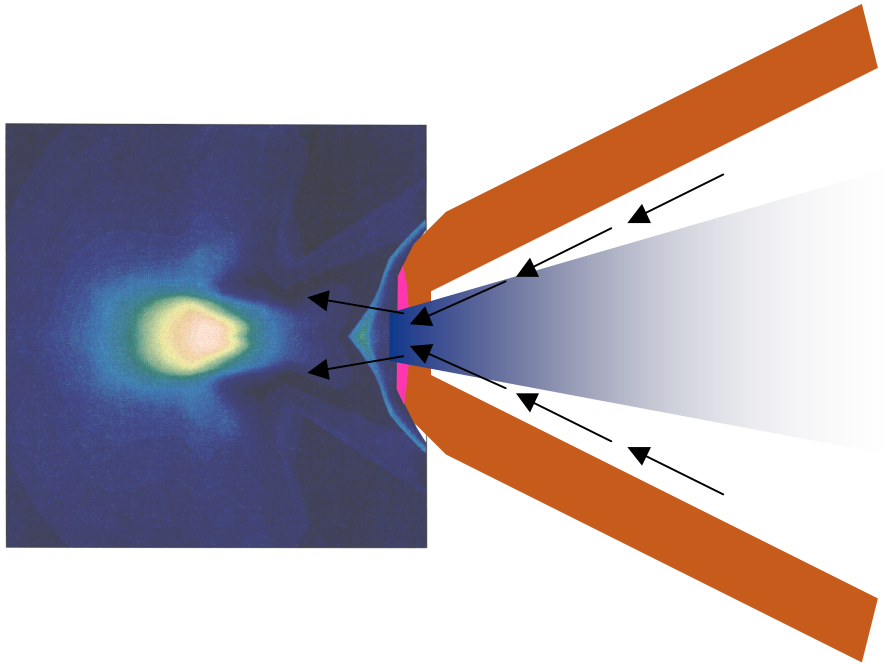

Indirect drive looks easier than direct drive

- Direct Drive puts more constraints on reactor
  - Drive symmetry
    - Laser drivers must be distributed over more of reactor wall? (using flat-topped beams, can get modest uniformity on NIF 26% p-v - is that sufficient for FI?)
  - Target survival
    - Reactor wall must be cooler, gas pressure lower
    - Target surface must be highly reflective or highly transmissive
  - Debris problems
    - Cone must be long and heavy (Hogan J/US FI WS)
- But
  - Can tolerate drive asymmetry so no problem?
  - Cold shell can tolerate much more heating
  - Cone can protect from asymmetric gas heating
  - Hohlraum losses reduce potential gain
  - Minimal absorption

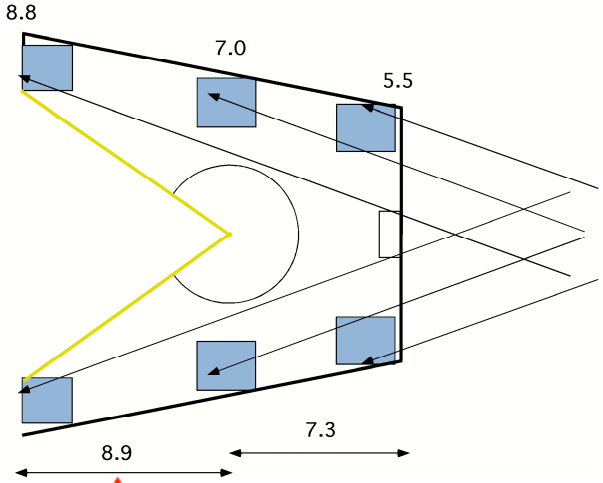

Fast Ignition targets present opportunities

- Complex to make but construction shortcuts
- Thermal layering is difficult but low temperatures feasible
- Minimize mixing but relax symmetries
- Cone massive but protects during injection

But we can't yet evaluate the tradeoffs

Integrated Fast-Ignitor Experiments on the Proposed OMEGA-EP Facility at LLE

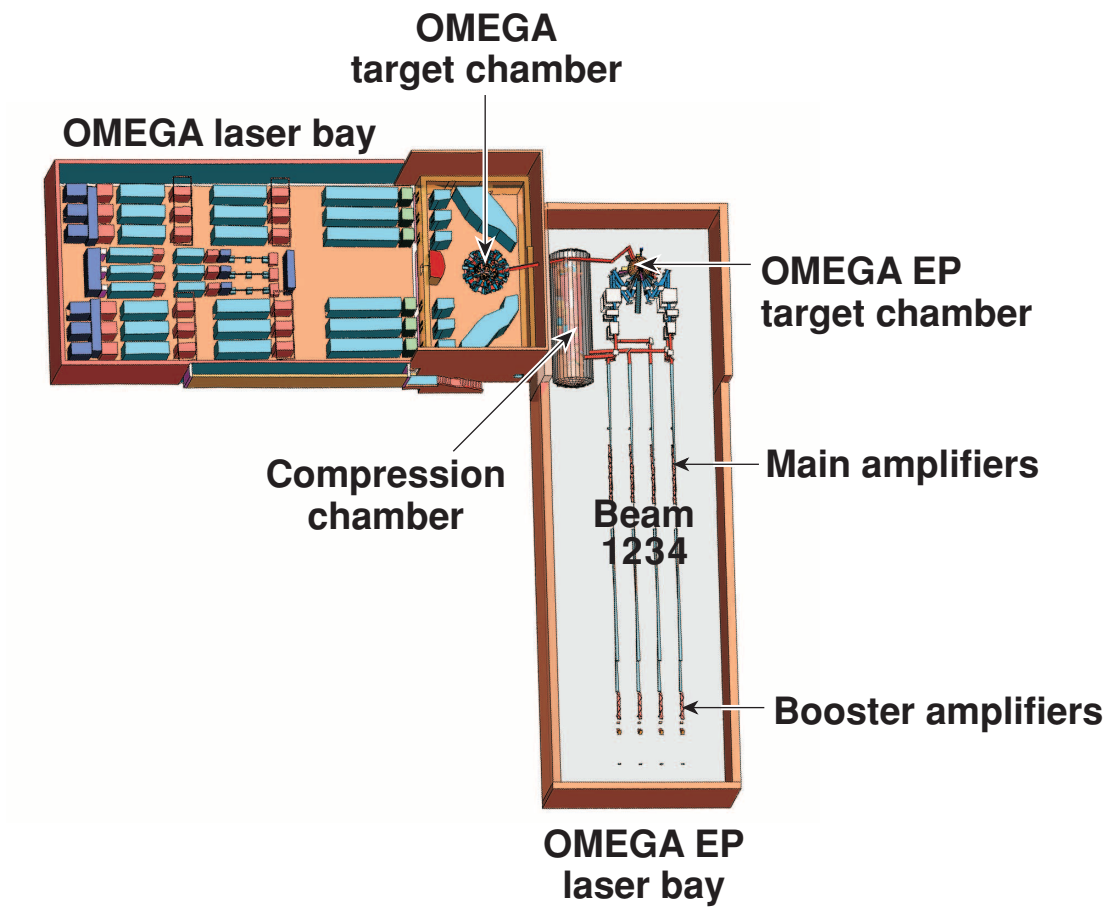

C. Stoeckl *et al.*
University of Rochester
Laboratory for Laser Energetics

6th Workshop on
Fast Ignition of Fusion Targets
St. Pete Beach, FL
16–19 November 2002

Summary

LLE is conducting FI-relevant experiments on OMEGA and will use OMEGA EP in the future

- Near-term fast-ignition research on OMEGA includes
  - cryo fuel assembly (symmetric and asymmetric illumination)
  - cone-focused targets (direct and indirect drive)
  - Target R & D: cryo layers inside cone capsules and ice-layer shimming
- Properly scaled experiments on OMEGA EP (and collaboratively on international facilities) will include
  - laser absorption
  - channel formation
  - igniter beam transport (channeling and cone)
  - hot-electron conversion efficiency
  - electron transport
- Integrated FI experiments on OMEGA EP will fully validate electron transport and core heating.

E11707a

The two viable fast-ignition concepts share fundamental issues: hot-electron production and transport to the core

UR LLE

Channeling

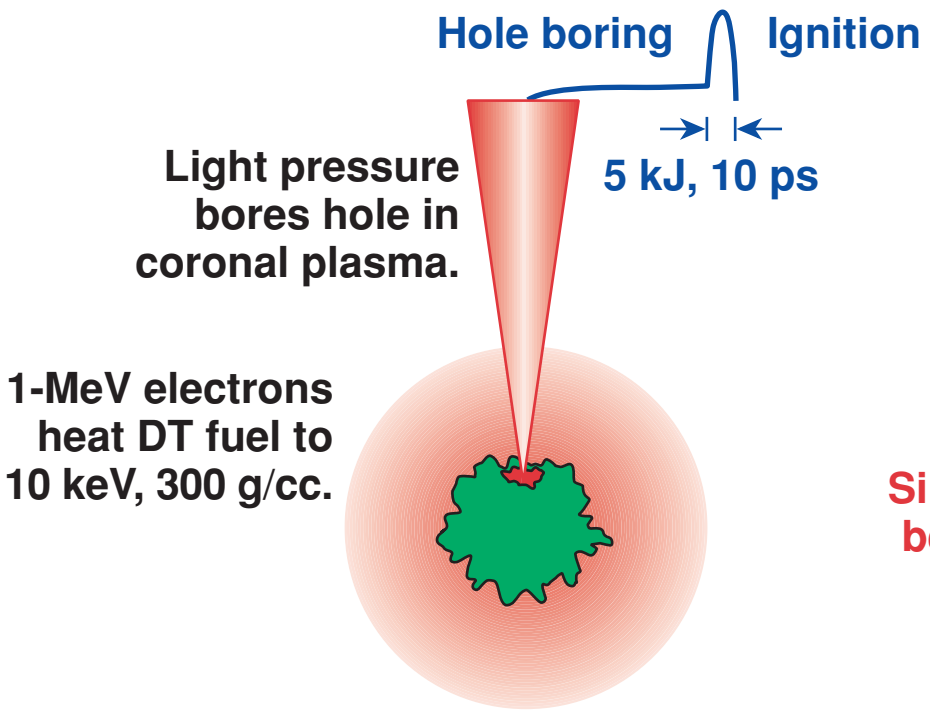

OMEGA EP would validate this concept with existing shperical cryo capsules.

Cone-focused ignition

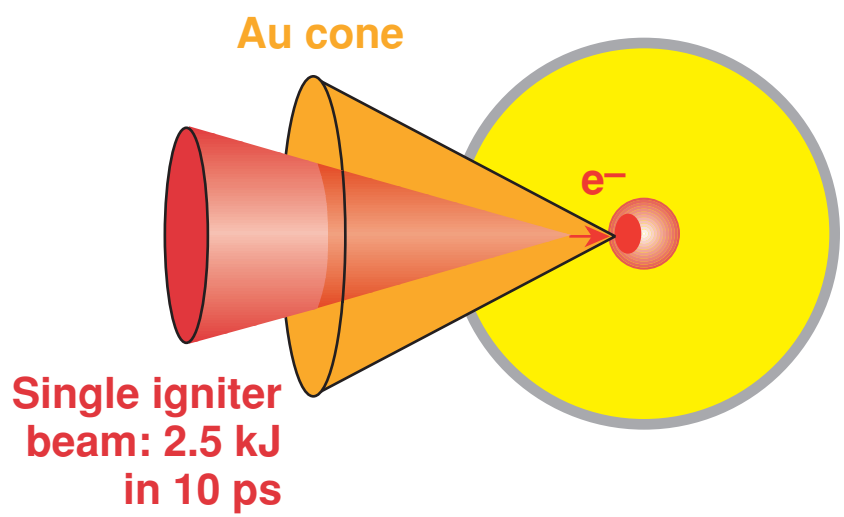

LLE has the cryogenic infrastructure to develop and shoot cryogenic cone-focused capsules.

E11710

Approximately 1 kJ of hot-electron energy is required to exploit the compression capability of OMEGA

25 kJ × 0.6 absorbed × 0.07 hydro ~ 1.0 kJ in core

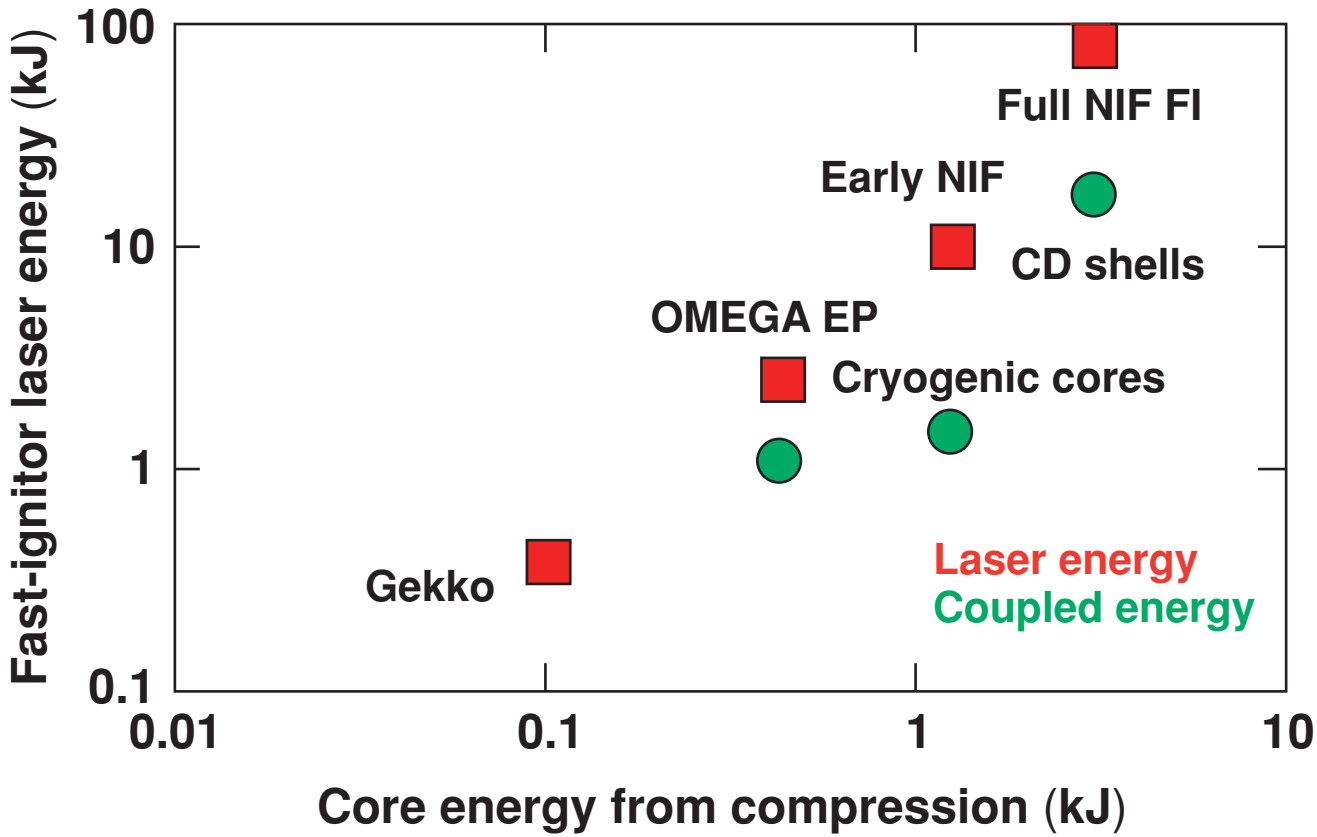

Laser and core coupled energies courtesy of S. Hatchett (LLNL).

Integrated Fast-Ignition experiments on OMEGA EP are an important stepping stone to high-yield Fast Ignition on the NIF.

E11956b

The OMEGA EP beams will be located next to the existing OMEGA facility

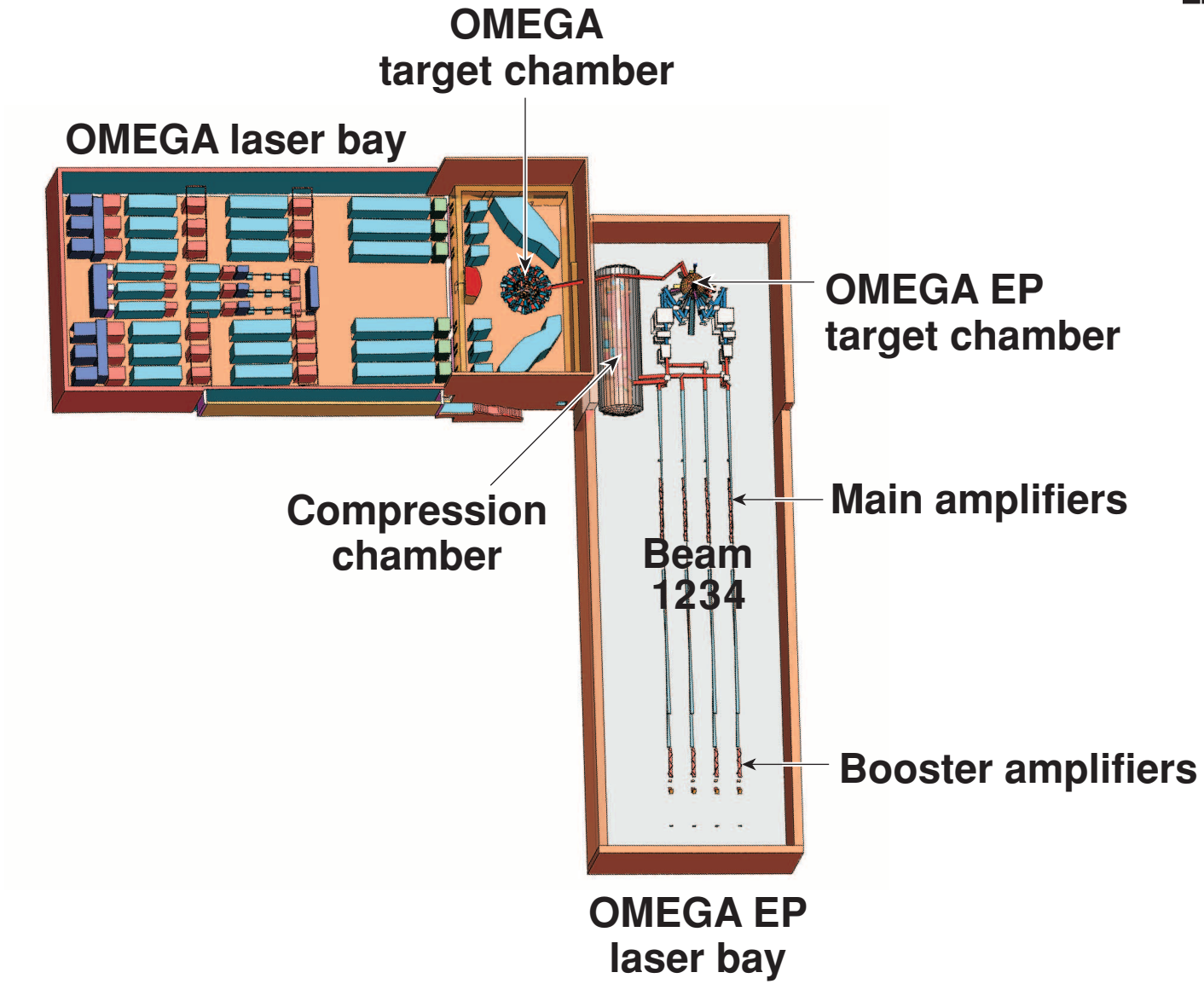

G5546a

OMEGA EP beamline architecture is NIF-like for both short- and long-pulse configurations

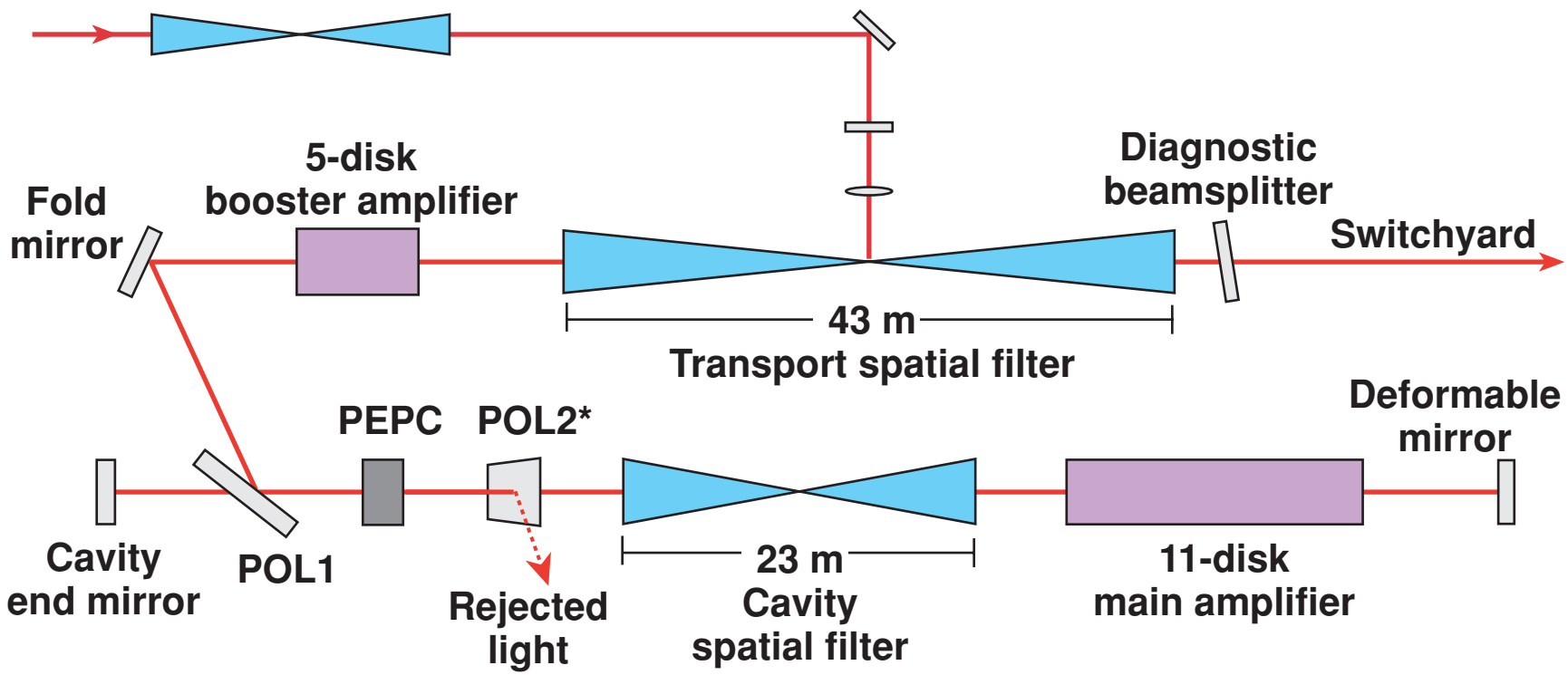

*Used only for two-pass operation (one round trip) for chirped-pulse beams

G5221d

The amplifiers use NIF disks in an LLE-engineered, water-cooled-flash-lamp, single-segment amplifier

- Optimized illumination uniformity of end disks for better gain uniformity
- Designed for LLE-style handling equipment to reduce maintenance cost
- Water-cooled flash lamps for improved (<2 h) rep rate (pump module shown removed for clarity)
- Low-voltage (15-kV) power conditioning for compatibility with existing OMEGA

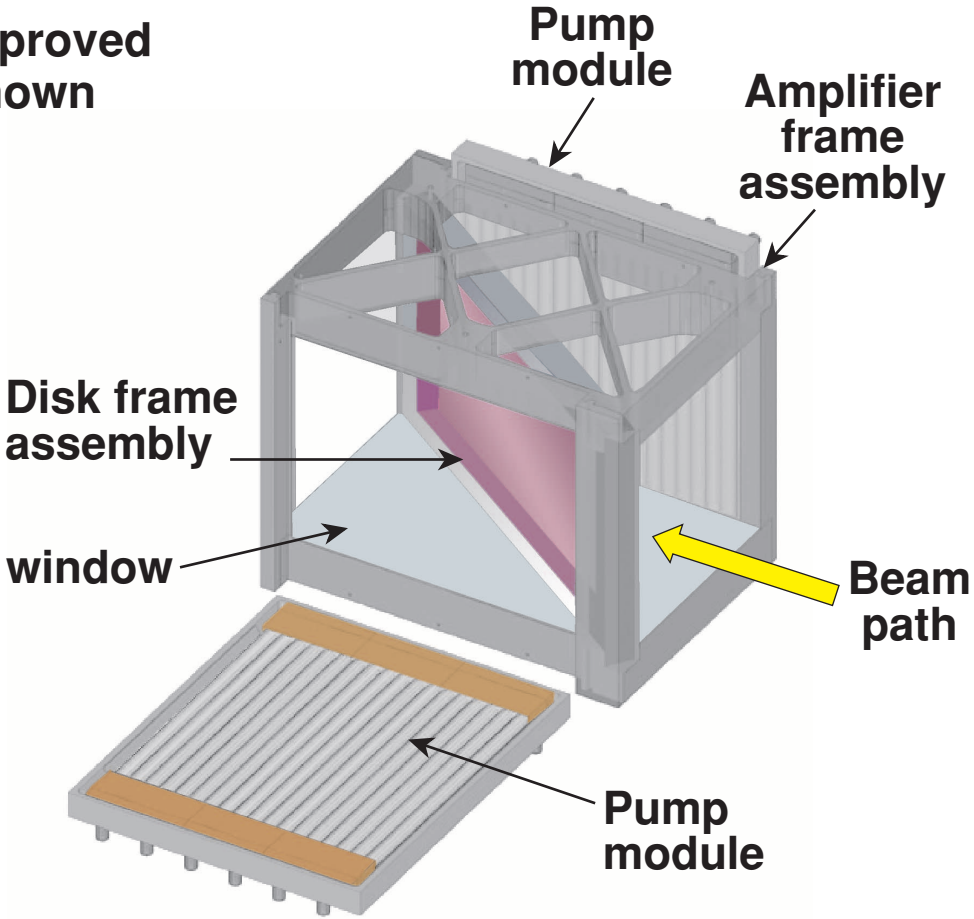

G5565

Amplifiers and integrated system performance will support short-pulse and long-pulse requirements

Short-pulse performance	Beam 1	Beam 2
Short pulse (IR)	1 to 100 ps	35 to 100 ps
IR energy on-target (kJ)	0.55 to $\geqslant$ 2.6*	0.55 to $\geqslant$ 2.6*
Intensity (W/cm^2)	0.2 to 1.0 $\times$ 10^{21}	~4 $\times$ 10^{18}

* With technology improvements to 2 J/cm^2

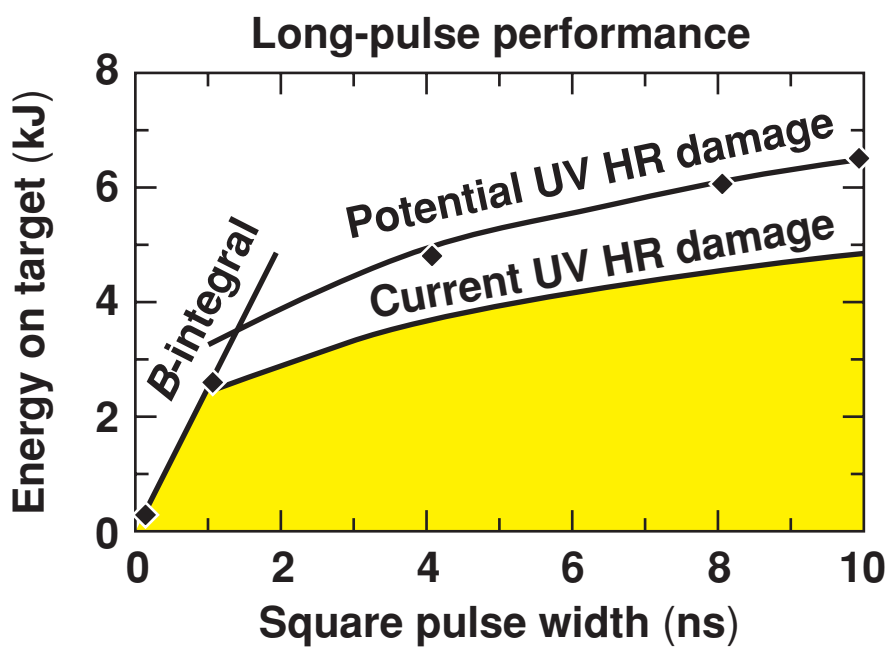

G5566

The OMEGA EP facility will have the flexibility to deliver the optimal hot-electron spectrum

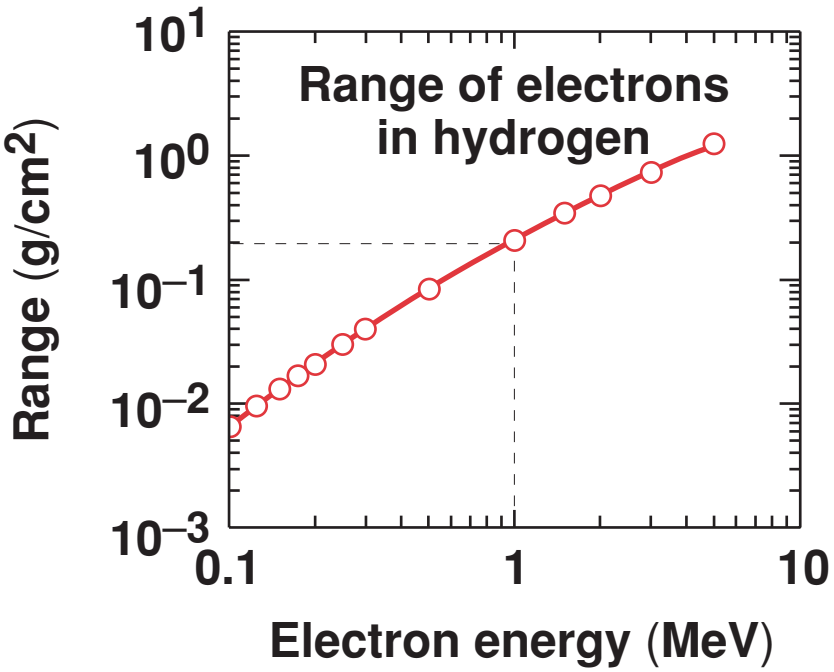

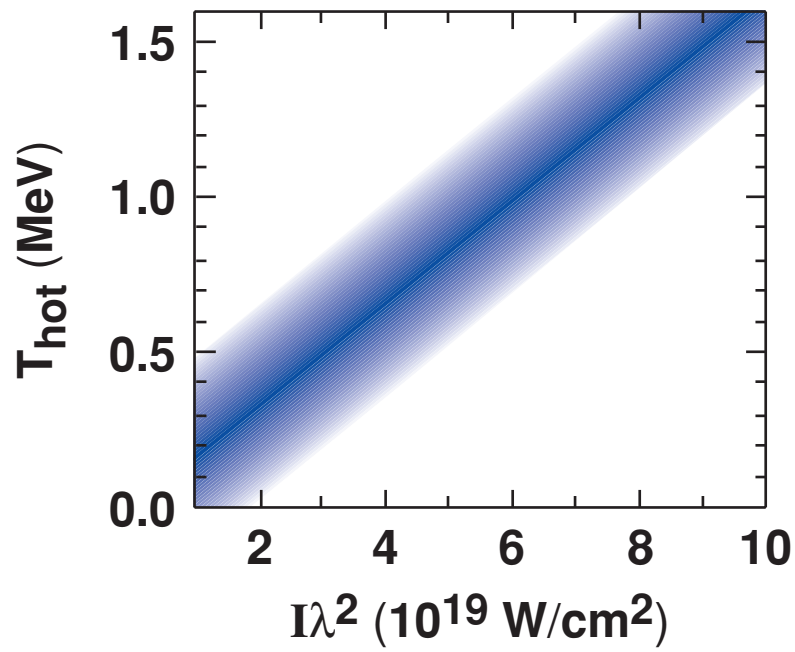

M. J. Berger *et al.*, NIST (1999).

Scaling used in EP P-CDR based on Lasinski *et al.*, Phys. Plasma 6, 2041 (1999); Wharton *et al.*, Phys. Rev. Lett. 81, 822 (1998).

The range of available intensities with the proposed OMEGA EP heater beam is larger than the uncertainties in the T_{hot} scaling.

E11714

Laser propagation, absorption, and conversion efficiency will be studied in planar experiments on OMEGA EP

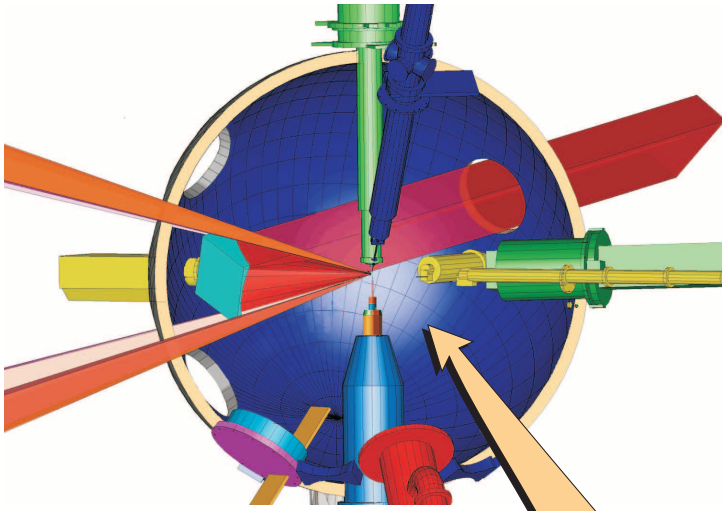

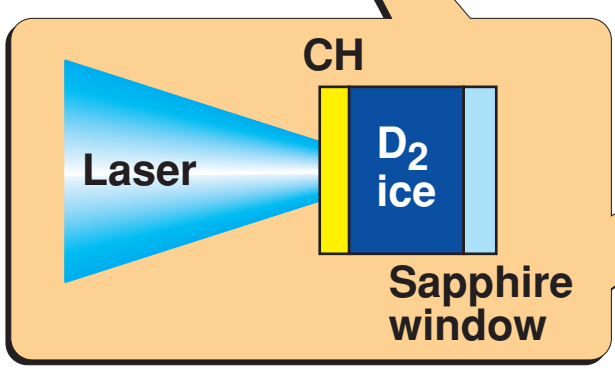

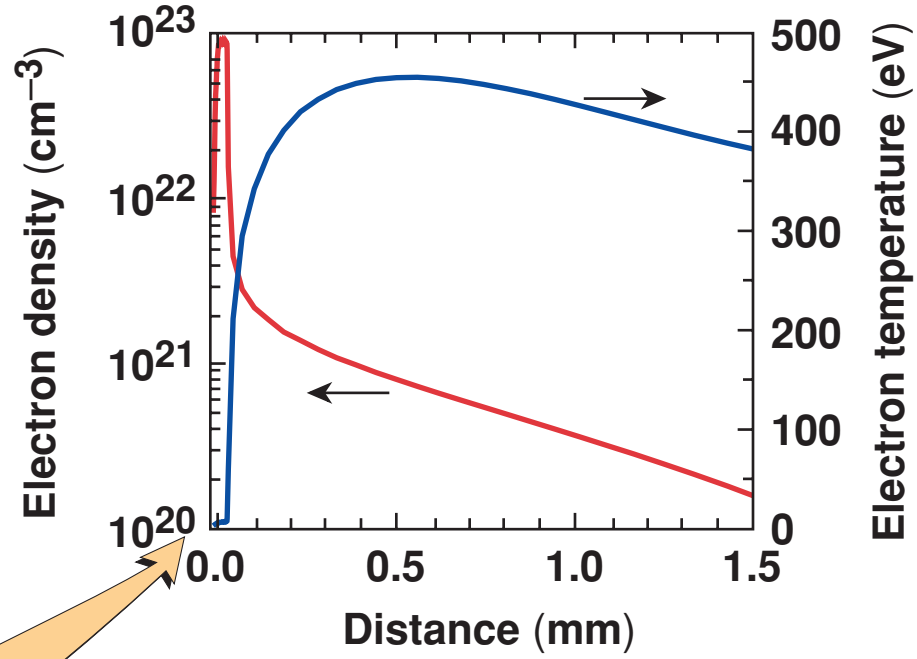

- Planar cryogenic targets
- Standard OMEGA TIM's and diagnostics
- Up to 20 kJ on planar targets with pulse lengths of up to 10 ns

E11719

Integrated cryogenic DD FI experiments validate/compare both channeling and cone concepts on a single facility

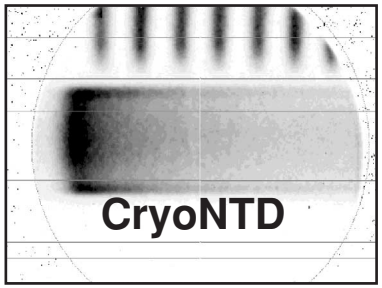

Neutronics

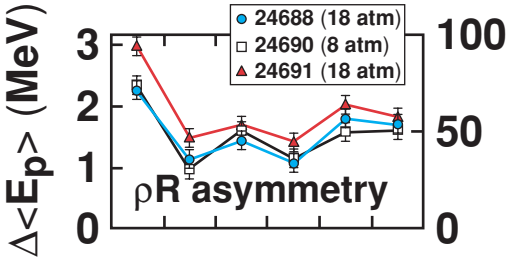

Charged-particle spectroscopy

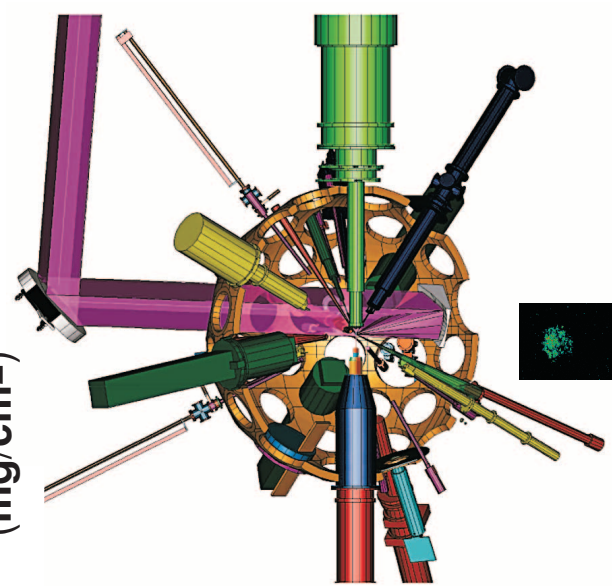

- Dedicated program
- High throughput
- Proven diagnostics
- Proven cryogenics

X-ray imaging

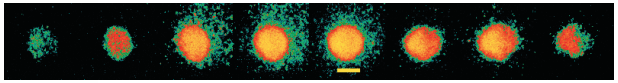

Neutron imaging

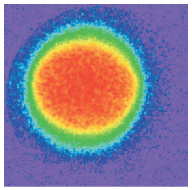

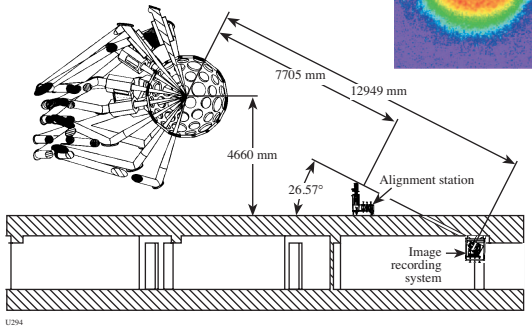

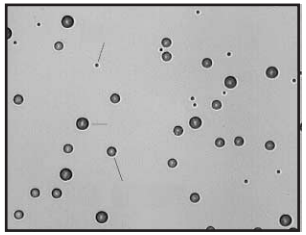

CR-39 track data

Direct-drive DT cryo capsules and slide cone targets

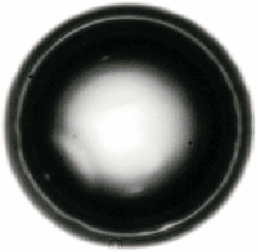

E11738

Diagnostics developed for DD cryogenic implosions will be essential for the FI fuel assembly experiments

UR LLE

Geneseo

OMEGA shot 26477

Spherical cryo performance to date:

- YOC ~ 100% (square pulse)
- ρR_n ~ 60 mg/cm^2 (α ~ 5 pulse)
- T_{ion} ~ 2.2 keV (α ~ 5 pulse)

CD, CH, and layered shells;
δr to control implosion stability

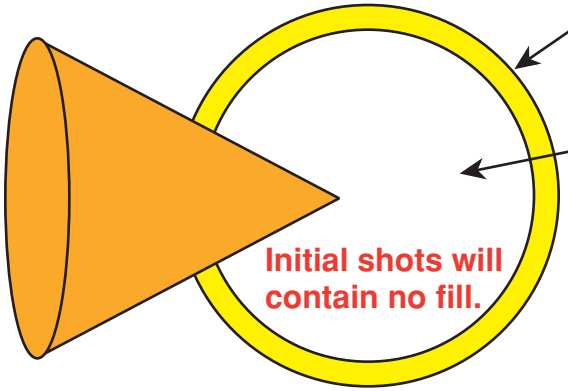

D^2, ^3He, and D^3He fill gases

For example:

$D + {}^3He > p\ (14.7\ MeV) + {}^4He$

→ proton dE/dx gives total ρR.

E11712c

Fuel assembly experiments with cone-focused targets have begun on OMEGA

Indirect drive cone targets shot on OMEGA in FY02 (LLNL, Ga)

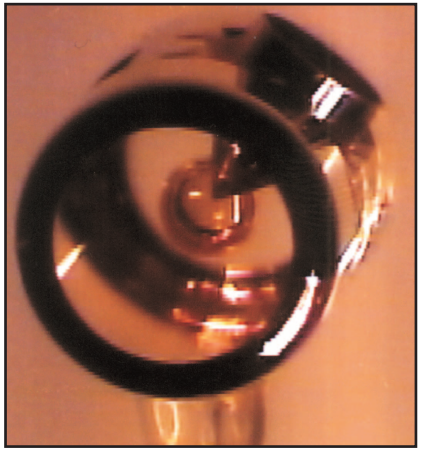

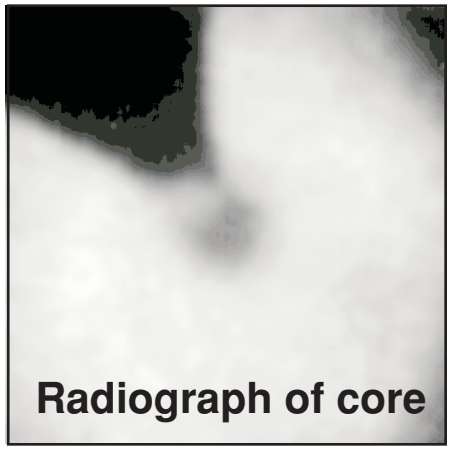

Direct drive cone targets shot on OMEGA in FY02 (LLNL, Ga)

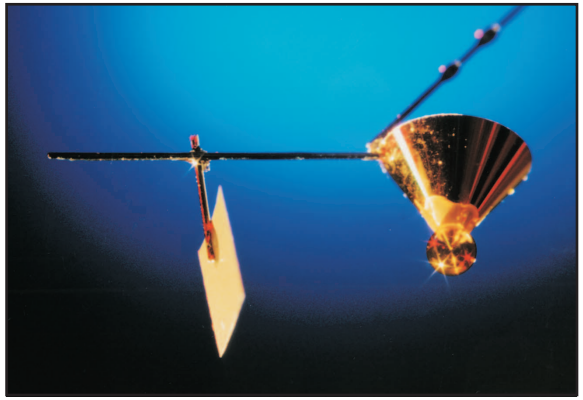

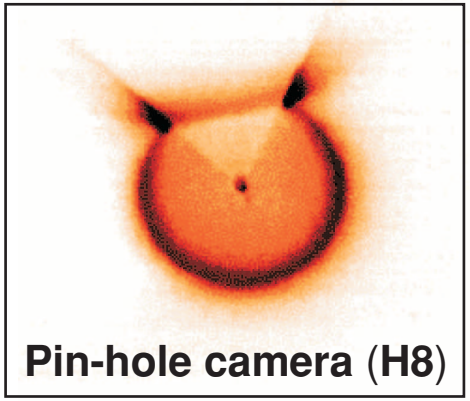

Raw framing camera images: Top shows early in time, bottom near stagnation.

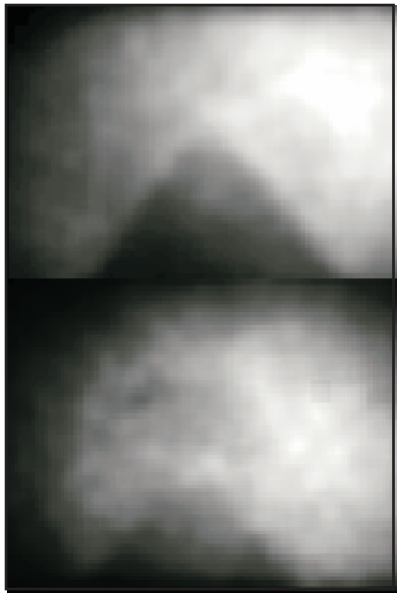

Note that near stagnation, the tip of the Au cone has started to disappear.

E11959

Uniform ice thickness within a “cone” target will require careful control of target design around the cone

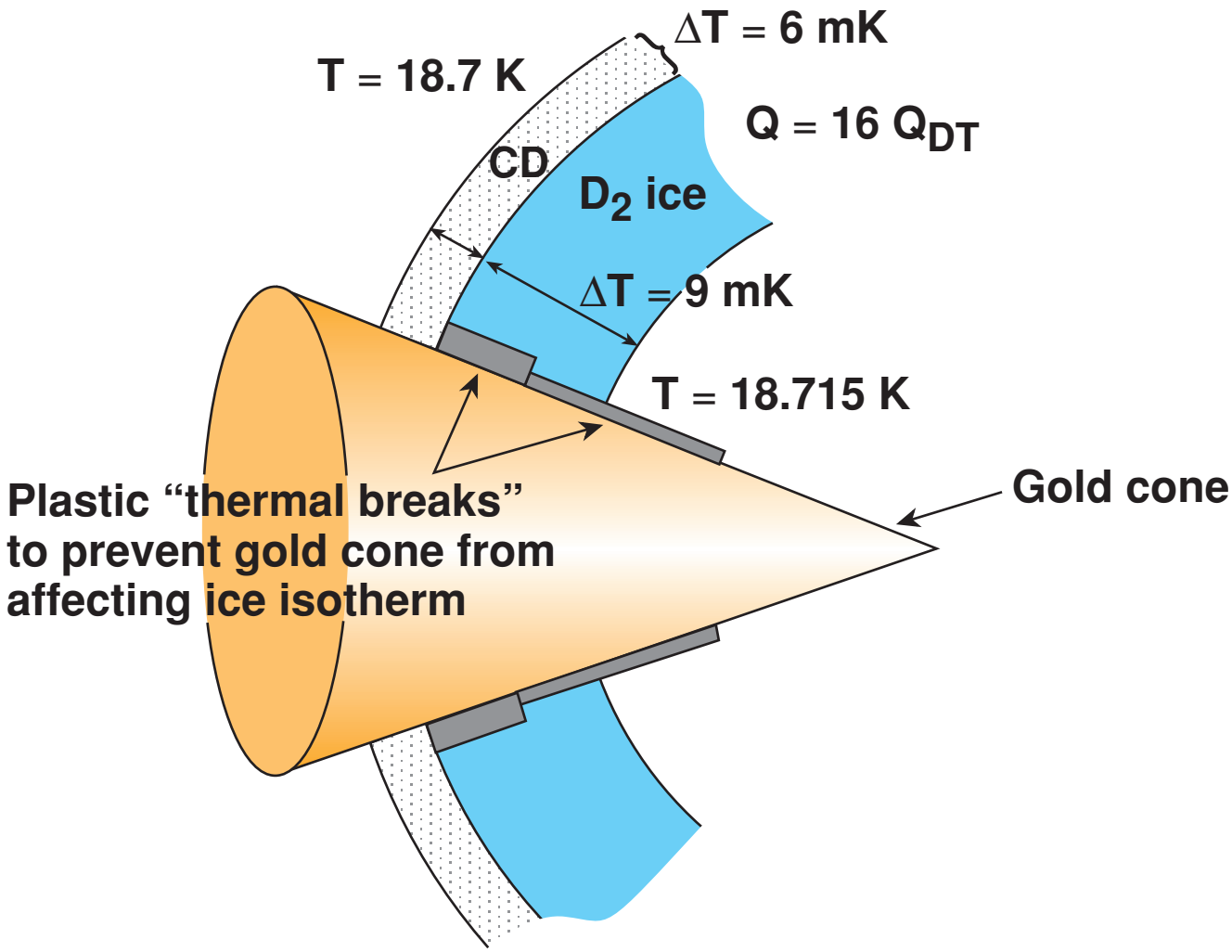

E11717

OMEGA EP is designed to perform integrated fast-ignition experiments with cryogenic implosions

Co-propagating OMEGA EP ignitor and channeling beams test both concepts.

Channeling beam:

- $I > 10^{18}$ W/cm^2
- E ~ 0.5 to 2.6 kJ in 100 ps
- r_{focus} ~ 15 μm
- shot cycle time < 2 h

Ignitor beam:

- $I > 10^{19}$ W/cm^2
- E ~ 0.5 to 2.6 kJ in <10 ps
- r_{focus} < 10 μm
- shot cycle time < 2 h

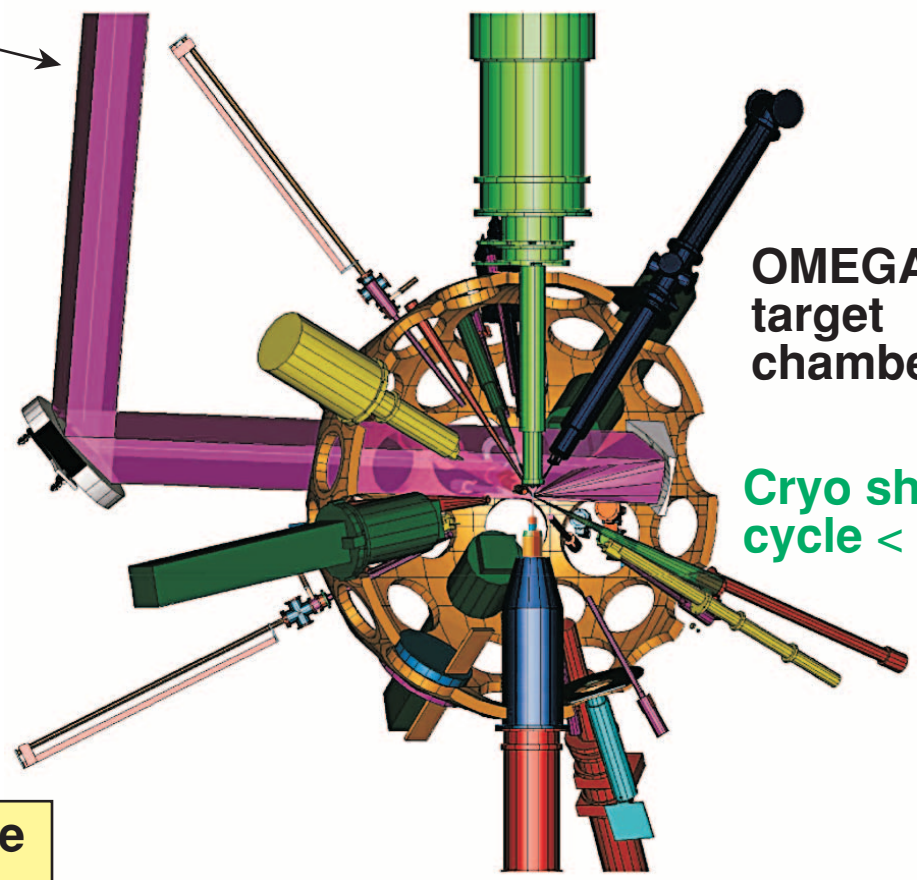

These experiments will validate hot-electron transport and core-heating physics.

E11715

OMEGA can assemble fast-ignition-relevant cryogenic fuel densities

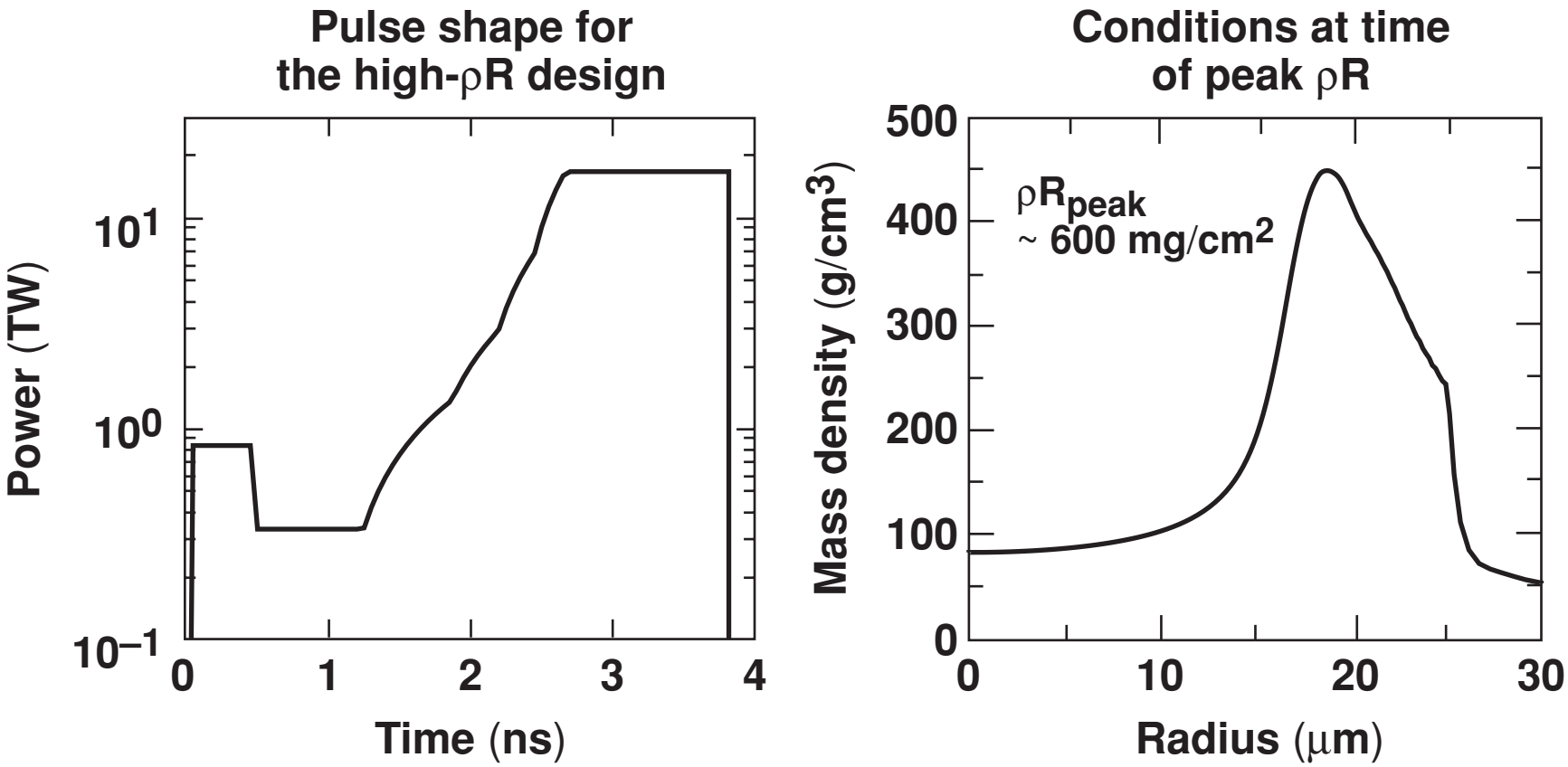

Expect neutron-averaged ρR_{fuel} to approach ~ 150 mg/cm^2 by the end of CY02 and ~ 500 mg/cm^2 (peak) over the next few years.

E11709

A significant yield enhancement should be observed with the OMEGA EP short-pulse beams coupled to OMEGA

- α = 1 implosions leading to ρR = 0.6 g/cm^2 (from earlier viewgraph).
- Energy deposited at 10 n_c^{IR}
- τ_e = 10-ps Gaussian e^- source; multi-group e^- transport

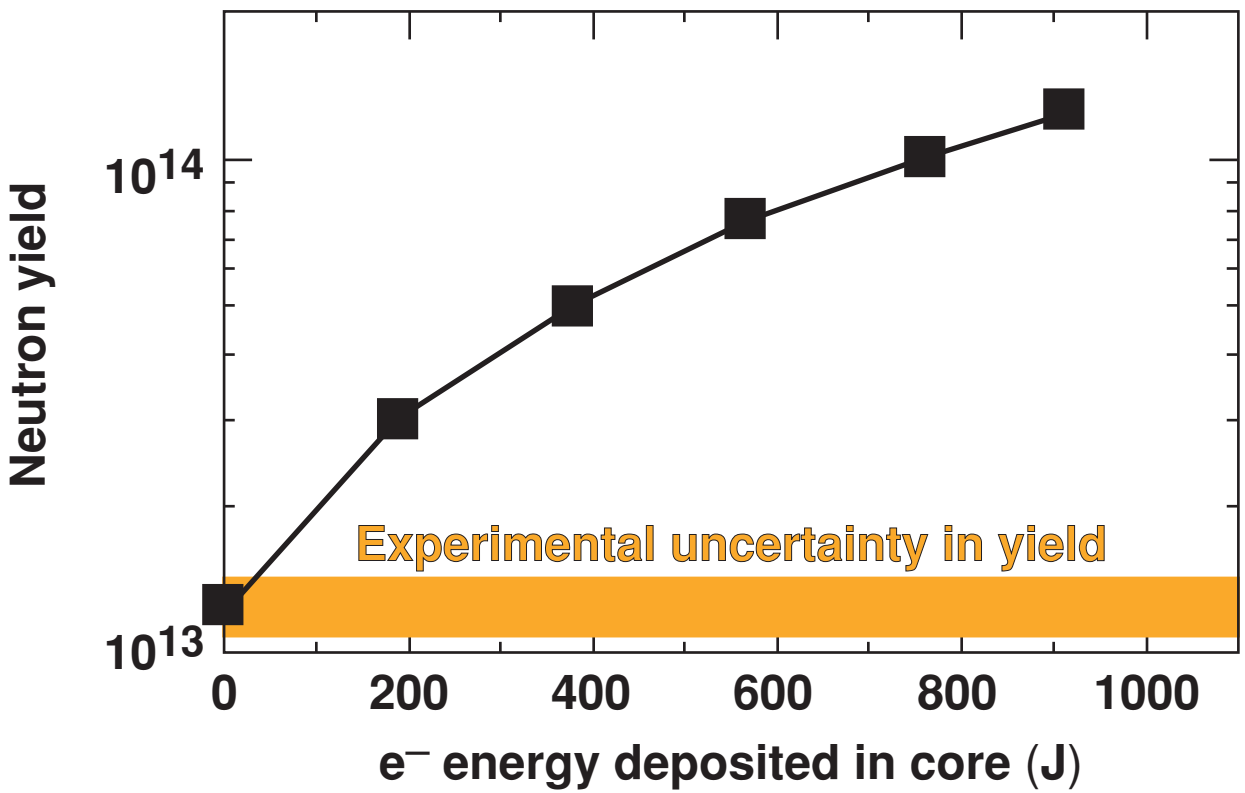

E11731a

Summary/Conclusion

LLE is conducting FI relevant experiments on OMEGA and will use OMEGA EP in the future

- Near-term fast ignition research on OMEGA includes
  - cryo fuel assembly (symmetric and asymmetric illumination)
  - cone-focused targets (direct and indirect drive)
  - Target R & D: cryo layers inside cone capsules and ice layer shimming
- Properly scaled experiments on OMEGA EP (and collaboratively on international facilities) will include
  - laser absorption
  - channel formation
  - igniter beam transport (channeling and cone)
  - hot-electron conversion efficiency
  - electron transport
- Integrated FI experiments on OMEGA EP will fully validate electron transport and core heating.

E11707a

Electron transport for Fast Ignition

APS/DPP Conference

Orlando,Florida

November 11-16,2002

k
'own
.asinski
.ruer
Langdon
e Livermore National Laboratory

Dale Welch

Mission
Research
Corporation

This work was performed under the a
of the U.S. Department of Energy by
University of California
Lawrence Livermore National Labora
under contract No. W-7405-Eng-48.

The LSP code[1] is being used to examine fast electron transport in short-pulse experiments

- The LSP code uses a direct implicit particle-in-cell algorithm in 3 dimensions to solve for the beam particles. The background particles are treated as a fluid.
- An electron beam is injected into a solid density CH plasma which contains a high conductivity region to simulate the effect of the fluor.
- An attempt is made to include effect of beam halo
- The importance and likelihood of electrons running away from the background distribution is discussed.

[1] D. R. Welch, et al, Nucl. Inst. Meth. Phys. Res. A 242, 134 (2001).

For 1 PW, 500J, 500fs pulses the intensity reaches $3x10^{20}$ Wcm^{-2} with a broad spectrum of intensities

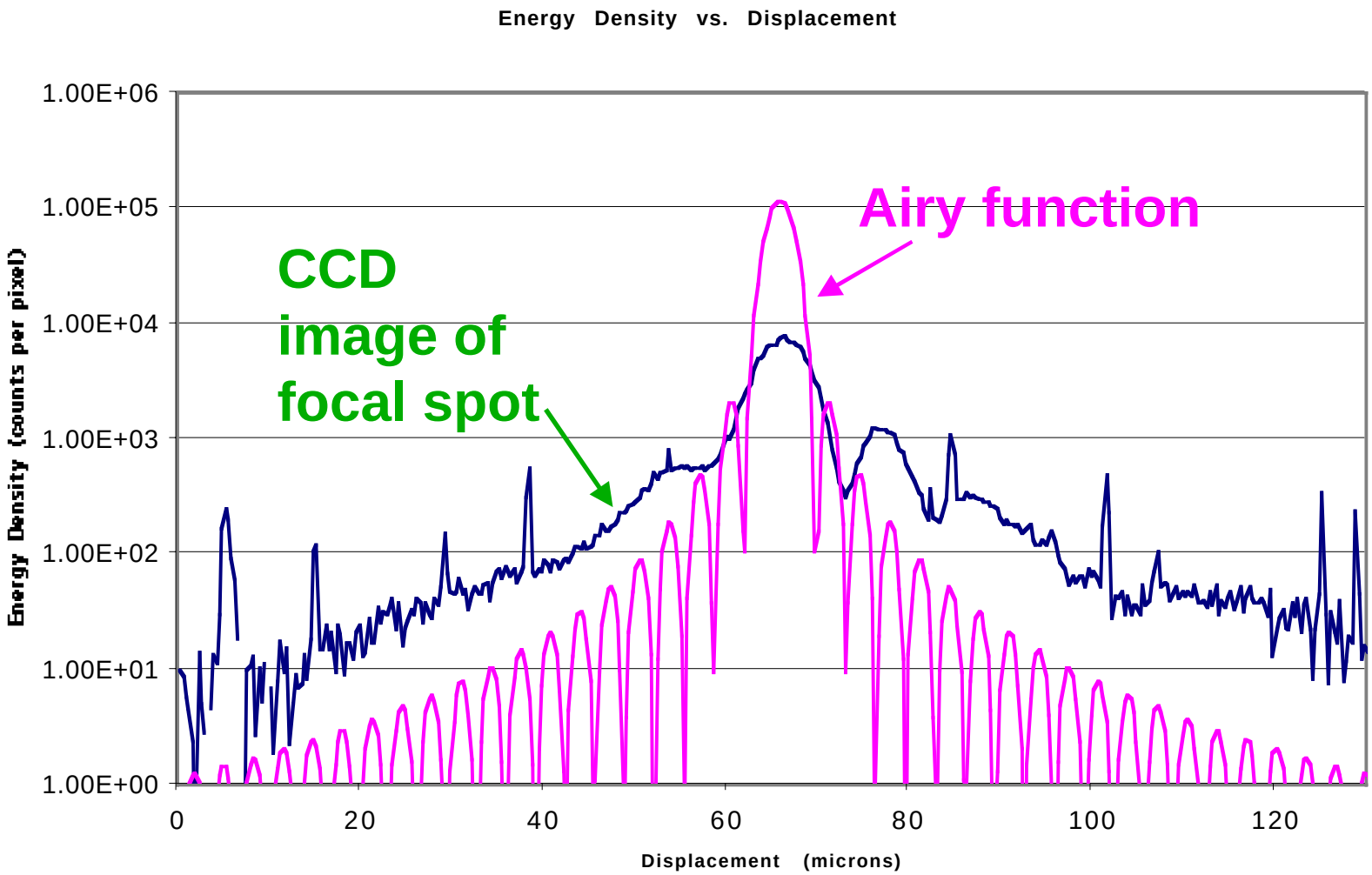

The short pulse laser halo produces energetically important electrons that produce a large K-α spot

- Assume half laser energy is in central spot and remainder is in spot with 5x radius

- Halo intensity ~ 4% of peak => electron particle energy 20% of peak

- Coupling efficiency in halo ~ 1/3 that in peak
  => #electrons in halo/# electrons in core ~ 5/3

- But dE/dx(K-α) ~ threshold factor *$1/\beta^2$
  - K-α efficiency at 200 keV ~3X η at 1-2 MeV
  - K-α intensity in halo ~20% in core(E&B probably enhance this)
  - Need MC calculations to check this

Small bremsstrahlung spot in experiments may be due to hard electrons that preferentially beam photons forward. K-α is isotropic.

Problem characteristics

Central spot:
5 μ radius
20 J e^-
2 MeV drift
500 keV temp

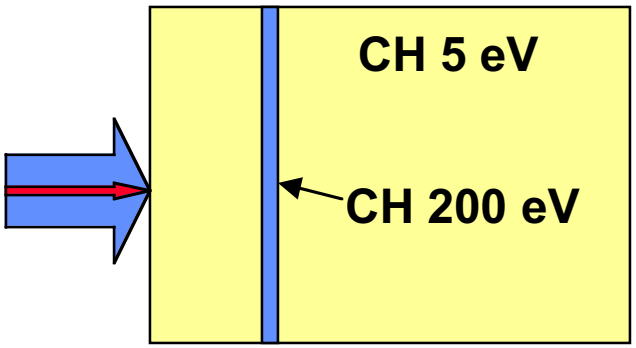

Pulse shape:
Triangular pulse with
Full width 1.5 ps

Big spot:
20 μ radius
120 J e^-
1 MeV drift
300 keV temp

There are ghosts of agreement with experiment in a "poor man's" K-α signal

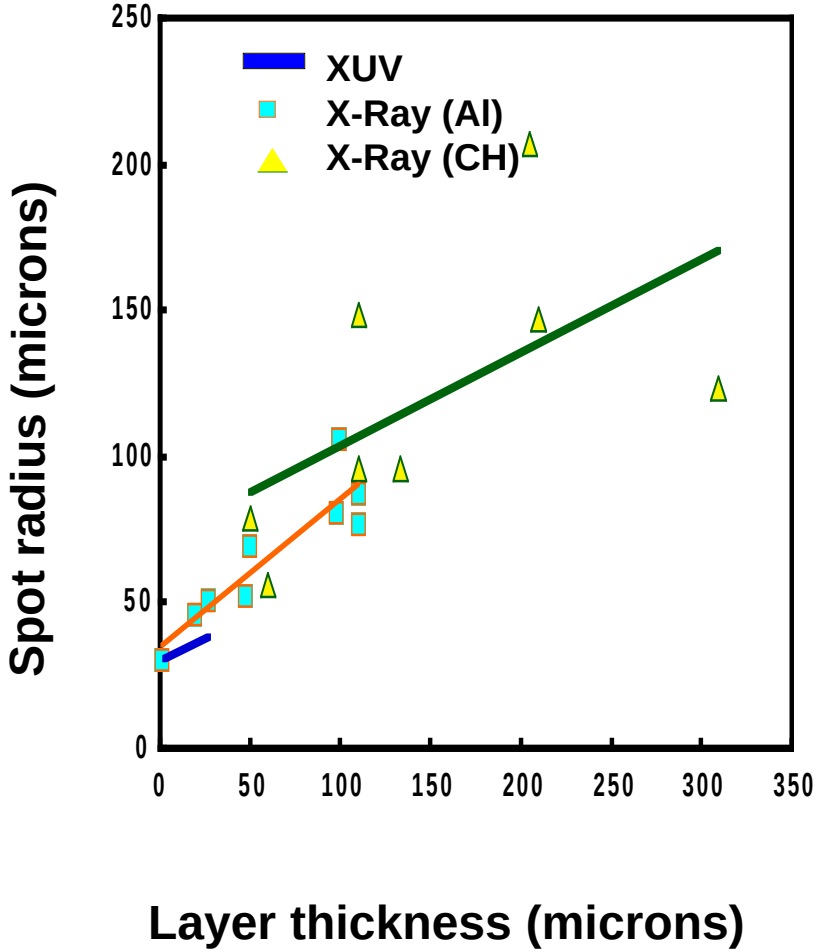

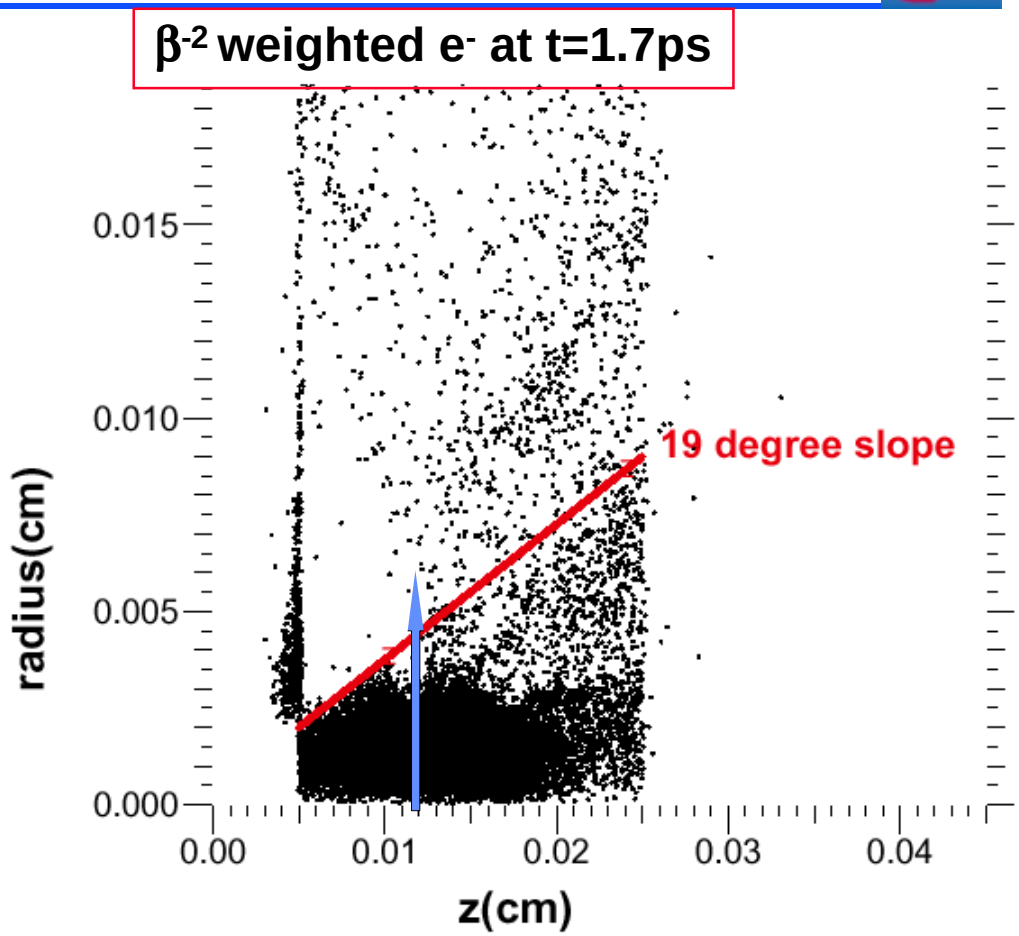

Slab section initially heated to 200 eV

Unweighted particle positions

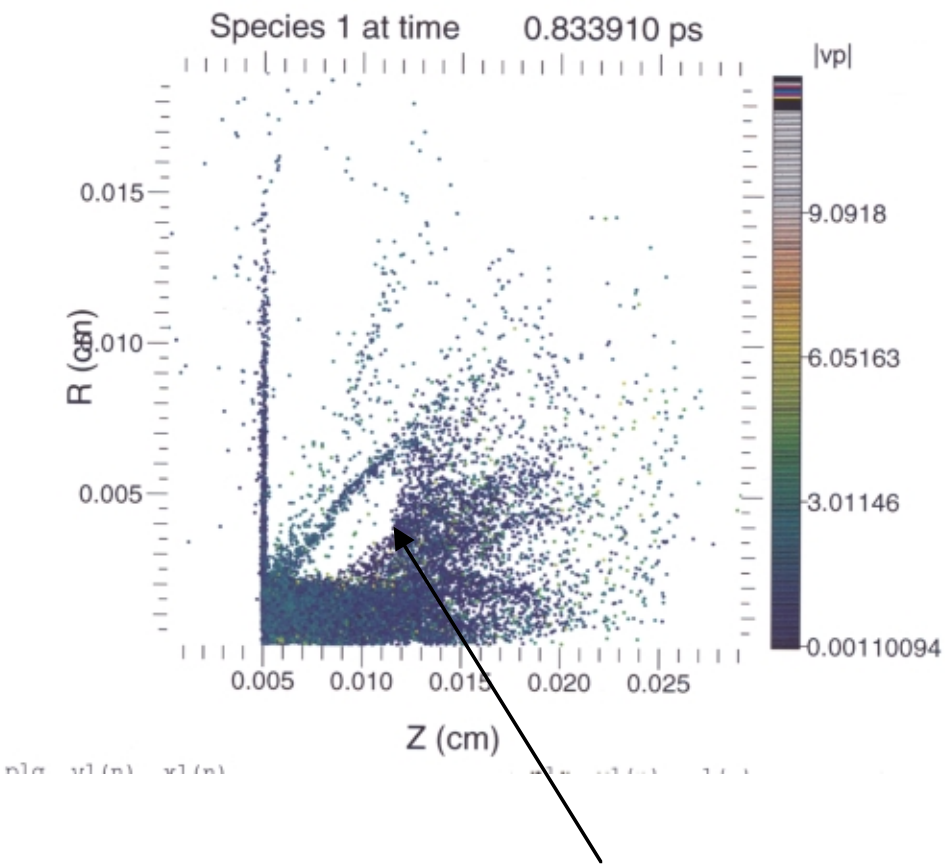

Spreading at heated foil

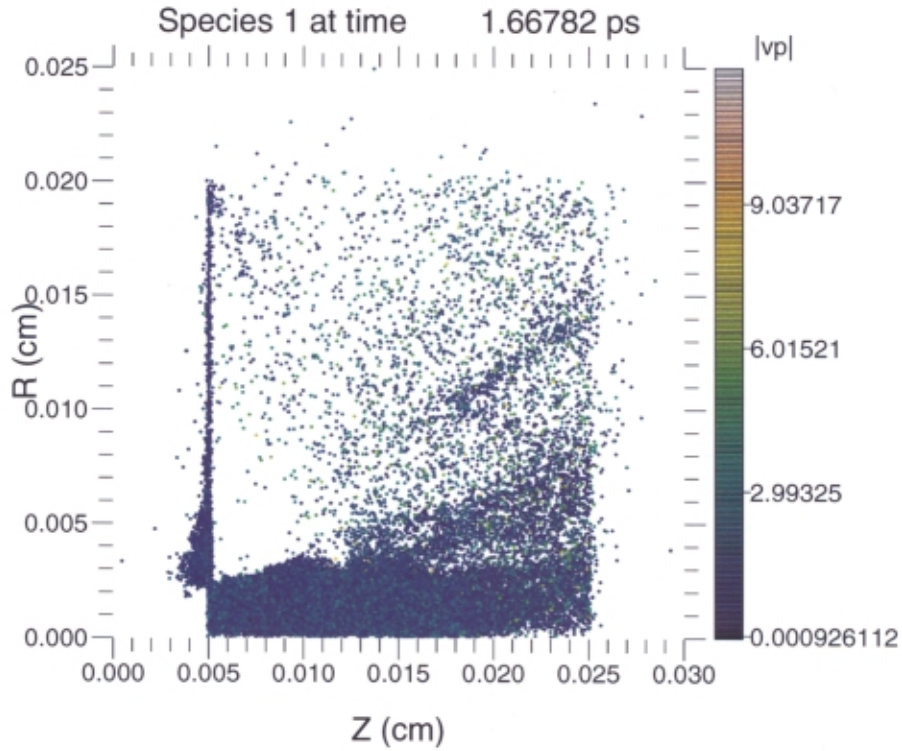

Spreading at heated foil
Not apparent at later time

Particle distribution functions in region of large E fields

- **Many issues:**
- **Are particle distributions much broader than initial?**
- **What effects of macro fields ,plasma instabilities or numerical artifacts?**
- **Is existing distribution stable?**

Future work !

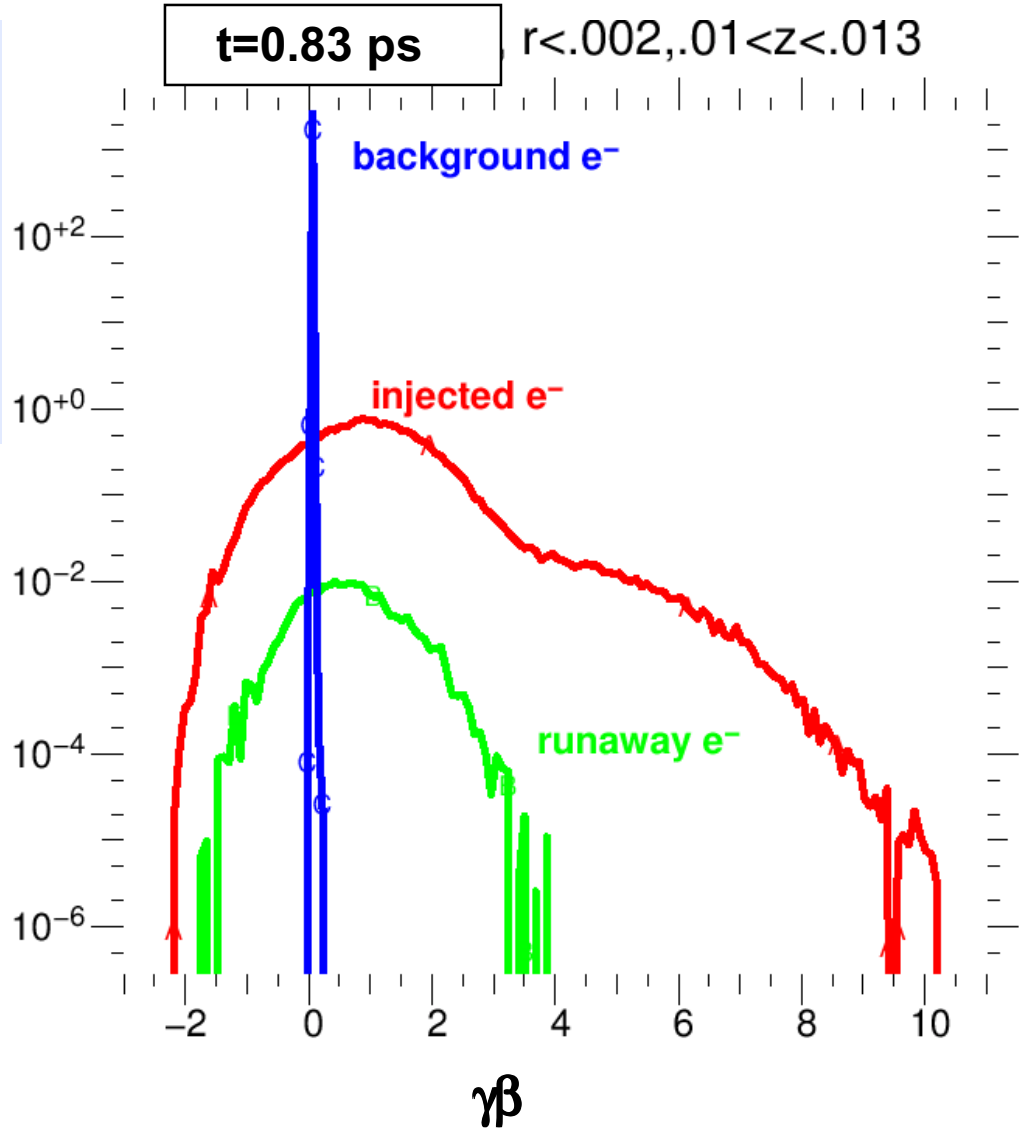

Field strengths at 0.8 ps

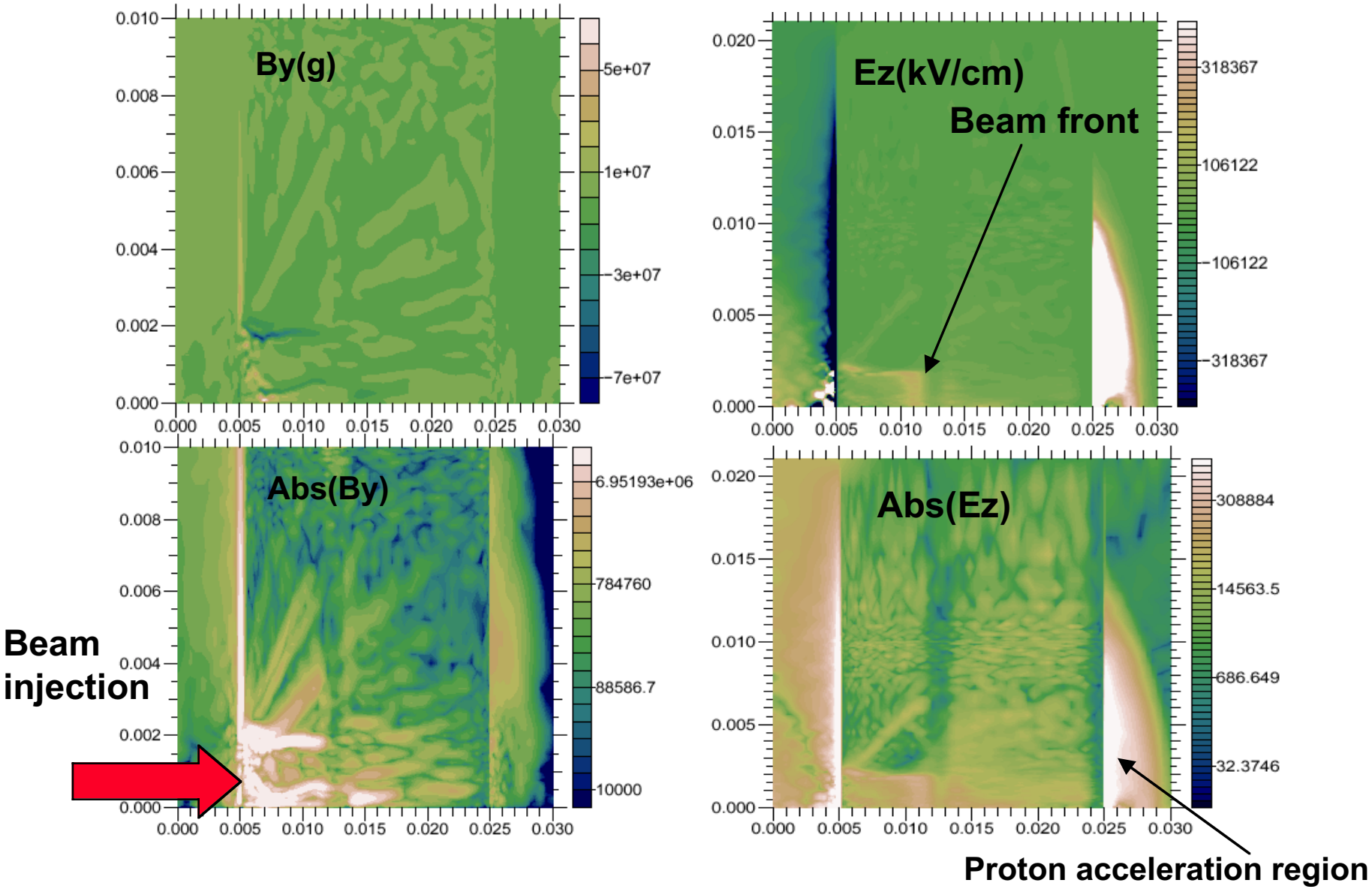

We use results of Fokker-Planck calculation* to estimate runaway rates(at t=.83 ps)

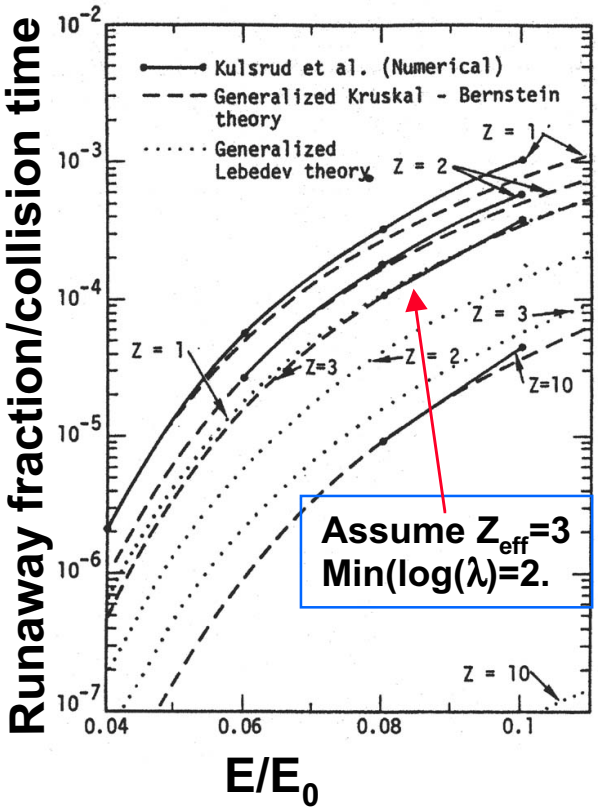

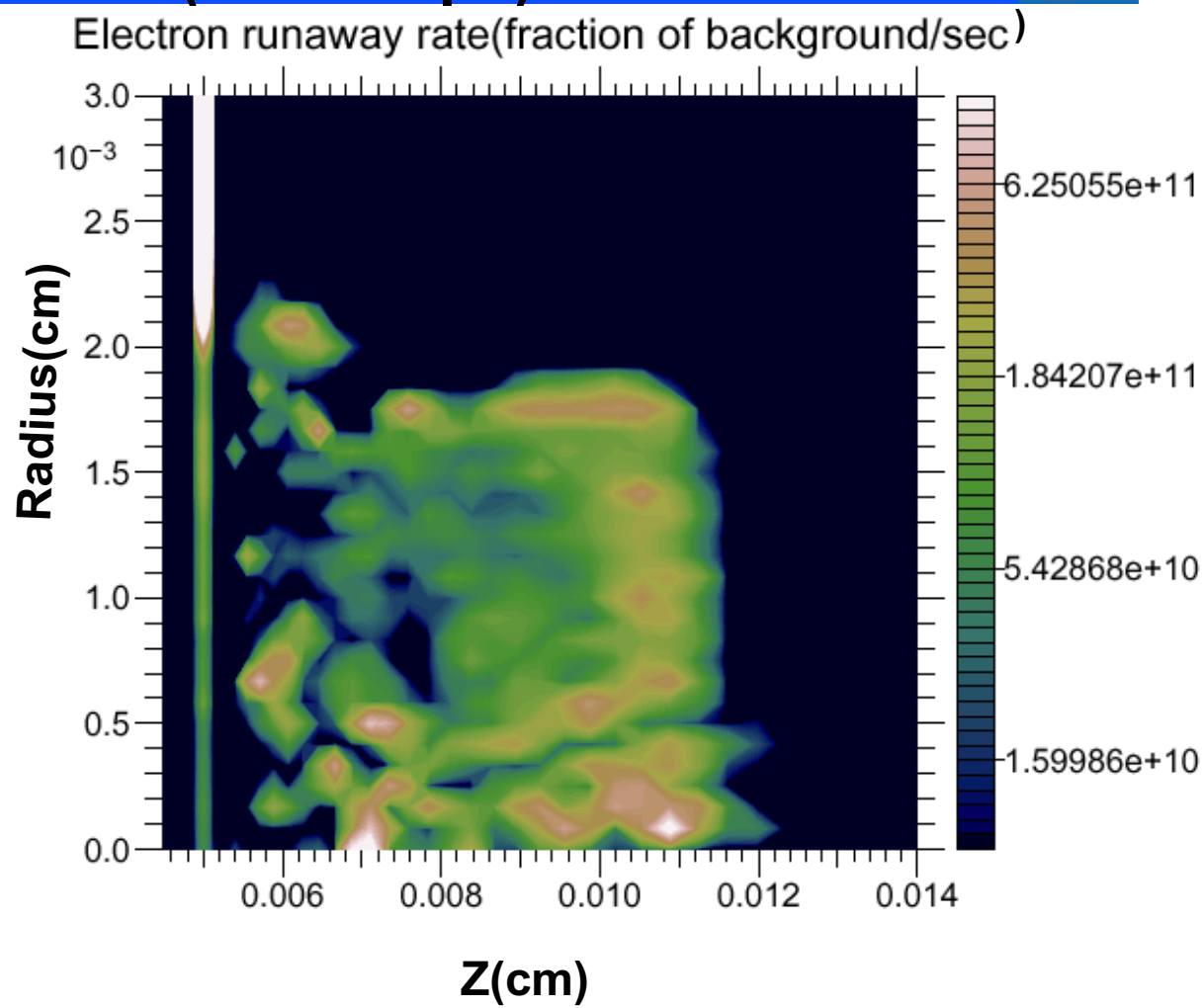

Significant fraction of background distribution should run away!

Not observed in LSP run. Why not?

*R.H.Cohen,Phys.Fluids19,2(1976),239

Where and for what electron population will magnetized flow be important?

In regions of highest B, even thermal electrons are magnetized

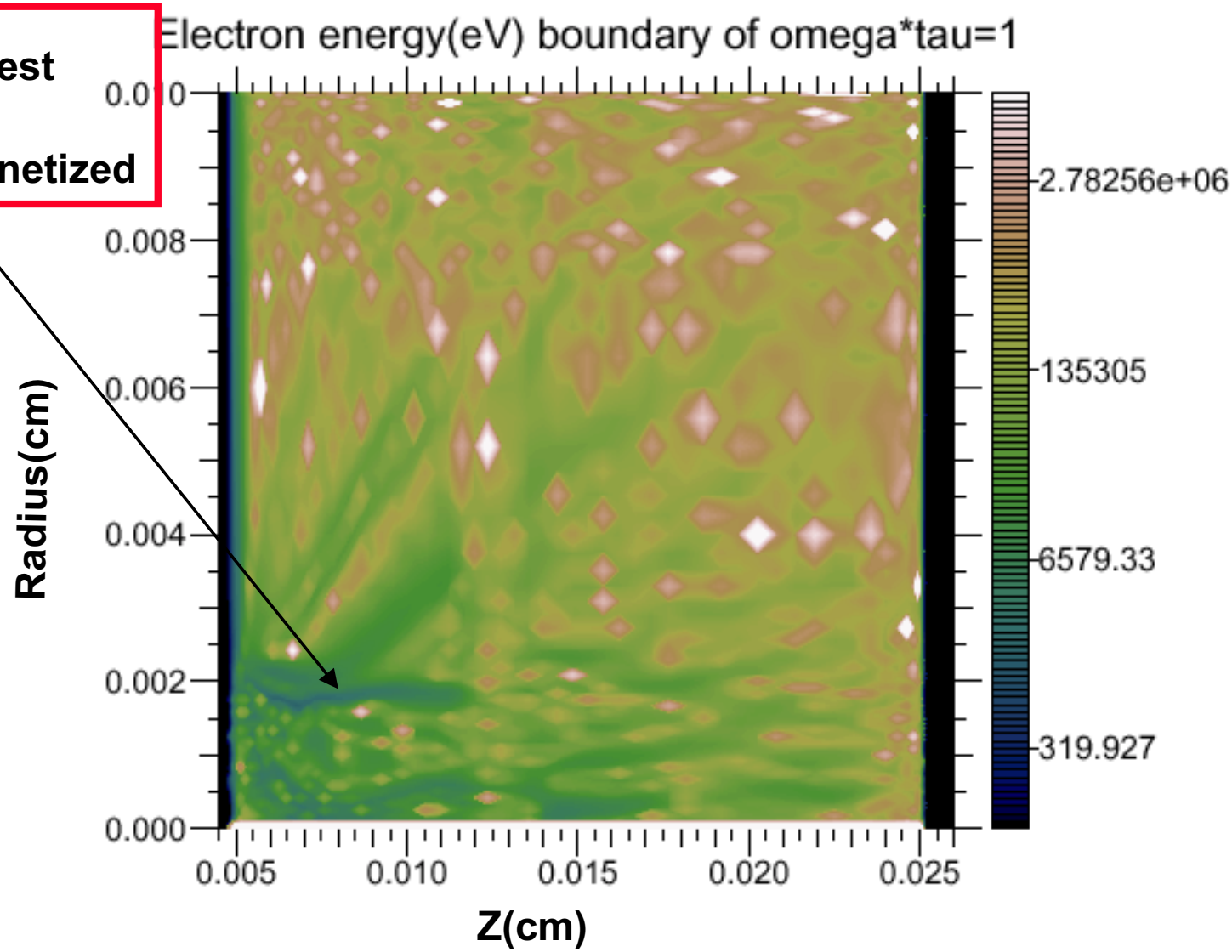

Where will B strongly affect trajectories?

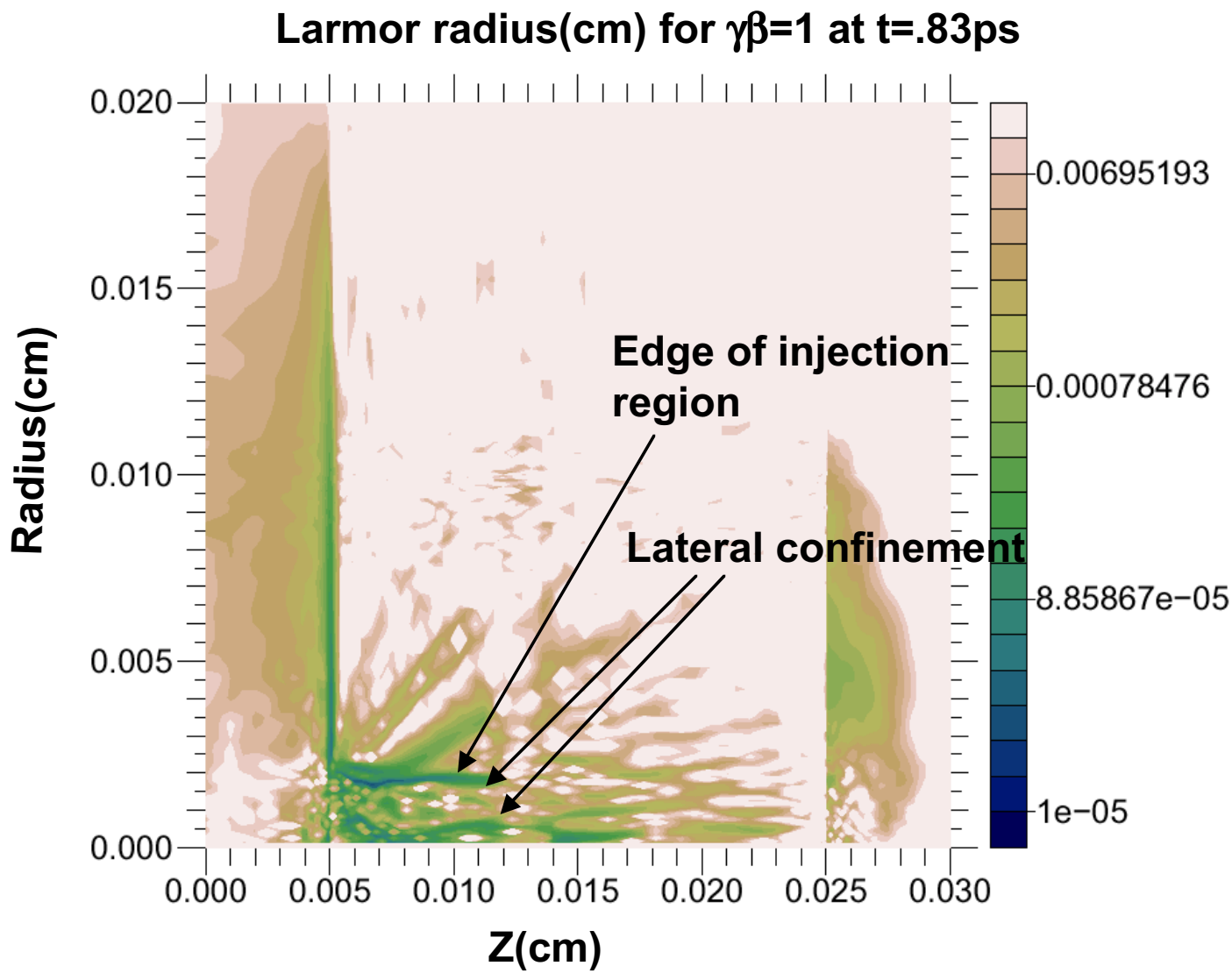

Are there limits to maximum velocity runaways can achieve?

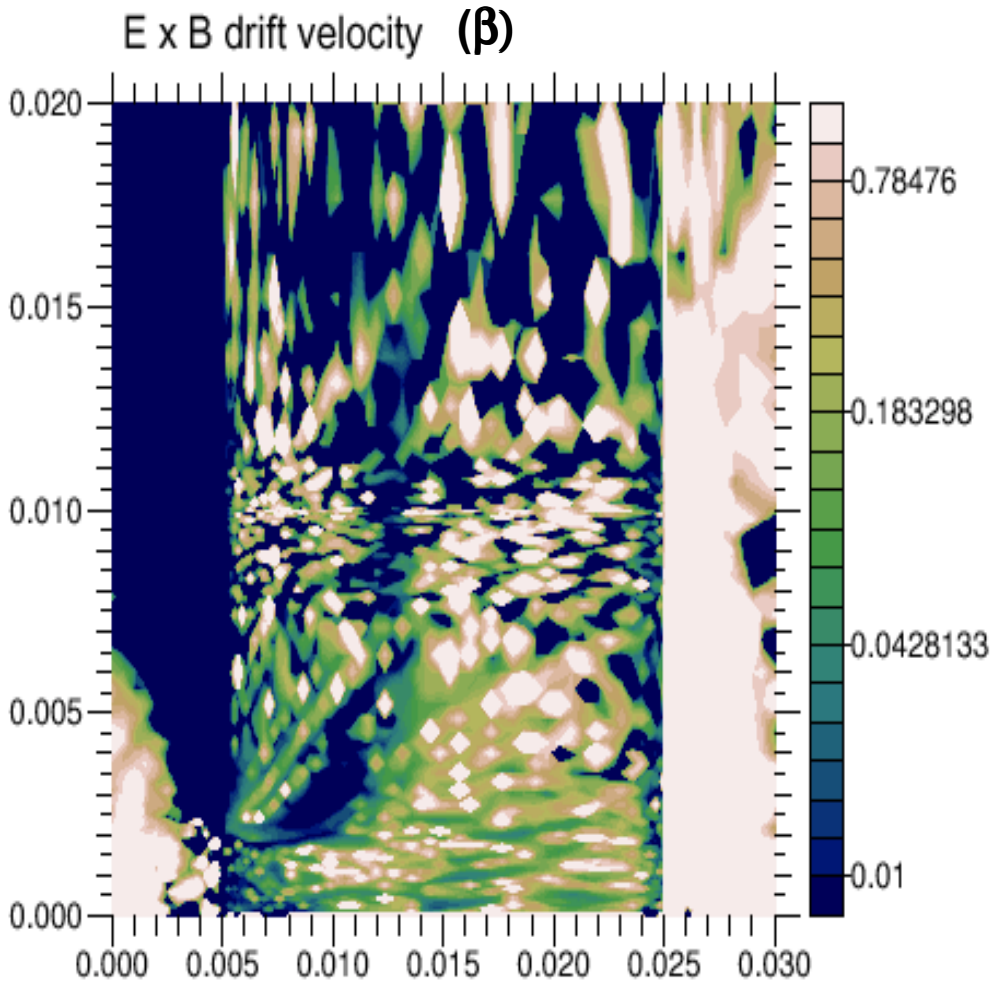

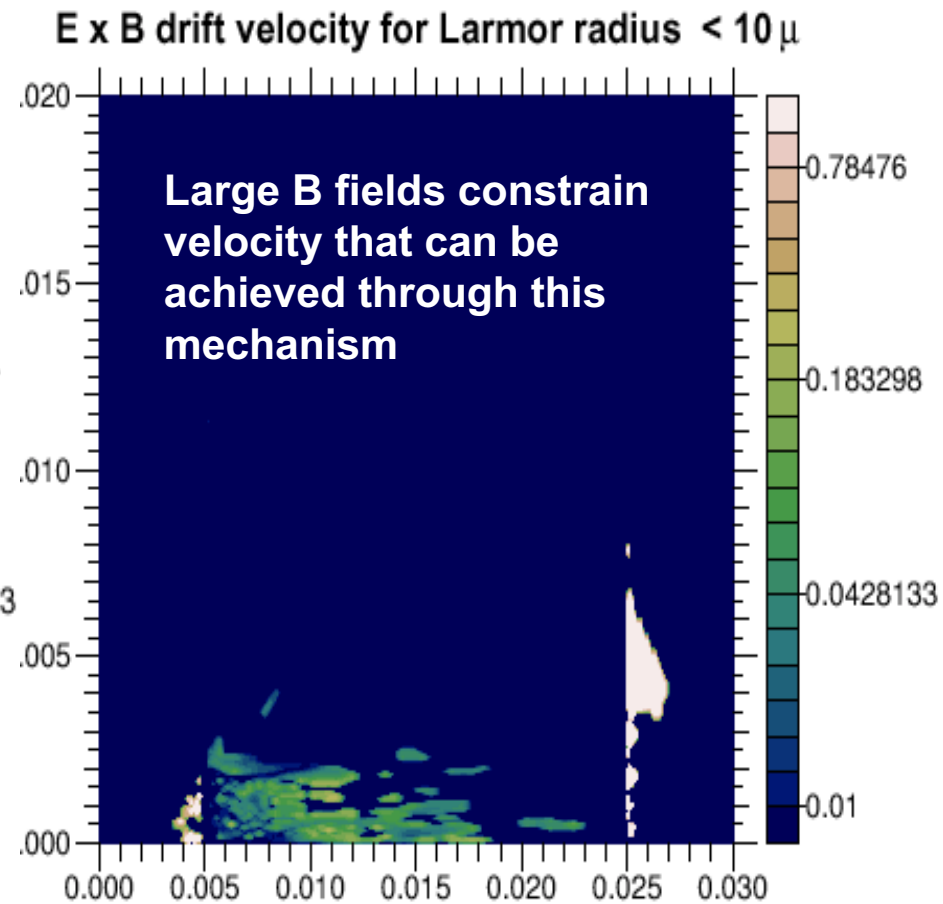

Conclusions and prospects

- There may be significant numbers of runaway electrons produced in these experiments, but it is difficult for them to reach high energy because they are quickly magnetized

- The influence of the hot electron distribution function on instability growth needs further study

- The wings of the laser beam may influence target energetics and apparent spot sizes

- The background electron transport and heat capacity models need to be improved

  - Will install Lee&More conductivity model and QEOS heat capacity model

Fast Ignition Tutorial

Fast Ignition Workshop

St.Petersburg,Fl

November 17-19,2002

Max Tabak

Lawrence Livermore National Laboratory

This work was performed under the auspices of the U.S. Department of Energy by the University of California Lawrence Livermore National Laboratoryunder contract No. W-7405-Eng-48.

Conflicting heating and compression requirements determine gain curves

Why is there a non-trivial energy requirement to achieve ignition and burn?

Little energy is required to assemble enough fuel to bootstrap and achieve high gain

$E_{comp} \propto M_c \rho_c^{2/3}$
Vanishes for
$\rho_c = \rho_{solid}$

Little energy is required to heat bootstrap region to ignition temperature

$E_{hotspot} \propto (\rho R)_{HS}^3 T/\rho^2_{HS}$
Vanishes for $\rho \rightarrow \infty$
for fixed ρR

Want to maximize $\phi M(/E_{tot})$ including both energies
$\phi = \rho R /(\rho R + 6)$

What are possible relations between hotspot and mainfuel?

- **Isochoric => uniform density(and huge pressure jump)**
- **Isobaric => uniform pressure(and low density hotspot)**

e isochoric (constant density) model produces gher gains with lower compressions

operty	Isobaric model	Isochoric model
in	$1.5 \cdot 10^3\ \eta\ (\eta E)^{0.3}$	$3 \cdot 10^4\ \eta\ (\eta E)^{0.4}$
lotspot (μm)	$190\ (\eta E)^{0.5}$	$120\ (\eta E)^{0.5}$
lainFuel(μm)	$280\ (\eta E)^{0.5}$	$1200\ (\eta E)^{0.6}$
ainFuel(g/cc)	$358\ (\eta E)^{-0.3}$	$33\ (\eta E)^{-0.5}$
stag(Mbar)	$8.4 \cdot 10^4\ (\eta E)^{-0.5}$	$780\ (\eta E)^{-0.8}$
ss(mg)	$19\ (\eta E)^{1.2}$	$230\ (\eta E)^{1.3}$

sochoric model: lower $\rho \Rightarrow$ more mass to burn($E_C \propto M\rho^{2/3}$)

For isobaric model:fuel at twice Fermi-degenerate isentrope

$R_{Hotspot}$ at triple value for maximum gain

e isochoric model produces higher gains with ess stressing implosion

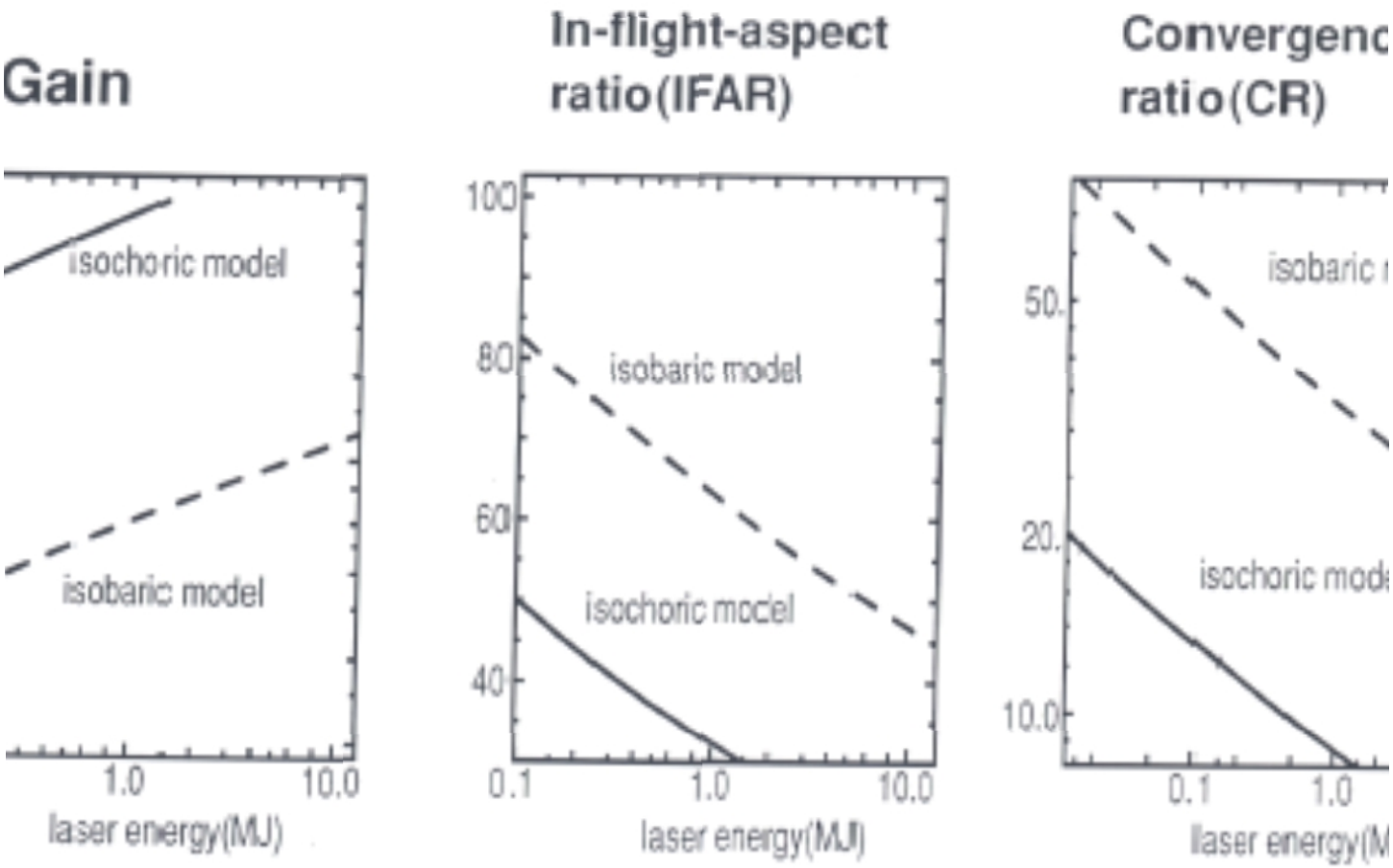

$I_{aric} = 2 \cdot 10^{14}$ W/cm^2 $I_{isochoric} = 3 \cdot 10^{13}$ W/cm^2

e electron-ion collision and disassembly times set e required ignition laser duration and intensity.

1
laser couples
to hot electrons

$\tau_{\gamma e} \sim 10^{-15}$ sec

2
hot e⁻'s couple
to thermal e⁻'s

$\tau_{ee} \sim 10^{-13}$ sec

3
thermal e-
couple to
DT ions

$\tau_{ei} \sim 1$ psec

4
core disassemb
$\tau_D \sim R/C_s$

$\tau_D \sim 10$ psec

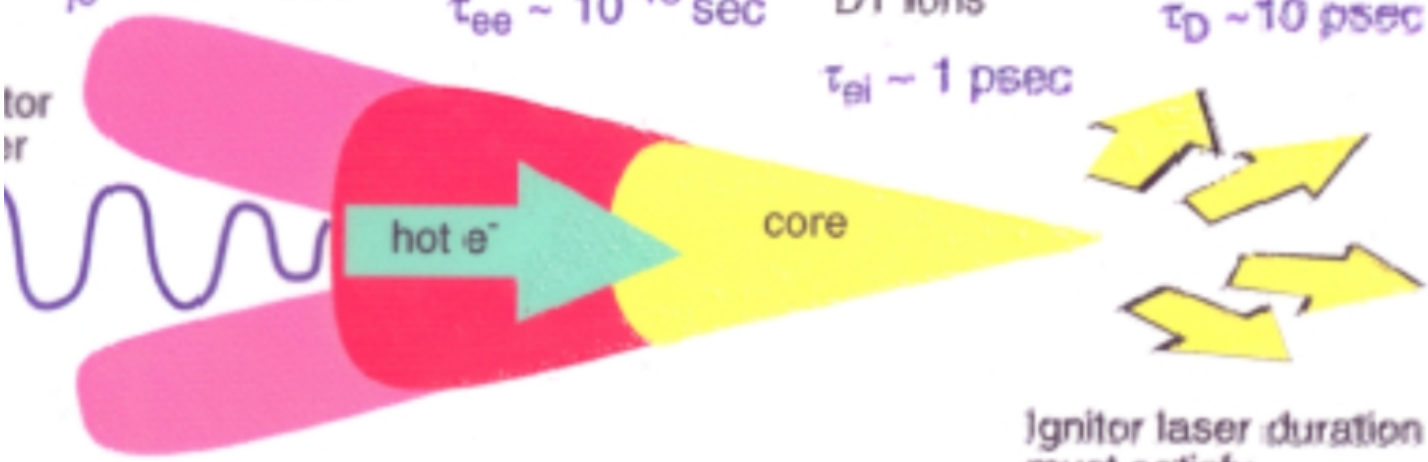

d ignition energy of
$\varepsilon_{ignt} = 3$ kJ
he laser power must be
$= \varepsilon_{ignt}/\tau_L = 3\times10^{14}$ W

$I_L = 10^{20}$ W/cm^2

Ignitor laser duration
must satisfy
$\tau_{ei} < \tau_L < \tau_D$

$\Rightarrow \tau_L \leq 10$ psec

*Note: All calculations are for
$\rho = 300$ gm/cc, $T_i = 10$ keV, and
$\rho R_{hs} = 0.4$ gm/cm^2

What is effect of ignition dynamics on gain curves

- Is it legitimate to assume that both isochoric and isobaric models have the same ignition criteria? No!!

- Ignition means that hotspot reaches 30 keV where burn efficiency is calculated.
  - -Lower temp OK because σv becomes quite large
  - -But need "ignition time" to bootstrap to burn temperature
  - -Include power loss from hydro&electron conduction

	pressure	radius	Stagnation time
isobaric	Stagnation pressure	Main fuel radius	100's of ps
isochoric	Ignition pressure	Hotspot radius	~ 10 ps

- Atzeni has charted Fast Ignition requirements

Atzeni,et.al., have found ignition windows and gain curves including loss terms

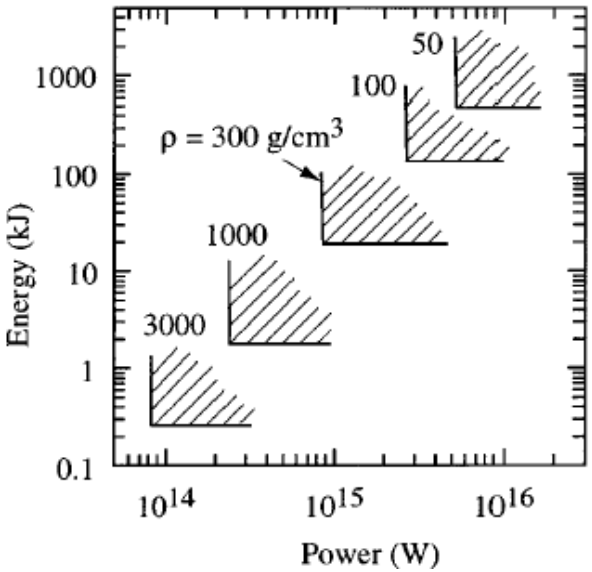

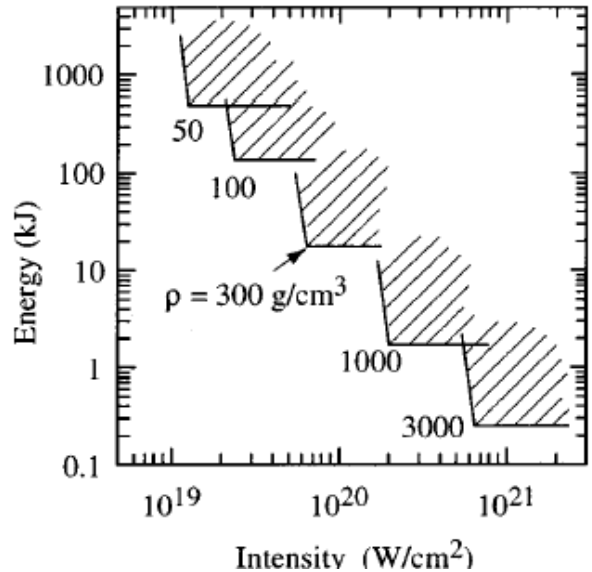

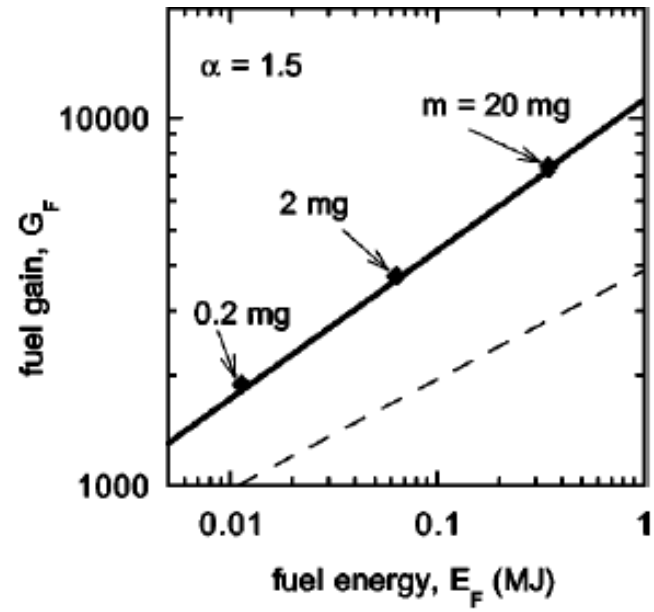

Ignition criteria:
T=12 keV, ρR=0.5 gm/cm^2
E_{ign}(kJ)=140(100 gm/cc/ρ)$^{1.85}$

What are the details that will allow us to achieve these gain curves?

- How to assemble fuel
  - Efficiently produce high density fuel without low density center

- How to couple energy to fuel

  - Laser transport(get energy close to fuel)
    - Filamentation and hole boring
    - Cone focus geometries
    - Asymmetric implosions
    - Other ideas

  - Laser plasma interaction and coupling efficiency(make hot e^-)

  - Electron transport(deliver energy from critical surface to fuel)

  - Proton generation and transport(another route)

High intensity light can couple efficiently to dense matter via collisionless mechanisms

Two mechanisms:

If E points into plasma,

- **oscillatory excursion > plasma scale height**
- **Electron doesn't feel decelerating field**
- **'Not-so-resonant resonant absorption"**

If large E parallel to plasma

- **B field will rotate motion into plasma**
- **Electron in vacuum would have figure 8**
- **Absorption increases with intensity**
- **"J x B heating"**

Rippling of surface increases absorption

PIC simulations see absorption 40-50%

- **Sometimes 90% with holeboring at high I**

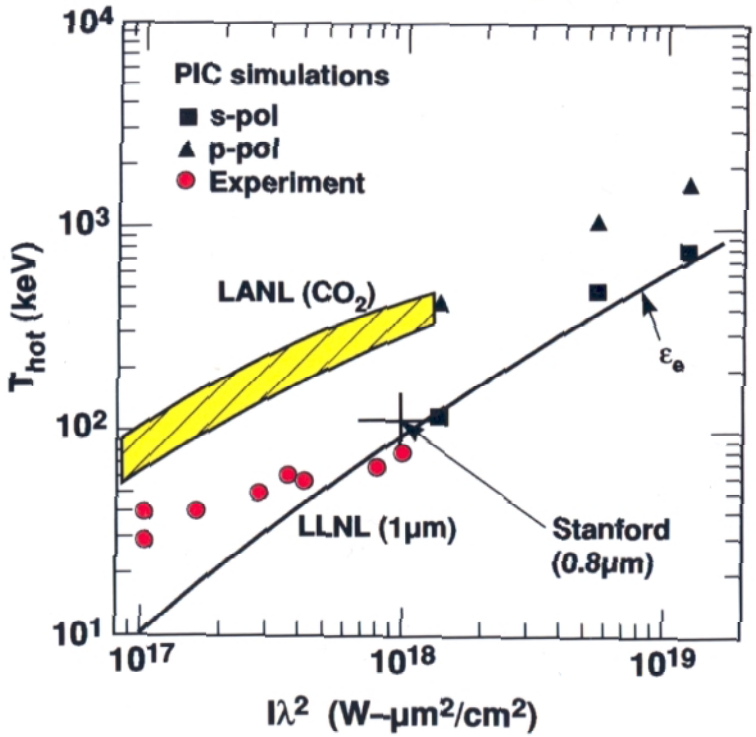

Several schemes to shorten distance between critical density and the ignition region were explored

The compressed fuel is produced by an implosion
The critical surface has radius ~ initial radius ~ mm
How can we hit 30µm spot from this distance?

Ponderomotive holeboring ,relativistic transparency and/or cone focus geometry are possible routes to reduce this distance

P=2I/c for mirror

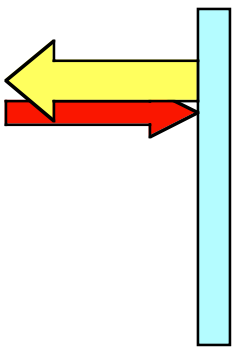

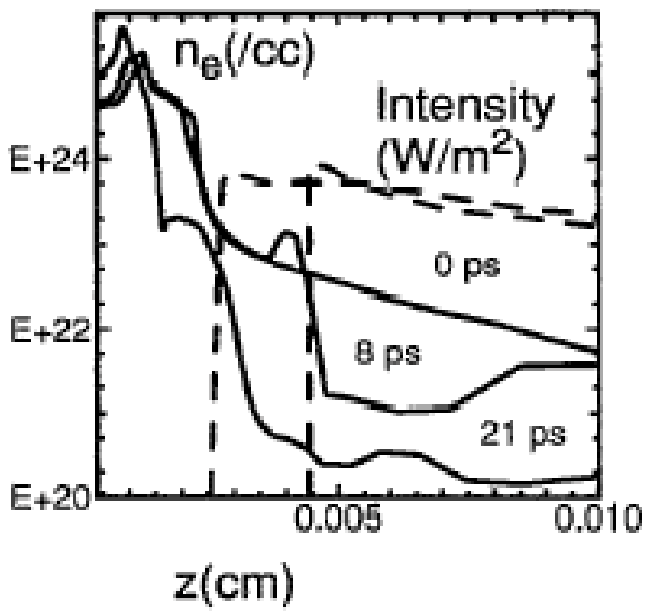

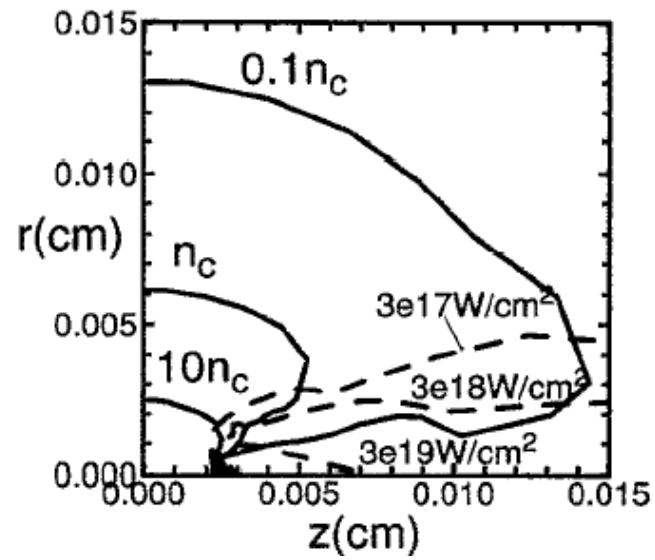

Early experiments showed that moderate intensity beams could penetrate 100's of μ of n_c plasma with thermal filamentation

I_{peak}=5 10^{15}W/cm^2
gaussian pulse

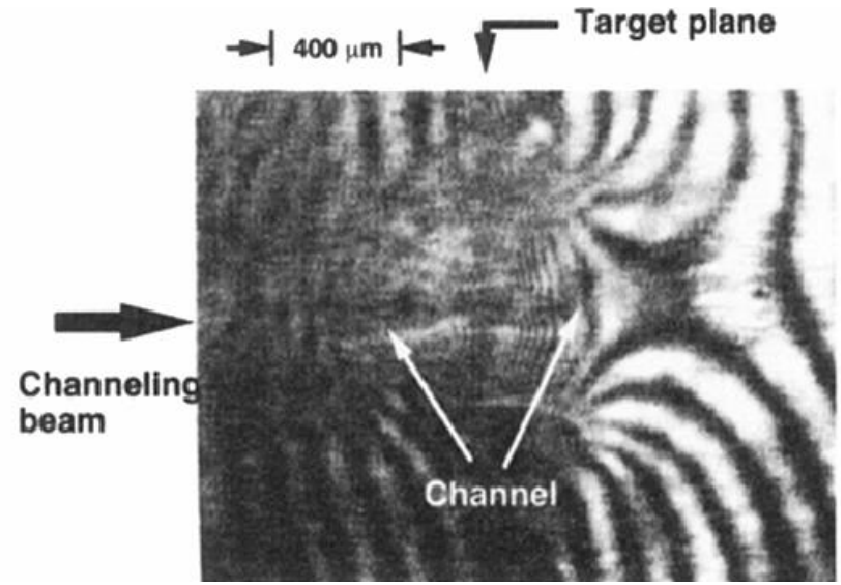

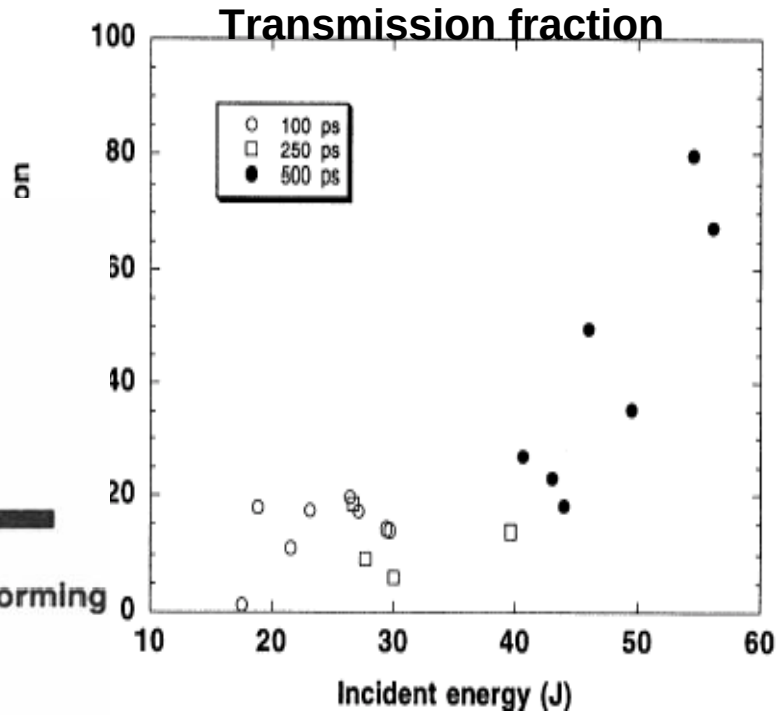

n_e(peak)=0.3n_c

Young,et.al.

But, coronal plasmas are have mm extent
Holeboring pulse took 100's of ps even for 500 μ plasma
Transmitted pulse may be filamented

As the sole technique to reduce the distance between critical and high density, hole boring is probably insufficient

Aberrated beams likely to filament

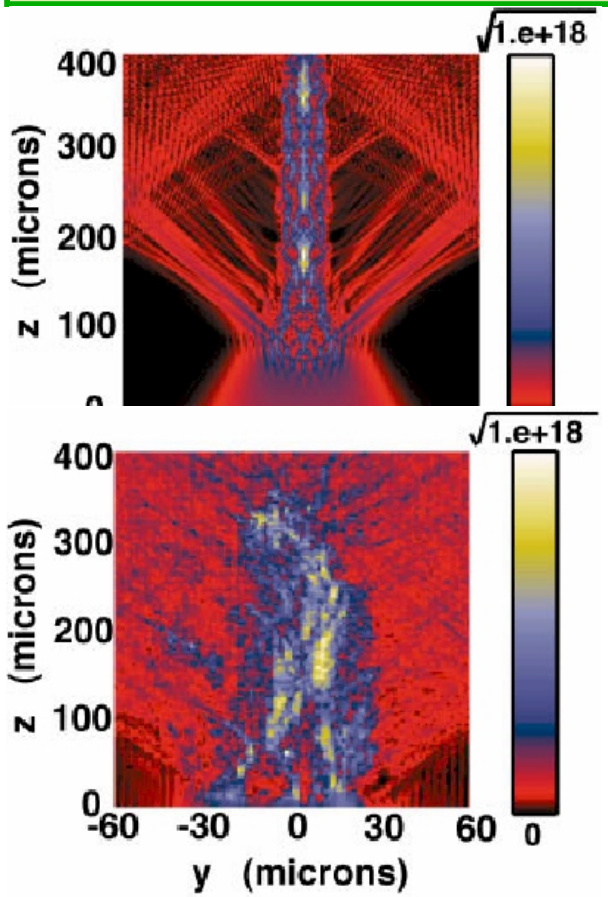

Large channel aspect ratio will lead to significant losses on walls

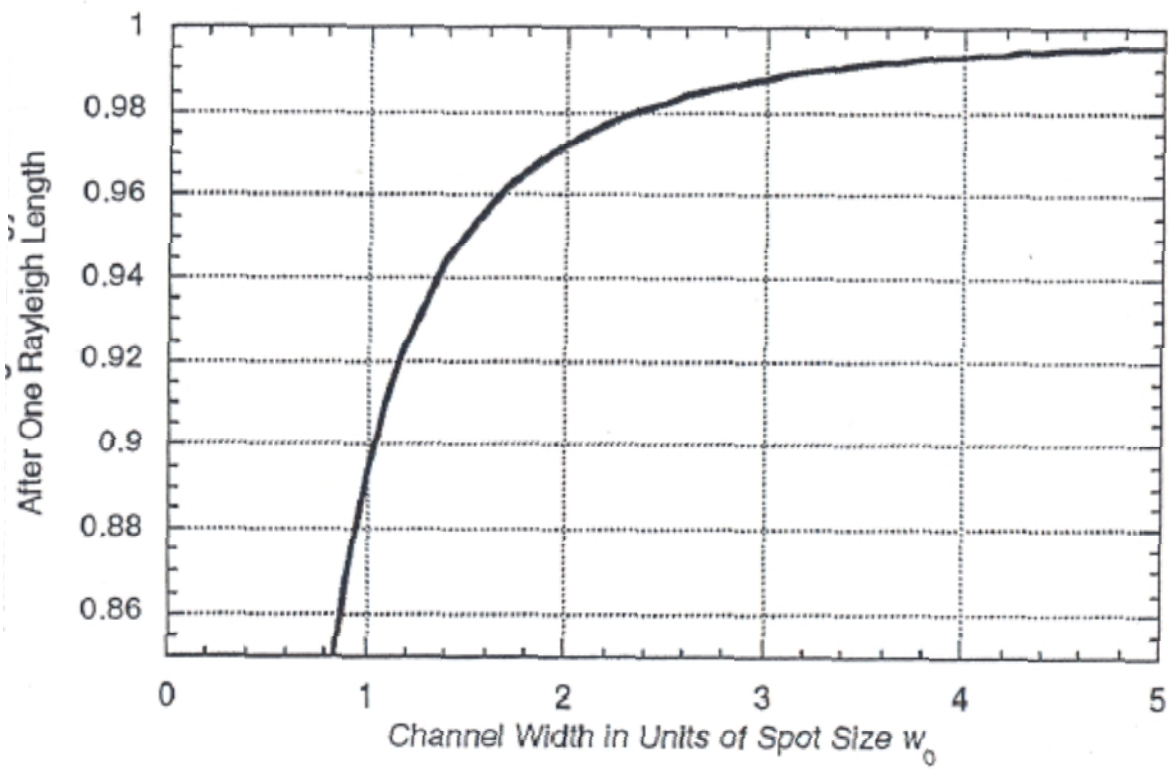

No experiment has demonstrated propagation through mm's of plasma with good efficiency

Cone focus designs provide access to assembled core

A NIF-like scheme

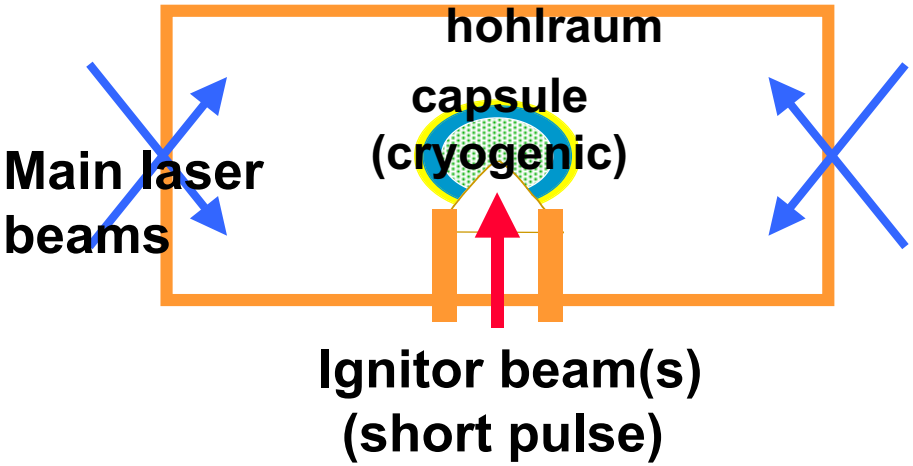

Issues:

- Entrainment of cone material
- Produce imploded core without
- central void
- Assemble core with good
- efficiency

$E_{beam,min}$ ~ 30 kJ

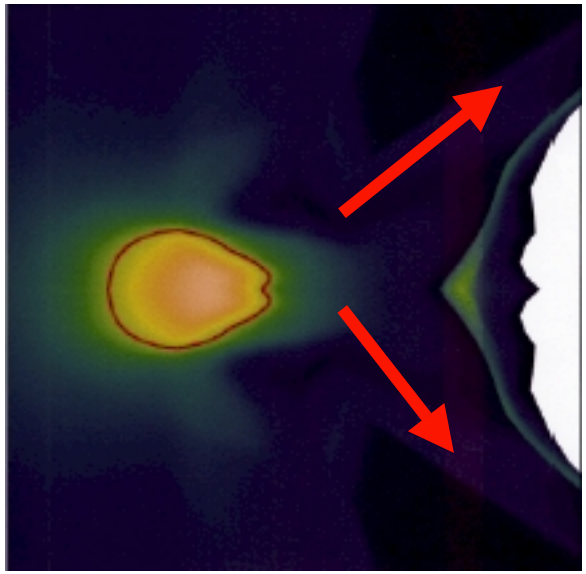

Neutron Image at end of deposition

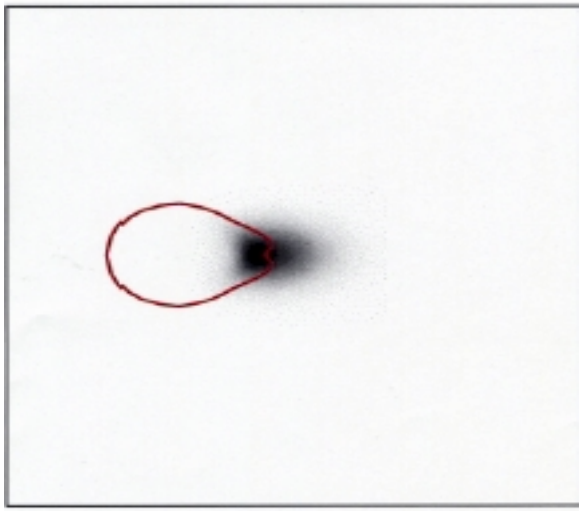

Yield = 27 MJ

Are there any ideas to reduce the central low density region in implosion?

Low density region halves ρR

⇒ϕ down 30% and ignition more difficult

Reduce central entropy by allowing mass to escape through aneurysm

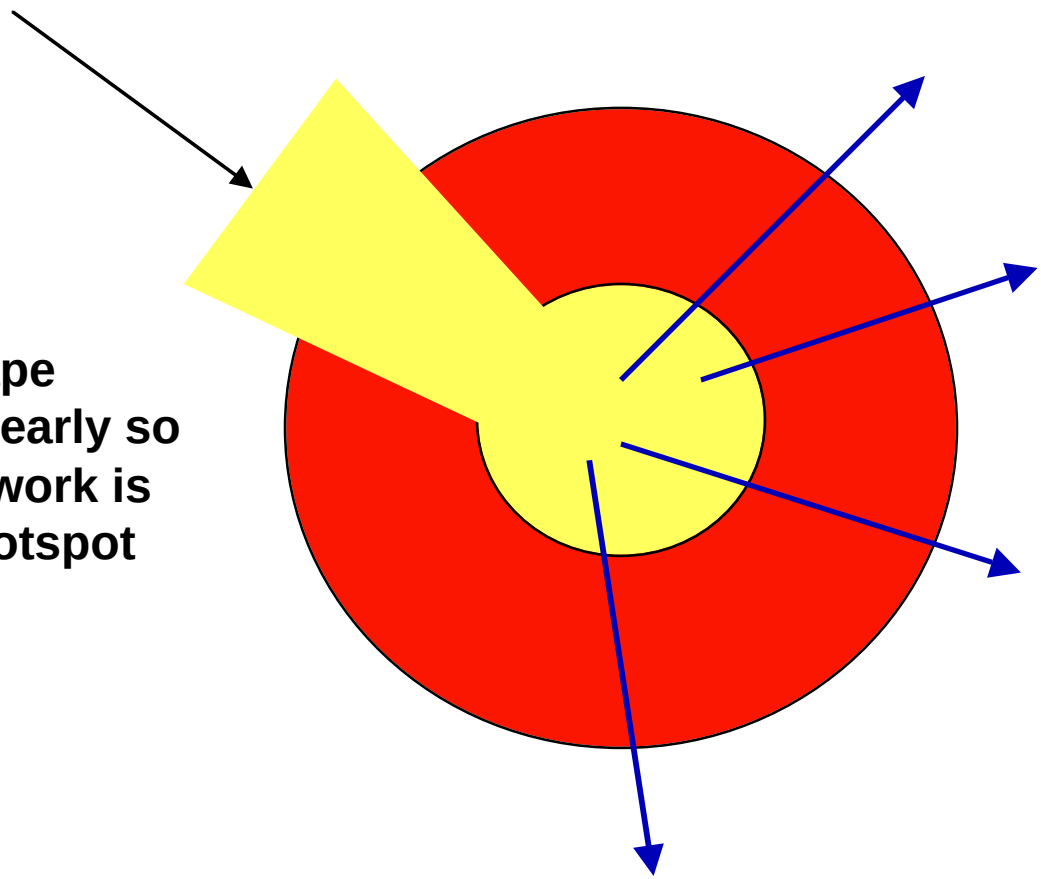

Poison center to produce radiative collapse

Mass escape should be early so minimum work is done on hotspot

Omega capsules were roughly 1/5 ignition scale; all CH.

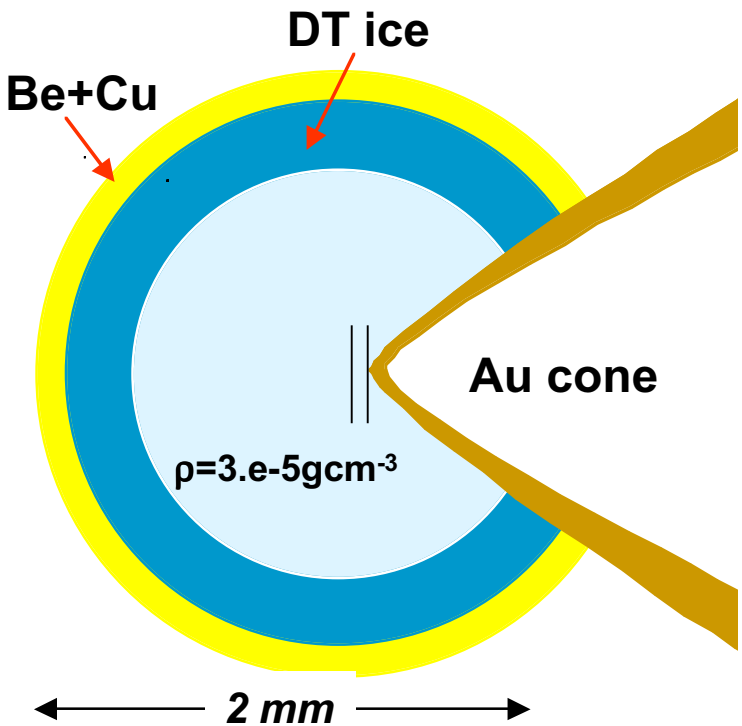

Ignition scale

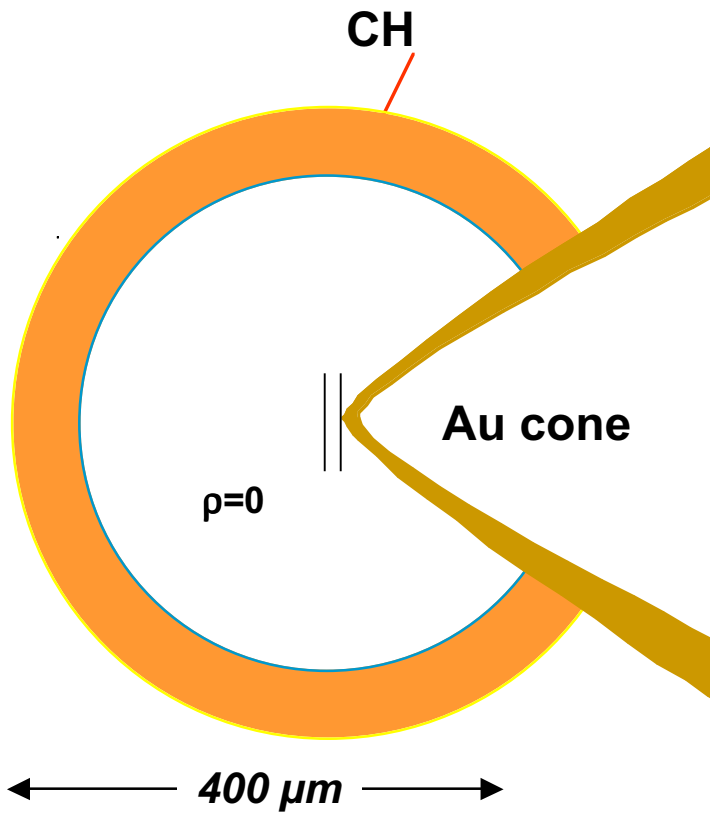

Omega scale

Backlit images (@8 keV) show convergence of cone-focussed targets was very similar to prediction — with perhaps a small time offset.

Experiment

225 μm

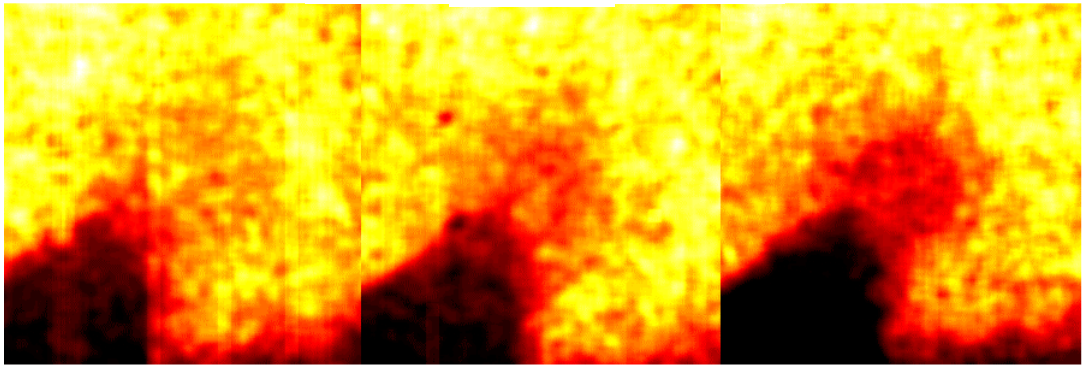

t = 3.0 ns 3.1 ns 3.2 ns

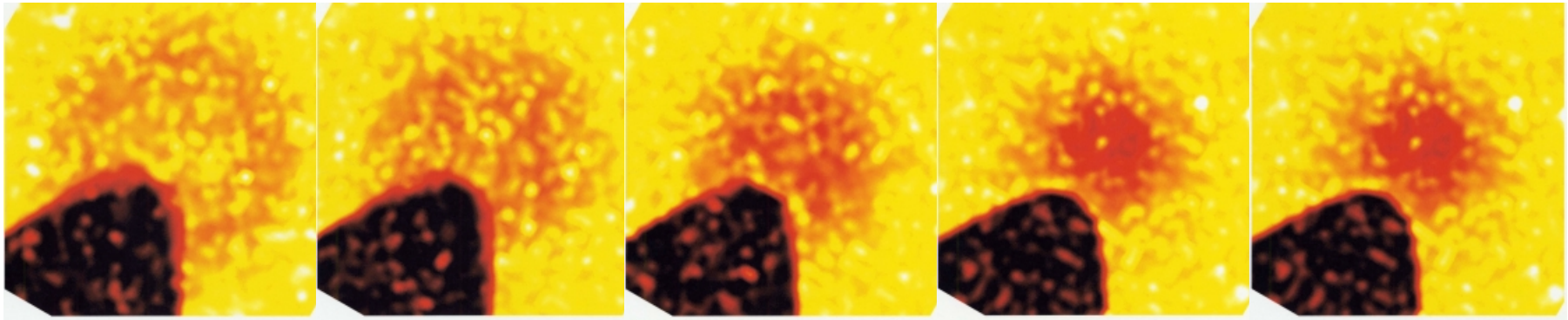

t = 3.0 ns 3.1 ns 3.2 ns 3.3 ns 3.4 ns

Prediction (with pixelation, noise, and smoothing like exp. images)

Comparison shows some exp. evidence for gold entrainment near tip of cone.

Apparent experimental convergence of cone-focussed targets is probably much less than their true convergence.

Prediction for 8 keV backlit images

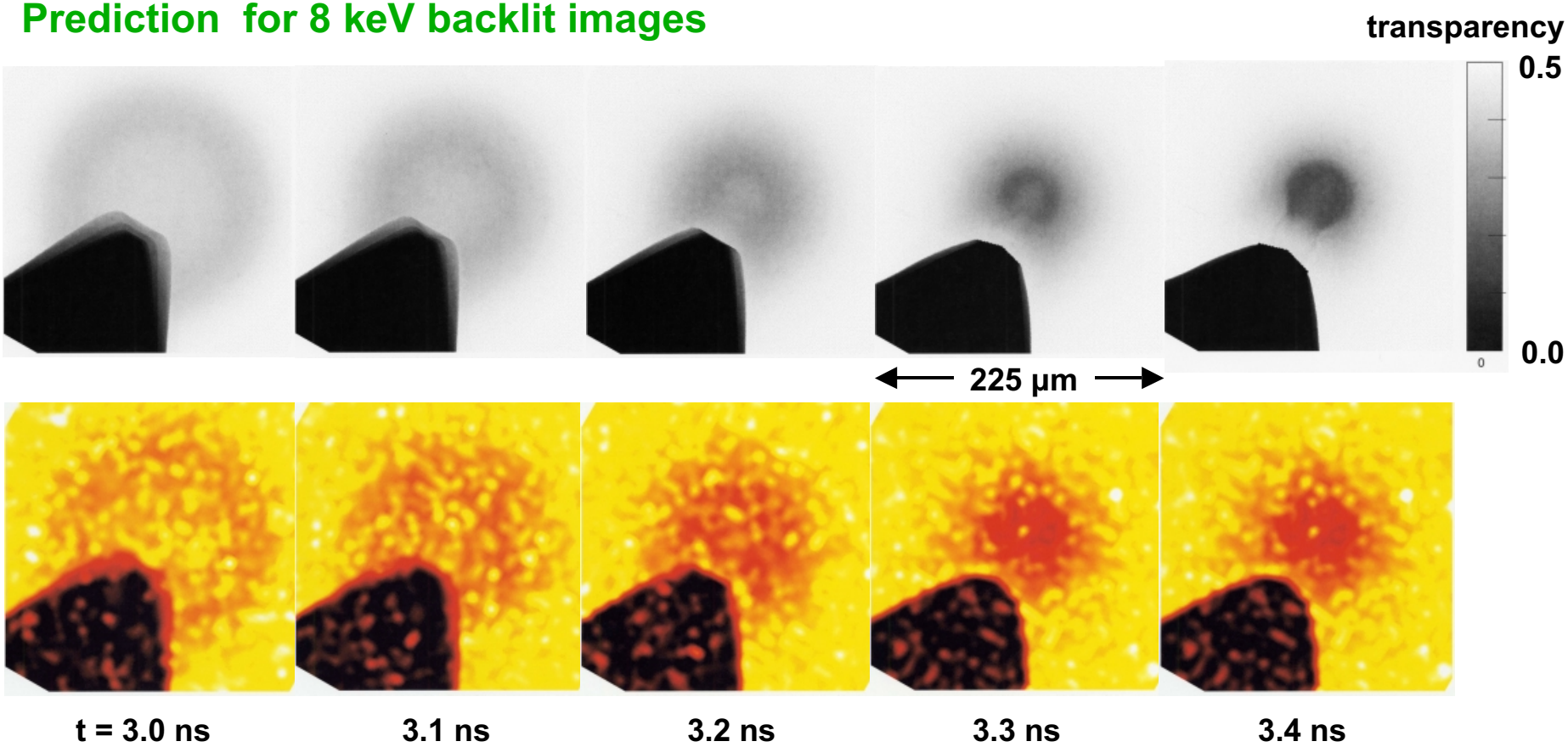

Prediction — with pixelation, noise, and smoothing like exp. images.

The transport of electrons is controlled by multiple scattering, effects of macroscopic E&B fields and possibly by microinstabilities

Scattering affects range and angular distribution

$dE/dx \sim Z_{eff}^2 n_e/\beta^2 * \mathrm{Log}\,\Lambda$ => for relativistic e^- $\rho(\delta x) \sim E$

Deutsch has suggested $Z_{eff} \neq 1$

Hots are so dense and fast that multiple electrons can scatter before shielding electrons move

$\langle\Theta^2\rangle \sim Z_{eff}^2\, \rho(\delta x)/L_{rad} p^2$

Charges and currents produced by the laser are so large that nothing can move without significant neutralization

Power = I V or 10^{15}W = 1 MV * 10^9A (Alfven current ~ $5*10^4$A)

Curl B = $j*\mu_0$ => $B=I\,\mu_0/(2\pi r)$ or for r=30microns B=6.7 10^{10} gauss

Energy=QV or 10^5J = 1 MV * 0.1 Coulombs

Div $E=\rho/\varepsilon_0$ => $E= Q/(\varepsilon_0 2\pi r^2)$ or for r=30microns E= 9 10^{16} V/m

In some simulations microinstabilities(Weibel,2 stream) show stopping Power ~10^4 classical, but not seen in normal density experiments

MHD models(Jim Hammer,Tony Bell) and hybrid code calculations predict fields in 5-30MG range and particles propagating as warm beams

MHD models treat hot and cold electrons as two fluids with stationary ion background

Fluids characterized by:

- $n_{H,C}$ **particle densities**
- $T_{H,C}$ **fluid temperature**
- $P_{H,C}$ **fluid pressures**
- $v_{H,C}$ **fluid drift velocities**
- ν_{HC} **drag coefficient between hots and colds**

Newton's law for two species:

$$n_H m_H \frac{d\vec{v}_H}{dt} = -\nabla P_H - e n_H \left(\vec{E} + \frac{\vec{v}_H}{c} \times \vec{B} \right) - n_H m_H \nu_{HC} \left(\vec{v}_H - \vec{v}_C \right)$$

Assume hots are collisionless; net force on hots much less than individual terms; there is a steady state

$$\Rightarrow \frac{\nabla P_H}{e n_H} + \vec{E} + \frac{\vec{v}_H}{c} \times \vec{B} \cong 0$$

MHD models II

Colds are also in steady state:

$$\vec{E} + \frac{\vec{v}_C}{c} \times \vec{B} = \eta_C J_{cold}$$

Scattering of colds from ions only

Currents must approximately cancel or magnetic and electric fields get crazy

$$J_{cold} \cong -J_{hot}$$

Magnetic force on colds << force on hots and maybe electric force on colds

$$\vec{E} = -\eta_C J_{hot}$$

Hot force law becomes:

$$\Rightarrow \frac{\nabla P_H}{e n_H} - \eta J_H + \frac{\vec{v}_H}{c} \times \vec{B} \cong 0$$

MHD models III

Remaining hot equations:

$$\dot{n}_H + \nabla \cdot n_H \vec{v}_H = 0$$

Current conservation

$$\dot{\vec{B}} = -c\nabla \times \vec{E} = c\nabla \times \left(\eta J_H\right)$$

Faraday's law

Limiting cases:
Electric force on hots << magnetic force

$$\Rightarrow \frac{\nabla P_H}{e n_H} + \frac{\vec{v}_H}{c} \times \vec{B} \cong 0$$

Bennett pinch condition but driven by Faraday's law, not $\nabla \times \vec{B} = 4\pi J / c$

In cylindrical geometry

$$v_{H_z} = \frac{c T_H}{e n_H B} \frac{\partial n_H}{\partial r}$$

$$\dot{B} = c \frac{\partial E_z}{\partial r} = \frac{\partial}{\partial r} \frac{\eta c^2 T_H}{B} \frac{\partial n}{\partial r}$$

MHD models IV

An ansatz for a solution

$$n_H = n_0 \exp\left(\frac{-r^2}{2r_0^2}\right)$$

$$B = B_0 \frac{r}{r_0} \exp\left(\frac{-r^2}{4r_0^2}\right)$$

$$B_0 = \sqrt{\frac{\eta T_H c^2 n_0 t}{r_0^2}}$$

Warm beam of constant radius composed of a magnetized plasma

Magnetic field grows as forward and currents diffusively separate

Drift velocity decreases as B increases
Effectively reduces practical range

Quiet about divergent flows

More detailed descriptions are provided by code calculations

Hybrid calculations are used to model kinetic particles traversing dense collisional plasmas

Hybrid codes have been used to model electron transport relevant to Fast Ignition

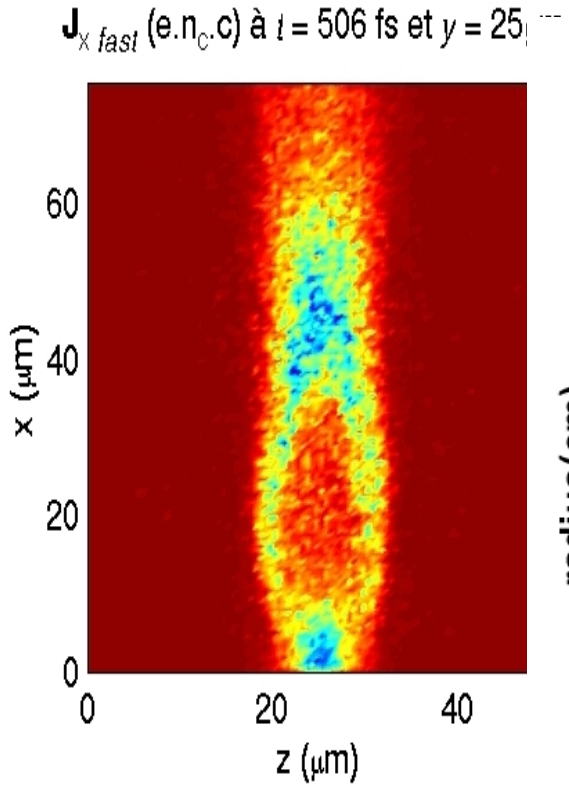

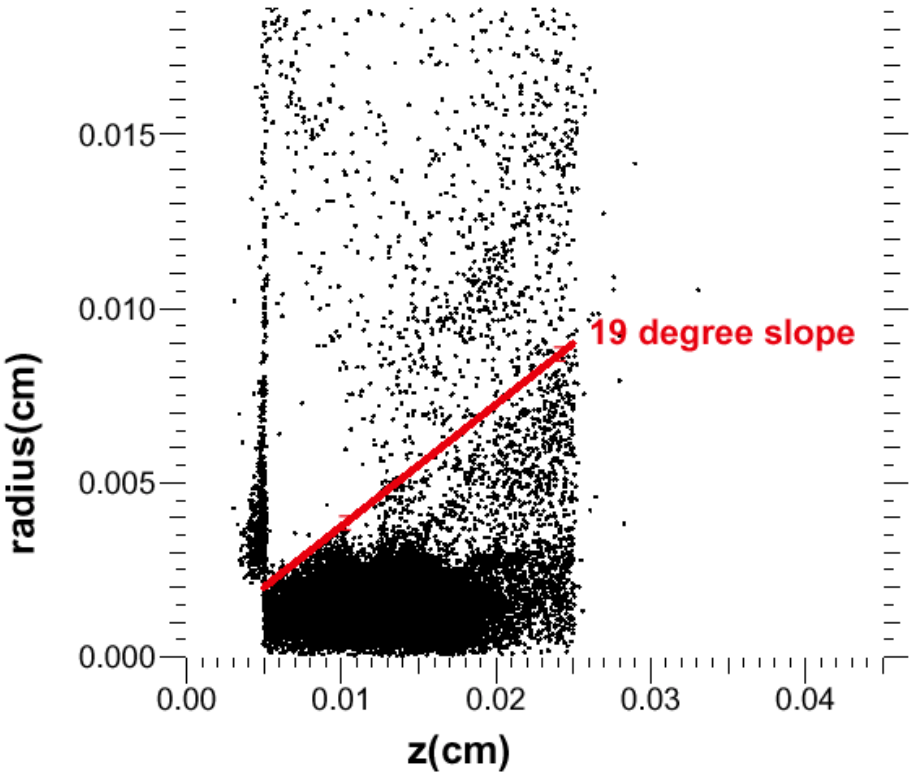

ANTHEM showed propagation as warm beam up gradient to 10^{26}

PARIS showed magnetic guiding, the filamentation Instability and annular current

LSP showed beam divergence and magnetic breakup near jumps in Conductivity. 3D code

Anomalous stopping due to micro-instabilities has been investigated with PIC codes

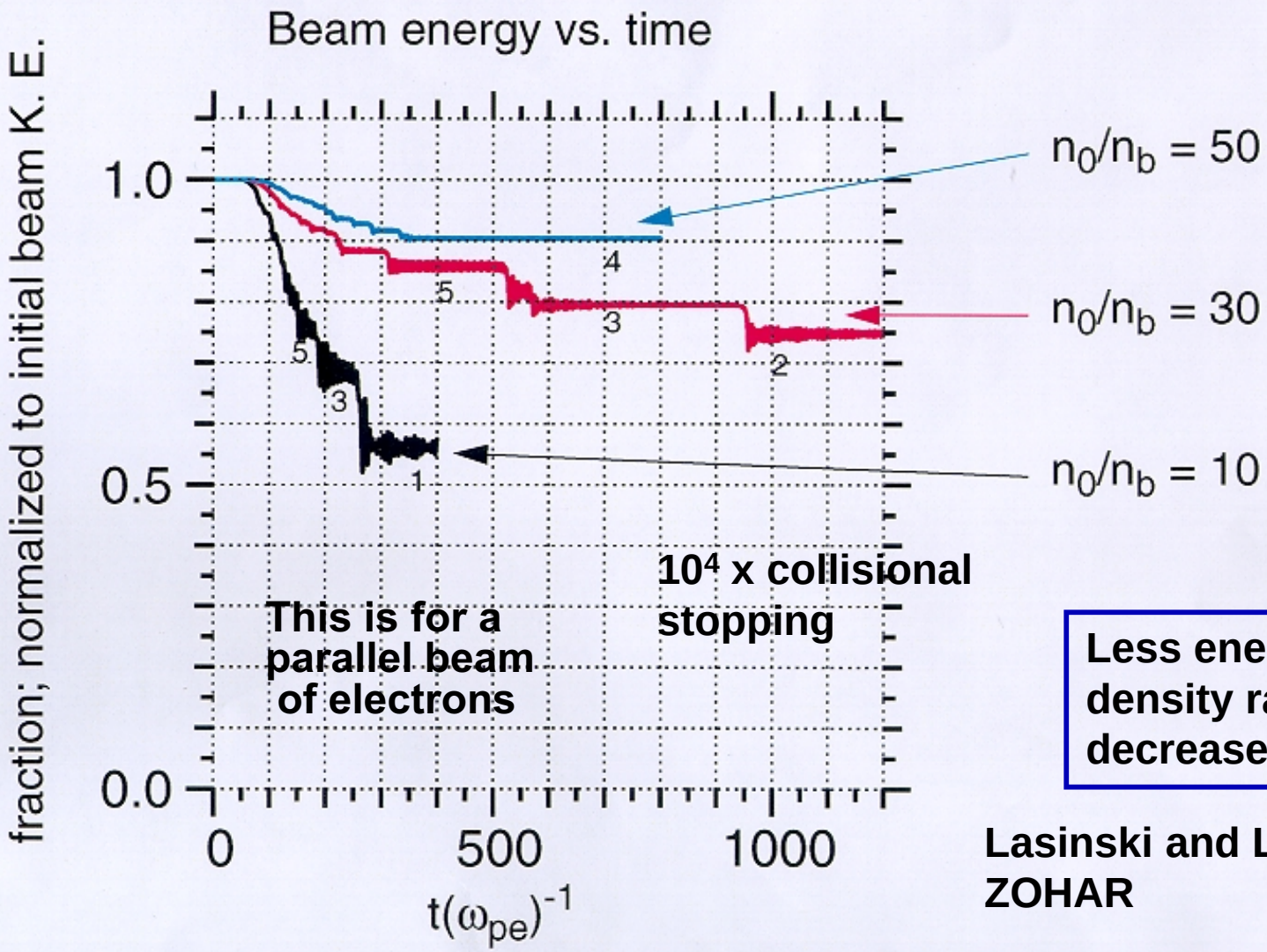

This is for a parallel beam of electrons

10^4 x collisional stopping

Less energy is lost as density ratio decreases

Lasinski and Langdon ZOHAR

Analytic models show that microinstabilities are suppressed by beam temperature and large n_e/n_b (but by different amounts)

Weibel instability threshold

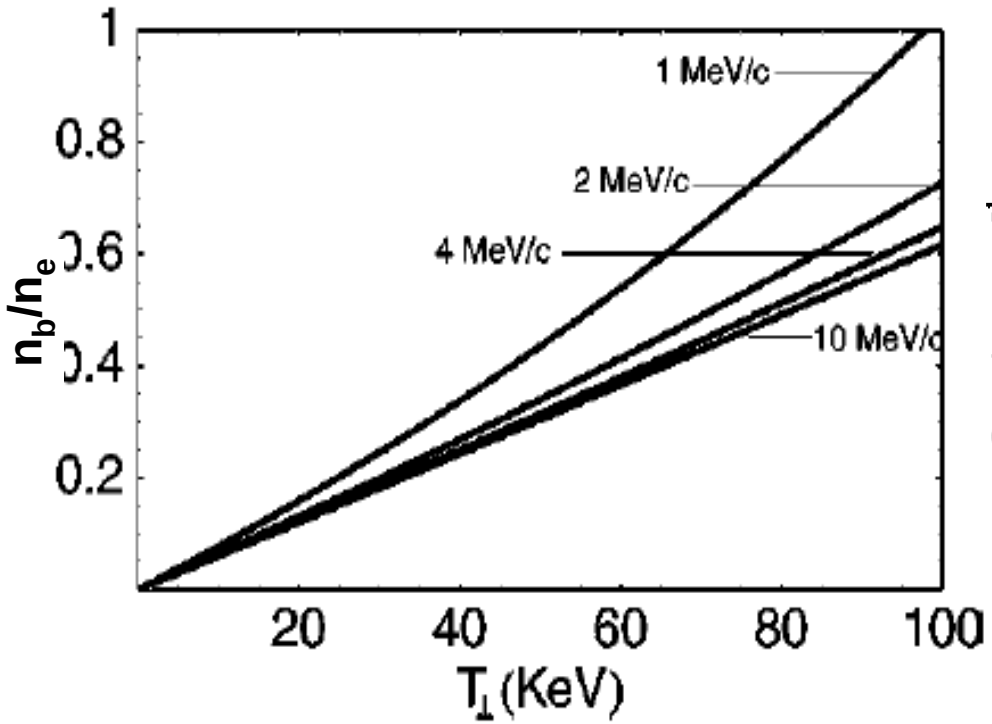

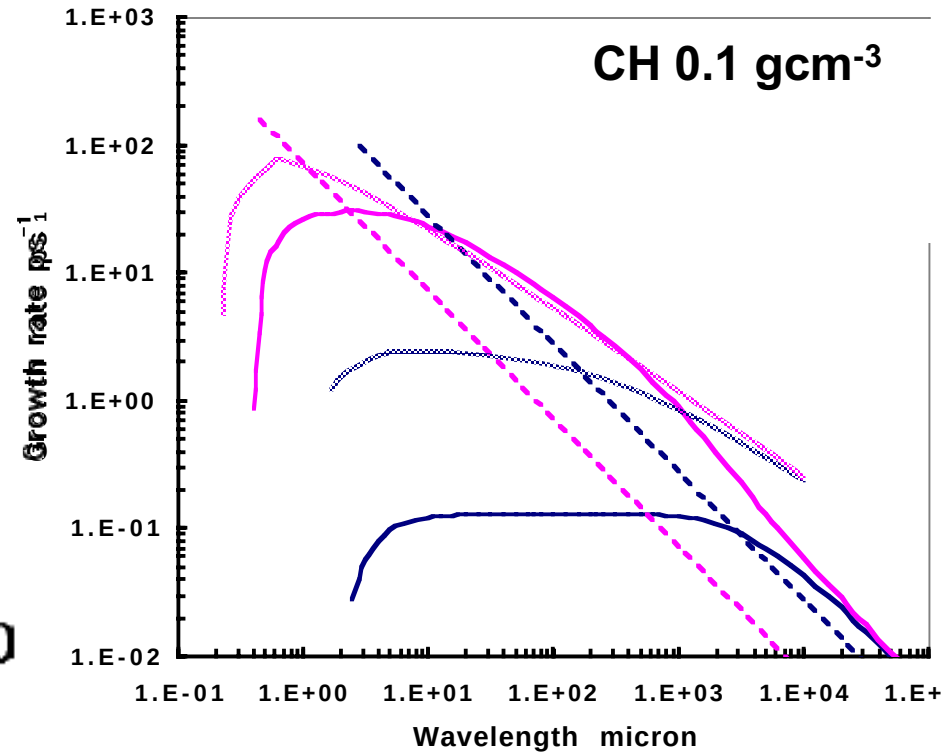

Fluid Temp 300keV
Fluid Temp 10 keV
Vfl=Vth 300keV
Vfl=Vth 10 keV
Parks - Kinetic 300keV
Parks - Kinetic 10keV

Uses waterbag distribution:
Fixed longitudinal momentum with tophat transverse distribution

Silva,et.al.

S 1

Ion acceleration by sudden creation of hot electrons has higher field and greater power in steeper initial gradients.

Schematic 1-D model

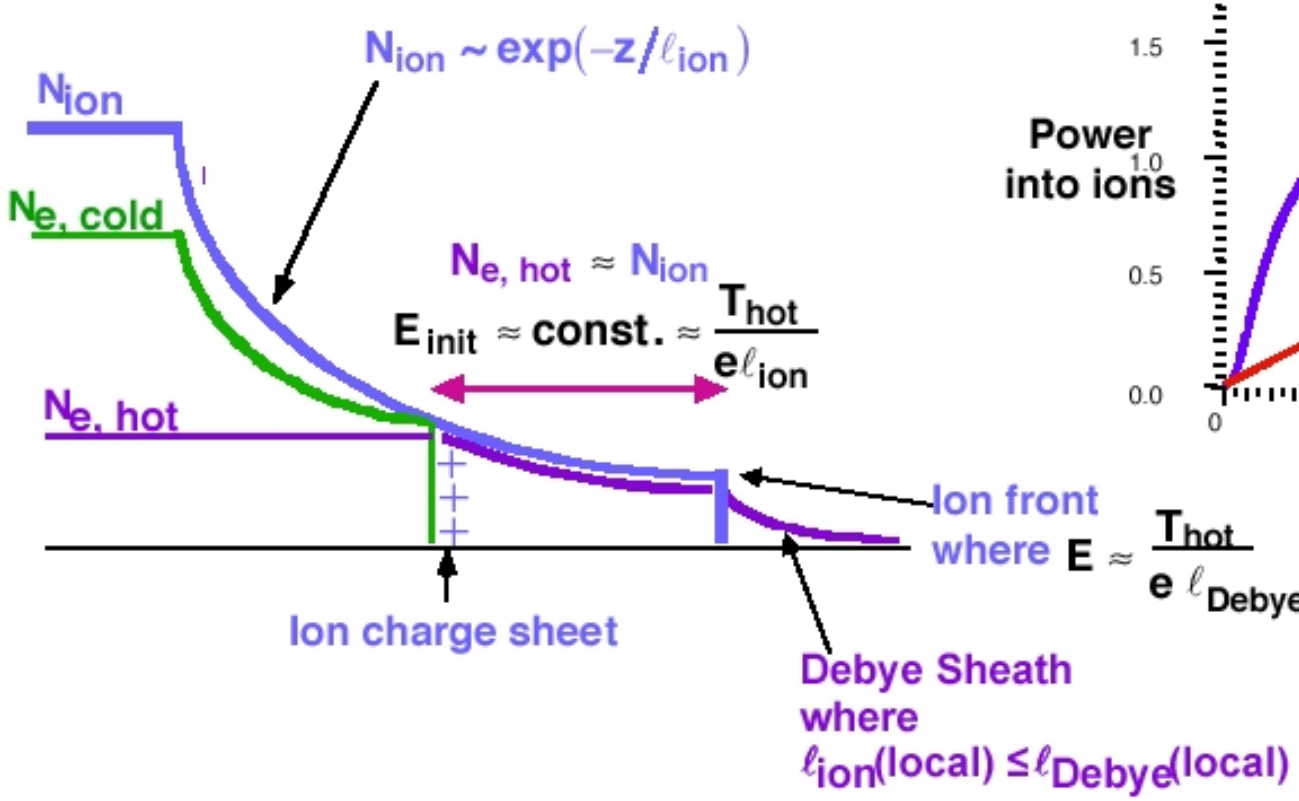

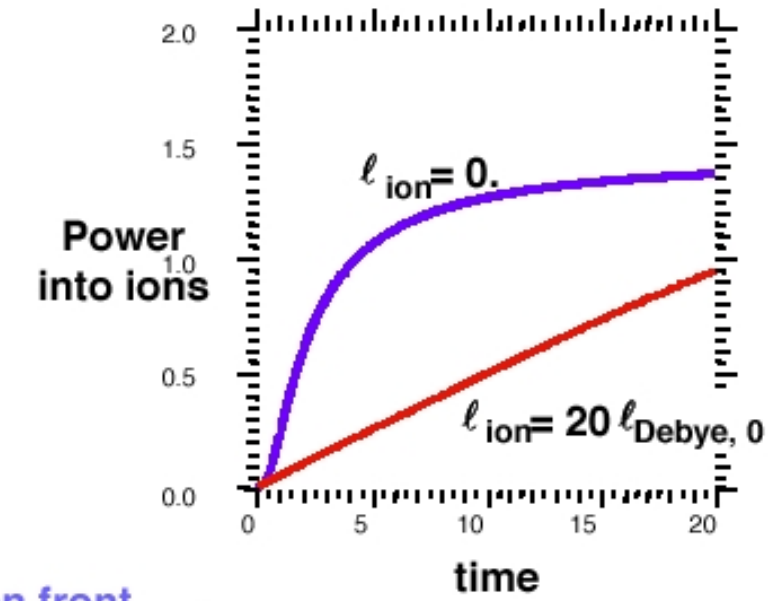

Ion acceleration continues until hots are energetically depleted — by dE/dx or by accelerating ions — in a few ps.

sph_APS99_ionschem

The energy and density of the hot electrons set the scales of things in the physics.

1. Length: Debye length of hots

$$\ell_0 \equiv \sqrt{\frac{T_{hot}}{4\pi e^2 N_{hot}}} = 2.4\mu m \left(\frac{T_{hot}}{1MeV}\right)^{1/2} \left(\frac{N_{hot}}{10^{19}}\right)^{-1/2}$$

2. Velocity: ("sound" speed)

$$c_s \equiv \sqrt{\frac{T_{hot}}{m_{ion}}} = 9.8\ \mu m\ ps^{-1} \left(\frac{T_{hot}}{1MeV}\right)^{1/2} \left(\frac{m_{ion}}{m_p}\right)^{1/2}$$

3. Time:

$$\tau \equiv \sqrt{\frac{\ell_0^2 m_{ion}}{T_{hot}}} = 0.24\ ps \left(\frac{N_{hot}}{10^{19}}\right)^{-1/2}$$

4. Sheath Electric field:

$$\boxed{E \cong \frac{T_{hot}}{e\ell_0} = \frac{MegaVolts}{microns}}$$

Ion acceleration mechanism is a new variation on an old theme: sheath field from hot electrons.

1. Laser <u>suddenly</u> creates large number of hot electrons:

$$\langle E_e \rangle \sim T_{hot} \sim U_{ponderomotive} \sim \text{few MeV} \quad \text{at } I\lambda^2 \sim 10^{20}\ \text{W cm}^{-2}\ \mu\text{m}^2$$

$$\#\ \text{hots} \sim \frac{\eta E_{laser}}{\langle E_e \rangle} \sim \frac{200\ \text{J}}{\text{few MeV}} \sim \text{several} \leftrightarrow 10^{14}$$

2. Hots <u>fly through</u> "thin" (~1mm x 1mm x 100 μm) targets; a small fraction escape, charging target to $eV_{target} > \langle E_e \rangle$

3. Hots circulate in and near target, set up sheath and sheath electrostatic field (>> charge-up field): ie Colds sag inward isolating a + surface charge of ions whose field contains the sheath of hots.

$$N_{e,\ hot} \sim \frac{\text{several } 10^{14}}{10^{-4}\text{cm}^3} \sim \text{several } 10^{18}\ \text{cm}^{-3}$$

4. Sheath field accelerates the ions.

Integrated results from ILE,Osaka are encouraging

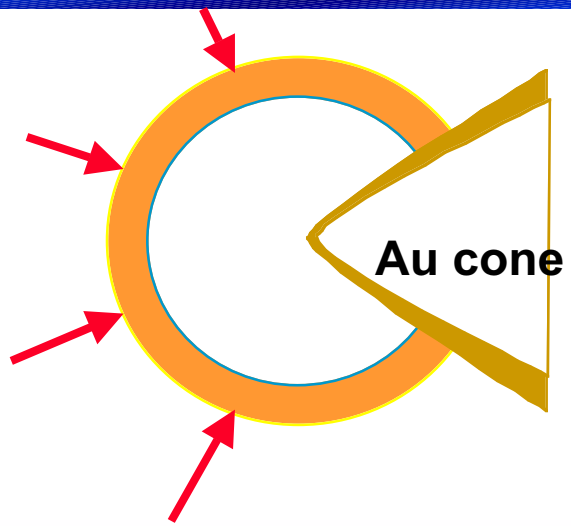

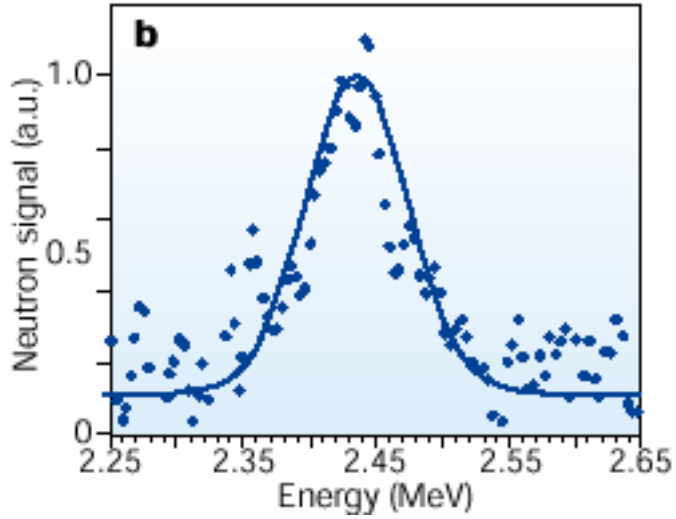

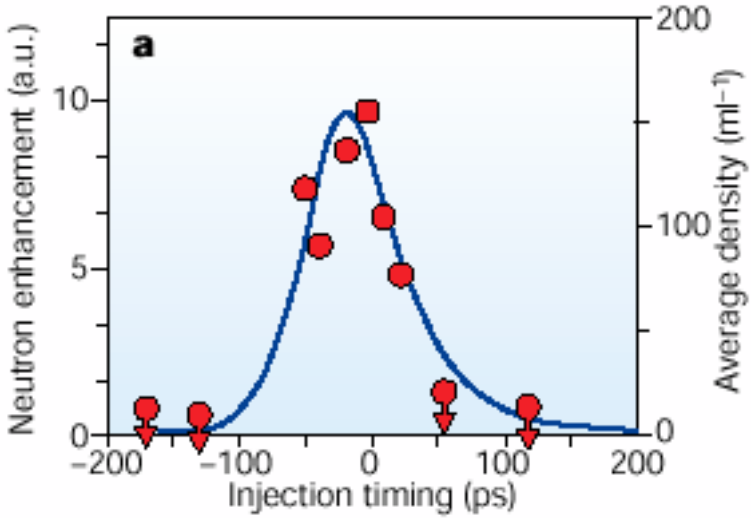

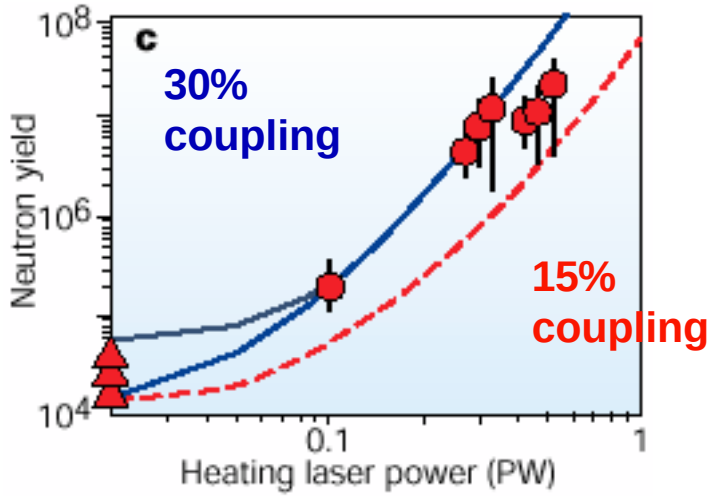

Infer 15-25% coupling efficiency from laser to compressed fuel!

After 10 years, there are still no showstoppers apparent for Fast Ignition

- Coupling efficiency appears adequate at 15-25%
- Lots of challenges remain
  - Improved implosion and ignition schemes
    - Reduce distance between critical high density
    - Improve efficiency of producing compressed core
    - Optimal energy deposition profile for short pulse
  - Develop detailed understanding of electron transport
  - Focus ion beams to high intensity and produce them with good efficiency
  - Understand scaling to high energy and long pulses
  - Need reactor scenario utilizing Fast Ignition

High intensity KrF laser pulse interaction with solid targets

Eiichi Takahashi, Isao Matsushima, Hirotaka Nakamura[a], Susumu Kato, and Yoshiro Owadano

National Institute of Advanced Industrial Science and Technology (AIST), 1-1-1 Umezono, Tsukuba, Ibaraki 305-8568 Japan

a. Tokyo University of Science , Yamazaki, Noda, Chiba, Japan

Motivation

UV laser is believe to be suitable for Fast ignitor driver, because

1) $I\lambda^2$ scaling of 0.25μm lasers to 10^{20} W/cm^2 yields hot electron temperatures of 1MeV.

2) Cut-off density of 0.25μm lasers is much closer to the compressed core than that of 1.06μm lasers.

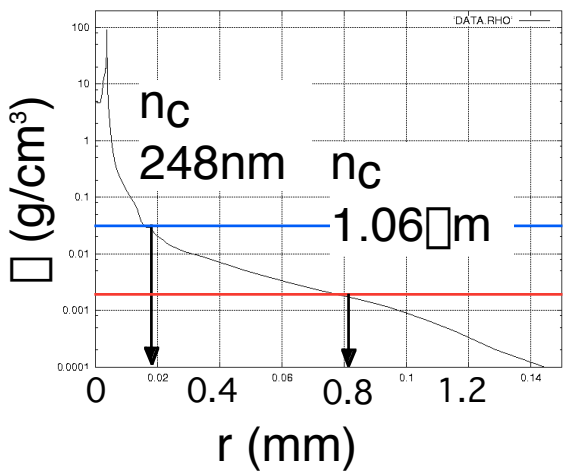

Motivation

However very few experimental results has been reported so far. Most intense KrF laser (λ=248nm) interaction experiment was reported by U. Teubner up to 10^{18}W/cm^2.

So, more experimental validations are necessary.

U. Teubner, et. al., "Absorption and hot electron production by high intensity femtosecond uv-laser pulses in solid targets",Phys. Rev. E, Vol.54, No.4, 1996, p. 4167.

Research Aim

At KrF (λ =248nm) wavelength,

1) The achievement of high focused intensity (a ~ 1, i.e. 10^{19}W/cm^2) for relativistic laser plasma interaction study.

2) The validation of $I\lambda^2$ scaling for hot electron temperature.

3) The study of hot electron propagation physics.

Because if J = nev $\sim$ $n_c$ec, very large electron current density is expected, $\sim$ 8x10^{13}A/cm^2.

"ASHURA" KrF Laser System

Characteristic Features,

1) Full vacuum laser beam propagation duct system (L ~ 100m)

2) No refractive optics

-> Lower the accumulation of B-integral (for direct short pulse amplification)

3) Special Short pulse oscillator (using stimulated scattering)

-> Lower the prepulse intensity

This system is only intense 4ω irradiation facility in the world.

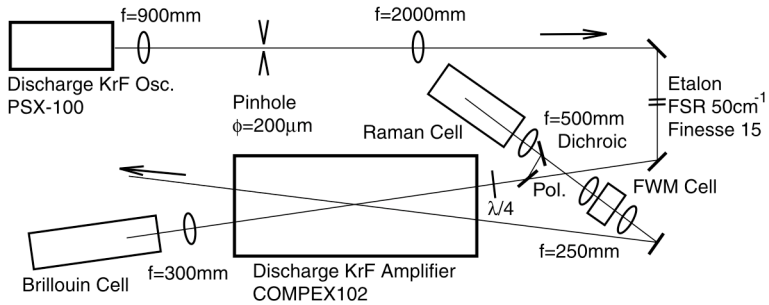

Short KrF laser pulse

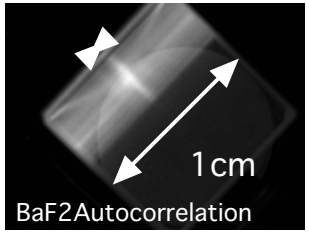

Amplified short pulse
Pulse width <1ps
Energy 2.2J
(ASE 250mJ, Total 2.45J)

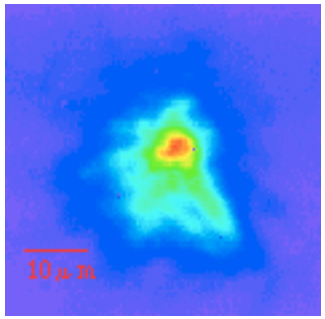

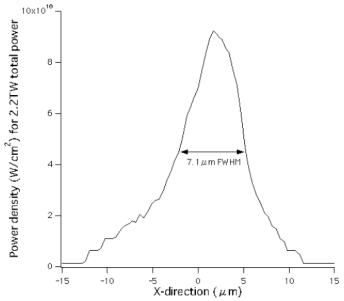

Focal spot diameter ~7um (50% of energy)

-> **$3x10^{18}W/cm^2$ has been achieved.**

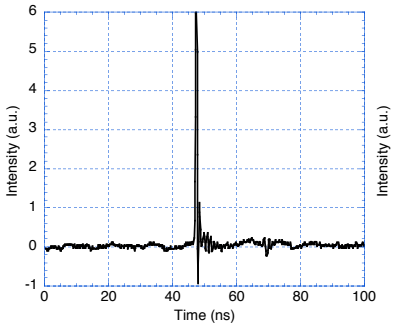

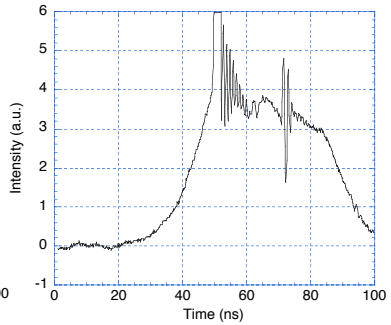

Prepulse / Main pulse focused intensity ratio
= 10^-10
$4x10^8W/cm^2$

Experimental Setup

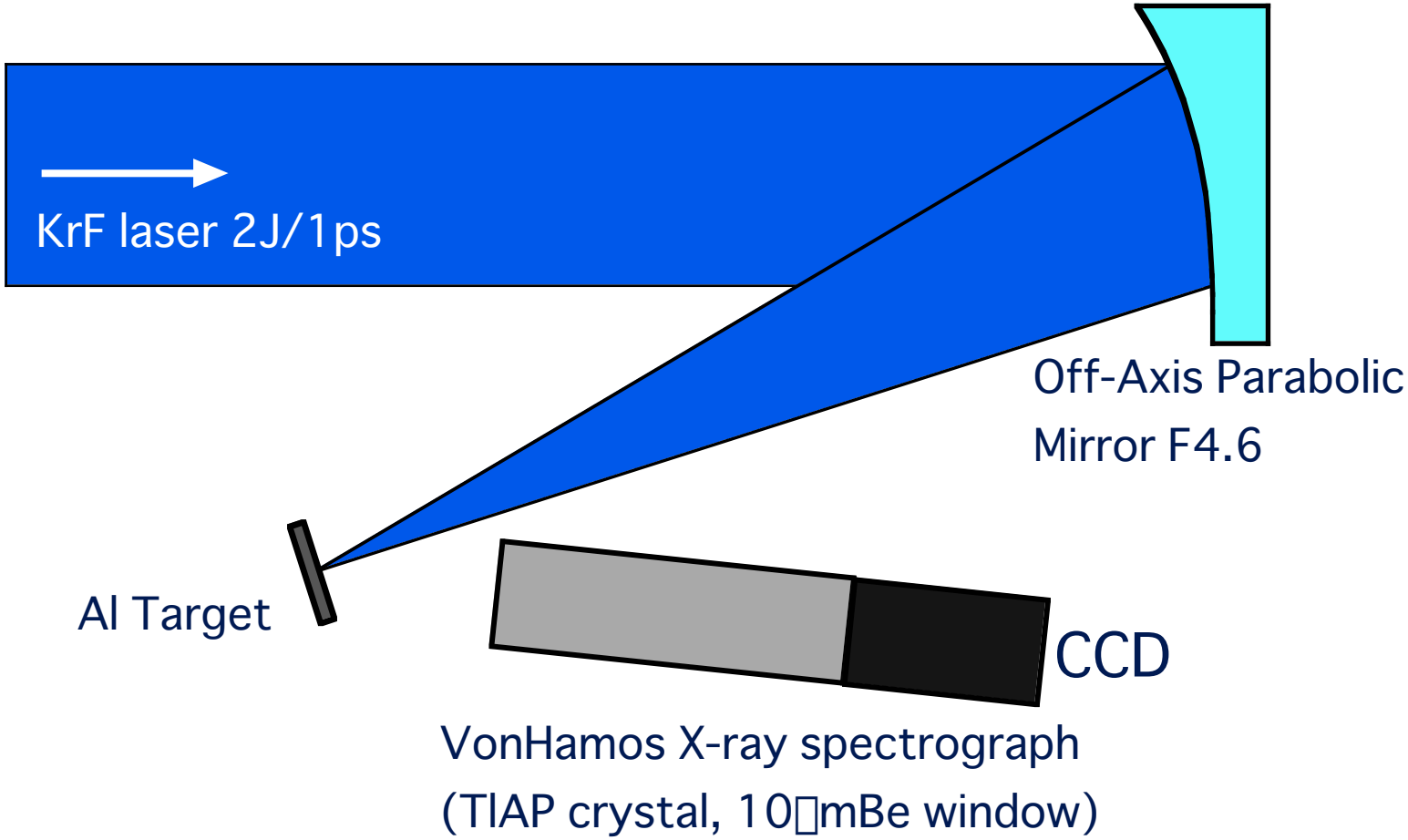

X-ray Spectra

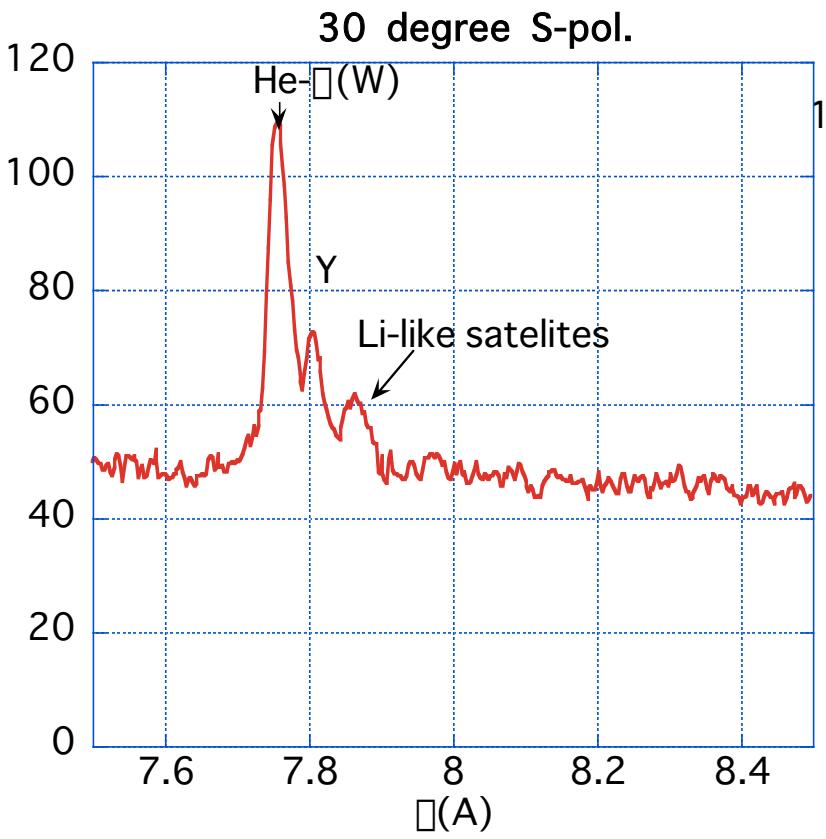

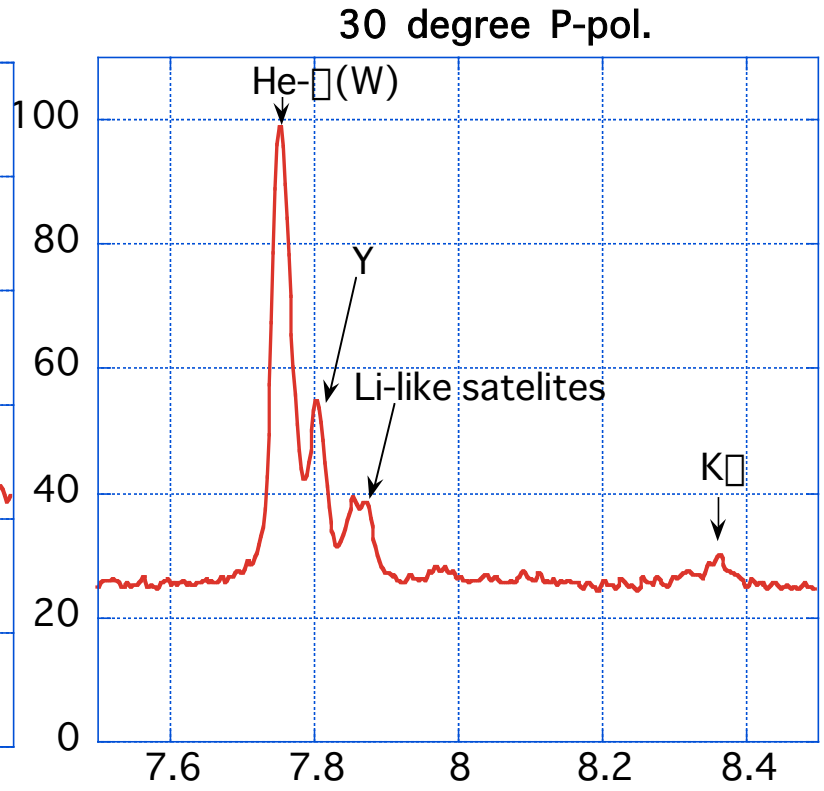

X-ray Spectra

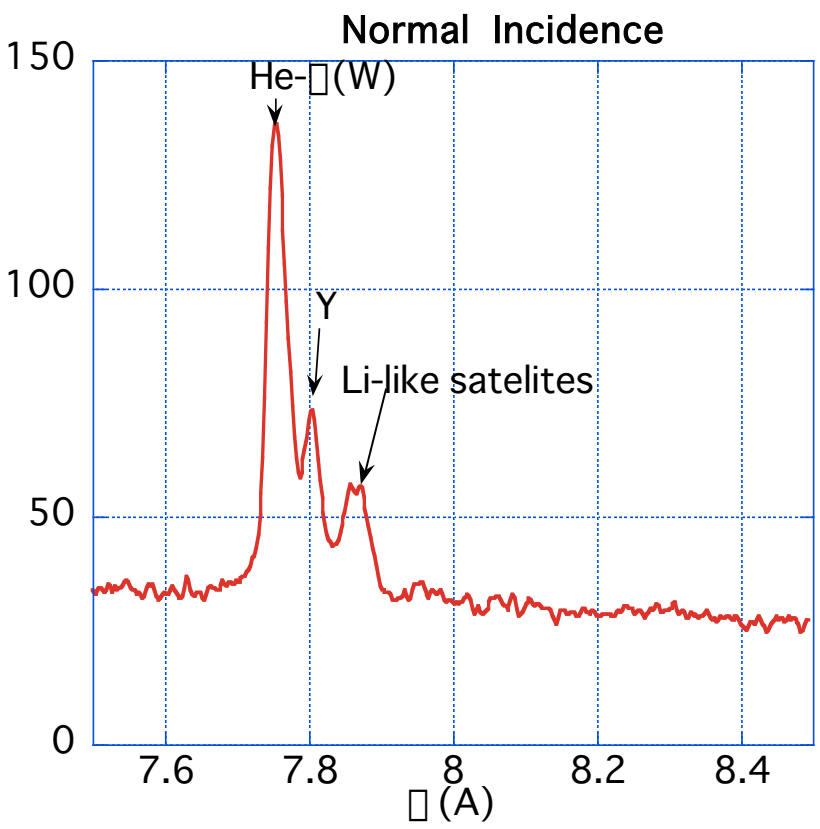

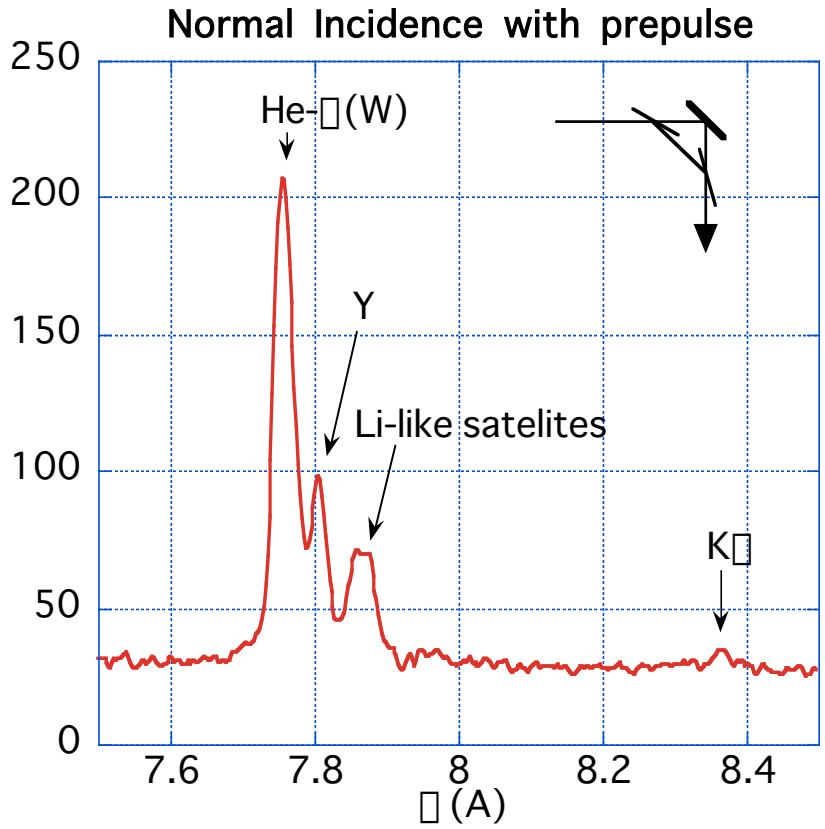

Hot electron generation

K□ emission has been observed for P-pol. (□=30) and normal incidence with prepulse.

These indicate that the hot electrons are generated by the intense KrF laser pulse irradiation.

Boosted 1-D Particle in Cell Simulation

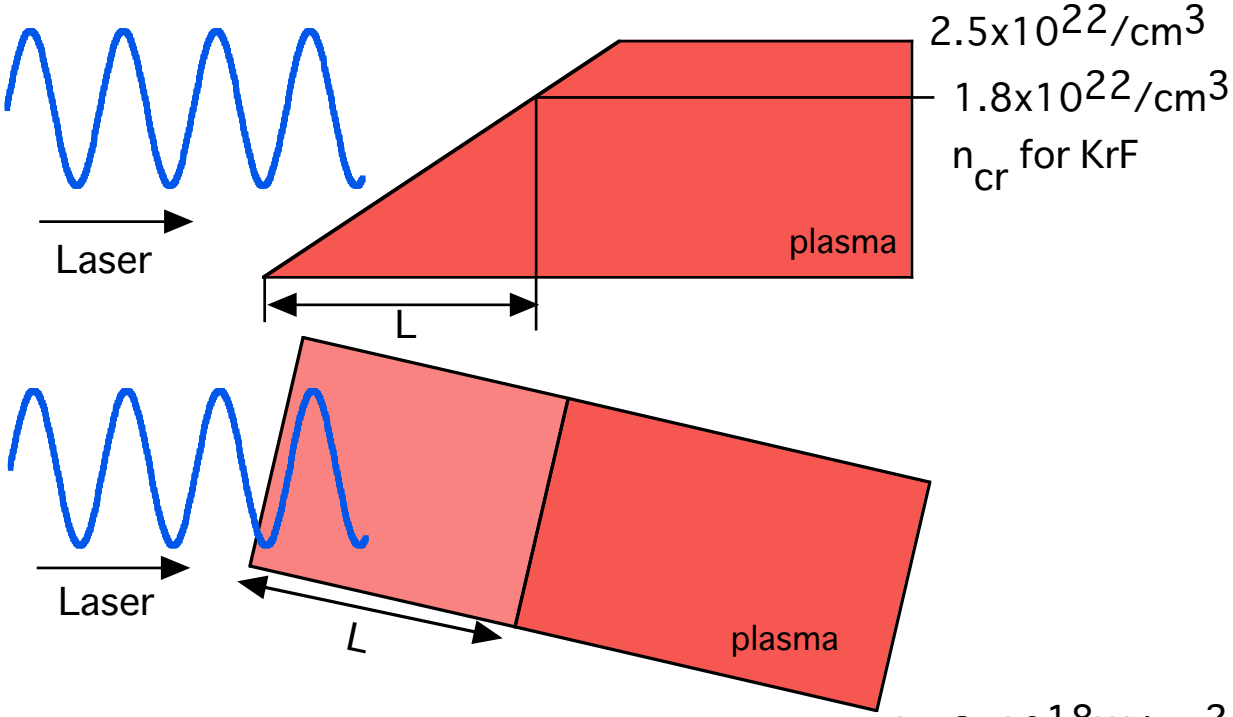

$I = 3\times10^{18} W/cm^2$

$\lambda = 248nm$

Initial Te = 300eV

Moving Ions

Laser riseup time: 10 fs and Constant

Laser Incident angle: Normal and 30°

Electron Distribution Function

Normal Incidence 3x10^18W/cm2 Te = 300eV t = 50fs

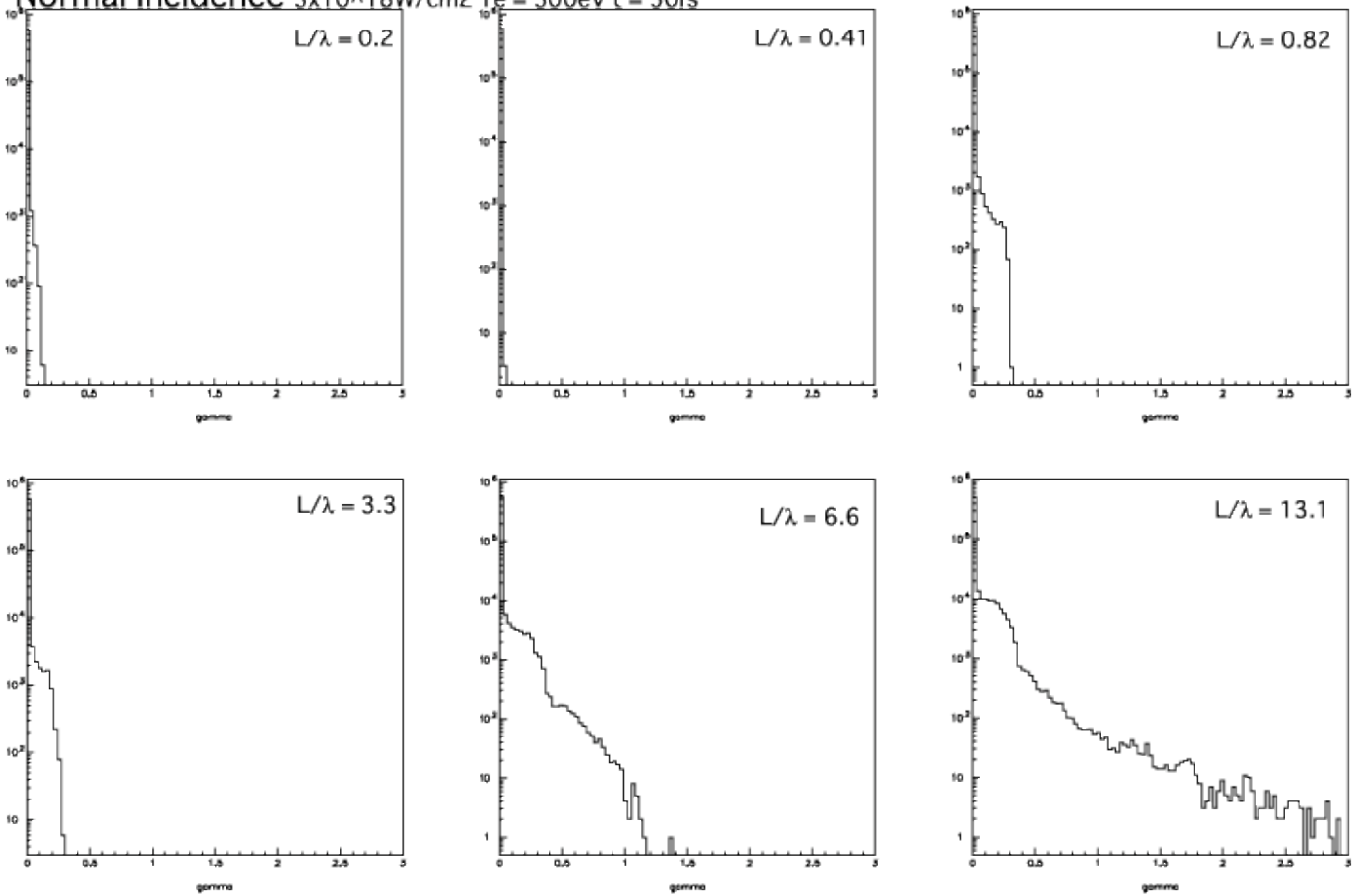

Normal incidence

L/ λ = 0.2

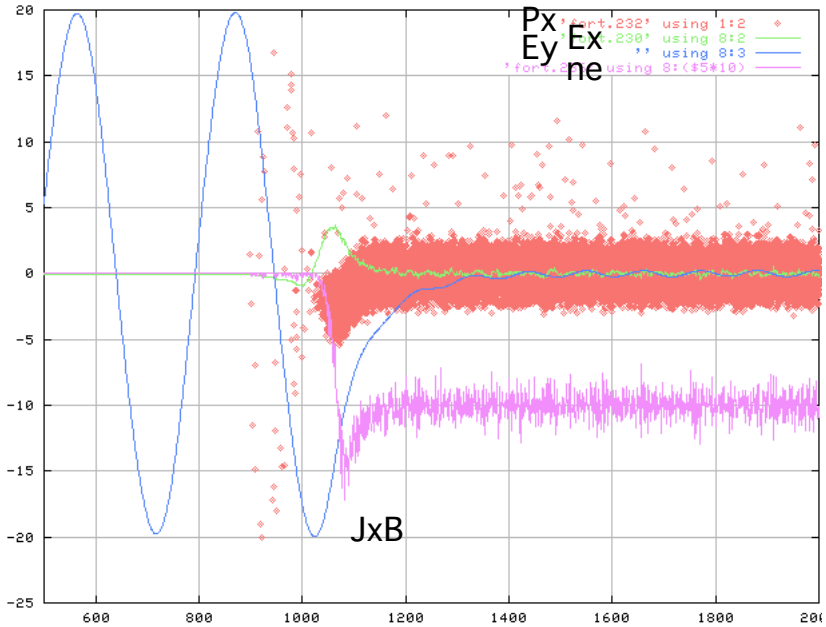

L/ λ = 13.1

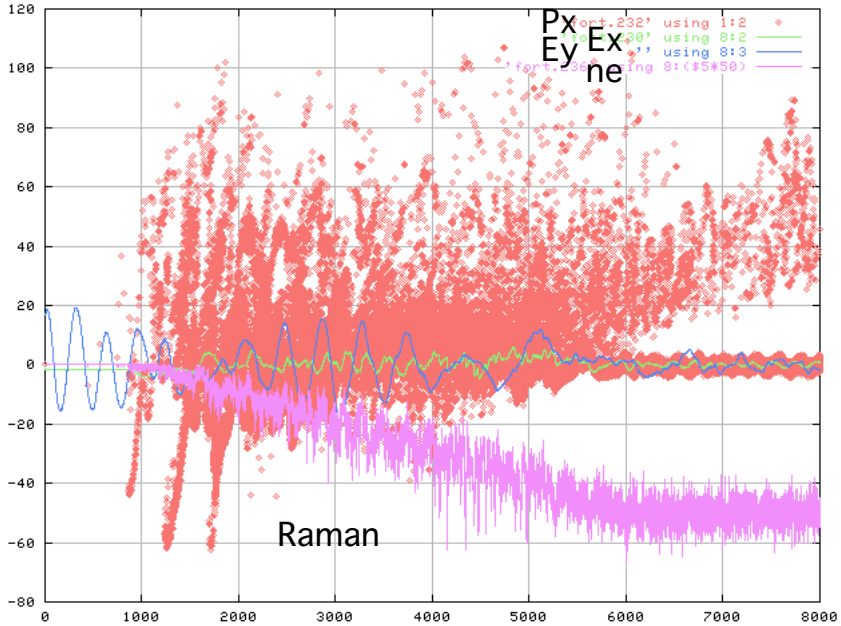

L/ λ = 0.41

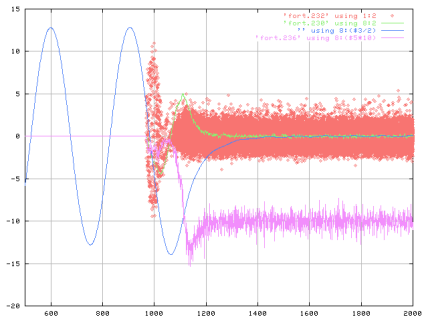

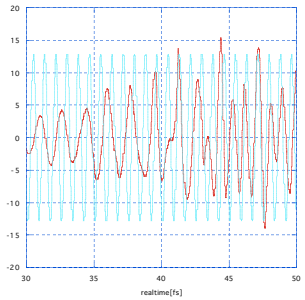

Electron Distribution Function

Oblique Incidence 30° 3x10^18W/cm2 Te = 300eV t = 50fs

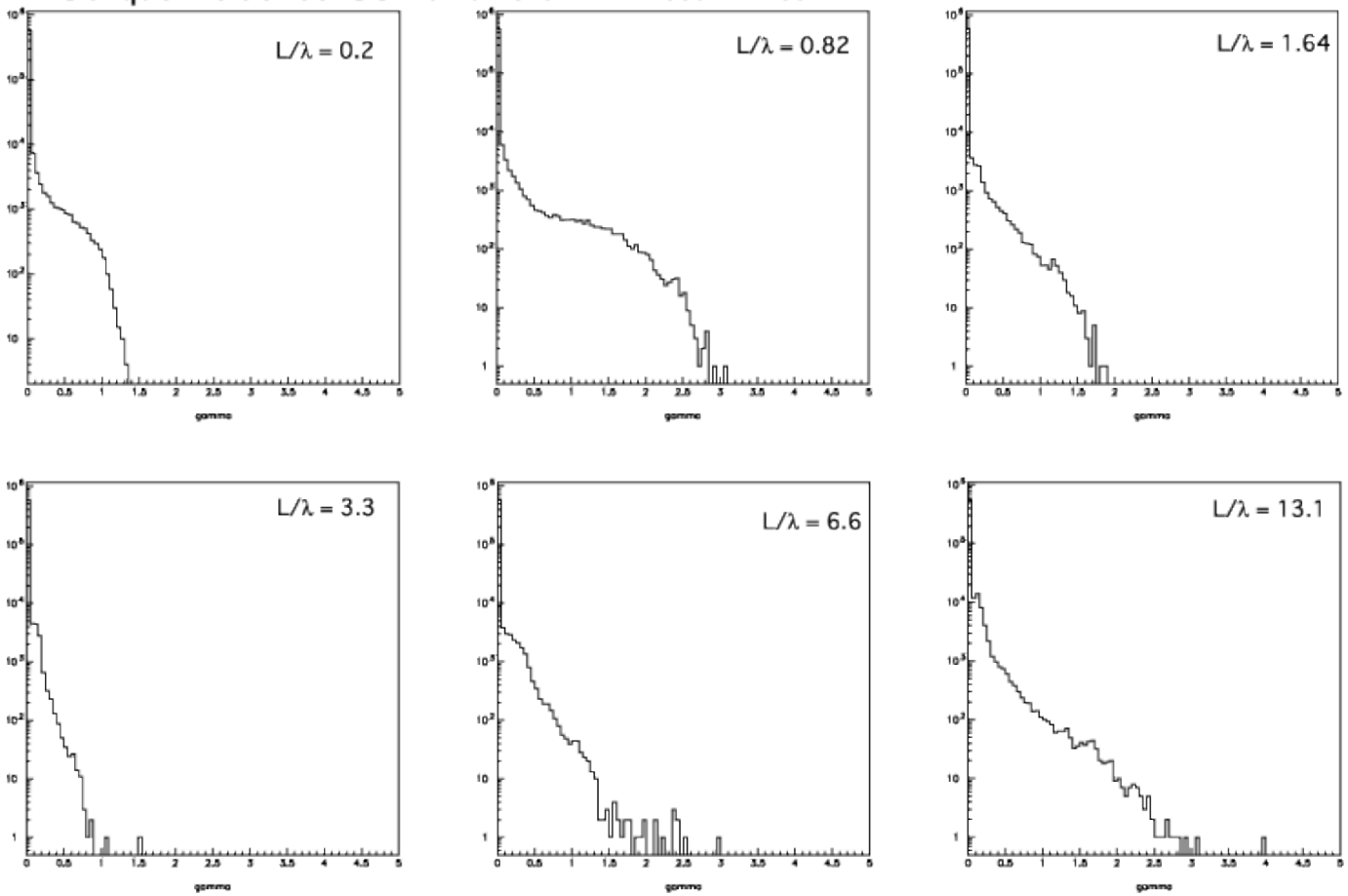

Obleque incidence 30°

L/ λ = 0.82

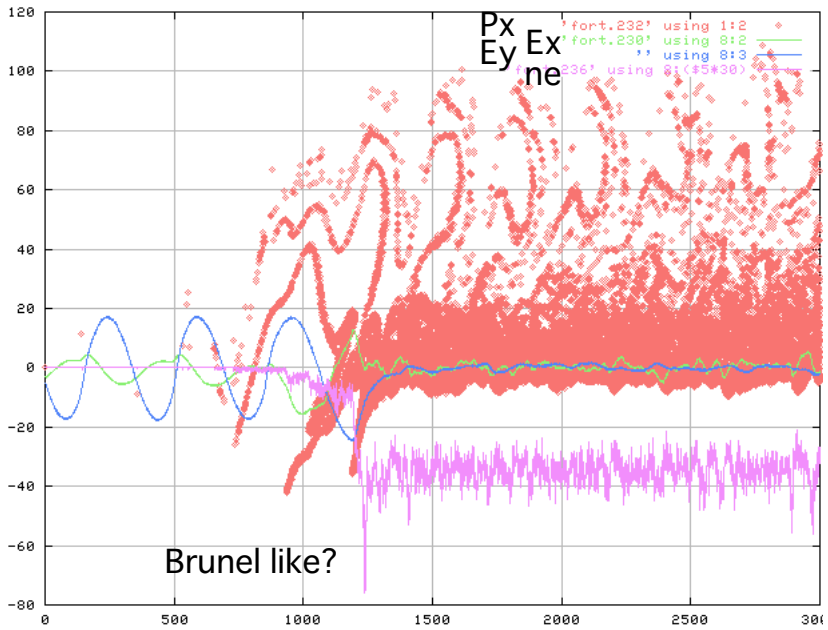

L/ λ = 13.1

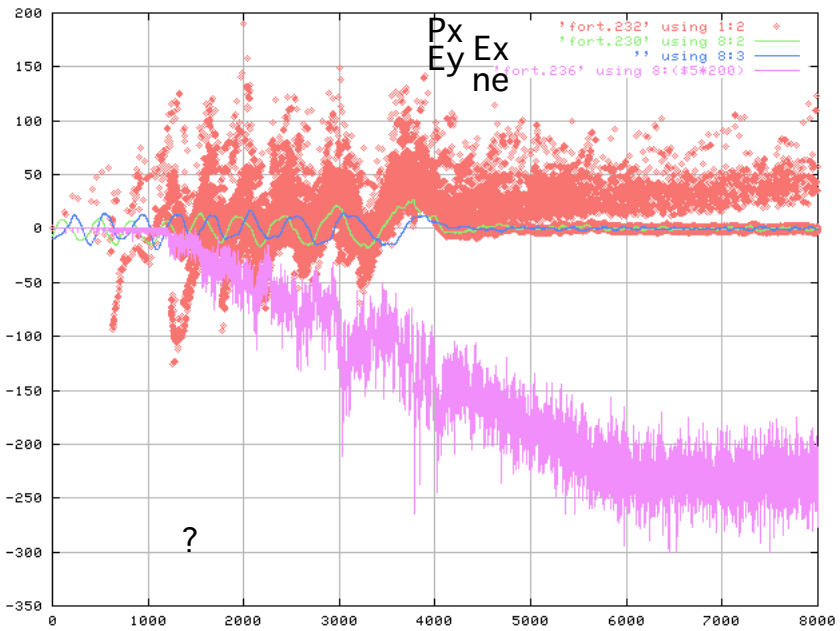

Summary

1. The intense KrF laser irradiation of $3 \times 10^{18} W/cm^2$ has been achieved by the newly installed vacuum beam propagation duct system.
2. Hot electrons were generated by intense KrF laser pulse irradiation.
3. PIC simulations suggested that the origin of these electrons could be Brunel like heating for oblique incidence and Raman scattering for normal incidence.

We will achieve focused intensity of $10^{19} W/cm^2$ by the improvement of focal spot size.
The hot electron temperature will be examined.

Calculations of Electron Transport in Fast Ignition Targets

Presentation to

6th Workshop on
Fast Ignition of Fusion Targets
St. Petes Beach, FL
November 16-19, 2002

R. P. J. Town, W. L. Kruer, A. B. Langdon, B. F. Lasinski, and M. Tabak
Lawrence Livermore National Laboratory
D. R. Welch
Mission Research Corp.

This work was performed under the auspices of the U.S. Department of Energy by the University of California, Lawrence Livermore National Laboratory under contract No. W-7405-Eng-48.

Summary

The LSP code has been used to study fast ignition relevant transport experiments

- A critical issue for Fast Ignition is understanding the transport of the ignitor electrons to the fuel.
- Experiments have shown a rapid increase in beam width followed by reasonable collimation.
- The LSP code has been used to study the effect on beam transport of:
  - a buried “fluor” layer;
  - a “halo” around the central high intensity laser spot;
  - a low resistivity channel; and
  - the initial beam divergence.

A critical issue for fast ignition is understanding the transport of the ignitor electrons to the fuel

Laser couples efficiently to the core

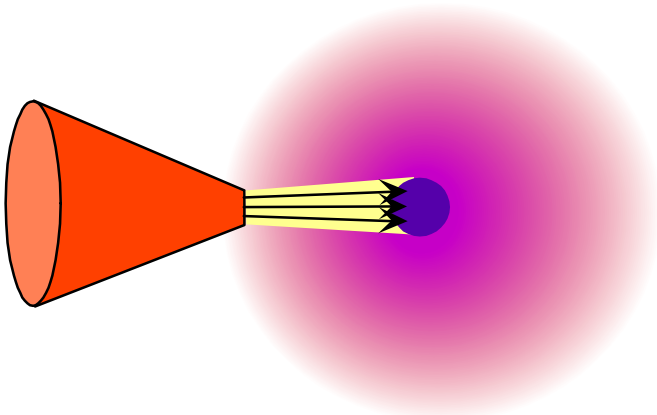

Laser couples inefficiently to the core

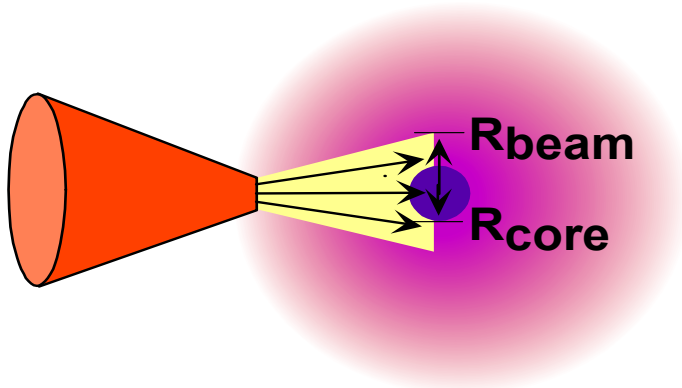

$$E_{laser} \approx E_{min}\left(\frac{R_{beam}}{R_{core}}\right)^2 \text{ for } R_{beam} \geq R_{core}$$

Experiments on MeV electron transport have been performed by researchers around the world

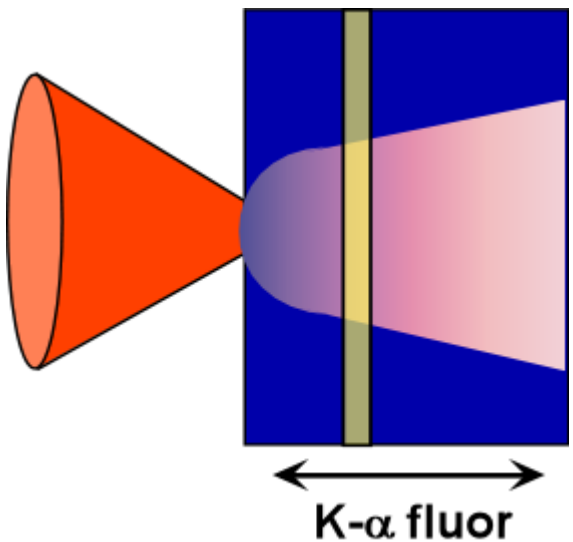

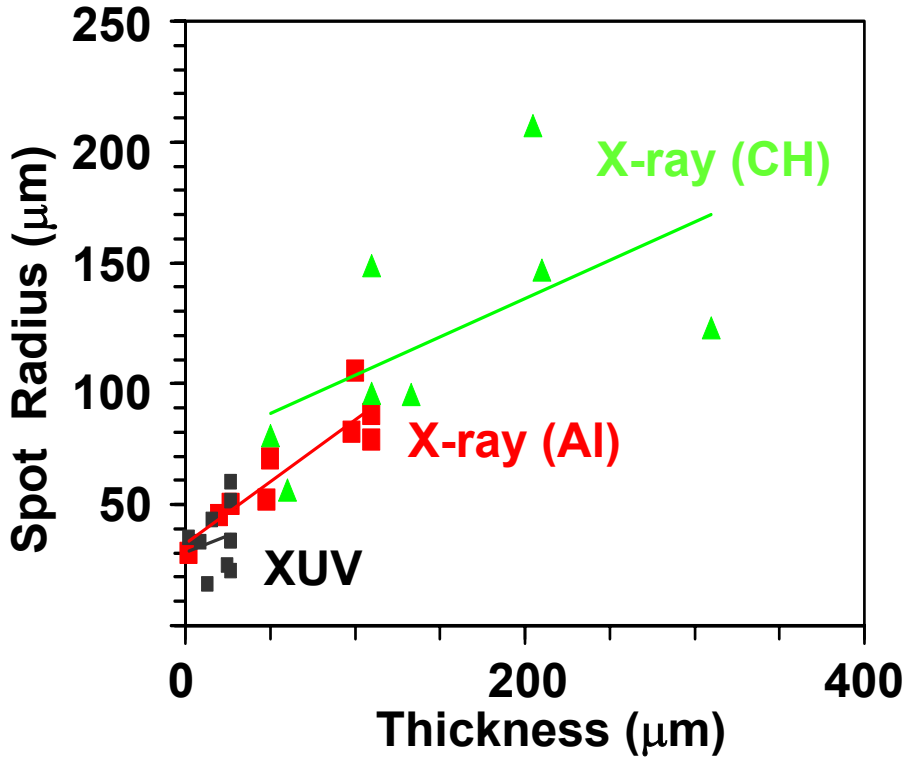

- Experimental data[1] show:
  - a rapid increase in beam size in the first few microns; and
  - a fairly collimated (20º half angle) beam in the bulk of the material.

[1]M. H. Key, et al, 5th Workshop on Fast Ignition of Fusion Targets (2001).

LSP[1] is a hybrid particle code used extensively in the ion beam community

- Performed simulations using:
  - 2-D in cylindrical geometry; and
  - 3-D in cartesian geometry.
- Employs a “direct implicit” energy conserving electromagnetic algorithm.
- Hybrid fluid-kinetic descriptions for electrons with dynamic reallocation.
- Scattering between the beam and background plasma included.
  - Ionization and excitation ignored.
- Beam created by two methods:
  - Injection at target boundary;
  - Promotion from the background plasma.

[1]D. R. Welch, et al, Nucl. Inst. Meth. Phys. Res. A 242, 134 (2001).

LSP captures the important features of electron transport

- The beam particles penetrates into the plasma generating an electric field.

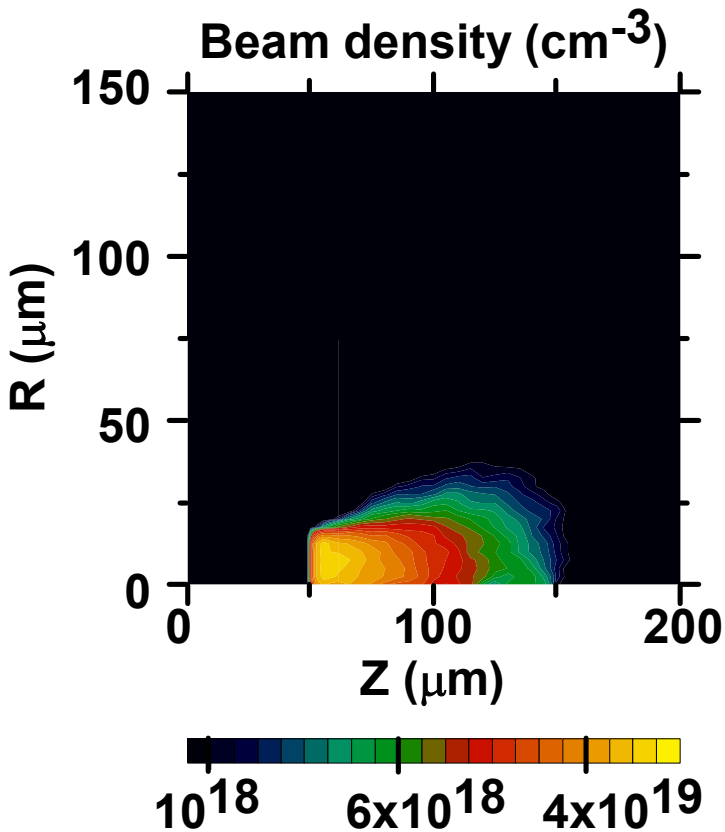

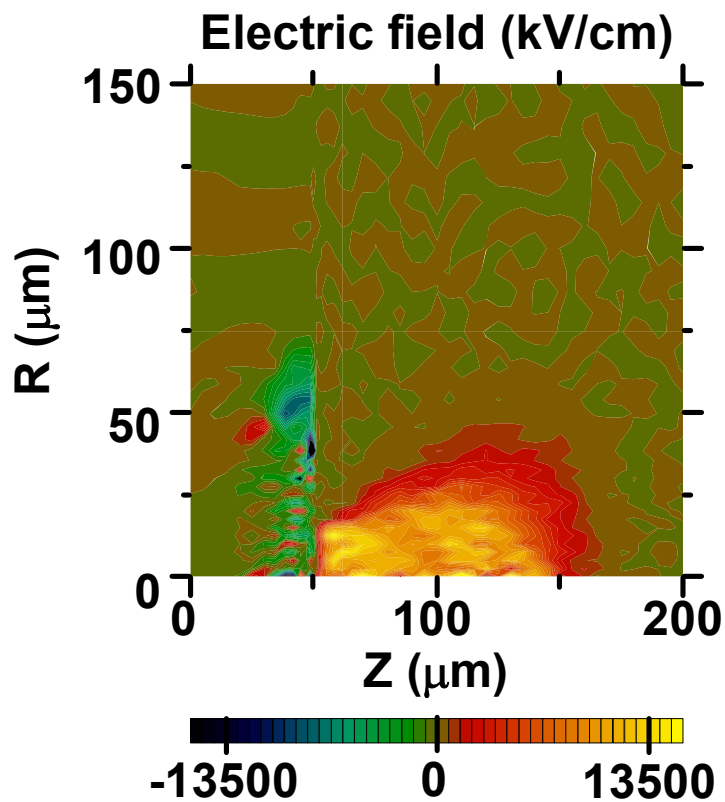

A magnetic field is generated because the electric field is not curl free

- The magnetic field collimates the beam.
- The electric field draws a return current from the background electrons (which may runaway[1].)

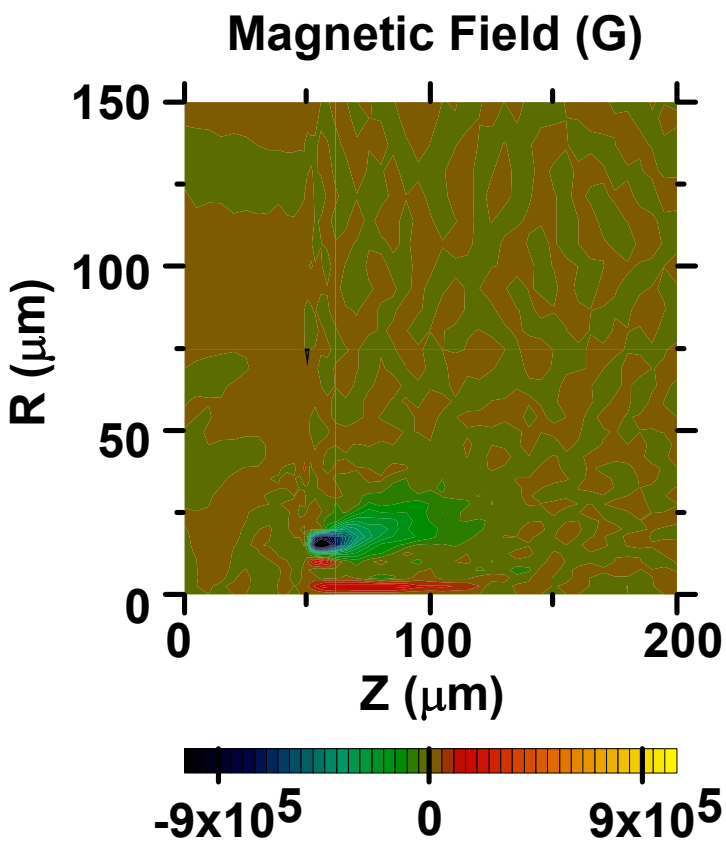

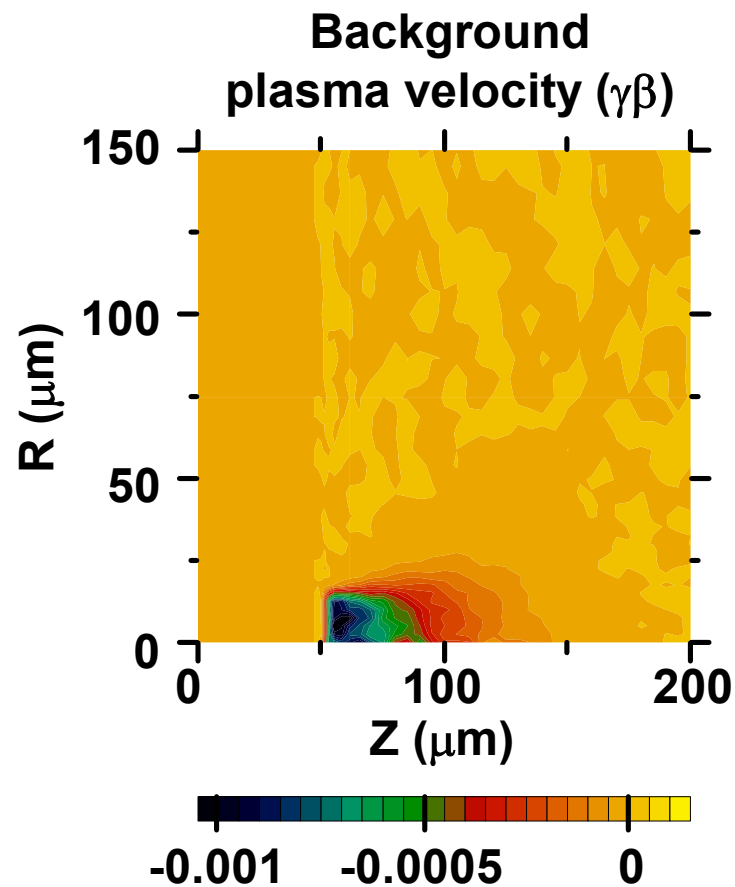

[1]M. Tabak, et al, CP1.113.

When the beam reaches the back a large electric field is generated

- This electric field:
  - accelerates protons out of the back surface[1]; and
  - reflects the beam back into the target.

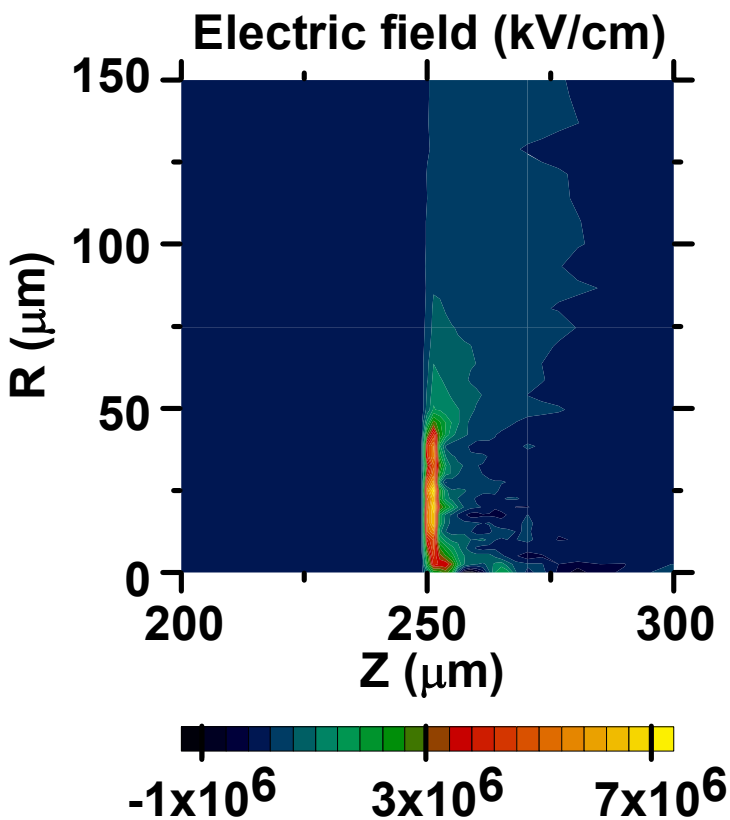

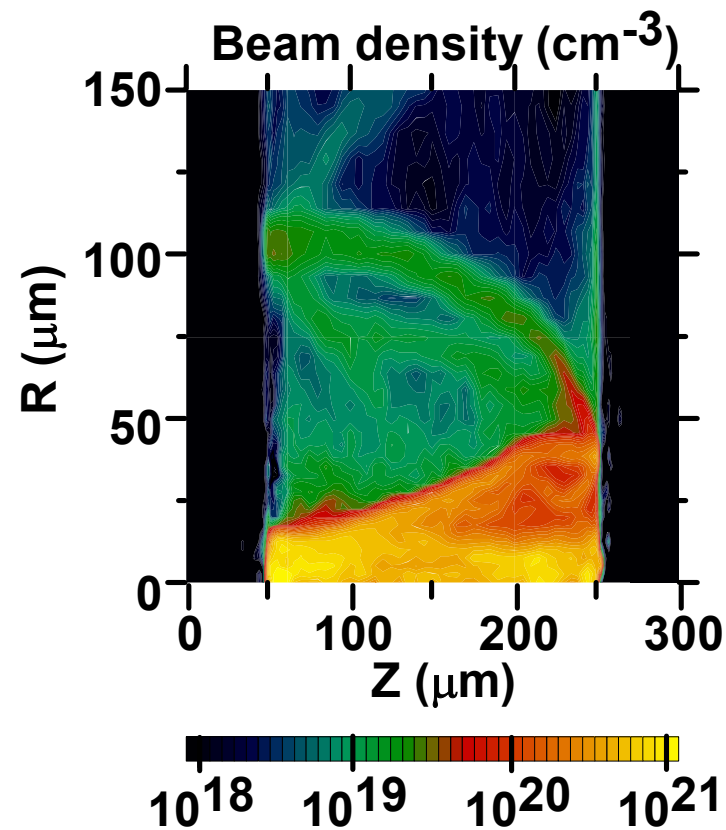

[1]B. Lasinski et al, CP1.112.

LSP was used to investigate the effect of a buried "fluor" in the target on electron transport

- An electron beam, with a 1-MeV drift velocity and a 300keV temperature, was injected into a solid density CH plasma at 5eV.
- Two layers to simulate the corona and the fluor with various conductivities (achieved by varying the temperature) were placed in the target.

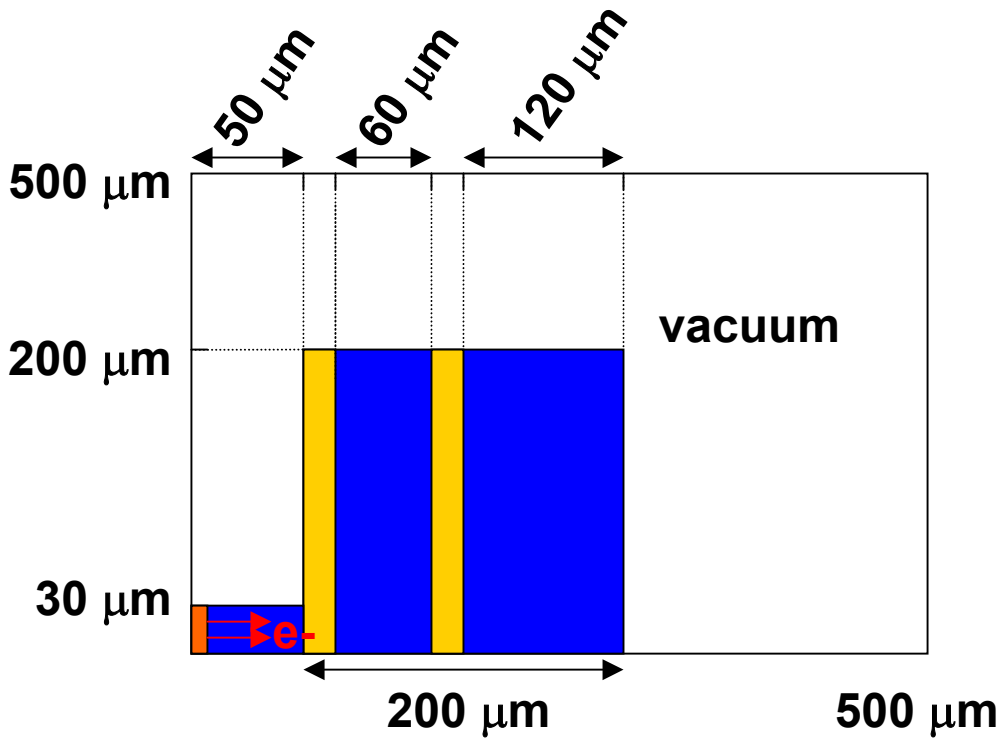

The presence of a high conductivity layer has a marginal effect on the beam

- Compared to the nominal low conductivity case the presence of a high conductivity region leads to:
  - a less filamented beam; and
  - no significant increase in beam width.

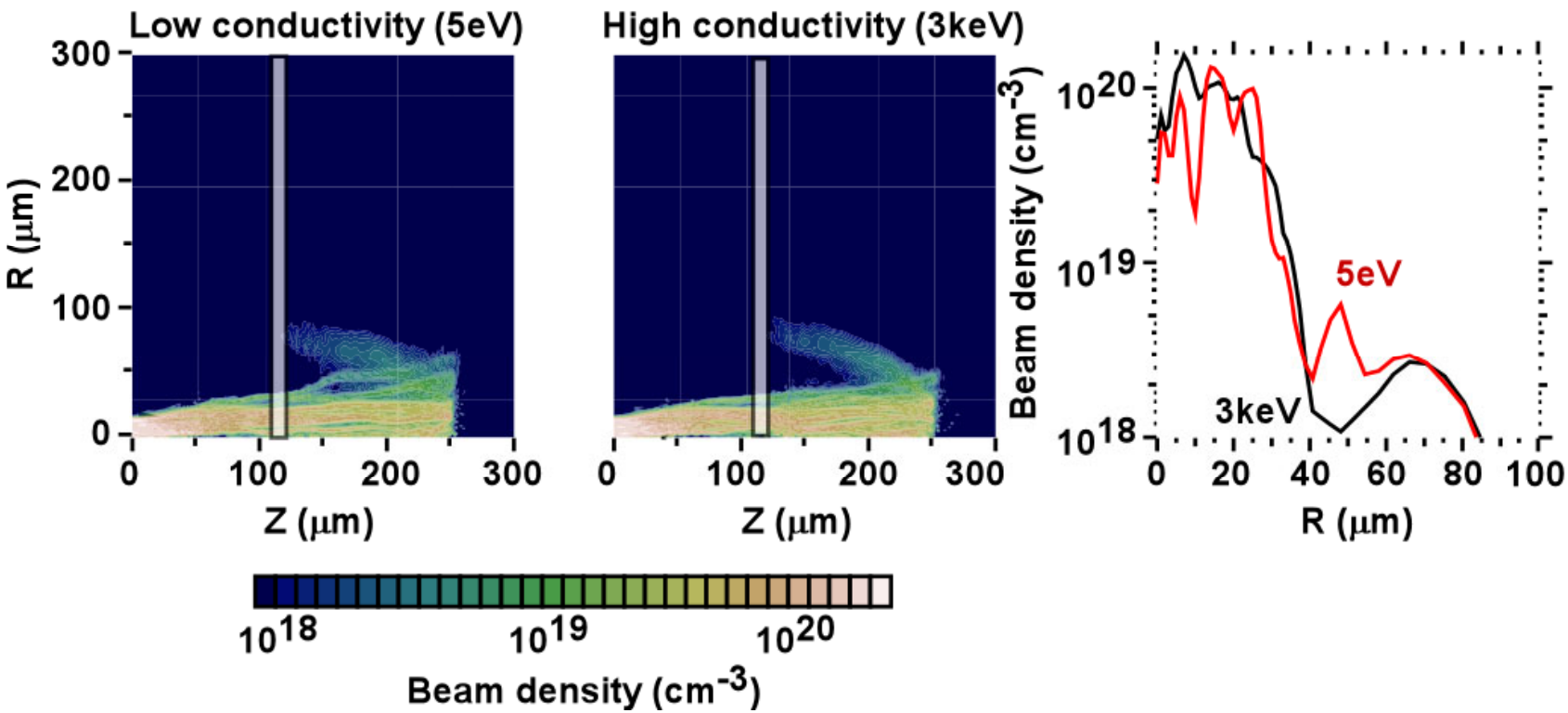

A significant "halo" surrounds the short-pulse high intensity spot

- Data from the Nova Petawatt showed:
  - 30-40% of the energy contained within a central 9 μm central spot.
  - Approximately 10^{-4} energy contained within a prepulse which existed for approximately 2-ns before the main pulse

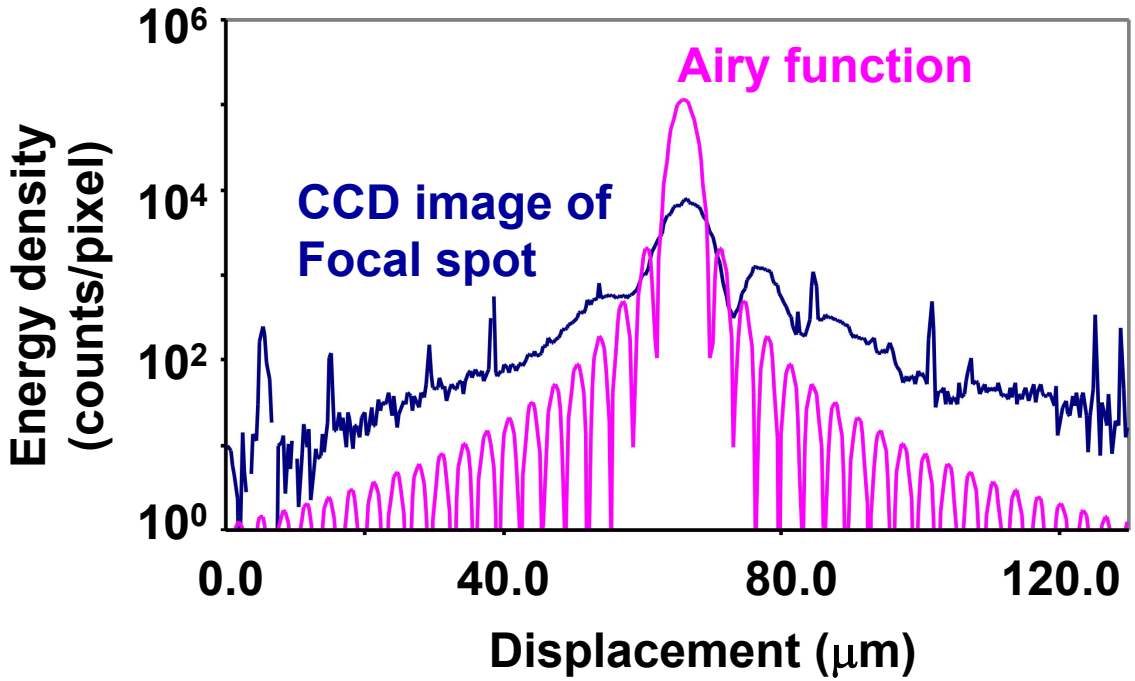

A “halo” appears to cause the beam to spread more

- A 100 μm fwhm Gaussian “halo” surrounds the 10 μm original beam.
- The particles in the “halo” may also contribute to the K-α signature.

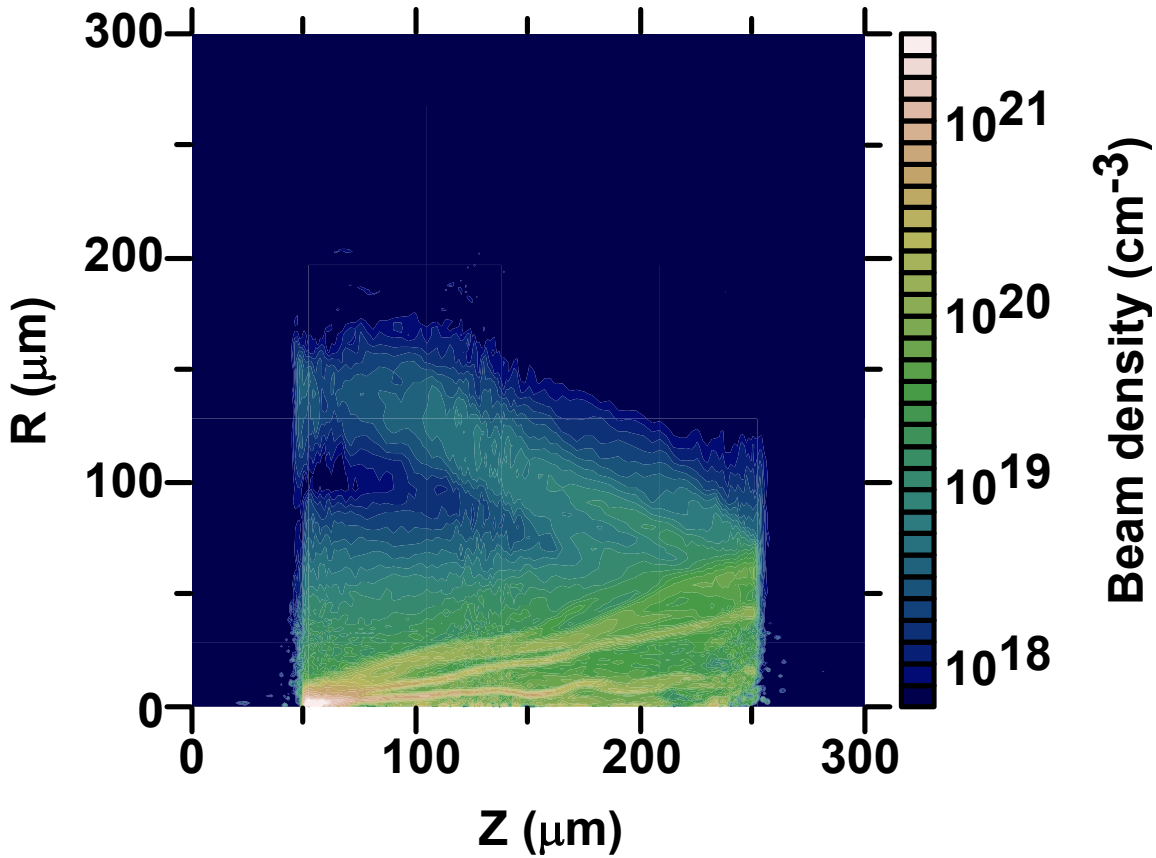

The presence of a high conductivity channel may help confine the electron beam

- The hot channel seems to help to constrict the electron beam, but there is still a significant "halo" surrounding the beam.
- The cold plasma case shows filamentation and *less* spreading than the hot channel case.

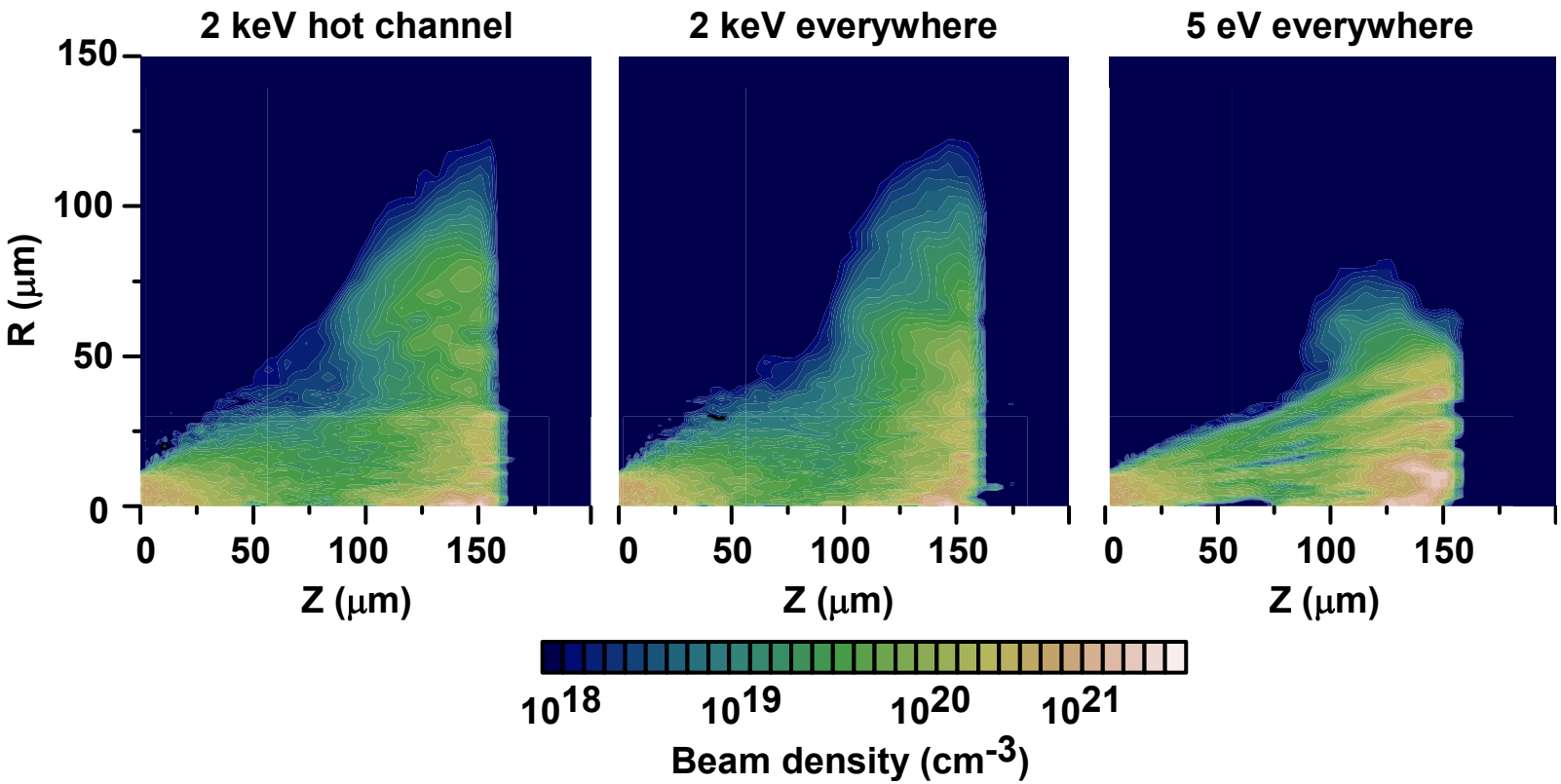

Increasing the thermal spread increases the beam divergence

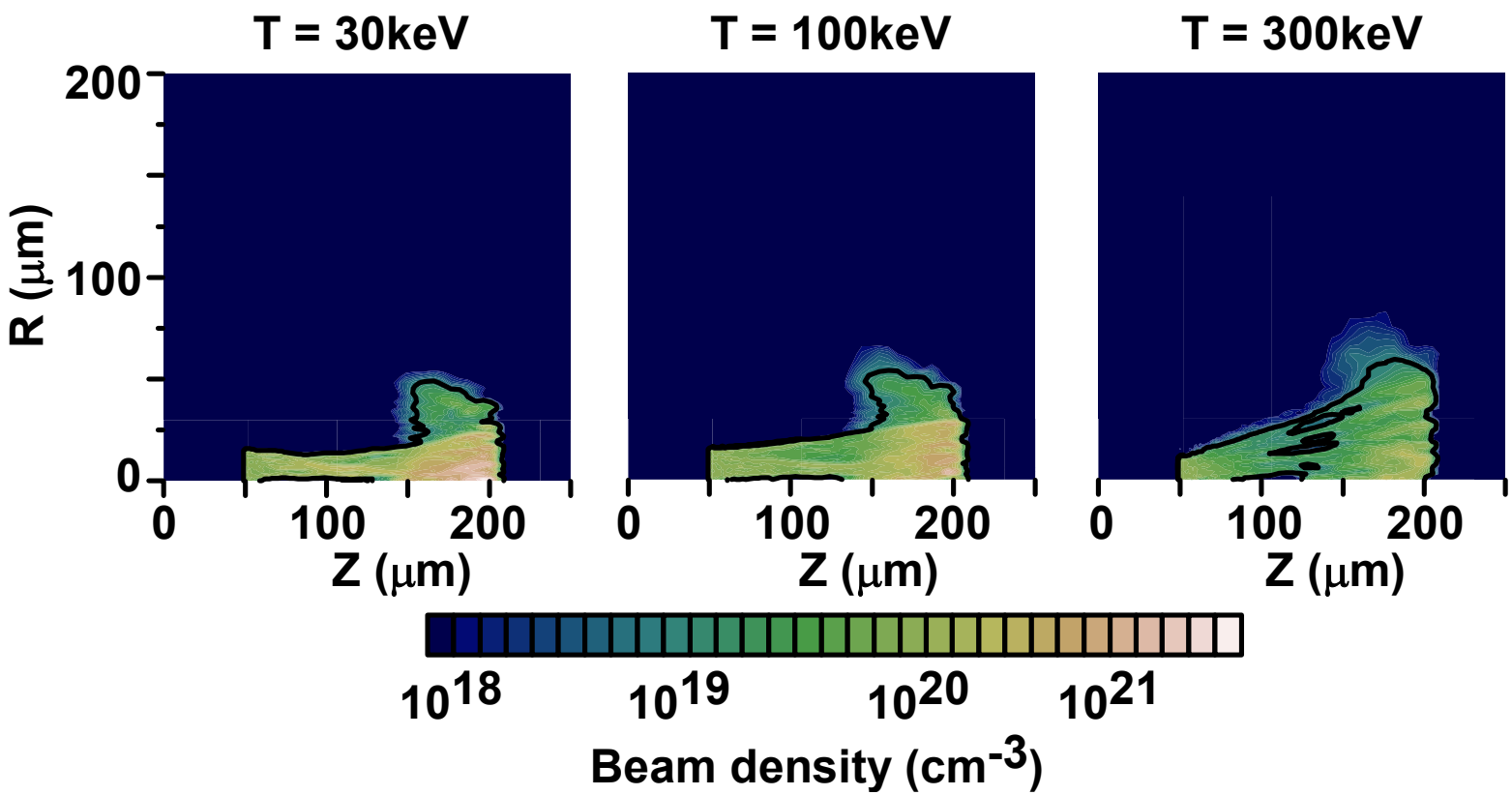

Beam dispersion is sensitive to the initial thermal spread of the beam

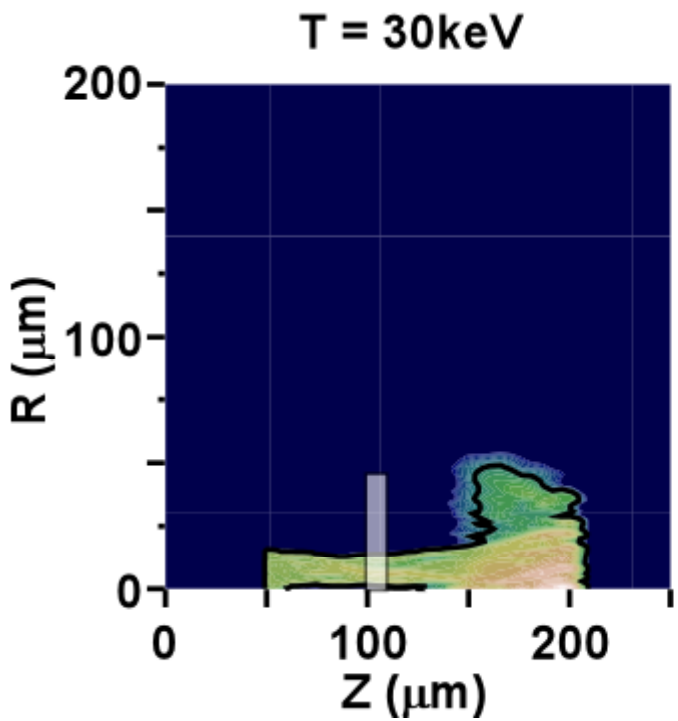

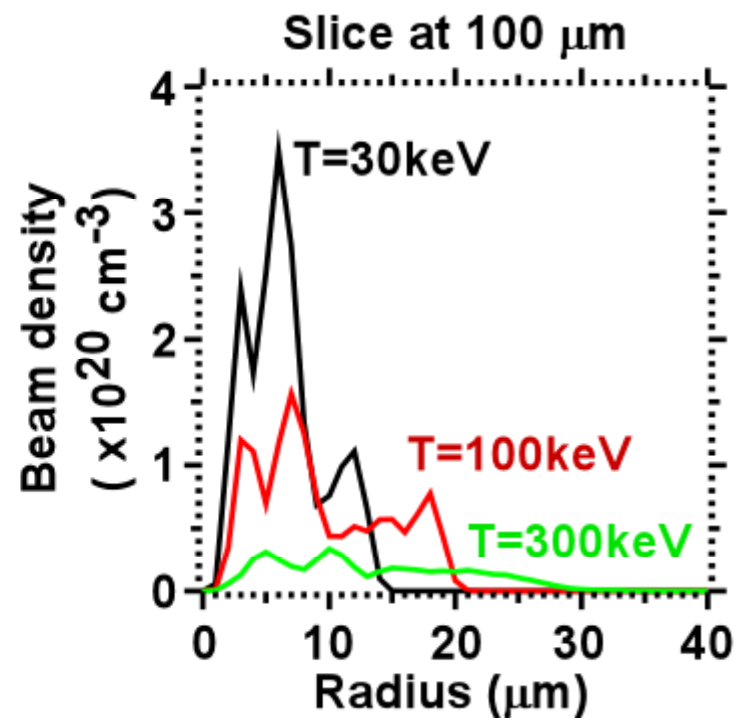

3-D simulations allow the beam to be injected at an angle

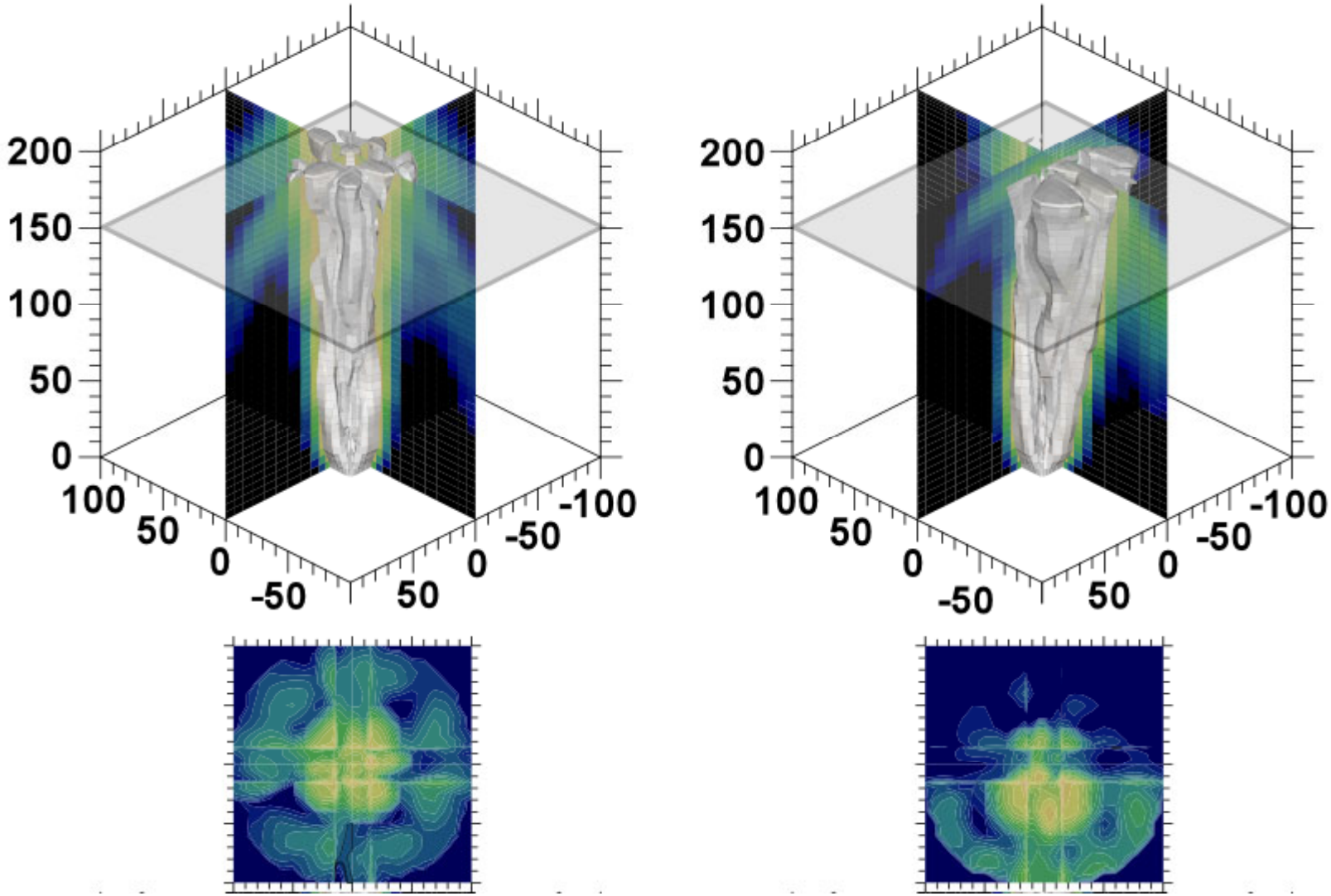

The LSP code has been used to study fast ignition relevant transport experiments

- A critical issue for Fast Ignition is understanding the transport of the ignitor electrons to the fuel.
- Experiments have shown a rapid increase in beam width followed by reasonable collimation.
- The LSP code has been used to study the effect on beam transport of:
  - a buried “fluor” layer;
  - a “halo” around the central high intensity laser spot;
  - a low resistivity channel; and
  - the initial beam divergence.
- Future work will involve adding:
  - real EOS;
  - real resistivity model ; and
  - K-α diagnostic.

Calculations of Electron Transport in Fast Ignition Targets.

R. P. J. Town, W. L. Kruer, A. B. Langdon, B. F. Lasinski, and M. Tabak
Lawrence Livermore National Laboratory
D. R. Welch
Mission Research Corp.

A crucial issue for the viability of the fast ignition approach [1] to inertial fusion energy is the transport of the ignition pulse energy from the critical surface to the high-density compressed fuel. For example, the ignition beam energy depends on the cross section area of the electron beam. Experiments of the interaction of short-pulse high intensity lasers with surrogate solid-density thin targets with buried K-α diagnostic layers have shown a fairly well collimated beam although with a larger radius than the laser beam spot [2]. We report on LSP calculations of these experiments. These calculations include the effects of non-normal electron beam injection, an effect previously not included in simulations. The LSP code [3] uses a direct implicit particle-in-cell algorithm in 3 dimensions to solve for the beam particles. The background particles are treated as a fluid. The implications for fast ignition will be discussed. This work was performed under the auspices of the U.S. Department of Energy by the University of California, Lawrence Livermore National Laboratory under contract W-7405-ENG-48.

[1] M. Tabak, et al, Phys. Plasmas 1, 1626 (1994).
[2] J. A. Koch, et al, Phys. Rev. E 65, 016410-1 (2001).
[3] D. R. Welch, D. V. Rose, B. V. Oliver, and R. E. Clark, Nucl. Inst. Meth. Phys. Res. A 242, 134 (2001).

Full Set of Equations for Relativistic Weibel and Tearing instal

We start from the following simplified set of equations describing both We
instabilities:

$$\dot{n}_b + \nabla \cdot (n_b \vec{v}_{b\perp}) = 0,$$

$$\frac{d}{dt}(\gamma_b \vec{v}_{b\perp}) = -\frac{e v_{bz0}}{mc}\nabla\psi + \frac{e^2}{2m^2c^2}(1 - \frac{1}{\gamma_b^3})\nabla\psi^2 - \frac{\partial}{\partial t}(\frac{n_b}{n_e}\vec{v}_{b\perp}) +$$
$$+\frac{\partial}{\partial t}\left(\frac{c}{4\pi e n_e}[\vec{e}_z \times \nabla B_z]\right) + \frac{eB_z}{mc}[\vec{e}_z \times \vec{v}_{b\perp}] + \nabla(\frac{v_{e\perp}^2}{2}),$$

$$\vec{v}_{e\perp} = -\frac{n_b}{n_e}\vec{v}_{b\perp} + \frac{c}{4\pi e n_e}[\vec{e}_z \times \vec{\nabla} B_z],$$

$$(\nabla^2 - k_{pe}^2 - k_{pb}^2\langle\frac{1}{\gamma_b^3}\rangle)\psi = \frac{4\pi e v_{bz0}}{c} n_b,$$

$$(\nabla^2 - \nabla \ln n_e \cdot \nabla - k_{pe}^2)B_z = \frac{4\pi e n_e}{c} e_z \cdot \nabla \times (\frac{n_b}{n_e}\vec{v}_{b\perp}),$$

$$\gamma_b v_{bz} = \gamma_{b0} v_{bz0} + \frac{e(\psi - \psi_0)}{mc}, \quad v_{bz} = v_{bz0} + \frac{e(\psi - \psi_0)}{mc\gamma_{b0}^3} + O(\psi -$$

Linearized Equations for Weibel and Tearing

$$\delta\dot{n}_b + \nabla\cdot(\delta n_b \vec{v}_{b\perp}) + \nabla\cdot(n_b \delta\vec{v}_{b\perp}) = 0,$$

$$\frac{\partial}{\partial t}(\gamma_b \delta\vec{v}_{b\perp}) = -\frac{e v_{bz0}}{mc}\nabla\delta\psi + \frac{e^2}{m^2c^2}(1-\frac{1}{\gamma_b^3})\nabla(\psi\delta\psi) - \frac{\partial}{\partial t}\left[(1+\frac{n_b^2}{n_e^2})\frac{\delta n_b}{n_b}\right.$$
$$-\frac{\partial}{\partial t}(\frac{n_b}{n_e}\delta\vec{v}_{b\perp}) + \frac{\partial}{\partial t}\left(\frac{c}{4\pi e n_e}[e_z\times\nabla B_z]\right) + \frac{eB_z}{mc}[\vec{e}_z\times\vec{v}_{b\perp}] + \nabla(\vec{v}_e$$

$$\delta\vec{v}_{e\perp} = -\frac{n_b}{n_e}\delta\vec{v}_{b\perp} - \frac{\delta n_b}{n_e}(1+\frac{n_b}{n_e})\vec{v}_{b\perp} + \frac{c}{4\pi e n_e}[\vec{e}_z\times\vec{\nabla}B_z],$$

$$(\nabla^2 - k_{pe}^2 - k_{pb}^2\langle\frac{1}{\gamma_b^3}\rangle)\delta\psi = k_{pb}^2\psi(1+\langle\frac{1}{\gamma_b^3}\rangle)\frac{\delta n_b}{n_b} + \frac{4\pi e v_{bz0}}{c}\delta n_b,$$

$$(\nabla^2 - \nabla\ln n_e\cdot\nabla - k_{pe}^2)B_z = \frac{4\pi e n_e}{c}e_z\cdot\vec{\nabla}\times\left(\frac{n_b}{n_e}\delta\vec{v}_{b\perp} + \frac{\delta n_b}{n_e}(1+\frac{n_b}{n_e})\vec{v}\right.$$
$$-\frac{4\pi e\delta n_b}{c}\vec{e}_z\cdot\vec{\nabla}\times(\frac{\vec{v}}{n}$$

We have already assumed that the non-perturbed (equilibrium) value of B
also suppose that the non-perturbed transverse velocities are zero as well. We
there is no z-dependence of non-perturbed quantities, and hence, due to con
$\dot{n}_e = \dot{n}_b = 0$.

Dimensionless set of equations describing linear stage of Weibe
ing instability

It is convenient (for both theoretical and numerical purposes) to rewrite th
dimensionless form. We introduce dimensionless quantities:

$$\tilde{x} = x/L, \quad \tilde{t} = \frac{c}{L}t, \quad \tilde{\psi} = \frac{e}{mc^2}\psi, \quad \tilde{B}_z = \frac{eL}{mc^2}B_z, \quad \tilde{k}^2 = (k_{pe}L)$$
$$\tilde{k}_0^2 = (k_{pe0}L)^2, \quad \tilde{n}_{e,b} = n_{e,b}/n_{e0}, \quad \chi = \frac{n}{n}$$

So, we rewrite linearized equations in dimensionless variables (omitting all

$$\frac{\partial}{\partial t}(\gamma_b \delta\vec{v}_{b\perp}) = -v_{bz0}\nabla\delta\psi + (1 - \frac{1}{\gamma_b^3})\nabla(\psi\delta\psi) - \frac{\partial}{\partial t}(\chi\delta\vec{v}_{b\perp}) + \frac{\partial}{\partial t}\left(\frac{1}{k^2}[e_z \times\right.$$

$$(\nabla^2 - k^2(1 + \chi\frac{1}{\gamma_b^3}))\delta\psi = k_0^2(\psi(1 + \frac{1}{\gamma_b^3}) + v_{b0})\delta n_b,$$

$$(\nabla^2 - \nabla \ln n_e \cdot \nabla - k^2)B_z = k^2 e_z \cdot \vec{\nabla} \times (\chi\delta\vec{v}_{b\perp}).$$

Now we consider the case of flat beam (infinite in y-direction and havin
x-direction), so that $\psi = \psi(x), n_b = n_b(x)$, and assume that linear perturba
$a(t, x, y)$ (which may represent any quantity in our problem) has the form a
hence,

$$(\gamma + \chi)i\omega\delta\vec{v}_{b\perp} = -v_{b0}\nabla\delta\psi + (1 - \gamma^{-3})\nabla(\psi\delta\psi) + \frac{i\omega}{k_0^2 n_e}(e_z \times \nabla$$

Final equation for eigenmodes of relativistic Weibel instability

In the case $B_z = 0$ we arrive with this huge equation for $\delta\psi$:

$$\delta\psi''\Big[\frac{-\omega^2}{k_0^2}(\gamma+\chi) - n_b(v_{b0} + \psi(1+\gamma^{-3}))(v_{b0} - \psi$$

$$+\delta\psi'\Big[2n_b(1-\gamma^{-3})\psi' - n_b'\frac{\gamma-\chi^2}{\gamma+\chi}(v_{b0} - \psi(1-\gamma^{-3}))\Big](v_{b0} + \psi$$

$$+\delta\psi\Big[-\frac{-\omega^2}{k_0^2}(\gamma+\chi)(k_y^2 + k_0^2 n_e(1+\chi\gamma^{-3})) + (v_{b0} + \psi(1+\gamma^{-3}))\Big(n_b k_y^2(v_{b0} - \psi$$

$$+n_b(1-\gamma^{-3})\psi'' + n_b'(1 -$$

which can be simplified in many regimes to much more simpler forms.

The equilibrium value (which serves as initial condition for our task) $\psi($ equation

$$\psi'' - k_0^2 n_e(x)(1+\chi(x)\gamma^{-3})\psi = k_0^2 n_b(x) v_{b0}.$$

Knowing the eigenfrequency ω and eigenmode $\delta\psi(x)$, one can evaluate the axi generated by this perturbation:

$$B_z'' - \frac{n_e'}{n_e}B_z' - k_0^2 n_e(x) B_z = \frac{k_0^2 v_{b0} k_y}{\gamma\omega}\frac{n_e'}{n_e}\delta\psi.$$

But this axial magnetic field has little influence on the beam: its contribution force on a beam electron

$$\vec{F}_\perp = (-e)\vec{v}_z \times \vec{B}_\perp + (-e)\vec{E}_\perp + (-e)\vec{v}_\perp \times \vec{B}_z$$

is a second-order correction, because both B_z and $v_\perp$ are small.

Exact solution of equilibrium equations in case of constant densi geometry.

For the homogeneous beam penetrating homogeneous plasma (n_b = const, can solve the equation for ψ exactly. Let the beam occupy the space between Equations for dimensionless $\tilde{\psi} \equiv \frac{e}{mc^2}\psi$ within and outside the beam layer are

$$(\partial_{\tilde{x}}^2 - k_1^2)\tilde{\psi} = a, \quad |\tilde{x}| < 1$$
$$(\partial_{\tilde{x}}^2 - k_2^2)\tilde{\psi} = 0, \quad |\tilde{x}| > 1,$$

where the dimensionless quantities in this equation are defined as $k_1^2 = \frac{4\pi e^2 n_e}{mc^2}$ $n_b)L^2$, $k_2^2 = \frac{4\pi e^2}{mc^2} n_{e0} L^2$, and $a = k_{pb}^2 L^2 \frac{v_{bz0}}{c}$ in our case.

Requirements of continuity select the unique solution

$$\tilde{\psi} = \begin{cases} \alpha \frac{\cosh(k_1 \tilde{x})}{\cosh k_1} - \frac{a}{k_1^2}, & |\tilde{x}| < 1 \\ (\alpha - \frac{a}{k_1^2}) e^{-k_2 |\tilde{x} - 1|}, & |\tilde{x}| > 1 \end{cases},$$

where α is proportional to a:

$$\alpha = \frac{a k_2}{k_1^2 (k_1 \tanh k_1 + k_2)}$$

The maximum of absolute value of ψ is reached at $x = 0$ and equals

$$\max |\tilde{\psi}| = |\tilde{\psi}(0)| = \frac{a}{k_1^2} \left| \frac{1}{1 + \frac{k_1 \tanh k_1}{k_2}} \cdot \frac{1}{\cosh k_1} - 1 \right| \approx \frac{a}{k_1^2} \sim \frac{v_{bz0}}{c} \frac{n}{n_{e0}}$$

Solution of the eigenvalue equation for homogeneous finite-size

The dispersion relation for the case of inhomogeneous density requires solving
problem. Taking only Weibel instability into account (no B_z), and making s
assumptions (like $n_b \ll n_e$), we can write the eigenvalue equation for $\delta\psi$ in th

$$(\nabla^2 - k_{pe}^2)\delta\psi = -\frac{v_b^2 k_{pb}^2}{\gamma_b \omega^2}\nabla^2\delta\psi,$$

or, after introducing $\lambda = \frac{-\gamma_b\omega^2}{v_b^2 k_{pb}^2}$,

$$\nabla^2\delta\psi + \frac{\lambda k_{pe}^2}{1-\lambda}\delta\psi = 0.$$

In the 1D-case (parallel layers with no y-dependence) and for the constan
$-L < x < L$ we can immediately write down the eigenvalues for this equatio
boundary condition is either $\delta\psi(\pm L) = 0$ or $\delta\psi(L) = 0, \delta\psi'(0) = 0$):

$$\frac{\lambda k_{pe}^2}{1-\lambda} = \left(\frac{\pi(2n+1)}{2L}\right)^2, \quad n = 0, 1, 2, \ldots$$

and finally

$$-\omega_n^2 = \frac{k_{pb}^2 v_b^2}{\gamma_b\left(1 + \left(\frac{2k_{pe}L}{\pi(2n+1)}\right)^2\right)}.$$

Axial magnetic field generated by Weibel instability

Let's apply our results for a homogeneous flat beam to evaluate the axial mag
Weibel instability. If a perturbation has a form $a(x)e^{ik_y y - i\omega t}$, then we arrive w
(17) for B_z, which can be easily solved in case of step-function profile for the be
only point with density gradient, which is necessary for non-zero B_z, is the poi
drops from some n_{b0} down to zero outside of the beam. The analytical soluti
$B_z(x)$ is an odd function and tends to zero at infinity:

$$B_z = \begin{cases} \alpha \sinh(k_1 x), & x < 1, \quad k_1^2 = (1 - n_{b0})k_0^2; \\ \alpha \sinh(k_1) \exp(-k_0 x), & x > 1. \end{cases}$$

Here

$$\alpha = -\frac{k_y k_0^2 v_{b0}}{\gamma_b \omega} \left(\frac{n_b}{n_e}\right) \frac{\delta\psi(1)}{k_0 \sinh k_1 + \frac{k_1}{1-n_{b0}} \cosh k_1},$$

and hence, the maximum axial magnetic field generated by Weibel kind of pe

$$|B_z|_{\max} = |B_z(\text{beam boundary})| = \frac{k_y k_0^2 v_{b0}}{\gamma_b |\omega|} \left(\frac{n_b}{n_e}\right) \frac{|\delta\psi(1)|}{k_0 + \frac{k_1}{1-n_{b0}} \coth k}$$

Weibel instability eigenvalues in case of arbitrary density profil

Again consider plane geometry case, but now $n_b = n_b(x)$ is an arbitrary even
$n_b(0)$. Numerical estimates show that all eigenmodes are unstable with growt

$$\Gamma_n = \sqrt{\frac{k_{pb0}^2 v_b^2 \lambda_n}{\gamma_b}},$$

where $k_{pb0}^2 = \frac{4\pi e^2 n_{b0}}{mc^2}$, and dimensionless (normalized) eigenvalues λ_n are distri
and 1, and the plot λ_n versus n follows a smooth curve, which was found b
instability in an infinitely wide beam:

$$\Gamma(k_x) = \sqrt{\frac{k_{pb0}^2 v_b^2}{\gamma_b(1 + \frac{k_{pe}^2}{k_x^2})}}$$

Differences between Weibel instability in finite-size beam and infinitely wide c

• In finite size beam we have a discrete (but infinite) set of eigenmodes.

• In finite size beam the lowest growth rate eigenmode exists, which grows w
~ 0.1 (depending on parameters) of the maximum growth rate (which is ap
same in any geometry), unlike instability in infinite medium, where $-\omega^2$ can

Common features in these two cases are:

• Maximum growth rate $\Gamma_{max} = \frac{k_{pb0} v_b}{\sqrt{\gamma_b}}$.

• The dependence of growth rate on the "effective wave number" of perturb
imately the same.

Field equations

- Out-of-plane component of magnetic field:

$$\left(\nabla^2 - \vec{\nabla}\ln n_e \cdot \vec{\nabla} - \frac{\omega_{pe}^2}{c^2}\right) B_z = \frac{4\pi n_e}{c}\vec{\nabla}\cdot\left(\frac{\vec{e}_z \times \vec{J}_b}{n_e}\right).$$

- In-plane magnetic field (described by potential $\psi \equiv A_z$):

$$\nabla^2\psi = \frac{\omega_{pe}^2 + \omega_{pb}^2 < \gamma_j^{-3} >}{c^2}\psi + \frac{4\pi e v_{b0}}{c} n_b.$$

Equation of motion for beam particles

$$\frac{d(\gamma_j \vec{v}_{j\perp})}{dt} = -\frac{e v_{jz0}}{mc}\vec{\nabla}\psi + \frac{e^2}{2m^2c^2}\left(1 - \frac{1}{\gamma_j^3}\right)\vec{\nabla}\psi^2 + \frac{\partial}{\partial t}\left(\frac{\vec{J}_{b\perp}}{e n_e}\right)$$
$$\frac{\partial}{\partial t}\left(\frac{c\vec{e}_z \times \vec{\nabla} B_z}{4\pi e n_e}\right) + \frac{e B_z}{mc}\vec{e}_z \times \vec{v}_j + \vec{\nabla}\left(\frac{\vec{v}_{e\perp}^2}{2}\right).$$

Experimental observations of the Weibel instability in high intensity laser solid interactions

M.S. Wei[1], F.N. Beg[1], E.L Clark[4], A.E.Dangor[1], A. Gopal[1], K.W.D. Ledingham[3], P. Mckenna[3], P.A. Norreys[2], I. Spencer[3], K. Lancaster[2], M. Tatarakis[1], M. Zepf[5], K. Krushelnick[1]

1. *The Blackett Laboratory, Imperial College, London*
2. *Central Laser Facility, CLRC Rutherford Appleton Laboratory*
3. *Department of Physics and Astronomy, University of Glasgow*
4. *Radiation Physics Department, AWE plc, Aldermaston*
5. *Department of Physics, The Queen's University Belfast*

Double Sided Illumination Experiments Layout

VUCAN laser facility, RAL(UK)

Basic set-up (Top view)

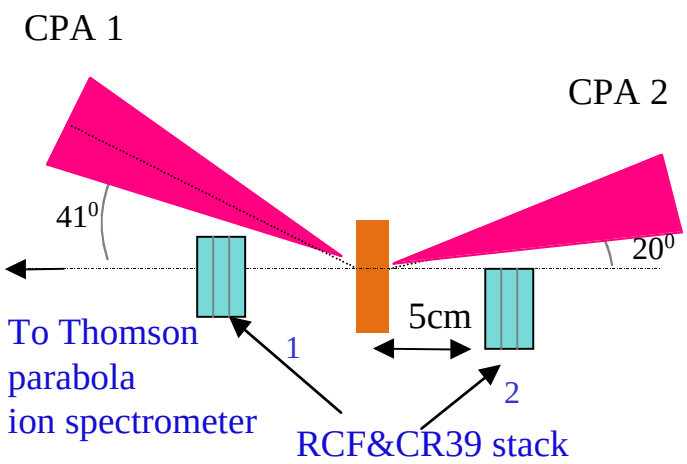

Both stacks (5cm ×5cm) were put parallel to the target. Stack1 looked at top half beam. Stack2 collected right half emission.

Two CPA Laser Pulse:

λ=1.054 μm, τ~1 ps
Up to 30 J and 20J on the target from CPA1 and CPA2 respectively
Focal spots size: 10 μm FWHM
Intensity up to 3×10^{19} Wcm^{-2}

Target :

Thin gold foil (20 μm thick) 5mm×8mm

Diagnostics:

Sandwich stack of radiochromic films and CR39 track detectors
Copper Activation Stack
Thomson Parabola Ion Spectrometer

Off-normal electron beams were consistently observed in the double illumination shots no matter two laser pulses were coincident or mismatching in time.

Shot 1: CPA1and CPA2 coincidence

RC film absorbed dose(Gy)

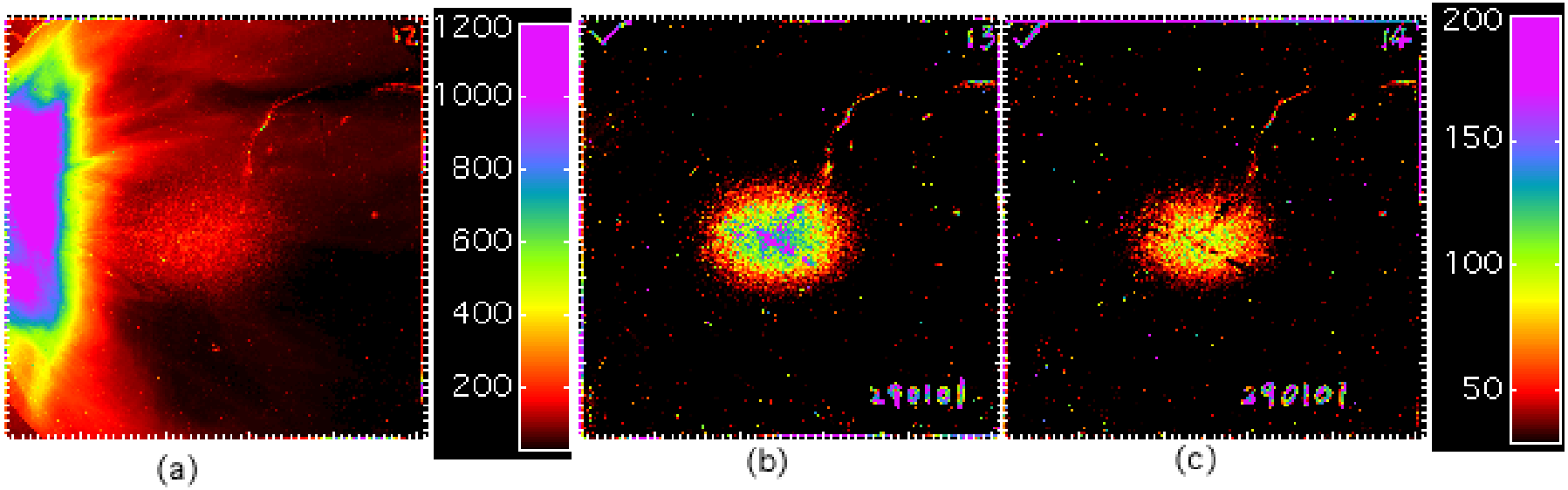

Total electron number in the off-normal direction beam: 10^{12}

Off-normal electron beams (continued)

Shot 2: CPA1and CPA2 coincidence

RC film absorbed dose(Gy)

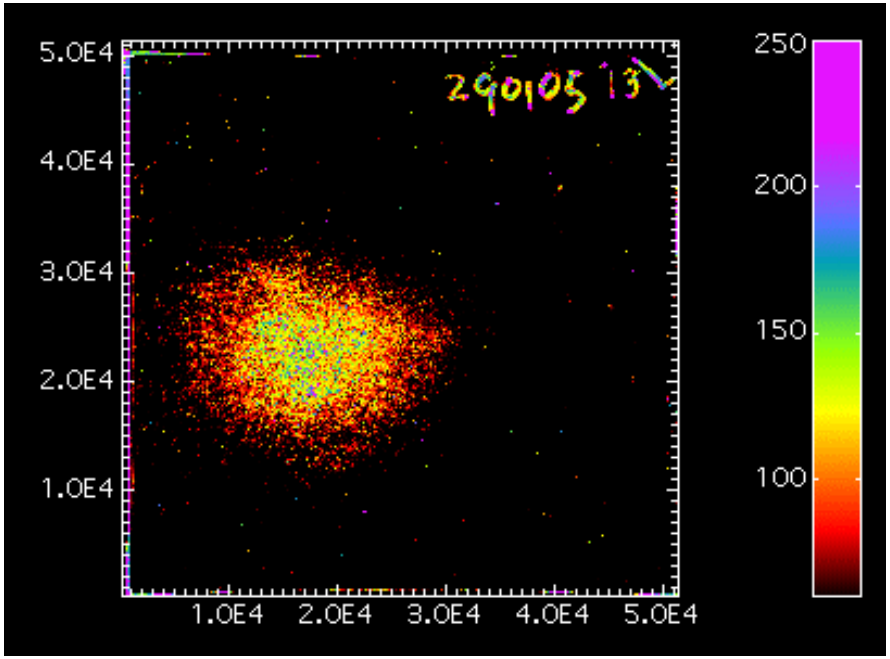

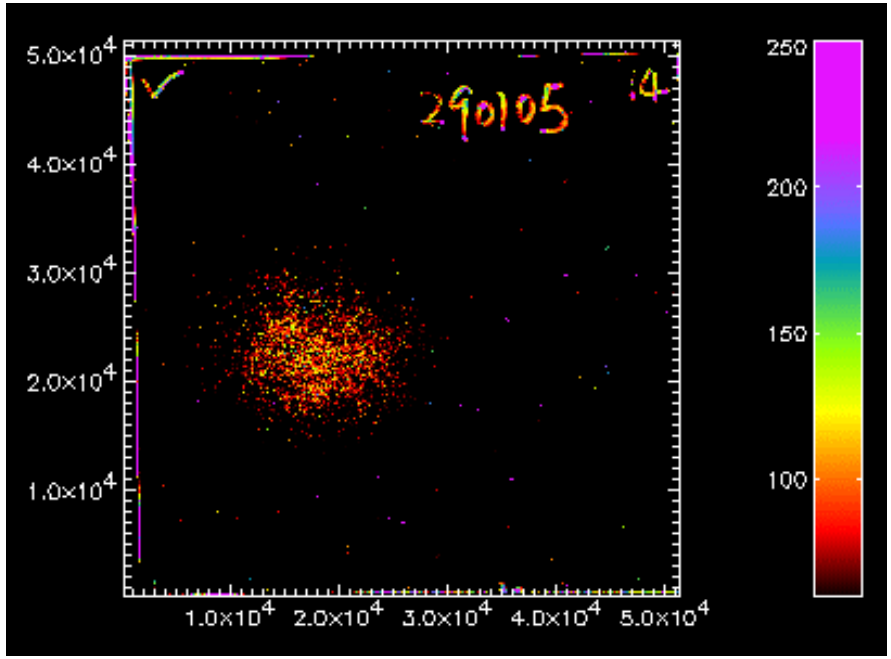

Off-normal electron beams (continued)

Shot 3: CPA1 1 ps than CPA2
RC film absorbed dose(Gy)

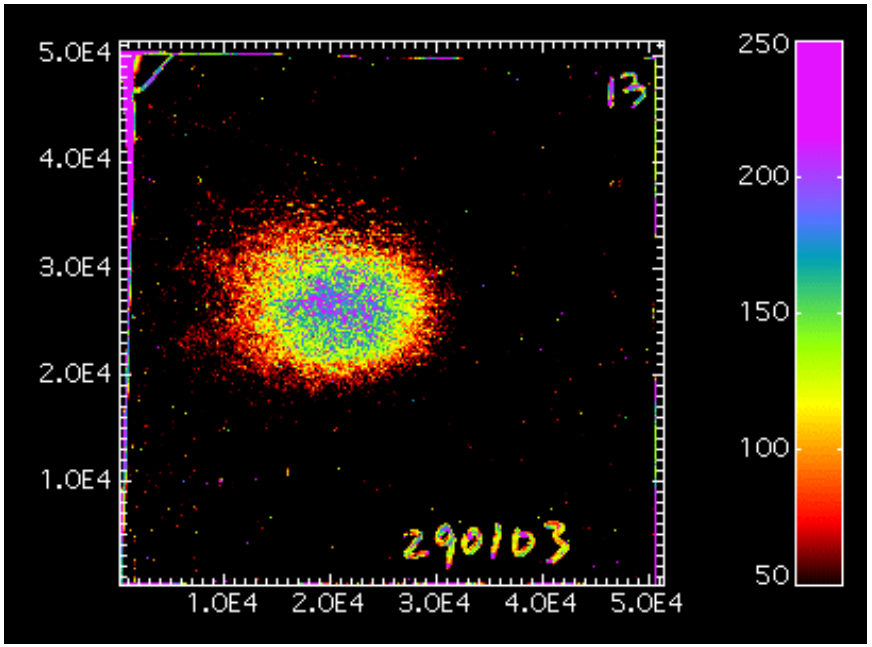

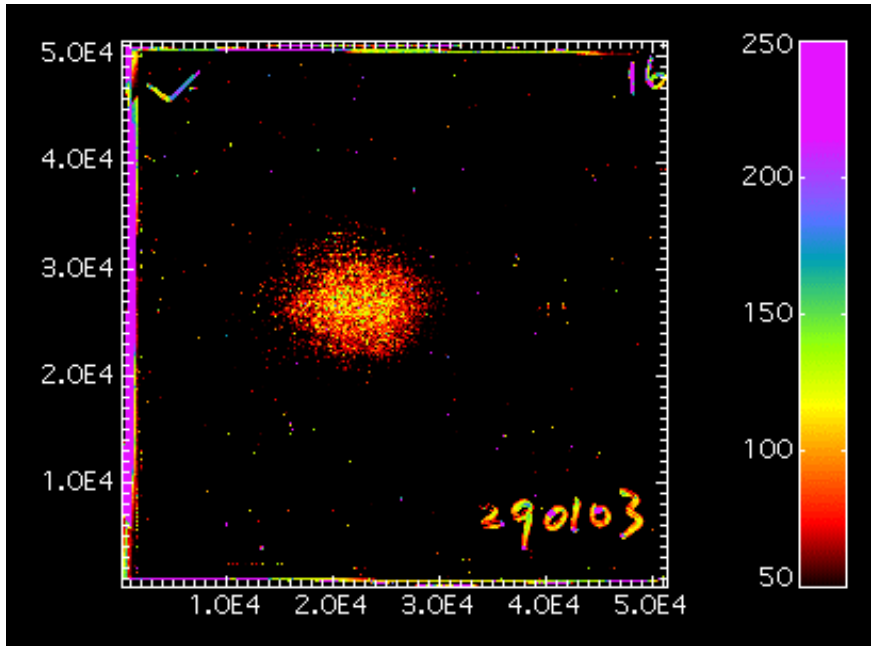

Characteristics of these off-normal electron beams using double sided illumination

- The direction of the beams was between target normal and CPA1 laser axis, about 20° off normal

- Highly collimated:
  the full cone angle of the emission is about 11°

- Very fine emission pattern:
  Speckle-like tiny beamlets

RCF scanned raw data in the single illumination shot (only CPA1 was used). It is clear that large filamented electron beams are emitted in the off-normal direction

a-c images from a detector stack behind the target.

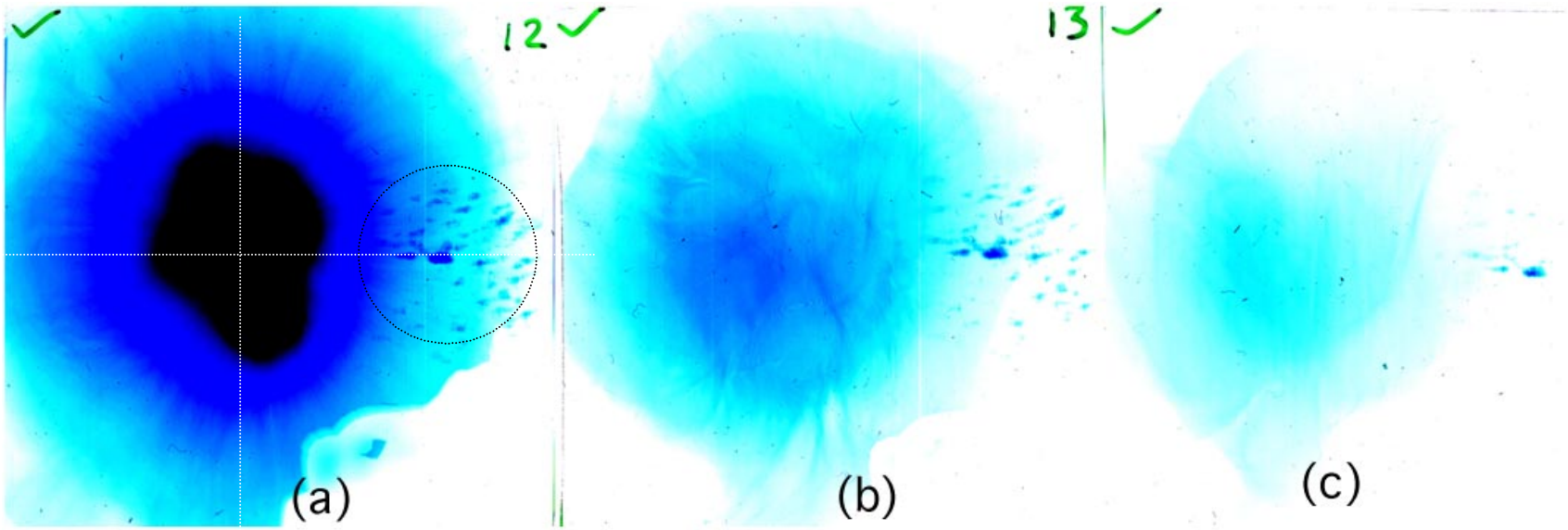

The bulk signals along the target normal direction are mainly due to energetic protons.

There is also a distinct emission feature due to dozens of electron beamlets ejected from the rear of the target.

Optical density of the RC films from the same single illumination shot

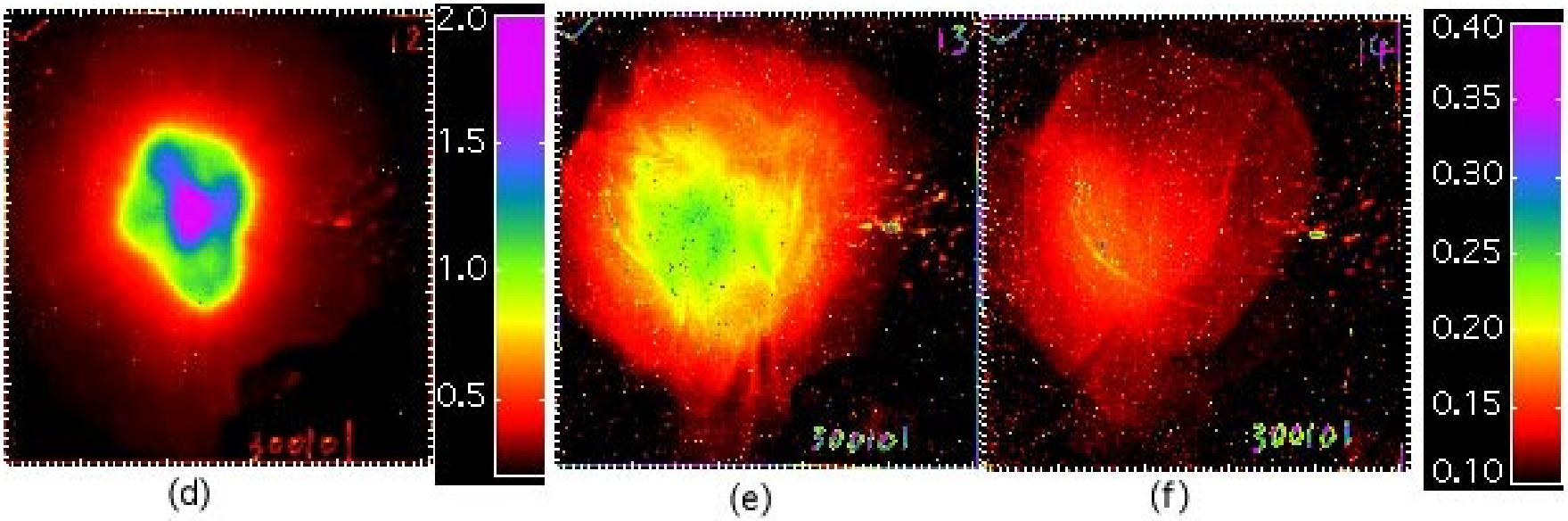

The observed growth rate of the Weibel instability in our experiments agrees with 2D PIC simulations

Experimental observation:
The off normal electron beamlets are much larger in the single illumination case than with double-sided irradiance.

2D PIC simulation results (Y. Sentoku, Phys. Plasmas, **7**, 689(2000))

- In the case of a collisional plasma, the growth rate of higher modes of Weibel instability are strongly suppressed, and the spectral peak of the growth rate shifts to the lower wave number.

- When the initial plasma temperature is high, the growth rate of the instability is strongly reduced.

Observation of Radiation from laser and Magnetized Plasma Interaction Experiments

N. Yugami, H. Kawakami, D.Dorranian, C.Rajyagru

M. Stradubtsev, H. Ito and Y. Nishida

(Utsunomiya University, Japan)

FIW2002, FL
Nov 16-20,2002

Department of Energy and Environmental Science,
Graduate School of Engineering,
Utsunomiya University

7-1-2 Yoto, Utsunomiya, Tochigi 321-8585, JAPAN, TEL: +81-28-689-6082, FAX: +81-28-689-7020

Outline

A proof-of-principle experiment demonstrates the generation of the radiation from the Cerenkov wake excited by a ultra short and ultra high power pulse laser in a perpendicularly magnetized plasma. The frequency of the radiation is in the millimeter range(up to 200 GHz). The intensity of the radiation is proportional to the magnetic field intensity as the theory expected. Polarization of the emitted radiation is also detected. The difference in the frequency of the emitted radiation between the experiments and previous theory can be explained by the electrons' oscillation in the electric field of a narrow column of ions in the focal region.

Oscillating Current in Plasma Wave

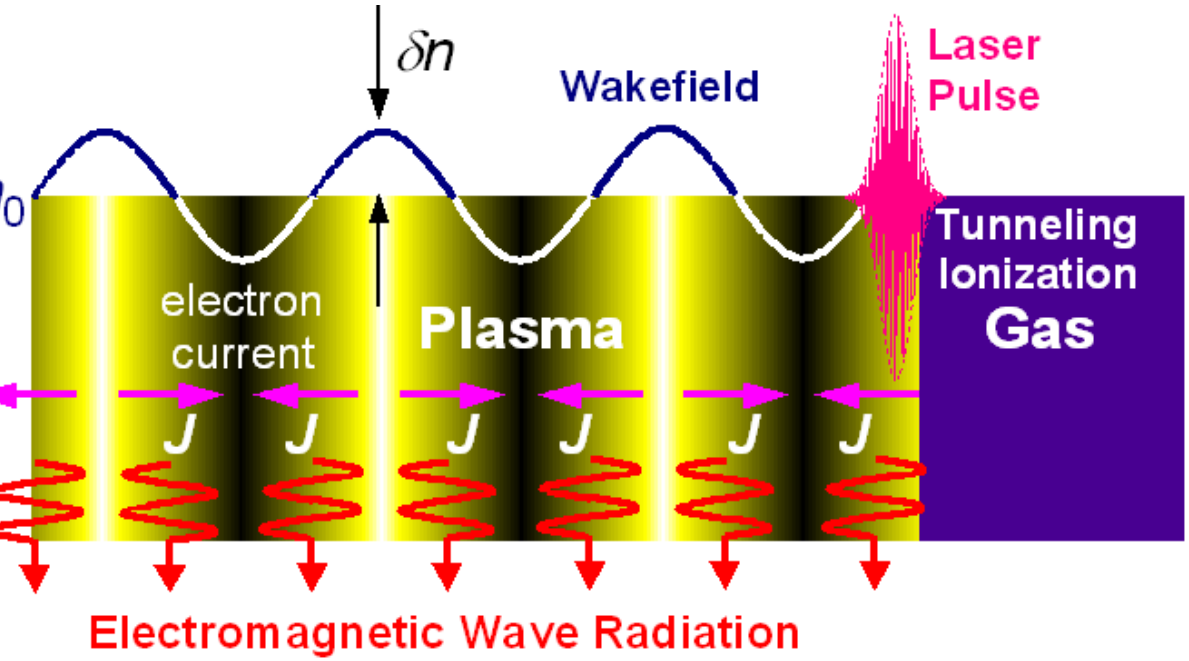

Electron Current

$$\frac{\partial \rho}{\partial t} + \nabla \cdot \mathbf{j} = 0$$

$$-\mathrm{i}\omega\rho + \mathrm{i}kj_x = 0$$

$$j_x = \frac{\omega}{k}\rho$$

Skin depth ; $\delta \approx c/\omega_p$

$n_0 = 10^{16}\ \mathrm{cm}^{-3}$

$\lambda_p = 300\ \mu\mathrm{m}$

$\delta \approx 50\ \mu\mathrm{m}$

Frequency ; $\omega \approx \omega_p$ (plasma freq.)

n=1.0x10^{16} cm^{-3} → f=0.9 THz

[1] J. Yoshii *et al.*, Phys. Rev. Lett. 79, 4194 (1997).

Experimental Setup for Radiation

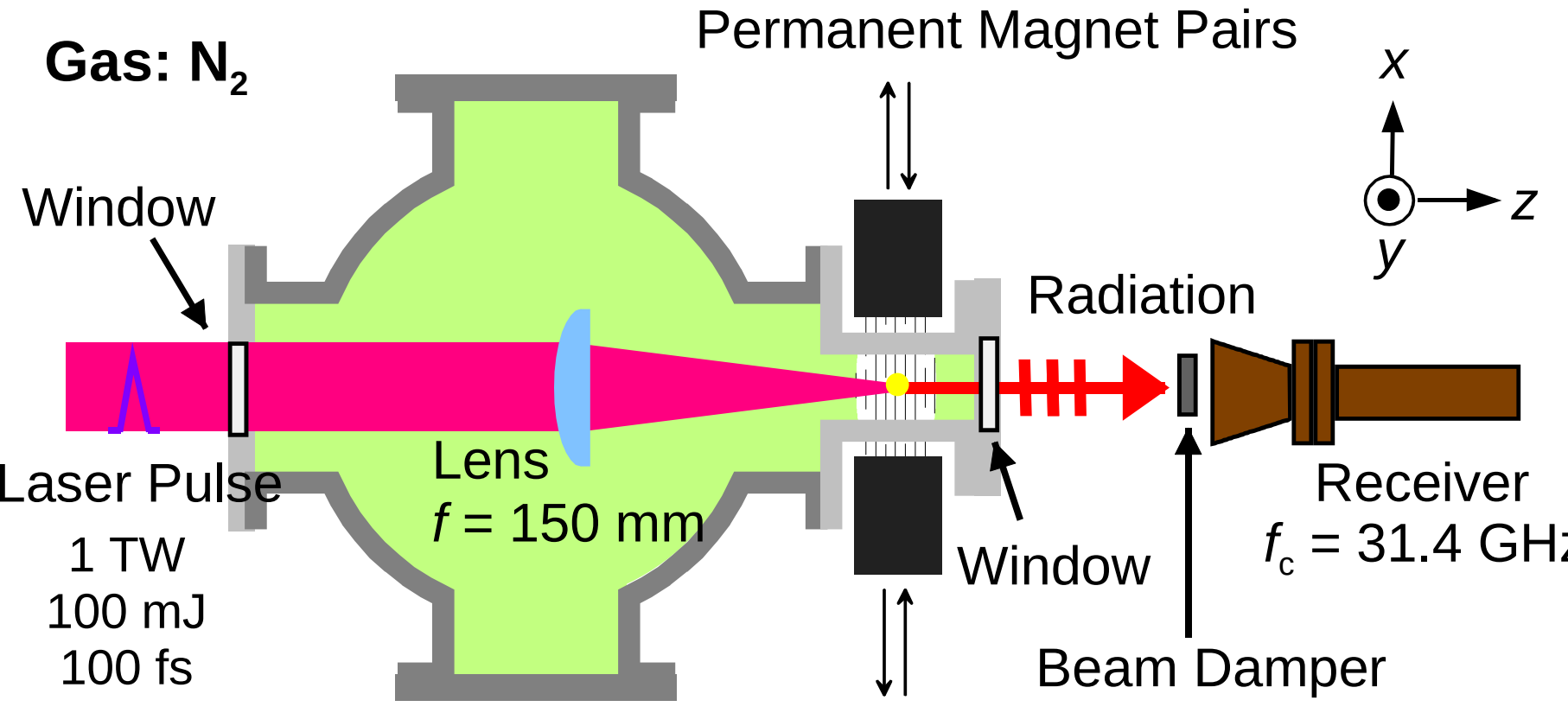

Typical Example of Emitted Radiation

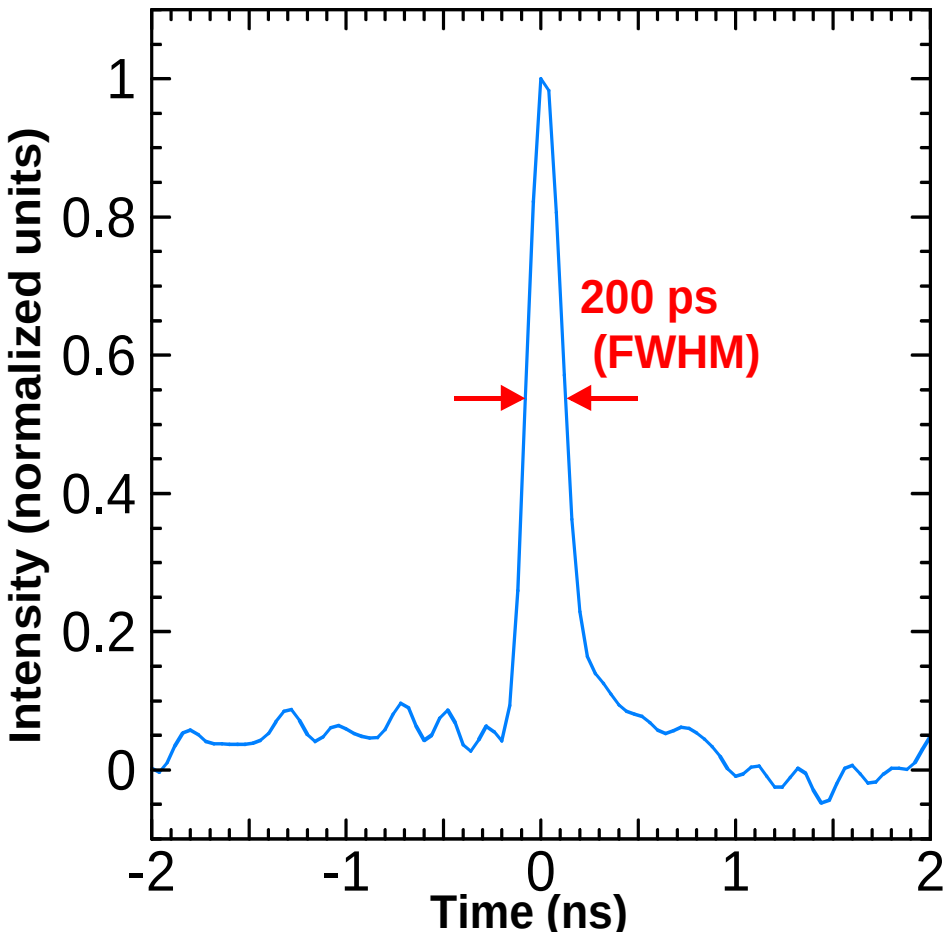

Experimental condition

Laser Power: 0.5 TW

B_0: 8.5 kG, He 375 mTorr

Expected Pulse Width

$$x_R = \frac{\pi w_0^2}{\lambda_0} : \text{Rayleigh length}$$

$$x_R = 0.4\ \text{mm}$$

$$\text{at } w_0 = 10\ \mu\text{m}, \lambda_0 = 800\ \text{nm}$$

$$\tau \approx \frac{L_p}{v_g} = \frac{2x_R}{c}\frac{\omega_p^2}{\omega_c^2} \approx 190\ \text{ps}$$

$$\text{for } L_p \approx 2x_R \text{ and } \omega_p >> \omega_c$$

Radiation intensity was proportional to the strength of B field

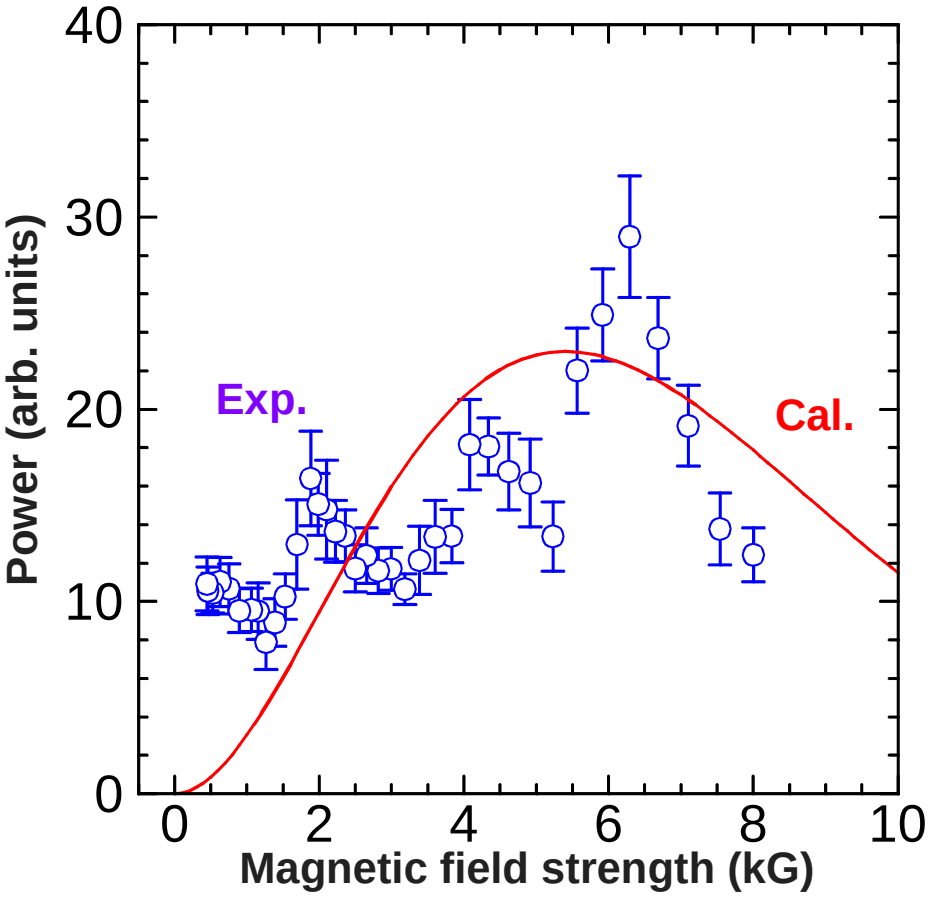

Laser Power ; 0.5 TW
N_2 750 mTorr

$$p \propto \left(\Gamma^2, B_0^2, E_x^2\right)$$

Plasma cavity for radiation

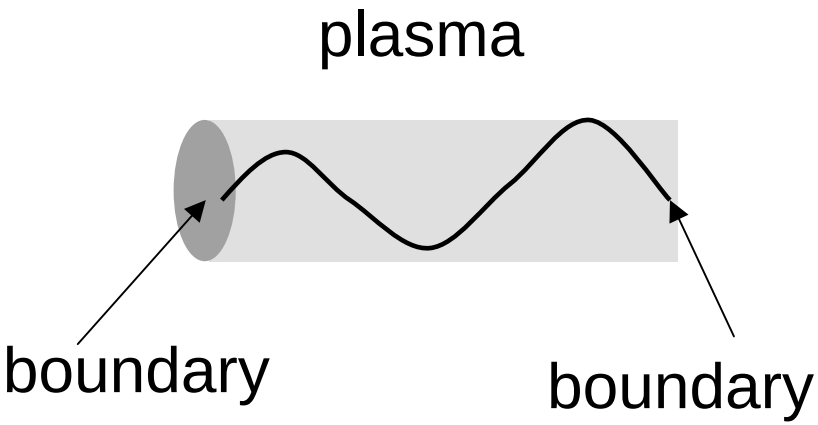

Plasma column works as “cavity” for radiation

Wavelength of the radiation is satisfied the matching condtion,

$$L = n\lambda$$

Strong radiation is expected to observe.

The data suggests the wavelength(frequency) depends on the strength of B field.

Damping at the plasma-vacuum surface

boundary

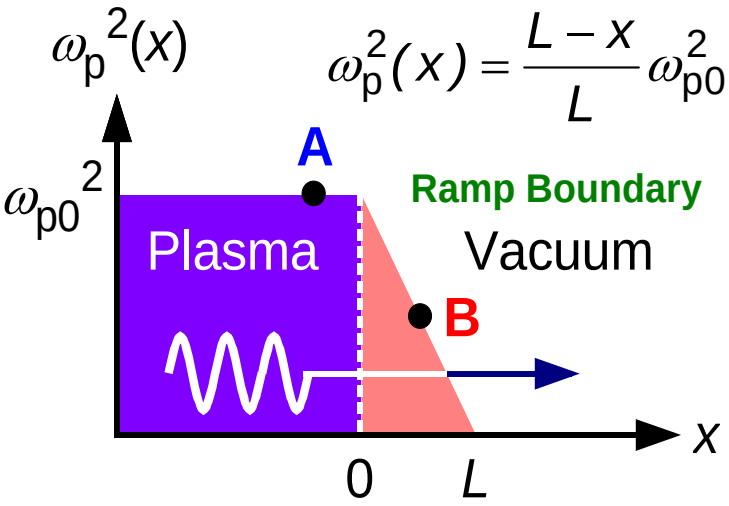

$$\omega_p^2(x) = \frac{L-x}{L}\omega_{p0}^2$$

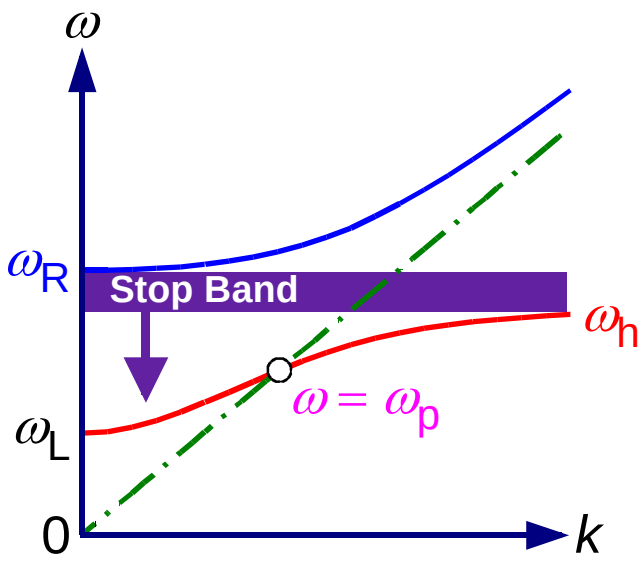

Ratio

$$\Gamma = \frac{E_{\text{vacuum}}}{E_{\text{plasma}}} = \exp\left(\frac{\alpha L \omega_0}{c}\right)$$

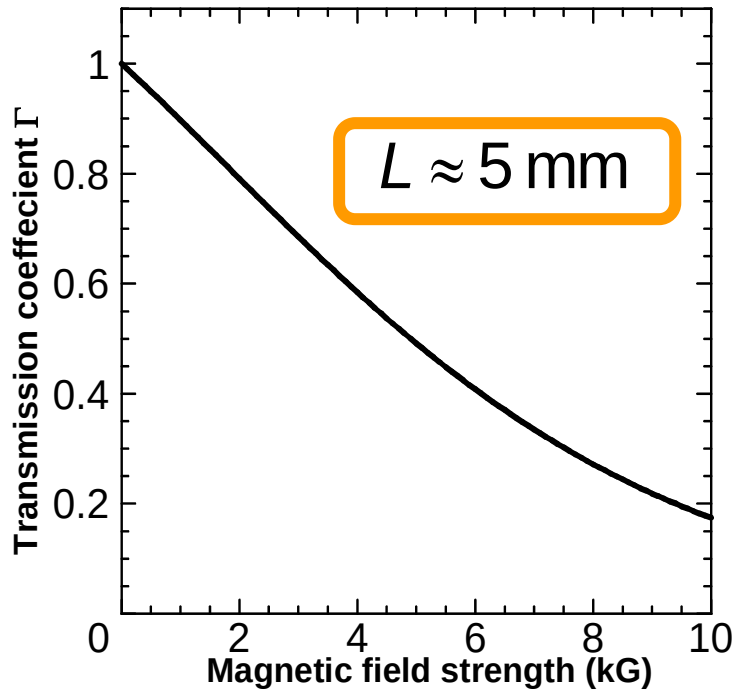

Typical Waveform of Radiation
--- 2 peaks were observed ---

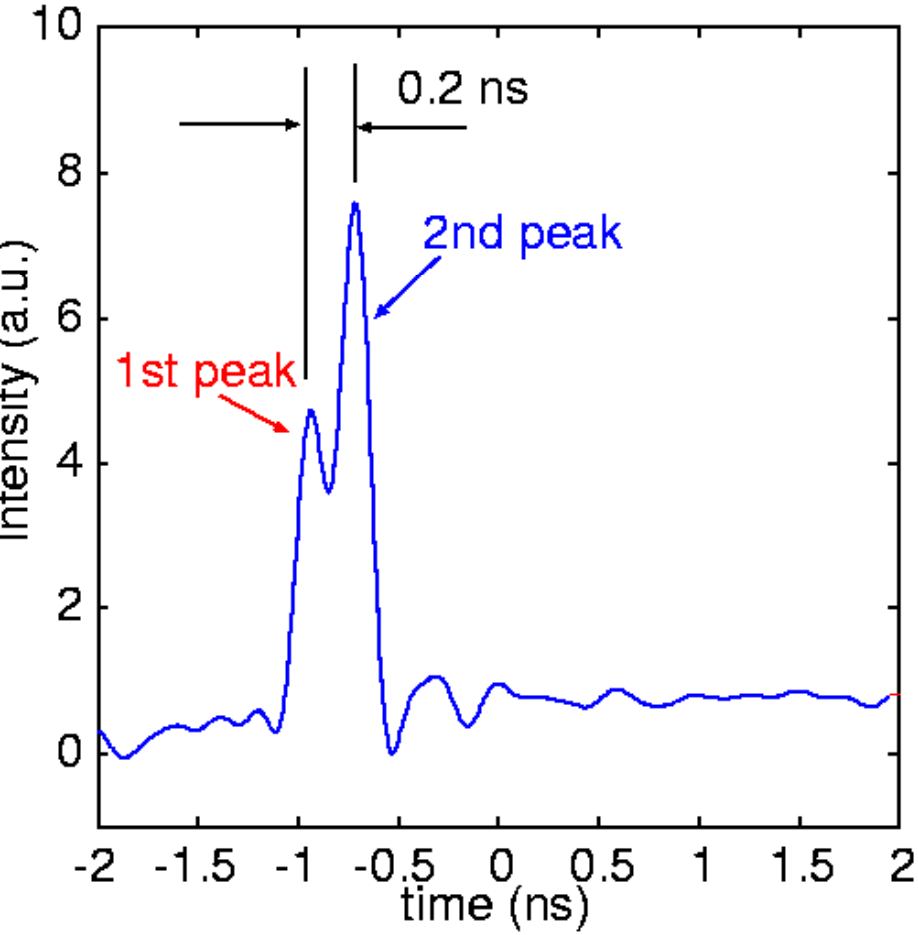

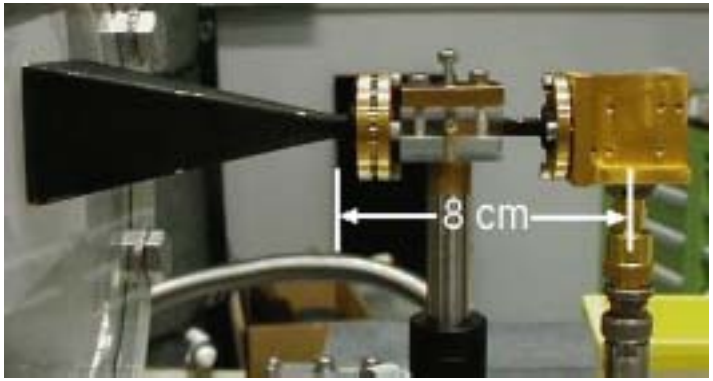

Cut-off freq. of waveguide

f_c = 31.4 GHz

Pulse width

200-250 ps

Each peak of radiation has different polarization

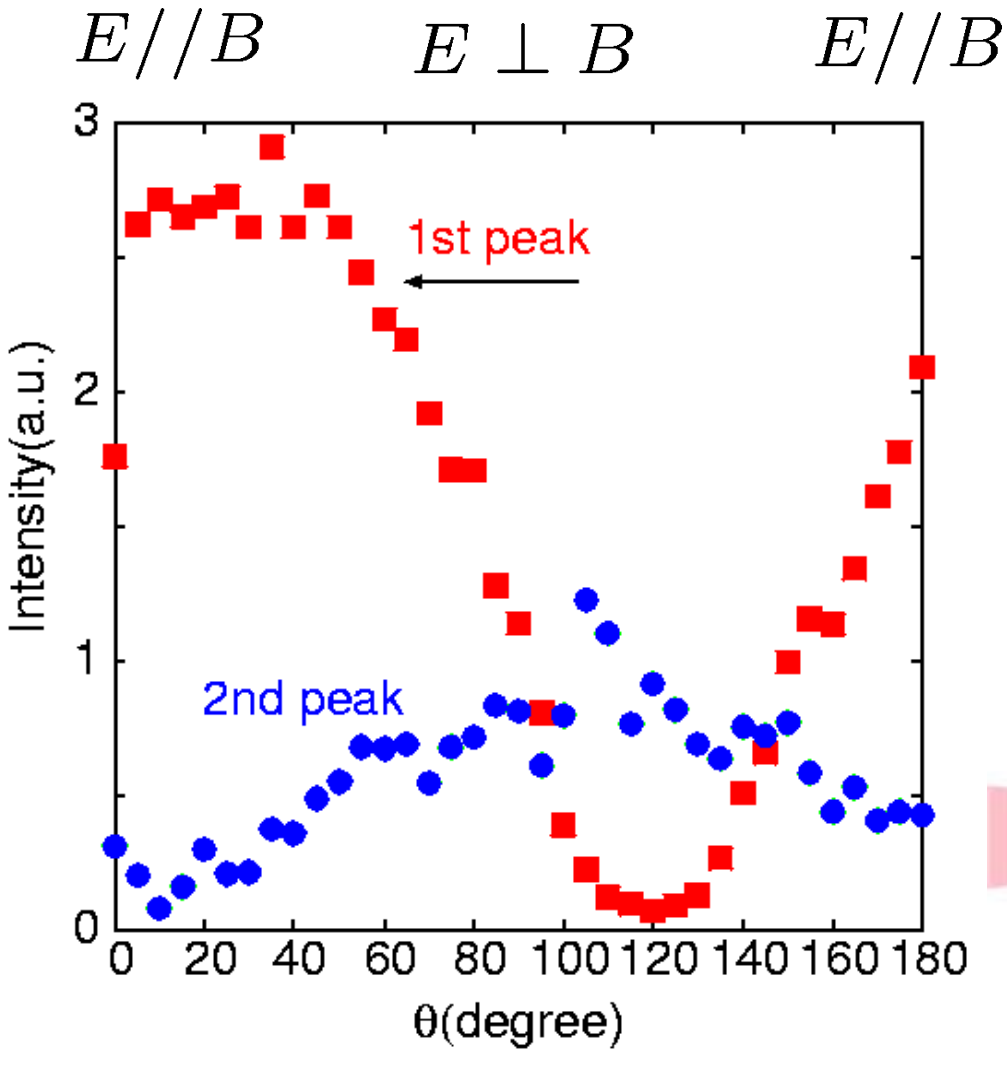

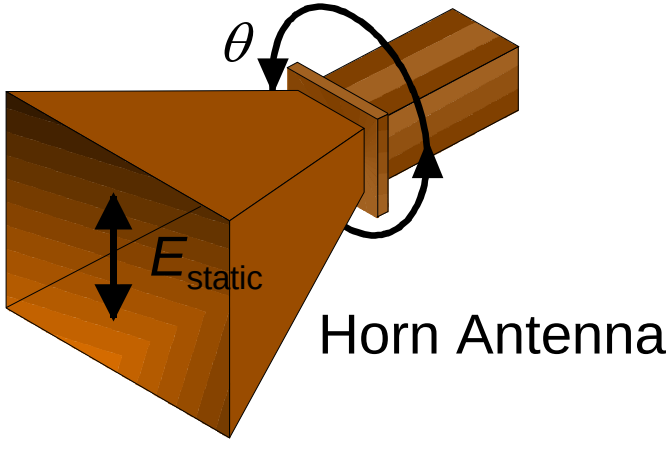

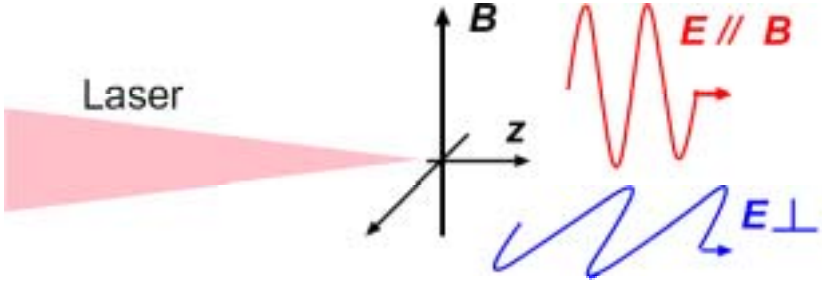

Two kinds of radiation in GHz region

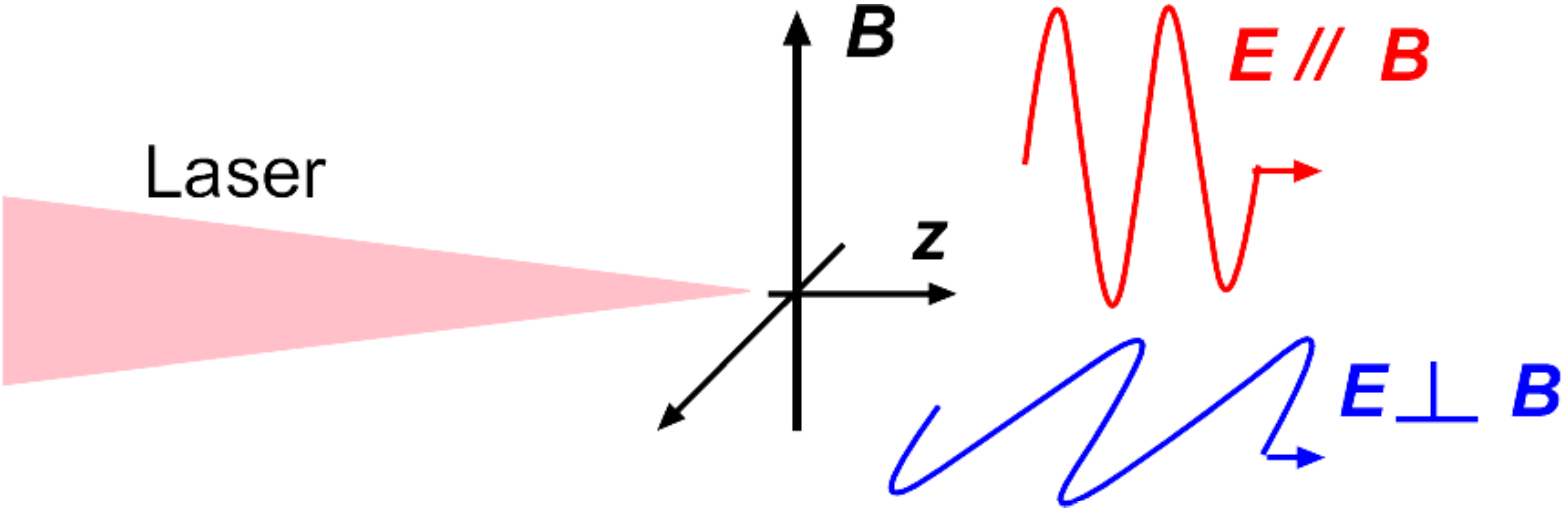

Freq. Spectrum measured by TOF **method**
--- Each peak has different freq. ---

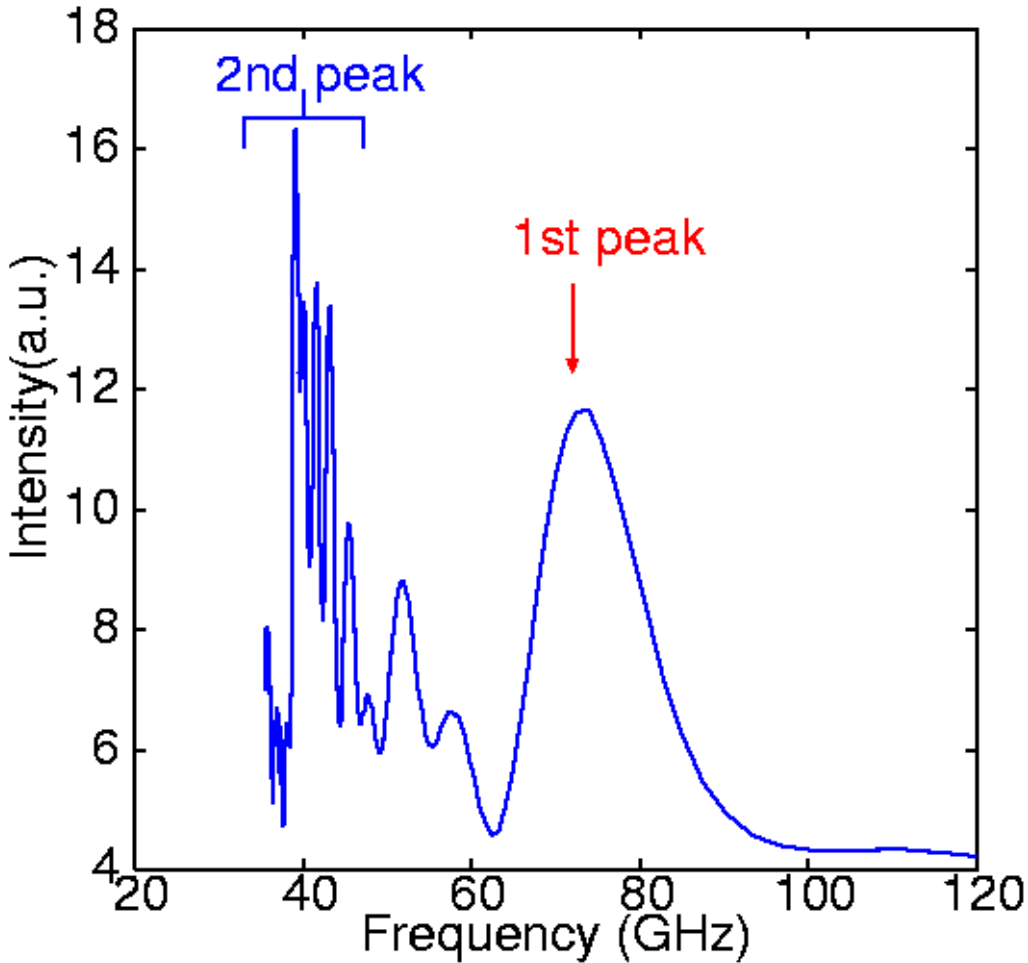

Flight length L = 1.2 m

1st peak ~74 GHz
2nd peak ~40 GHz

Freq. of 1st peak does NOT depend on B field
Freq. of 2nd peak depends on B field.

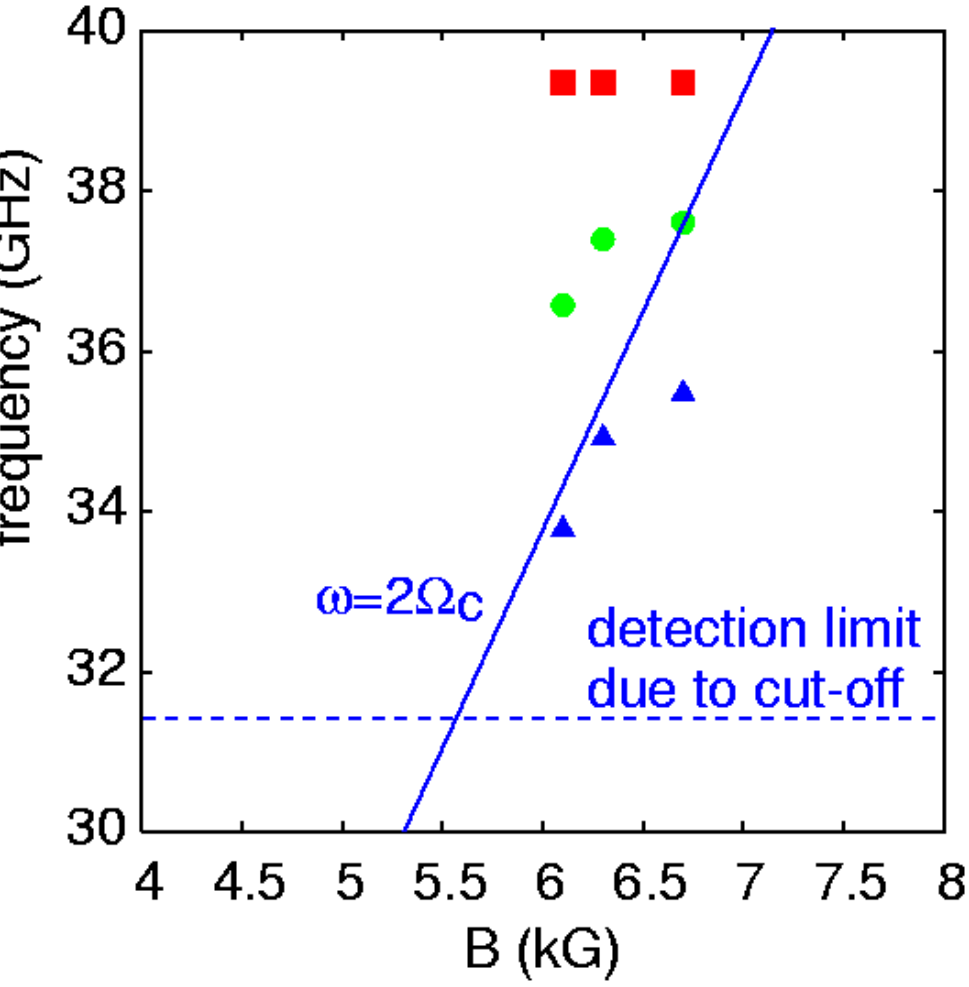

$$\Omega_c \propto B$$

1st peak of Radiation

- Freq. : 74 GHz.
- Polarization of radiation // B field
- Frequency of radiation dose not depend on the strength of B field

Electrons' oscillation in the electric field of a narrow column of ions in the focal region.

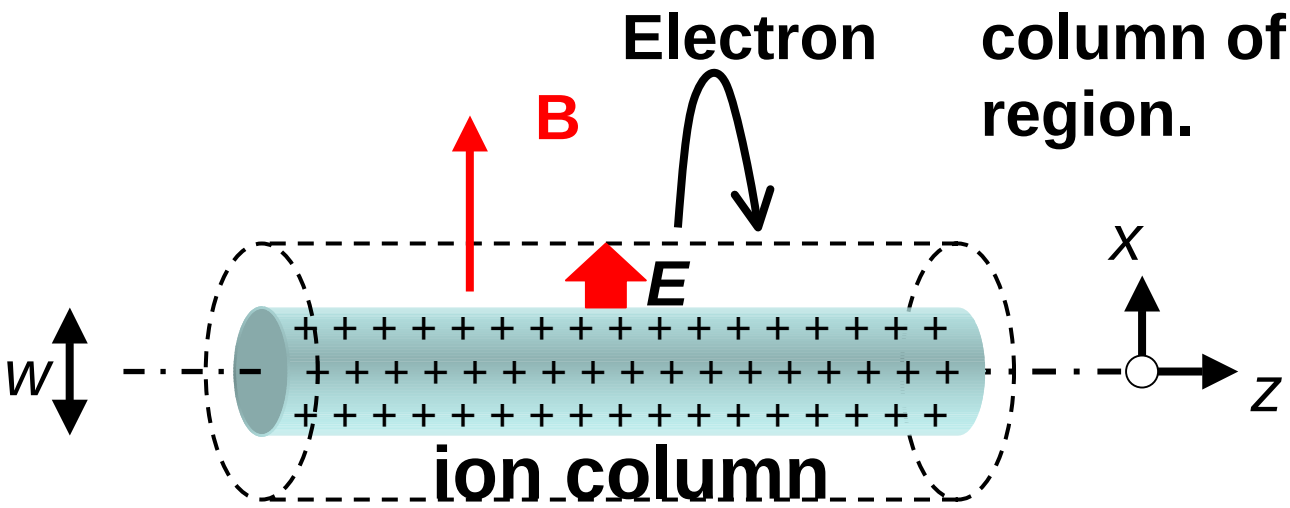

2nd peak pulse

- Freq. : ~40 GHz.
- Polarization of radiation ⊥ B field
- Frequency of radiation depends on the strength of B field

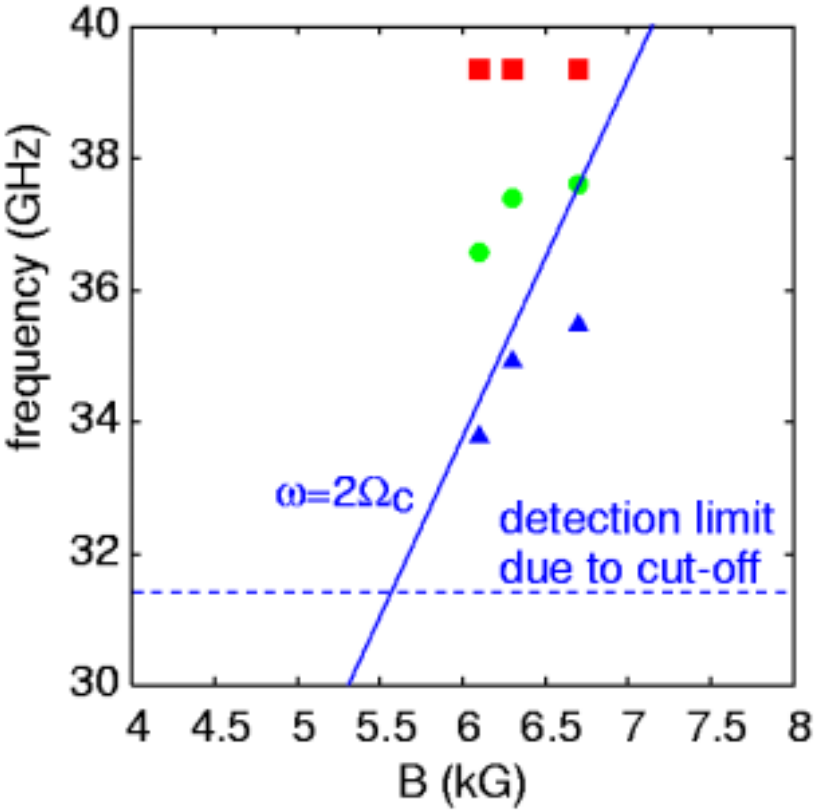

Bernstein mode

$$\omega = n\Omega_c \quad (n = 1, 2, 3, \cdots$$

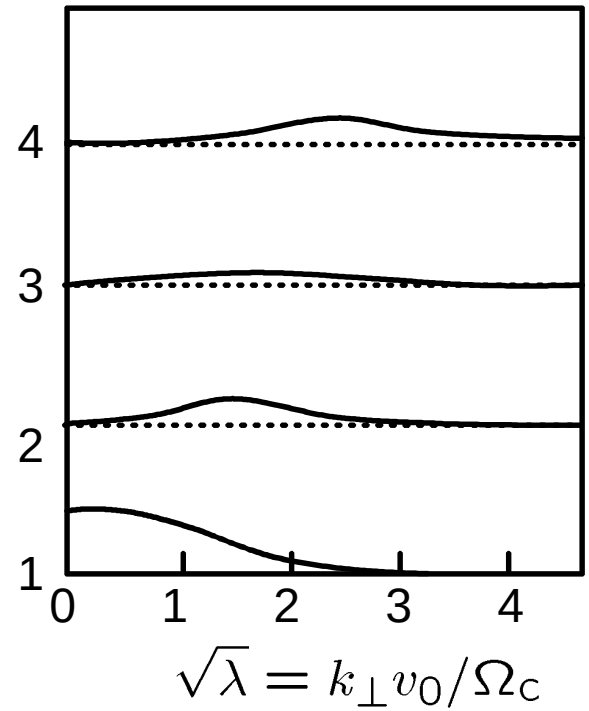

Conclusion

- The radiation from the interaction between laser and magnetized plasma was observed.
- Higher freq. and lower freq. components were observed.

- Higher Freq. Component
  - Freq : 74 GHz
  - Polarization …. Parallel to B field
  - Frequency does not depend on the strength of B field.
  - Due to the electron motion parallel to the B field.
- Lower Freq. Component
  - Polarization …. Perpenducular to B field
  - Frequency does depends on the strength of B field.
  - Bernstein mode?

Proton acceleration from high intensity laser interactions with thin foil targets.

Matthew Zepf
School of Mathematics and Physics, Queen's University, Belfast, UK

K. Krushelnick, F. Beg, A.E. Dangor, A. Gopal, M. Tatarakis,M. Wei
Blackett Laboratory, Imperial College, London, UK

E. Clark
AWE, Aldermaston, UK

P.A. Norreys
Central Laser Facility, Rutherford Appleton Laboratory, Didcot, UK

Overview

- Background and acceleration mechanisms
- Origin of the protons - a topic of lively debate
- Experiment
- Summary

Typical proton acceleration experiment.

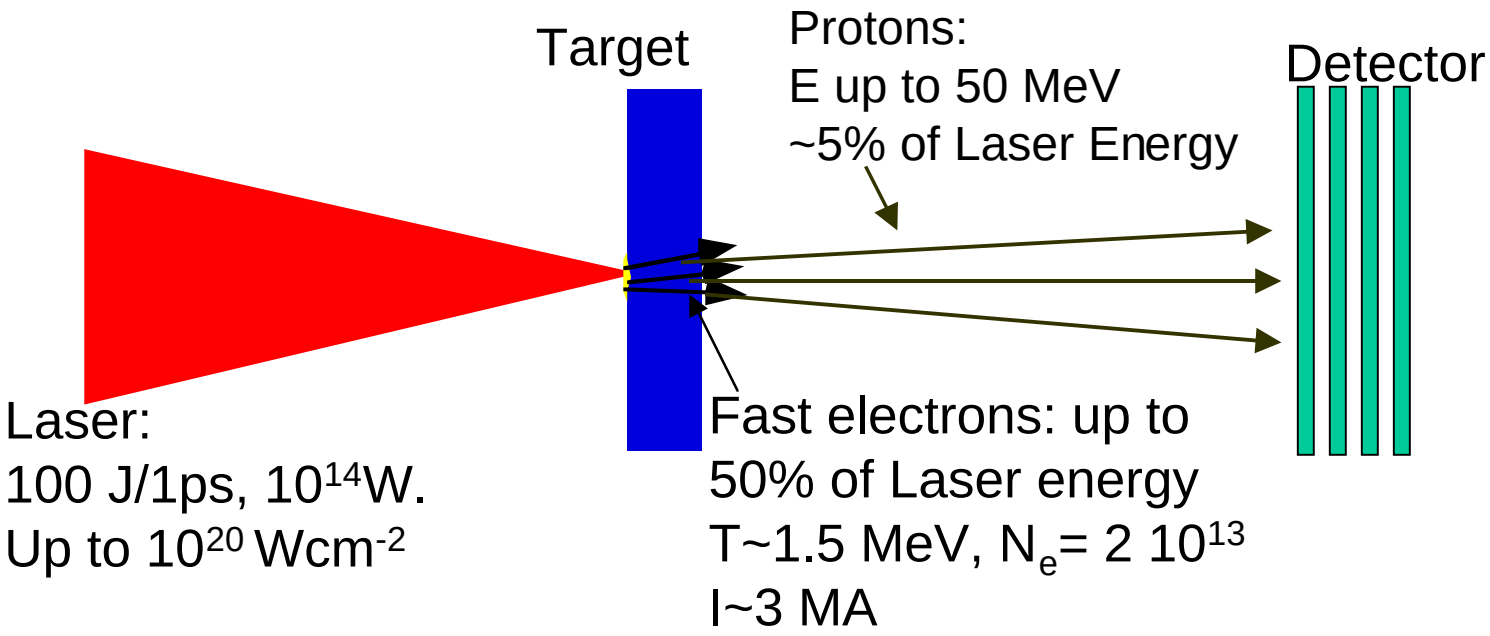

A large fraction of the laser energy is absorbed into fast electrons
⇒ Current exceeds the Alfvén limit by far
⇒ Strong electric fields are set up in response throughout the target
⇒ Significant fraction of electron energy is converted into MeV protons

So how can fast protons be accelerated?

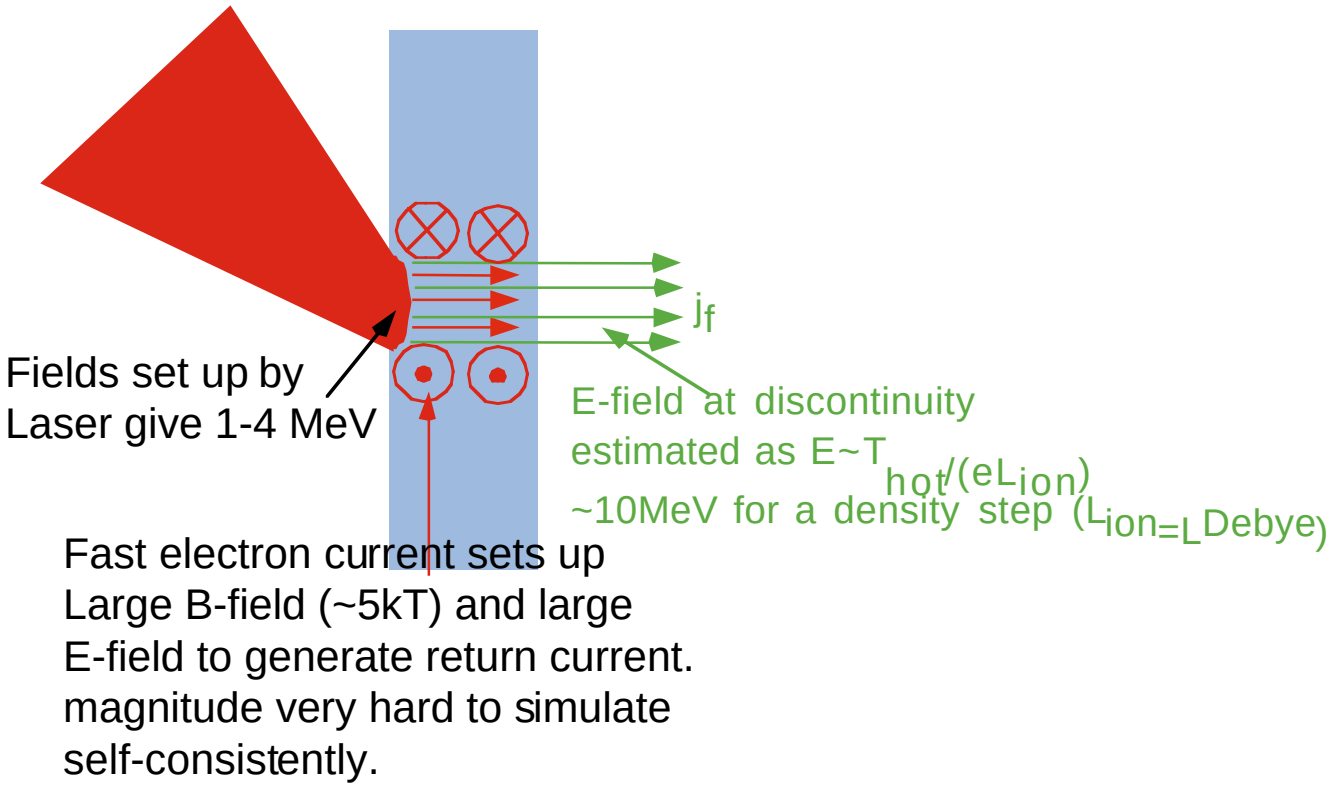

- Large fields are expected to exist throughout the target
- Fields in the interior hard to access with simulations or experiments

Angular distribution

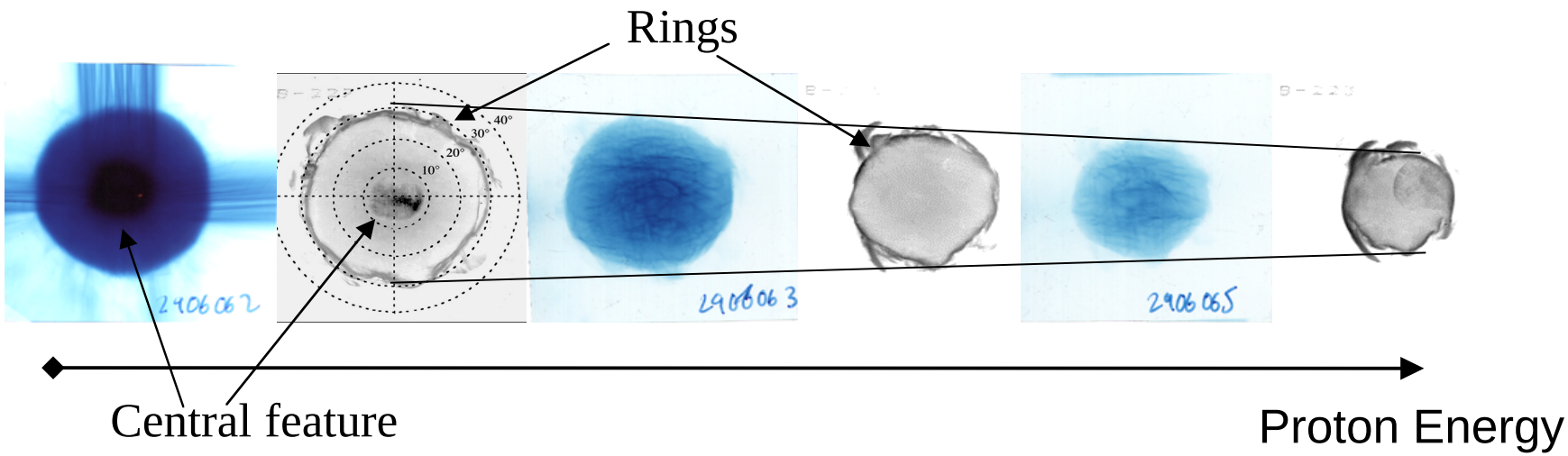

- CR39 and RCF detectors depicting proton energy surfaces
  - Half angle decreases with increasing energy
  - Strong, low divergence signal at the centre, extends to a few MeV
  - Contracting ring component extends to high energies.
    - Rings broaden for plastic targets, disks observed for thin targets.
  - RCF vs CR39
    - CR39: Sensitive to narrow band of proton energies (at end of range)
    - RCF: sensitive to all types of radiation and a broad band of energies.

Some data suggests, that the protons are from the front.

- Proton energy is sharply correlated with angle
  - Hence they are likely from the front.
    E. Clark et al., PRL 84, pp670 (2000): " It is more probable that the protons (in the ring structure) are generated at the front of the target and subsequently transported through the target. This is .. consistent with measurements of beam-plasma fusion reactions (Disdier et al, PRL 82, pp1454, 1999) Norreys et al Plas. Phys. Contr. Fus., 40, 175, (1998).

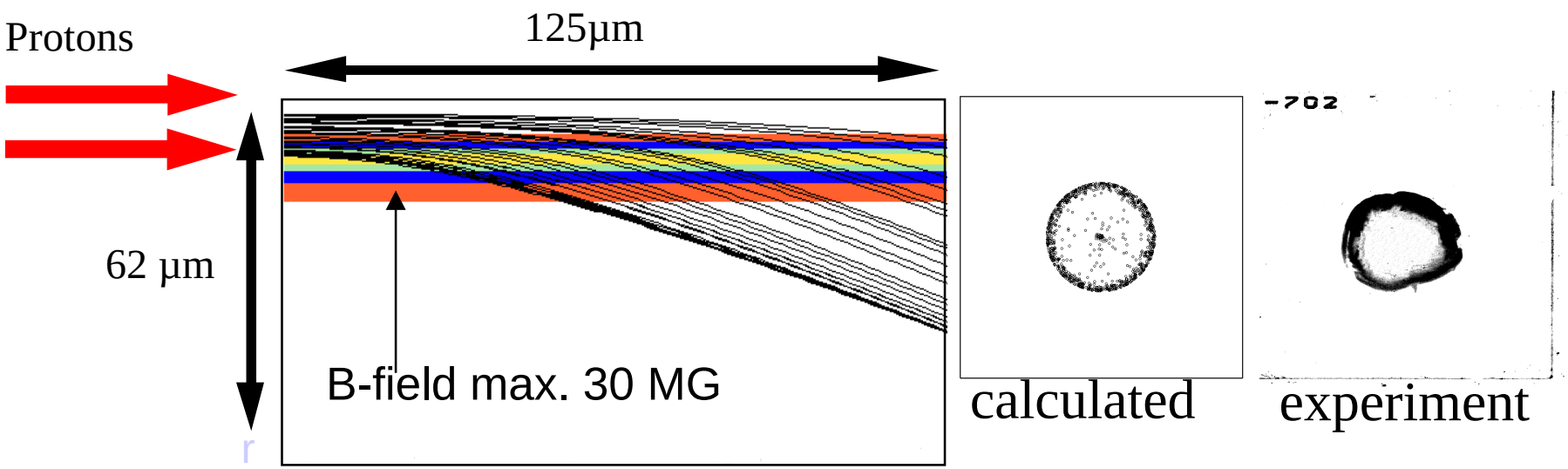

Thin targets produce large divergence disks, in accordance with expectations

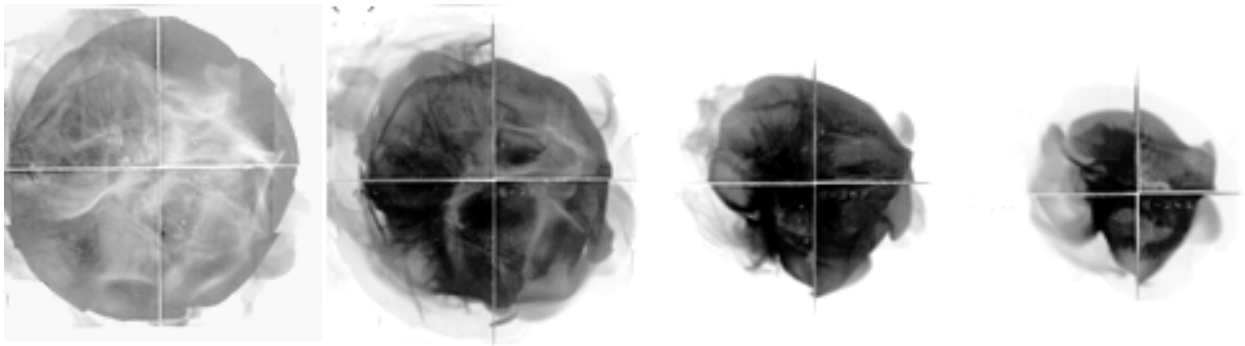

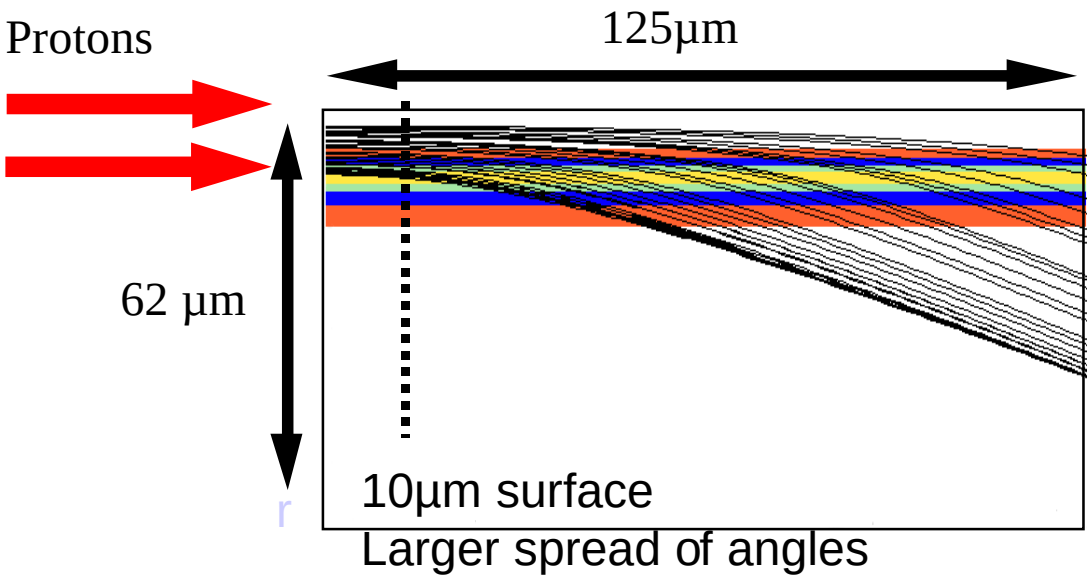

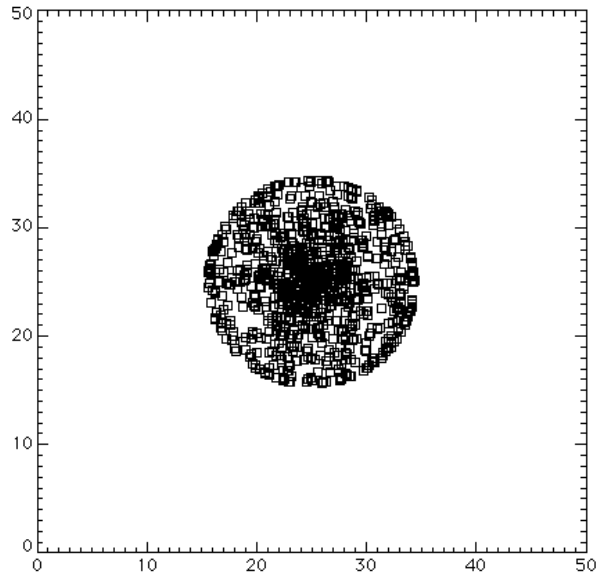

And we also have direct evidence.

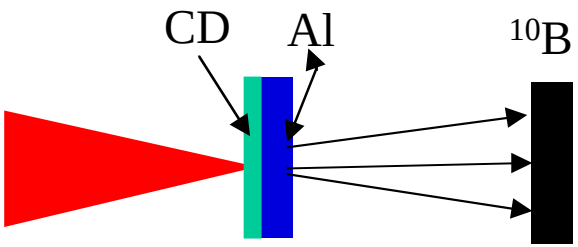

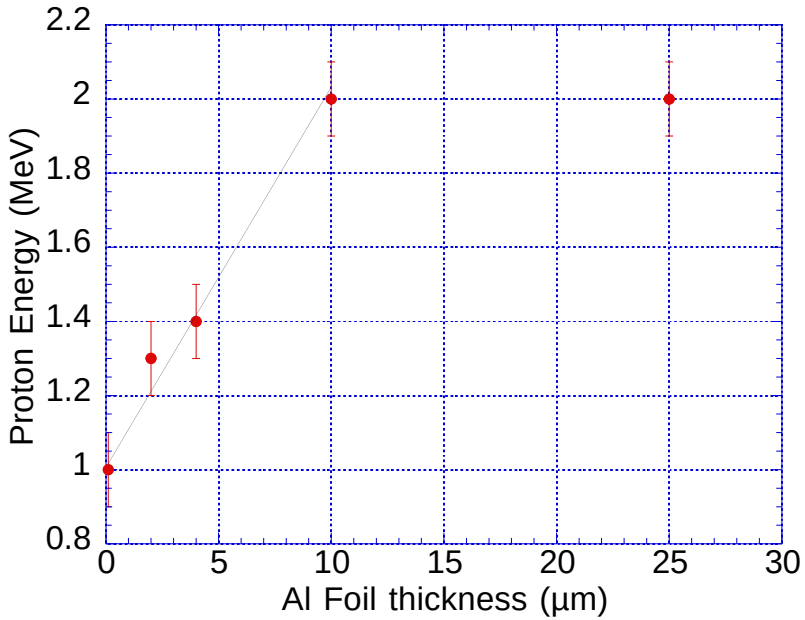

- Maksimchuk et al. show that at $I=10^{18}$ Wcm^{-2}
  PRL 84, pp4108 (2000), Appl. Phys. Lett, 78, pp595, (2001)
  - Deuteron activation of ^{10}B sample occurs only with D on front
  - Proton energy *increases* with target length.
    ⇒Consistent with protons from the front.

Strong influence of the rear surface - does rear surface acceleration dominate ?

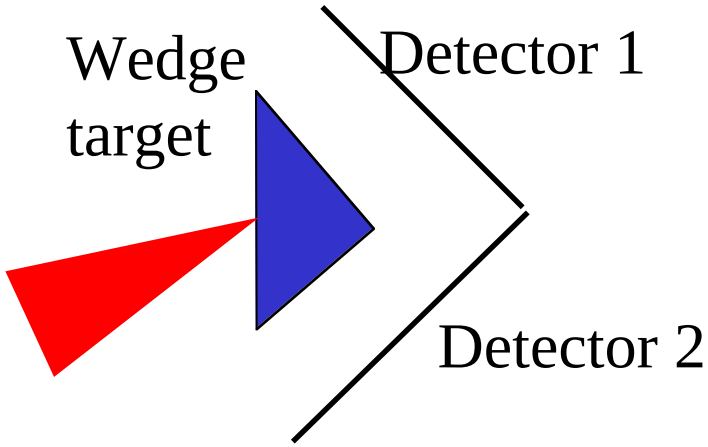

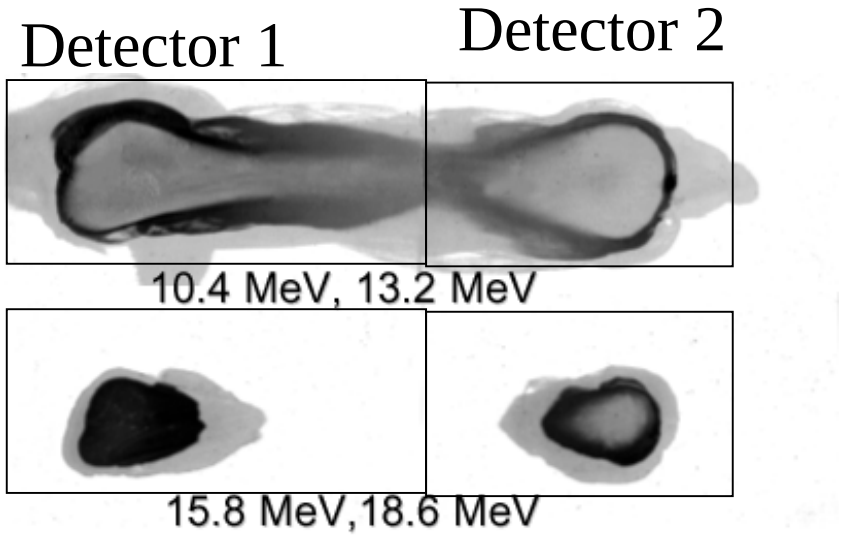

- The signal from wedge targets is centred on the rear surface normal. (R. Snavely et al.,PRL, 85, pp2945 (2000)
  - Top and bottom surfaces of target do not produce similar proton beams ⇒ More complicated than simple target charging.
- Forming a plasma on the rear surface suppresses proton production. (A. MacKinnon et al., PRL, 86, 1769 (2001)
- Large fields directly measured at rear. Hegelich et al, PRL, 89, 085002 (2002)

The Experiment

- **Idea:** Selectively contaminate target with protons
- **Problem:** Surface layer is contaminated with impurities (CH chains)
  - Protons are naturally everywhere
- **Solution:**
  - Heat targets to reduce contamination
  - Then **contaminate selectively**:
    Coat targets with high melting plastic (PEEK coating)

Control of contamination by heating an Al target

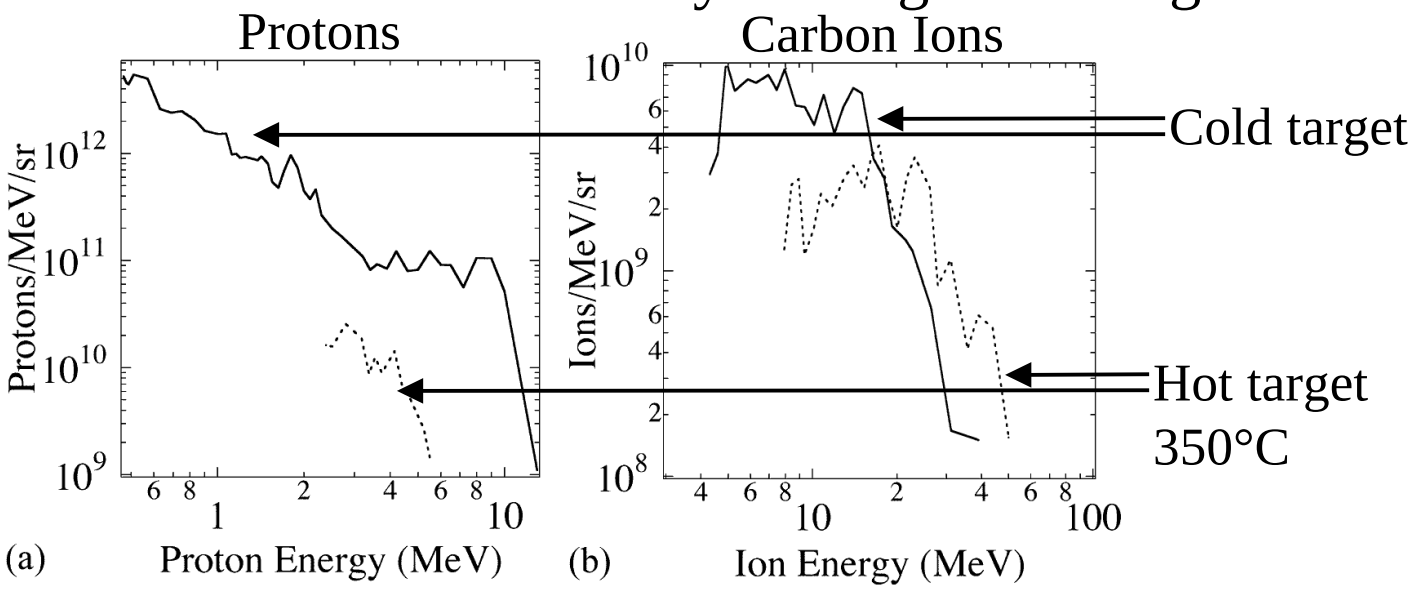

Selectively contaminated, heated targets

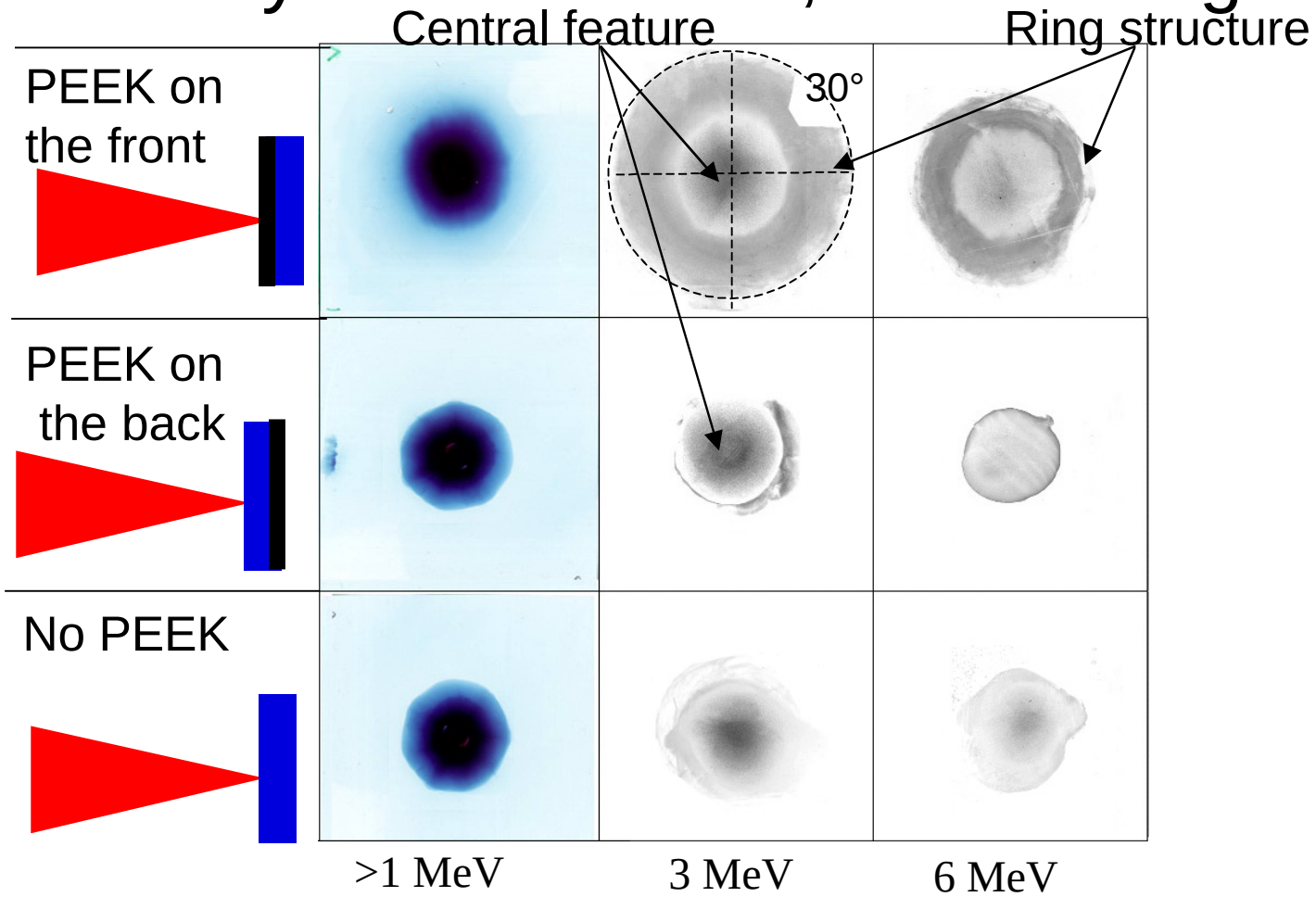

Biggest change is in the spatial structure!

Ring structure almost vanishes when no coating is present on the front of the target.
> 30 times the number of protons > 3 Mev measured at the rear with PEEK on the front

Spatial Structure

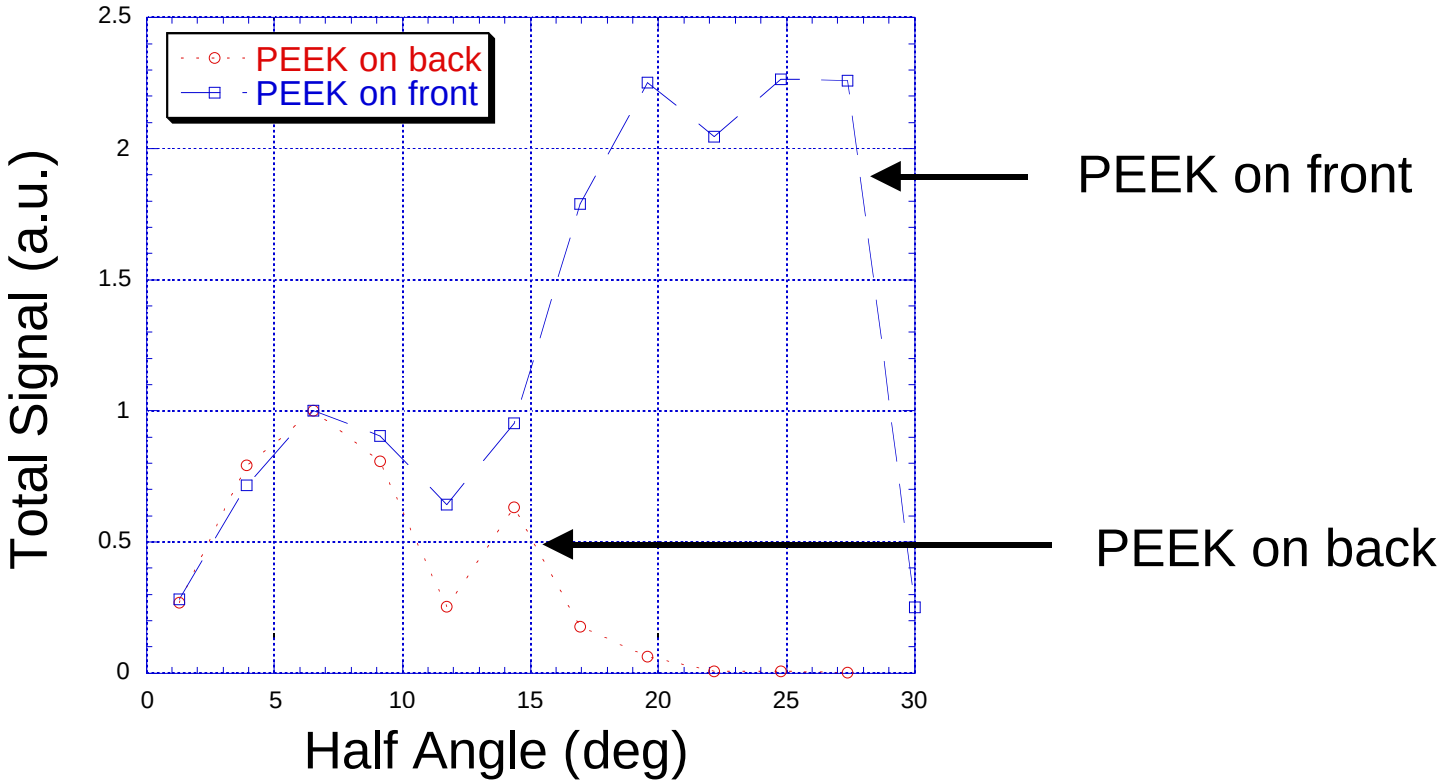

- CR39 signal clearly show the suppression of the outer ring when the coating is on the rear.

Central feature agrees with 3D PIC

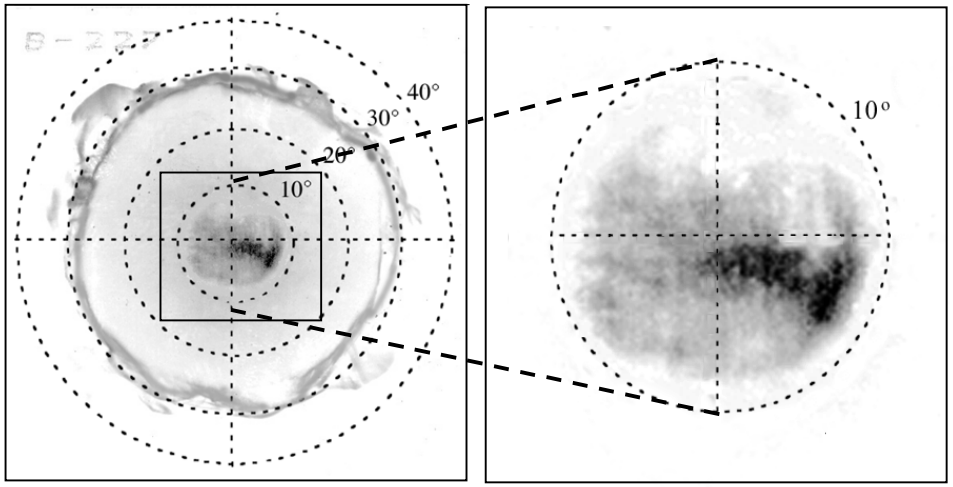

- Proton energy and angular distribution of central feature agrees well with 3D PIC by A. Pukhov.

Interplay of acceleration mechanisms

Acceleration during the Pulse

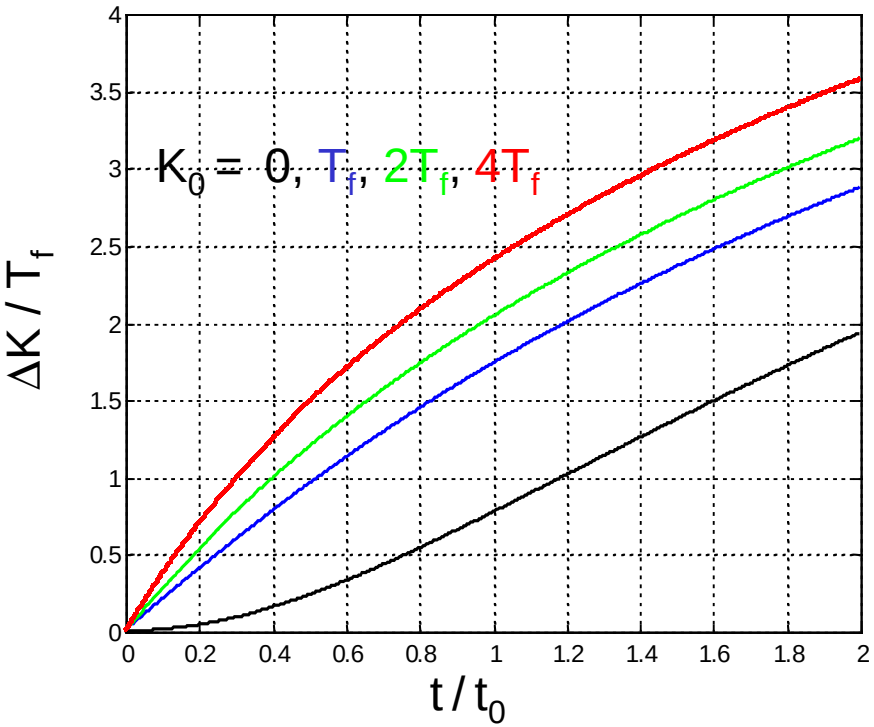

Finite pulse duration

$t_{pulse} = 0.25, 0.5, 1, 2\ t_0$

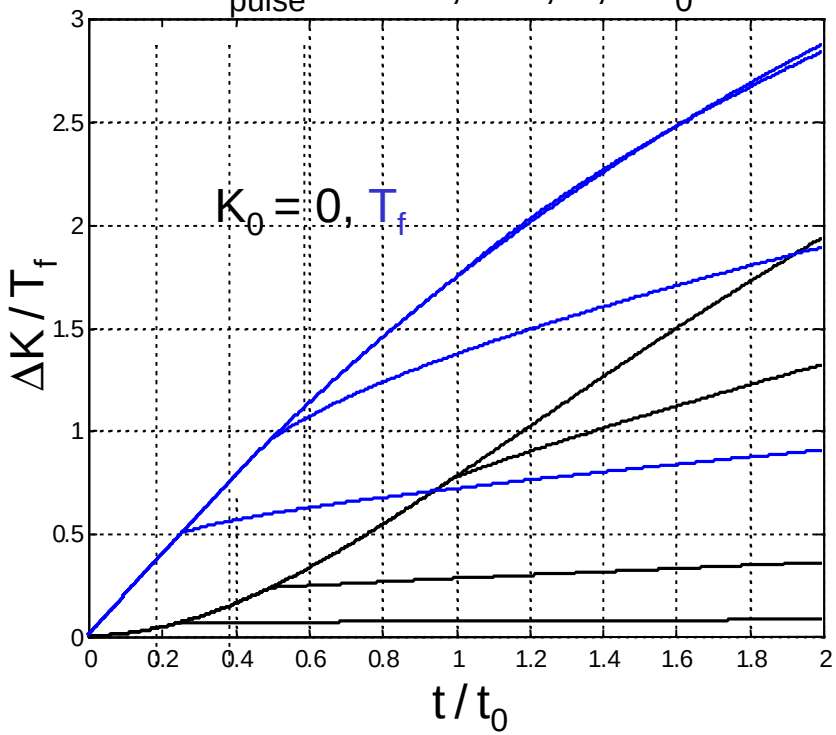

Calculations by JR Davies, to be published in Laser and Particle Beams

- Energy gain increases with time **and initial energy**
- Large energy gains are possible in the target as well for $K_0 \neq 0$
  - This is the case due to the acceleration at the front surface

Construct a picture to fit the experimental results.

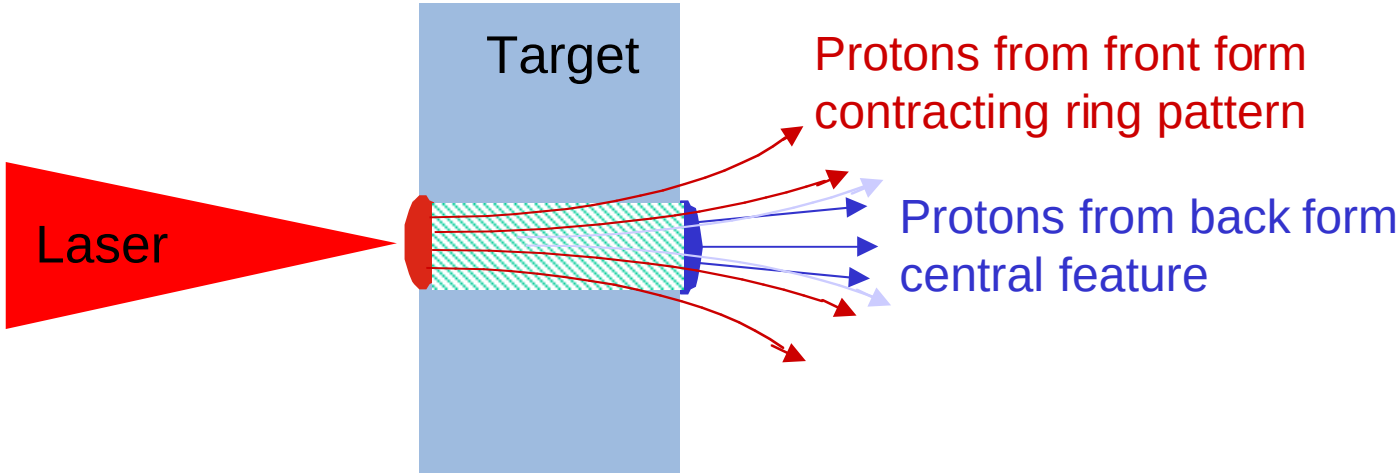

- Some Protons are accelerated at the critical surface.
  ⇒ these protons will gain most energy in the target.
  ⇒ these protons will gain most energy at the rear.
- Protons traversing the target will suffer deflection due to B-fields in the target
  ⇒ Ring structure.
  ⇒ Sharp minimum energy cut-off for outer ring.
- Large fields do exist at rear
  – Protons starting at rear are less likely to gain maximum energy.

Proton energy scaling

Flat spectrum consistent with front surface acceleration. L. Silva, Tuesday morning.

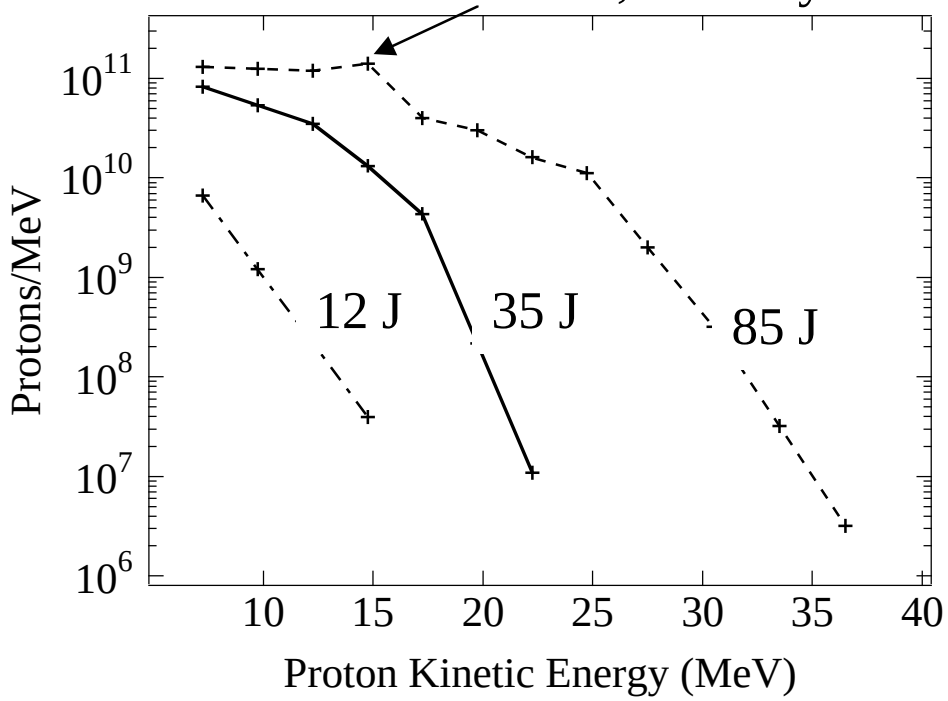

- Target: 10µm Al
- Temperature
  ~ 1.8 MeV for 12 J
  ~ 5 MeV for 85J
- Energy conversion
  $\eta \sim 2\ 10^{-3}$ for 12 J
  $\eta \sim 5\ 10^{-2}$ for 85 J
  $\eta \sim 1\ 10^{-1}$ for 400 J(LLNL)

Proton energy and efficiency scale rapidly with intensity.

Data acquired for constant focusing conditions.

Results

- Protons originating from front and rear have been identified.
  - Protons with multi-MeV energies originate both from the front and the rear of the target.
  - Consistent with previous experiments
  - Everybody is right…
- Different origin results in specific spatial signature
  - Wide angle signal from the front of the target.
    - Ring structure for thick targets, disk structure for thin targets
    - extends to the highest energies observable.
  - Central feature protons directly accelerated from rear.
    - Gain less energy
    - dominates low energy (up to 4-5 MeV) protons signal.

Summary and Caveats

- Complicated parameter space
  - Protons in Michigan experiments from the front
  - Protons in in high energy, ps experiments -> front and rear front dominates in RAL experiments
  - Thin foil JanUSP experiments probably from rear
- Relative strength of signals will depend on experiment.
  - Target thickness, pulse duration, intensity and prepulse
- Results will depend on detector type and size.
- Some more work is required to explain all experiments satisfactorily.
  - Wedges and plasma formation beams make experiments much more complicated.